Technical Report EL-94-4
May 1994

US Army Corps of Engineers
Waterways Experiment Station

Three-Dimensional Eutrophication Model of Chesapeake Bay

Volume I: Main Report

by Carl F. Cerco, Thomas M. Cole

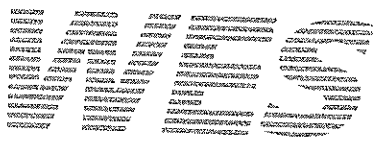

Approved For Public Release; Distribution Is Unlimited

Prepared for U.S. Environmental Protection Agency
and U.S. Army Engineer District, Baltimore

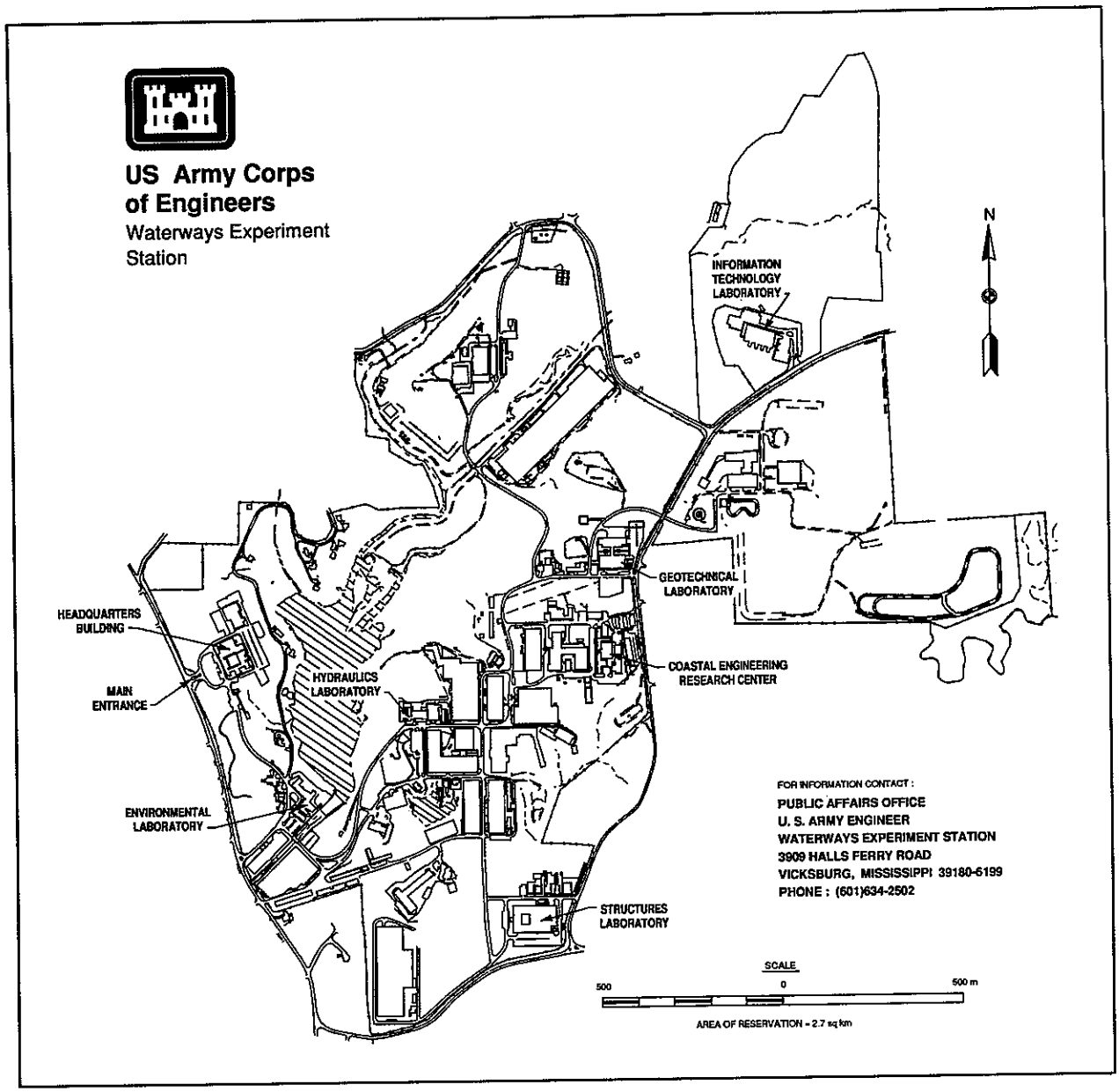

Waterways Experiment Station Cataloging-in-Publication Data

Cerco, Carl F.
Three-dimensional eutrophication model of Chesapeake Bay. Volume I, Main report / by Carl F. Cerco, Thomas M. Cole ; prepared for Chesapeake Bay Program Office, U.S. Environmental Protection Agency and U.S. Army Engineer District, Baltimore.
658 p. : ill. ; 28 cm. -- (Technical report ; EL-94-4 v.1)
Includes bibliographic references.
1. Eutrophication -- Chesapeake Bay (Md. and Va.) -- Mathematical modelss. 2. Water quality -- Chesapeake Bay (Md. and Va.) -- Mathematical models. 3. Sedimentation and deposition -- Chesapeake Bay (Md. and Va.) -- Mathematical models. 4. Algal blooms. I. Cole, Thomas M. II. United States. Army. Corps of Engineers. Baltimore District. III. United States. Environmental Protection Agency. Chesapeake Bay Program. IV. U.S. Army Engineer Waterways Experiment Station. V. Title. VI. Series: Technical report (U.S. Army Engineer Waterways Experiment Station) ; EL-94-4 v.1.
TA7 W34 no.EL-94-4 v.1

Contents

Preface vii

I—Introduction 1-1

Requirements for Present Study 1-2
The Technical Workshops 1-3
The Chesapeake Bay Model Package 1-6

II—The Study System 2-1

Physical Description 2-1
Hydrology 2-3
Eutrophication Processes 2-13

III—Hydrodynamic Model and Computational Grid 3-1

Introduction 3-1
The Hydrodynamic Model 3-1
Linkage to the Water Quality Model 3-2
Volumetric Flows 3-6

IV—The Water Quality Model 4-1

Introduction 4-1
Conservation of Mass Equation 4-4
Algae 4-5
Organic Carbon 4-22
Phosphorus 4-27
Nitrogen 4-37
Silica 4-44
Chemical Oxygen Demand 4-47
Dissolved Oxygen 4-47
Total Active Metal 4-50
Salinity 4-51
Temperature 4-54

V—Loads to the System 5-1

Introduction 5-1
Fall-Line Loads 5-1
Below-Fall-Line Nonpoint-Source Loads 5-3
Point-Source Loads 5-5

Atmospheric Loads 5-7
Summary 5-9

VI—Linking in the Loads 6-1

Introduction 6-1
Guidelines from Observations 6-2
Model Parameters 6-5

VII—The Data Bases 7-1

Monitoring Data 7-1
Supplementary Monitoring Data 7-6
Primary Production 7-7

VIII—Boundary Conditions 8-1

Introduction 8-1
Fall-Line Boundary Conditions 8-1
Oceanic Boundary Conditions 8-3

IX—Parameter Evaluation 9-1

Introduction 9-1
Algae 9-1
Hydrolysis and Mineralization Rates 9-21
Detrital Settling Rates 9-22
Nitrification 9-23
Chemical Oxygen Demand 9-25
Particulate Biogenic Silica 9-26
Reaeration 9-26
Total Active Metal 9-27

X—Coupling with the Sediment Model 10-1

Introduction 10-1
Description of Sediment Model 10-3
Flux 10-5
Data Bases 10-7
Coupling the Water Column and Sediment Submodel 10-10

XI—Mainstem Bay Calibration Results 11-1

Introduction 11-1
Time-Series Plots 11-7
Longitudinal Transects 11-12
Spatial Dissolved Oxygen Distribution 11-16
Additional State Variables 11-16
Observed and Modelled Eutrophication Processes 11-17
Suggested Improvements 11-41
Performance of Open-Mouth Boundary Conditions 11-47
Mass Balance and Flux Analyses 11-50

XII—Tributary Calibration Results 12-1

Introduction 12-1
Time-Series Plots 12-1
Longitudinal Transects 12-3
Carbon and Nutrient Budgets 12-3
The James River 12-3
The Potomac River 12-16
Rappahannock, York, and Patuxent Rivers 12-35
Conclusions 12-39

XIII—Statistical Summary of Calibration 13-1

Introduction 13-1
Presentation Format 13-1
Evaluation of Results 13-3
Sediment Model Performance 13-16
Comparison with Alternate Models 13-18

XIV—Thirty-Year Analysis 14-1

Introduction 14-1
The Data Base 14-1
Approach and Objectives 14-8
Hydrology and Hydrodynamics 14-9
Loads 14-12
Thirty-Year Simulation Results 14-29
Hydrodynamics or Loads? 14-76
Nitrogen or Phosphorus? 14-80
Summary and Conclusions 14-81

XV—Scenarios and Load Sensitivity Analyses 15-1

Introduction 15-1
How Long to Steady State? 15-2
Analytical Approach 15-2
Empirical Approach 15-13
Comparison of Analytical and Empirical Results 15-19
Discussion 15-25
Scenario Design--Duration, Hydrology, and Hydrodynamics 15-28
Scenario Nutrient Loads 15-33
Point Sources 15-33
Fall-Line Loads 15-35
Below-Fall-Line Loads 15-38
Atmospheric Loads 15-39
Oceanic Nutrient Loads 15-39
Load Summary 15-41
Scenario Descriptions 15-44
Management Scenarios 15-45
Response Scenarios 15-53
System Response to Nitrogen and Phosphorus Loads 15-55
Mainstem Bay Under LOT and All-Forested Conditions 15-72

Influence of Nitrogen and Phosphorus on Anoxia 15-101
Summary 15-107

XVI—Summary and Conclusions 16-1

Background 16-1
The Study System 16-3
Hydrodynamic Model and Computational Grid 16-8
The Water Quality Model 16-12
Existing Loads to the System 16-21
The Data Bases 16-23
Coupling with the Sediment Model 16-25
Mainstem Bay Calibration 16-28
Tributary Calibration 16-30
Statistical Summary of Calibration 16-34
Thirty-Year Analysis 16-37
Scenarios and Load Sensitivity Analyses 16-42
Comparison with Current Paradigms 16-47
In Conclusion 16-50

References Ref-1

SF 298

Preface

The Chesapeake Bay Three-Dimensional Model Study was sponsored by the Chesapeake Bay Program Office (CBPO), U.S. Environmental Protection Agency, and the U.S. Army Engineer District, Baltimore (CENAB). Project monitors were Mr. Lewis Linker, CBPO, and Mr. Larry Lower, CENAB.

The water-quality model portion of the study was conducted by Dr. Carl F. Cerco and Mr. Thomas Cole, Water Quality and Contaminant Modeling Branch (WQCMB), Environmental Laboratory (EL), U.S. Army Engineer Waterways Experiment Station (WES). Supervision of the water-quality model activities was provided by Dr. Mark Dortch, Chief, WQCMB. Project management was provided by Mr. Donald Robey, Chief, Environmental Processes and Effects Division, EL. Overall supervision was provided by Dr. John W. Keeley, Director, EL.

At the time of publication of this report, Director of WES was Dr. Robert W. Whalin. Commander was COL Bruce K. Howard, EN.

This report should be cited as follows:

> Cerco, C. F., and Cole, T. M. (1994). "Three-dimensional eutrophication model of Chesapeake Bay; Volume 1, Main report," Technical Report EL-94- , U.S. Army Engineer Waterways Experiment Station, Vicksburg, MS.

Chapter I: Introduction

The present study commenced with a series of technical workshops held in Annapolis and Baltimore, Maryland, in autumn, 1987. The roots of the study extend back to 1983, however. In that year, a technical synthesis (Flemer et al. 1983) concluded that the volume of anoxic water in the Bay had increased by an order of magnitude from 1950 to 1980. The conclusion was controversial; an alternate, contemporary, synthesis (Heinle et al. 1980) reported that dissolved oxygen concentration in the Bay had not changed greatly. The existing data base was insufficient to conclusively determine whether anoxia was increasing or not. Other indicators, however, including diminished fisheries harvest and shrinking distribution of submerged aquatic vegetation, supported the judgement that natural resources of the Bay were deteriorating. The potential loss of Bay resources spawned increased activity in Bay monitoring, ecological research, and modeling for management purposes.

The first management model completed after the reported increase in anoxic volume was a two-dimensional, vertically-averaged, hydrodynamic and water quality model (Chen et al. 1984). Examination of the results of this rapidly-completed study indicated greatly expanded efforts were required to produce a model sufficient for management of eutrophication in the Bay. Required improvements included a fully three-dimensional model applied to an expanded, contemporary data base.

The succeeding modeling effort (HydroQual 1987) applied three-dimensional hydrodynamic and eutrophication models to data collected in 1965, 1984, and 1985. Summer-average, steady-state conditions were modeled independently in each year. The model provided credible representations of historic and contemporary conditions in the Bay and tributaries. Results of the study indicated that:

> Dissolved oxygen declined from 1965 to 1985 due to increased sediment oxygen demand and increased benthic nutrient releases.
>
> Bottom sediments were the largest sources of phosphate and ammonium during summer of 1984 and 1985.

Dissolved oxygen and algae were controlled largely by sediment oxygen demand, sediment nutrient release, and degree of vertical stratification.

Only management strategies that decreased sediment oxygen demand and sediment nutrient releases would significantly improve dissolved oxygen and algal conditions.

Despite the success of the modeling effort, limitations were apparent. The chief limitation was absence of a predictive model of sediment-water interactions. The study indicated that sediment release was the dominant source of nitrogen and phosphorus during summer conditions. Sediment oxygen demand was a major dissolved oxygen sink. No means existed to predict how these sediment processes would respond to nutrient load reductions, however. Neither was the time scale for completion of the responses predictable. A second limitation was the steady-state nature of the analysis. The steady-state model allowed no influence of conditions in previous years or seasons on summer-average water quality.

The HydroQual study provided the technical basis for the 1987 Chesapeake Bay Agreement. In the agreement, the chief executives of Pennsylvania, Maryland, Virginia, and the District of Columbia pledged to reduce by forty percent the amounts of nitrogen and phosphorus entering the mainstem of Chesapeake Bay. In view of uncertainties associated with the model study, however, a portion of the Chesapeake Bay Agreement called for a 1991 reevaluation of the forty-percent nutrient reduction goal.

Requirements for Present Study

The EPA Chesapeake Bay Program Office formulated requirements for a model to address remaining technical issues in time for the 1991 reevaluation. Requirements included:

Ability to analyze the current origins and extent of anoxia.

Ability to predict the future of the Bay as a result of management action or inaction.

Ability to reconstruct the processes that have led the Bay to its present condition.

Eight capacities were envisioned in order for a model to meet the requirements. These were:

Simulation of responses of water quality and sediment processes to point and nonpoint-source control actions.

Performance of short-term (annual) and long-term (decades) simulations.

Determination of the effect of spring runoff events on summer anoxia.

Simulation of lateral water quality variations.

Determination of Bay response to area-specific management activities.

Determination of response time of the Bay to management actions.

Evaluation of frequency of critical water-quality events.

Evaluation of historical changes in anoxia.

The Technical Workshops

Negotiations between the EPA Chesapeake Bay Program Office, the U.S. Army Engineer District, Baltimore, and the U.S. Army Engineer Waterways Experiment Station led to selection of the Waterways Experiment Station to conduct the next phase of eutrophication modeling in the Bay. Four workshops were convened to guide formulation of a technical approach for the model study. The workshops were attended by members of government, academia, and industry within and outside the Bay community.

Workshop I: Water Column State Variables and Aquatic Processes

The first workshop was convened to recommend the water quality processes and state variables to be represented in the eutrophication model. Participants first identified biogeochemical processes that affect eutrophication in the Bay. Recommendation to include a process in the model depended on the importance of the process, the level of understanding of the process, and the availability of data. When possible, suggestions for mechanistic formulation were presented along with recommendations for inclusion in the model. Participants also identified additional data and research needs to enhance model calibration and verification.

Workshop recommendations were:

Include twenty-two state variables in the eutrophication model:

Salinity,

Suspended Solids,

Three phytoplankton groups: diatoms, non-diatoms, and blue-green algae,

Zooplankton,

Three carbon forms: dissolved organic, labile particulate organic, and refractory particulate organic,

Five nitrogen forms: ammonium, nitrate+nitrite, dissolved organic, labile particulate organic, and refractory particulate organic,

Five phosphorus forms: dissolved inorganic, particulate inorganic, dissolved organic, labile particulate organic, and refractory particulate organic,

Dissolved oxygen, and

Two silica forms: dissolved and particulate biogenic.

Defer until a subsequent workshop a decision to include methane and sulfide as state variables.

A mechanistic model of submerged aquatic vegetation was not feasible. Treat effects of submerged aquatic vegetation on water quality through specified sources and sinks.

Add total silica to the monitoring program.

Measure labile and refractory fractions and decay rates of particulate organic nutrient forms.

Investigate sensitivity to inclusion of bacteria and multiple zooplankton groups in the model.

Workshop II: Sediment Processes and Sediment Modeling

The second workshop was convened to recommend formulation and state variables for a predictive model of sediment oxygen demand and nutrient fluxes. The workshop commenced with presentation of a proposed sediment model. The model was based on an existing model of oxygen demand and nitrogen flux in freshwater sediments (DiToro et al. 1990). Three processes were represented in the proposed model: deposition of particulate matter to the sediments, diagenesis (decay) within the sediments, and flux to the water column. Activity focused on coupling between the models of the water column and sediments and on employment of data for model calibration and verification. Participants identified existing sediment composition and flux

data and reviewed a plan to collect additional data sufficient to calibrate and verify a predictive sediment model.

The workshop provided a large number of recommendations. The most significant were:

> The diagenesis portion of the model would consider three organic matter fractions: labile, refractory, and inert.
>
> Model calibration required measurement of sediment oxygen demand and sediment-water fluxes of ammonium, nitrate, phosphate and silica. Measures were to be collected at a minimum of fifteen mainstem stations four to six times per year.
>
> Additional measures should be collected including sulfate depletion, sulfide release, CO_2 production, and nitrogen gas production.
>
> Burial rates should be determined from analysis of sediment cores using pollen or lead-210 dating techniques.
>
> Two to four particle traps should be deployed in the water column to measure deposition of particulate matter.
>
> The recommendation of the first workshop to measure labile and refractory fractions and decay rates of organic particles was repeated. Measures were recommended of particles in point and nonpoint load sources and in the water column.

Workshop III: Hydrodynamic and Water Quality Model Interfacing

In large-scale eutrophication model studies, models of hydrodynamic and water quality processes are often executed separately. Output from the hydrodynamic model is stored on magnetic media and read as input by the water quality model. Transfer of information from the hydrodynamic to the water quality model is described as "linkage" or "interfacing." Treatment of information during the transfer can greatly affect the results of the water quality modeling effort.

The third workshop focused on several issues. Temporal and spatial resolution required in the hydrodynamic model to adequately represent transport processes were examined. Calibration data sets were identified. The time period for model application was determined. Tests and procedures for linkage of the two models were specified. The most substantial recommendations were:

Three years should be simulated: 1984, 1985, 1986. The three-year period covered a range of hydrologic conditions from extremely wet to extremely dry.

The hydrodynamic grid should contain roughly 600 cells in the surface plane. Vertical resolution should include at least ten layers.

The feasibility of averaging hydrodynamic output prior to water quality input should be examined as quickly as possible. Feasibility should be examined on multiple time scales from two to twelve hours.

Techniques must be developed for computing the dispersion coefficient resulting from temporal and spatial averaging of hydrodynamic output.

Workshop IV: Long-Term Modeling of Chesapeake Bay

The final workshop convened to examine techniques for long-term (decades) modeling of the Bay. Two considerations made long-term modeling desirable. The first was the time scale of management scenarios. The simulated period had to exceed the time required for bottom sediments to respond to load reductions. The response time was unknown but a time scale of decades was suspected. A second intention of long-term modeling was identification and examination of long-term trends in Bay water quality.

Computational feasibility of long-term model runs was a prime consideration in the workshop. Early in the proceedings, participants recognized that creation of decades of hydrodynamics, computed at intervals of minutes, exceeded the computational and storage capabilities of the largest supercomputers. Consequently, an approach was adopted in which hydrodynamics from 1984, 1985, and 1986, representative of wet, dry, and average hydrological conditions, would be pieced together to approximate long-term transport processes. Additional recommendations were:

A thirty-year period, beginning in the 1950's should be simulated.

Initial long-term model runs should be performed using the existing steady-state model.

The Chesapeake Bay Model Package

A package of interactive models (Figure 1-1) was assembled to comply with requirements and recommendations for the eutrophication model study.

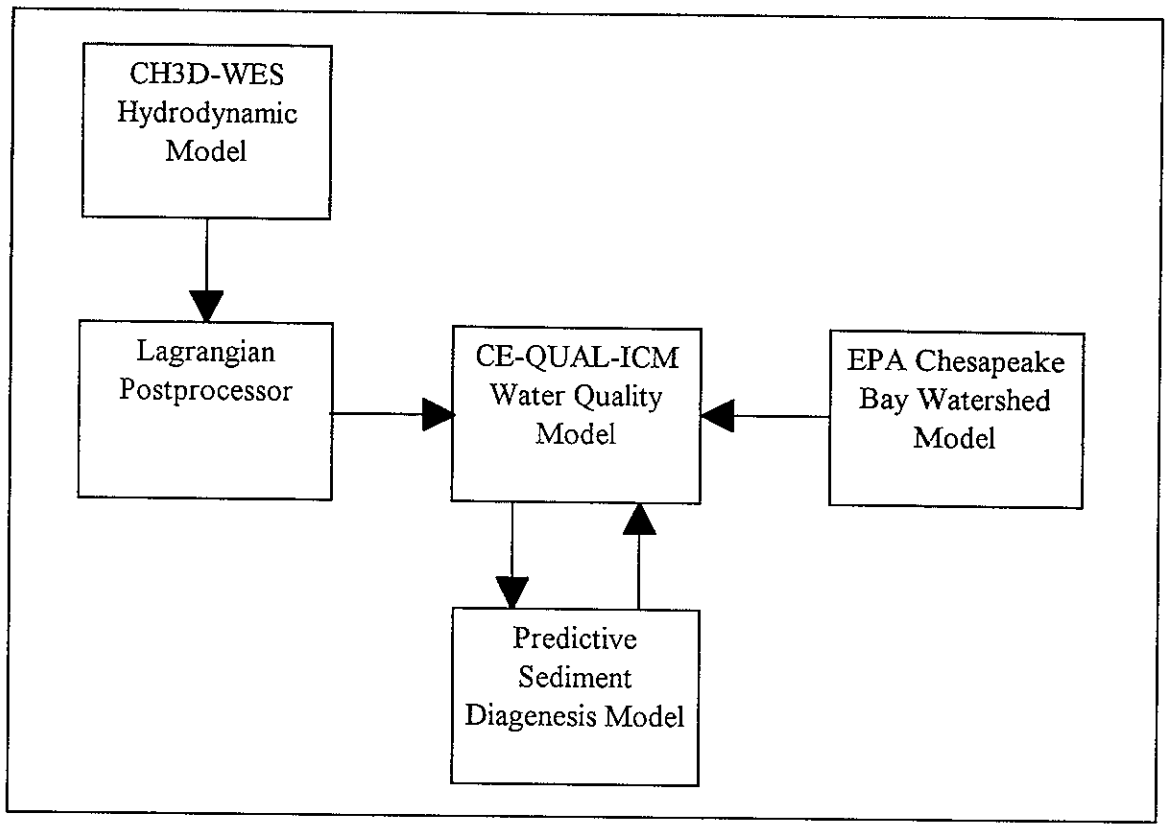

Figure 1-1. The Chesapeake Bay Model Package

The CH3D-WES hydrodynamic model (Johnson et al. 1991) produced three-dimensional predictions of velocity, diffusion, surface elevation, salinity, and temperature on an intratidal (five-minute) time scale. A processor appended to CH3D-WES filtered intratidal details from hydrodynamic output but maintained intertidal (twelve-hour) transport (Dortch 1990). Intertidal flows, vertical diffusion, and surface elevation were written to disk for subsequent use by the water quality model, dubbed CE-QUAL-ICM. Computation of eutrophication processes within the water quality model was conducted on a two-hour time scale. The water quality model interacted dynamically with a predictive sediment diagenesis model (DiToro and Fitzpatrick 1993). Fall-line loads and below-fall-line non-point source loads were supplied to the eutrophication model by the EPA's Chesapeake Bay Watershed model (Donigian et al. 1991).

The present report is the primary reference for the formulation of the CE-QUAL-ICM water quality model and application to Chesapeake Bay. Summary descriptions of the hydrodynamic and sediment modeling efforts are included as well.

Chapter II: The Study System

Physical Description

The Chesapeake Bay system (Figure 2-1) consists of the mainstem bay, five major western-shore tributaries, and a host of lesser tributaries and embayments. Urban centers along the Bay and tributaries include Norfolk and Richmond Va., Washington, D.C., and Baltimore, Md. The mainstem is roughly 300 km long, 8 to 48 km wide, and 8 m average depth. A deep trench with depths to 50 m runs up the center of the mainstem.

Table 2-1
Physical Characteristics of Chesapeake Bay (Cronin, cited by Flemer et al. 1987)

Length	290 km
Width	8 to 48 km
Depth	53 m maximum, 8.4 m mean (open Bay), 6.5 m mean (with tributaries)
Surface Area	6,500 km^2 (open Bay), 11,500 km^2 (with tributaries)
Shoreline	13,000 km
Volume	52 x 10^9 m^3 (open Bay, low tide), 74 x 10^9 m^3 (total, low tide)

Total drainage area of the Bay is 166,000 km^2. The primary source of freshwater to the system is the Susquehanna River (≈ 64% of total gauged freshwater flow) which empties into the northernmost extent of the Bay. Other major freshwater sources are the Potomac (≈ 19%) and James Rivers (≈ 12%). The remaining western-shore tributaries, the York (≈ 3%), the Rappahannock (≈ 3%), and the Patuxent (< 1%) contribute only small fractions of the total freshwater flow to the Bay.

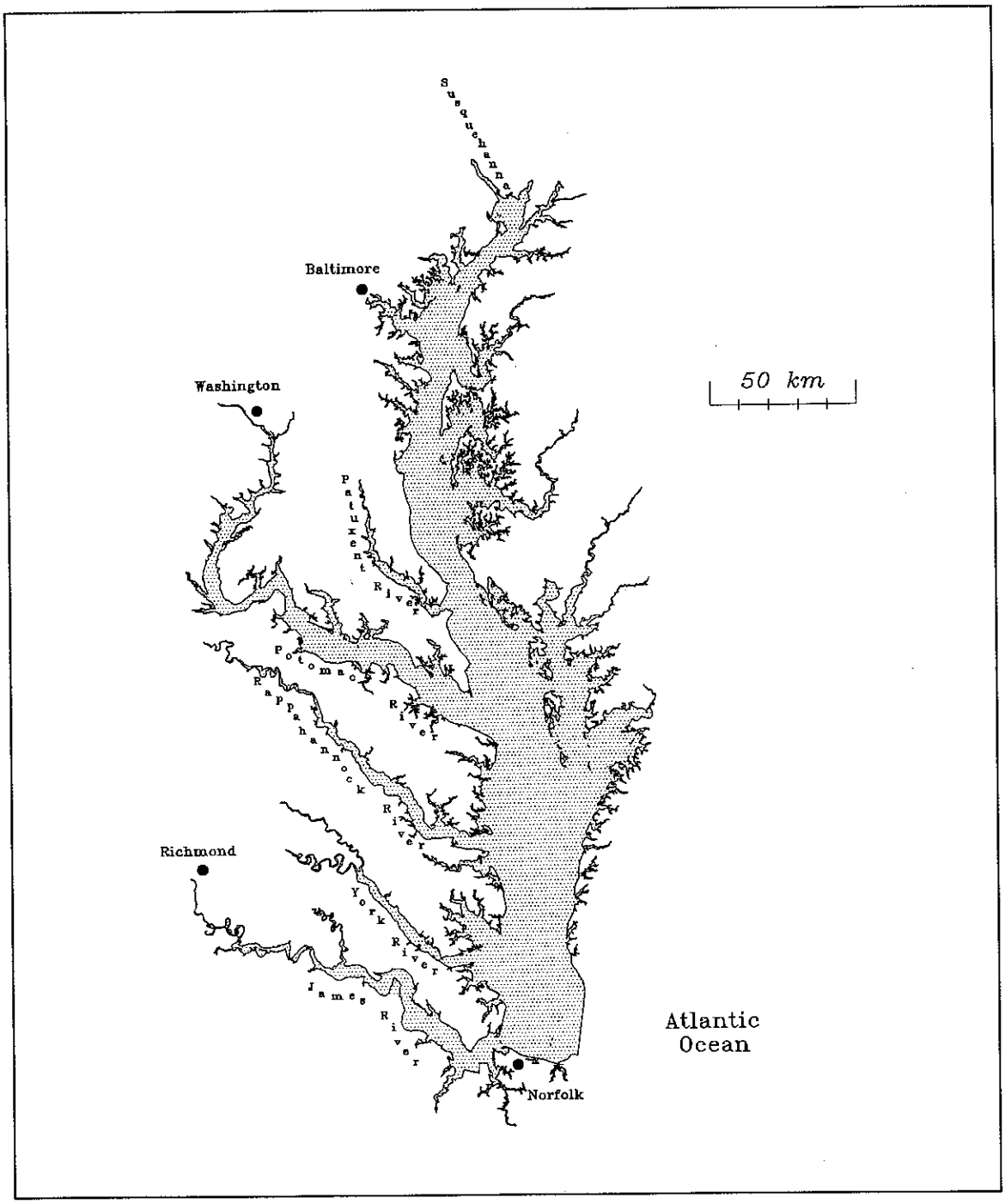

Figure 2-1. The Chesapeake Bay System

The mainstem Bay and major tributaries are classic examples of partially-mixed estuaries (Pritchard 1967). When flows in these estuaries are averaged over lengthy time periods, generally more than fifteen days, a net longitudinal circulation is evident. Longitudinal density gradients push bottom water

Table 2-2
Freshwater Inflow to Chesapeake Bay (Cronin, cited by Flemer et al. 1987)

Mean	2,178 m^3 sec^{-1}
Lowest Annual Mean	1,387 m^3 sec^{-1}
Highest Annual Mean	3,720 m^3 sec^{-1}
Extreme Low	134 m^3 sec^{-1}
Extreme High	28,320 m^3 sec^{-1}

upstream and enhance flow of surface water downstream. The volume of the density-induced flow vastly exceeds the volume of freshwater runoff.

Effects of the earth's rotation on long-term circulation induce flow predominance towards the right. The level of no net motion is tilted so that the depth of the downstream-flowing surface layer is less along the right-hand side, looking upstream, than along the left. In the mainstem, rotational effects are evident in surface salinity which is higher along the eastern shore than along the western shore (Figure 2-2). Under some circumstances, the level of no net motion intersects the surface so that net surface flow is upstream along the eastern portion of the bay.

Net long-term circulation is altered by forcing functions which act on a variety of time scales. Tidal cycling of flow occurs with a period of 12.4 hours. Winds acting on the surface of the Bay induce lateral and longitudinal motions with time scales of two to five days (Wang and Elliott 1978). Wind effects on coastal sea level force water into and out of the Bay with time scales of 20 days (Wang and Elliott 1978).

Hydrology

An annual runoff cycle exists in the major bay tributaries. Peak flows typically occur in March or April while minimum flows occur in August and September. On a logarithmic scale, the cycling between high and low flows is roughly sinusoidal. Both floods and droughts cause daily and monthly flows to deviate from the long-term pattern. The occurrence of maximum annual flow is particularly susceptible to flood events. As a result of tropical storms, maximum flow may occur in late summer or in autumn rather than in spring. The Susquehanna River is, by far, the major source of freshwater to the bay. The runoff volume and location of the fall line at the head of the bay make the Susquehanna a prime determinant of stratification and circulation in the mainstem. Flow in the Susquehanna exhibits typical annual cycling (Figure 2-3). Deviations from long-term flows occur as a result of flow regulation at the fall line as well as meteorological events. Regulation at the Conowingo Dam

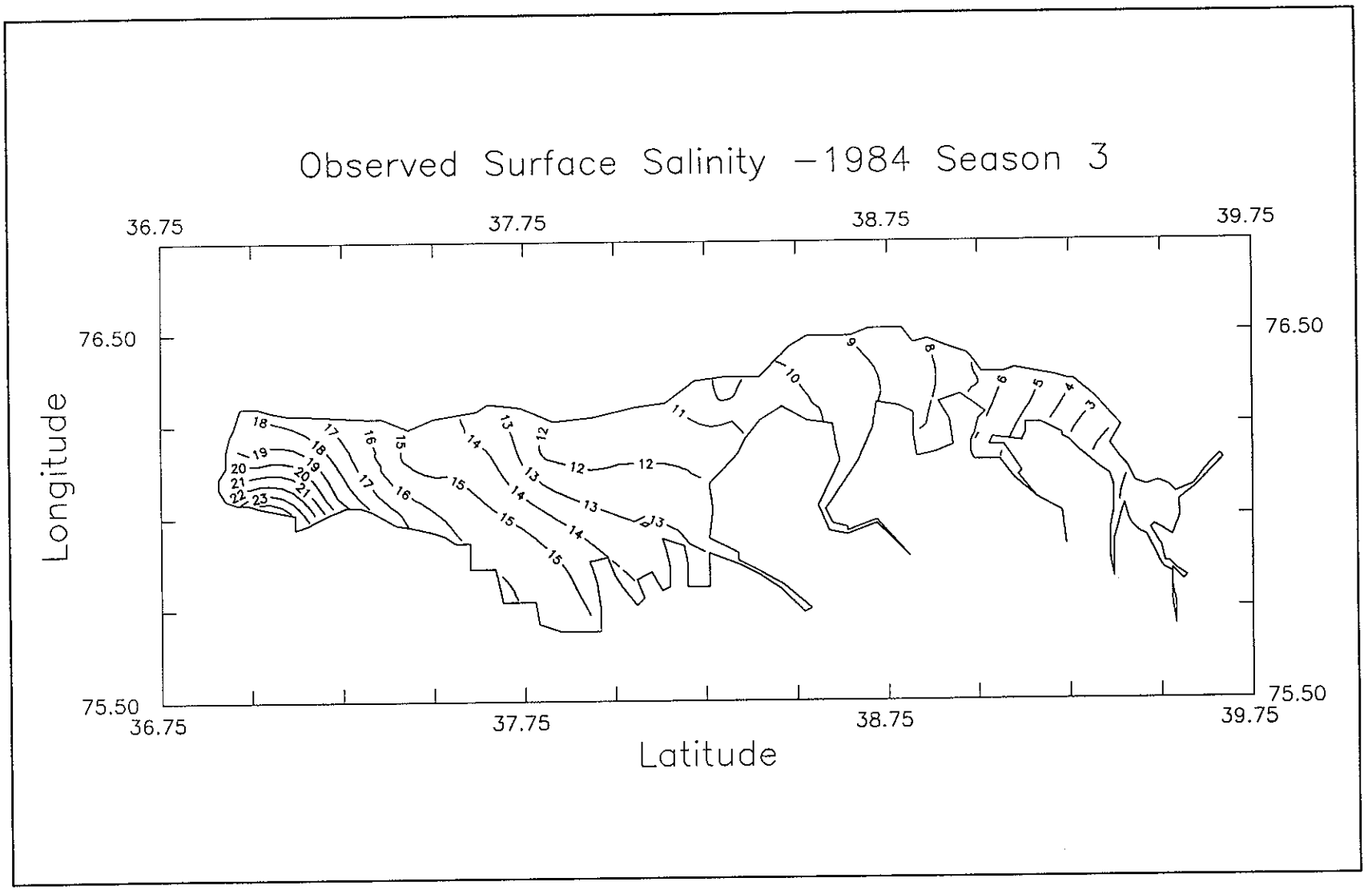

Figure 2-2. Surface Salinity in Mainstem Bay, Summer 1984

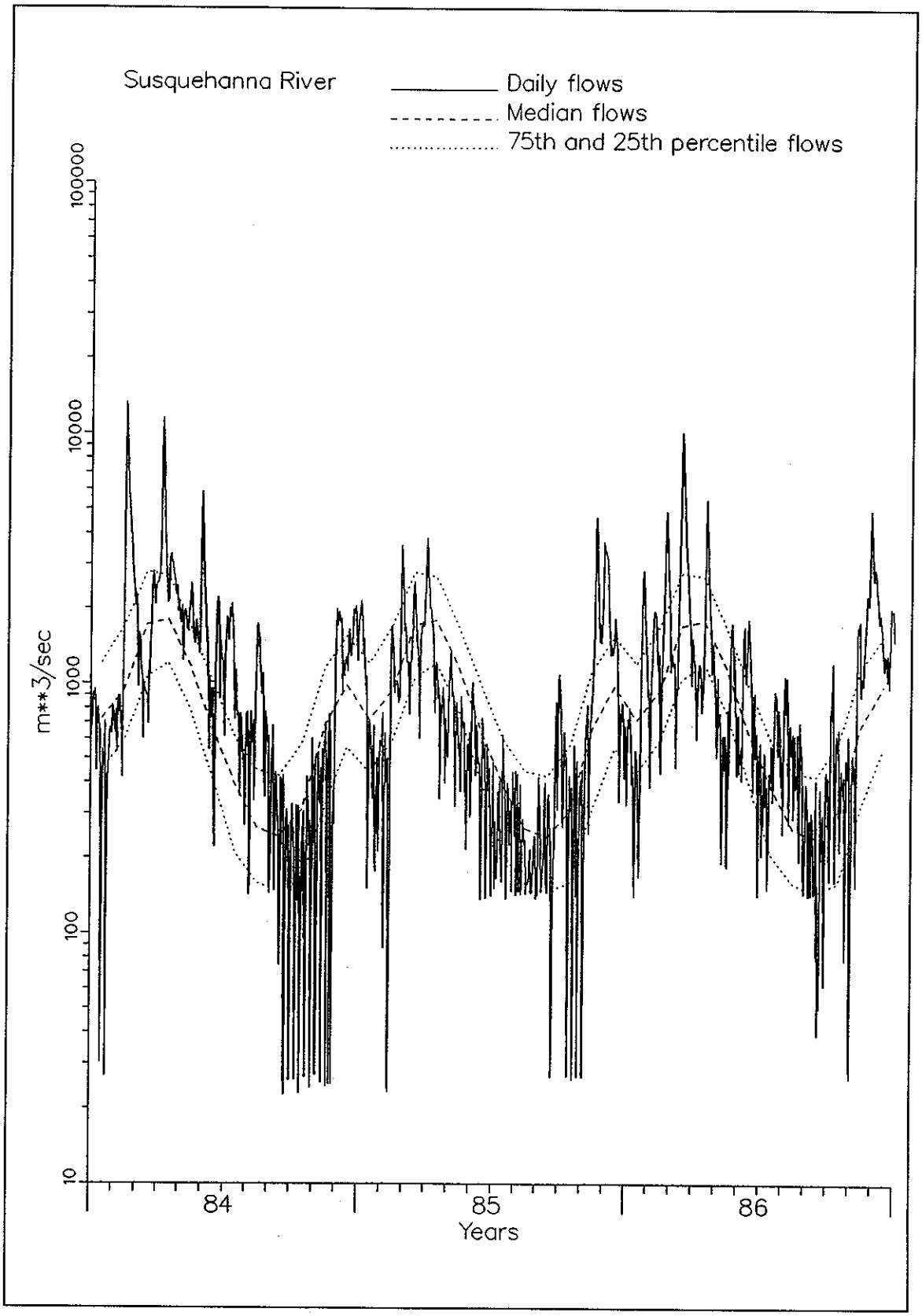

Figure 2-3. Susquehanna River Hydrograph, 1984-1986

Table 2-3
Gauges Employed in Hydrologic Analysis

River	USGS Gauge	Location	Drainage Area, km^2
Susquehanna	01578310	Conowingo, MD	70,189
Potomac	01646580	Chain Bridge, DC	29,966
James	02035000	Cartersville, VA	16,206
Rappahannock	01668000	Fredericksburg, VA	4,134
Pamunkey	01673000	Hanover, VA	2,800
Mattaponi	01674500	Beulahville, VA	1,557
Patuxent	01594440	Bowie, MD	901

imposes high-frequency, almost daily, flow fluctuations which are especially noticeable during low-flow periods.

Hydrology, 1984-1986

Mean Susquehanna runoff in 1984 (Table 2-4) was well above mean flow in the period of record, 1959-1988. In fact, mean flow exceeded 90% of the annual mean flows on record. The year 1984 was a "wet" year. By contrast, flow in 1985 was unusually low. Roughly 80% of the years on record had mean flow which exceeded 1985. The year 1985 was a "dry" year. Mean flow in 1986 was near the mean long-term flow. Susquehanna hydrology in 1986 was "average".

Mean flow in the Potomac for 1984 was also well above average (Table 2-4). The relative order of 1985 and 1986 was reversed from the Susquehanna, however. Flow through most of 1985 fluctuated about the median while flow in 1986 was well below-average for half the year (Figure 2-4). The defining event of 1985 was an autumn flood in which highest flows in the study period, 1984-1986 occurred.

Flows in the Virginia tributaries generally corresponded to the pattern observed in the Potomac. Highest mean flows were in 1984, moderate flows in 1985, and lowest flows in 1986. All Virginia tributaries experienced the November 1985 flood. The effect in the James was especially pronounced (Figure 2-5). In the James, highest flows in the study period occurred in autumn, 1985. In the remaining Virginia tributaries, autumn 1985 flows were roughly equivalent to peak spring runoff in 1984 (Figures 2-6 to 2-8).

As with the other western-shore tributaries, the Patuxent experienced highest flows in 1984. The November 1985 storm did not affect the Patuxent,

Table 2-4
Hydrologic Statistics

River	Year	Mean Flow, $m^3 sec^{-1}$	25% Exceedence, $m^3 sec^{-1}$	Median Flow, $m^3 sec^{-1}$	75% Exceedence, $m^3 sec^{-1}$
Susquehanna	1984	1410	448	925	1853
	1985	863	303	578	1207
	1986	1168	419	793	1465
	1959–88	1086	326	697	1387
Potomac	1984	468	119	242	564
	1985	331	86	201	357
	1986	234	47	130	254
	1959–88	319	79	178	377
James	1984	267	93	153	309
	1985	213	70	126	197
	1986	119	42	92	139
	1959–88	196	58	118	220
Rappahannock	1984	72	17	37	75
	1985	43	7	24	40
	1986	25	6	17	33
	1959–88	46	11	25	50
Pamunkey	1984	46	10	27	53
	1985	31	6	15	29
	1986	18	5	11	24
	1959–88	29	6	16	32
Mattaponi	1984	27	8	17	32
	1985	15	4	11	18
	1986	9	2	6	13
	1959–88	17	4	11	21
Patuxent	1984	12	5	8	17
	1985	6	3	4	6
	1986	6	2	4	7
	1959–88	10	5	7	10

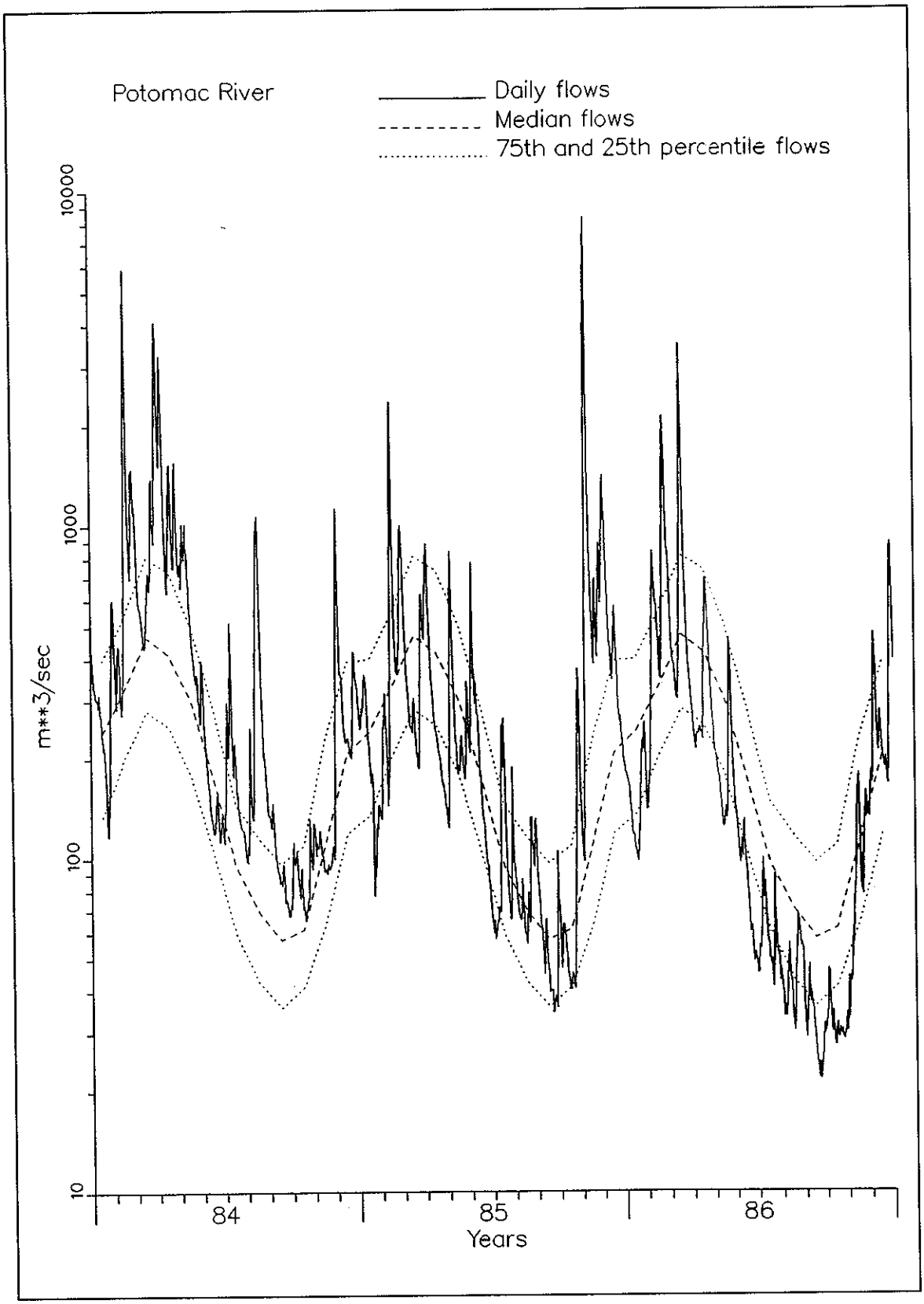

Figure 2-4. Potomac River Hydrograph, 1984-1986

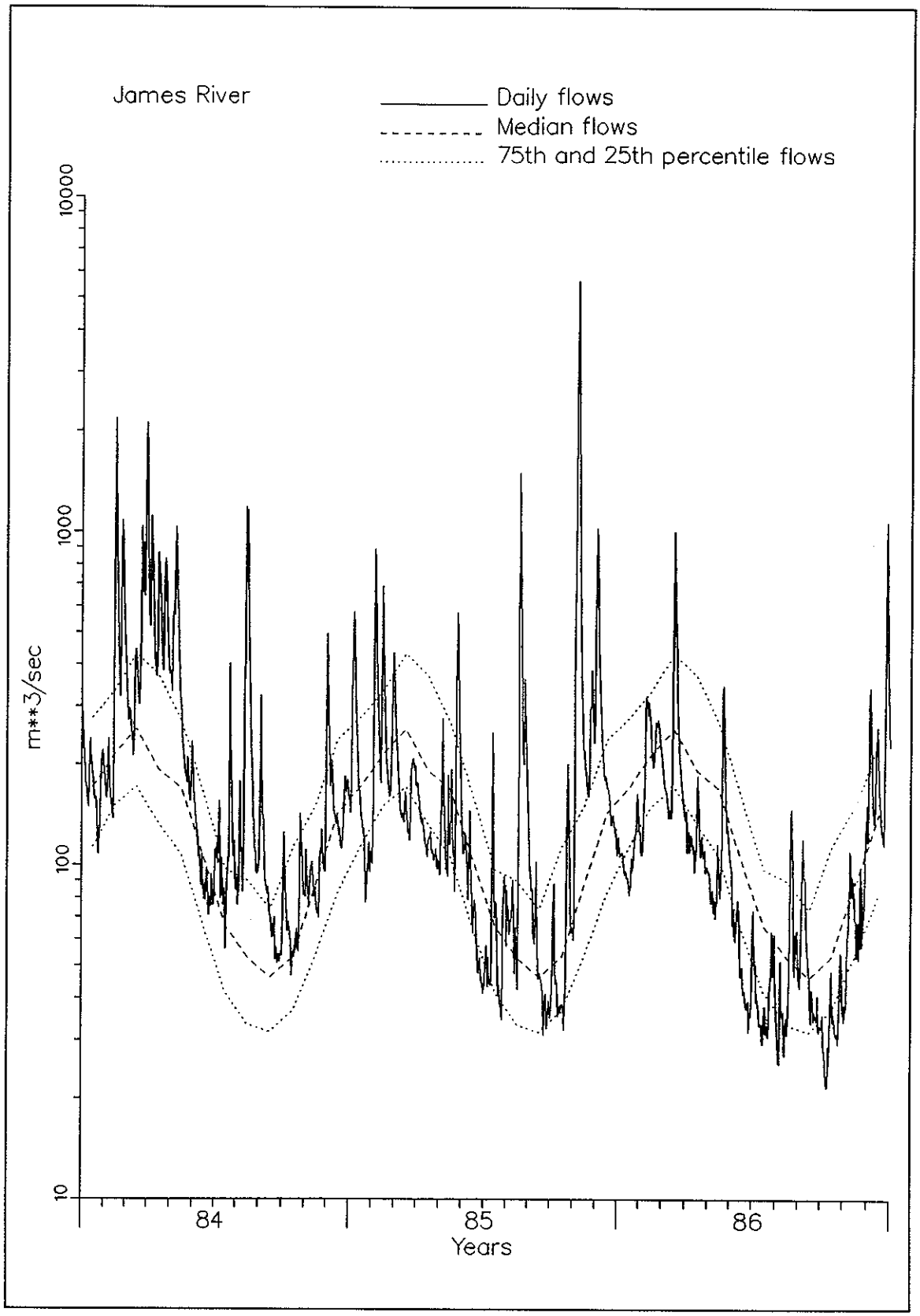

Figure 2-5. James River Hydrograph, 1984-1986

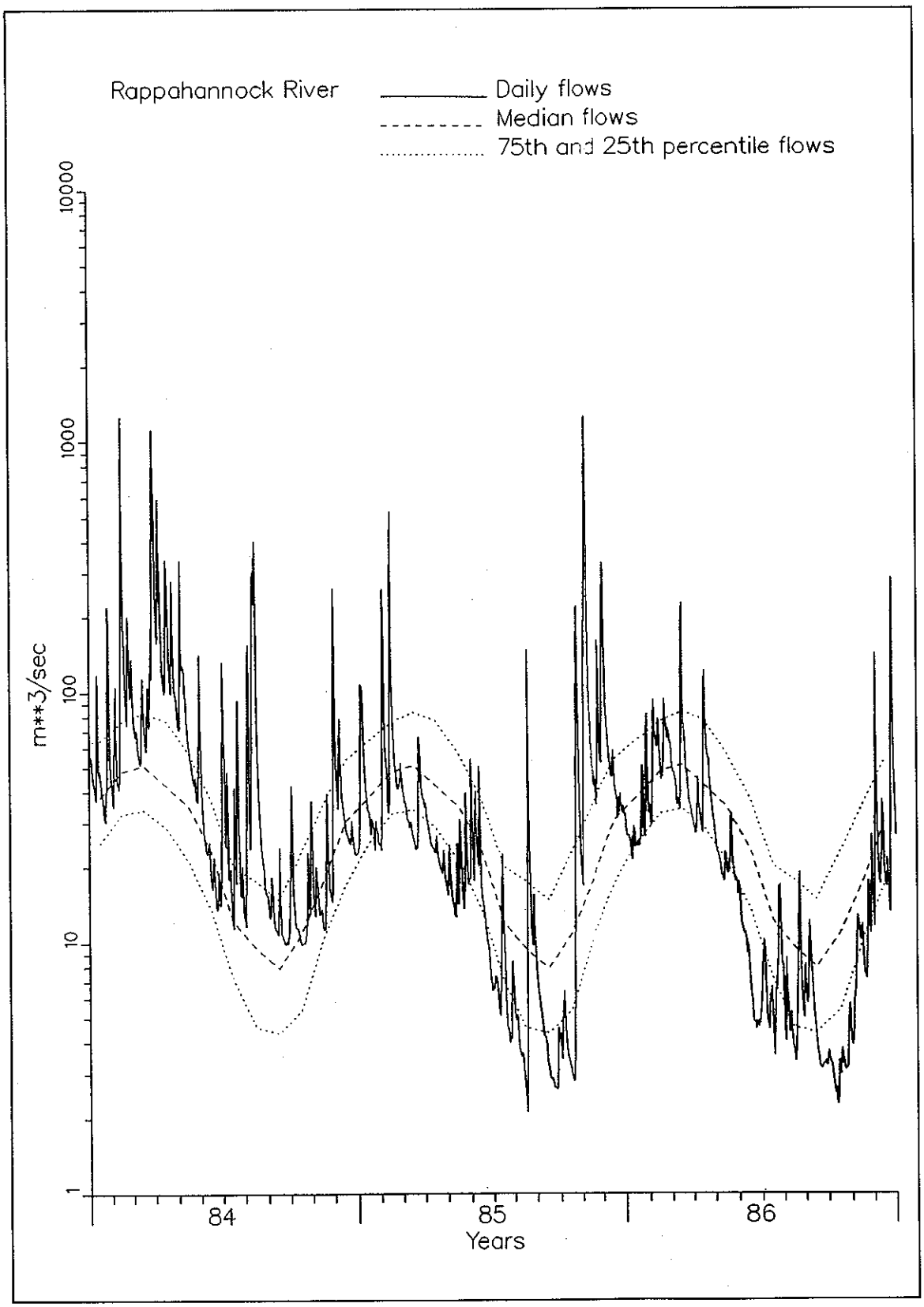

Figure 2-6. Rappahannock River Hydrograph, 1984-1986

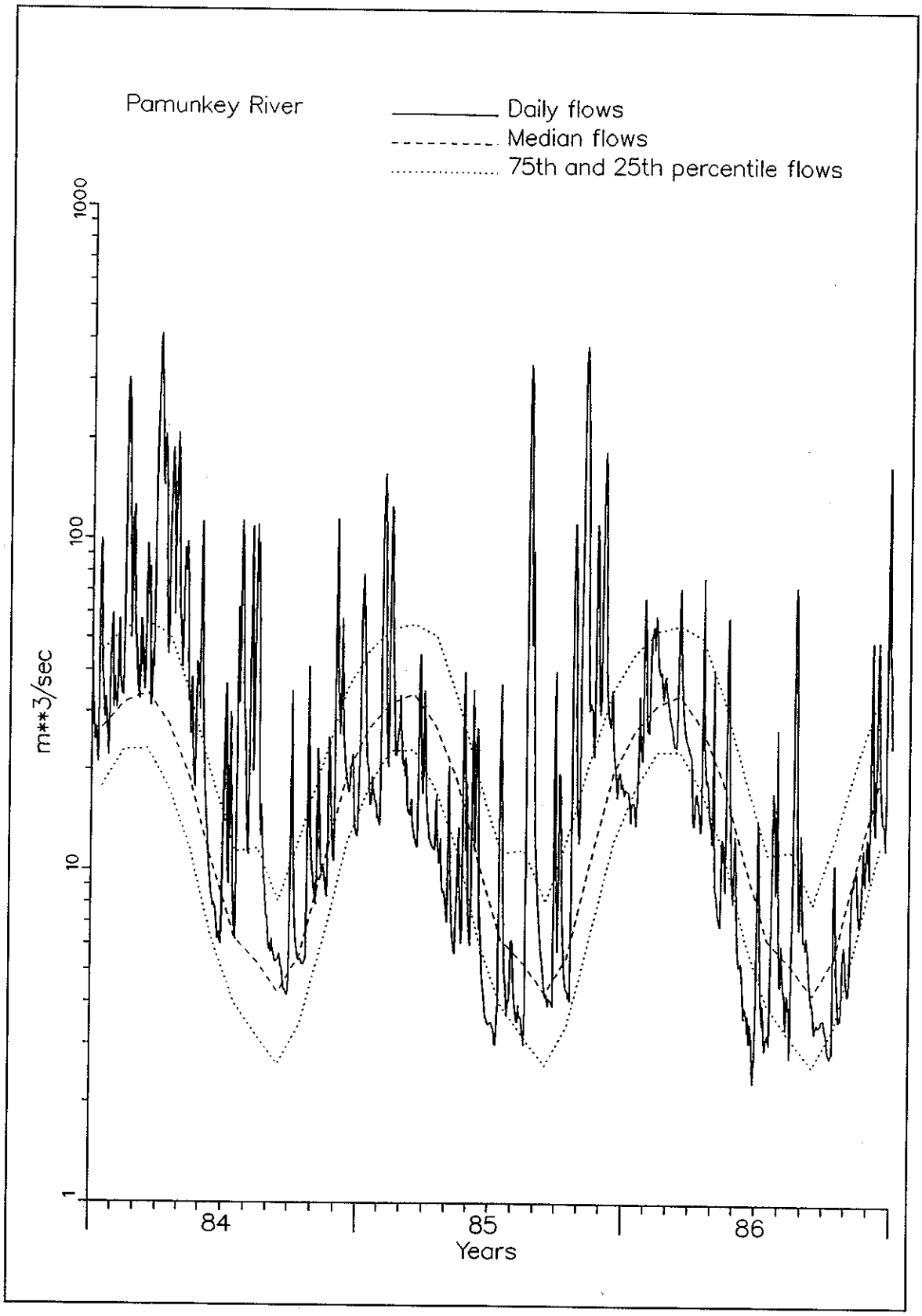

Figure 2-7. Pamunkey River Hydrograph, 1984-1986

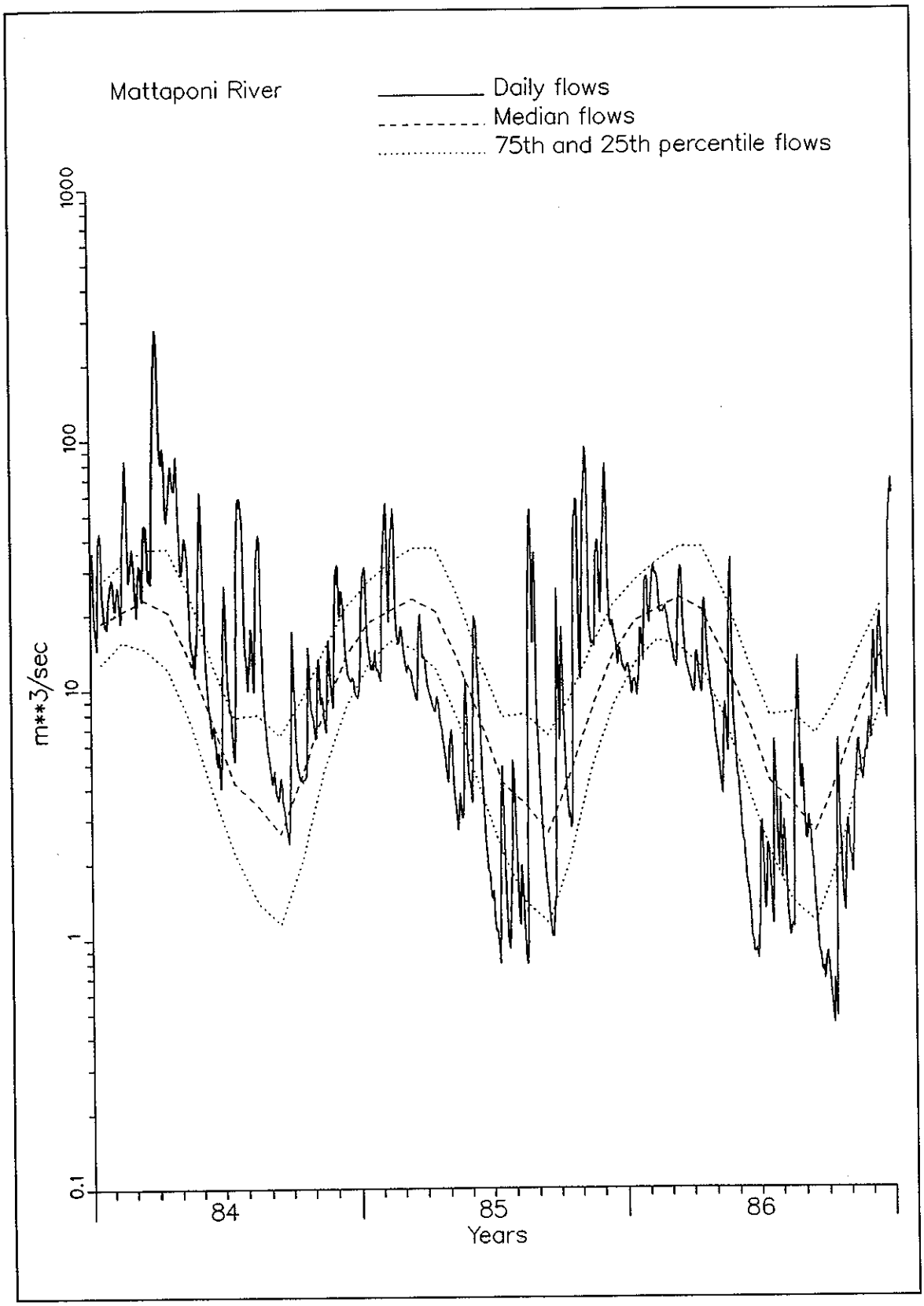

Figure 2-8. Mattaponi River Hydrograph, 1984-1986

however, and hydrologic distinctions between the study years were not as evident as in other tributaries (Figure 2-9).

Eutrophication Processes

Chesapeake Bay is perhaps the most intensively studied estuary in the world. An extensive data base exists as a product of biological, chemical, and ecological research. Characteristic eutrophication processes and phenomena have been identified. Consensus exists on the mechanisms that influence many of these processes. Reasonable hypotheses have been posed to explain processes that are not yet fully understood. Processes and phenomena relevant to the present study are reviewed below.

Bottom-Water Hypoxia

During the summer months, bottom waters of the mainstem bay are characterized by hypoxic (low dissolved oxygen) or anoxic (no dissolved oxygen) conditions (Figure 2-10). Longitudinal and lateral extent of hypoxia are determined by the geometry of the trench that runs up the center of the Bay. On occasion, hypoxic water extends from the bottom to within a few meters of the surface but summer-average oxygen concentration within the surface mixed layer is usually 6 gm m^{-3} or greater.

Bottom-water hypoxia occurs at recurrent, predictable time intervals (Figure 2-11). The onset is in late May when spring warming enhances respiration in benthic sediments. Decay of material deposited in spring and in previous years removes oxygen from bottom water. Density stratification prevents mixing of oxygenated surface water downwards. Low-oxygen conditions continue through the summer, maintained by respiration in bottom water. In mid-September, autumn winds end the hypoxic period by mixing surface water down to the bottom. Respiration in bottom water, diminished by cool temperature, is insufficient to re-establish hypoxia following the mixing event.

The extent of hypoxia in prehistoric and historic times is controversial. Dissolved oxygen observations less than 1 gm m^{-3} are present in the earliest records, which date from the late 1930's (CSC 1991). Concentrations less than 0.1 gm m^{-3} were not observed until 1958, however (CSC 1991). Analysis of sediment cores suggests anoxic conditions were not present in the mid-Bay trench until circa 1940 (Cooper and Brush 1991). Together, observations in the water and cores indicate that hypoxic water has been present in the Bay for decades, at least, but that strictly anoxic water has not been present until relatively recent times.

A call to arms was sounded when a summary report concluded the volume of anoxic bay water increased by an order of magnitude from 1950 to 1980 (Flemer et al. 1983). A subsequent investigation concluded no trend in anoxia

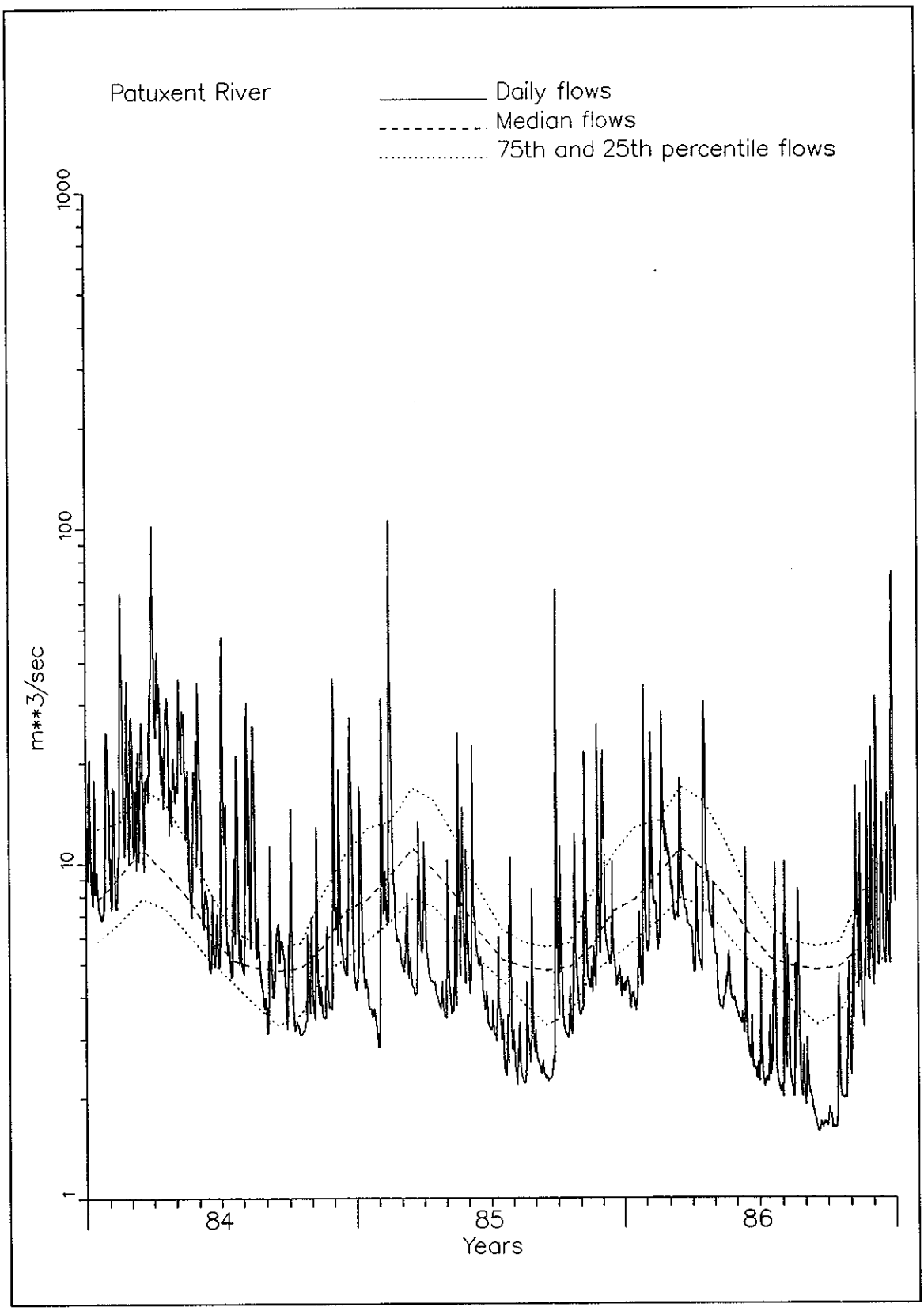

Figure 2-9. Patuxent River Hydrograph, 1984-1986

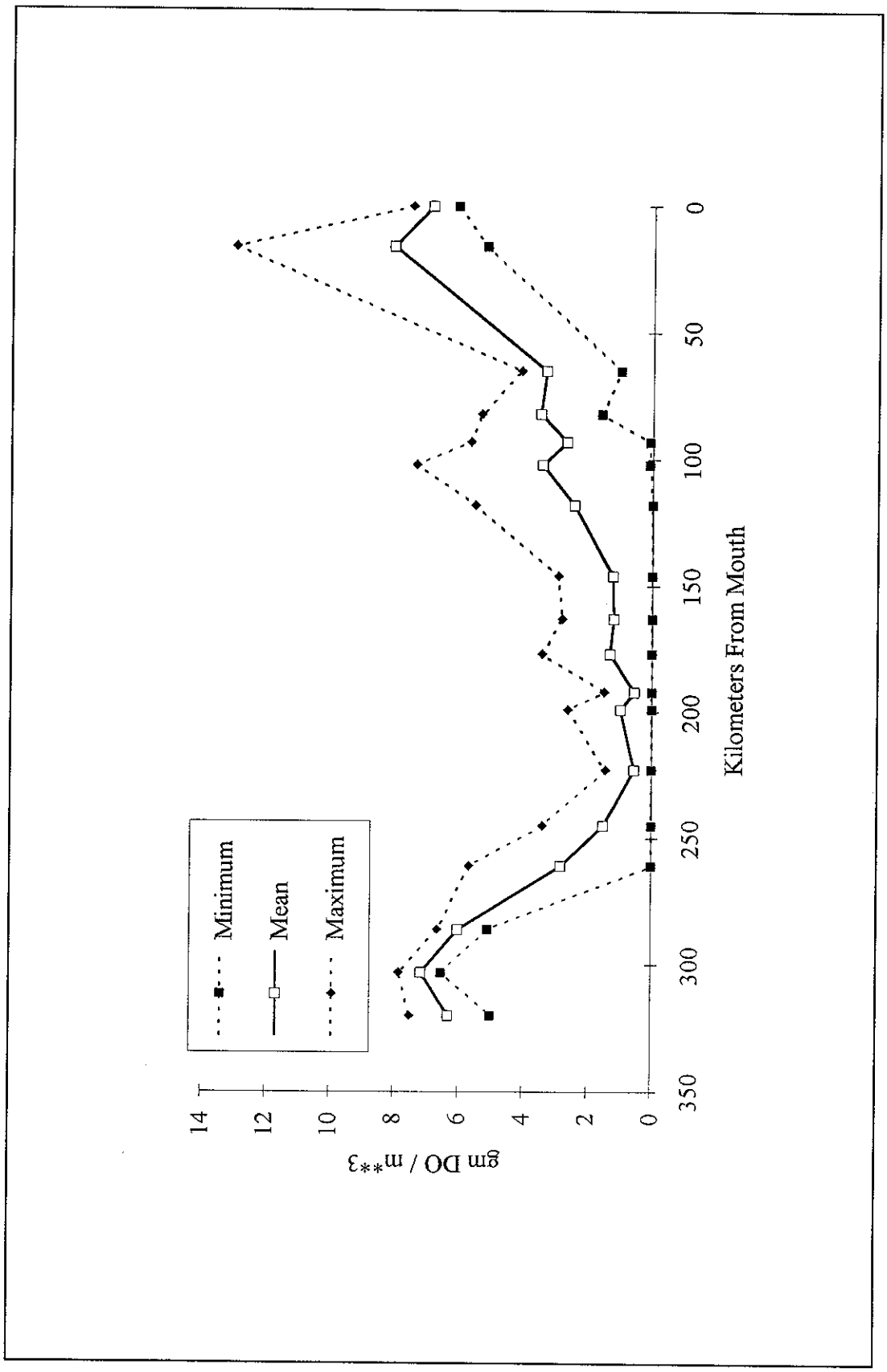

Figure 2-10. Bottom Dissolved Oxygen, Summer 1984

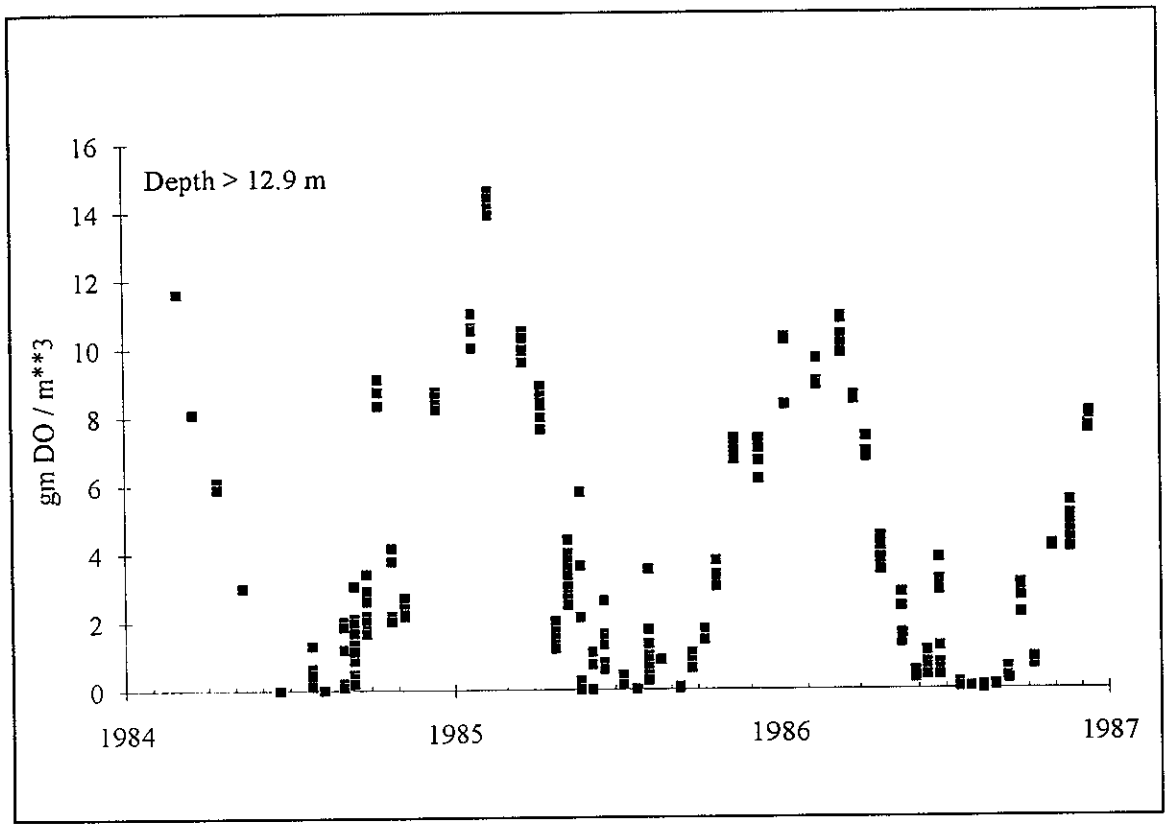

Figure 2-11. Dissolved Oxygen Near Bottom at Upper Bay Station CB3.3C

existed (Seliger and Boggs 1988). Rather, anoxic volume was linked to volume of spring runoff in the Susquehanna River. Yet another data analysis detected a small upward temporal trend in anoxia but only a weak link to runoff volume (Bahner, Reynolds, and Batuik 1990). The disparate conclusions were due largely to the nature of the historic data base. Observations in earlier years were an order of magnitude fewer than in the present monitoring program (Figure 2-12). Synoptic sampling was commenced in 1984. In prior years, sampling was sporadic in space and time. Faced with incomplete data, investigators were forced to employ data selectively. The selection process influenced the conclusions of their investigations.

Present consensus (Harding, Leffler, and Mackiernan 1992) is that anoxic volume is strongly linked to runoff from the Susquehanna. Two factors contribute to the linkage. First, large runoff induces strong density stratification which inhibits oxygenation of bottom water. Second, large runoff supplies nutrients which promote phytoplankton production. Excess production settles to the bottom of the bay, decays, and consumes oxygen. The relative influence of stratification versus loading cannot be determined since the two forcing functions co-vary (Boicourt 1992). Consensus also indicates that year-to-year variations in anoxic volume, associated with variations in runoff, prevent detection of trends in the historic record.

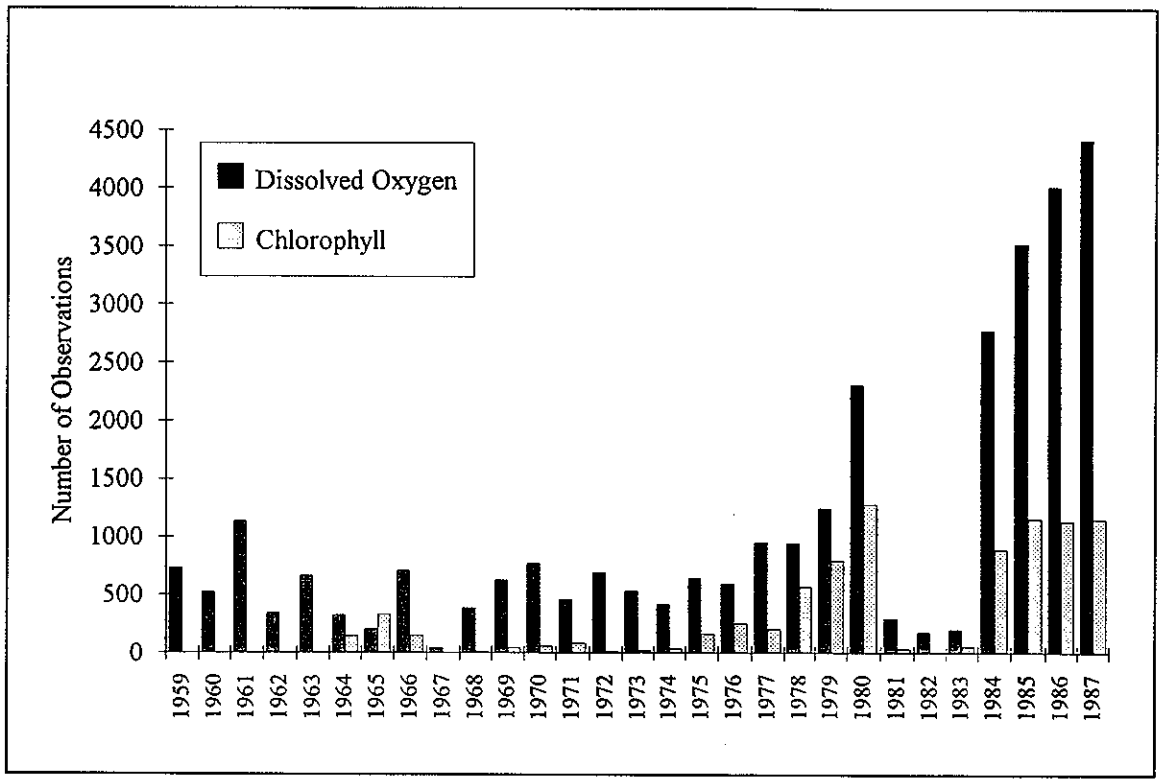

Figure 2-12. Number of Oxygen and Chlorophyll Observations, 1959-1987

Spring Phytoplankton Bloom

A second recurring phenomenon in the Bay is the spring phytoplankton bloom. The spring bloom primarily consists of three genera of marine diatoms: *Cerataulina*, *Rhizosolina*, and *Thalassiosira* (Sellner 1990). The bloom usually commences in February, reaches a maximum in April, and ends precipitously in May (Figure 2-13). The bloom is characterized by high chlorophyll concentrations throughout the water column. At times, a subsurface chlorophyll maximum occurs. Elevated chlorophyll throughout the water column marks the spring bloom as the period of maximum algal biomass. During summer, chlorophyll concentrations are generally less than in spring and restricted to surface waters. Despite the disparity in biomass, however, primary production in summer exceeds production in spring (Malone et al. 1988).

Although the bloom occurs regularly, the magnitude and spatial extent of the bloom vary from year to year. Factors affecting this variability are not well-known. The occurrence and apparent propagation of viable algae at great depth, in the absence of light, also remain unexplained.

Strong consensus exists that the occurrence and magnitude of the spring bloom are linked to subsequent bottom-water anoxia. A spring peak in carbon deposition to sediments occurs coincident with the algal bloom (Boynton et al.

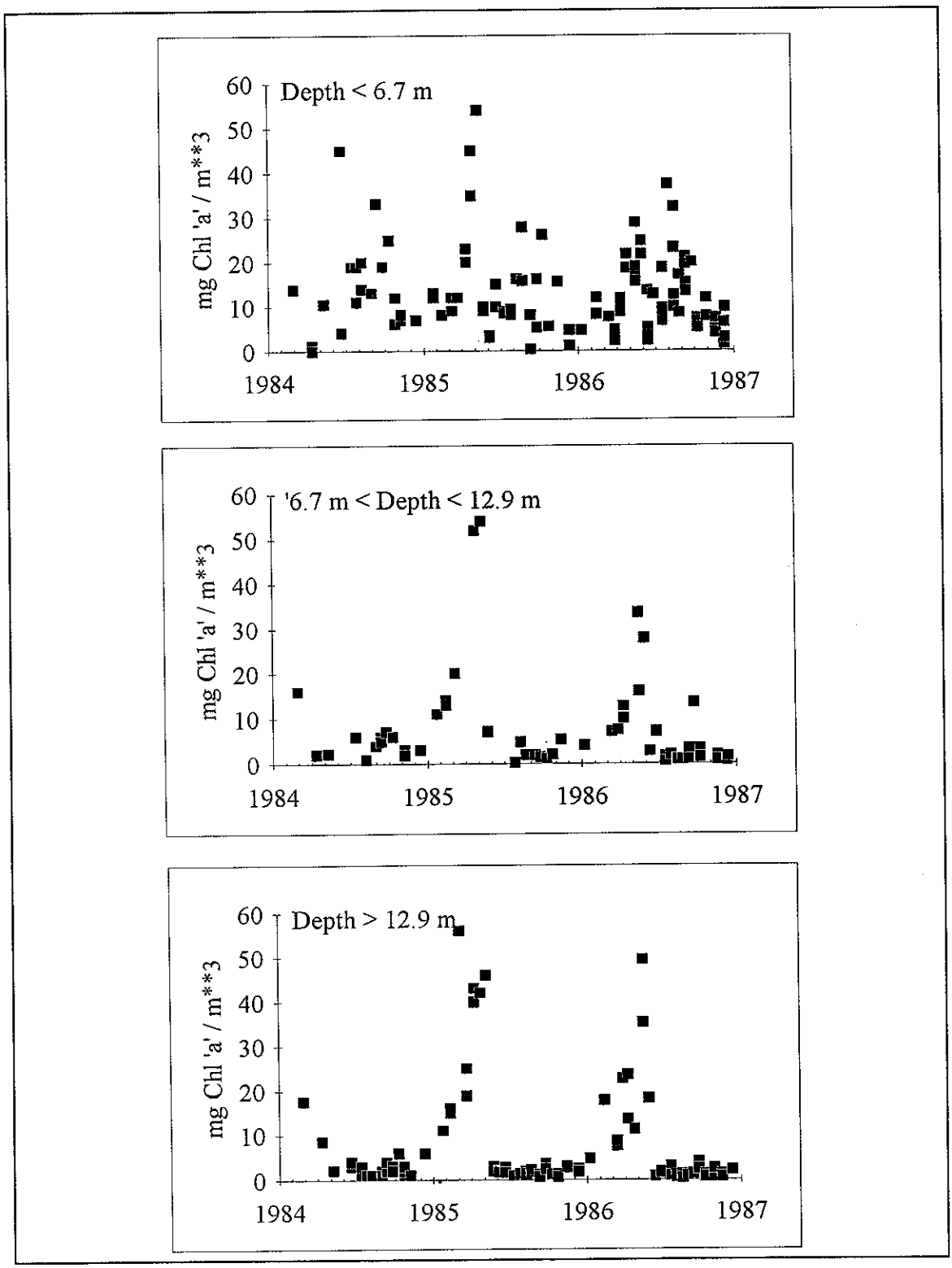

Figure 2-13. Chlorophyll at Upper Bay Station CB3.3C

1988). The deposition and decay of fresh organic matter contributes to oxygen demand during the onset of the anoxic period.

A subtle, and potentially more important link, is through a nutrient trapping mechanism (Malone et al. 1988). Nutrients in spring runoff are taken up by algae during the bloom. Predation and algal mortality result in the transfer of nutrients, in particulate organic form, to benthic sediments (Figure 2-14). In summer, the nutrients are mineralized in the sediments and released to the water column. Nutrients released from the sediments support summer algal production. Carbon produced by algae settles to bottom waters, decays, and consumes oxygen. Diminished oxygen in bottom water enhances sediment nutrient release, especially of ammonium. The nutrient release continues the cycle of benthic release, algal production, and oxygen consumption.

Nutrient Limitations

Algae require three major nutrients for growth: carbon, nitrogen, and phosphorus. Diatoms require silica, as well, from which they synthesize their distinctive skeletons. Algal production is diminished or eliminated in the prolonged absence of one or more of the required nutrients.

Nutrients are supplied in various ratios from natural and anthropogenic sources. The ratio of nutrient utilization by algae is within a limited range, however, largely determined by algal composition. The classic Redfield ratios (Redfield, Ketchum, and Richards 1966) indicate the ratio of carbon to nitrogen required by algae is 6 to 1 by mass. The ratio of carbon to phosphorus required is 42 to 1. The carbon to silica requirement is ≈1.25 to 1 (Strickland 1960). Disparity in the ratio of nutrients supplied and nutrients required often leads to depletion of one nutrient, due to algal uptake, while the others remain available. The depleted nutrient is referred to as "limiting" since algal production is limited by the supply of this nutrient.

Inorganic carbon is seldom in short supply and is usually not considered in analyses of nutrient limitations. Silica receives little emphasis in management studies since the supply from natural sources is beyond control and usually abundant. Tremendous emphasis is placed on limitations by nitrogen and phosphorus since the supply of these nutrients can be altered through management of release from municipalities, industry, agriculture, and other sources.

A "rule of thumb" is that phosphorus is the limiting nutrient in freshwater systems (Hecky and Kilham 1988) while nitrogen is limiting in estuarine (Boynton, Kemp, and Keefe 1982) and marine waters. The phosphorus limit in freshwater is influenced by the relative natural abundance of the two nutrients. At the Susquehanna fall line, for example, mass loading of nitrogen to phosphorus is ≈20 to 1. Algae in the vicinity of the fall line, taking up nitrogen to phosphorus in a ratio of 7 to 1, will deplete phosphorus before nitrogen.

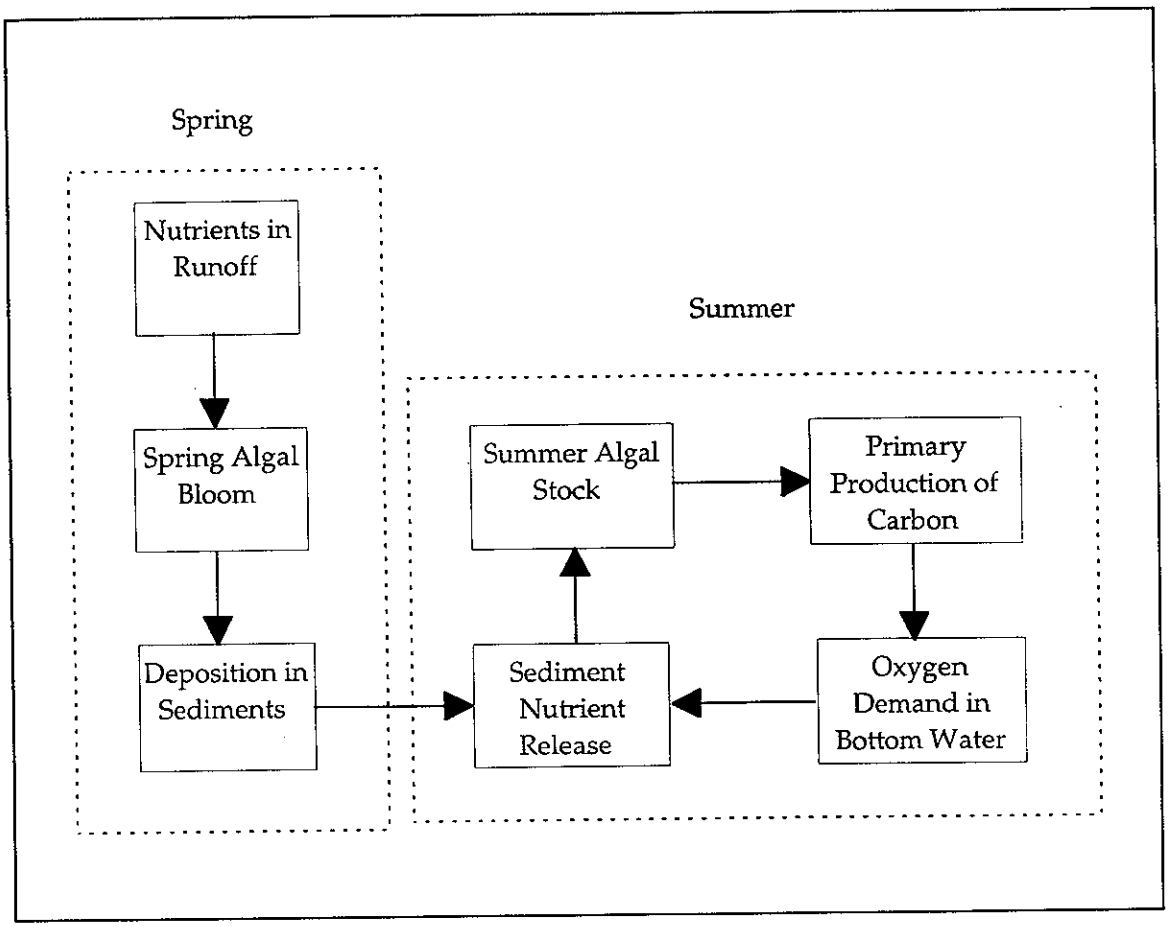

Figure 2-14. Coupling of Spring Algal Bloom to Summer Algal Production

In downstream portions of estuaries and in coastal waters, the ratio of nitrogen to phosphorus is altered from the ratio in runoff by internal recycling processes. Sediment-water interactions greatly diminish the availability of nitrogen relative to phosphorus (Nixon 1981). Particulate organic nitrogen and phosphorus enter the sediments roughly in Redfield proportions as organic detritus. Within the sediments, total phosphorus is conservative. The only pathways for removal are recycling of inorganic phosphorus back to the water column or burial to deep, isolated sediments. Total nitrogen is non-conservative, however. A significant fraction is lost through denitrification to nitrogen gas. The nitrogen loss is such that the nitrogen returned to the water column is roughly half the amount expected based on nitrogen to phosphorus ratio of the incoming material. The reduced nitrogen to phosphorus ratio of dissolved fluxes leaving the sediments, compared to particle fluxes entering the sediments, acting over lengthy time scales, pushes the water column towards nitrogen rather than phosphorus limitation.

The principle of phosphorus limitation in freshwater and nitrogen limitation in saltwater presents a reasonable pattern for the Chesapeake Bay system. Phosphorus tends to be limiting in tidal fresh water and near the Susquehanna

fall line. In the lower tributaries and in most of the mainstem nitrogen is of more importance as the limiting nutrient.

Seasonality is also apparent in the nutrient limitations. Bioassays (D'Elia, Sanders, and Boynton 1986) and data analyses (Fisher et al. 1992) indicate phosphorus is important as a limiting nutrient in estuarine waters in late winter and spring while nitrogen is more important in summer. The predominance of phosphorus in spring is an effect of high runoff volume. Nitrogen-rich runoff is pushed downstream from the fall lines and comprises a large fraction of surface water. In summer, the runoff volume is low and is rapidly diluted in the wide expanses of the lower tributaries and mainstem. Internal recycling processes, which favor nitrogen limitation, predominate.

The seasonal switch from phosphorus to nitrogen indicates much of the system is phosphorus-limited during the spring bloom and nitrogen-limited during the period of summer maximum productivity. The spring bloom is also a period of potential silica limitation. Silica is diminished by diatom uptake simultaneously with phosphorus. The role of silica in limiting the spring bloom is ambiguous. Two investigations reported silica "occasionally approaches levels limiting to diatom growth" (D'Elia, Nelson, and Boynton 1983) and silica "may limit diatom abundance" (Fisher et al. 1992) while a third concluded "silicate controls the magnitude of diatom production and causes the collapse of the spring bloom" (Conley and Malone 1992).

Sediment-Water Interactions

Over time scales of years, benthic sediments are sinks of oxygen, nitrogen, phosphorus, and silica removed from the water column. Oxygen is consumed, directly or indirectly, in the oxygenation of organic carbon and in the nitrification of ammonium. Substantial fractions of particulate nitrogen, phosphorus, and silica that settle into surficial sediments are buried to deep sediments from which recycling to the water column is impossible.

Over seasonal time scales, sediments can be significant sources of dissolved nutrients to the overlying water. The role of sediments in the system-wide nutrient budget is especially important in summer when seasonal low flows diminish riverine nutrient input. During summer, warm temperature enhances biological processes in the sediments. Diagenesis (decay) of organic matter produces ammonium, phosphate, and silica that are released to the water column. Sediment ammonium release supplies an estimated 13% to 40% of algal nutrient requirements during August in Chesapeake Bay (Boynton and Kemp 1985). Silica nutrient limitation is not seen in summer because sediment release exceeds fluvial input by a factor of five or more (D'Elia, Nelson, Boynton 1983).

Seasonal effects are also evident in sediment oxygen consumption. While temperature effects are significant, the seasonal pattern of sediment oxygen consumption is also affected by carbon supply to the sediments and by oxygen

availability in the water column. Peak sediment oxygen consumption typically occurs in late spring (Boynton et al, 1991; Kemp et al. 1992) when water warms, when fresh organic matter is available from the spring bloom, and when oxygen is freely available in the water column. During summer, sediment oxygen consumption in much of the Bay is diminished from the spring peak. The depression occurs because organic matter is consumed in the water column before it reaches the sediments and because hypoxic conditions limit supply of oxygen to the sediment-water interface. Under hypoxic conditions, oxygen demand created in the sediments is released to the water column, primarily in the form of sulfide.

Oxygen consumption in the sediments (or of sulfide released from sediments) is generally about one-third of total oxygen consumption in the system (Kemp et al. 1992). At times, however, sediment processes account for the majority of oxygen consumption. Oxygen consumption due to sediment processes predominates during the spring peak, and in late summer concurrent with maximum sulfide release.

A sediment process of potential importance in eutrophication management is the coupled nitrification/denitrification sequence (Figure 2-15). The nitrification reaction, in which ammonium is oxidized to nitrate, requires oxygen. The denitrification reaction, in which nitrate is reduced to a gaseous nitrogen form, usually takes place under anoxic conditions. Denitrification is a potential major pathway for removal of nitrogen from the system. In the Bay, nitrification and denitrification are closely coupled (Jenkins and Kemp 1984). The primary source of nitrate for denitrification is from previously nitrified ammonium. Maximum denitrification, an anoxic process, occurs when oxygen is available for nitrification. When oxygen is absent, denitrification is diminished and limited to the rate at which nitrate is supplied by diffusion from the water column.

When oxygen is freely available, a large fraction of ammonium produced in sediments is nitrified/denitrified to gaseous nitrogen, a form unavailable to algae. When oxygen is absent, virtually all ammonium produced is released to the water column and is available to algae. The coupling of nitrification and denitrification indicate existence of a vicious cycle in the eutrophication process. Conditions that lead to hypoxia diminish denitrification. Ammonium is instead released to the water column and supplies algal production. Algal carbon settles to the bottom, consumes oxygen, and further diminishes denitrification. The same mechanism suggests that a slight improvement in bottom dissolved oxygen can start a positive feedback reaction (Figure 2-16). Enhanced dissolved oxygen would promote denitrification at the expense of ammonium release. Diminished release would limit algal production and diminish carbon supplied to the bottom. Diminished carbonaceous oxygen demand leads to increased dissolved oxygen which leads to still more denitrification.

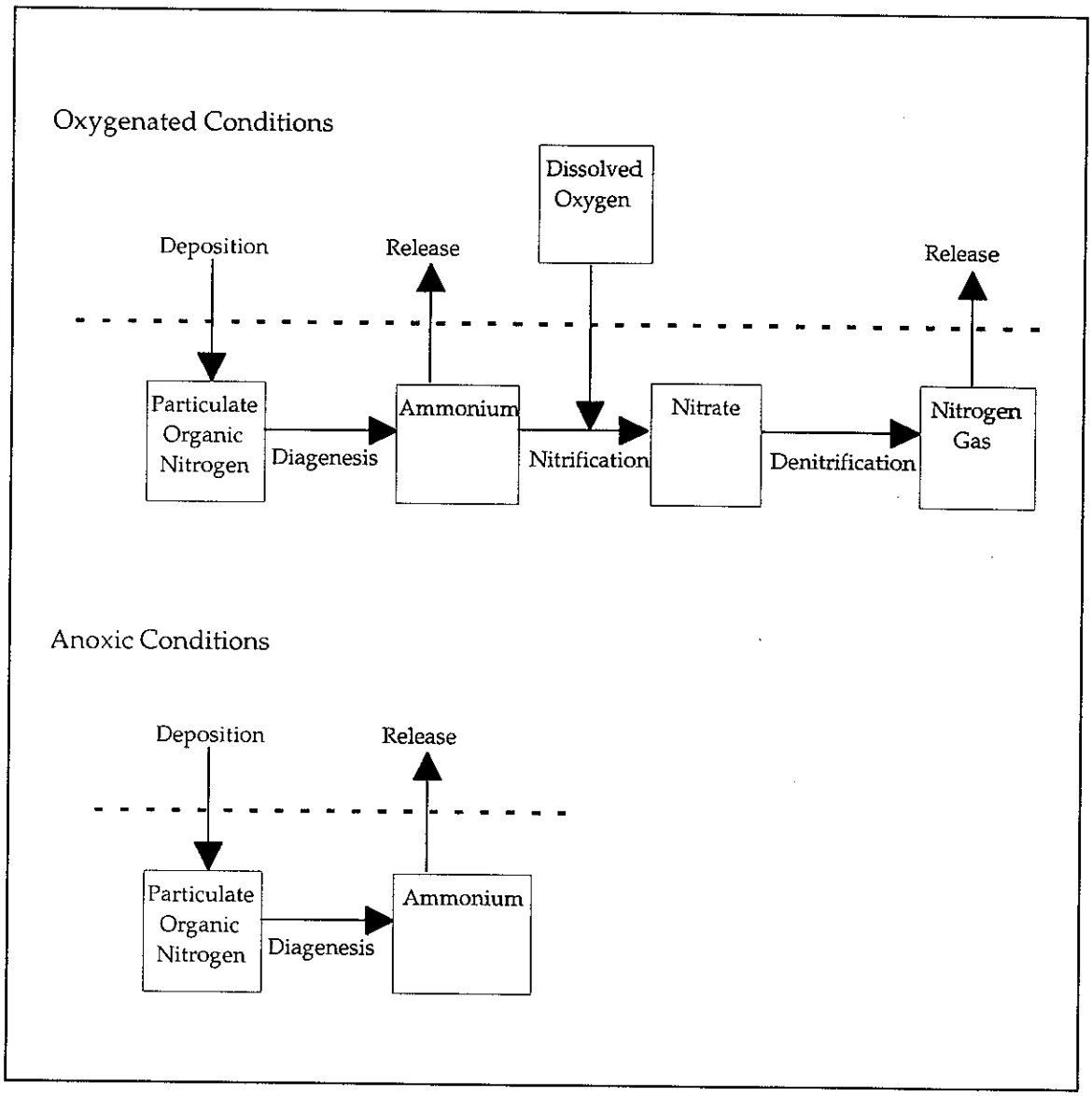

Figure 2-15. Nitrification/Denitrification Under Oxic and Anoxic Conditions

Nitrogen and Phosphorus Budgets

Annual nutrient budgets for the bay were completed as part of the 1982 Technical Synthesis (USEPA 1982). The largest nitrogen sources to the bay were identified as fall-line loads, direct loads (point-source plus nonpoint-source), and atmospheric loads, respectively (Figure 2-17). The largest phosphorus sources were direct loads, fall-line loads, and atmospheric loads (Figure 2-18). Prominent features of the nitrogen and phosphorus budgets were the large fractions of nutrient loads buried to deep, unavailable sediments. Virtually all nutrient load to the bay was buried. The bay exported nitrogen to

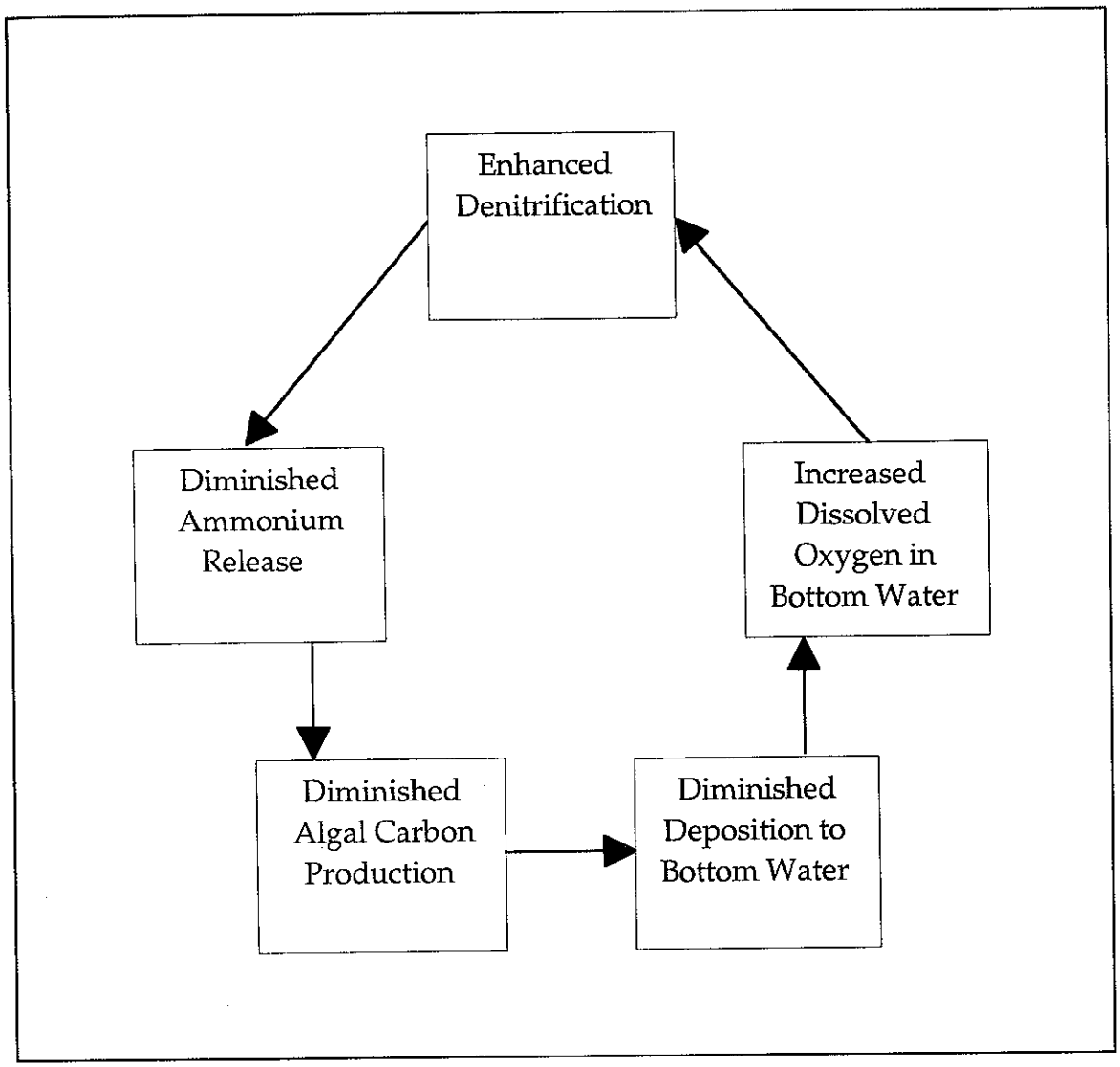

Figure 2-16. Role of Enhanced Dentrification in Diminished Hypoxia

the ocean and imported phosphorus. Net imports and exports through the mouth were small, however, compared to nutrient loads and burial terms.

Magnitude and direction of net loads at the bay mouth cannot be measured in the presence of tidal oscillations and short-term major events such as storm flows. Consequently, fluxes at the mouth are usually assigned to balance the budget once loads and burial are evaluated. Fall-line loads, direct loads, and atmospheric loads can be quantified with reasonable accuracy. Estimation of the burial term has a large variance, however, which impacts the estimation of flux at the mouth. If large fractions of the loads are buried, little remains for export out the mouth. Calculation of net import may result if burial exceeds loading. If burial estimates are a small fraction of loading, then most load must be exported to the ocean. Alternate estimates of burial terms in the 1982 budget were formulated which indicated only 3% to 6% of nitrogen load and

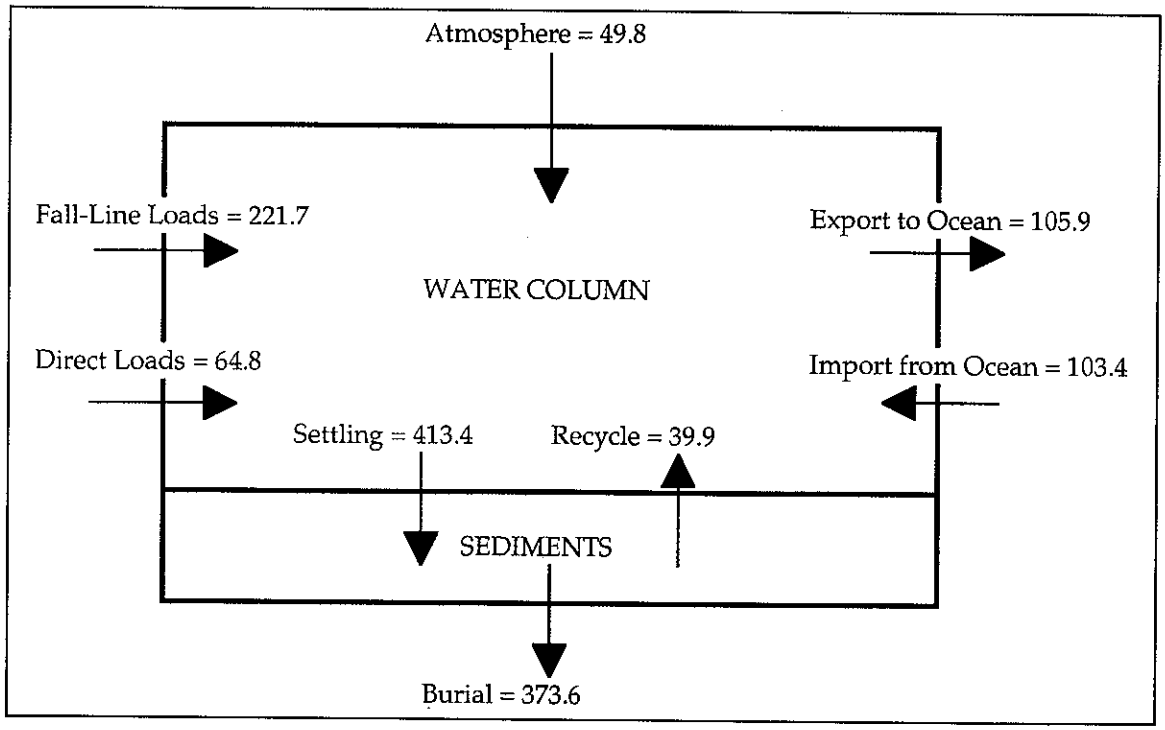

Figure 2-17. Annual Nitrogen Budget in 1000 kg/day (Modified from USEPA 1982)

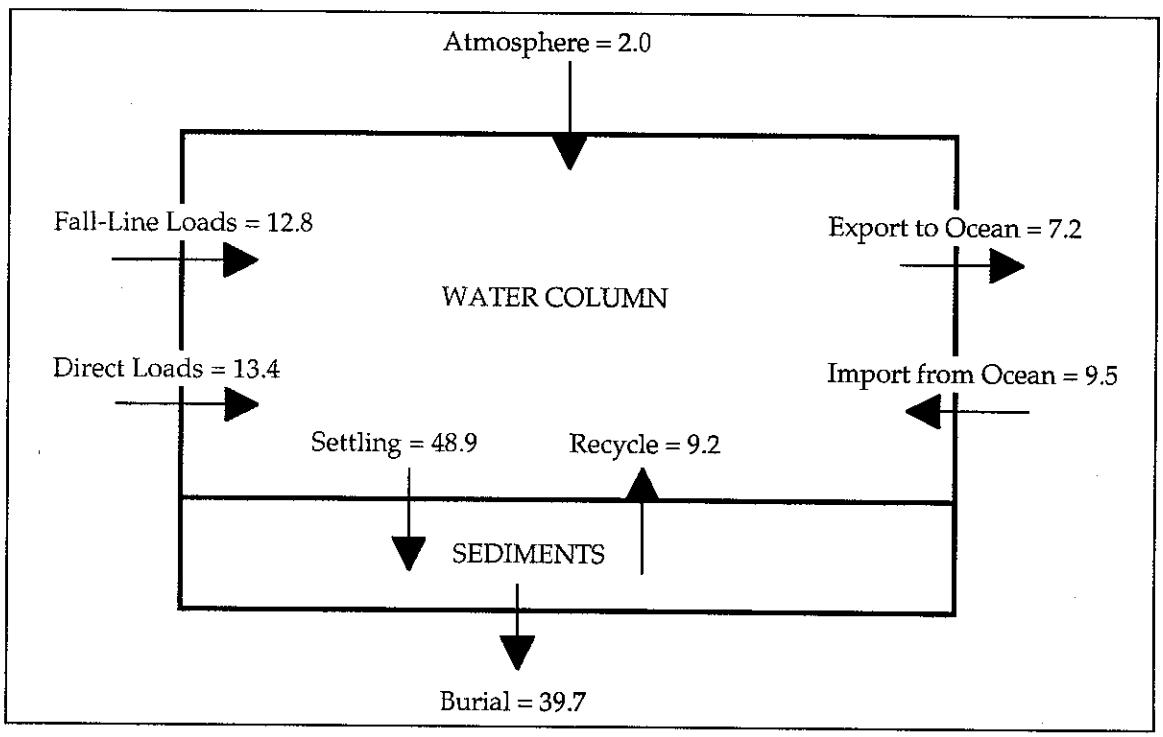

Figure 2-18. Annual Phosphorus Budget in 1000 kg/day (Modified from USEPA 1982)

11% to 17% of phosphorus load were buried (Nixon 1987). These burial estimates implied large fractions of nutrient loads were exported to the ocean.

Most recent budget estimates have identified pathways not quantified in the Technical Synthesis. Recent estimates assign roughly forty percent of the nitrogen loss in sediments to denitrification rather than burial (Figure 2-19). Commercial fishery harvest is identified as a significant sink of nitrogen and phosphorus (Figure 2-20).

All budgets agree that fall-line loads are the major nitrogen source. All budgets indicate that fall-line loading is a significant phosphorus source but not as dominant as for nitrogen. All budgets agree that the system exports nitrogen to the ocean. Estimates of the fraction exported vary widely however, from a negligible quantity to the majority of the load. Both direction and magnitude of net phosphorus flux at the mouth are controversial. The three budgets available indicate negligible import, significant export, and significant import. The contradictory results are strongly affected by estimates of burial and the requirement to balance the budget.

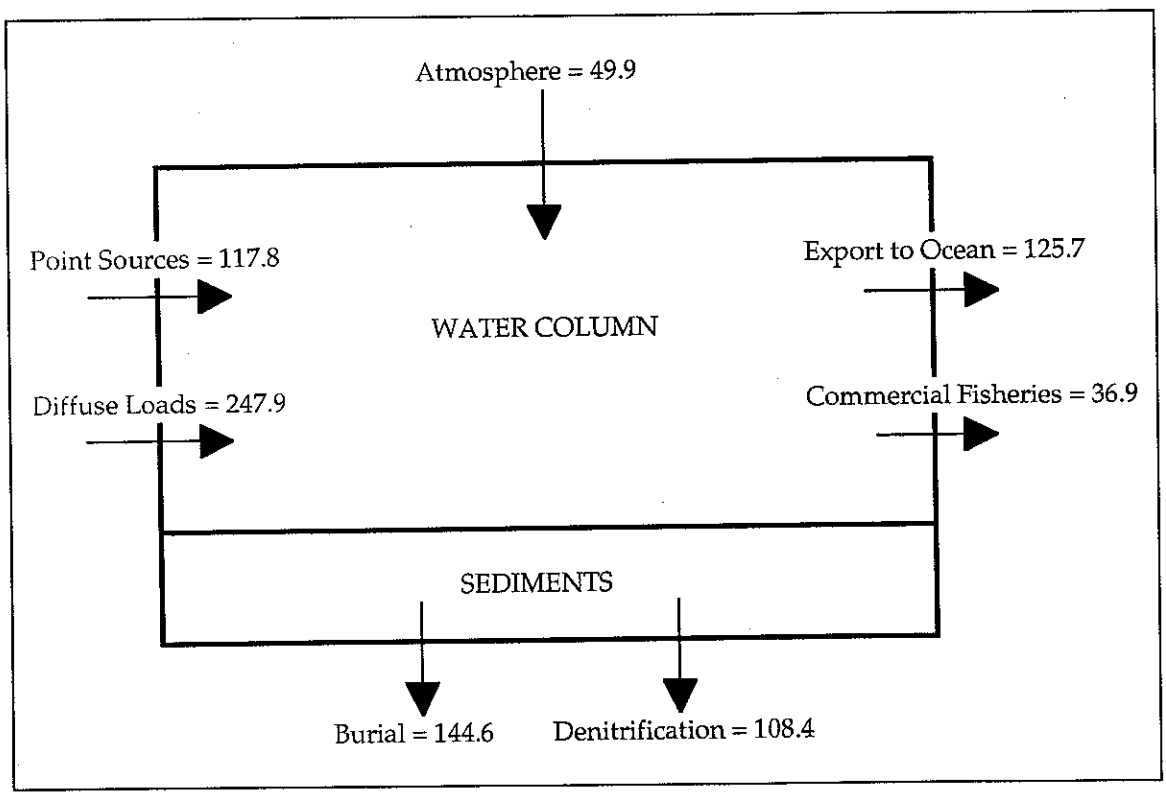

Figure 2-19. Annual Nitrogen Budget in 1000 kg/day (Courtesy of Dr. Walter Boynton, Center for Environmental and Estuarine Studies, University of Maryland)

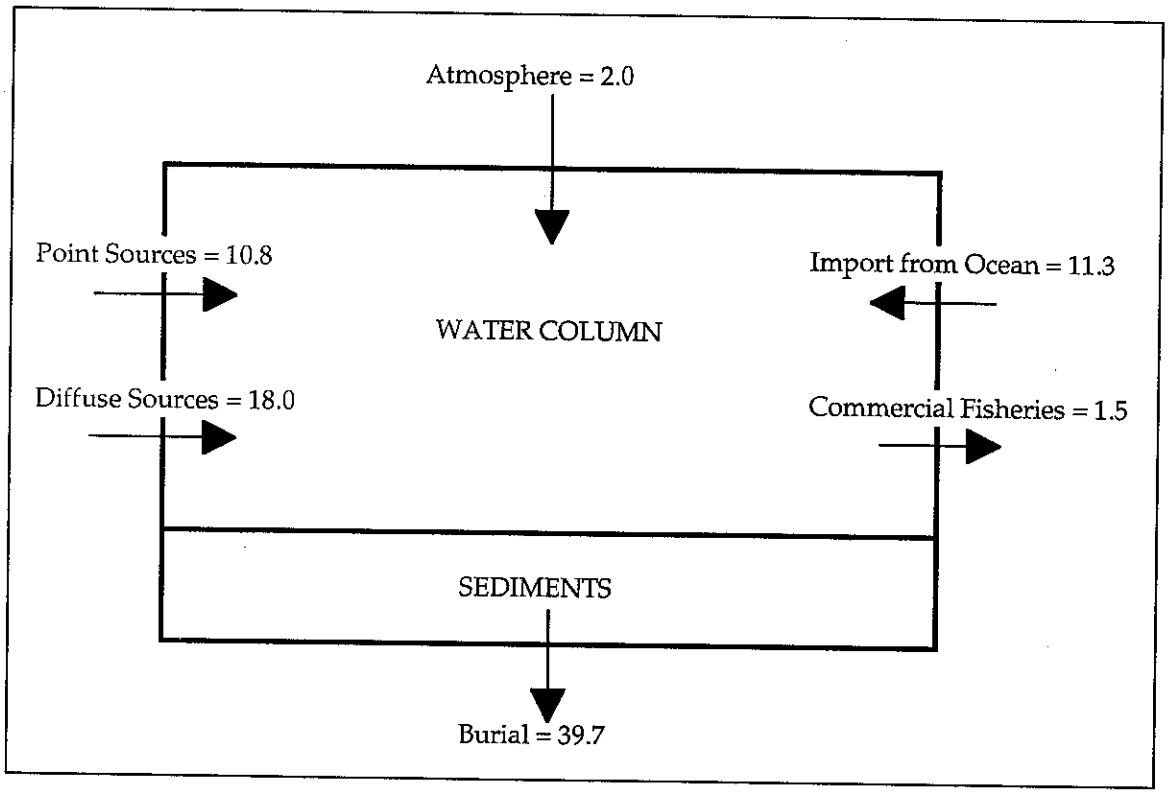

Figure 2-20. Annual Phosphorus Budget in 1000 kg/day (Courtesy of Dr. Walter Boynton, Center for Environmental and Estuarine Studies, University of Maryland)

Chapter III: Hydrodynamic Model and Computational Grid

Introduction

Modeling the physics, chemistry, and biology of the Bay required a package of models. Transport processes were modeled by a three-dimensional hydrodynamic model which operated independently of the water quality model. Transport information from the hydrodynamic model was processed and stored on magnetic media for subsequent use by the water quality model.

The Hydrodynamic Model

CH3D-WES

The CH3D-WES (Computational Hydrodynamics in Three Dimensions - Waterways Experiment Station) hydrodynamic model was a substantially revised version of the CH3D model originally developed by Sheng (1986). Model formulation was based on principles expressed by the equations of motion, conservation of volume, and conservation of mass. Quantities computed by the model included three-dimensional velocities, surface elevation, vertical viscosity and diffusivity, temperature, salinity, and density. Details of the model formulation and application to Chesapeake Bay were presented by Johnson et al. (1991).

Computational Grid

The basic equations of CH3D-WES were solved via the finite-difference method. The finite-difference solution algorithm replaced continuous derivatives in the governing differential equations with ratios of discrete quantities. Solutions to the hydrodynamics were obtained using five-minute intervals for the discrete time steps. The spatial continuum of the Bay was divided into a grid of discrete cells. To achieve close conformance of the grid to Bay geometry, cells were represented in curvilinear rather than rectangular coordinates.

Velocities were computed on the boundaries between cells. Temperature, salinity, and density were computed at the center of each cell.

The grid contained 729 cells, roughly 5 x 10 km, in the surface plane (Figure 3-1). The number of cells underlying each surface cell varied, depending on local depth (Figure 3-2). Number of cells in the vertical ranged from two to fifteen (Figure 3-3). Surface cells were 2.14 m thick. All other cells were 1.53 m thick. Total number of cells in the grid was 4073.

Calibration and Verification

The hydrodynamic model was calibrated and verified against a large body of observed tidal elevations, currents, and densities. Particular attention was devoted to replication, in the model, of Bay processes during an April 1983 spring runoff event and an October 1983 wind mixing event. The final check on performance was demonstrated by comparison of modeled and observed salinity over a three-year period 1984-1986. Details of model performance were presented by Johnson et al. (1991).

Linkage to the Water Quality Model

Hydrodynamics for employment in the water quality model were produced for three years, 1984, 1985, 1986. Each year was a single, continuous production run. A processor imbedded in the CH3D-WES code transformed velocities, surface elevations, and vertical diffusivities computed on a five-minute basis into tidal-average values output every 12.4 hours. Lagrangian averaging (Dortch 1990) was performed so that employment of a tidal dispersion coefficient, to compensate for tidal averaging, was not required. Employment of the Lagrangian algorithm reduced the storage requirements for the hydrodynamic output by an order of magnitude.

The water quality model operated on a grid identical to the hydrodynamic grid. Extensive testing was conducted to ensure that transport processes in the water quality model were identical to transport processes in the hydrodynamic model. Tests included comparisons of transport of conservative substances in both models. Initial tests compared "dye dumps" in the hydrodynamic and water quality models. Secondary tests were examinations of salinity computed in both models. The tests proved that information was correctly transferred from the hydrodynamic model to the water quality model. Performance of the Lagrangian averaging algorithm was excellent. Dye and salinity distributions computed in the water quality model, using Lagrangian-averaged velocities, agreed closely with distributions computed by the hydrodynamic model using transport computed at five-minute intervals. Details of the testing were provided by Dortch (1990).

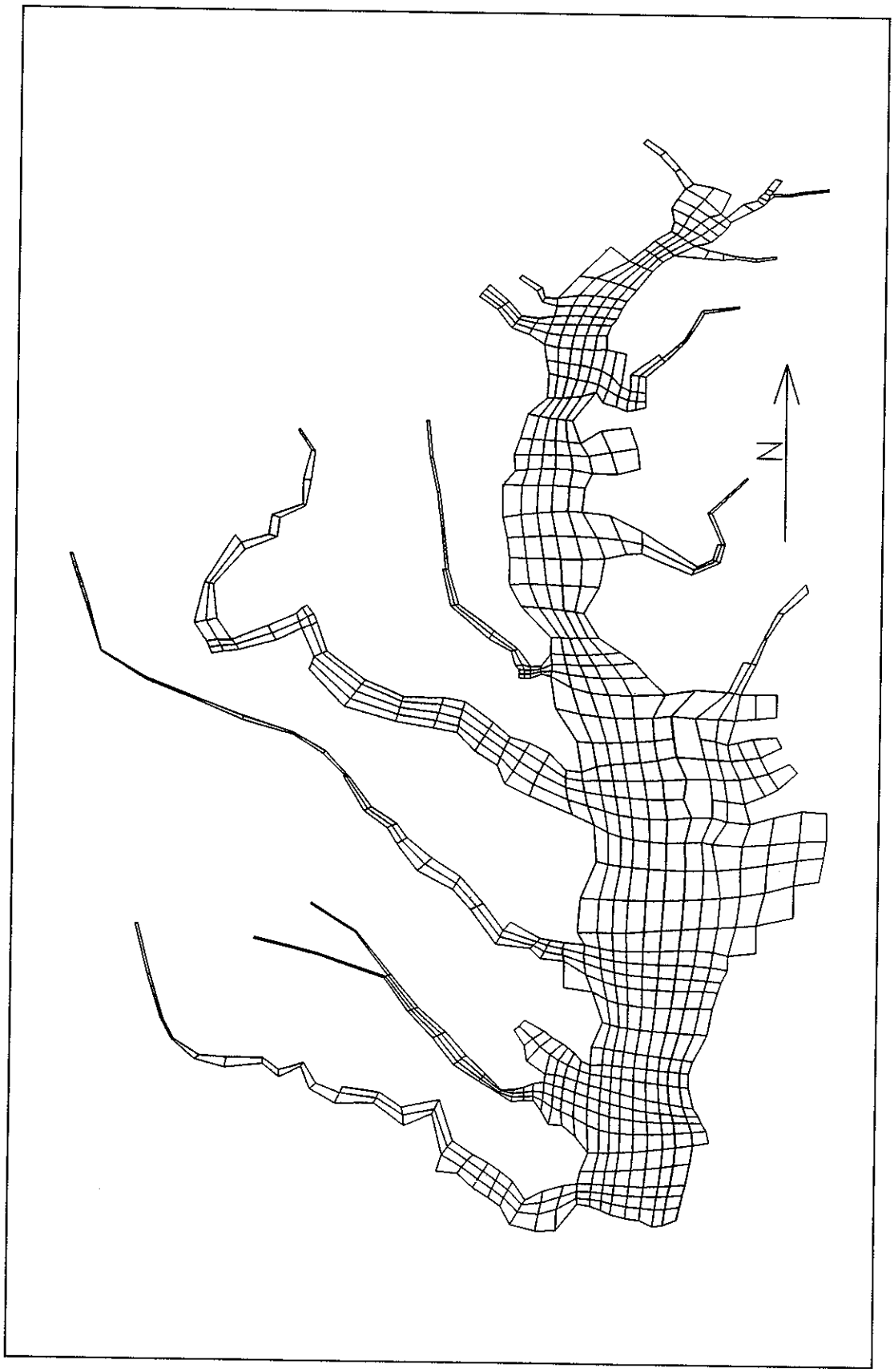

Figure 3-1. Plan View of Computational Grid

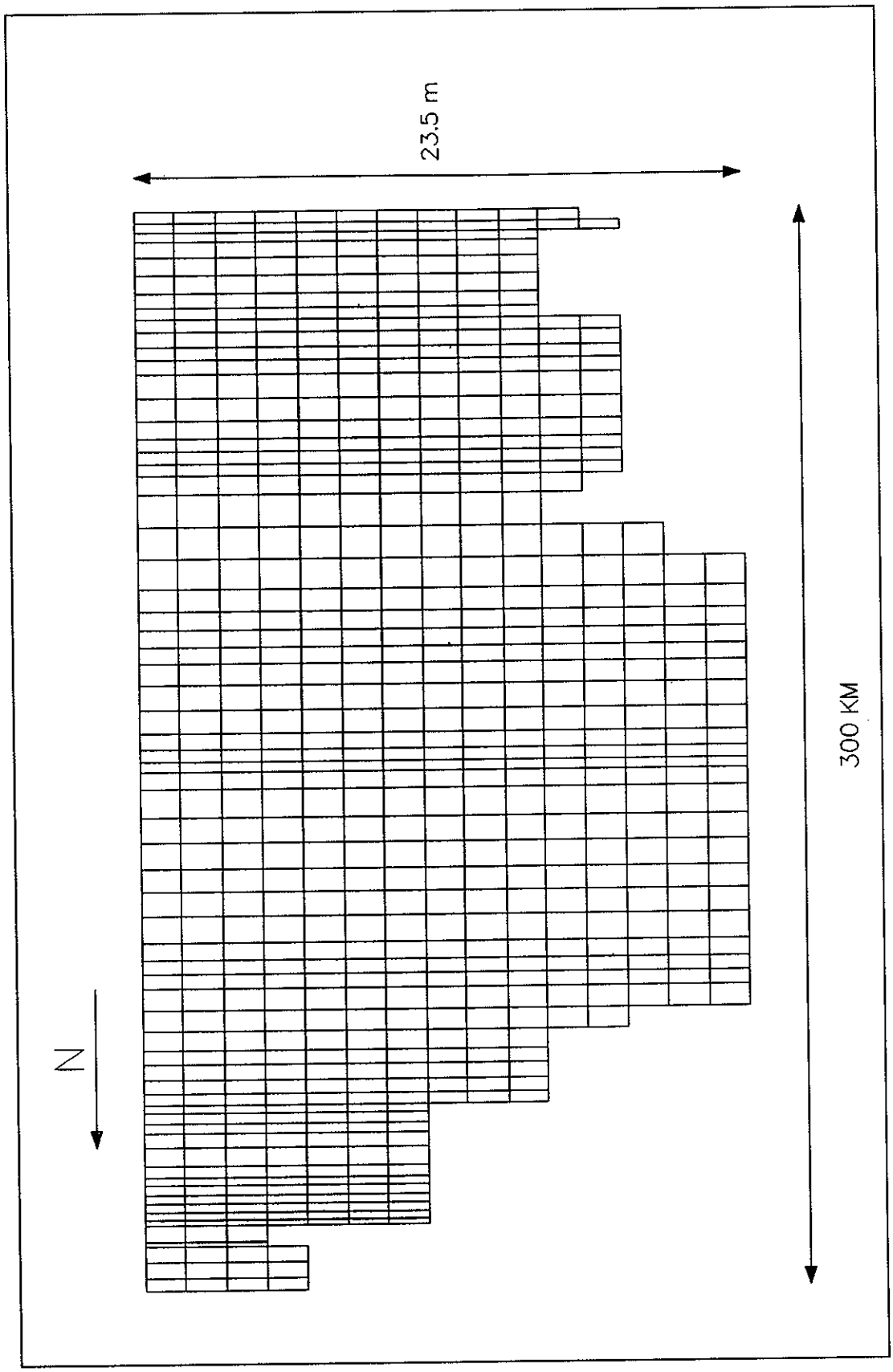

Figure 3-2. Elevation of Computational Grid Along Longitudinal Bay Axis

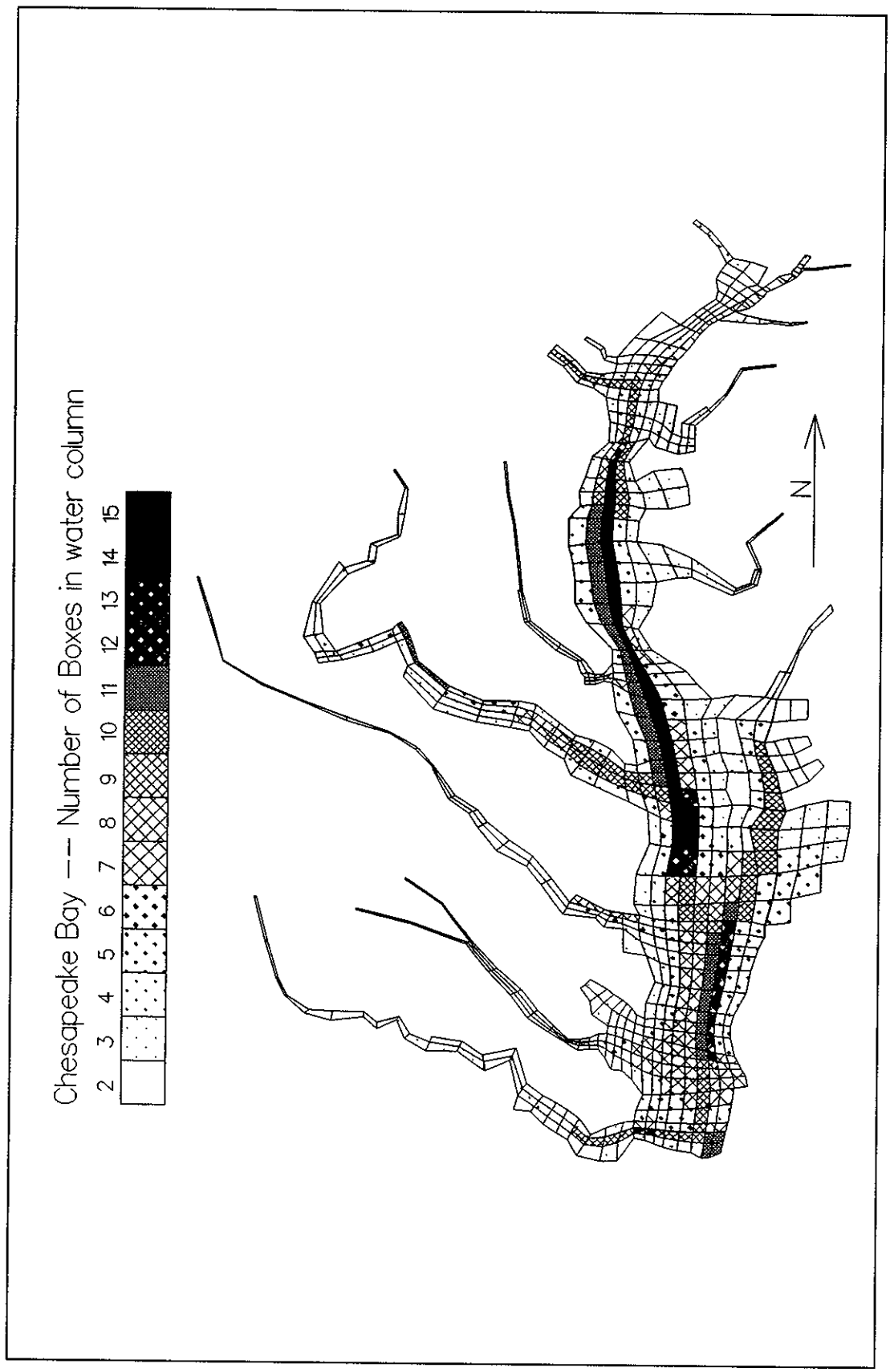

Figure 3-3. Plan View Showing Number of Cells in Vertical Dimension

Volumetric Flows

The massive quantity of hydrodynamic information precluded ready examination and interpretation. To aid in interpretation of predictions from the water quality model, various summaries of transport processes were produced. One summary was an examination of volumetric flow between regions of the Bay. Nine regions were defined (Figure 3-4). Eight were along the main axis of the Bay and the ninth comprised the Tangier sound adjacent to the Eastern Shore. Volumetric flows were summarized for each cell interface along transects dividing adjacent regions. Flows were produced from averages of Lagrangian velocities for the summer months, June to September, of 1986. The year 1986 was selected since it was a year of average flow in the Susquehanna River.

Spatial distribution of flows at the transects (Figures 3-5 to 3-13) conformed to expectations based on theory and observations. Flows near the surface of the Bay were mostly downstream, towards the ocean. Flows near the bottom were mostly upstream, towards the Susquehanna. The division between upstream and downstream flows was tilted, however, rather than horizontal. The tilting was sufficient that net upstream flows occurred at the surface at many transects. At the junction with the ocean (Figure 3-5) and in the lower Bay (Figure 3-6 to 3-10), upstream flow showed a predominance towards the right, looking upstream. The right-hand predominance indicated effects of the earth's rotation upon flow in the stratified Bay. At two transects in the upper Bay (Figures 3-11 and 3-12), upstream predominance was towards the left, and suggested influences of channel geometry.

At each transect, summaries of upstream, downstream, and net flows were produced. Magnitude of upstream and downstream flows was greatest in the lower Bay and diminished with distance upstream towards the Susquehanna River (Figure 3-14). Lateral volumetric exchanges between the mainstem and Tangier Sound were less than longitudinal flows along the mainstem in mid-Bay. Net flows (Figure 3-15) were usually an order of magnitude less than upstream and downstream flows. Net flows revealed an interesting phenomenon. Strong net lateral flows occurred from the mainstem into Tangier Sound. Primary downstream transport was through Tangier Sound. A net upstream flow occurred along the mainstem adjacent to the Sound.

At the mouths of major tributaries, net flows induced by freshwater runoff were negligible compared to huge Bay-tributary volume exchanges caused by density-driven circulation (Figure 3-16). Magnitude of the flows into and out of the tributaries was generally proportional to cross-sectional area. Largest circulation, at the mouth of the York River, was influenced by the location of the transect which defined the river entrance. Substantial upstream and downstream circulation also occurred at the mouths of the Potomac and James Rivers.

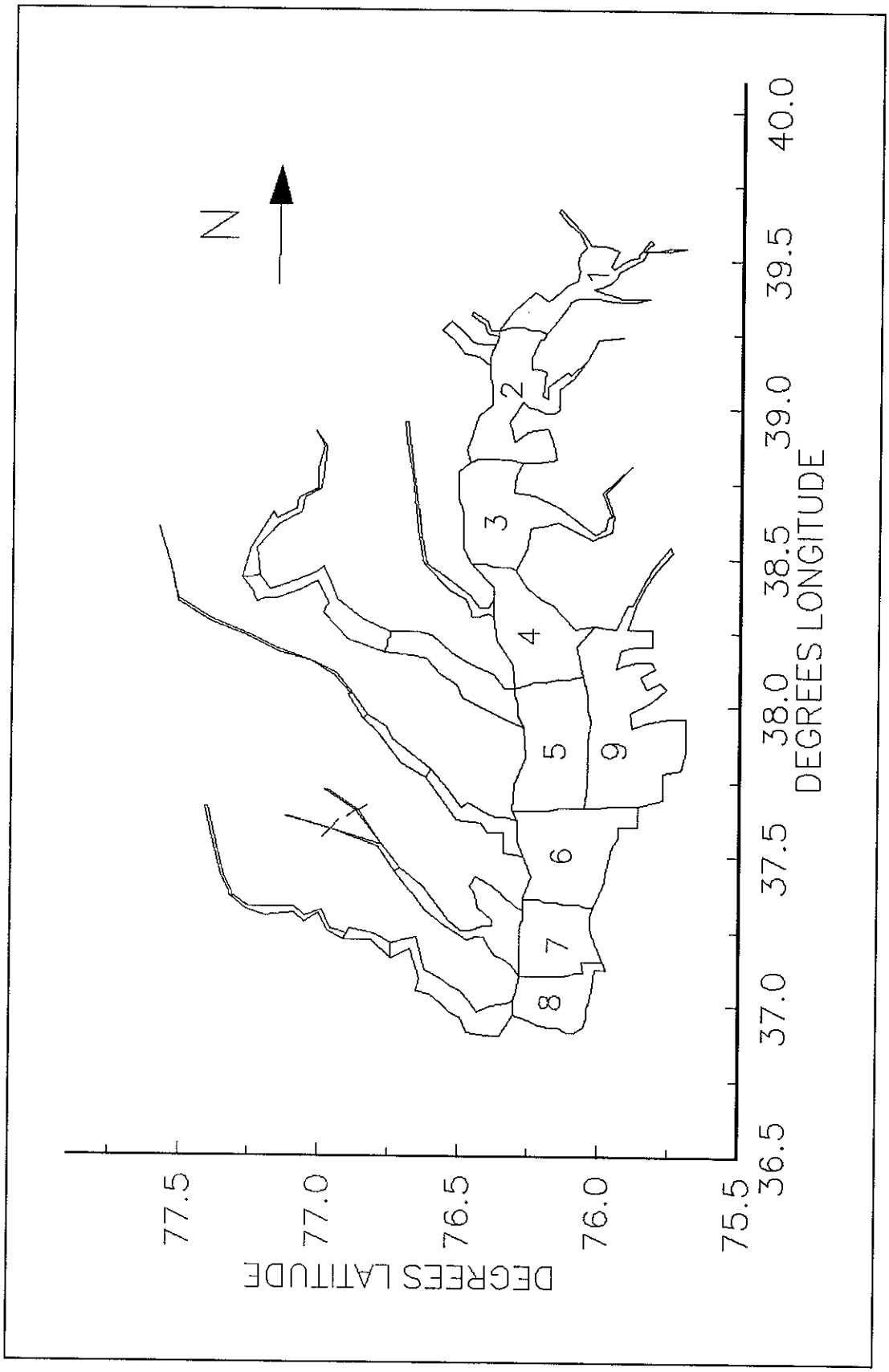

Figure 3-4. Zones for Summaries of Volumetric Flows

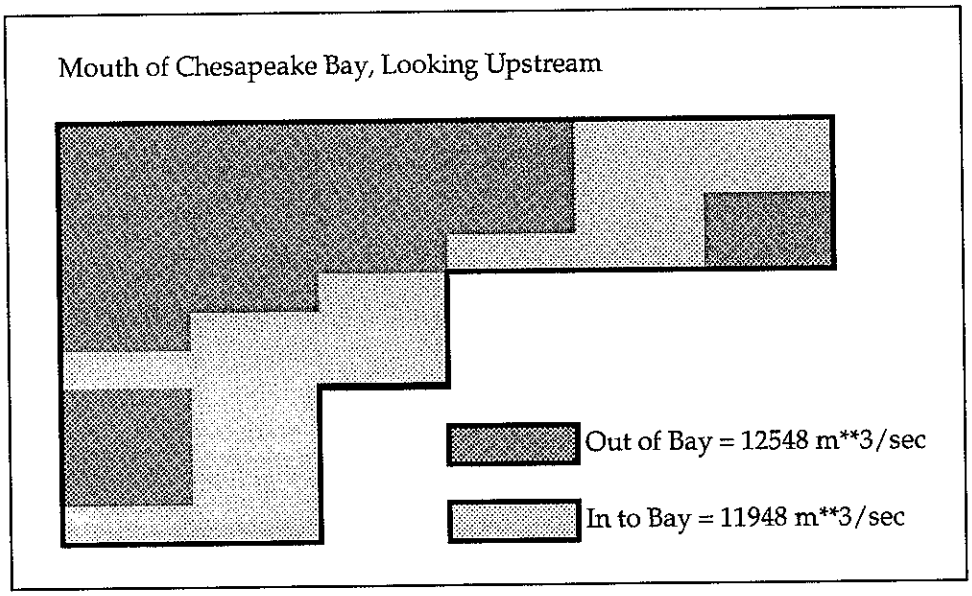

Figure 3-5. Spatial Flow Distribution at Bay Mouth, Summer 1986

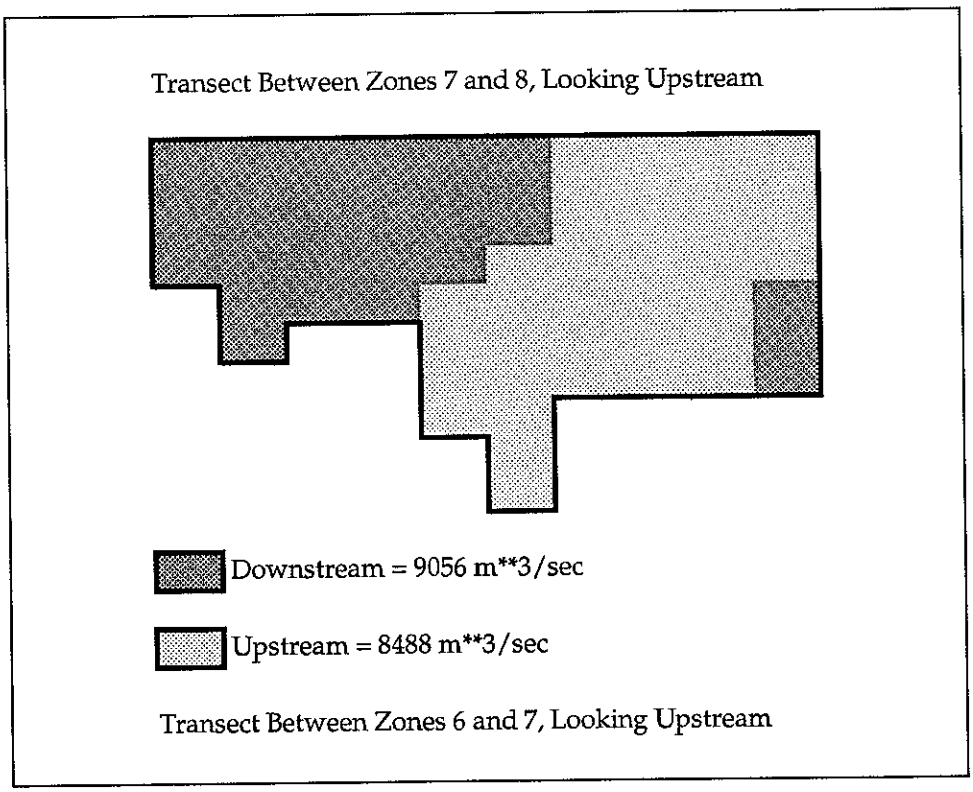

Figure 3-6. Spatial Flow Distribution at Transect Between Zones 7 and 8, Summer 1986

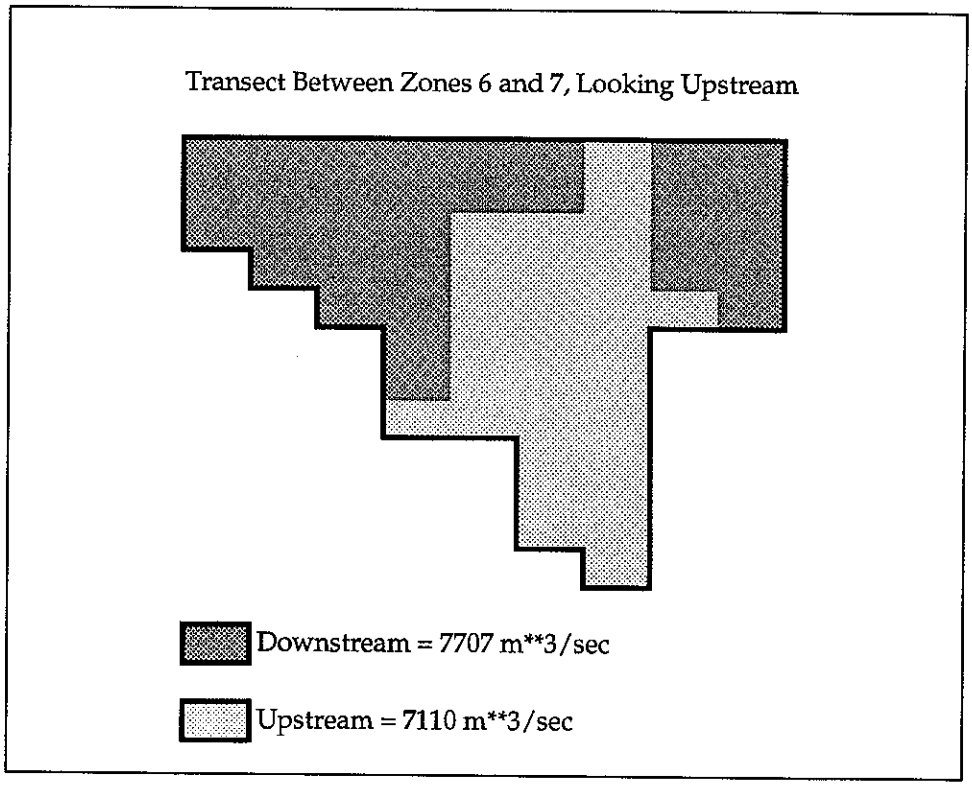

Figure 3-7. Spatial Flow Distribution at Transect Between Zones 6 and 7, Summer 1986

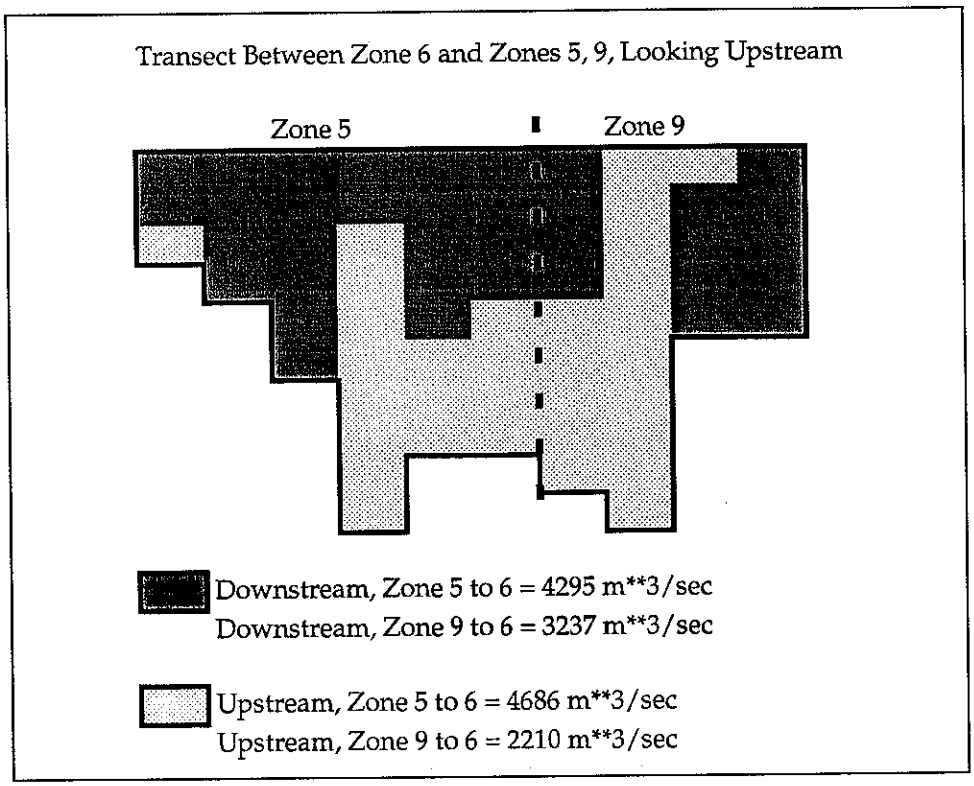

Figure 3-8. Spatial Flow Distribution at Transect Between Zones 6 and 5, 9, Summer 1986

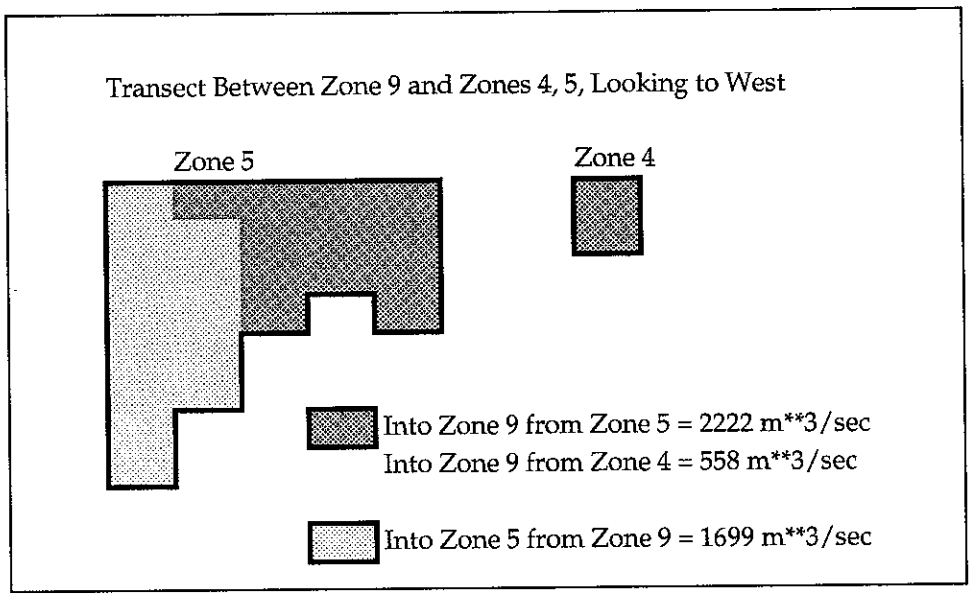

Figure 3-9. Spatial Flow Distribution at Transect Between Zones 9 and 4, 5, Summer 1986

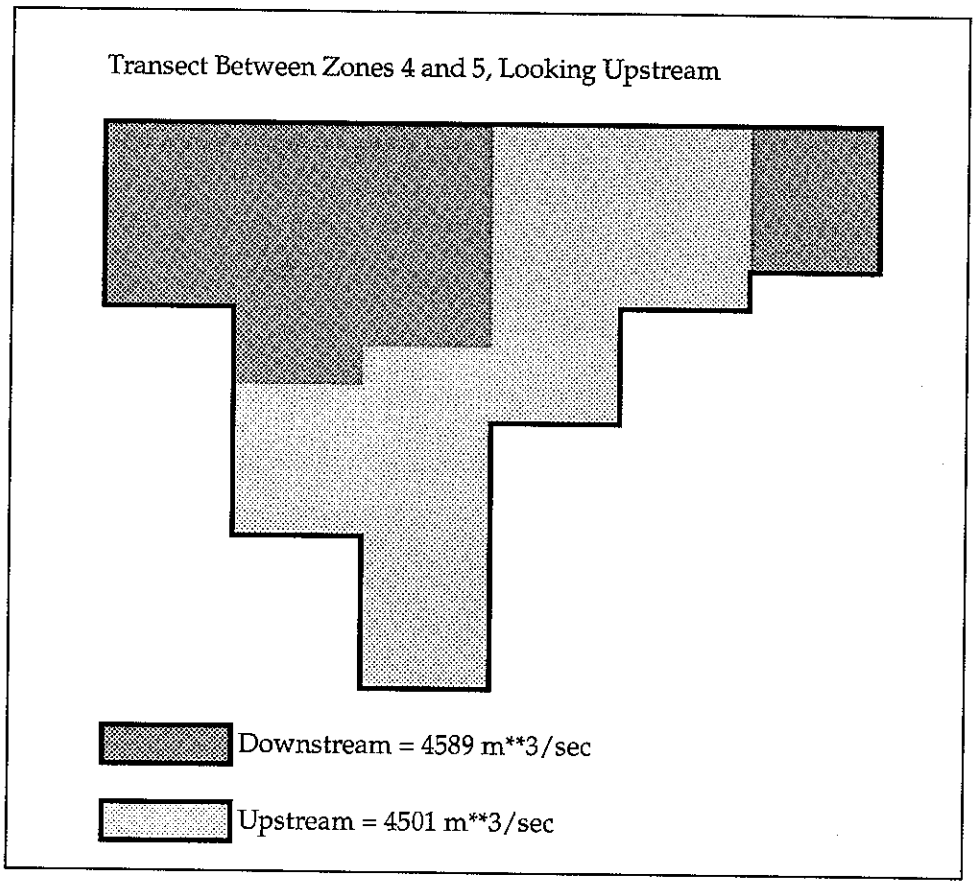

Figure 3-10. Spatial Flow Distribution at Transect Between Zones 4 and 5, Summer 1986

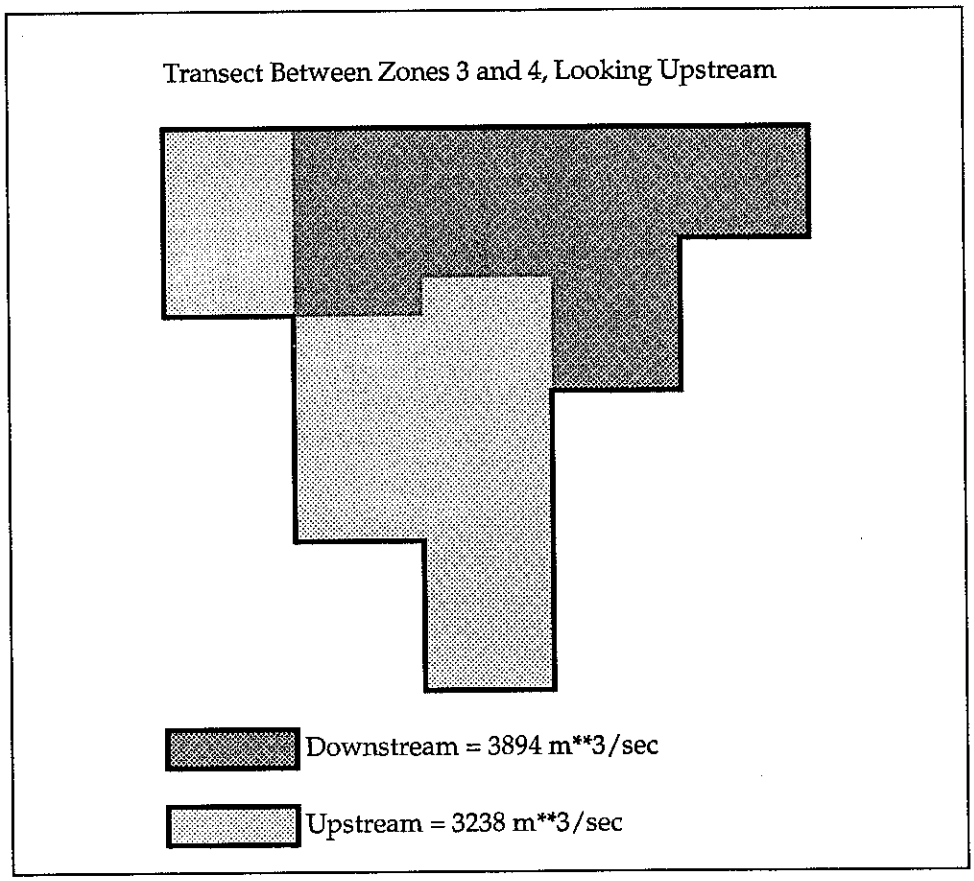

Figure 3-11. Spatial Flow Distribution at Transect Between Zones 3 and 4, Summer 1986

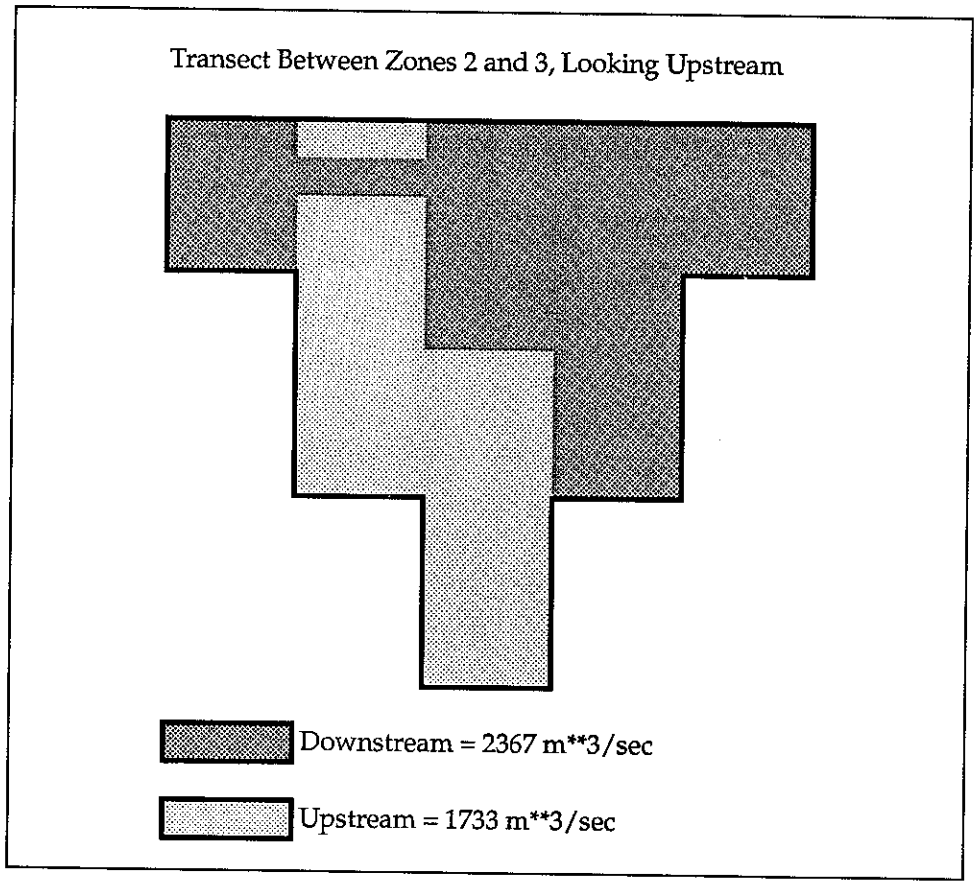

Figure 3-12. Spatial Flow Distribution at Transect Between Zones 2 and 3, Summer 1986

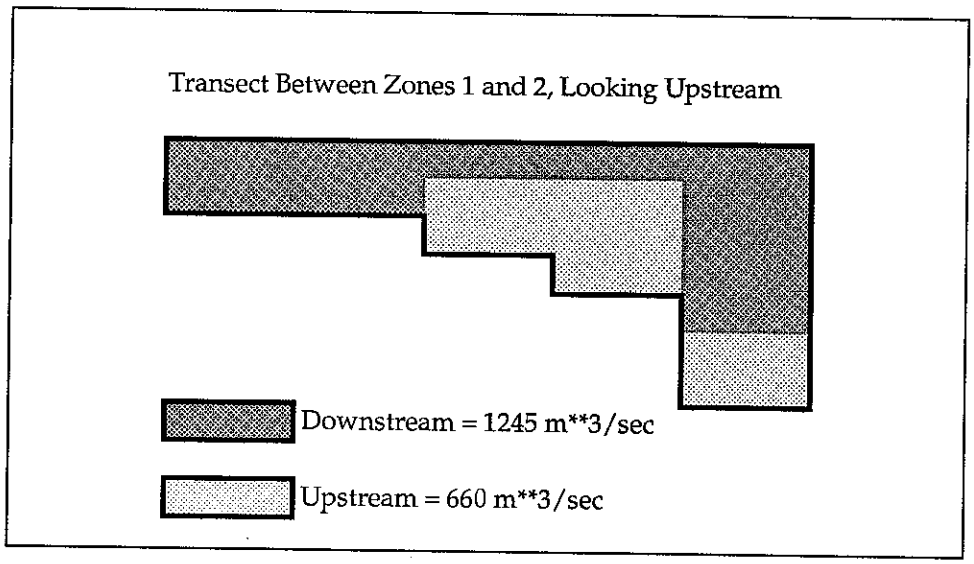

Figure 3-13. Spatial Flow Distribution at Transect Between Zones 1 and 2, Summer 1986

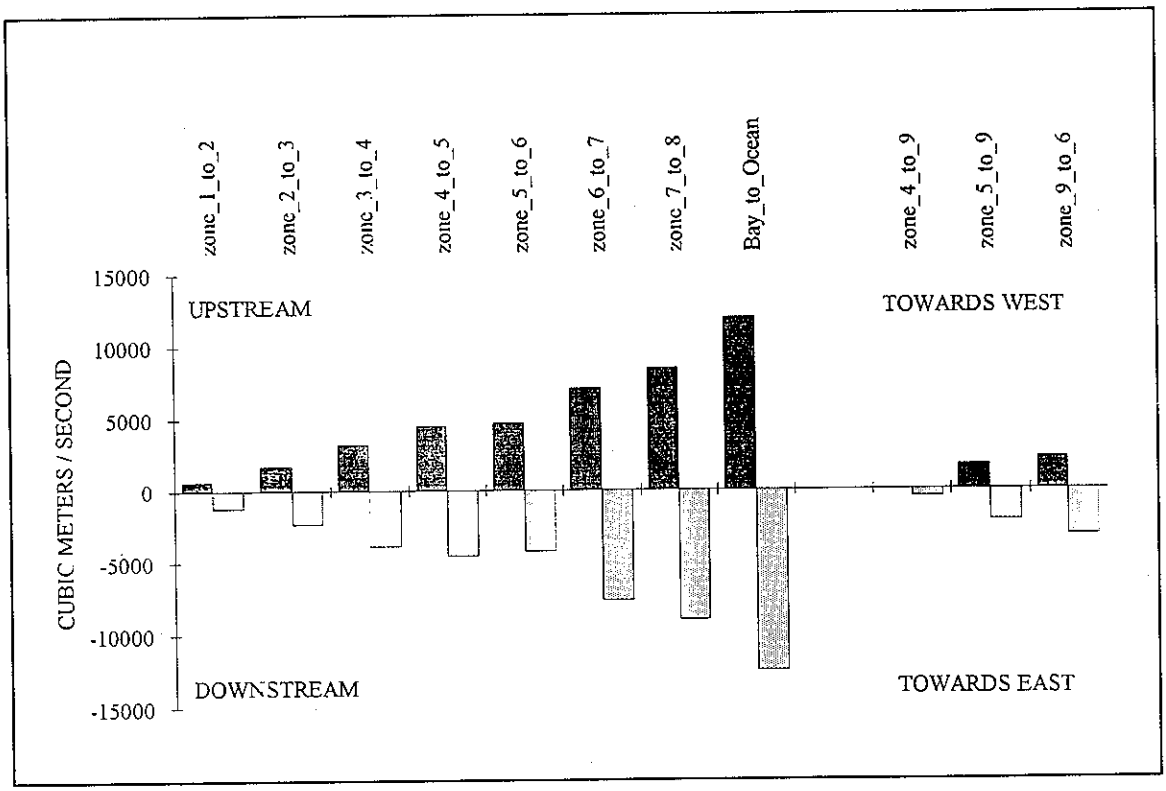

Figure 3-14. Upstream and Downstream Flows at Bay Transects, Summer 1986

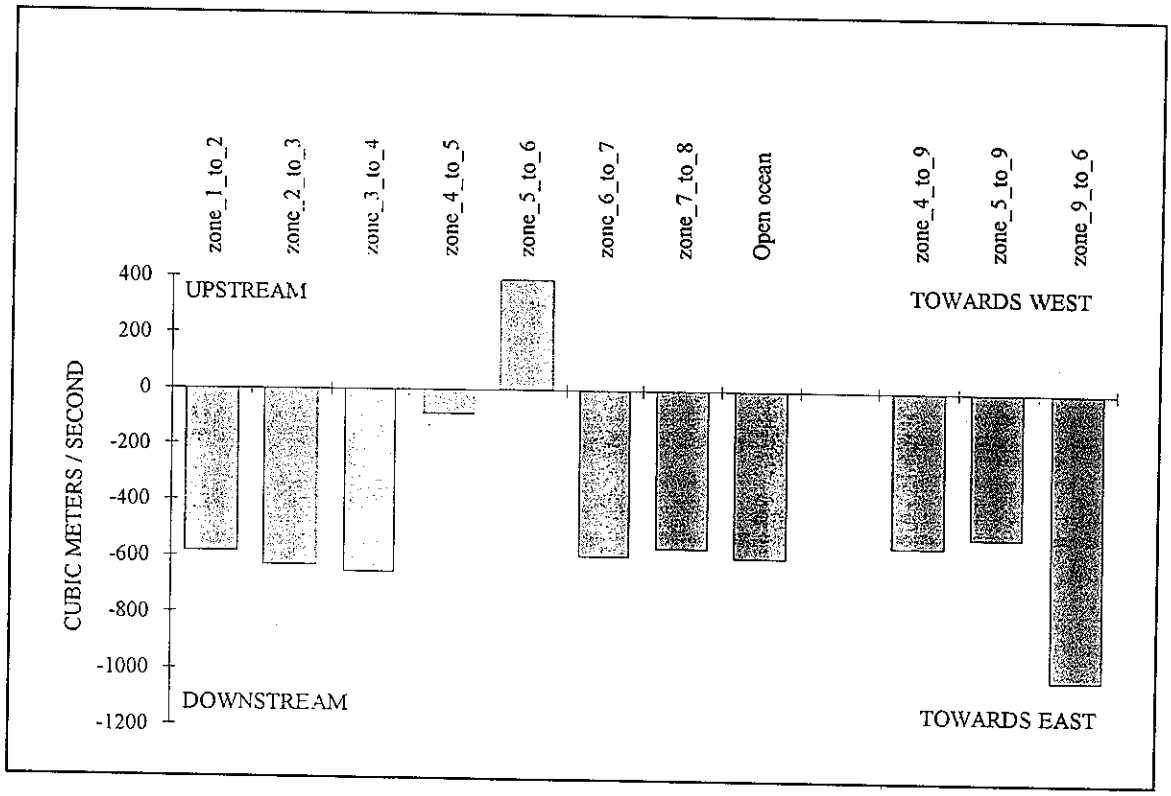

Figure 3-15. Net Flows at Bay Transects, Summer 1986

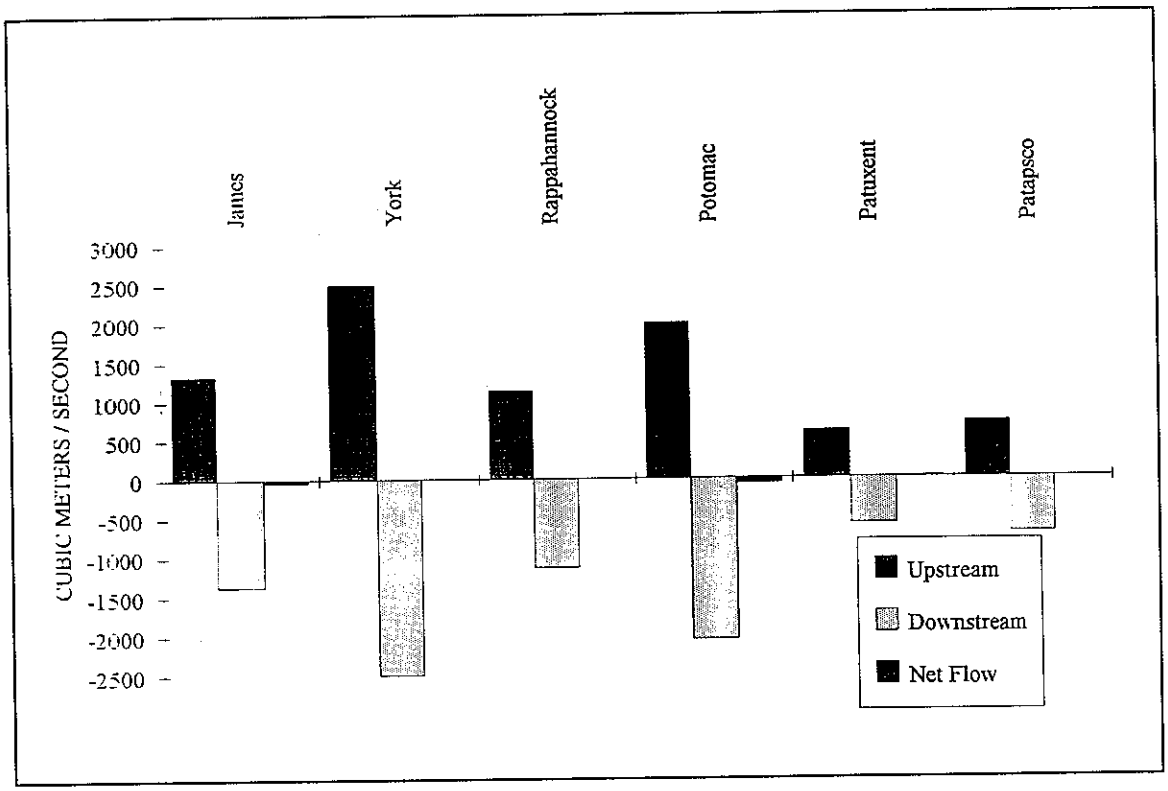

Figure 3-16. Upstream, Downstream, and Net Flows at Mouths of Major Tributaries

Chapter IV: The Water Quality Model

Introduction

The central issues in the water quality model are primary production of carbon by algae and concentration of dissolved oxygen. Primary production provides the energy required by the ecosystem to function. Excessive primary production is detrimental, however, since its decomposition, in the water and sediments, consumes oxygen. Dissolved oxygen is necessary to support the life functions of higher organisms and is considered an indicator of the "health" of estuarine systems. In order to predict primary production and dissolved oxygen, a large suite of model state variables is necessary (Table 4-1).

Table 4-1
Water Quality Model State Variables

Temperature	Salinity
Total Active Metal	Cyanobacteria
Diatoms	Green Algae
Dissolved Organic Carbon	Labile Particulate Organic Carbon
Refractory Particulate Organic Carbon	Ammonium
Nitrate	Dissolved Organic Nitrogen
Labile Particulate Organic Nitrogen	Refractory Particulate Organic Nitrogen
Total Phosphate	Dissolved Organic Phosphorus
Labile Particulate Organic Phosphorus	Refractory Particulate Organic Phospho–rus
Chemical Oxygen Demand	Dissolved Oxygen
Particulate Biogenic Silica	Available Silica

Algae

Algae are grouped into three model classes: cyanobacteria, diatoms, and greens. The grouping is based upon the distinctive characteristics of each class and upon the significant role the characteristics play in the ecosystem. Cyanobacteria, commonly called blue-green algae, are characterized by their abundance (as picoplankton) in saline water and by their bloom-forming characteristics in fresh water. Cyanobacteria are unique in that some species fix atmospheric nitrogen although nitrogen fixers are not predominant in the Chesapeake Bay system. The Cyanobacteria distinguished in the model are the bloom-forming species found in the tidal, freshwater Potomac River. They are characterized as having negligible settling velocity and are subject to low predation pressure. The picoplankton are combined with the green algae group since insufficient data exists to consider them separately. Diatoms are distinguished by their requirement of silica as a nutrient to form cell walls. Diatoms are large algae characterized by high settling velocities. Settling of spring diatom blooms to the sediments may be a significant source of carbon for sediment oxygen demand. Algae that do not fall into the preceding two groups are lumped into the heading of green algae. Green algae settle at a rate intermediate between cyanobacteria and diatoms and are subject to greater grazing pressure than cyanobacteria.

Organic Carbon

Three organic carbon state variables are considered: dissolved, labile particulate, and refractory particulate. Labile and refractory distinctions are based upon the time scale of decomposition. Labile organic carbon decomposes on a time scale of days to weeks while refractory organic carbon requires more time. Labile organic carbon decomposes rapidly in the water column or the sediments. Refractory organic carbon decomposes slowly, primarily in the sediments, and may contribute to sediment oxygen demand years after deposition.

Nitrogen

Nitrogen is first divided into organic and mineral fractions. Organic nitrogen state variables are: dissolved organic nitrogen, labile particulate organic nitrogen, and refractory particulate organic nitrogen. Two mineral nitrogen forms are considered: ammonium and nitrate. Both are utilized to fulfill algal nutrient requirements although ammonium is preferred from thermodynamic considerations. The primary reason for distinguishing the two is that ammonium is oxidized by nitrifying bacteria into nitrate. This oxidation can be a significant sink of oxygen in the water column and sediments. An intermediate in the complete oxidation of ammonium, nitrite, also exists. Nitrite concentrations are usually much less than nitrate and for modeling purposes nitrite is combined with nitrate. Hence the nitrate state variable actually represents the sum of nitrate plus nitrite.

Phosphorus

As with carbon and nitrogen, organic phosphorus is considered in three states: dissolved, labile particulate, and refractory particulate. Only a single mineral form, total phosphate, is considered. Total phosphate exists as several states within the model ecosystem: dissolved phosphate, phosphate sorbed to inorganic solids, and phosphate incorporated in algal cells. Equilibrium partition coefficients are used to distribute the total among the three states.

Silica

Silica is divided into two state variables: available silica and particulate biogenic silica. Available silica is primarily dissolved and can be utilized by diatoms. Particulate biogenic silica cannot be utilized. In the model, particulate biogenic silica is produced through diatom mortality. Particulate biogenic silica undergoes dissolution to available silica or else settles to the bottom sediments.

Chemical Oxygen Demand

In the context of this study, chemical oxygen demand is the concentration of reduced substances that are oxidizable by inorganic means. The primary component of chemical oxygen demand is sulfide released from sediments. Oxidation of sulfide to sulfate may remove substantial quantities of dissolved oxygen from the water column.

Dissolved Oxygen

Dissolved oxygen is required for the existence of higher life forms. Oxygen availability determines the distribution of organisms and the flows of energy and nutrients in an ecosystem. Dissolved oxygen is a central component of the water quality model.

Total Active Metal

Both phosphate and dissolved silica sorb to inorganic solids, primarily iron and manganese. Sorption and subsequent settling is one pathway for removal of phosphate and silica from the water column. Consequently, the concentration and transport of iron and manganese are represented in the model. Limited data do not allow a complete treatment of iron and manganese chemistry, however. Rather, a single state variable, total active metal, is defined as the total concentration of metals that are active in phosphate and silica transport. Total active metal is partitioned between particulate and dissolved phases by an oxygen-dependent partition coefficient.

Salinity

Salinity is a conservative tracer that provides verification of the transport component of the model and facilitates examination of conservation of mass. Salinity also influences the dissolved oxygen saturation concentration and is used in the determination of kinetics constants that differ in saline and fresh water.

Temperature

Temperature is a primary determinant of the rate of biochemical reactions. Reaction rates increase as a function of temperature although extreme temperatures result in the mortality of organisms.

Conservation Of Mass Equation

The foundation of CE-QUAL-ICM is the solution to the three-dimensional mass-conservation equation for a control volume. The control-volume structure was selected to allow maximum flexibility in linkage of CE-QUAL-ICM to alternate hydrodynamic models. Control volumes in CE-QUAL-ICM correspond to cells in x-y-z space on the CH3D grid. CE-QUAL-ICM solves, for each volume and for each state variable, the conservation of mass equation:

$$\frac{\delta V_i C_i}{\delta t} = \sum_{j=1}^{n} Q_j C_j^* + \sum_{j=1}^{n} A_j D_j \frac{\delta C}{\delta x_j} + \sum S_i \qquad (4\text{-}1)$$

V_i = volume of ith control volume (m^3)
C_i = concentration in ith control volume (gm m^{-3})
Q_j = volumetric flow across flow face j of ith control volume (m^3 sec^{-1})
C^*_j = concentration in flow across flow face j (gm m^{-3})
A_j = area of flow face j (m^2)
D_j = diffusion coefficient at flow face j (m^2 sec^{-1})
n = number of flow faces attached to ith control volume
S_i = external loads and kinetic sources and sinks in ith control volume (gm sec^{-1})
t, x = temporal and spatial coordinates

Solution to the mass-conservation equation is via the finite-difference method using the QUICKEST algorithm (Leonard 1979) in the horizontal directions and a Crank-Nicolson scheme in the vertical direction.

The remainder of this chapter details the kinetics portion of the mass-conservation equation for each state variable. Parameters are defined where

they first appear. All parameters are listed, in alphabetical order, in an appendix. For consistency with reported rate coefficients, kinetics are detailed using a temporal dimension of days. Within the CE-QUAL-ICM code, kinetics sources and sinks are converted to a dimension of seconds before employment in the mass-conservation equation.

Algae

Algae play a central role in the carbon and nutrient cycles that comprise the model ecosystem. Equations governing the three algal groups are largely the same. Differences among groups are expressed through the magnitudes of parameters in the equations. In describing the parameters, the letter "x" is used as a "wild card." As needed in this text, the wild card is replaced with a letter that indicates a specific algal group. Characters that indicate each algal group are:

c = cyanobacteria
d = diatoms
g = green algae

Sources and sinks of algae are:

Growth (production)
Basal metabolism
Predation
Settling

The governing equation for algal biomass is:

$$\frac{\delta}{\delta t} Bx = \left(Px - BMx - PRx - WSx \frac{\delta}{\delta z} \right) Bx \qquad (4\text{-}2)$$

Bx = algal biomass, expressed as carbon (gm C m^{-3})
Px = production (day^{-1})
BMx = basal metabolism (day^{-1})
PRx = predation (day^{-1})
WSx = settling velocity (m day^{-1})
z = vertical coordinate (m)

Production

Production by phytoplankton is determined by the availability of nutrients, by the intensity of light, and by the ambient temperature. The effects of each are considered to be multiplicative:

$$Px = PMx\ f(N)\ f(I)\ f(T) \quad (4\text{-}3)$$

PMx = production under optimal conditions (day^{-1})
f(N) = effect of suboptimal nutrient concentration ($0 \leq f \leq 1$)
f(I) = effect of suboptimal illumination ($0 \leq f \leq 1$)
f(T) = effect of suboptimal temperature ($0 \leq f \leq 1$)

The Cyanobacteria found in the Potomac are freshwater organisms that undergo rapid mortality in salt water. This effect is noted by including a salinity toxicity term in the Cyanobacteria production equation:

$$Pc = PMc\ f(N)\ f(I)\ f(T)\ f(S) \quad (4\text{-}4)$$

f(S) = effect of salinity on Cyanobacteria production ($0 \leq f \leq 1$)

Nutrients

Carbon, nitrogen, and phosphorus are the primary nutrients required for algal growth. Diatoms require silica, as well. Inorganic carbon is usually available in excess and is not considered in the model. The effects of the remaining nutrients on growth are described by the formulation commonly referred to as "Monod kinetics" (Monod 1949). In the Monod formulation (Figure 4-1) growth is dependent upon nutrient availability at low nutrient concentrations but is independent of nutrients at high concentrations. A key parameter in the formulation is the "half-saturation concentration". Growth rate is half the maximum when available nutrient concentration equals the half-saturation concentration. Liebig's "law of the minimum" (Odum 1971) indicates growth is determined by the nutrient in least supply. For cyanobacteria and greens:

$$f(N) = \text{minimum}\left(\frac{NH_4 + NO_3}{KHnx + NH_4 + NO_3}, \frac{PO_4d}{KHpx + PO_4d}\right) \quad (4\text{-}5)$$

NH_4 = ammonium concentration (gm N m^{-3})
NO_3 = nitrate concentration (gm N m^{-3})
KHnx = half-saturation constant for nitrogen uptake (gm N m^{-3})
PO_4d = dissolved phosphate concentration (gm P m^{-3})
KHpx = half-saturation constant for phosphorus uptake (gm P m^{-3})

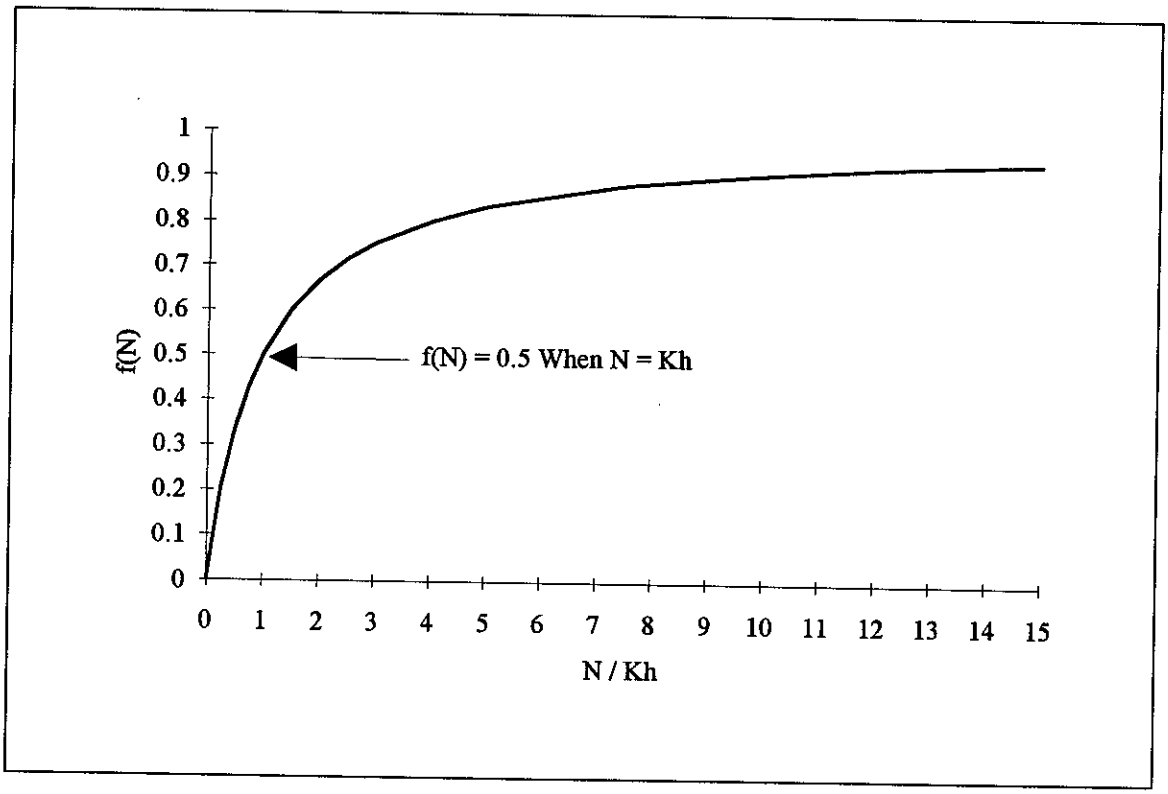

Figure 4-1. The Monod formulation for nutrient-limited growth

Some cyanobacteria, notably the bloom-forming genus *Anabaena*, can use atmospheric nitrogen to supply their nutrient requirements. At present, a non-fixing genus, *Microcystis*, is the predominant cyanobacteria in the freshwater Potomac River (Thomann et al. 1985). Consequently, the nitrogen limitation expressed in Equation 4-5 applies to cyanobacteria represented in the model. The potential growth of nitrogen fixers, such as *Anabaena*, can be estimated, if desired, by removing from the model the nitrogen limitation on cyanobacteria.

Diatoms require silica, as well as nitrogen and phosphorus, for growth. For diatoms, the nutrient limitation is the minimum of the limitations expressed in Equation 4-5 or the following:

$$f(N) = \frac{SAd}{KHs + SAd} \qquad (4\text{-}6)$$

SAd = dissolved available silica concentration (gm Si m^{-3})
KHs = half-saturation constant for silica uptake by diatoms (gm Si m^{-3})

Light

Algal production increases as a function of light intensity until an optimal intensity is reached. Beyond the optimal intensity, production declines as intensity increases. Steele's equation (DiToro et al. 1971) describes this phenomenon:

$$f(I) = \frac{I}{Is} e^{1 - \frac{I}{Is}} \tag{4-7}$$

I = illumination rate (Langleys day^{-1})
Is = optimal illumination (Langleys day^{-1})

Steele's equation describes the instantaneous light limitation at a point in space. The model, however, computes processes integrated over discrete time intervals and aggregated spatially into model segments. Therefore, Steele's equation must be integrated over an appropriate time interval and averaged over the thickness of each model segment. The integration interval selected is one day. This interval does not preclude computation steps less than a day but frees the model from accounting for illumination in "real time." Daily averaging does preclude computation of diurnal fluctuations in algal production. This restriction is not severe, however, since the classic equations for algal growth are not appropriate for short time scales.

Assuming light intensity declines exponentially with depth, the integrated, averaged form of Steele's equation is:

$$f(I) = \frac{2.72\,FD}{Kess\,\Delta z}\left(e^{\alpha b} - e^{\alpha t}\right) \tag{4-8}$$

$$\alpha b = -\frac{Io}{FD\,Is} e^{-Kess\,(ZD + \Delta z)} \tag{4-9}$$

$$\alpha t = -\frac{Io}{FD\,Is} e^{-Kess\,ZD} \tag{4-10}$$

Io = daily illumination at water surface (Langleys day^{-1})
FD = fractional daylength ($0 \leq FD \leq 1$)
Kess = total light attenuation coefficient (m^{-1})

Δz = model segment thickness (m)
ZD = distance from water surface to top of model segment (m)

Light attenuation in the water column is composed of two fractions: a background value dependent on water color and concentration of suspended particles, and extinction due to light absorption by ambient chlorophyll:

$$Kess = Keb + Kechl \sum_{x=c,d,g} \frac{1}{CChlx} Bx \qquad (4\text{-}11)$$

Keb = background light attenuation (m^{-1})
Kechl = light attenuation coefficient for chlorophyll 'a' (m^2 mg^{-1})
CChlx = carbon-to-chlorophyll ratio of algal group x (gm C mg^{-1} chl)

Optimal illumination for photosynthesis depends on algal taxonomy, duration of exposure, temperature, nutritional status, and previous acclimation. Variations in optimal illumination are largely due to adaptations by algae intended to maximize production in a variable environment. Steele (1962) noted the result of adaptations is that optimal illumination is a consistent fraction (≈ 50%) of daily illumination. Kremer and Nixon (1978) reported an analogous finding that maximum algal production occurs at a constant depth (≈ 1m) in the water column. Their approach is adopted here so that optimal illumination is expressed:

$$Isx = Ioavg\, e^{-Kess\ Doptx} \qquad (4\text{-}12)$$

Ioavg = adjusted surface illumination (Langleys day^{-1})
Doptx = depth of maximum algal production (m)

A minimum, Ismin, is specified for optimal illumination so that algae do not thrive at extremely low light levels. The time required for algae to adapt to changes in illumination is recognized by computing Is based on a time-weighted average of daily illumination:

$$Ioavg = 0.7\, Io + 0.2\, I1 + 0.1\, I2 \qquad (4\text{-}13)$$

I1 = daily illumination one day preceding model day (Langleys day^{-1})
I2 = daily illumination two days preceding model day (Langleys day^{-1})

Insight into the interactions of light and algal production can be gained by averaging the light effect, f(I), over the entire water column. For this case, ZD = 0, and Δz = H, the total water column depth. Four independent parameters determine the light effect: FD, Ke, Dopt, and H. The parameters Ke

and Dopt, and Ke and H occur as products, however, so the number of independent parameters that determine the light effect is actually three: FD, Ke * Dopt, and Ke * H.

Fractional daylength, FD, occurs as a multiplier and in the exponential terms of the integrated form of Steele's equation (Equation 4-8). The net effect of FD on the light function is nearly linear, however (Figure 4-2). At the latitude of Chesapeake Bay, FD is limited to the range ≈0.4 to 0.6 so that f(I) varies by ≈50% from the shortest to longest day of the year.

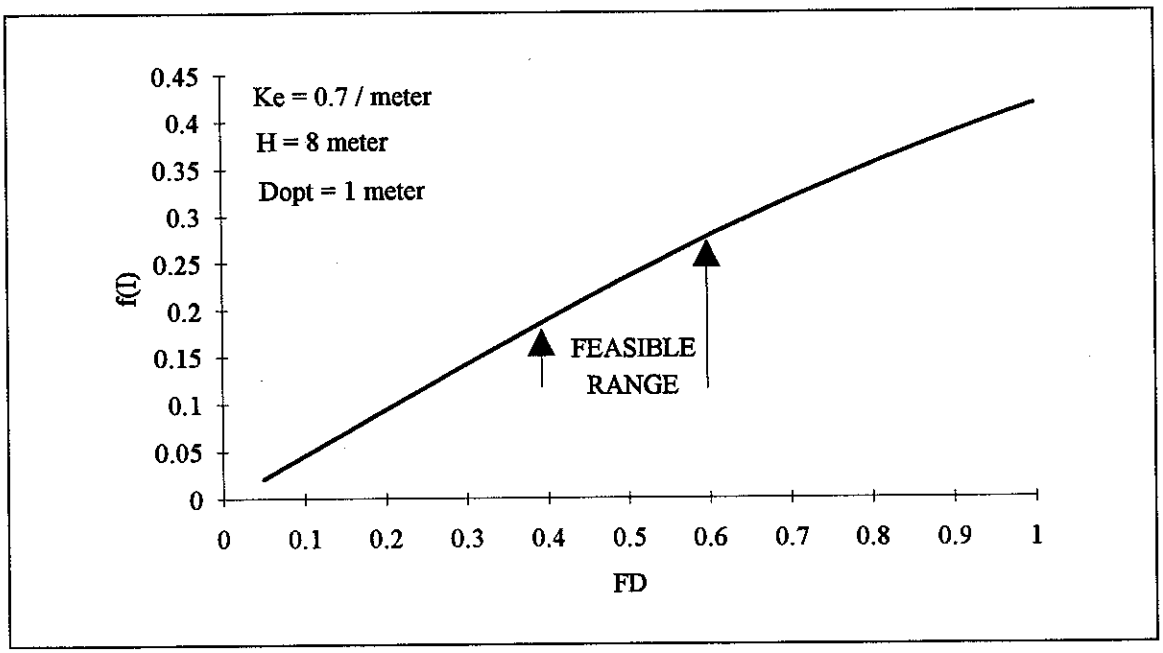

Figure 4-2. Effect of fractional daylength on algal light limitation

A plot of the effects on growth of the pairs Ke * H and Ke * Dopt (Figure 4-3) has numerous interpretations. For Ke * H >> Ke * Dopt, growth diminishes as Ke * H increases. In other words, averaged over the water column, growth goes down as light extinction and/or depth increase. For much of the feasible range of Ke * H, growth is only weakly dependent on Dopt. This weak dependence was one factor in the selection of the light-effect formulation. Maximum growth occurs when Ke * H is slightly larger than Ke * Dopt (when H is slightly larger than Dopt). When Ke * H $\leq$ Ke * Dopt (H $\leq$ Dopt), growth is diminished from the maximum due to light levels in the majority of the water column occupying the supersaturated range for algal growth. For small Ke * H (shallow systems with little light attenuation) maximum growth occurs when Dopt = 0. When Dopt = 0, no portion of the water column is in the supersaturated range. For much of the feasible range of Ke * H, however, maximum production occurs when Dopt > 0. For this case, diminished production due to light supersaturation near the surface is offset by increased production at deeper depths.

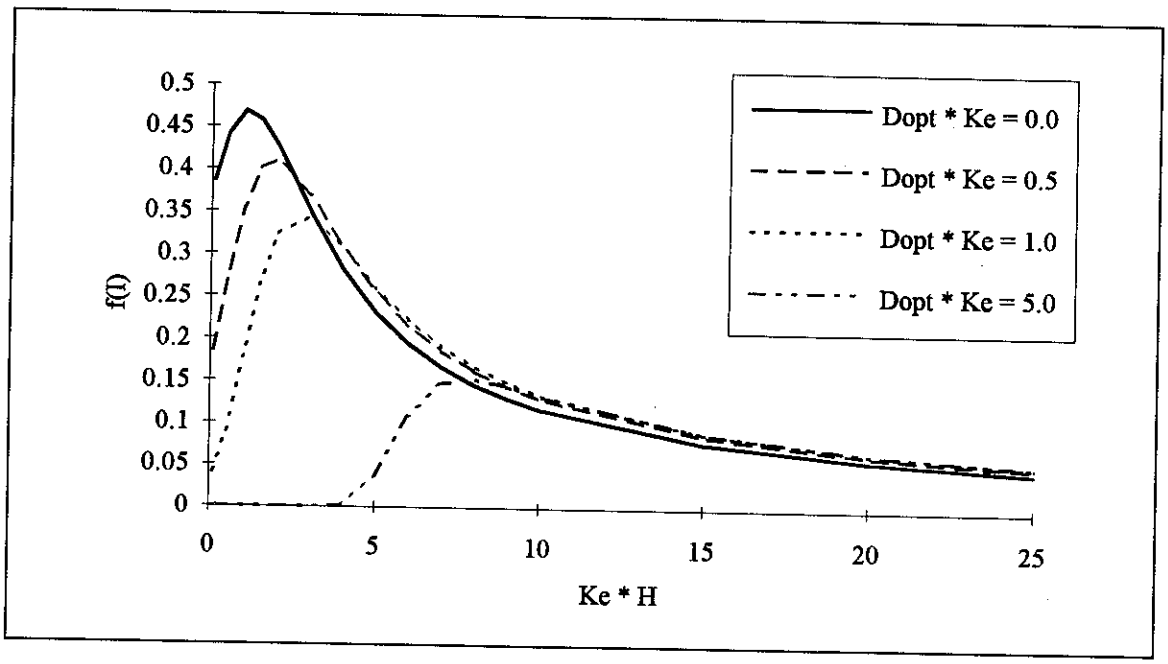

Figure 4-3. Effect of light extinction, total depth, and optimal depth on algal light limitation

Temperature

Algal production increases as a function of temperature until an optimum temperature or temperature range is reached. Above the optimum, production declines until a temperature lethal to the organisms is attained. Numerous functional representations of temperature effects are available. Inspection of growth versus temperature curves indicates a function similar to a Gaussian probability curve (Figure 4-4) provides a good fit to observations:

$$f(T) = e^{-KTgx1\,(T - Tmx)^2} \text{ when } T \leq Tmx$$
$$= e^{-KTgx2\,(Tmx - T)^2} \text{ when } T > Tmx \qquad (4\text{-}14)$$

T = temperature (C^o)
Tmx = optimal temperature for algal growth (C^o)
KTgx1 = effect of temperature below TMx on growth ($C^{o\,-2}$)
KTgx2 = effect of temperature above TMx on growth ($C^{o\,-2}$)

Salinity Toxicity

The effect of salinity on freshwater Cyanobacteria is represented by an empirical equation:

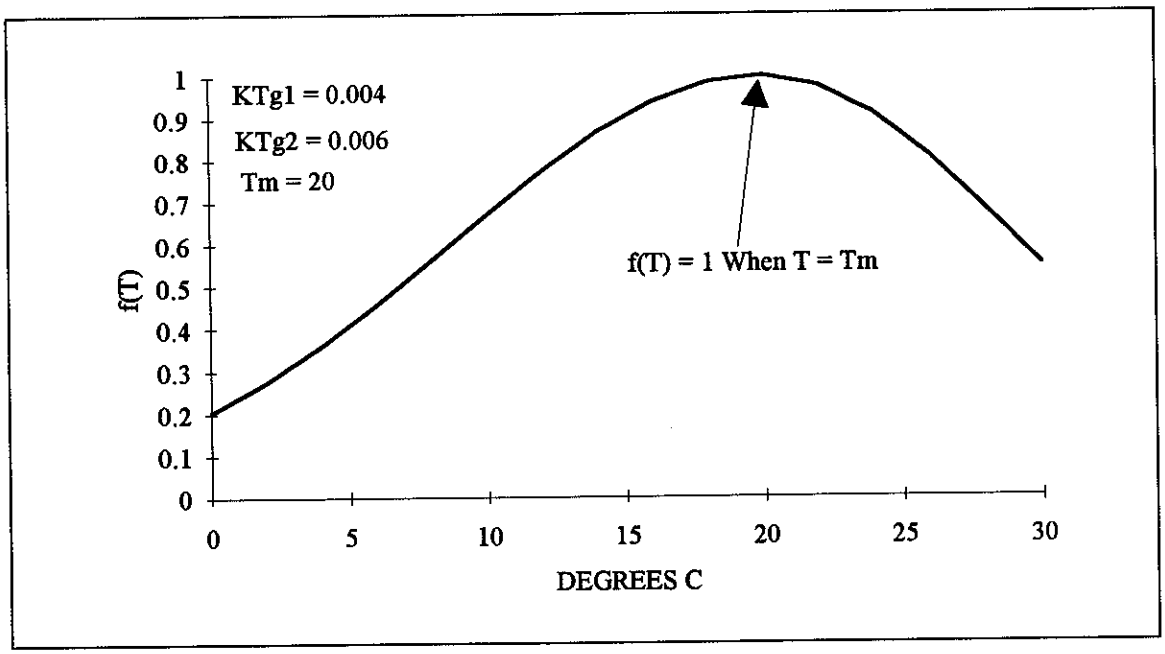

Figure 4-4. Effect of temperature on algal production

$$f(S) = \frac{Stox^2}{Stox^2 + S^2} \qquad (4\text{-}15)$$

Stox = salinity which Microcystis growth is halved (ppt)

Settling

Species comprising the diatom population of the Bay vary according to season and location. In late winter and early spring, diatom population in the Bay and lower tributaries is characterized by large species with high settling velocities. At the end of spring, large diatoms are replaced by populations of smaller individuals with lower settling velocities. Seasonal variations in settling velocity may be one factor that influences formation of the subsurface chlorophyll maximum during the spring phytoplankton bloom. Diatom settling is represented in the model:

$$WSd = WSdb + Prdval\ WSds \qquad (4\text{-}16)$$

WSdb = base diatom settling velocity (m day^{-1})
WSds = enhanced settling velocity of large diatoms (m day^{-1})
Prdval = piecewise function used to specify seasonal diatom settling velocity

Basal Metabolism

As employed here, basal metabolism is the sum of all internal processes that decrease algal biomass. A portion of metabolism is respiration which may be viewed as a reversal of production. In respiration, carbon and nutrients are returned to the environment accompanied by the consumption of dissolved oxygen. A second internal sink of biomass is the excretion of dissolved organic carbon.

Respiration cannot proceed in the absence of oxygen. Basal metabolism cannot decrease in proportion to oxygen availability, however, or algae would approach immortality under anoxic conditions. To solve this dilemma, basal metabolism is considered to be independent of dissolved oxygen concentration but the distribution of metabolism between respiration and excretion is oxygen-dependent. When oxygen is freely available, respiration is a large fraction of the total. When oxygen is restricted, excretion becomes dominant. Formulation of this process is detailed in the text that describes algal effects on carbon and dissolved oxygen.

Basal metabolism is commonly considered to be an exponentially increasing (Figure 4-5) function of temperature:

$$BMx = BMrx\, e^{KTbx\,(T - Trx)} \qquad (4\text{-}17)$$

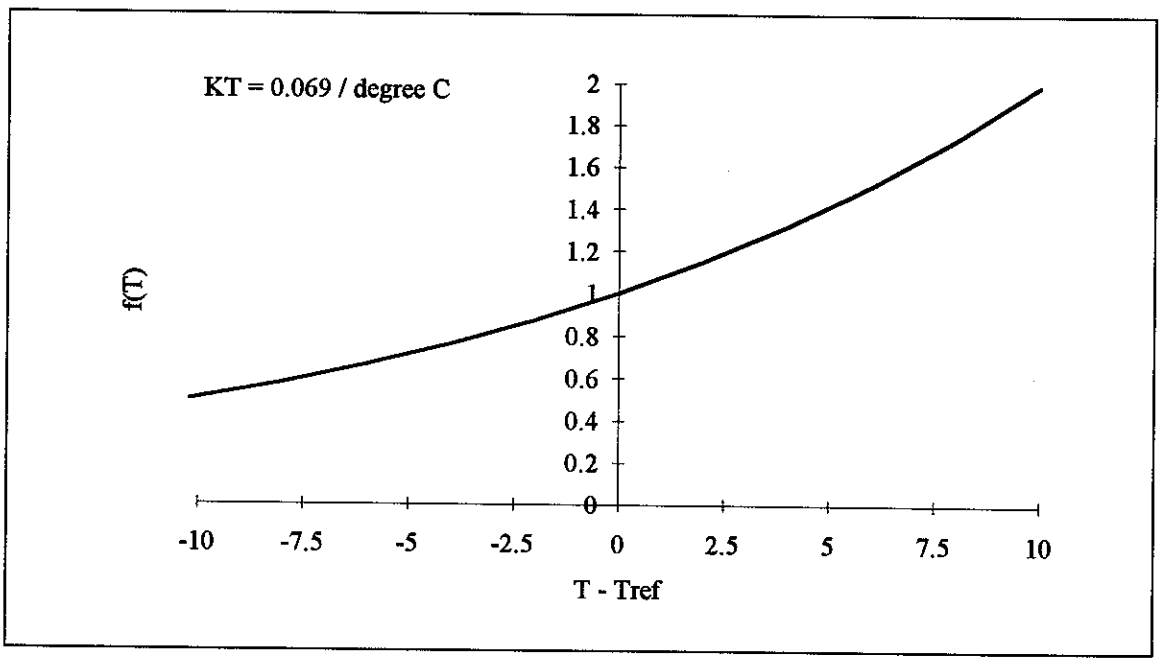

Figure 4-5. Exponential temperature function

BMrx = metabolic rate at Trx (day^{-1})
KTbx = effect of temperature on metabolism ($C^{o\,-1}$)
Trx = reference temperature for metabolism (C^{o})

Predation

Detailed specification of predation rate requires predictive modeling of zooplankton biomass and activity. At present, zooplankton are not included in the model. Consequently, a constant predation rate is specified. This specification implicitly assumes zooplankton biomass is a constant fraction of algal biomass. Zooplankton activity is assumed to be influenced by temperature and is taken into account by incorporating an exponential temperature relationship (Figure 4-5) into the predation term. The predation formulation is identical to basal metabolism. The difference in predation and basal metabolism lies in the distribution of the end products of these processes.

$$PRx = BPRx\, e^{KTbx\,(T\,-\,Trx)} \tag{4-18}$$

BPRx = predation rate at Trx (day^{-1})

Effect of Algae on Organic Carbon

During production and respiration, algae primarily take up and produce carbon dioxide, an inorganic form not considered in the model. A small fraction of basal metabolism is exuded as dissolved organic carbon, however, and in the model this fraction increases as dissolved oxygen becomes scarce. Algae also produce organic carbon through the effects of predation. Zooplankton take up and redistribute algal carbon through grazing, assimilation, respiration, and excretion. Since zooplankton are not included in the model, routing of algal carbon through zooplankton is simulated by empirical distribution coefficients. The effects of algae on organic carbon are expressed:

$$\frac{\delta}{\delta t} DOC = \left(\left(FCDx + (1 - FCDx)\frac{KHrx}{KHrx + DO}\right)BMx + FCDP\,PRx\right)Bx \tag{4-19}$$

$$\frac{\delta}{\delta t} LPOC = FCLP\,PRx\,Bx \tag{4-20}$$

$$\frac{\delta}{\delta t} RPOC = FCRP\ PRx\ Bx \qquad (4\text{-}21)$$

DOC = dissolved organic carbon concentration (gm C m^{-3})
DO = dissolved oxygen concentration (gm O_2 m^{-3})
LPOC = labile particulate organic carbon concentration (gm C m^{-3})
RPOC = refractory particulate organic carbon concentration (gm C m^{-3})
FCDx = fraction of basal metabolism exuded as dissolved organic carbon
KHrx = half-saturation concentration for algal dissolved organic carbon excretion (gm O_2 m^{-3})
FCDP = fraction of dissolved organic carbon produced by predation
FCLP = fraction of labile particulate carbon produced by predation
FCRP = fraction of refractory particulate carbon produced by predation

The sum of the three predation fractions must equal unity.

Effect of Algae on Phosphorus

Algae take up dissolved phosphate during production and release dissolved phosphate and organic phosphorus through mortality. As with carbon, the fate of algal phosphorus released by metabolism and predation is represented by distribution coefficients. Since the total phosphate state variable includes both intra and extracellular phosphate, no explicit representation of the effect of algae on phosphate is necessary. Distribution of total phosphate is determined by partition coefficients as detailed in the "PHOSPHORUS" section of this chapter. The equations that express the effects of algae on organic phosphorus are:

$$\frac{\delta}{\delta t} DOP = (BMx\ FPDx + PRx\ FPDP)\ APC\ Bx \qquad (4\text{-}22)$$

$$\frac{\delta}{\delta t} LPOP = (BMx\ FPLx + PRx\ FPLP)\ APC\ Bx \qquad (4\text{-}23)$$

$$\frac{\delta}{\delta t} RPOP = (BMx\ FPRx + PRx\ FPRP)\ APC\ Bx \qquad (4\text{-}24)$$

DOP = dissolved organic phosphorus concentration (gm P m^{-3})
LPOP = labile particulate organic phosphorus concentration (gm P m^{-3})
RPOP = refractory particulate organic phosphorus concentration (gm P m^{-3})
APC = phosphorus-to-carbon ratio of all algal groups (gm P gm^{-1} C)
FPDx = fraction of dissolved organic phosphorus produced by metabolism

FPLx = fraction of labile particulate phosphorus produced by metabolism
FPRx = fraction of refractory particulate phosphorus produced by metabolism
FPDP = fraction of dissolved organic phosphorus produced by predation
FPLP = fraction of labile particulate phosphorus produced by predation
FPRP = fraction of refractory particulate phosphorus produced by predation

The sums of the metabolism and respiration fractions must each be less than or equal to unity.

Effect of Algae on Nitrogen

Algae take up ammonium and nitrate during production and release ammonium and organic nitrogen through mortality. Nitrate is internally reduced to ammonium before synthesis into biomass occurs (Parsons et al. 1984). Trace concentrations of ammonium inhibit nitrate reduction so that, in the presence of ammonium and nitrate, ammonium is utilized first. The "preference" of algae for ammonium can be expressed empirically (Thomann and Fitzpatrick 1982):

$$PNx = NH_4 \frac{NO_3}{(KHnx + NH_4)(KHnx + NO_3)} + NH_4 \frac{KHnx}{(NH_4 + NO_3)(KHnx + NO_3)} \quad (4\text{-}25)$$

PNx = algal preference for ammonium uptake ($0 \leq PNx \leq 1$)

The ammonium preference function (Figure 4-6) has two limiting values. When nitrate is absent, the preference for ammonium is unity. When ammonium is absent, the preference is zero. In the presence of ammonium and nitrate, the preference depends on the abundance of both forms relative to the half-saturation constant for nitrogen uptake. When both ammonium and nitrate are abundant, the preference for ammonium approaches unity. When ammonium is scarce but nitrate is abundant, the preference decreases in magnitude and a significant fraction of algal nitrogen requirement comes from nitrate.

The fate of algal nitrogen released by metabolism and predation is represented by distribution coefficients. The effects of algae on the nitrogen state variables are expressed:

$$\frac{\delta}{\delta t} NH_4 = (BMx\, FNIx + PRx\, FNIP - PNx\, Px)\, ANCx\, Bx \quad (4\text{-}26)$$

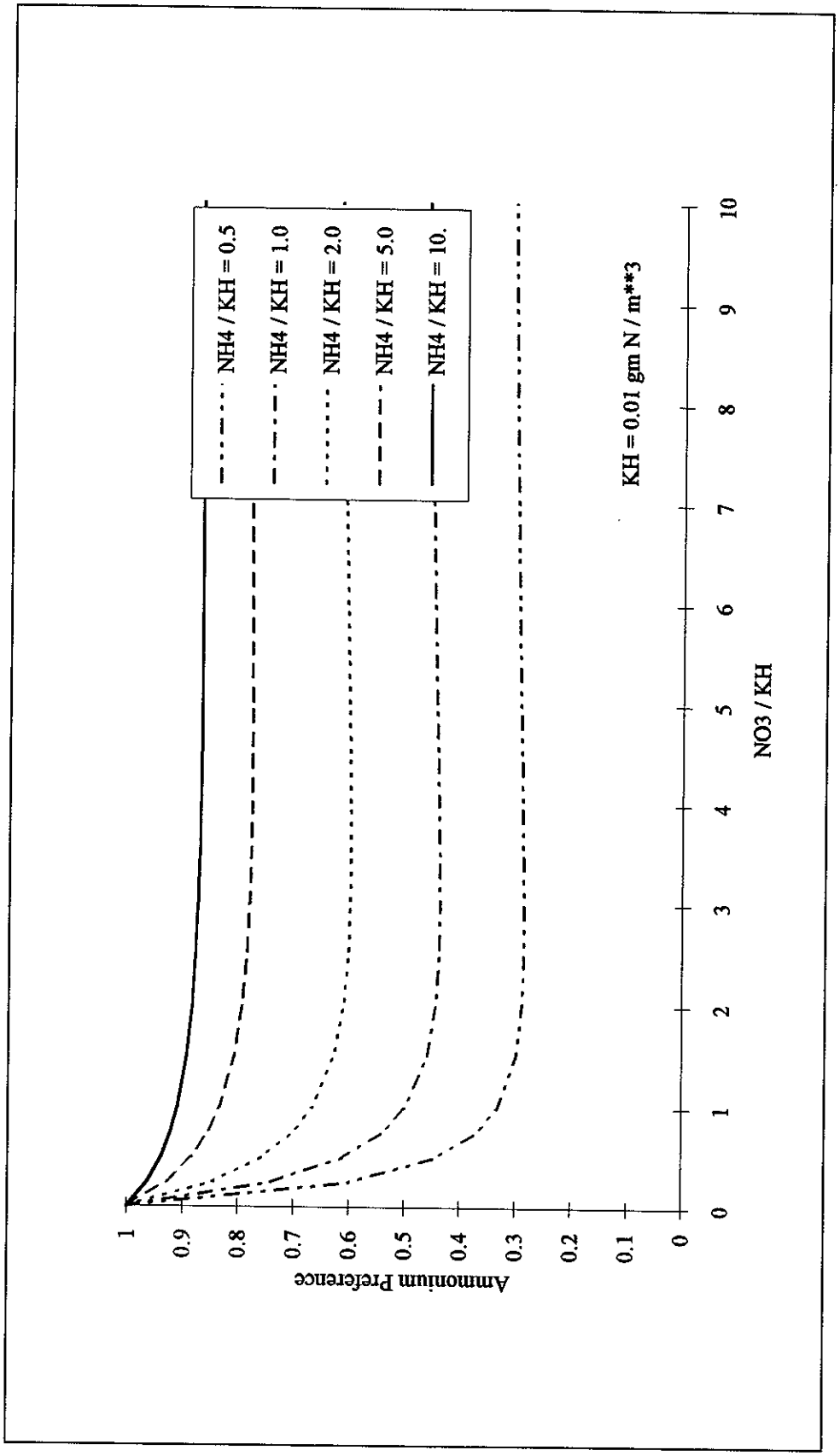

Figure 4-6. Ammonium preference function

$$\frac{\delta}{\delta t} NO_3 = (PNx - 1)\, Px\, ANCx\, Bx \qquad (4\text{-}27)$$

$$\frac{\delta}{\delta t} DON = (BMx\, FNDx + PRx\, FNDP)\, ANCx\, Bx \qquad (4\text{-}28)$$

$$\frac{\delta}{\delta t} LPON = (BMx\, FNLx + PRx\, FNLP)\, ANCx\, Bx \qquad (4\text{-}29)$$

$$\frac{\delta}{\delta t} RPON = (BMx\, FNRx + PRx\, FNRP)\, ANCx\, Bx \qquad (4\text{-}30)$$

DON = dissolved organic nitrogen concentration (gm N m^{-3})
LPON = labile particulate organic nitrogen concentration (gm N m^{-3})
RPON = refractory particulate organic nitrogen concentration (gm N m^{-3})
ANCx = nitrogen-to-carbon ratio of algae (gm N gm^{-1} C)
FNIx = fraction of inorganic nitrogen produced by metabolism
FNDx = fraction of dissolved organic nitrogen produced by metabolism
FNLx = fraction of labile particulate nitrogen produced by metabolism
FNRx = fraction of refractory particulate nitrogen produced by metabolism
FNIP = fraction of inorganic nitrogen produced by predation
FNDP = fraction of dissolved organic nitrogen produced by predation
FNLP = fraction of labile particulate nitrogen produced by predation
FNRP = fraction of refractory particulate nitrogen produced by predation

The sums of the metabolism fractions and the predation fractions must each equal unity.

Algal Stoichiometry

Algal biomass is quantified in units of carbon. In order to express the effects of algae on nitrogen and phosphorus, the ratios of nitrogen-to-carbon and phosphorus-to-carbon in algal biomass must be specified. Global mean values of these ratios are well known (Redfield et al. 1966). Algal composition varies, however, especially as a function of nutrient availability. As nitrogen and phosphorus become scarce, algae adjust their composition so that smaller quantities of these vital nutrients are required to produce carbonaceous biomass (Droop 1973; DiToro 1980; Parsons et al. 1984).

Observations from upper Chesapeake Bay were examined to assess the potential variability of algal stoichiometry. Data employed were collected by the Maryland Department of the Environment from June 1985 to December 1987. This subset of the monitoring data base was selected since it contained direct laboratory analysis of particulate nutrients. Examination was restricted to surface ($\leq$2m) data to maximize the fraction of algae in the particulate analyses. The ratio of particulate carbon-to-nitrogen was plotted as a function of ammonium plus nitrate concentration (Figure 4-7). The ratio of particulate carbon-to-phosphorus was plotted as a function of dissolved phosphate concentration (Figure 4-8). (These ratios were plotted to correspond to conventional reporting of algal composition. Their inverses are used in the model.) The variation of carbon-to-nitrogen stoichiometry in the upper Bay was small. No altered composition as a function of diminished nutrient availability was evident. As a consequence of these observations, the model formulation specified constant algal nitrogen-to-carbon ratio, ANCx. Large variations in carbon-to-phosphorus ratio occurred, however. The carbon-to-phosphorus ratio in seston more than doubled as dissolved phosphate concentration diminished. To account for this effect, a variable algal phosphorus-to-carbon ratio, APC, was specified in the model. The ratio was described by an empirical approximation to the trend apparent in Figure 4-8:

$$APC = \frac{1}{PCprm1 + PCprm2\, e^{-PCprm3\, PO_4d}} \qquad (4\text{-}31)$$

PCprm1 = minimum carbon-to-phosphorus ratio (gm C gm^{-1} P)
PCprm2 = difference between minimum and maximum carbon-to-phosphorus ratio (gm C gm^{-1} P)
PCprm3 = effect of dissolved phosphate concentration on carbon-to-phosphorus ratio (m^3 gm^{-1} P)

Effect of Algae on Dissolved Oxygen

Algae produce oxygen during photosynthesis and consume oxygen through respiration. The quantity produced depends on the form of nitrogen utilized for growth. More oxygen is produced, per unit of carbon fixed, when nitrate is the algal nitrogen source than when ammonium is the source. Equations describing algal uptake of carbon and nitrogen and production of dissolved oxygen (Morel 1983) are:

$$106\, CO_2 + 16\, NH_4^+ + H_2PO_4^- + 106\, H_2O \longrightarrow \qquad (4\text{-}32)$$

$$\text{protoplasm} + 106\, O_2 + 15\, H^+$$

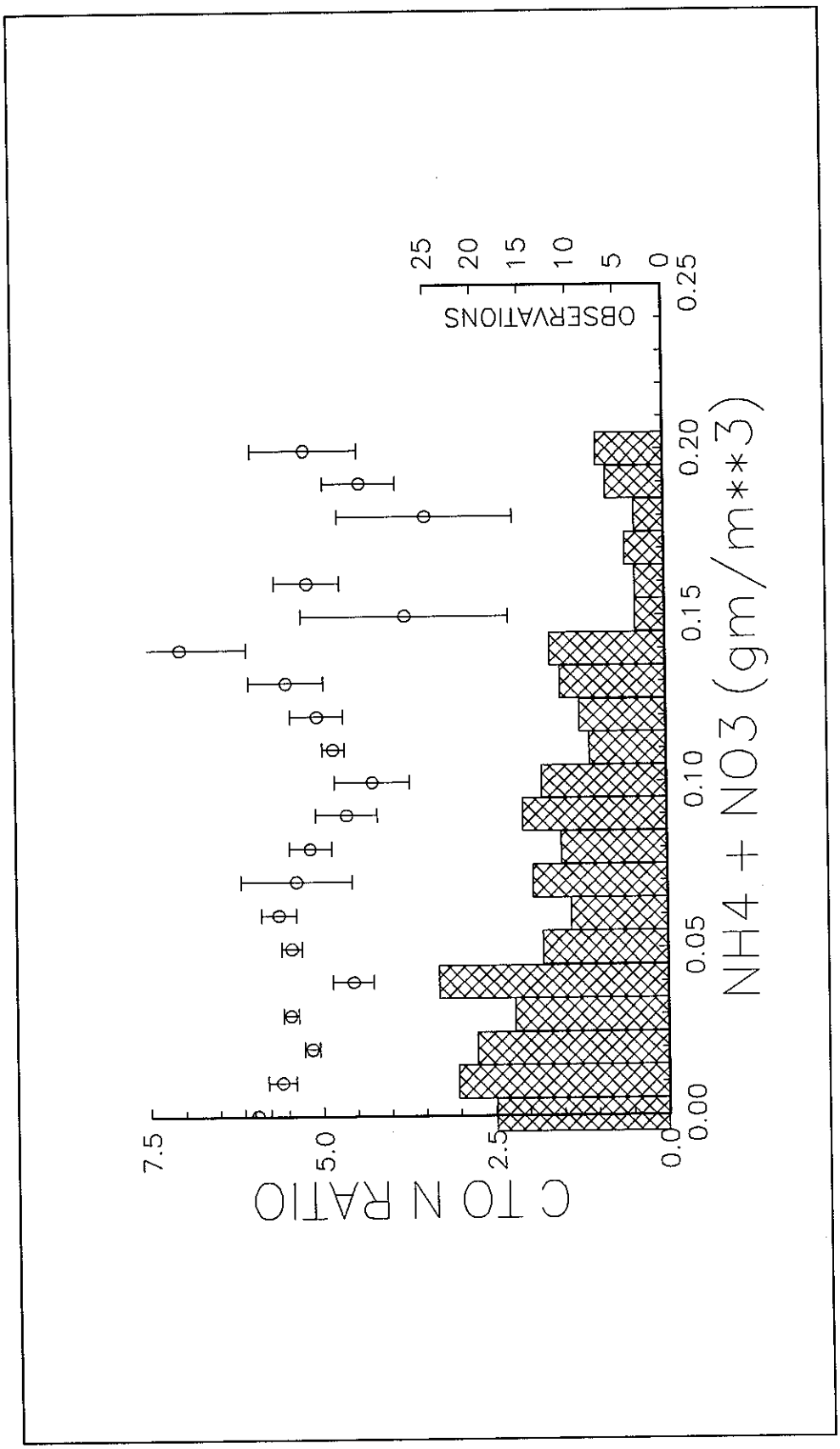

Figure 4-7. Carbon-to-nitrogen ratio of seston in upper Chesapeake Bay. Total inorganic nitrogen observations are grouped in intervals of 0.01 gm m^{-3}. Mean and standard error or carbon-to-nitrogen ratio are shown for each group. Bars show number of observations in each group

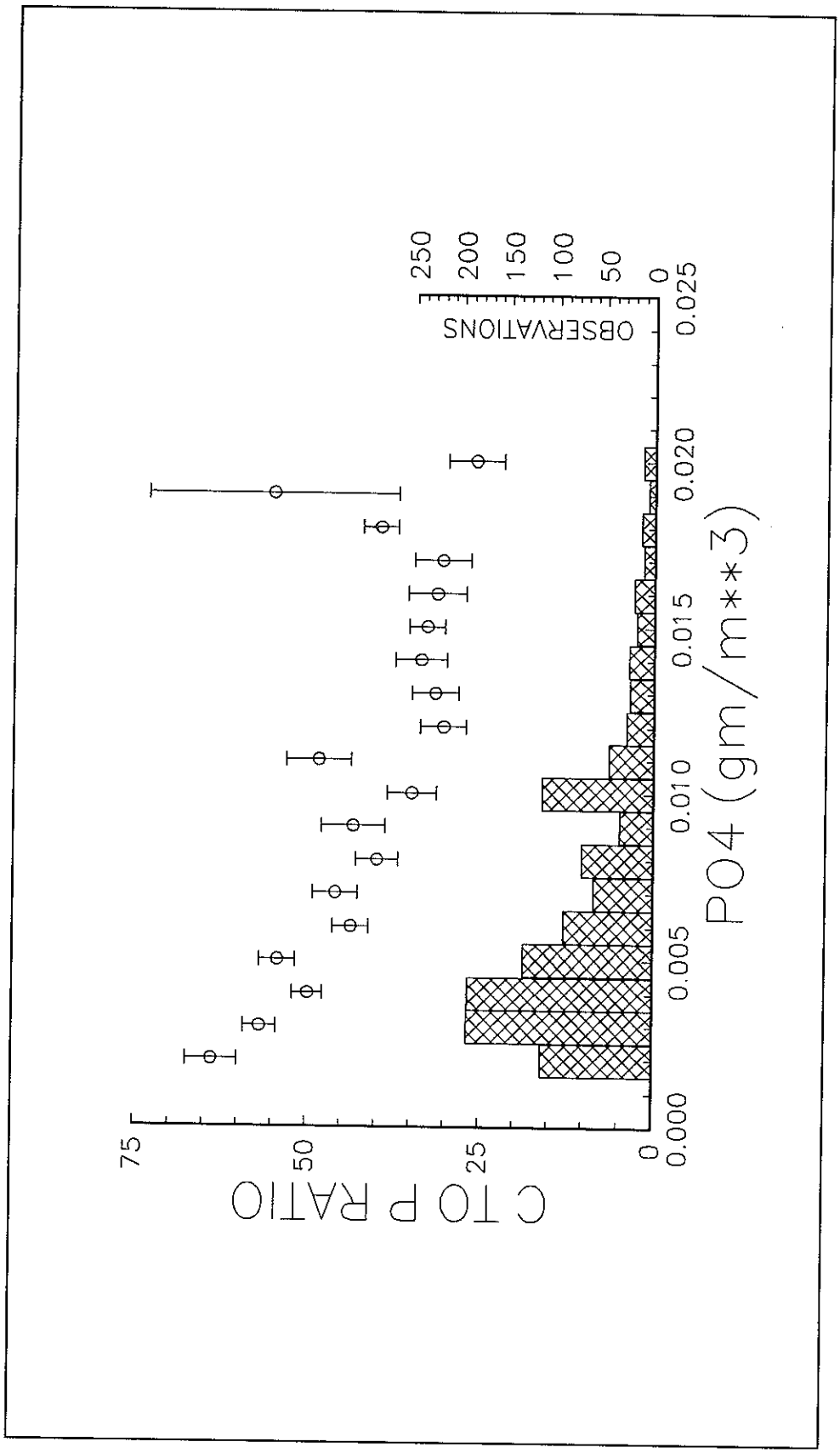

Figure 4-8. Carbon-to-phosphorus ratio of seston in upper Chesapeake Bay. Dissolved phosphate observations are grouped in intervals of 0.001 gm m^{-3}. Mean and standard error or carbon-to-phosphorus ratio are shown for each group. Bars show number of observations in each group

$$106\,CO_2 + 16\,NO_3^- + H_2PO_4^- + 122\,H_2O + 17\,H^+ \rightarrow \text{protoplasm} + 138\,O_2 \quad (4\text{-}33)$$

When ammonium is the nitrogen source, one mole oxygen is produced per mole carbon dioxide fixed. When nitrate is the nitrogen source, 1.3 moles oxygen are produced per mole carbon dioxide fixed.

The equation that describes the effect of algae on dissolved oxygen in the model is:

$$\frac{\delta}{\delta t} DO = \left((1.3 - 0.3\,PNx)\,Px - (1 - FCDx)\,\frac{DO}{KHrx + DO}\,BMx \right) AOCR\,Bx \quad (4\text{-}34)$$

AOCR = dissolved oxygen-to-carbon ratio in respiration (2.67 gm O_2 gm^{-1} C)

The magnitude of AOCR is derived from a simple representation of the respiration process:

$$CH_2O + O_2 = CO_2 + H_2O \quad (4\text{-}35)$$

The quantity (1.3 - 0.3 PNx) is the photosynthesis ratio and expresses the molar quantity of oxygen produced per mole carbon fixed. The photosynthesis ratio approaches unity as the algal preference for ammonium approaches unity.

Organic Carbon

Organic carbon undergoes innumerable transformations in the water column. The model carbon cycle (Figure 4-9) consists of the following elements:

Phytoplankton production
Phytoplankton exudation
Predation on phytoplankton
Dissolution of particulate carbon
Heterotrophic respiration
Denitrification
Settling

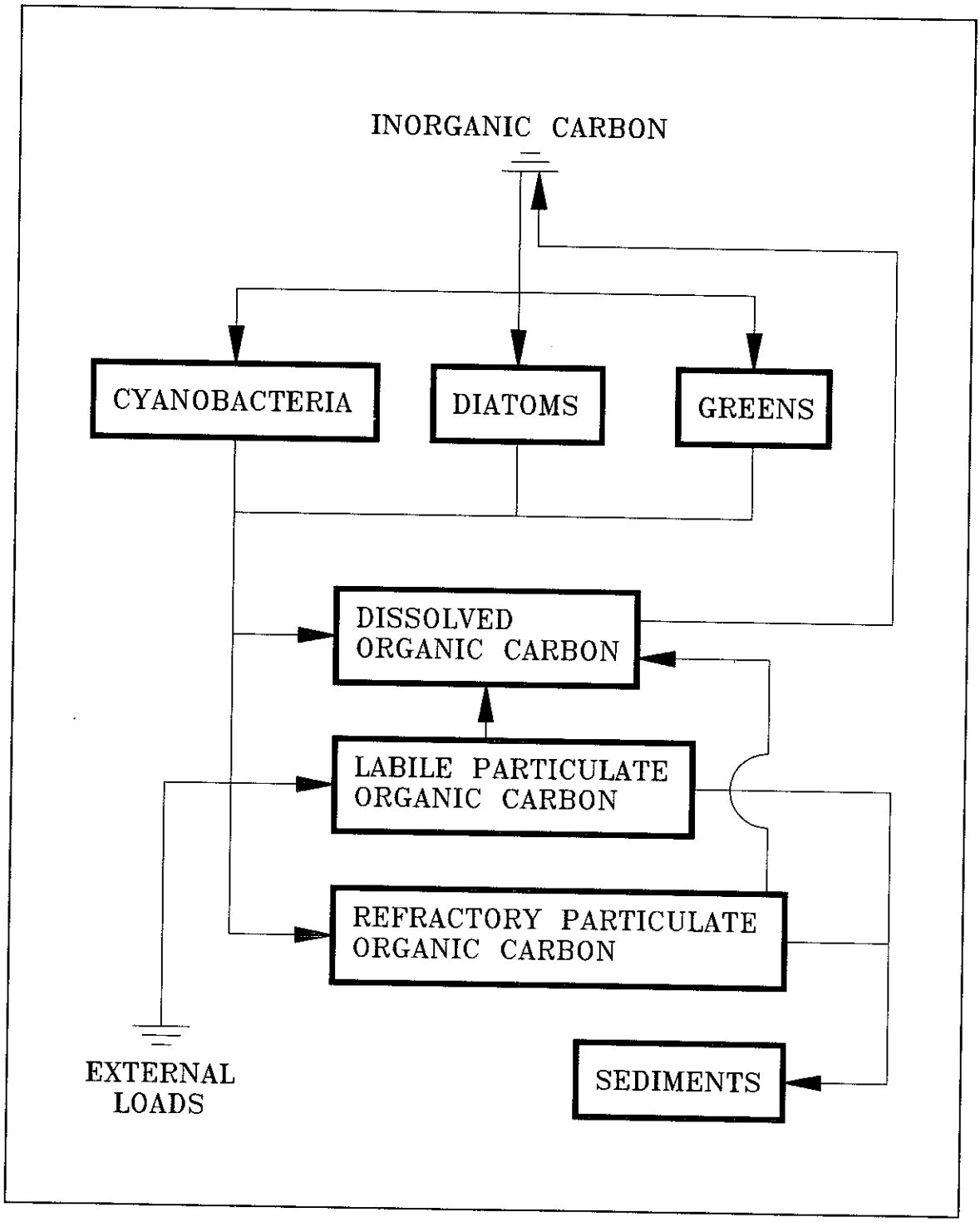

Figure 4-9. The model carbon cycle

Algal production is the primary carbon source although carbon also enters the system through external loading. Predation on algae releases particulate and dissolved organic carbon to the water column. A fraction of the particulate organic carbon undergoes first-order dissolution to dissolved organic

carbon. The remainder settles to the sediments. Dissolved organic carbon produced by phytoplankton exudation, by predation, and by dissolution is respired or denitrified at a first-order rate to inorganic carbon. No carbon is recycled from the sediments to the water column although oxygen demand created by carbon diagenesis is included in the model.

Dissolution and Respiration Rates

Dissolution and respiration rates depend on the availability of carbonaceous substrate and on heterotrophic activity. Heterotrophic activity and biomass have been correlated with algal activity and biomass across a wide range of natural systems (Bird and Kalff 1984; Cole et al. 1988). Consequently, algal biomass can be incorporated into dissolution and respiration rate formulations as a surrogate for heterotrophic activity. The correlation between algae and heterotrophs occurs because algae produce labile carbon that fuels heterotrophic activity. Dissolution and respiration processes do not require the presence of algae, however, and may be fueled entirely by external carbon inputs. Representation of dissolution and respiration in the model allows specification of algal-dependent and algal-independent rates:

$$Kdoc = Kdc + Kdcalg \sum_{x=c,d,g} Bx \qquad (4\text{-}36)$$

Kdoc = respiration rate of dissolved organic carbon (day^{-1})
Kdc = minimum respiration rate (day^{-1})
Kdcalg = constant that relates respiration to algal biomass ($m^3\ gm^{-1}\ C\ day^{-1}$)

$$Klpoc = Klc + Klcalg \sum_{x=c,d,g} Bx \qquad (4\text{-}37)$$

Klpoc = dissolution rate of labile particulate organic carbon (day^{-1})
Klc = minimum dissolution rate (day^{-1})
Klcalg = constant that relates dissolution to algal biomass ($m^3\ gm^{-1}\ C\ day^{-1}$)

$$Krpoc = Krc + Krcalg \sum_{x=c,d,g} Bx \qquad (4\text{-}38)$$

Krpoc = dissolution rate of refractory particulate organic carbon (day^{-1})
Krc = minimum dissolution rate (day^{-1})
Krcalg = constant that relates dissolution to algal biomass ($m^3\ gm^{-1}\ C\ day^{-1}$)

An exponential function (Figure 4-5) relates dissolution and respiration to temperature.

Denitrification

As oxygen is depleted from natural systems, oxidation of organic matter is effected by the reduction of alternate oxidants (referred to as "alternate electron acceptors"). The sequence in which alternate acceptors are employed is determined by the thermodynamics of oxidation-reduction reactions. The first substance reduced in the absence of oxygen is nitrate. A representation of the denitrification reaction can be obtained by balancing standard half-cell redox reactions (Stumm and Morgan 1981):

$$4\,NO_3^- + 4\,H^+ + 5\,CH_2O \rightarrow 2\,N_2 + 7\,H_2O + 5\,CO_2 \qquad (4\text{-}39)$$

Equation 4-39 describes the stoichiometry of the denitrification reaction. The kinetics of the reaction, represented in the model, are first-order. The dissolved organic carbon respiration rate, Kdoc, is modified so that significant decay via denitrification occurs only when nitrate is freely available and dissolved oxygen is depleted (Figure 4-10). A parameter is included so that the anoxic respiration rate is slower than oxic respiration:

$$Denit = \frac{KHodoc}{KHodoc + DO}\,\frac{NO_3}{KHndn + NO_3}\,AANOX\,Kdoc \qquad (4\text{-}40)$$

Denit = denitrification rate of dissolved organic carbon (day^{-1})
AANOX = ratio of denitrification to oxic carbon respiration rate ($0 \leq AANOX \leq 1$)
KHodoc = half-saturation concentration of dissolved oxygen required for oxic respiration (gm O_2 m^{-3})
KHndn = half-saturation concentration of nitrate required for denitrification (gm N m^{-3})

An exponential function (Figure 4-5) relates denitrification to temperature. Parameter values in the function are the same as for dissolved organic carbon respiration.

Dissolved Organic Carbon

The complete representation of all dissolved organic carbon sources and sinks in the model ecosystem is:

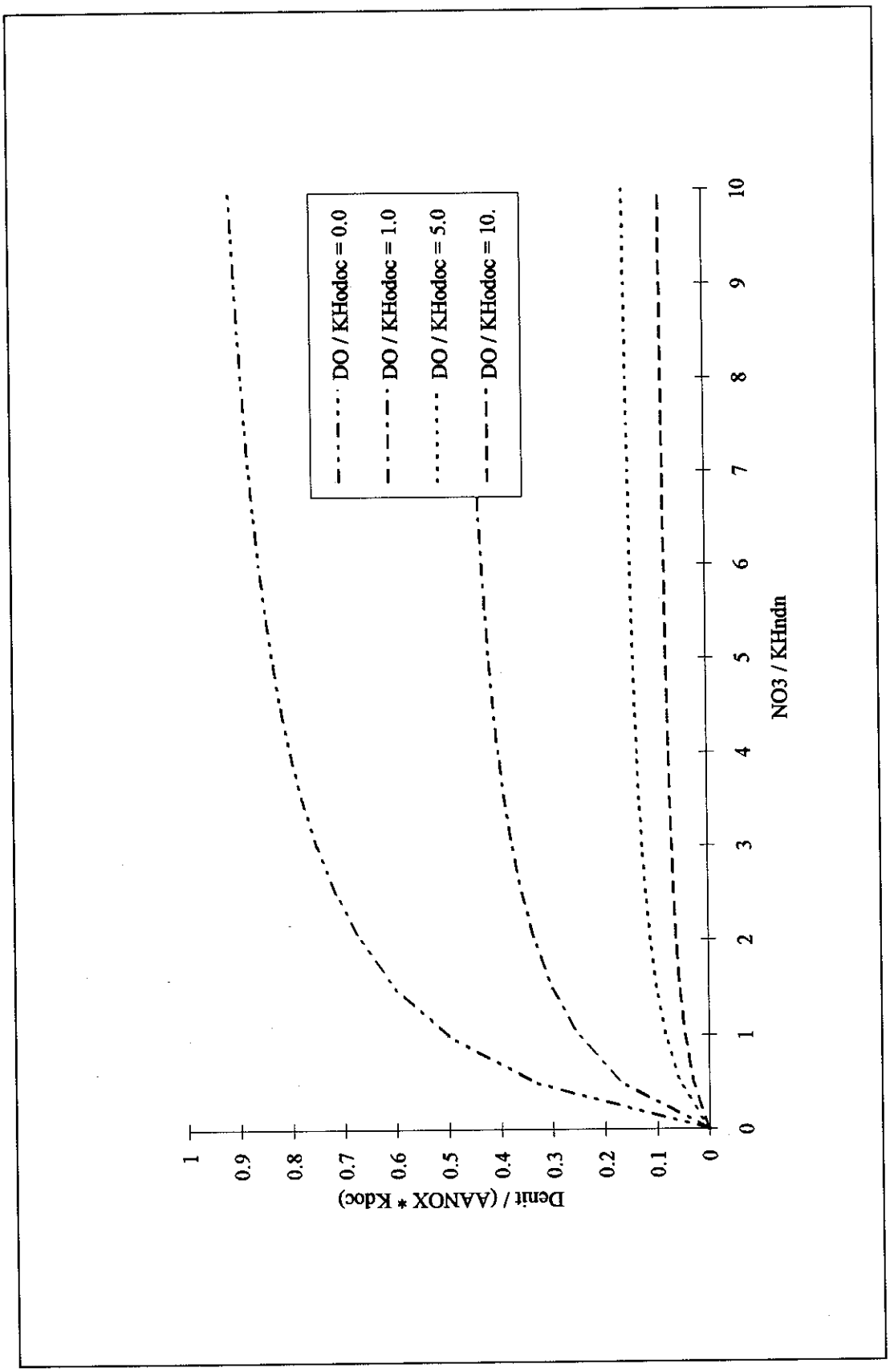

Figure 4-10. Effect of nitrate and dissolved oxygen on denitrification rate

$$\frac{\delta}{\delta t} DOC =$$

$$\sum_{x=c,d,g} \left(\left(FCDx + (1 - FCDx) \frac{KHrx}{KHrx + DO} \right) BMx + FCDP\, PRx \right) Bx \quad (4\text{-}41)$$

$$+ Klpoc\, LPOC + Krpoc\, RPOC - \frac{DO}{KHodoc + DO} Kdoc\, DOC$$

$$- Denit\, DOC$$

Labile Particulate Organic Carbon

The complete representation of all labile particulate organic carbon sources and sinks in the model ecosystem is:

$$\frac{\delta}{\delta t} LPOC =$$

$$\sum_{x=c,d,g} FCLP\, PRx\, Bx - Klpoc\, LPOC - WSl \frac{\delta}{\delta z} LPOC \quad (4\text{-}42)$$

WSl = settling velocity of labile particles (m day^{-1})

Refractory Particulate Organic Carbon

The complete representation of all refractory particulate organic carbon sources and sinks in the model ecosystem is:

$$\frac{\delta}{\delta t} RPOC =$$

$$\sum_{x=c,d,g} FCRP\, PRx\, Bx - Krpoc\, RPOC - WSr \frac{\delta}{\delta z} RPOC \quad (4\text{-}43)$$

WSr = settling velocity of refractory particles (m day^{-1})

Phosphorus

The model phosphorus cycle (Figure 4-11) includes the following processes:

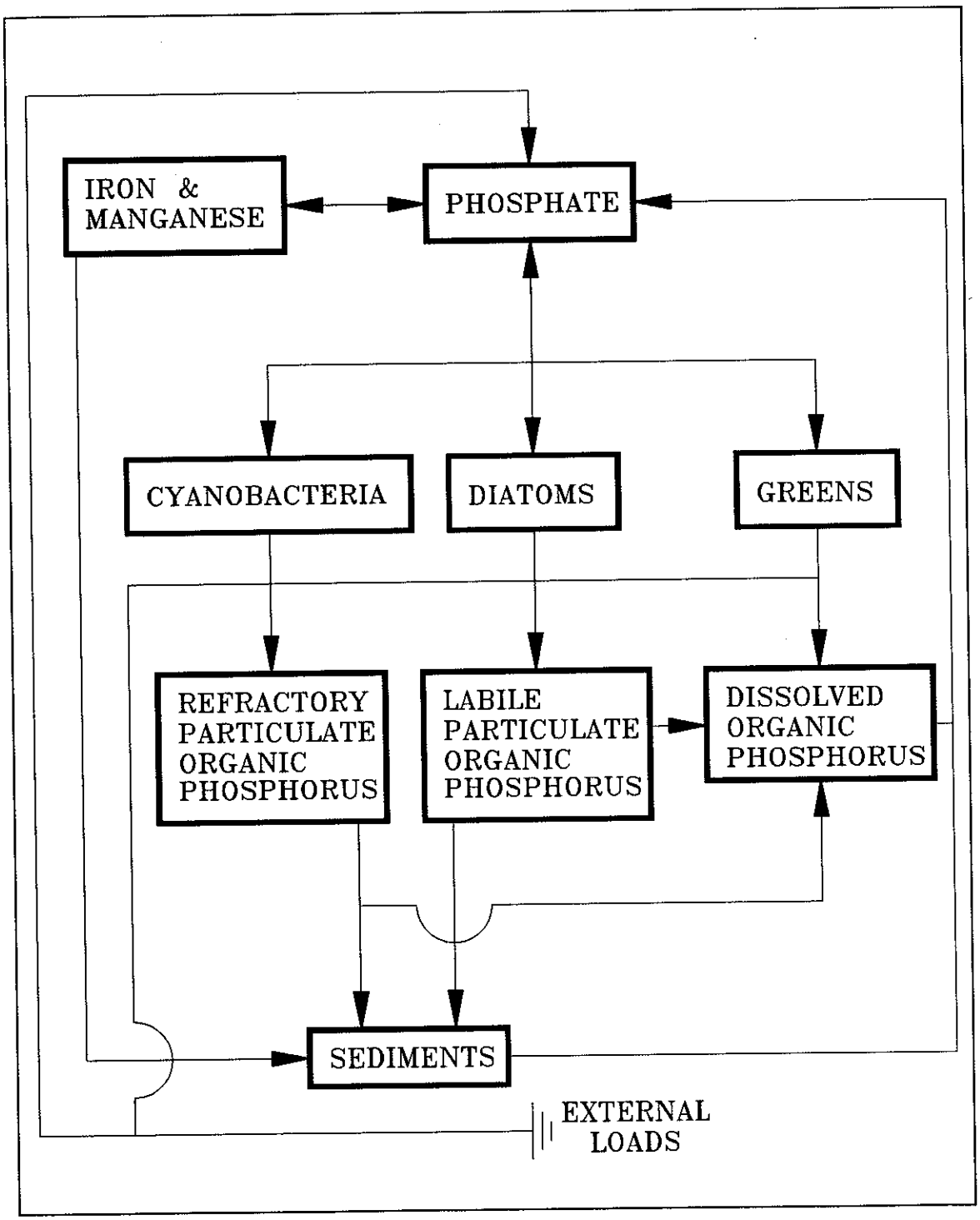

Figure 4-11. The model phosphorus cycle

Algal production and metabolism
Predation
Hydrolysis of particulate organic phosphorus
Mineralization of dissolved organic phosphorus
Settling
Exchange with inorganic solids

External loads provide the ultimate source of phosphorus to the system. Dissolved phosphate is incorporated by algae during growth and released as phosphate and organic phosphorus through respiration and predation. A portion of the particulate organic phosphorus hydrolyzes to dissolved organic phosphorus. The balance settles to the sediments. Dissolved organic phosphorus is mineralized to phosphate. A portion of the phosphate sorbs to inorganic solids and settles to the sediments. Within the sediments, particulate phosphorus is mineralized and recycled to the water column as dissolved phosphate.

Effects on phosphorus of algal production, metabolism, and predation have already been detailed. Descriptions of hydrolysis and mineralization and of the total phosphate system follow.

Hydrolysis and Mineralization

Within the model, hydrolysis is defined as the process by which particulate organic substances are converted to dissolved organic form. Mineralization is defined as the process by which dissolved organic substances are converted to dissolved inorganic form. Conversion of particulate organic phosphorus to phosphate proceeds through the sequence of hydrolysis and mineralization. Direct mineralization of particulate organic phosphorus does not occur.

Mineralization of organic phosphorus is mediated by the release of nucleotidase and phosphatase enzymes by bacteria (Ammerman and Azam 1985; Chrost and Overbeck 1987) and algae (Matavulj and Flint 1987; Chrost and Overbeck 1987; Boni et al. 1989). Since the algae themselves release the enzyme and since bacterial abundance is related to algal biomass, the rate of organic phosphorus mineralization is related, in the model, to algal biomass. A most remarkable property of the enzyme process is that alkaline phosphatase activity is inversely proportional to ambient phosphate concentration (Chrost and Overbeck 1987; Boni et al. 1989). Put in different terms, when phosphate is scarce, algae stimulate production of an enzyme that mineralizes organic phosphorus to phosphate. This phenomenon is simulated by relating mineralization to the algal phosphorus nutrient limitation. Mineralization is highest when algae are strongly phosphorus limited and is least when no limitation occurs.

Expressions for mineralization and hydrolysis rates are:

$$Kdop = Kdp + \frac{KHp}{KHp + PO_4d} Kdpalg \sum_{x=c,d,g} Bx \qquad (4\text{-}44)$$

Kdop = mineralization rate of dissolved organic phosphorus (day^{-1})
Kdp = minimum mineralization rate (day^{-1})
KHp = mean half-saturation constant for algal phosphorus uptake ($gm\ P\ m^{-3}$)
= (KHpc + KHpd + KHpg)/3
Kdpalg = constant that relates mineralization to algal biomass ($m^3\ gm^{-1}\ C\ day^{-1}$)

$$Klpop = Klp + \frac{KHp}{KHp + PO_4d} Klpalg \sum_{x=c,d,g} Bx \qquad (4\text{-}45)$$

Klpop = hydrolysis rate of labile particulate phosphorus (day^{-1})
Klp = minimum hydrolysis rate (day^{-1})
Klpalg = constant that relates hydrolysis to algal biomass ($m^3\ gm^{-1}\ C\ day^{-1}$)

$$Krpop = Krp + \frac{KHp}{KHp + PO_4d} Krpalg \sum_{x=c,d,g} Bx \qquad (4\text{-}46)$$

Krpop = hydrolysis rate of refractory particulate phosphorus (day^{-1})
Krp = minimum hydrolysis rate (day^{-1})
Krpalg = constant that relates hydrolysis to algal biomass ($m^3\ gm^{-1}\ C\ day^{-1}$)

An exponential function (Figure 4-5) relates mineralization and hydrolysis rates to temperature.

Potential effects of algal biomass and nutrient limitation on mineralization and hydrolysis rates shown in Figure 4-12. When nutrient concentration greatly exceeds the half-saturation concentration for algal uptake, the rate roughly equals the minimum. Algal biomass has little influence. As nutrient becomes scarce relative to the half-saturation concentration, the rate increases. The magnitude of increase depends on algal biomass. Factor of two to three increases are feasible.

The Total Phosphate System

One fraction of total phosphorus in the water column is phosphorus incorporated in algal biomass. This fraction is computed in the model as the product of algal biomass and APC, the phosphorus-to-carbon ratio. In the environment, algae adjust their phosphorus content in response to external

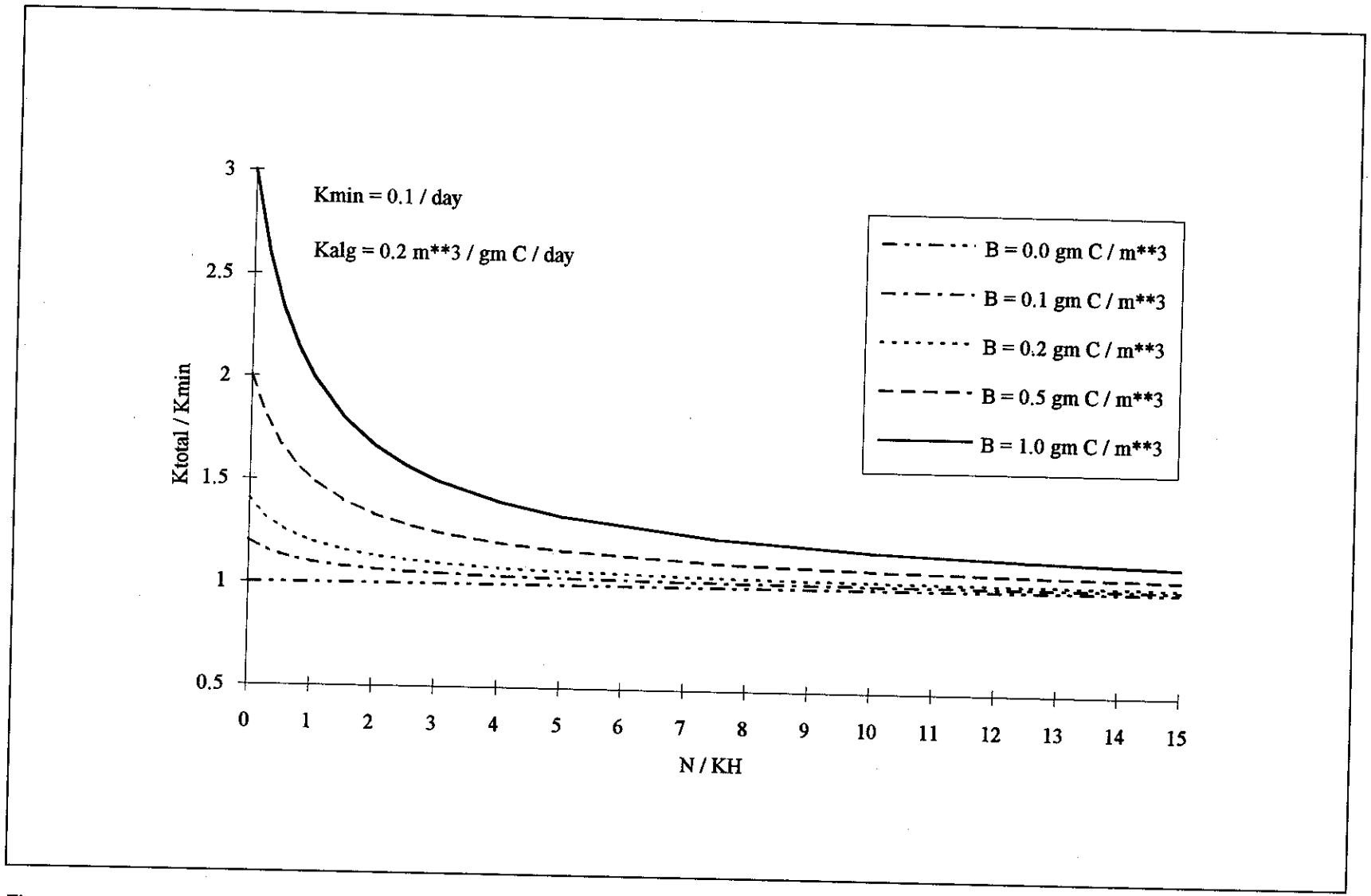

Figure 4-12. Effect of algal biomass and nutrient concentration on hydrolysis and mineralization

conditions. Algal phosphorus content is high when external phosphorus is abundant and phosphorus content is low when phosphorus is scarce. The adaptation of algae to their environment indicates phosphorus-to-carbon ratio should be a variable in the model. Treatment of the ratio as a variable, however, greatly complicates computation of phosphorus transport due to the mixture of algal masses of different composition. The complication is avoided if intracellular and extracellular phosphorus are treated and transported as a single state variable. Intracellular and extracellular concentrations are determined by equilibrium partitioning of their sum.

Adsorption is the process in which ions or molecules are attracted to the surface of a solid. Phosphate ions exhibit a strong adsorption to particulate species of metals including iron and manganese. Sorption to metals is included in the model based on phenomenon observed in the monitoring data (Figure 4-13). Phosphate was rapidly depleted from anoxic bottom waters during the autumn reaeration event. Our hypothesis was that reaeration of bottom waters caused dissolved iron and manganese to precipitate. Phosphate sorbed to the newly-formed metal particles and rapidly settled to the bottom. Computation of transport of sorbed and dissolved fractions is facilitated when the model state variable represents the sum of both fractions. Particulate and dissolved fractions are determined by equilibrium partitioning of their sum.

The model phosphate state variable is defined as the sum of dissolved phosphate, sorbed phosphate, and algal phosphorus content:

$$PO_4t = PO_4d + PO_4p + PO_4a \qquad (4\text{-}47)$$

PO_4t = total phosphate (gm P m^{-3})
PO_4d = dissolved phosphate (gm P m^{-3})
PO_4p = particulate (sorbed) phosphate (gm P m^{-3})
PO_4a = algal phosphorus (gm P m^{-3})

Exchange With Particulate Metals

Detailed treatment of iron and manganese is beyond the scope of this model. Instead, the state variable "total active metal" is defined as the sum of all metals that act as sorption sites. Phosphate sorbs to only the particulate fraction of the total metal, however. Therefore the total metal is partitioned into particulate and dissolved fractions via an equilibrium partition coefficient. Extracellular phosphate is partitioned by a linear sorption isotherm so that dissolved and particulate fractions are computed:

$$PO_4d = \frac{1}{1 + \text{Kadpo4 TAMp}} (PO_4t - PO_4a) \qquad (4\text{-}48)$$

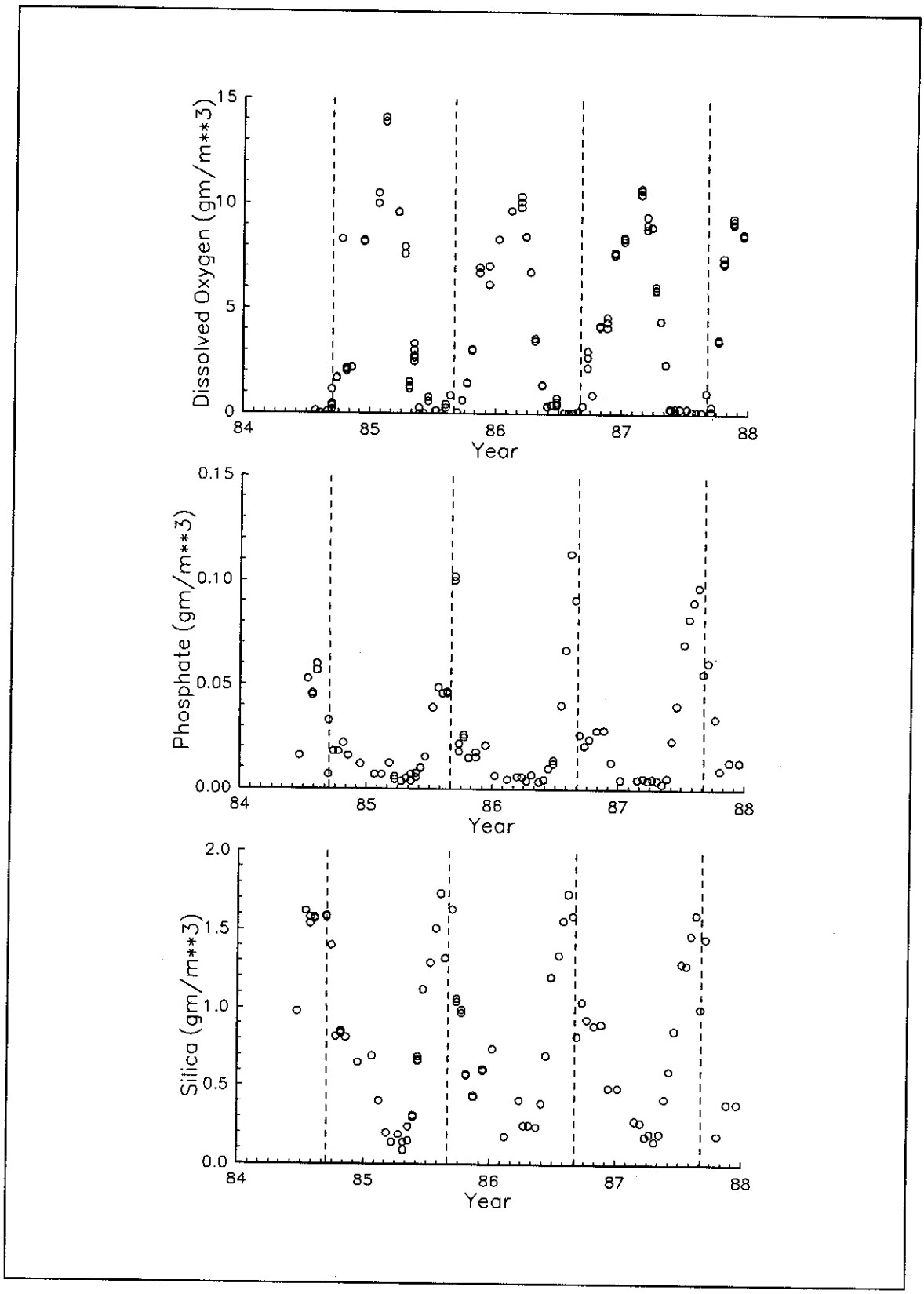

Figure 4-13. Dissolved oxygen, dissolved phosphate, and dissolved silica at Chesapeake Bay station CB3.3C. Data collected one meter from bottom

$$PO_4p = \frac{Kadpo4\ TAMp}{1 + Kadpo4\ TAMp} (PO_4t - PO_4a) \qquad (4\text{-}49)$$

Kadpo4 = partition coefficient of sorbed vs. dissolved phosphate ($m^3\ mol^{-1}$)
TAMp = particulate total active metal ($mol\ m^{-3}$)

Computation of Algal Phosphorus

Algal phosphorus is defined:

$$PO_4a = APC \sum_{x=c,d,g} Bx \qquad (4\text{-}50)$$

The phosphorus-to-carbon ratio is calculated by the empirical function expressed in Equation 4-31.

The equations 4-31, 4-48, 4-49, 4-50, form an implicit system. The implicit nature of the system can be seen by substituting the expressions for dissolved phosphate (Equation 4-48) and algal phosphate (Equation 4-50) into the expression for phosphorus-to-carbon ratio (Equation 4-31). For notational simplicity, assume negligible TAMp. Then:

$$APC = \frac{1}{PCprm1 + PCprm2\, e^{-PCprm3\,(PO_4t - APC \sum Bx)}} \qquad (4\text{-}51)$$

The phosphorus-to-carbon ratio appears on both sides of the equation and cannot be obtained explicitly. Within the model code, phosphorus-to-carbon ratio is obtained by iterative solution of Equation 4-51 in each control volume at each time step. Following computation of phosphorus-to-carbon ratio, algal phosphorus is computed (Equation 4-50). Next, extra-cellular phosphate is partitioned into dissolved and particulate fractions (Eqs. 4-48 and 4-49).

Effect of Variable Phosphorus Stoichiometry

The effect of the variable phosphorus-to-carbon ratio and the operation of the total phosphate system is best seen by an example. The model was applied to a chemostat supplied with unlimited inorganic nitrogen. Phosphorus recycling was eliminated in the water and sediments so that only the initial phosphate was available to the algae. The chemostat was simulated for thirty days. Midway through the simulation, a phosphate load, equivalent to the initial

mass in the chemostat, was injected. Simulations were conducted with and without variable stoichiometry.

Algal production was initially identical with and without variable stoichiometry (Figure 4-14). As dissolved phosphate became scarce in the constant-stoichiometry chemostat, algal production diminished so that respiration exceeded growth prior to day five. Biomass decreased until the phosphate injection at day fifteen. In the variable-stoichiometry chemostat, algae responded to diminished phosphate availability by reducing their phosphorus-to-carbon ratio. Because less phosphorus was required per unit carbonaceous biomass formed, growth exceeded respiration beyond day five and maximum biomass exceeded biomass formed under constant stoichiometry. Upon injection of new phosphate, algal production increased with and without variable stoichiometry. Algae with variable stoichiometry responded with increased phosphorus-to-carbon ratio as well as increased production. As a result of the altered ratio, dissolved phosphate peaked at a lower concentration in the presence of variable stoichiometry. The ability of algae to diminish phosphorus-to-carbon ratio still allowed algae in the variable-stoichiometry chemostat to exceed biomass formed in the constant-stoichiometry chemostat, however.

This example is an analog to our simulation of the spring algal bloom and late autumn flood periods in Chesapeake Bay. We found that variable stoichiometry provided the minimum phosphorus-to-carbon ratio necessary to simulate the spring bloom. As an alternative, we could have specified a constant, extremely low phosphorus-to-carbon ratio. We found, however, that algal phosphorus uptake in autumn and winter was too low when a constant, minimum ratio was employed. Predicted dissolved phosphate exceeded observations during these seasons. In multi-year simulations, the excess phosphate "carried over" into the subsequent spring and confounded simulation of the spring bloom. Variable stoichiometry allowed reasonable simulations of dissolved phosphate over lengthy periods spanning seasons of high and low dissolved phosphate concentrations.

Phosphate

Once the interactions of dissolved, particulate, and algal phosphate are made explicit, the balance of the equations describing phosphorus are straightforward summations of previously-described sources and sinks:

$$\frac{\delta}{\delta t} PO_4t = - \sum_{x=c,d,g} WSx \frac{\delta}{\delta z} APC\,Bx - WSs \frac{\delta}{\delta z} PO_4p + Kdop\,DOP \qquad (4\text{-}52)$$

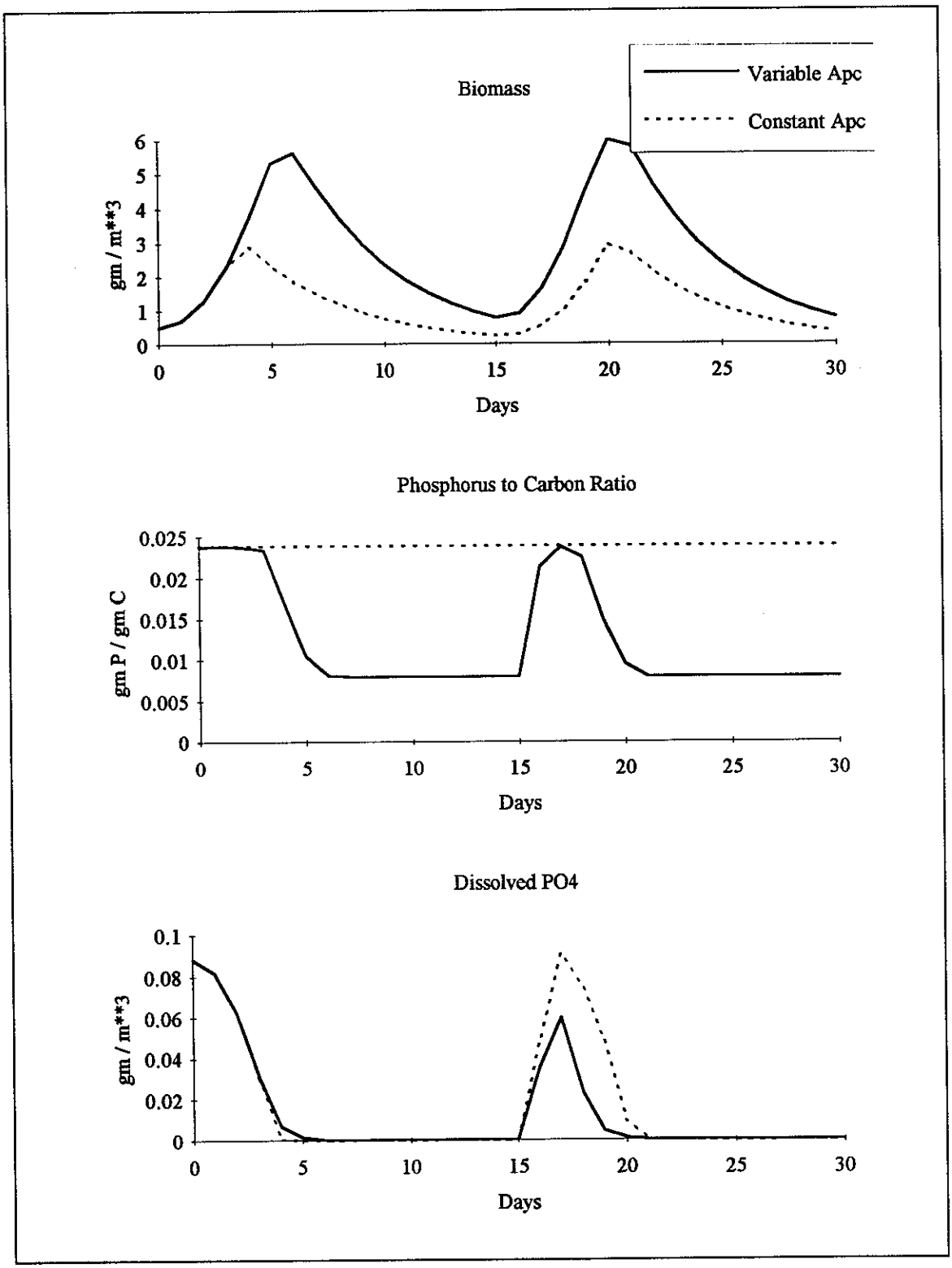

Figure 4-14. Chemostat simulation with and without variable phosphorus stoichiometry

WSs = settling velocity of particulate metal (m day^{-1})

Algal uptake and release of phosphate represents an exchange of phosphate fractions rather than a phosphate source or sink. Consequently, no algal source or sink terms are included in the phosphate mass-conservation equation. The settling terms are required to represent the settling of particulate phosphate incorporated in algal biomass or sorbed to particles.

Dissolved Organic Phosphorus

$$\frac{\delta}{\delta t} DOP = \sum_{x=c,d,g} (BMx\ FPDx + PRx\ FPDP)\ APC\ Bx + Klpop\ LPOP + Krpop\ RPOP - Kdop\ DOP \quad (4\text{-}53)$$

Labile Particulate Organic Phosphorus

$$\frac{\delta}{\delta t} LPOP = \sum_{x=c,d,g} (BMx\ FPLx + PRx\ FPLP)\ APC\ Bx - Klpop\ LPOP - WSl \frac{\delta}{\delta z} LPOP \quad (4\text{-}54)$$

Refractory Particulate Organic Phosphorus

$$\frac{\delta}{\delta t} RPOP = \sum_{x=c,d,g} (BMx\ FPRx + PRx\ FPRP)\ APC\ Bx - Krpop\ RPOP - WSr \frac{\delta}{\delta z} RPOP \quad (4\text{-}55)$$

Nitrogen

The model nitrogen cycle (Figure 4-15) includes the following processes:

Algal production and metabolism
Predation
Hydrolysis of particulate organic nitrogen
Mineralization of dissolved organic nitrogen
Settling

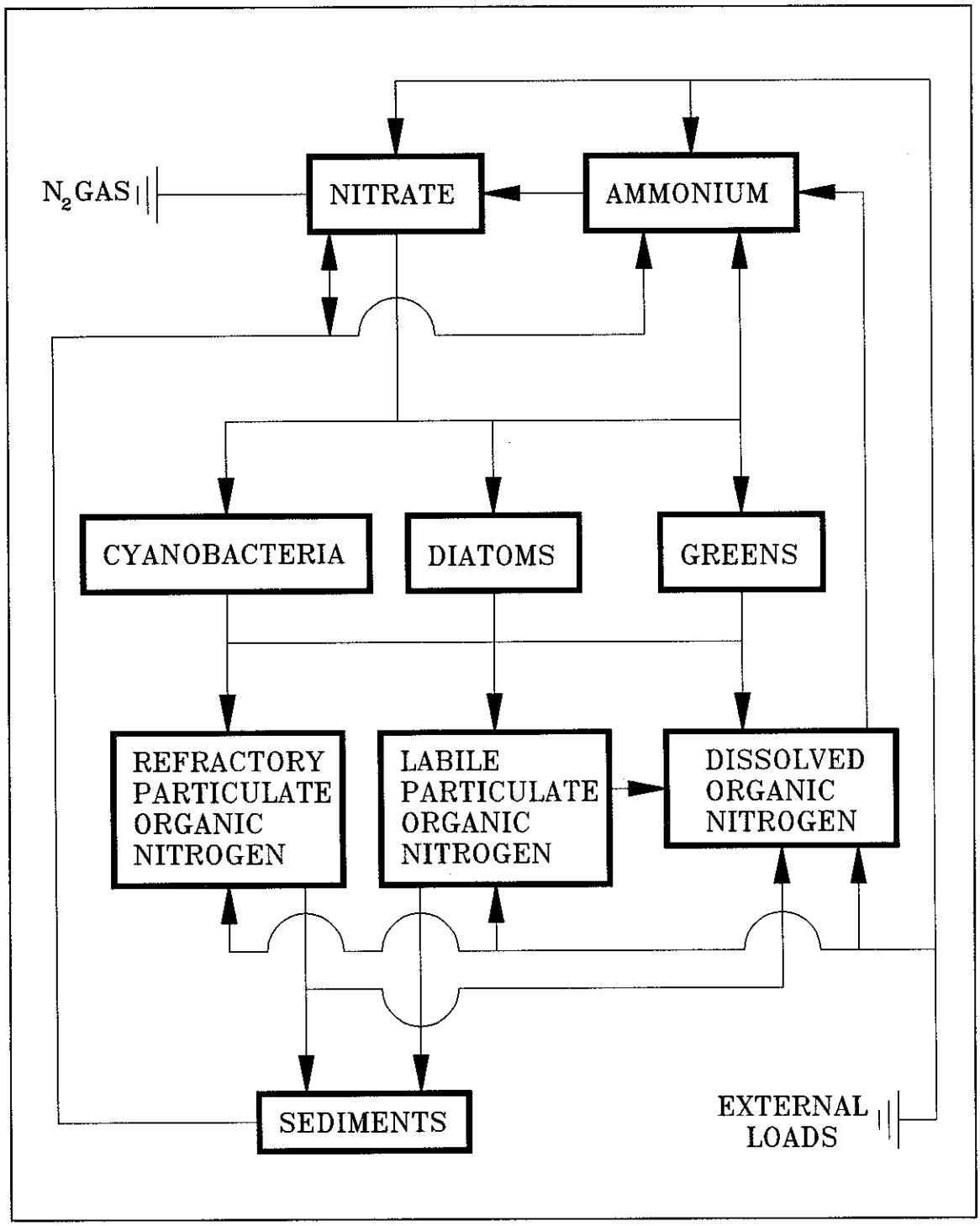

Figure 4-15. The model nitrogen cycle

Nitrification
Denitrification

External loads provide the ultimate source of nitrogen to the system. Inorganic nitrogen is incorporated by algae during growth and released as ammonium and organic nitrogen through respiration and predation. A portion of the particulate organic nitrogen hydrolyzes to dissolved organic nitrogen. The balance settles to the sediments. Dissolved organic nitrogen is mineralized to ammonium. In an oxygenated water column, a fraction of the ammonium is subsequently oxidized to nitrate through the nitrification process. In anoxic water, nitrate is lost to nitrogen gas through denitrification. Particulate nitrogen that settles to the sediments is mineralized and recycled to the water column, primarily as ammonium. Nitrate moves in both directions across the sediment-water interface, depending on relative concentrations in the water column and sediment interstices.

Effects on nitrogen of algal production, metabolism, and predation have already been detailed. Descriptions of hydrolysis, mineralization, nitrification and denitrification follow.

Hydrolysis and Mineralization

In the model, particulate organic nitrogen is converted to the dissolved organic form via hydrolysis. Dissolved organic nitrogen is converted to ammonium through mineralization. Conversion of particulate nitrogen to ammonium proceeds through the sequence of hydrolysis and mineralization. Direct mineralization of particulate nitrogen does not occur. The argument for accelerated hydrolysis and mineralization during nutrient-limited conditions is not as clear for nitrogen as for phosphorus. The same formulations are made available for nitrogen as for phosphorus, however. Accelerated processes can be activated or deactivated through parameter selection. The nitrogen hydrolysis and mineralization formulations are:

$$Kdon = Kdn + \frac{KHn}{KHn + NH_4 + NO_3} Kdnalg \sum_{x=c,d,g} Bx \qquad (4\text{-}56)$$

Kdon = mineralization rate of dissolved organic nitrogen (day^{-1})
Kdn = minimum mineralization rate (day^{-1})
KHn = mean half-saturation constant for algal nitrogen uptake (gm N m^{-3})
= (KHnc + KHnd + KHng)/3
Kdnalg = constant that relates mineralization to algal biomass
(m^3 gm^{-1} C day^{-1})

$$Klpon = Kln + \frac{KHn}{KHn + NH_4 + NO_3} Klnalg \sum_{x=c,d,g} Bx \qquad (4\text{-}57)$$

Klpon = hydrolysis rate of labile particulate nitrogen (day^{-1})
Kln = minimum hydrolysis rate (day^{-1})
Klnalg = constant that relates hydrolysis to algal biomass ($m^3\ gm^{-1}\ C\ day^{-1}$)

$$Krpon = Krn + \frac{KHn}{KHn + NH_4 + NO_3} Krnalg \sum_{x=c,d,g} Bx \qquad (4\text{-}58)$$

Krpon = hydrolysis rate of refractory particulate nitrogen (day^{-1})
Krn = minimum hydrolysis rate (day^{-1})
Krnalg = constant that relates hydrolysis to algal biomass ($m^3\ gm^{-1}\ C\ day^{-1}$)

An exponential function (Figure 4-5) relates mineralization and hydrolysis rates to temperature.

Nitrification

Nitrification is a process mediated by specialized groups of autotrophic bacteria that obtain energy through the oxidation of ammonium to nitrite and oxidation of nitrite to nitrate. A simplified expression for complete nitrification (Tchobanoglous and Schroeder 1987) is:

$$NH_4^+ + 2\,O_2 \longrightarrow NO_3^- + H_2O + 2\,H^+ \qquad (4\text{-}59)$$

The equation indicates that two moles of oxygen are required to nitrify one mole of ammonium into nitrate. The simplified equation is not strictly true, however. Cell synthesis by nitrifying bacteria is accomplished by the fixation of carbon dioxide so that less than two moles of oxygen are consumed per mole ammonium utilized (Wezernak and Gannon 1968).

The kinetics of complete nitrification are modelled as a function of available ammonium, dissolved oxygen, and temperature:

$$NT = \frac{DO}{KHont + DO} \frac{NH_4}{KHnnt + NH_4} f(T)\, NTm \qquad (4\text{-}60)$$

NT = nitrification rate (gm N m^{-3} day^{-1})
KHont = half-saturation constant of dissolved oxygen required for nitrification (gm O_2 m^{-3})
KHnnt = half-saturation constant of NH_4 required for nitrification (gm N m^{-3})
NTm = maximum nitrification rate at optimal temperature (gm N m^{-3} day^{-1})

The kinetics formulation (Figure 4-16) incorporates the products of two "Monod" functions. The first function diminishes nitrification at low dissolved oxygen concentration. The second function expresses the influence of ammonium concentration on nitrification. When ammonium concentration is low, relative to KHnnt, nitrification is proportional to ammonium concentration. For NH4 << KHnnt, the reaction is approximately first-order. (The first-order decay constant ≈ NTm/KHnnt.) When ammonium concentration is large, relative to KHnnt, nitrification approaches a maximum rate. This formulation is based on a concept proposed by Tuffey et al. (1974). Nitrifying bacteria adhere to benthic or suspended sediments. When ammonium is scarce, vacant surfaces suitable for nitrifying bacteria exist. As ammonium concentration increases, bacterial biomass increases, vacant surfaces are occupied, and the rate of nitrification increases. The bacterial population attains maximum density when all surfaces suitable for bacteria are occupied. At this point, nitrification proceeds at a maximum rate independent of additional increase in ammonium concentration.

The optimal temperature for nitrification may be less than peak temperatures that occur in coastal waters. To allow for a decrease in nitrification at superoptimal temperature, the effect of temperature on nitrification is modelled in the Gaussian form of Equation 4-14.

Effect of Nitrification on Ammonium

$$\frac{\delta}{\delta t} NH_4 = - NT \qquad (4\text{-}61)$$

Effect of Nitrification on Nitrate

$$\frac{\delta}{\delta t} NO_3 = NT \qquad (4\text{-}62)$$

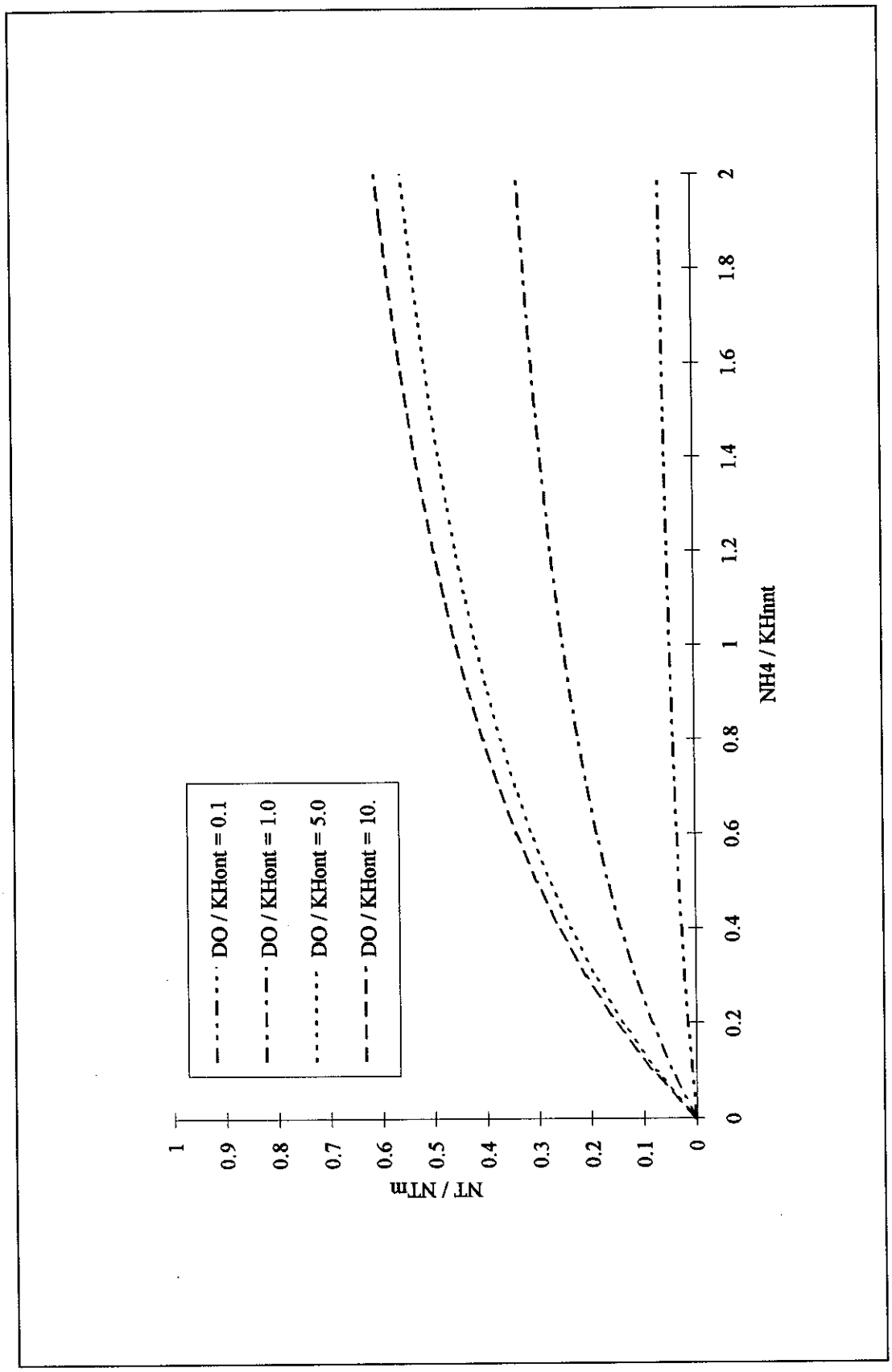

Figure 4-16. Effect of dissolved oxygen and ammonium concentration on nitrification rate

Effect of Nitrification on Dissolved Oxygen

$$\frac{\delta}{\delta t} DO = - AONT\, NT \qquad (4\text{-}63)$$

AONT = mass dissolved oxygen consumed per mass ammonium-nitrogen nitrified (4.33 gm O_2 gm^{-1} N)

Effect of Denitrification on Nitrate

The effect of denitrification on dissolved organic carbon has been described. Denitrification removes nitrate from the system in stoichiometric proportion to carbon removal as determined by Equation 4-39:

$$\frac{\delta}{\delta t} NO_3 = - ANDC\, Denit\, DOC \qquad (4\text{-}64)$$

ANDC = mass nitrate-nitrogen reduced per mass dissolved organic carbon oxidized (0.933 gm N gm^{-1} C)

Nitrogen Mass Balance Equations

The mass-balance equations for nitrogen state variables are written by summing all previously-described sources and sinks:

Ammonium

$$\frac{\delta}{\delta t} NH_4 = \sum_{x=c,d,g} (BMx\, FNIx + PRx\, FNIP - PNx\, Px)\, ANCx\, Bx + Kdon\, DON - NT \qquad (4\text{-}65)$$

Dissolved Organic Nitrogen

$$\frac{\delta}{\delta t} DON = \sum_{x=c,d,g} (BMx\ FNDx + PRx\ FNDP)\ ANCx\ Bx + Klpon\ LPON + Krpon\ RPON - Kdon\ DON \quad (4\text{-}66)$$

Labile Particulate Organic Nitrogen

$$\frac{\delta}{\delta t} LPON = \sum_{x=c,d,g} (BMx\ FNLx + PRx\ FNLP)\ ANCx\ Bx - Klpon\ LPON - WSl \frac{\delta}{\delta z} LPON \quad (4\text{-}67)$$

Refractory Particulate Organic Nitrogen

$$\frac{\delta}{\delta t} RPON = \sum_{x=c,d,g} (BMx\ FNRx + PRx\ FNRP)\ ANCx\ Bx - Krpon\ RPON - WSr \frac{\delta}{\delta z} RPON \quad (4\text{-}68)$$

Nitrate

$$\frac{\delta}{\delta t} NO_3 = \sum_{x=c,d,g} (PNx - 1)\ Px\ ANCx\ Bx + NT - ANDC\ Denit\ DOC \quad (4\text{-}69)$$

Silica

The model incorporates two siliceous state variables, available silica and particulate biogenic silica. For practical purposes, available silica is equivalent to dissolved silica although sorption of available silica to inorganic solids occurs. The silica cycle (Figure 4-17) is a simple one in which diatoms take

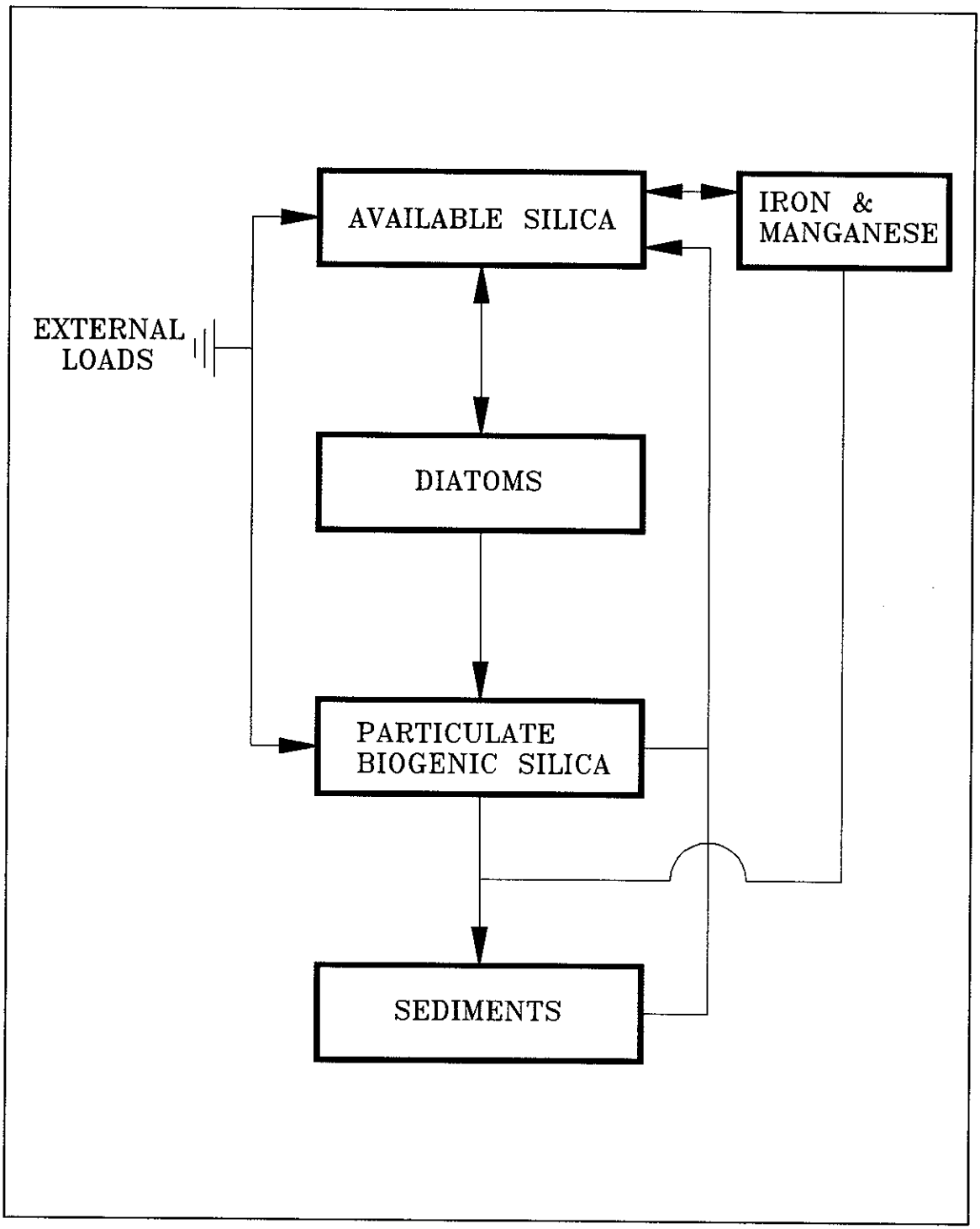

Figure 4-17. The model silica cycle

up available silica and recycle available and particulate biogenic silica through the actions of metabolism and predation. Particulate silica dissolves in the water column or settles to the bottom. A portion of the settled particulate

biogenic dissolves within the sediments and returns to the water column as available silica. Sources and sinks represented are:

Diatom production and metabolism
Predation
Dissolution of particulate to dissolved silica
Settling
Exchange with inorganic solids

Available Silica

Analysis of monitoring data indicated depletion of dissolved silica from anoxic bottom water following reaeration events (Figure 4-13). The phenomenon was similar to, and concurrent with, phosphate depletion. Our hypothesis to explain the phenomenon was the same as for phosphorus. Reaeration of bottom waters caused dissolved iron and manganese to precipitate. Dissolved silica sorbed to the newly-formed metal particles and rapidly settled to the bottom. To represent this process, available silica was partitioned into dissolved and particulate fractions according to a linear sorption isotherm:

$$SAd = \frac{1}{1 + Kadsa\ TAMp} SA \qquad (4\text{-}70)$$

$$SAp = \frac{Kadsa\ TAMp}{1 + Kadsa\ TAMp} SA \qquad (4\text{-}71)$$

SA = available silica concentration (gm Si $m^{-3)}$
SAd = dissolved available silica (gm Si m^{-3})
SAp = particulate available silica (gm Si m^{-3})
Kadsa = partition coefficient of sorbed vs. dissolved available silica ($m^3\ mol^{-1}$)

The kinetics equation for available silica is:

$$\frac{\delta}{\delta t} SA = (FSAP\ PRd - Pd)\ ASCd\ Bd - WSs \frac{\delta}{\delta z} SAp + Ksua\ SU \qquad (4\text{-}72)$$

SU = particulate biogenic silica concentration (gm Si m^{-3})
FSAP = fraction of diatom silica made available by predation ($0 \leq FSAP \leq 1$)

ASCd = silica-to-carbon ratio of diatoms (gm Si gm^{-1} C)
Ksua = particulate silica dissolution rate (day^{-1})

Particulate Biogenic Silica

The kinetics equation for particulate biogenic silica is:

$$\frac{\delta}{\delta t} SU = (BMd + (1 - FSAP) PRd) ASCd\, Bd - WSs \frac{\delta}{\delta z} SU - Ksua\, SU \quad (4\text{-}73)$$

An exponential function (Figure 4-5) describes the effect of temperature on silica dissolution.

Chemical Oxygen Demand

In this study, chemical oxygen demand is the concentration of reduced substances that are oxidizable through inorganic means. The source of chemical oxygen demand in saline water is sulfide released from sediments. A cycle occurs in which sulfate is reduced to sulfide in the sediments and reoxidized to sulfate in the water column. In freshwater, methane is released to the water column by the sediment model. Both sulfide and methane are quantified in units of oxygen demand and are treated with the same kinetics formulation:

$$\frac{\delta}{\delta t} COD = - \frac{DO}{KHocod + DO} Kcod\, COD \quad (4\text{-}74)$$

COD = chemical oxygen demand concentration (gm O2-equivalents m^{-3})
KHocod = half-saturation concentration of dissolved oxygen required for exertion of chemical oxygen demand (gm O_2 m^{-3})
Kcod = oxidation rate of chemical oxygen demand (day^{-1})

An exponential function (Figure 4-5) describes the effect of temperature on exertion of chemical oxygen demand.

Dissolved Oxygen

Sources and sinks of dissolved oxygen in the water column (Figure 4-18) include:

Algal photosynthesis
Atmospheric reaeration
Algal respiration
Heterotrophic respiration
Nitrification
Chemical oxygen demand

Reaeration

The rate of reaeration is proportional to the dissolved oxygen deficit in model segments that form the air-water interface:

$$\frac{\delta}{\delta t} DO = \frac{Kr}{\Delta z} (DOs - DO) \qquad (4\text{-}75)$$

Kr = reaeration coefficient (m day^{-1})
DOs = dissolved oxygen saturation concentration (gm O_2 m^{-3})

The surface renewal concept, attributed to Danckwerts by O'Connor and Dobbins (1958), indicates:

$$Kr = \sqrt{Dl\,R} \qquad (4\text{-}76)$$

Dl = molecular diffusivity of oxygen in water ($\approx$1.7 x 10-4 m^2 day^{-2})
R = surface renewal rate (day^{-1})

Specification of the surface renewal rate is the fundamental problem in reaeration theory. O'Connor and Dobbins (1958) state that, in isotropic turbulence, surface renewal can be approximated as the ratio of stream velocity to depth. The renewal rate is also influenced by wind, however (O'Connor 1983). Influences on reaeration of temperature (ASCE 1961) and salinity (Wen et al. 1984), most likely effected through changes in diffusivity, have been measured. No single theory that unites all these factors into a formulation of reaeration in an estuary is available. The surface renewal concept is retained in this study with the renewal rate treated as a calibration parameter.

Saturation dissolved oxygen concentration diminishes as temperature and salinity increase. An empirical formula that describes these effects (Genet et al. 1974) is:

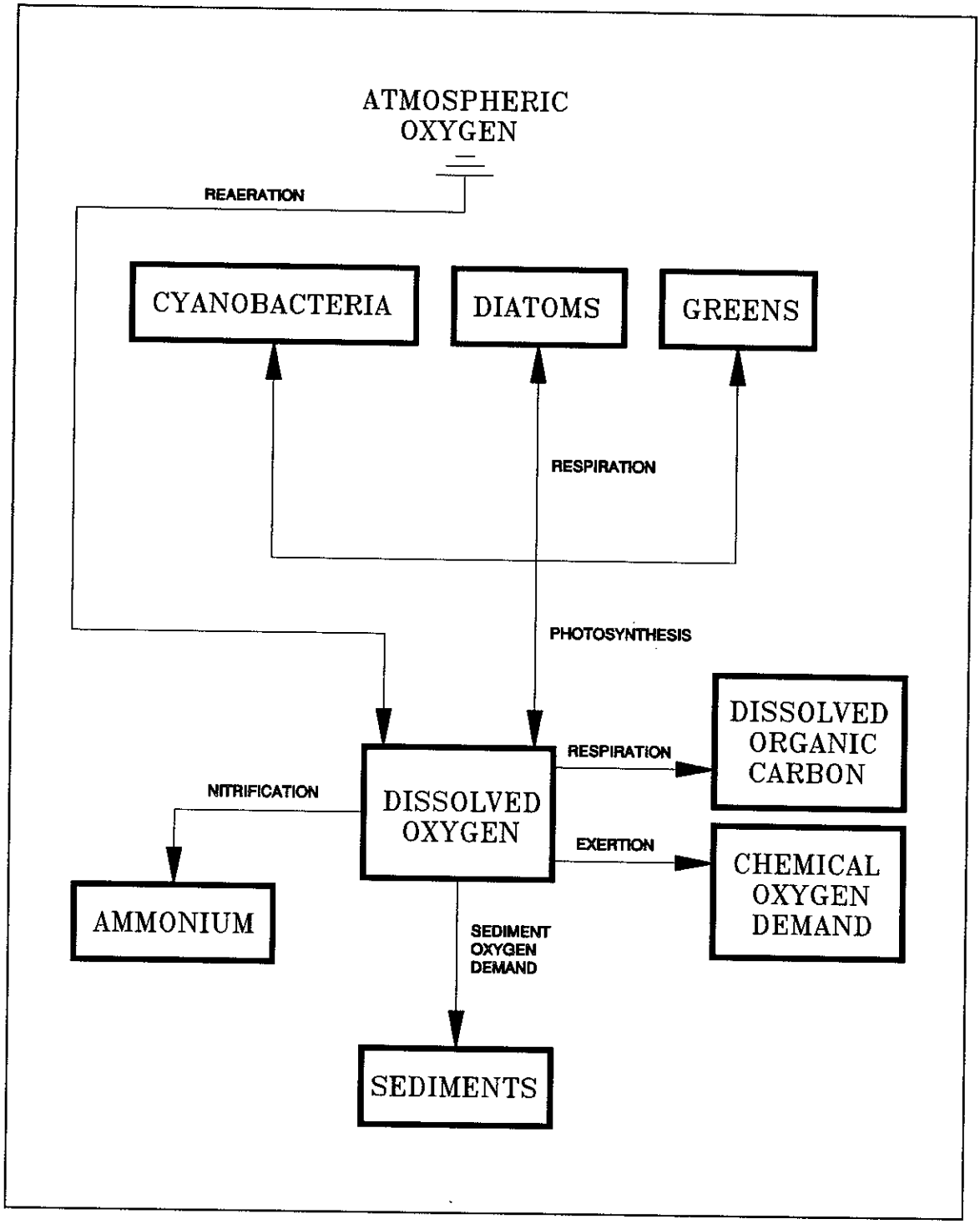

Figure 4-18. Dissolved oxygen sources and sinks

$$DOs = 14.5532 - 0.38217\,T + 0.0054258\,T^2 - CL\,(1.665 \times 10^{-4} - 5.866 \times 10^{-6}\,T + 9.796 \times 10^{-8}\,T^2) \quad (4\text{-}77)$$

CL = chloride concentration (= salinity/1.80655)

Summary of Dissolved Oxygen Sources and Sinks

The complete kinetics for dissolved oxygen are:

$$\frac{\delta}{\delta t} DO = \sum_{x=c,d,g} \left((1.3 - 0.3\,PNx)\,Px - \frac{DO}{KHrx + DO} BMx \right) AOCR\,Bx - AONT\,NT - \frac{DO}{KHodoc + DO} AOCR\,Kdoc\,DOC - \frac{DO}{KHocod + DO} Kcod\,COD + \frac{Kr}{\Delta z}(DOs - DO) \quad (4\text{-}78)$$

Total Active Metal

The total active metal state variable is the sum of iron and manganese concentrations. Iron and manganese exist in particulate and dissolved forms in estuaries. The prime determinant of the species is dissolved oxygen. In the oxygenated water, total iron and manganese are almost completely particulate. Under anoxic conditions, large fractions of total iron and manganese are dissolved although solid-phase sulfides and carbonates exist and may predominate. The simplified partitioning of particulate and dissolved phases of total active metal employed here notes that total active metal concentration must achieve a minimum level before precipitation occurs. The minimum level is a function of dissolved oxygen:

$$TAMd = \text{minimum}\left(TAMdmx\,e^{-Kdotam\,DO}, TAM\right) \quad (4\text{-}79)$$

$$TAMp = TAM - TAMd \quad (4\text{-}80)$$

TAM = total active metal concentration (mol m^{-3})
TAMd = dissolved total active metal (mol m^{-3})
TAMp = particulate total active metal (mol m^{-3})
TAMdmx = solubility of total active metal under anoxic conditions (mol m^{-3})
Kdotam = constant that relates total active metal solubility to dissolved oxygen concentration (m^3 gm^{-1} O_2)

Behavior of the functions expressed in Equations 4-79 and 4-80 is shown in Figures 4-19 and 4-20. In the first figure, total active metal concentration exceeds the maximum solubility, TAMdmx. Particulate metal is present at all dissolved oxygen concentrations. The particulate fraction increases as oxygen concentration increases. When dissolved oxygen >> Kdotam, virtually all metal is in particulate form. In the second figure, total active metal concentration is less than the maximum solubility. All metal is in dissolved form until oxygen-dependent solubility falls below total metal concentration. At that oxygen concentration, precipitation of particulate metal occurs. Following precipitation, the particulate fraction increases as a function of oxygen concentration until virtually all metal is particulate when dissolved oxygen >> Kdotam.

The origin of total active metal in the model is benthic sediments. Since metal release is not explicit in the sediment model, release is incorporated into the kinetics portion of the water-column model. Release is treated as a spatially-uniform, empirical function of temperature and dissolved oxygen concentration. The only other source or sink in the water column is settling of the particulate fraction. In the mass balance equation that follows, the benthic source is understood to operate only in model cells that adjoin the bottom:

$$\frac{\delta}{\delta t} TAM = - WSs \frac{\delta}{\delta z} TAMp + \frac{KHbmf}{KHbmf + DO} \frac{BENTAM}{\Delta z} \quad (4\text{-}81)$$

BENTAM = anoxic total active metal release rate release rate (mol m^{-2} day^{-1})
KHbmf = dissolved oxygen concentration at which total active metal release is half the anoxic rate (gm O_2 m^{-3})

Release of metal from the bottom is maximum when dissolved oxgyen is absent from the overlying water (Figure 4-21). Release declines as oxygen concentration increases and is negligible when dissolved oxygen >> KHbmf.

Sediment release of total active metal is treated as an exponential function of temperature (Figure 4-5).

Salinity

No internal sources or sinks of salinity exist.

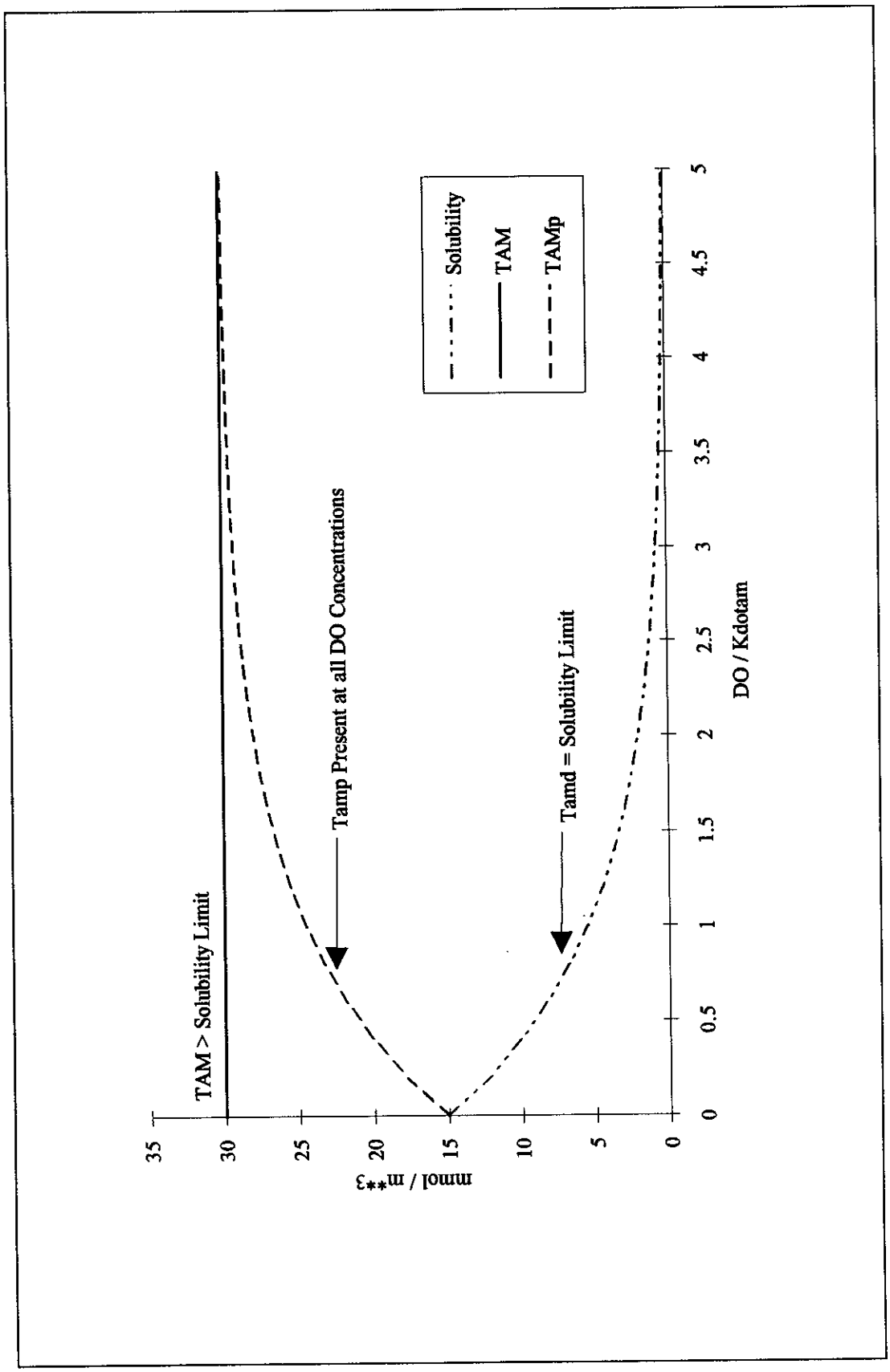

Figure 4-19. Total active metal partitioning when concentration exceeds maximum solubility

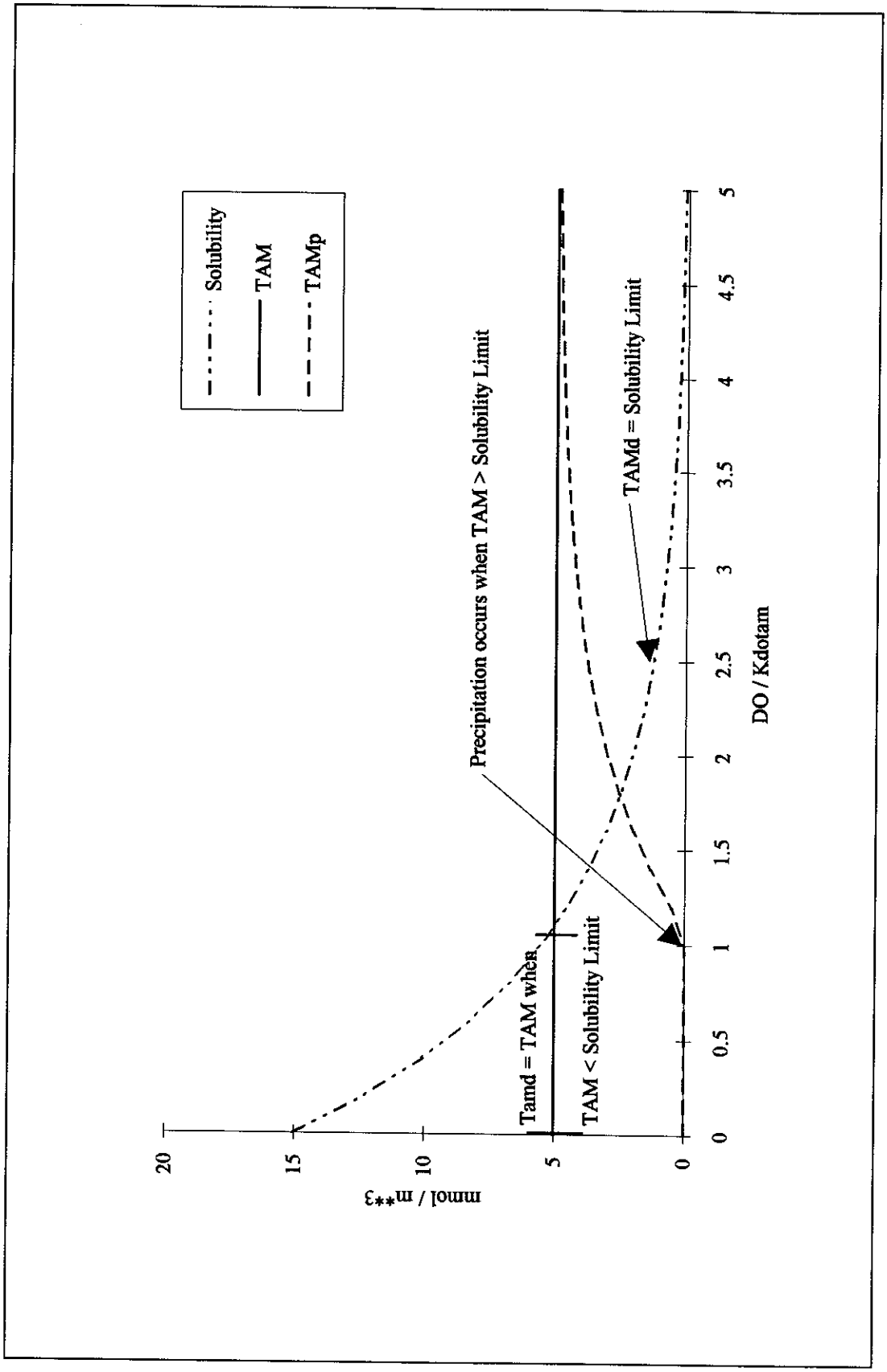

Figure 4-20. Total active metal partitioning when concentration is less than maximum solubility

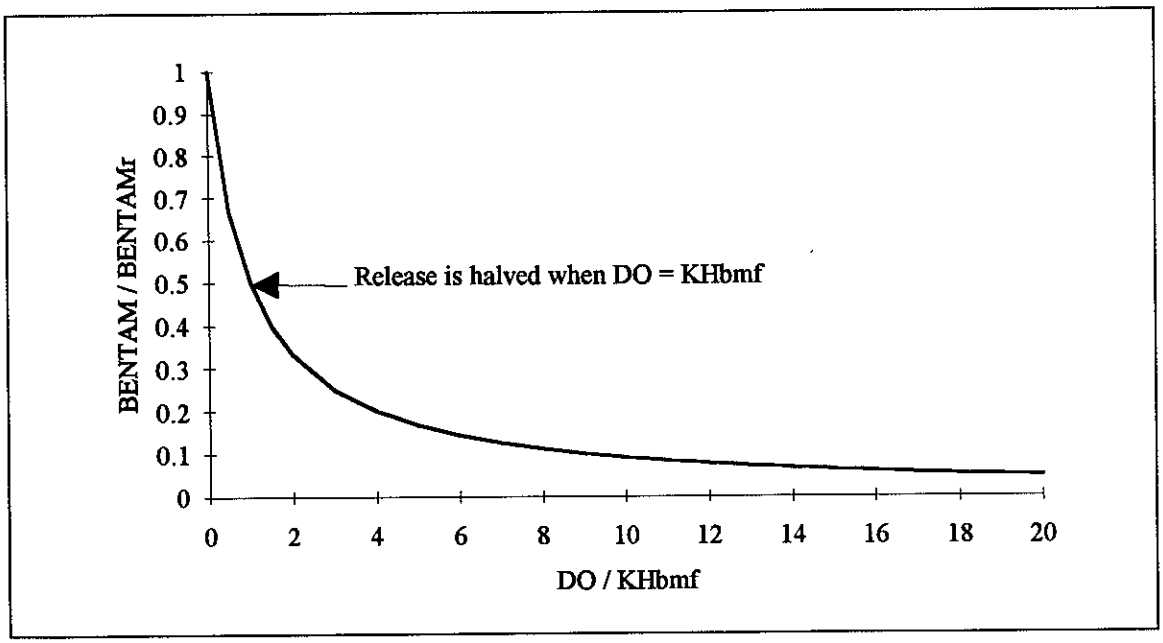

Figure 4-21. Effect of dissolved oxygen on benthic metal release

Temperature

A conservation of internal energy equation can be written analogous to the conservation of mass equation. The only source or sink of internal energy considered is exchange with the atmosphere. Although solar radiation can penetrate several meters into the water column, radiation-induced increases in internal energy are here assigned entirely to the surface model layer.

For practical purposes, the internal-energy equation can be written as a conservation of temperature equation. Change of temperature due to atmospheric exchange is considered proportional to the temperature difference between the water surface and a theoretical equilibrium temperature (Edinger et al. 1974):

$$\frac{\delta}{\delta t} T = \frac{KT}{\rho \, Cp \, \Delta z} (Te - T) \qquad (4\text{-}82)$$

Te = equilibrium temperature (C^o)
KT = Heat exchange coefficient (watt m^{-2} $C^{0\ -1}$)
Cp = specific heat of water (4200 watt sec kg^{-1} $C^{o\ -1}$)
ρ = density of water (1000 kg m^{-3})

Chapter V: Loads to the System

Introduction

External loads of nutrients and oxygen demand were divided into four classes. Fall-line loads were carried by freshwater flows that entered the Bay and tidal tributaries at the upper limit of tidal excursion. Location of this limit, the fall line, defined the transition from freeflowing to tidal water bodies. Below-fall-line, nonpoint-source loads were associated with distributed overland flows that entered the Bay and tidal tributaries directly. Point-source loads were discharges from municipal treatment plants, industries, and similar facilities. Atmospheric loads were transfers from the atmosphere to the water surface via rainfall, wind, and other processes.

Fall-Line Loads

Carbon, nitrogen, and phosphorus were the only substances treated as mass loads at the fall lines. Inflows of algae, dissolved oxygen, and silica were treated through specification of concentration boundary conditions (Chapter IX). Fall-line loads were generated by the EPA Chesapeake Bay Watershed Model (Donigian et al. 1991). Loads provided by the watershed model resulted from computation of loading, transport, and transformations throughout the Chesapeake Bay watershed above the fall lines. The domain of the watershed model included portions of New York, Pennsylvania, Virginia, West Virginia, District of Columbia, and Delaware (Figure 5-1).

The watershed model provided daily loads at seven major fall lines: the James, Mattaponi, Pamunkey, Rappahannock, Potomac, Patuxent, and Susquehanna Rivers. Loads at fall lines of lesser tributaries were combined with below-fall-line nonpoint sources. Daily output from the watershed model was averaged into bi-weekly loads before input to the water quality model. Annual summaries of fall-line loads are presented in Table 5-1. For summary purposes, loads from the Mattaponi and Pamunkey are summed into a single quantity for the York River.

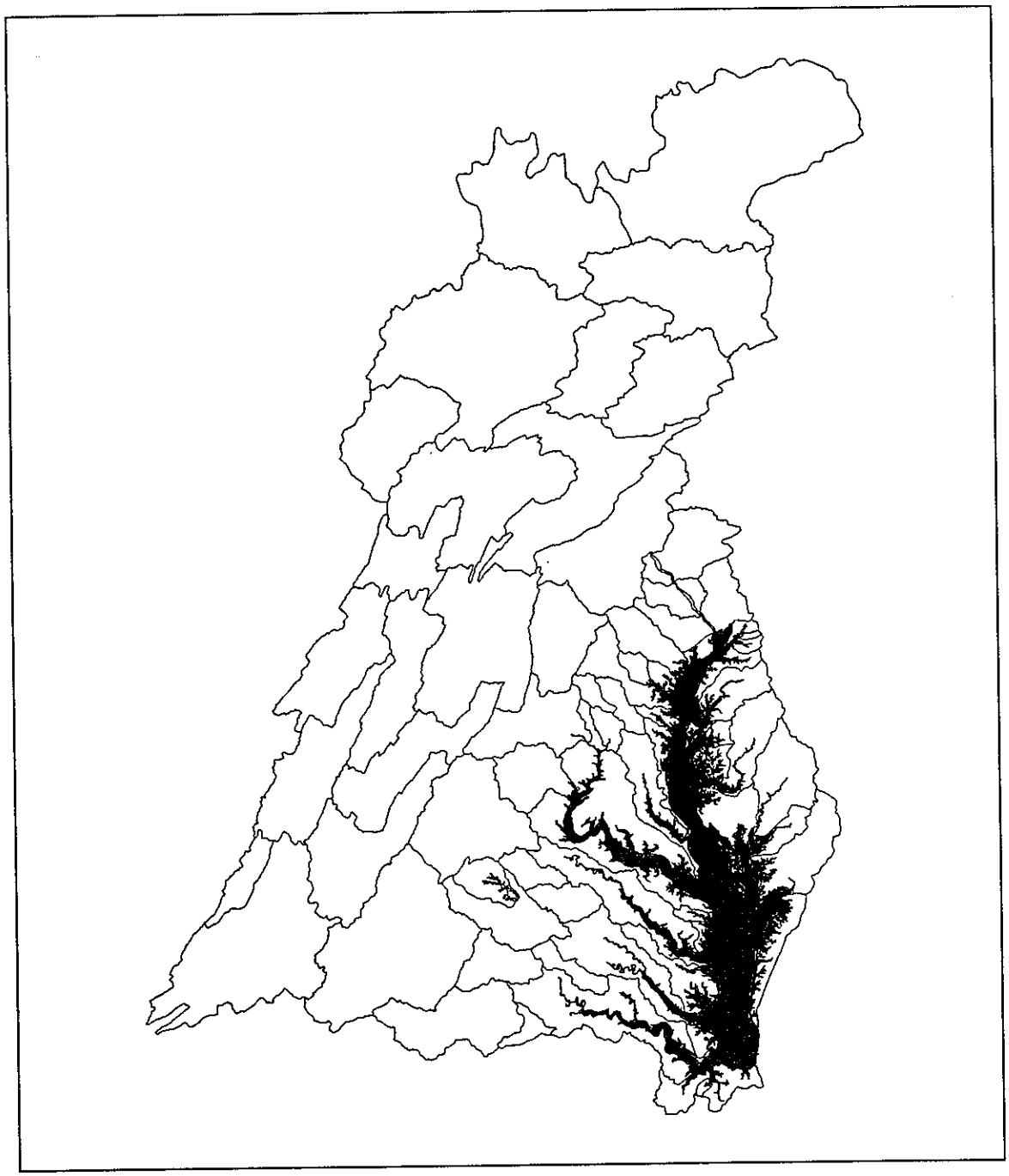

Figure 5-1. The Chesapeake Bay Watershed

Table 5-1
Fall-Line Loads, 1984-1986

Year, Fall Line	Carbon, kg day^{-1}	Nitrogen, kg day^{-1}	Phosphorus, kg day^{-1}
1984			
James	126858	19045	2800
York	28584	4153	489
Rappahannock	28337	6732	634
Potomac	393170	86980	9763
Patuxent	5280	3039	345
Susquehanna	787811	240516	11760
Total	1370039	360463	25792
1985			
James	211397	17250	4159
York	35979	2578	463
Rappahannock	19794	4343	452
Potomac	169553	52909	6472
Patuxent	2552	2099	269
Susquehanna	293608	134674	6239
Total	732882	213853	18054
1986			
James	20240	6561	833
York	5470	1140	129
Rappahannock	4379	2217	189
Potomac	93047	36339	3484
Patuxent	3183	2187	185
Susquehanna	416029	172379	8229
Total	542346	220823	13050

Below-Fall-Line Nonpoint-Source Loads

Below-fall-line loads of carbon, nitrogen, and phosphorus were also provided by the watershed model. Loads of algae, dissolved oxygen, and other substances were considered negligible. The watershed model generated daily loads for twenty-nine watersheds along the shore of the Bay and tidal tributaries (Figure 5-2). Loads from each watershed were distributed evenly into adjoining water quality model cells in the surface plane of the grid. Daily loads were averaged into monthly loads prior to input to the water quality model.

Annual summaries of below-fall-line loads are provided in Table 5-2. For summary purposes, loads from individual watersheds are combined into loads to the mainstem and major tributaries.

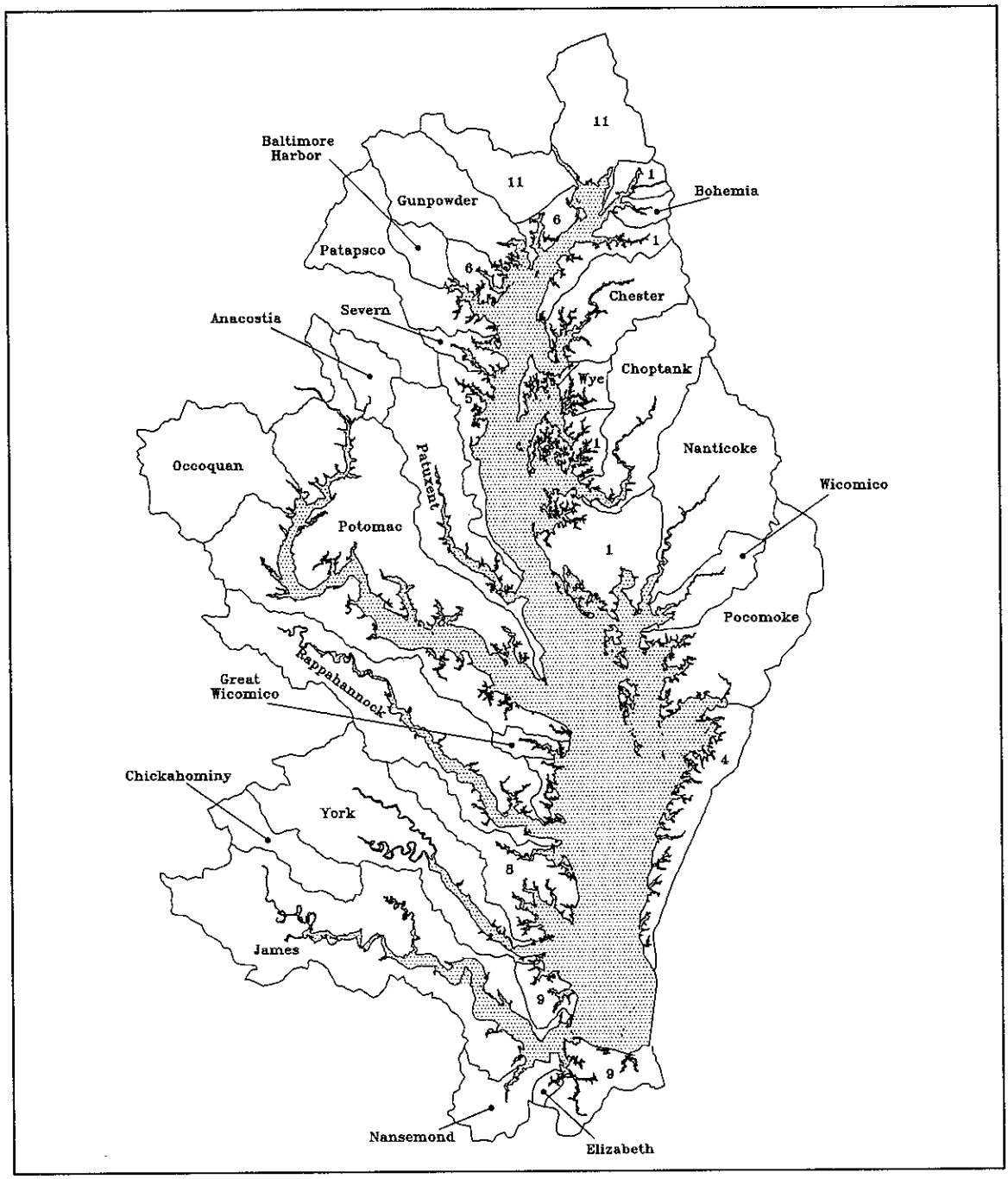

Figure 5-2. Below-Fall-Line Drainage Basins

Table 5-2
Below-Fall-Line, Nonpoint-Source Loads, 1984-1986

Year, Basin	Carbon, kg day^{-1}	Nitrogen, kg day^{-1}	Phosphorus, kg day^{-1}
1984			
James	41163	15570	1000
York	4892	4552	283
Rappahannock	5311	6135	438
Potomac	13647	15917	991
Patuxent	3163	3253	252
Baltimore Harbor	2388	3528	241
Mainstem Bay	35473	60634	3144
Total	106424	110127	6385
1985			
James	55559	9766	888
York	5484	2403	237
Rappahannock	6417	3097	395
Potomac	12584	8799	767
Patuxent	2939	2153	224
Baltimore Harbor	1592	2152	172
Mainstem Bay	58398	26554	2431
Total	143243	55266	5142
1986			
James	11223	6589	346
York	1805	2182	135
Rappahannock	1453	2689	153
Potomac	8673	9175	644
Patuxent	1857	1903	152
Baltimore Harbor	2311	2540	234
Mainstem Bay	30265	27485	2077
Total	57967	52976	3779

Point-Source Loads

Point-source dischargers to the Chesapeake range in size from one of the world's largest, the Blue Plains Treatment Facility, down to trailer parks and highway rest stops. Municipal dischargers in Maryland and the District of Columbia were considered in the model only if daily flow exceeded 0.4 mgd (million gallons per day). Industrial dischargers were considered if BOD load exceeded 100 ppd (pounds per day), if nitrogen load exceeded 40 ppd, or if phosphorus load exceeded 12 ppd. All identifiable point sources in Virginia were considered. In total, nearly 150 point sources (Appendix A) were represented in the model.

Point-source loads from each facility were computed as the product of flow rate and concentration. Quantification of loads was conducted on a monthly basis. Availability of data for computation of monthly loads was highly variable. Excellent records of flow, total nutrient concentration, and nutrient speciation were available from many large, modern municipal plants. At the other extreme, only design flow and BOD_5 were available for many of the smallest facilities. Default concentrations and speciation (Table 5-3), supplied by the Chesapeake Bay Program Office, were employed when records were unavailable. Annual flows were employed when monthly flows were not recorded.

Table 5-3
Default Concentrations for Point Sources

Treatment Level, State	Nitrogen				Phosphorus		
Primary	**Total, gm m^{-3}**	**NH_4, %**	**NO_3, %**	**Org N,%**	**Total, gm m^{-3}**	**PO_4, %**	**Org P, %**
Maryland	20.7	66	0	34	7.2 – 8.0	45	55
Virginia	20.7	66	0	34	7.2	45	55
Secondary	**Total, gm m^{-3}**	**NH_4, %**	**NO_3, %**	**Org N, %**	**Total, gm m^{-3}**	**PO_4, %**	**Org P, %**
Maryland	18.5	50	35	15	7.0 – 8.0	85	15
Virginia	18.5	50	35	15	6.4	85	15
Advanced	**Total, gm m^{-3}**	**NH_4, %**	**NO_3, %**	**Org N, %**	**Total, gm m^{-3}**	**PO_4, %**	**Org P, %**
Maryland	TKN < 10	15	62	23	< 2.0	45	55
Virginia	TKN < 10	15	62	23	< 1.0	45	55

Five-day biochemical oxygen demand was reported for the point sources. Since biochemical oxygen demand was not a model state variable, BOD_5 concentrations were converted to total organic carbon for use in the model. A relationship obtained for New York City municipal wastewaters (HydroQual 1991) was employed:

$$TOC = 18 + 0.7\,BOD_5 \qquad (1)$$

in which:

TOC = total organic carbon (gm m^{-3})

BOD_5 = five day biochemical oxygen demand (gm m^{-3})

Point-source loads are summarized by basin in Table 5-4. Assignment of point sources to basins is arbitrary in some cases. For example, industries at the mouth of the York River can be assigned to the York or the mainstem Bay. Alternate summaries have been produced by the Chesapeake Bay Program Office and should be regarded as authoritative.

Table 5-4
Point-Source Load Summary, 1984-1986

Year, Basin	Carbon, kg day^{-1}	Nitrogen, kg day^{-1}	Phosphorus, kg day^{-1}
1984			
James	41919	24649	3817
York	3463	1486	473
Rappahannock	826	424	147
Potomac	38534	27318	473
Patuxent	804	647	119
Baltimore Harbor	41310	24551	1596
Virginia Mainstem Bay	2242	2515	465
Maryland Mainstem Bay	6108	3608	708
Total	135204	85202	7798
1985			
James	45920	26463	3850
York	3976	1564	506
Rappahannock	759	410	144
Potomac	35402	28318	404
Patuxent	765	595	120
Baltimore Harbor	33370	23306	1241
Virginia Mainstem Bay	2346	2381	391
Maryland Mainstem Bay	5721	3272	703
Total	128259	86313	7359
1986			
James	42603	28077	3964
York	4346	1557	477
Rappahannock	816	433	153
Potomac	33827	26899	309
Patuxent	818	649	46
Baltimore Harbor	34168	22258	1007
Virginia Mainstem Bay	2212	2772	485
Maryland Mainstem Bay	5982	3553	406
Total	124772	86202	6848

Atmospheric Loads

Atmospheric loads are typically divided into two categories. "Wetfall" is the loading associated with dissolved substances in rainfall. Settling of dust particles and similar processes contribute to "dryfall". Observations of concentrations in rainwater, for computation of wetfall, are frequently available. Dryfall is usually estimated as a fraction of wetfall.

Annual mean concentrations of ammonium and nitrate in wetfall were obtained from data published by the National Atmospheric Data Program

(NADP 1989). Seasonal wetfall concentrations of organic nitrogen, phosphate, and organic phosphorus were obtained from the Chesapeake Bay Program Technical Synthesis (USEPA 1982). Wetfall was input to the model as daily-average rainfall and concentration. These were specified on a monthly basis (Table 5-5). Dryfall nitrogen load was assumed equal to the wetfall nitrate load. Dryfall phosphorus load was assumed to be negligible. Annual mean atmospheric loads, on an areal basis, were 1.51 gm N m^{-2} yr^{-2} and 0.064 gm P m^{-2} yr^{-1}. These were identical to loads employed in the watershed model.

Table 5-5
Precipitation Rate and Wetfall Concentrations

Month	Rainfall, cm day^{-1}	NH_4, gm m^{-3}	NO_3, gm m^{-3}	Org. N, gm m^{-3}	PO_4, gm m^{-3}	Org. P, gm m^{-3}
December, January, February	0.24	0.18	0.33	0.21	0.016	0.022
March, April, May	0.28	0.18	0.33	1.25	0.015	0.065
June, July, August	0.33	0.18	0.33	0.74	0.014	0.065
September, October, November	0.26	0.18	0.33	0.39	0.021	0.029

Atmospheric loads to each model cell in the surface plane were computed within the model as a function of precipitation, concentration, and cell surface area. Load summaries, by basin, are presented in Table 5-6.

Table 5-6
Summary of Atmospheric Loads

Basin	Nitrogen, kg day^{-1}	Phosphorus, kg day^{-1}
James	2114	90
York	1924	82
Rappahannock	1510	64
Potomac	3934	167
Patuxent	472	20
Baltimore Harbor	414	18
Mainstem Bay	32517	1378
Total	42885	1819

Summary

The importance of nutrient loading sources differed among basins. In the mainstem (Figure 5-9) and Potomac (Figure 5-6), fall-line loads greatly exceeded nonpoint-source and atmospheric loads. The ratio reflected the extensive above-fall-line drainage area of the Susquehanna and Potomac Rivers. In the remaining basins, relative magnitude of fall-line loads, nonpoint-source loads, and atmospheric loads varied but the disparity between these three sources was not large.

The dominant source of nutrients in the James River (Figure 5-3) and in Baltimore Harbor (Figure 5-8) was point-source loading. Point-source phosphorus loads to the James River exceeded every other basin in magnitude. The York River (Figure 5-4) was also heavily loaded with point-source phosphorus relative to other sources. Point-source nitrogen loads to the Potomac were extensive but did not exceed fall-line loads. Magnitude of Potomac point-source phosphorus loads was among the least of all basins due to extensive controls in the vicinity of Washington.

Total nutrient loads to each basin were largely proportional to drainage area. Largest nitrogen loads were to the mainstem, Potomac, and James (Figure 5-10). These reflected the fall-line loads to each basin although point sources were a significant contributor in the James. Nitrogen loads to Baltimore Harbor were almost entirely from point sources. Nitrogen loads to remaining basins were minor due to small drainage area and few point-source dischargers.

The mainstem also received the largest direct phosphorus load (Figure 5-11) due to runoff from the Susquehanna. Under average hydrologic conditions, total phosphorus load in the James exceeded the Potomac despite the lesser drainage area of the James. The exceedance was due to the large disparity in point-source loading between the two basins. Phosphorus loads to remaining basins were much less than the first three and roughly equivalent.

The predominant nitrogen load to the system was at the fall lines (Figure 5-12). Fall-line loads were proportional to runoff volume. The year of highest runoff, 1984 had the greatest load. Loads in 1985 and 1986 were equivalent despite the description of 1985 as "dry" year and 1986 as an "average" year. Annual fall-line loads in 1985 were influenced by the autumn storm in the western tributaries. Loads in the Susquehanna, the primary runoff source to the mainstem were less in 1985 than in 1986. In 1985 and 1986, point sources were the second largest nitrogen source although nonpoint sources exceeded point sources in 1984. Atmospheric nitrogen loads were the least of all sources.

Fall-line loading was also the predominant phosphorus source (Figure 5-13). Despite lesser flow in the Susquehanna in 1985 than in 1986, total fall-line loading was greater in 1985. Excess load in 1985 was due to the autumn storm that affected the tributaries. Second largest phosphorus loading

was from point sources in all years. Atmospheric phosphorus loads were the least of all sources.

On an annual basis, total nitrogen loads to the system (Table 5-7) reflected runoff volume in the Susquehanna. Nitrogen loads were largest in 1984, less in 1986 and least in 1985. Total phosphorus loads were also largest in 1984 but the least loads occurred in 1986 rather than 1985. The excess loading in 1985 was due to the loading associated with the major autumn storm in the western tributaries.

Table 5-7
Total Direct Loads to System, 1984-1986

Year	Carbon	Nitrogen	Phosphorus
1984	1611667	598677	41794
1985	1004384	398317	32374
1986	725085	402886	25496

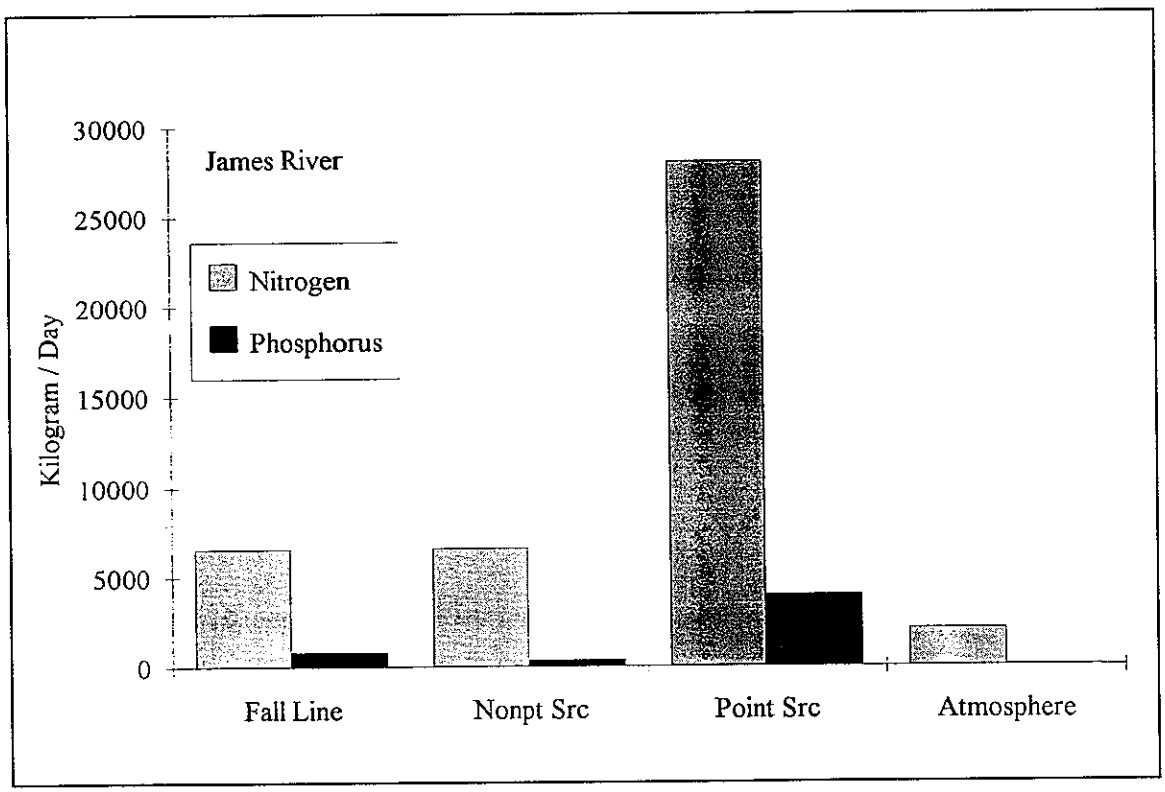

Figure 5-3. Nutrient Loads to James River Basin, 1986

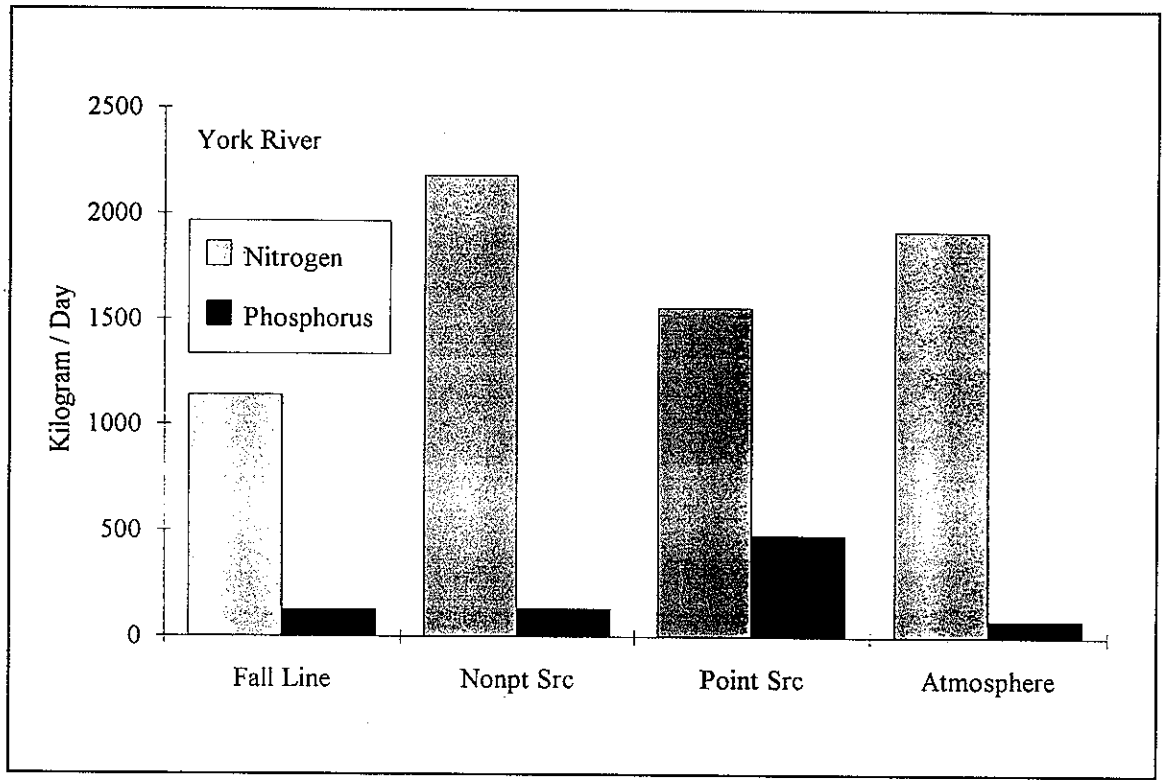

Figure 5-4. Nutrient Loads to York River Basin, 1986

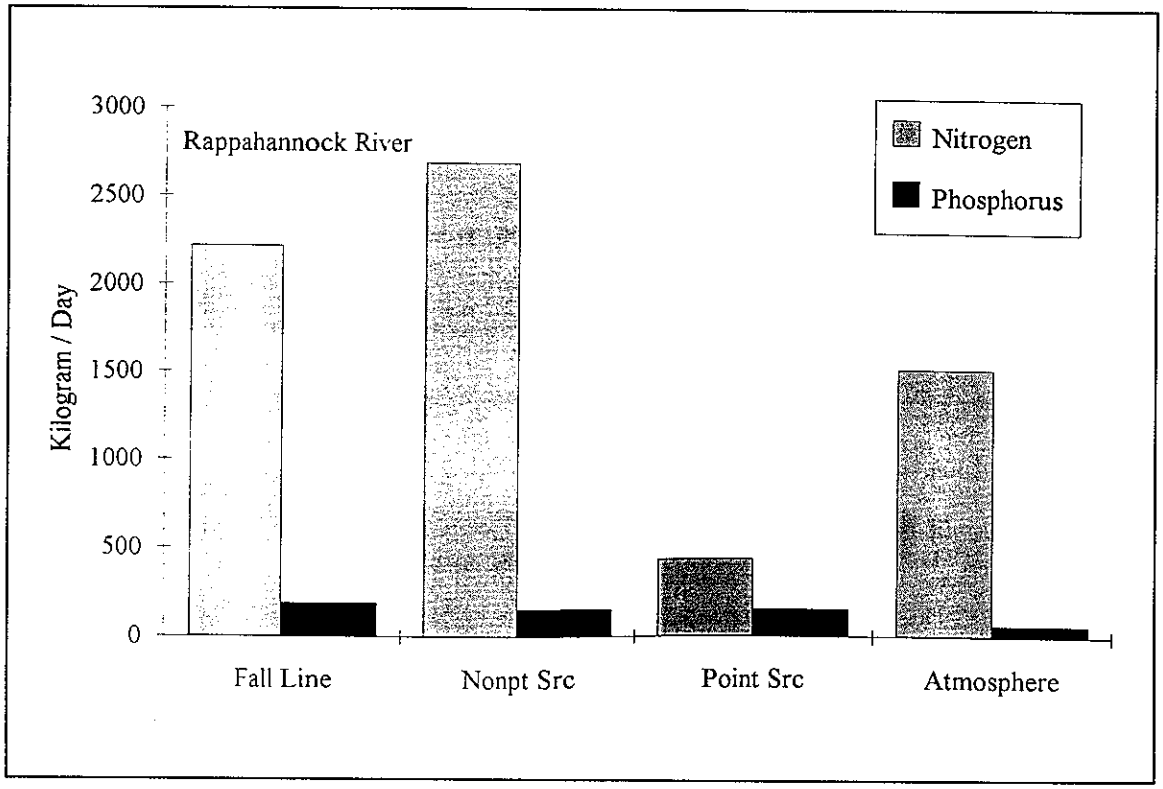

Figure 5-5. Nutrient Loads to Rappahannock River Basin, 1986

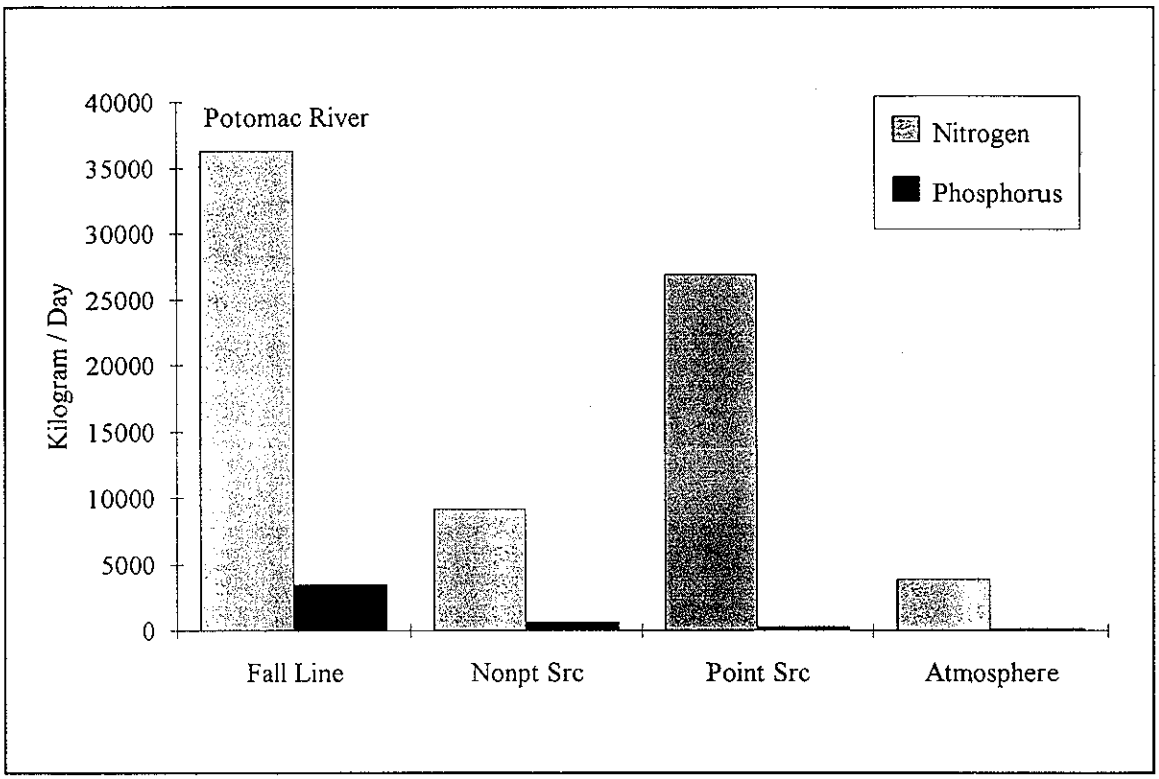

Figure 5-6. Nutrient Loads to Potomac River Basin, 1986

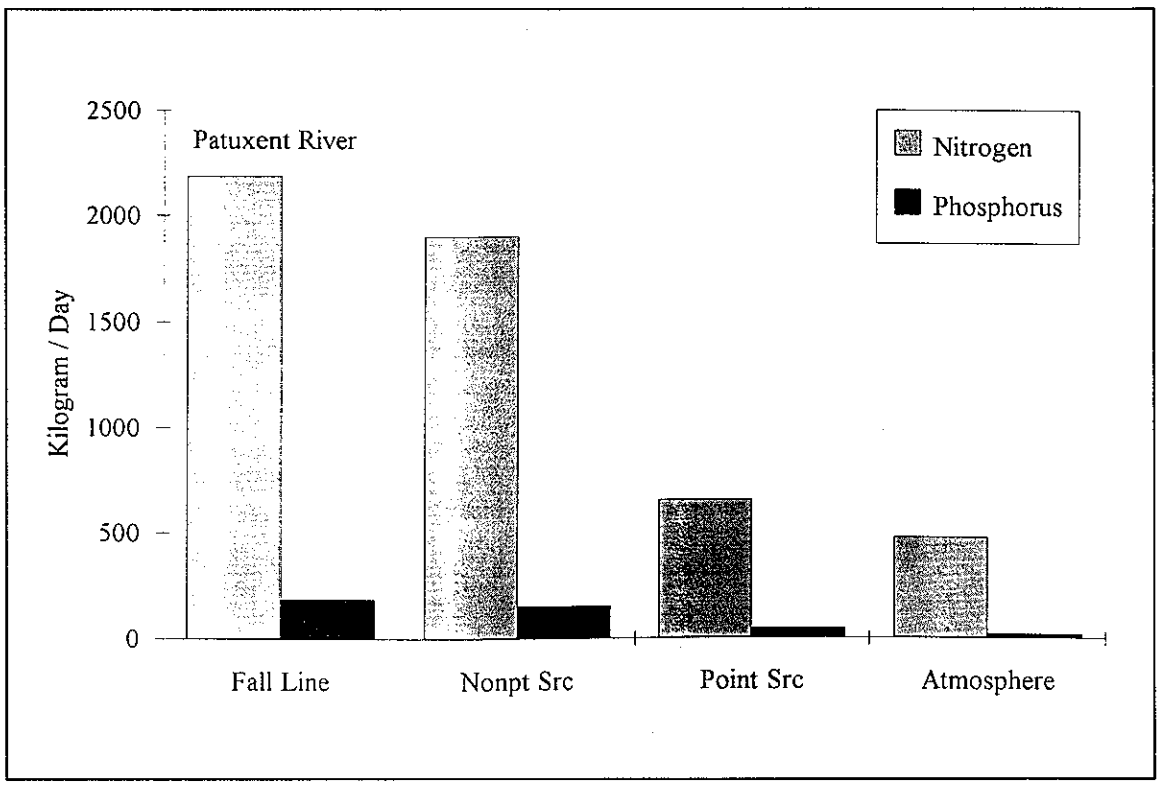

Figure 5-7. Nutrient Loads to Patuxent River Basin, 1986

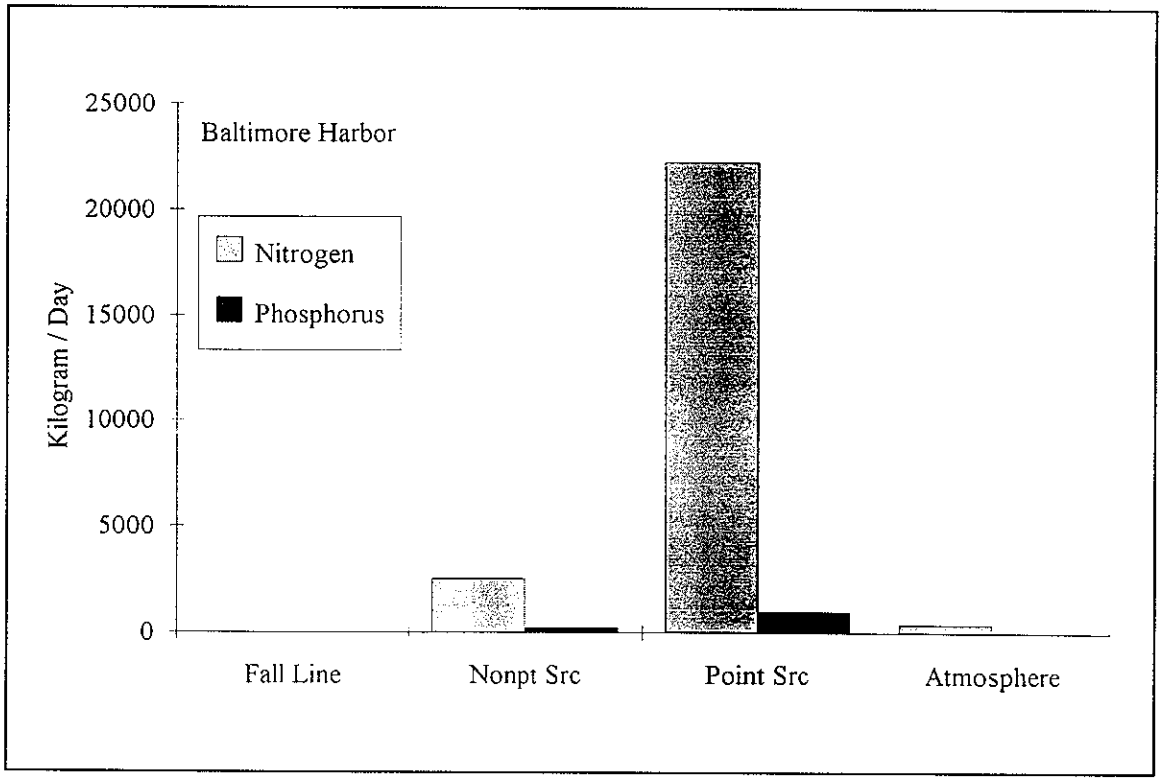

Figure 5-8. Nutrient Loads to Baltimore Harbor, 1986

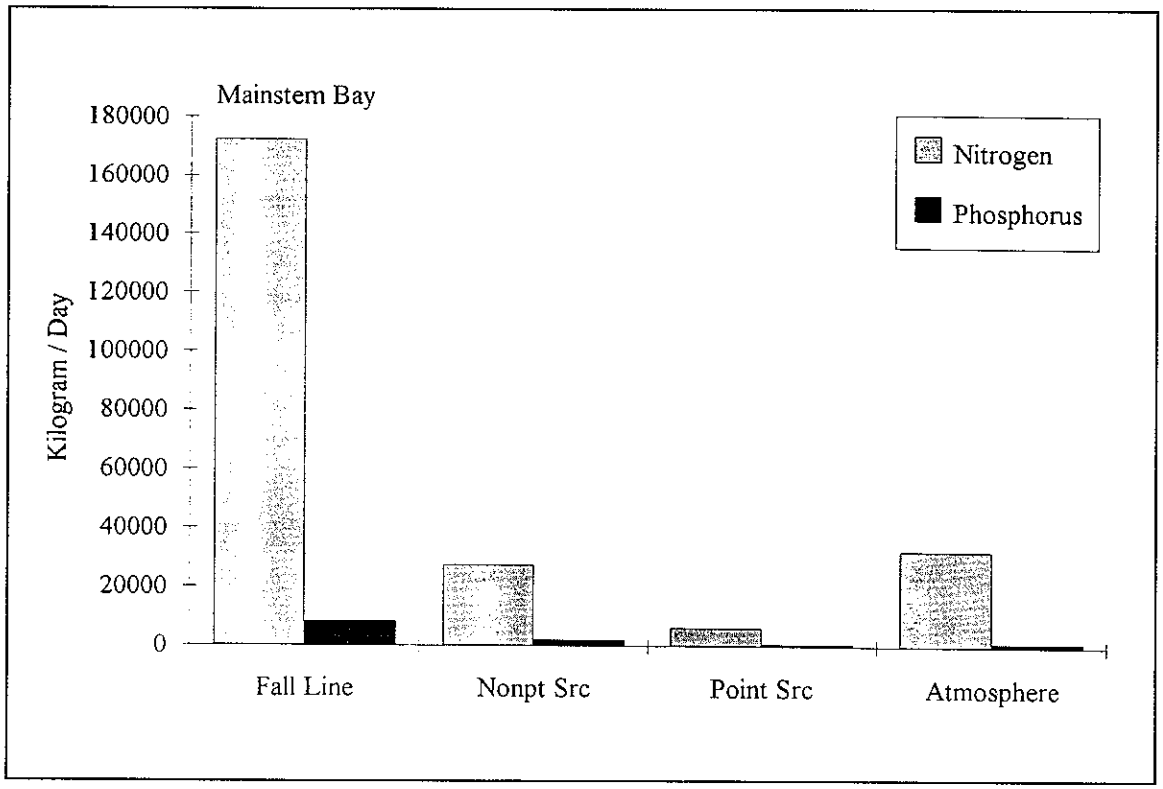

Figure 5-9. Nutrient Loads to Mainstem Bay, 1986

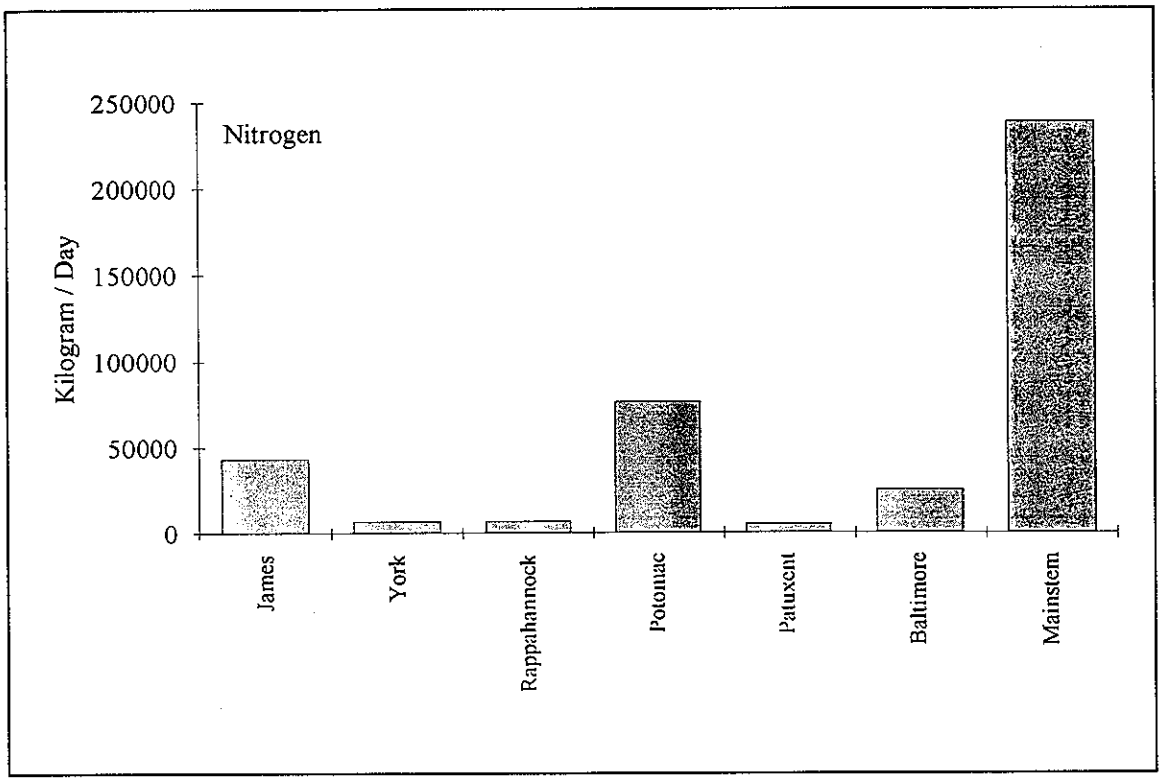

Figure 5-10. Nitrogen Loads by Basin, 1986

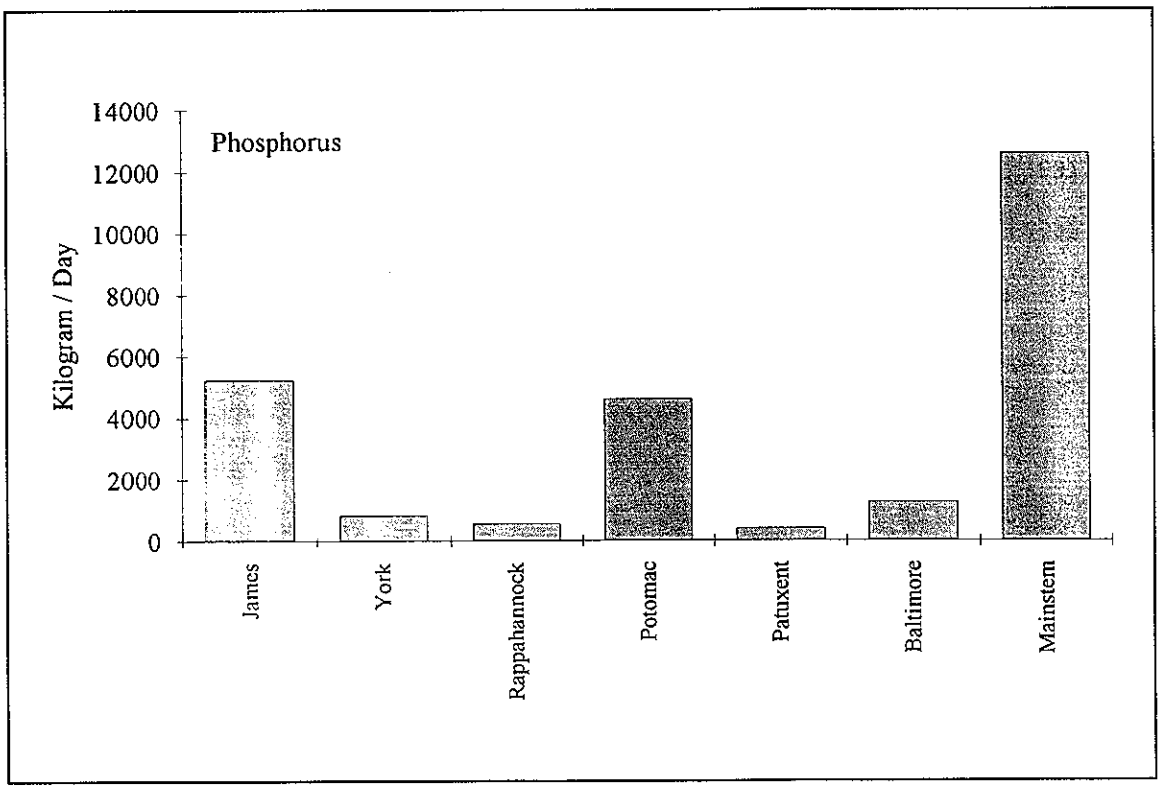

Figure 5-11. Phosphorus Loads by Basin, 1986

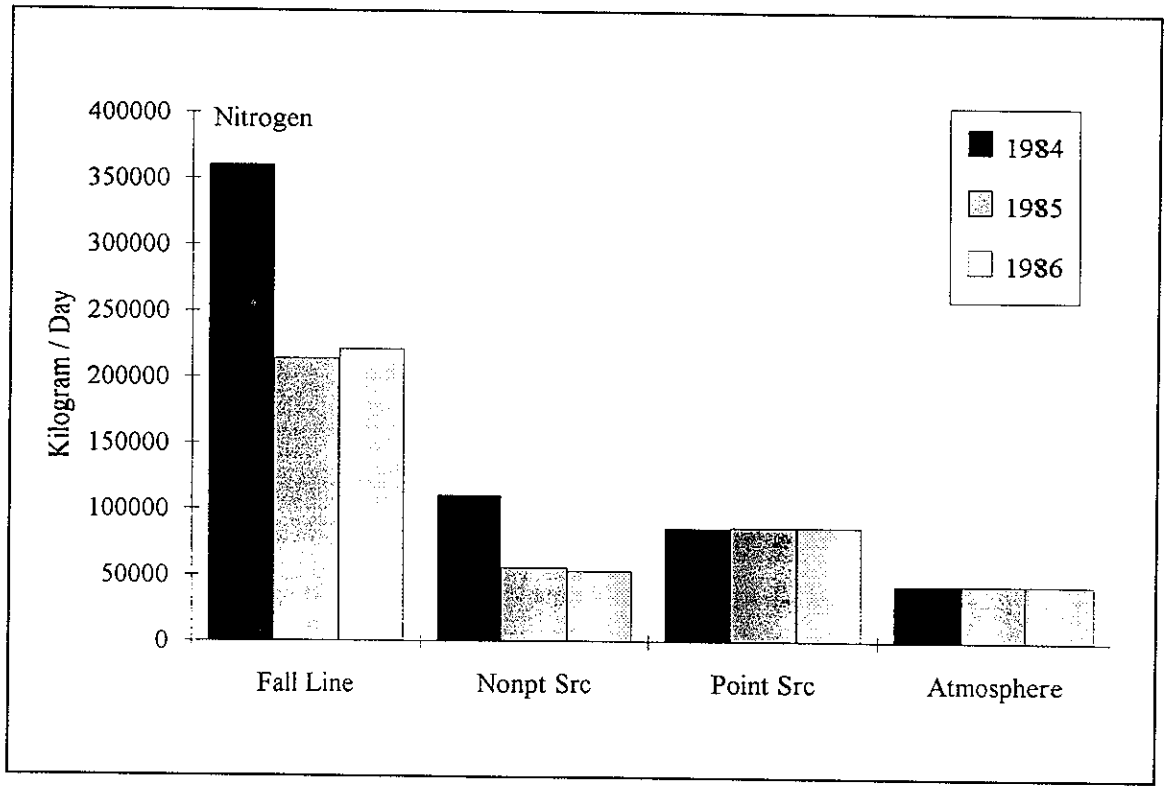

Figure 5-12. Total Nitrogen Loads, 1984-1986

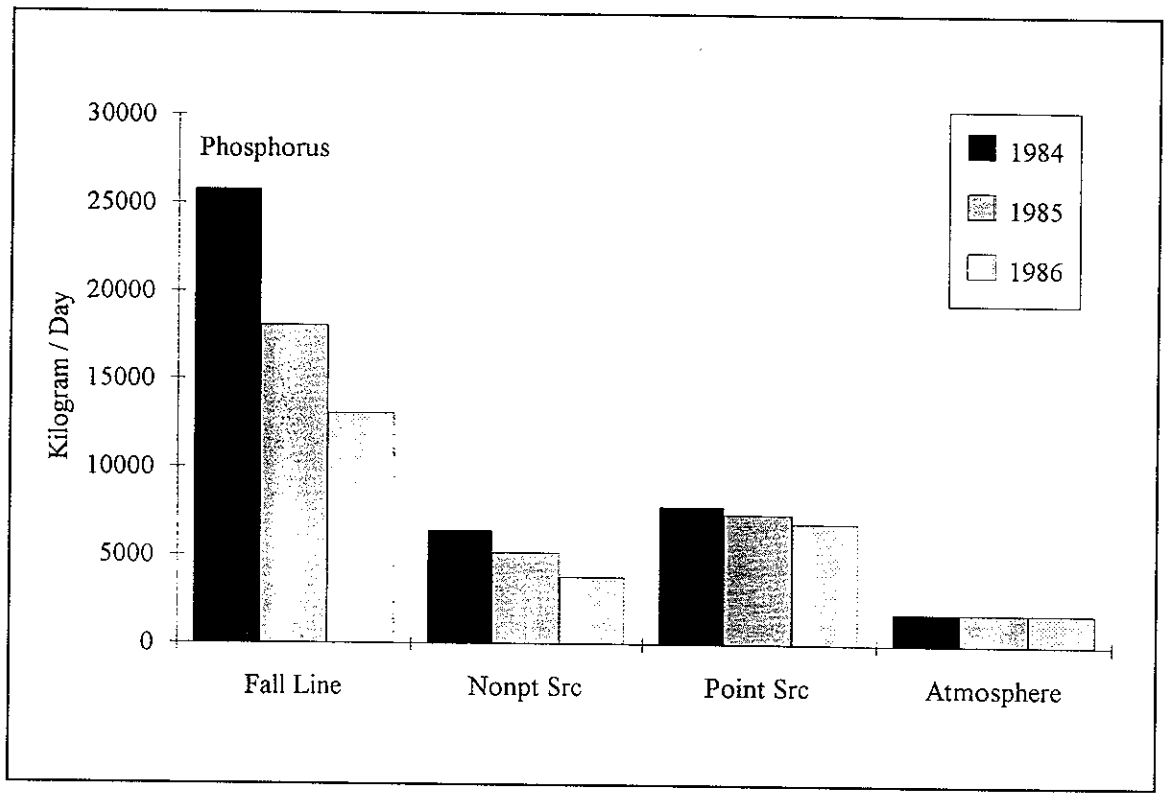

Figure 5-13. Total Phosphorus Loads, 1984-1986

Chapter VI: Linking in the Loads

Introduction

Transfer of fall-line and below-fall-line loads from the watershed model to the water-quality model was largely a software problem. FORTRAN programs were created that read watershed-model output and wrote water-quality-model input files. As part of the transfer, watershed-model state variables required conversion into water-quality-model state variables (Table 6-1). Organic forms of carbon, nitrogen, and phosphorus had to be split into dissolved, labile particulate, and refractory particulate fractions. Similar conversion of substances observed at point sources into water-quality-model state variables was required. The present chapter describes development, from observations, of conversion guidelines and lists parameter values employed in the conversions.

Table 6-1
Variables in Loads and Water-Quality Model

Load Variable	Maps to	Model Variable
Ammonium	—>	Ammonium
Nitrate	—>	Nitrate
Organic Nitrogen	—>	Dissolved Organic Nitrogen, Labile Particulate Organic Nitrogen, Refractory Particulate Organic Nitrogen
Phosphate	—>	Phosphate
Organic Phosphorus	—>	Dissolved Organic Phosphorus, Labile Particulate Organic Phosphorus, Refractory Particulate Organic Phosphorus
Total Organic Carbon	—>	Dissolved Organic Carbon, Labile Particulate Organic Carbon, Refractory Particulate Organic Carbon

Guidelines From Observations

Laboratory Experiments

Labile/refractory splits of loads to the Bay were investigated in a laboratory study. Volumes of water were collected at several fall lines and point sources under dry-weather and storm conditions. The volumes were incubated for fifty days during which seven samples were collected and analyzed for quantities noted in Table 6-2. Fall-line samples were concentrated by centrifuging prior to incubation. The purpose was to determine decay coefficients and labile/refractory splits of organic particles in the volumes. Sampling of multiple point sources and under varying weather conditions was intended to differentiate the splits as a function of treatment level and stormflow.

Table 6-2
Substances Analyzed in Labile/Refractory Experiment

Total Organic Carbon	Nitrate
Dissolved Organic Carbon	Total Phosphorus
Total Kjeldahl Nitrogen	Filtered Total Phosphorus
Filtered Total Kjeldahl Nitrogen	

Analytical procedures in the laboratory prevented full employment of the data as planned. Particle concentrations were determined as the difference between analyses of total and dissolved concentrations. The precision of the dissolved and total analyses was limited such that the difference between the two was often insignificant. Particle concentration was sometimes negative. For some volumes, particle concentration appeared to increase during the incubation. Information was obtained from the data by pooling results of multiple measures and eliminating obviously bad analyses. Isolation of the effects of treatment level and storms was impossible, however.

Dissolved and Particulate Fractions

The particulate and dissolved fractions in the initial point-source samples (Table 6-3) provided guidance for splitting point-source loads of organic substances into dissolved and particulate components.

Since the fall-line volumes were concentrated, the experiments were not utilized to determine dissolved/particulate splits in fall-line loads. Particulate and dissolved fractions from fall-line observations that contained this information were employed. Regression was utilized to determine the dissolved fractions of the total organic concentrations (Table 6-3). Carbon and nitrogen observations at some fall lines (Figure 6-1) indicated a break or maximum in

Table 6-3
Observed Dissolved Fraction of Total Organics

	Carbon		Nitrogen		Phosphorus
	Fraction Dissolved	Maximum, gm m^{-3}	Fraction Dissolved	Maximum, gm m^{-3}	Fraction Dissolved
Point Sources, median	0.80 (n=11)		0.95 (n=11)		0.59 (n=11)
James	0.87	4.4	0.49	0.37	0.04
Mattaponi			0.69		0.19
Pamunkey			0.55		0.14
Rappahannock			0.63		0.15
Potomac	0.74	3.7	0.59	0.44	0.03
Patuxent			0.78		0.13
Susquehanna	0.75	3.8	0.62	0.47	0.04

dissolved concentration. When this break was noted, it was accounted for in the regression and in the determination of model loads.

Labile Fraction of Particles

Labile organic matter is defined in the sediment model as organic matter with a decay coefficient of 0.035 day^{-1} @ 20 C^{o}. At that rate, more than eighty percent of labile (G1) organic matter decays away in fifty days. Less than ten percent of the refractory (G2) component decays away in fifty days. Thus the fraction of organic particles that dissolved during the fifty-day incubations was a first approximation to the labile fraction of the particles. Median labile fractions were defined in this manner for fall-line and point source groupings of the data (Table 6-4).

Table 6-4
Observed Labile Fraction of Organic Particles

	Carbon	Nitrogen	Phosphorus
Point Sources, median	0.70 (n=11)	0.48 (n=6)	0.02 (n=11)
Fall Lines, median	0.22 (n=16)	0.61 (n=14)	0.18 (n=17)

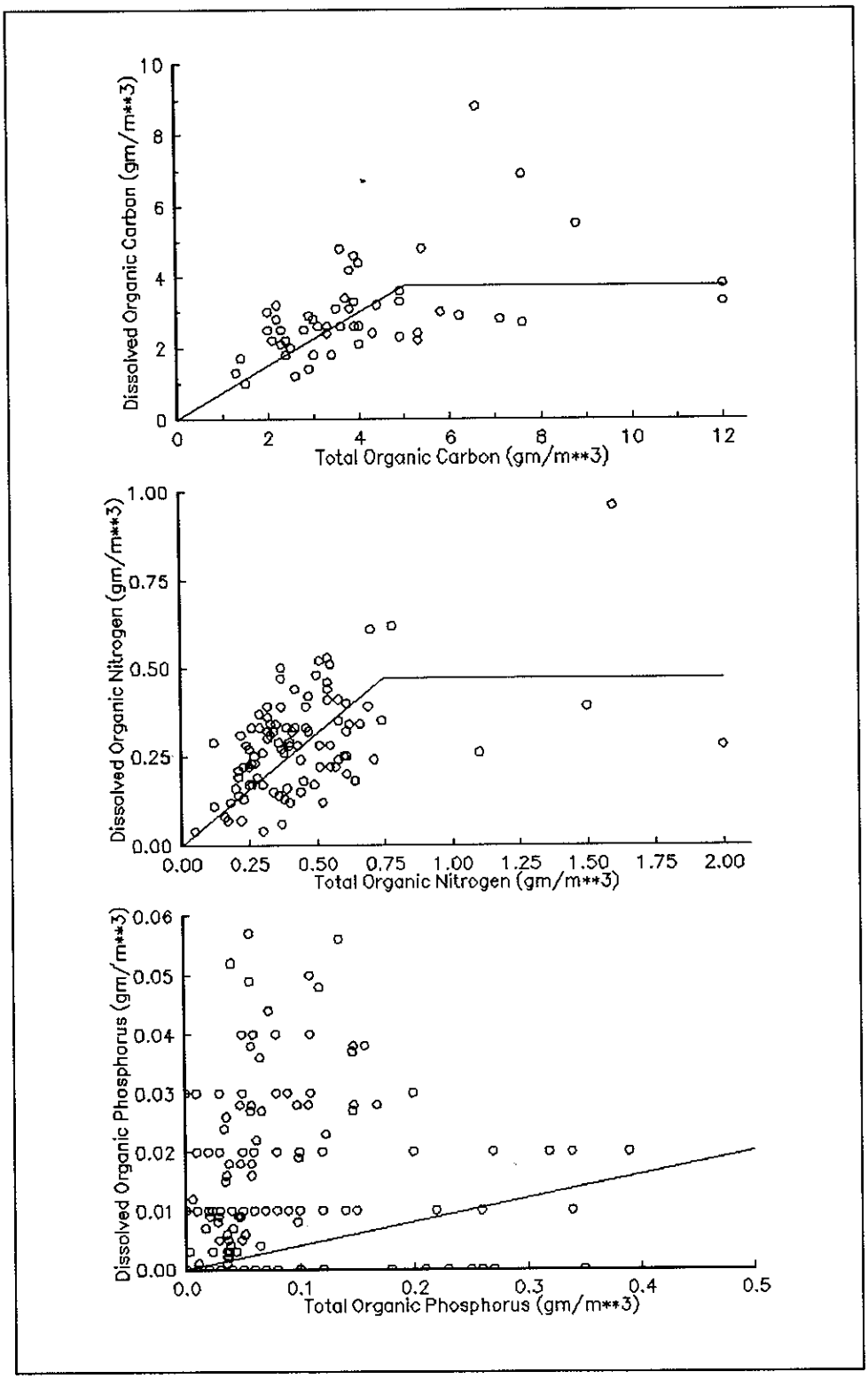

Figure 6-1. Concentrations of Dissolved and Total Organics at Susquehanna Fall Line

Model Parameters

Fractions used to split point-source and fall-line loads of organic substances into dissolved and particulate components were close to observational guidelines (Table 6-5). Below-fall-line loads were split based on adjacent fall lines. Upper limits were enforced on dissolved organic carbon and nitrogen concentrations in fall-line loads.

Table 6-5
Model Dissolved Fraction of Total Organics

	Carbon		Nitrogen		Phosphorus
	Fraction Dissolved	Maximum, gm m^{-3}	Fraction Dissolved	Maximum, gm m^{-3}	Fraction Dissolved
Point Sources	0.8		0.8		0.4
James	0.87	5.0	0.49	0.75	0.04
Mattaponi	0.87	5.0	0.55	0.75	0.14
Pamunkey	0.87	5.0	0.55	0.75	0.14
Rappahannock	0.87	5.0	0.63	0.75	0.15
Potomac	0.74	5.0	0.59	0.75	0.04
Patuxent	0.74	5.0	0.78	0.75	0.13
Susquehanna	0.75	5.0	0.62	0.75	0.04

Labile/refractory splits of particles in point-source loads were based on observed guidelines (Table 6-6). The labile fraction of particles in fall-line and below-fall-line loads was set to zero despite observed indications of a labile component. The refractory nature of the particles was determined during the model calibration process. Sediment nutrient releases near fall lines were excessive when significant fractions of the fall-line loads were considered to be labile.

Table 6-6
Model Labile Fraction of Organic Particles

	Carbon	Nitrogen	Phosphorus
Point Sources	0.7	0.5	0.1
Fall Lines	0.0	0.0	0.0

A rationale for the refractory nature of fall-line loads is that the labile/refractory split depends on season and flow. During low flow and warm weather, fall-line particles are autochthonous and contain a labile component. During cool, wet weather (especially storms), fall-line particles are from land runoff or bed erosion. These particles are refractory. Since the majority of the annual particle load accompanies stormflows, the volume-weighted labile fraction of fall-line loads is negligible.

Chapter VII: The Data Bases

Monitoring Data

The primary source of water-column observations was the monitoring data base maintained by the Chesapeake Bay Program Office. Monitoring data were available from initiation of the program, in June 1984, through the end of 1986. Observations were collected in bay-wide surveys conducted twice monthly in March through October and once monthly in the remaining months. In the Maryland portion of the Bay and in the Virginia portion of the Bay overlying the deep trench, four samples were collected at each station: one meter below the surface, one meter above the bottom, above the pyncnocline, and below the pyncnocline. At the remaining Bay stations and in the tributaries, surface and bottom samples only were collected. Stations sampled and employed in the present study are shown in Figure 7-1.

Sample analyses differed depending upon sample location and analytical laboratory. Substances directly analyzed (or derived from direct analyses) in the mainstem bay, the Patuxent River, and the lower Potomac River are presented in Table 7-1. Substances directly analyzed (or derived from direct analyses) in the upper Potomac River and Virginia tributaries are presented in Table 7-2.

Monitoring data was received from the EPA Chesapeake Bay Program Office in the form of SAS data sets in December 1990 (1986 data), and August 1991 (1984-1985 data). These SAS data sets were appended and processed into a model data base employed for calibration of the water-quality model. Several corrections and revisions were performed on the raw data in preparation of the model data base:

Corrections to Total Kjeldahl Nitrogen

Total Kjeldahl nitrogen in the Maryland portion of the Bay was analyzed using a helix digestion method from June 1984 to May 1985. In May 1985, a block digestion method was introduced. Total Kjeldahl nitrogen analyzed by the helix method was underestimated and inconsistent with the block analysis. Corrections (Bergstrom 1989) were applied to the helix data:

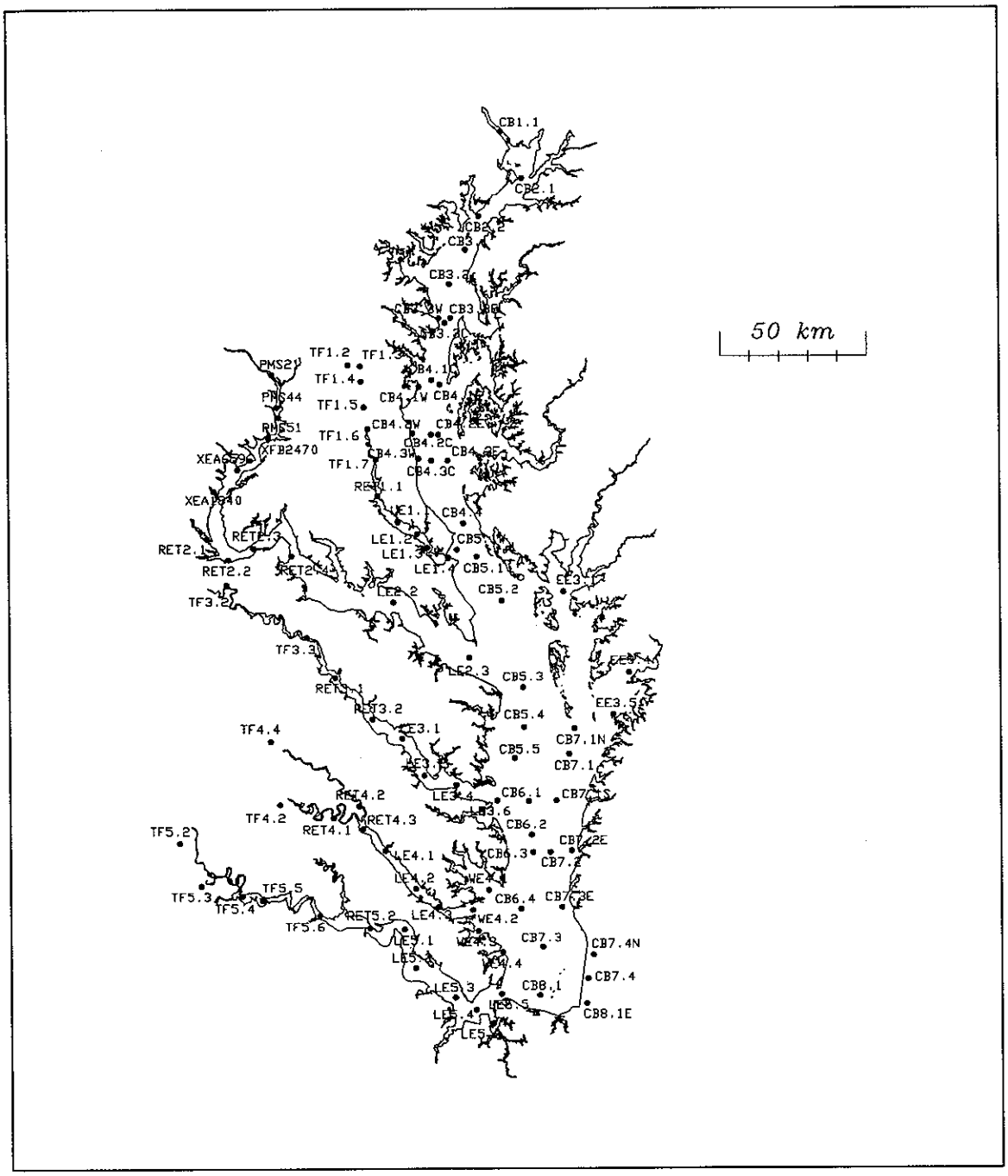

Figure 7-1. Monitoring Program Stations

Table 7-1
Sampled or Derived Substances in Chesapeake Bay, Patuxent, and Lower Potomac Rivers

Temperature	Salinity
Chlorophyll 'a'	Dissolved Organic Carbon
Particulate Organic Carbon	Ammonium
Nitrate+Nitrite	Dissolved Organic Nitrogen
Particulate Organic Nitrogen	Total Nitrogen
Dissolved Phosphate	Dissolved Organic Phosphorus
Particulate Phosphorus	Total Phosphorus
Dissolved Oxygen	Dissolved Silica
Disk Visibility	

Table 7-2
Sampled or Derived Substances in Virginia Tributaries and Upper Potomac River

Temperature	Salinity
Chlorophyll 'a'	Total Organic Carbon
Ammonium	Nitrate+Nitrite
Total Kjeldahl Nitrogen	Total Nitrogen
Dissolved Phosphate	Total Phosphorus
Dissolved Oxygen	Dissolved Silica
Disk Visibility	

$$TKNW_{HA} = 1.75\left(TKNW_{HEL} - 0.07306 + 0.0377 \ln (CHLa)\right) \quad (7\text{-}1)$$

$$TKNF_{HA} = \left(1.55\,(TKNF_{HEL} - 0.1726)\right)^{1/2} \quad (7\text{-}2)$$

in which:

$TKNW_{HA}$ = Corrected whole total Kjeldahl nitrogen (gm m^{-3})
$TKNF_{HA}$ = Corrected filtered total Kjeldahl nitrogen (gm m^{-3})
$TKNW_{HEL}$ = Helix-analyzed whole total Kjeldahl nitrogen (gm m^{-3})

$TKNF_{HEL}$ = Helix-analyzed filtered total Kjeldahl nitrogen (gm m^{-3})
CHLa = chlorophyll 'a' (mg m^{-3})

Deletion of Organic Carbon

At the commencement of the monitoring program, organic carbon in the Maryland portion of the Bay was analyzed via a manual injection method employing Beckman instrumentation. In May 1985, analysis was switched to an automatic injection method employing Ionics instrumentation. A step change occurred in reported organic carbon at the time of the change in methodologies. Due to the lack of precision of the earlier method, organic carbon samples collected in the upper Bay from June 1984 to May 1985 were dropped from the model data base.

Correction to Total Phosphorus

Total phosphorus and total dissolved phosphorus analyses in the Potomac and Patuxent Rivers were mistakenly reported due to failure to adjust sample analyses for blanks. A constant 0.04 gm P m^{-3} was subtracted from Potomac and Patuxent phosphorus measures in the model data base.

Light Extinction Coefficient

Light extinction in Chesapeake Bay was monitored as disk visibility (Secchi depth). Several steps were required to employ these observations in the model. First, an in-situ light extinction coefficient was determined from each observation of disk visibility. Next, extinction due to ambient chlorophyll was removed from the in-situ extinction in order to determine the background extinction due solely to water color and non-algal solids. Finally, spatial and temporal gaps in the discrete observations were filled to provide a continuous light extinction field.

The relationship between disk visibility and light extinction, attributed to Poole and Atkins (Walker 1982), is:

$$Ke\,DV = \kappa \tag{7-3}$$

in which:

Ke = light extinction coefficient (m^{-1})
DV = disk visibility (m)
κ = empirical constant

The value of κ usually ranges from 1 to 2 (Davies-Colley and Vant 1989; Effler 1985; Holmes 1970). Observations in the York River (Webb 1988) and elsewhere (Holmes 1970; Walker 1982) indicate $\kappa \approx 1.4$ in turbid coastal

waters. The value $\kappa = 1.44$ was used to convert in-situ secchi depths to extinction coefficients.

A linear relationship was employed to remove the effect of chlorophyll from in-situ extinction coefficients:

$$Keb = Ke - Kechl\ CHLa \qquad (7\text{-}4)$$

in which:

Keb = background light extinction (m^{-1})
Kechl = light attenuation coefficient of chlorophyll 'a' ($m^2\ mg^{-1}$)
CHLa = chlorophyll 'a' ($mg\ m^{-3}$)

The magnitude of Kechl is ≈ 0.01 to $0.03\ m^2\ mg^{-1}$ (Pennock 1985). The value Kechl = 0.017 was employed on the monitoring data. (The algal component of light extinction, based on predicted chlorophyll, was recombined with background extinction during model computations.)

Daily time series of light extinction at each monitoring station were created by relating extinction to fall-line flow:

$$Keb = Keo + \gamma Q \qquad (7\text{-}5)$$

in which:

Keo = minimum light extinction (m^{-1})
Q = fall-line flow ($ft^3\ sec^{-1}$)
γ = incremental effect of flow on extinction ($sec\ ft^{-3}\ m^{-1}$)

The relationship employed fall-line flow as a surrogate for suspended solids load and location of the turbidity maximum, two factors that influence extinction. Parameters in the relationship were evaluated via regression of derived background extinction on flow. Significant relationships occurred at stations in the upper Bay and in major tributaries (Table 7-3). Superior correlations were obtained for some stations when flow was lagged several days. The lag was interpreted as the time required for the influence of fall-line flows to travel down the estuary.

Monthly averages of daily extinction were employed as model input. For stations where no significant regression was obtained, monthly averages of observed extinction were employed. The model grid was divided into regions, each containing a monitoring station. Extinction in model cells within the region was specified as the monthly value at the monitoring station.

Table 7-3
Relation of Light Extinction to Fall-Line Flow

Basin	Station	R^2	$p \leq$	Keo, m^{-1}	γ, 10^{-6} sec ft^{-3} m^{-1}	lag, days
James	TF5.3	0.72	0.0001	1.07	101	3
	TF5.4	0.39	0.0058	2.21	104	10
	TF5.5	0.78	0.0001	1.62	126	10
	TF5.6	0.56	0.0008	1.17	370	10
	LE5.1	0.70	0.0002	0.83	471	11
	RET5.2	0.62	0.0001	1.57	308	11
	LE5.2	0.40	0.0117	0.57	321	11
	LE5.3	0.52	0.0003	1.51	24.5	11
	LE5.4	0.35	0.0208	0.89	94.3	18
	LE5.6	0.55	0.0038	0.70	192	18
York	LE4.2	0.52	0.0002	1.09	321	18
	RET4.3	0.47	0.0098	1.66	496	17
Rappahannock	TF3.3	0.91	0.0001	2.02	1320	7
	RET3.1	0.33	0.0051	2.12	996	7
Potomac	PMS01	0.21	0.0278	2.10	134	0
	PMS21	0.65	0.0001	0.90	95.4	0
	PMS29	0.51	0.0001	1.37	73.3	0
	PMS37	0.53	0.0001	1.55	71.9	0
	PMS44	0.60	0.0001	1.58	76.7	0
	PMS51	0.48	0.0007	1.49	79.7	0
	RET2.1	0.83	0.0001	2.06	96.9	16
	RET2.2	0.74	0.0001	2.20	39.3	16
	RET2.3	0.75	0.0001	2.21	37.8	16
	RET2.4	0.45	0.0001	1.55	10.0	16
	XEA1840	0.52	0.0001	2.35	38.5	16
	XFB1433	0.37	0.0058	1.97	131	1
	LE2.2	0.18	0.0032	0.95	19.4	19
Chesapeake Bay	CB1.1	0.53	0.0001	1.09	16.3	4
	CB2.2	0.38	0.0001	1.81	19.3	4
	CB3.1	0.37	0.0001	1.27	21.6	4
	CB3.2	0.42	0.0001	0.97	16.1	4
	CB3.3C	0.37	0.0001	0.78	7.18	9
	CB3.3E	0.45	0.0001	0.69	8.30	9
	CB3.3W	0.39	0.0001	0.90	7.86	9
	CB4.1C	0.28	0.0001	0.60	3.67	9
	CB3.1E	0.24	0.0001	0.62	2.81	9
	CB4.2C	0.16	0.0005	0.57	1.49	9

Supplementary Monitoring Data

The interval selected for model application commenced in January 1984 while the EPA monitoring program did not start until June 1984. Observations for the first five months of 1984 were obtained from two sources. Data

collected by Mary Tyler was obtained by WES in July 1989. The Tyler data base contained only salinity, temperature, chlorophyll, and dissolved oxygen, but was spatially extensive (Figure 7-2).

Observations collected during trial surveys prior to commencement of regular monitoring were obtained from the Maryland Department of the Environment, also in 1989. The Maryland observations included most of the analyses listed in Table 7-1 but were limited to three locations, coincident with monitoring stations CB3.3C, CB5.1, CB5.1W (Figure 7-1).

Primary Production

Primary production observations in the upper Bay, Potomac and Patuxent Rivers (Figure 7-3) were supplied by the Academy of Natural Sciences (Sellner 1989). The observations were short-term ($\approx$ 1 hour) measures of carbon-14 fixation in surface water samples. Measures were conducted on shipboard at saturated light intensity. Sellner converted measured hourly rates to estimated daily rates:

$$NPPD = NPPH\ EZH\ \beta_1\ \beta_2\ HDL \qquad (7\text{-}6)$$

in which:

NPPD = daily net primary production (gm C m^{-2} day^{-1})
NPPH = hourly net primary production (gm C m^{-3} hr^{-1})
EZH = euphotic zone depth (depth to 1% light penetration) (m)
β_1 = factor that converts light-saturated primary production to average over photic zone ($\beta_1 = 0.5$)
β_2 = factor that accounts for light-limited primary production at sunrise and sunset ($\beta_2 = 0.8$)
HDL = hours of daylight (hr day^{-1})

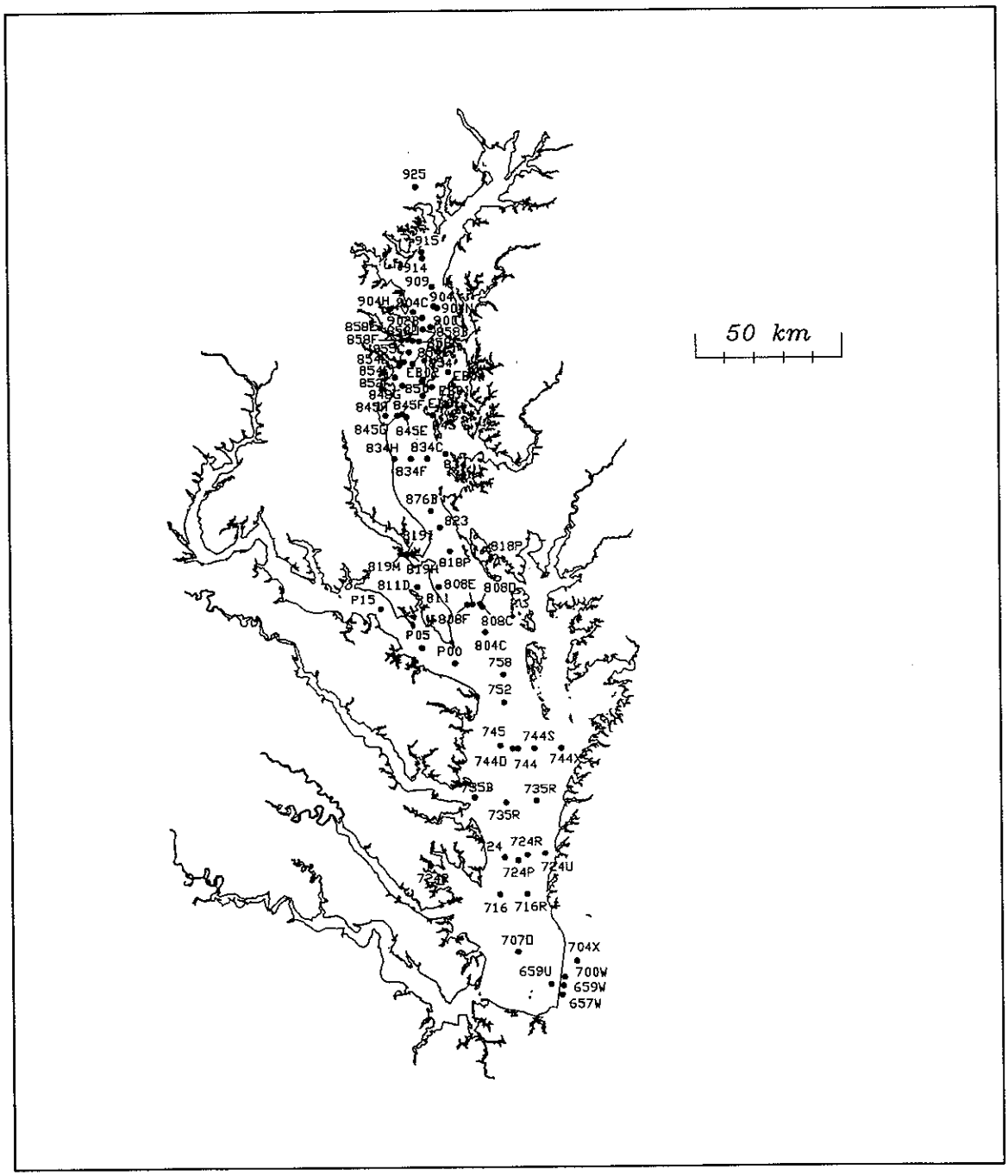

Figure 7-2. Tyler Data Stations

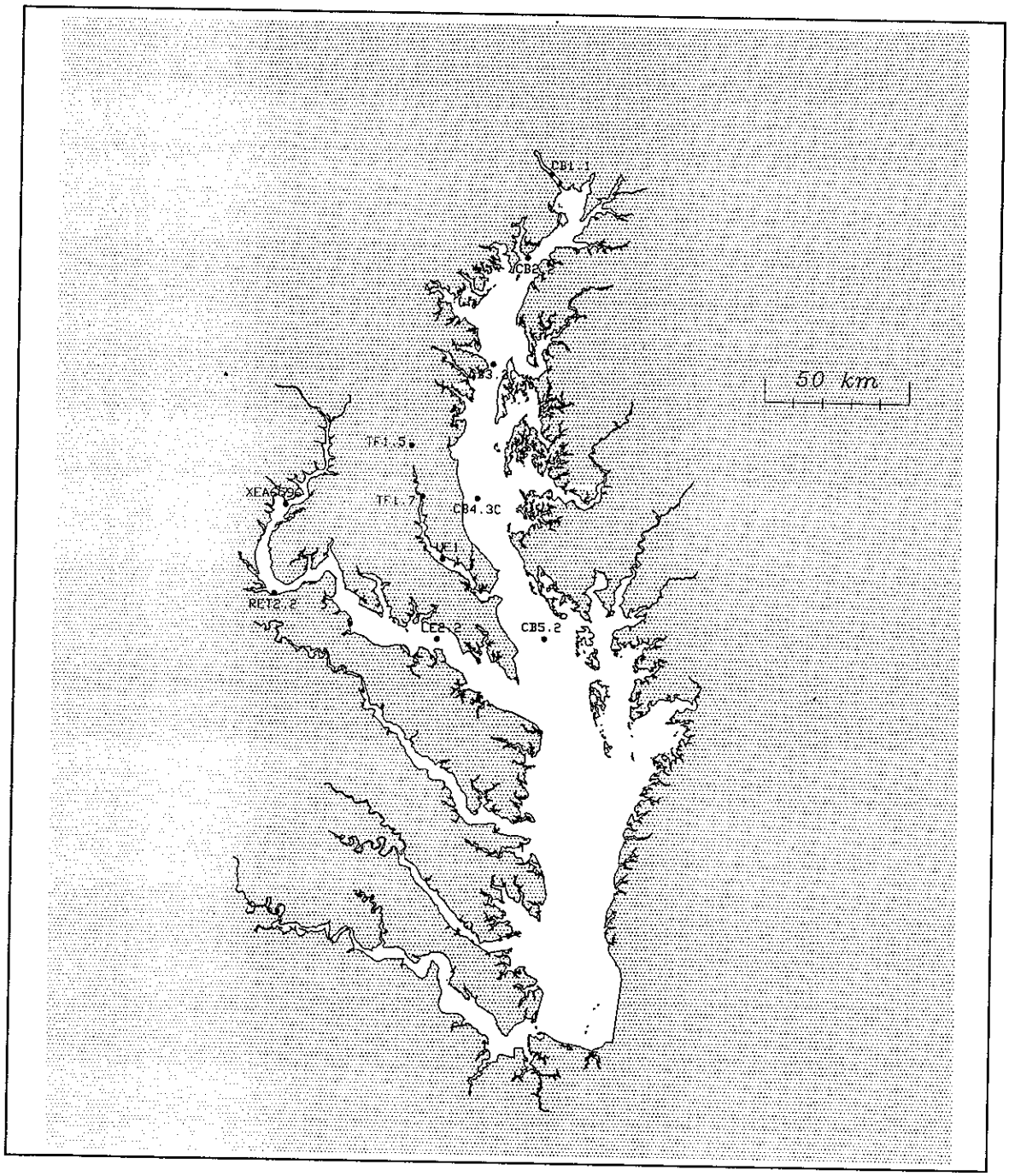

Figure 7-3. Primary Production Stations

Chapter VIII: Boundary Conditions

Introduction

Specification of boundary conditions was required at the fall lines of major tributaries and at the interface with the ocean. Specification of boundary conditions amounted to evaluation at the boundary of the concentration C^* and the longitudinal derivative $\delta C/\delta x$ in the conservation of mass equation (Equation 4-1). Advective boundary conditions in the Bay model were of the "upwind" type. Evaluation of C^* depended on the direction of flow at the boundary. When flow was out of the model, as near the surface at the ocean interface, C^* was assigned the concentration in the model cell immediately upstream of the boundary. When flow was into the model, as at the fall lines and near the bottom at the ocean interface, C^* was assigned a specified value representative of conditions outside the model domain. Diffusive boundary conditions were set by specifying $\delta C/\delta x = 0$ at the boundaries.

Fall-Line Boundary Conditions

Inflow boundary conditions were required at the fall lines of major tributaries: the James, Mattaponi, Pamunkey, Rappahannock, Potomac, Patuxent, and Susquehanna Rivers. Inflows at lesser tributaries were considered negligibly small and not included in the model. Boundary conditions were specified at monthly intervals. Temperature of inflowing water was set to monthly mean equilibrium temperature. Concentrations of total active metal and chemical oxygen demand in inflowing water were considered to be zero. Concentrations of nitrogen, phosphorus, and carbon were also set to zero. These constituents were input to the model directly as loads rather than as the product of concentration and flow crossing boundary interfaces.

Algae

Algal concentrations at the fall lines were derived from chlorophyll observations. Characteristic chlorophyll concentrations (Table 8-1) were converted

Table 8-1
Chlorophyll Concentrations at Fall Lines

River	Chlorophyll, (mg m^{-3})	River	Chlorophyll, (mg m^{-3})
James	3.0	Potomac	5.0
Pamunkey	3.0	Patuxent	3.0
Mattaponi	3.0	Susquehanna	5.0
Rappahannock	3.0		

to carbonaceous biomass using the model carbon-to-chlorophyll ratio. No temporal variability was considered. Fall-line algae were considered half diatoms and half green algae. No blue-greens were included in fall-line loads. As an alternative to a fall-line boundary, a blue-green algal seed (100 kg/day) was planted in the Potomac River, in the vicinity of Gunston Cove, in the spring of each year.

Dissolved Oxygen

A sinusoidal function was fit to dissolved oxygen observations at each fall line:

$$DO = a_1 + a_2 \sin\frac{2\pi\,jday}{365} + a_3 \cos\frac{2\pi\,jday}{365} + a_4 \sin\frac{2\pi\,jday}{182.5} + a_5 \cos\frac{2\pi\,jday}{182.5} \quad (8\text{-}1)$$

in which:

DO = dissolved oxygen (gm m^{-3})
a_1, a_2, a_3, a_4, a_5 = empirical constants (gm m^{-3})
jday = julian day

Constants in the relationship were derived by linear regression on the observations (Table 8-2). The function was used to calculate daily dissolved oxygen concentrations which were averaged into monthly values (Figure 8-1) for input to the model.

Silica

Fall-line dissolved silica loads were computed using an MVUE (minimum variance, unbiased estimator) regression package (Cohn et al. 1989). Loads for each month of the simulation were converted to concentrations (Figure 8-1)

Table 8-2
Constants in Fall-Line Dissolved Oxygen Relationship

River	a_1	a_2	a_3	a_4	a_5	R^2
James	10.06	1.37	2.73		0.40	0.85
Pamunkey	9.38	1.38	3.18	0.41	0.49	0.87
Mattaponi	9.37	1.10	2.81	0.27	0.56	0.89
Rappahannock	10.3	0.9	2.93			0.83
Potomac	11.2	1.14	3.19	0.14	0.14	0.84
Patuxent	8.22	1.98	3.08	0.39		0.86
Susquehanna	9.61	2.97	4.13	-0.50		0.91

through division by monthly flows. Fall-line concentrations of particulate silica were set to zero.

Oceanic Boundary Conditions

Oceanic boundary conditions for salinity, temperature, algae, organic carbon, dissolved oxygen, and dissolved silica were specified based on monitoring data collected at stations spanning the Bay mouth (Figure 3-1). Observations were averaged by month into three depth intervals: 0 to 6.7 m, 6.7 to 12.8 m, and > 12.8 m (Figure 8-2). Concentrations in oceanic water flowing into model cells were assigned according to the depth interval of the cell. Chlorophyll concentrations were converted to carbonaceous biomass using the model carbon-to-chlorophyll ratio. Oceanic algae were considered half diatoms and half green algae. Oceanic concentrations of total active metal, chemical oxygen demand, and particulate biogenic silica were set to zero.

Nitrogen and Phosphorus

Dissolved and particulate substances that exit the Bay mouth are not permanently removed from the system. Water that leaves the Bay mixes with shelf water and is returned to the Bay by interactions of physical processes including wind, along-shelf currents, and density-driven circulation (Boicourt et al. 1987, Goodrich et al. 1989). Strong evidence exists that physical processes trap and return crab larvae that are advected out of the Bay (Goodrich et al. 1989). Nutrients leaving the Bay must also be recycled along with water volumes and associated particulates. Recycling of nutrients outside the Bay mouth suggests a linkage between nutrient loads to the Bay and nutrient concentration in inflowing water. If nutrient concentration in water leaving the Bay declines due to load reductions, then concentration in the mixture entering the Bay declines as well.

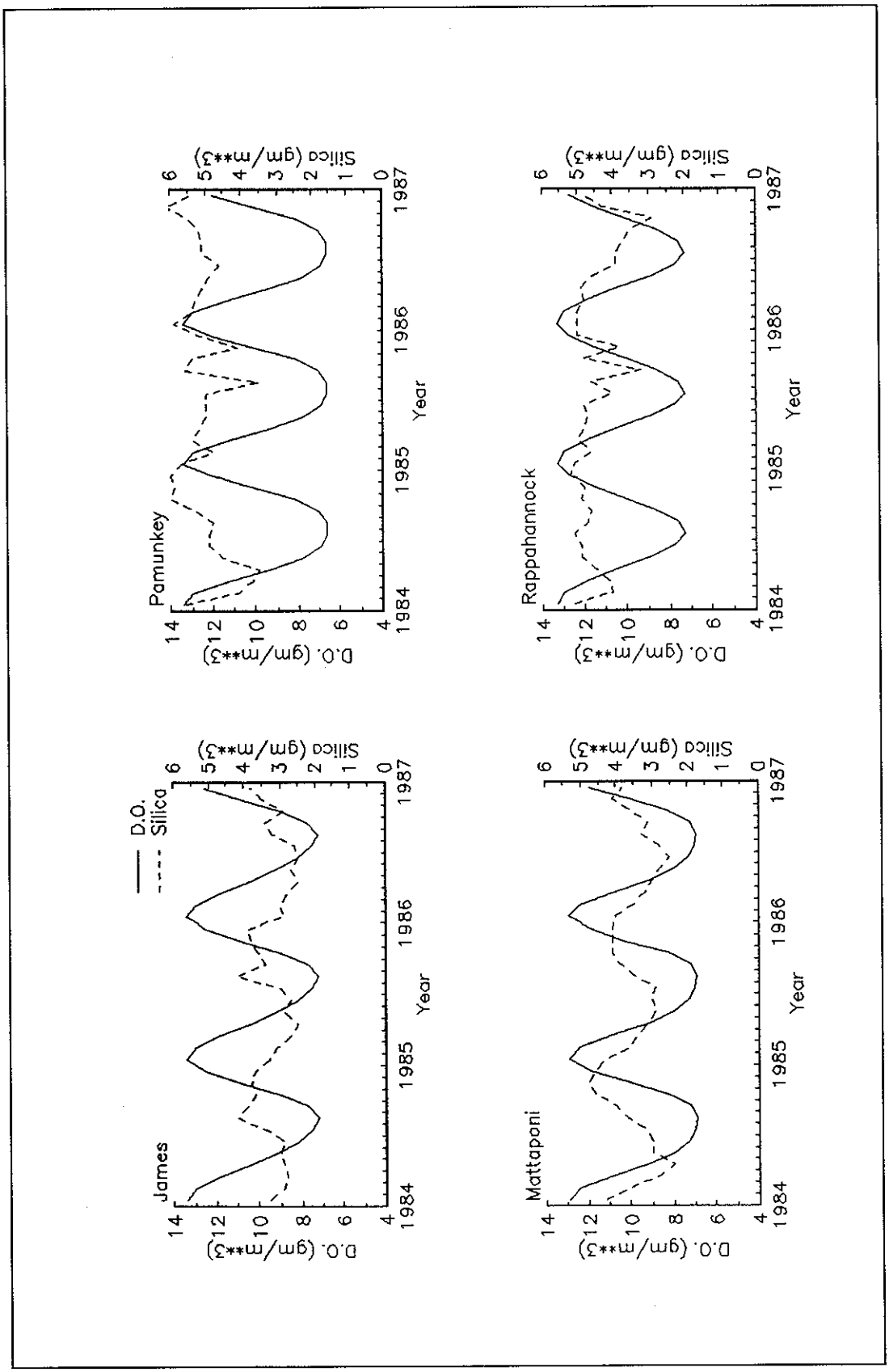

Figure 8-1. Fall-line Dissolved Oxygen and Dissolved Silica Concentrations (Continued)

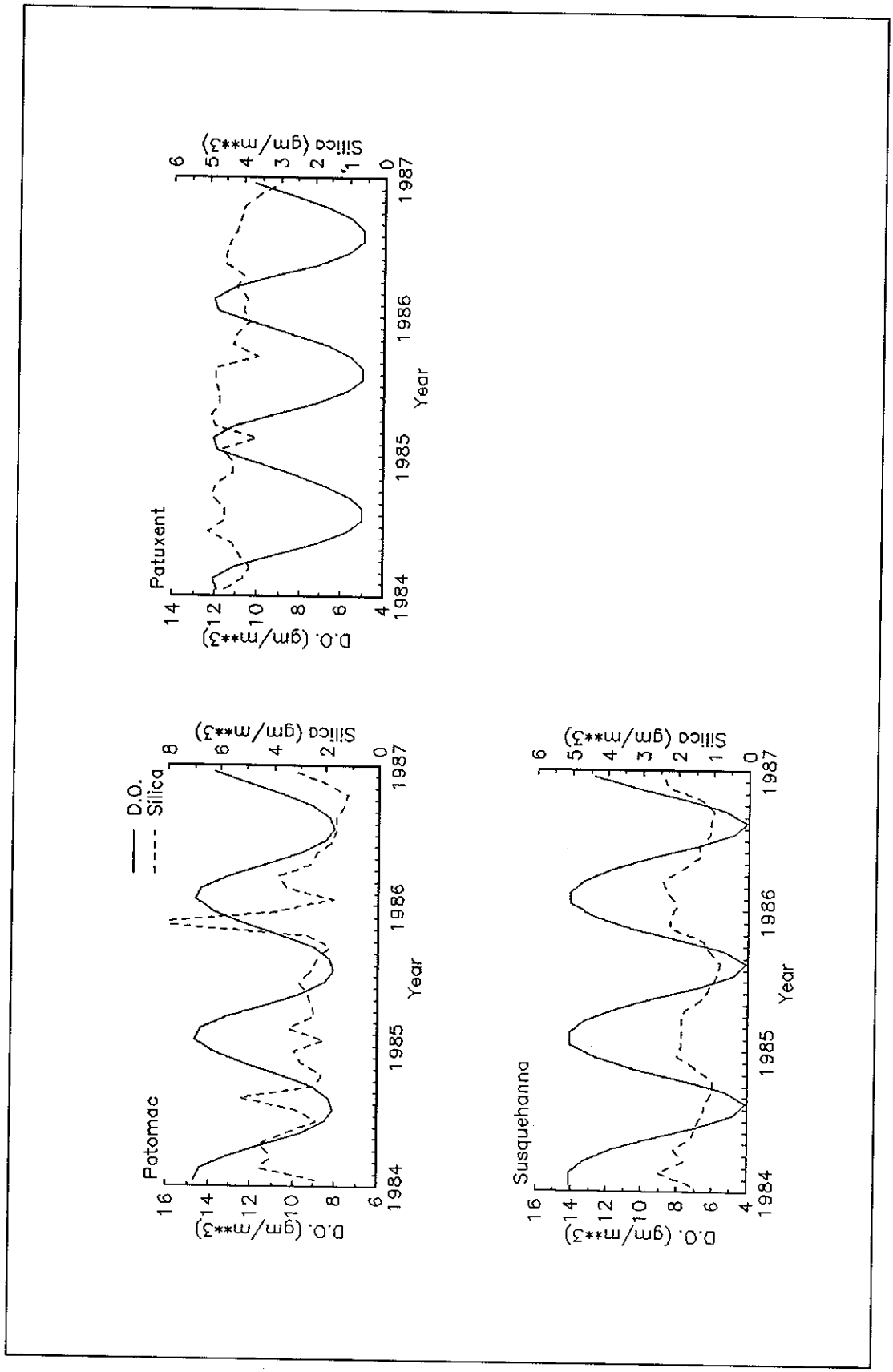

Figure 8-1. (Concluded)

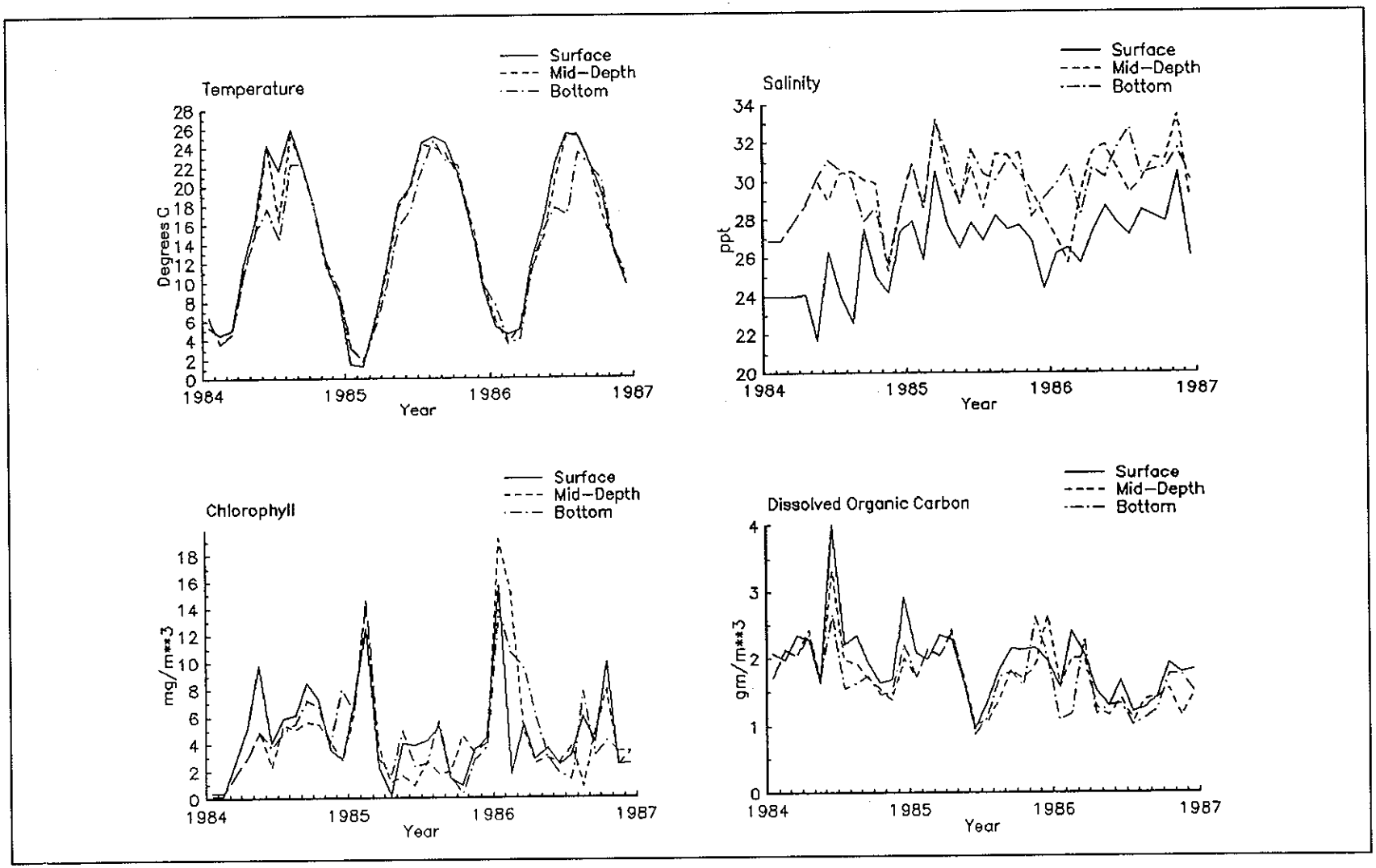

Figure 8-2. Temperature, Salinity, Chlorophyll, Organic Carbon, Dissolved Oxygen, and Dissolved Silica Concentrations Specified at Bay Mouth (Continued)

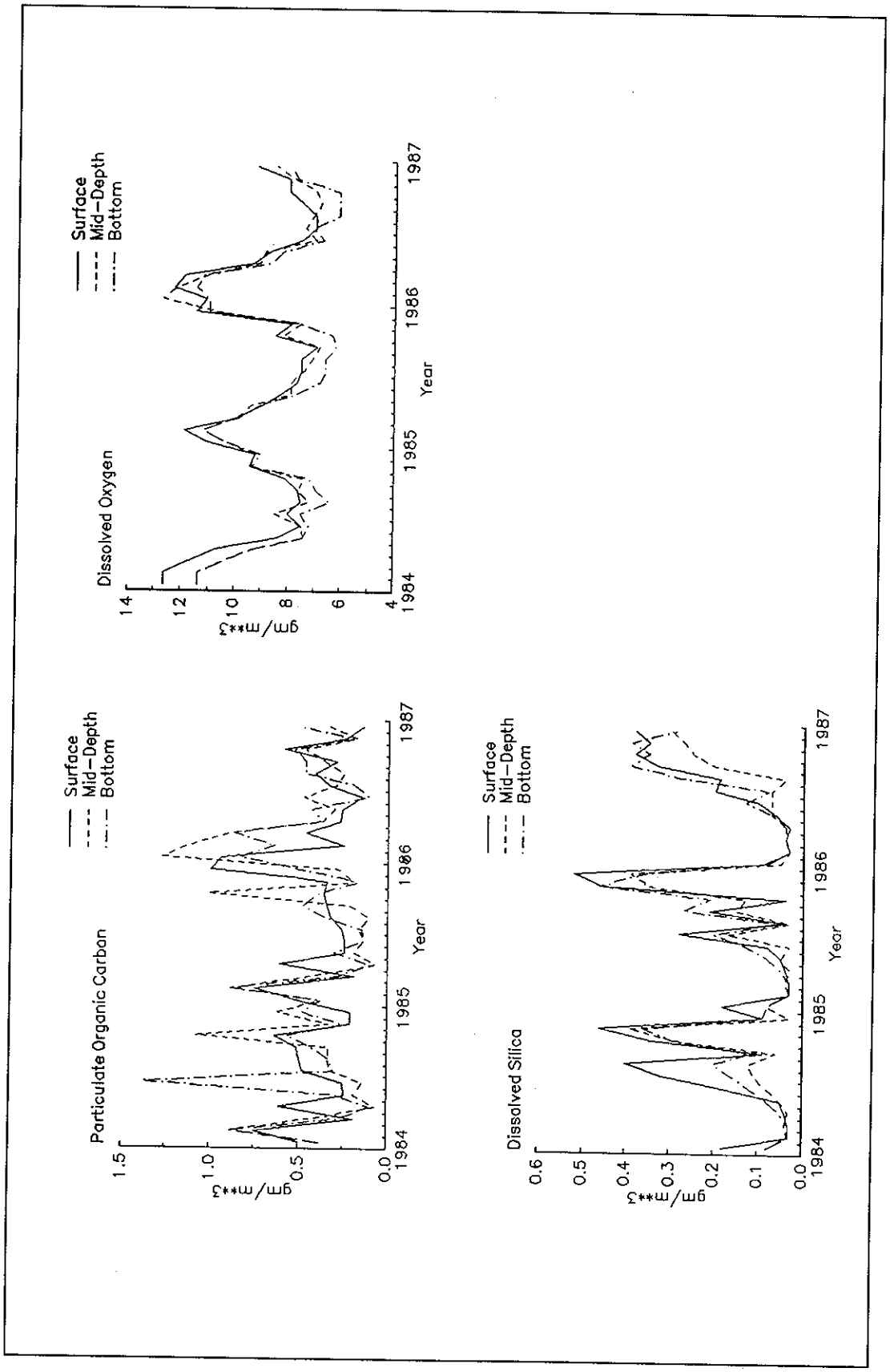

Figure 8-2. (Concluded)

Table 8-3
Median Nutrient Concentrations Entering Chesapeake Bay

Nutrient	Station	1984-1986	1987-1990
Total Nitrogen, gm m^{-3}	CB7.4 (bottom)	0.43	0.23
	CB7.4N (bottom)	0.42	0.24
Total Phosphorus, gm m^{-3}	CB7.4 (bottom)	0.052	0.033
	CB7.4N (bottom)	0.054	0.036

The hypothesis of coupling between loads and inflow nutrient concentrations was supported by a summary of monitoring data (Bieber and Magnien 1991a; 1991b) that indicated a decline in nitrogen and phosphorus concentrations at the Bay mouth (Table 8-3). The decline in phosphorus occurred concurrent with a phosphate detergent ban in Virginia. The origin of the nitrogen decline was ambiguous and affected to an unknown extent by a change in analytical methods. The potential dependence of inflow boundary conditions on loads had large implications on specification of boundary conditions during load-reduction scenarios. If boundary conditions were affected by loads, then the scenario boundary conditions required alteration from existing conditions.

To account for potential changes in boundary conditions during load-reduction scenarios, a mass-balance boundary condition was derived and employed to set nutrient boundary conditions for the scenarios. To maintain consistency between calibration and scenarios, the mass balance was employed in the calibration as well.

Mass-Balance Boundary Condition[1]

Assume a well-mixed volume of water exists between the Bay mouth and an infinite reservoir of continental shelf water (Figure 8-3). A steady-state mass balance for the volume is:

$$Qu\,Cu + E\,(Csh - Cb) = Qf\,Cb + Qb\,Cb \qquad (8\text{-}2)$$

in which:

Qu = volumetric flow leaving Bay ($L^3\ T^{-1}$)
Cu = concentration in flow leaving Bay ($M\ L^{-3}$)

[1]This section was adapted from an analysis provided by Dominic DiToro of HydroQual, Inc.

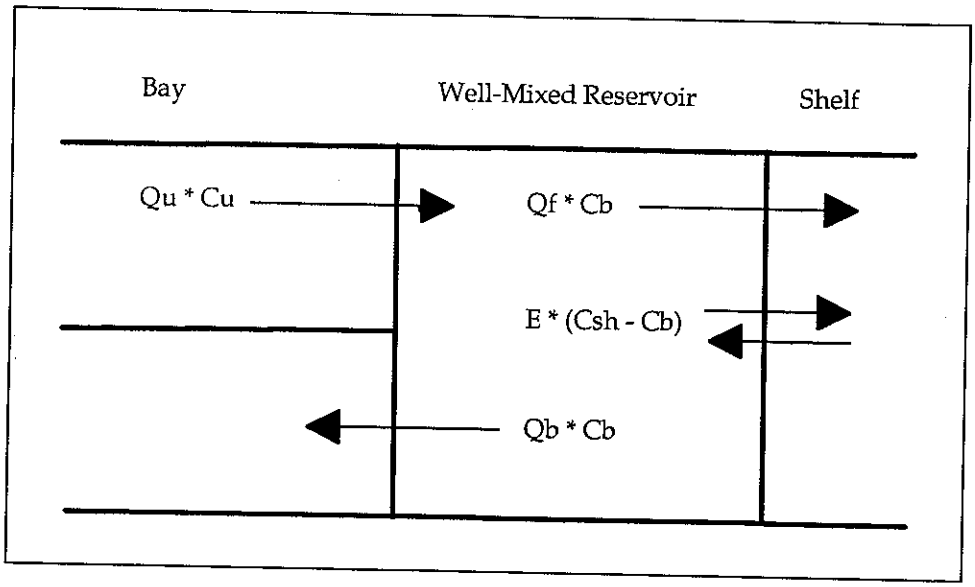

Figure 8-3. Mass-Balance Boundary Condition

E = exchange coefficient between well-mixed volume and shelf reservoir ($L^3\ T^{-1}$)
Csh = concentration in continental shelf reservoir ($M\ L^{-3}$)
Cb = concentration in well-mixed volume ($M\ L^{-3}$)
Qf = freshwater runoff into Bay ($L^3\ T^{-1}$)
Qb = volumetric flow from well-mixed volume into Bay ($L^3\ T^{-1}$)

The mass balance indicates concentration in water entering the Bay is a mixture of concentrations in shelf water and in water leaving the Bay:

$$Cb = \frac{Qu}{Qu + E} Cu + \frac{E}{Qu + E} Csh \qquad (8\text{-}3)$$

Equation 8-3 contains two unknowns: the proportions in the mixture and the concentration of the shelf reservoir. The proportions were determined from a salt balance on the well-mixed volume, employing the known salinity of the world's oceans. Equation 8-3 was simplified to yield:

$$Sb = \alpha\, Su + (1 - \alpha)\, Ssh \qquad (8\text{-}4)$$

in which:

Sb = salinity of water entering the Bay mouth (ppt)
Su = salinity of water leaving the Bay mouth (ppt)
Ssh = salinity of continental shelf (35 ppt)
α = proportionality constant ($0 \leq \alpha \leq 1$)

The constant α indicates the fraction of inflowing mass that is made up of mass that previously left the Bay.

A map was drawn of Lagrangian flows at the Bay mouth computed by the hydrodynamic model (Figure 8-4). This map was superimposed on station locations and sample depths to determine the observations that characterized water entering the Bay. These were the bottom samples collected at stations CB7.4 and CB7.4N. Once inflowing salinities were known, Equation 8-4 was solved on a monthly basis for the unknown α (Table 8-4). Evaluation of α indicated a large fraction of Bay water ($\approx$75%) was recycled during autumn and winter months while a lesser fraction ($\approx$50%) was recycled during spring and summer.

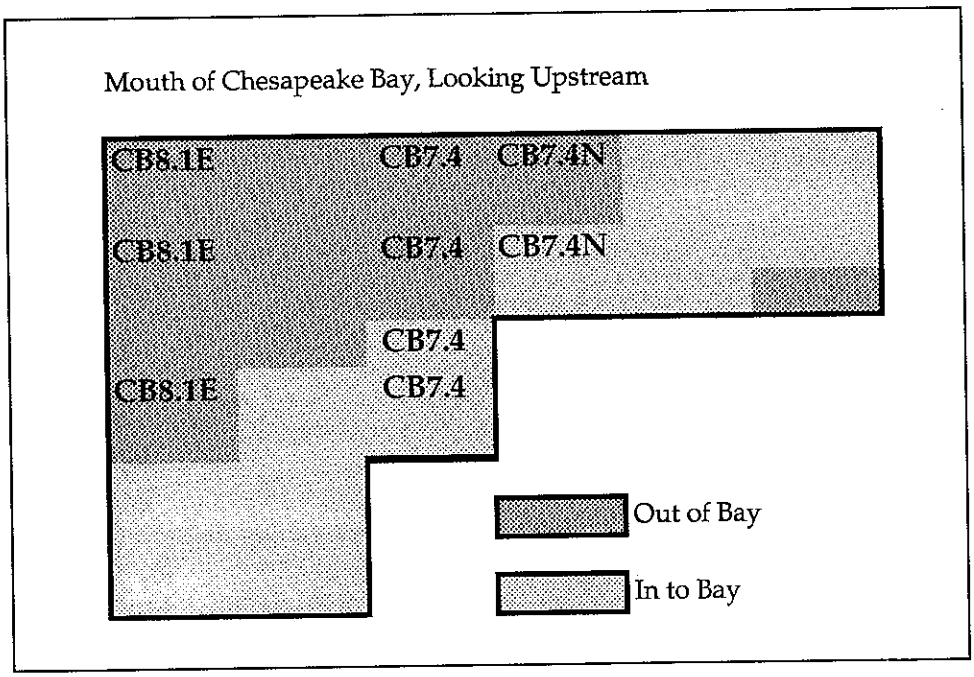

Figure 8-4. Annual Average Lagrangian Flows (1986) and sample Stations at Bay Mouth

Shelf concentrations of nitrogen and phosphorus were obtained by substituting into Equation 8-4 the proportionality constants and observed concentrations entering and leaving the Bay. Annual average shelf concentrations were derived for 1984-1986. These were averaged into a grand mean for use in the model (Table 8-5).

Comparison of 1984-1986 observations from stations assigned to outflow and stations assigned to inflow indicated no mean difference in total nitrogen (Table 8-6). At times, outflow concentration exceeded inflow concentration while at other times, inflow concentration exceeded outflow concentration (Figure 8-5). Inflow concentration computed by mass balance exhibited fluctuations but showed no distinct trends or cycles. Mean computed inflow concentration was less than mean observed outflow concentration.

Table 8-4
Proportionality Constants in Mass Balance

Month	α	Month	α
January	0.84	July	0.64
February	0.68	August	0.54
March	0.42	September	0.58
April	0.44	October	0.80
May	0.55	November	0.66
June	0.49	December	0.73

Table 8-5
Concentrations Derived for Shelf Reservoir

Constituent	gm m^{-3}	Constituent	gm m^{-3}
Ammonium	0.011	Phosphate	0.015
Nitrate	0.009	Dissolved Organic Phosphorus	0.01
Dissolved Organic Nitrogen	0.3	Particulate Organic Phosphorus	0.028
Particulate Organic Nitrogen	0.05		

Table 8-6
Mean Total Nitrogen and Phosphorus Boundary Conditions, 1984-1986

	Total Nitrogen, gm m^{-3}	Total Phosphorus, gm m^{-3}
Observed Outflow	0.45	0.043
Observed Inflow	0.45	0.056
Mass–Balance Inflow	0.42	0.047
Ocean, Computed by Mass–Balance	0.37	0.053

Observed inflow phosphorus concentrations were clearly and consistantly greater than outflow concentrations (Table 8-6). Particularly evident in the observations was a late 1985 event in which inflow concentrations were nearly double the concentrations observed in the remainder of 1984-1986 (Figure 8-6). The high inflow concentrations were not associated with corrresponding outflow observations, however. Periodicity was evident in computed

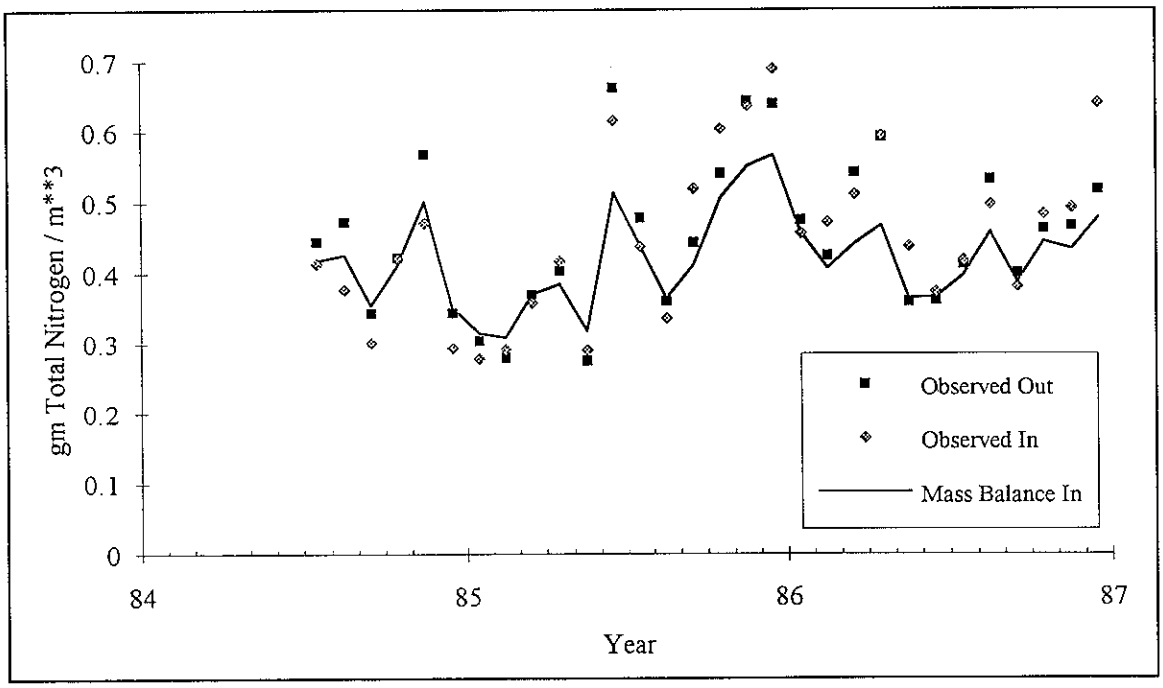

Figure 8-5. Total Nitrogen, Observed and Computed by Mass Balance, at Bay Mouth, 1984-1986

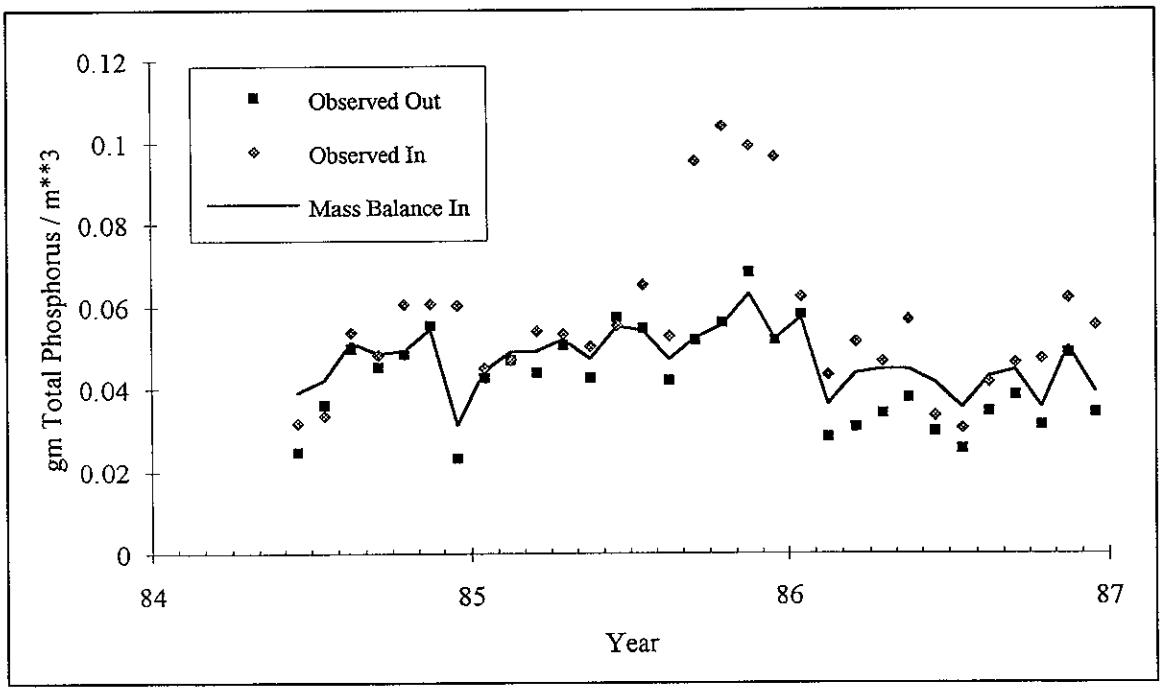

Figure 8-6. Total Phosphorus, Observed and Computed by Mass Balance, at Bay Mouth, 1984-1986

inflow concentrations while fluctuations were less pronounced than for nitrogen. Mean computed inflow concentration exceeded mean observed outflow concentration.

Chapter IX: Parameter Evaluation

Introduction

Model parameter evaluation is a recursive process. Parameters are selected from a range of feasible values, tested in the model, and adjusted until optimal agreement between predicted and observed variables is obtained. Ideally, the range of feasible values is determined by observation or experiment. For some parameters, however, no observations are available. Then, the feasible range is determined by parameter values employed in similar models or by the judgement of the modeler. The present chapter reports model parameter values selected for the final calibration of the water quality model. Parameters appear roughly in the order in which they were presented in Chapter IV. Experimental or observed parameter values, when available, are presented for comparison with model parameters.

Algae

Production

Maximum growth rates and their temperature dependence were based on observational summaries produced by Canale and Vogel (1974) supplemented with additional values provided by Collins and Wlosinski (1983). Reported growth rates were subject to in-situ nutrient limitations. Since the maximum growth rates employed by the model were for nutrient-unlimited situations, parameter values (Table 9-1) were selected to provide an envelope around maximum reported rates (Figures 9-1 to 9-3) based on the assumption that maximum reported rates were independent of nutrient limitations. Employment of the maximum rates reported for the cyanobacteria group proved unsuited for the *microcystis* genus found in the upper Potomac, however. The temperature relationship employed for *microcystis* was less than the cyanobacteria maximum at temperatures greater than ≈25 C°.

Table 9-1
Algal Growth Rates and Temperature Parameters

Group	Parameter	Value	Units
Cyanobacteria	PMc	2.5 (Upper Potomac only)	day^{-1}
	Tmc	27.5	C°
	KTgc1	0.005	$C^{\circ -2}$
	KTgc2	0.004	$C^{\circ -2}$
	Stox	1.0	ppt
Diatoms	PMd	2.25	day^{-1}
	Tmd	20.0	C°
	KTgd1	0.004	$C^{\circ -2}$
	KTgd2	0.006	$C^{\circ -2}$
Greens	PMg	2.50	day^{-1}
	Tmg	25.0	C°
	KTgg1	0.008	$C^{\circ -2}$
	KTgg2	0.010	$C^{\circ -2}$

The model included a salinity toxicity factor (Equation 4-15) that limited *microcystis* growth. The toxicity factor (Table 9-1) was set based on observations that the photosynthetic ability of Potomac River *microcystis* decreased rapidly at 1 to 2 ppt salinity (Sellner et al. 1988).

Mortality

Basal Metabolism. Metabolic rates were specified consistent with reported respiration rates (Table 9-2). Initial calibration efforts indicated diminished base rates were required to replicate the spring diatom bloom. Temperature effects were specified so that metabolism doubled for a 10 C° temperature increase.

Predation. Consider a phytoplankton system in which predation depends upon local zooplankton biomass. For simplicity, ignore settling and macrobenthic grazing. Then:

$$\frac{\delta}{\delta t} B = (P - R) B - G Z \qquad (1)$$

in which:

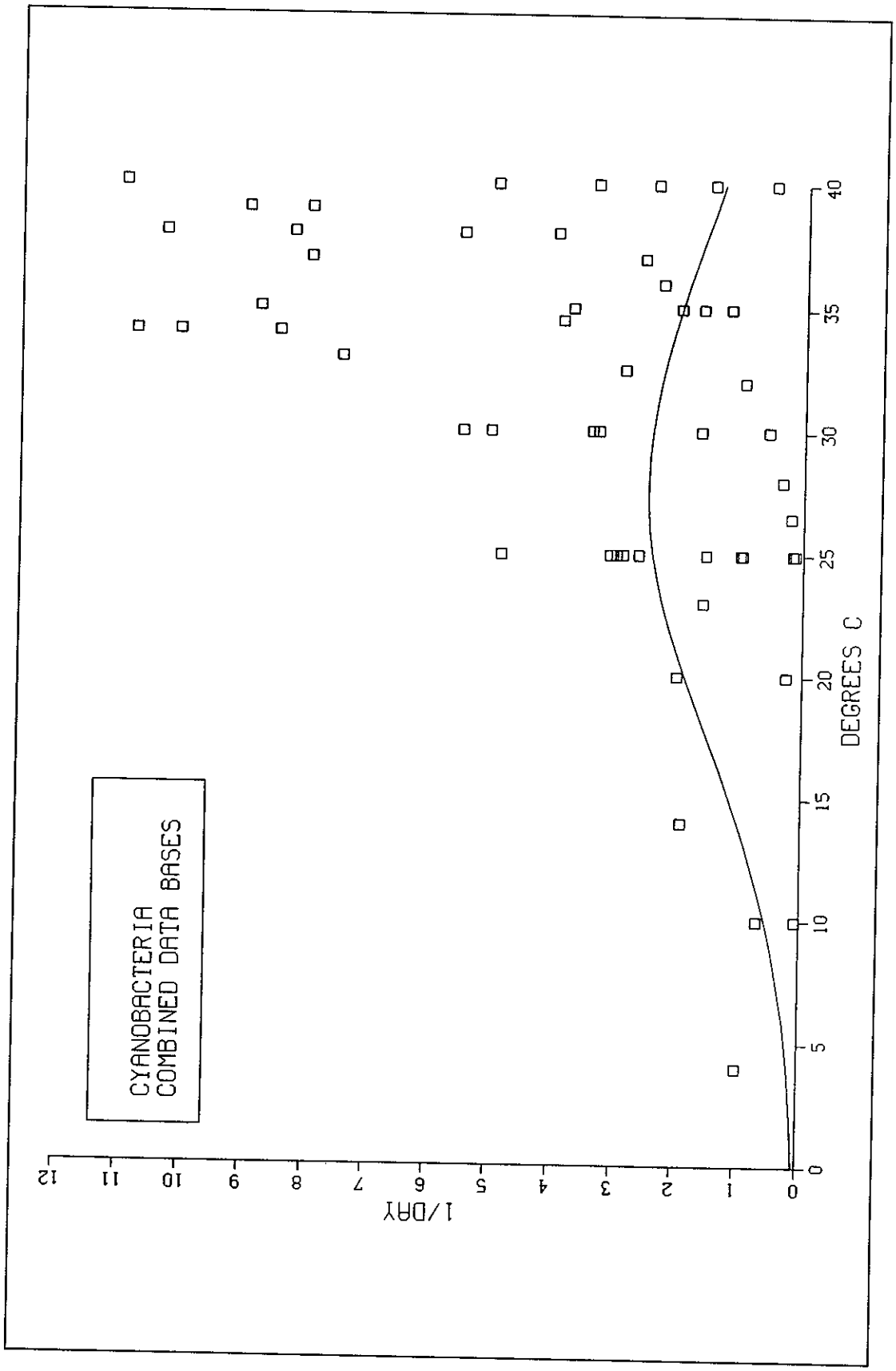

Figure 9-1. Reported and Modelled Growth Rate for Cyanobacteria

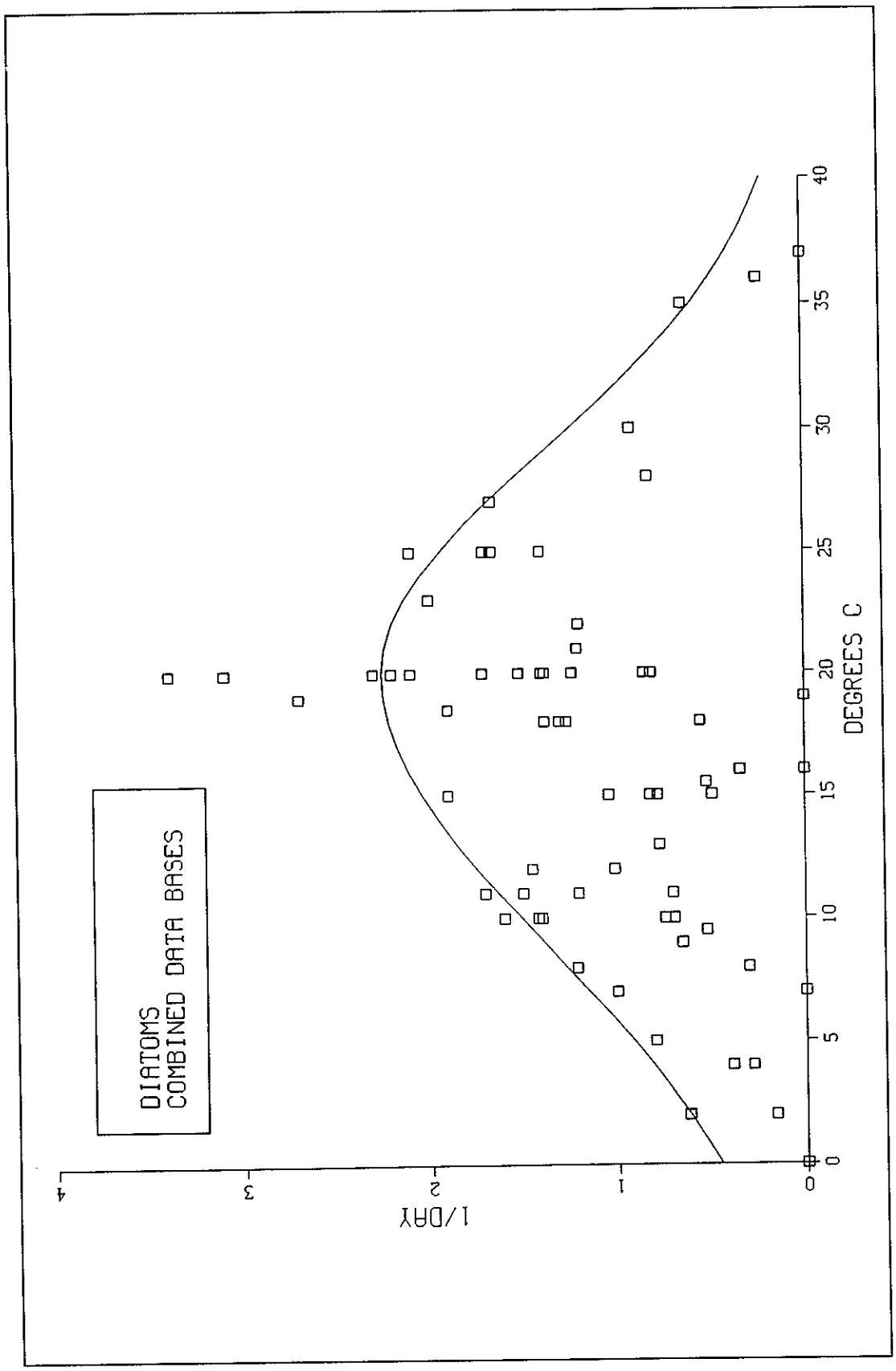

Figure 9-2. Reported and Modelled Growth Rates for Diatoms

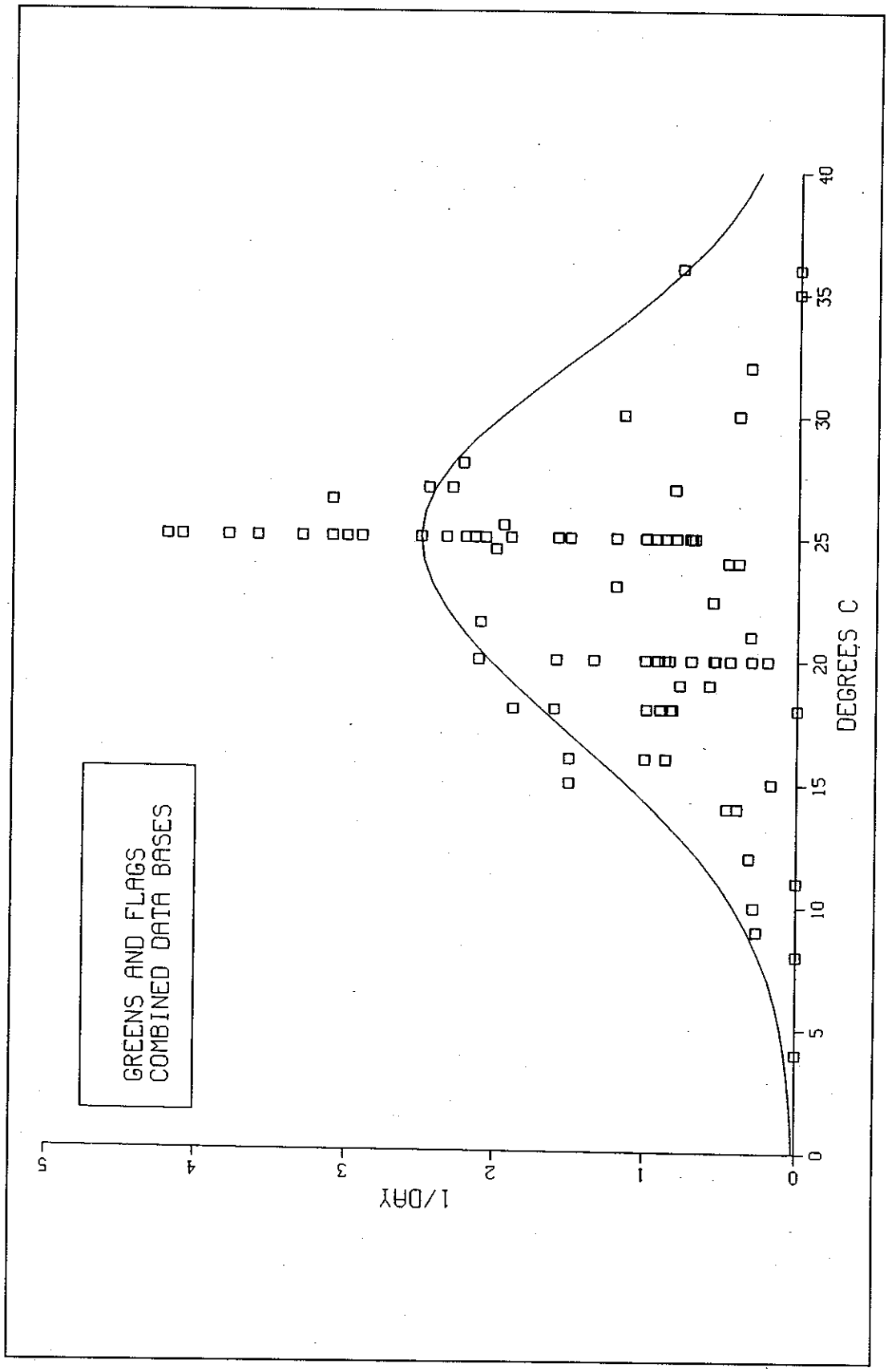

Figure 9-3. Reported and Modelled Growth Rates for Other Green Algae

Table 9-2
Basal Metabolic Rates

Group	Parameter	Value	Comments
	BMrx	0.03 – 0.09 day^{-1}	Experiments by Laws and Wong (1978)
	BMrx	0.02 – 0.36 day^{-1}	Raven and Beardall (1981)
Cyanobacteria	BMrc	0.04 day^{-1}	Model value
	Trc	20 C°	"
	KTbc	0.069 $C^{\circ-1}$	"
Diatoms	BMrd	0.01 day^{-1} 0.003 day^{-1}	Model value January – May in saltwater only
	Trd	20 C°	Model value
	KTbd	0.069 $C^{\circ-1}$	"
Greens	BMrg	0.01 day^{-1}	"
	Trg	20 C°	"
	KTbg	0.069 $C^{\circ-1}$	"

B = algal biomass as carbon (gm C m^{-3})
P = production (day^{-1})
R = respiration (day^{-1})
G = ingestion rate (gm algal C gm^{-1} zooplankton C day^{-1})
Z = zooplankton biomass (gm C m^{-3})

If zooplankton biomass is proportional to algal biomass, $Z = \alpha B$, Equation 9-1 can be rewritten:

$$\frac{\delta}{\delta t} B = (P - R - \alpha G) B \qquad (2)$$

Equation 9-2 is analogous to the governing equation for algal biomass, Equation 4-2. The problem of specifying the predation rate, PRx, in Equation 4-2 becomes a problem of specifying parameters α and G in Equation 9-2. Algal biomass estimates for the upper Bay (Figure 9-4) indicate biomass is 1 - 2 gm C m^{-3} during the spring bloom and 0.5 - 1 gm C m^{-3} otherwise. Zooplankton biomass in the same region is ≈ 0.05 - 0.1 gm C m^{-3} (OEP 1987). Consequently, α is of order 0.1. Specific grazing rates derived from published values are ≈ 1 - 2 gm algal C gm^{-1} zooplankton C day^{-1} (Table 9-3). The order-of-magnitude grazing rate should then be 0.1 - 0.2 day^{-1}.

Predation rates employed in the model (Table 9-3) were determined by calibration in the vicinity of the order-of-magnitude values derived above. Effects of temperature on predation were considered identical to effects of

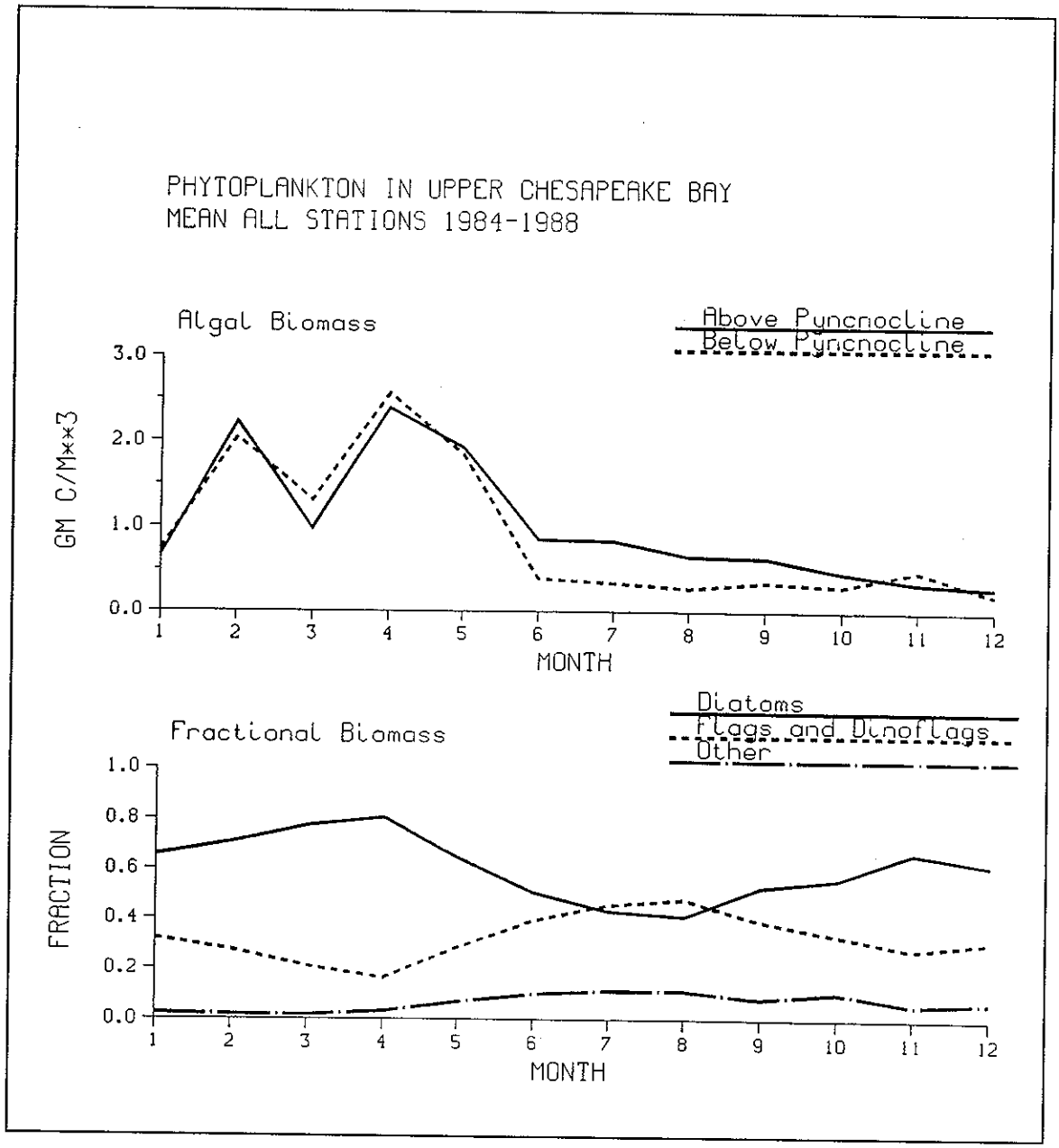

Figure 9-4. Monthly Mean Algal Biomass in Upper Chesapeake Bay, 1984-1988 (Data courtesy of Dr. Kevin Sellner, Benedict Estuarine Research Laboratory, Academy of Natural Sciences)

temperature on respiration. As with respiration, predation rates on diatoms in spring were reduced in order to simulate the bloom.

Macrobenthic Grazing. Although macrobenthic grazing may be a locally important phytoplankton sink (Cohen et al. 1984), grazing rates were set to zero in the model. Spatial and temporal specification of benthic biomass presented a complication that could not be addressed within the time and technical frame of the study. Proper implementation of benthic grazing also

Table 9-3
Predation Rates

Group	Parameter	Value	Comments
	G	1 – 2 day^{-1}	Copepod *Calanus Pacificus*, derived from Beers (1986)
	G	0.7 – 1.1 day^{-1}	*Acartia*, Patuxent River, derived from Storms (1974)
	G	2.6 day^{-1}	*Strombodium*, derived from Beers and Brownlee (1988)
Cyanobacteria	BPRc	0.01 day^{-1}	Model value
Diatoms	BPRd	0.215 day^{-1} 0.065 day^{-1}	Model value January – May, saltwater only
Greens	BPRg	0.215 day^{-1}	Model value

Macrobenthic Grazing. Although macrobenthic grazing may be a locally important phytoplankton sink (Cohen et al. 1984), grazing rates were set to zero in the model. Spatial and temporal specification of benthic biomass presented a complication that could not be addressed within the time and technical frame of the study. Proper implementation of benthic grazing also required modifications to the sediment submodel. Explicit treatment of benthic grazing may be a worthwhile future improvement in the water quality and sediment models. In the meanwhile, algal losses due to benthic grazing were lumped into the predation term.

Composition

Nitrogen. Determination of algal stoichiometry was based on the assumption that composition of organic particles near the surface of the Bay (depth $\leq$ 2 m) approximated the composition of viable algae. Algal carbon-to-nitrogen ratio was evaluated using the relationship:

$$POC = POC_b + CNR\,PON \qquad (3)$$

in which:

POC = particulate organic carbon (gm C m^{-3})
POC_b = non-algal particulate organic carbon (gm C m^{-3})
CNR = carbon-to-nitrogen ratio of algae (gm C gm^{-1} N)
PON = particulate organic nitrogen (gm N m^{-3})

Carbon-to-nitrogen ratio was evaluated via regression employing observed particulate organic nitrogen as the independent variable and observed particulate organic carbon as the dependent variable. Type II regression (Ricker 1972; Laws and Archie 1981), appropriate when the value of the independent variable is uncertain, was employed in the determination.

Analysis of algal composition required screening of the data. In the Virginia portion of the Bay and in the Maryland portion prior to June 1985, particle concentrations were determined as the difference between total and dissolved analyses. The determination by difference resulted in uncertainty in concentration sufficient to render regression results insignificant. Subsequent to June 1985, particle concentrations in the Maryland portion of the Bay were directly determined. Regressions on this portion of the monitoring data yielded significant results reported here.

Regressions were performed using data separated into seasons. The separation allowed for potential seasonal variation in algal composition and in the background concentration of non-algal particulate organic carbon (Figure 9-5). Seasonal differences in composition were apparent (Table 9-4) although the significance of the seasonal differences was not tested. Ratios were close to Redfield stoichiometry which was employed in the model (Table 9-5).

Phosphorus. Analysis indicated the carbon-to-phosphorus ratio of particles varied as a function of dissolved phosphate concentration (Figure 4-8). To account for the phenomenon, variable algal phosphorus stoichiometry was formulated (Equation 4-31). Parameters in the stoichiometry relationship (Table 9-5) were initially evaluated by visual fit to the observed particle composition. Initial values were subsequently adjusted during calibration of algae and phosphorus state variables. Modeled algal carbon-to-phosphorus ratio maintained the functional form suggested by the observations but was greater than observed particle composition (Figure 9-6). The offset between observations and model indicated a fraction of the observed particulate phosphorus was not incorporated in viable algae. Modeled algal composition approached Redfield stoichiometry (carbon-to-phosphorus = 42) at dissolved phosphate concentration greater than $\approx$0.02 gm m^{-3}. Algal carbon-to-phosphorus ratio increased when phosphate was less than $\approx$0.02 gm m^{-3}.

Silica. The silica content of diatoms was estimated by Type II regression of particulate biogenic silica on particulate organic carbon (Figure 9-7). Regression was performed on observations collected at Buoy R-64 (near monitoring station CB4.3C) from 1987 to 1990. Data were divided into seasons to allow for variations in the ratio as a function of diatom abundance. A significant relationship occurred only in Spring (March to May) coincident with the spring bloom. The model value was adjusted from the regression value to optimize predicted chlorophyll during the spring bloom (Table 9-6).

Carbon-to-Chlorophyll Ratio. Determination of carbon-to-chlorophyll ratio followed the pattern set for carbon-to-nitrogen ratio. Type II regression was performed on data segregated by season. Chlorophyll concentration was

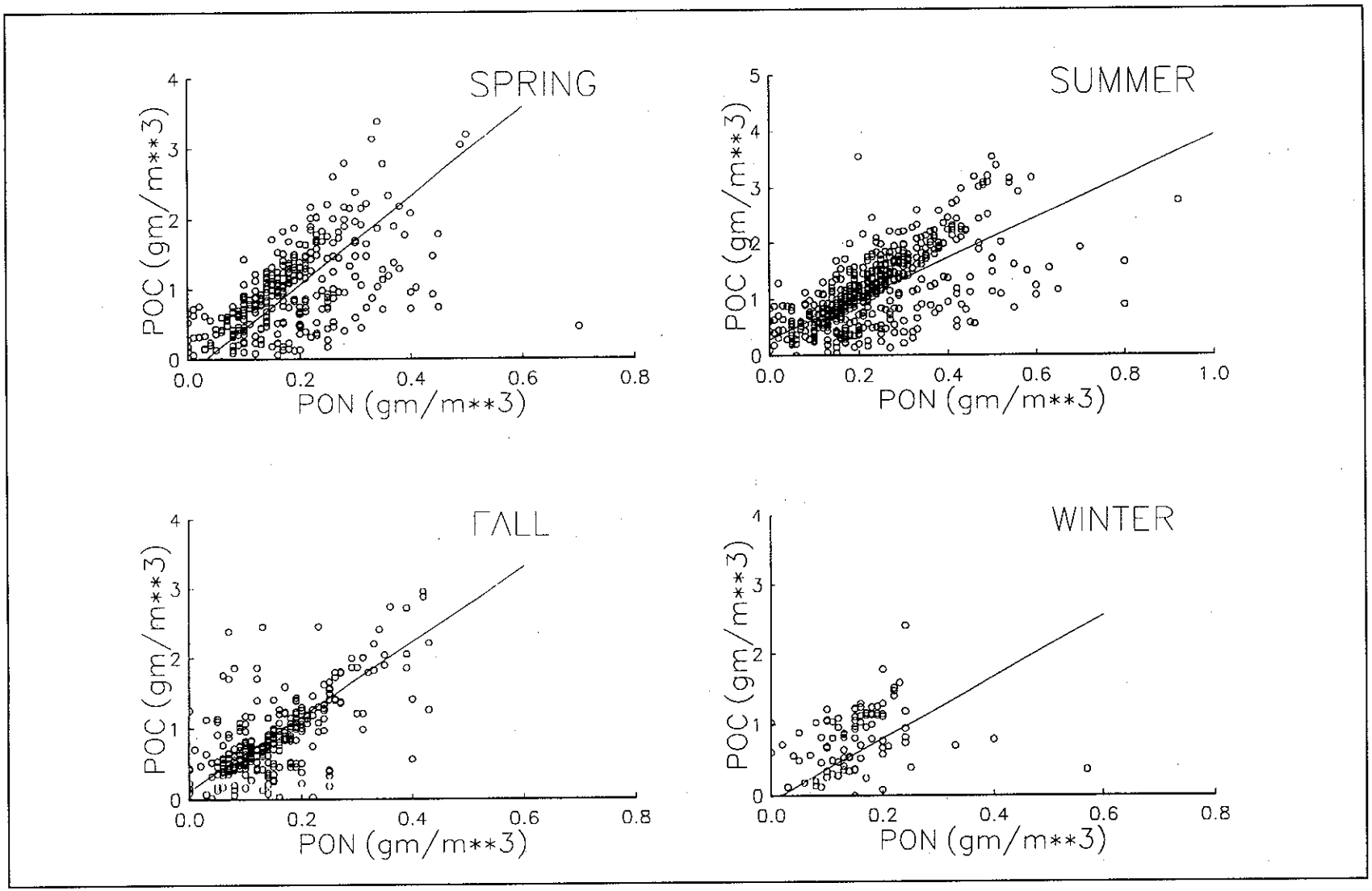

Figure 9-5. Carbon-to-Nitrogen Ratio in Upper Bay Seston

Table 9-4
Carbon-to-Nitrogen Ratio of Upper-Bay Particles

Season	Ratio, gm C gm^{-1} N	Observations	r	p
Spring	6.34	335	0.55	< 0.0001
Summer	3.64	667	0.68	< 0.0001
Autumn	5.32	377	0.54	< 0.0001
Winter	4.39	102	0.61	< 0.0001

Table 9-5
Model Algal Nitrogen and Phosphorus Stoichiometry

Parameter	Units	Value
ANCx	gm N gm^{-1} C	0.167, all groups
PCprm1	gm C gm^{-1} P	42.
PCprm2	gm C gm^{-1} P	85.
PCprm3	m^3 gm^{-1} P	200.

treated as the independent variable and particulate organic carbon was treated as the dependent variable (Figure 9-8). Significant regressions were obtained for three seasons (Table 9-7). Seasonal variations in carbon-to-chlorophyll ratio were apparent but the statistical significance of the variation was not tested. A constant ratio, consistent with the regressions and reported values was specified (Table 9-8).

Nutrient Uptake

Model half-saturation values for nutrient uptake are reported along with relevant literature values in Table 9-9.

Light

Model parameters that relate algal growth to light are reported in Table 9-10.

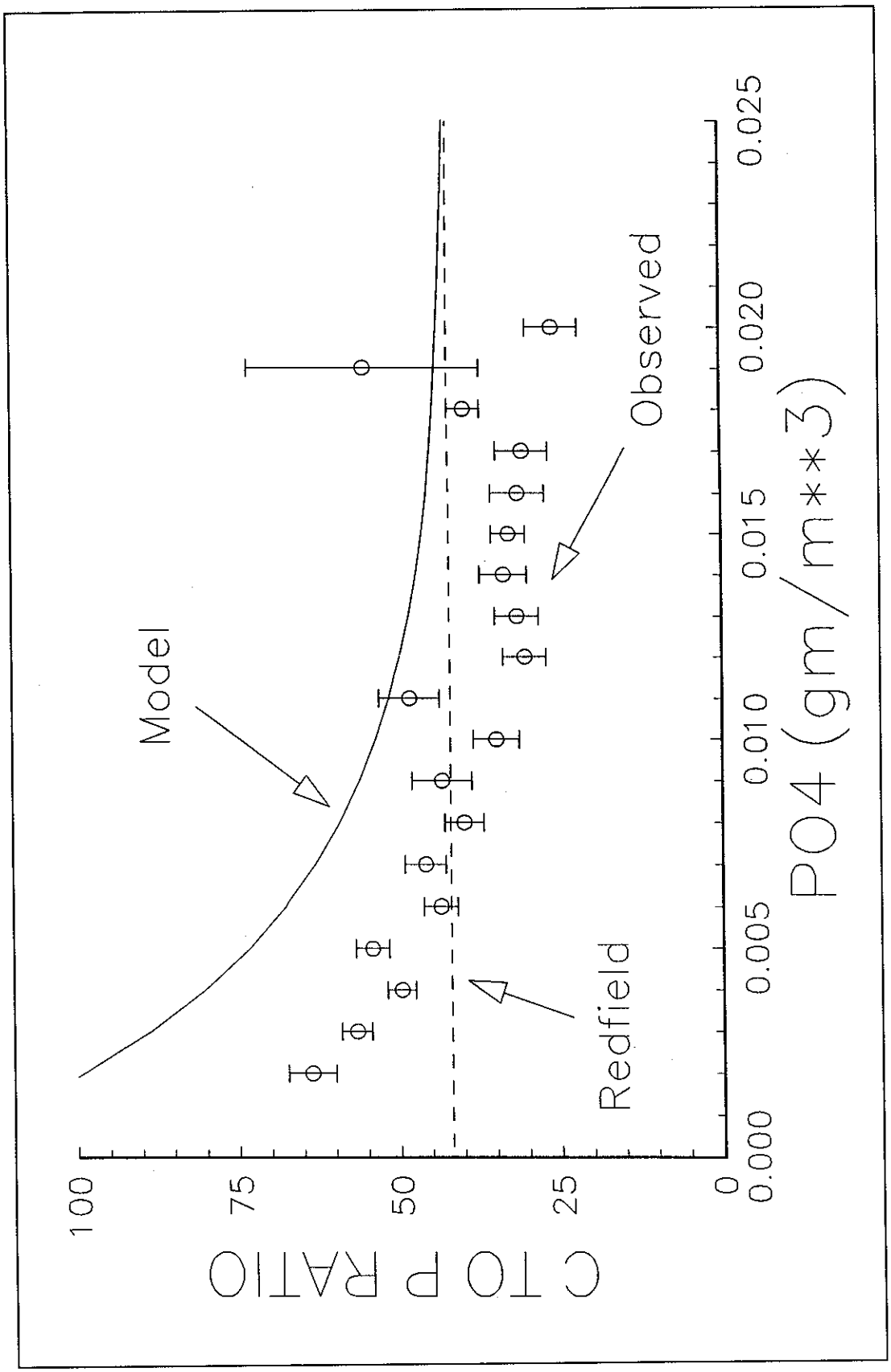

Figure 9-6. Modeled and Observed Carbon-to-Phosphorus Ratio as a Function of Dissolved Phosphate Concentration

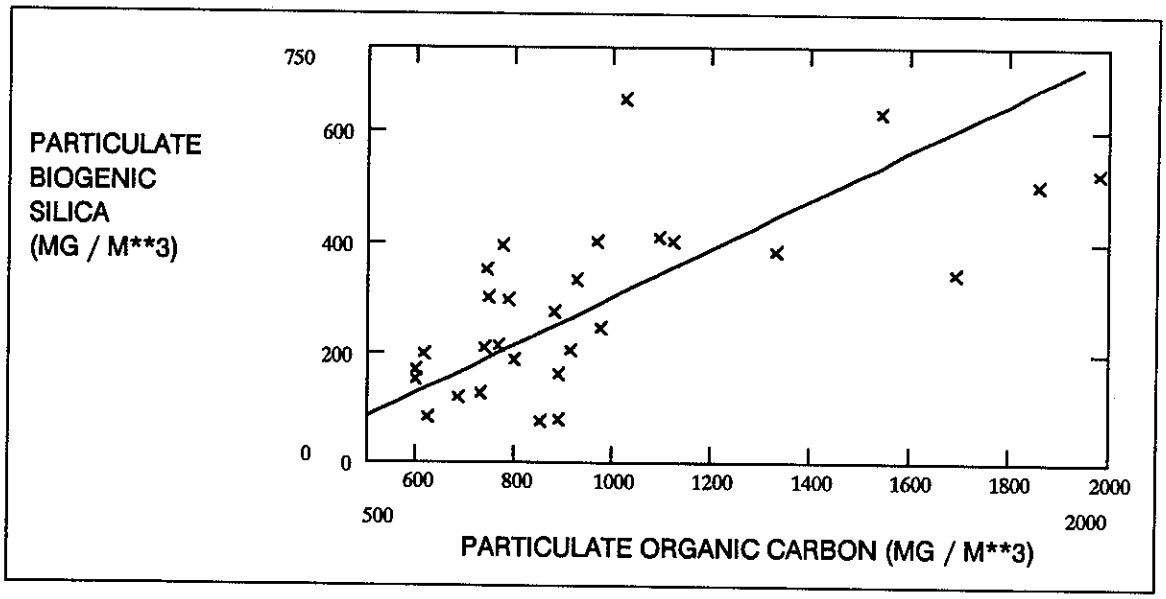

Figure 9-7. Particulate Biogenic Silica Versus Particulate Organic Carbon at Buoy R-64, March to May (Data courtesy of Dr. Walter Boynton, Center for Environmental and Estuarine Studies, University of Maryland)

Table 9-6
Silica Stoichiometry

Parameter	Value	Comments
ASCd (gm Si gm^{-1} C)	0.43	Regression on observations at R–64. $n = 38$, $R^2 = 0.45$, $p < 0.0001$
	0.29	Suggested by D'Elia et al. (1983) for Chesapeake Bay
	0.5 – 1.0	Summary by Parsons et al. (1984)
	0.50	Model value

Algal Settling Rates

Reported settling rates observed for diatoms (Figure 9-9) and other algae (Figure 9-10) vary over several orders of magnitude. In part, this variation is a function of physical factors related to algal size, shape, and density. The dramatic variability also reflects regulation of algal buoyancy as a function of light, nutrients, and other factors. Settling rates employed in the model (Table 9-11) were determined via calibration, aided by qualitative guidelines. One guideline was that settling of the large diatoms that characterize the spring bloom should be greater than settling of smaller diatoms and other species that predominate the remainder of the year. A second guideline was that net settling of cyanobacteria must be small as evidenced by formation of surface algal mats.

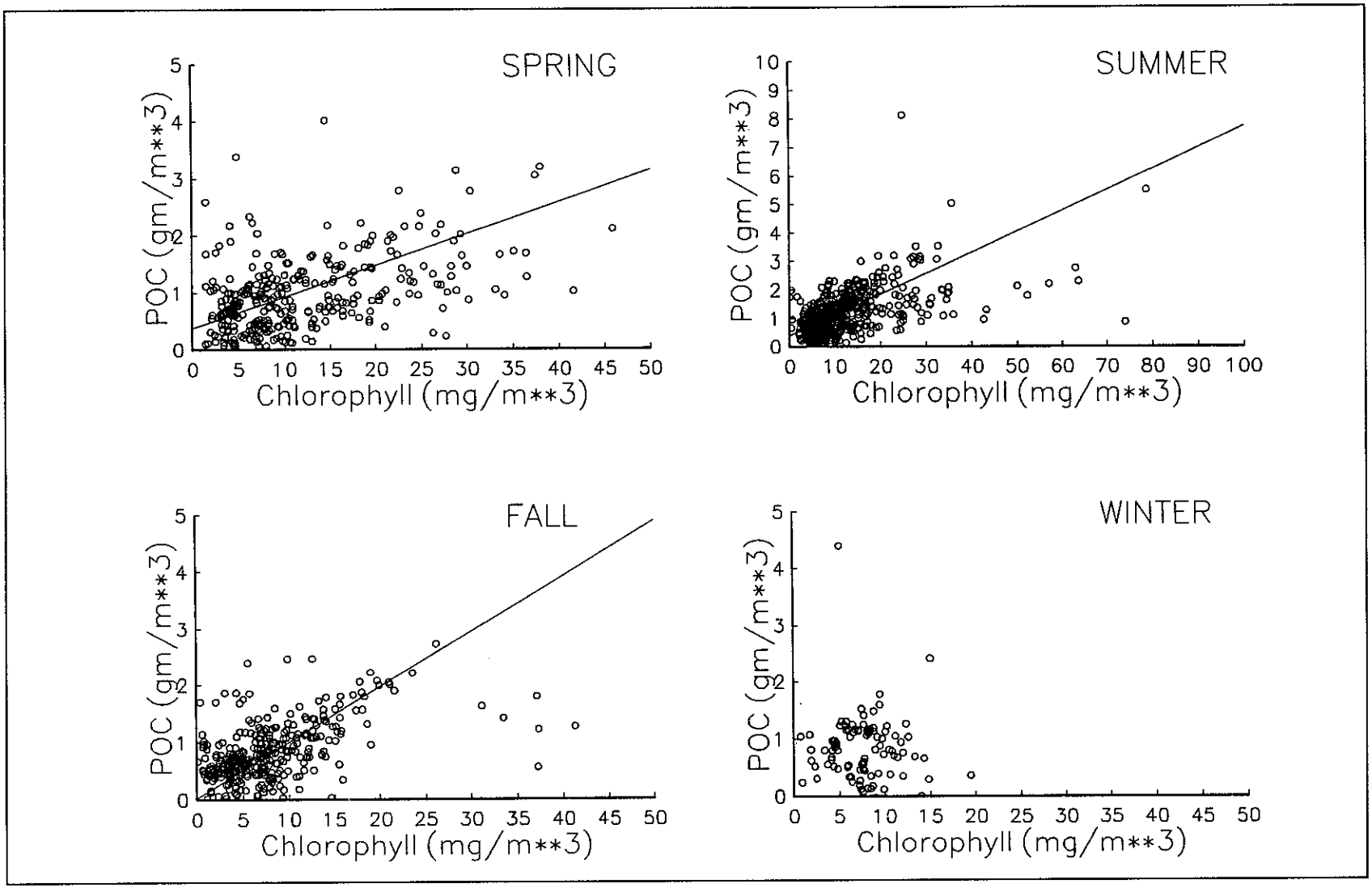

Figure 9-8. Particulate Organic Carbon Versus Chlorophyll in Surface Waters of Upper Chesapeake Bay

Table 9-7
Carbon-to-Chlorophyll Ratio of Upper-Bay Particles

Season	Ratio, gm C gm^{-1} Chl	Observations	r	p
Spring	77	320	0.45	< 0.0001
Summer	67	654	0.46	< 0.0001
Autumn	97	364	0.44	< 0.0001
Winter				> 0.59

Table 9-8
Reported and Modeled Carbon-to-Chlorophyll Ratio

CChl	Comments	Source
90	Proposed for Chesapeake Bay	Harding et al. (1986)
37 – 79	Marine phytoplankton	Antia et al., cited by Parsons et al. (1984)
48	Choptank River mesocosms	Roman et al. (1988)
30 – 143	Mesohaline Chesapeake Bay	Malone et al. (1988)
60	Model, all groups	

Effect of Algae on Organic Carbon and Dissolved Oxygen

Direct relation of experimental observations to the model distribution of biomass due to algal mortality is difficult. One problem is that experimental design is not intended to measure distribution as parameterized in the model. A second problem is that carbon and nutrient cycles in the model are affected by both the initial distribution of algal biomass and the recycling rates. Different combinations of initial distributions and recycling rates can yield equivalent concentrations of organic and inorganic substances. As a consequence, experiments should be viewed as qualitative guides only for selection of model parameters. The primary issue in recycling of algal carbon was the distribution of dissolved, labile particulate, and refractory particulate organic carbon. No universal distinction between labile and refractory exists. Definition in the present study was based on parameters employed in the sediment model. In the sediment model, the carbon fraction deemed labile (G1) had a decay rate of 0.035 day^{-1} @ 20 C^{o}. Ninety-percent of G1 carbon was mineralized in 65 days. Labile carbon in the water quality model was defined as the carbon that mineralizes in ≈ 60 days. In interpretation of experiments, carbon that

Table 9-9
Half-Saturation Constants for Algal Nutrient Uptake

Nutrient	Parameter	Value	Comments
Nitrogen	KHnc	0.16 ÷ 0.22	Literature search (Collins and Wlosinski 1983)
	KHnd	0.003 – 0.186	"
	KHng	0.006 – 0.589	"
		0.001 – 0.008	NH4 uptake in Chesapeake Bay (Wheeler et al. 1982)
	KHnx	0.010, all groups	Model Value
Phosphorus		0.001 – 0.105	Literature search (Collins and Wlosinski 1983)
		0.003 – 0.008	PO4 uptake in Chesapeake Bay (Taft et al. 1975)
	KHpx	0.001, all groups	Model Value
Silica	KHs	0.031	*Skelotenema Costatum* (Davis et al. 1978)
	KHs	0.02 – 0.10	Paasche cited by Parsons et al. (1984)
	KHs	0.082	Goering et al. cited by Parsons et al. (1984)
	KHs	0.050	Model Value

Table 9-10
Model Parameters Relating Algae to Light

Parameter	Model Value	Comments
Kechl	17 m^2 gm^{-1} Chl 'a'	Compares to 14 – 31 m^2 gm^{-1} Chl 'a' reported in summary by Pennock (1985)
Dopt	1 m, all groups	Obtained from Kremer and Nixon (1978)
Ismin	40 langley day^{-1}	Obtained from Kremer and Nixon (1978)

mineralized in ≈ 60 days or less corresponded to labile carbon in the model. Results of some relevant experiments (Table 9-12) were used to guide selection of initial model parameters. Final parameters (Table 9-13) were selected by adjustment of initial values to optimize agreement of predicted and observed state variables.

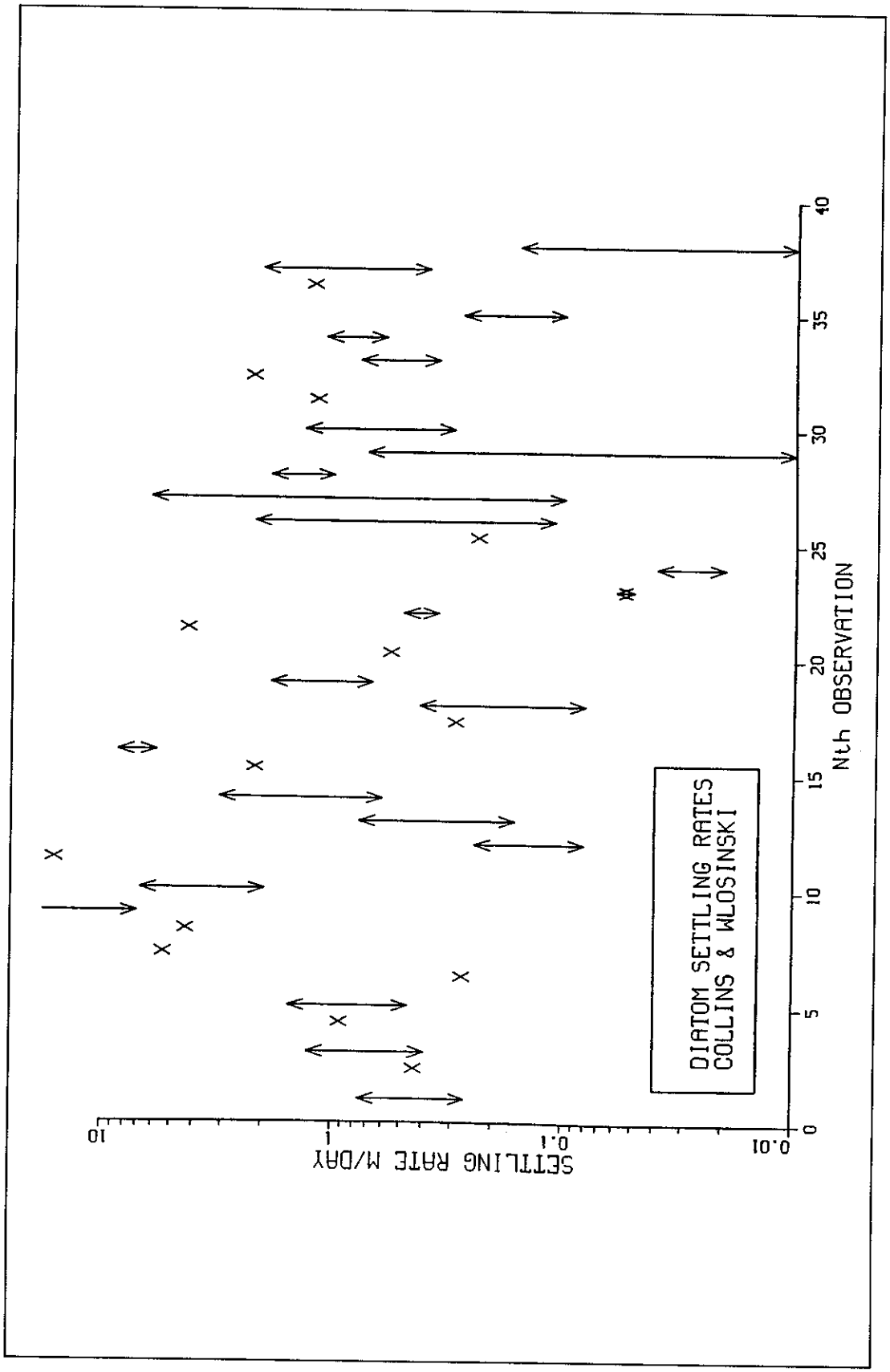

Figure 9-9. Diatom Settling Rates (Collins and Wlosinski 1983)

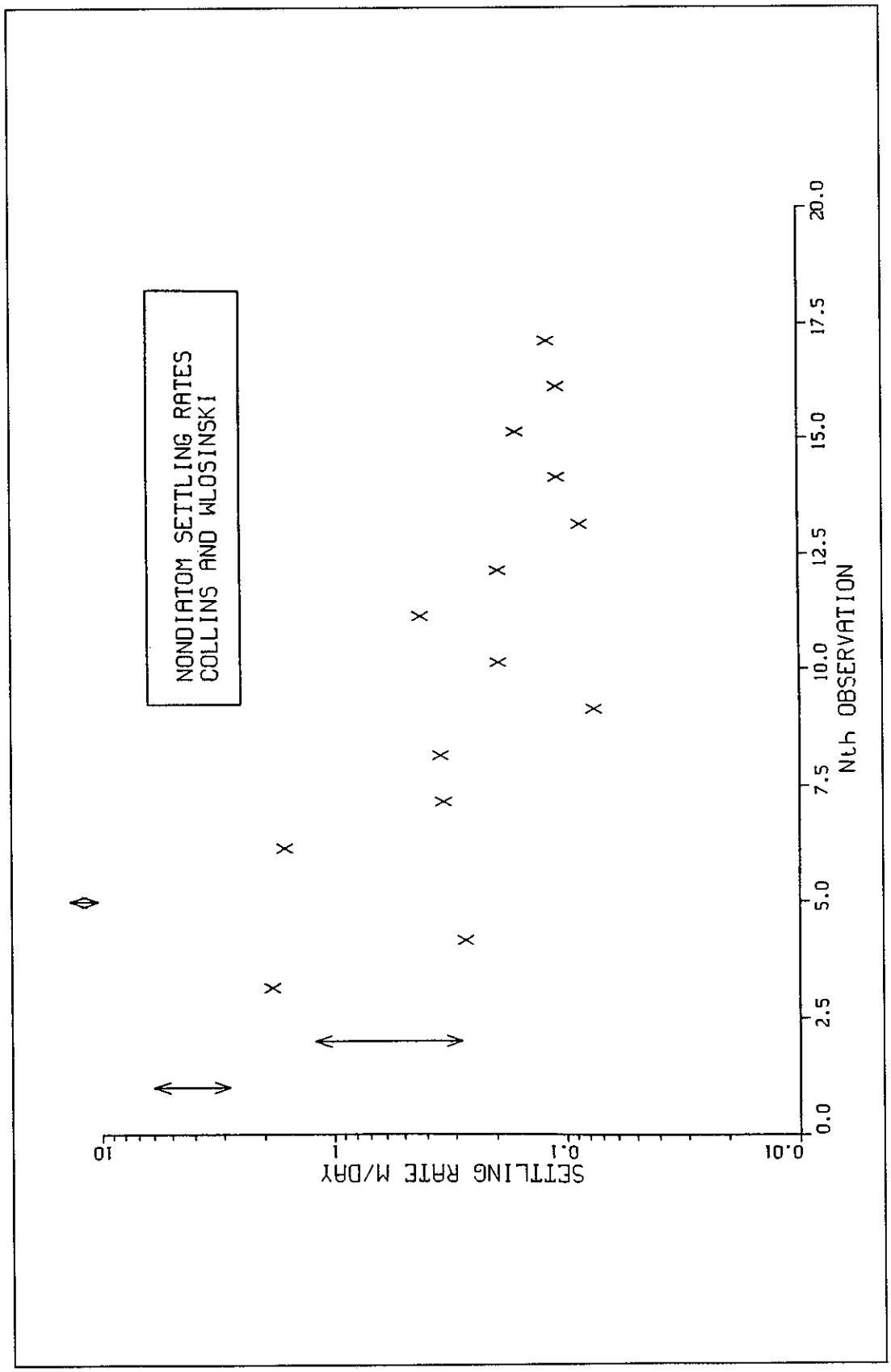

Figure 9-10. Settling Rates for Algae Other than Diatoms (Collins and Wlosinski 1983)

Table 9-11
Algal Settling Rates

Group	Parameter	Value
Cyanobacteria	WSc	0.0 m day^{-1}
Diatoms	WSdb	0.1 m day^{-1}
	WSds	0.25 m day^{-1}
	Prdval	1 (January – May) 0 (June – December)
Greens	WSg	0.1 m day^{-1}

Table 9-12
Reported Distribution of Algal Carbon

Distribution	Reference
Refractory fraction of algae averages 40% of ash-free dry weight	Foree and McCarty (1970)
22% dissolved, 73% labile particulate, 5% refractory particulate	Pett (1989)
33% dissolved, 33% labile particulate, 33% refractory particulate	Westrich and Berner (1984)
7% dissolved, 63% labile particulate, 30% refractory particulate	Otsuki and Hanya (1972)
dissolved organic carbon exudation from healthy cells < 15% of carbon fixed	Parsons et al. (1984)

Table 9-13
Modeled Effects of Algae on Organic Carbon and Dissolved Oxygen

Parameter	Value
FCDx	0.0, all groups
FCDP	0.10
FCLP	0.55
FCRP	0.35
KHrx	0.5 gm DO m^{-3}, all groups
AOCR	2.67 gm DO gm^{-1} C

Effect of Algae on Nitrogen and Phosphorus

Parameterization of the distribution of algal nutrients upon mortality was similar to distribution of algal carbon except that distribution into an inorganic pool was also required. As with carbon, experiments were interpreted so that organic matter that decayed on a time scale ≈ 60 days was considered labile. Results of relevant experiments (Table 9-14) guided selection of initial model parameters. Final nitrogen and phosphorus parameters (Table 9-15) were selected to optimize agreement of predicted and observed state variables.

Table 9-14
Reported Distribution of Algal Nitrogen and Phosphorus

Nutrient	Distribution	Reference
Nitrogen	5 to 7% dissolved inorganic, 30 to 50% dissolved organic, labile particulate > 22 to 44%, refractory particulate < 21 to 23%	Garber (1984)
	50% of particulate nitrogen is refractory	Grill and Richards (1964)
	6% dissolved organic, 64% labile particulate, 30% refractory particulate	Otsuki and Hanya (1972)
Phosphorus	24 to 27% dissolved inorganic, 42 to 56% dissolved organic, labile particulate > 4 to 16%, refractory particulate < 7 to 27%	Garber (1984)
	33% of particulate phosphorus is refractory	Grill and Richards (1964)

Table 9-15
Modeled Effects of Algae on Nitrogen and Phosphorus

Parameter	Value	Parameter	Value
FNIx	0.0, all groups		
FNDx	1.0, all groups	FPDx	1.0, all groups
FNLx	0.0, all groups	FPLx	0.0, all groups
FNRx	0.0, all groups	FPRx	0.0, all groups
FNIP	0.0		
FNDP	0.1	FPDP	0.5
FNLP	0.55	FPLP	0.2
FNRP	0.35	FPRP	0.1

Hydrolysis and Mineralization Rates

The model required specification of the rates at which particulate organic matter was solubilized into dissolved organic matter and the rates at which dissolved organic matter was converted to inorganic form. For carbon, these rates were referred to as dissolution and respiration rates. For nitrogen and phosphorus, the rates were referred to as hydrolysis and mineralization rates. Literature summaries (Bowie et al. 1985) indicated orders-of-magnitude variation in the rates employed in eutrophication models. Most often, the first-order rate constants were of order 10^{-2} to 10^{-1} day^{-1}. The base rates employed for dissolved and labile particulate organic matter in the present study (Table 9-16), selected to optimize agreement of predicted and observed state variables, were within the order-of-magnitude range most often employed elsewhere. Temperature parameters were specified so that rates doubled for a 10 C^{o} increase in temperature.

Table 9-16
Carbon, Nitrogen, and Phosphorus Recycle Rates

Parameter	Value	Parameter	Value	Parameter	Value
Kdc	0.010 day^{-1}	Kdn	0.015 day^{-1}	Kdp	0.100 day^{-1}
Klc	0.075 day^{-1}	Kln	0.075 day^{-1}	Klp	0.075 day^{-1}
Krc	0.005 day^{-1}	Krn	0.005 day^{-1}	Krp	0.005 day^{-1}
Kdcalg	0.0	Kdnalg	0.0	Kdpalg	0.2 m^3 day^{-1} gm^{-1} C
Klcalg	0.0	Klnalg	0.0	Klpalg	0.0
Krcalg	0.0	Krnalg	0.0	Krpalg	0.0
AANOX	0.5				
KHodoc	0.5 gm DO m^{-3}				
KHndn	0.1 gm N m^{-3}				
Trmnl	20 C^{o}				
KTmnl	0.069 C^{o-1}				
Trhdr	20 C^{o}				
KThdr	0.069 C^{o-1}				

Dissolution and hydrolysis rates for refractory particulates were arbitrarily set an order of magnitude ($\approx 10^{-3}$ day^{-1}) less than the rates for labile particulates. The refractory rates (Table 9-16) were negligibly small and their specification had no demonstrable effect on calibration.

The formulation of the model allowed relation of carbon, nitrogen, and phosphorus recycle rates to algal biomass, a surrogate for bacterial activity. For nitrogen and phosphorus, the formulation also accelerated hydrolysis and mineralization as nutrients become scarce. This option rested on a strong observational base for phosphorus. The option was originally included in the model in order to make phosphorus available during the spring bloom, a period of high algal biomass and phosphorus-limited conditions, without overestimating inorganic phosphorus concentration the remainder of the year. The acceleration option for phosphorus was activated in the calibration (Table 9-16). Assuming a characteristic algal biomass of 1 gm C m^{-3}, the phosphorus mineralization rate increased from 0.1 day^{-1} when phosphate was freely available to 0.3 day^{-1} when phosphate was 100% limiting to algal growth. During the calibration procedure, no advantage in relating carbon dissolution and respiration rates to algal biomass was noted. Calibration of nitrogen concentrations was satisfactory without relating recycle rates to algal biomass.

Detrital Settling Rates

The first estimate of detrital settling rates was obtained by computation of Stokes' velocity for a settling sphere (Scavia 1980):

$$W = \frac{2}{9} g r^2 \frac{\Delta\rho}{v} \qquad (4)$$

in which:

W = settling velocity (cm sec^{-1})
g = gravitational acceleration (980 cm sec^2)
r = equivalent radius (cm)
$\Delta\rho$ = excess density (gm cm^{-3})
v = kinematic viscosity of water ($\approx$ 0.01 gm sec^{-1} cm^{-1} @ 20 C^o)

The size and density of organic detritus, for use in Stokes' equation, were characterized by reported size and density of phytoplankton. The characteristic radius of phytoplankton was 10^0 to 10^2 µm (Beers 1986). Excess density was $\approx$ 0.2 gm cm^{-3} for diatoms and 0.03 gm cm^{-3} for other algae (Scavia 1980). The resulting computed range of settling velocities ranged from 10^{-2} to 10^2 m day^{-1} (a fairly large range from which to choose).

An alternate, more precise, initial estimate of detrital settling velocity was obtained employing data from a sediment trap at Buoy R-64 in the upper Bay. Dimensional analysis indicated detrital settling rate could be estimated:

$$W = \frac{Dpoc}{POC} \quad (5)$$

in which:

W = settling velocity (m day^{-1})
Dpoc = particulate organic carbon deposition rate measured in trap (gm C m^{-2} day^{-1})
POC = particulate organic carbon concentration in vicinity of trap (gm C m^{-3})

Particulate carbon deposition rates measured in the trap were 0.5 to 1 gm C m^{-2} day^{-1} (Figure 9-11). Water-column surface particulate organic carbon concentrations in the vicinity were 0.5 to 1.5 gm C m^{-3}. The characteristic settling velocity, given by Equation 5, was 0.5 to 1.5 m day^{-1}.

The sediment trap analysis provided a range of feasible settling velocities for use in the model. Final value of settling velocity (Table 9-17) was selected to optimize agreement of predicted and observed carbon, nitrogen, and phosphorus in the water column and benthic sediments.

Table 9-17
Detrital Settling Velocities

Parameter	Value	Comments
	$10^{-2} - 10^{2}$ m day^{-1}	Stokes' velocity for phytoplankton–size particles
	0.5 – 1.5 m day^{-1}	Characteristic of R–64 sediment trap
WSs	1.0 m day^{-1}	Model value
WSl	1.0 m day^{-1}	"
WSr	1.0 m day^{-1}	"

Nitrification

Representation of nitrification in the model required specification of maximum nitrification rate and effects of dissolved oxygen, ammonium, and temperature on the maximum. Parameters for the Bay model were selected from reported ranges (Table 9-18). Extensive calibration of the nitrification parameters was not conducted as the process was not a major factor in the oxygen budget or distribution of ammonium and nitrate.

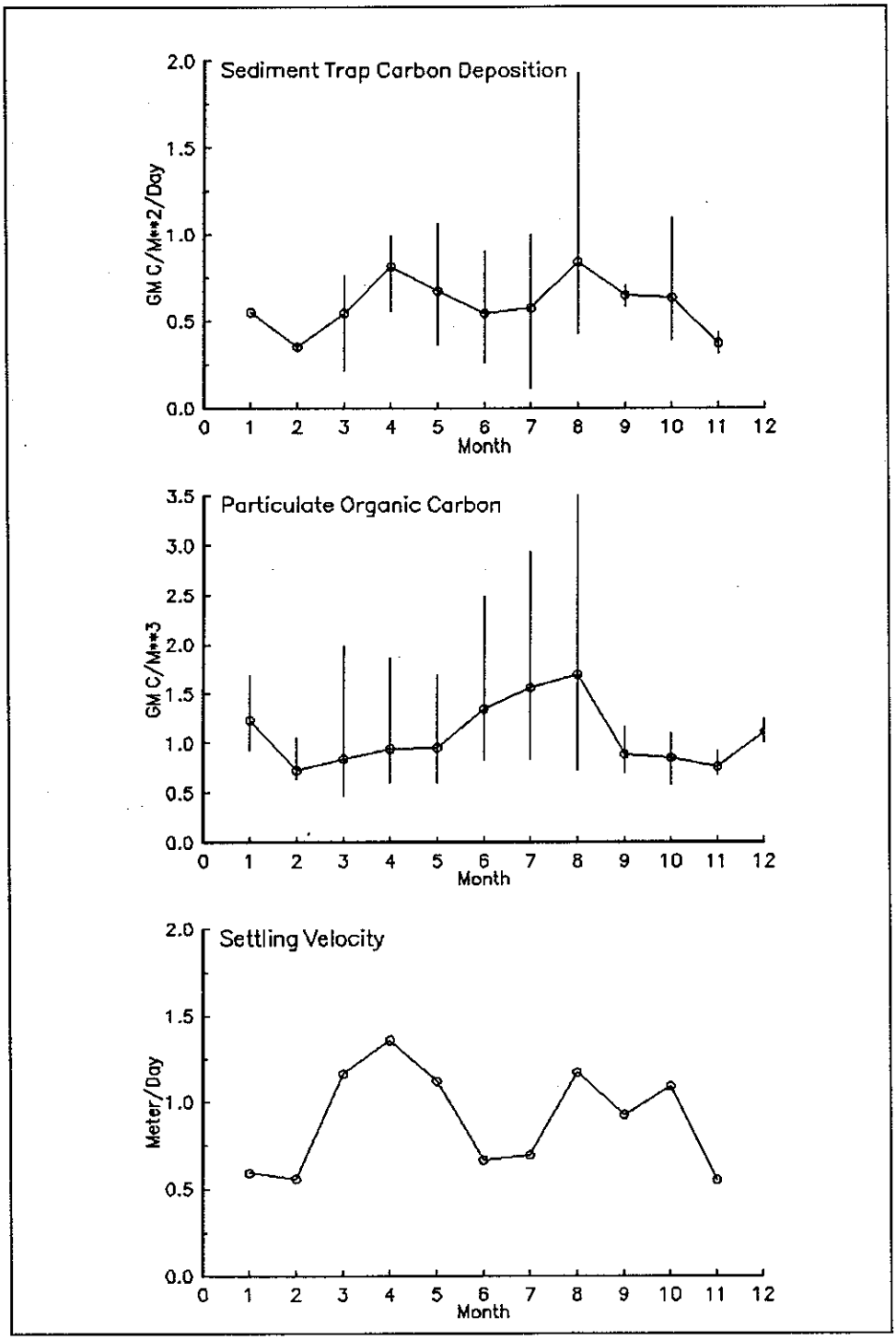

Figure 9-11. Particulate Organic Carbon Deposition, Concentration, and Set tling Velocity at Buoy R-64 (Data courtesy of Dr. Walter Boynton, Center for Environmental and Estuarine Studies, University of Maryland)

Table 9-18
Parameters in Nitrification Kinetics

NTm, gm N m^{-3} day^{-1}	KHnnt, gm N m^{-3}	KHont, gm DO m^{-3}	Tmnt, C^{o}	KTnt, $C^{o\,-2}$	Comments
0.006 – 0.446					Chesapeake Bay (Horrigan et al. 1990)
0.018					Enriched microcosm, Narragansett Bay (Berounsky and Nixon 1985)
0.027					James River (Kator 1990)
0.043					Tamar Estuary (Owens 1986)
0.004 – 0.11					Delaware Estuary (Lipschultz et al. 1986)
	0.78	1	25 – 35	≈0.006	For growth of *nitrosomonas* (Helder and DeVries 1983)
	1.6		15		Charley et al. (1980)
	1.3 – 2.6		> 25		Stratton and McCarty (1967)
	0.06 – 3.5	0.6 – 3	28 – 36		Review by Sharma and Ahlert (1977)
0.07	1.0	1.0	27	0.0045	Model

Chemical Oxygen Demand

The principal component of chemical oxygen demand in saline waters of Chesapeake Bay is the oxidation of sulfide. Parameters for chemical oxygen demand kinetics in the model (Table 9-19) were selected from reported rates for sulfide oxidation.

Table 9-19
Chemical Oxygen Demand Parameters

Kcod, day^{-1}	KHocod, gm DO m^{-3}	KTcod, C^{o-1}	Comments
1 to 42	≈ 1	0.041	Seawater (Almgren and Hagstrom 1974)
35 to 76	3	0.046	Domestic wastewater (Wilmot et al. 1988)
43 to 144			Chesapeake Bay bottom water (Millero 1991)
20	1.5	0.041	Model. Trcod = 20 C^o

Particulate Biogenic Silica

Parameters affecting the cycling of particulate biogenic silica were selected within the range of published values (Table 9-20) and adjusted to optimize agreement of predicted and observed silica and chlorophyll.

Table 9-20
Particulate Biogenic Silica Parameters

Ksua, day^{-1}	KTsua, C^o	FSAP	Comments
0.06			Wollast (1974)
0.04			Vanderborght et al. (1977)
0.017			Grill and Richards (1964)
	0.092		Lawson cited by Yamada and D'Elia (1984)
0.03	0.092	0.0	Model. Trsua = 20 C^o

Reaeration

Application of two reaeration formulae, one dependent on bottom stress and the other a wind-dependent formulation, indicated the order-of-magnitude reaeration coefficient for Chesapeake Bay is 1 m day^{-1} (Cerco 1989). The surface renewal rate in the model was set to R = 3.5 x 10^4 day^{-1}. The resulting reaeration coefficient in the model was Kr = 2.4 m day^{-1}.

Total Active Metal

Solubility and benthic release rate for total active metal were selected from iron and manganese data reported for estuaries (Table 9-21). The half-saturation dissolved oxygen concentration and temperature dependence were developed from the same sources. Order-of-magnitude phosphorus and silica partition coefficients were derived from O'Connor (1988) and converted to appropriate units employing a metal molecular weight of 55 gm mol^{-1}.

Table 9-21
Total Active Metal Parameters

Parameter	Value	Comments	Reference
BENTAM (mmol m^2 day^{-1})	0.73 0.36 1.1	Anoxic Fe release Oxic Mn release Anoxic Mn release	Kiel Bight (Balzer 1982)
	0.3 7.0	Oxic Mn release Anoxic Mn release	Chesapeake Bay (Eaton 1979)
	0.36	Oxic Mn release	Narragansett Bay (Graham et al. 1976)
	10.0	Model value @ 20C°	
TAMdmx (mmol m^{-3})	8 to 10 ≈80	Fe in anoxic water Mn in anoxic water	Kiel Bight (Balzer 1982)
	2 to 5 5 to 10	Fe in anoxic water Mn in anoxic water	Chesapeake Bay (Gavis and Grant 1986)
	5 to 12	Mn in anoxic water	Chesapeake Bay (Eaton 1979)
	15	Model value	
Kdotam (gm DO m^{-3})	1.0	Model value	
KHbmf (gm DO m^{-3})	0.5	Model value	
KTbmf (C^{o-1})	0.2	Model value	
Kadpo4 (m^3 mol^{-1})	6.0	Model value	
Kadsa (m^3 mol^{-1})	6.0	Model value	

Chapter X: Coupling with the Sediment Model

Introduction

The need for a predictive benthic sediment model was made apparent by the results of the steady-state model study (HydroQual 1987) which preceded this one. The study indicated sediments were the dominant sources of phosphorus and ammonium during the summer period of minimum dissolved oxygen. An increase in sediment oxygen demand and nutrient release was implicated in a perceived decline in dissolved oxygen from 1965 to 1985. Simultaneously, basic scientific investigations were indicating the importance of sediment-water exchange processes in Chesapeake Bay and other estuarine systems (Boynton and Kemp 1985; Seitzinger, Nixon, and Pilson 1984; Fisher, Carlson, and Barber 1982). For management purposes, a model was required with two fundamental capabilities:

Predict effects of management actions on sediment-water exchange processes, and

Predict time scale for alterations in sediment-water exchange processes.

A sediment model to meet these requirements was created for this study. The model (Figure 10-1) was driven by net settling of organic matter from the water column to the sediments. In the sediments, the model simulated the diagenesis (decay) of the organic matter. Diagenesis produced oxygen demand and inorganic nutrients. Oxygen demand, as sulfide (in saltwater) or methane (in freshwater), took three paths out of the sediments: export to the water column as chemical oxygen demand, oxidation at the sediment-water interface as sediment oxygen demand, or burial to deep, inactive sediments. Inorganic nutrients produced by diagenesis took two paths out of the sediments: release to the water column, or burial to deep, inactive sediments.

Additional details of the model, required to understand the coupling of the sediment submodel to the model of the water column, are provided below. Complete model documentation is provided by DiToro and Fitzpatrick (1993).

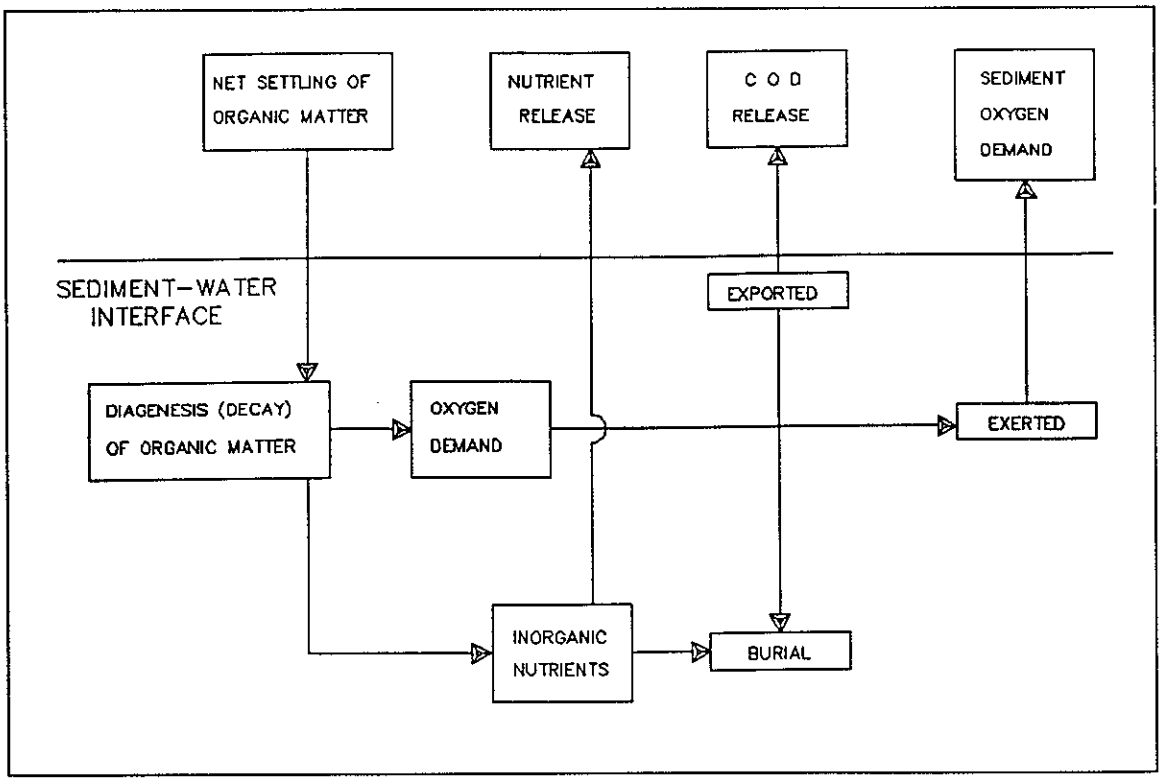

Figure 10-1. Sediment Model Schematic

A listing of sediment model state variables and predicted sediment-water fluxes is provided in Table 10-1.

Table 10-1
Sediment Model State Variables and Fluxes

State Variable	Sediment-Water Flux
Temperature	
Particulate Organic Carbon	Sediment Oxygen Demand
Sulfide/Methane	Release of Chemical Oxygen Demand
Particulate Organic Nitrogen	
Ammonium	Ammonium Flux
Nitrate	Nitrate Flux
Particulate Organic Phosphorus	
Phosphate	Phosphate Flux
Particulate Biogenic Silica	
Available Silica	Silica Flux

Description of Sediment Model

Benthic sediments are represented as two layers with a total depth of 10 cm (Figure 10-2). The upper layer, in contact with the water column, may be oxic or anoxic depending on dissolved oxygen concentration in the water. The lower layer is permanently anoxic. The thickness of the upper layer is determined by the penetration of oxygen into the sediments. At its maximum thickness, the oxic layer depth is only a small fraction of the total.

The sediment model consists of three basic processes. The first is deposition of particulate organic matter from the water column to the sediments. Due to the negligible thickness of the upper layer, deposition proceeds from the water column directly to the lower, anoxic layer. Within the lower layer, organic matter is subject to the second basic process, diagenesis (or decay). The third basic process is flux of substances produced by diagenesis to the upper sediment layer, to the water column, and to deep, inactive sediments. The flux portion of the model is the most complex. Computation of flux requires consideration of reactions in both sediment layers, of partitioning between particulate and dissolved fractions in both layers, of sedimentation from the upper to lower layer and from the lower layer to deep inactive sediments, of particle mixing between layers, of diffusion between layers, and of mass transfer between the upper layer and the water column.

Deposition

Deposition is one process which couples the model of the water column with the model of the sediments. Consequently, deposition is represented in both the sediment and water-column models. In the water column, deposition is represented with a modification of the mass-balance equation applied only to cells that interface the sediments:

$$\frac{\delta C}{\delta t} = [\text{transport}] + [\text{kinetics}] + \frac{WS}{\Delta z} C_{up} - \frac{W_{net}}{\Delta z} C \qquad (1)$$

C = concentration of particulate constituent (gm m^{-3})
WS = settling velocity in water column (m day^{-1})
C_{up} = constituent concentration two cells above sediments (gm m^{-3})
W_{net} = net settling to sediments (m day^{-1})
Δz = cell thickness (m)

Net settling to the sediments may be greater or lesser than settling in the water column. Sediment resuspension is implied when settling to the sediments is less than settling through the water column. Net settling that exceeds particle settling velocity implies active incorporation of particles into sediment by biota or other processes.

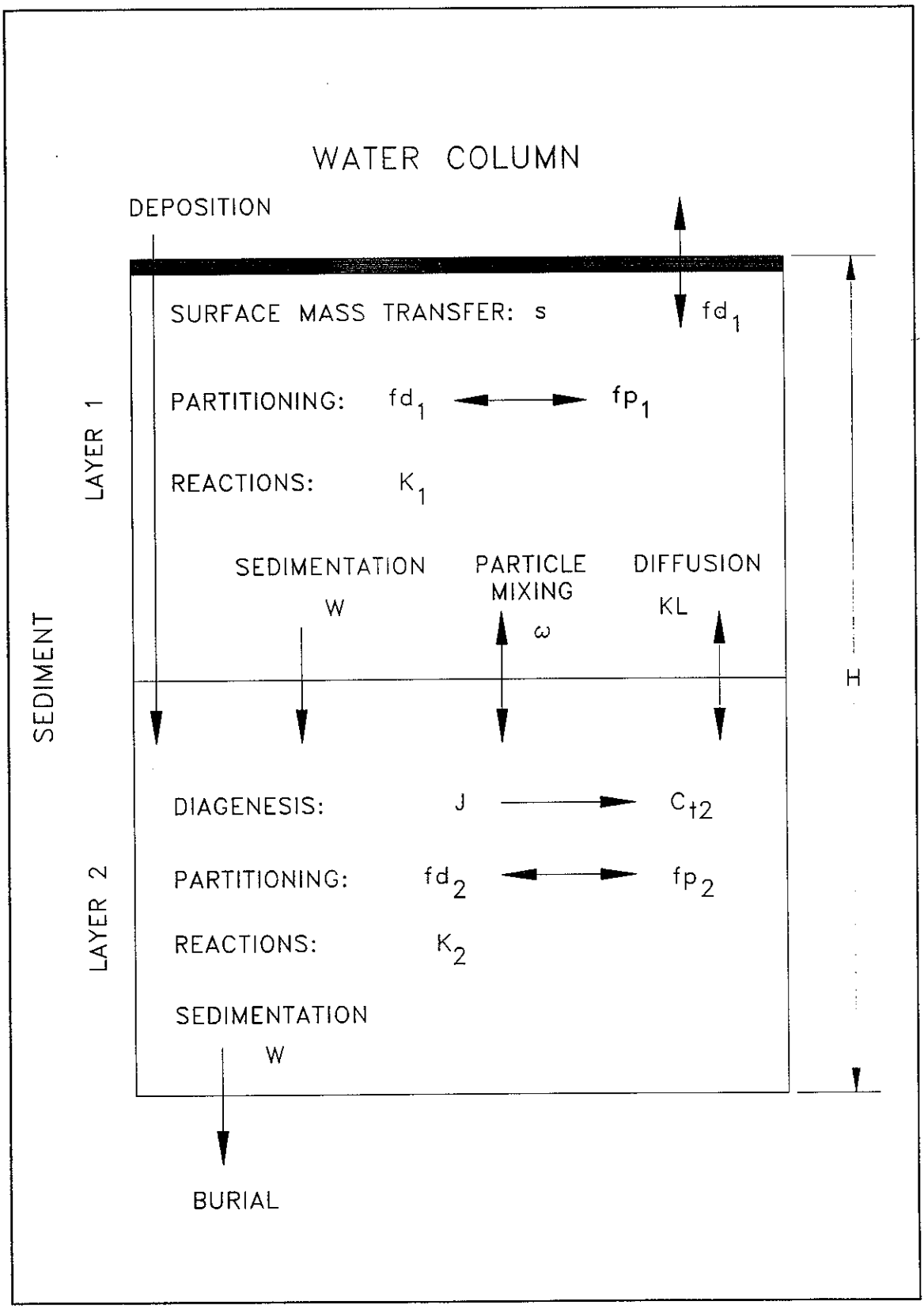

Figure 10-2. Sediment Layers and Processes

Diagenesis

Organic matter in the sediments is divided into three G classes or fractions, in accordance with principles established by Westrich and Berner (1984). Division into G classes accounts for differential decay rates of organic matter fractions. The G1, labile, fraction has a half life of 20 days. The G2, refractory, fraction has a half life of one year. The G3, inert, fraction undergoes no significant decay before burial into deep, inactive sediments. Each G class has its own mass-conservation equation:

$$H\frac{\delta Gi}{\delta t} = W_{net} f_i C - W Gi - H K_i Gi \theta_i^{(T-20)} \quad (2)$$

H = total thickness of sediment layer (m)
Gi = concentration organic matter in G class i (gm m^{-3})
f_i = fraction of deposited organic matter assigned to G class i
W = burial rate (m day^{-1})
K_i = decay rate of G class i (day^{-1})
θ_i = constant that expresses effect of temperature on decay of G class i

Since the G3 class is inert, $K_3 = 0$.

Total diagenesis is the rate at which oxygen demand and nutrients are produced by diagenesis of the G1 and G2 fractions:

$$J = H\left[K_1 G1 \theta_1^{(T-20)} + K_2 G2 \theta_2^{(T-20)}\right] \quad (3)$$

J = total diagenesis (gm m^{-2} day^{-1})

Flux

Total diagenesis provides the driving force for the flux portion of the model. Computation of flux requires mass-balance equations for oxygen demand and nutrients in both sediment layers. The upper layer is thin such that a steady-state approximation is appropriate:

$$s\, fd_1\, Ct_1 = \omega\left(fp_2 Ct_2 - fp_1 Ct_1\right) + KL\left(fd_2 Ct_2 - fd_1 Ct_1\right) - W Ct_1 \pm \sum K_1 \quad (4)$$

Ct_1 = total concentration in upper layer (gm m^{-3})
Ct_2 = total concentration in lower layer (gm m^{-3})
fd_1 = dissolved fraction of total substance in upper layer ($0 \le fd \le 1$)
fd_2 = dissolved fraction of total substance in lower layer
fp_1 = particulate fraction of total substance in upper layer
= $1 - fd_1$
fp_2 = particulate fraction of total substance in lower layer
s = sediment-water mass-transfer coefficient (m day^{-1})

ω = particle mixing velocity (m day^{-1})
KL = diffusion velocity for dissolved fraction (m day^{-1})
ΣK_1 = sum of all sources and sinks due to reactions in upper layer (gm m^{-2} day^{-1})

The left hand side of Equation 4 represents flux to the water column under the assumption that dissolved concentration in the water column is negligibly small compared to the sediments. The assumption is made here for notational simplicity. Effects of concentration in the overlying water are computed in the sediment model code. The terms on the right hand side are mass transport due to particle mixing, diffusion of dissolved substance, deposition to the lower layer, and reactive sources and sinks. The reactions include, for example, the oxidation of sulfide that results in sediment oxygen demand. The equation states that flux to the water column, deposition from surficial sediments, and reactive sources and sinks are balanced by mixing and diffusion from deeper sediments.

The mass balance equation for the lower layer accounts for temporal concentration variations:

$$\frac{\delta Ct_2}{\delta t} = \frac{J}{H} - \frac{\omega}{H}\left(fp_2 Ct_2 - fp_1 Ct_1\right) - \frac{KL}{H}\left(fd_2 Ct_2 - fd_1 Ct_1\right) + \frac{W}{H}\left(Ct_1 - Ct_2\right) \pm \sum K_2 \quad (5)$$

ΣK_2 = sum of all sources and sinks due to reactions in upper layer (gm m^{-2} day^{-1})

The first term on the right of equation 5 represents the diagenetic source of oxygen demand or nutrient. The second term represents exchange of the particulate fraction with the upper layer. The third term represents exchange of the dissolved fraction with the upper layer. The fourth term represents deposition of total substance from the upper layer to the lower layer and burial from the lower layer to deep, inactive sediments. The last term is the sum of all internal sources and sinks due to reactions.

The mass balance equations, with appropriate sources and sinks, are solved within the sediment model for sulfide, methane, ammonium, nitrate, phosphate, and silica. Details of the reactions and solution scheme may be found in the model documentation (DiToro and Fitzpatrick 1993).

The water quality and sediment models interact on a time scale equal to the integration time step of the water quality model. After each integration, predicted particle deposition, temperature, nutrient and dissolved oxygen concentrations are passed from the water quality model to the sediment model. The sediment model computes sediment-water fluxes of dissolved nutrients and oxygen based on predicted diagenesis and concentrations in the sediments and water. The computed sediment-water fluxes are incorporated by the water quality model into appropriate mass balances and kinetic reactions.

Data Bases

SONE and BEST Programs

Sediment water flux measures employed in model development, calibration, and performance evaluation were obtained from two programs. The SONE (sediment oxygen and nutrient exchange) program (Boynton et al. 1986) provided observations of sediment oxygen demand, and ammonium, nitrate, phosphate, and silica exchange at eight stations in the upper Bay, Patuxent and Potomac Rivers (Figure 10-3). Observations were collected four times per year during 1985 and 1986. The methodology employed intact sediment cores incubated in triplicate immediately upon collection. SONE data were obtained from the principal investigators by HydroQual Inc., coded on magnetic media, and supplied to WES in July 1989.

Data collected in the SONE program alone were insufficient to develop and calibrate the sediment model. The more extensive BEST (benthic exchange and sediment transformations) program (Garber et al. 1988) employed SONE methodology to measure sediment-water exchanges at fourteen stations throughout the mainstem Bay (Figure 10-4) during 1988. BEST and SONE flux measures were employed to calibrate the sediment model in a "stand-alone" mode.

BEST flux measures were outside the time period of eutrophication model application. Sediment composition measures collected as part of BEST were employed in calibration of the eutrophication model, however. We assumed that sediment composition measured in 1988 was not substantially different than composition in 1984-1986. Cores collected as part of BEST were analyzed for particulate organic carbon, particulate nitrogen, particulate phosphorus, and particulate biogenic silica. Analyses were conducted in 2 cm increments for the upper 22 cm of each core. BEST data were obtained from the principal investigators by HydroQual Inc., coded on magnetic media, and supplied to WES in January 1991.

Sediment Particulate Organic Carbon

Additional particulate organic carbon data were obtained from surveys conducted by the Maryland Geological Survey (Kerhin et al. 1983) and Virginia Institute of Marine Science (Byrne et al. 1983). Analyses were conducted on surficial grab samples collected in each square kilometer of the Maryland portion of the Bay and each square mile of the Virginia portion. Data were supplied by the Chesapeake Bay Program Office to HydroQual Inc., processed into transects and segments, and supplied to WES in January 1991.

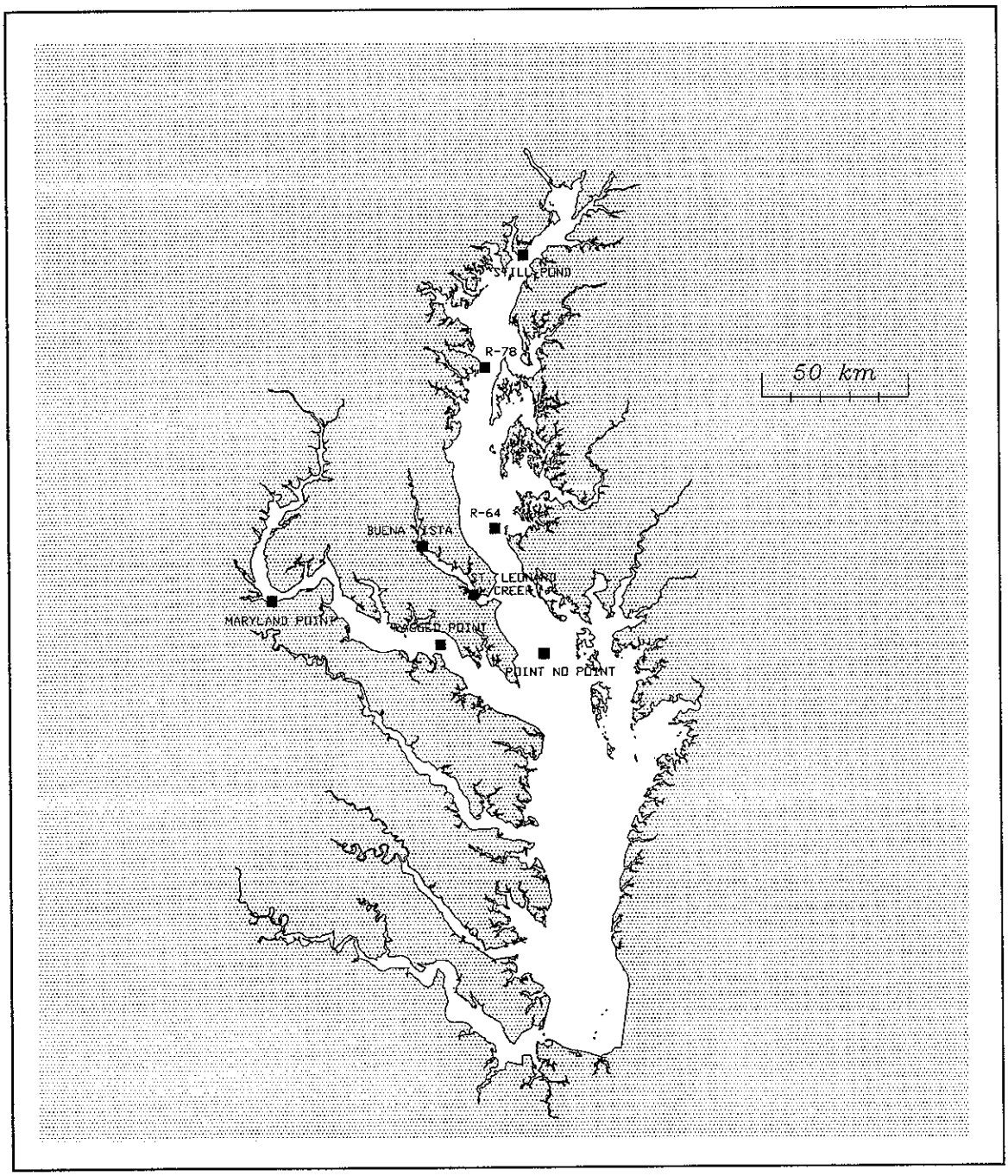

Figure 10-3. SONE Sample Stations

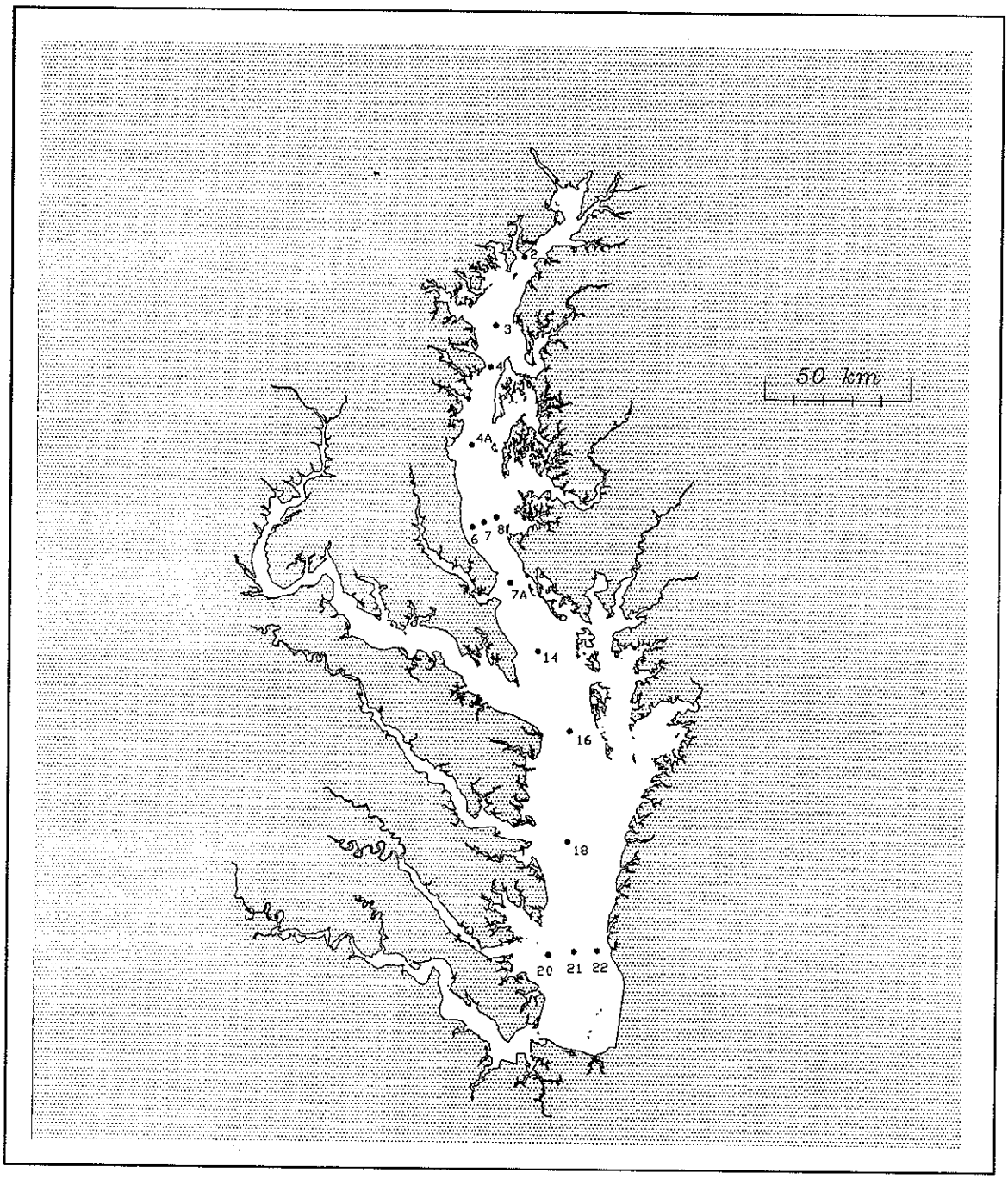

Figure 10-4. BEST Sample Stations

Burial Rates

Sedimentation (or burial) rates were measured via a pollen-dating method (Brush 1989) in cores collected in 1988-1989 (Figure 10-5). Results were reported as accumulation rates (cm yr^{-1}) and mass sedimentation rates (gm m^2 yr^{-1}) at various depths in each core. Results were provided by the principal investigator directly to WES.

Coupling the Water Column and Sediment Submodel

The primary challenge in development of the sediment model was in the flux component. To focus on the primary technical issue, the sediment model was operated in a "standalone" mode during initial development and application. Diagenesis in the "standalone" model was derived from the observed ammonium flux. Conditions in the overlying water were based on observations collected at the time sediment-water fluxes were measured. Spatial variations in model parameters were not considered. Operation of the sediment model in a coupled mode with the model of the water column required evaluation of parameters not employed or only roughly evaluated in the "standalone" application. Coupled operation also provided potential for spatially-varying specification of sediment model parameters.

Net Deposition Rates

Successful coupling of the water column and sediment models required deposition of particulate organic matter in quantities sufficient to produce the diagenesis rates that drove the "standalone" model. Sensitivity analyses indicated, however, that net settling velocity into the sediments was not a critical model parameter. Transport from the water into the sediments was largely determined by the primary production of particles and settling through the water column. No more particles could be incorporated into the sediments than were produced in the water, no matter how large the net settling velocity. Specification of net settling less than settling in the water caused concentration in the cells above the sediments to increase until the product of concentration and settling velocity equaled the delivery of particles from the surface region of the water column.

Net settling was specified identical to particle settling velocities in the water column (Tables 5-11, 5-17). The only exception was net settling of diatoms which was set to zero during the spring bloom period (January - May). Prevention of diatom settling into the sediments was essential to simulating the elevated subsurface diatom concentrations that define the spring bloom.

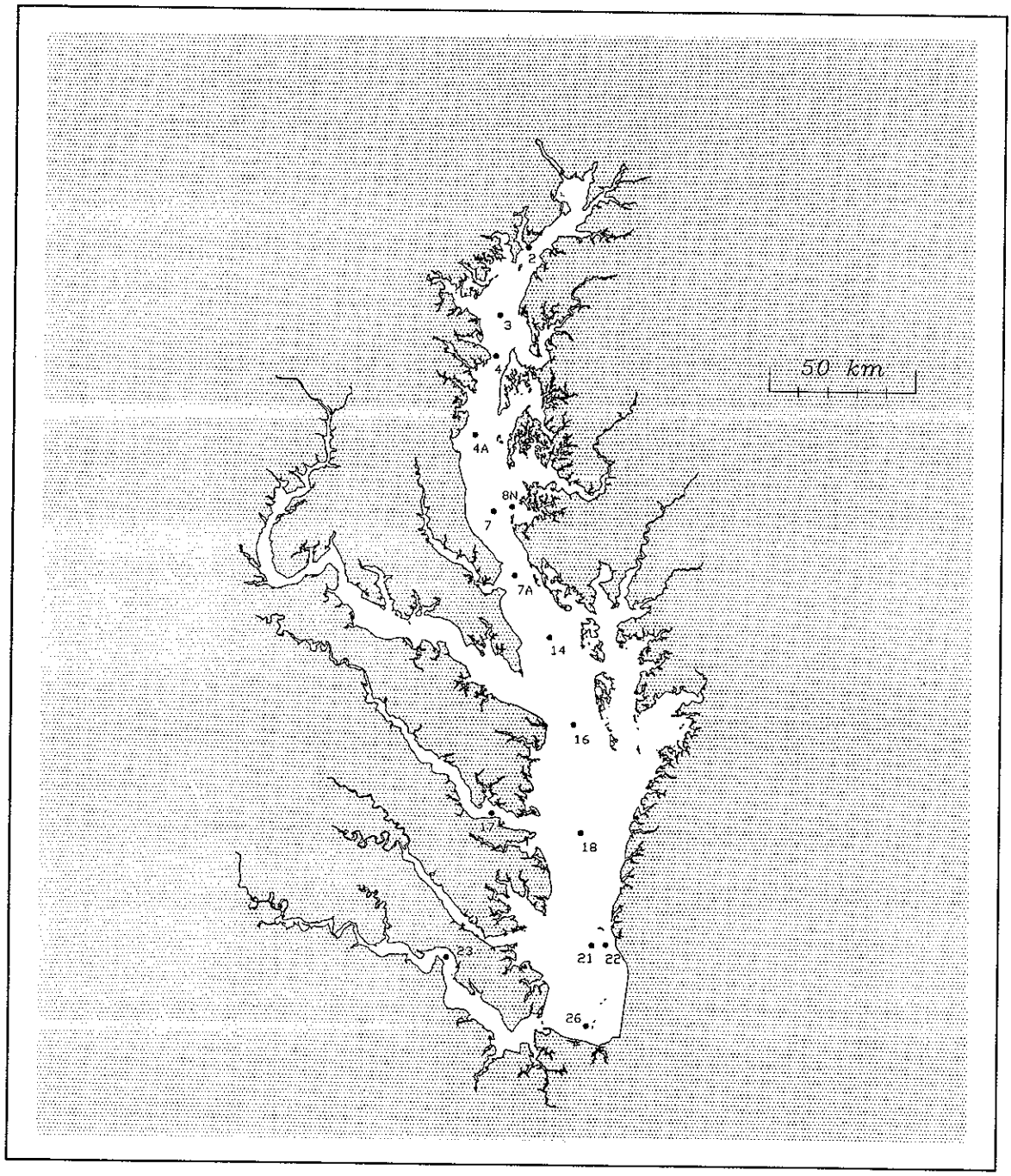

Figure 10-5. Locations of Sedimentation Rate Analyses

Assignment to G Classes

Upon deposition in the sediments, state variables representing particulate organic matter in the water quality model required conversion into sediment model state variables. The water quality model considered two classes of particulate organic matter: labile and refractory. The sediment model was

based on three classes of organic particles: labile (G1), refractory (G2), and inert (G3). Labile particles from the water quality model were transferred directly into the G1 class in the sediment model. Refractory particles from the water quality model had to be split into G2 and G3 fractions upon entering the sediments. Initial guidance for the splits was obtained from experiments (Westrich and Berner 1984) in which roughly even distribution between refractory and inert particulate organic carbon was noted. The final distribution (Table 10-1) was obtained from model calibration. Splits of organic detritus were specified by zone (Figure 10-6). In all zones, nitrogen was considered slightly more reactive than carbon or phosphorus. This treatment was determined by the observed carbon enrichment of sediment particles relative to the water column. The carbon-to-nitrogen ratio in Chesapeake Bay sediments is $\approx$ 10:1; the carbon-to-nitrogen ratio in the water column is $\approx$ 6:1. Detritus in the zones immediately below the fall lines was considered largely inert. This consideration was driven by observed water-column nutrient concentrations. Unless fall-line particles settling to the sediments were assigned minimal reactivity, sediment nutrient releases produced water column concentrations greatly in excess of observations.

Algae settling directly to the sediments also required routing into sediment model state variables (Table 10-1). The algal fraction routed into G1 particles was equivalent to the fraction of algal particles assigned to the labile pool following mortality in the water column. Routing of refractory algae into G2 and G3 classes was equivalent to the split employed for detritus throughout most of the Bay. No spatial variation in the reactivity of algae was considered.

Table 10-1
Routing Organic Particles into Sediment Classes

WQM Variable	Carbon, Phosphorus			Nitrogen		
	% G1	% G2	% G3	% G1	% G2	% G3
Labile Particles	100			100		
Refractory Particles, Bay and Tributary Zones 1		11	89		26	74
Refractory Particles, Bay Zones 2, 10		43	57		54	46
Refractory Particles, All Other Zones		73	27		82	18
Algae	65	25	10	65	28	7

Burial Rates

Particles were removed from the active sediment layer by burial into deep, non-reactive sediments. Initial estimates of burial velocity were obtained from

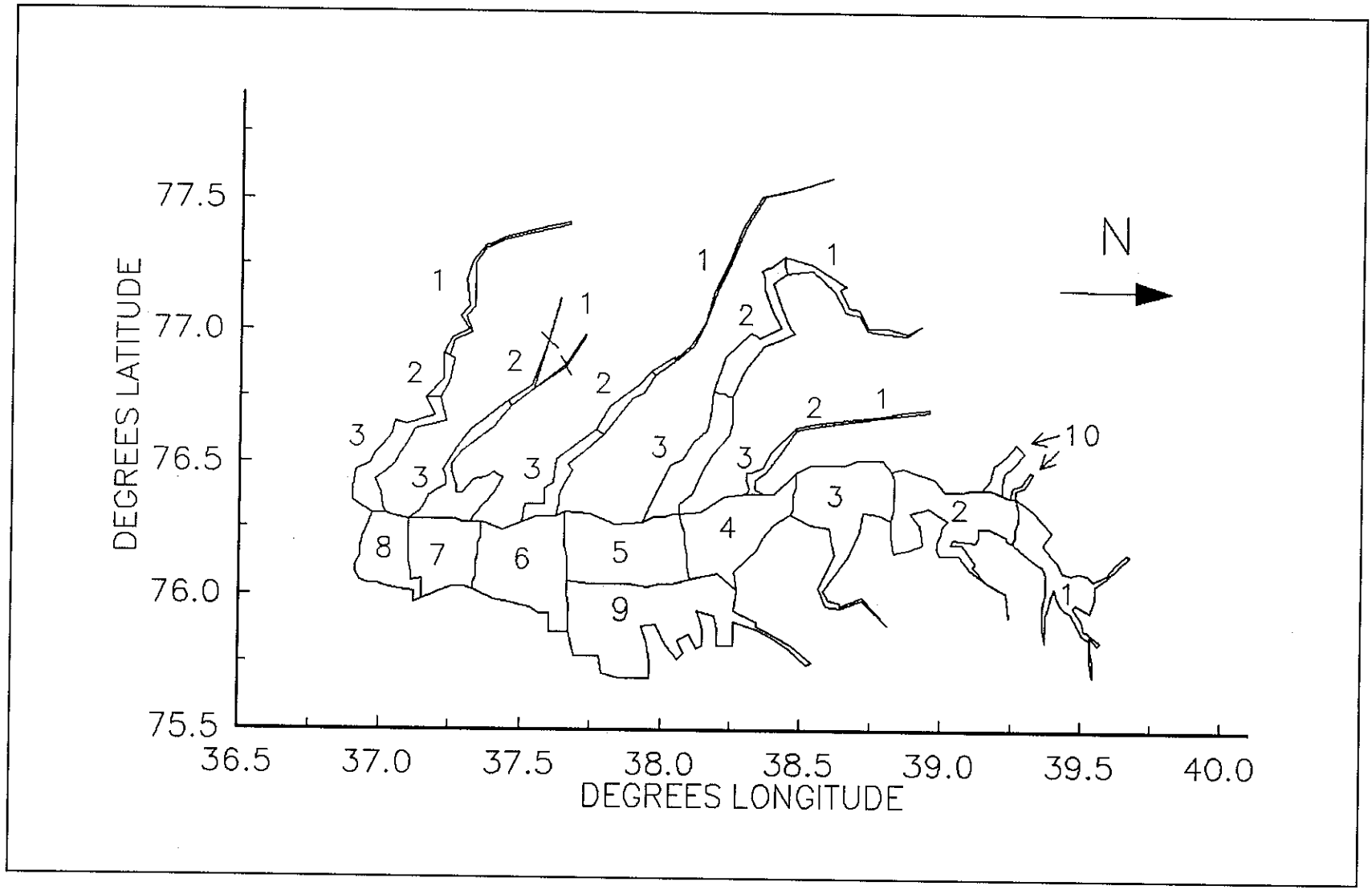

Figure 10-6. Zones for Assignment of Sediment Model Parameters

the Brush data set. Raw data supplied to WES included sedimentation rates specified by depth interval in the sediments. Depth intervals corresponded to age intervals. When possible, weighted mean sedimentation rates, from the earliest to most recent age intervals, were computed (Table 10-2). Weighting was proportional to the length of each age interval. No spatial or other patterns were apparent in the data. Final sedimentation rates in the mainstem Bay (Table 10-3) were set by adjusting burial velocity to achieve agreement between predicted and observed concentrations of sediment organic particles. The resulting axial distribution of sedimentation rates agreed with the tendency apparent in an extensive assemblage of observations (Officer et al. 1984).

Table 10-2
Observed Sedimentation Rates

Core	Earliest Year	Sedimentation Rate, cm yr^{-1}
2	1955	0.06
3	1937	0.16
4	1957	0.36
4A	1937	0.19
7	1941	0.21
8N	1941	0.11
7A	1945	0.07
14	1845	0.007
16	1944	0.29
18	1943	0.11
21	1969	0.16
22	1944	0.16
26		> 0.21
17		> 0.32
23		> 0.30

Table 10-3
Model Burial Velocity

Bay Zones	Velocity, cm yr^{-1}	Tributary Zones	Velocity, cm yr^{-1}
1, 2, 10	0.50	1	0.50
3 – 6, 9	0.25	2, 3	0.25
7, 8	0.37		

Burial rates were highest near the Susquehanna, least in the central Bay, and moderate near the Bay mouth.

Burial rates in the tributaries (Table 10-3) were patterned after the Bay. Highest burial rates were specified below the fall lines with lower rates further downstream. The decreasing trend in burial with distance away from the fall lines reflected findings in several Bay tributaries (Brush 1984).

Revisions to Sediment Model Calibration Parameters

Freshwater versus Saltwater. Calibration of the "standalone" sediment model was based primarily on sediment-water flux observations collected in saline regions of the Bay and tributaries. Spatial variations in model parameter values were not considered. The sediment oxygen demand portion of the model differentiated between fresh and saltwater but the nitrogen, phosphorus, and silica kinetics routines did not. During calibration of the water quality model, the need for adjustment of sediment model parameters in portions of the Bay system became apparent. Sediments adjacent to fall lines appeared to retain larger fractions of deposited nitrogen and phosphorus than sediments elsewhere. One way to readily parameterize this variation, especially in the tributaries, was assignment of different parameter values in fresh and saltwater. Increased nitrification and denitrification rates and phosphorus sorption coefficients were specified in freshwater relative to saltwater (Table 10-4). The division between the two regimes was set at 1 ppt salinity, the same salinity that determined employment of methane or sulfide in the SOD kinetics.

Table 10-4
Revisions to Sediment Model Parameters

Parameter	Standalone Sediment Model	Coupled Sediment - Water Quality Model
Nitrification Velocity, (m day^{-1})	0.131	0.200 freshwater, 0.140 saltwater
Denitrification Velocity, (m day^{-1})	0.100	0.300 freshwater, 0.125 saltwater
Phosphate Partition Coefficient, (L kg^{-1})	300	3000 freshwater, 300 saltwater
Half–Saturation Dissolved Oxygen Concentration, (gm m^{-3})	3.68	1.0

It's worth noting that adjustments for freshwater, forced by mass-balance considerations, were later independently validated. Experiments by Gardner, Seitzinger, and Malczyk (1991) determined that ammonium release from

sediments in freshwater was less than from the same sediments in synthetic seawater. They hypothesized that nitrification was favored in freshwater, over saltwater, by differential adsorption of ammonium to sediment particles.

In the sediment model documentation, DiToro and Fitzpatrick (1993) noted spatial variation in the ratio of dissolved to particulate sediment phosphate observed in the mainstem Bay. At the most upstream station (Still Pond, Figure 10-3), pore-water phosphate was lowest while particulate inorganic phosphate was highest. They indicated the partition coefficient was largest at the upstream station and decreased downstream.

Nitrification/Denitrification Rates. Predicted sediment ammonium release during hypoxic/anoxic intervals often exceeded observations. The enhanced anoxic release was due to blocking of the nitrification portion of the nitrification/denitrification process that removes nitrogen from the sediments. Excess ammonium release was countered, to the greatest extent possible, by lowering the half-saturation dissolved oxygen concentration for nitrification specified in the "standalone" sediment model to a value (Table 10-4) consistent with the half-saturation concentration specified for the water column (Table 9-18). Small adjustments were also made in the basic nitrification and denitrification rates specified in the final calibration of the "standalone" model.

Verification of Model Behavior

Development of the sediment model indicated the functional dependence of sediment-water fluxes on the sediment-water mass-transfer coefficient. Numerous fundamental relationships between sediment-water fluxes of different substances were revealed as well. To ensure the sediment model was correctly coupled to the water quality model, we determined that functional relationships identified in the "standalone" model occurred in the coupled model as well. One relationship was selected for each of the fluxes predicted by the sediment model: ammonium, nitrate, phosphate, silica, and SOD. Results from the coupled model are shown side-by-side with figures excerpted from the standalone model documentation (Figures 10-7 to 10-12). The fundamental relationships correspond closely which indicates that the sediment model performs the same whether operated in a standalone or coupled mode.

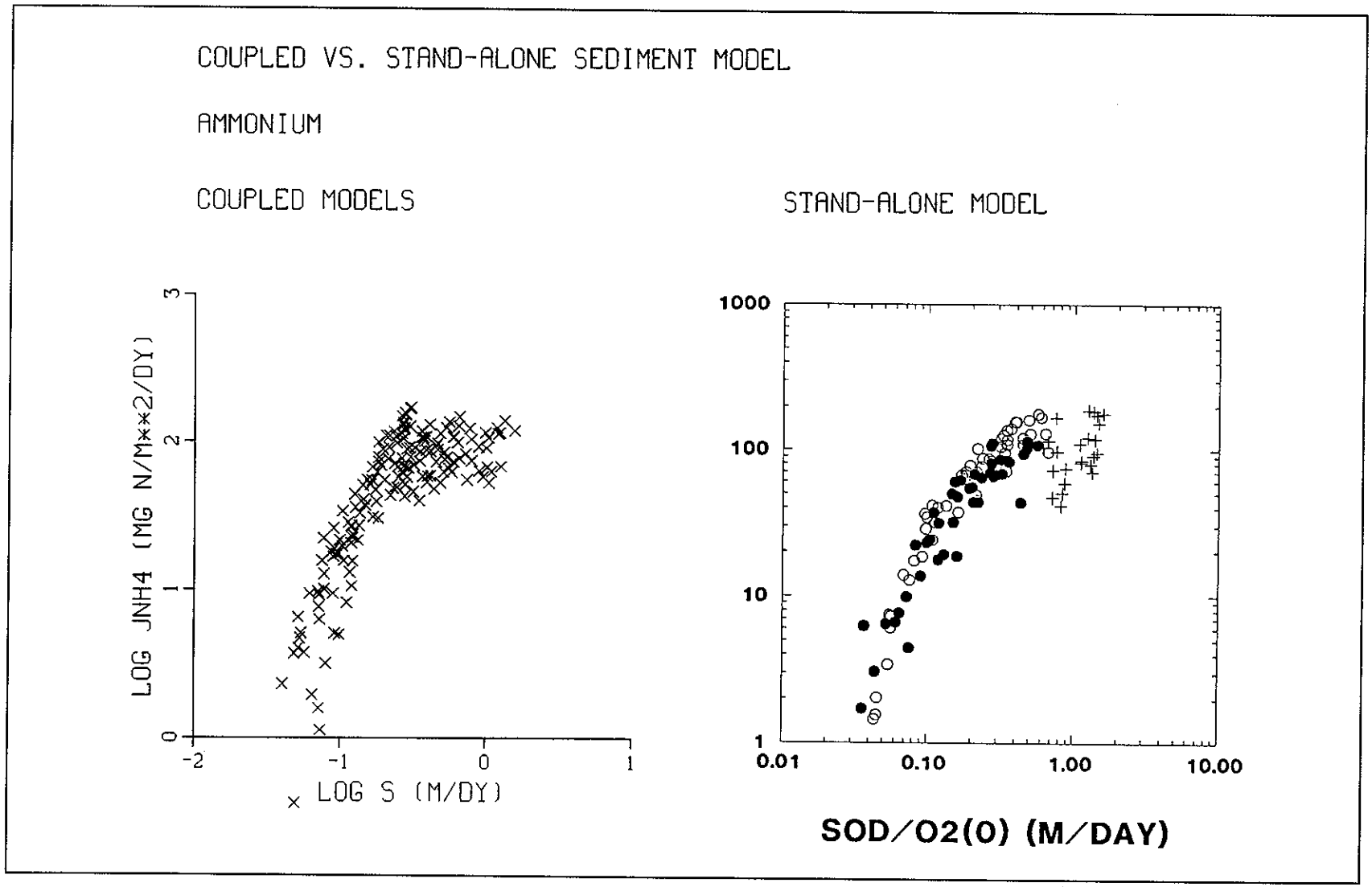

Figure 10-7. Ammonium Flux vs. Mass-Transfer Coefficient, Coupled and Standalone Models

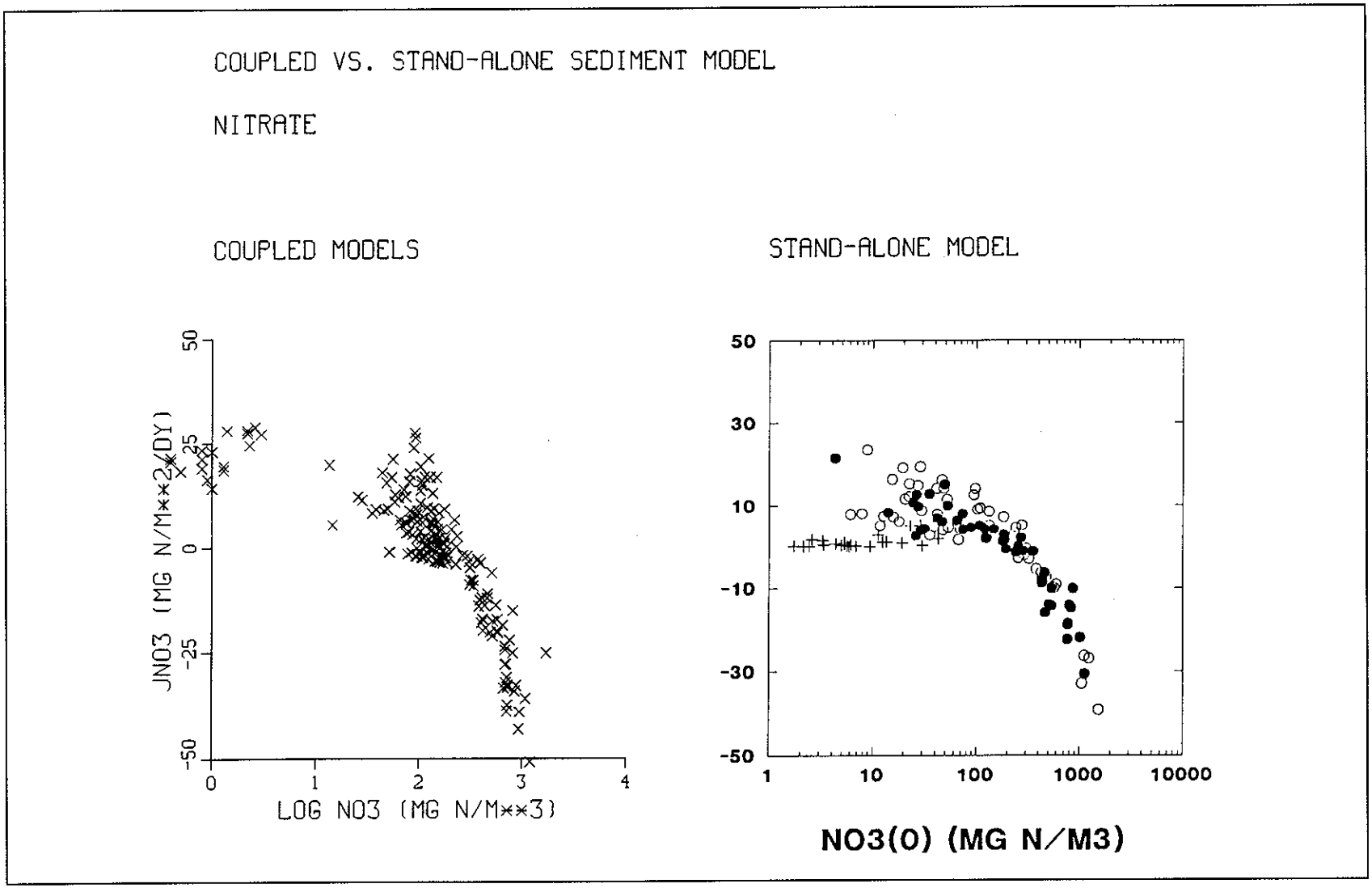

Figure 10-8. Nitrate Flux vs. Nitrate Concentration, Coupled and Standalone Models

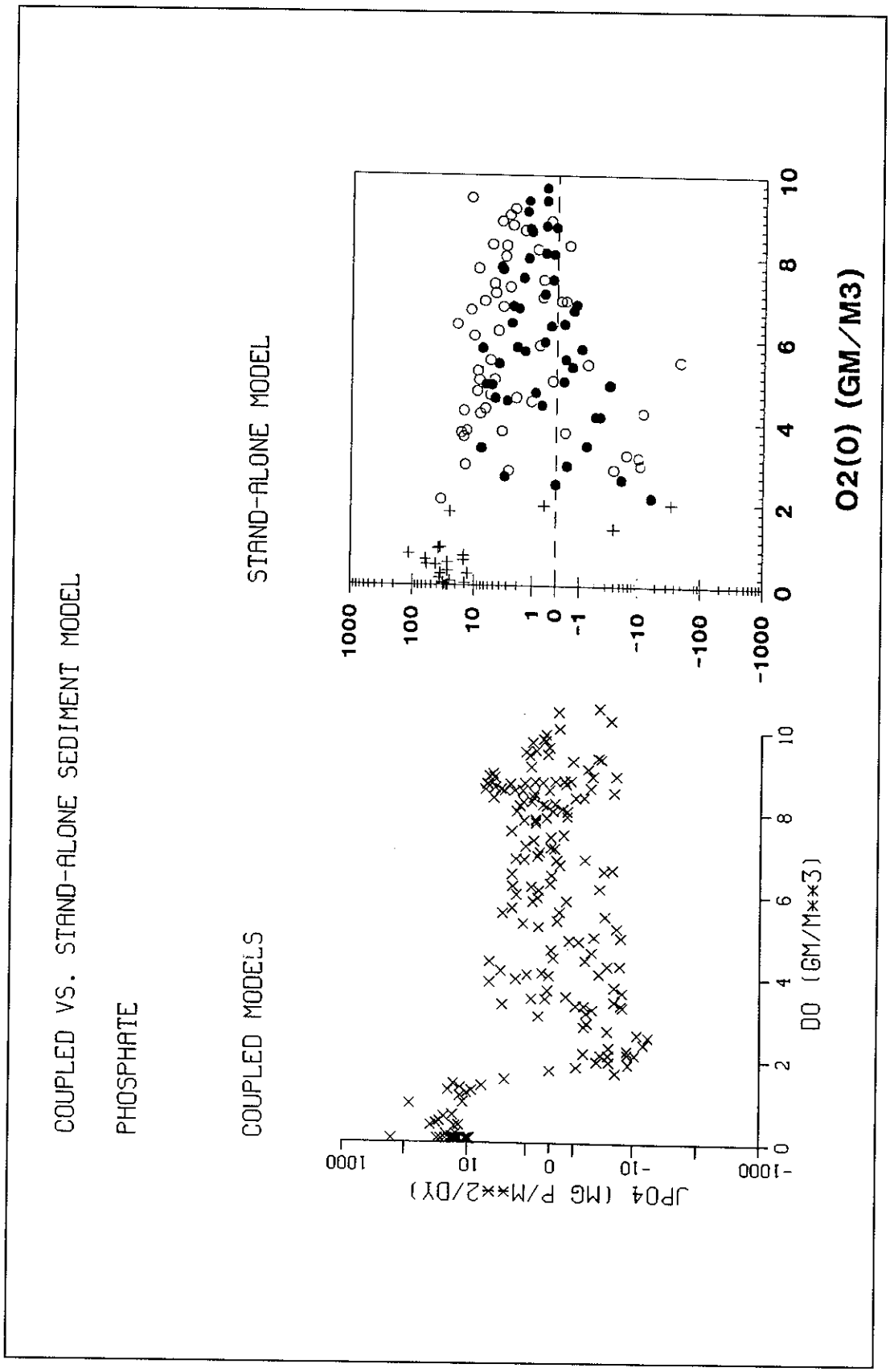

Figure 10-9. Phosphate Flux vs. Dissolved Oxygen Concentration, Coupled and Standalone Models

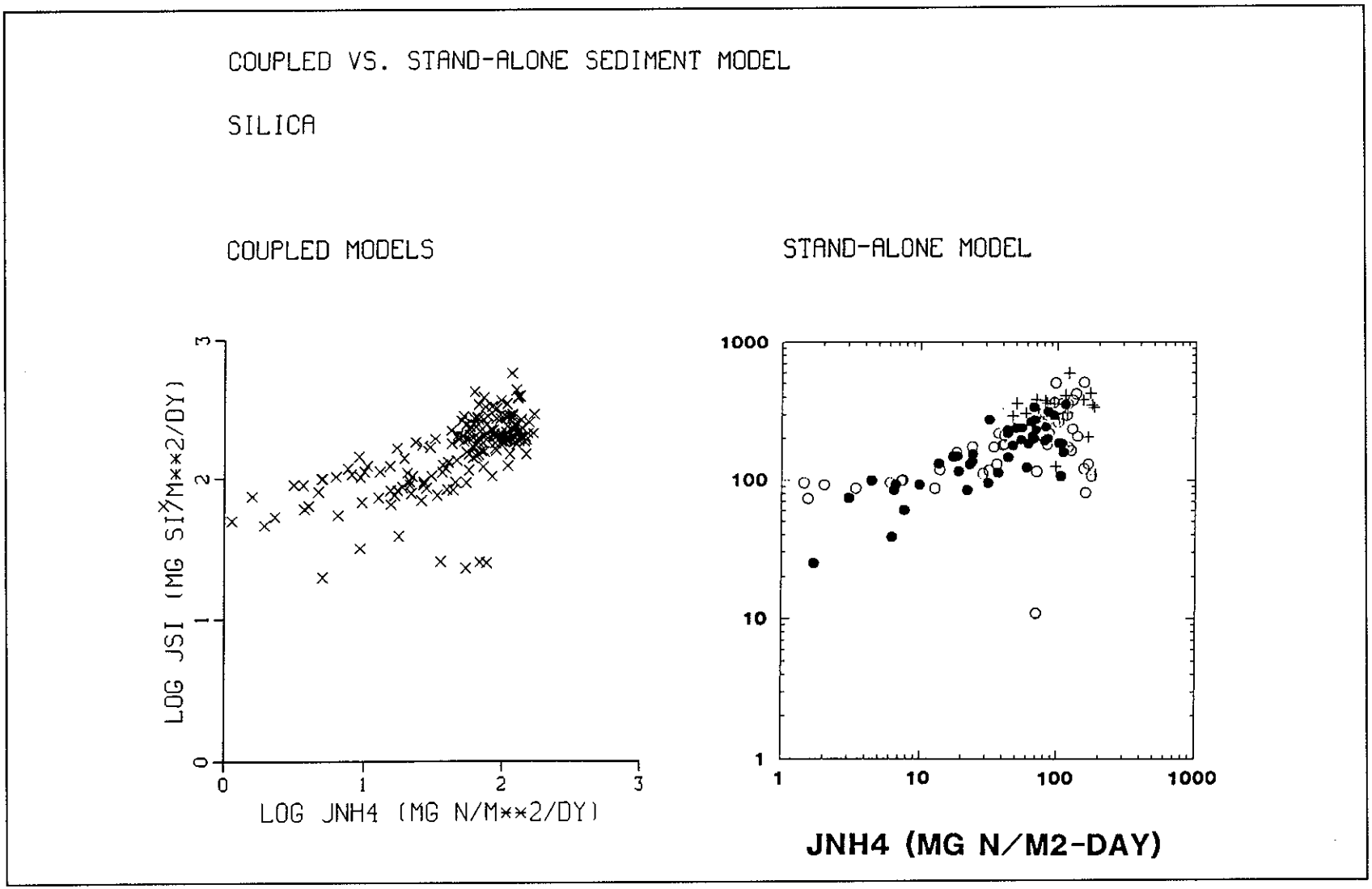

Figure 10-10. Silica Flux vs. Ammonium Flux, Coupled and Standalone Models

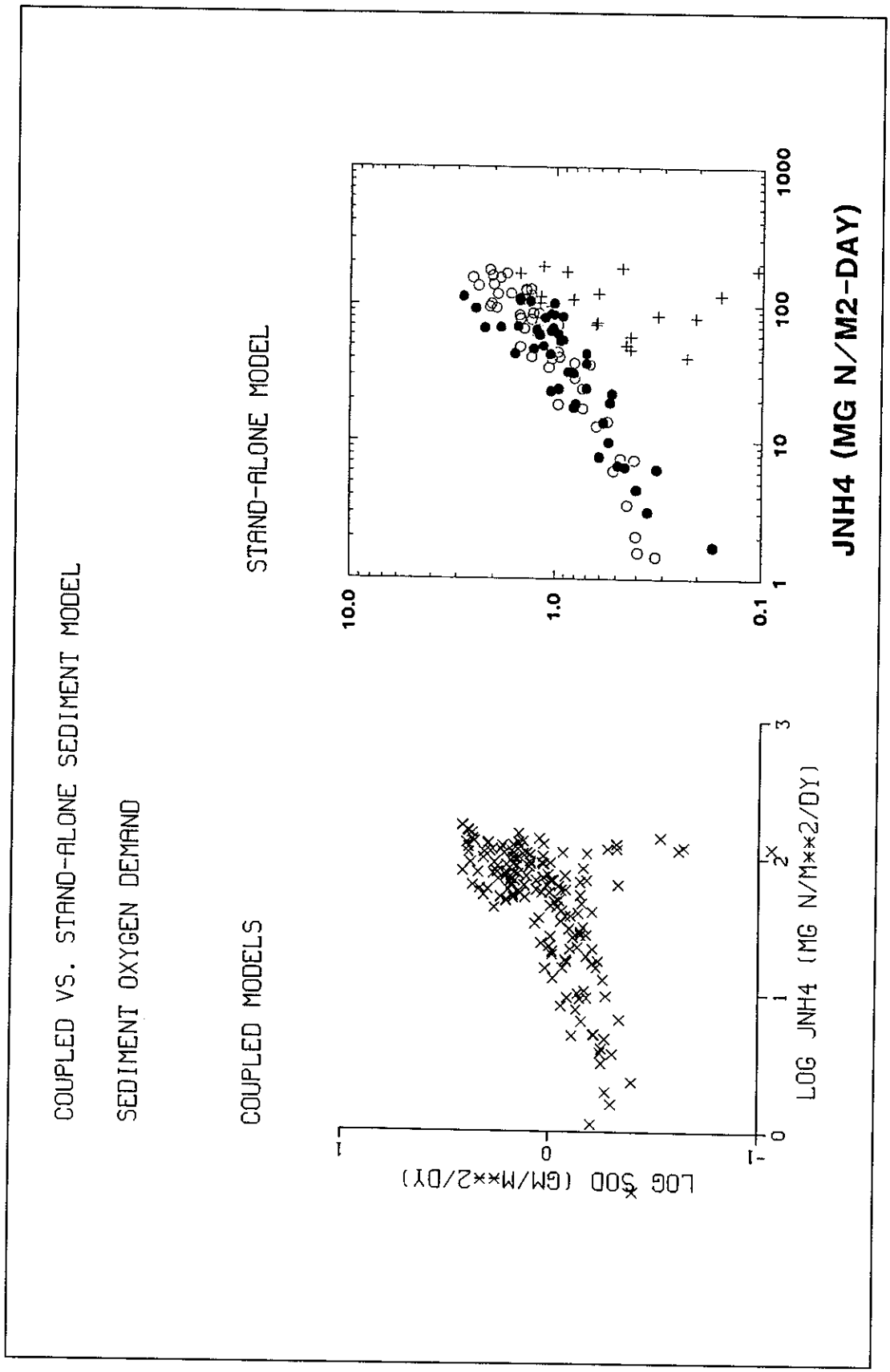

Figure 10-11. Sediment Oxygen Demand vs. Ammonium Flux, Coupled and Standalone Models

Chapter XI: Mainstem Bay Calibration Results

Introduction

Each observation in the monitoring program was collected at an instant in time at a single point in space. Time scales realistically represented in the model were determined by time scales of primary forcing functions: tidal-average hydrodynamics, daily meteorologic updates, fortnightly fall-line loads, and monthly direct loads. The minimum model spatial scales were determined by the size of the grid: kilometers in horizontal extent and meters in vertical extent. The disparity in temporal and spatial scales in the monitoring program and the model meant that individual observations were not directly comparable with model predictions for single time steps in single cells.

Interpretation of individual observations was clouded by spatial and temporal gaps between data points and by random physical and biological effects that occurred on time scales similar to the duration of the observation. Consequently, monitoring data were best interpreted when viewed as assemblages, to minimize effects of gaps, or when aggregated, to minimize effects of random variability.

Calibration of the model and presentation of results required aggregations of observations and predictions that provided meaningful information and allowed for direct comparison. Both temporal and spatial aggregations were necessary. The minimum temporal aggregation was determined by the sampling frequency of the monitoring program. Surveys were conducted once or twice monthly. Consequently, minimum temporal aggregation was one to two months in order to average several samples at each station. Aggregation seasons were defined through examination of characteristic, repetitive Bay behavior (Figure 11-1). Season One was defined from the beginning of the calendar year to the onset of the spring bloom, Julian days 1 - 60. Season Two was defined as the duration of the spring bloom, Julian days 61 - 150. The division between Seasons Two and Three roughly coincided with two events, the end of the bloom and the onset of anoxia. Season Three extended from the onset of anoxia to the fall overturn, Julian days 151 - 270. Season Four was

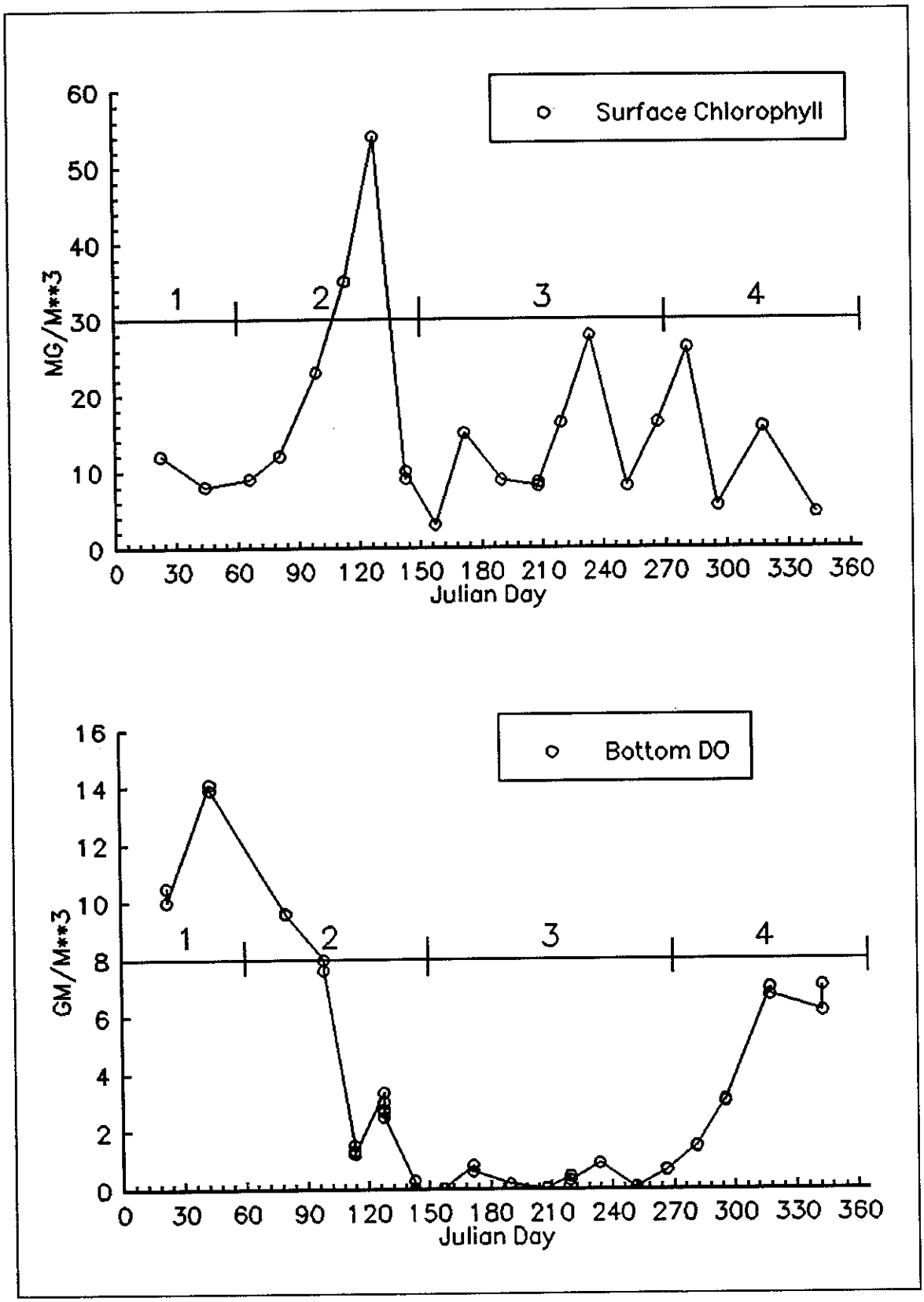

Figure 11-1. Aggregation Seasons (Data from Station CB3.3C, 1985)

Table 11-1
Aggregation Seasons

Sequence	Season	Julian Days
One	Winter	1 – 60
Two	Spring	61 – 150
Three	Summer	151 – 270
Four	Fall	271 – 365

defined as the period from fall overturn to the end of the calendar year, Julian days 271 - 365.

Spatial aggregation was required on two scales, horizontal and vertical. To illustrate temporal Bay behavior, model output and data were aggregated into zones and levels. Ten zones were defined in the longitudinal-lateral plane (Figure 11-2). Limits of eight of the zones were defined by entry of major Bay tributaries. The ninth zone was defined along the Eastern Shore and the tenth zone was defined as the Patapsco and Back Rivers. The characteristic length of the zones was ≈ 30 km. Zone width spanned the Bay except adjacent to Zone 9 at which the Bay was resolved laterally into two zones. Most zones contained three or more monitoring stations although, in the limit, two zones contained only one station each.

Vertical aggregation was into three levels which were defined through examination of vertical concentration profiles. Observations (Figure 11-3, 11-4) often indicated a well-mixed surface layer that extended roughly 6 meters down from the surface. Below the well-mixed layer, a pyncnocline or region of maximum vertical transition extended roughly an additional 6 meters. Below the pyncnocline, well-mixed conditions again prevailed. Layer One was defined to coincide with the surface mixed layer (0 to 6.7 m) and comprised the upper four model layers. Layer Two approximated the pyncnocline region (6.7 - 12.8 m) and included the next four layers from the surface. Layer Three corresponded to the bottom mixed layer (depth > 12.8 m) and included all model layers beyond the eight uppermost.

Table 11-2
Aggregation Layers

Sequence	Layer	Depth, m
One	Surface Mixed Layer	0 – 6.7
Two	Pyncnocline	6.7 – 12.8
Three	Bottom Mixed Layer	> 12.8

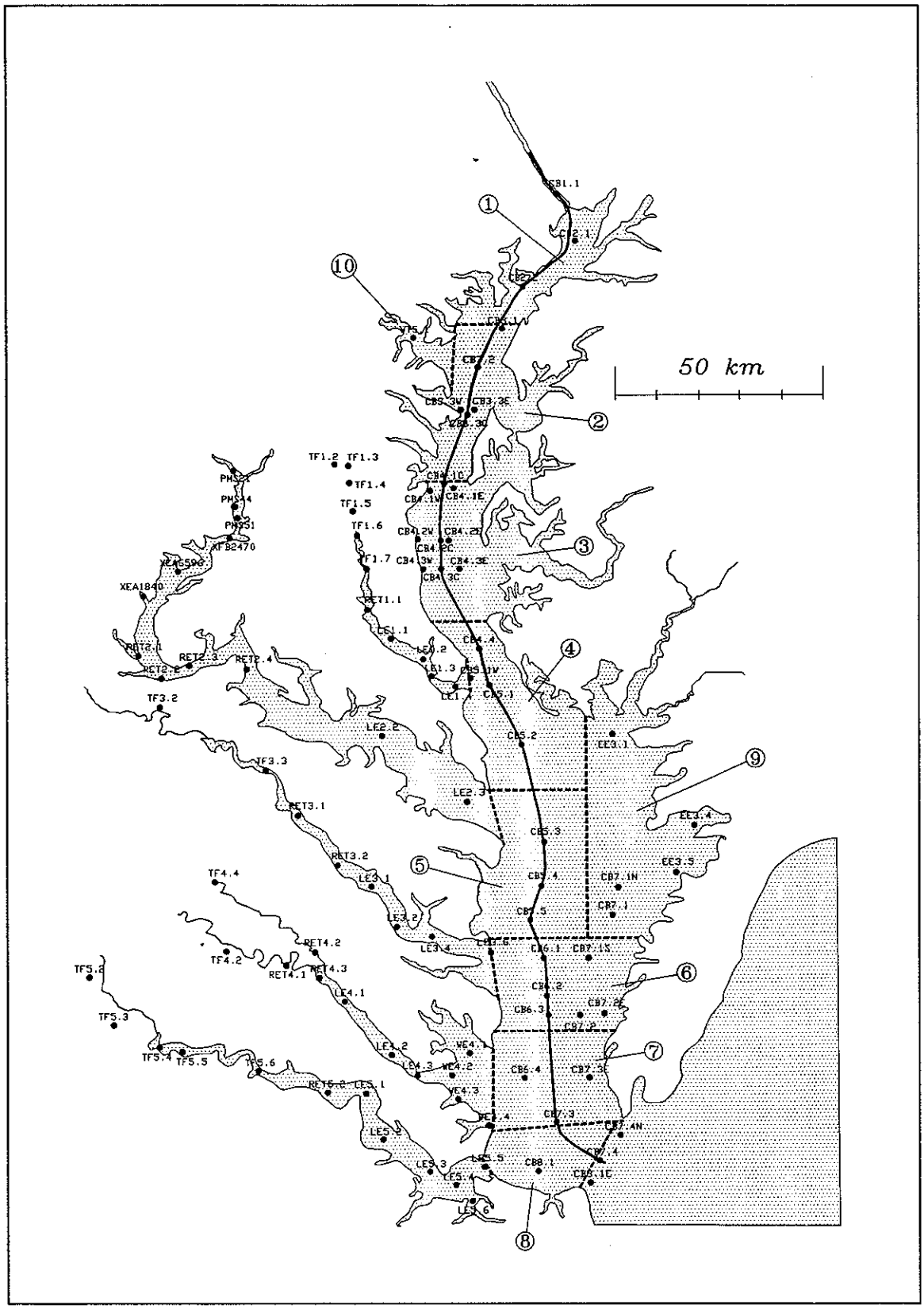

Figure 11-2. Mainstem Bay Aggregation Zones

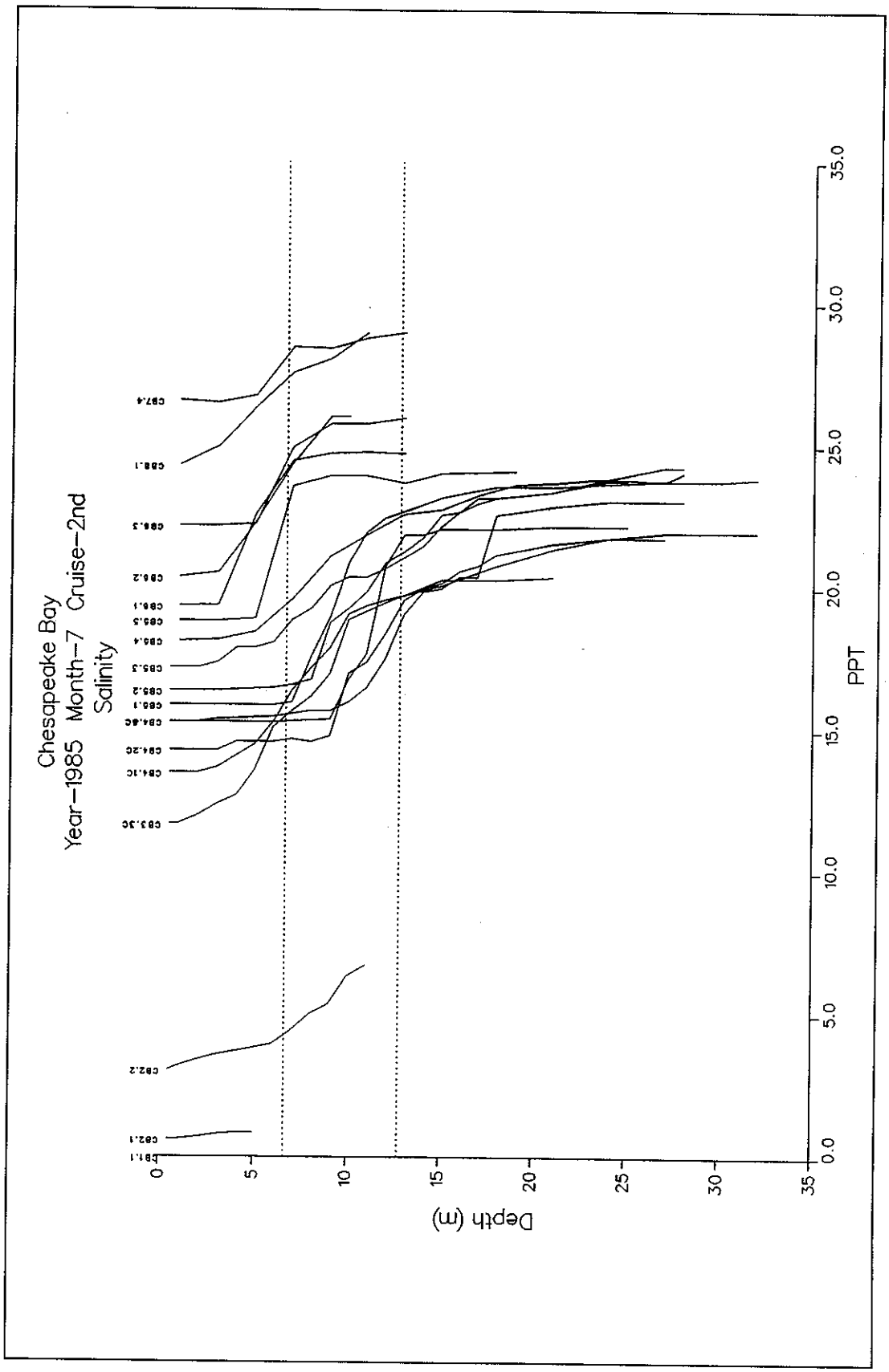

Figure 11-3. Salinity versus Depth Along Mainstem Bay Axis (Dashed lines show extent of surface-mixed layer and pyncnocline)

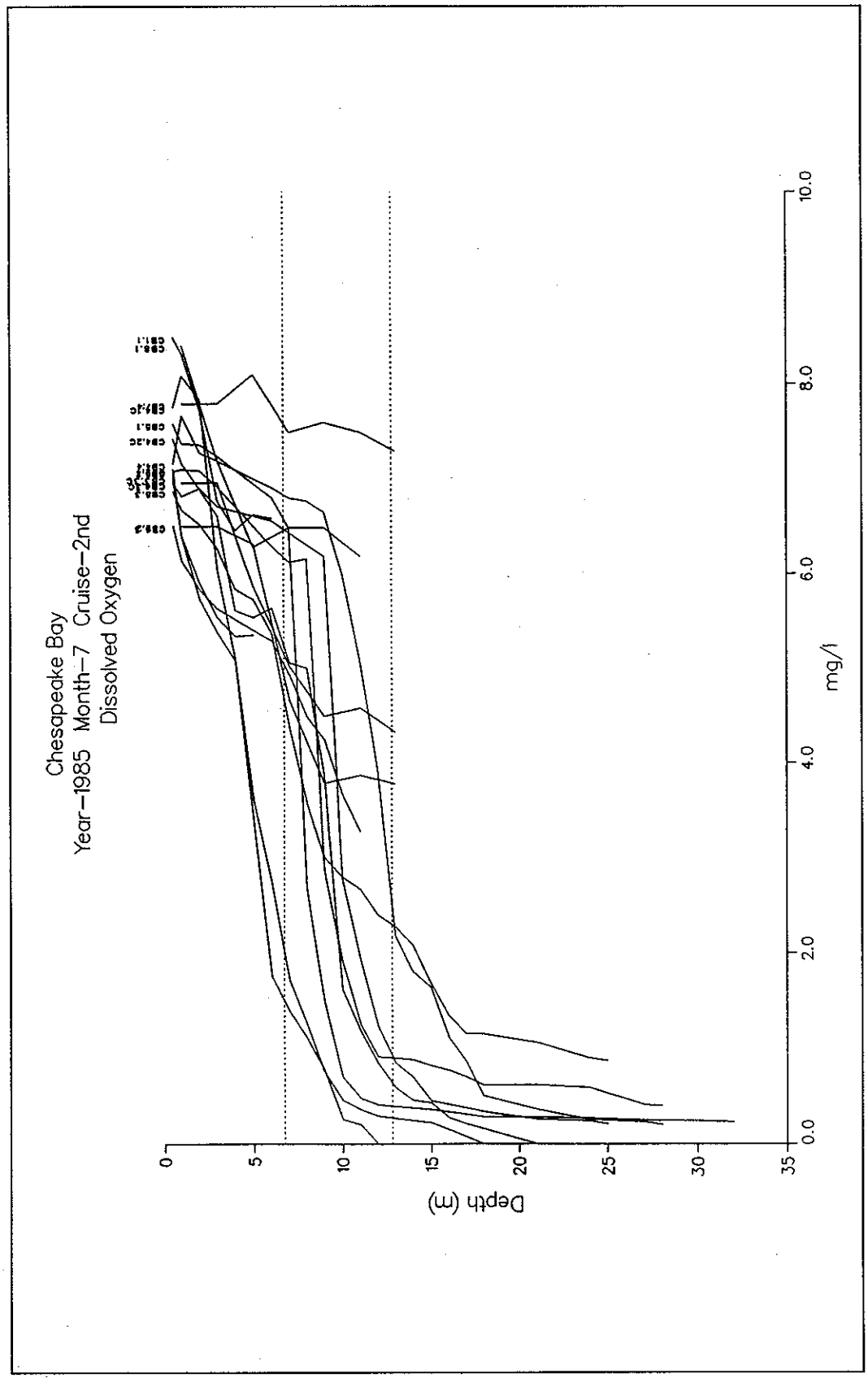

Figure 11-4. Dissolved Oxygen versus Depth Along Mainstem Bay Axis (Dashed lines show extent of surface-mixed layer and pyncnocline)

The primary presentation modes were time series in ten zones and longitudinal transects from the Bay mouth to the Susquehanna fall line (Figure 11-2). For the time series, observations and model output were aggregated by season, zone, and level. Along the transect, observations and model output were aggregated by season and level but no spatial aggregation was performed. Even after aggregation, the quantity of plots illustrating calibration was overwhelming. The present volume contains time series for four zones only. Longitudinal plots are provided for 1986, the average hydrologic year. Remaining calibration plots are provided in an appendix produced as a second volume.

Time-Series Plots

Concentration

Time-series plots are presented for Bay Zones Two (Figure 11-5), Four (Figure 11-9), Six (Figure 11-13), and Nine (Figure 11-17). The horizontal axis on each plot extends three years with the origin at January 1, 1984. Model and data are averaged by season and level. Mean and range of the observations are plotted against the predicted mean. The observed mean is the arithmetic mean of the data. The model mean is weighted to account for varying length of the integration time step and volume of individual model cells. Predicted minimum dissolved oxygen is also shown.

Sediment Fluxes

Sediment-water flux observations were sparse such that aggregation was not appropriate. Zone Two contained only one SONE station, R-78 (coincident with CB3.3C in Figure 11-2). Zone Four contained one SONE station located at Point-No-Point (coincident with CB5.2 in Figure 11-2). Observations were conducted once or twice per season. No observations were available in the lower Bay during the calibration period. For presentation, individual observations in Zones Two (Figure 11-6) and Four (Figure 11-10) were plotted against modelled fluxes in the single cell that contained the SONE station. Instantaneous model fluxes were output at ten-day intervals. In the lower Bay, model output only (Figure 11-14) was examined in the cell containing Station CB6.2 (Figure 11-2).

The horizontal axis on each plot extends three years with the origin at January 1, 1984. The vertical axis indicates sediment-water flux. Positive fluxes are from sediment to water, negative fluxes from water to sediment. In addition to predicted and observed fluxes of ammonium, nitrate, phosphate, silica, and oxygen, the plots also indicate predicted COD release and organic particle deposition. A second series of plots (Figures 11-7, 11-11, 11-15) indicates the predicted particle concentrations in the sediments. For nitrogen and carbon, concentrations of the G1, G2, and G3 fractions are shown. For

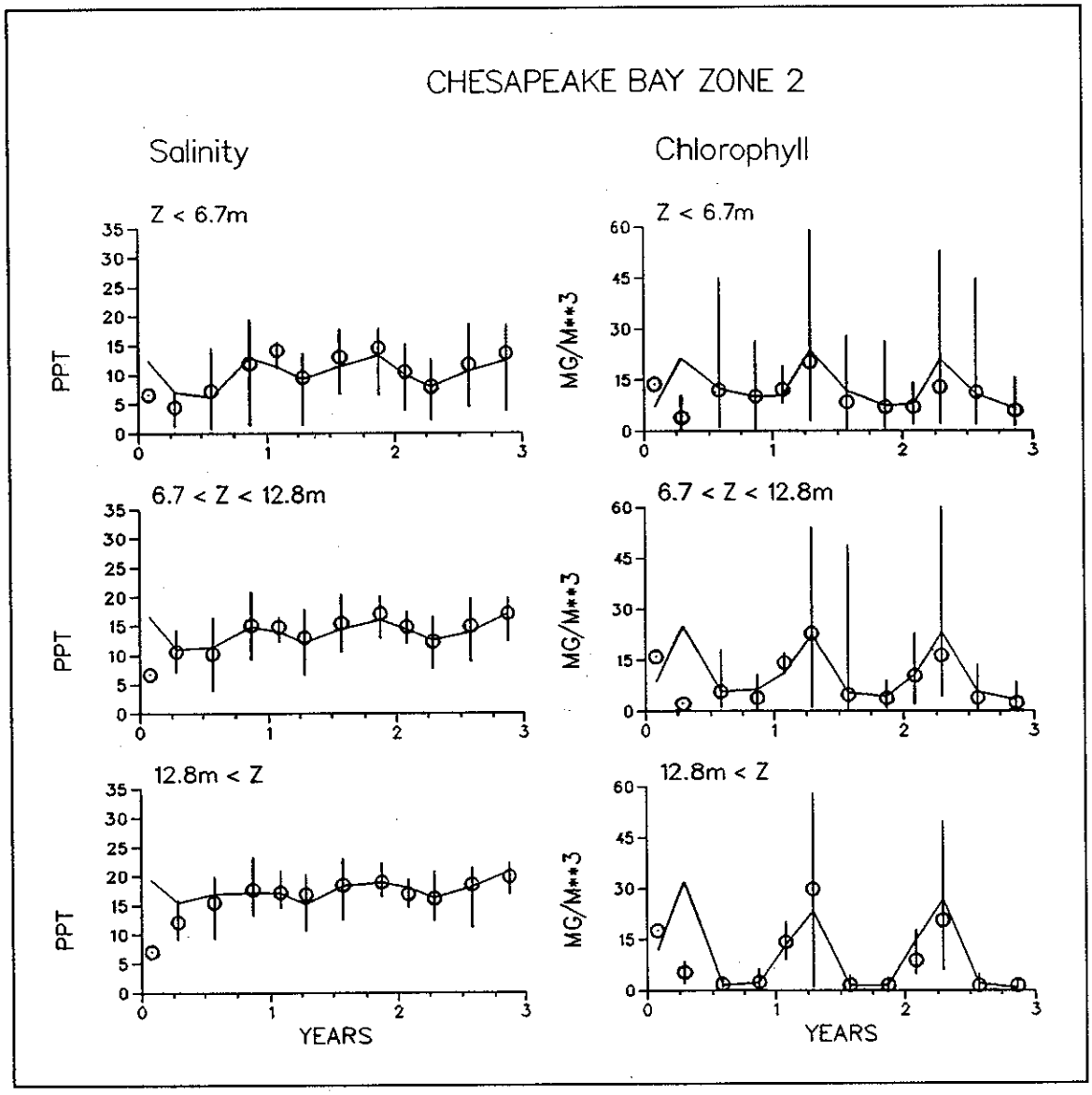

Figure 11-5. Time Series of Predicted and Observed Concentrations in Zone Two (Sheet 1 of 5)

phosphorus, the G1 and G2 fractions are combined and particulate inorganic phosphorus (TPO4) is indicated.

Diagnostic Plots

A series of plots denoted "Diagnostic Plots" are presented for Zones Two (Figure 11-8), Four (Figure 11-12) and Six (Figure 11-16). Diagnostic information includes algal growth limitations, primary production, light extinction, and respiration. As with the sediment plots, observations for comparison with model output are sparse and aggregation is not appropriate. When available,

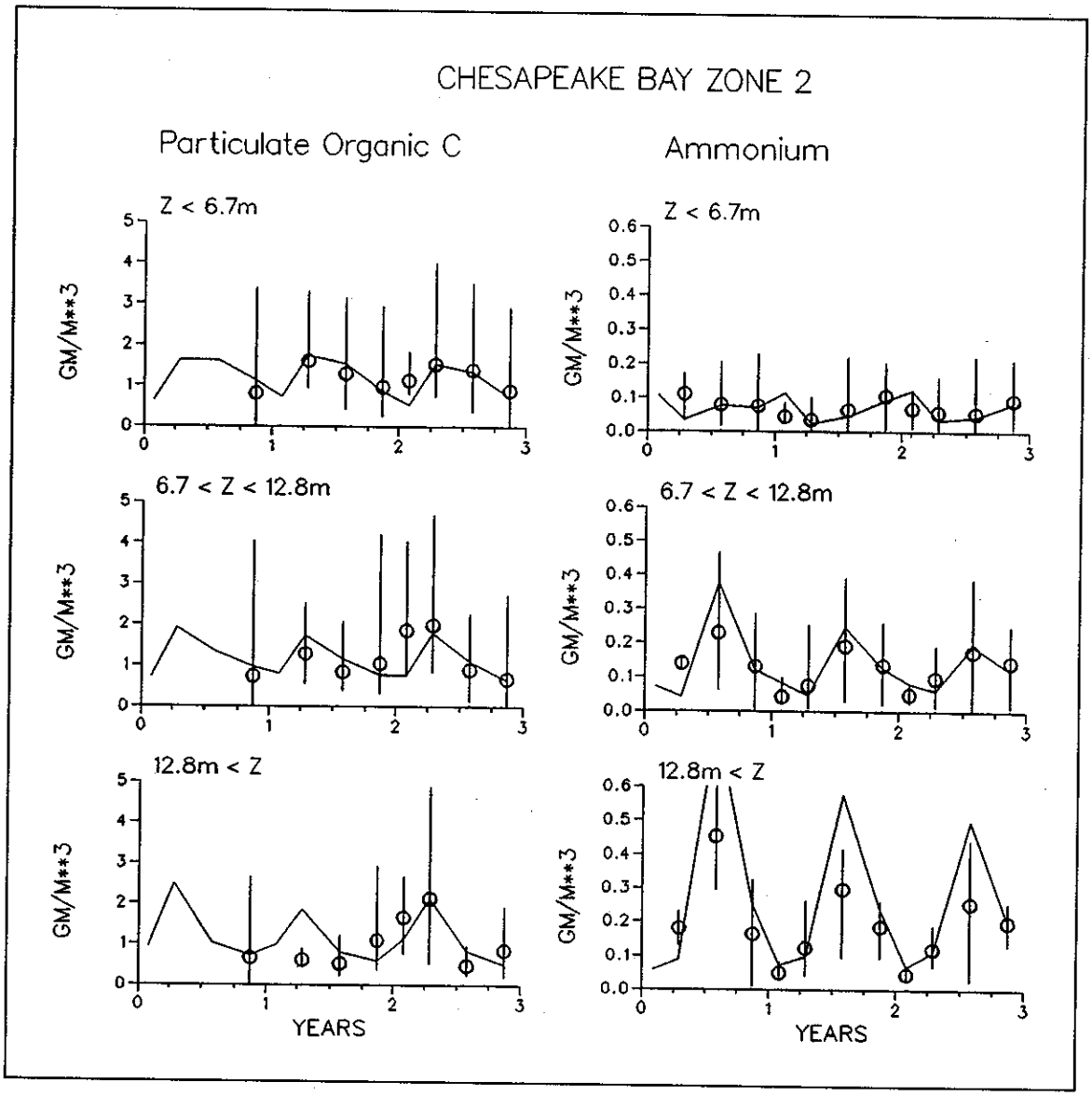

Figure 11-5. (Sheet 2 of 5)

observations are compared with instantaneous model results output at ten-day intervals in cells corresponding to Stations CB3.3C, CB5.2, and CB6.2 (Figure 11-2).

The first diagnostic plot illustrates growth limitations for diatoms in the surface cell (depth < 2.14 m). The range of limitation runs from zero, indicating complete inhibition of growth, to unity, indicating no limitation. The nutrient limitations are computed by Equations 4-5 and 4-6. The light limitation is computed by Equation 4-8. According to model formulation, the diminution from maximum algal growth is the product of the light limitation and the minimum nutrient limitation.

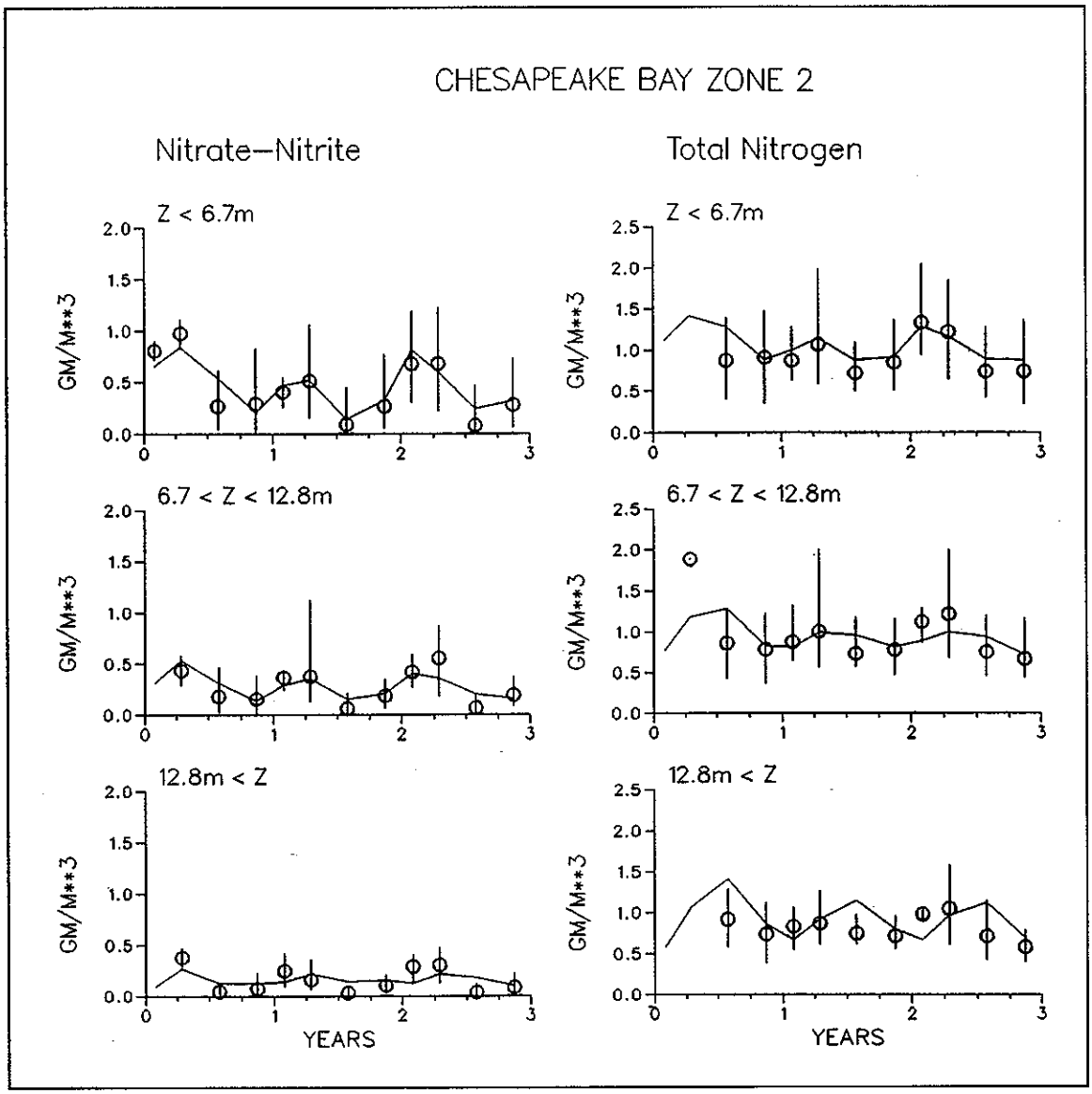

Figure 11-5. (Sheet 3 of 5)

The second diagnostic plot illustrates growth limitations for green (non-diatomaceous) algae. Since, at the current stage of calibration, no differentiation of nitrogen, phosphorus, or light limitations is made among algal groups, the green algal limitation plot is identical to the diatom plot except for the omission of silica.

The next diagnostic plot illustrates primary production. To maintain compatibility with the observations, model values are analogs to the computation used to convert short-term deck incubations to daily estimates (Equation 7-6).

One diagnostic plot compares observed light extinction with light extinction employed in the model. Data are derived from in-situ observations of disk

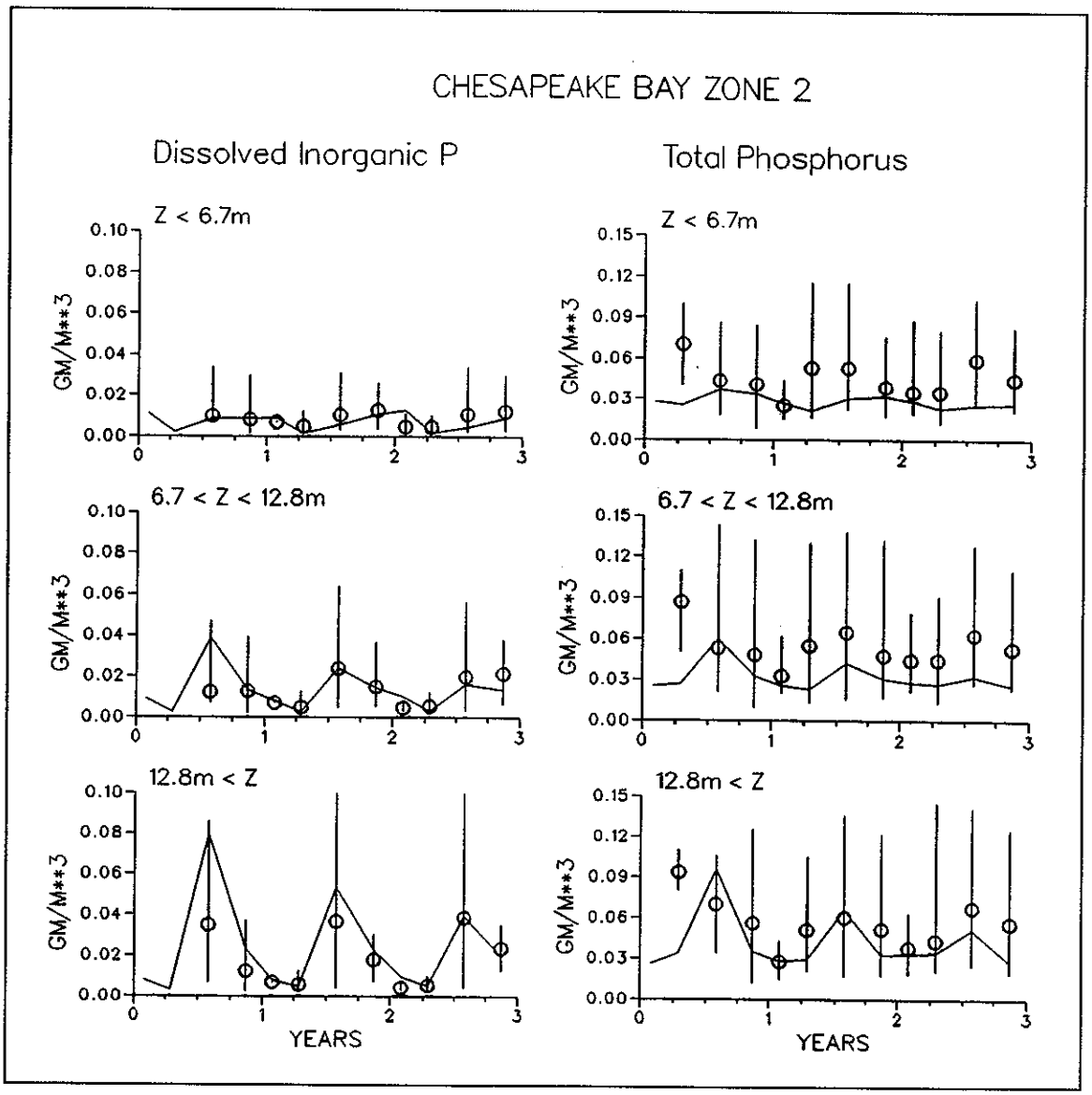

Figure 11-5. (Sheet 4 of 5)

visibility and include the influence of ambient chlorophyll. Model results are the sum of background extinction, based on regression and input to the model, and the influence of predicted chlorophyll concentration.

Limited measurements of microbial oxygen consumption were available from a transect located in Zone 2 (Tuttle et al. 1986). These were shipboard, six-hour BOD incubations. Measurements were compared to the sum of oxygen consumption processes in the model at mid-depth in the water column.

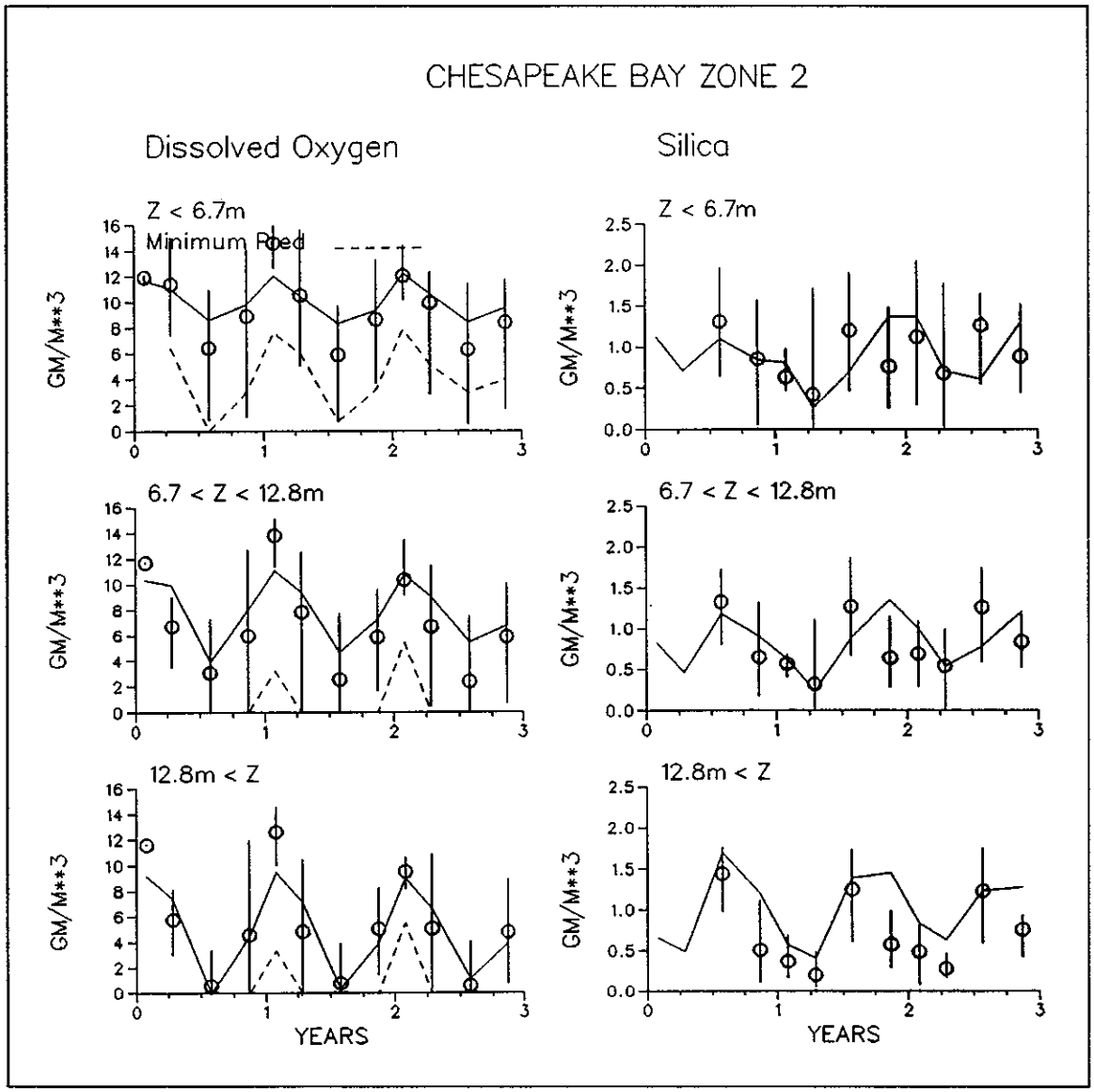

Figure 11-5. (Sheet 5 of 5)

Longitudinal Transects

Concentration

Longitudinal transects are presented for Seasons One (Figure 11-18), Two (Figure 11-21), Three (Figure 11-24), and Four (Figure 11-28) of 1986. The horizontal axis represents kilometers from the mouth and is measured on a line that extends from the Atlantic Ocean to the Susquehanna fall line (Figure 11-2). Arithmetic mean and range of observations from stations on or adjacent to the transect are shown. Model mean for cells along the transect is weighted to

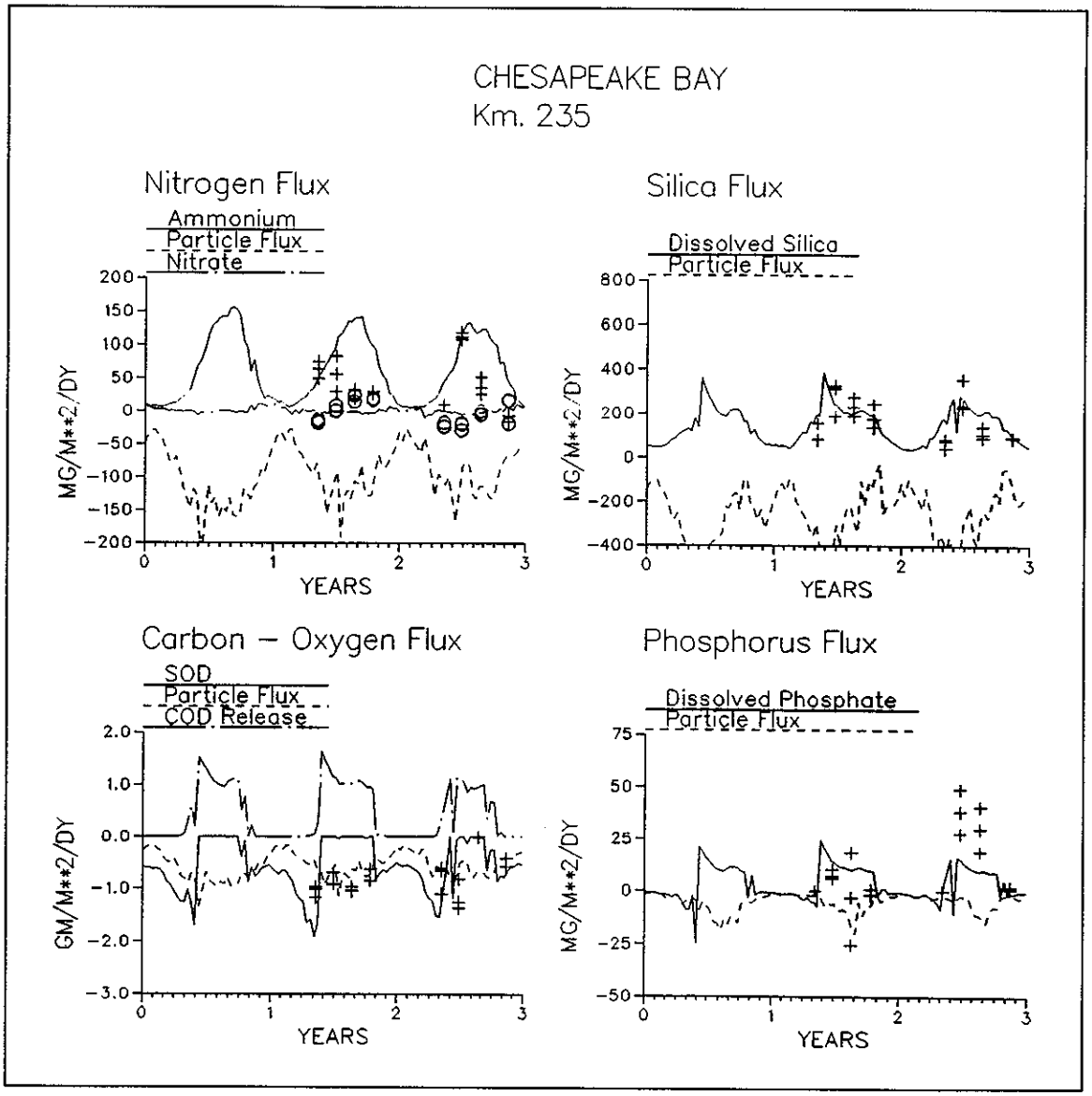

Figure 11-6. Time Series of Predicted and Observed Sediment-Water Fluxes in Zone Two

account for integration time step and cell volume. Predicted minimum dissolved oxygen is also shown. Predictions in the pyncnocline and bottom layer extend only to Km 270 since the model contains no cells in Layers Two or Three beyond this point.

Sediment-Water Fluxes

Longitudinal plots of predicted and observed sediment-water fluxes are presented along the transect employed for concentration plots (Figures 11-19, 11-22, 11-25, 11-29). Quantities plotted are the same as the sediment time series. Predictions and observations are averaged by season. The only

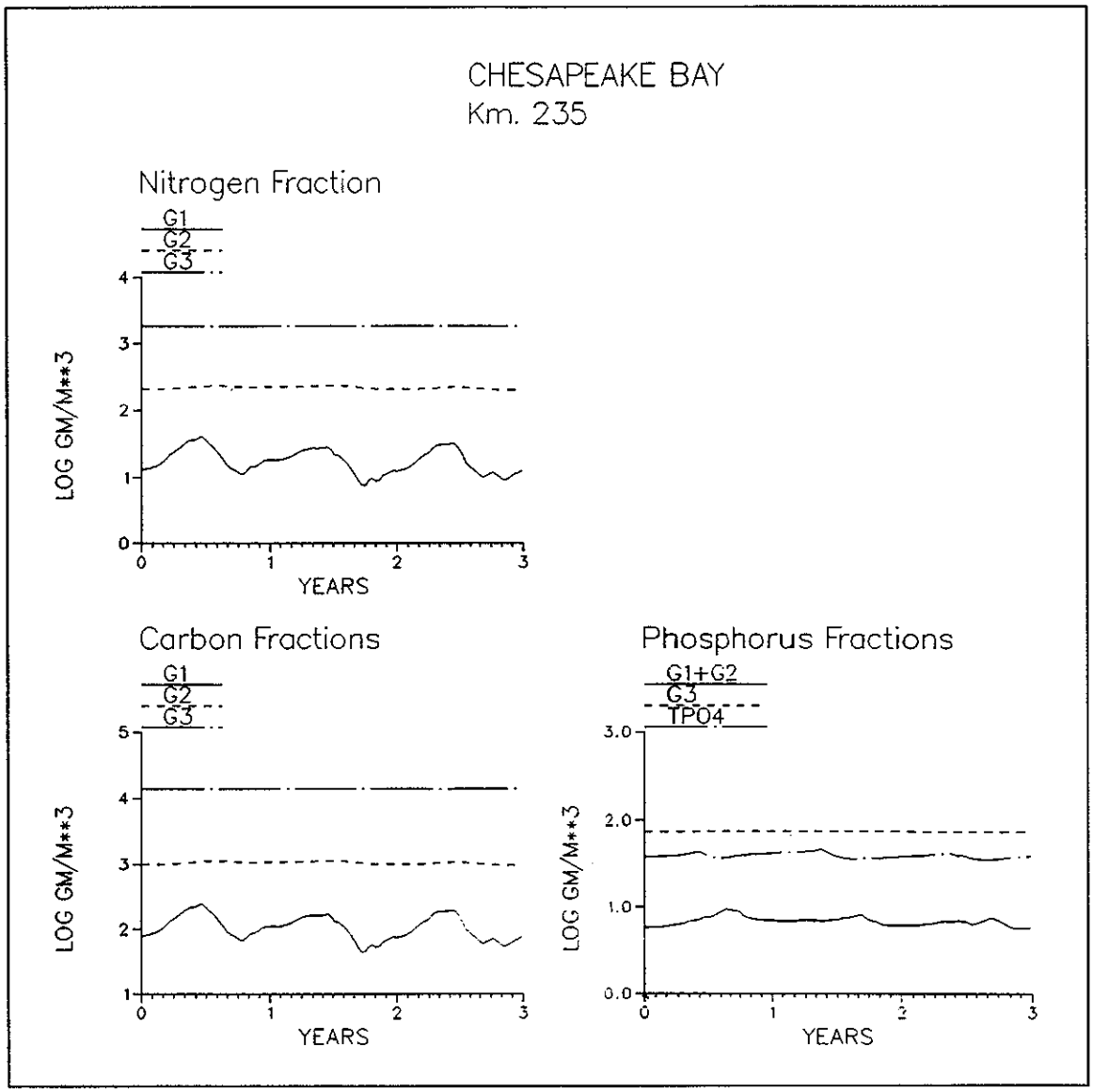

Figure 11-7. Time Series of Predicted Sediment Particulate Carbon, Nitrogen, and Phosphorus in Zone Two

temporal aggregation of the data occurs in Season Three, however, in which two triplicate measures at each station are averaged. In Seasons Two and Four, seasonal averages at each station are actually the average of a triplicate measure collected at one instance. The limited availability of data renders these plots more valuable as indicators of model predictions than as comparators of predictions and observations.

Comparisons of predicted and observed sediment particulate organic carbon, particulate nitrogen, and particulate phosphorus are also presented along the main Bay axis. Total concentrations of these substances do not change

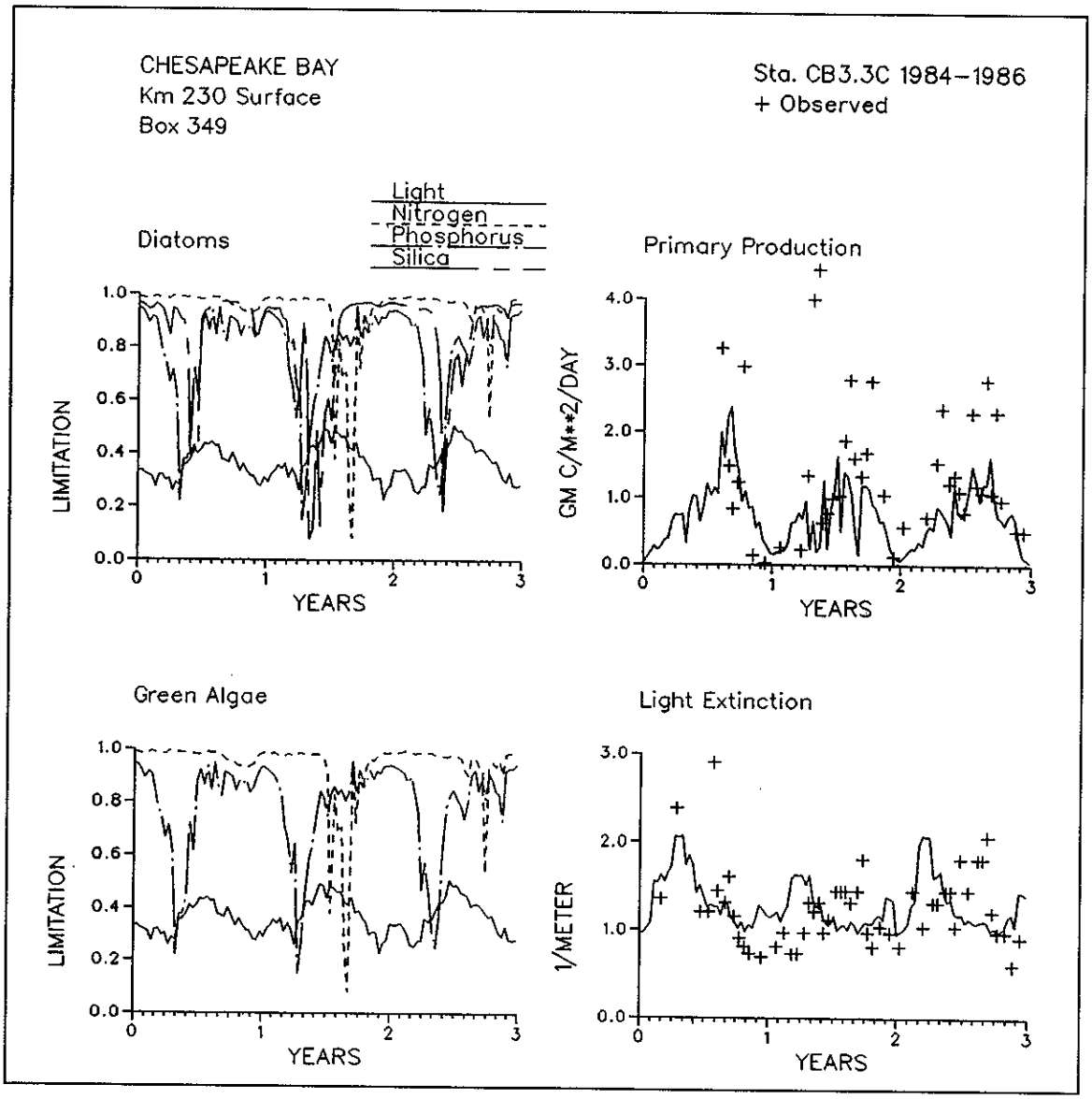

Figure 11-8. Time Series of Predicted and Observed Diagnostic Information in Zone Two (Continued)

noticeably from season to season so presentation is limited to Season Three (Figure 11-26).

Diagnostic Plots

Diagnostic information presented along the main Bay axis corresponds to diagnostic information presented in time series. In the longitudinal plots, however, model output and observations are presented as seasonal averages (Figures 11-20, 11-23, 11-27, 11-30).

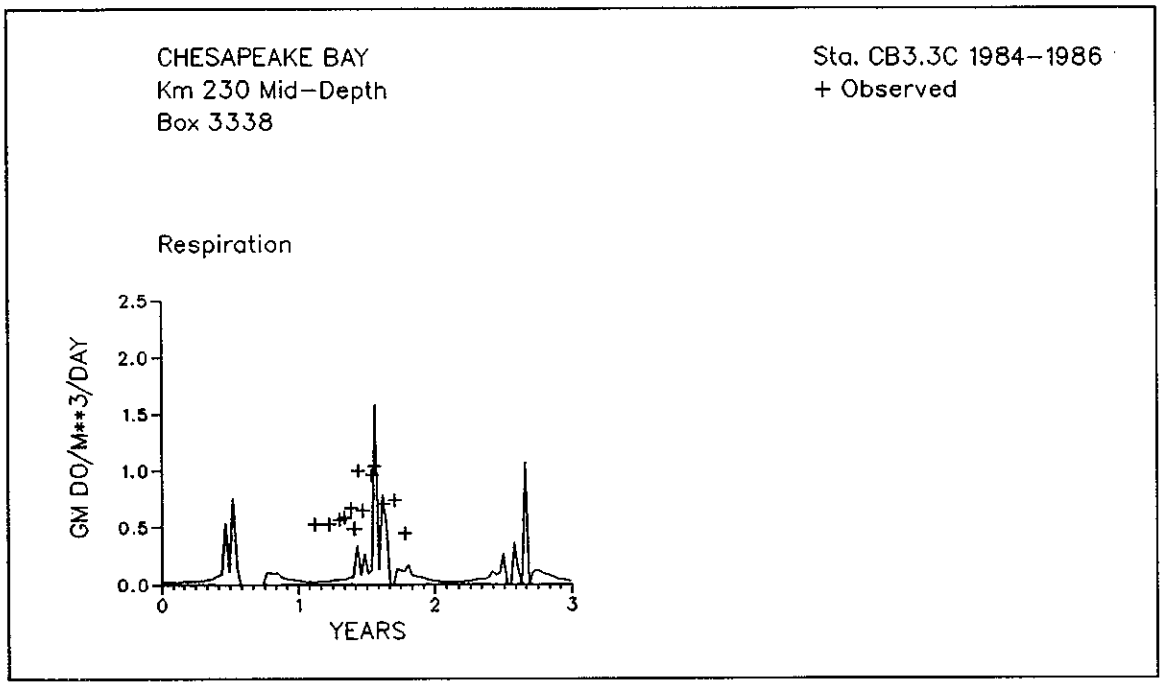

Figure 11-8. (Concluded)

Spatial Dissolved Oxygen Distribution

A system-wide representation of modelled bottom-water dissolved oxygen is shown as Figure 11-31. Predicted dissolved oxygen in the bottom-most model cells is averaged for Season Three of 1986.

An vertical profile of predicted dissolved oxygen is shown as Figure 11-32. Summer-average predictions along a north-south transect down the middle of the Bay are shown. The mouth of the Bay is towards the right.

Additional State Variables

Three model state variables, total active metal, chemical oxygen demand, and particulate biogenic silica, were not sampled in the monitoring program. Model calculations of total active metal and chemical oxygen demand are compared to observations collected in Zone Two in Table 11-3. Particulate biogenic silica concentrations, predicted and observed in Zone Three, are compared in Figure 11-33. Model results are averaged by season, zone, and level during the calibration period. Observations are seasonal mean and range of data collected at Buoy R-64, 1987-1990.

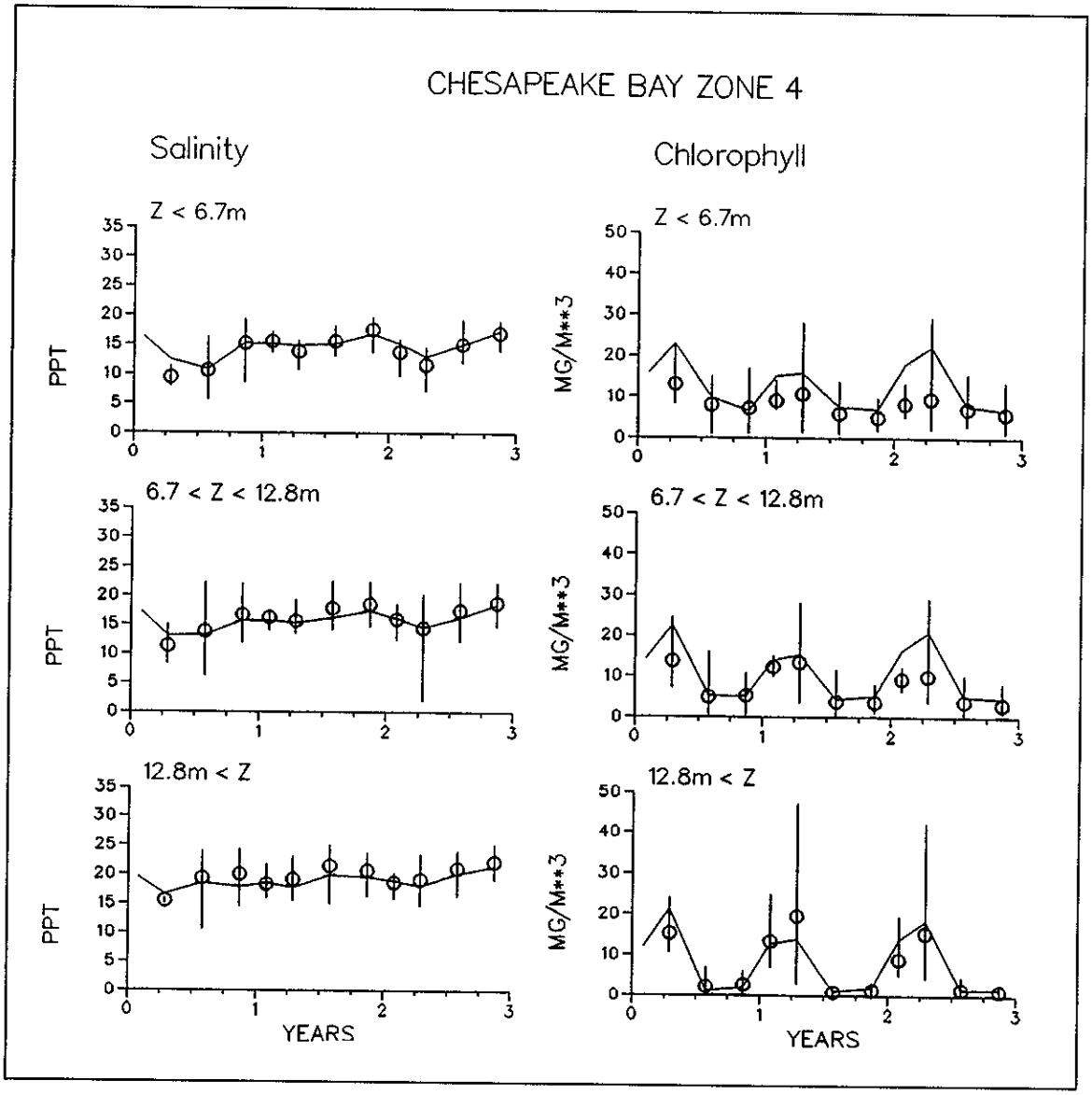

Figure 11-9. Time Series of Predicted and Observed Concentrations in Zone Four (Sheet 1 of 5)

Observed and Modelled Eutrophication Processes

The model presented a realistic representation of conditions that prevailed in the mainstem Bay from 1984 to 1986. Seasonal cycling and spatial distribution of concentrations in the water column were well represented as were major eutrophication precesses.

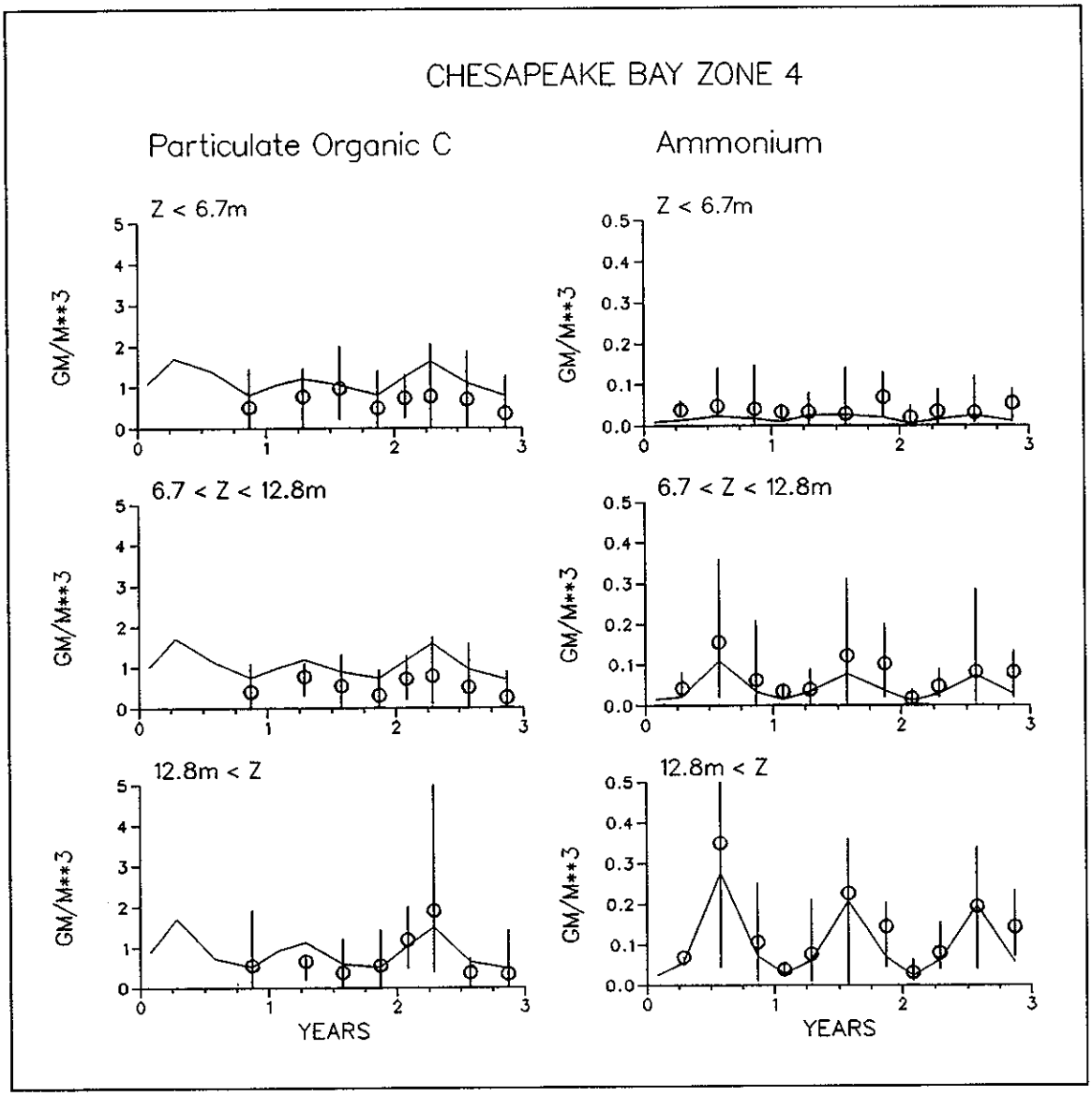

Figure 11-9. (Sheet 2 of 5)

Season One, Winter

Season One was characterized by the onset of the spring phytoplankton bloom. In the lower Bay (Figures 11-13, 11-18) chlorophyll usually attained its annual maximum during the months of January and February. In the mid and upper Bay (Figures 11-12, 11-5), Season One was usually the period of second-highest chlorophyll concentration. Inorganic nitrogen and silica were abundant in the upper 200 km of the Bay due to runoff from the Susquehanna River. Inorganic phosphorus was also available for algal uptake although not in the excess concentrations apparent for nitrogen and silica. Dissolved oxygen was nearly at saturation concentrations throughout the water column.

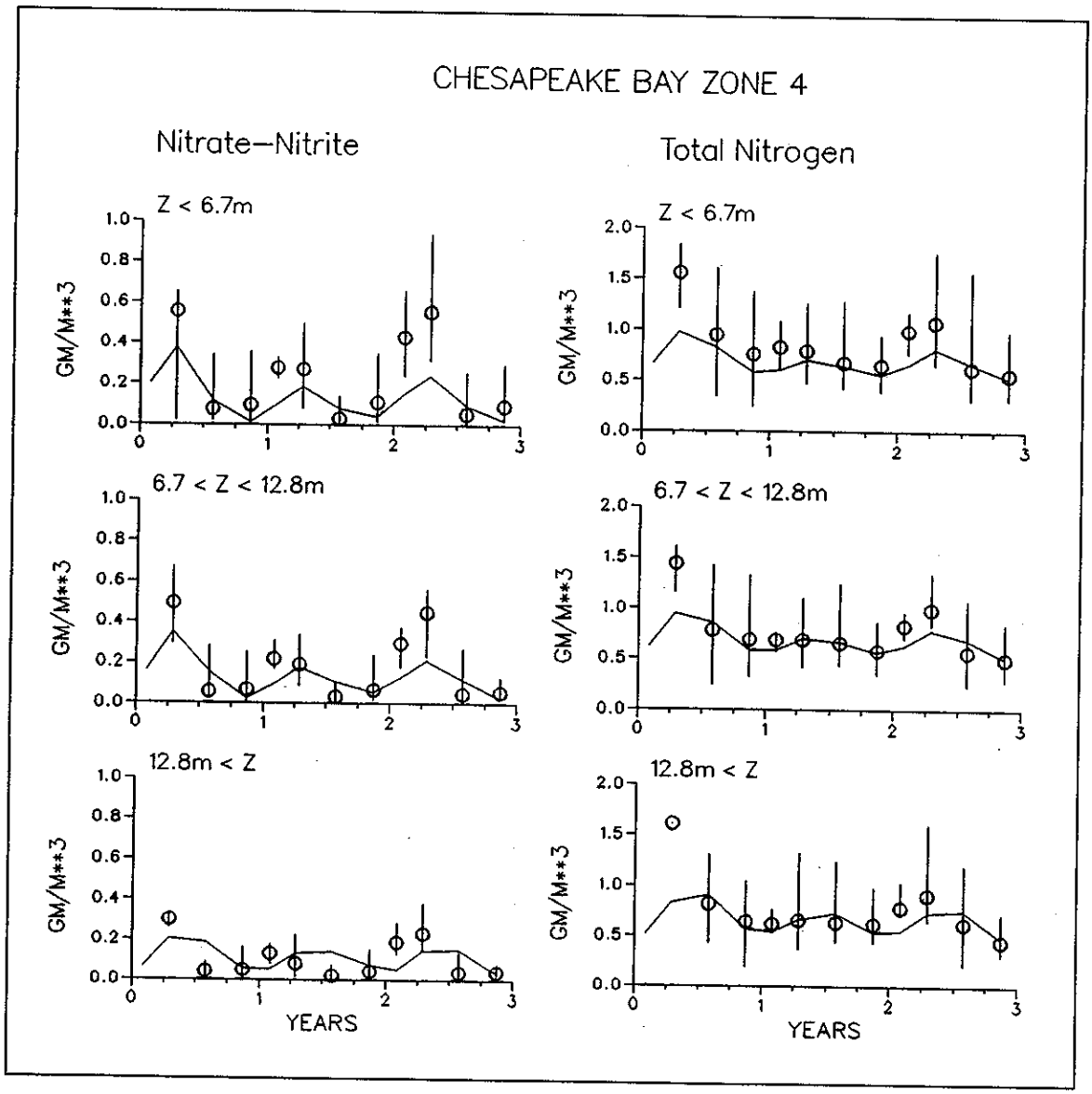

Figure 11-9. (Sheet 3 of 5)

The model reproduced the observed characteristics of the water column in Season One. In particular, the onset of the bloom and the predominance of diatoms at all depths were simulated. Simulation of the bloom required several ad-hoc modifications to algal kinetics. First, the respiration and predation rates were reduced to 30% of the rates employed the rest of the year (Tables 9-2, 9-3). These rates were further diminished due to the influence of temperature below 20 C°. Second, algae were permitted to settle through the water column but not into the sediments. These modifications presented insights into conditions necessary for occurrence of the spring bloom at all depths. First, predation pressure and other mortality factors during winter and spring must be very low. Second, diatoms must maintain their buoyancy in the water column above the sediments.

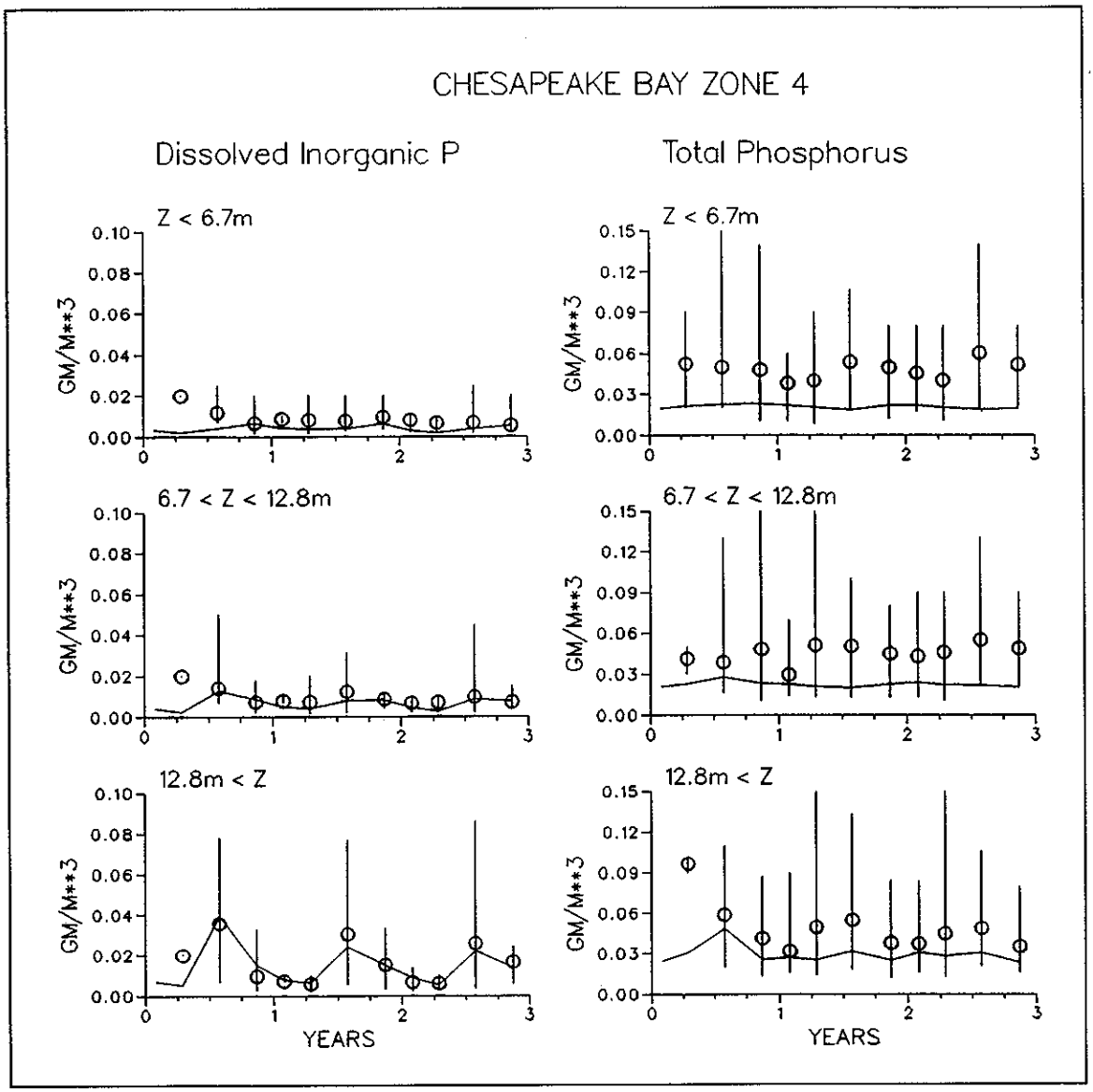

Figure 11-9. (Sheet 4 of 5)

No observations were available to characterize sediment-water fluxes during Season One. Model predictions (Figures 11-6, 11-10, 11-14, 11-19) indicated particle deposition was at an annual minimum. Deposition was limited by algal buoyancy and by reduced predation which diminished production of algal detritus. Sediment-water fluxes of nutrients were nearly zero, limited by temperature effects on sediment diagenesis. Sediment oxygen demand, ≈0.5 gm m^{-2} day^{-1}, was apparent, however, caused by chemical oxidation of particulate sulfide accumulated in previous seasons.

Primary production measures were sparse during Season One but suggested that production was minimal during the winter months. Model results agreed with the trend of the measures. The model indicated significant nutrient

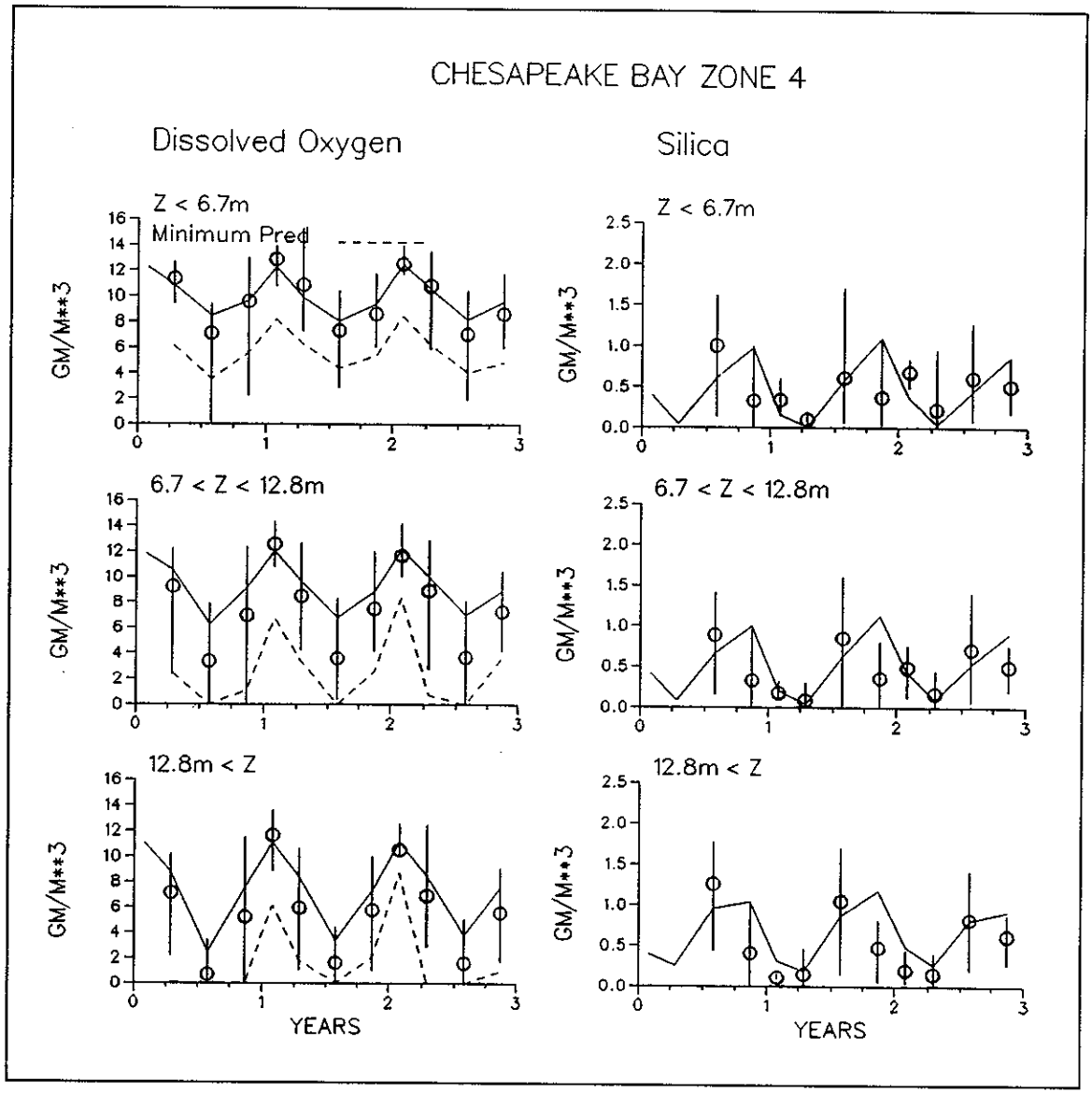

Figure 11-9. (Sheet 5 of 5)

limitations did not occur in the upper (Figure 11-8) and middle Bay (Figure 11-12). Limitations that did occur in Season One indicated nitrogen as limiting in the lower 100 km of the Bay (Figure 11-16, 11-20). The model predictions were not entirely reliable, however, due to discrepancies in predicted and observed nitrogen and silica in the lower Bay. Observations suggested silica was the more likely the limiting nutrient near the mouth of the Bay in winter.

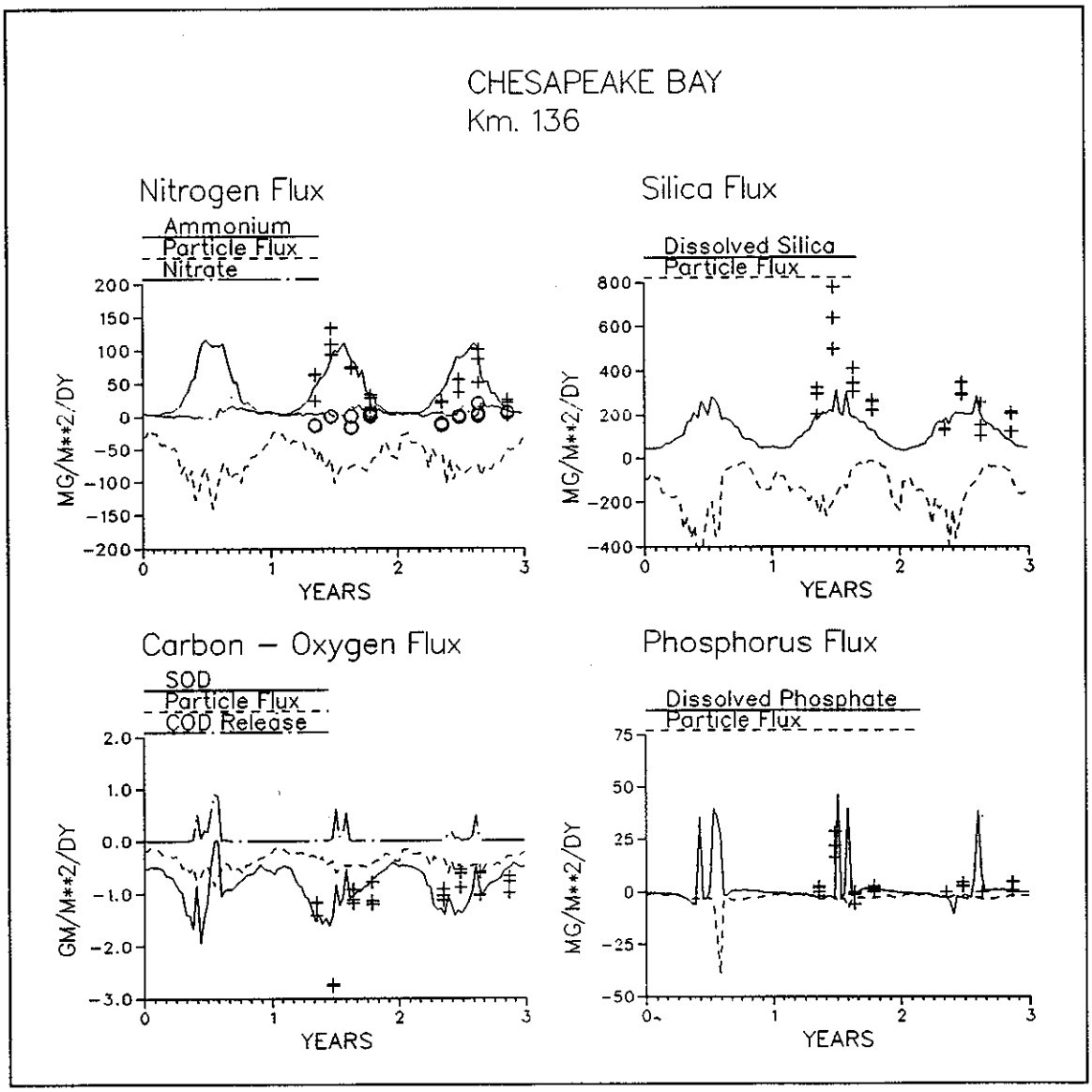

Figure 11-10. Time Series of Predicted and Observed Sediment-Water Fluxes in Zone Four

Season Two, Spring

The defining event in Season Two was the occurrence of the spring algal bloom. In the upper and middle Bay, chlorophyll concentrations at all levels attained their annual peaks (Figures 11-5, 11-9, 11-23). Concentrations in the lower Bay also remained high (Figure 11-13) following the earlier peak in Season One. Inorganic nitrogen remained abundant due to continued spring runoff. Inorganic phosphorus approached depletion throughout the Bay, however, as did silica in the lower 150 km. Seasonal-mean dissolved oxygen generally exceeded 5 gm m^{-3} throughout the mainstem but at the head of the deep trench around km 250, the onset of bottom-water anoxia was apparent.

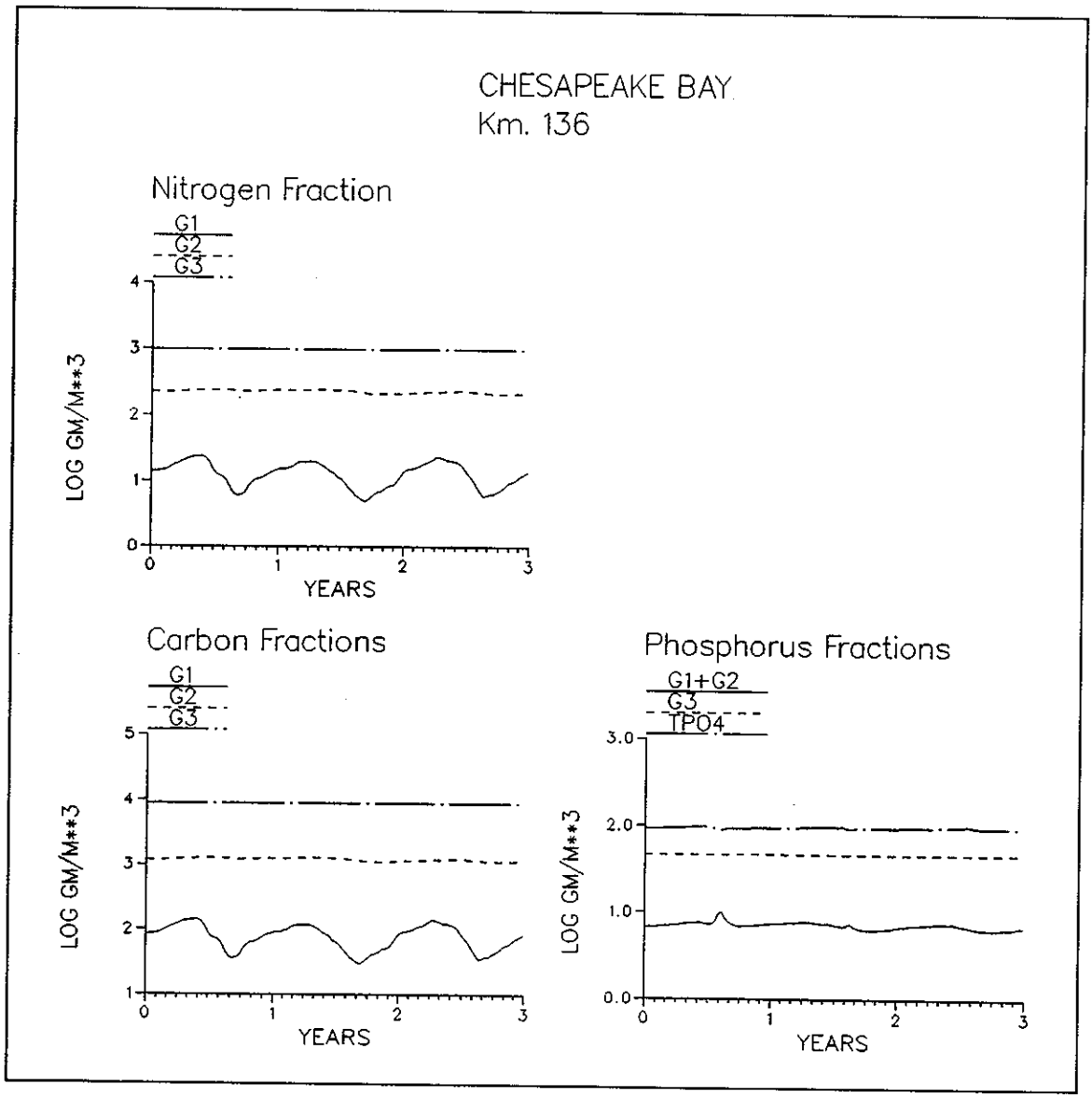

Figure 11-11. Time Series of Predicted Sediment Particulate Carbon, Nitrogen, and Phosphorus in Zone Four

The model performed well in reproducing observations collected in Season Two, especially the occurrence of maximum chlorophyll concentrations at all depths. Little variation was apparent in the predicted bloom from year to year, however. Variations that were present were linked to nutrient loading. In the middle Bay, the bloom was diminished in 1985, a dry year (Figure 11-9). In the lower Bay, the bloom was prominent in 1984, a wet year (Figure 11-13).

Depletion of inorganic phosphorus and silica were very-well represented during Season Two. Accuracy in these substances indicated the model provided an accurate representation of limiting nutrients during the spring bloom.

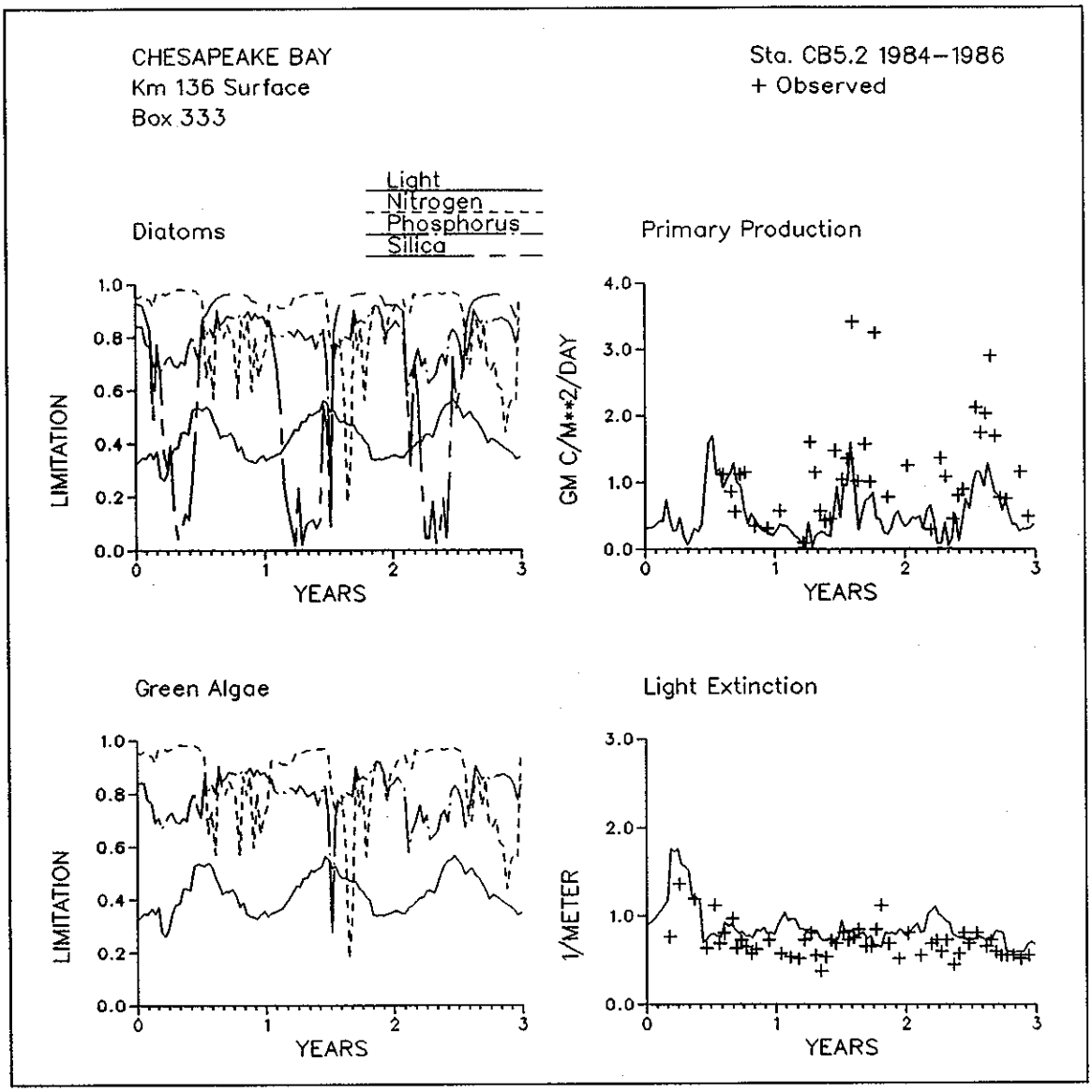

Figure 11-12. Time Series of Predicted and Observed Diagnostic Information in Zone Four

The model also successfully simulated the onset of bottom-water anoxia at the end of the season.

Predicted deposition to the sediments increased throughout Season Two and approached the annual maximum at the transition to Season Three, coincident with the collapse of the spring bloom (Figures 11-6, 11-10, 11-14). Spatial trends in deposition were evident. Peak carbon, nitrogen, and phosphorus deposition were at the head of the Bay, adjacent to the Susquehanna fall line (Figure 11-22). Secondary peaks in carbon, nitrogen, and phosphorus and the primary peak in silica deposition were at the head of the trench, beneath the maximum bloom. Observations revealed the onset of sediment ammonium and silica release. Observed sediment oxygen demand was substantial,

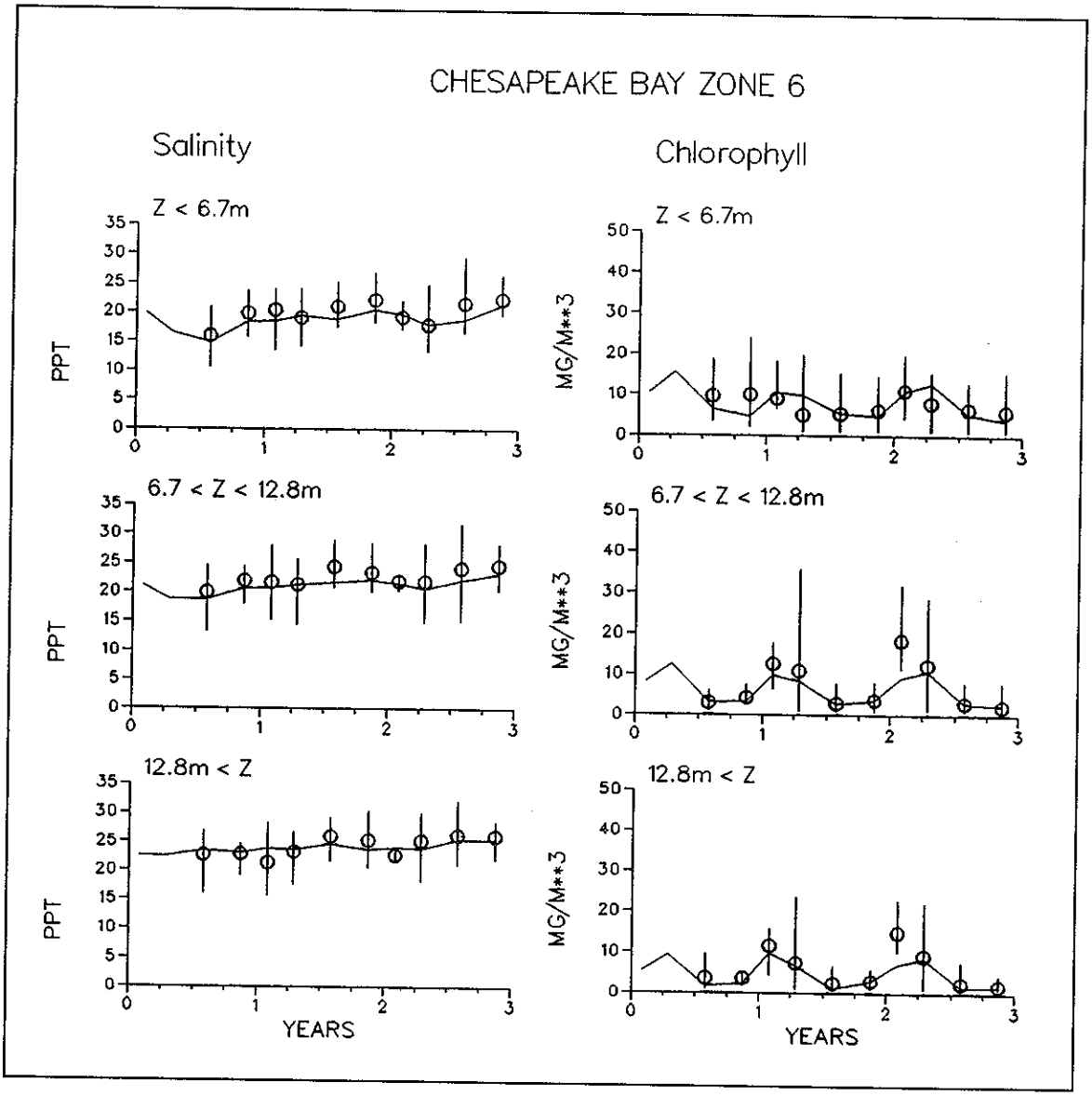

Figure 11-13. Time Series of Predicted and Observed Concentrations in Zone Six (Sheet 1 of 5)

≈1 gm m^{-2} day^{-1}. The model also indicated the onset of nutrient release and calculated annual maximum sediment oxygen demand during Season Two.

The most important information in the diagnostic series was the indication of limiting nutrient during the spring bloom. Averaged over the season, phosphorus was limiting in the upper half of the Bay and silica was limiting in the lower half (Figure 11-23). Although phosphorus limitation dominated most of the season in the upper Bay, time series plots indicated a transition to silica limitation towards the termination of the bloom (Figure 11-8).

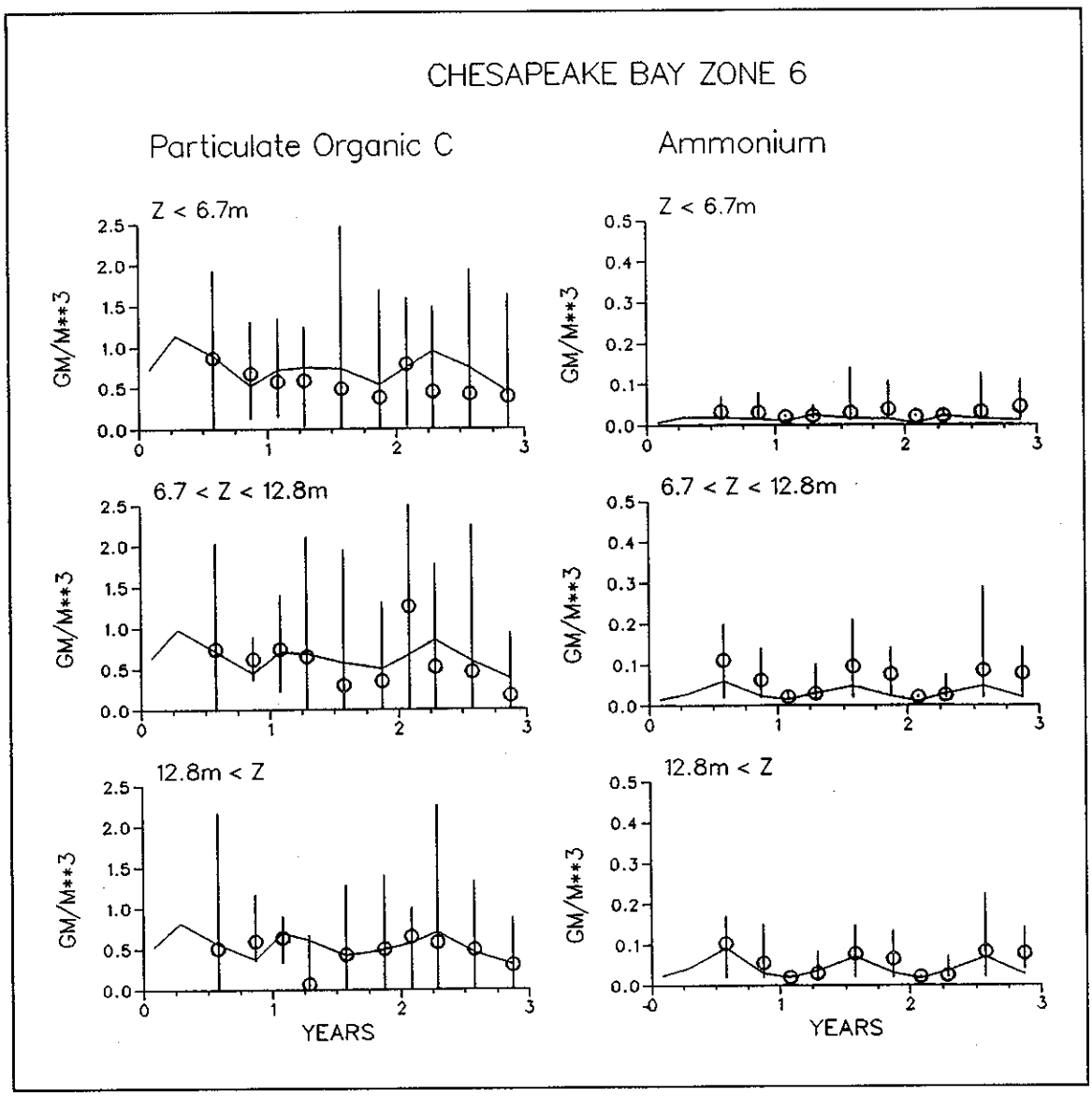

Figure 11-13. (Sheet 2 of 5)

Season Three, Summer

The transition from Season Two to Season Three was rapid and dramatic. Chlorophyll virtually disappeared from the bottom of the water column and was greatly diminished at the surface (Figures 11-5, 11-9, 11-13, 11-24). Nitrate concentration attained an annual minimum due to diminished freshwater runoff. Ammonium and inorganic phosphorus were removed from surface water by algal uptake. These nutrients were abundant in subsurface water, however, due to sediment release. Two factors contributed to silica availability. Diatoms comprised a lesser fraction of the algal community, thereby reducing demand, and temperature-enhanced sediment release occurred, thereby increasing supply.

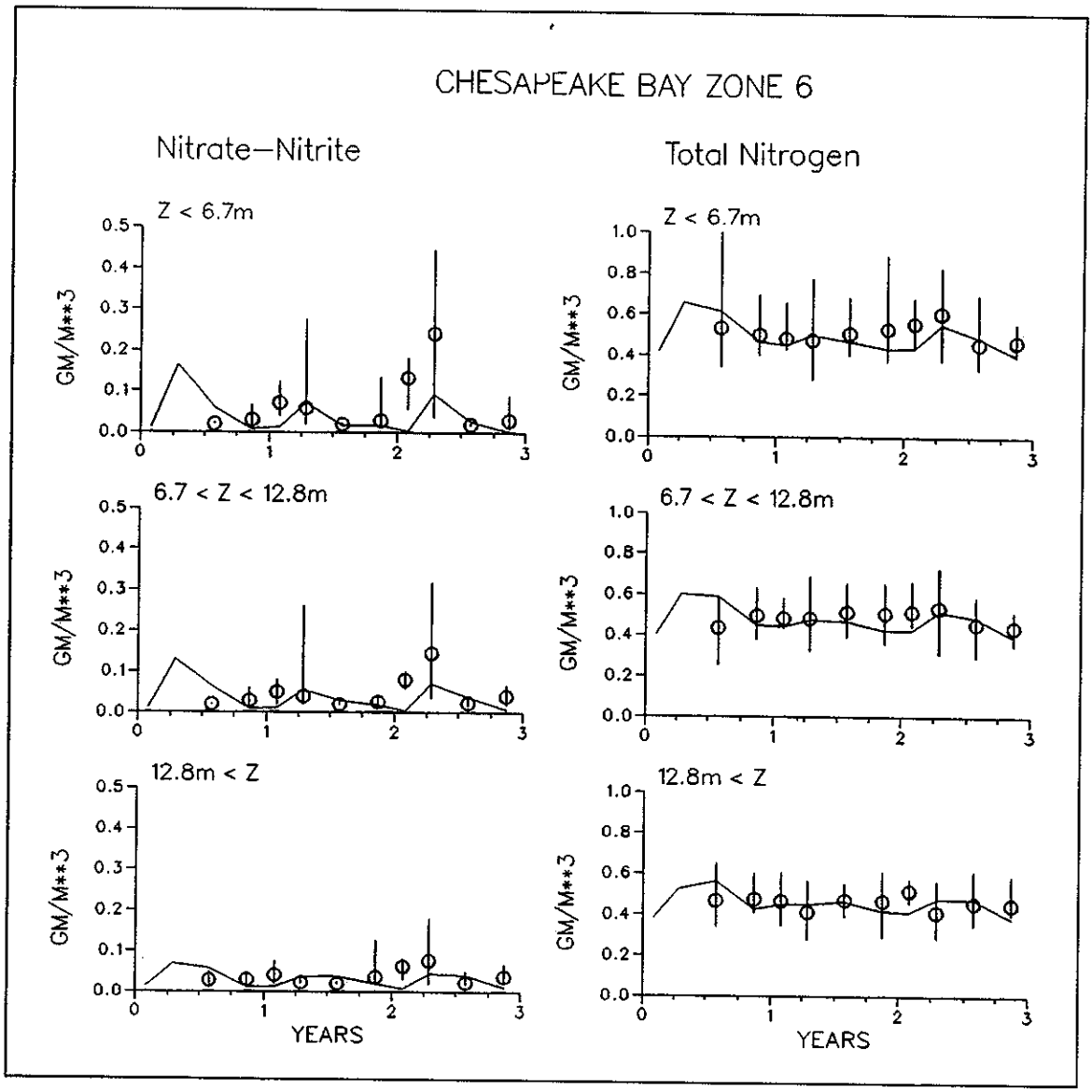

Figure 11-13. (Sheet 3 of 5)

Anoxia was occasionally present in Layers Two and Three at all stations between km 100 and 250. Seasonal-average dissolved oxygen concentrations in Layer Three approached zero in a 50 to 100 km reach of the mainstem. Bottom-water dissolved oxygen was definitely linked to hydrology. In the wet year, 1984, essentially anoxic bottom water extended downstream to km 150. In dry and average years, however, anoxia was limited to the region above km 200.

The model performed well in reproducing observed concentrations and processes during Season Three. As in the observations, the spring bloom died off rapidly and was replaced with an algal population concentrated at the water surface. Concentrations of ammonium, nitrate, and phosphate in surface

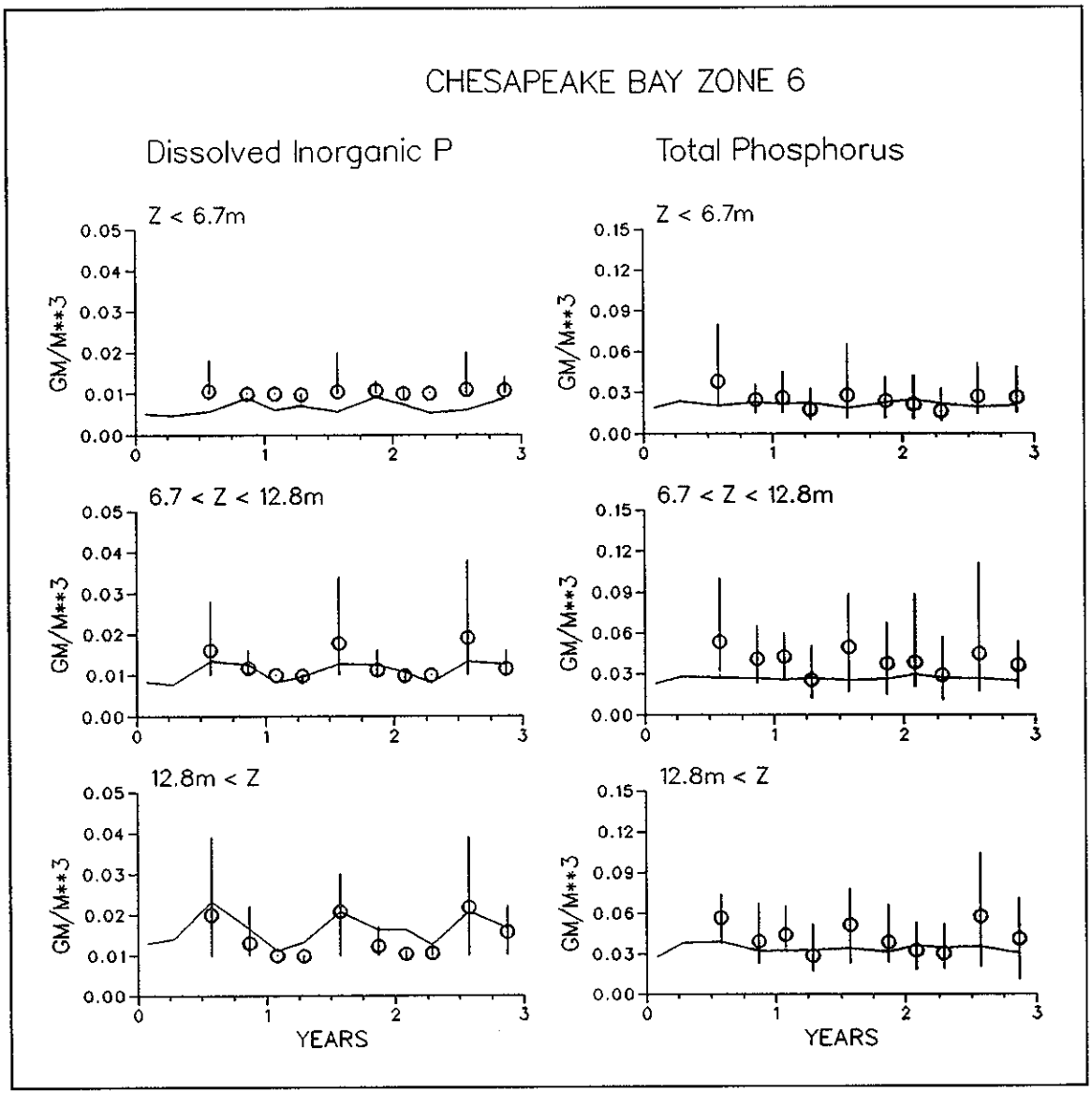

Figure 11-13. (Sheet 4 of 5)

waters were accurately predicted. The accurate predictions indicated a high degree of model reliability in predicting the effect of nutrient reductions on summer algal production.

The interactions between system geometry and hypoxia were well-represented in the model (Figure 11-31). Lowest predicted dissolved oxygen concentrations occurred at the head of the deep trench and penetrated up the channel into Baltimore Harbor. Hypoxia followed the trench down the Bay and penetrated into the connecting channel at the mouth of the Potomac. Substantial anoxia was also indicated in the secondary channel that runs along the Eastern Shore. Hypoxic water was virtually absent from shoal areas of the

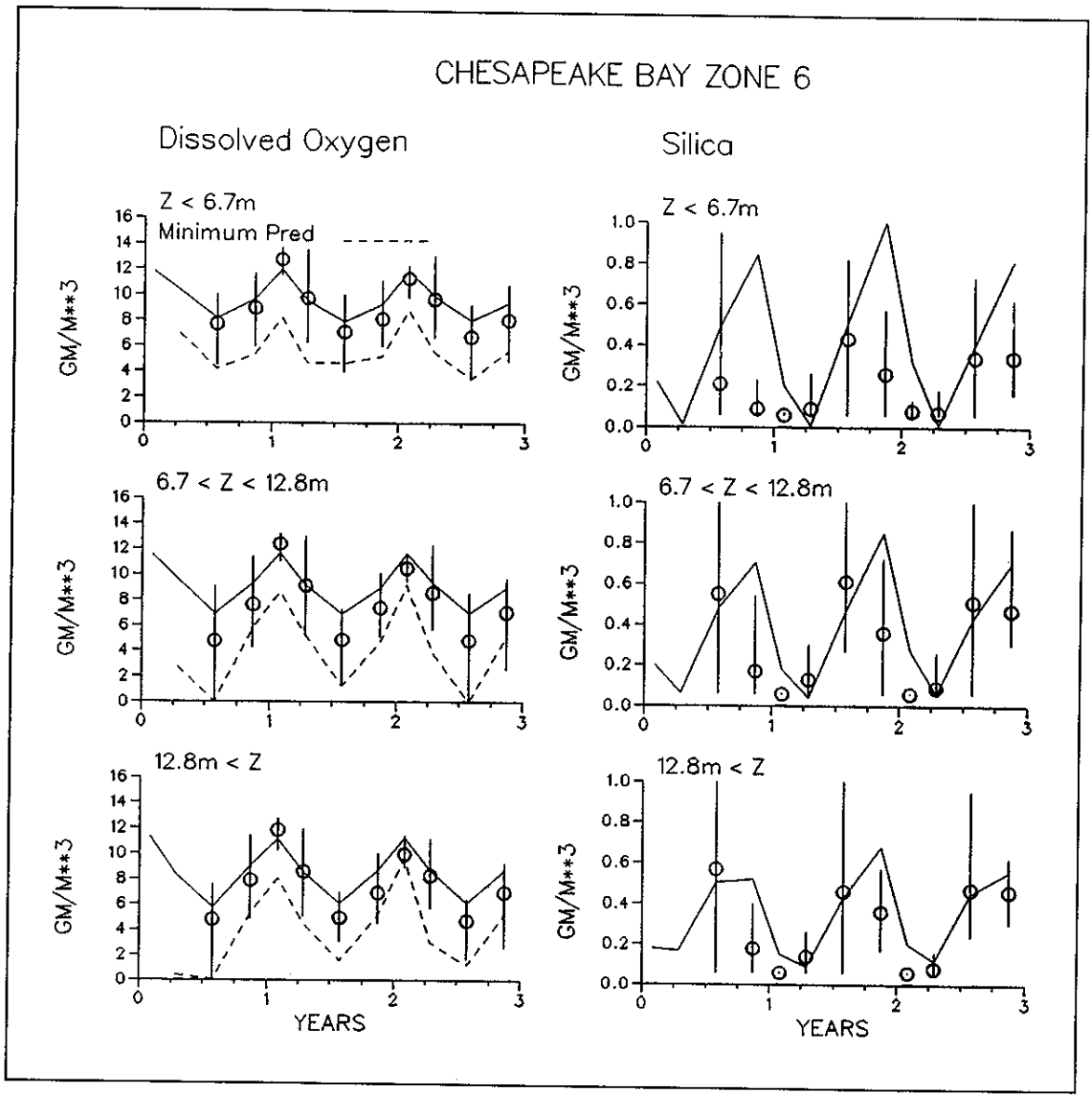

Figure 11-13. (Sheet 5 of 5)

mainstem although hypoxia was indicated in shallow portions of some tributaries.

The model accurately represented the recurrence of anoxic water at the head of the deep trench (Figures 11-5, 11-24). In the middle (Figure 11-9) and lower Bay (Figure 11-13) predicted bottom dissolved oxygen was less in 1984, the wet year, than in 1985 or 1986. The model well represented the minimum dissolved oxygen that occurred in the trench but summer average predictions in the bottom layer often exceeded observations. The discrepancy appeared related to the modelled vertical profile of dissolved oxygen (Figure 11-32). Hypoxic or anoxic water occurred in model cells immediately above the bottom but did not extend the full depth of the layer considered in averaging.

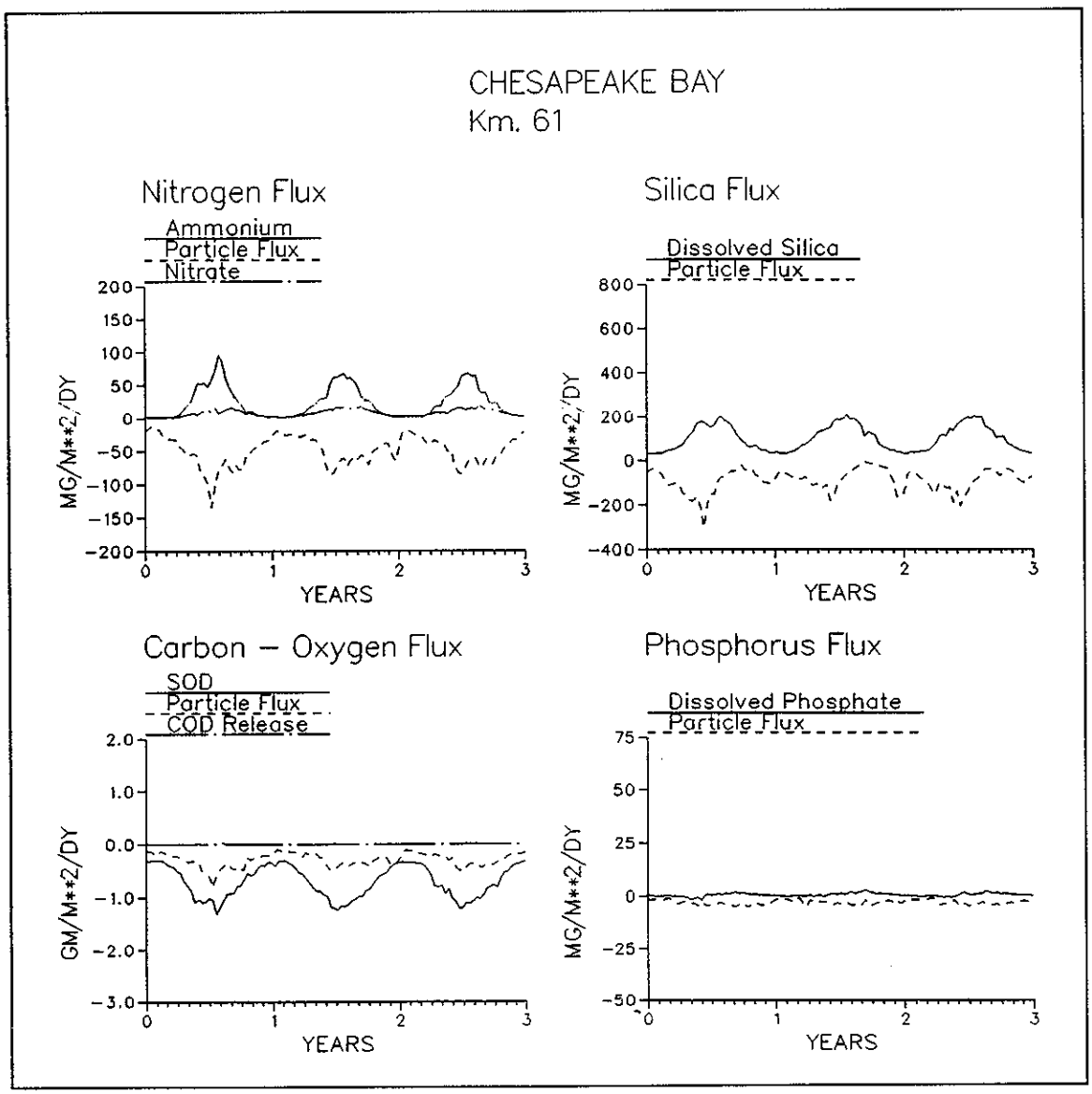

Figure 11-14. Time Series of Predicted Sediment-Water Fluxes in Zone Six

Consequently, model minimum in the layer matched observed minimum but model average exceeded observed average.

Observed sediment ammonium and silica releases attained their maximum values during Season Three (Figures 11-6, 11-10, 11-25). Three factors contributed to the maxima: the deposition of labile organic matter, temperature enhanced diagenesis, and bottom water hypoxia. Rapid diagenesis of fresh organic matter resulted in maximum production of ammonium and silica. Hypoxia blocked the nitrification/denitrification sequence so that a large fraction of ammonium was released.

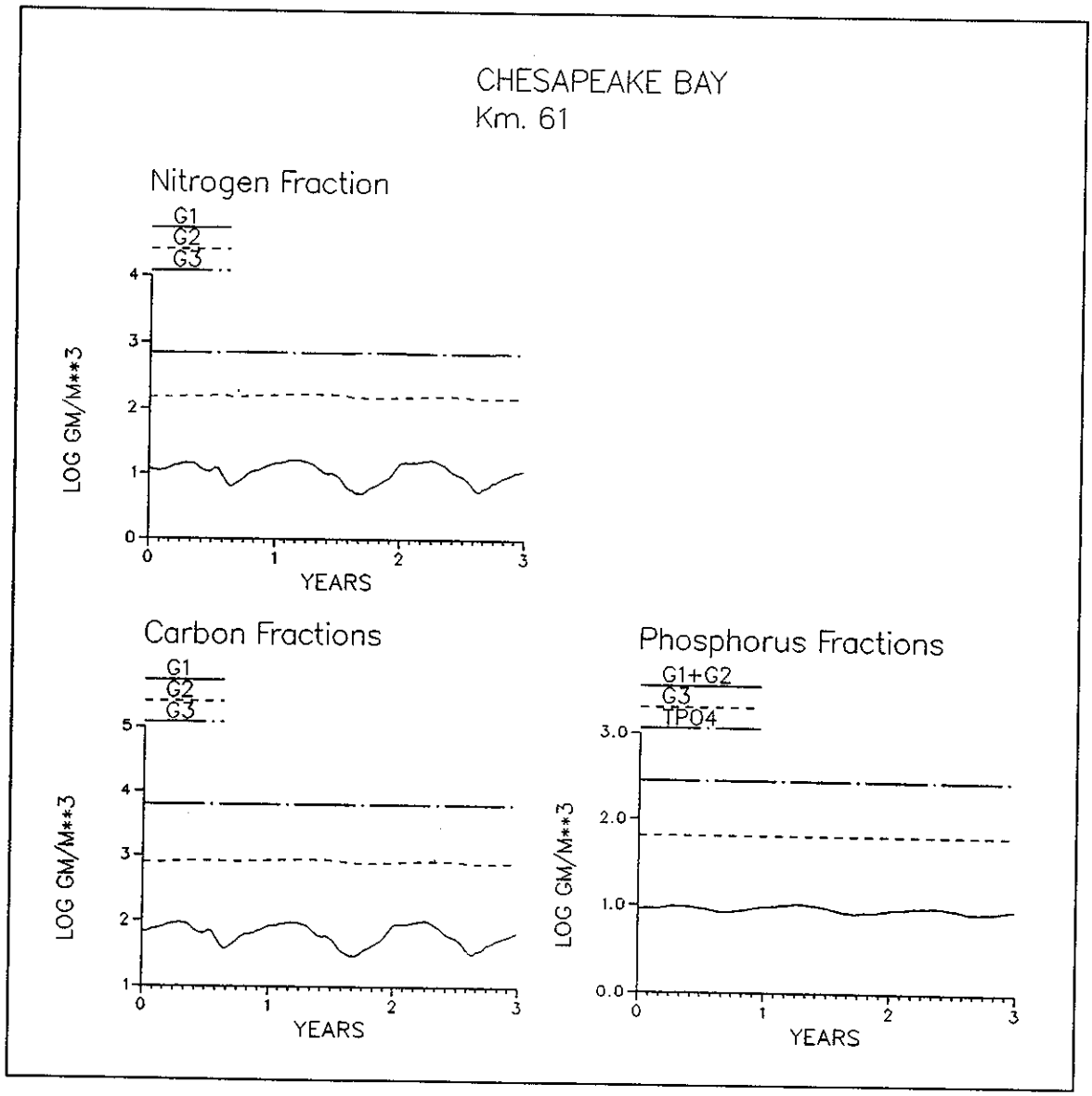

Figure 11-15. Time Series of Predicted Sediment Particulate Carbon, Nitrogen, and Phosphorus in Zone Six

Maximum observed sediment phosphorus release also occurred in Season Three. Although diagenesis contributed to the seasonal maximum, sharp release peaks were primarily the result of bottom-water hypoxia. Under anoxic conditions, iron oxides in surface sediments, which sorb phosphate under oxic conditions, were reduced to soluble forms, allowing free diffusion of sediment phosphate to overlying water.

Observed sediment oxygen demand was erratic. Although large demands were measured in Season Three, observations suggested that sediment oxygen demand was diminished for most of the season from a peak in Season Two or at the transition between seasons.

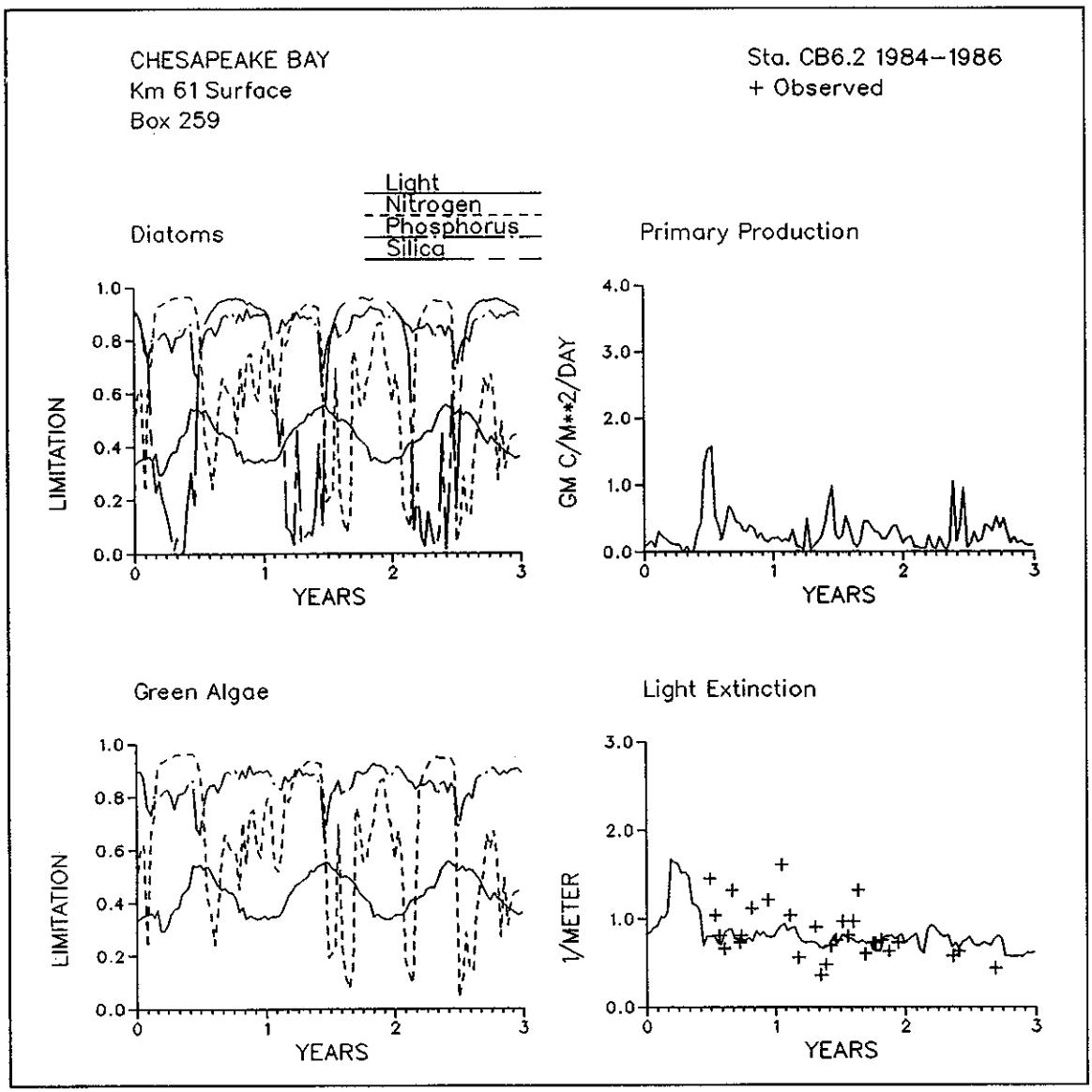

Figure 11-16. Time Series of Predicted and Observed Diagnostic Information in Zone Six

The model faithfully reproduced the trends apparent in the nutrient flux observations. Predicted maximum ammonium and silica release occurred in Season Two. The time series of predicted fluxes was smooth with a broad peak indicating the dominant influence of temperature which changed slowly throughout the season. At the upper-Bay station (Figure 11-6), the pattern of phosphorus release was also broad and smooth due to the seasonal duration of anoxia. At the mid-Bay station (Figure 11-10) predicted release was erratic and coincided with sporadic occurrence of hypoxia in overlying water. Sediment phosphorus release was inhibited at the lower Bay station (Figure 11-14) by continuous presence of dissolved oxygen in overlying water.

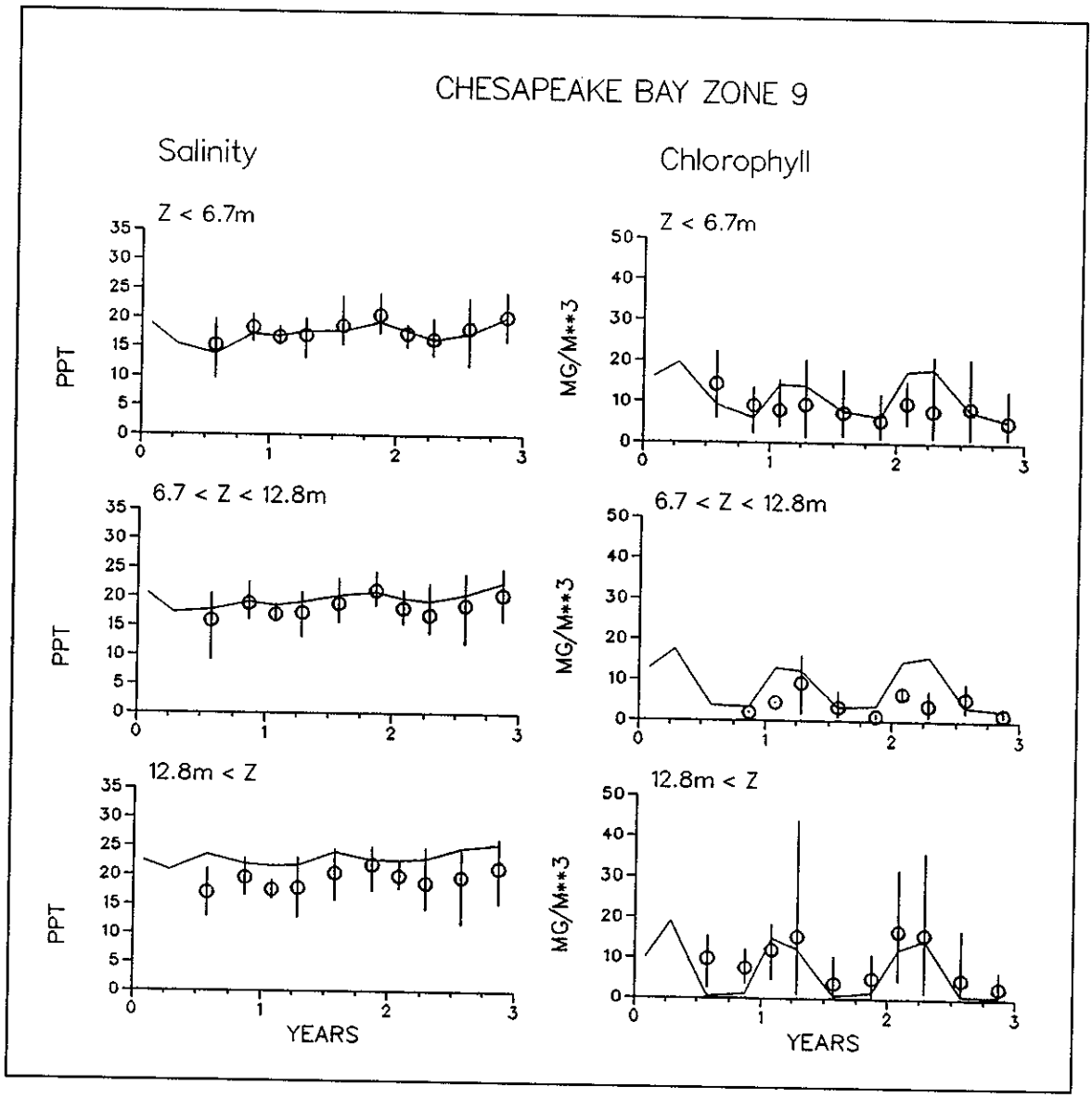

Figure 11-17. Time Series of Predicted and Observed Concentrations in Zone Nine (Sheet 1 of 5)

Predicted maximum sediment oxygen demand occurred at the transition between Seasons Two and Three, coincident with collapse of the spring algal bloom. At the upper-Bay station, exertion of sediment oxygen demand was inhibited by anoxia in the overlying water. Instead, chemical oxygen demand was released to the water column. Resulting COD concentrations in the water column agreed reasonably with measures conducted in the vicinity (Table 11-3). At the mid-Bay station COD release occurred occasionally, coincident with sporadic anoxia. No COD release occurred in the lower Bay.

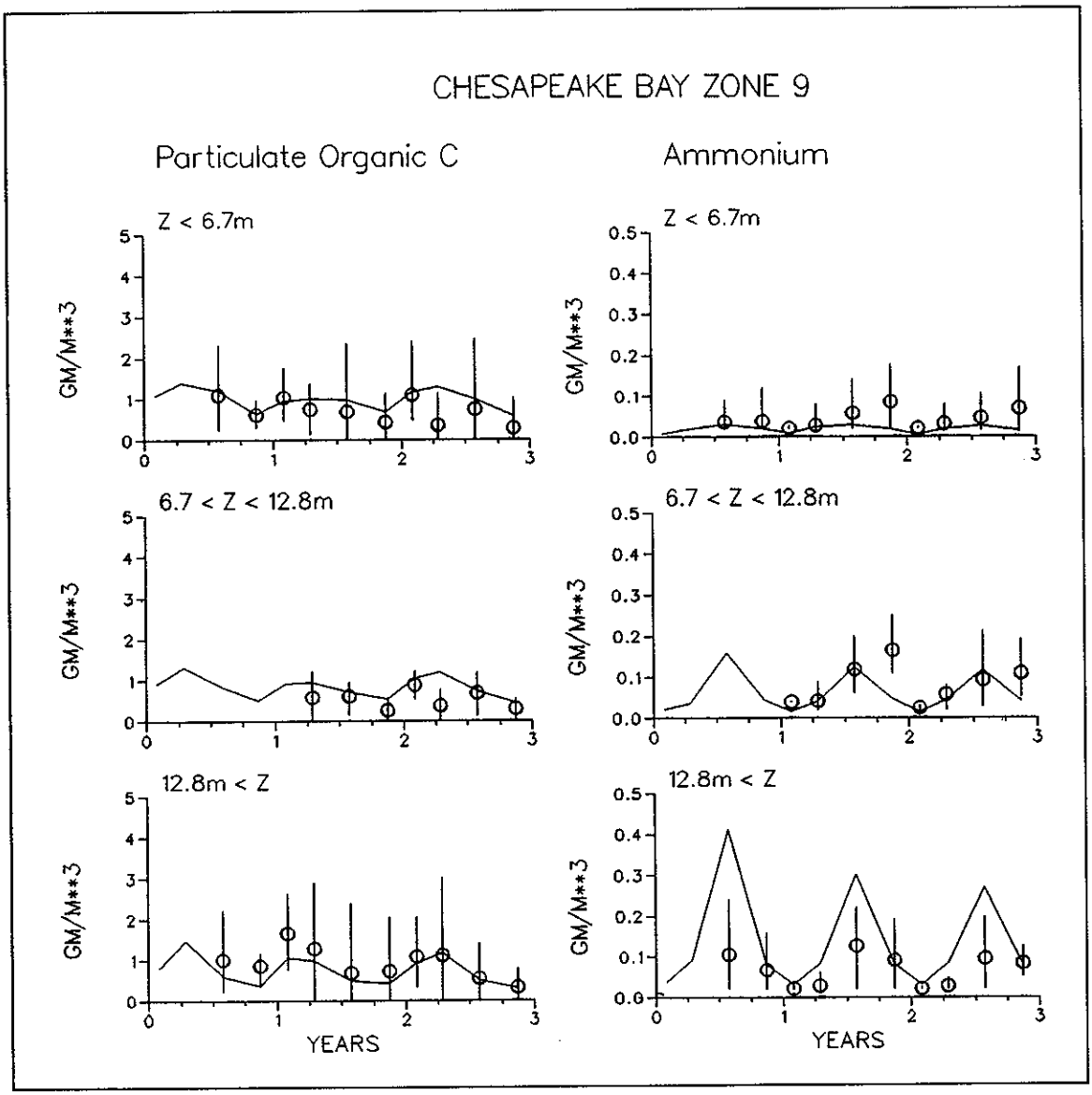

Figure 11-17. (Sheet 2 of 5)

Agreement between observed and modelled sediment particulate organic carbon was excellent (Figure 11-26). Observations and model exhibited a sharp decrease in the upper 50 km of the Bay followed by a gradual decrease towards the mouth in the remainder of the mainstem. The enormous concentration near the fall line resulted from deposition of particles in Susquehanna River runoff. In the remainder of the Bay, deposition was largely from algal primary production. Most of the sediment carbon was inert G3 material (Figures 11-7, 11-11, 11-15). Excellent reproduction of observations was a validation of G-splits (Table 10-1) and burial rates (Table 10-3) employed in the model.

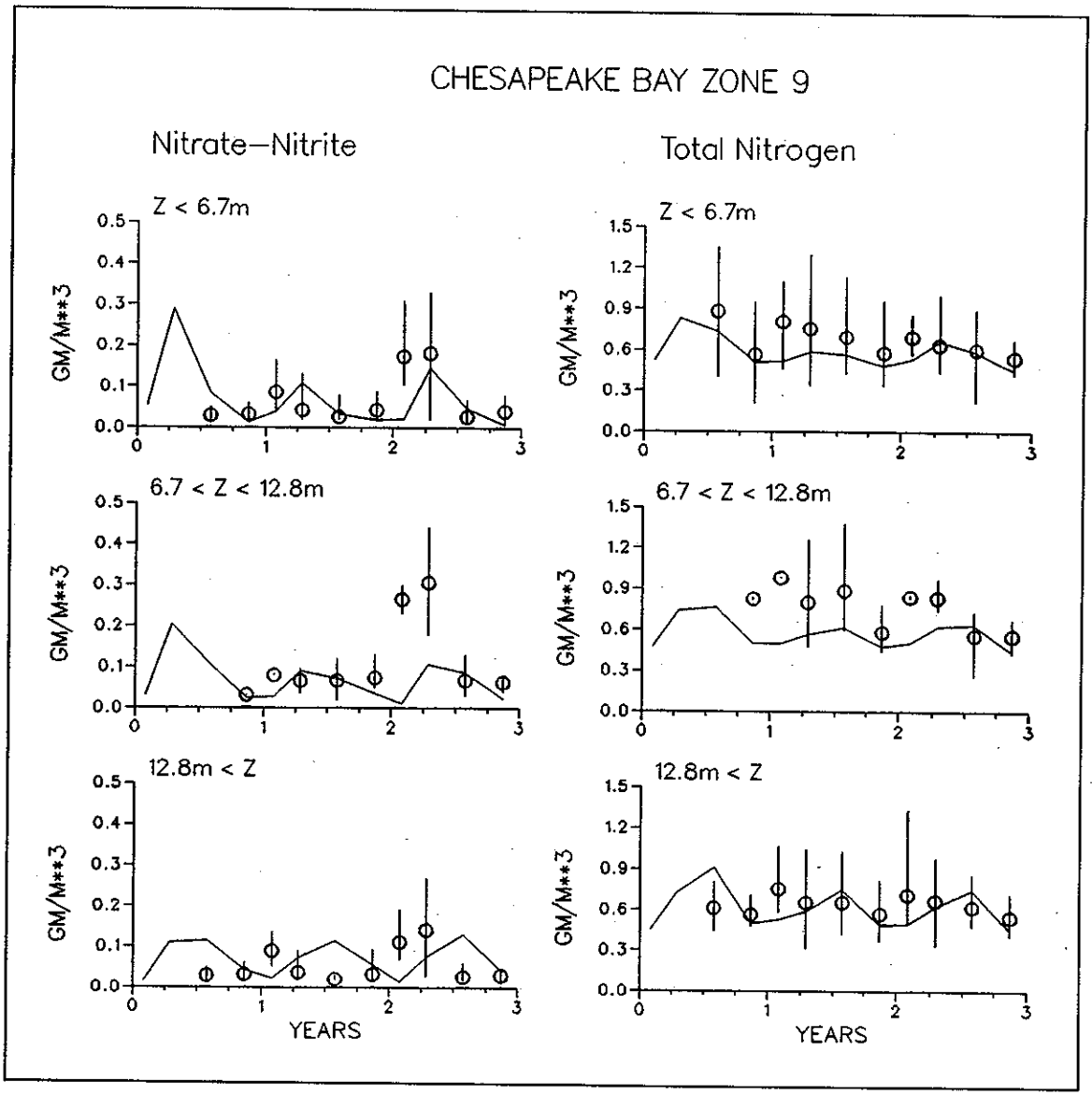

Figure 11-17. (Sheet 3 of 5)

Predicted sediment particulate organic nitrogen followed the pattern observed for carbon. A precipitous decline downstream of the fall line was succeeded by a gradual decline towards the mouth. Both predictions and observations exhibited a ten-to-one carbon to nitrogen ratio in the sediments.

The spatial distribution of sediment particulate phosphorus differed from carbon and nitrogen. A sharp upturn occurred at the mouth of the Bay which indicated phosphorus deposition. The upturn occurred in a reach in which deposition of clay from the continental shelf has been identified (Skrabal 1991). The model and observations suggested import of a particulate phosphorus form from the shelf and deposition near the mouth of the Bay.

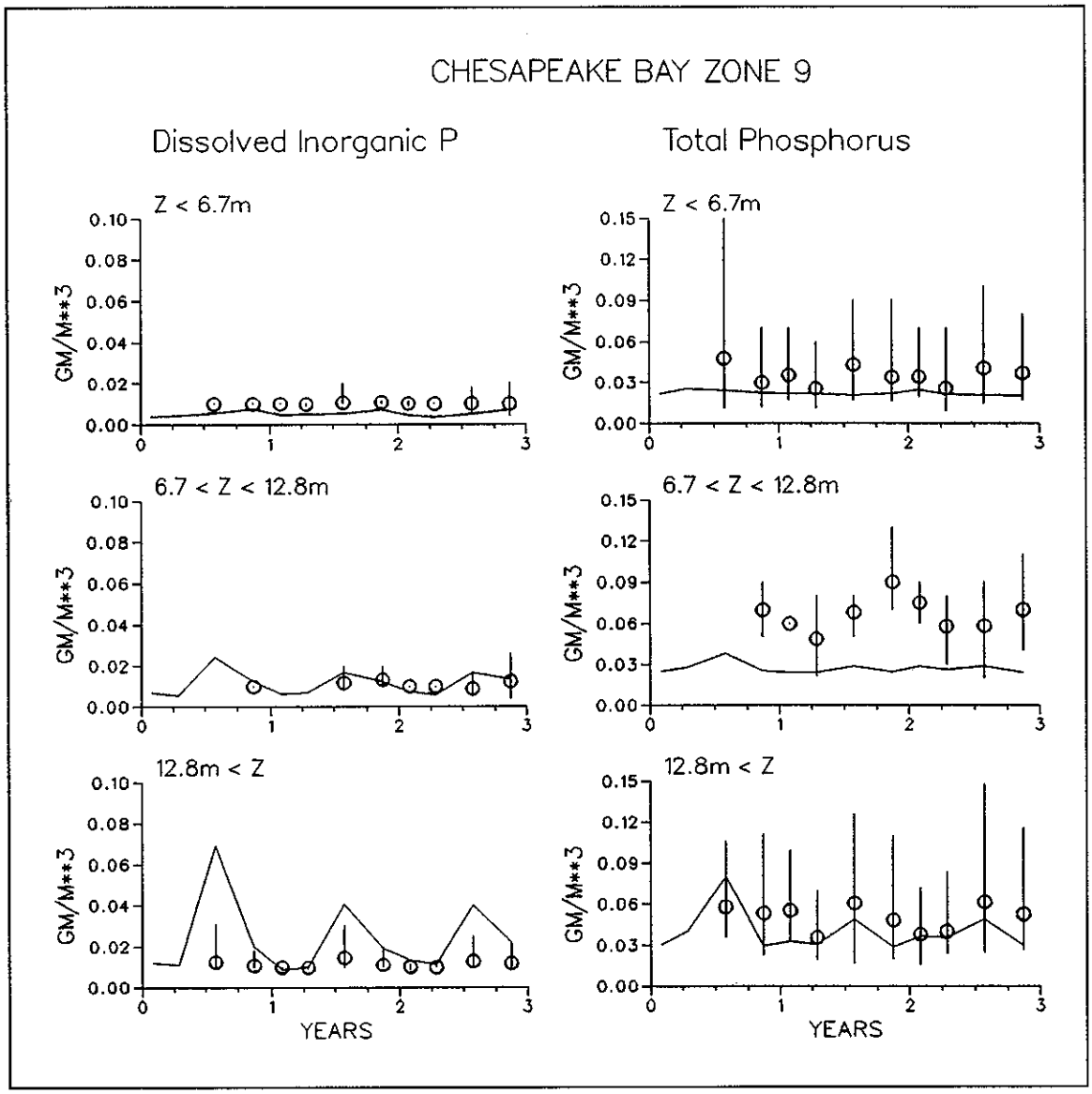

Figure 11-17. (Sheet 4 of 5)

The composition of sediment phosphorus was variable. At the upper-Bay station (Figure 11-7), the dominant predicted form was inert, G3, organic matter. In the middle (Figure 11-11) and lower Bay (Figure 11-15), the dominant form was particulate inorganic phosphorus. The inorganic fraction increased with distance downstream. The pattern indicated that retention of phosphate in sediments, through sorption to particles, was diminished at the upper station by recurrent anoxia.

Both observations and model identified summer as the season of maximum primary production (Figures 11-8, 11-12, 11-16). The model indicated spatial variability in limiting nutrient (Figure 11-27). During summer, phosphorus was identified as the limiting nutrient in the upper half of the Bay while

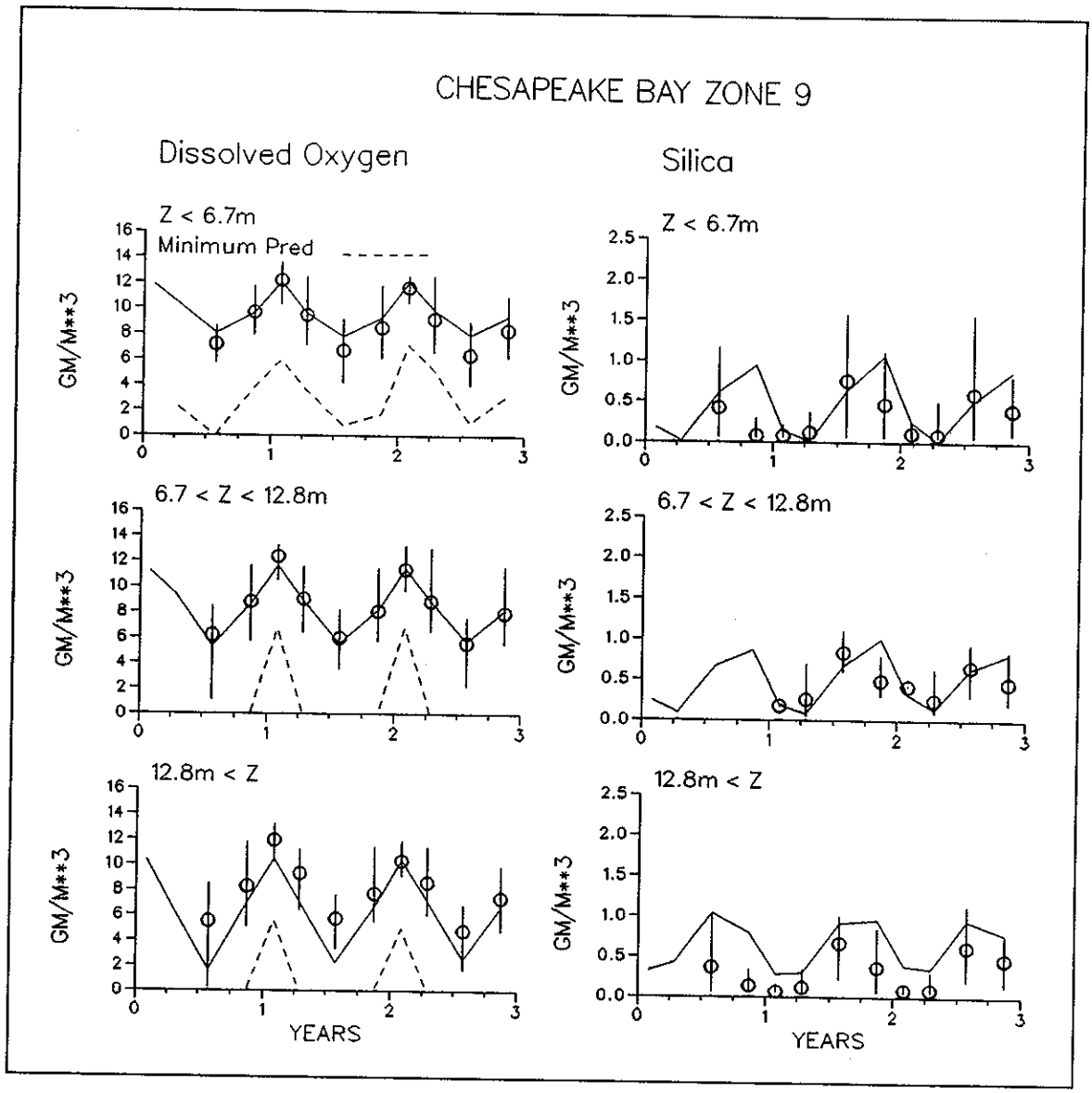

Figure 11-17. (Sheet 5 of 5)

nitrogen limitation was predominant in the lower half. The model indicated silica limitation was roughly equivalent to phosphorus limitation at mid-Bay. The limitation did not affect the large green algal population in summer nor was the limitation supported by the observations.

Season Four, Fall

Autumn was characterized by annual minimum chlorophyll concentrations throughout the Bay (Figures 11-5, 11-9, 11-13, 11-28). In the upper Bay, nitrate was available in non-limiting quantities from surface runoff. Ammonium released from sediments remained in the water column. In the middle

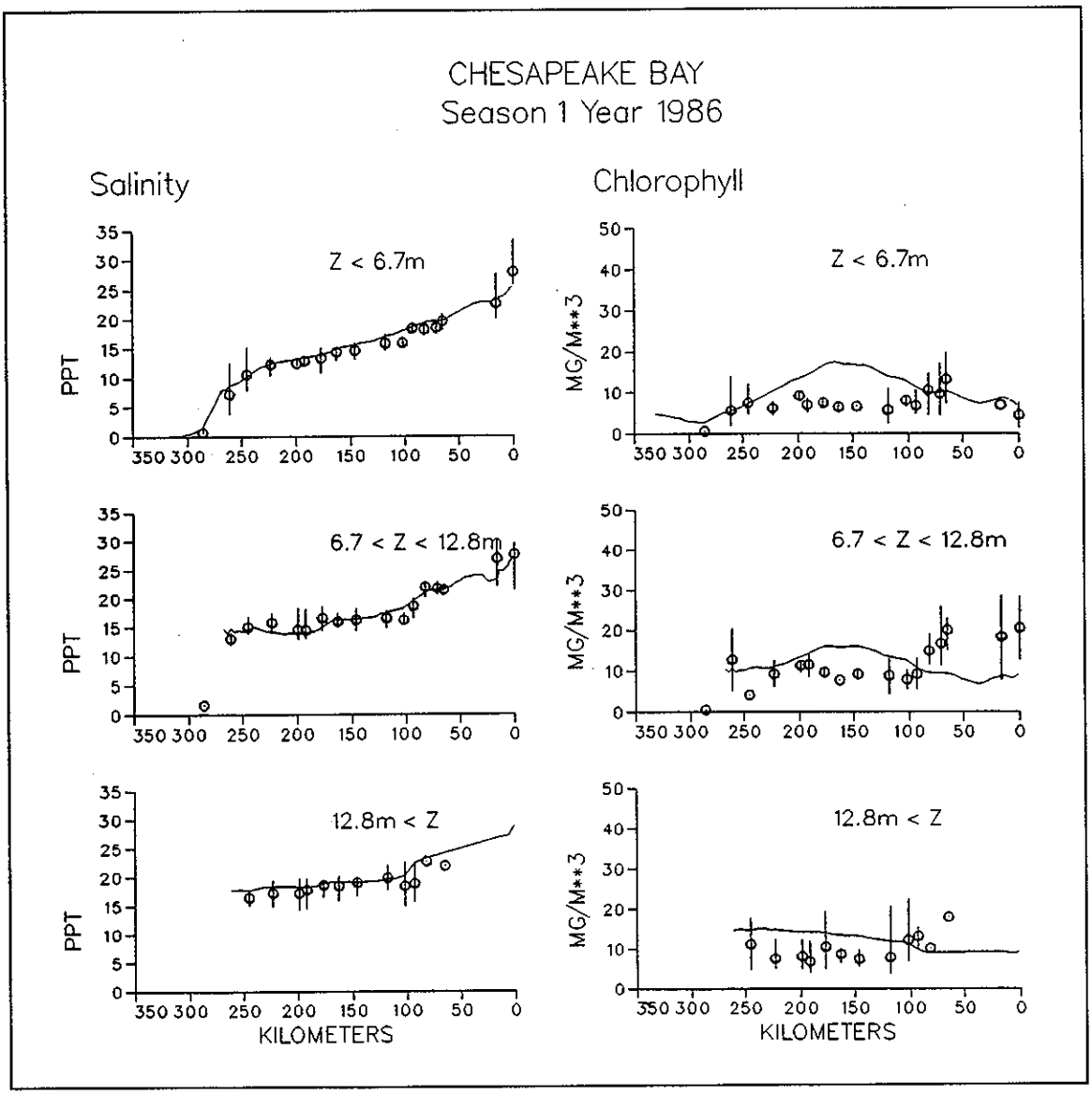

Figure 11-18. Predicted and Observed Concentrations Along Mainstem Bay Transect, Season One, 1986 (Sheet 1 of 8)

and lower Bay, however, inorganic nitrogen was scarce. Phosphate concentrations were low in surface waters throughout the Bay while silica was abundant. The defining process in Season Four was the fall overturn. In late September, autumn winds caused vertical mixing in the water column and ended the period of summer hypoxia. Seasonal-mean dissolved oxygen was ≈5 gm m^{-3} or greater everywhere although remnants of hypoxia were occasionally observed, especially in Layer Three.

Results of the model conformed to the pattern of the observations. Predicted chlorophyll was minimum during Season Four. Availability of inorganic nitrogen in the upper Bay but not in the lower Bay was represented

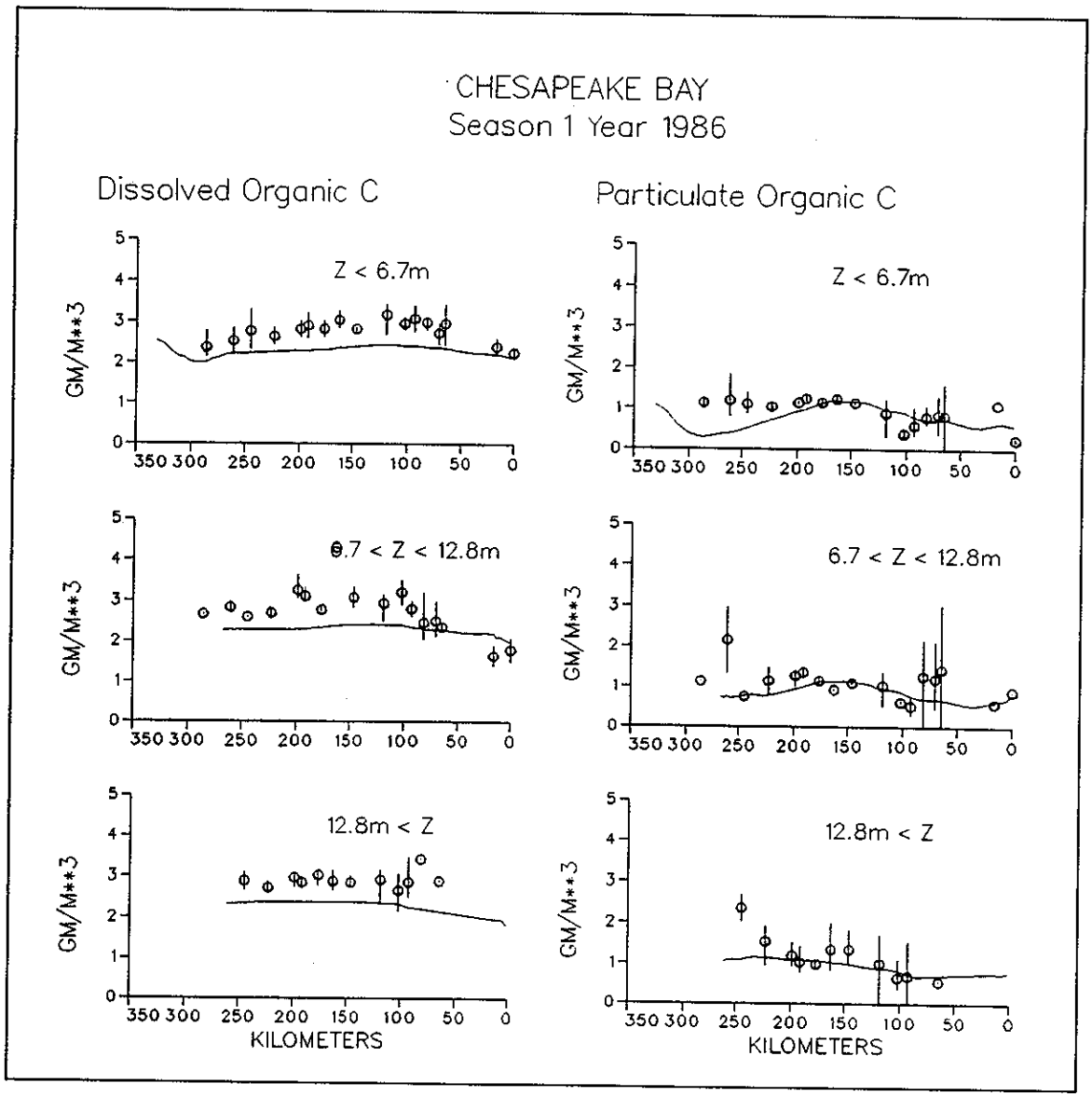

Figure 11-18. (Sheet 2 of 8)

although seasonal-average ammonium was underestimated in the lower Bay. Inorganic phosphorus predictions were nearly perfect and predicted silica was readily available for algal uptake.

The transition from hypoxic to oxygenated conditions was reproduced. The model provided reasonable agreement with observed seasonal-average dissolved oxygen and with minimum observations that occurred near the head of the deep trench.

Sediment nutrient releases in Season Four were among the lowest observed (Figures 11-6, 11-10, 11-29). Diminished release was caused by depletion of fresh organic matter in the sediments and by temperature effects on diagenesis.

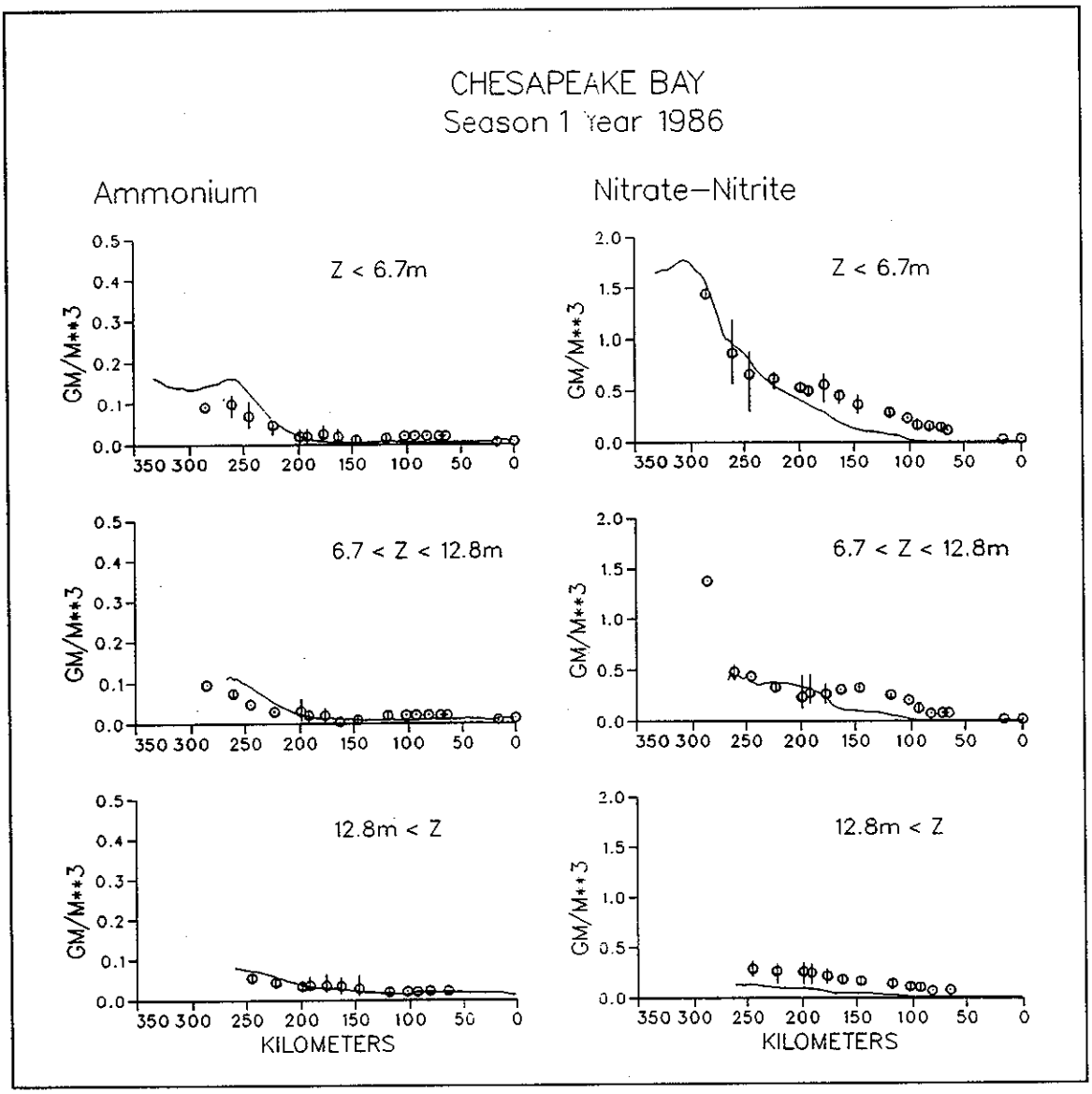

Figure 11-18. (Sheet 3 of 8)

Substantial sediment oxygen demand was observed, 0.5 to 1 gm m^{-2} day^{-1}, due largely to oxidation of sulfide previously stored in the sediments. Trends and magnitudes of fluxes in the model corresponded to the observations.

Both observations and the model indicated minimal primary production during Season Four (Figures 11-8, 11-12, 11-16). Growth in the upper Bay was virtually unlimited by nutrients (figure 11-30). In the lower Bay, the model indicated a nitrogen limitation which was partially an artifact of low ammonium predictions. The primary limit on growth was diminished temperature.

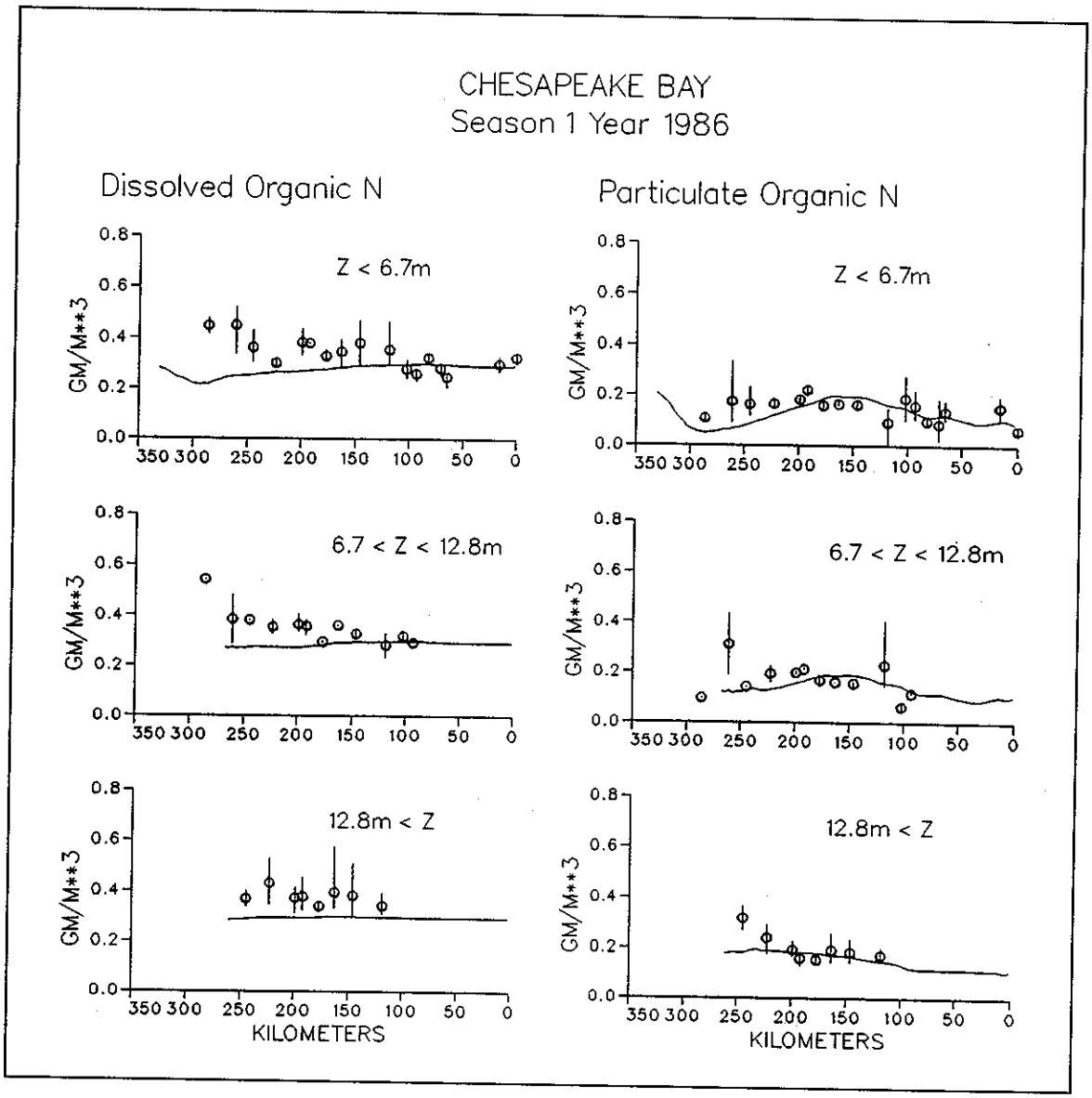

Figure 11-18. (Sheet 4 of 8)

Suggested Improvements

The model provided a realistic representation of eutrophication processes in the mainstem Bay. Spatial and temporal trends and magnitude of the observations were well reproduced. The extensive effort allotted to calibration indicates no improvement in model-data agreement is possible with the present model. Improvement may be obtained, however, after model modification. Suggested improvements are unlikely to alter the utility or reliability of the model but will enhance realism and agreement with observations.

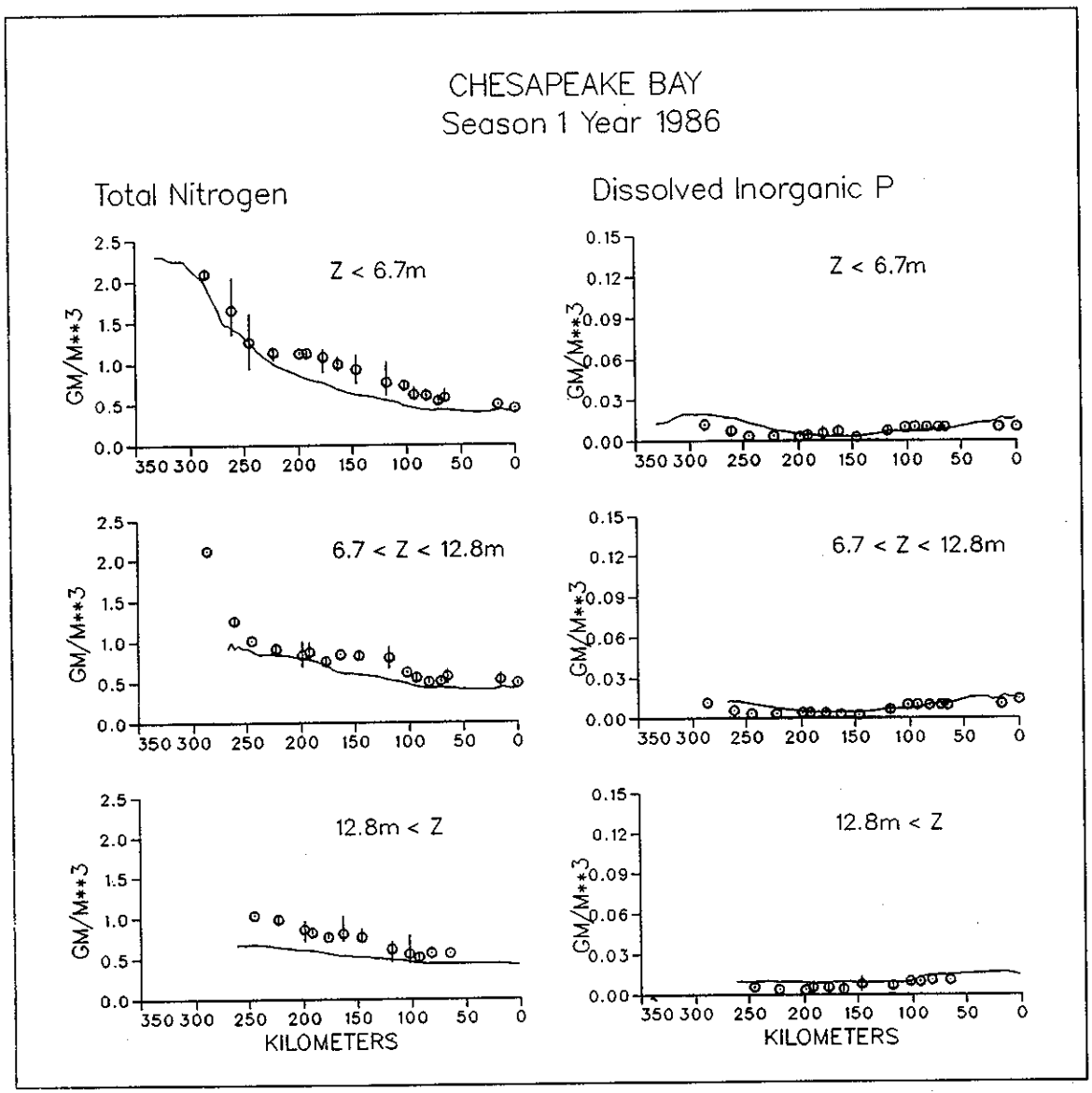

Figure 11-18. (Sheet 5 of 8)

Addition of Zooplankton

Hypoxia in the mainstem Bay starts with primary production of organic carbon by algae. The carbon settles to bottom waters and is oxidized in the water column and sediments, consuming dissolved oxygen. Key elements in the process were represented in the model. Magnitudes of several components were underestimated, however. In Season Three, modelled primary production was generally less than observed (Figure 11-27) as was predicted dissolved organic carbon (Figure 11-24). Respiration, in the model, was less than indicated by available observations (Figure 11-8) and average dissolved oxygen exceeded observations through much of the water column (Figure 11-24).

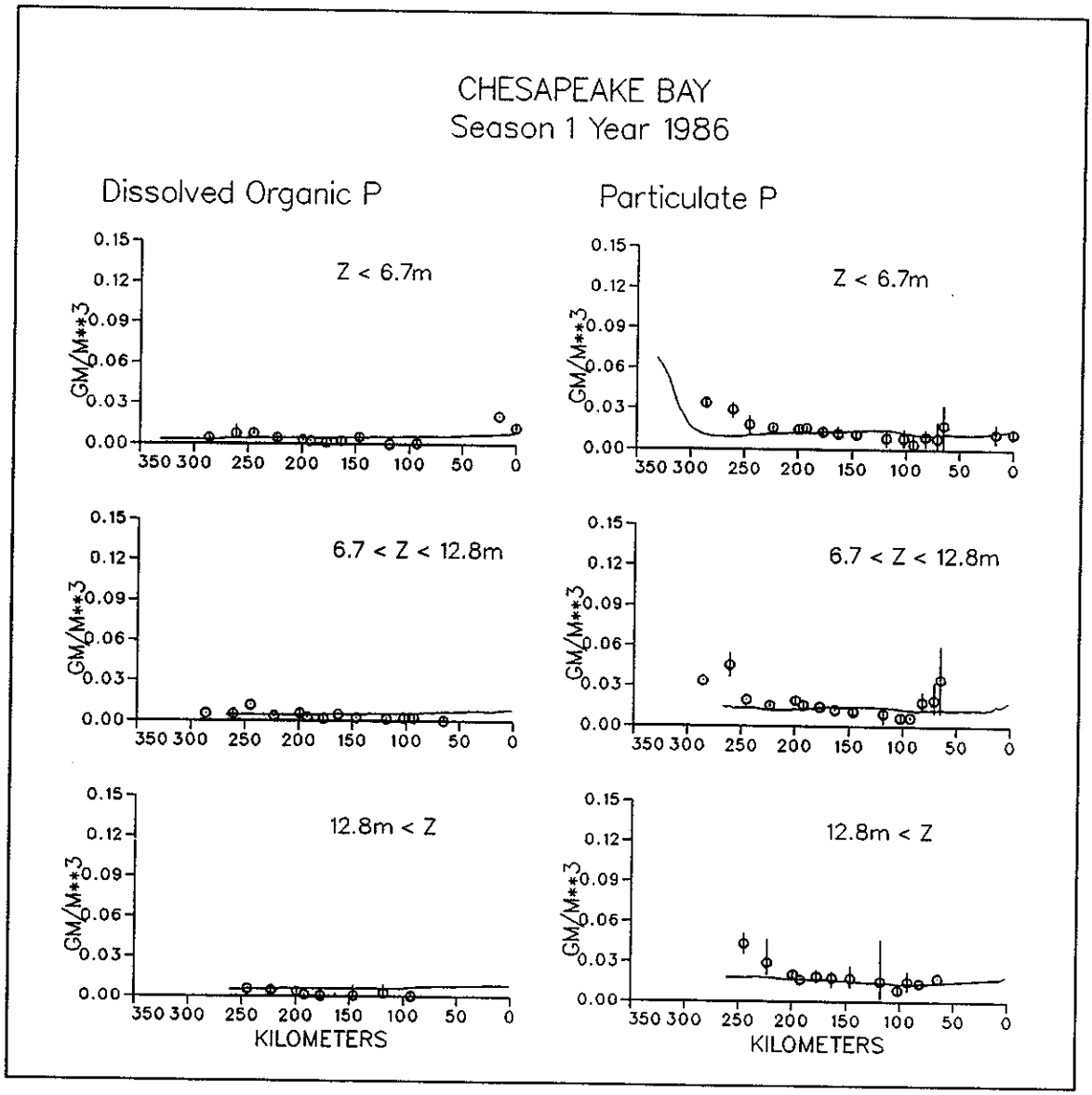

Figure 11-18. (Sheet 6 of 8)

Predicted dissolved oxygen can be diminished through primary production and respiration of additional carbon. The trick is to achieve additional primary production while maintaining the current, accurate, predictions of algal standing stock. Attempts to increase production while maintaining reasonable chlorophyll predictions have been unsuccessful. Production increases have been accompanied by intolerable increases in algal biomass. The inability to increase production while maintaining biomass originates in the disparate formulations of algal source and sink terms. Algal production is a Gaussian function of temperature (Equation 4-12) and a non-linear function of nutrients (Equation 4-5) and light (Equation 4-8). Respiration and predation are exponential functions of temperature only (Equation 4-17). Balance between source and sink terms is difficult to accomplish due to the different

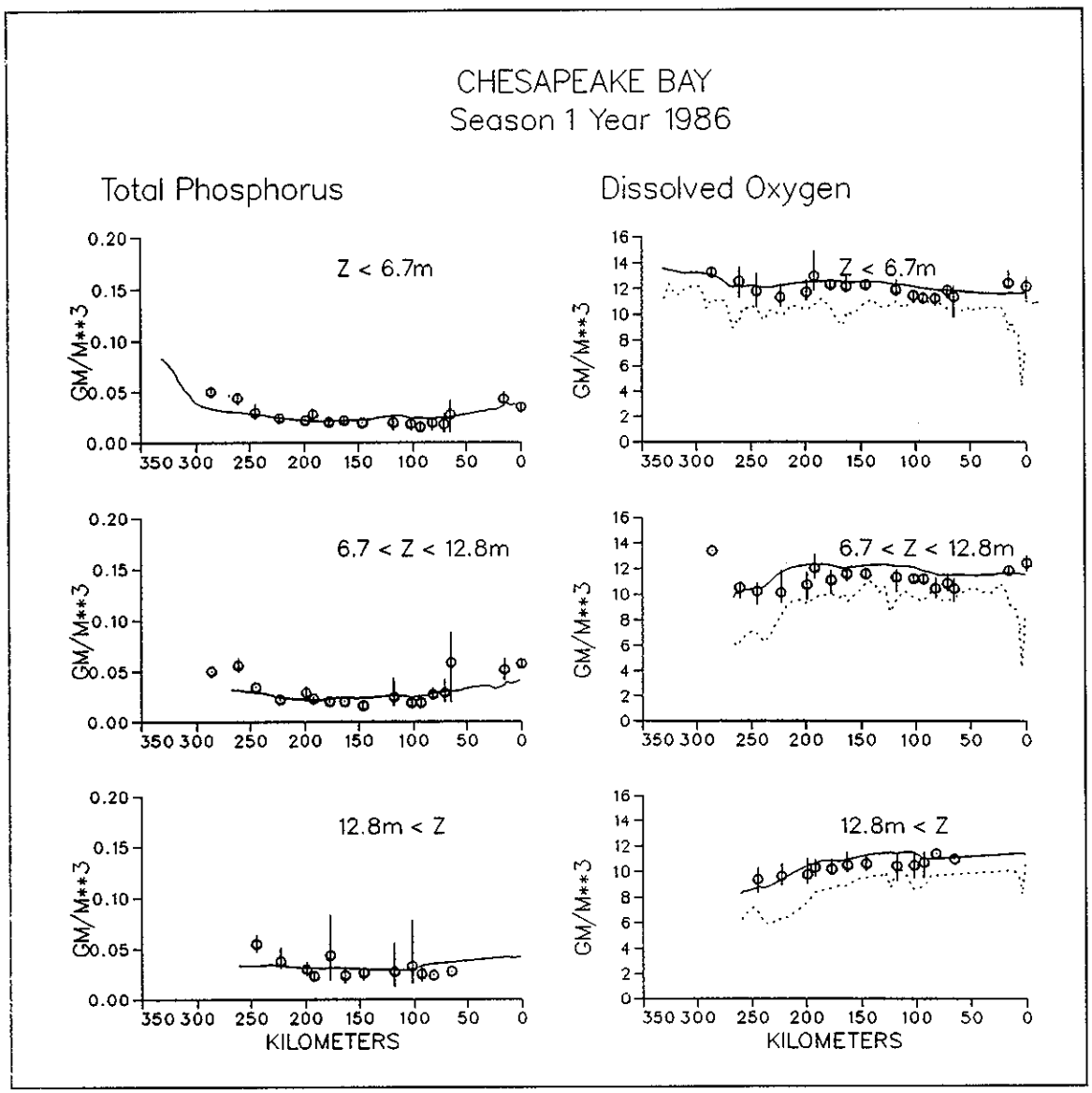

Figure 11-18. (Sheet 7 of 8)

formulations. A means of increasing production while maintaining acceptable algal biomass might be the addition of zooplankton to the model. In this hypothesis, the zooplankton biomass would track the algal biomass and provide close coupling of algal source and sink terms.

The initial formulation of the model included two zooplankton groups. The initial version could not be calibrated within the time frame of the project, however, so the zooplankton were dropped. Now that initial application of the model is complete, addition of zooplankton, to provide advanced closure on the phytoplankton, appears feasible.

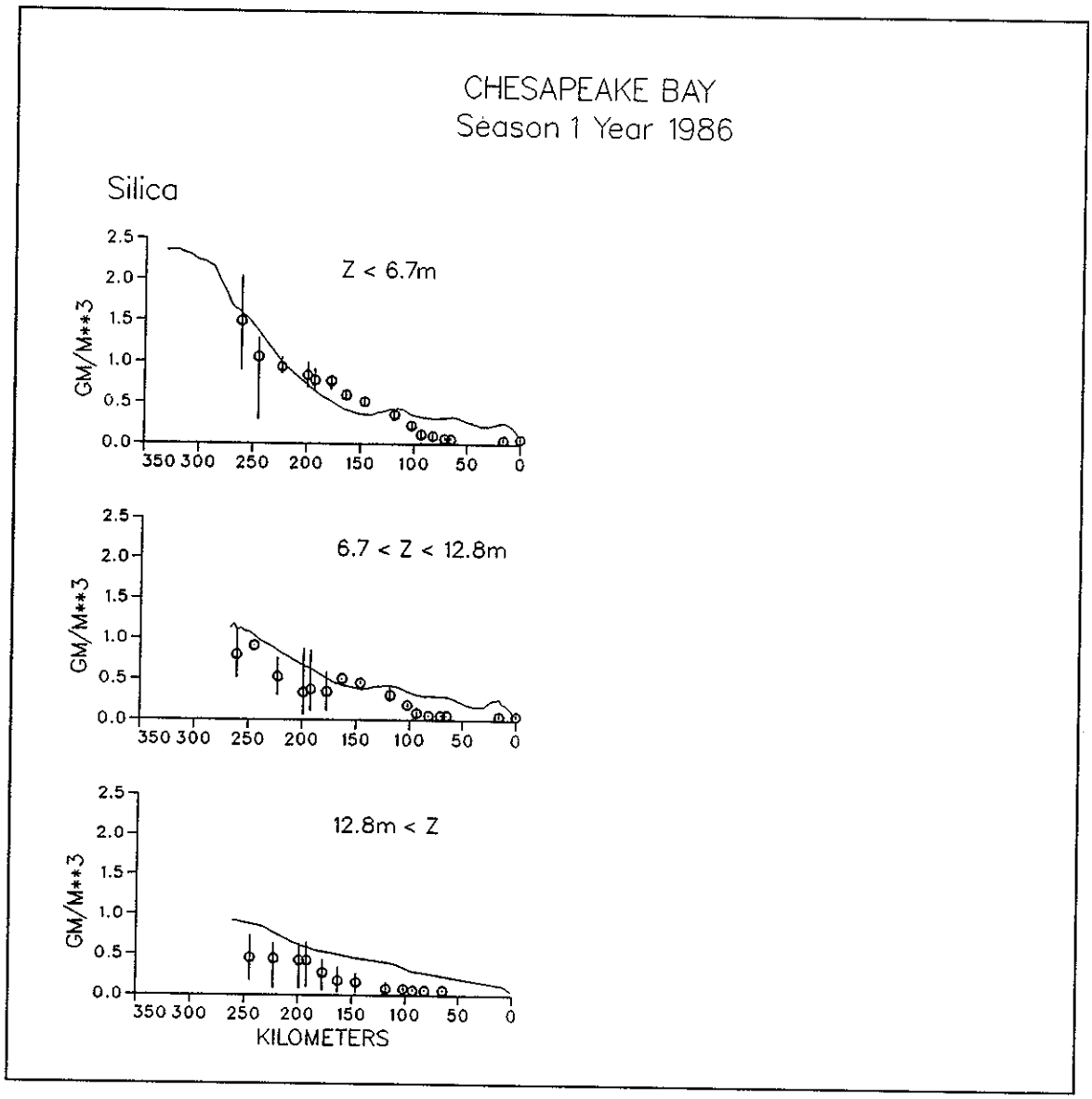

Figure 11-18. (Sheet 8 of 8)

Particulate Inorganic Phosphorus

Extensive effort was devoted to producing highly accurate predictions of dissolved phosphate, a crucial algal nutrient, in the mainstem. Predictions of total phosphorus were less accurate than the dissolved inorganic fraction, however. A shortfall of predicted particulate phosphorus often accounted for overall underestimation of total phosphorus (Figures 11-21, 11-24, 11-28).

The underestimation of total phosphorus suggests omission a phosphorus source. One potential source is bank erosion, roughly estimated at 6000 kg day^{-1} (CBPO 1991) or ≈ 18% of the loads considered in the model (Table 5-7).

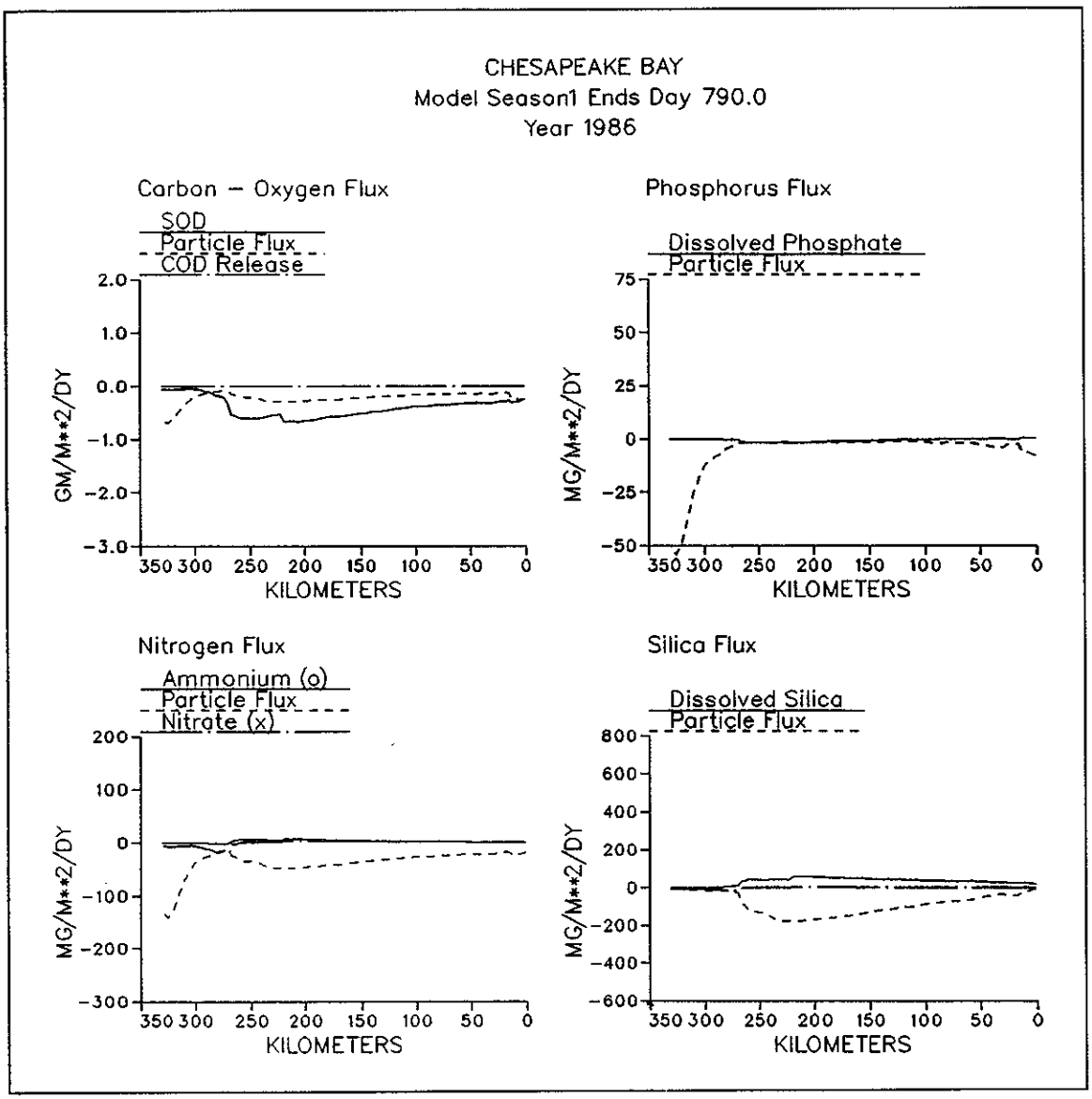

Figure 11-19. Predicted Sediment-Water Fluxes Along Mainstem Bay Transect, Season One, 1986

The idea that phosphorus loading from bank erosion is significant fits neatly with the second factor thought responsible for the phosphorus shortfall. A particulate inorganic fraction remains in suspension throughout the Bay. The particulate fraction comprises 23% to 86% of total particulate phosphorus in the water column (Keefe 1993). Distribution and transport of the particulate inorganic phosphorus are apparently similar to suspended sediment. Greatest concentrations of particulate phosphorus occur around km 300, coincident with the turbidity maximum.

The availability of the particulate inorganic phosphorus to biota in the water column is unknown. If the major source is erosion, the phosphorus may be

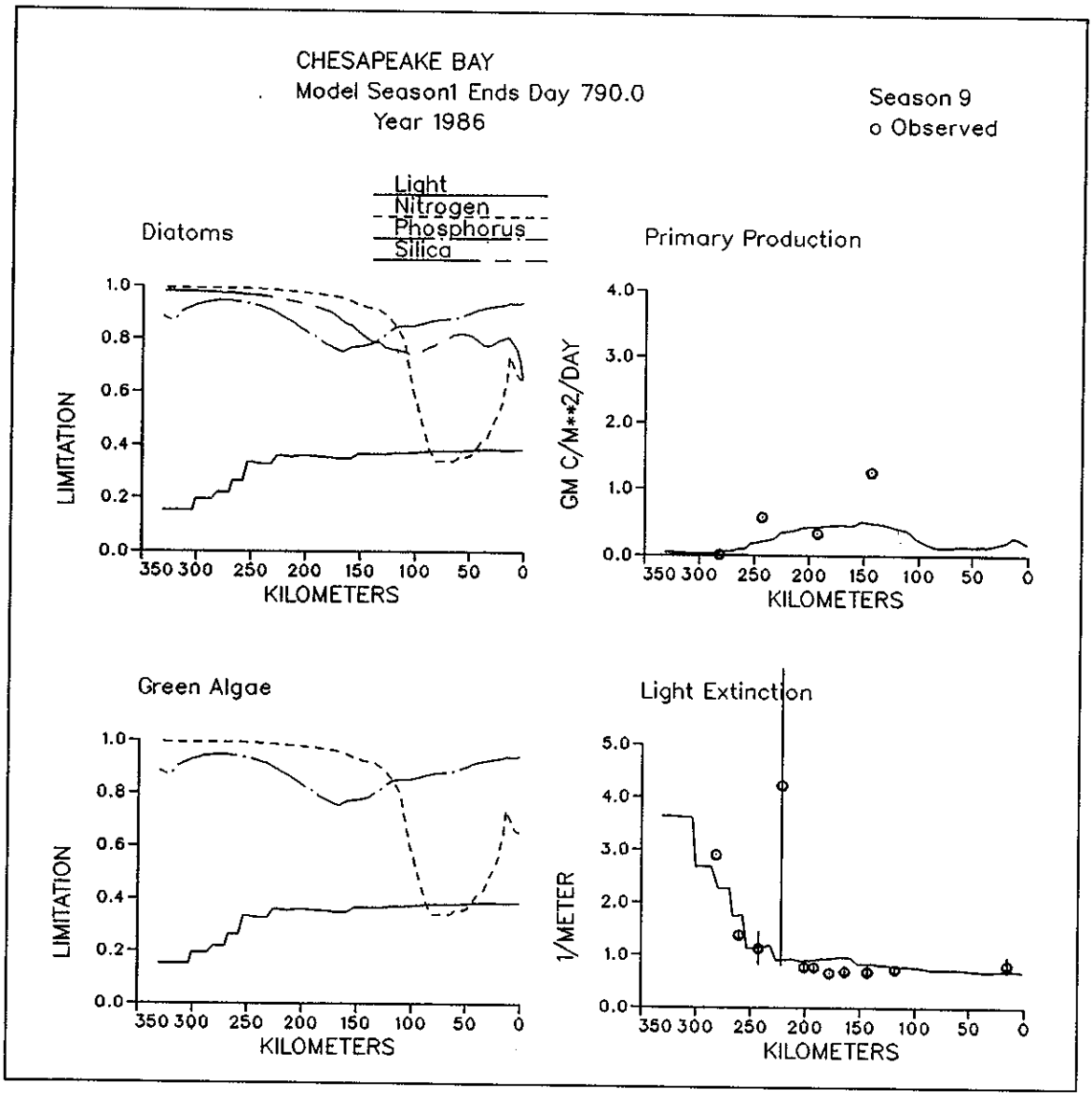

Figure 11-20. Predicted and Observed Diagnostic Information Along Mainstem Bay Transect, Season One, 1986

tightly bound in unavailable mineral form. The careful calibration of dissolved inorganic phosphate suggests the conclusions of the present study will be unaffected by addition of particulate inorganic phosphorus. The predictions of particulate and total phosphorus will be much improved, however, by addition of particulate inorganic phosphorus to the suite of state variables.

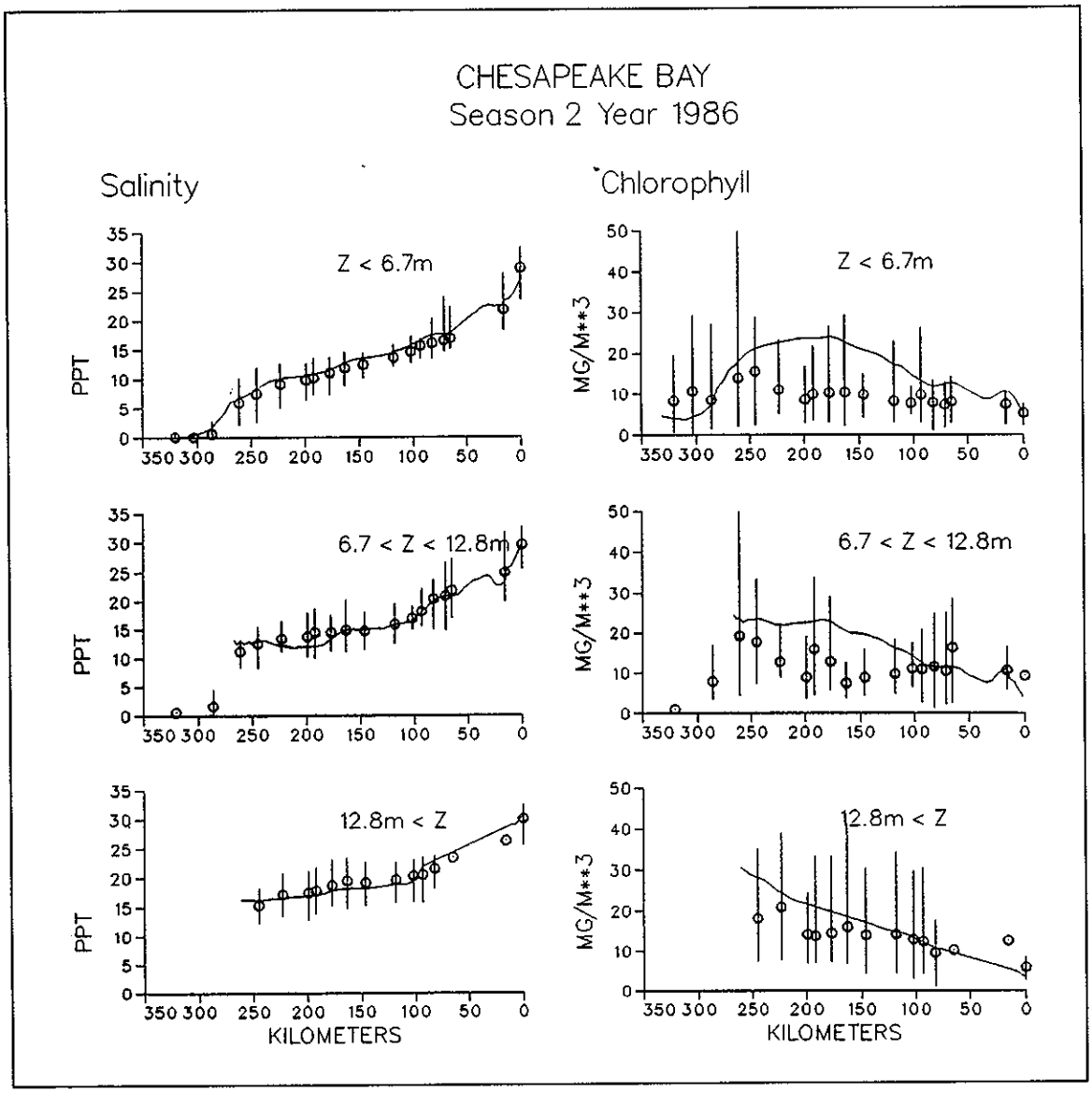

Figure 11-21. Predicted and Observed Concentrations Along Mainstem Bay Transect, Season Two, 1986 (Sheet 1 of 8)

Performance of Open-Mouth Boundary Conditions

In initial evaluation of the boundary-condition algorithm, outflow concentrations were specified based on observations (Figures 8-5, 8-6). During model application, however, outflow concentrations were predicted as functions of loading and internal processes. Performance of the algorithm was verified with the model operating in predictive mode. Observations from Stations CB8.1E, CB7.4, and CB7.4N (Figure 11-2) were compared to predictions in model cells immediately adjacent to the ocean boundary. Model and data were

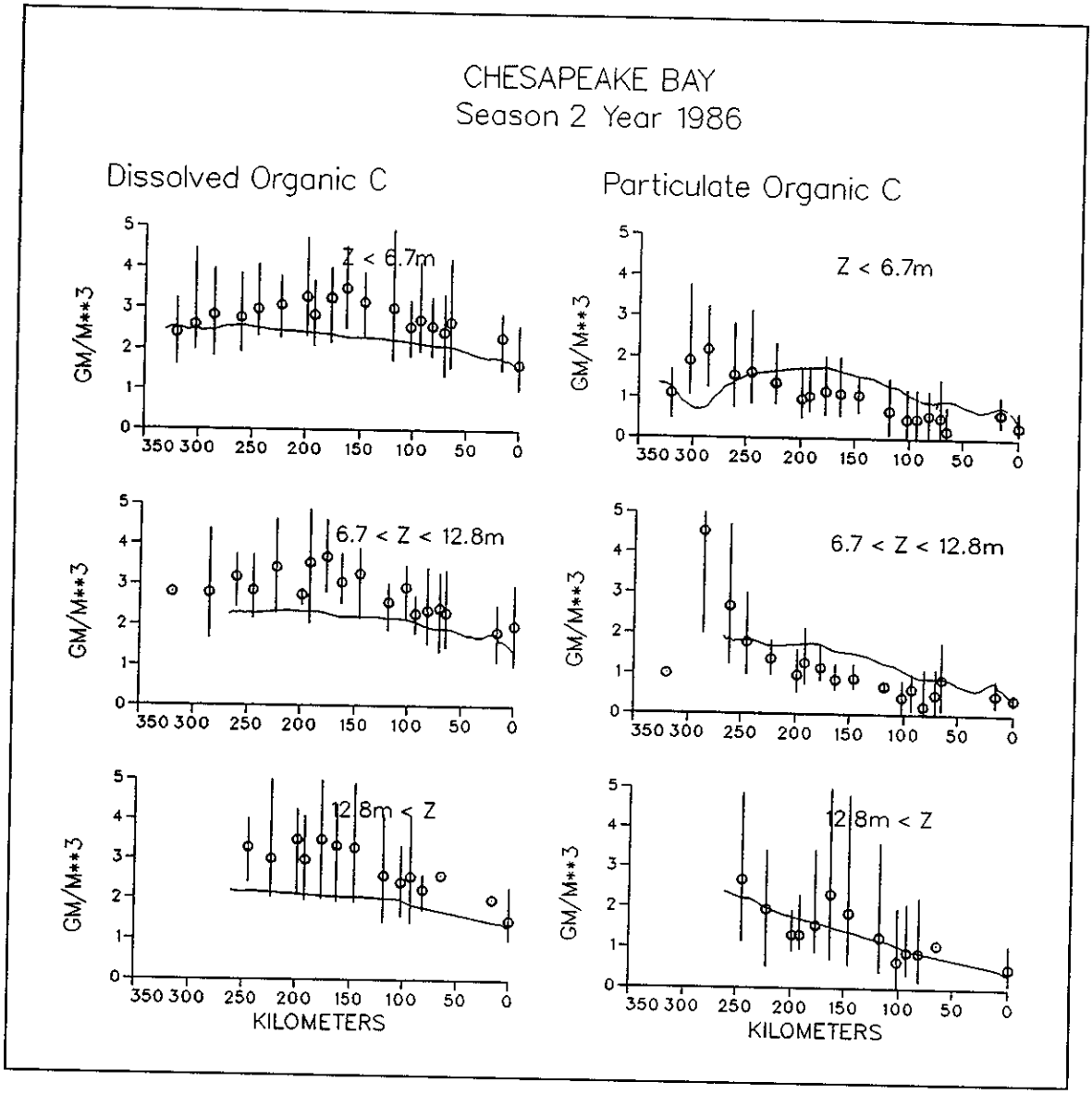

Figure 11-21. (Sheet 2 of 8)

aggregated by season and into inflow and outflow regimes. Inflow and outflow were determined by the same mapping scheme employed in development of the mass-balance boundary conditions (Chapter VIII).

Predicted total nitrogen conformed to the central tendency of the observations (Figure 11-34) although the variability present in the observations was averaged out of the model. An important characteristic of the observations, reproduced in the model, was the absence of definitive differences in inflow and outflow concentrations.

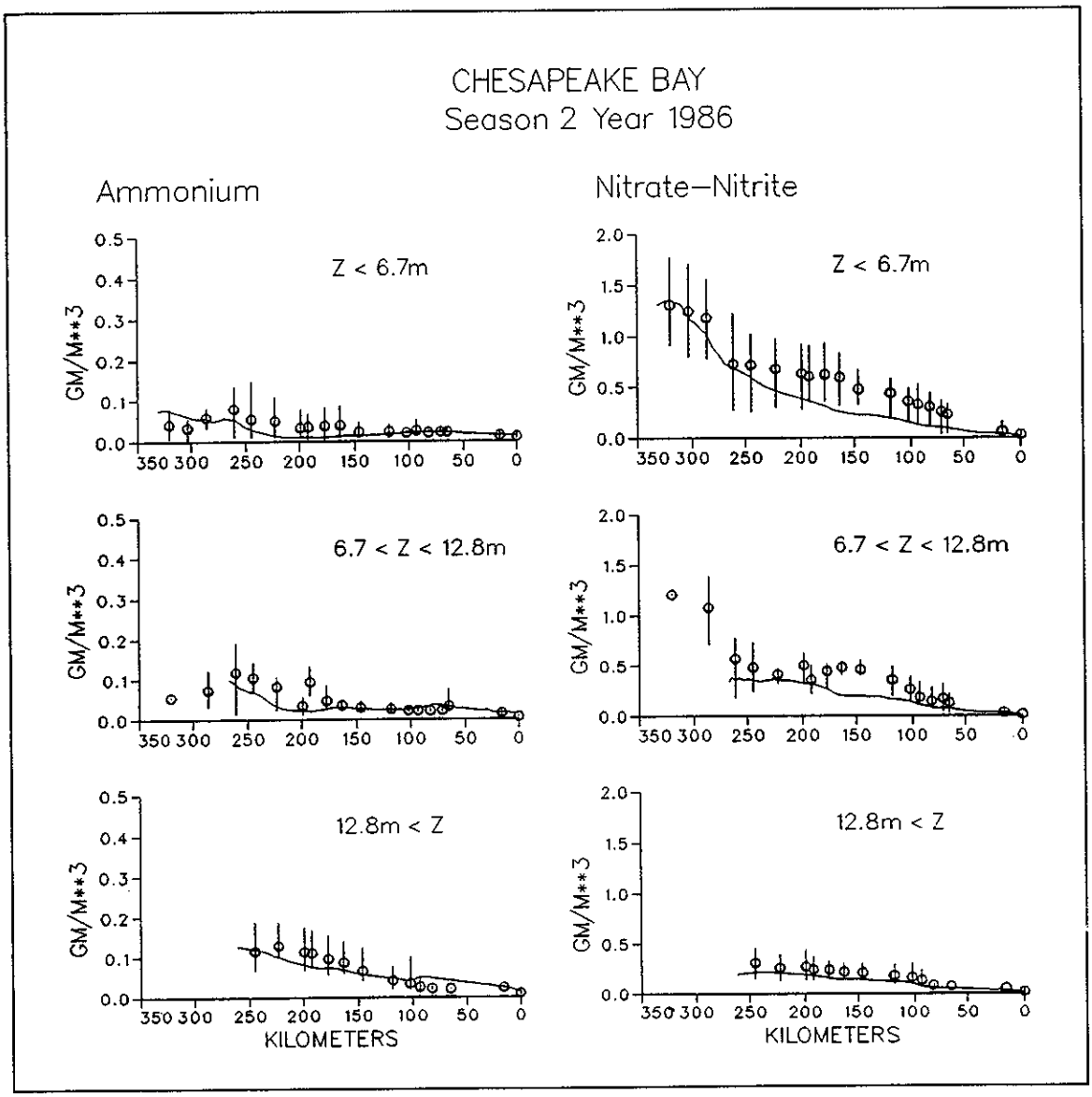

Figure 11-21. (Sheet 3 of 8)

Predicted total phosphorus conformed closely to observations. Neither model nor observations showed much variability. An exception was an observed peak in late 1985 coincident with the November storm that flooded the tributaries. Inflow concentrations exceeded outflow concentrations by a small (< 0.01 gm m^{-3}) but consistent amount in both observations and model.

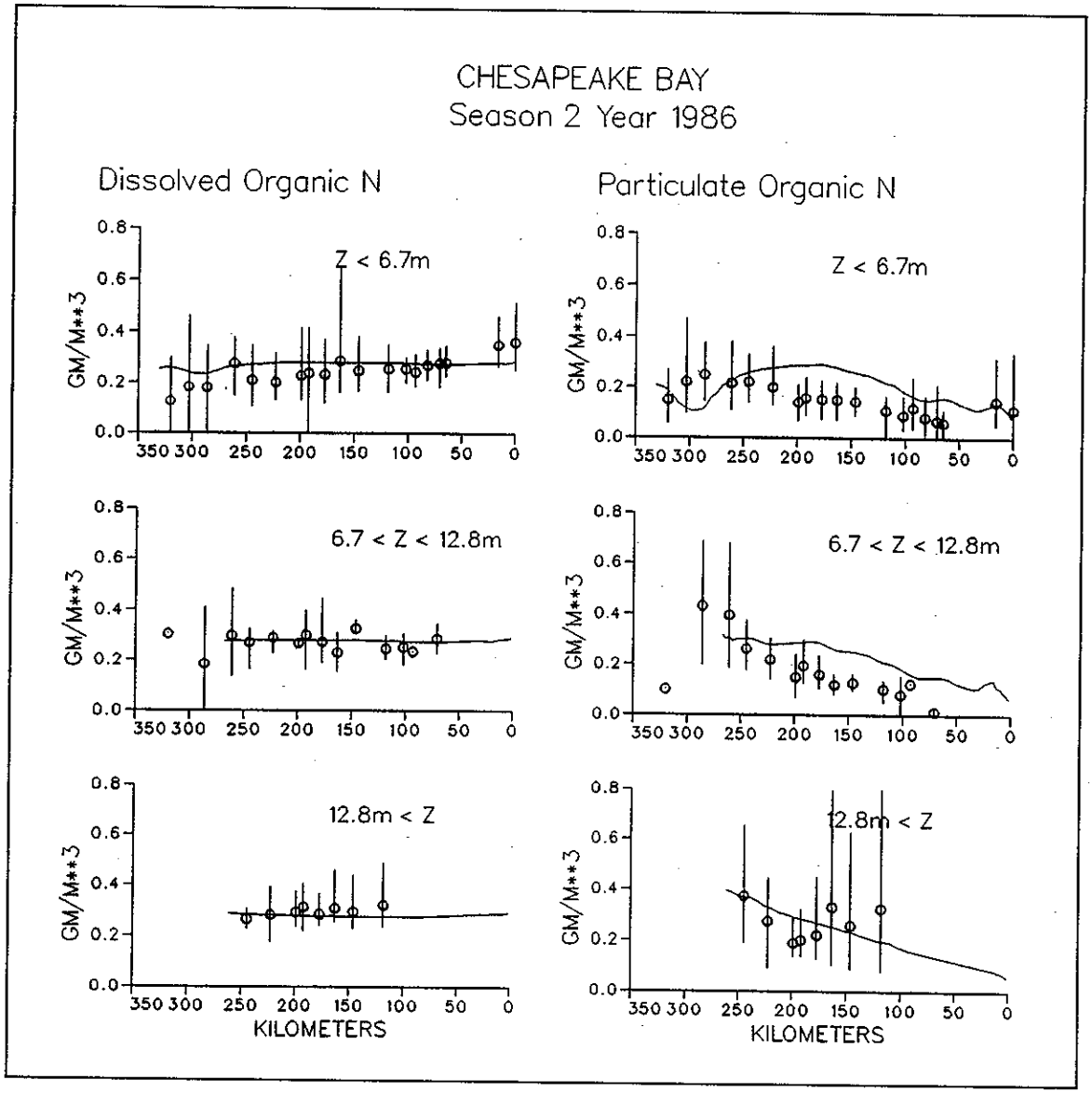

Figure 11-21. (Sheet 4 of 8)

Mass Balance and Flux Analyses

Transport

Transport of carbon, nitrogen, and phosphorus among regions of the Bay (Figure 11-2) was analyzed for 1986, the average hydrologic year. Based on annual mean flows, cell faces in transects between regions were identified as "upstream" or "downstream" flow faces. At transects dividing the mainstem from the Eastern Shore, downstream was defined as flow from west to east. Annual mass transport at each cell face was summed into upstream and downstream totals for each transect.

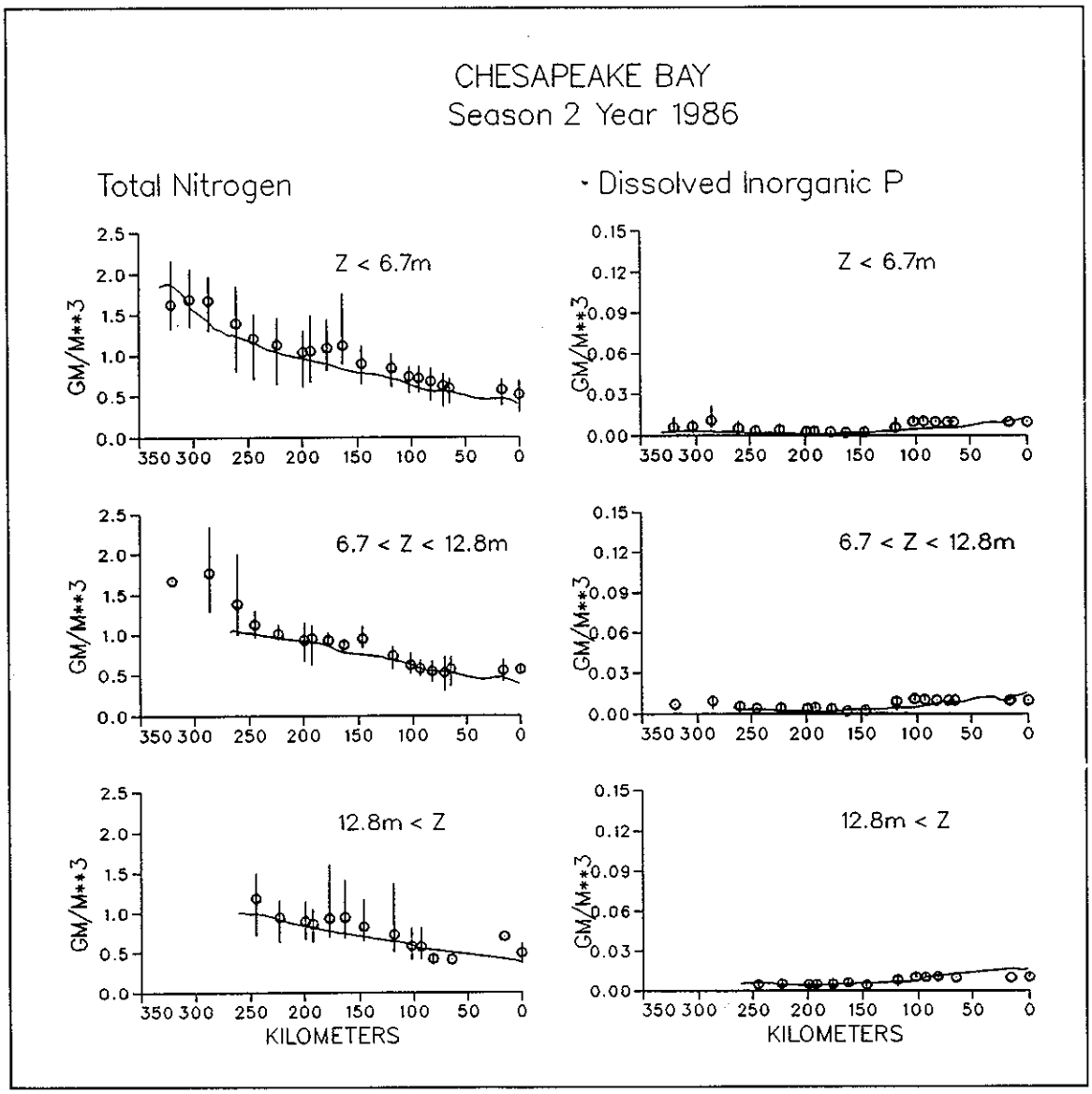

Figure 11-21. (Sheet 5 of 8)

Patterns of annual carbon (Figure 11-35), nitrogen (Figure 11-36), and phosphorus (Figure 11-37) transport are largely similar to the volumetric flows (Figures 3-14, 3-15). Large masses of carbon and nutrients are transported upstream and downstream. Mass flows increase with distance downstream as does volumetric flow. Mass transport along the mainstem exceeds lateral exchange between the mainstem and Eastern Shore.

Net carbon transport is exclusively downstream (Figure 11-38). The primary pathway for net transport is through the Eastern Shore. This path conforms to the pattern of net flow (Figure 3-15). Net carbon flow throughout the mainstem is downstream, however, while net volumetric flow is upstream in the mainstem adjacent to the Eastern Shore. The discrepancy between

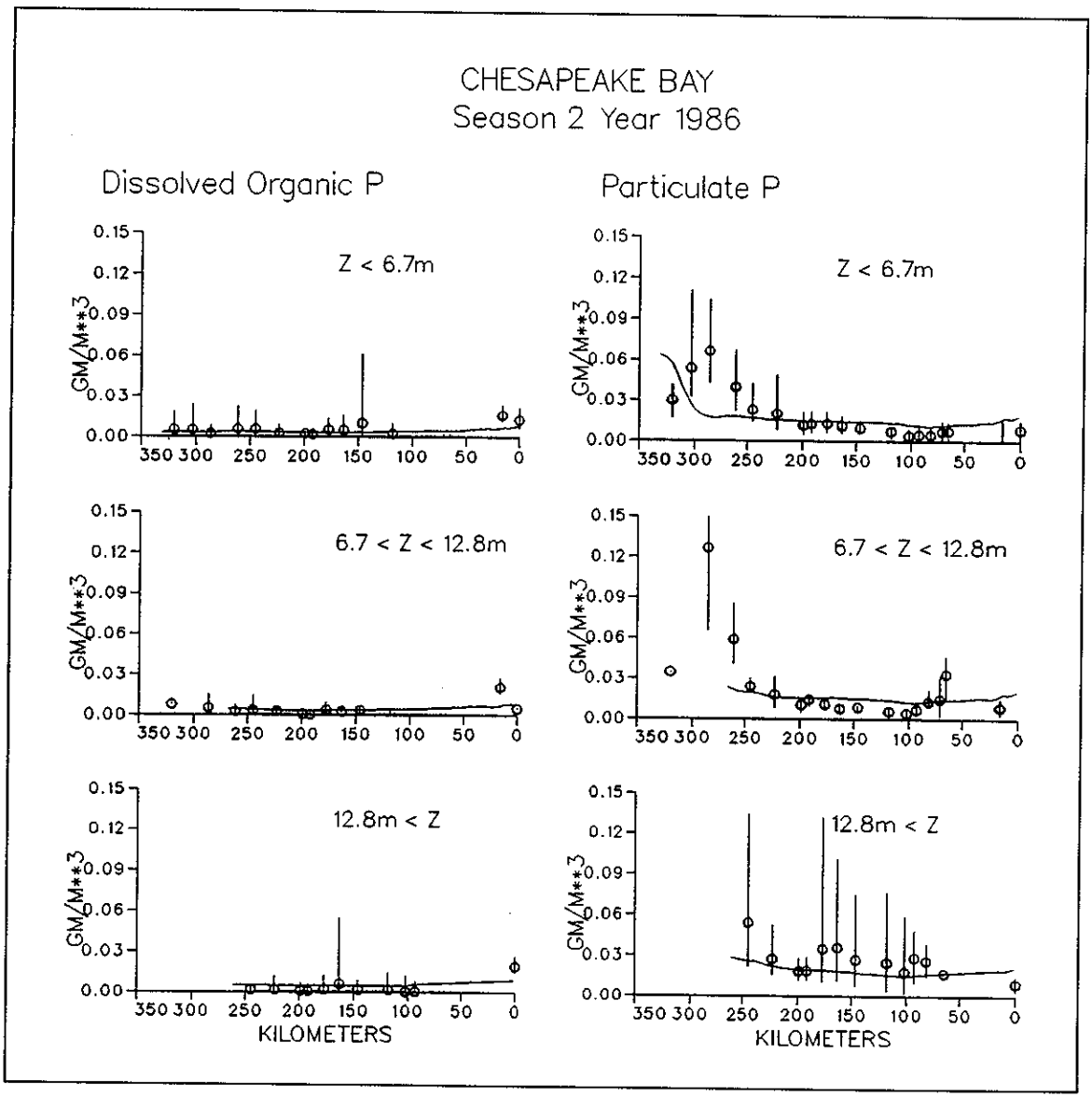

Figure 11-21. (Sheet 6 of 8)

carbon transport and flow may reflect higher carbon concentration in surface waters or may be due to differences in analysis. The flow summaries were for summer only.

The pattern of net nitrogen transport (Figure 11-39) differs from carbon. Net transport is greatest in the upper Bay and diminishes with distance downstream. The large mass transported through the upper Bay is nitrogen supplied by the Susquehanna River. Diminished transport with distance indicates nitrogen is lost from the water column as net flow transports it from the river to the sea. An important feature of the transport analysis is nitrogen loss from the estuary to the ocean. The transport to the ocean is due to flow predominance

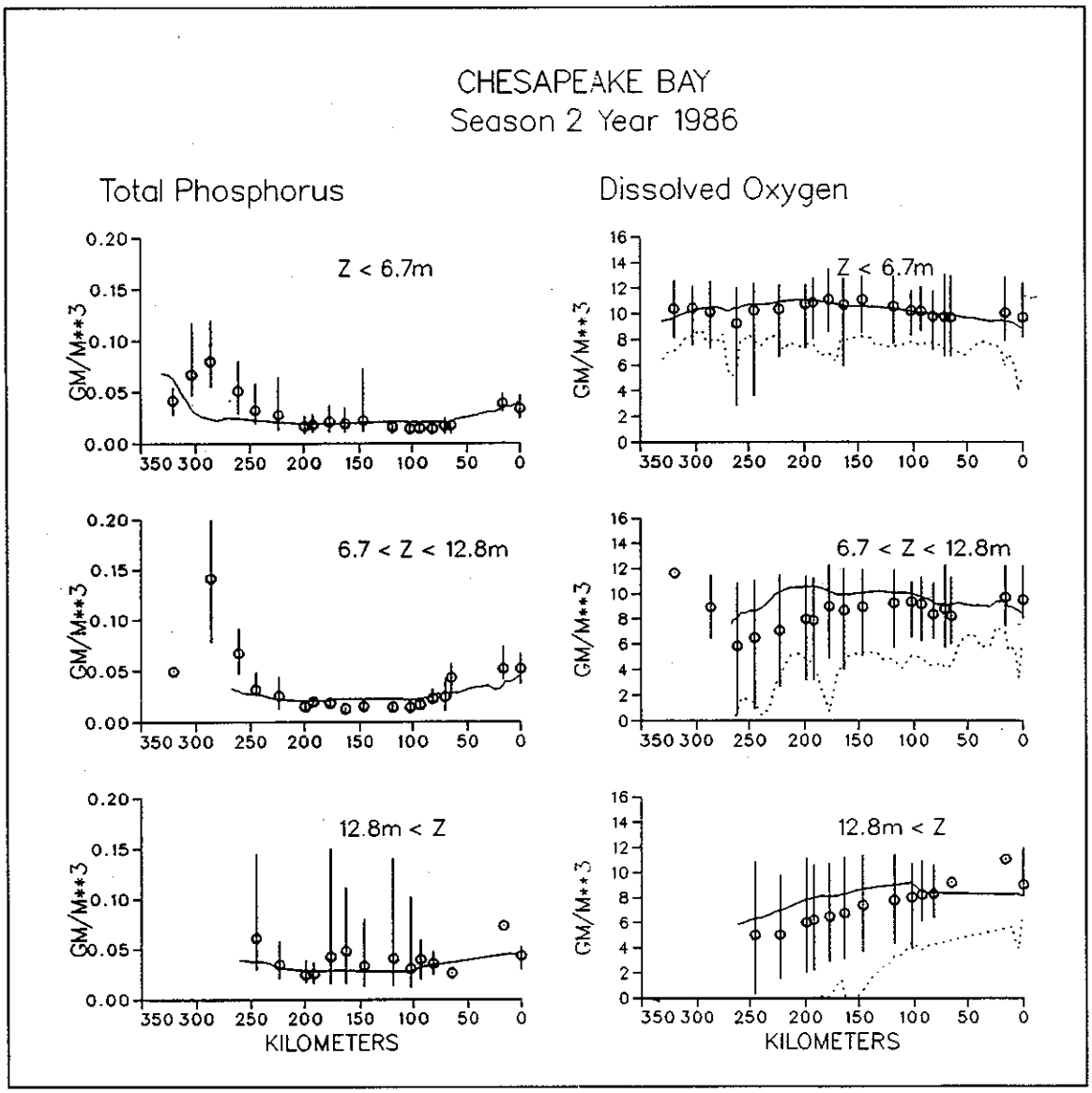

Figure 11-21. (Sheet 7 of 8)

at the mouth. Net freshwater runoff leaves the system and carries nitrogen with it.

Net phosphorus transport is distinctive (Figure 11-40). Greatest net transport is at the mouth of the Bay and is upstream, into the Bay. The net transport from the ocean occurs because phosphorus concentration is greater in inflowing water. Net upstream transport predominates as far Zone Four, adjacent to the Patuxent River mouth. From the Susquehanna to the Patuxent, phosphorus transport is downstream. Diminished transport downstream from the Susquehanna and upstream from the mouth indicates phosphorus is lost from the water column as it travels from the river and the ocean.

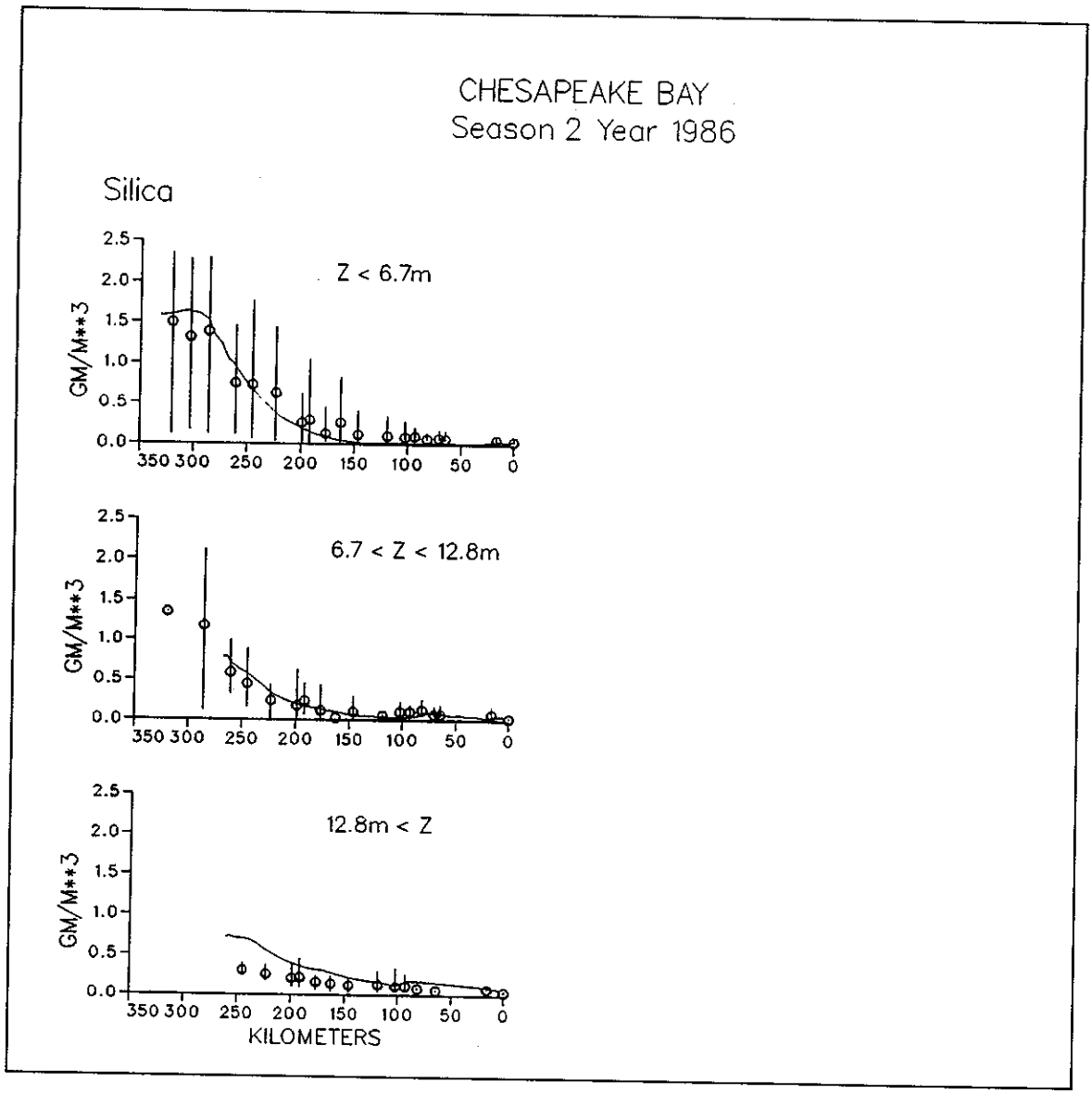

Figure 11-21. (Sheet 8 of 8)

The pattern of net transport corresponds well with phosphorus observations in the water column and sediments. Often, observations indicate total phosphorus concentration is higher at the mouth and head of the Bay than at mid-Bay (Figures 11-18, 11-21, 11-28). The basic concept that substances flow from regions of higher concentration to regions of lesser concentration suggests phosphorus travels downstream from the Susquehanna and upstream fom the Bay mouth. The spatial pattern in sediment phosphorus near the mouth of the Bay (Figure 11-26) supports the concept that phosphorus is lost from the water column as it travels upstream.

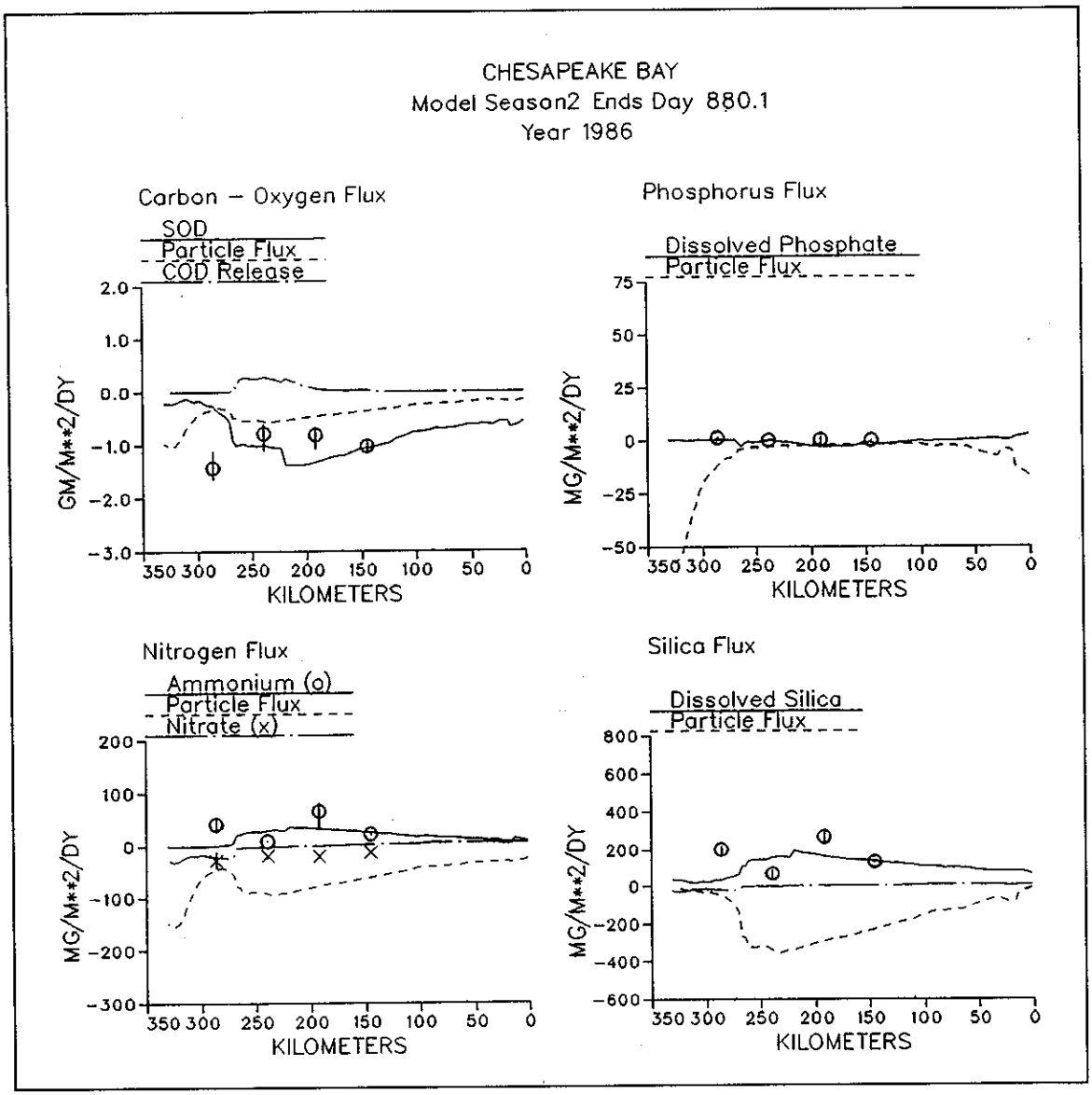

Figure 11-22. Predicted and Observed Sediment-Water Fluxes Along Mainstem Bay Transect, Season Two, 1986

Mass Balance

A valuable feature of the model was the ability to perform system mass balances. Mass balances provided both a check on computational accuracy and insights into Bay behavior. Annual mass balances were performed on the mainstem Bay and on each of the major tributaries. Mainstem mass balances are presented here for 1986, the average hydrologic year.

Water-column (Figure 11-41) and sediment (Figure 11-42) mass balances were completed for total nitrogen, total phosphorus, and organic carbon. Net sources to the water column were assigned positive values. Net sinks were

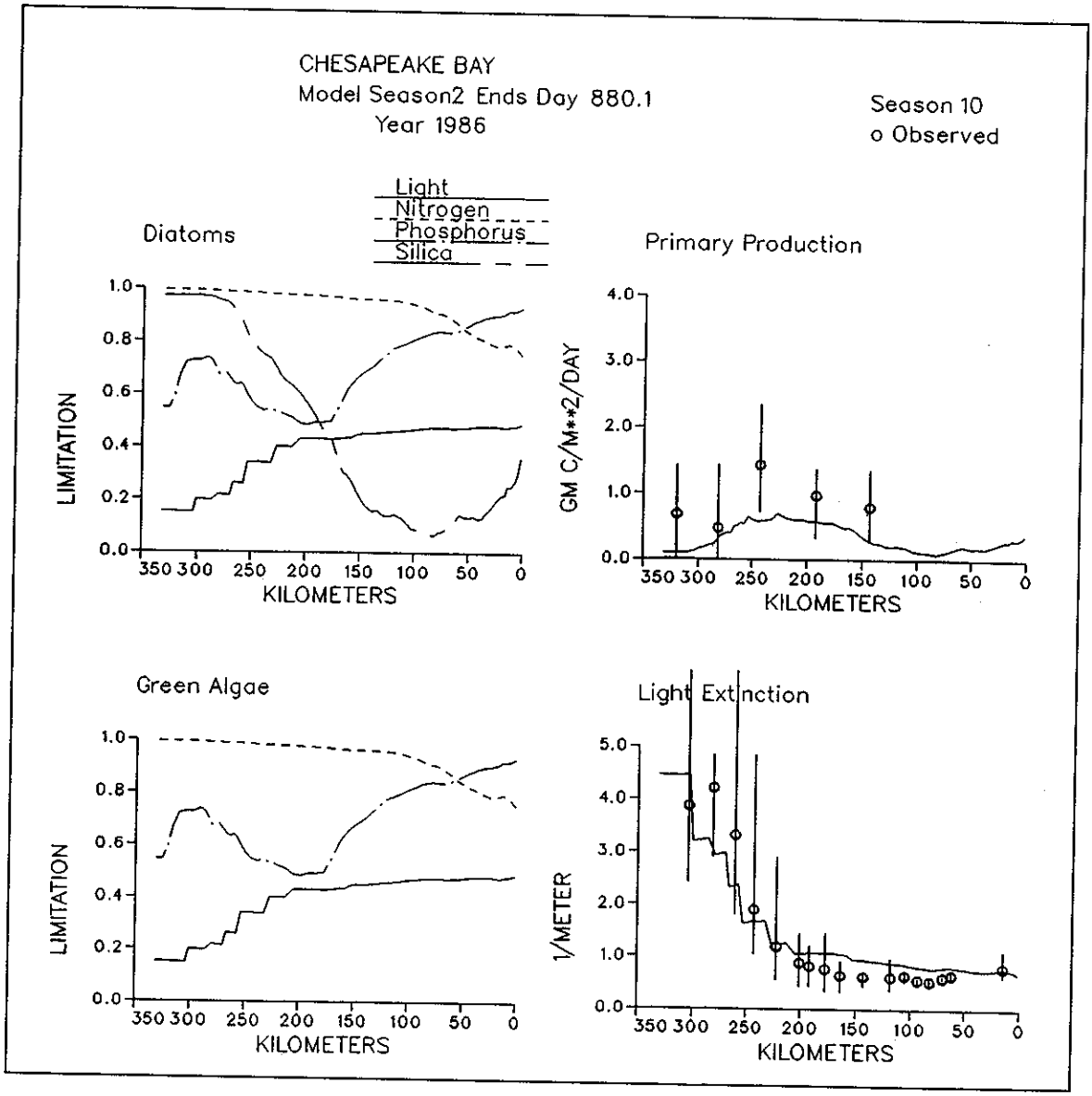

Figure 11-23. Predicted and Observed Diagnostic Information Along Mainstem Bay Transect, Season Two, 1986

assigned negative values. An identical convention was employed for the sediment balances. By this convention, settling of particles was assigned a negative value as sink in the water-column budget and a positive value as a source in the sediment budget. Sediment nutrient release was a source in the water-column budget and a sink in the sediment budget.

For water-column nitrogen, the "Other" category is the atmospheric load to the water surface less denitrification in the water column. The "Other" category for water-column phosphorus is solely the atmospheric load to the water surface. "Primary Production" of carbon is algal production minus algal respiration and dissolved organic carbon oxidation. "Direct" loads of all

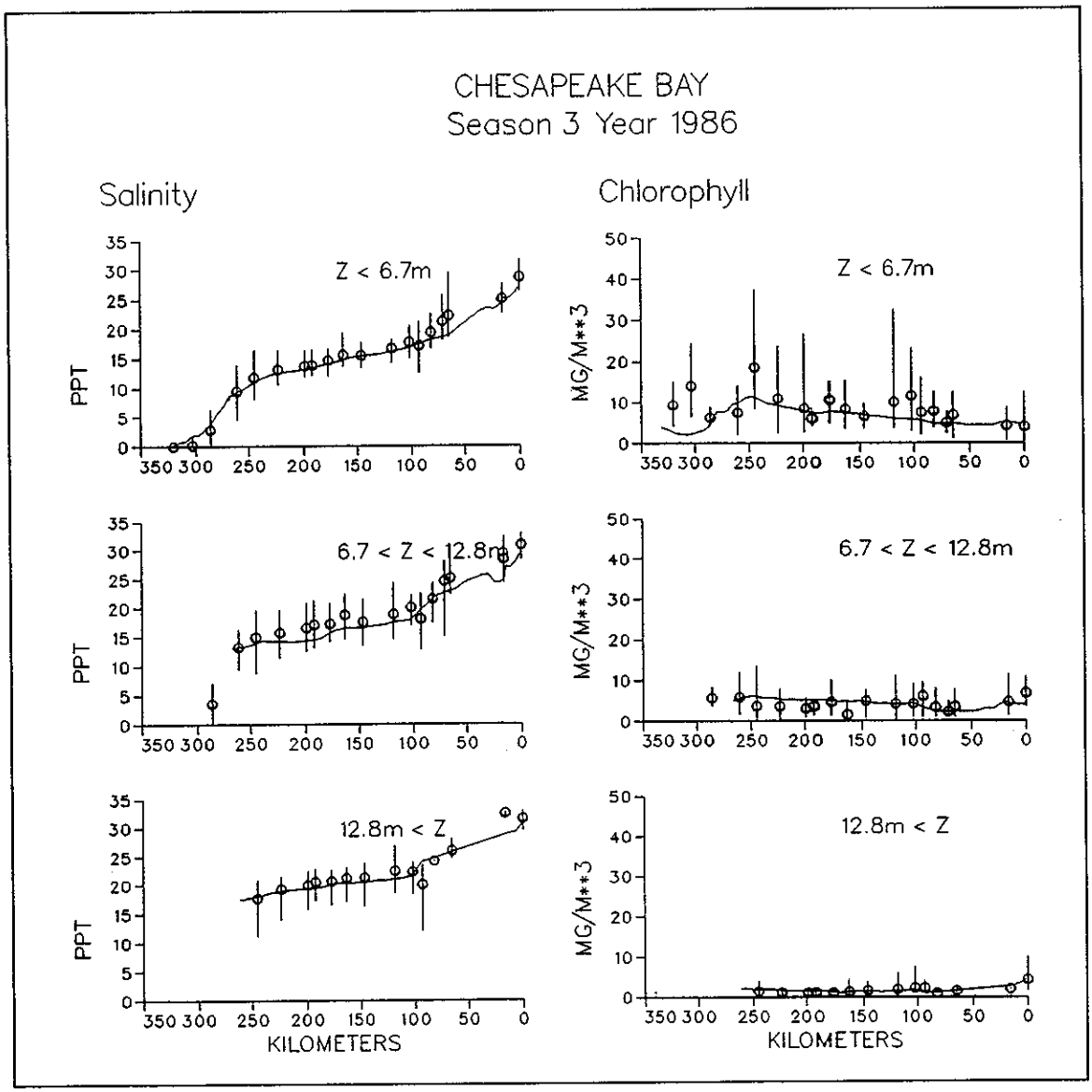

Figure 11-24. Predicted and Observed Concentrations Along Mainstem Bay Transect, Season Three, 1986 (Sheet 1 of 8)

substances are point-source discharges and nonpoint-source runoff into the mainstem Bay.

In the sediment mass balances, "Settling" is the transfer of particles from the water to sediments. "Burial" is the loss of material, primarily particles, into deep, isolated, sediments that underlay the active layer considered in the model. "Diagenesis" is the loss of organic carbon through oxidation.

The largest source of carbon, by far, to the water column is net primary production (Figure 11-41). Virtually all primary production of carbon is deposited in the sediments. In the sediments (Figure 11-42), 80% of the

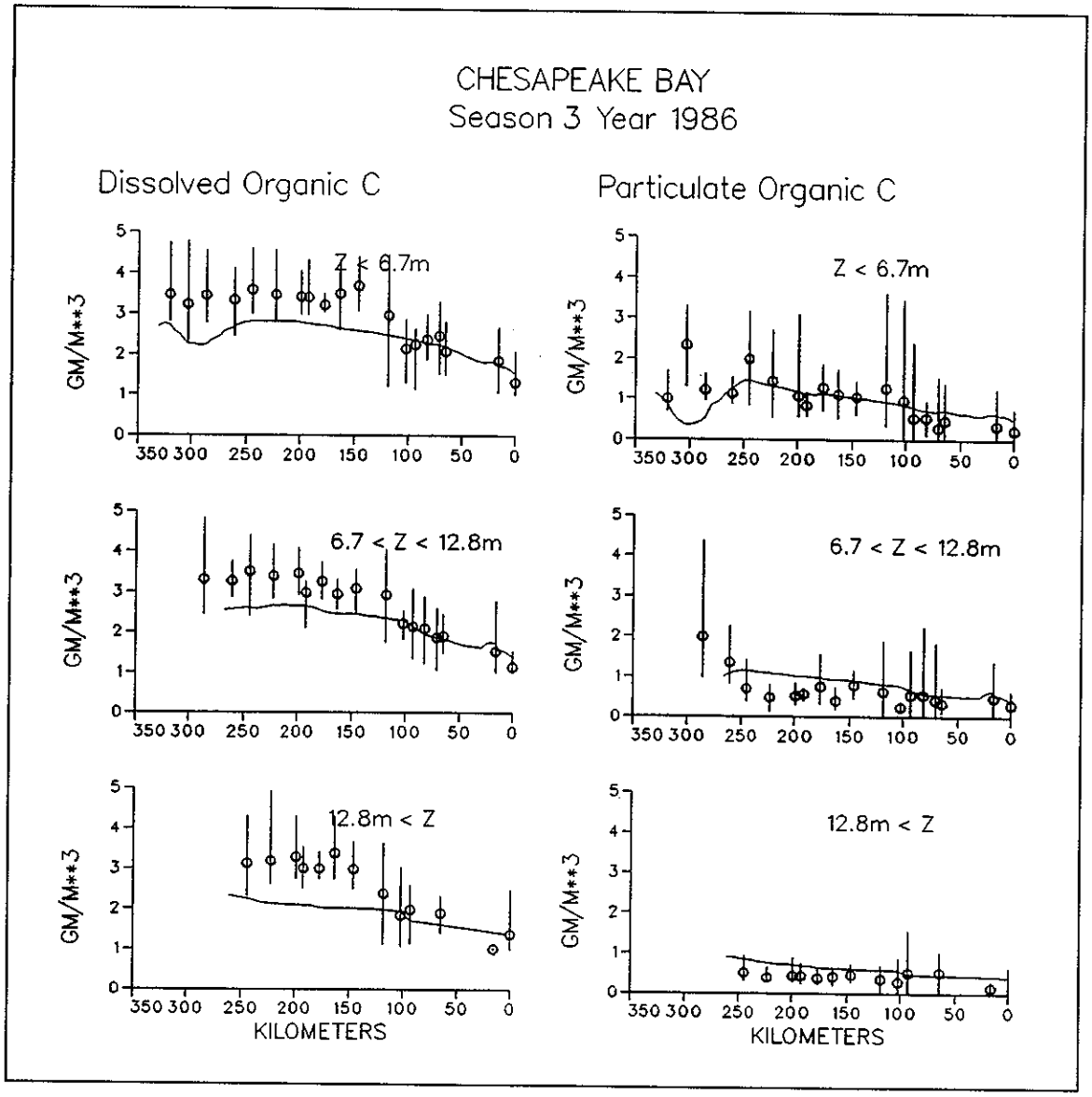

Figure 11-24. (Sheet 2 of 8)

carbon undergoes diagenesis, creating oxygen demand. The remainder, largely inert, G3, carbon is buried to deep, isolated sediments.

The second largest carbon source is fall-line loading followed by lesser amounts from tributaries and direct loads. Some fraction of the tributary loads is also from primary production, however. The dominant role of primary production as the source of oxygen demand indicates that carbon (or BOD) loads to the mainstem play a negligible role in occurrence of anoxia.

The dominant nitrogen source to the mainstem is the Susquehanna fall line. Predominant secondary sources include direct loads, the Potomac River, and Baltimore Harbor. Sediments are the major net sink. Roughly 70% of the

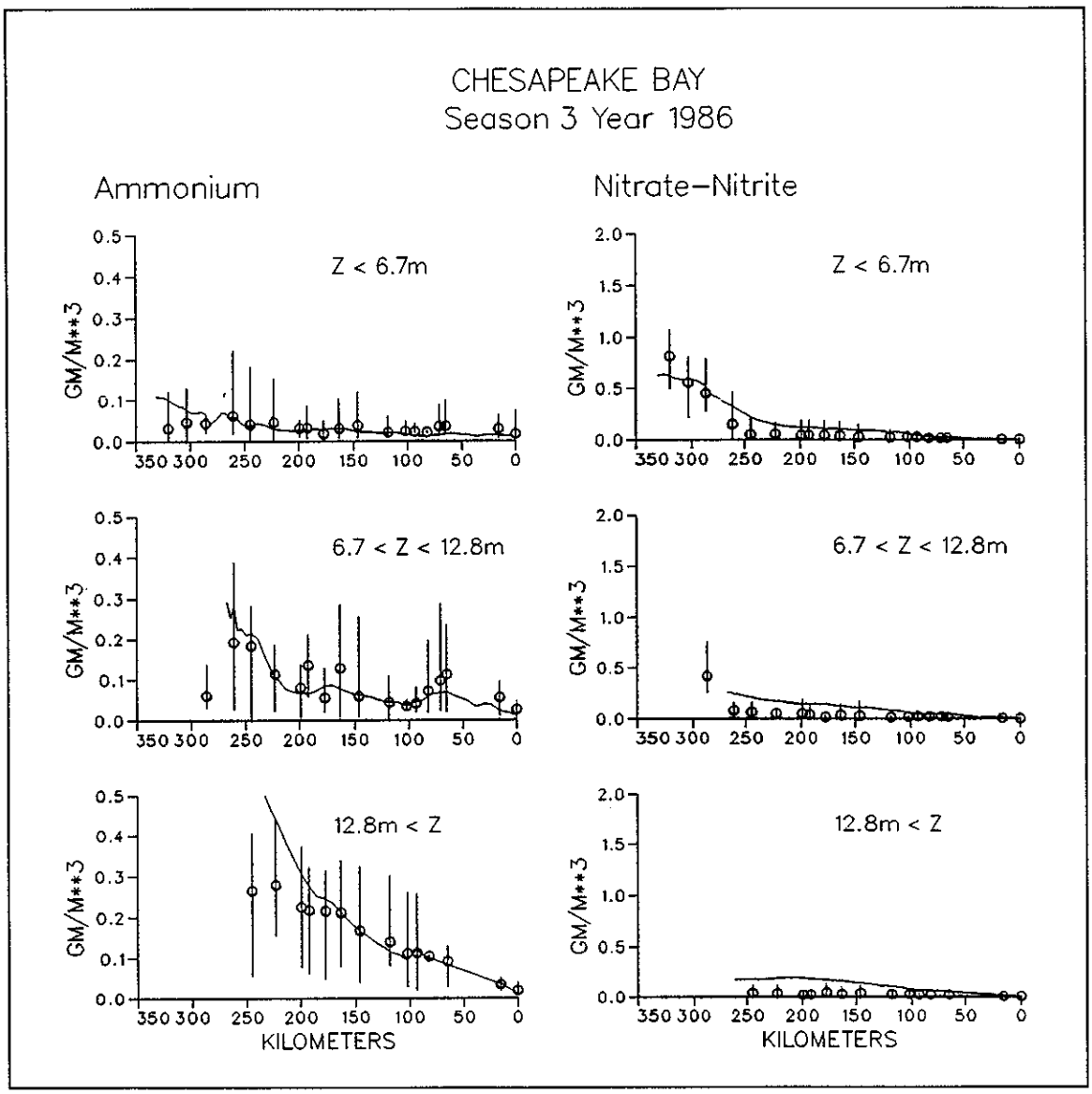

Figure 11-24. (Sheet 3 of 8)

nitrogen load to the mainstem is lost to the sediments while the remainder is exported to the ocean. The amount lost to the sediments corresponds to the denitrification and burial terms in the sediment budget.

Roughly half the nitrogen deposited in the sediments is returned to the water column through diagenetic processes. Denitrification losses account for 28% of the nitrogen deposited while burial to deep, isolated sediments accounts for the remainder.

The dominant phosphorus source to the mainstem is fall-line loading. The oceanic source is nearly equivalent, however. Predominant secondary sources are direct loads, the James River, and atmospheric loads. Virtually all net

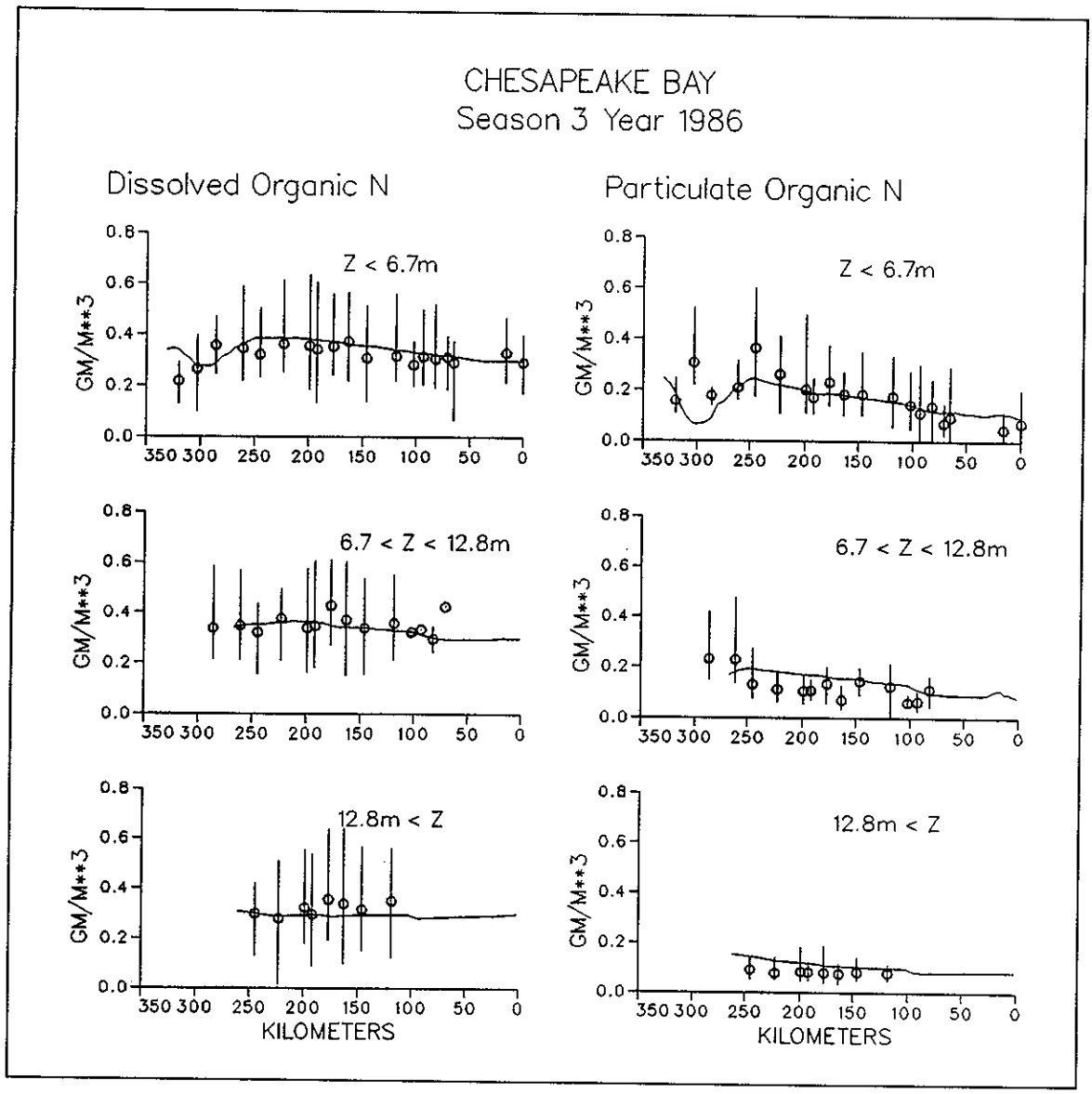

Figure 11-24. (Sheet 4 of 8)

phosphorus load to the mainstem is deposited in the sediments. Roughly 22% of phosphorus deposited is returned to the water column through diagenesis. The remainder is buried to deep, isolated sediments. Net loss from the water column corresponds to burial in the sediment budget.

Direct numerical comparison of the model nutrient budgets with alternate estimates is complicated by differences in time periods and classifications of sources and sinks. Reasonable comparisons can be made to relative magnitude and direction of fluxes, however.

The model distribution of nitrogen loss to the ocean and sediments corresponds best with the recent estimates provided by Boynton (Figure 2-19).

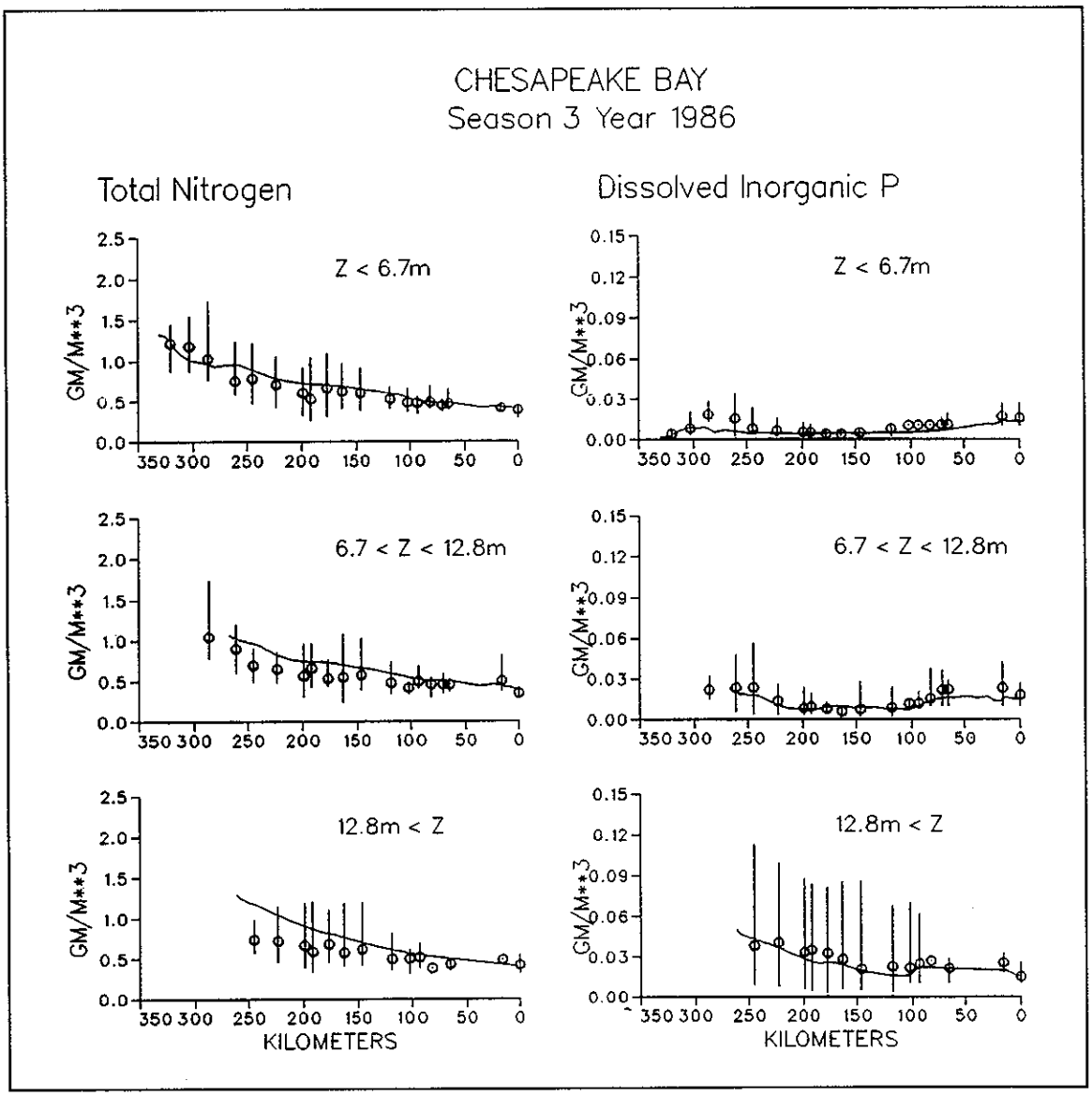

Figure 11-24. (Sheet 5 of 8)

Both budgets indicate the majority of nitrogen loading is lost to the sediments. Nitrogen loss to the ocean is a lesser but still substantial fraction of the loads. The model indicates the major loss from the sediments is through denitrification, however, while Boynton indicates burial is the dominant term.

The model phosphorus budget also corresponds best with the recent Boynton estimates (Figure 2-20). Both budgets identify the ocean as a major phosphorus source, almost equivalent to fall-line loading. Both budgets identify burial as the major phosphorus pathway out of the system.

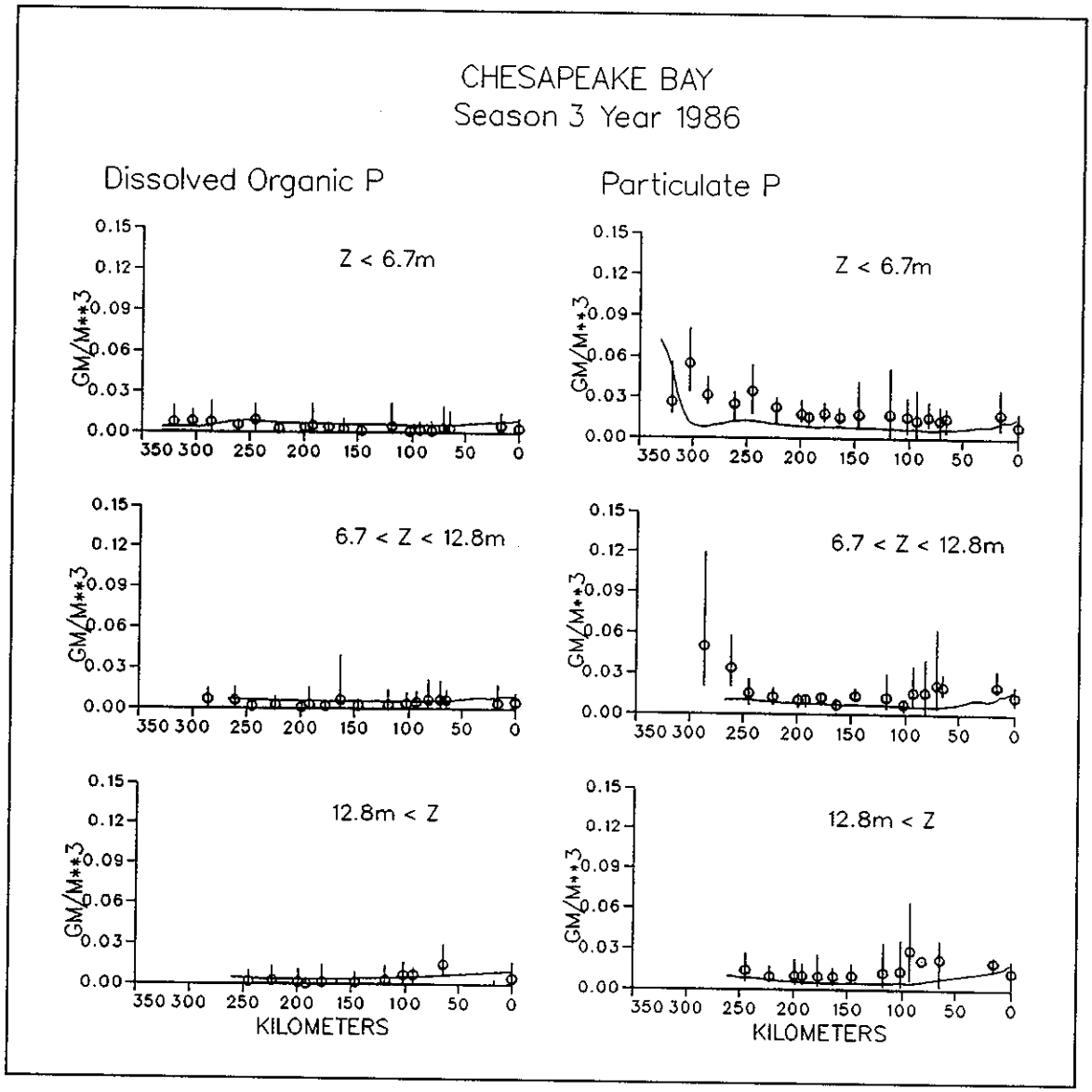

Figure 11-24. (Sheet 6 of 8)

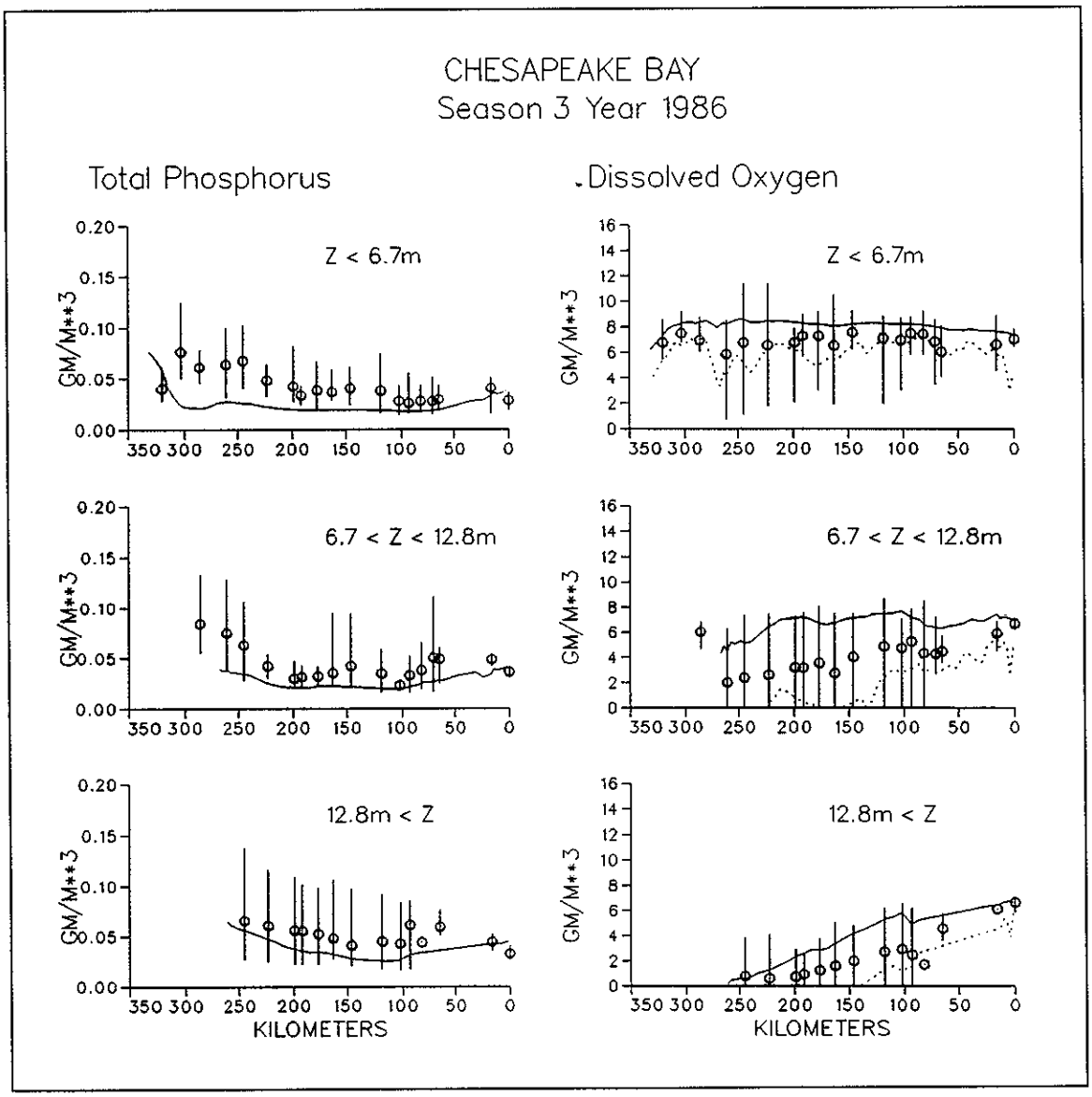

Figure 11-24. (Sheet 7 of 8)

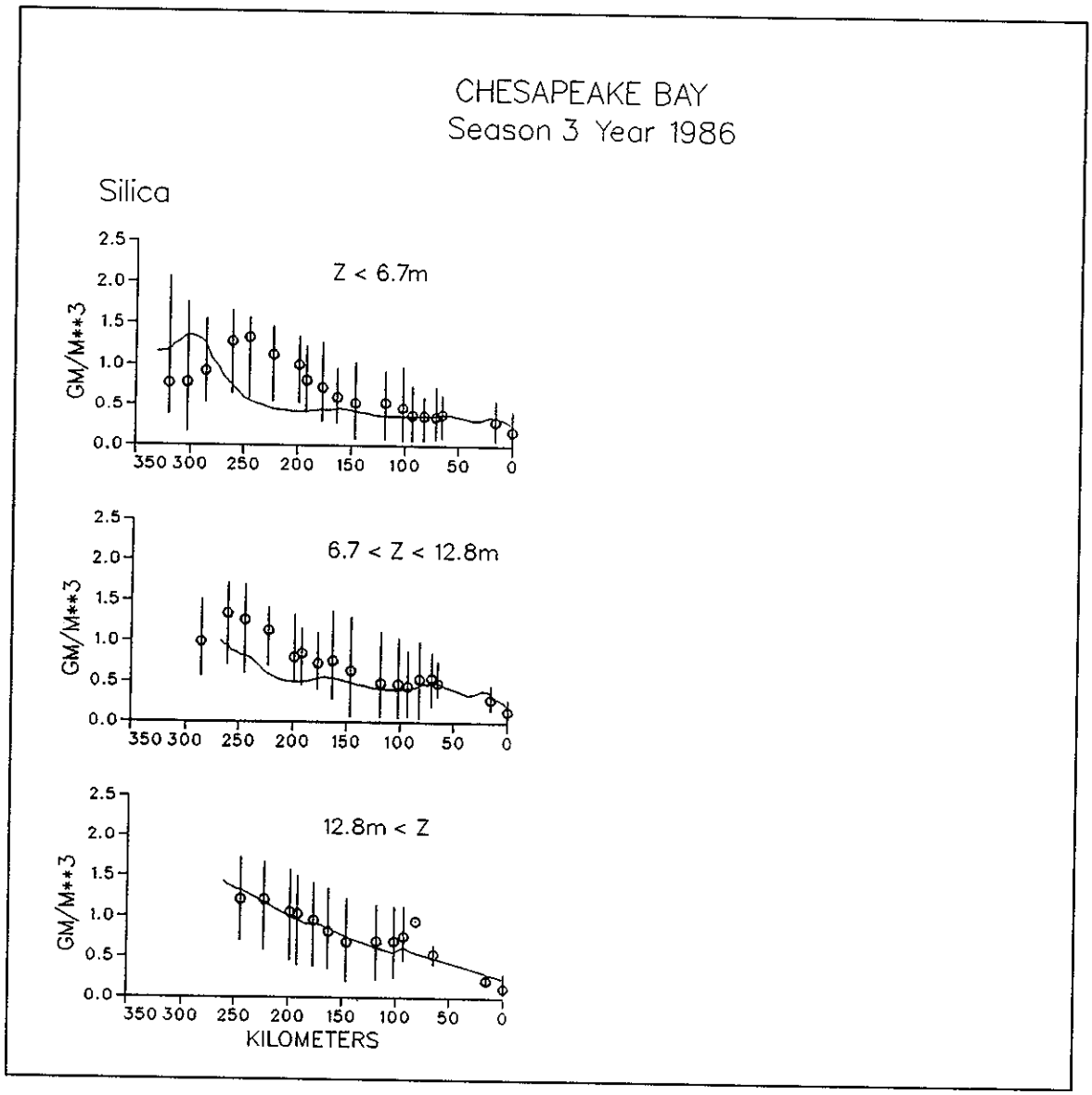

Figure 11-24. (Sheet 8 of 8)

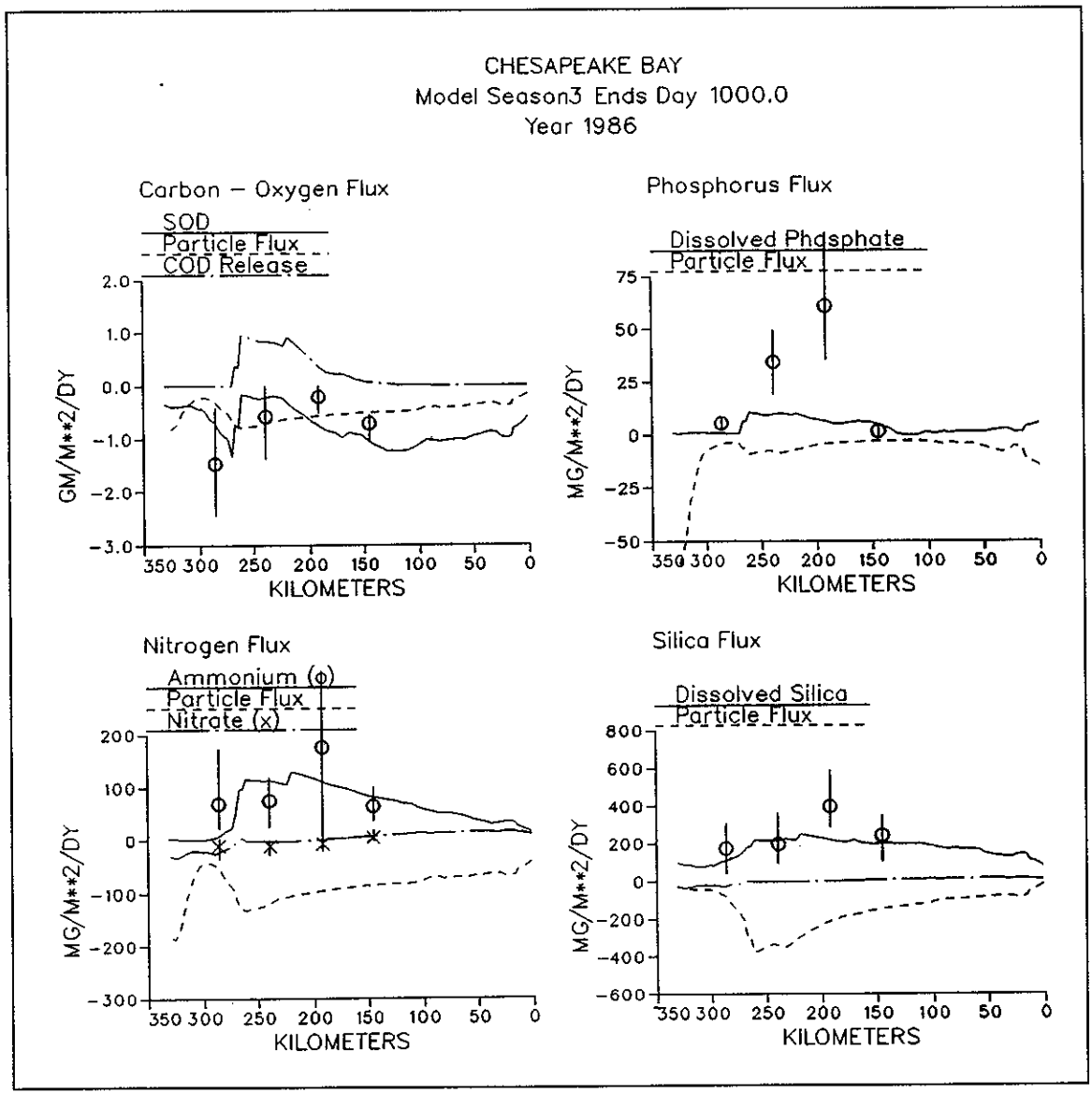

Figure 11-25. Predicted and Observed Sediment-Water Fluxes Along Mainstem Bay Transect, Season Three, 1986

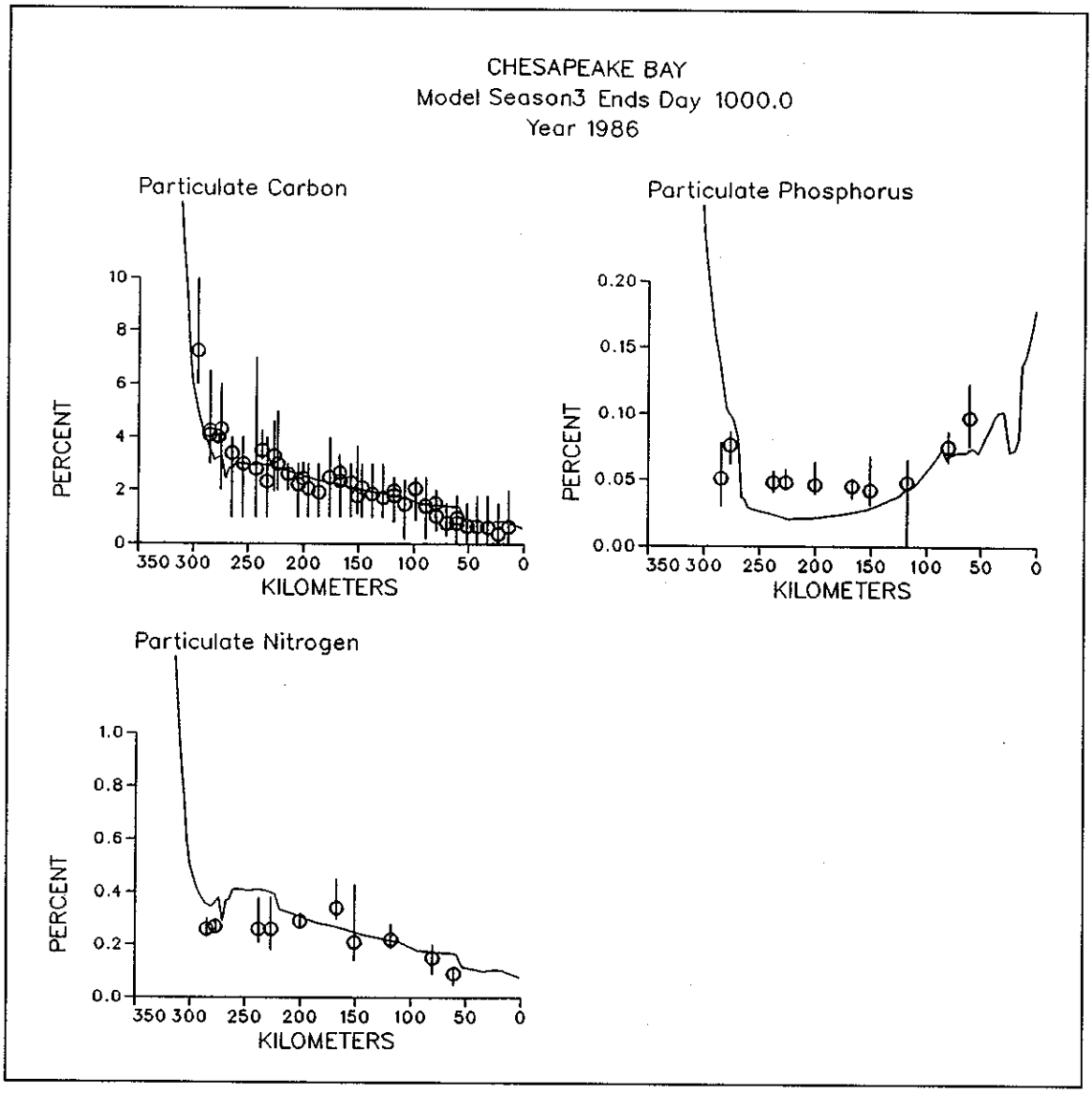

Figure 11-26. Predicted and Observed Sediment Particulate Carbon, Nitrogen, and Phosphorus Along Mainstem Bay Transect

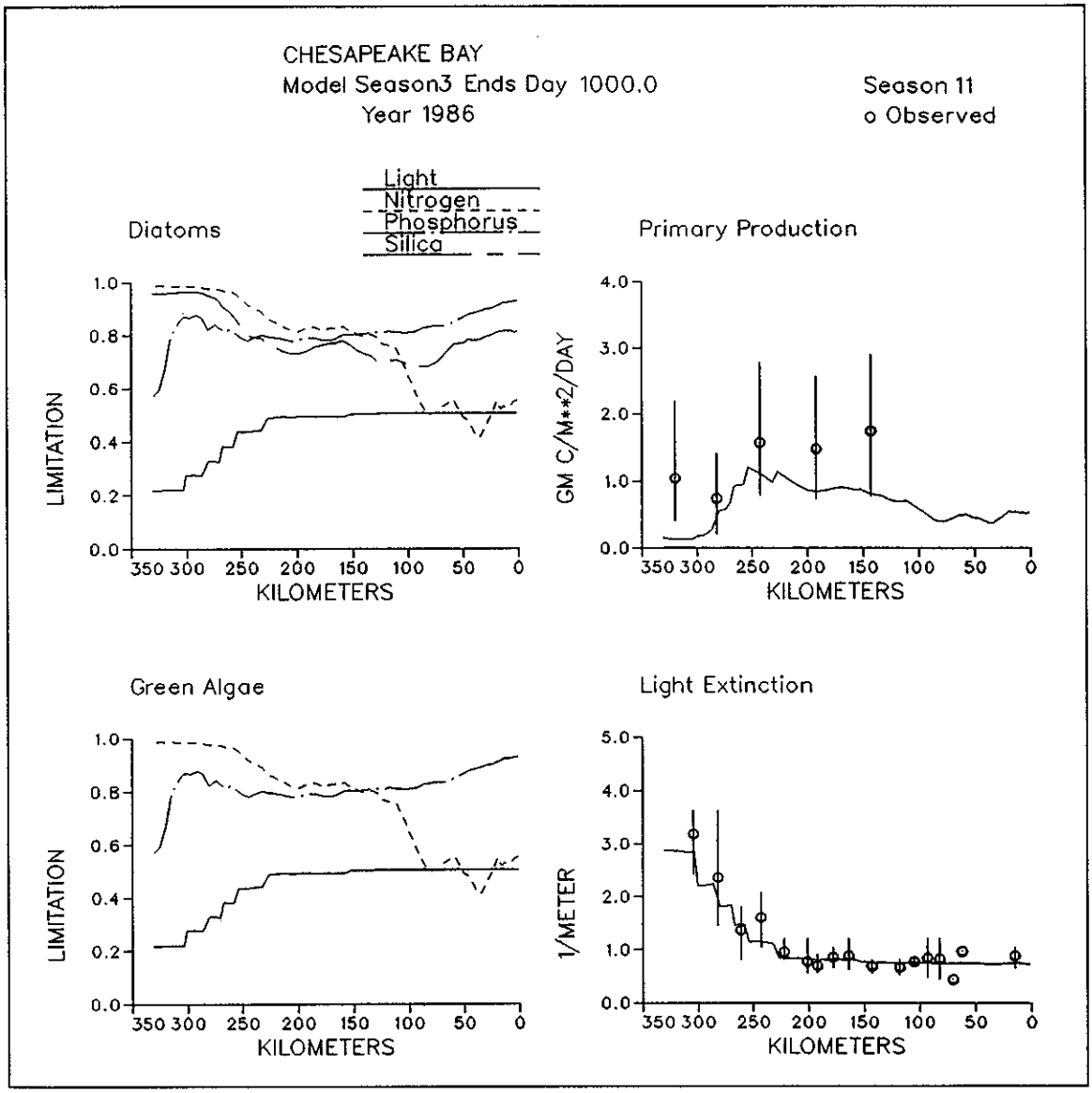

Figure 11-27. Predicted and Observed Diagnostic Information Along Mainstem Bay Transect, Season Three, 1986

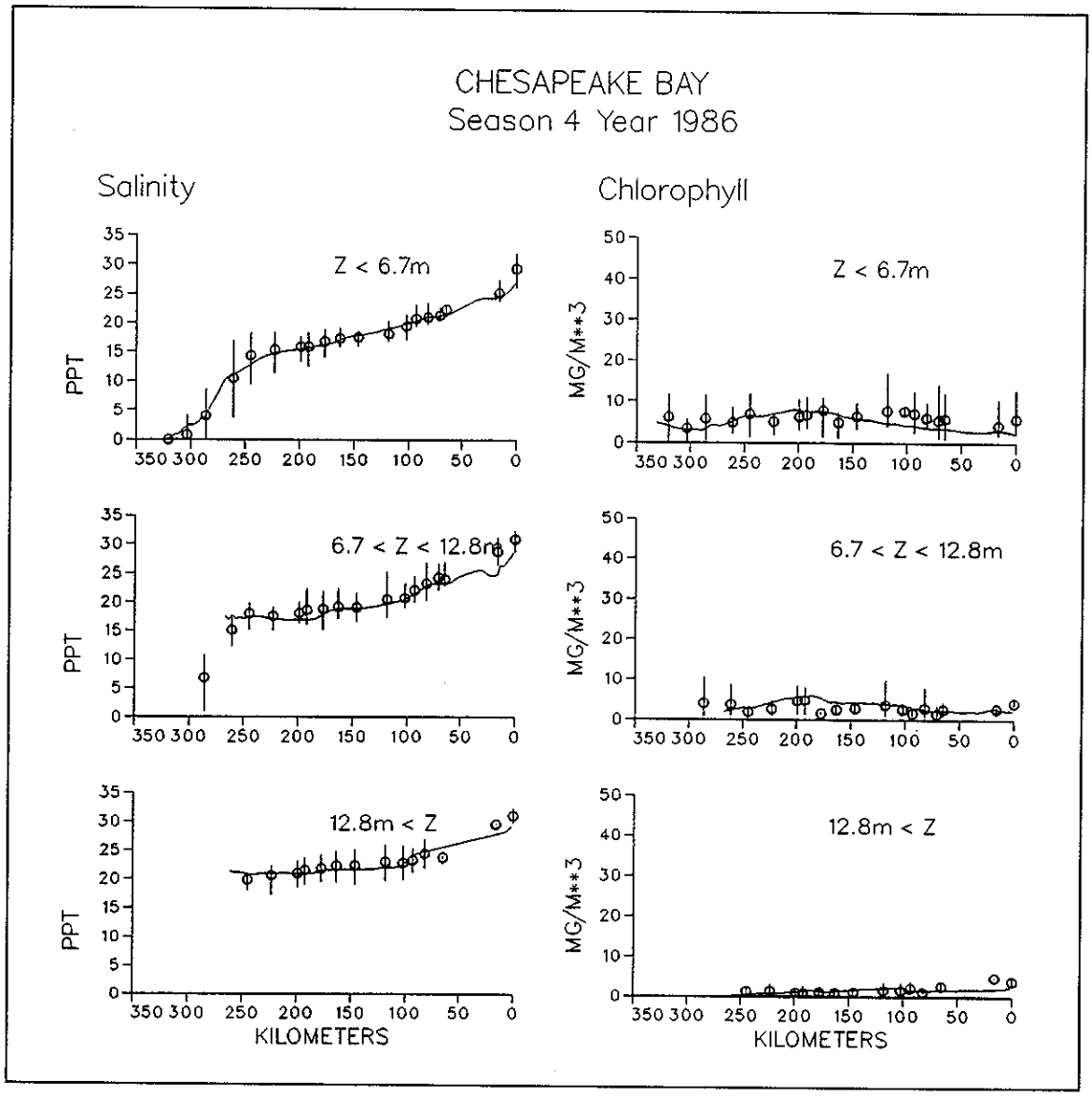

Figure 11-28. Predicted and Observed Concentrations Along Mainstem Bay Transect, Season Four, 1986 (Sheet 1 of 8)

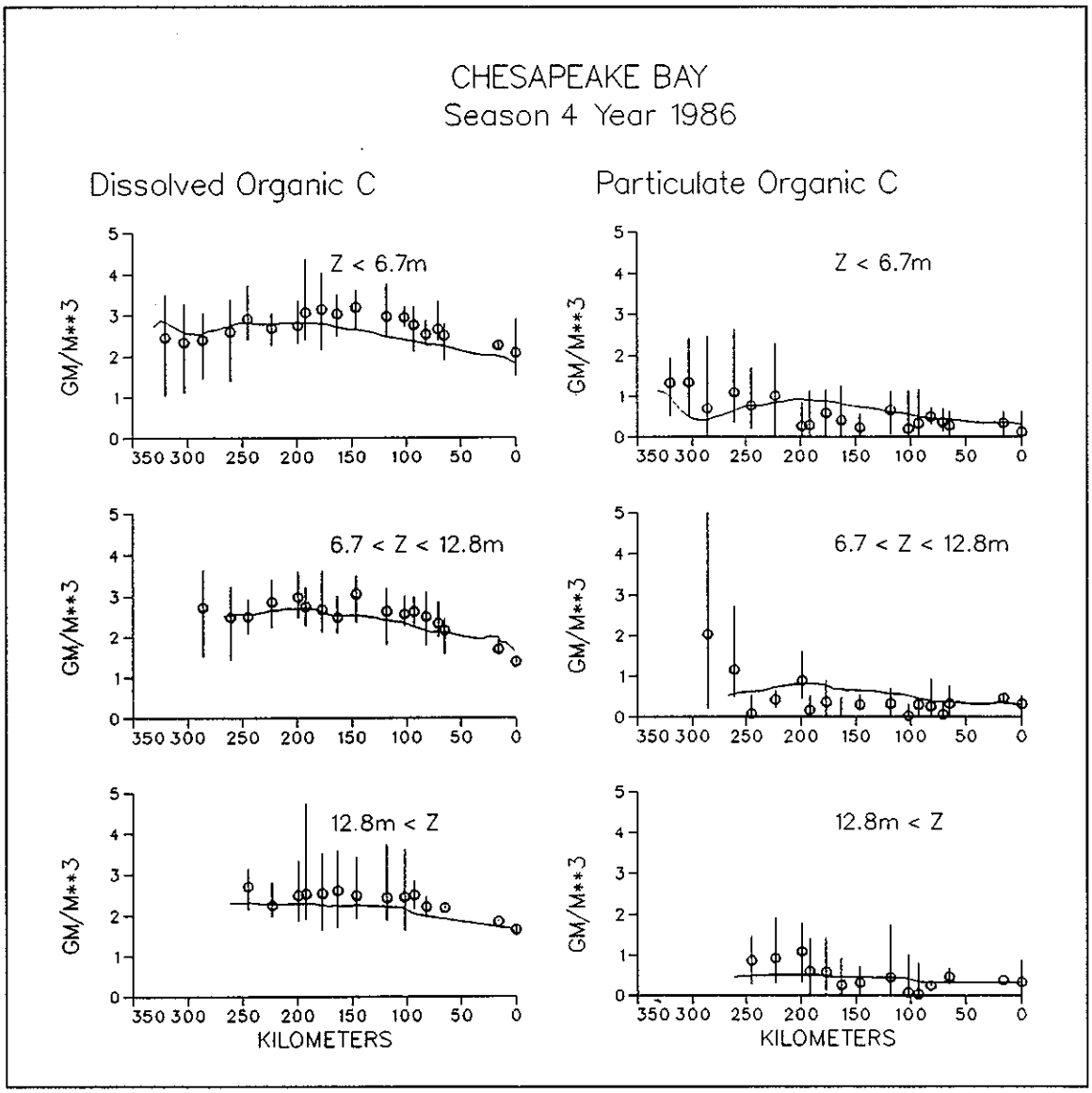

Figure 11-28. (Sheet 2 of 8)

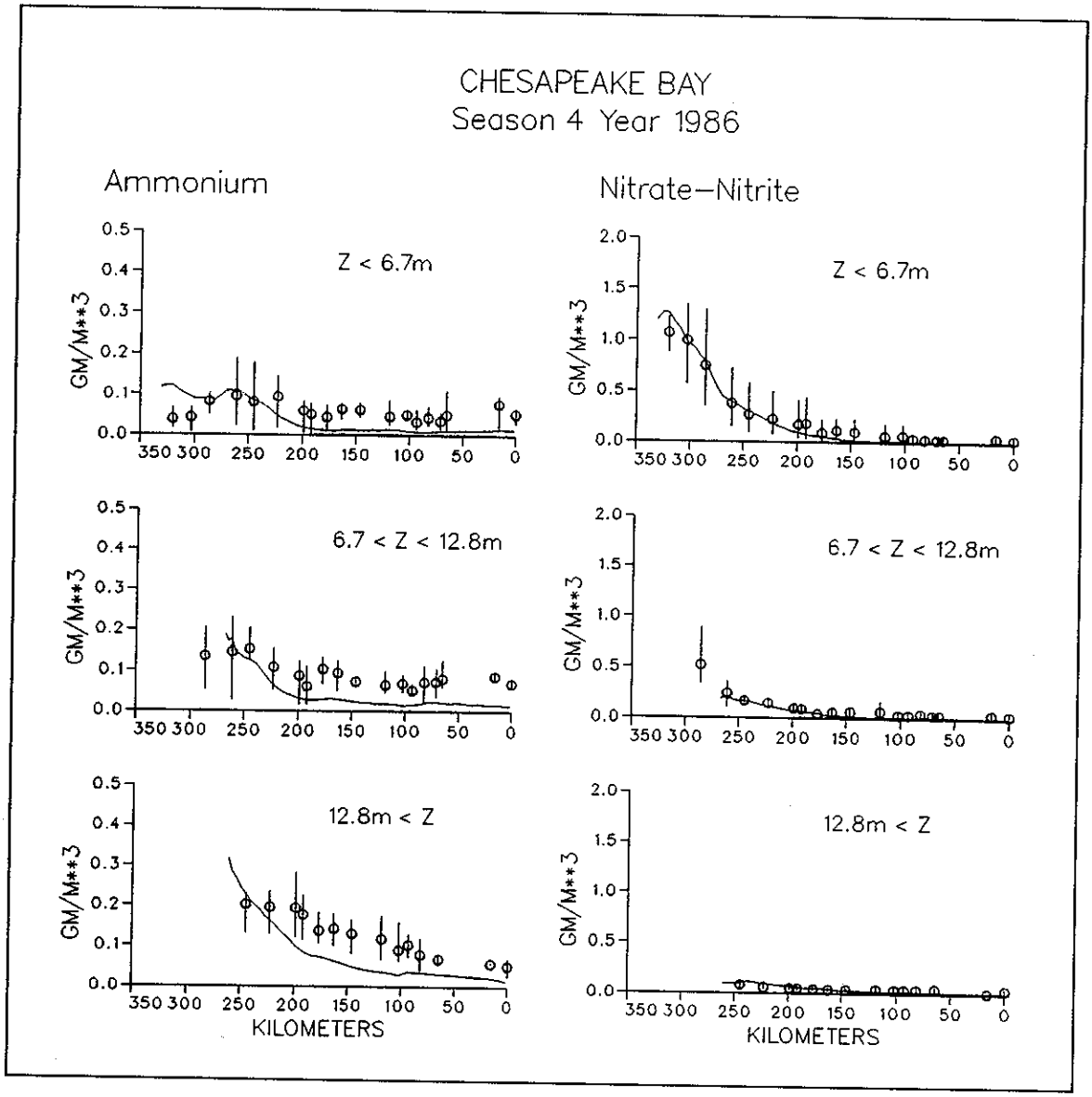

Figure 11-28 (Sheet 3 of 8)

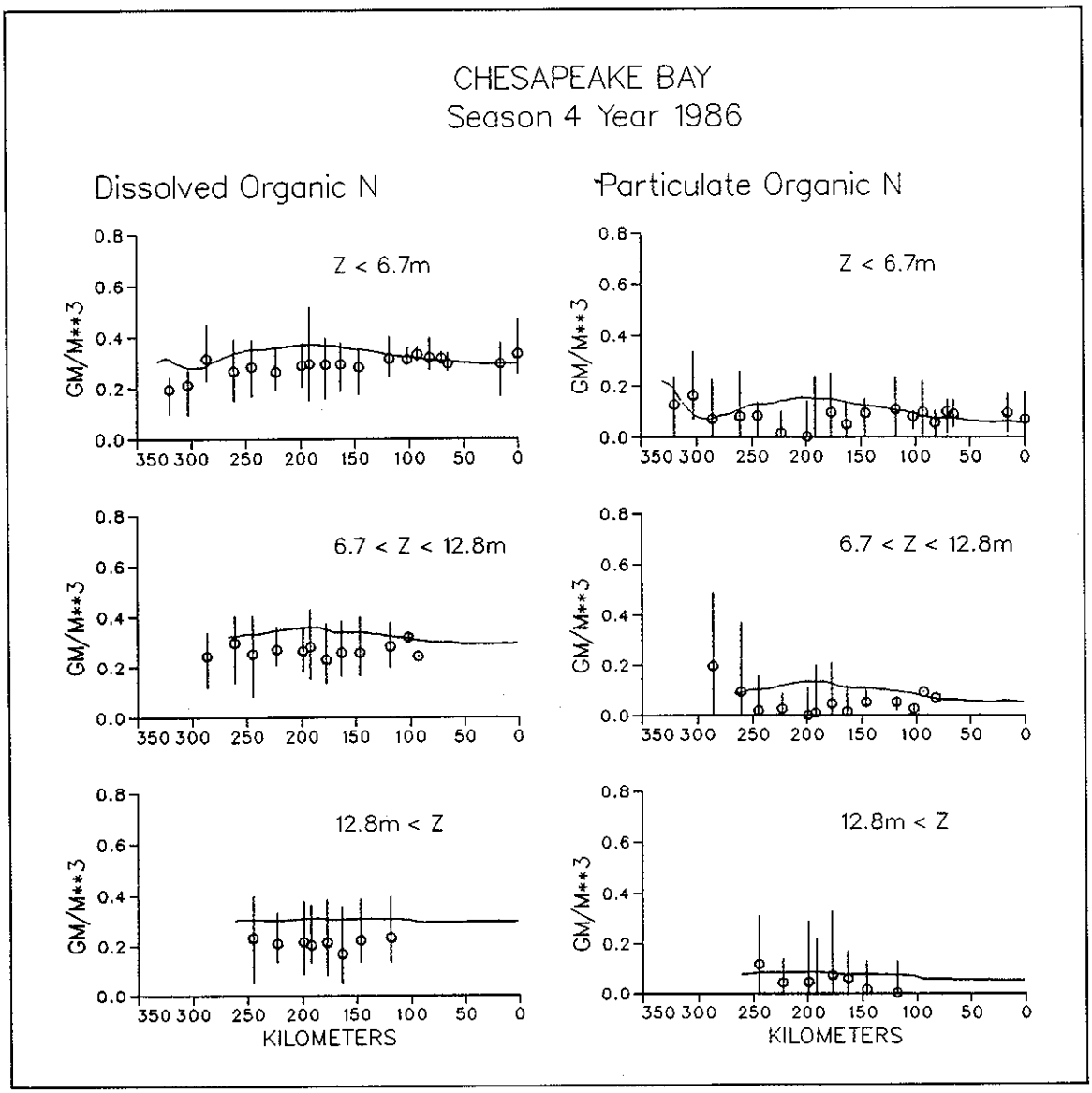

Figure 11-28. (Sheet 4 of 8)

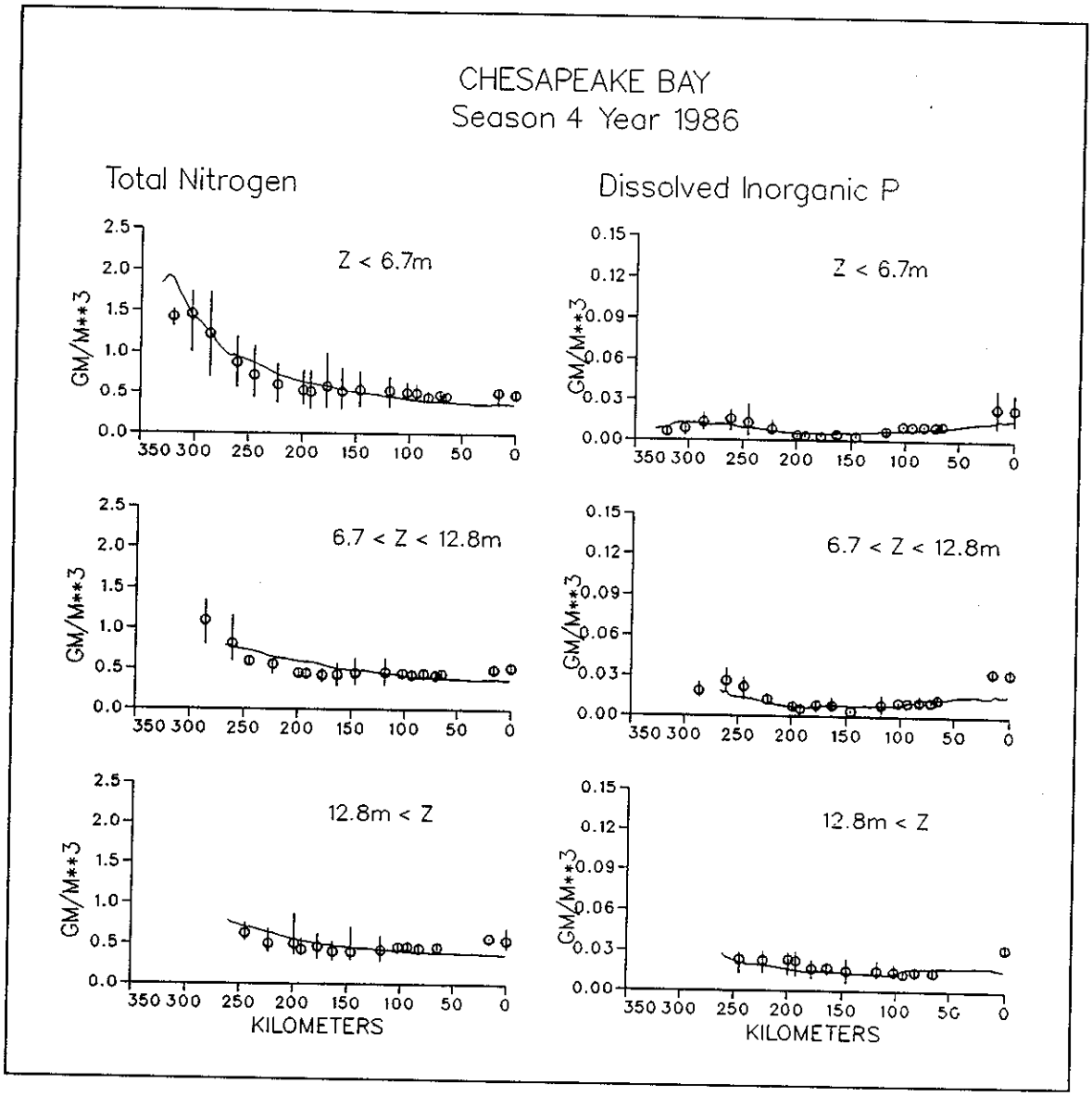

Figure 11-28. (Sheet 5 of 8)

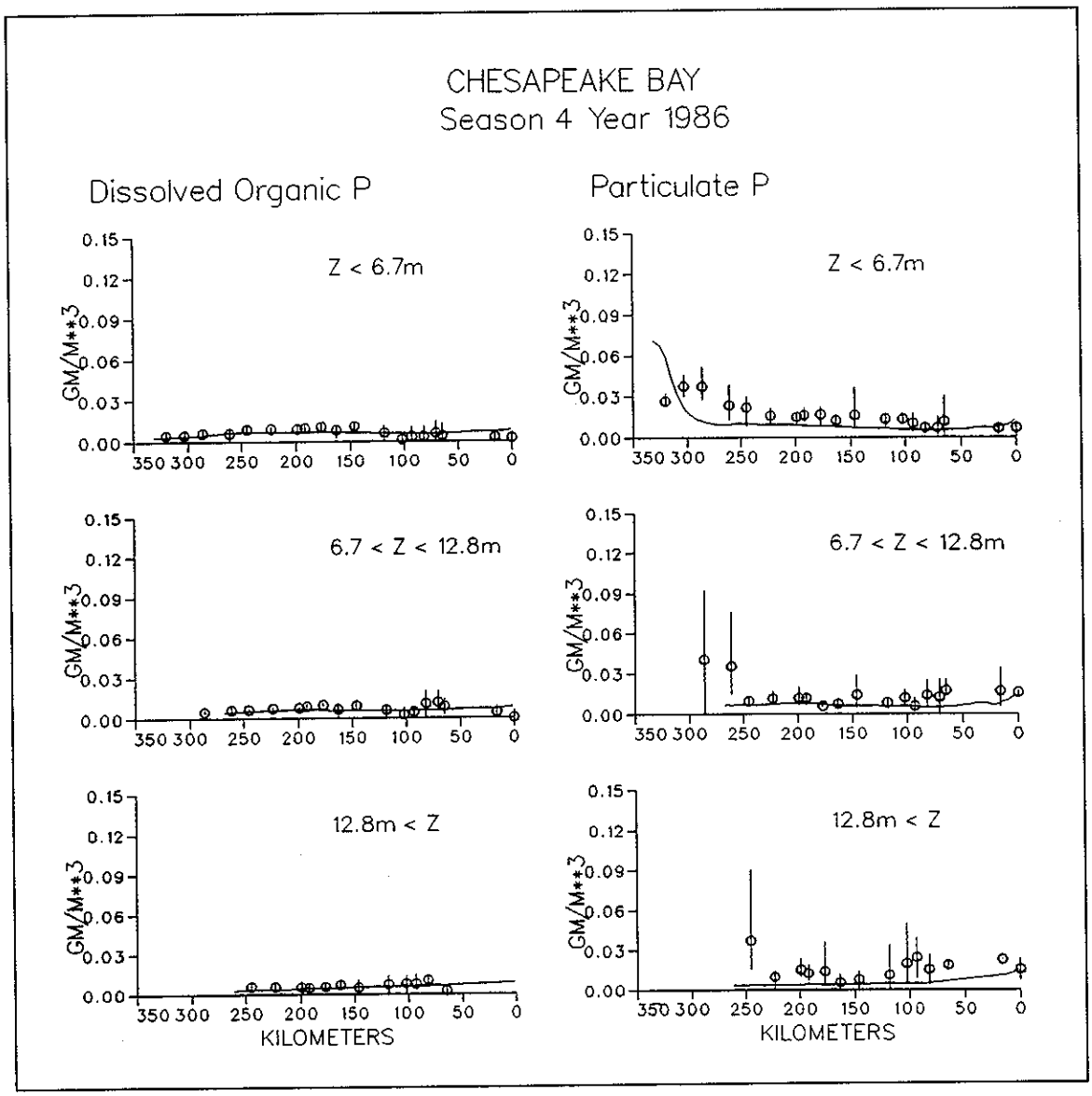

Figure 11-28. (Sheet 6 of 8)

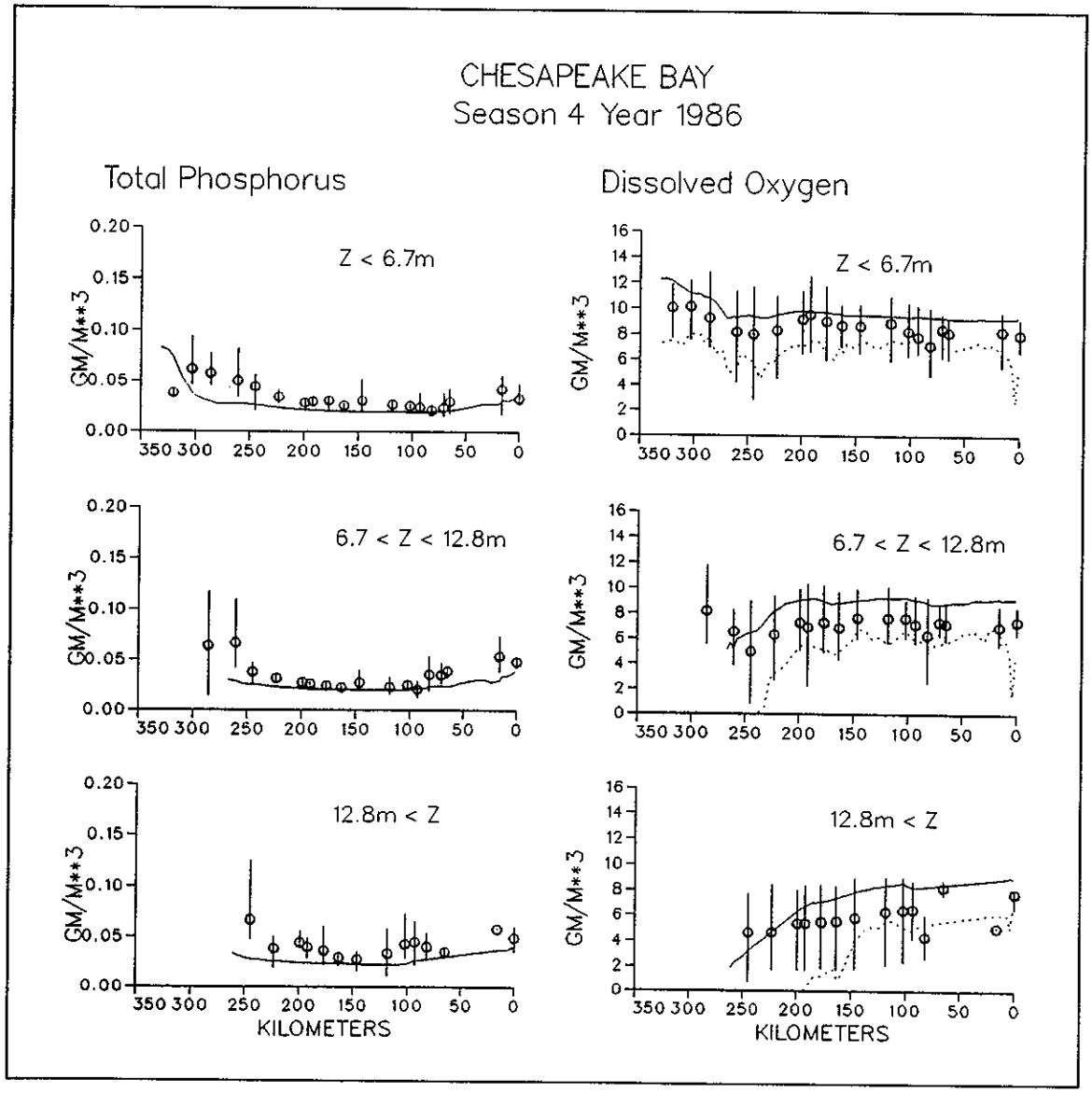

Figure 11-28. (Sheet 7 of 8)

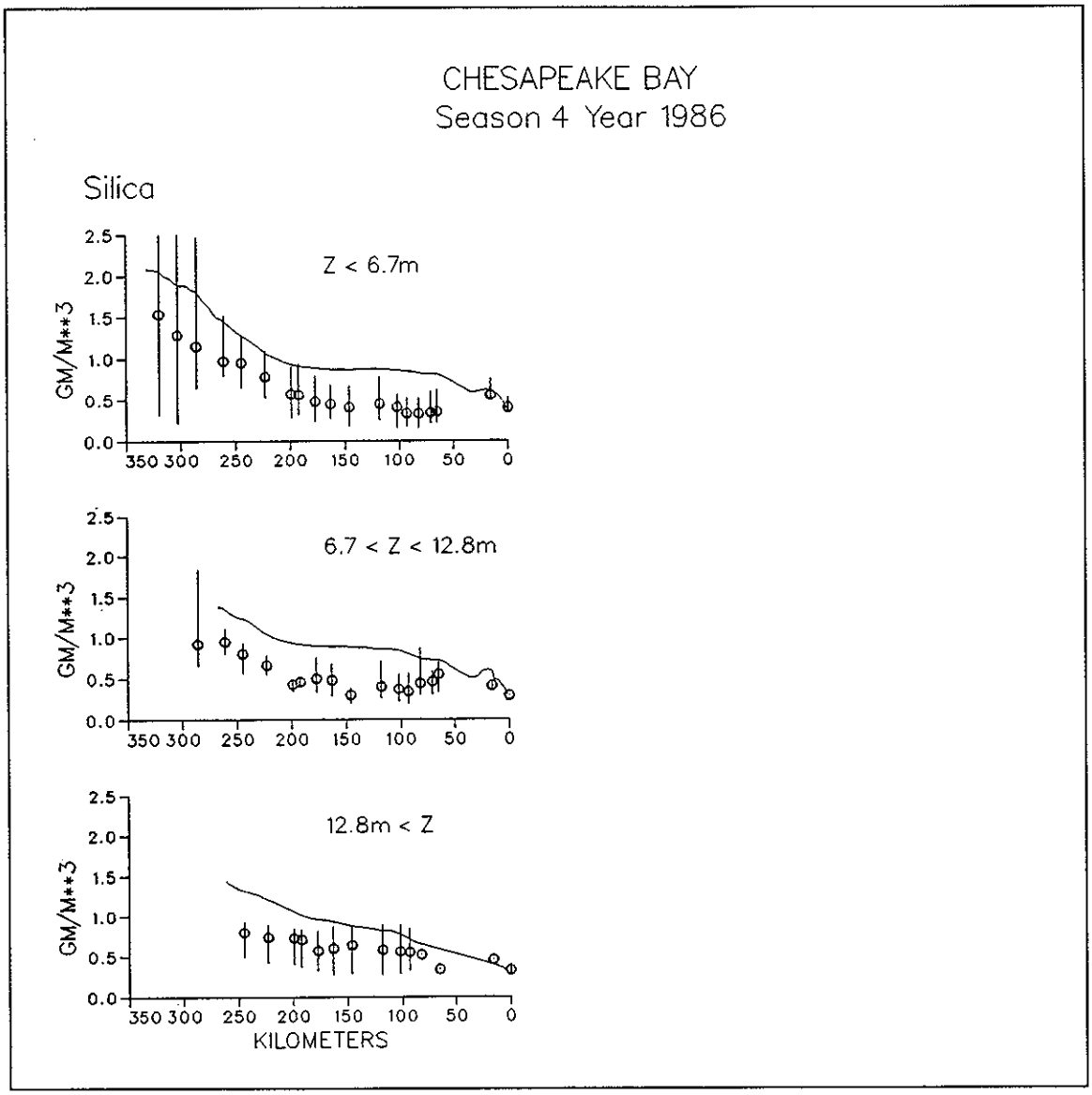

Figure 11-28. (Sheet 8 of 8)

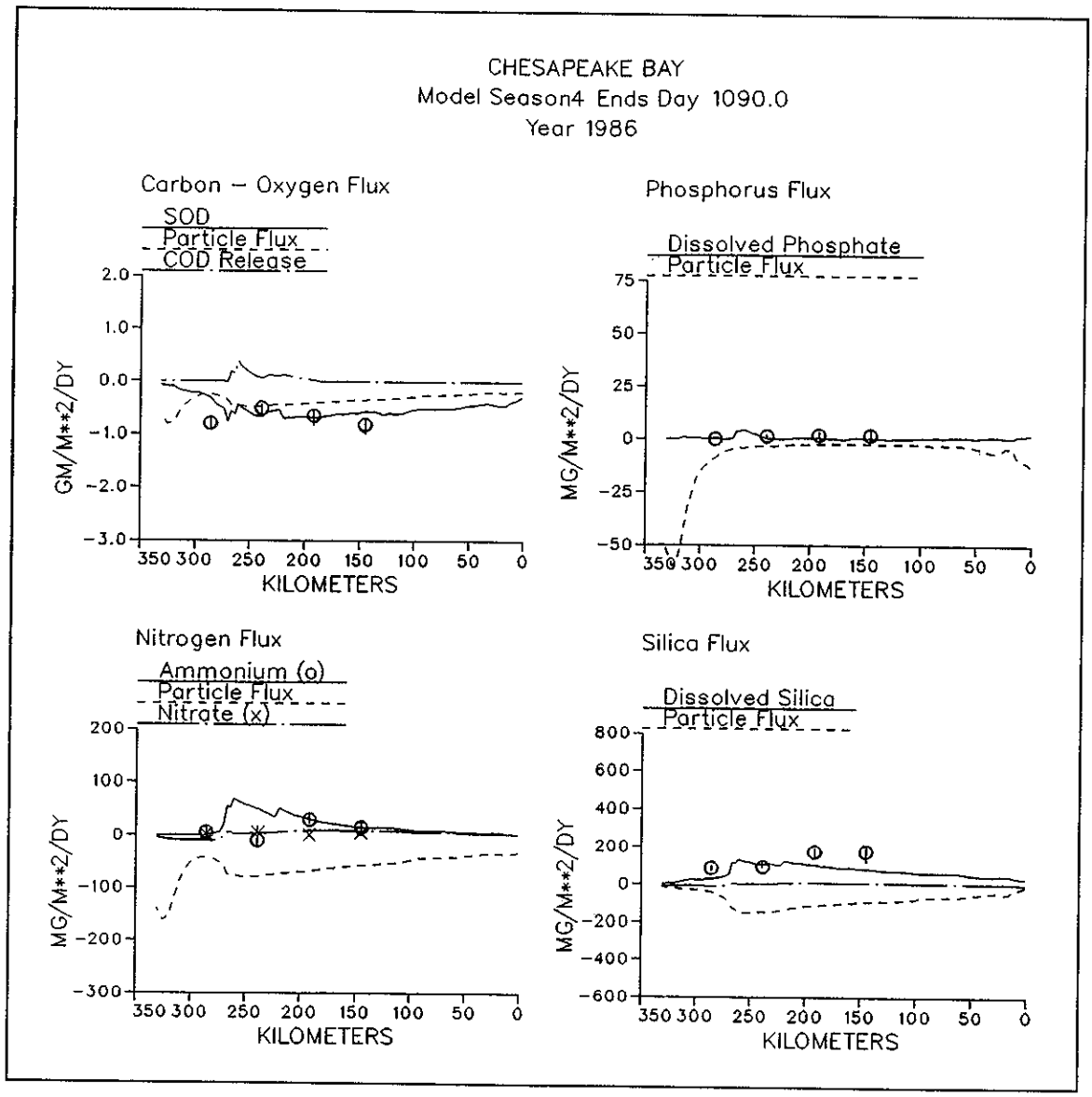

Figure 11-29. Predicted and Observed Sediment-Water Fluxes Along Mainstem Bay Transect, Season Four, 1986

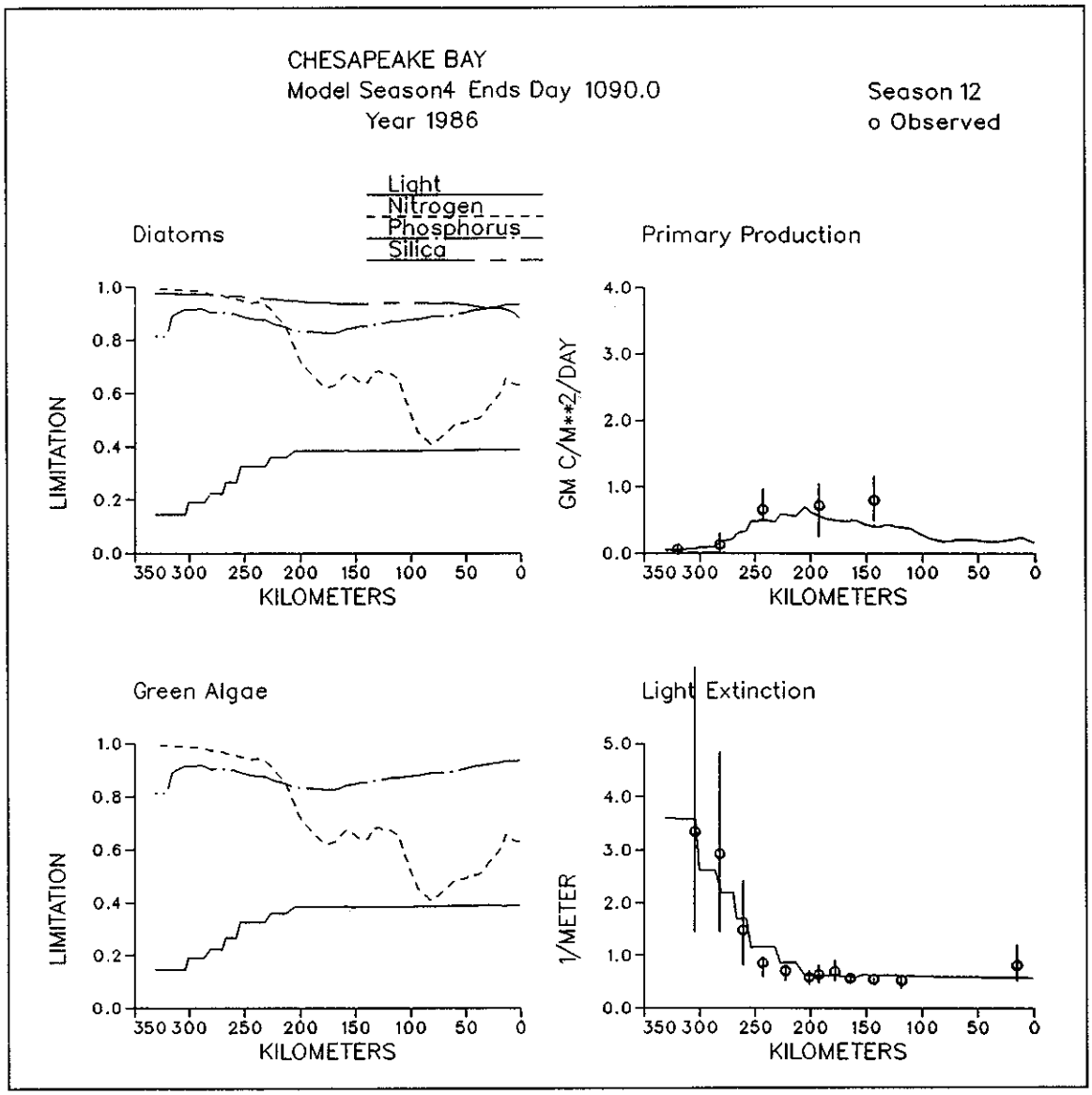

Figure 11-30. Predicted and Observed Diagnostic Information Along Mainstem Bay Transect, Season Four, 1986

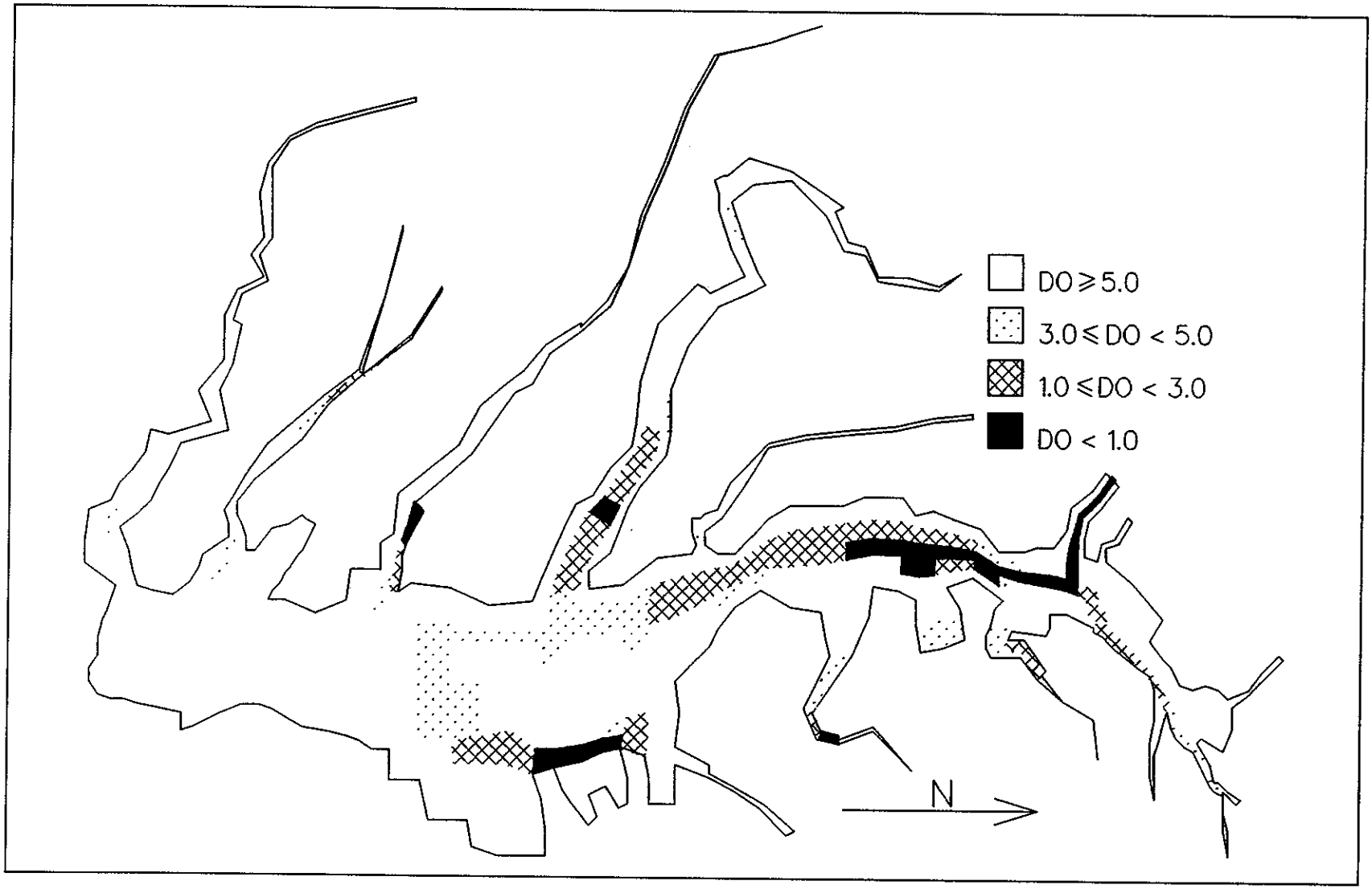

Figure 11-31. Plan View of Predicted Bottom Dissolved Oxygen, Season Three, 1986

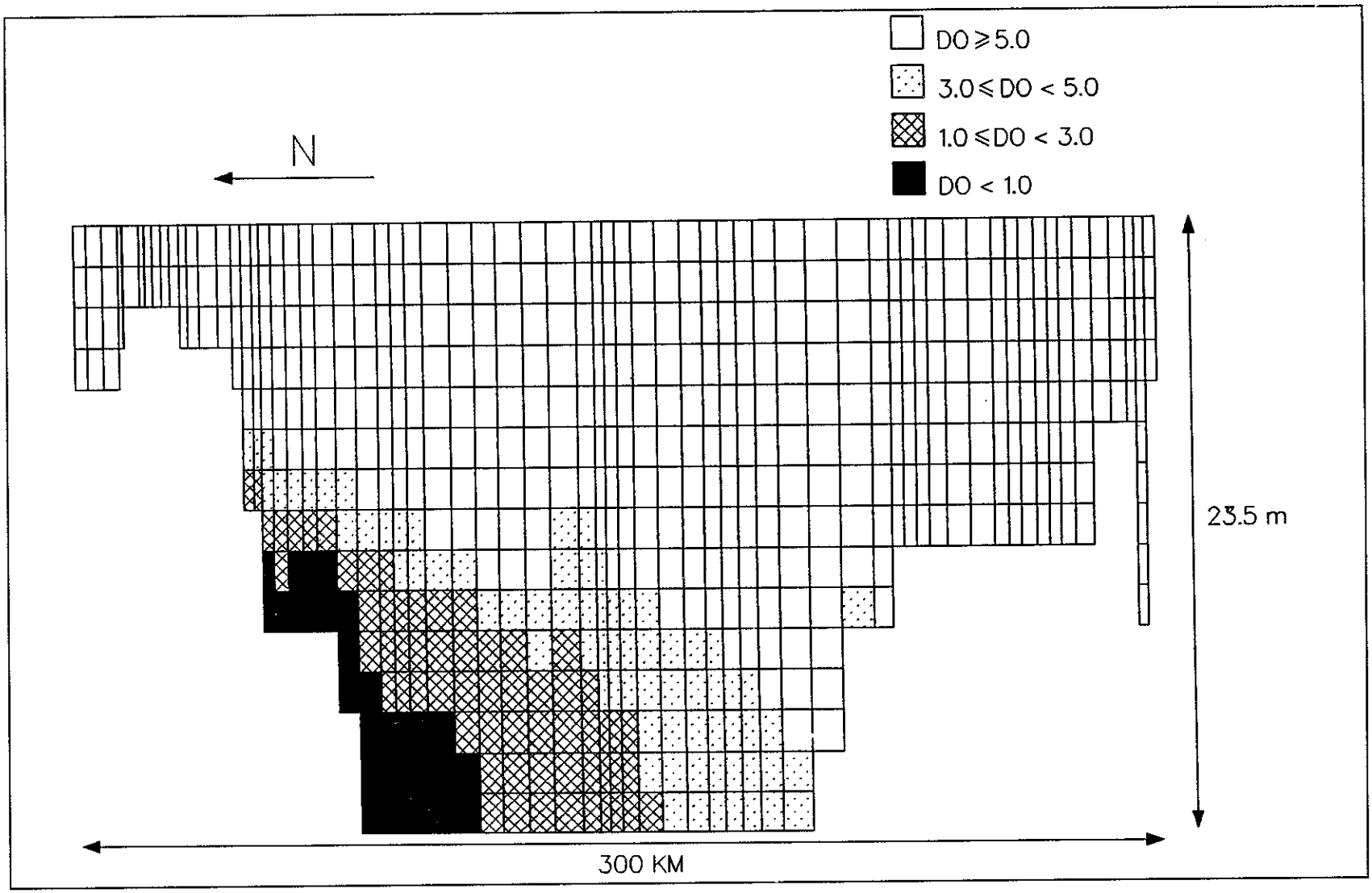

Figure 11-32. Profile of Predicted Dissolved Oxygen Along Mainstem Bay Transect, Season Three, 1986

Table 11-3
Modelled and Observed Total Active Metal and Chemical Oxygen Demand

Variable	Value	Comments
Total Active Metal	19 to 24 μM	Model Mean, Season III, Zone 2, Level III
Total Active Metal	10 to 30 μM	Observed near bottom, Zone 2, June and July 1981 (Gavis and Grant 1986)
Chemical Oxygen Demand	0.7 to 1.4 gm^{-1} m^{-3}	Model Mean, Season III, Zone 2, Level III
Chemical Oxygen Demand	0.6 to 60 gm^{-1} m^{-3}	Observed near bottom, Zone 2, June and July 1981 (Gavis and Grant 1986)
Chemical Oxygen Demand	2 to 4 gm^{-1} m^{-3}	Observed near bottom, Zone 2, June and July 1987 (Luther et al. 1988)

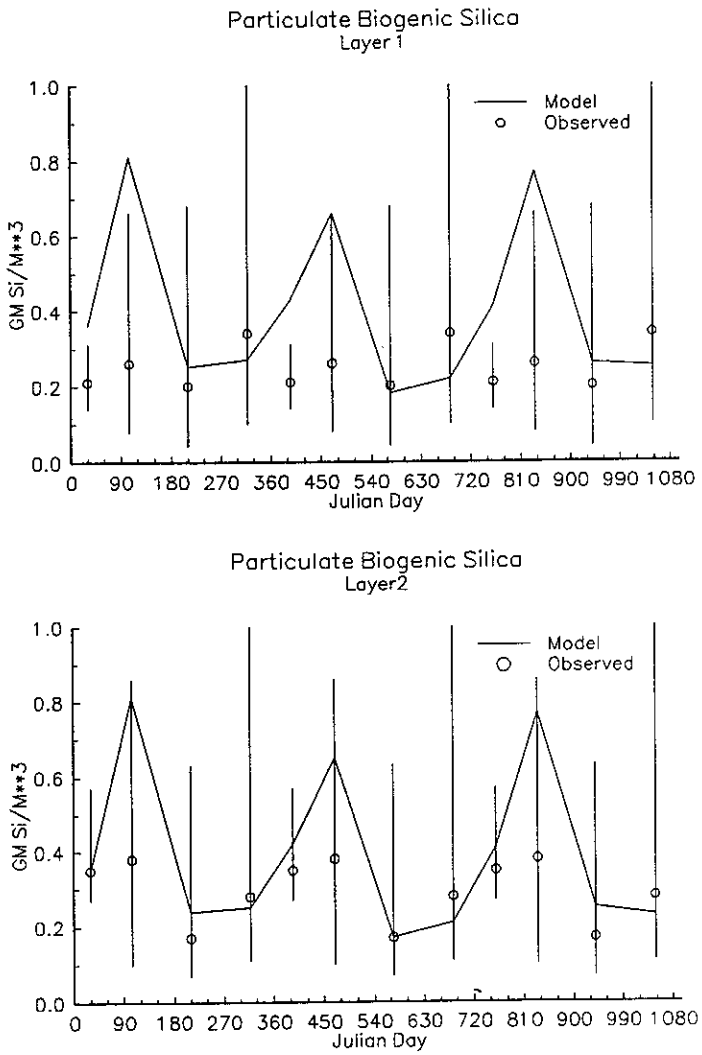

Figure 11-33. Predicted and Observed Particulate Biogenic Silica in Zone Three (Data courtesy of Dr. Walter Boynton, Center for Environmental and Estuarine Studies, University of Maryland)

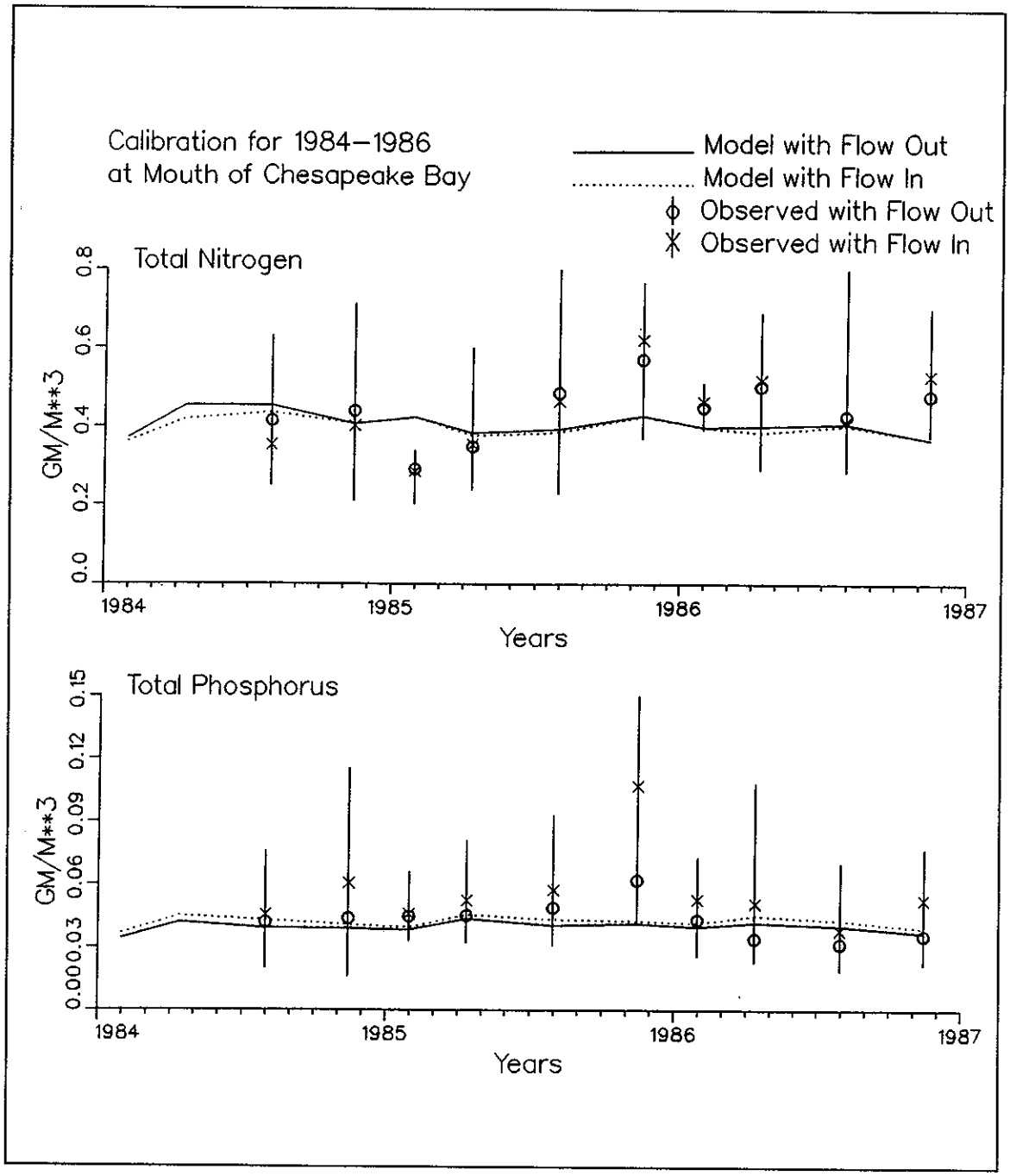

Figure 11-34. Predicted and Observed Total Nitrogen and Phosphorus Concentrations at Ocean Boundary

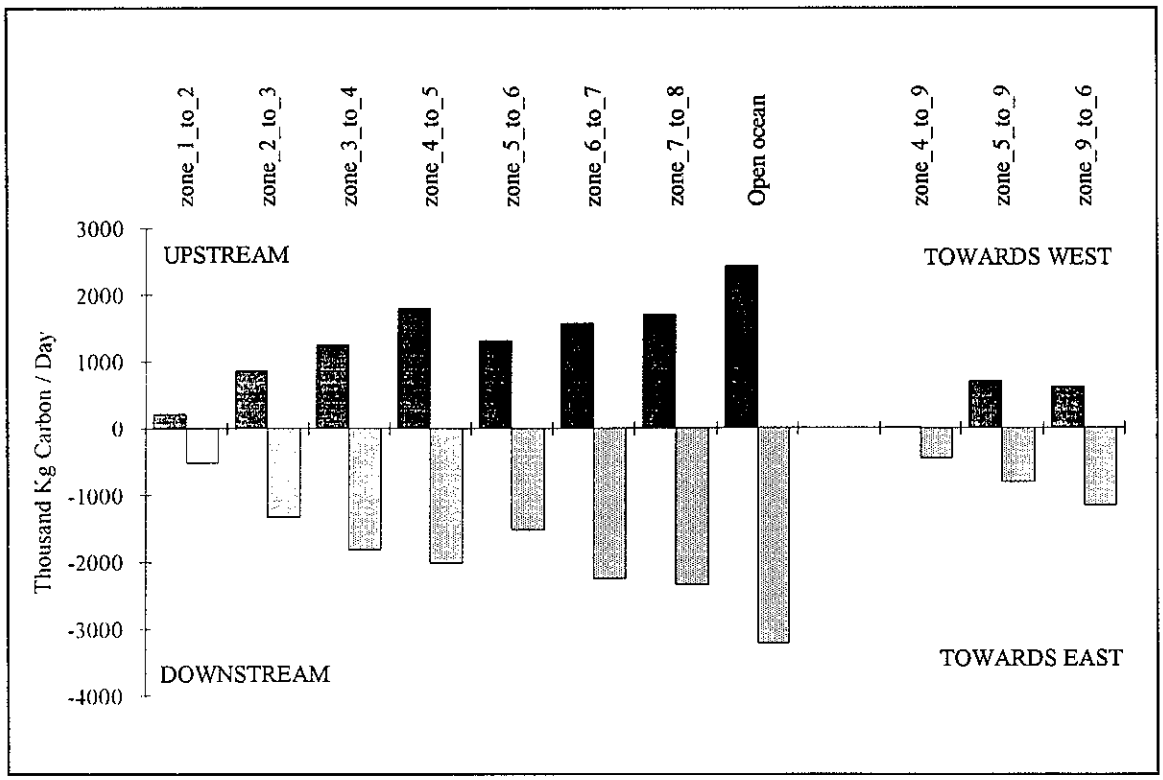

Figure 11-35. Annual Upstream and Downstream Transport of Total Organic Carbon, 1986

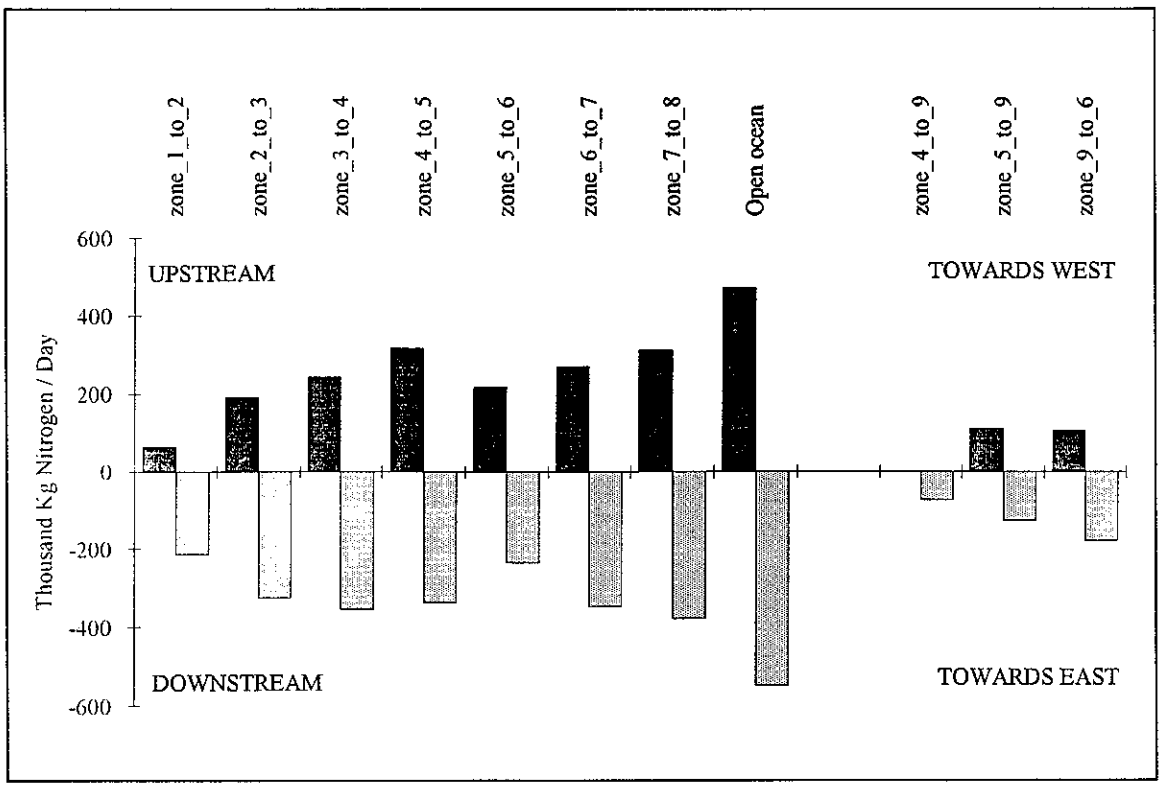

Figure 11-36. Annual Upstream and Downstream Transport of Total Nitrogen, 1986

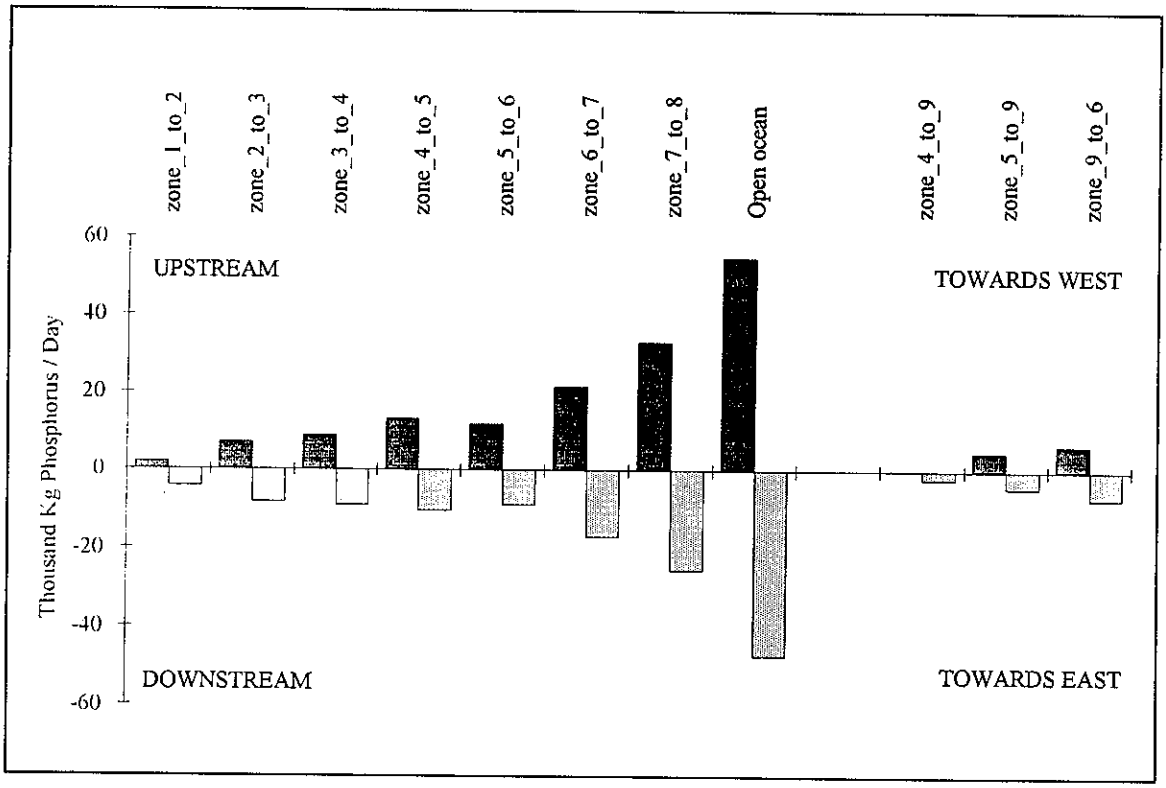

Figure 11-37. Annual Upstream and Downstream Transport of Total Phosphorus, 1986

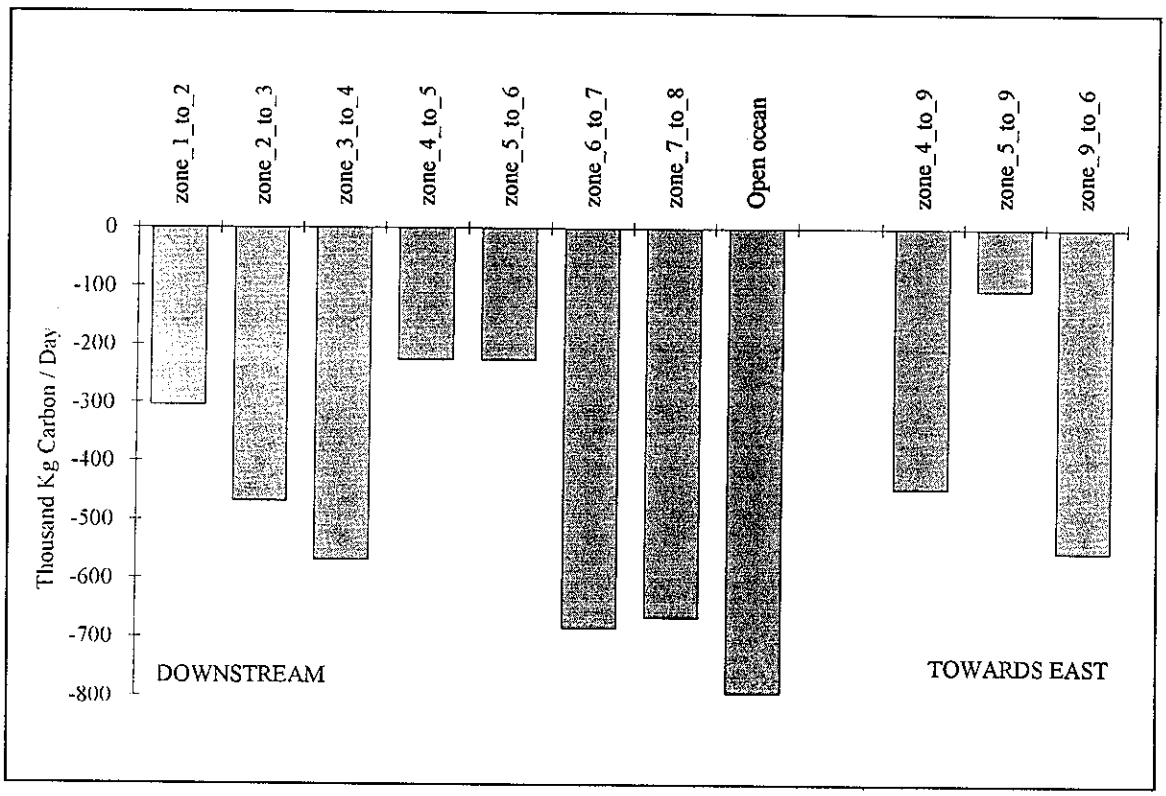

Figure 11-38. Annual Net Transport of Total Organic Carbon, 1986

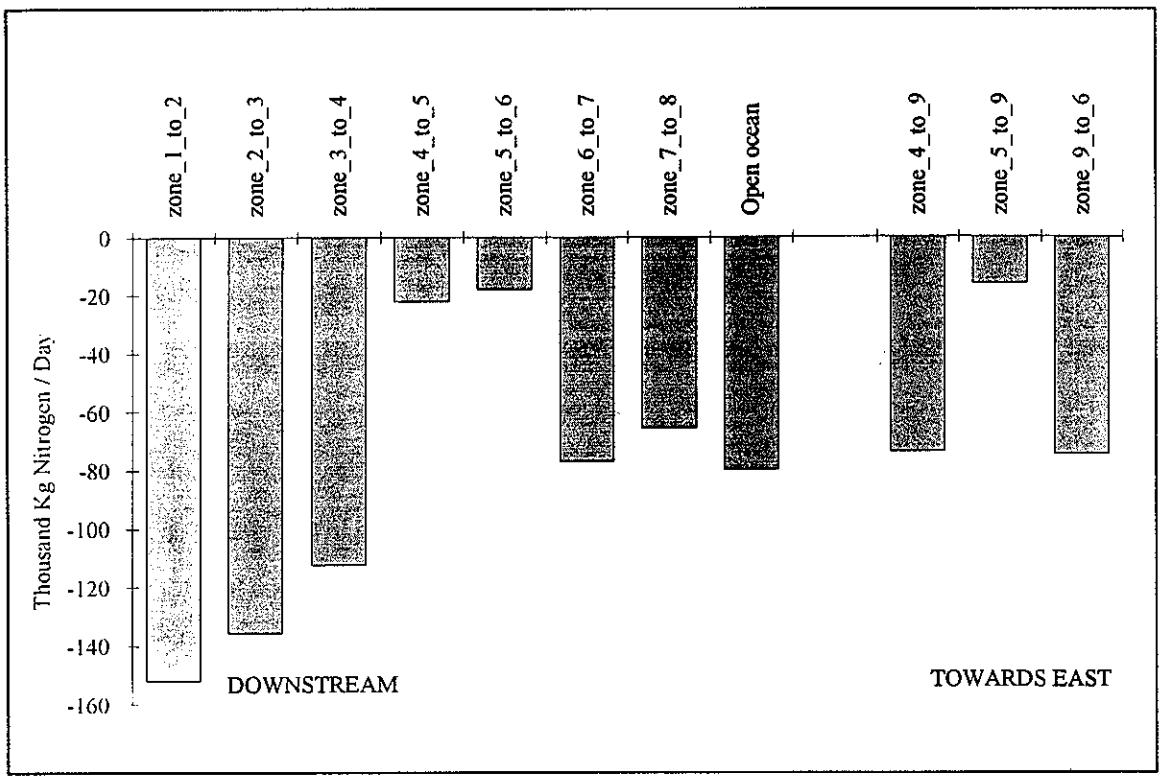

Figure 11-39. Annual Net Transport of Total Nitrogen, 1986

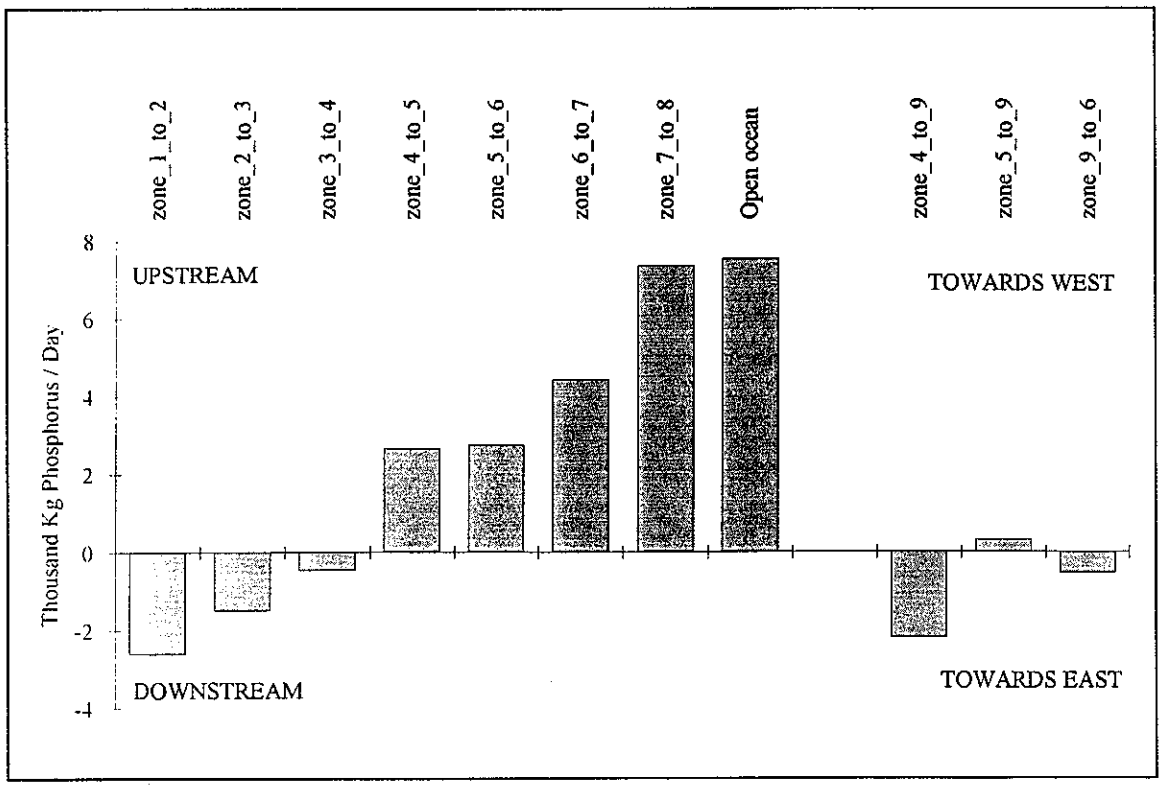

Figure 11-40. Annual Net Transport of Total Phosphorus, 1986

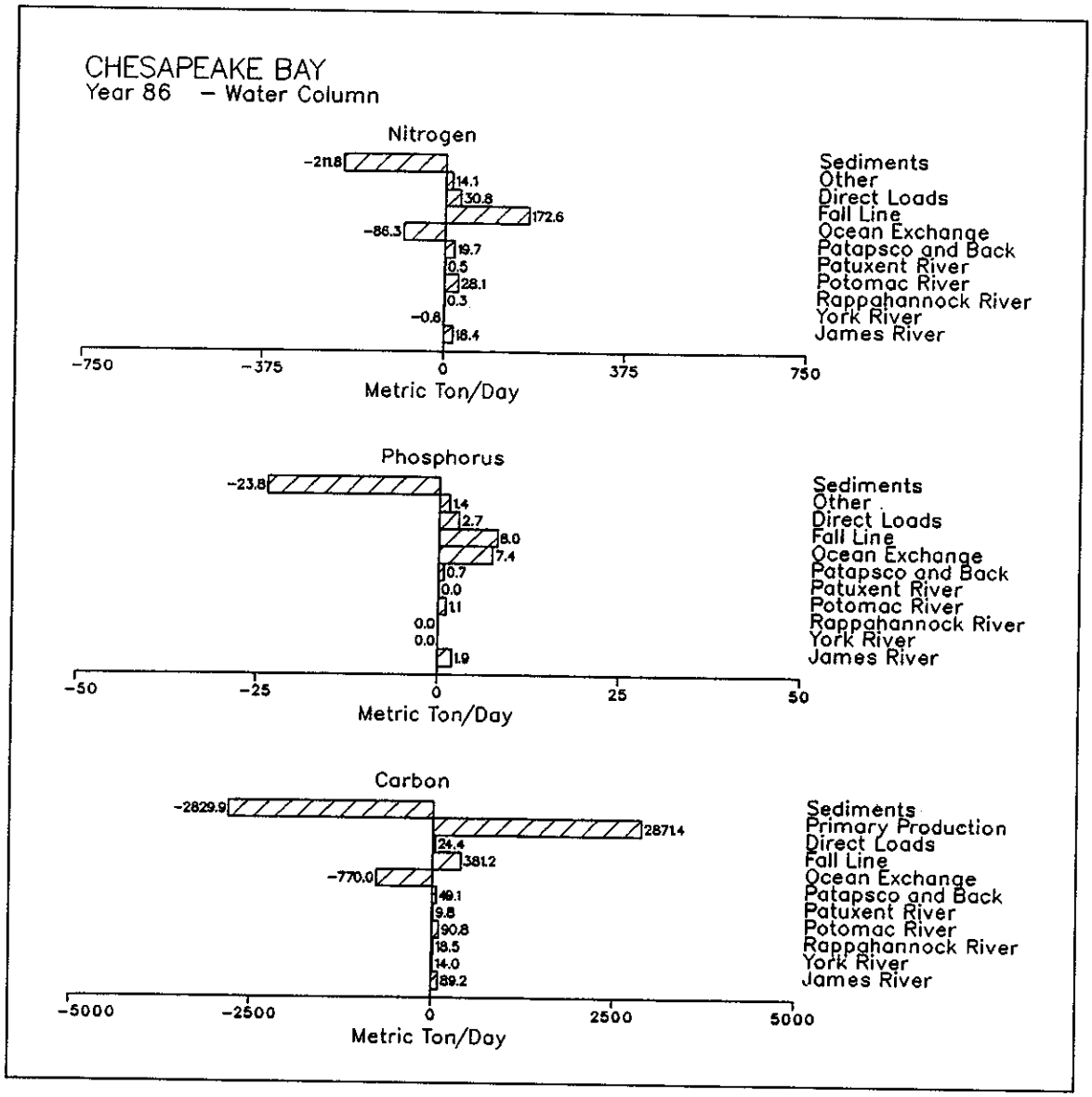

Figure 11-41. Annual Mass Balance for Mainstem Bay Water Column, 1986

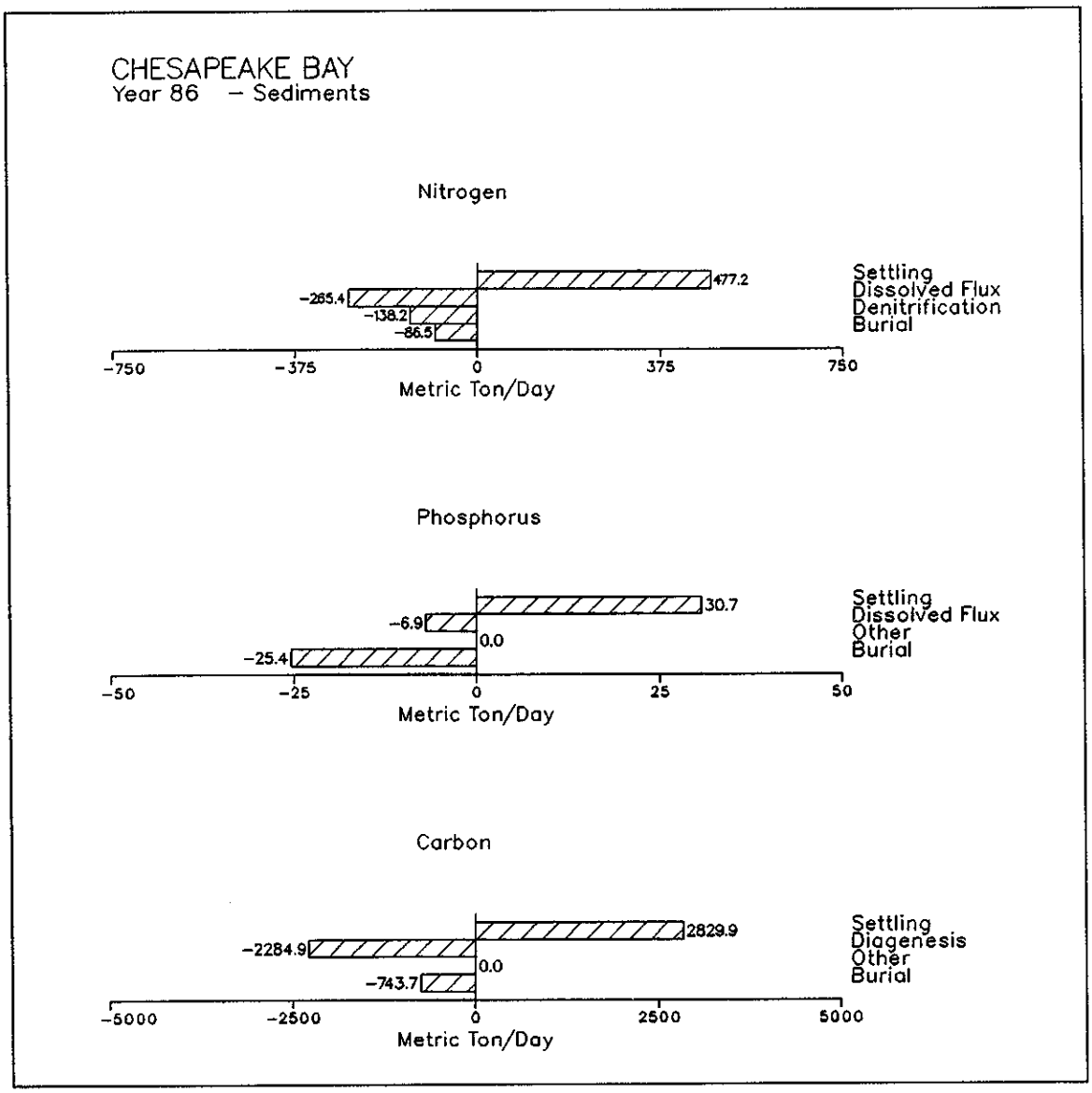

Figure 11-42. Annual Mass Balance for Mainstem Bay Sediments, 1986

Chapter XII: Tributary Calibration Results

Introduction

Five major tributaries were sampled and modelled in detail sufficient to warrant individual presentation. These were the James, York, Rappahannock, Potomac, and Patuxent Rivers. Analysis of observations and model results in the tributaries followed the pattern for the mainstem Bay. Time series and longitudinal transects of concentrations, sediment fluxes, and diagnostic information were produced. Individual carbon and nutrient budgets for each tributary were prepared. As with the mainstem, the quantity of resulting plots was overwhelming. Selected results are included in the present chapter. Remaining tributary plots are included in the appendix.

Time-Series Plots

Observed and modeled concentrations were aggregated by season, zone, and level. Each tributary was divided into three zones (Figure 12-1) corresponding to station delineations in the monitoring program. Zone One was the tidal fresh region immediately below the fall line (station prefix TF). Zone Two was the region of transition from fresh to salt water (station prefix RET). Zone Three was the lower estuarine region adjoining the mainstem Bay (station prefix LE). Seasons and levels were defined identical to the mainstem. Presentation of less than three levels for a zone indicates no model cells occupied the missing levels.

Observations of sediment-water fluxes and diagnostic information were available in the Potomac and Patuxent only. These were compared with model results in cells containing the sample stations. No aggregation was performed. For the Virginia tributaries, model results only were plotted in cells corresponding to selected stations in the tributary monitoring program.

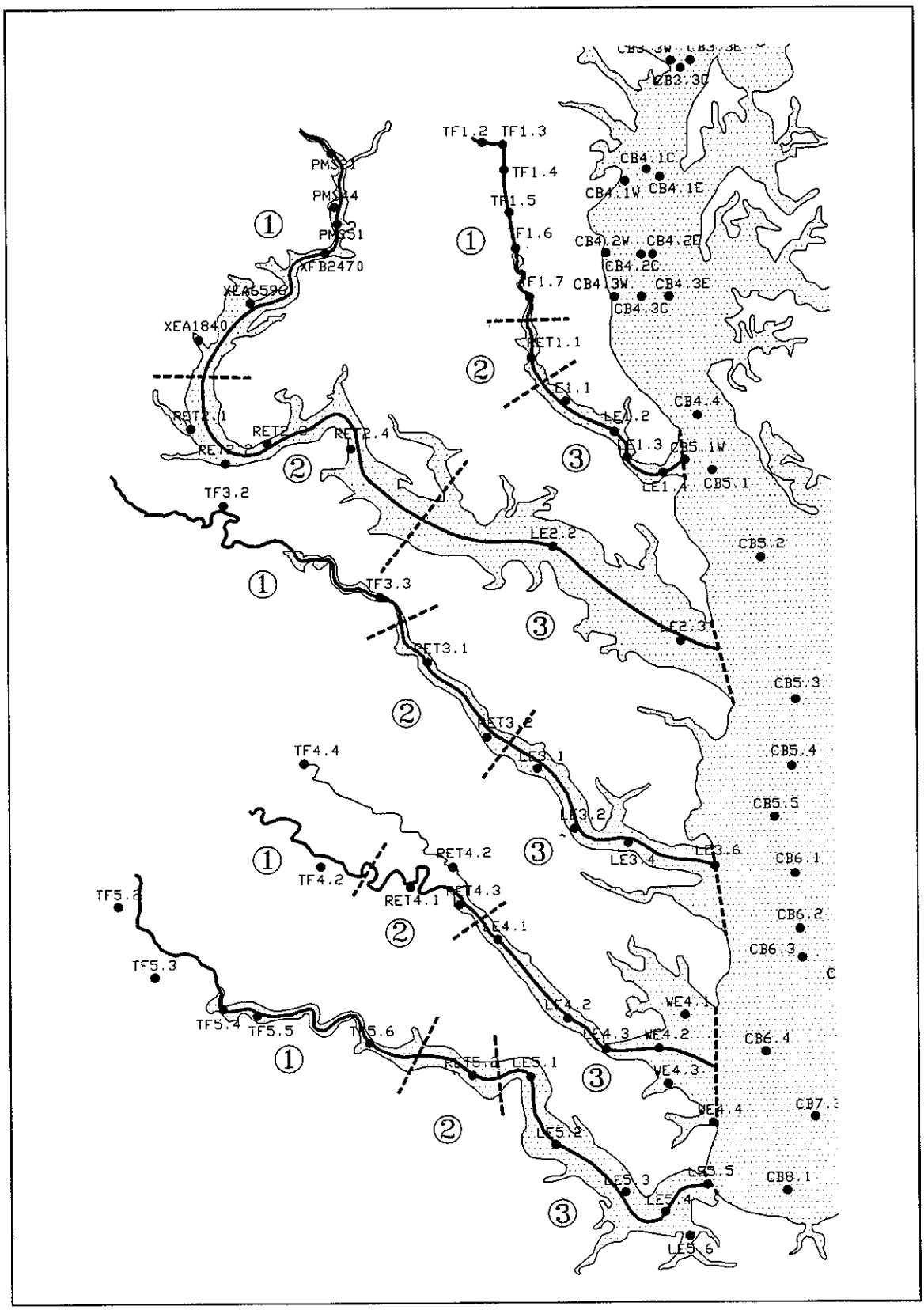

Figure 12-1. Aggregation Zones in Major Tributaries

Longitudinal Transects

Predictions and observations were aggregated into seasons for presentation along longitudinal transects (Figure 12-1). Samples in the tributaries were collected at two depths only: surface and bottom. Consequently, observations and model results were not aggregated by depth. Longitudinal transects in the tributaries show the mean and range of surface and bottom samples plotted against the mean of predictions in the surface and bottom boxes. The horizontal axis represents kilometers from the junction with the mainstem Bay.

Longitudinal plots of sediment-water fluxes and diagnostic information correspond to similar plots presented for the mainstem Bay.

Carbon and Nutrient Budgets

Budgets for the water column and sediments were prepared for each tributary. Elements in the budgets and sign convention largely corresponded with the budgets prepared for the mainstem. In the tributaries, however, atmospheric nitrogen and phosphorus loads were specifically identified. The "Other" category in the water-column nitrogen budget was solely loss due to denitrification.

The James River

The present chapter contains time-series plots for the three aggregation zones and longitudinal plots for the summer of 1986. Although 1986 was a year of average hydrology in the Susquehanna, mean flow in the James was below average (Table 2-4). Annual carbon and nutrient budgets for 1986 are also presented.

Concentrations

The time-series plots (Figures 12-2, 12-6, 12-7) demonstrate a high degree of correspondence between observations and model, although exceptions occur. The longitudinal plot (Figure 12-11) reveals more discrepancies than are apparent in the aggregations. Together, the presentations indicate the model performs well in predicting concentrations characteristic of large segments of the river. Spatial details, on scales of five to ten kilometers, however, are often missed by the model.

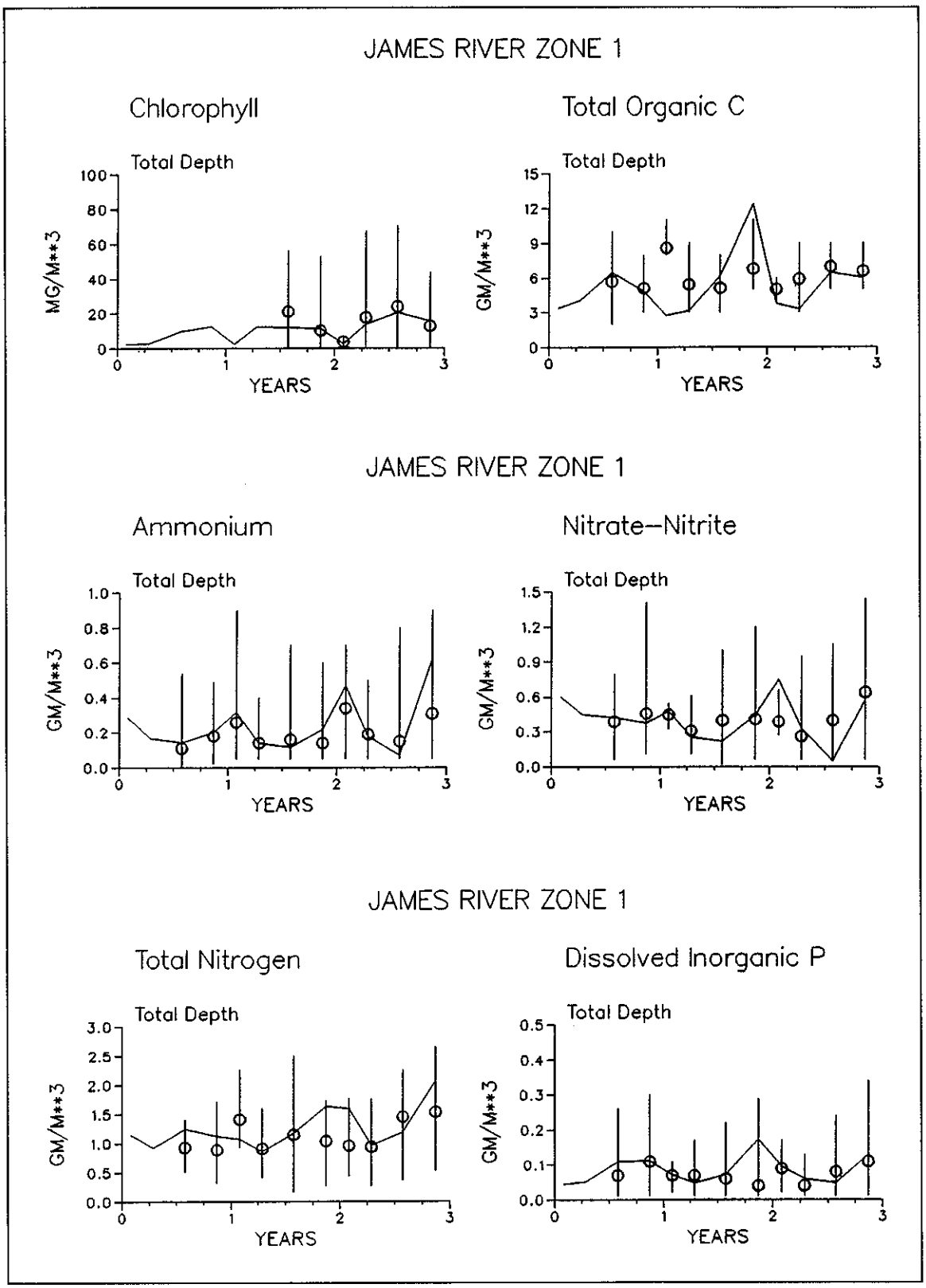

Figure 12-2. Time Series of Predicted and Observed Concentrations in James River Zone One (Continued)

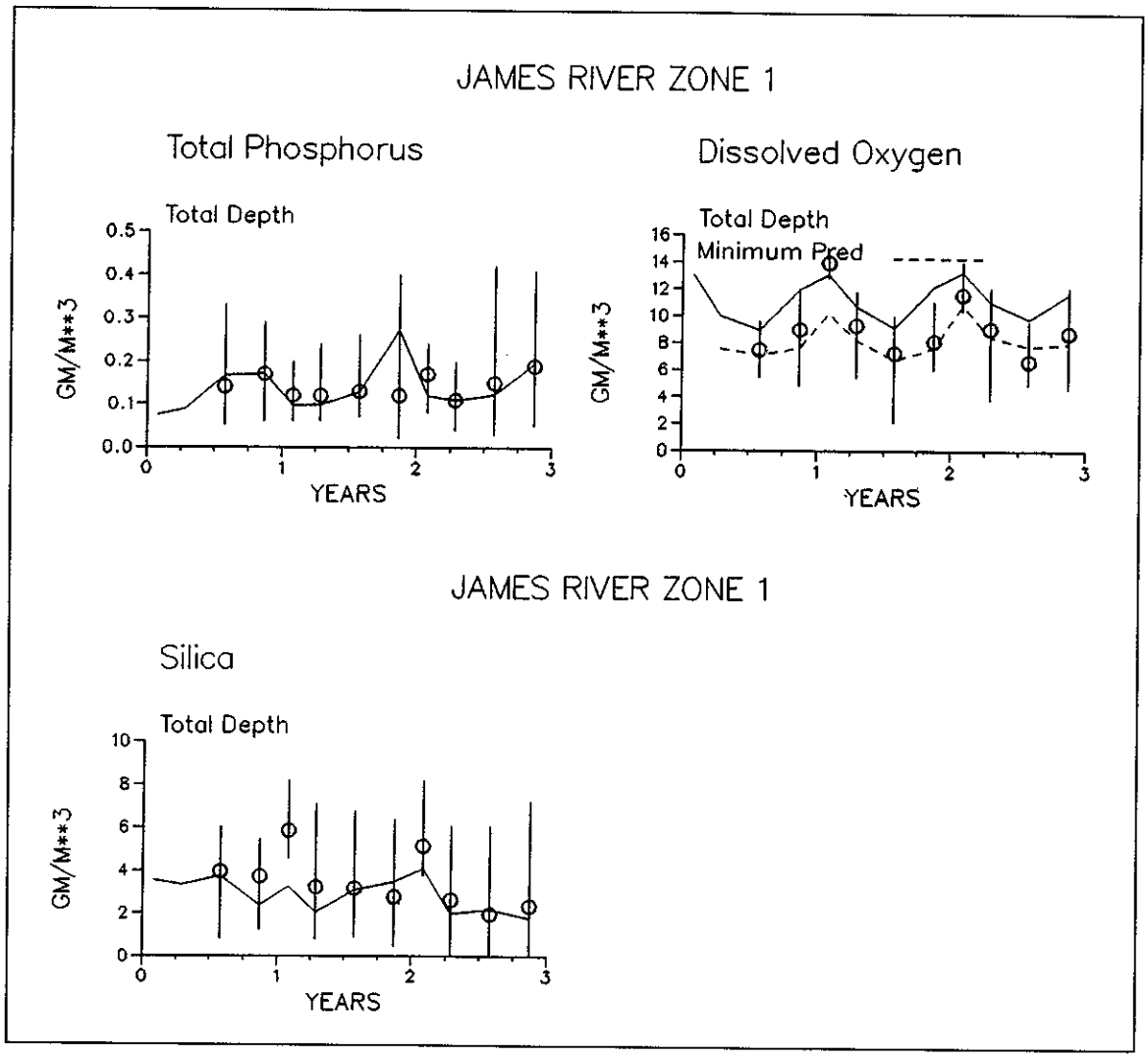

Figure 12-2. (Concluded)

Sediment-Water Fluxes

In the model, James River sediments were virtual nutrient traps. Little of the particulate nitrogen and phosphorus deposited was recycled to the overlying water (Figures 12-3, 12-8, 12-12). In the upper James, dissolved phosphate was scavenged by sediments from the water column. Phosphate scavenging and minimal ammonium release, through much of the river, concurred with observations conducted during 1983 and 1984 (Cerco 1985a). The magnitude of predicted sediment oxygen demand, ≈1 gm m^{-2} day^{-1} during summer, was also supported by observations. Immense observed ammonium releases near the fall line and large nitrate fluxes into the sediments near Hopewell were not reproduced in the model, however. Substrate for the observed ammonium releases was likely provided by combined-sewer overflows not represented in the model. Model nitrate flux into the sediments near km 100

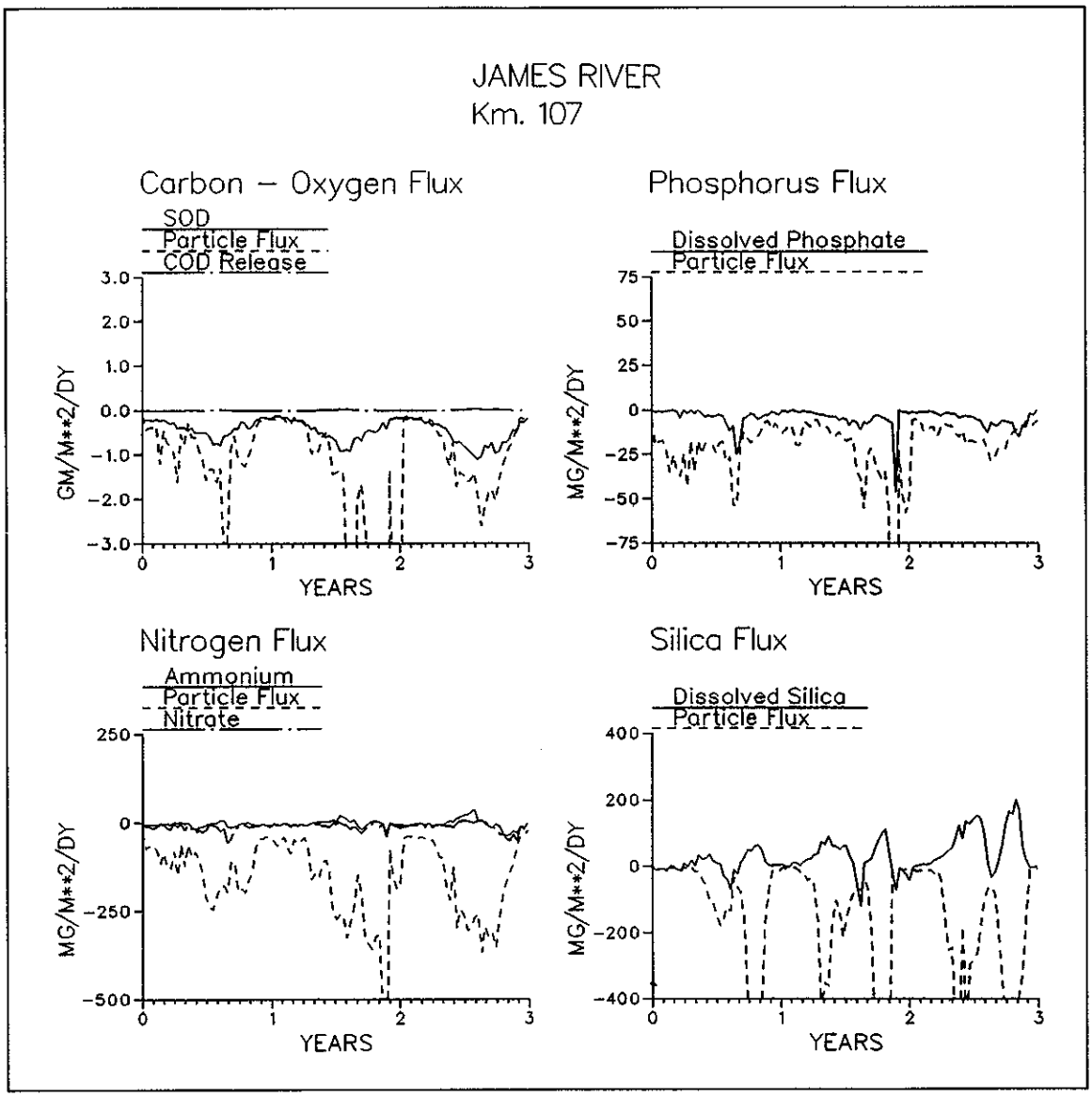

Figure 12-3. Time Series of Predicted Sediment-Water Fluxes in James River Zone One

was restricted by absence of nitrate in the water column at the same location (Figure 12-11).

Diagnostic Information

The model identified nitrogen as the only nutrient limiting in the James River at any time (Figure 12-5, 12-10, 12-13). The paradigm of freshwater phosphorus limitation did not apply in the upper James. Phosphorus loads from the fall line and point sources were sufficient to supply virtually all algal requirements.

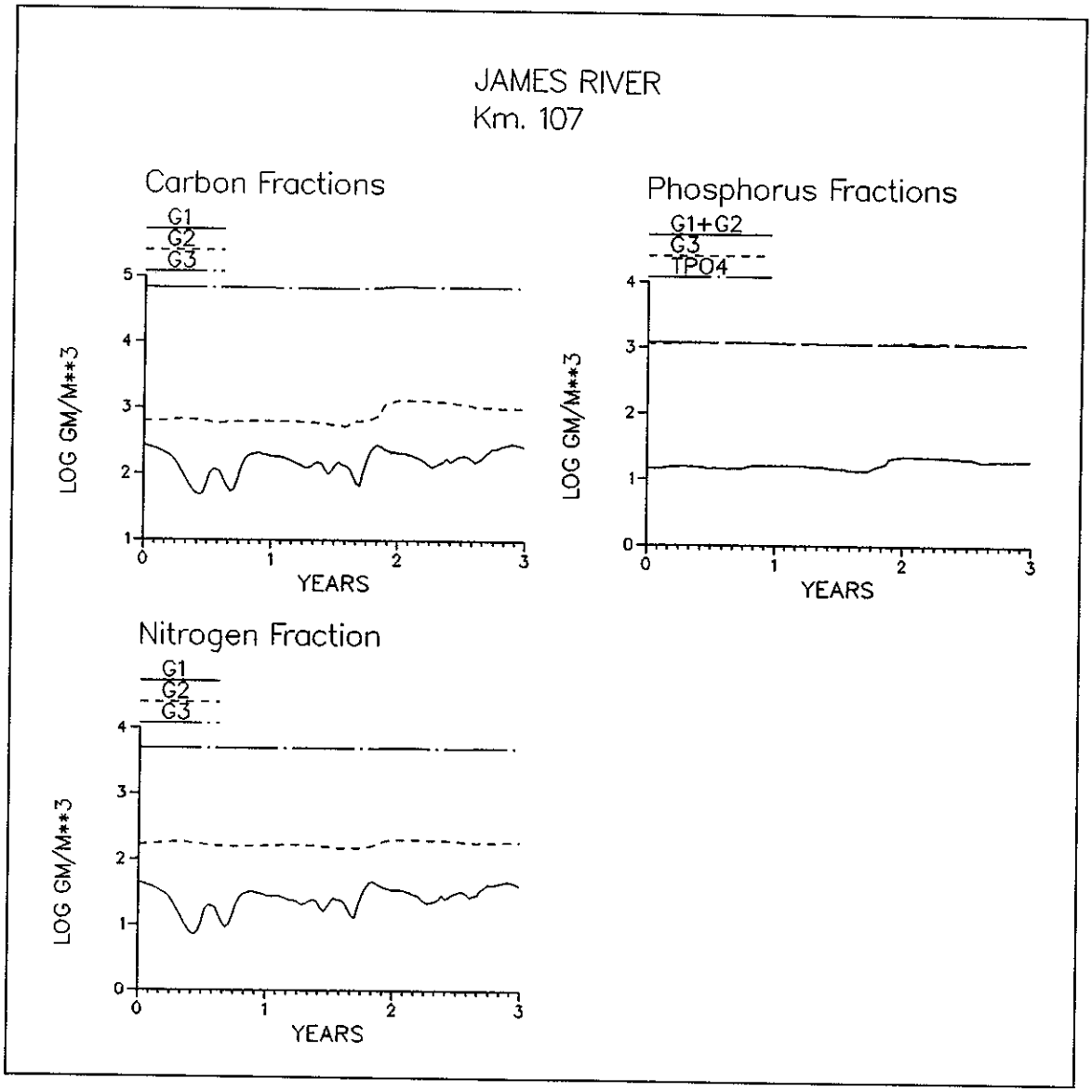

Figure 12-4. Time Series of Predicted Sediment Particulate Carbon, Nitrogen, and Phosphorus in James River Zone One

Carbon and Nutrient Budgets

As with the mainstem Bay, primary production was the major source of carbon (and oxygen demand) in the James River (Figure 12-14). Direct loads, primarily from point sources, were the second largest source. Roughly 70% of total carbon load was deposited in the sediments. The rest was exported to the mainstem. In the sediments, 80% of deposited carbon was oxidized (Figure 12-15) and the remainder was buried to deep, isolated sediments.

Direct loads, primarily from point sources, were, by far, the largest source of nitrogen and phosphorus to the James. Roughly 40% of the nutrient loads

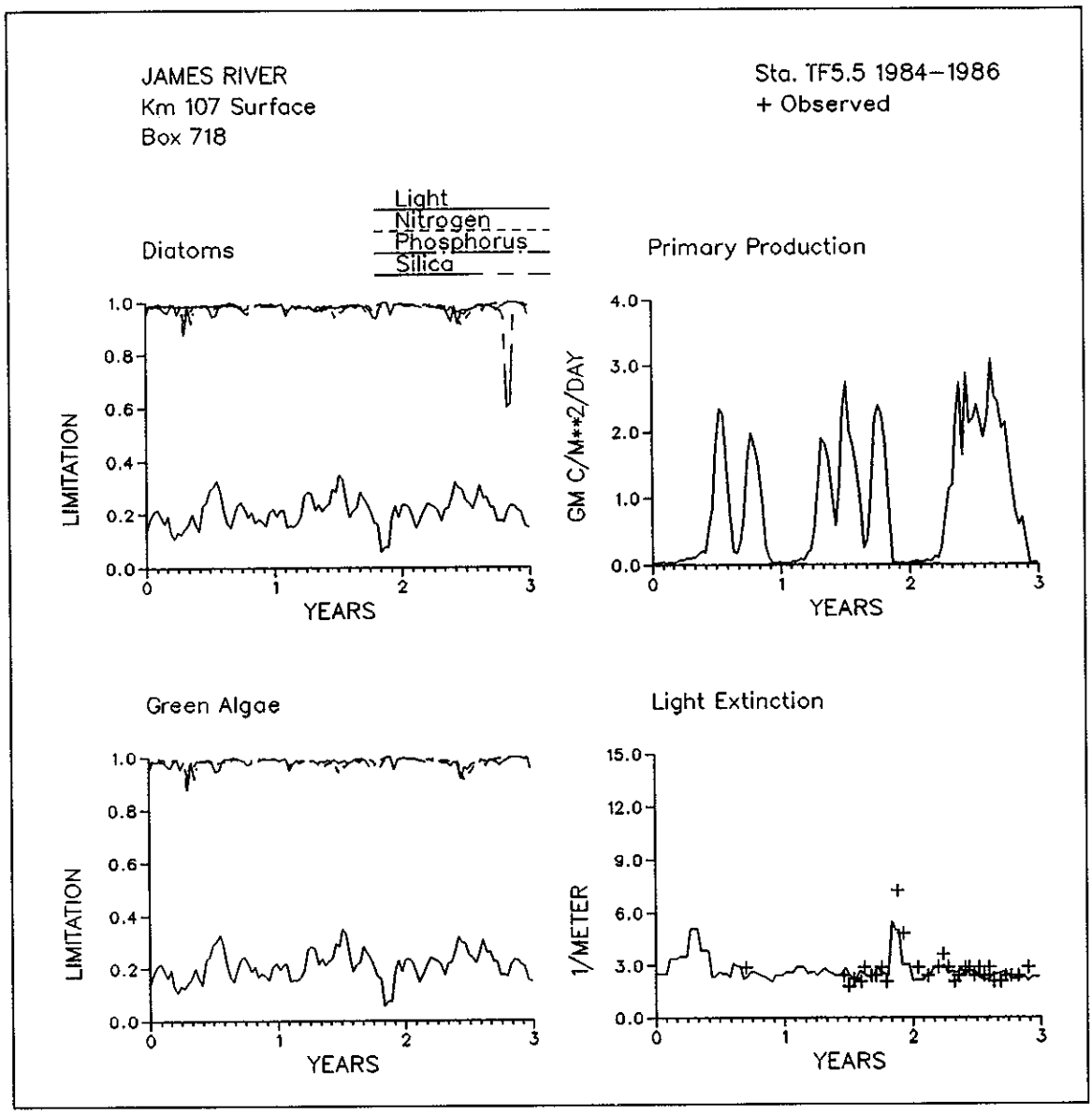

Figure 12-5. Time Series of Predicted Diagnostic Information in James River Zone One

were exported to the mainstem Bay. The remainder was lost in James River sediments. Denitrification was the primary pathway for removal of sediment nitrogen. Burial was the sole sediment sink of phosphorus.

Potential Improvements

The present calibration is the best that can be obtained with the current model. Origins of model-data discrepancies and requirements for improved calibration in the James River are listed below.

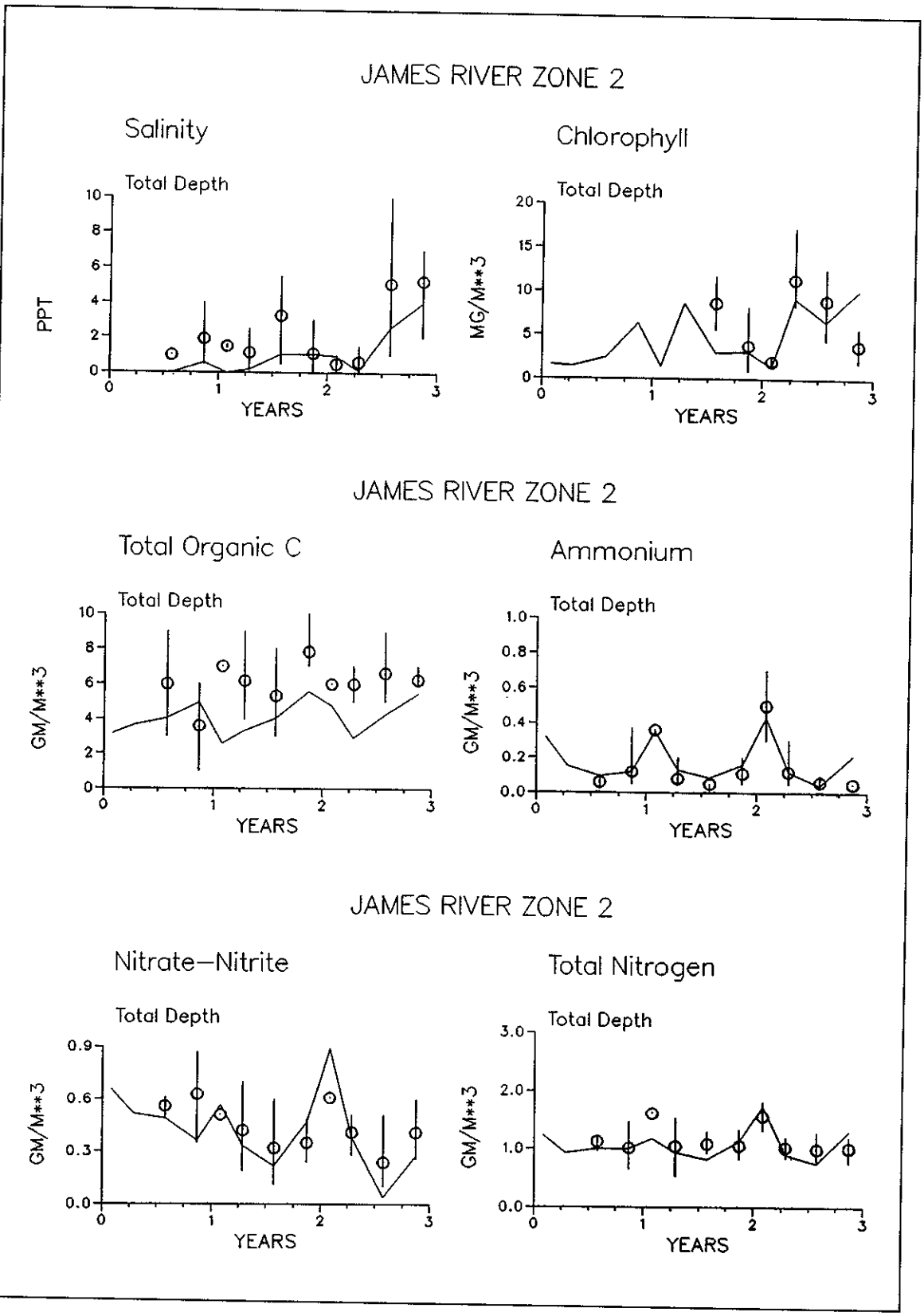

Figure 12-6. Time Series of Predicted and Observed Concentrations in James River Zone Two (Continued)

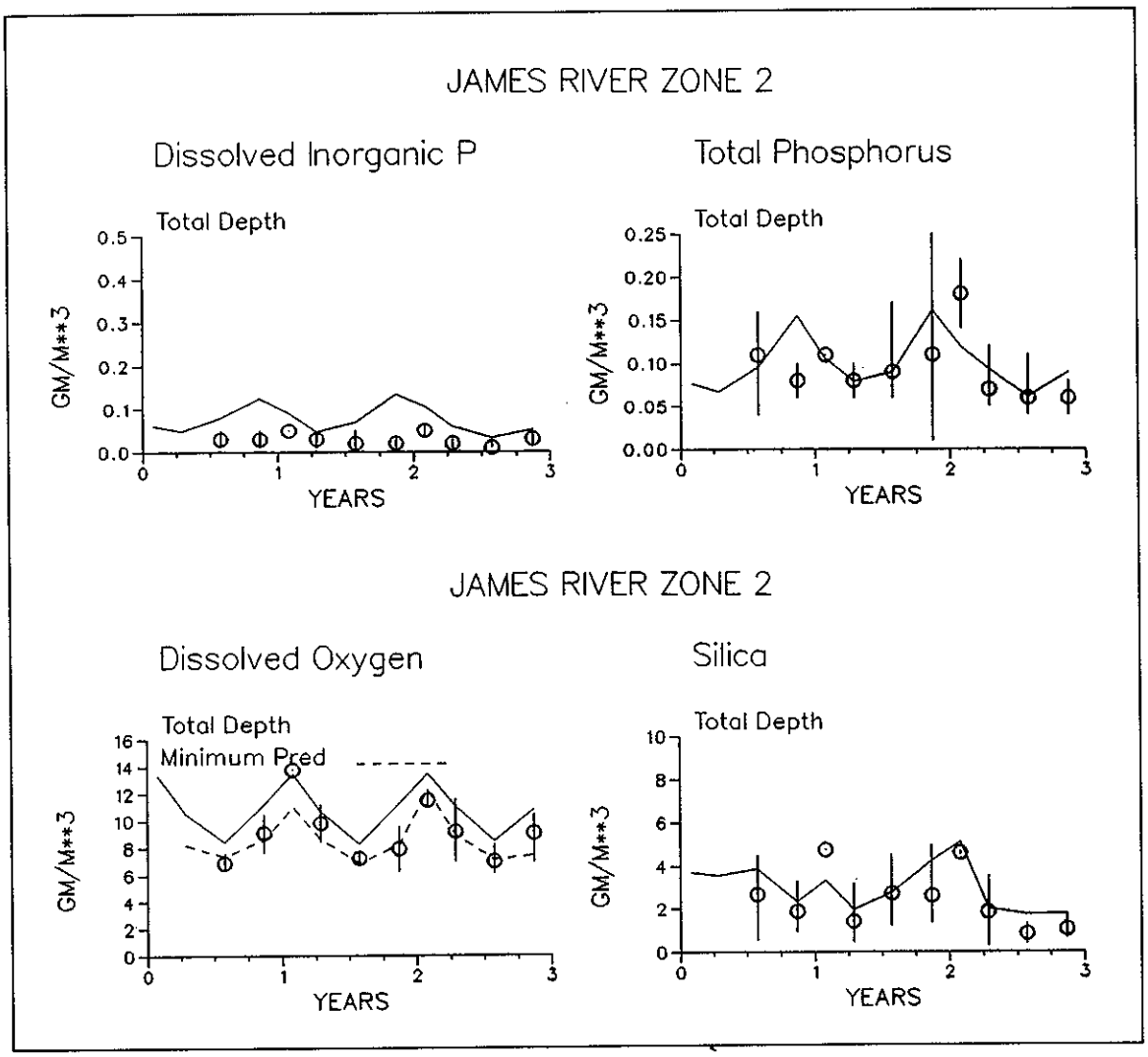

Figure 12-6. (Concluded)

Loading

The model incorporated loads from twenty-four below-fall-line point-source facilities in the James River basin. Accurate modeling of carbon and nutrients in the James required accurate quantification of loads from these sources. In 1986, however, all point-source nitrogen concentrations and the vast majority of phosphorus concentrations were obtained by default or by reference to alternate years. Consequently, the exact loads from individual point sources and the distribution of total nutrients into fractions were not well known.

The use of defaults is acceptable in summations of large numbers of loads. Underestimates at one source will compensate for overestimates at another. The initial distribution of nutrient fractions declines in significance as a function of distance from the source. The fractionation becomes dominated by internal recycling processes rather than initial distribution. On time scales of

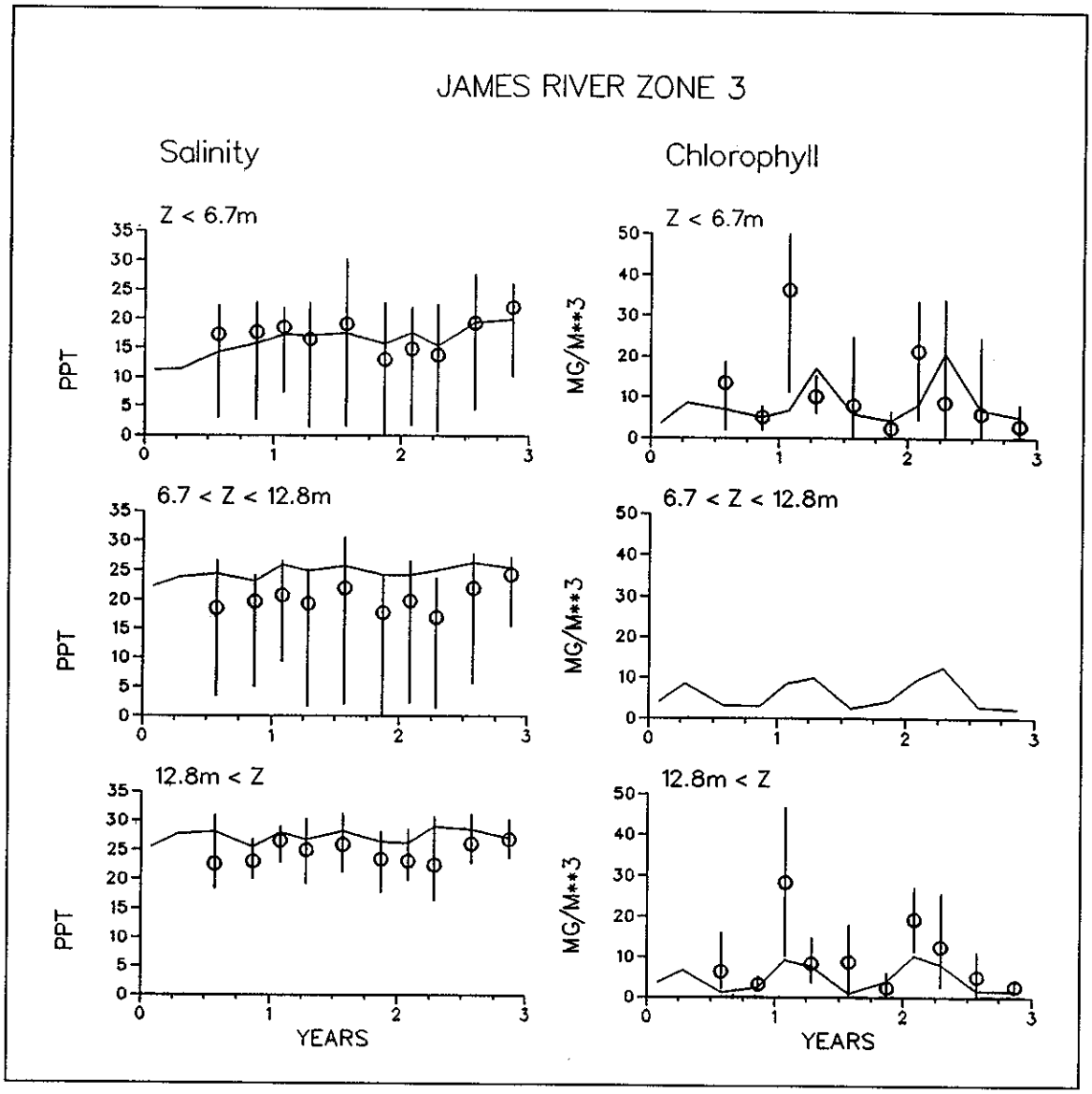

Figure 12-7. Time Series of Predicted and Observed Concentrations in James River Zone Three (Sheet 1 of 5)

months, in the immediate vicinity of point sources, however, absence of detailed loading information will be reflected in model results. The discrepancies between predicted and observed ammonium and nitrate around km 100 (Figure 12-11), downstream of the point sources concentrated near Hopewell, are likely examples of point-source loading problems.

In the vicinity of the fall line, accuracy in the water-quality model depended heavily on accuracy in the Watershed Model which generated fall-line loads. The Watershed Model performed exceptionally well in computing these loads. Occasional shortfalls in performance occurred, however, notably in total organic carbon concentration. Alternate estimates of carbon load, as

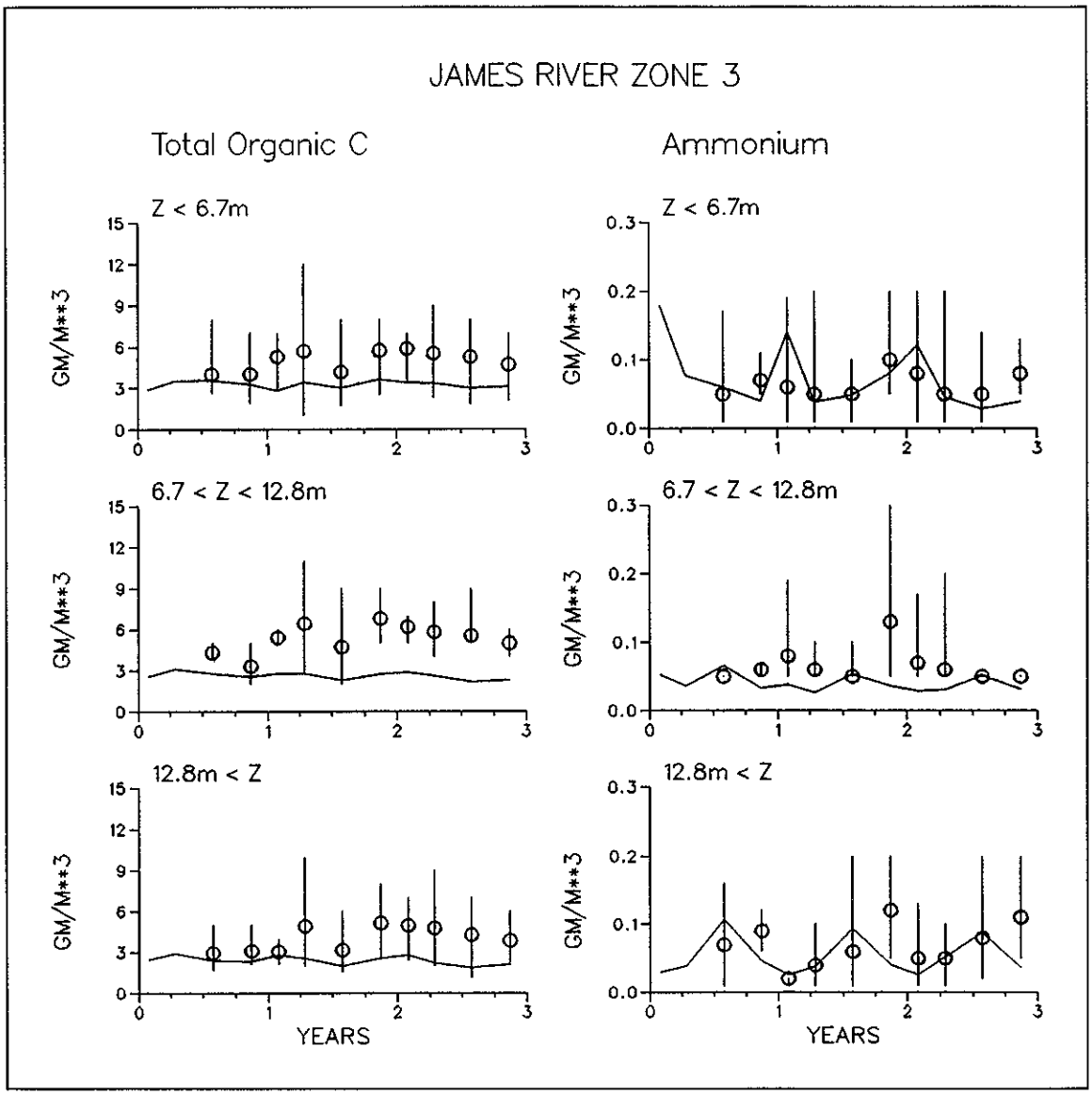

Figure 12-7. (Sheet 2 of 5)

from a regression relationship, would have provided more accurate model results (Figure 12-16). Occasional discrepancies in predicted nitrogen and phosphorus concentrations also originated in the fall-line loads and were beyond remedy in the water-quality model. As with the point-source loads, inaccuracies in individual events or in fractionation were of little significance at large distances from the fall line.

Particulate Inorganic Phosphorus

Dissolved phosphate and total phosphorus were well-represented in Zone One (Figure 12-2). Downstream, however, predicted dissolved phosphate was

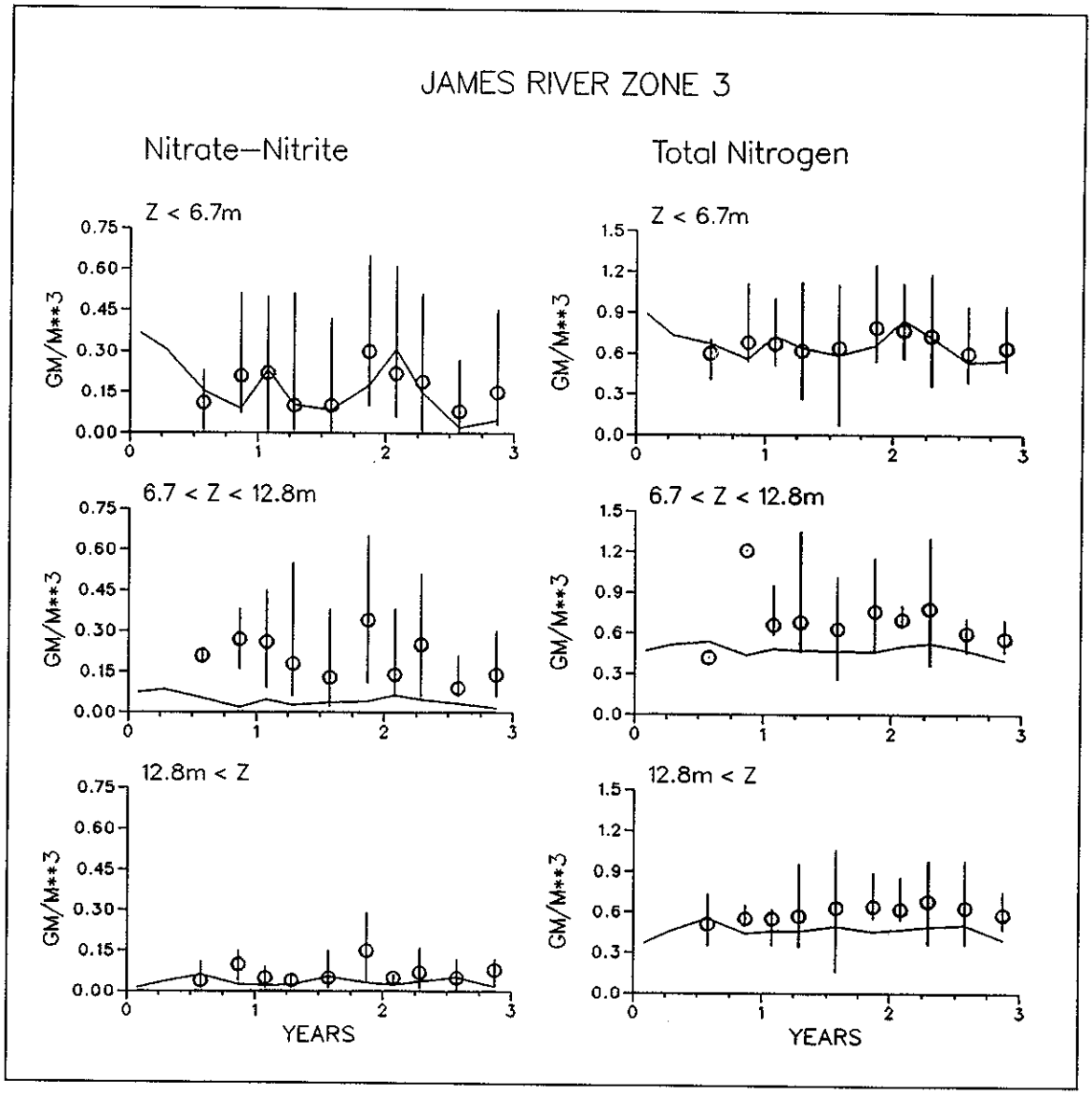

Figure 12-7. (Sheet 3 of 5)

often in excess of observations (Figure 12-7). Sensitivity analysis indicated a prototype process was converting dissolved phosphate into particulate form. The most plausible explanation is that phosphorus sorbed onto suspended sediments. This process was not represented in the model and could not be mimicked by manipulation of calibration parameters. Accurate modeling of dissolved phosphate in the middle and lower James requires addition of phosphate exchange with inorganic solids to the model framework.

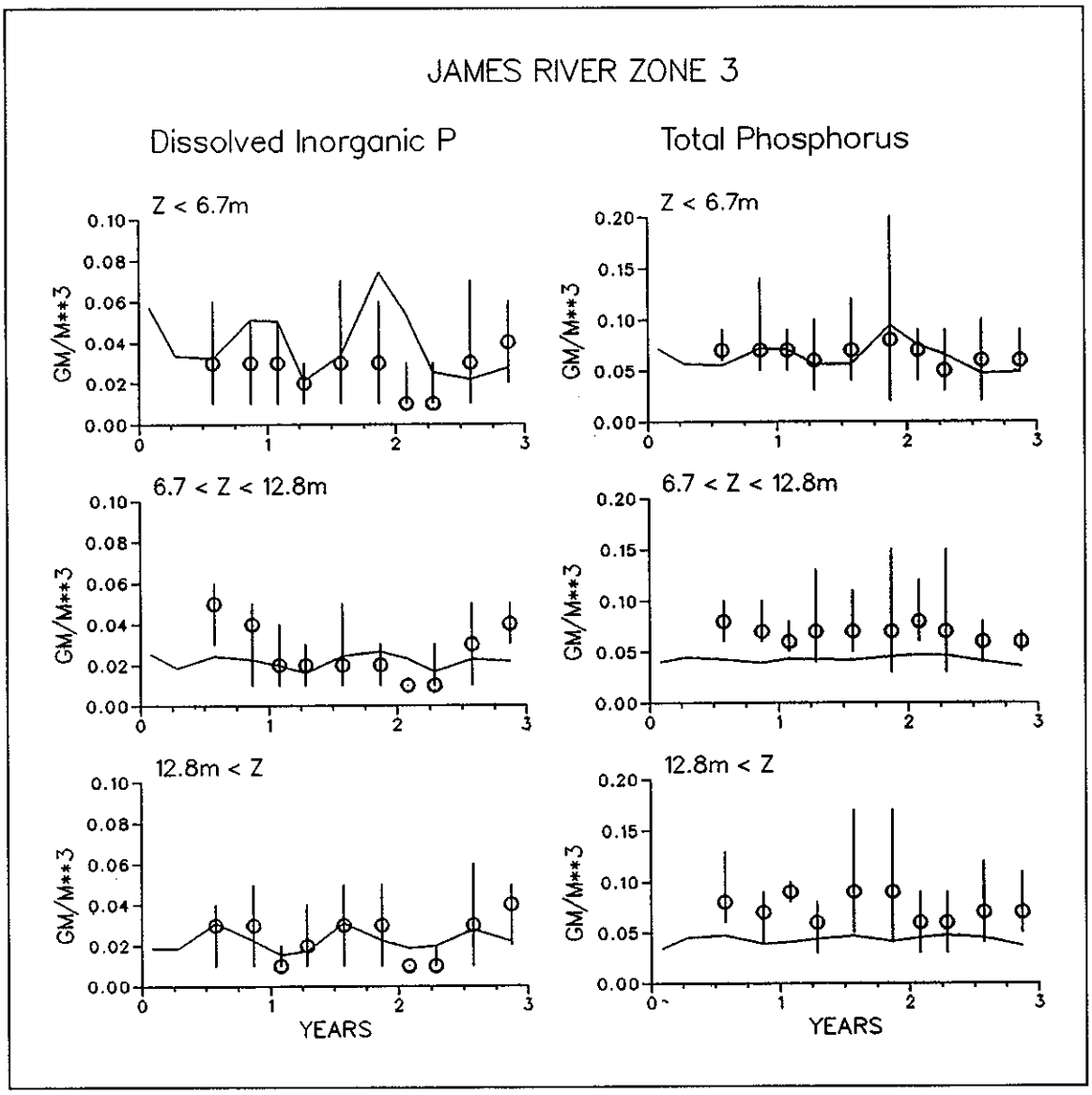

Figure 12-7. (Sheet 4 of 5)

Grid Resolution

Accuracy in the James can be enhanced by additional grid resolution in the longitudinal and lateral dimensions. The present grid (characteristic length ≈6 km) is insufficient to resolve the spatial distribution of point sources in the upper James. The influence of these sources is closely reflected in observations at adjacent monitoring stations. Additional longitudinal resolution will enhance accuracy in regions of sharp gradients as between km 100 and 125 (Figure 12-11).

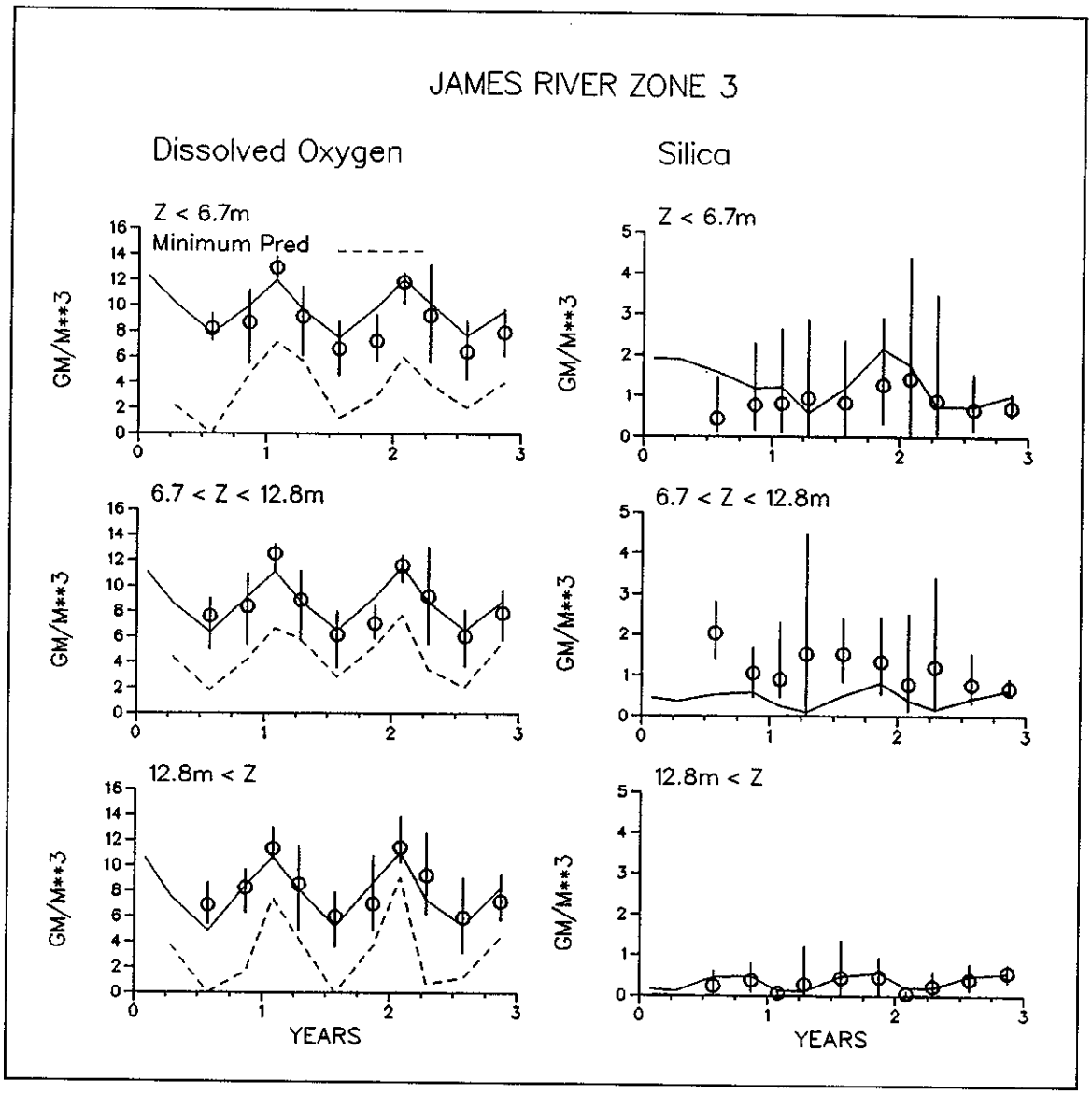

Figure 12-7. (Sheet 5 of 5)

Additional lateral resolution is especially needed in the lower James (km 0 to 50) and near Hopewell (km 100). In the lower James, the current grid is three cells wide. As a consequence the deep central channel is roughly one-third of the total width. This over-represents channel width and influences computed density-driven circulation in the saline portion of the river. The extensive shoals at the mouth of the Appomattox, near Hopewell, are not represented at all. Consequently, effects of sediment-water exchange processes, which are dependent on average depth, are underestimated in this region.

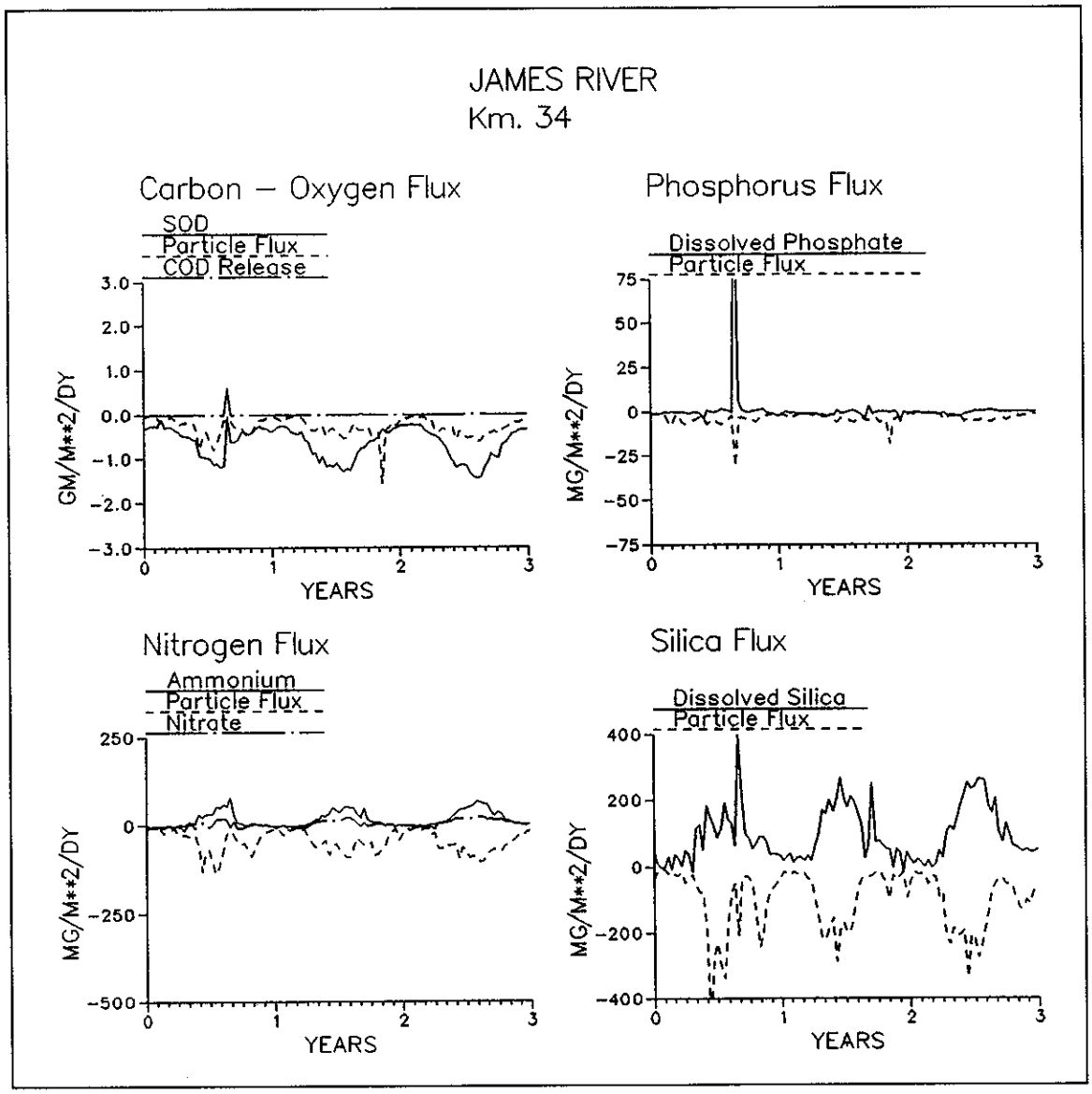

Figure 12-8. Time Series of Predicted Sediment-Water Fluxes in James River Zone Three

The Potomac River

The present chapter contains time-series plots for the three aggregation zones and longitudinal plots for the summer of 1986. Although 1986 was a year of average hydrology in the Susquehanna, mean flow in the Potomac was below average (Table 2-4). Annual carbon and nutrient budgets for 1986 are also presented.

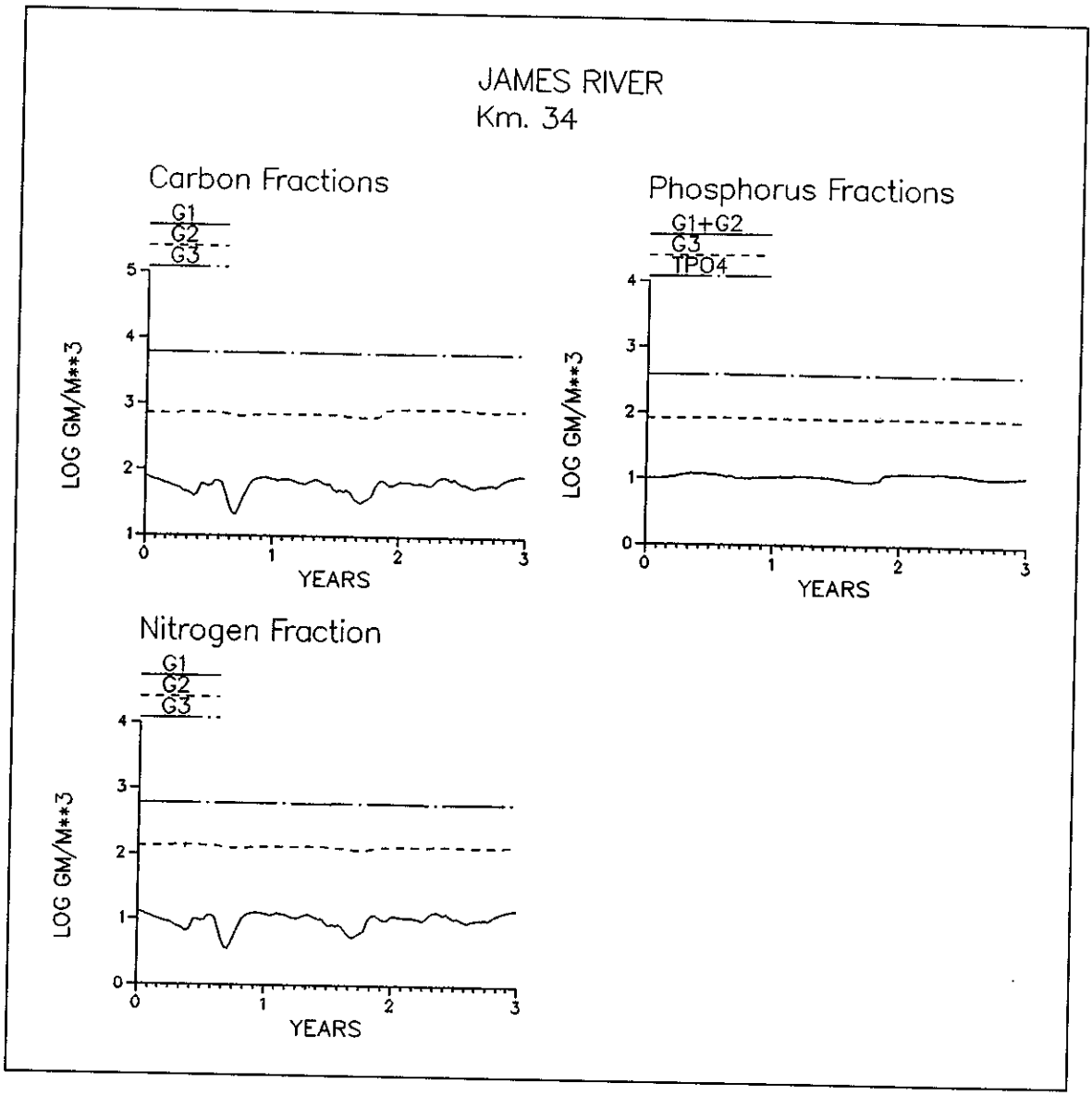

Figure 12-9. Time Series of Predicted Sediment Particulate Carbon, Nitrogen, and Phosphorus in James River Zone Three

Concentrations

Comparisons of observations and model results in the Potomac River presented a mixed picture. Agreement was largely successful in Zone Three (Figure 12-25). Zone Three comprised a large volume, distant from most loading sources. Hydrodynamics and eutrophication processes resembled the adjacent region of the mainstem Bay. In the upper (Figure 12-17) and middle Potomac (Figure 12-21), discrepancies were often observed between observations and model results. Discrepancies were largely attributable to loading and to tributary-specific processes not represented in the model framework.

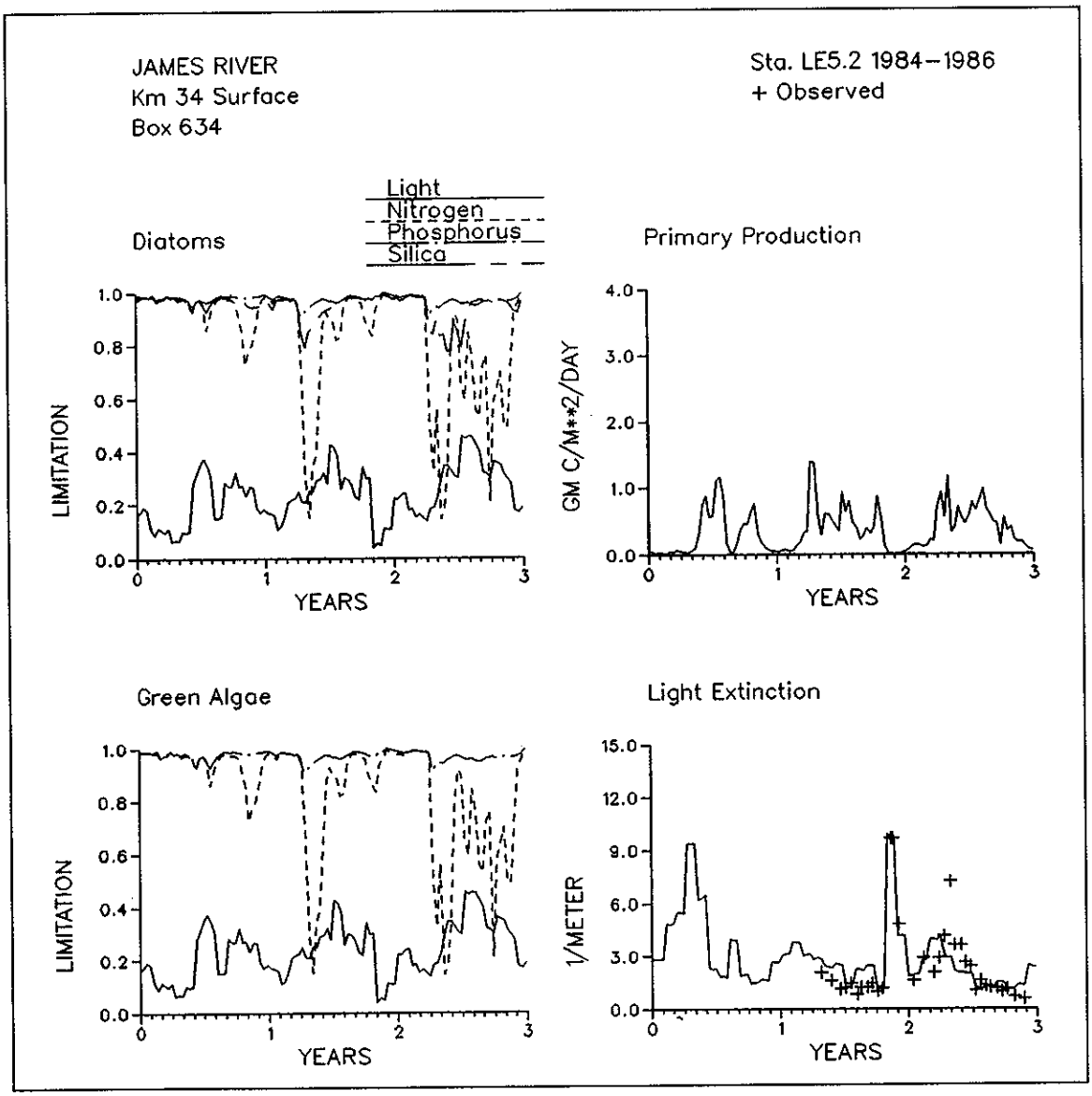

Figure 12-10. Time Series of Predicted Diagnostic Information in James River Zone Three

Zone One exhibited problems in two areas, fall-line phosphorus loading and cyanobacteria dynamics. The Watershed model consistently overestimated the fraction of dissolved phosphate in total phosphorus loading. Total phosphorus loads appeared to be overestimated, as well, in late 1984 and early 1985. Phosphate predictions in Zone One were much improved when phosphorus concentrations were specified by regression rather than by the Watershed Model (Figure 12-33).

Zone One was the site of cyanobacteria predominance not observed elsewhere in the Bay system. The freshwater cyanobacteria were assigned a unique model state variable to allow for specific calibration of the upper Potomac. Prediction of cyanobacteria was partly confounded by the

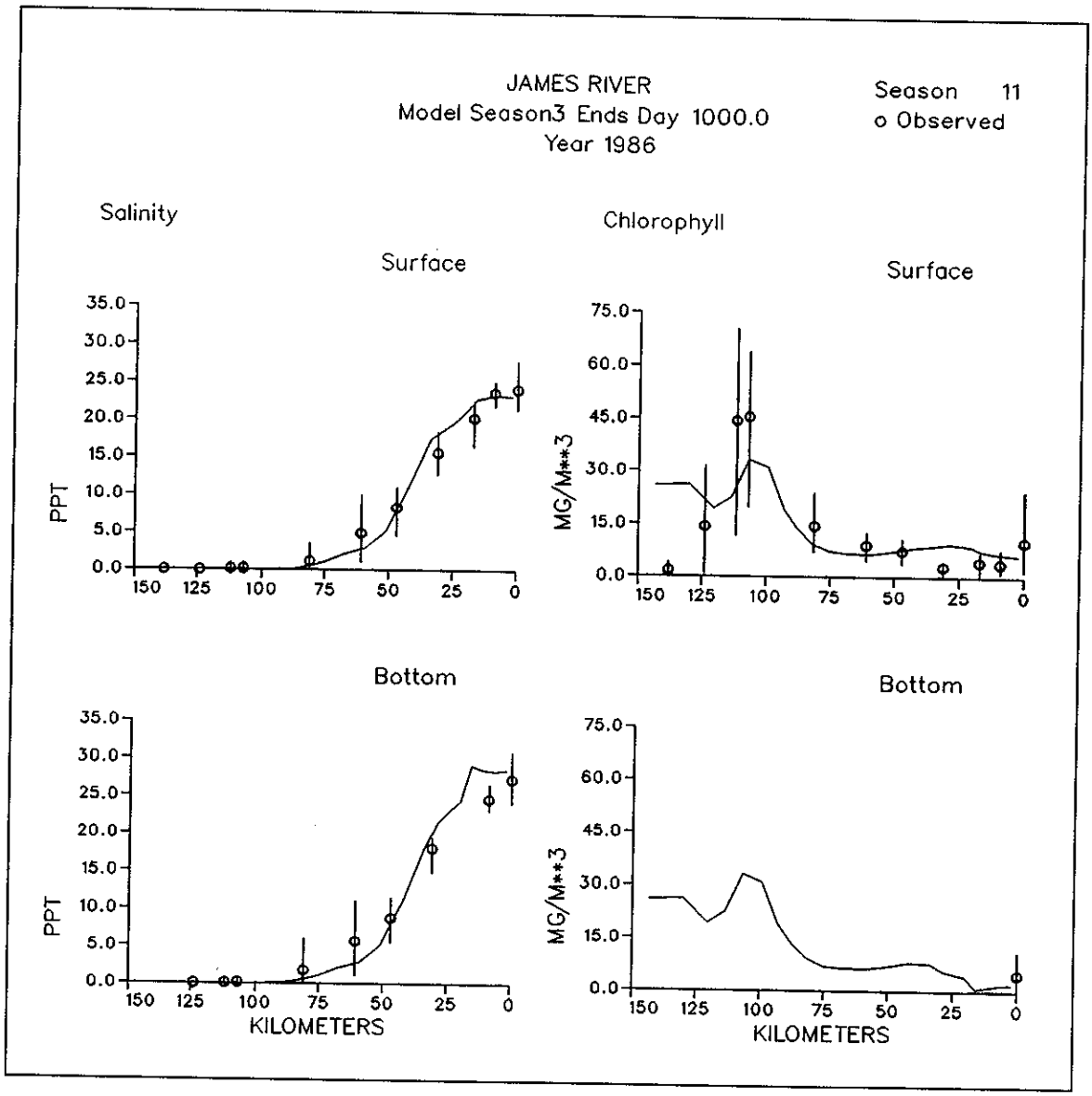

Figure 12-11. Predicted and Observed Concentrations Along James River Longitudinal Transect, Season Three, 1986 (Sheet 1 of 5)

phosphorus loading issue. Aside from improvements in load specification, however, refinements to formulation or parameter values are required to improve representation of cyanobacteria.

In the present calibration, the summer bloom persists into autumn. An adjustment in parameter values or formulation is required to terminate the bloom in Season Three. Adjustments to growth rate and carbon-to-chlorophyll ratio are also suggested. At present, total organic carbon is overpredicted even when chlorophyll predictions are accurate (Figure 12-17). The excess carbon is algal biomass. The growth rate should be reduced to improve total carbon predictions. Next, the carbon-to-chlorophyll ratio should be adjusted

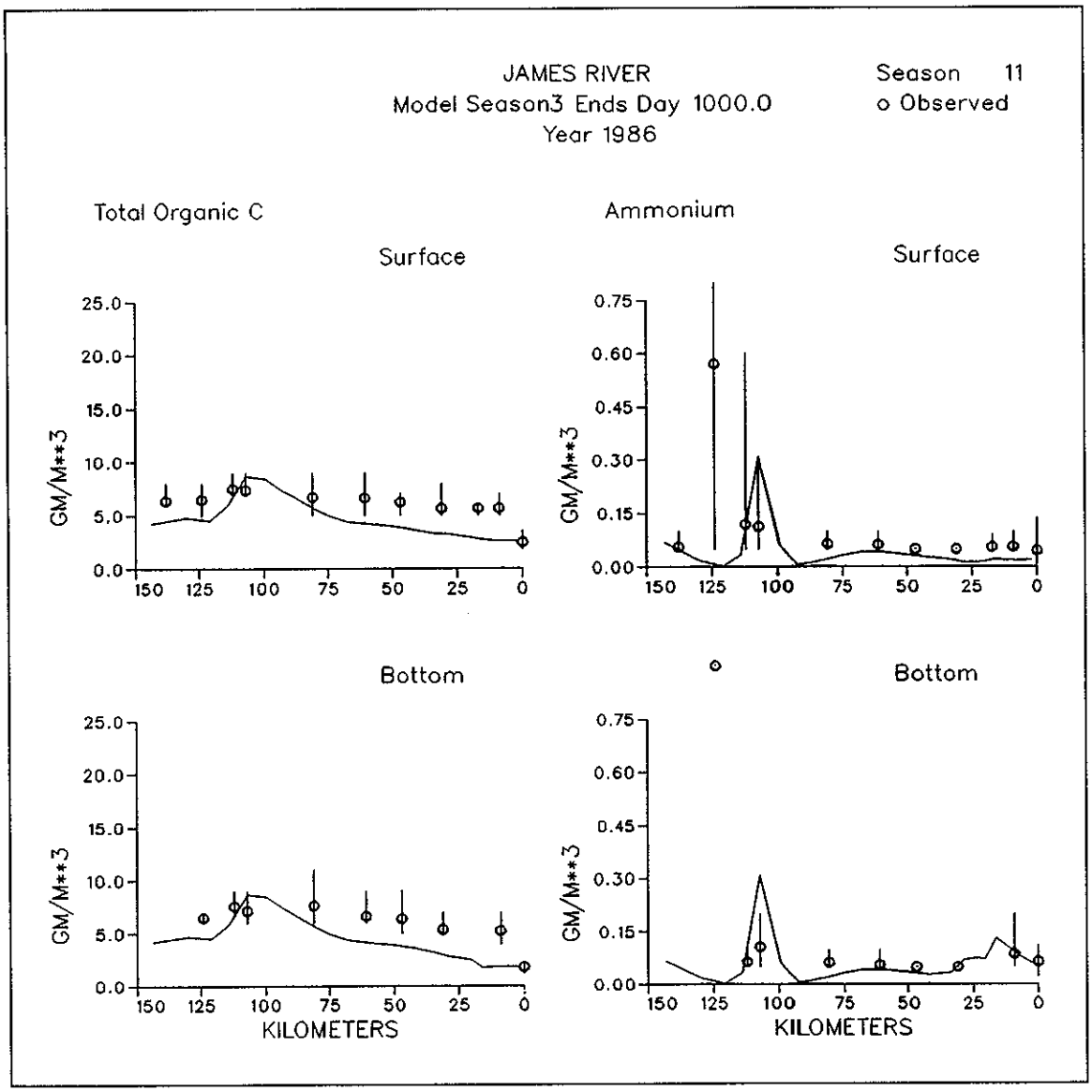

Figure 12-11. (Sheet 2 of 5)

downward until predicted chlorophyll approximates the existing chlorophyll concentration. At present the carbon-to-chlorophyll ratio is 60 gm C gm^{-1} Chl. A more appropriate ratio for cyanobacteria in the Potomac is 20 to 45 gm C gm^{-1} Chl (Thomann and Fitzpatrick 1982).

Zone Two was the site of anomalous phosphorus behavior. Concentration peaked around km 100, far from any loading sources (Figure 12-29). The peak was a persistent feature of the river (Figure 12-34) and was coincident with the peak solids concentration characteristic of the turbidity maximum (Figure 12-35).

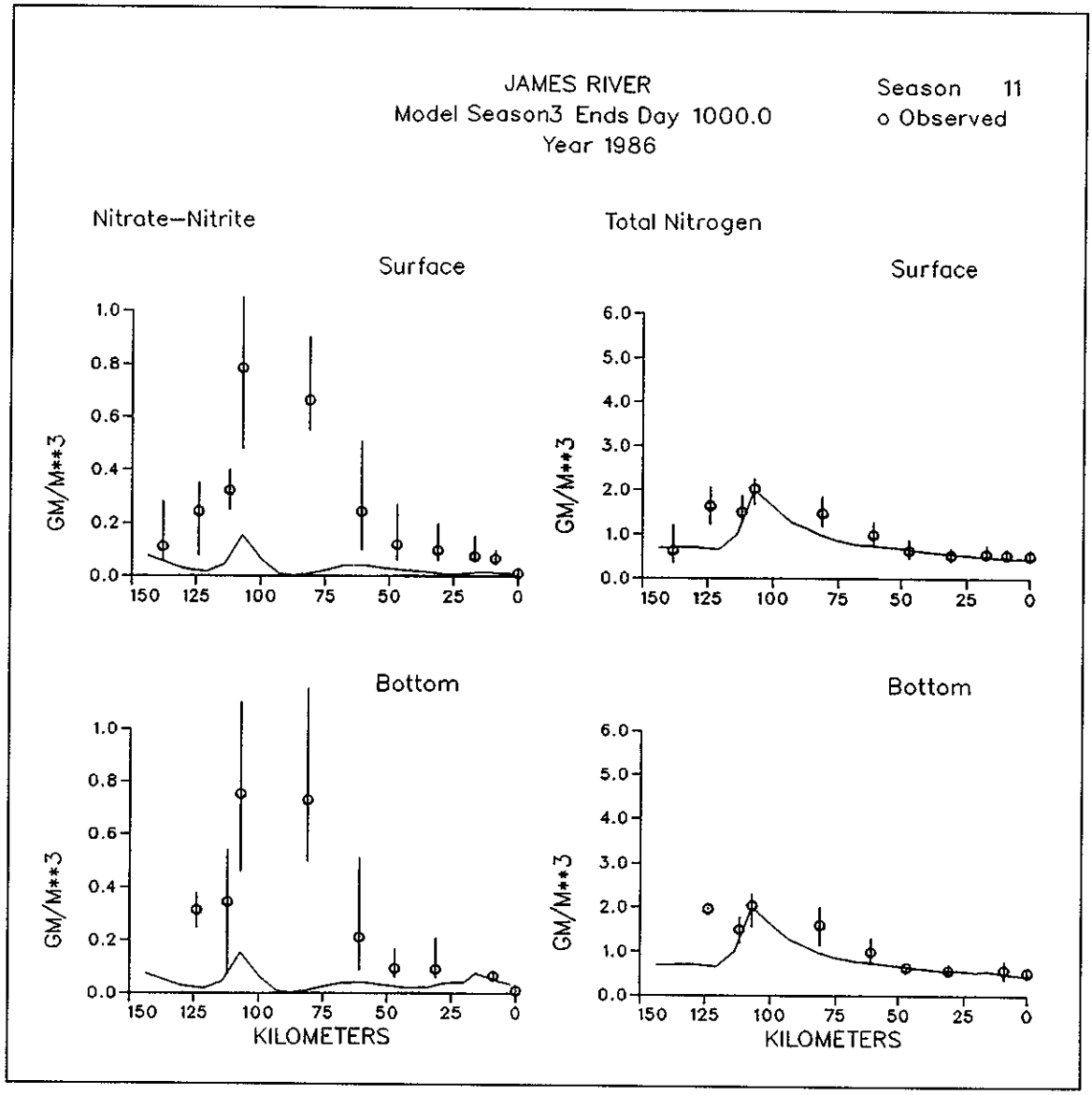

Figure 12-11. (Sheet 3 of 5)

Zone Two was also the site of a chlorophyll maximum located upstream of maximum solids concentration (Figure 12-36). Similar chlorophyll maxima have been observed in other estuaries, notably the Rappahannock (Anderson 1986) and James (Moon and Dunstan 1990), although the mechanisms responsible for the maxima are controversial.

The model was unable to reproduce the features associated with the freshwater-saltwater transition region. In order to reproduce the phosphorus maximum, suspended solids and phosphate exchange with the solids must be added to the model. The chlorophyll maximum occurs coincident with the highest extinction in the river (Figure 12-37). If algae are to grow there, revision of the existing light-growth relationship is required. Reproduction of both the

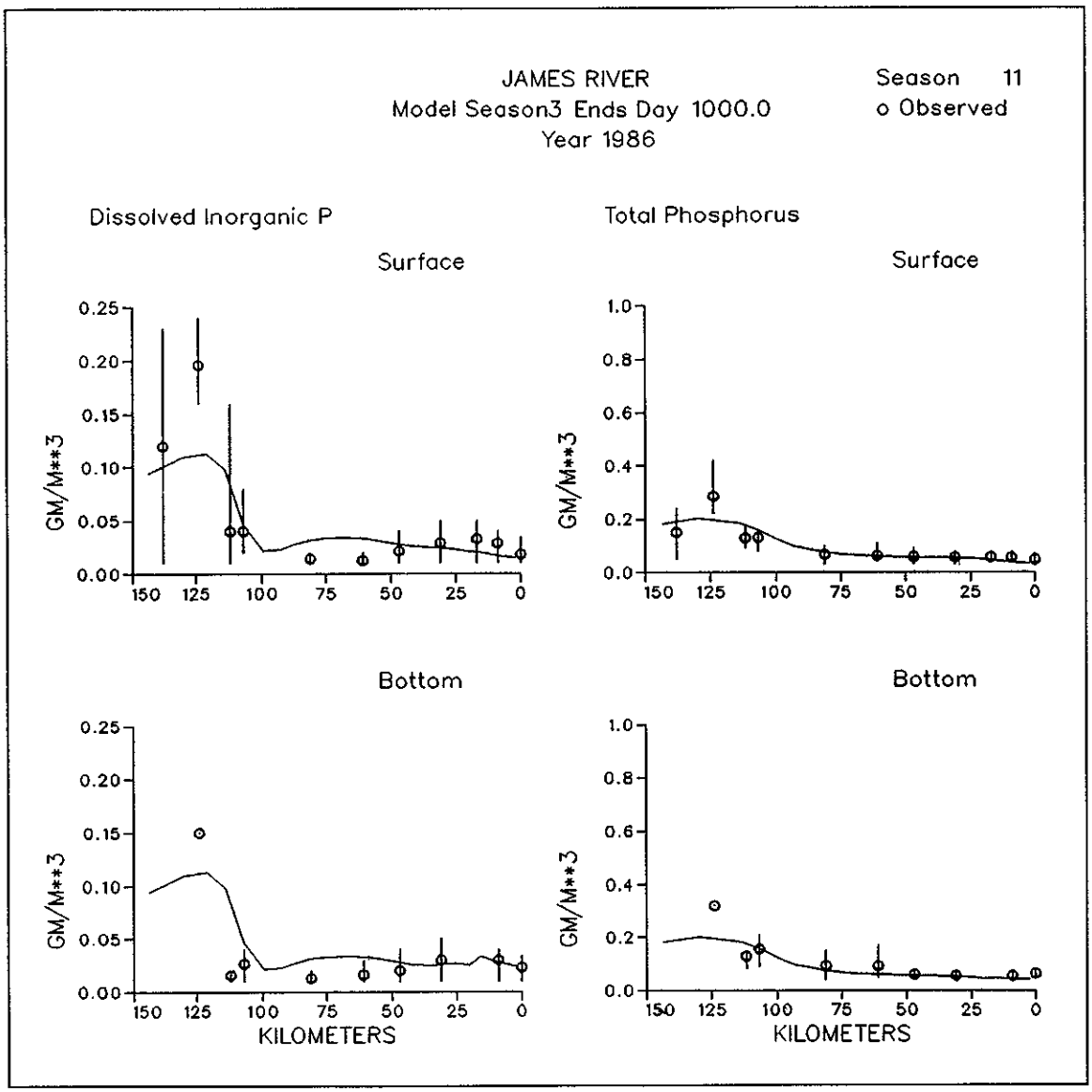

Figure 12-11. (Sheet 4 of 5)

phosphorus and chlorophyll maxima require accurate representation of hydrodynamics near the limit of salt intrusion.

Sediment-Water Fluxes

Sediments in the Potomac exhibited a range of behaviors. In the upper Potomac, sediments were an exclusive sink of nitrogen and phosphorus (Figure 12-18). Virtually all particulate nitrogen and phosphorus deposited was retained and dissolved phosphate was occasionally scavenged from the water column. Deposition and retention of phosphorus were a result of parameter

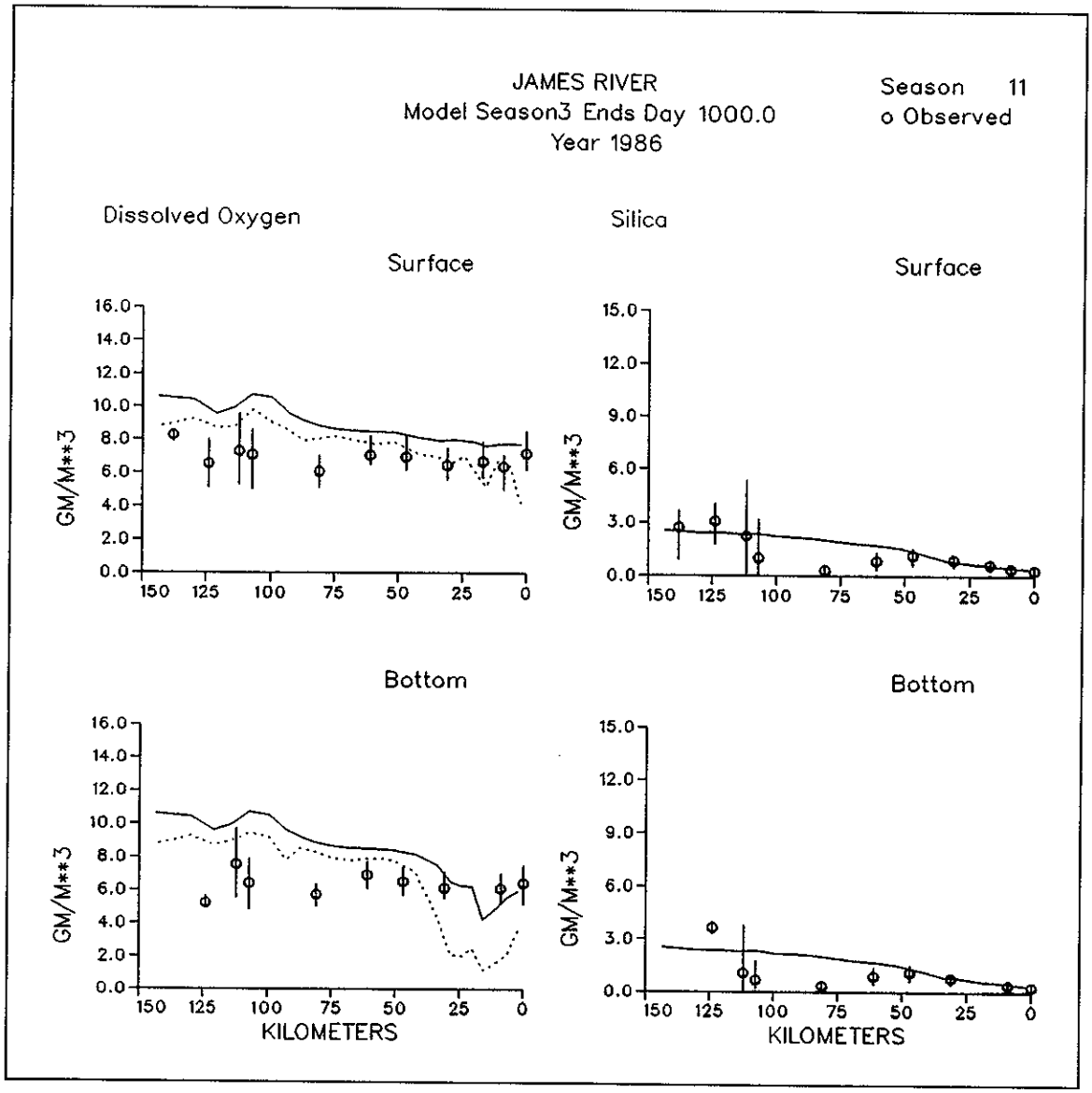

Figure 12-11. (Sheet 5 of 5)

adjustments performed to calibrate phosphorus concentration in the overlying water. Phosphorus scavenging has been observed in the vicinity, however (Cerco 1985b). Substantial phosphorus recycling from the sediments is usually episodic and associated with algal-induced pH fluctuations (Thomann et al. 1985).

In the middle (Figure 12-22) and lower (Figure 12-26) Potomac, correspondence between observed and modeled sediment-water fluxes was good. As in the mainstem, temperature was the prime determinant of sediment oxygen demand, ammonium release, and silica release. Phosphorus release was most dependent on dissolved oxygen concentration in the overlying water. In the middle Potomac, release was sporadic, corresponding to sporadic hypoxic

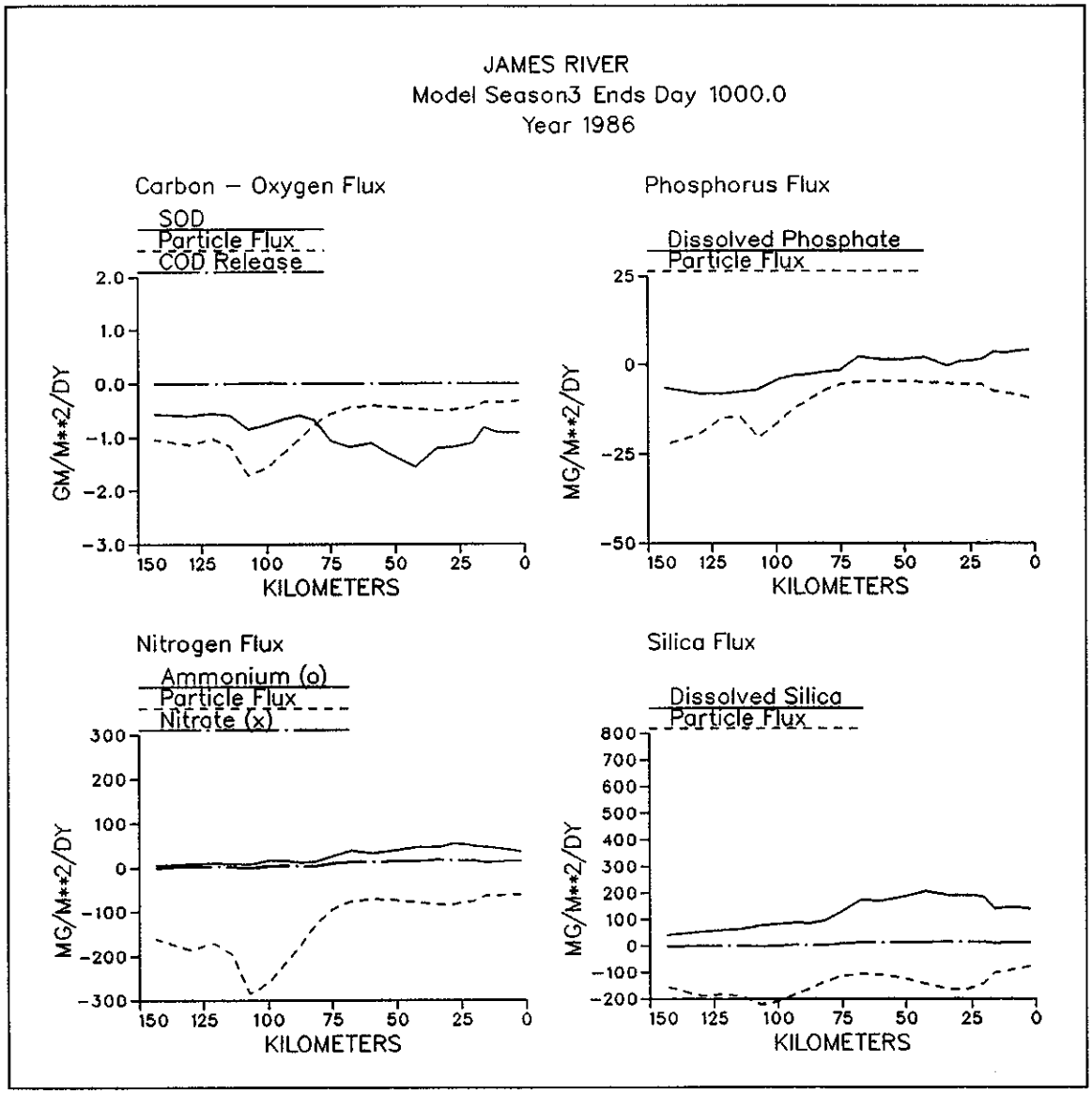

Figure 12-12. Predicted Sediment-Water Fluxes Along James River Longitudinal Transect, Season Three, 1986

events. In the lower Potomac, release was persistent, corresponding to persistent anoxia. The model predicted sediment oxygen demand as high as 2 gm m^{-2} day^{-1}, which often corresponded well with observations. Extreme observations, up to 3 gm m^{-2} day^{-1}, were not reproduced by the model, however.

Limited sediment carbon, nitrogen, and phosphorus observations, circa 1980, were available for the Potomac (Goodwin et al. 1984). Model correspondence with these observations was reasonable in the lower 100 km of the estuary (Figure 12-31). In the upper 75 km, predicted concentrations were

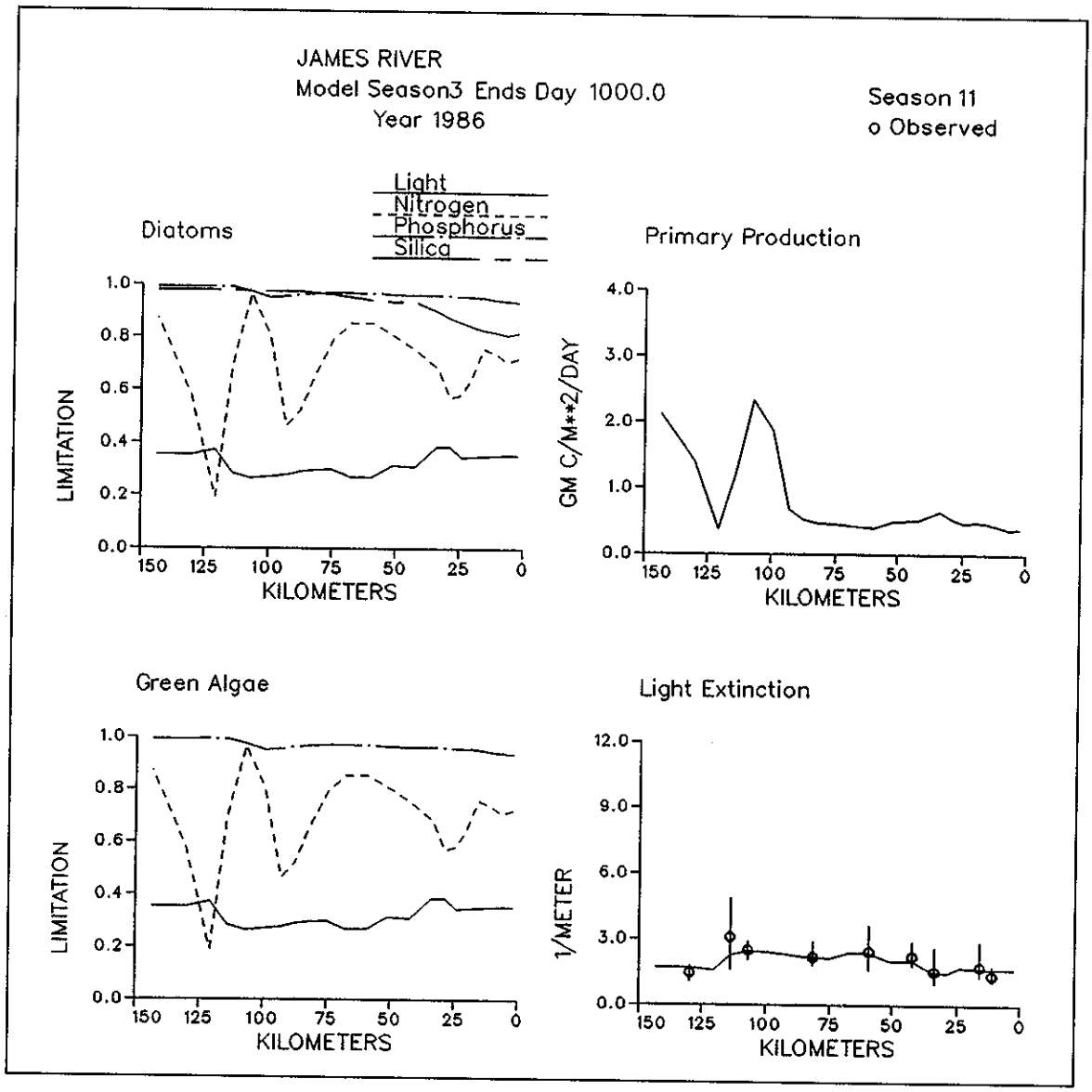

Figure 12-13. Predicted Diagnostic Information Along James River Longitudinal Transect, Season Three, 1986

well in excess of the observations. Increased burial to deep, isolated sediments was required in the model to match observations.

Diagnostic Information

Agreement between modelled and observed primary production in the upper Potomac was excellent (Figure 12-20). Occasional phosphorus nutrient limitation was computed by the model. Phosphorus is commonly accepted as the limiting nutrient in the freshwater Potomac but the computed limitation was

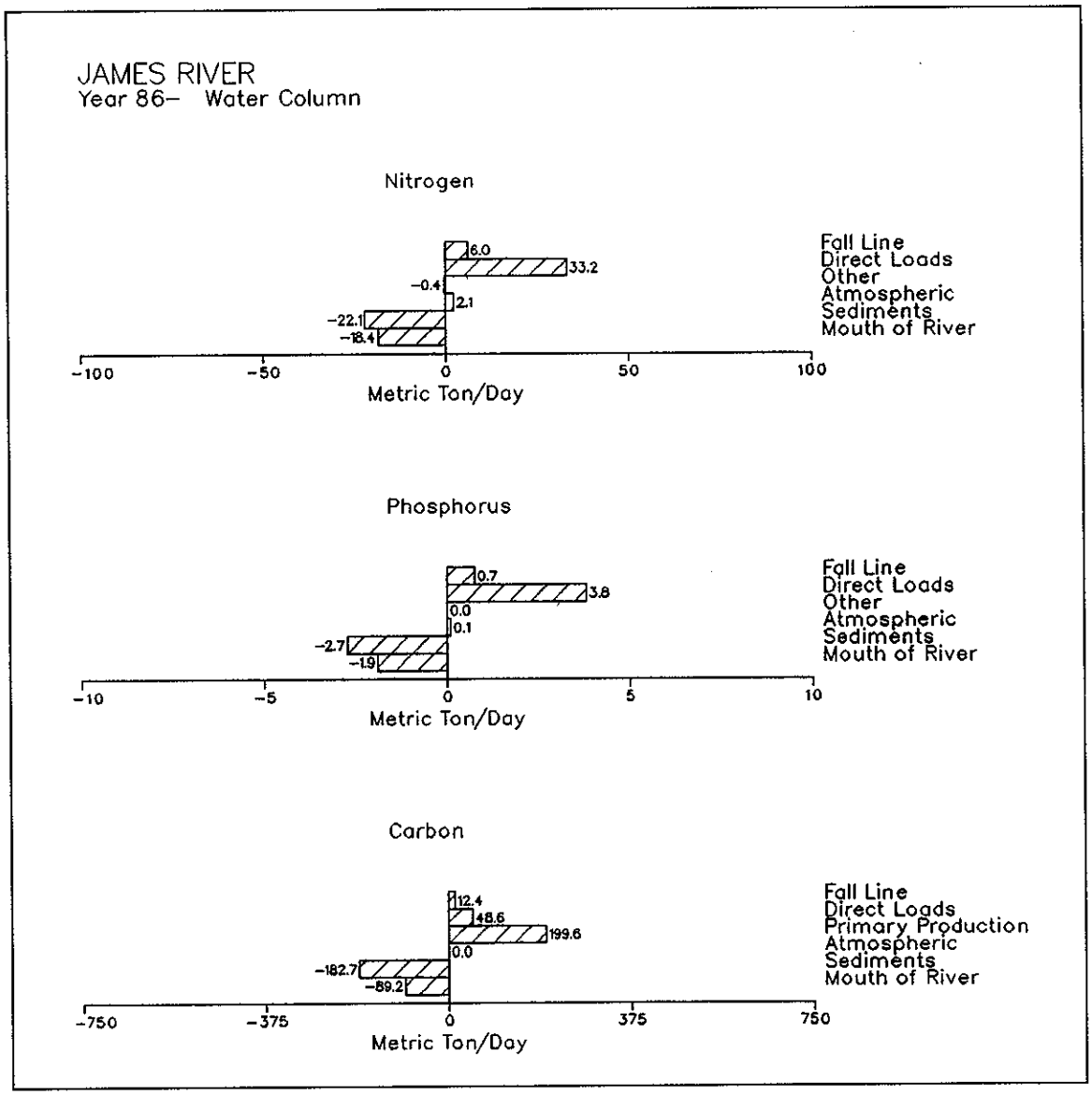

Figure 12-14. Annual Mass Balance for James River Water Column, 1986

less than expected based on stringent phosphorus discharge controls in the vicinity.

Virtually no nutrient limitation was computed in the middle Potomac (Figure 12-24). In Zone Two, algae were strongly constrained by light limitation. Due to light limitation, net primary production in summer was negligible in the model although measurements indicated otherwise.

The lower Potomac exhibited a spring diatom bloom coincident with the bloom in the mainstem. The model indicated the bloom was limited by silica rather than phosphorus (Figure 12-28). In summer, minimal phosphorus limitation was computed in the lower Potomac. Phosphate predictions in Zone

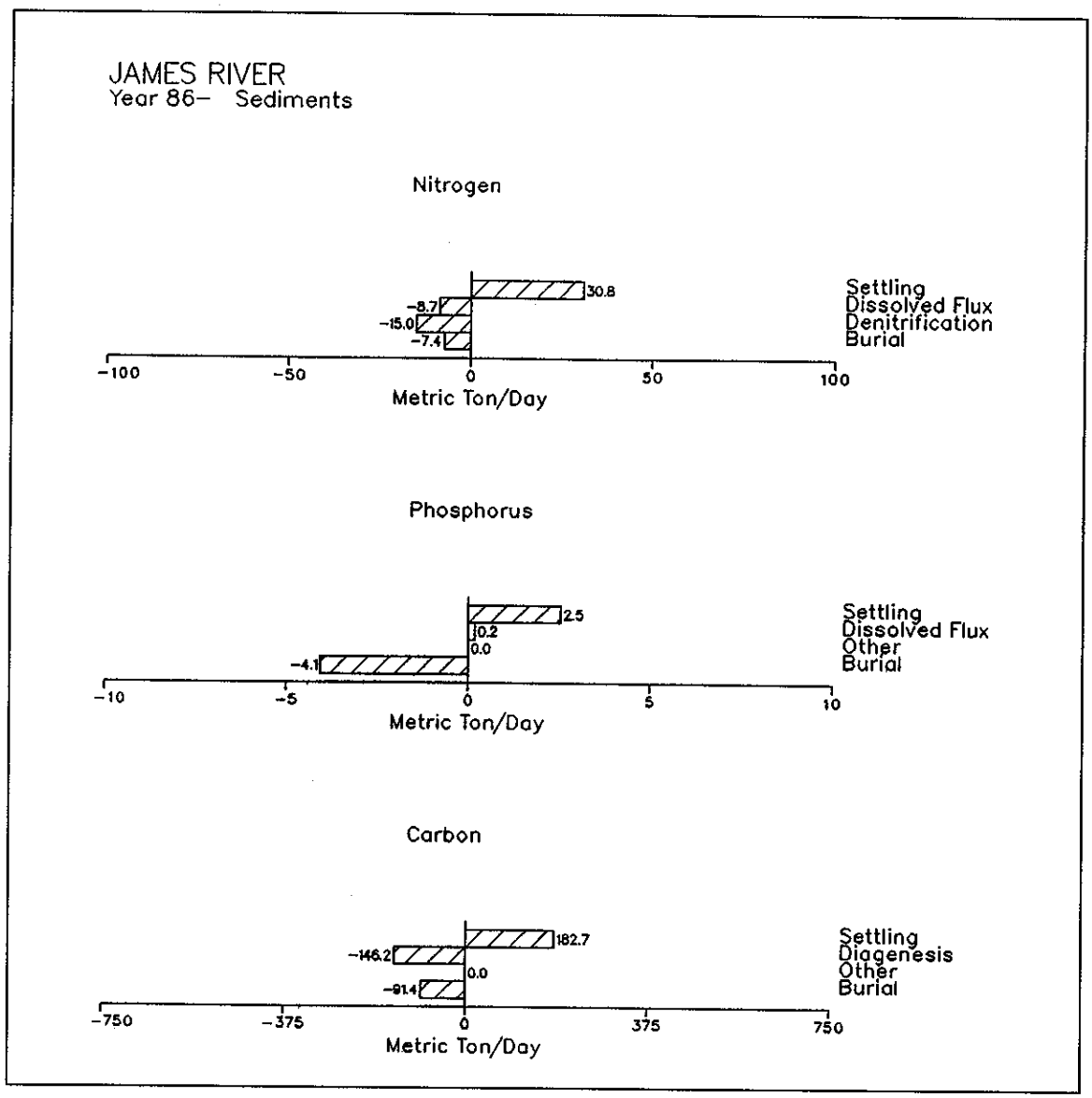

Figure 12-15. Annual Mass Balance for James River Sediments, 1986

Three were largely accurate (Figure 12-25) so the magnitude of the computed phosphorus limitation was correct. Computed nitrate was often in excess of observations, however. As a result, the model under-computed the extent of nitrogen limitation in the lower Potomac. The single limiting nutrient, nitrogen or phosphorus, could not be evaluated. Computed primary production was usually less than observed.

Carbon and Nutrient Budgets

As with the mainstem Bay, primary production was the major source of carbon (and oxygen demand) in the Potomac River (Figure 12-38). Fall-line

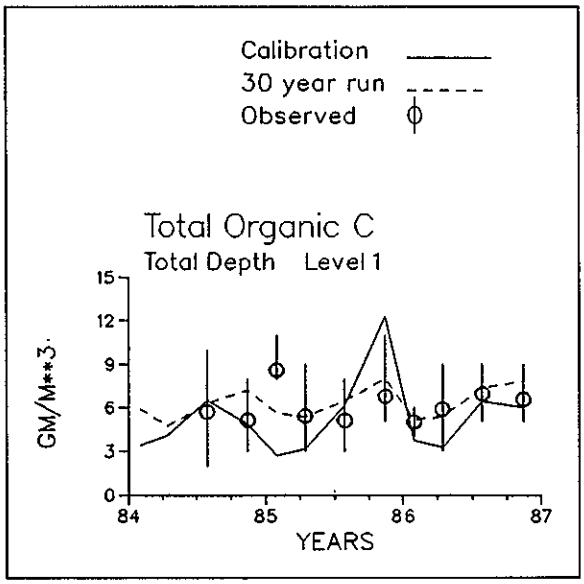

Figure 12-16. Comparison of Regression and Watershed Model Total Organic Carbon in James River Zone One (Calibration is from Watershed Model, 30-year run is from regression)

loading was second largest source. Nearly 80% of total carbon load was deposited in the sediments. The rest was exported to the mainstem. In the sediments, nearly 80% of deposited carbon was oxidized (Figure 12-39) and the remainder was buried to deep, isolated sediments.

In the 1986 budget, fall-line and direct nitrogen loads were roughly equivalent. The fall-line contribution was influenced by the dry hydrology, however. Fall-line loads were, by far, the major source of phosphorus to the Potomac. A larger fraction of nitrogen loads, ≈38%, was exported to the mainstem than phosphorus loads, ≈26%. A small quantity of nitrogen was lost through water-column denitrification but most of the nitrogen, and all of the phosphorus, not exported to the mainstem was deposited in the sediments. Denitrification was the primary pathway for removal of sediment nitrogen. Burial was the sole sediment sink of phosphorus.

Suggested Improvements

The present calibration is nearly the best that can be obtained in the Potomac with the existing model. Some improvement is possible in the calibration of cyanobacteria near the fall line. Substantial improvements throughout the estuary require revision of loads and additions to the model structure, however.

Loading

The Watershed model was calibrated to exacting standards and generally performed well throughout the system. In the Potomac, however, the model apparently over-computed the fraction of dissolved phosphorus in the total fall-line phosphorus load. Occasional over-estimation of the total phosphorus load was apparent also. Improved predictions of both phosphorus and algae in the upper Potomac require revisions to the computation of fall-line phosphorus loads.

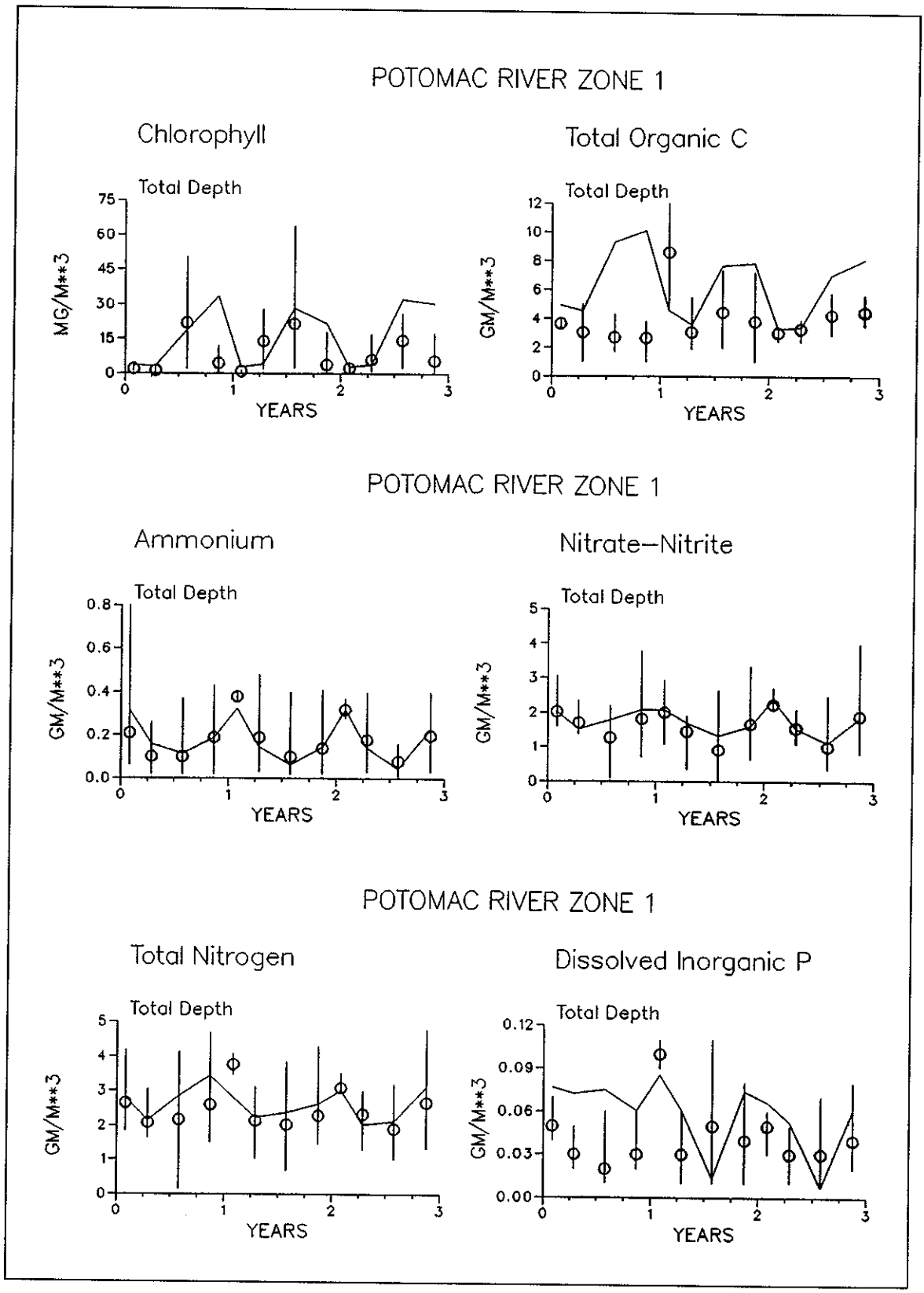

Figure 12-17. Time Series of Predicted and Observed Concentrations in Potomac River Zone One (Continued)

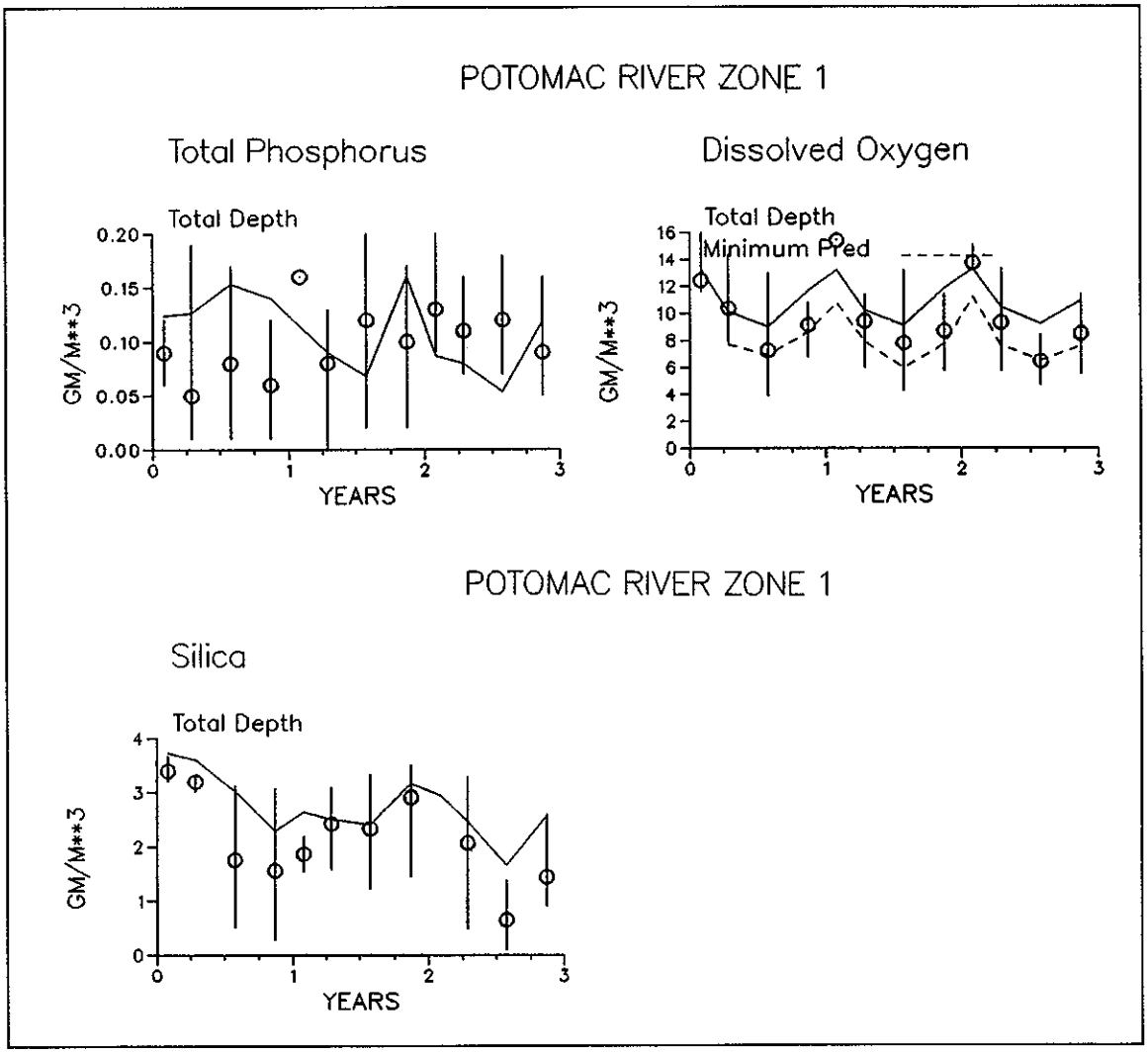

Figure 12-17. (Concluded)

The point-source loads in the Potomac were the most accurately quantified in the system. At times, however, the fraction of ammonium in the loads appeared under-estimated while the nitrate was over-estimated. The influence of the existing fractionation is apparent to a small extent in the figure in the present volume (Figure 12-29) and to a large extent in figures in the appendix. The fractionation of nitrogen in Potomac point-source loads should be re-examined.

The Transition Zone

The Potomac exhibits several characteristic phenomena near the transition from tidal freshwater to saline water. In this region, flow convergence occurs as density-driven upstream circulation meets downstream flowing freshwater. Suspended particles are concentrated near the convergence and form the

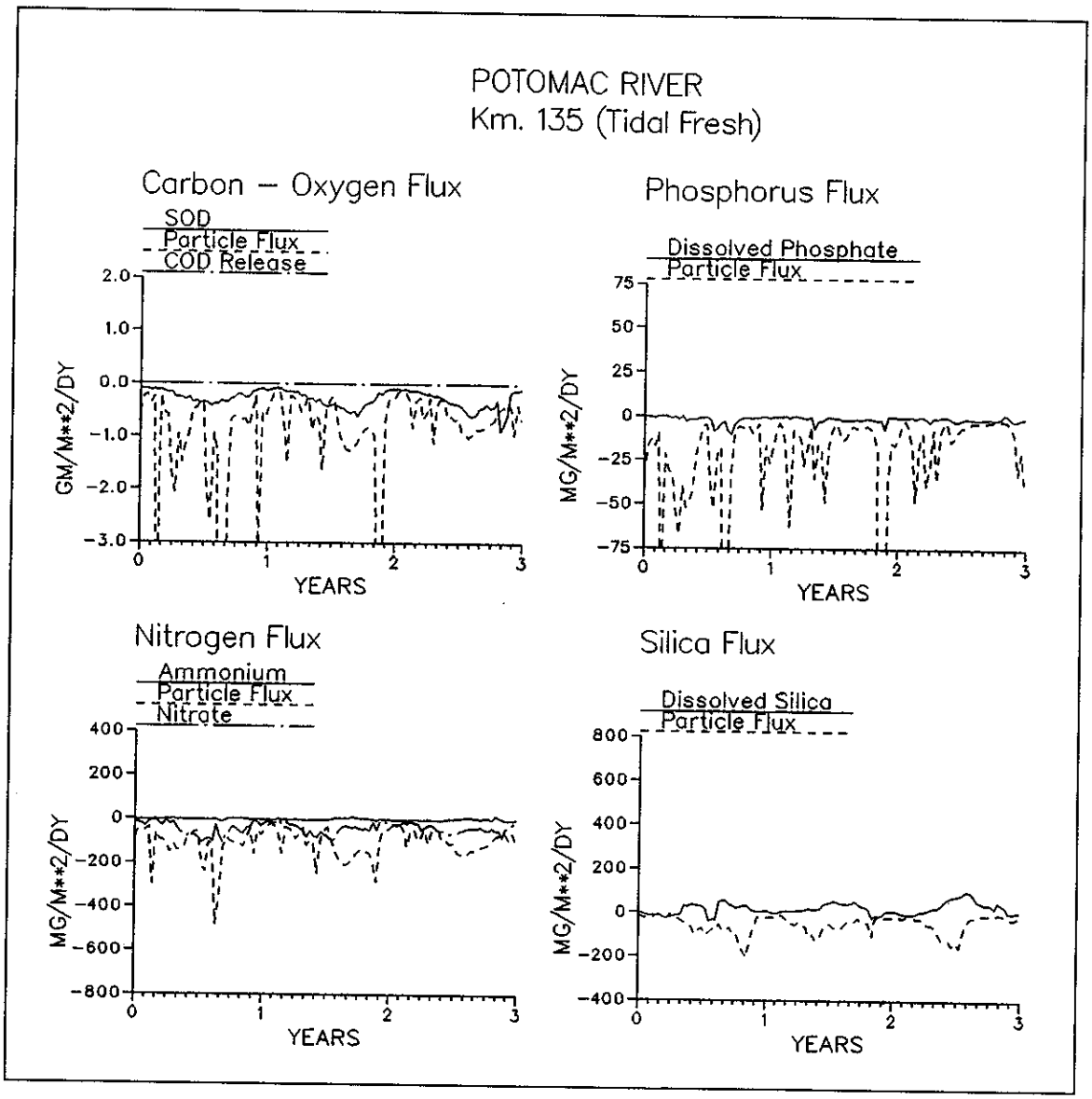

Figure 12-18. Time Series of Predicted Sediment-Water Fluxes in Potomac River Zone One

turbidity maximum. Particulate phosphorus is also trapped and concentrated in the turbidity maximum. Upstream of the maximum, a concentration of algae occurs. Reasons for the algal concentration are not well-known. The concentration may indicate physical aggregation or production of algae in a region of nutrient availability.

The present model does not represent the characteristic phenomena in the transition region. Physical concentration of particles does not occur to a great extent. Absence of concentration may reflect coarse representation of hydrodynamics in the convergence. Particle concentration is not solely a function of transport, however. Settling velocity in the water column and net deposition to the sediments are additional influences. Representation of particle

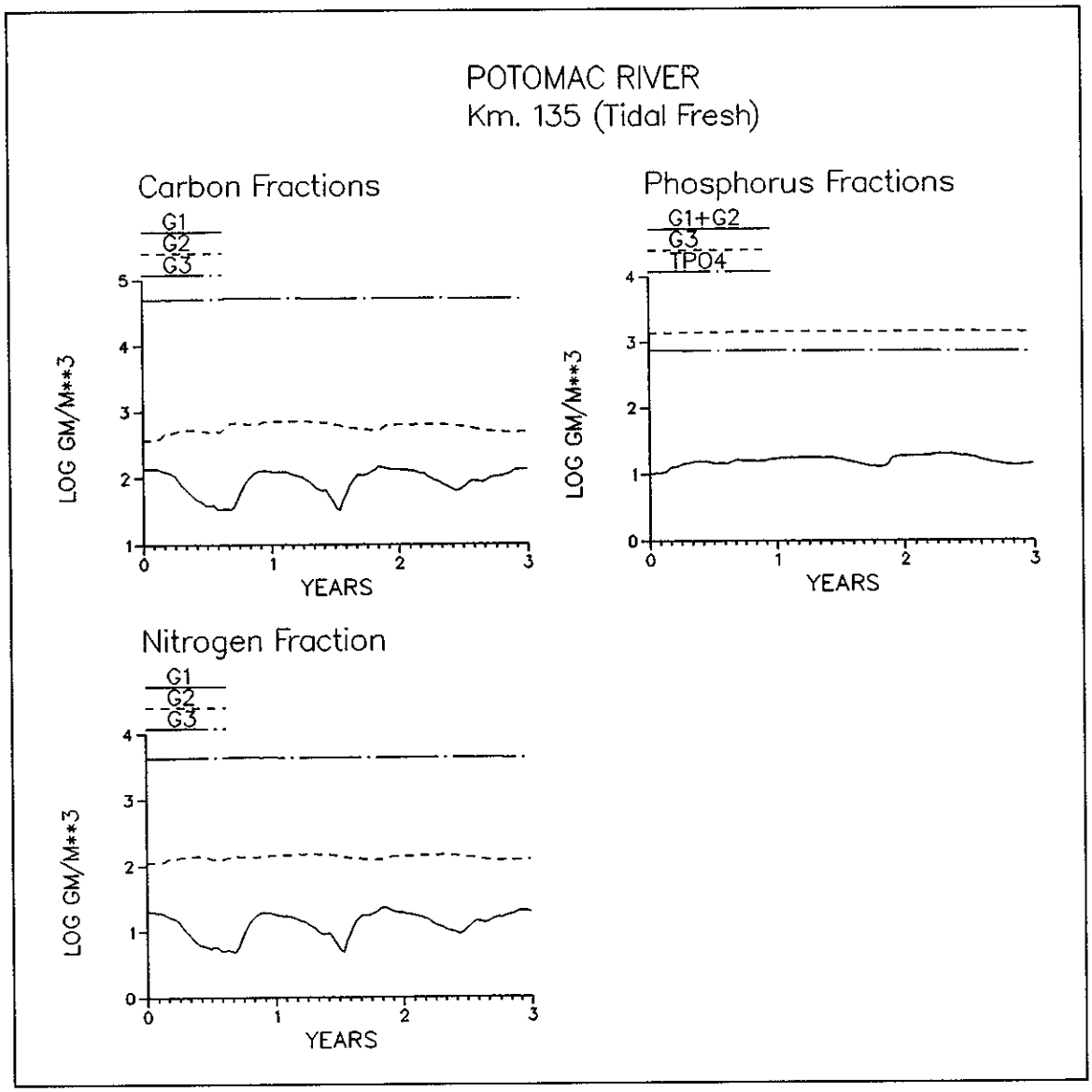

Figure 12-19. Time Series of Predicted Sediment Particulate Carbon, Nitrogen, and Phosphorus in Potomac River Zone One

concentration in the transition zone is required to accurately match observations but may be beyond the predictive capabilities of a water-quality model.

Independent of the problems associated with particle concentration, computation of phosphorus in the transition region requires addition of particulate inorganic phosphorus to the suite of state variables.

Primary production data indicate algae grow in the turbid waters of the transition region. Revision to the growth-light formulation, to allow this production, is required.

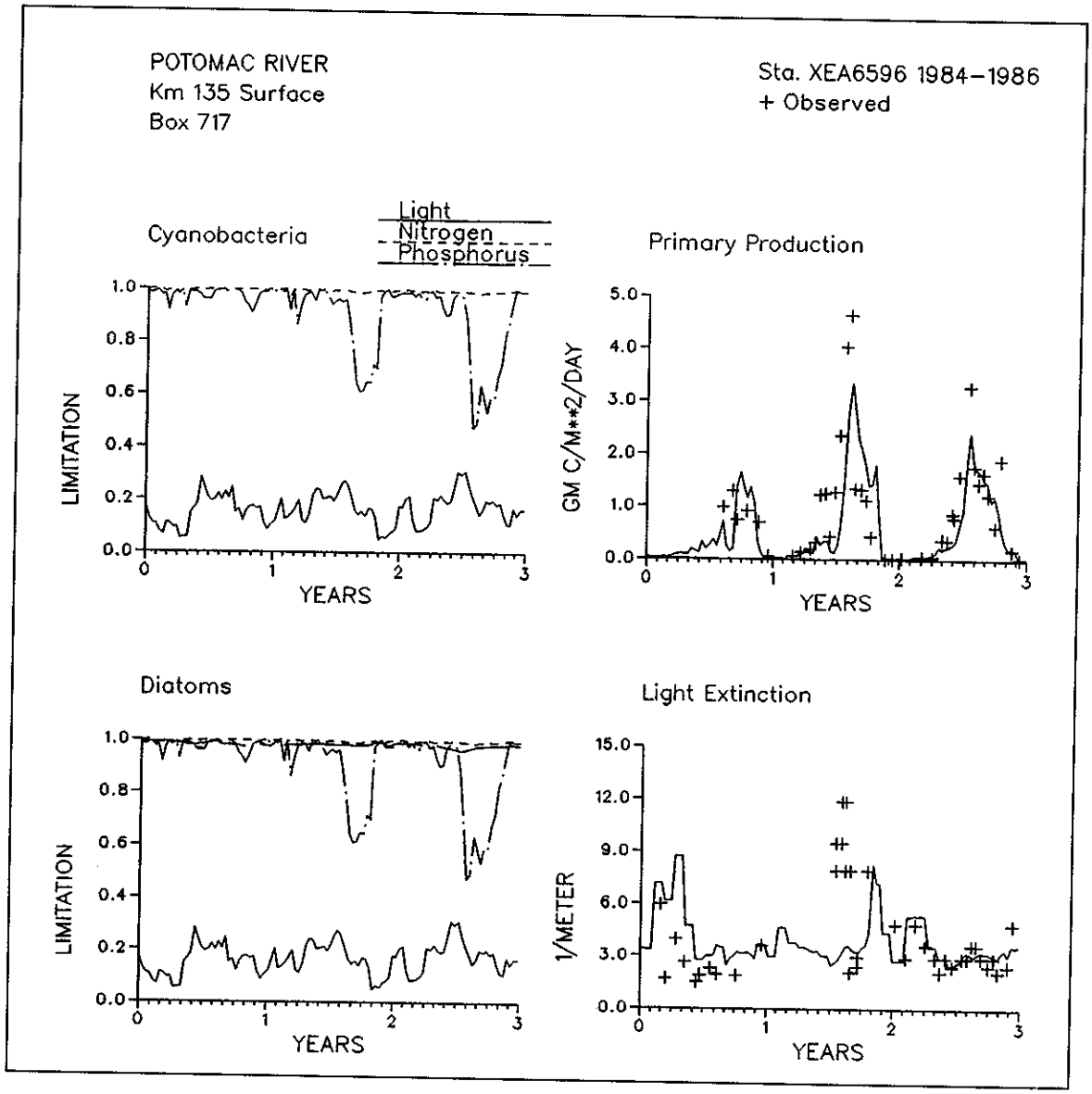

Figure 12-20. Time Series of Predicted and Observed Diagnostic Information in Potomac River Zone One

Grid Resolution

The central portion of the Potomac estuary is characterized by sharp bends and rapid transitions in depth. The present grid provides coarse representation of these transitions. Grid size is responsible for the "jumpy" longitudinal salinity distribution (Figure 12-29) and influences the computation of hydrodynamics in the saltwater-freshwater transition region. Additional longitudinal resolution will smooth computed concentration gradients in regions of steep geometrical change and may be required to accurately model the phenomena characteristic of the freshwater-saltwater transition region.

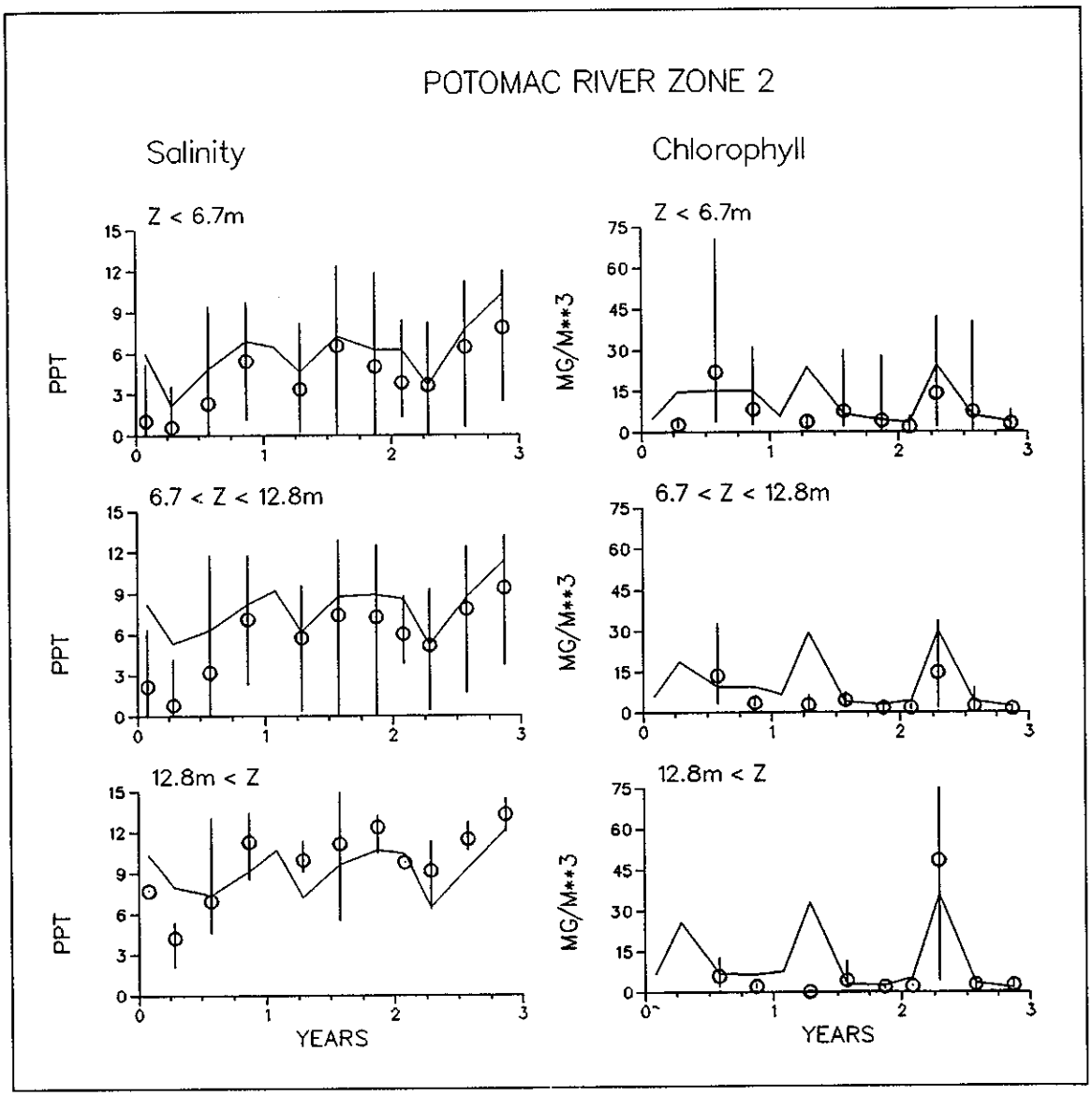

Figure 12-21. Time Series of Predicted and Observed Concentrations in Potomac River Zone Two (Sheet 1 of 5)

Additional lateral resolution is especially needed immediately downstream of the fall line. In the present grid, this region is only one cell wide. The width of the modelled channel is exaggerated and the extensive shoals and embayments of the prototype are not represented at all. The shoals and embayments are regions of extensive deposition and should be represented in order to correctly compute effects of sediment-water exchanges. The over-computation of sediment carbon and nutrients in the existing calibration is partially a result of settling fall-line loads exclusively into a narrow channel instead of a wide, shoal area.

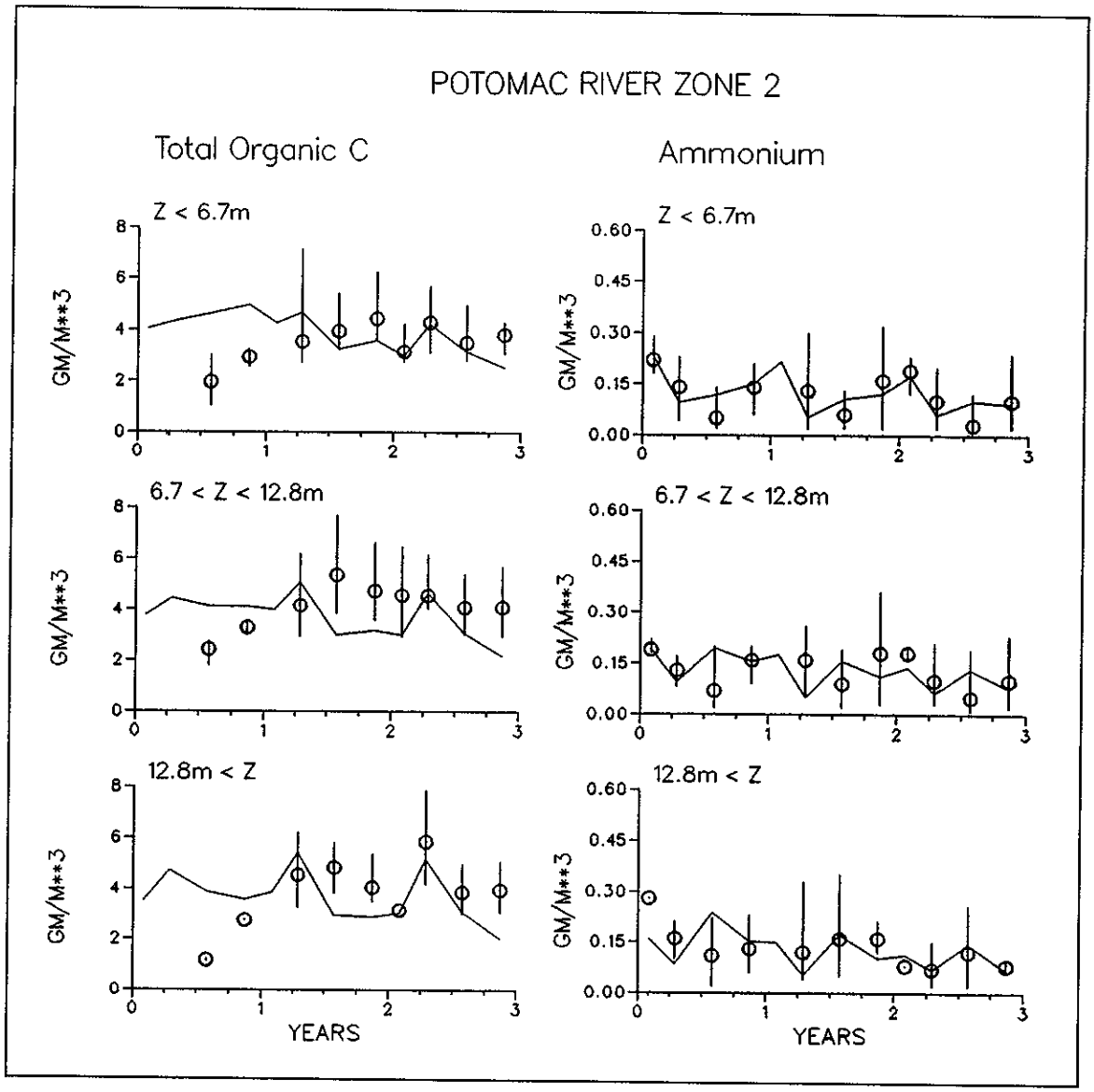

Figure 12-21. (Sheet 2 of 5)

Rappahannock, York, and Patuxent Rivers

Presentations for the remaining tributaries are limited to longitudinal plots of concentration, sediment-water fluxes, and diagnostic information. Plots are for Season Three of 1986. Runoff in all three rivers in 1986 was below the long-term mean (Table 2-4). Remaining plots are in the appendix.

In a qualitative sense, correspondence between predictions and observations is less satisfactory in the lesser tributaries than in the mainstem Bay and in the Potomac and James Rivers. The discrepancies partially originate in the

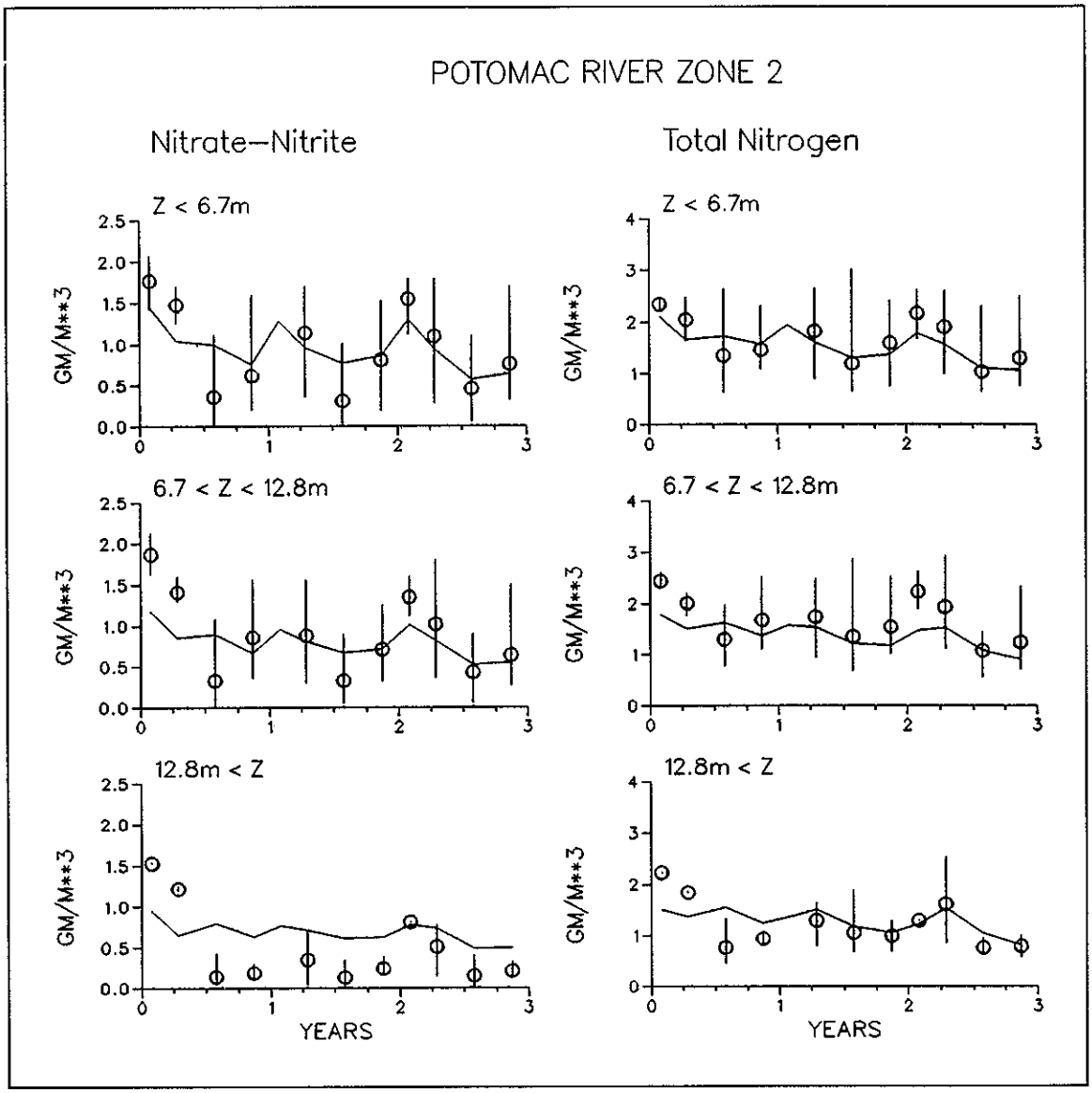

Figure 12-21. (Sheet 3 of 5)

diminished spatial scale of the lesser tributaries. The size of grid elements is roughly the same in all tributaries. Relatively, grid resolution is more coarse in the lesser tributaries than in larger water bodies. Channel width, depth, and geometrical transitions are only approximately represented. Diminished size also amplifies the influence of individual point sources and storm events on predicted concentrations.

The importance of extremely accurate loading information in the lesser tributaries cannot be over-emphasized. Correspondence between model and observations in the upper reaches of these bodies is determined more by loading than by evaluation of calibration parameters. A comparison of concentrations in Zone One of the Rappahannock, based on alternate estimates of

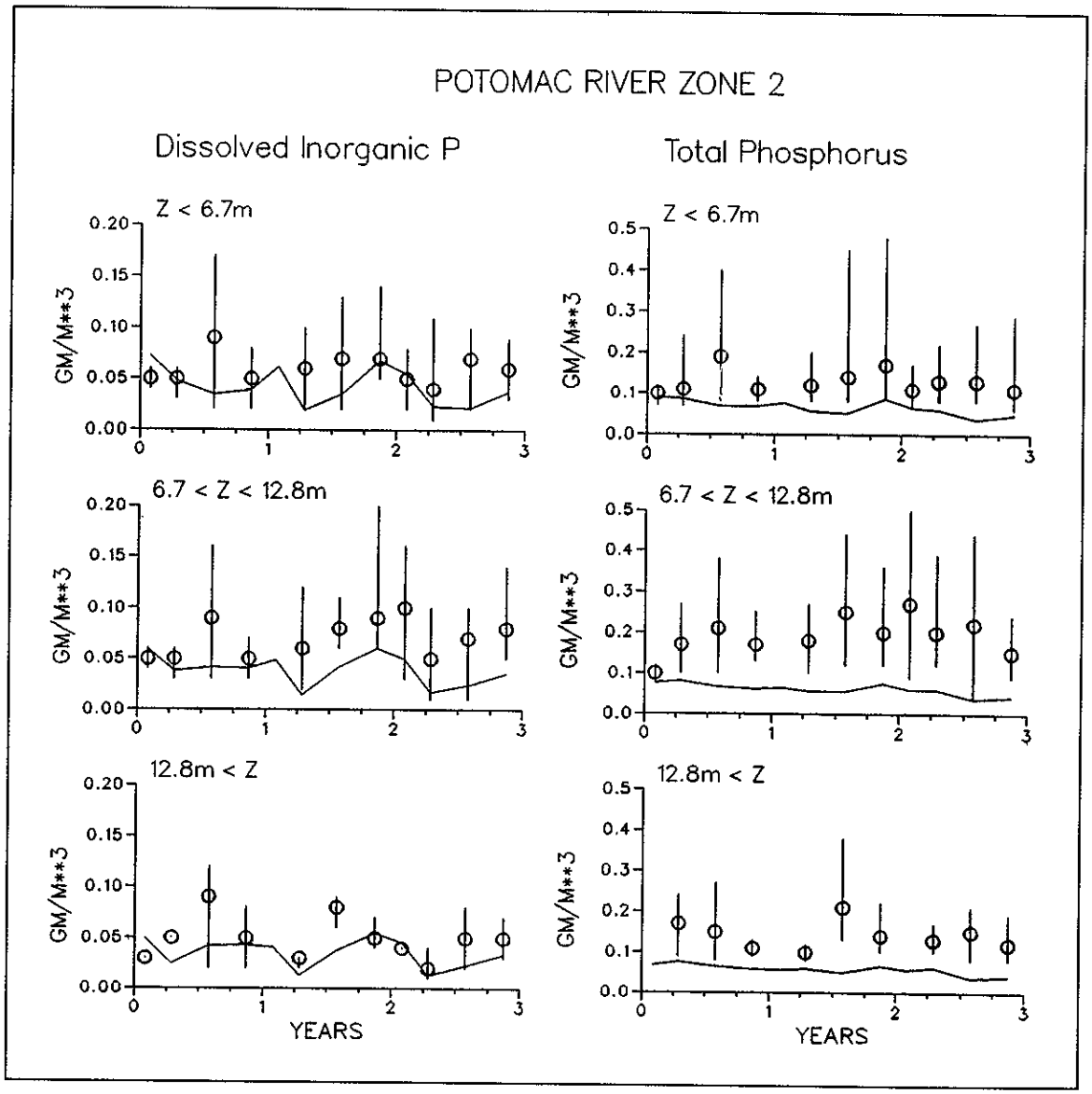

Figure 12-21. (Sheet 4 of 5)

fall-line loads, illustrates this point (Figure 12-49). Water-quality model predictions of total organic carbon, ammonium, and nitrate based on regression loads are clearly superior to predictions based on Watershed-Model loads. Water-quality predictions of total nitrogen differ based on the two loading sources but neither is superior. Little can be done to "calibrate" away these loading uncertainties.

Concentrations of phosphate and total phosphorus diverge from observations regardless of the source of fall-line load estimates. Insensitivity to fall-line loads suggests a discrepancy in another loading source. In 1986, no phosphorus observations were available at the Fredericksburg STP, the major point source on the river.

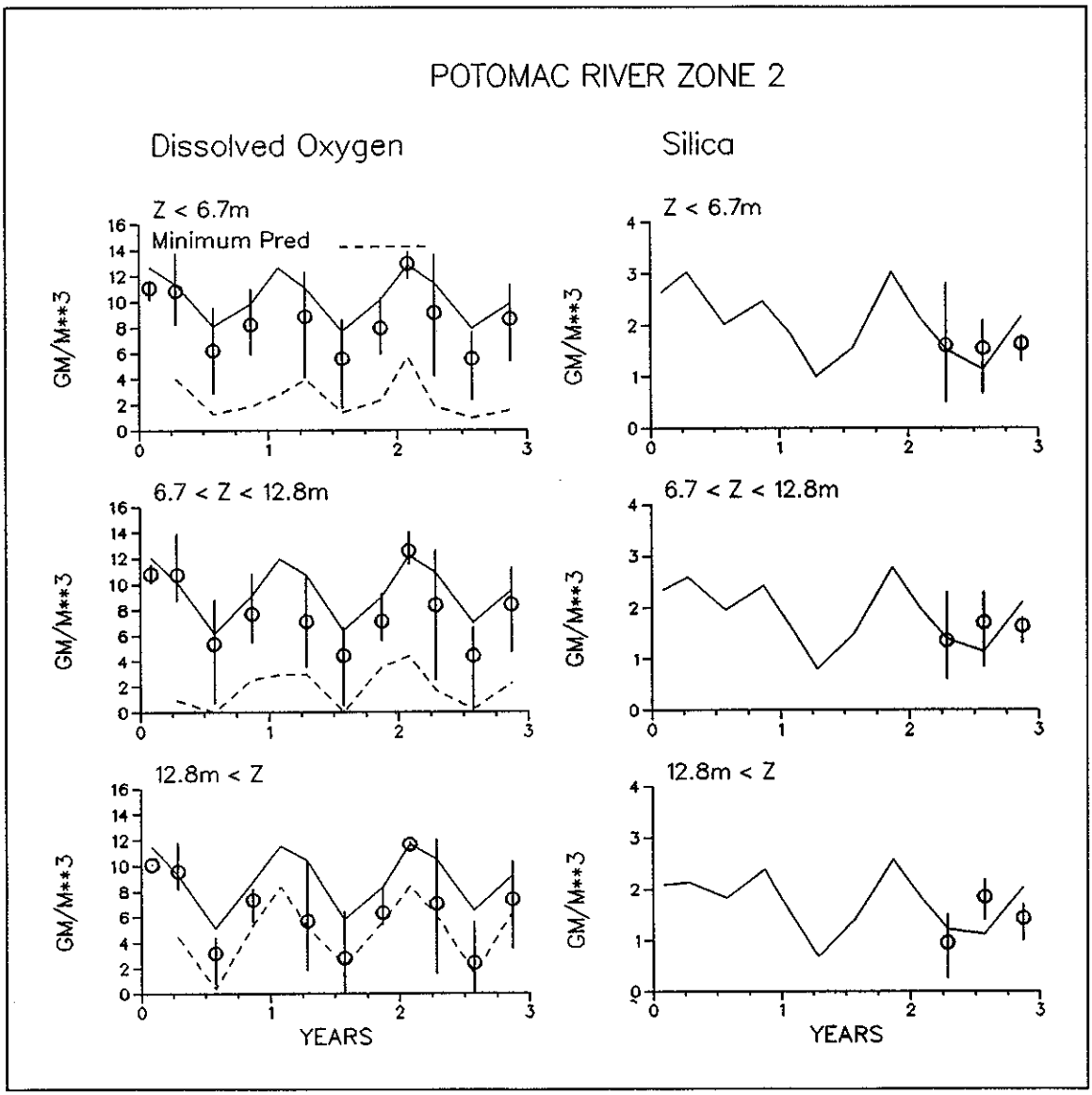

Figure 12-21. (Sheet 5 of 5)

Loads to the Rappahannock, York, and Patuxent are small fractions of the total loads to the Chesapeake Bay system. Uncertainty in the magnitude or composition of these loads has little influence on eutrophication processes in the mainstem or on the major findings of this study. Within the tributaries, however, careful quantification of loads is required before the model can be used for management purposes.

The lesser tributaries frequently exhibited the phenomena associated with the freshwater-saltwater transition noted for the Potomac. In summer, 1986, the Rappahannock chlorophyll maximum was located between km 100 and 125 (Figure 12-40), near the limit of salt intrusion and coincident with an observed peak in total phosphorus. In the Patuxent, the chlorophyll peak was at km 70

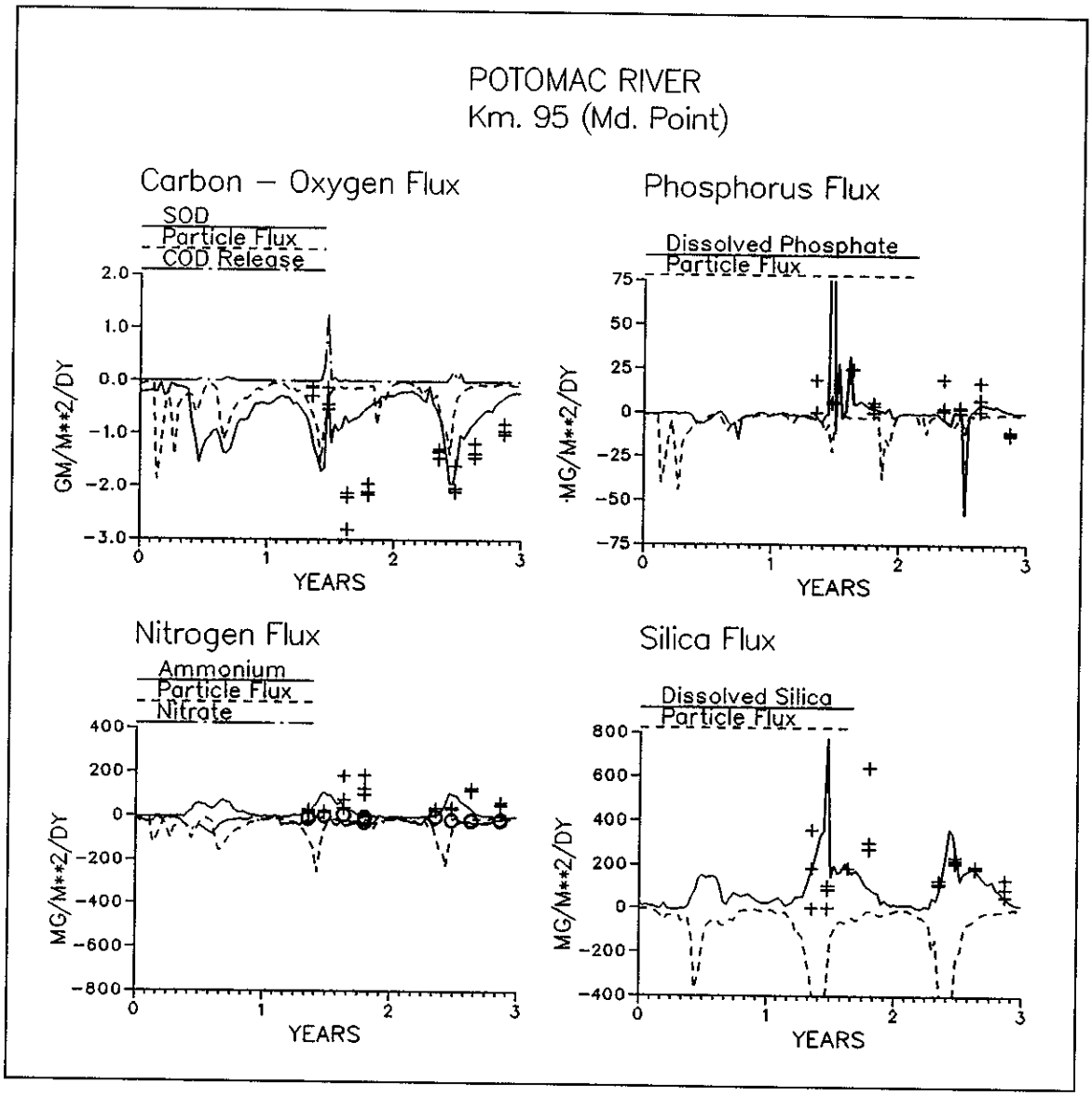

Figure 12-22. Time Series of Predicted and Observed Sediment-Water Fluxes in Potomac River Zone Two

(Figure 12-46), coincident with the highest light extinction observed in the river (Figure 12-48). Previous recommendations to improve the model in the transition region apply to the lesser tributaries as well.

Conclusions

Model performance in the two largest tributaries, the James and the Potomac, is largely satisfactory although model-data discrepancies occur. Performance in the Rappahannock, York, and Patuxent Rivers is less

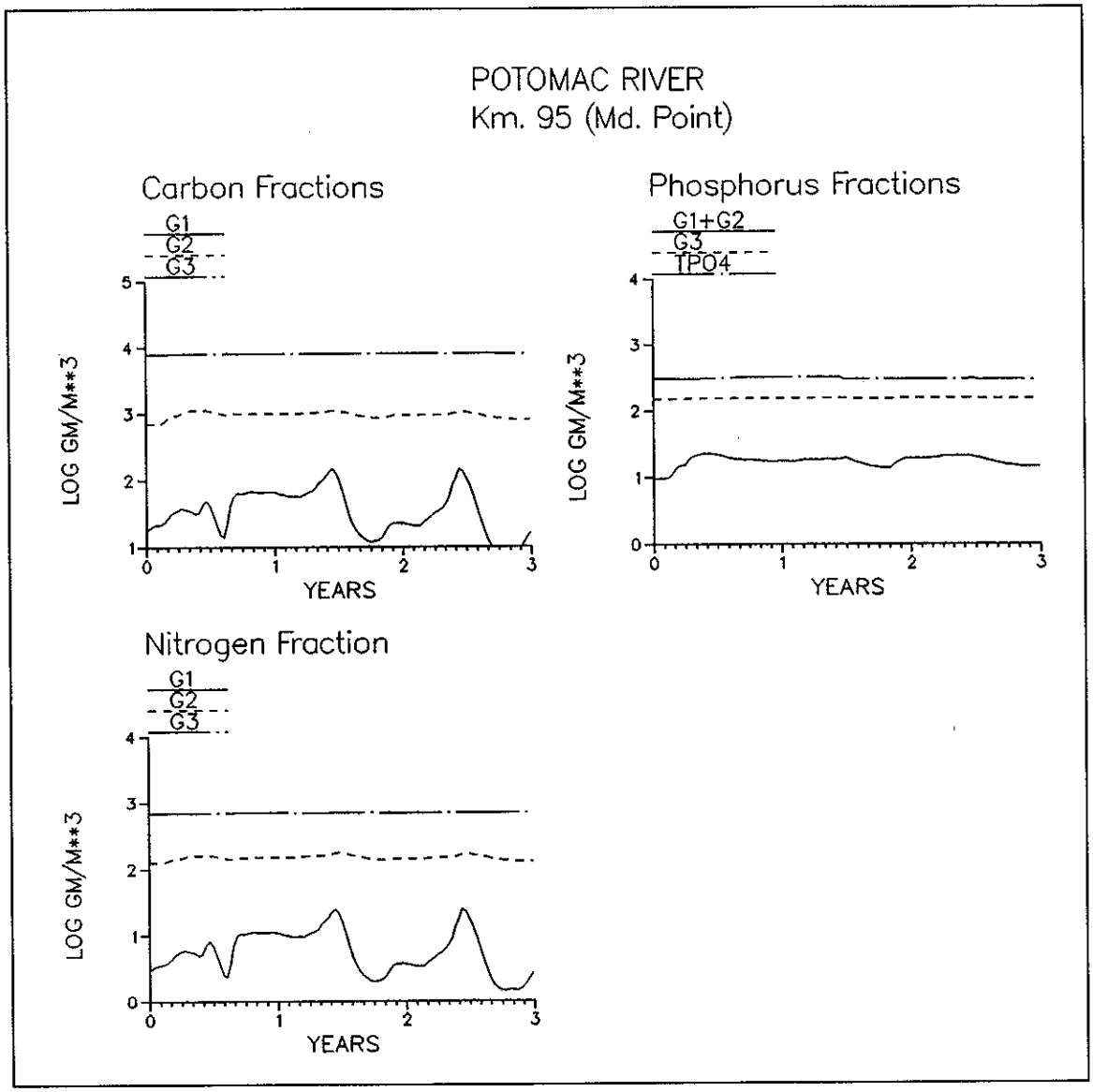

Figure 12-23. Time Series of Predicted Sediment Particulate Carbon, Nitrogen, and Phosphorus in Potomac River Zone Two

satisfactory and not consistent with the standards established for the mainstem Bay. The function of the tributaries as conduits of loads to the mainstem is simulated in the present model. The existing representation is of limited utility, however, in management of eutrophication processes within the tributaries.

The effort required to improve the current representation of the tributaries should not be underestimated. Each tributary presents a unique challenge. Optimal modeling of each tributary requires human and computational effort comparable to the investment in the present model of the system. Starting

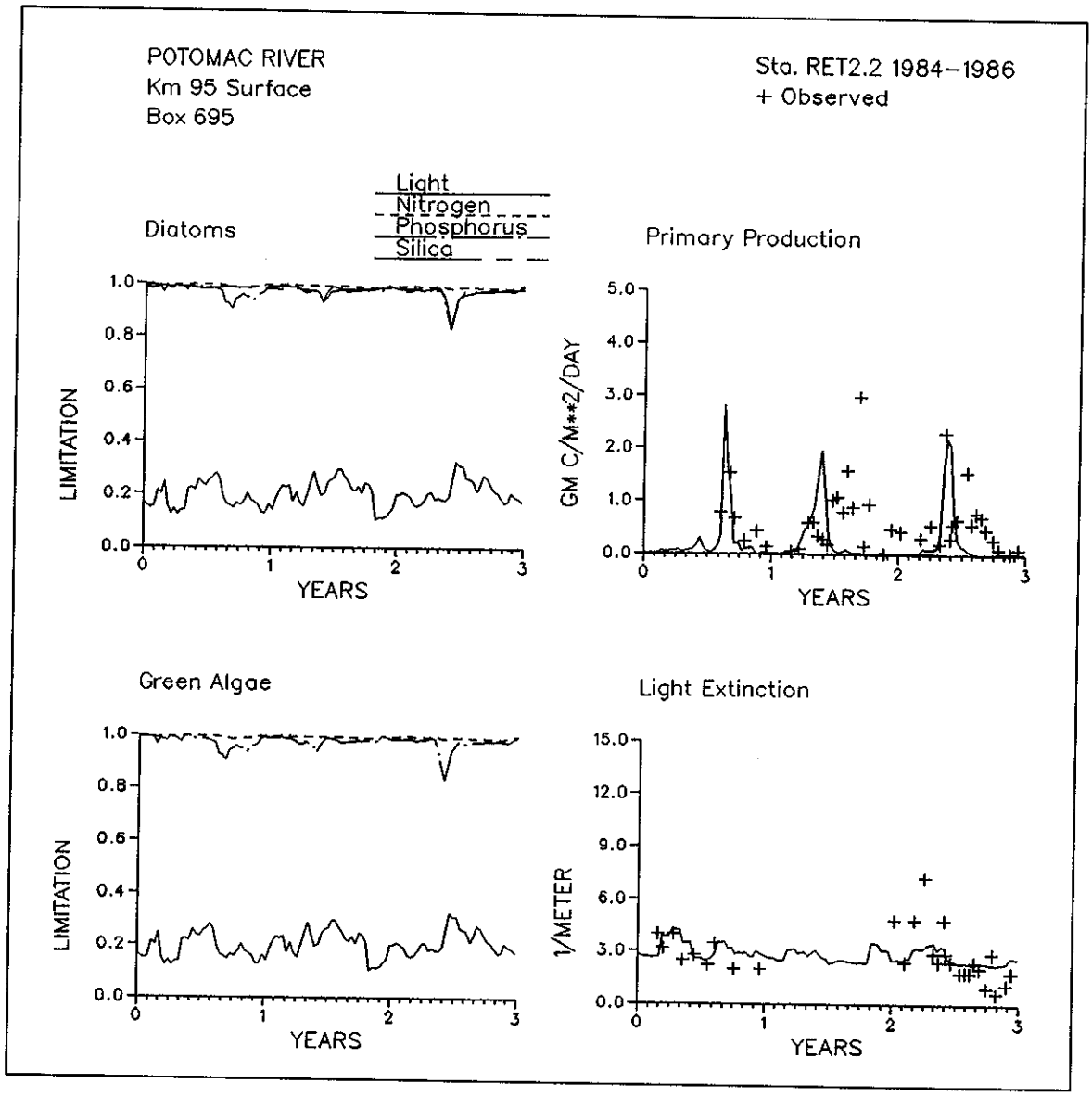

Figure 12-24. Time Series of Predicted and Observed Diagnostic Information in Potomac River Zone Two

points for improved representation, common to all tributaries, have been identified. These are:

1) Magnitude and composition of loads must be quantified with extreme accuracy.

2) Phenomena occurring near the limit of salt intrusion must be represented. These include convergent flows, physical concentration of particulate phosphorus, and the chlorophyll maximum.

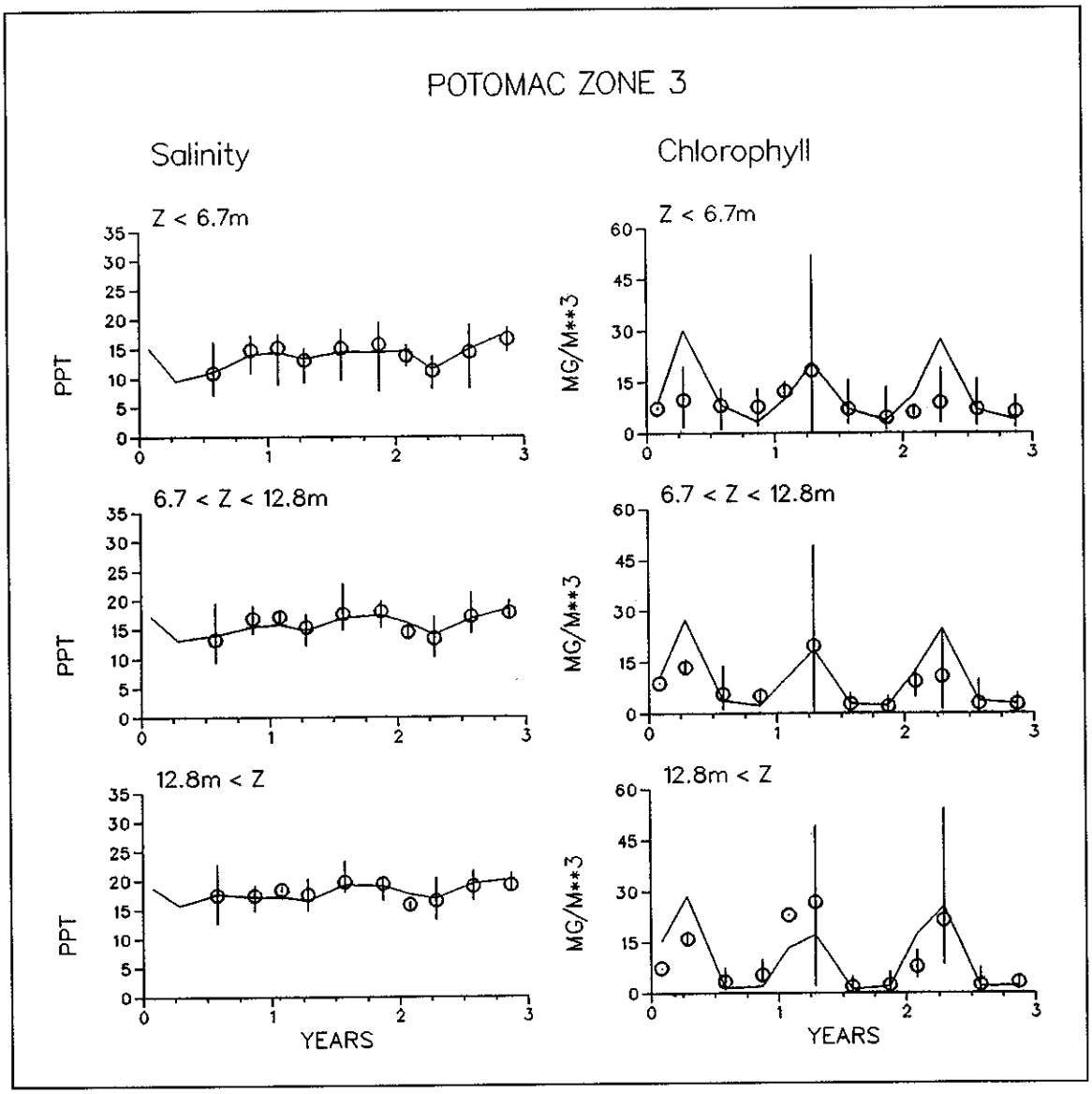

Figure 12-25. Time Series of Predicted and Observed Concentrations in Potomac River Zone Three (Sheet 1 of 5)

3) Longitudinal and lateral resolution of the tributary grids should be improved.

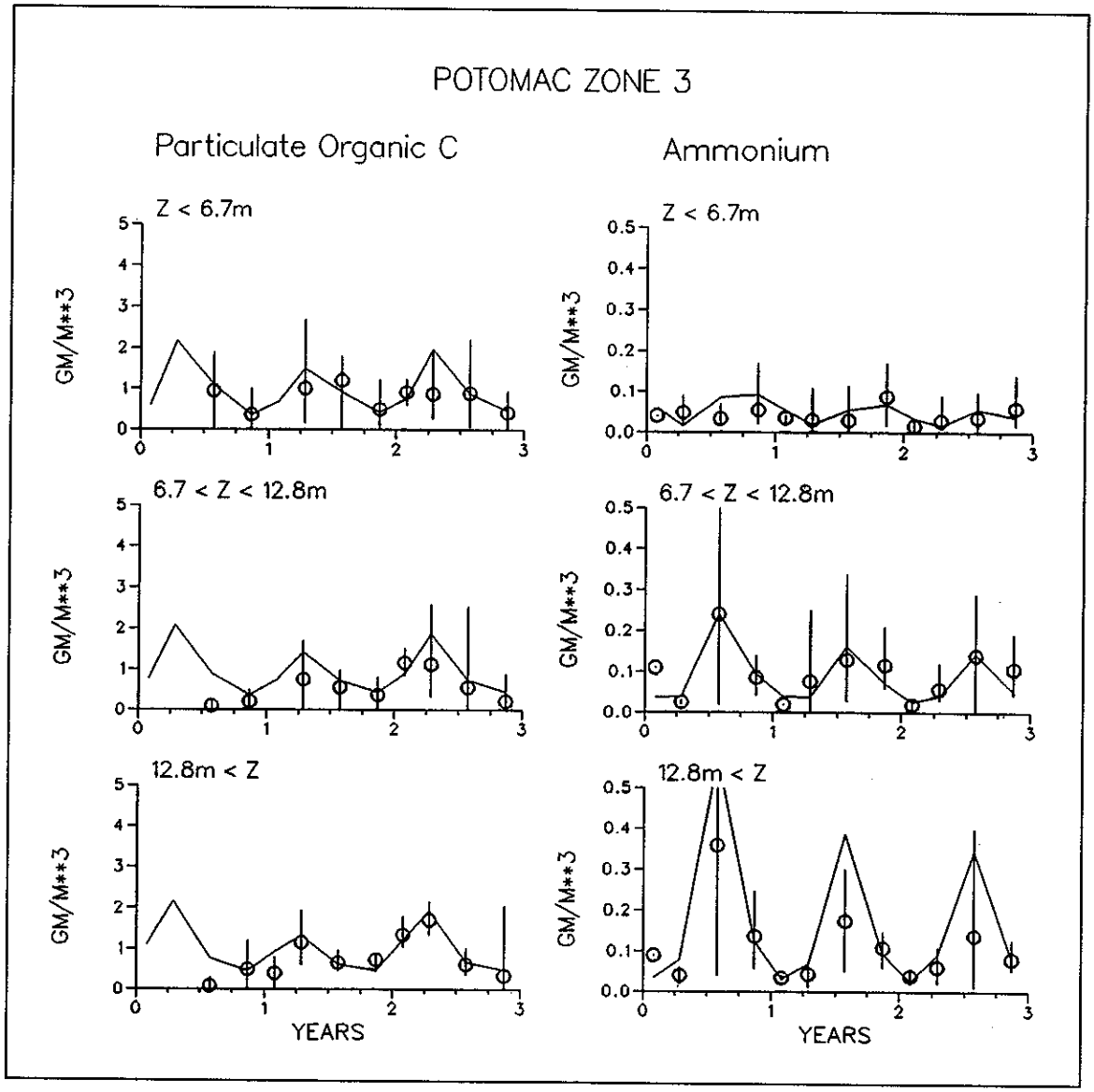

Figure 21-25. (Sheet 2 of 5)

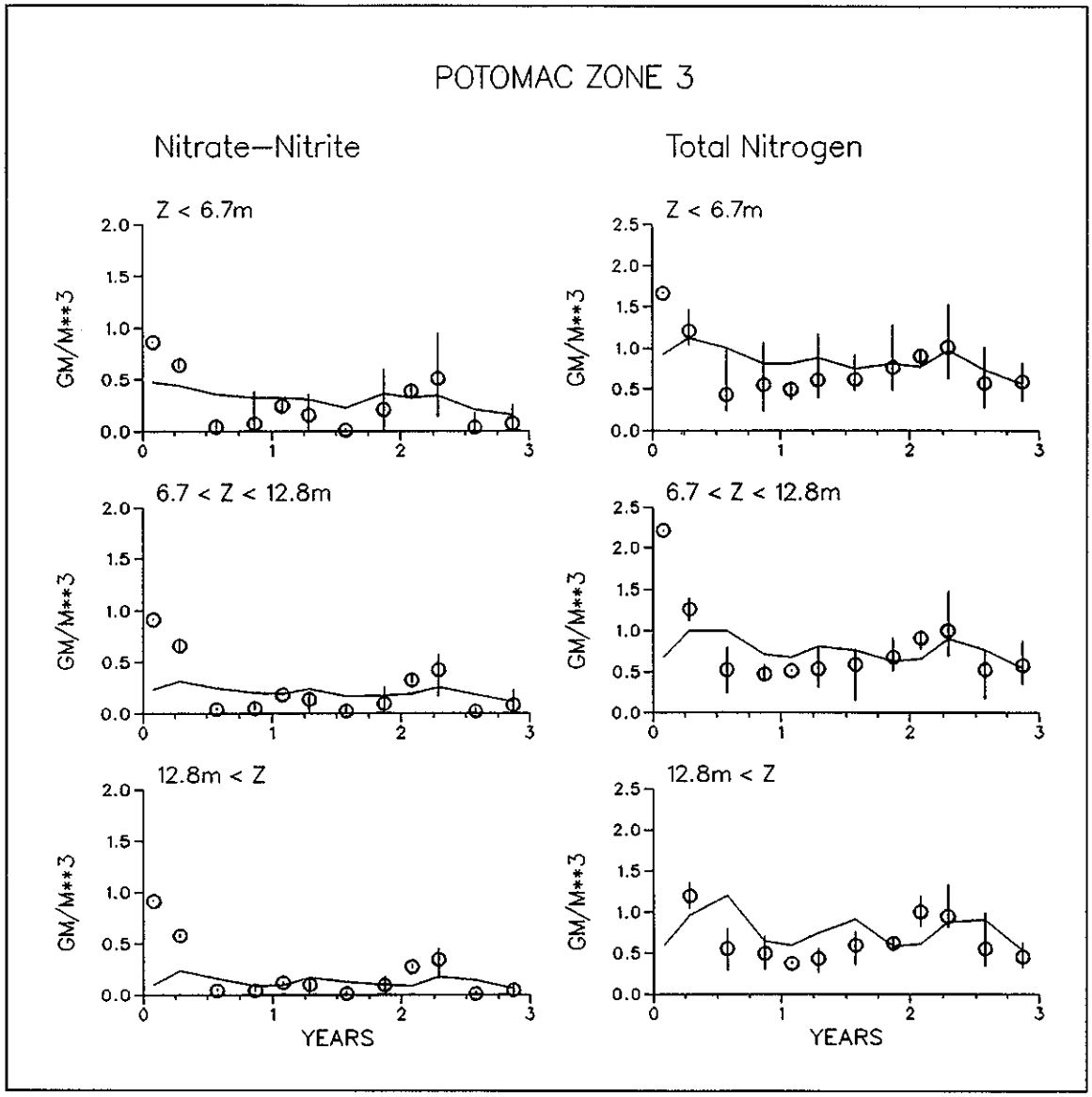

Figure 12-25. (Sheet 3 of 5)

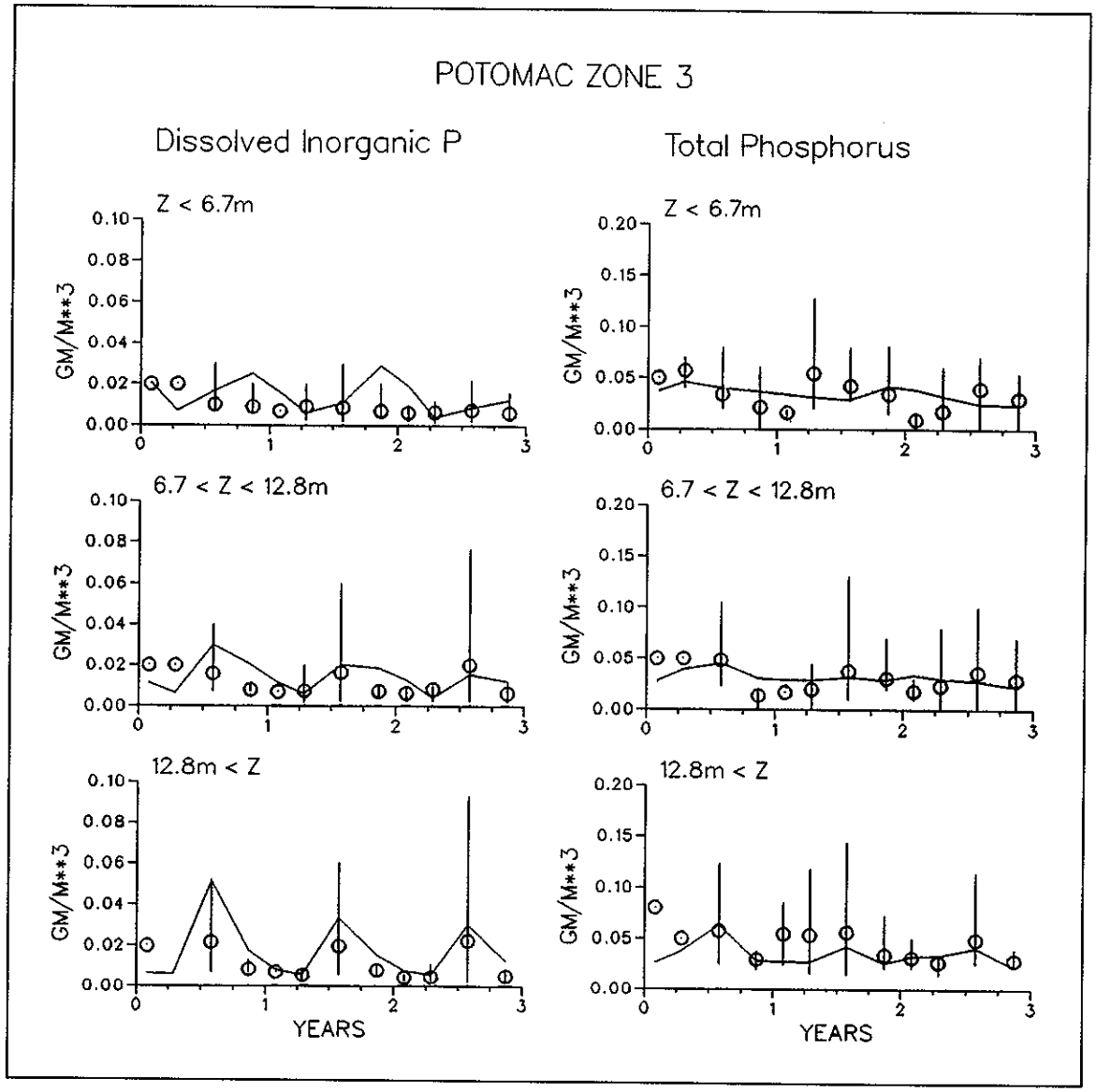

Figure 12-25. (Sheet 4 of 5)

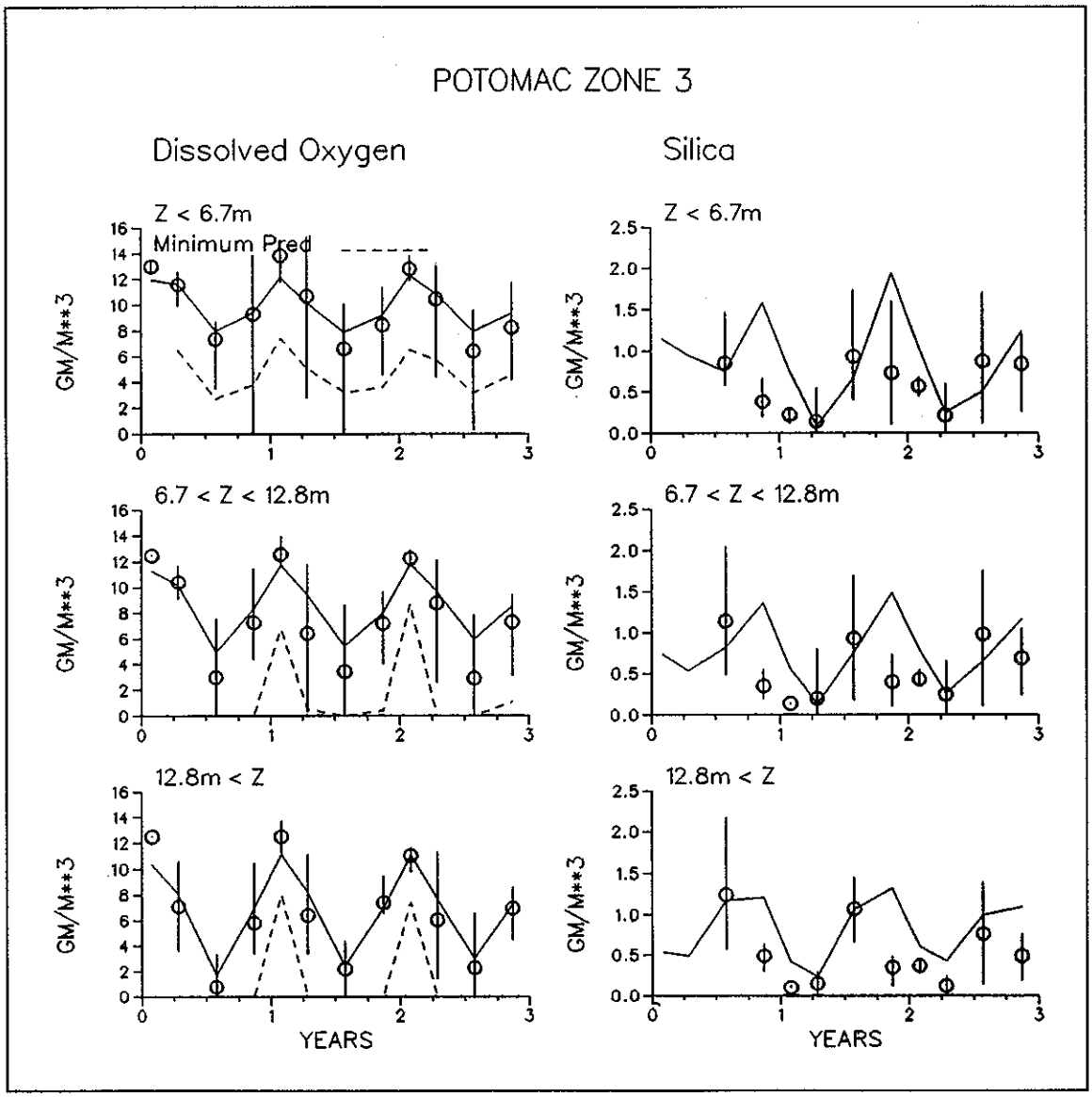

Figure 12-25. (Sheet 5 of 5)

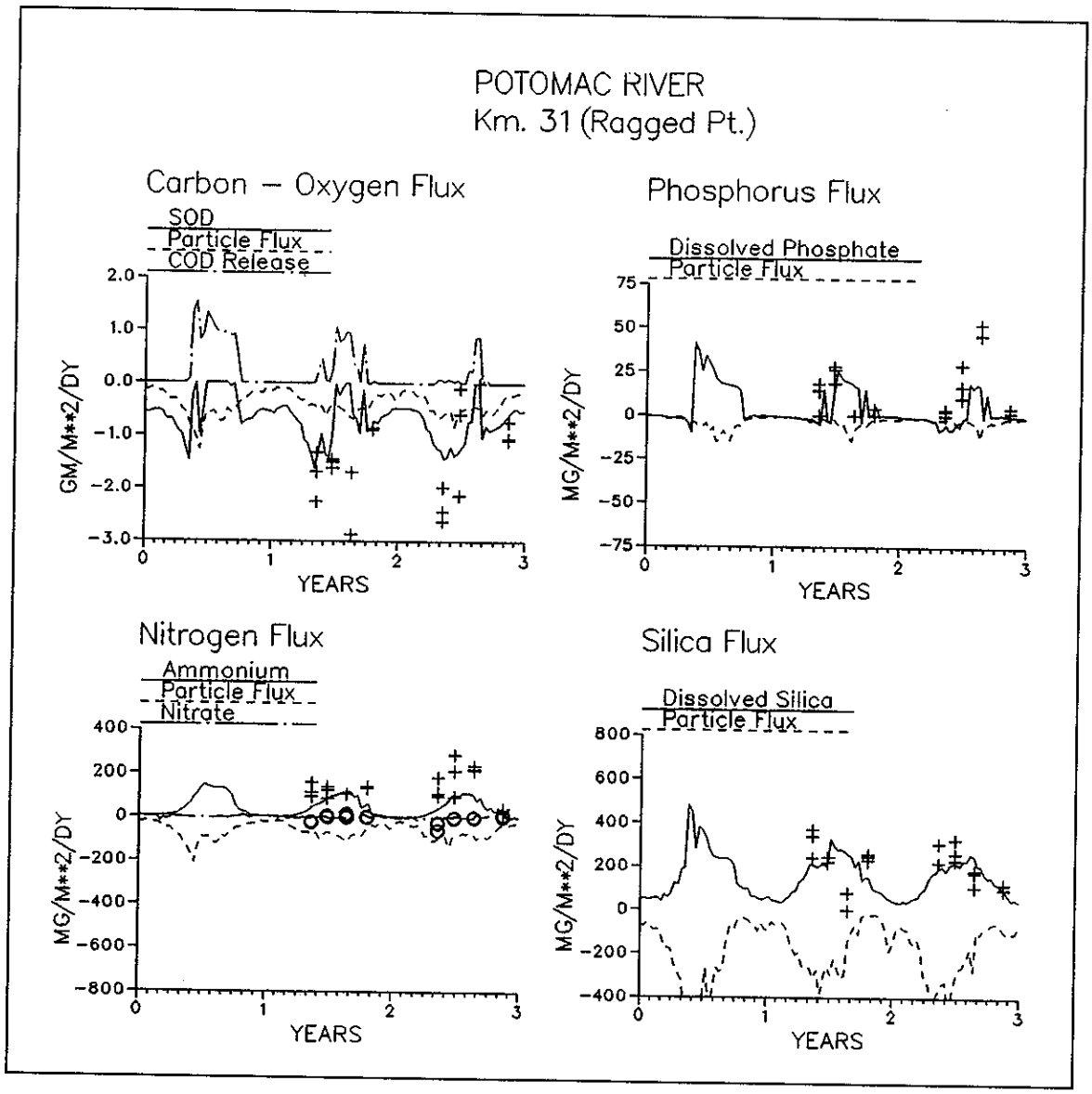

Figure 12-26. Time Series of Predicted and Observed Sediment-Water Fluxes in Potomac River Zone Three

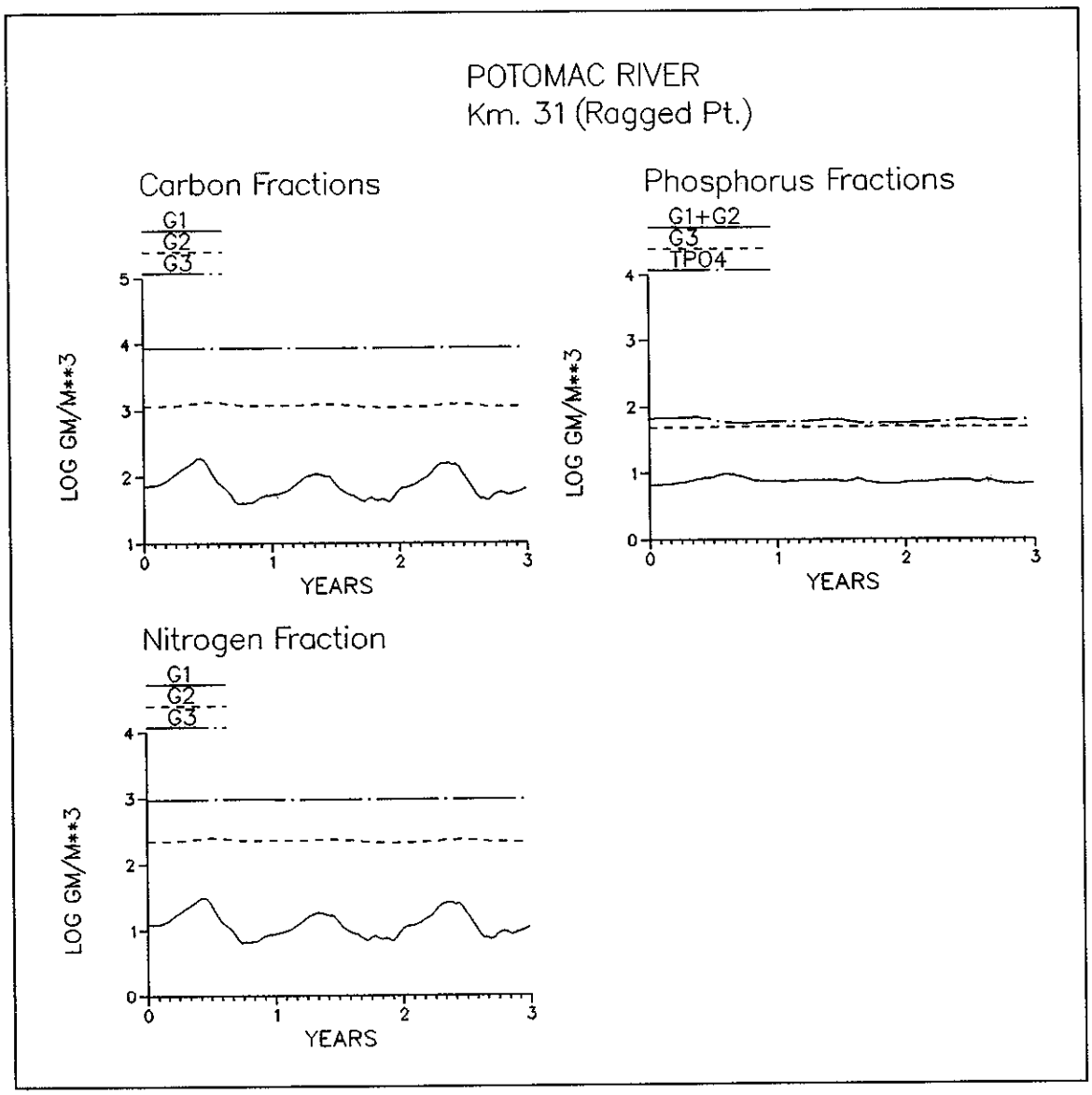

Figure 12-27. Time Series of Predicted Sediment Particulate Carbon, Nitrogen, and Phosphorus in Potomac River Zone Three

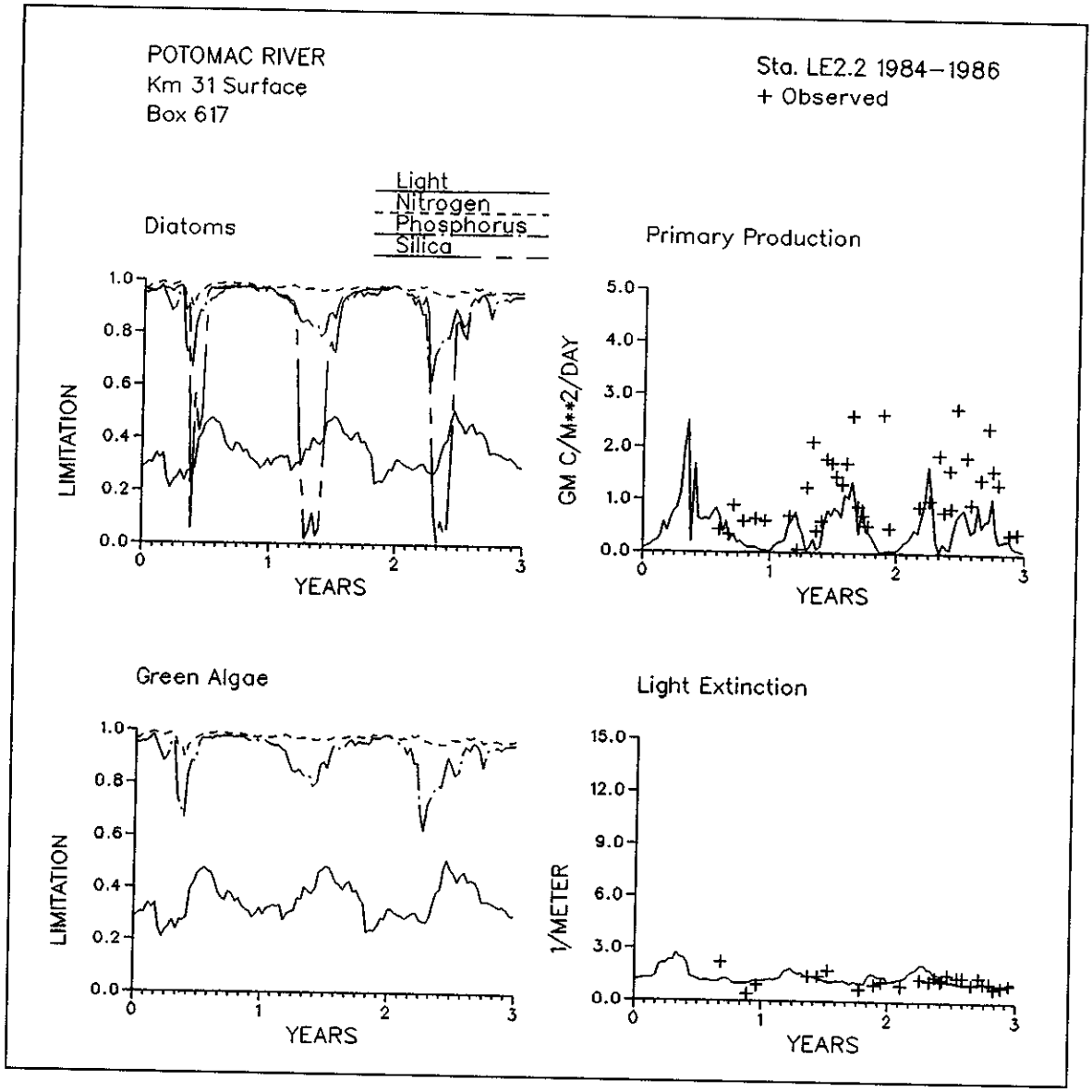

Figure 12-28. Time Series of Predicted and Observed Diagnostic Information in Potomac River Zone Three

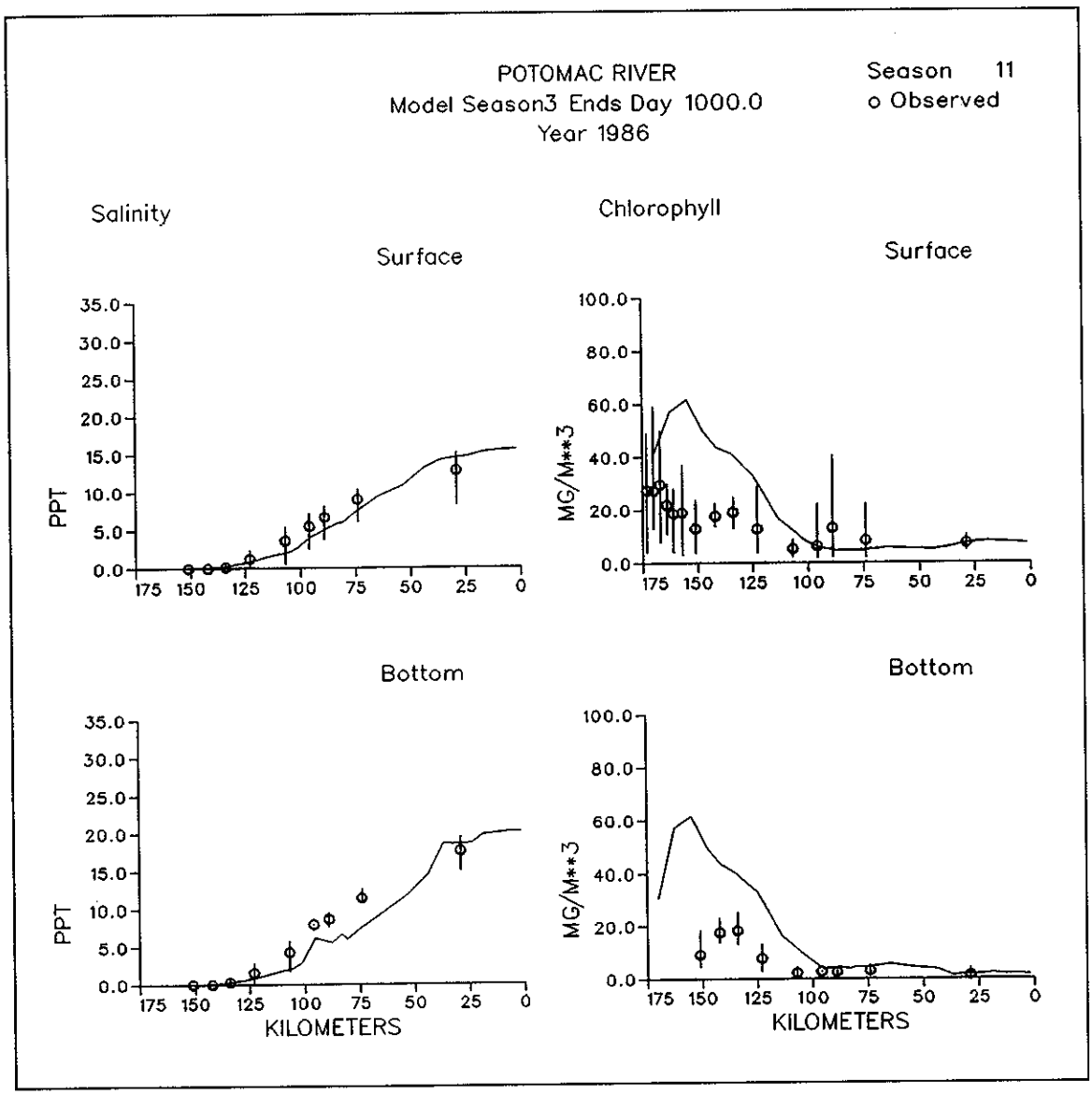

Figure 12-29. Predicted and Observed Concentrations Along Potomac River Longitudinal Transect, Season Three, 1986 (Sheet 1 of 5)

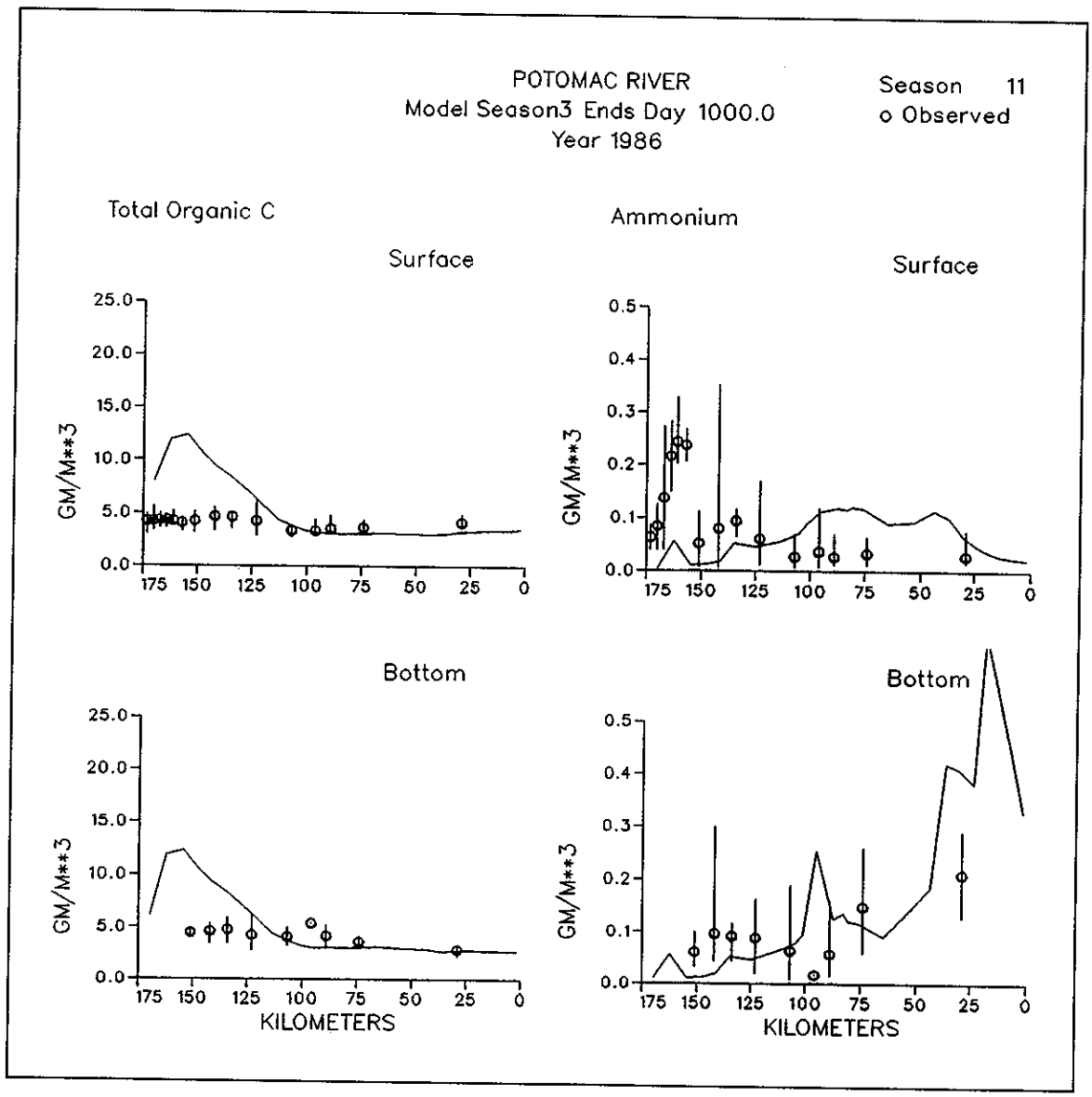

Figure 12-29. (Sheet 2 of 5)

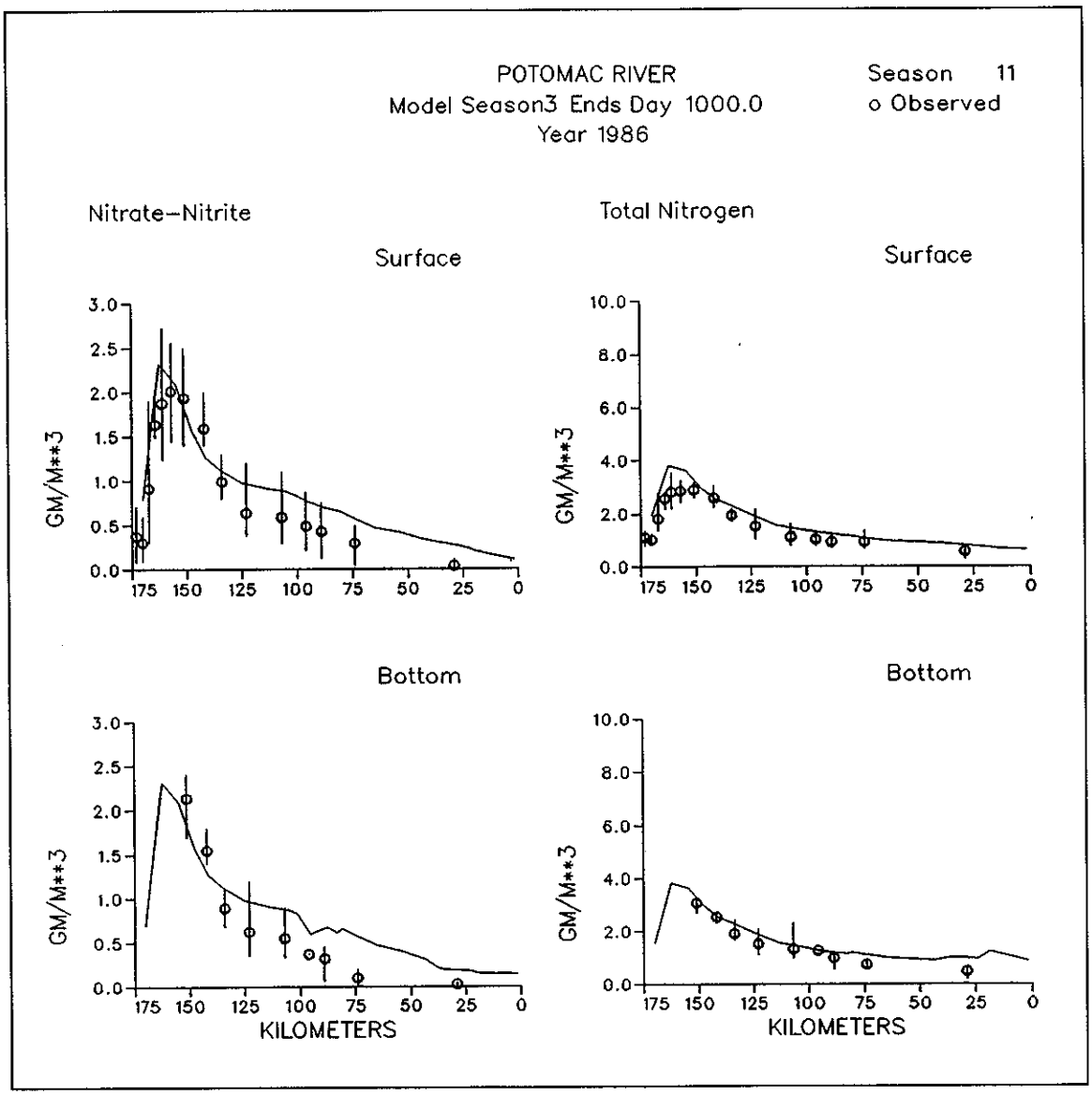

Figure 12-29. (Sheet 3 of 5)

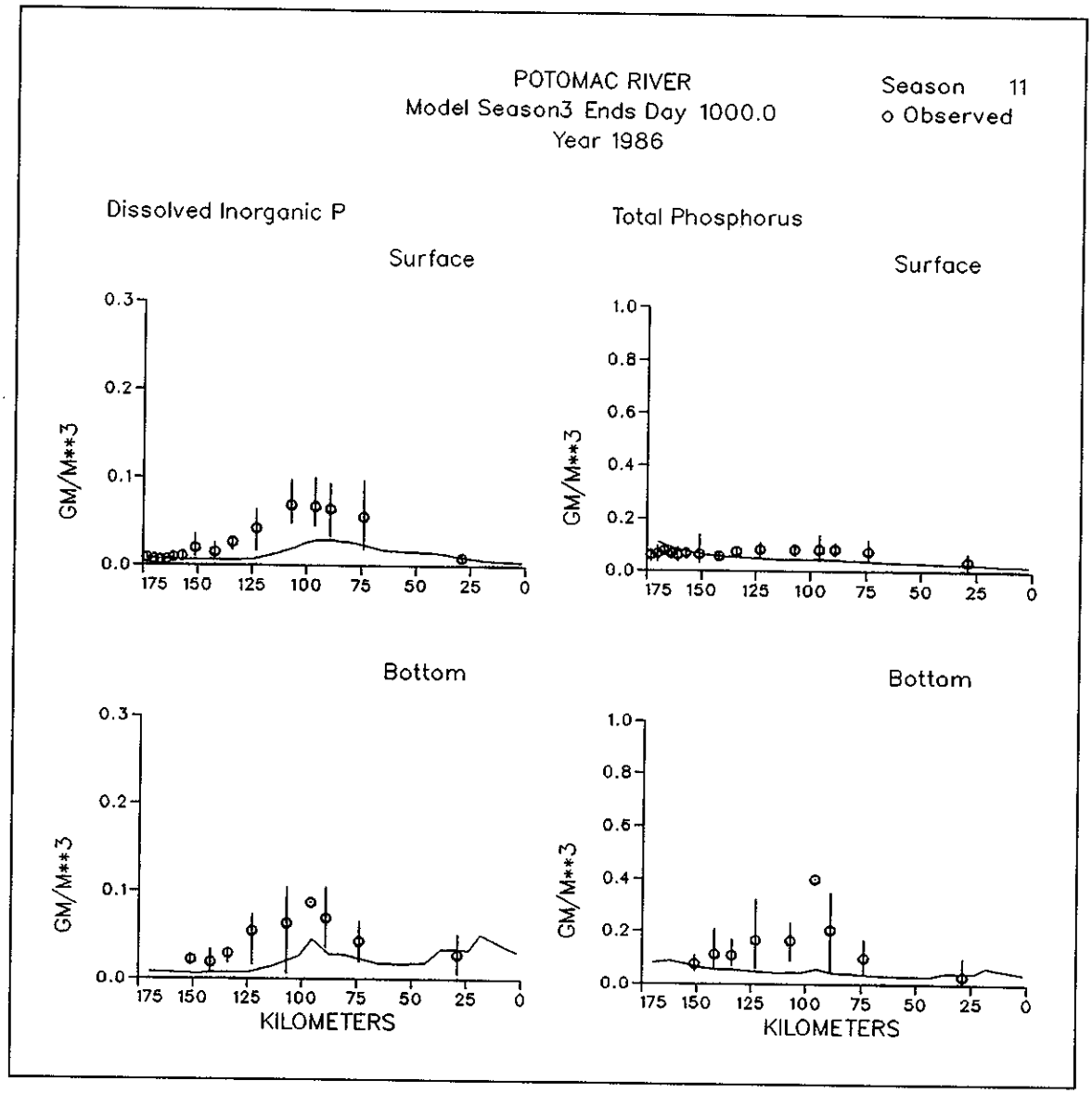

Figure 12-29. (Sheet 4 of 5)

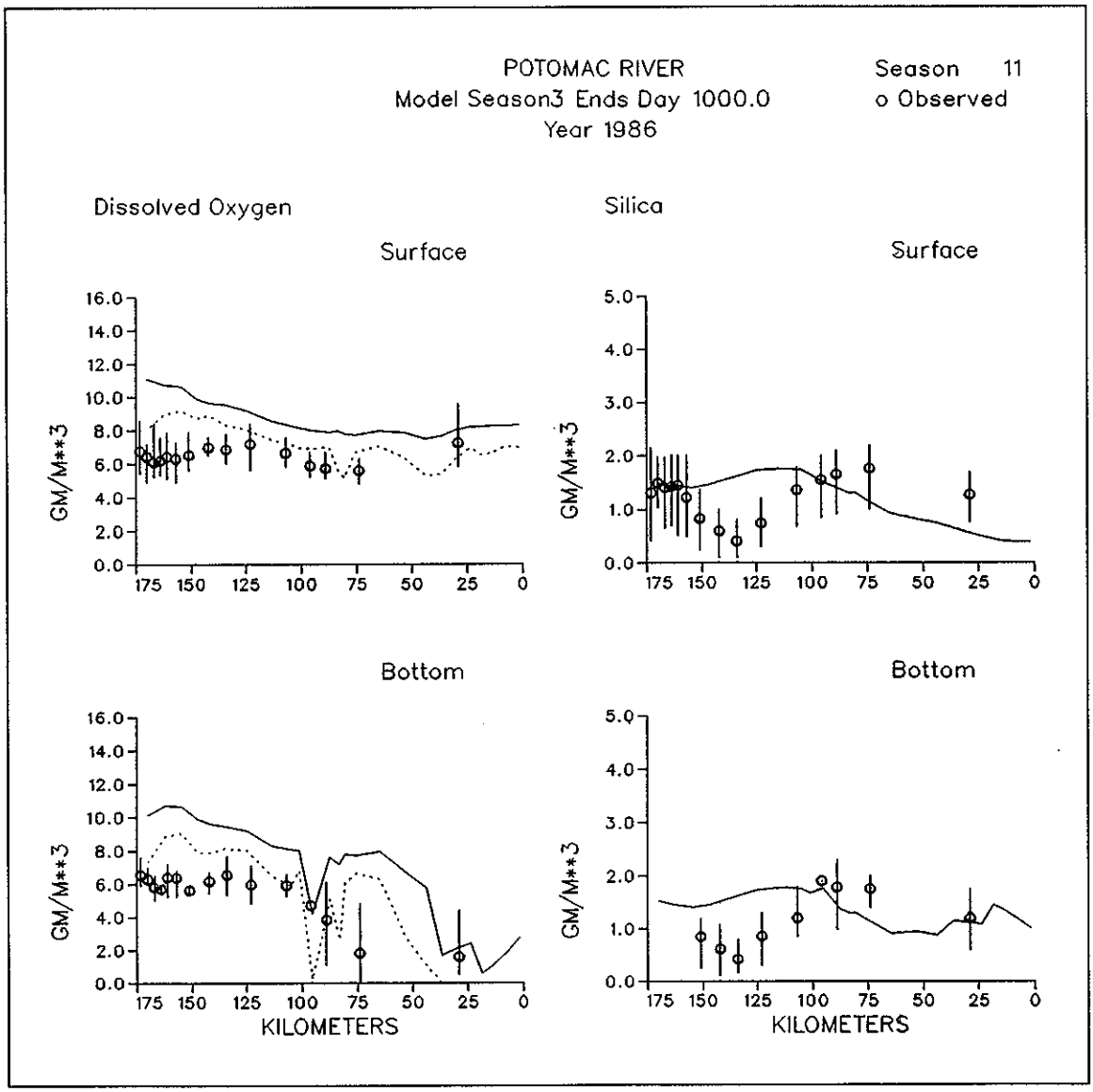

Figure 12-29. (Sheet 5 of 5)

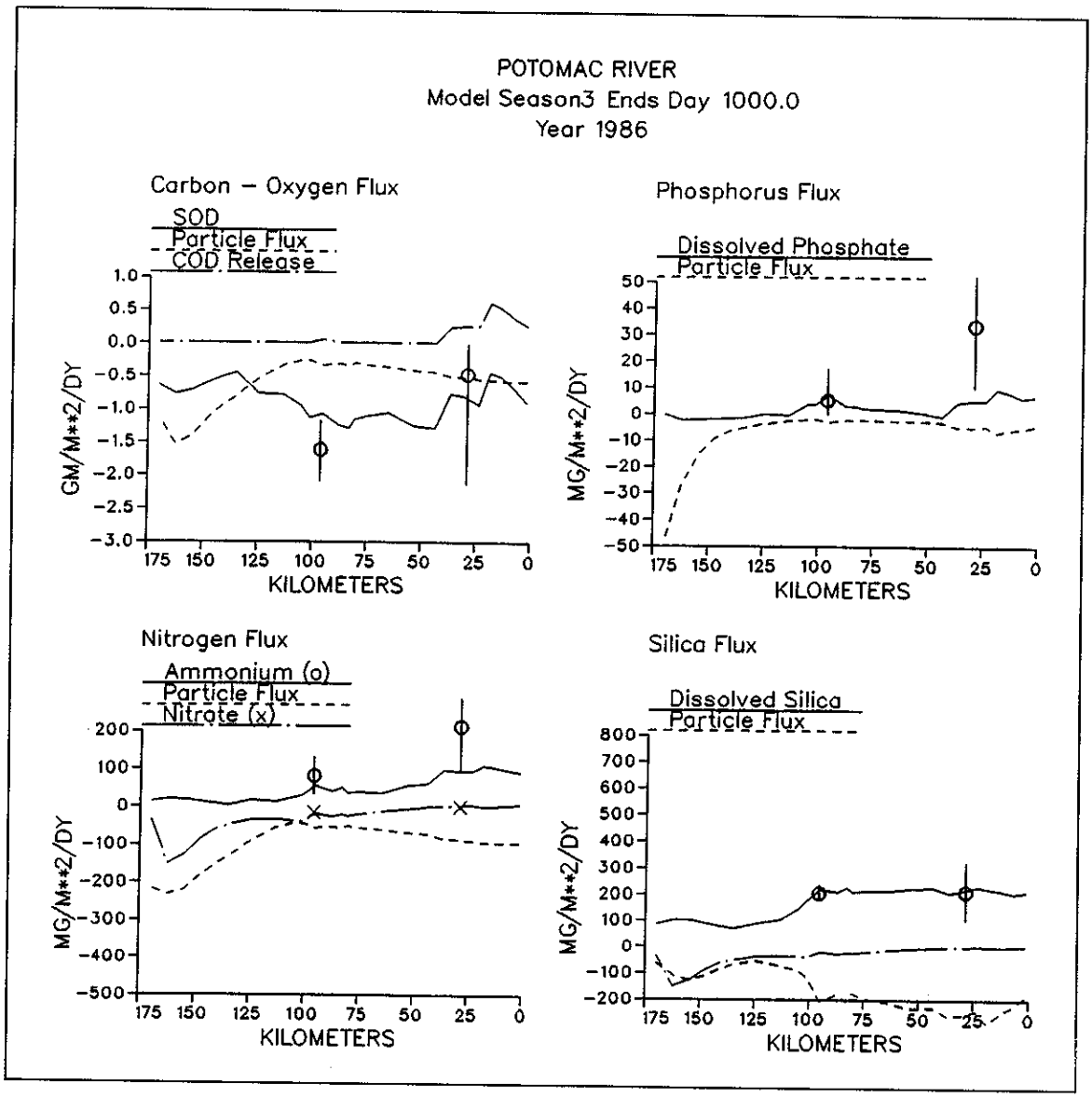

Figure 12-30. Predicted and Observed Sediment-Water Fluxes Along Potomac River Longitudinal Transect, Season Three, 1986

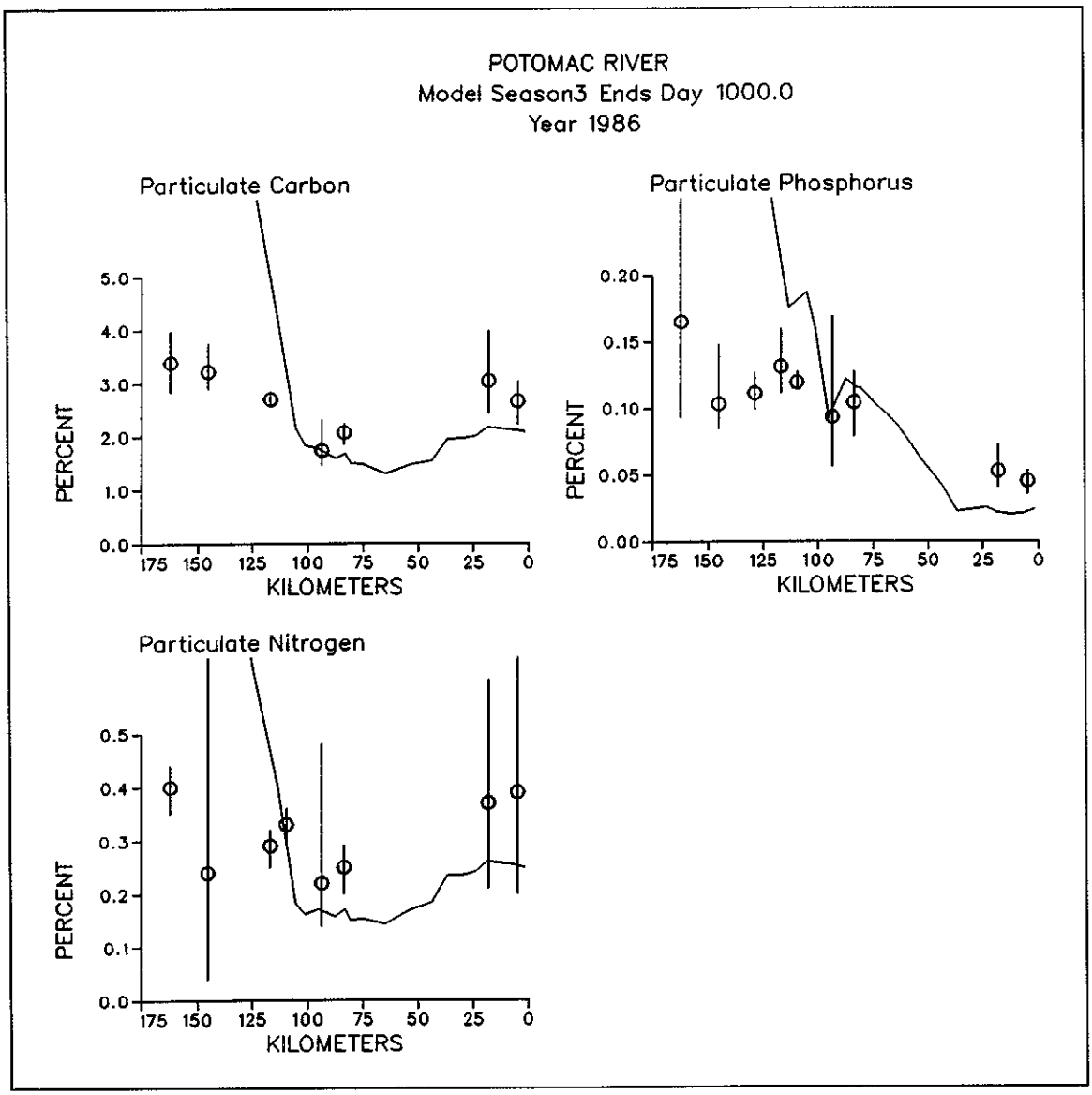

Figure 12-31. Predicted and Observed Sediment Particulate Carbon, Nitrogen, and Phosphorus Along Potomac River Longitudinal Transect

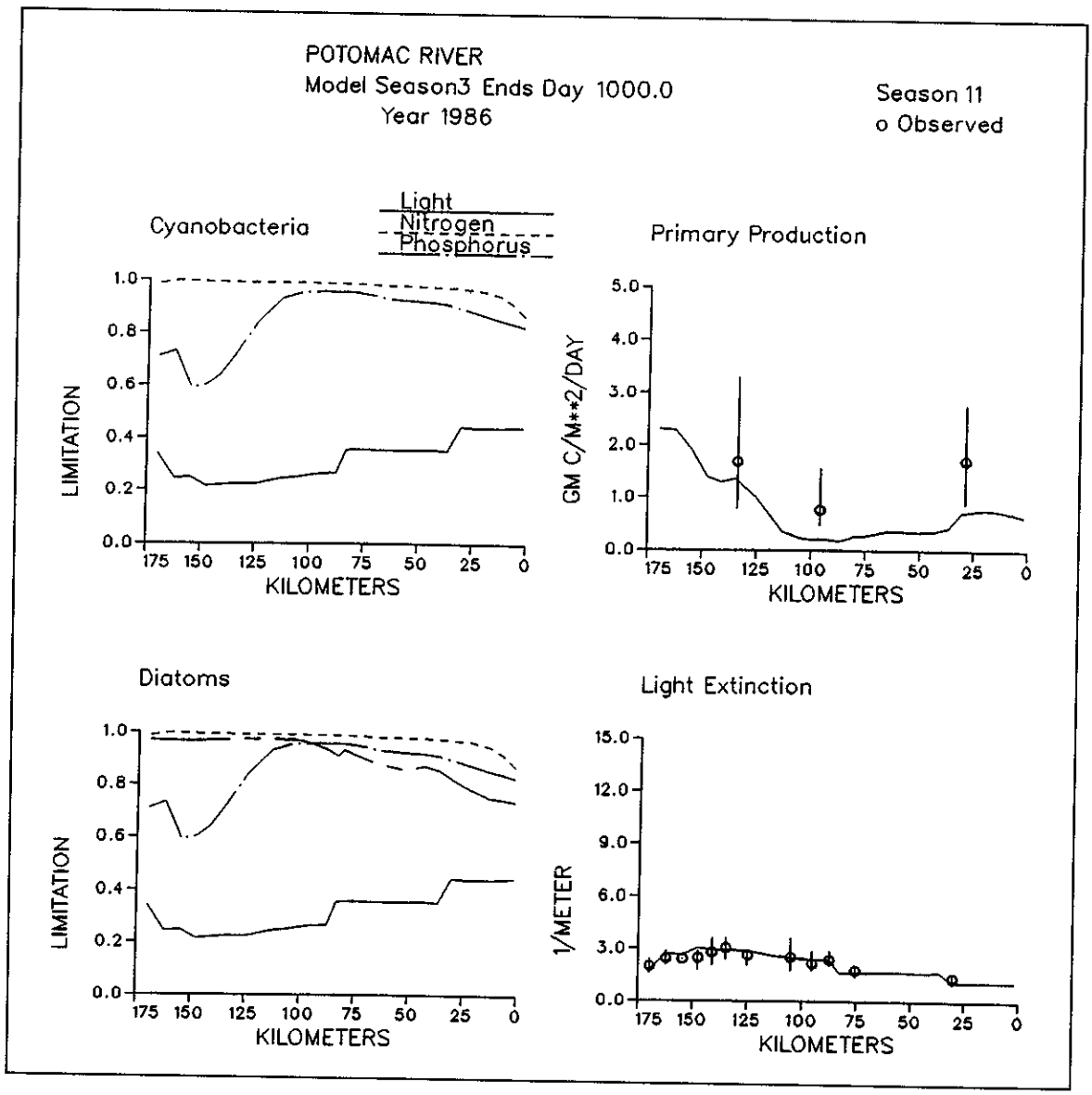

Figure 12-32. Predicted and Observed Diagnostic Information Along Potomac River Longitudinal Transect, Season Three, 1986

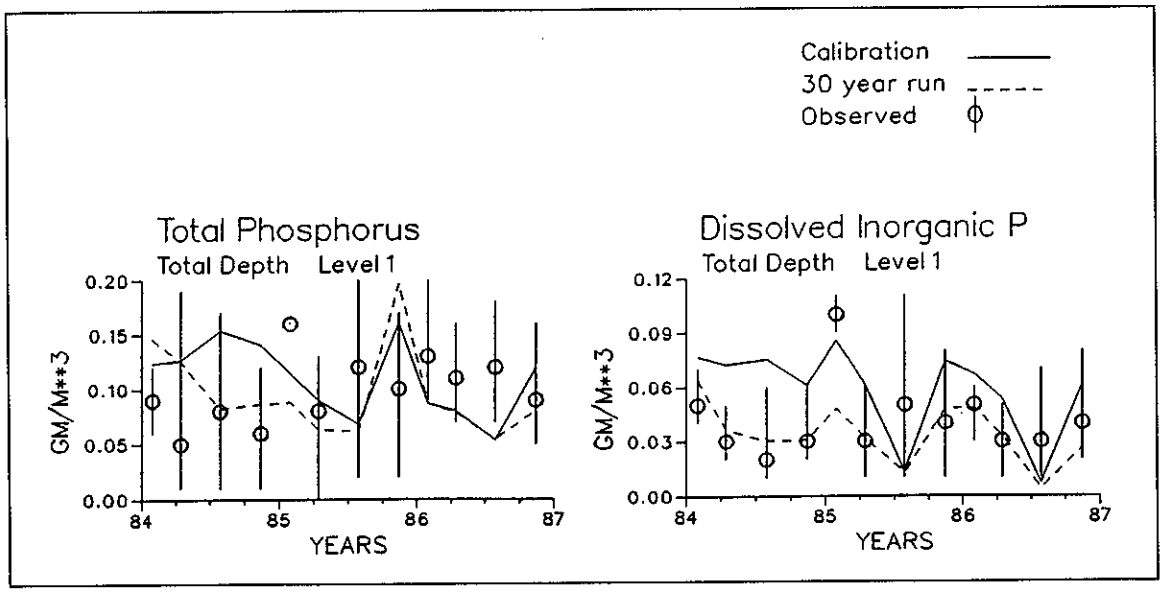

Figure 12-33. Phosphorus Concentrations in Potomac Zone One Resulting From Watershed Model (Calibration) and Regression (30 Year Run) Fall-Line Loads

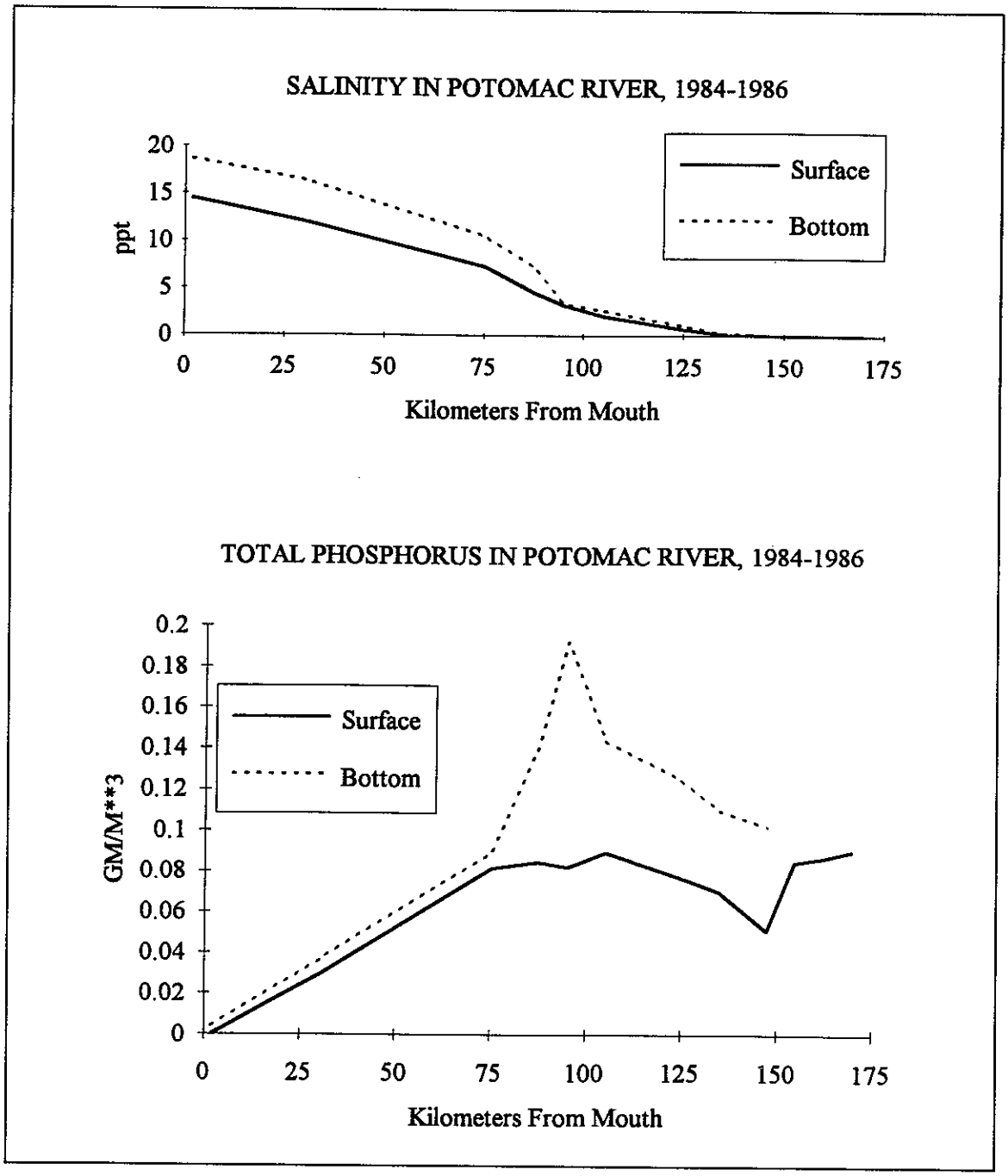

Figure 12-34. Salinity and Total Phosphorus in the Potomac River, 1984-1986

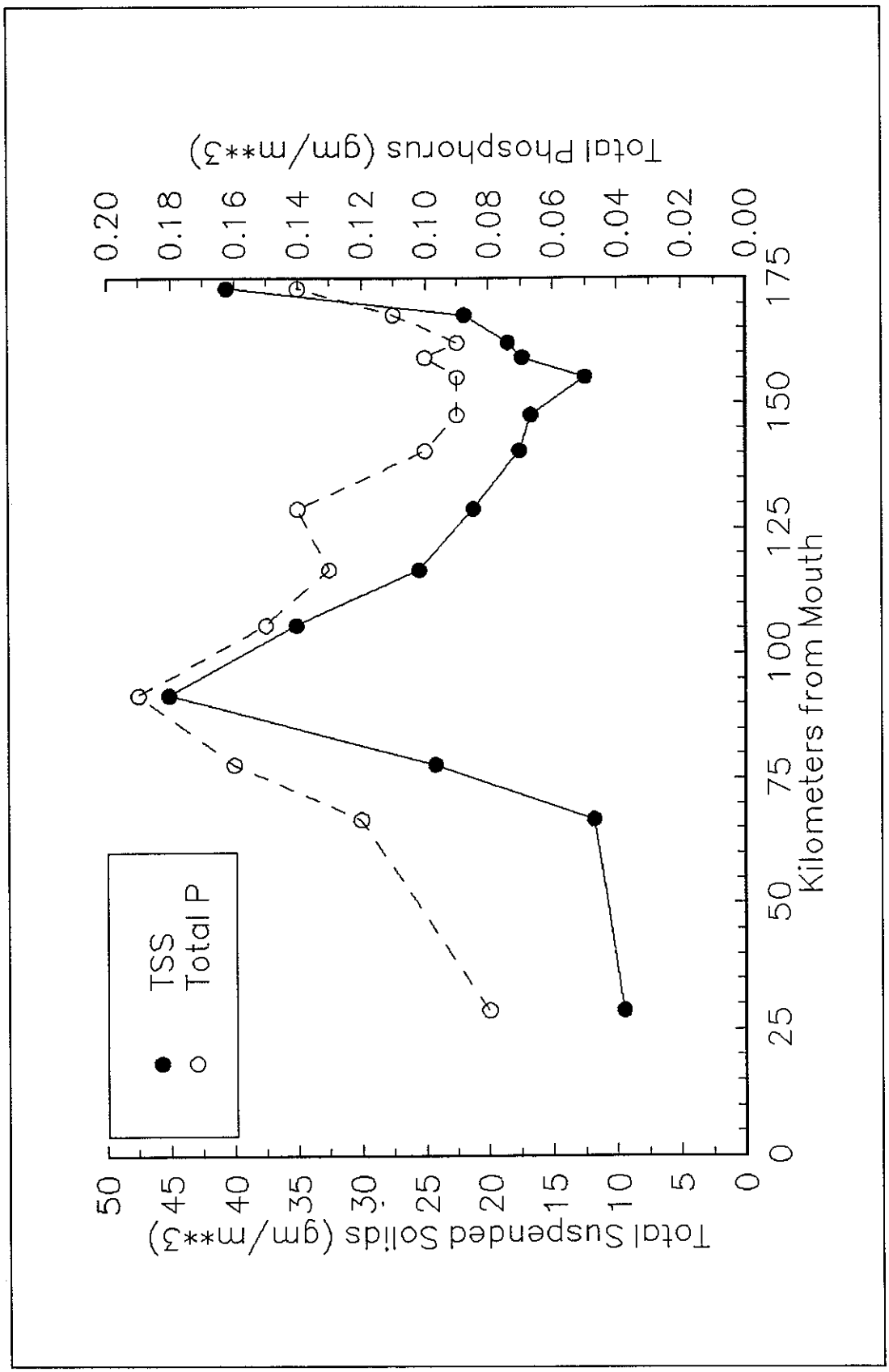

Figure 12-35. Total Suspended Solids and Phosphorus in Potomac River Surface Samples, 1985

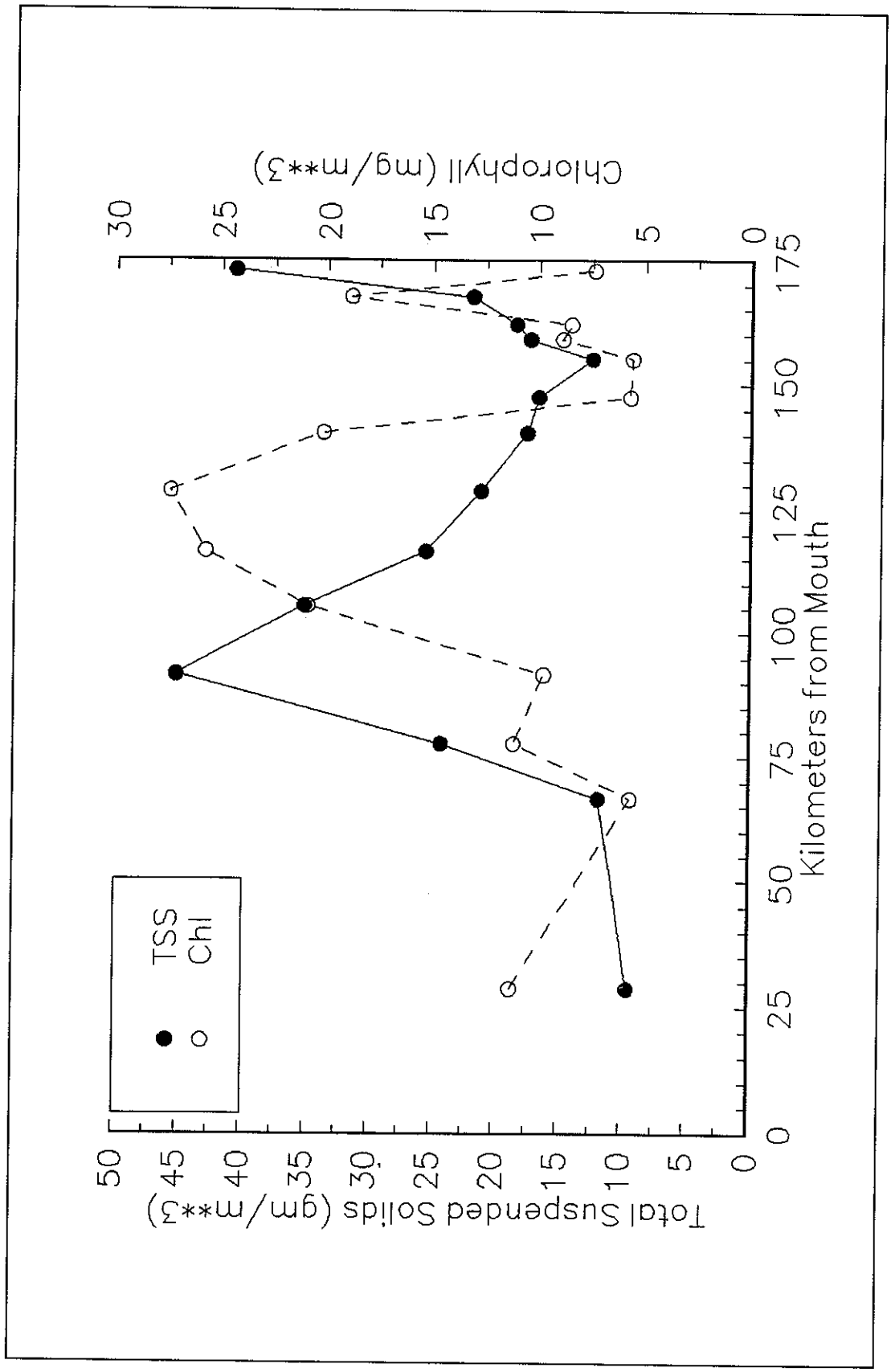

Figure 12-36. Total Suspended Solids and Chlorophyll in Potomac River Surface Samples, 1985

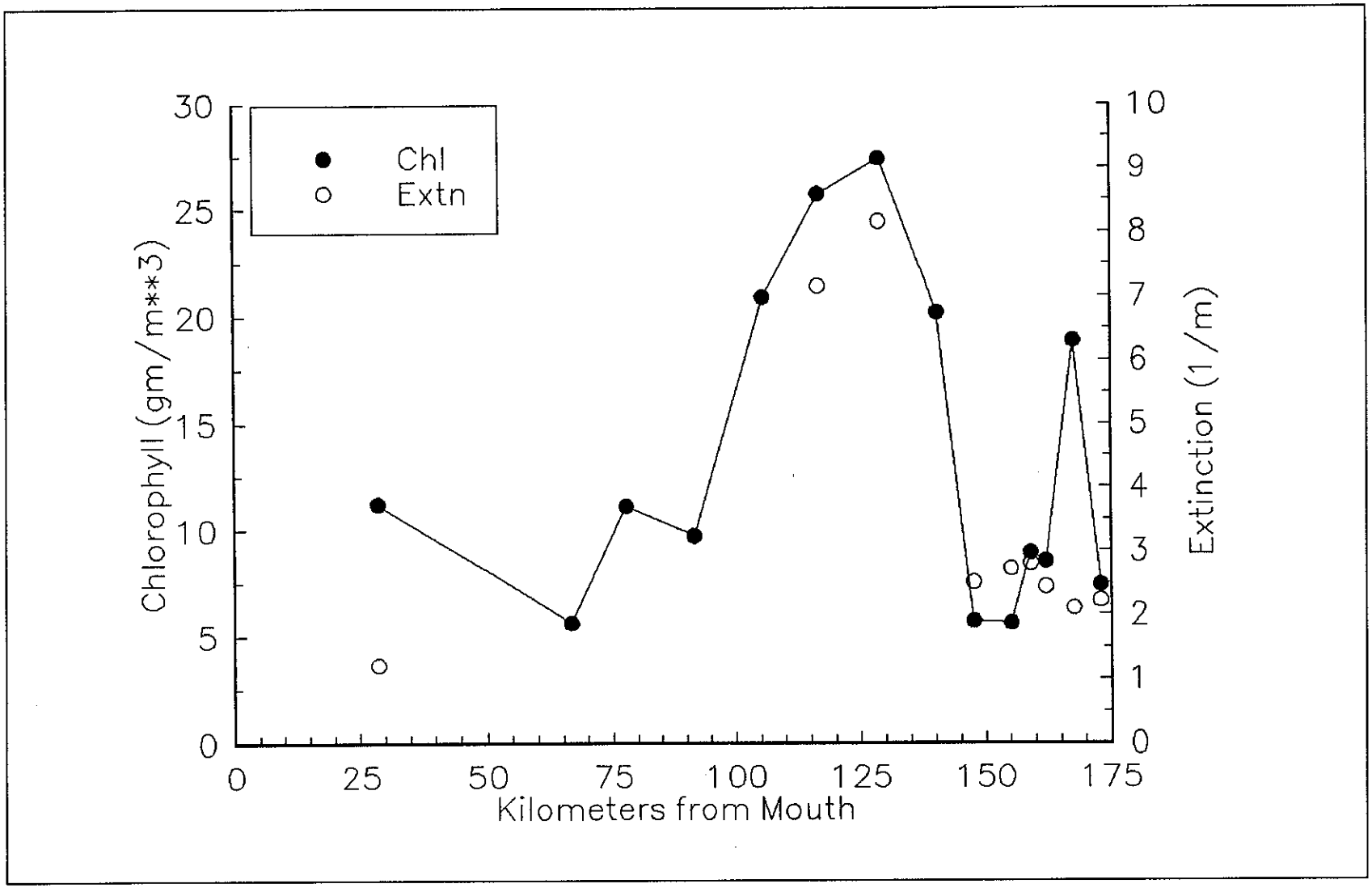

Figure 12-37. Chlorophyll and Chlorophyll-Corrected Light Extinction in Potomac River Surface Samples, 1985

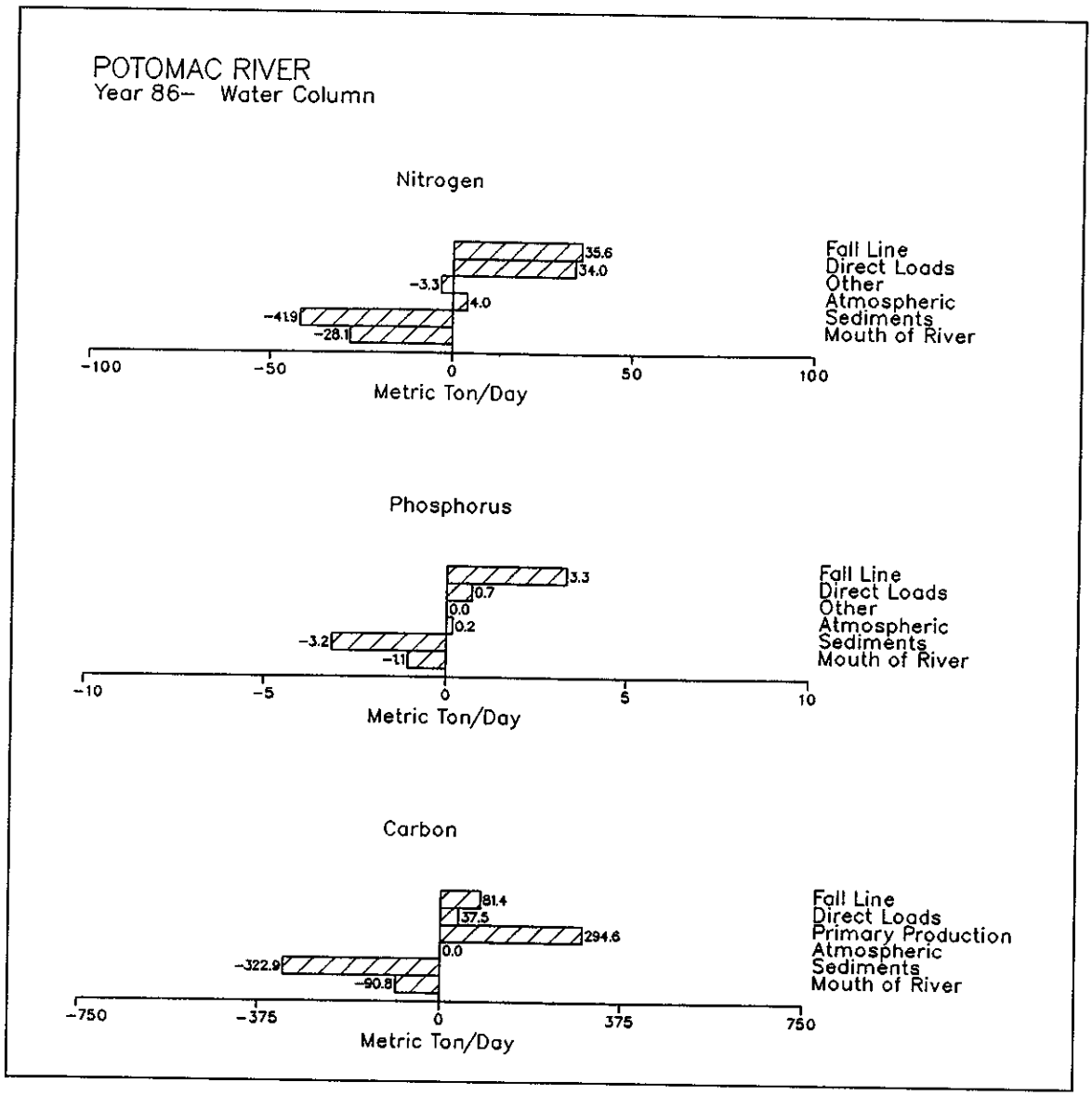

Figure 12-38. Annual Mass Balance for Potomac River Water Column, 1986

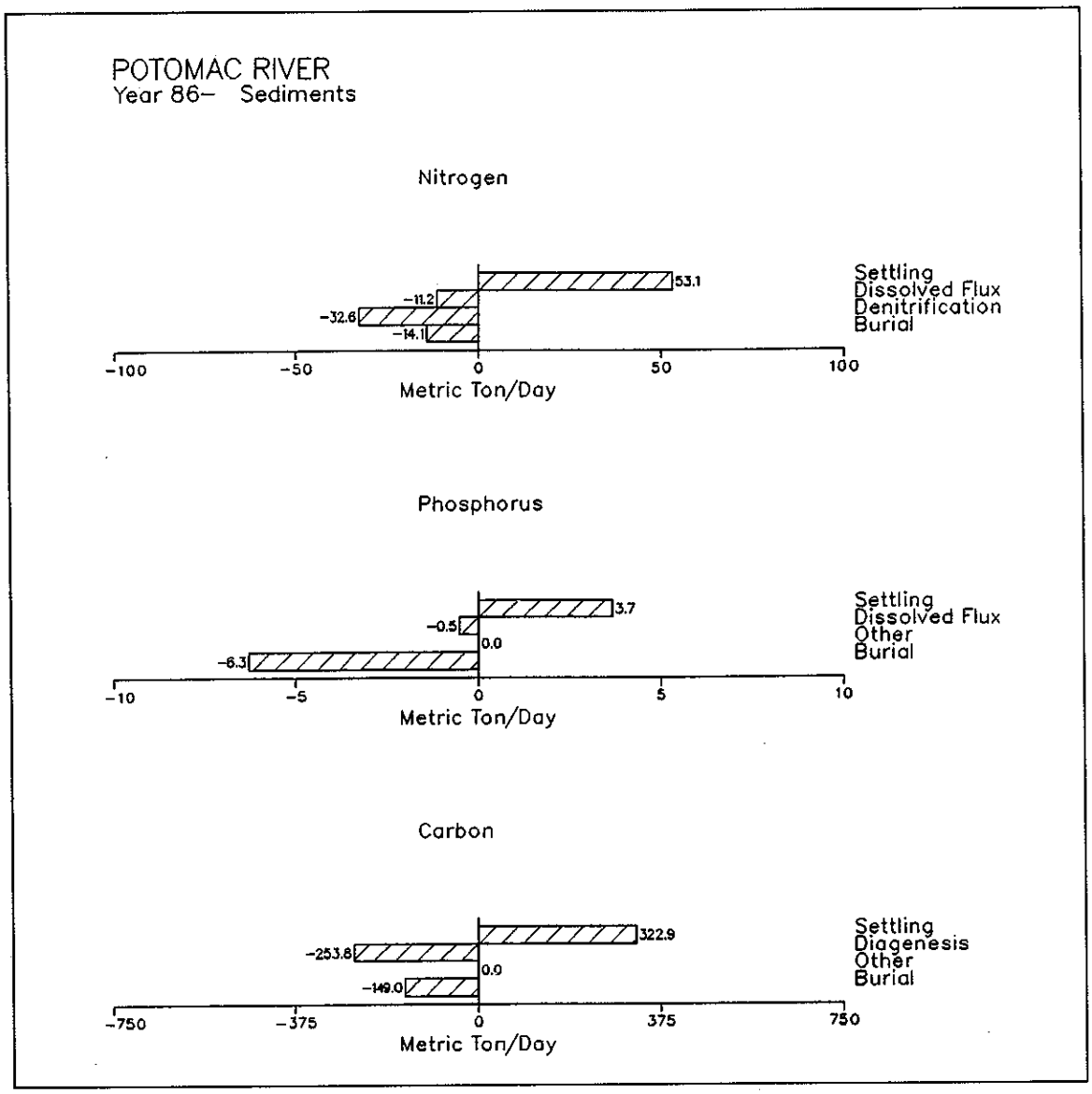

Figure 12-39. Annual Mass Balance for Potomac River Sediments, 1986

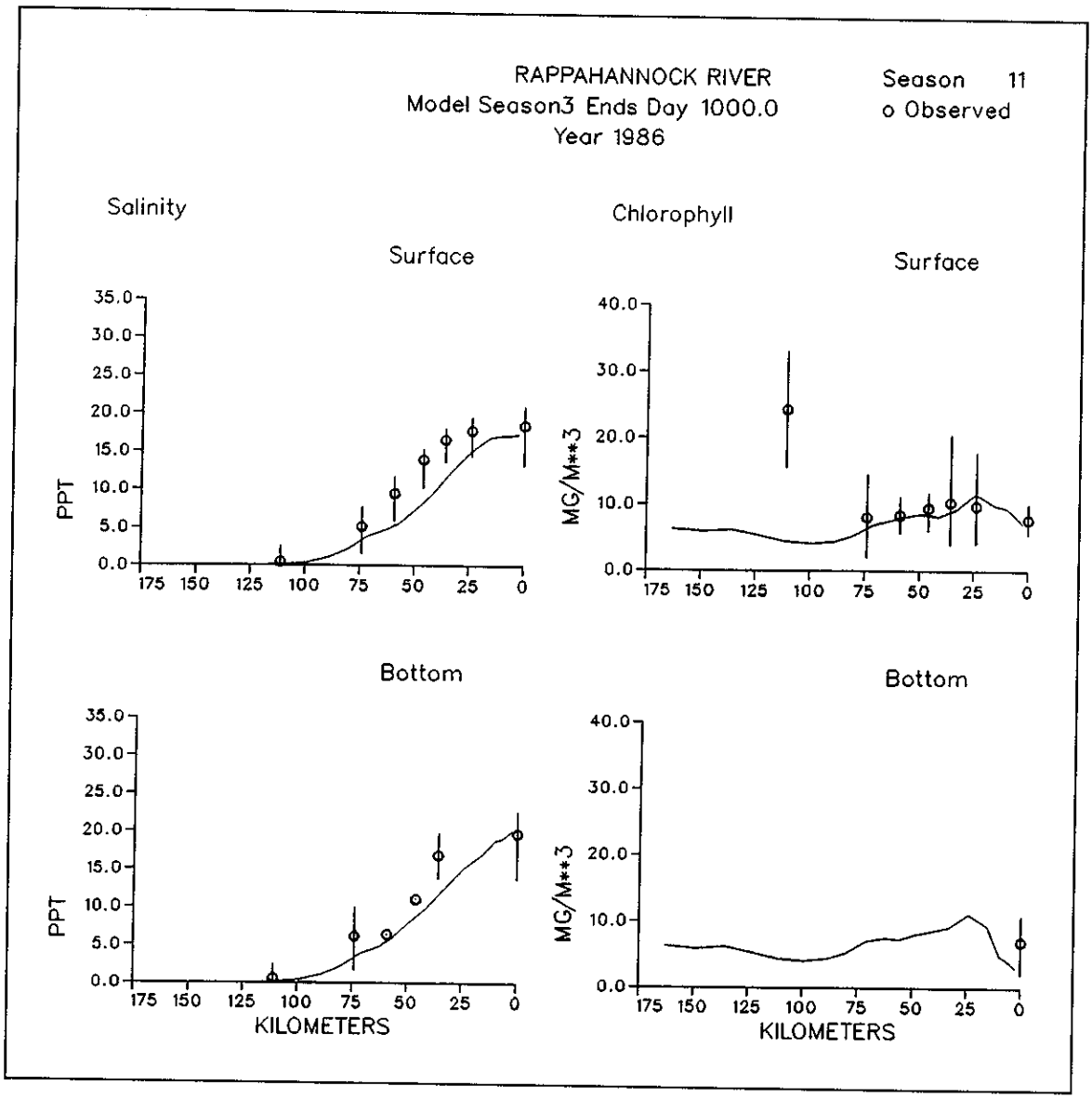

Figure 12-40. Predicted and Observed Concentrations Along Rappahannock River Longitudinal Transect, Season Three, 1986 (Sheet 1 of 5)

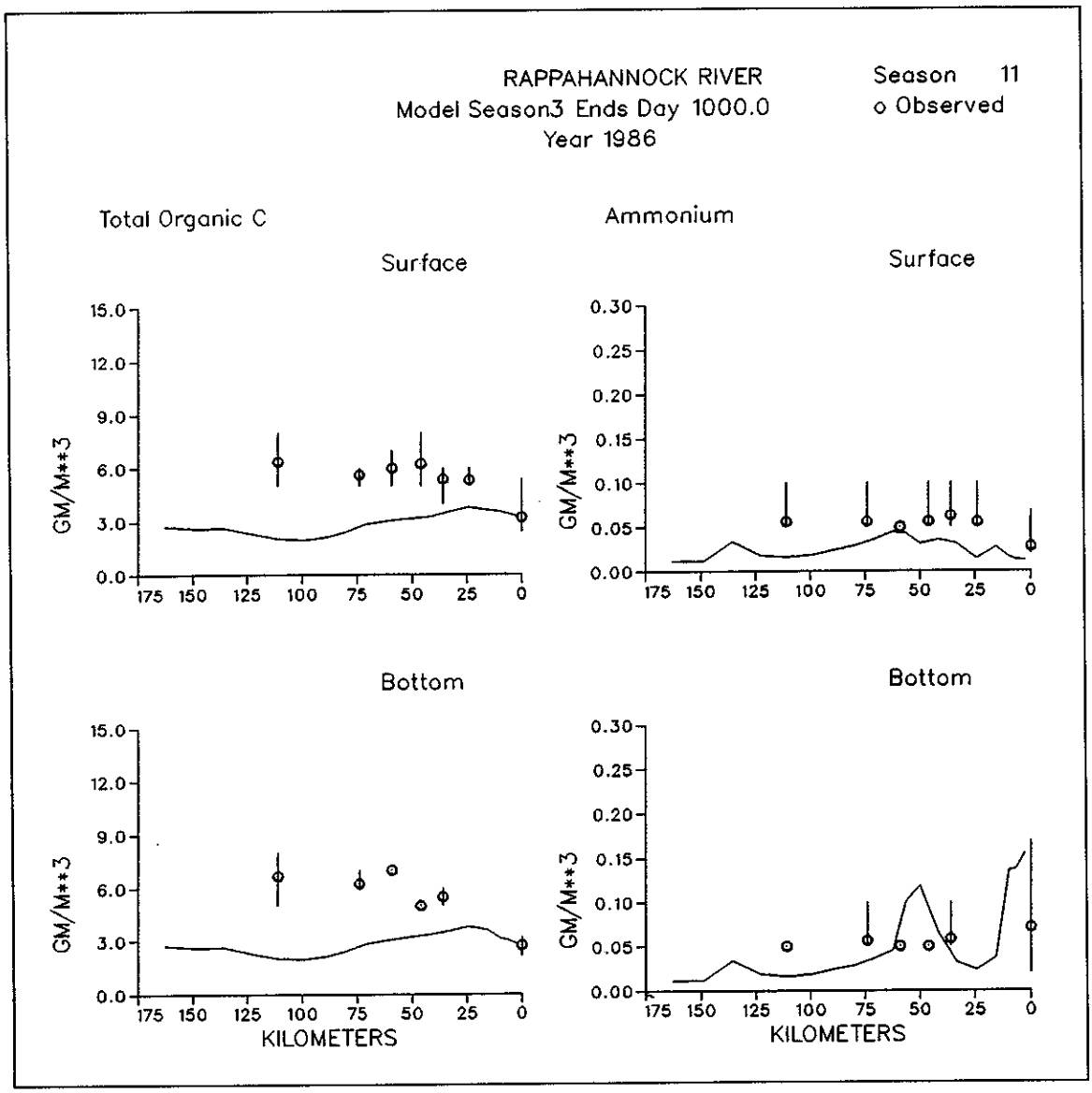

Figure 12-40. (Sheet 2 of 5)

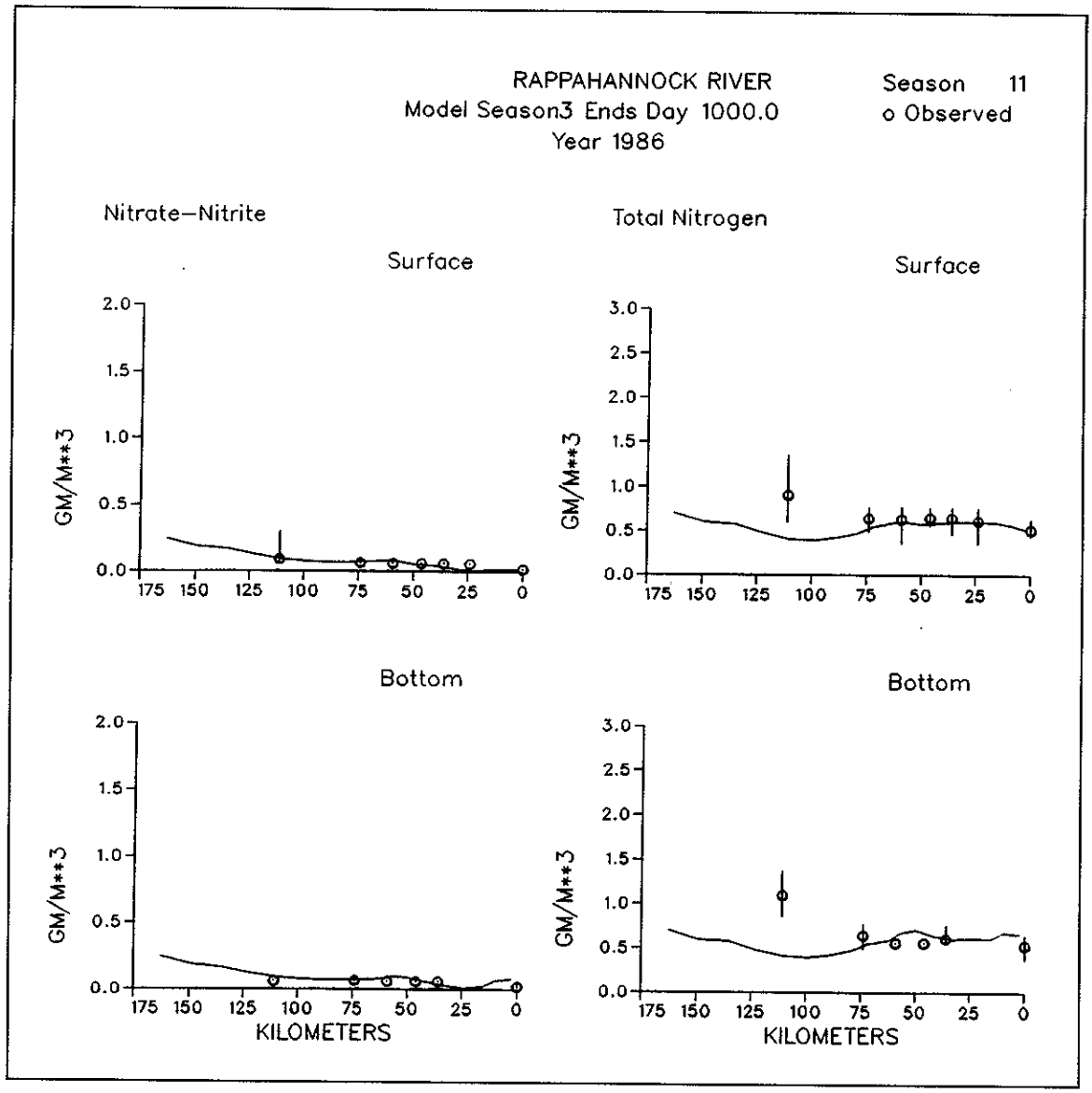

Figure 12-40. (Sheet 3 of 5)

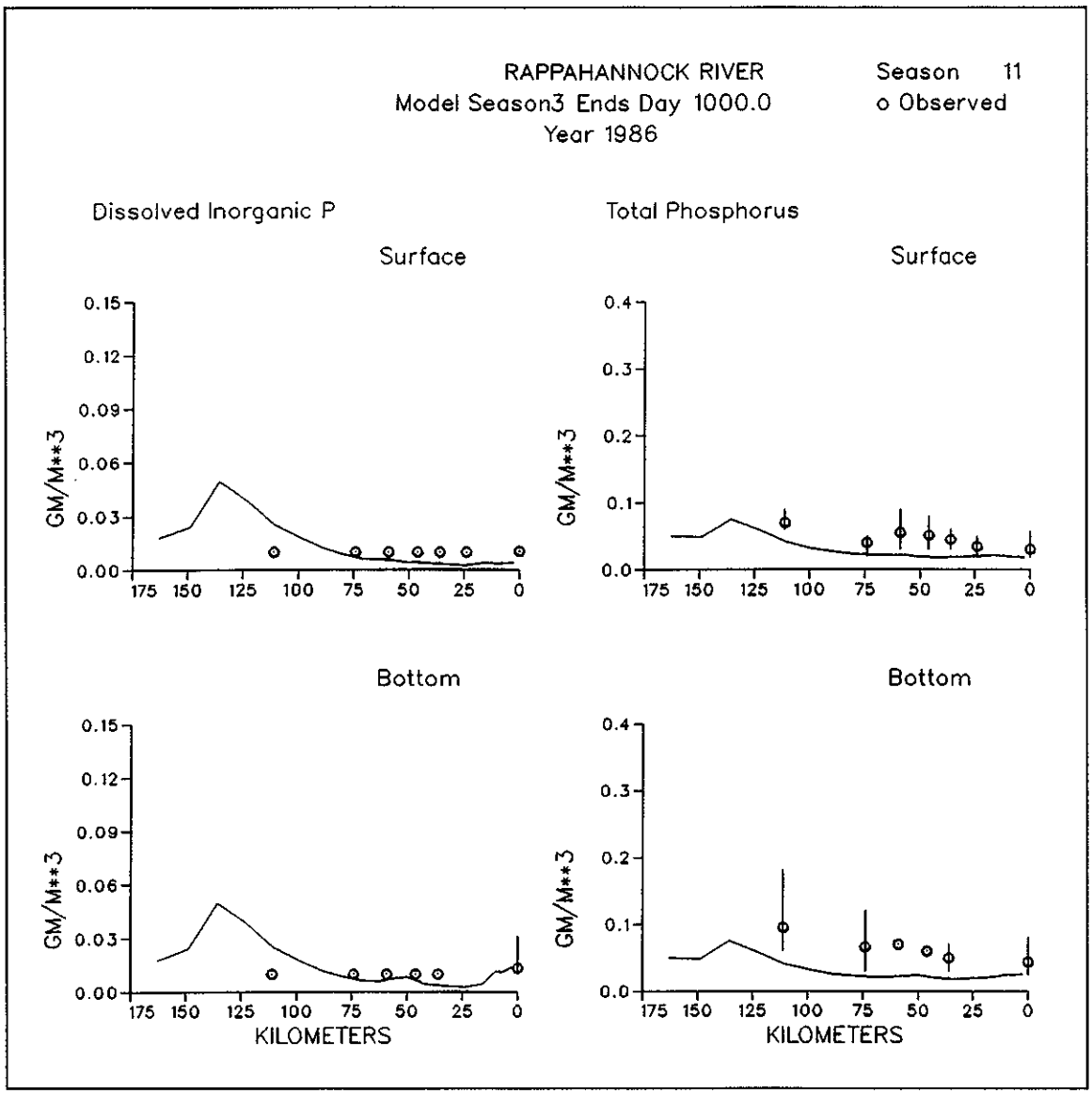

Figure 12-40. (Sheet 4 of 5)

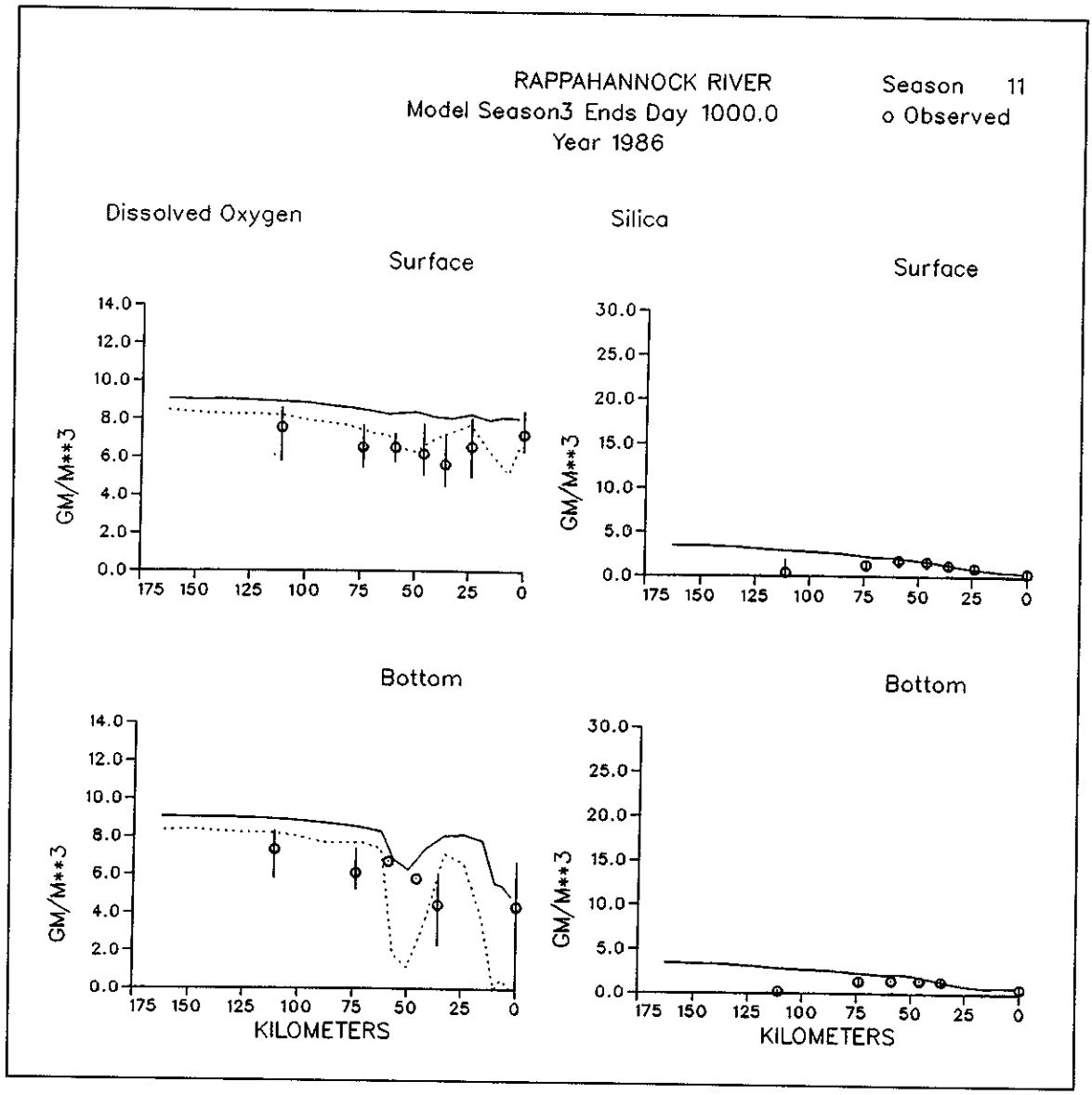

Figure 12-40. (Sheet 5 of 5)

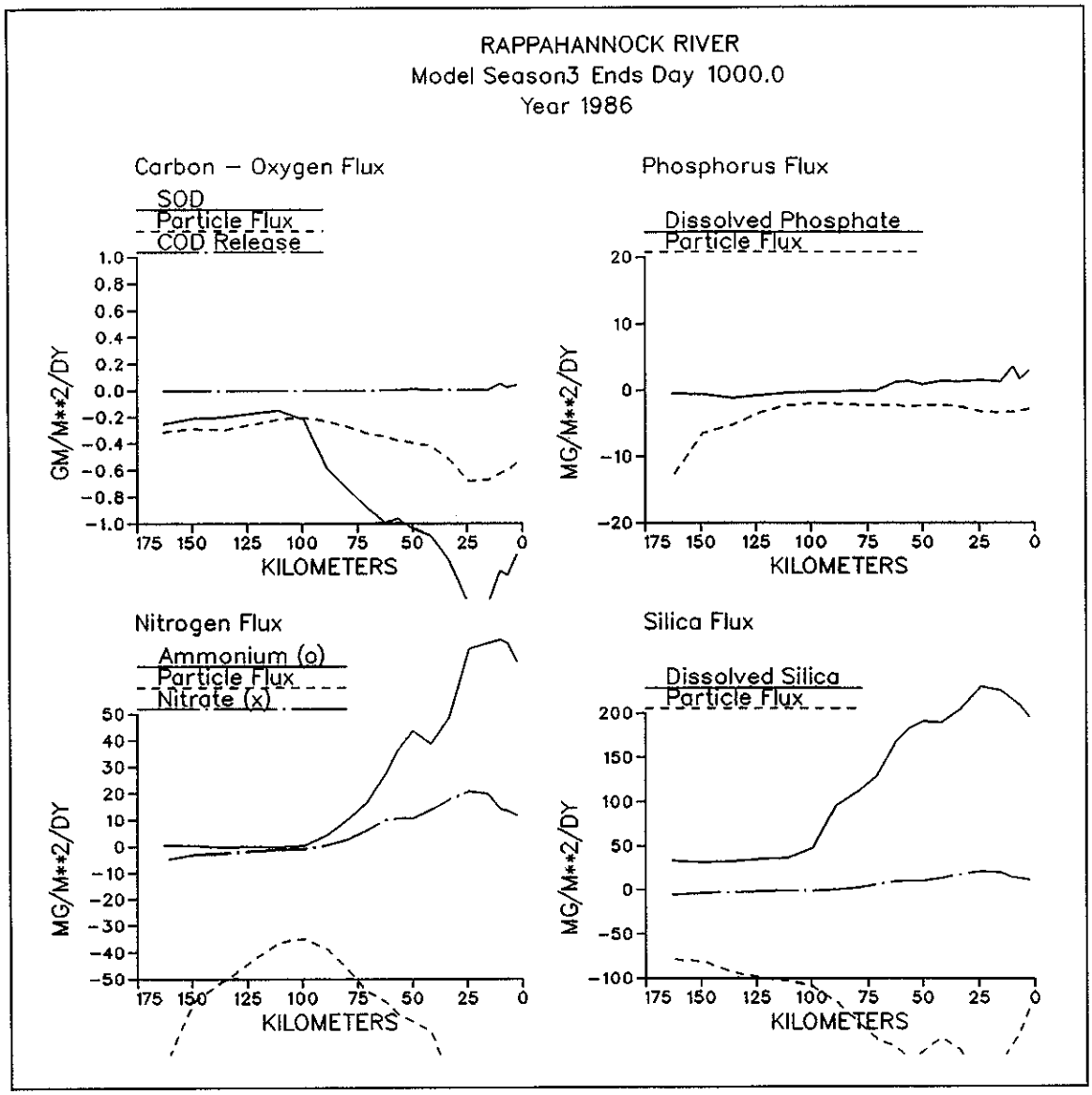

Figure 12-41. Predicted Sediment-Water Fluxes Along Rappahannock River Longitudinal Transect, Season Three, 1986

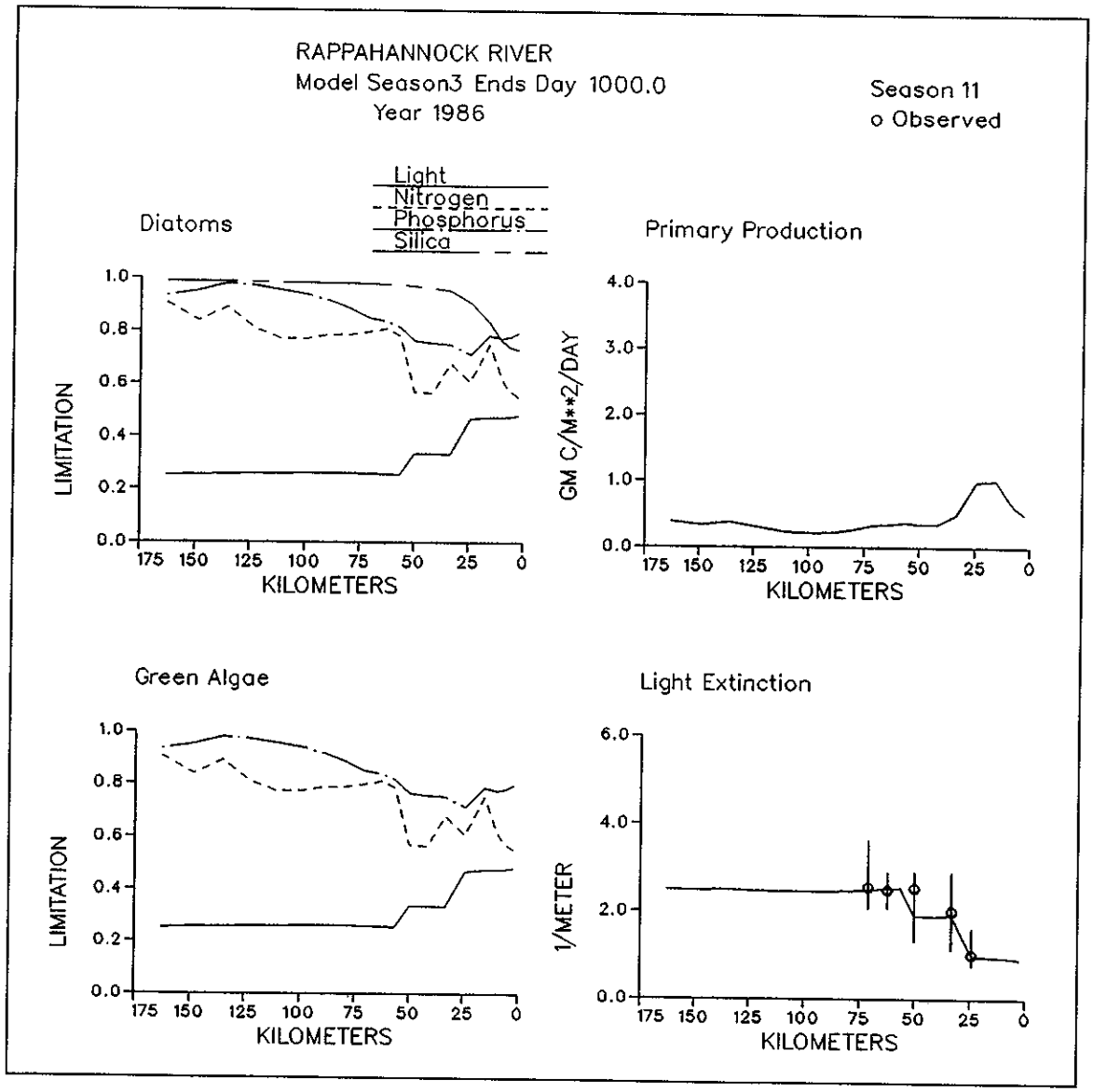

Figure 12-42. Predicted Diagnostic Information Along Rappahannock River Longitudinal Transect, Season Three, 1986

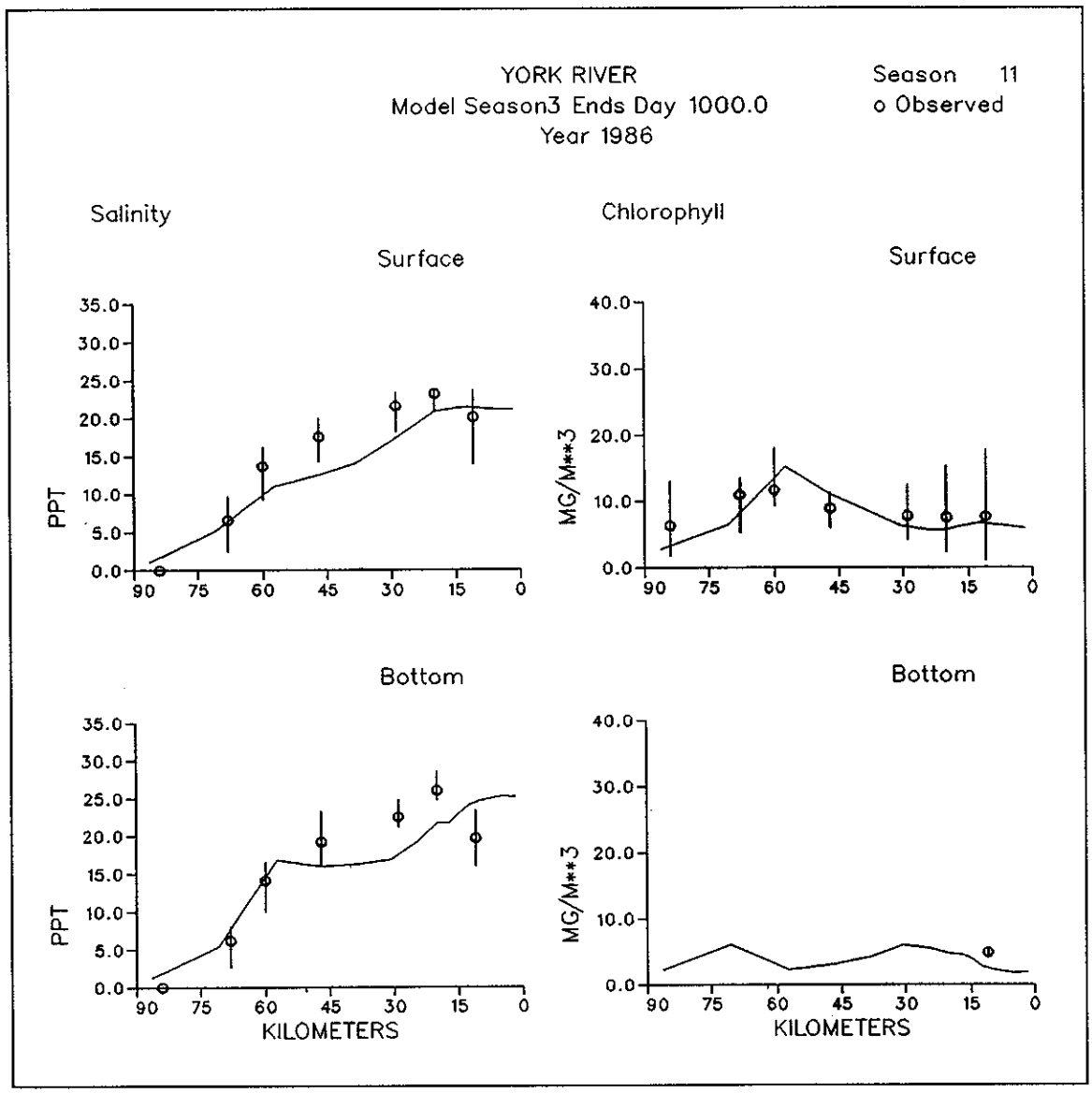

Figure 12-43. Predicted and Observed Concentrations Along York River Longitudinal Transect, Season Three, 1986 (Sheet 1 of 5)

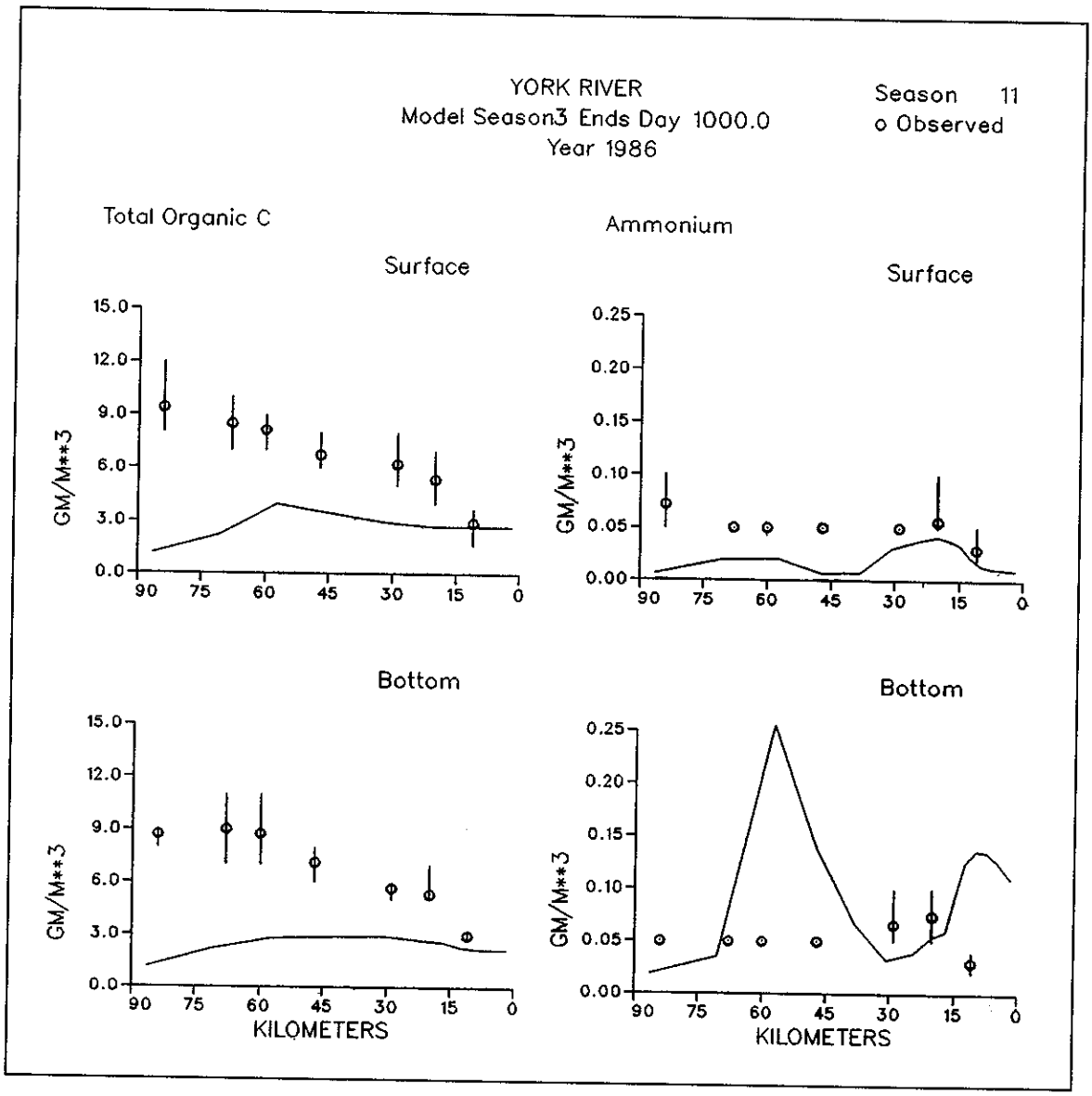

Figure 12-43. (Sheet 2 of 5)

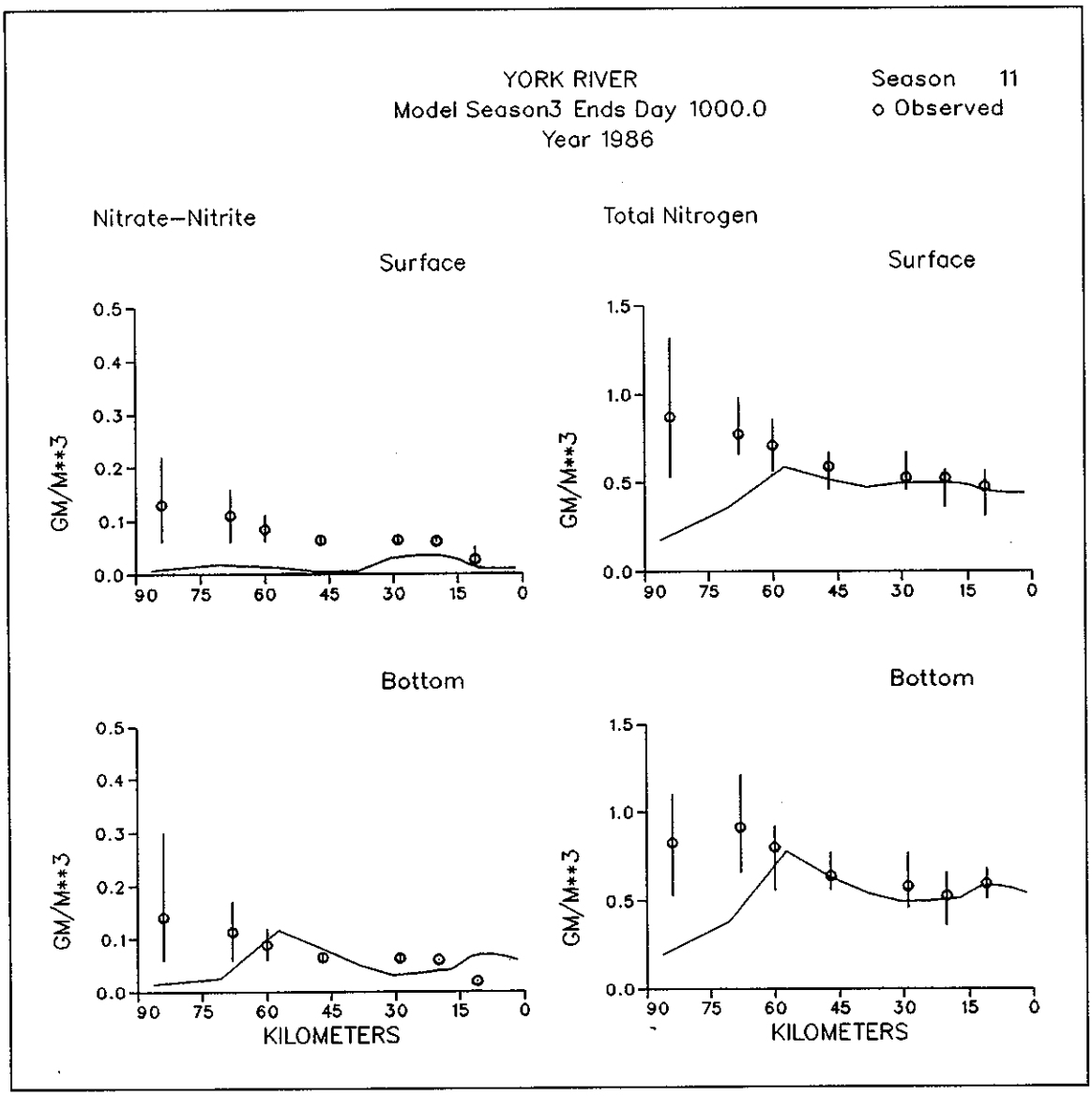

Figure 12-43. (Sheet 3 of 5)

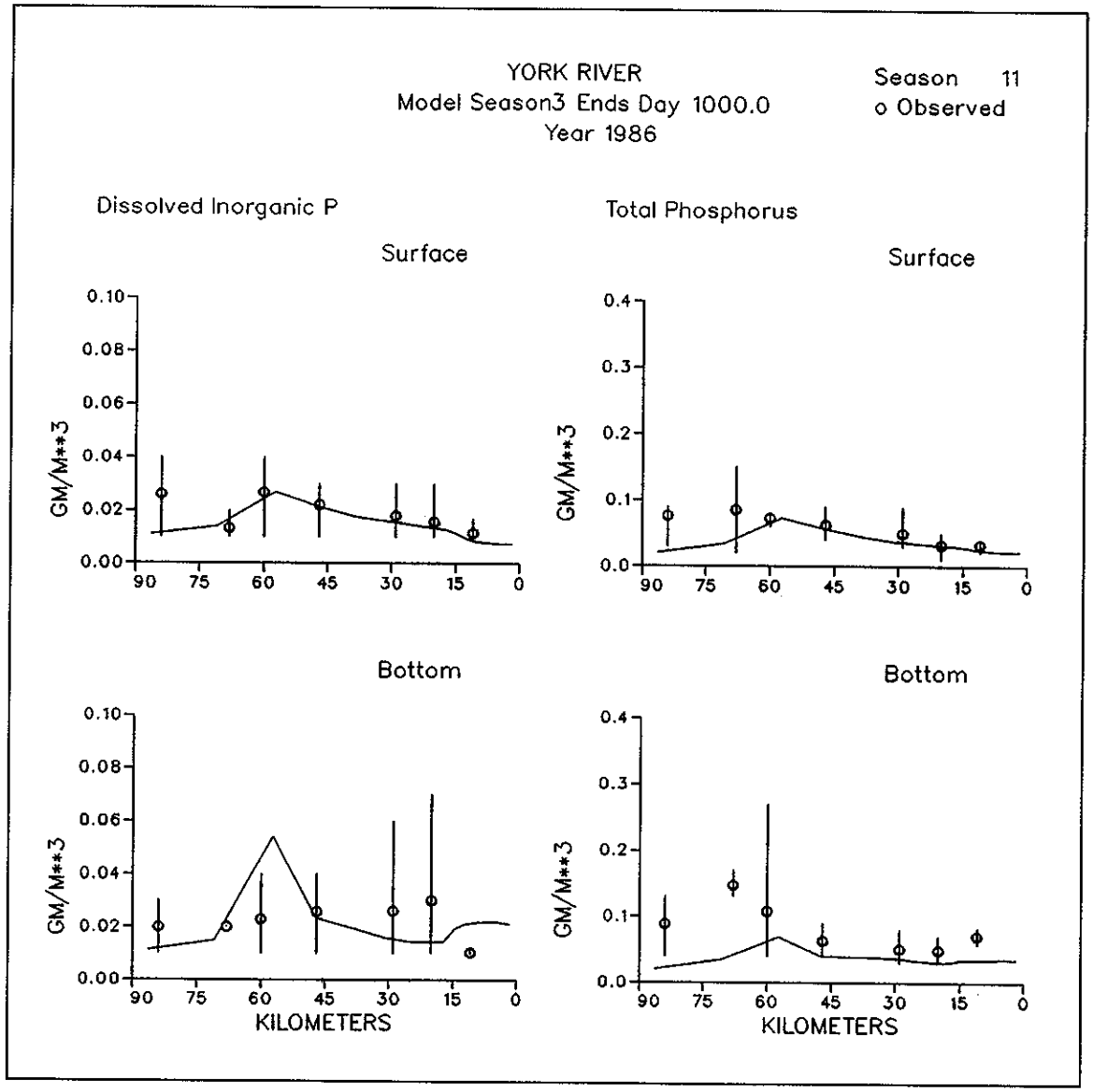

Figure 12-43. (Sheet 4 of 5)

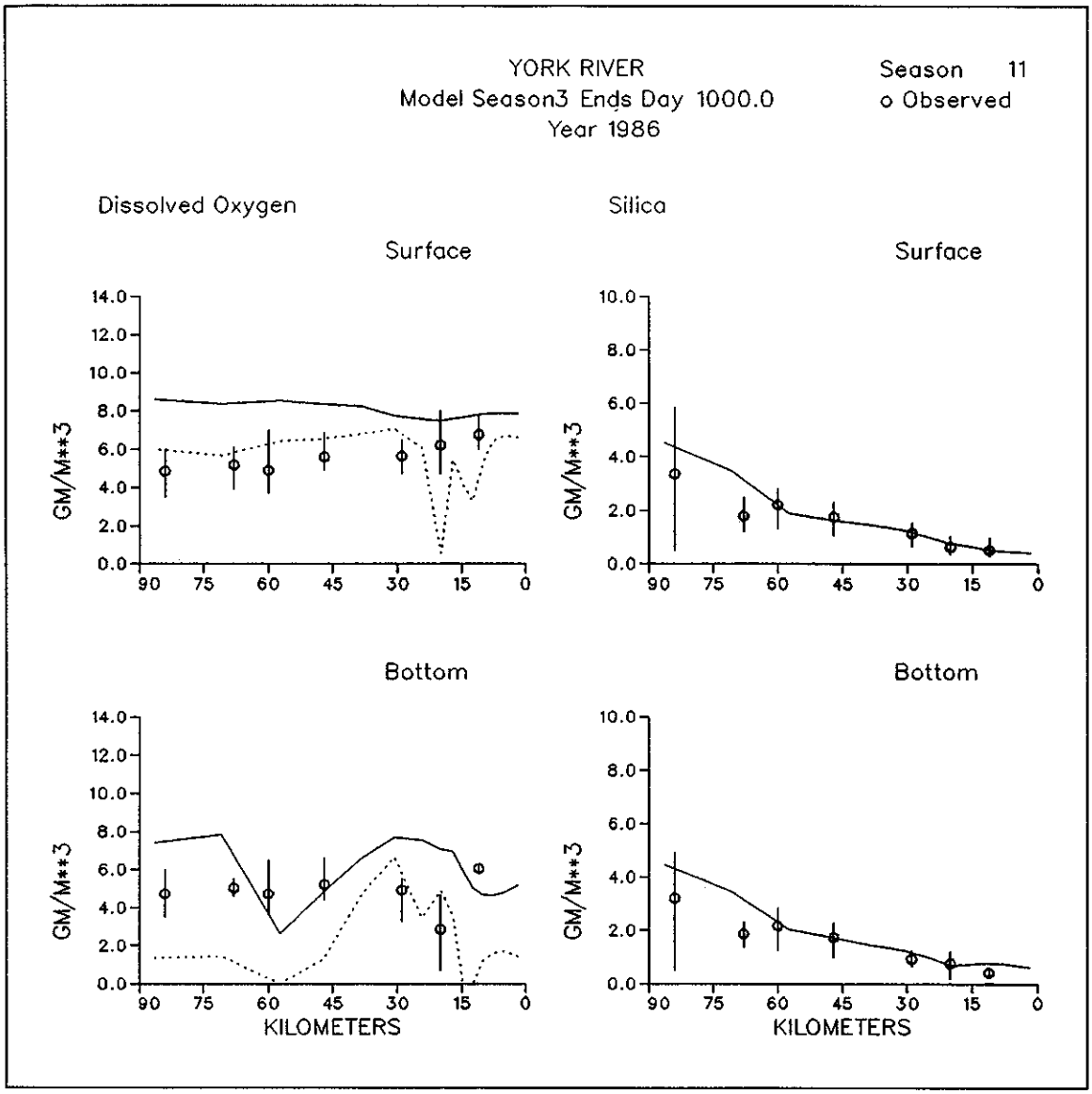

Figure 12-43. (Sheet 5 of 5)

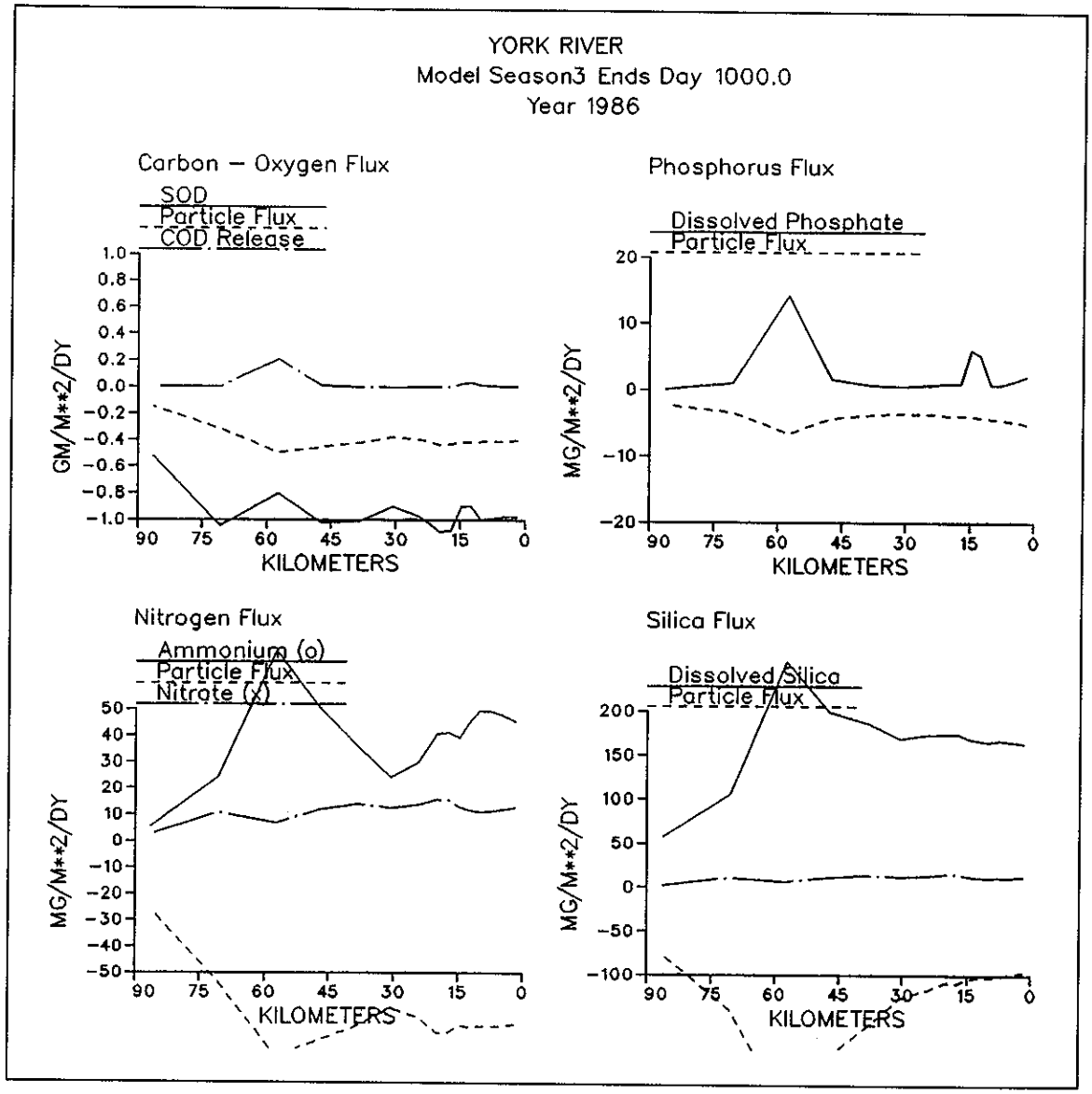

Figure 12-44. Predicted Sediment-Water Fluxes Along York River Longitudinal Transect, Season Three, 1986

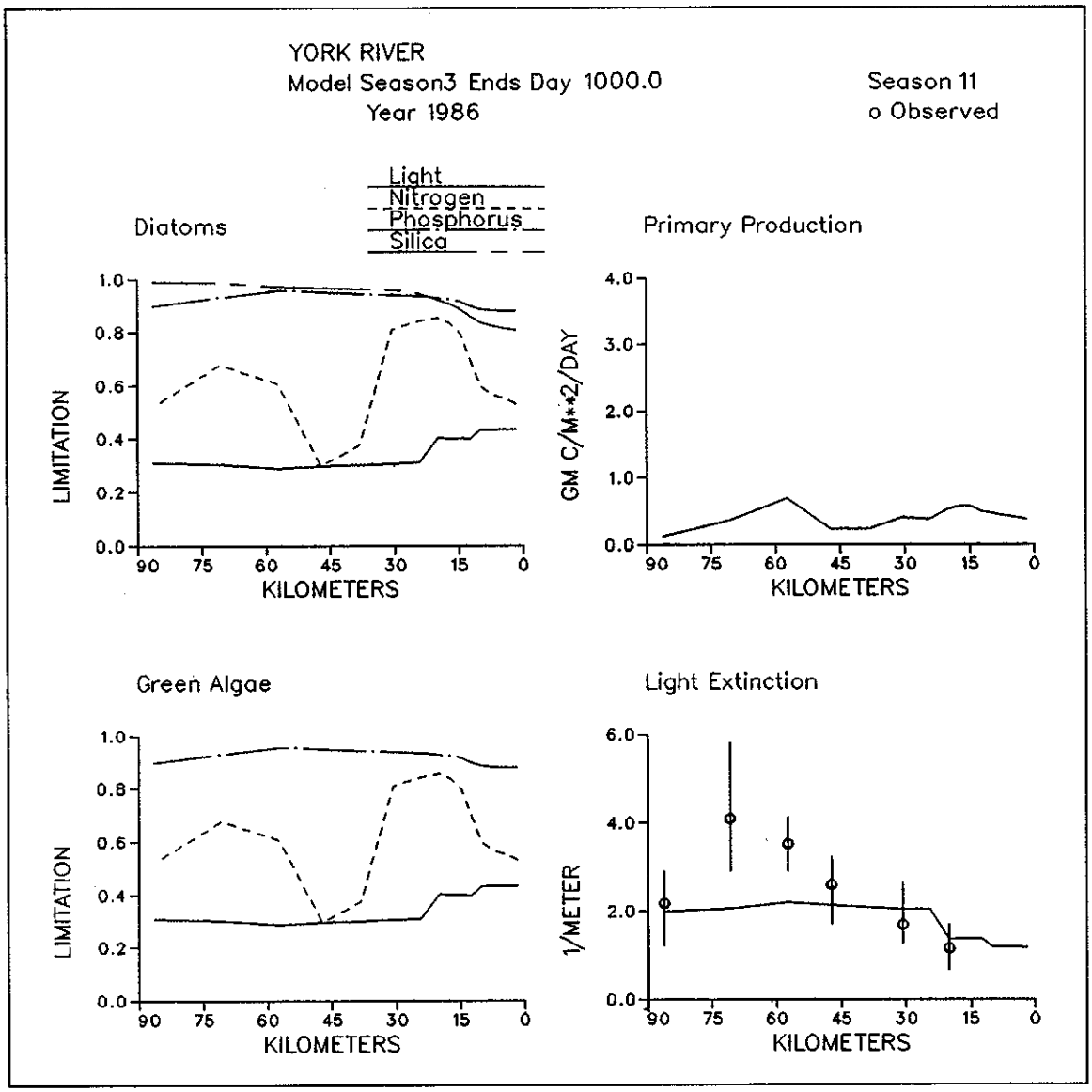

Figure 12-45. Predicted Diagnostic Information Along York River Longitudinal Transect, Season Three, 1986

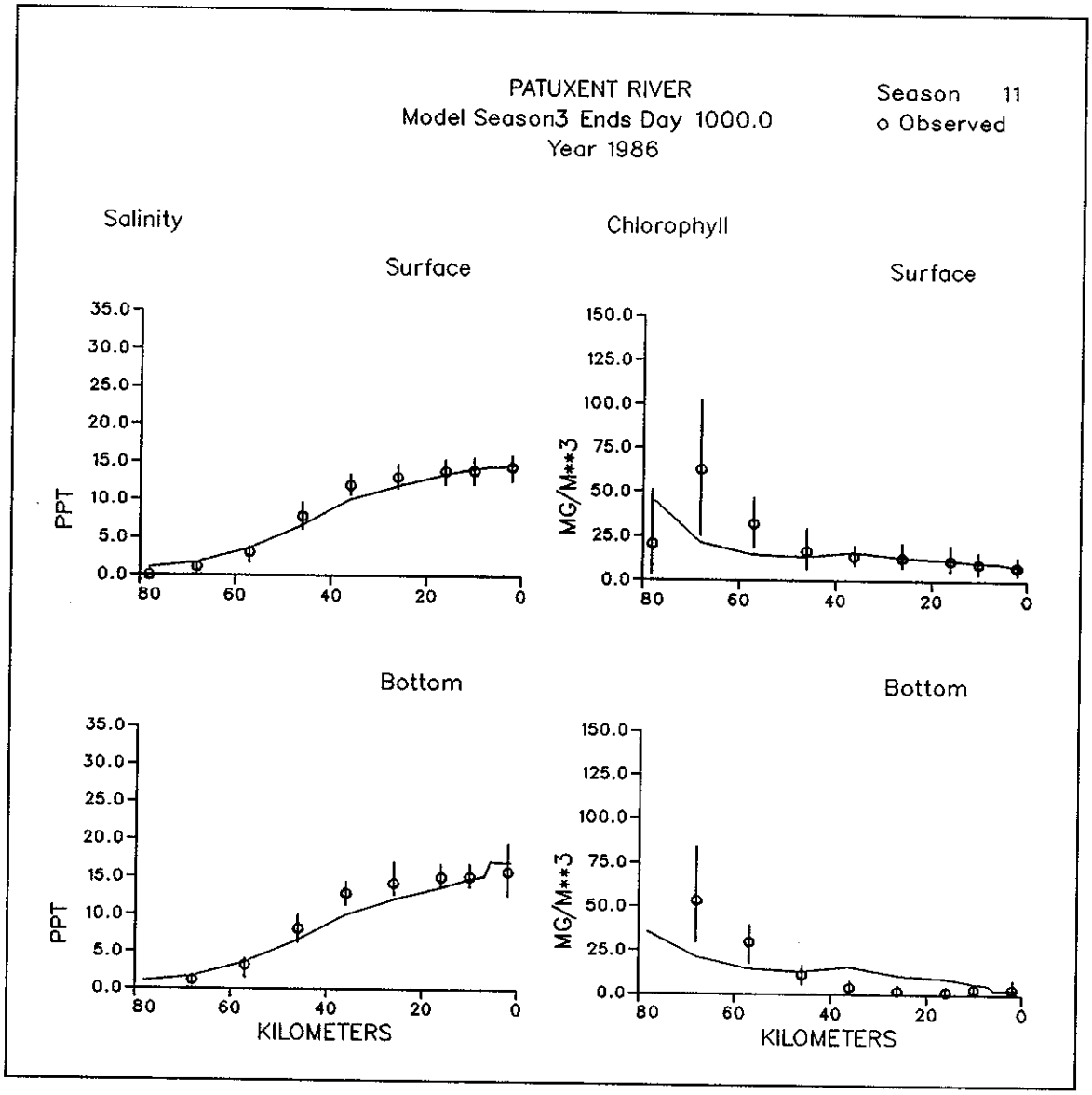

Figure 12-46. Predicted and Observed Concentrations Along Patuxent River Longitudinal Transect, Season Three, 1986 (Sheet 1 of 5)

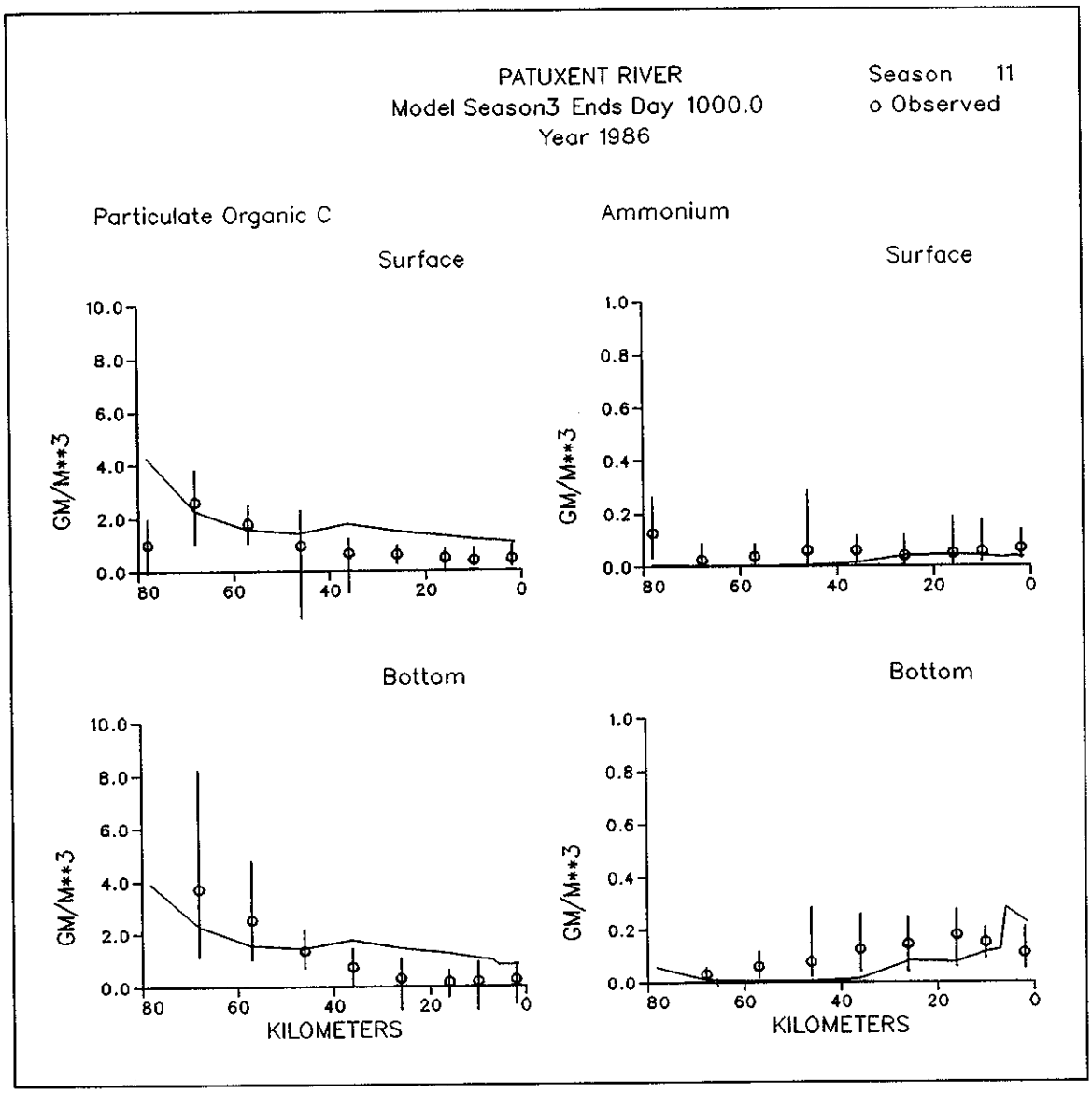

Figure 12-46. (Sheet 2 of 5)

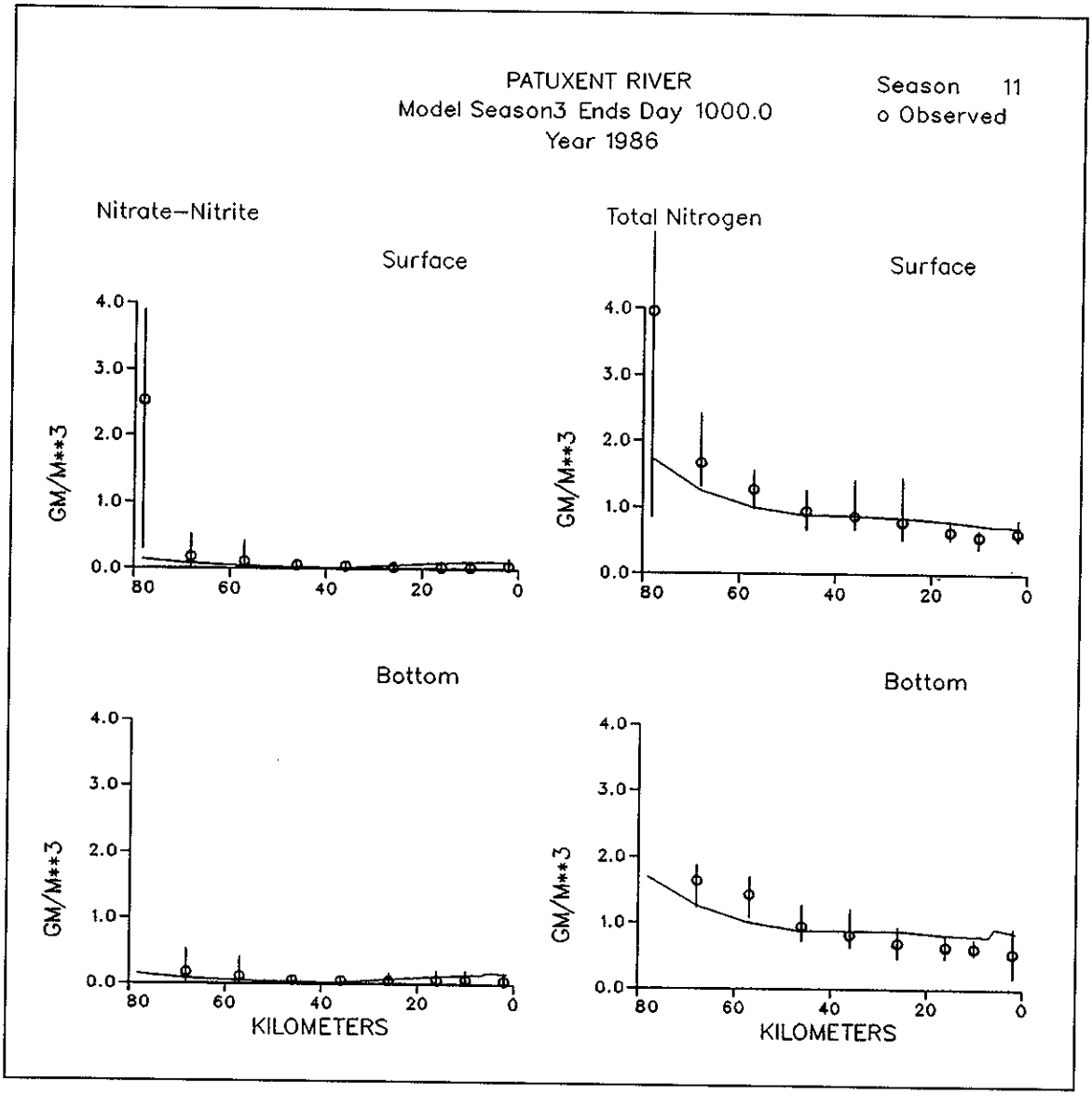

Figure 12-46. (Sheet 3 of 5)

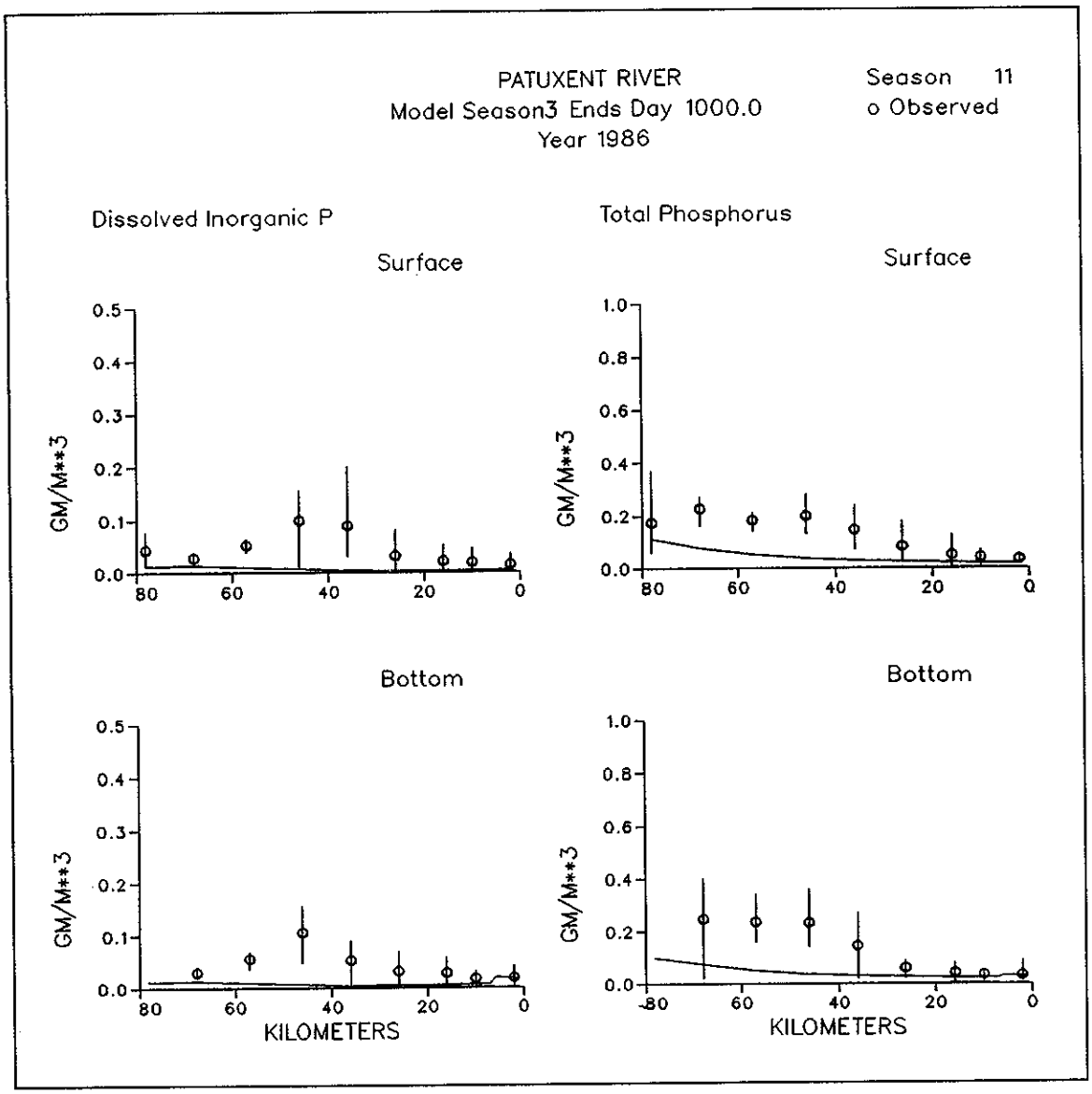

Figure 12-46. (Sheet 4 of 5)

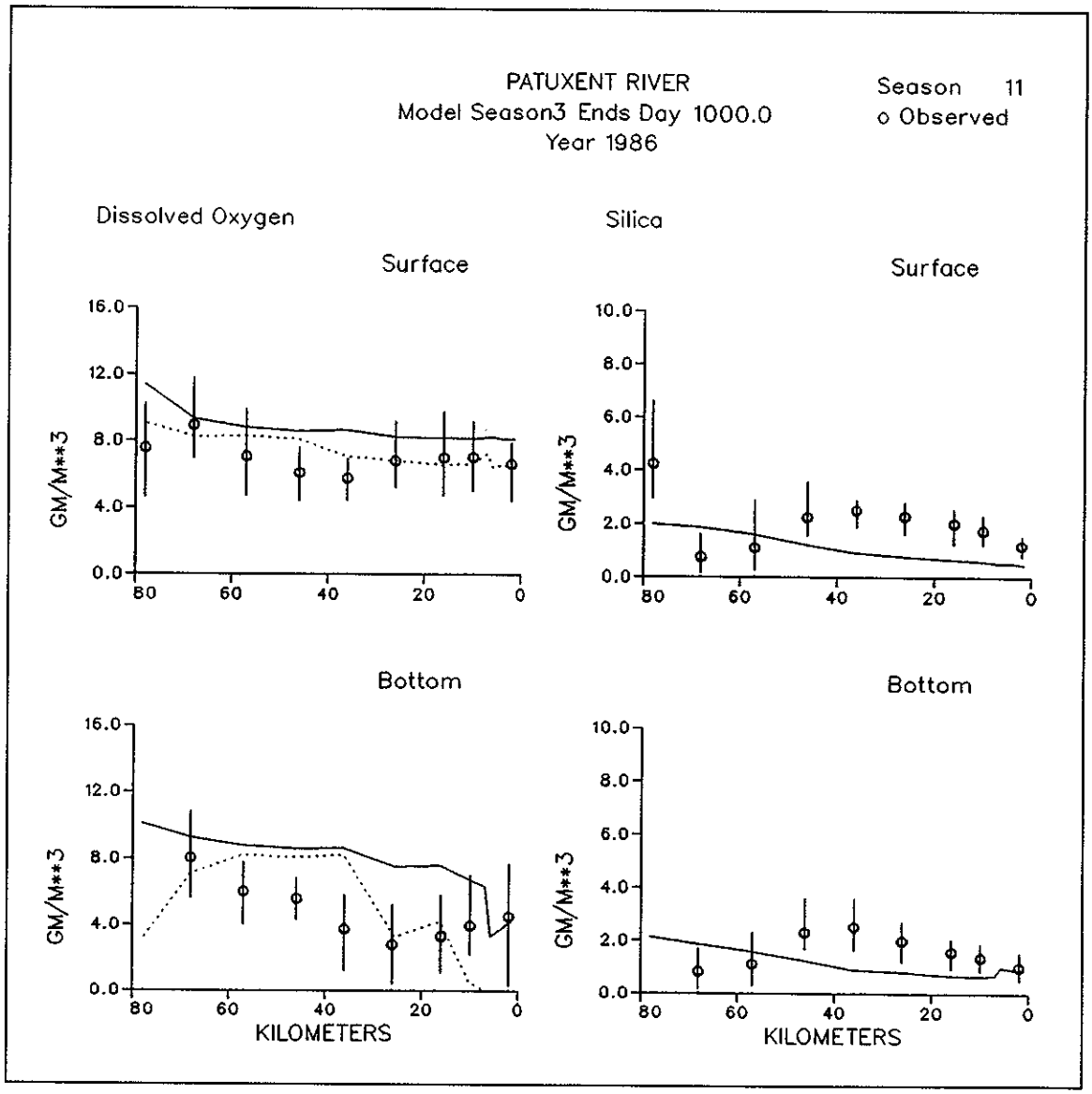

Figure 12-46. (Sheet 5 of 5)

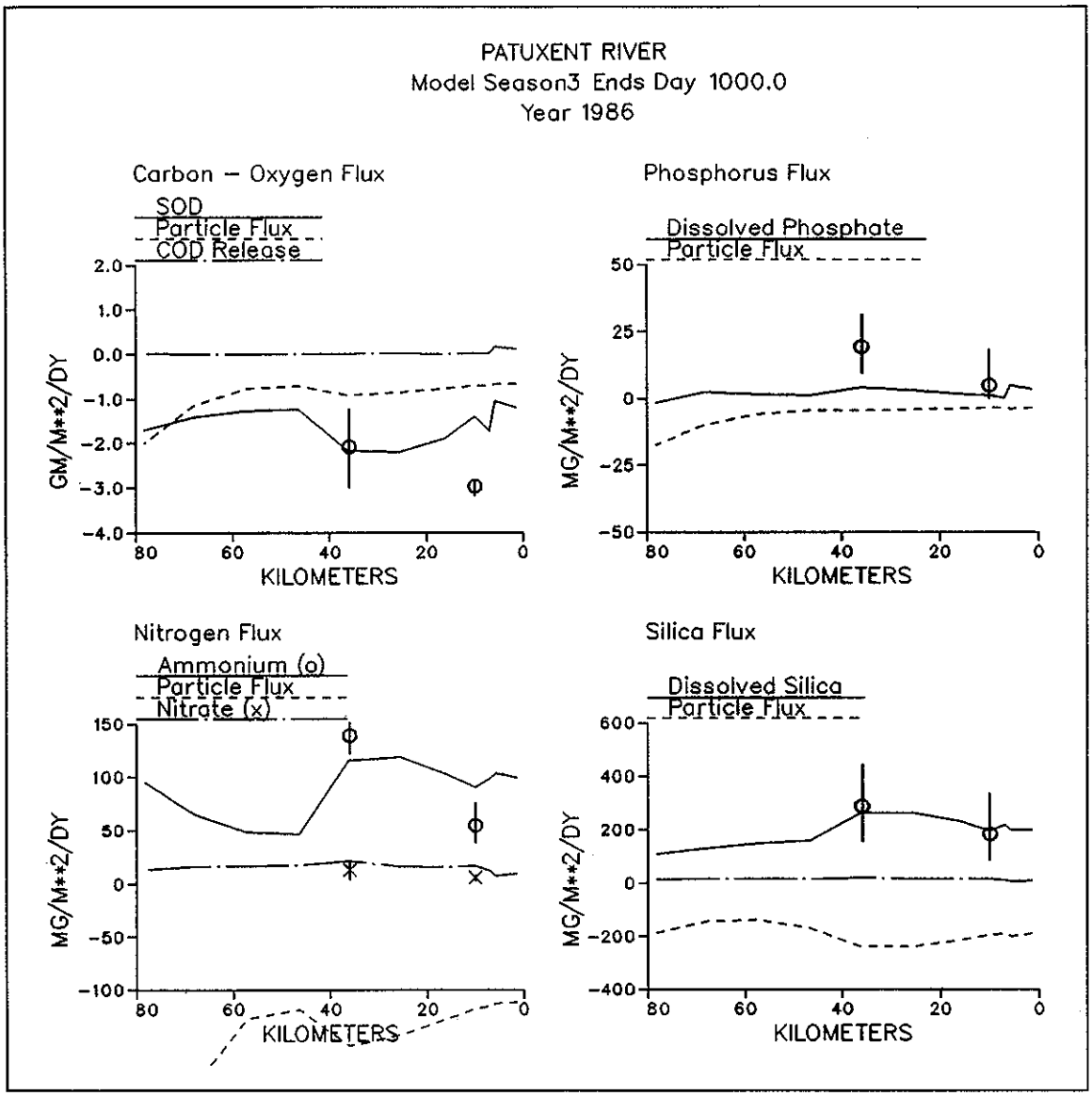

Figure 12-47. Predicted and Observed Sediment-Water Fluxes Along Patuxent River Longitudinal Transect, Season Three, 1986

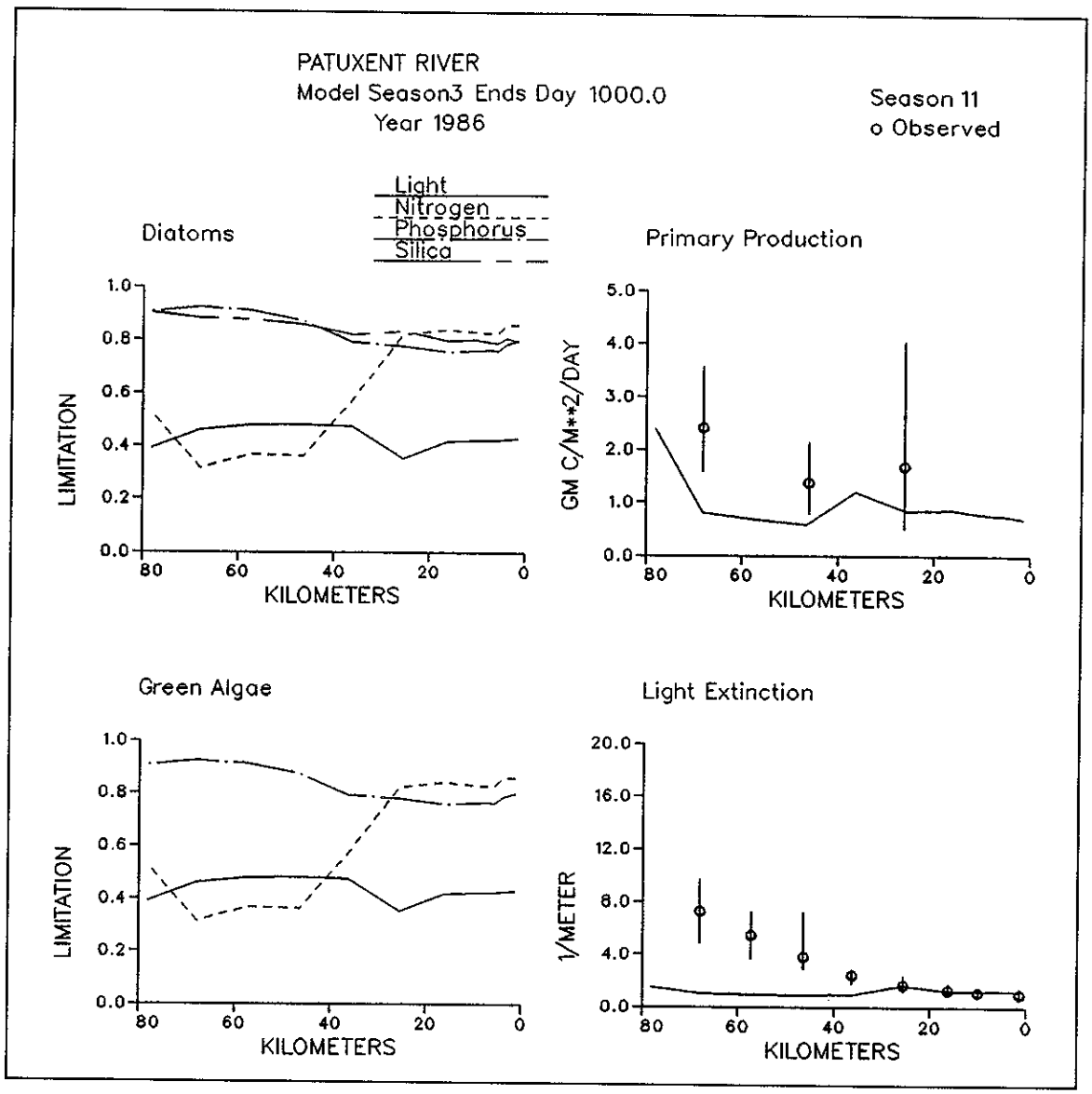

Figure 12-48. Predicted and Observed Diagnostic Information Along Patuxent River Longitudinal Transect, Season Three, 1986

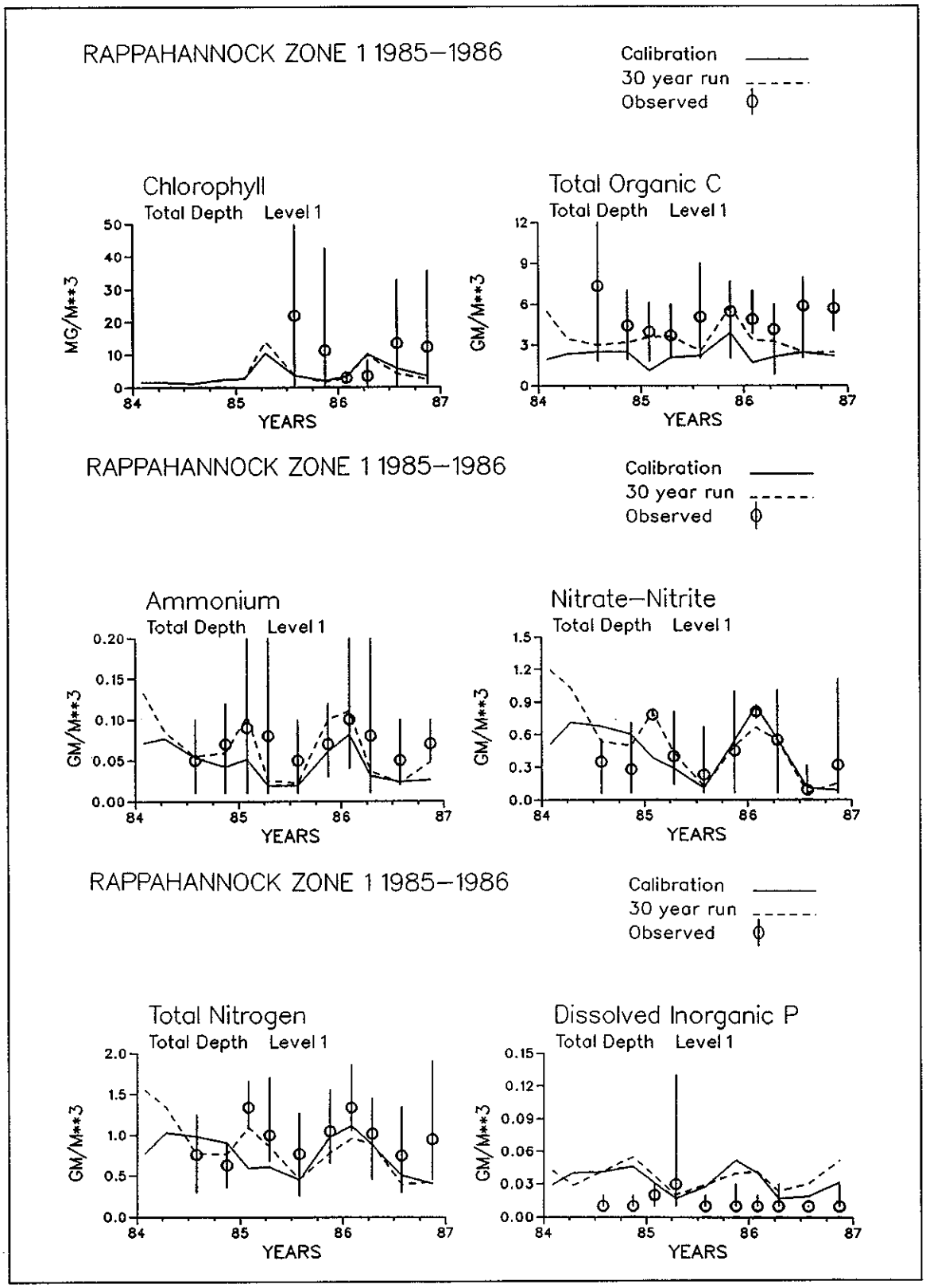

Figure 12-49. Concentrations in Rappahannock Zone One Based on Watershed Model (Calibration) and Regression (30-Year Run) Fall-Line Loads (Continued)

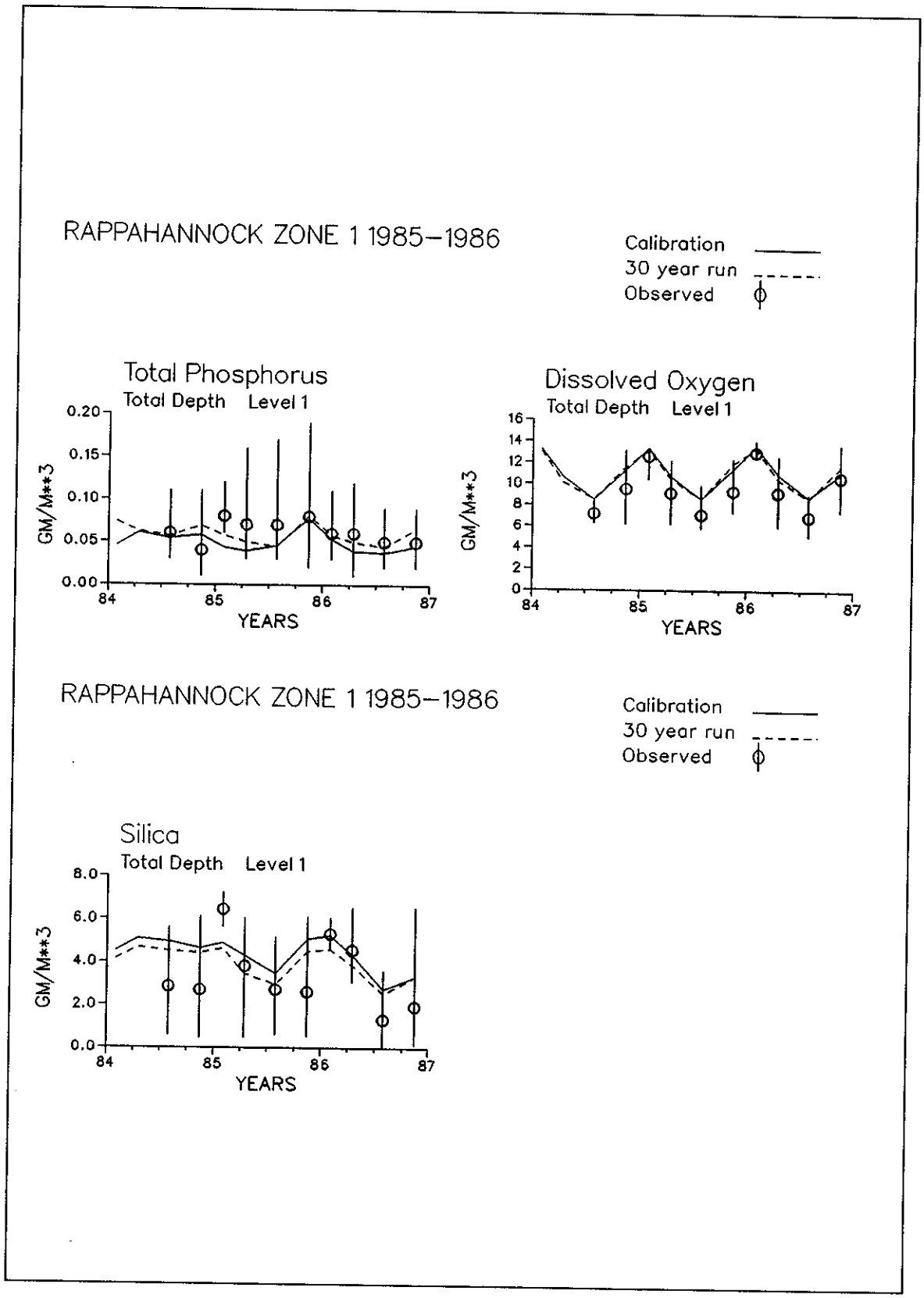

Figure 12-49. (Concluded)

Chapter XIII: Statistical Summary of Calibration

Introduction

The model-data comparisons in the preceding chapters provide a qualitative evaluation of the model calibration. Experienced viewers can examine the plots and form an instinctive judgement on the status of the calibration. Graphical summaries and quantitative, statistical, examinations of the calibration are also possible. These presentations provide new insights as well as exact quantification of the calibration state.

Numerous summaries and analyses of model performance are available. No consensus exists on a standard analytical suite. The basic comparison employed here is between predictions and observations aggregated by season, zone, and level. The mainstem Bay and major tributaries are treated individually. Definitions of the summaries and statistics are provided since these are not standardized.

Presentation Format

Scatterplots

Scatterplots were produced for major water-quality constituents. Model predictions were plotted on the horizontal axis versus observations on the vertical axis. One-to-one correspondence was indicated by a solid, diagonal line. Scatterplots for several substances, when plotted on an arithmetic scale, demonstrated characteristic behavior in which deviation from the one-to-one line increased with the magnitude of the observation. This behavior occurred because the magnitude of the observations was limited at zero on the lower end but was unlimited on the upper end. For these substances, variance about the one-to-one line was normalized by plotting on a logarithmic scale.

Cumulative Error Plots

These plots indicate the percentage of model predictions (vertical axis) that differed from observations by less than an arbitrary amount (horizontal axis). The median absolute difference between predictions and observations can be obtained from these plots by moving across from the 50th percentile until the curve is intersected and then moving down to read the difference on the horizontal axis. Extremes of model performance can be obtained in similar fashion.

Regression Statistics

One popular form of model-data comparison is treatment of predictions as independent variates and observations as dependent variates in regression analysis. The basis of this analysis is that a high degree of correspondence between predictions and observations is indicated by a correlation coefficient that approaches unity, an intercept near zero, and a slope near unity. Regression statistics are provided here but the regression line is not plotted.

Mean Error

The mean error between predictions and observations is defined:

$$E = \frac{\sum (O - P)}{n} \qquad (1)$$

in which:

E = mean error
O = observation, aggregated by season, zone, level
P = prediction, aggregated by season, zone, level
n = number of observations

A mean error of zero is ideal. Positive mean error indicates model predictions are less than observations, on average. A negative mean error indicates model predictions exceed observations, on average.

Absolute Mean Error

The absolute mean error between predictions and observations is defined:

$$E_{abs} = \frac{\sum |O - P|}{n} \qquad (2)$$

in which:

E_{abs} = absolute mean error

An absolute mean error of zero is ideal. The magnitude of the absolute mean error indicates the average deviation between predictions and observations.

Root-Mean-Square Error

The root-mean-square error is defined:

$$E_{rms} = \sqrt{\frac{\sum (O - P)^2}{n}} \quad (3)$$

in which:

E_{rms} = root-mean-square error

A root-mean-square error of zero is ideal. The root-mean-square error is an indicator of the deviation between predictions and observations. The root-mean-square is an alternative to (and usually larger than) the absolute mean error.

Relative Error

The relative error is defined:

$$E_{rel} = \frac{\sum |O - P|}{\sum O} \quad (4)$$

in which

E_{rel} = relative error

The relative error is the ratio of the absolute mean error to the mean of the observations.

Evaluation of Results

Summary plots and statistics for the mainstem Bay are included in the present volume (Figure 13-1). Summary plots and statistics for each tributary are in the appendix.

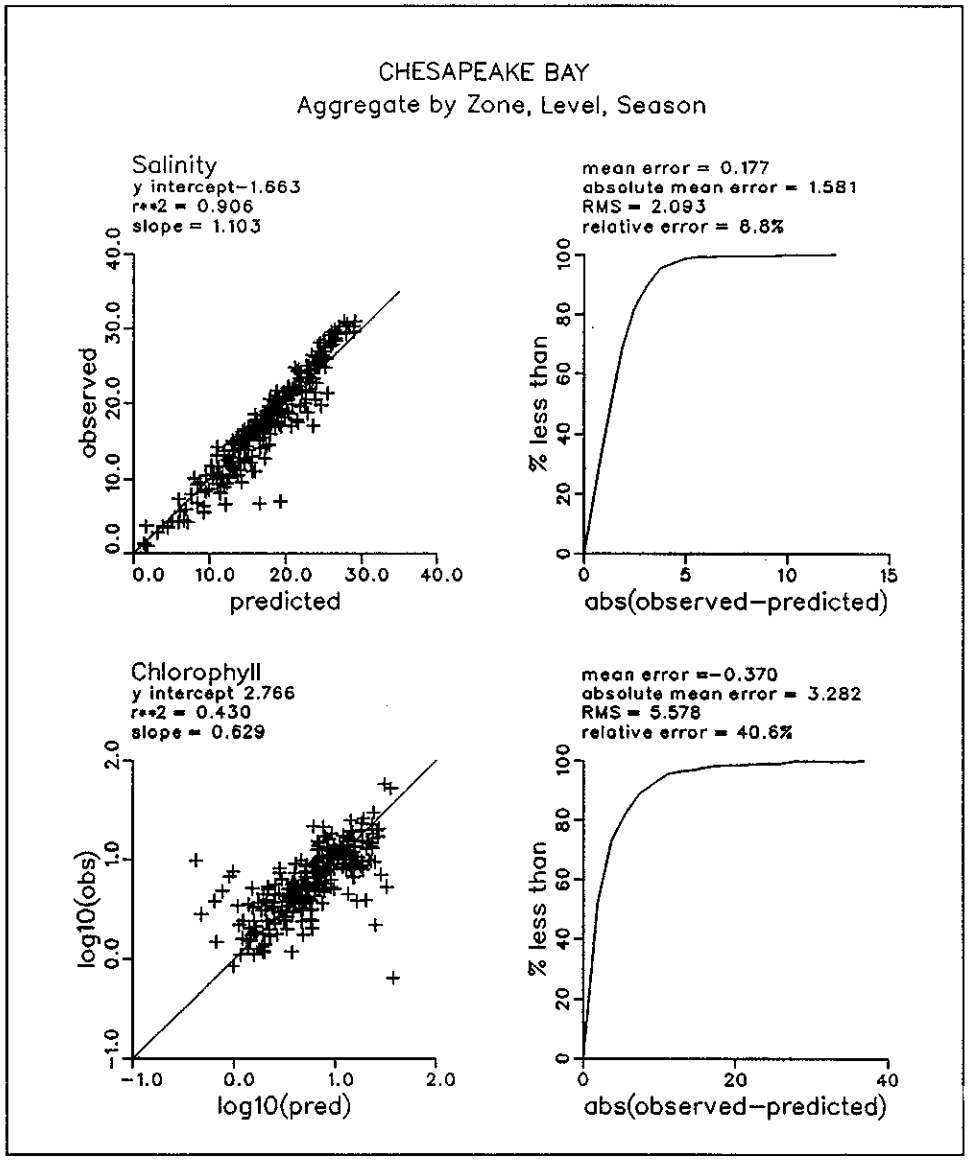

Figure 13-1. Graphical Summary and Statistics for Mainstem Bay (Sheet 1 of 5)

Mainstem Scatter Plots

The salinity scatter plot demonstrated nearly ideal correspondence of model and data. Predictions and observations were close to the one-to-one line throughout the range of observations. Deviations from the one-to-one line were minor and random. The minor discrepancies were inevitable results of sampling protocol, analytical uncertainty, aggregation of model and data, and similar effects.

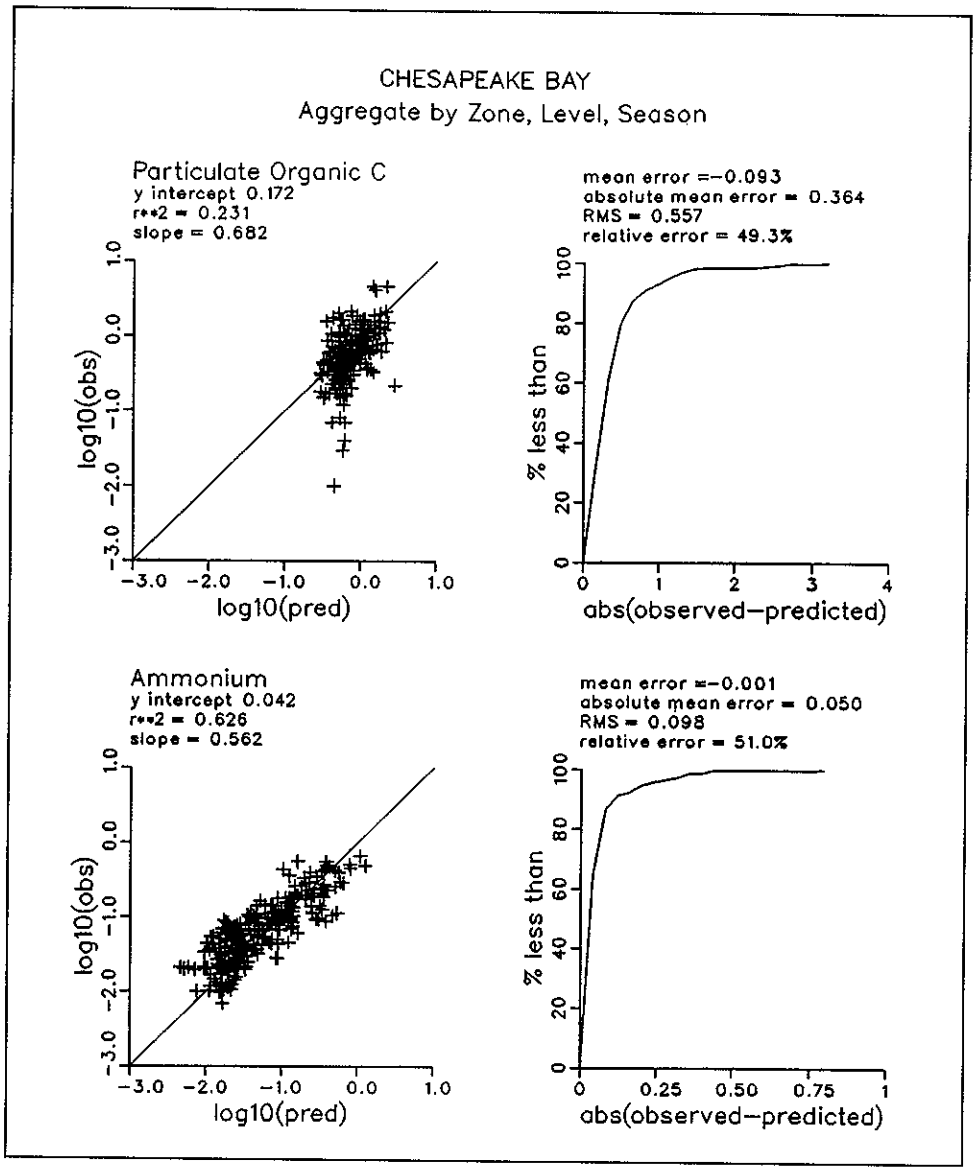

Figure 13-1. (Sheet 2 of 5)

One-to-one correspondence of model and data was also evident for chlorophyll, ammonium, nitrate, total nitrogen, and dissolved oxygen. Conformance of individual data points to the line of exact correspondence was not as close as for salinity, however. Several chlorophyll observations differed by an order of magnitude from predictions. These indicated the natural algal population exhibited behavior that was not always predictable by a mechanistic, mathematical model. Predicted dissolved oxygen often exceeded observations when observed dissolved oxygen was less than 5 gm m^{-3}.

The particulate organic carbon plot indicated model and data were largely in the same range. A few predictions exceeded observations by an order of magnitude, however. Most particulate carbon was algal biomass or detritus.

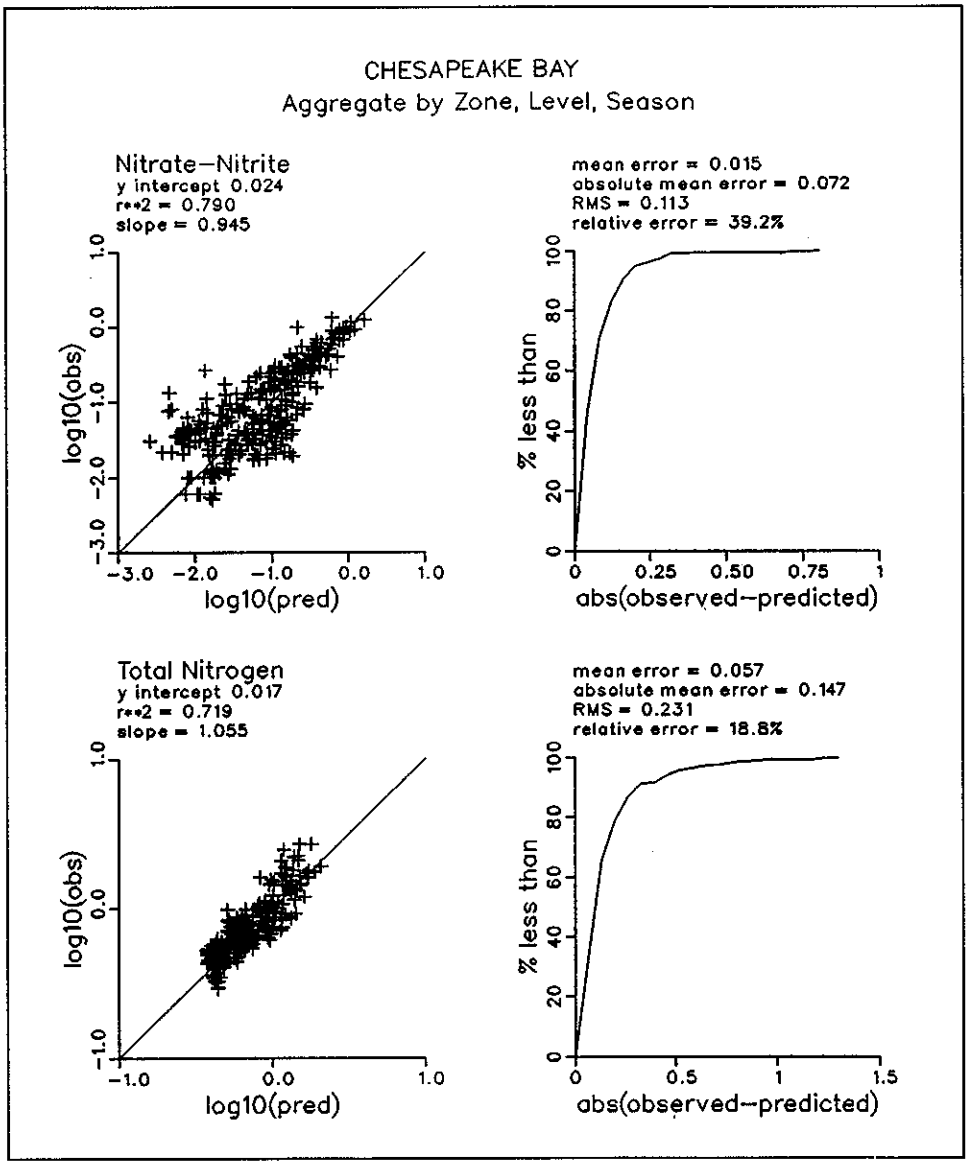

Figure 13-1. (Sheet 3 of 5)

As with chlorophyll, the deviations illustrated the difficulty in predictive modeling of a naturally-variable population.

A large majority of total phosphorus observations exceeded predictions. The systematic excess suggested a shortfall in loading. Dissolved phosphate observations also exceeded predictions when predictions were less than 0.01 gm m^{-3}. The apparent disagreement was partially an artifact, however, of minimum phosphate detection level in the observations.

The silica plot illustrated curvilinear behavior. Minimum observations, ≈0.1 gm m^{-3}, exceeded minimum predictions, ≈0.01 gm m^{-3}, while observations greater than ≈0.3 gm m^{-3} were usually exceeded by predictions. The

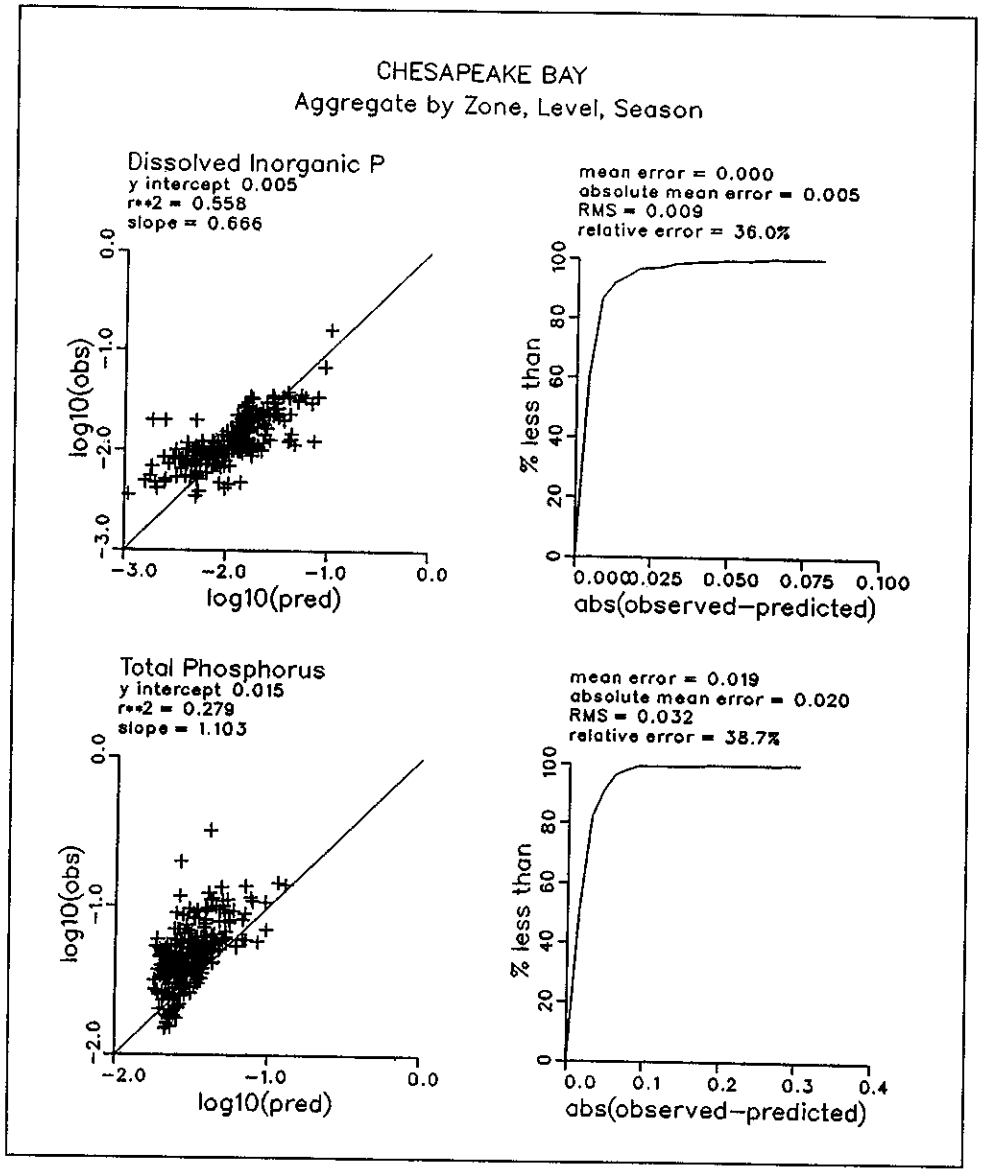

Figure 13-1. (Sheet 4 of 5)

origin of the cross-over between under-prediction and over-prediction was not apparent but detection limits may have had a role.

Mean Error in Bay and Tributaries

The mean error statistic in the mainstem and tributaries (Figure 13-2) supported observations already made in the review of calibration and scatter plots. In particular, a shortfall in predicted total phosphorus was evident throughout the system. In the mainstem, the mean error was 38% of the observed mean concentration. The mean error indicated a deficiency in total phosphorus loading.

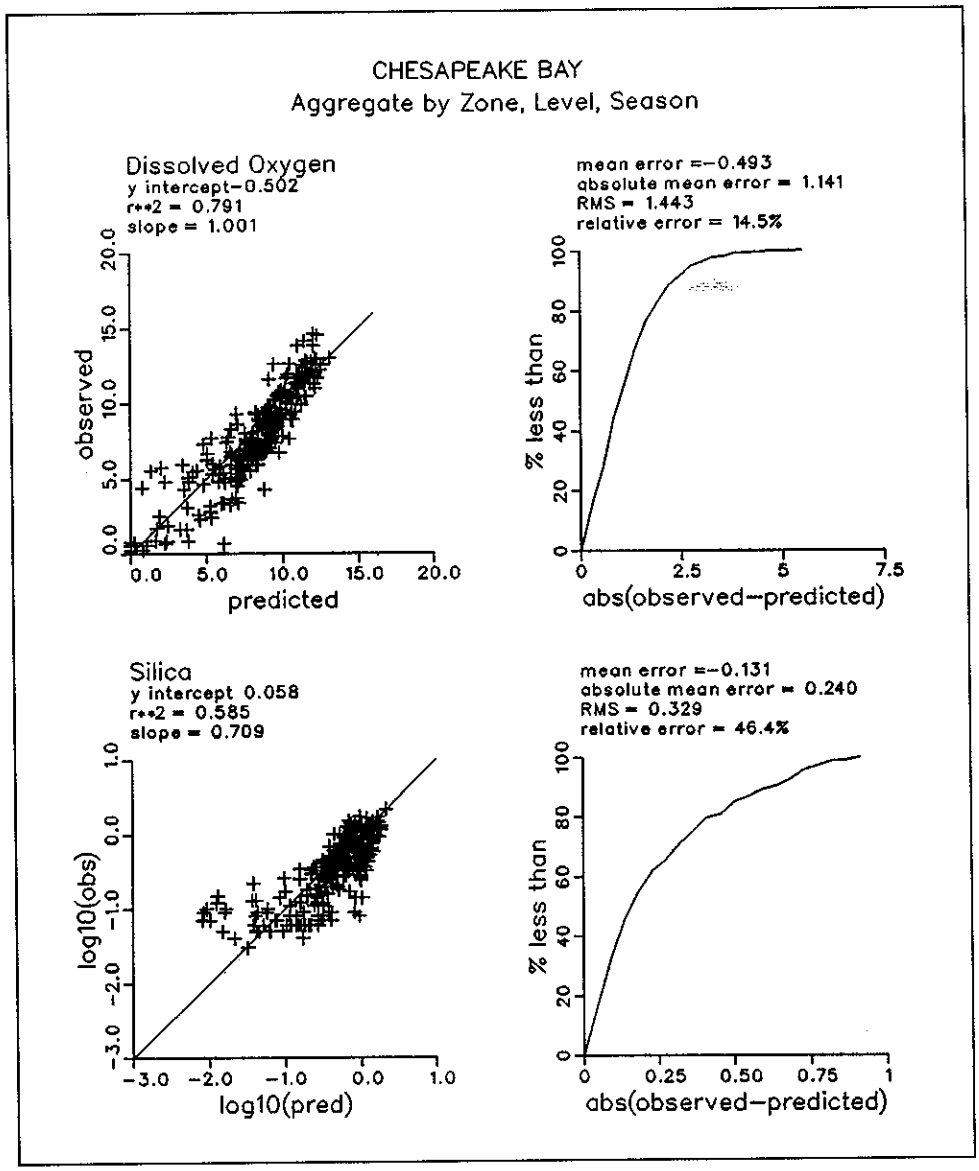

Figure 13-1. (Sheet 5 of 5)

Total nitrogen was also under-predicted, on average. The bias was not apparent in preceding analyses. In the mainstem, the mean error was 5% of the observed mean concentration.

Bank erosion is the likely origin of the missing phosphorus. Estimated erosion loads, 6000 kg day^{-1} (CBPO 1991), are roughly 18% of the loads presently considered in the model.

Loads from bank erosion are not the source of the missing nitrogen, however. Nitrogen loads from bank erosion are minor, 4500 kg day^{-1} (CBPO 1991), roughly 1% of the loads considered in the model. A potential source of additional nitrogen is atmospheric loading. Estimated atmospheric load to the

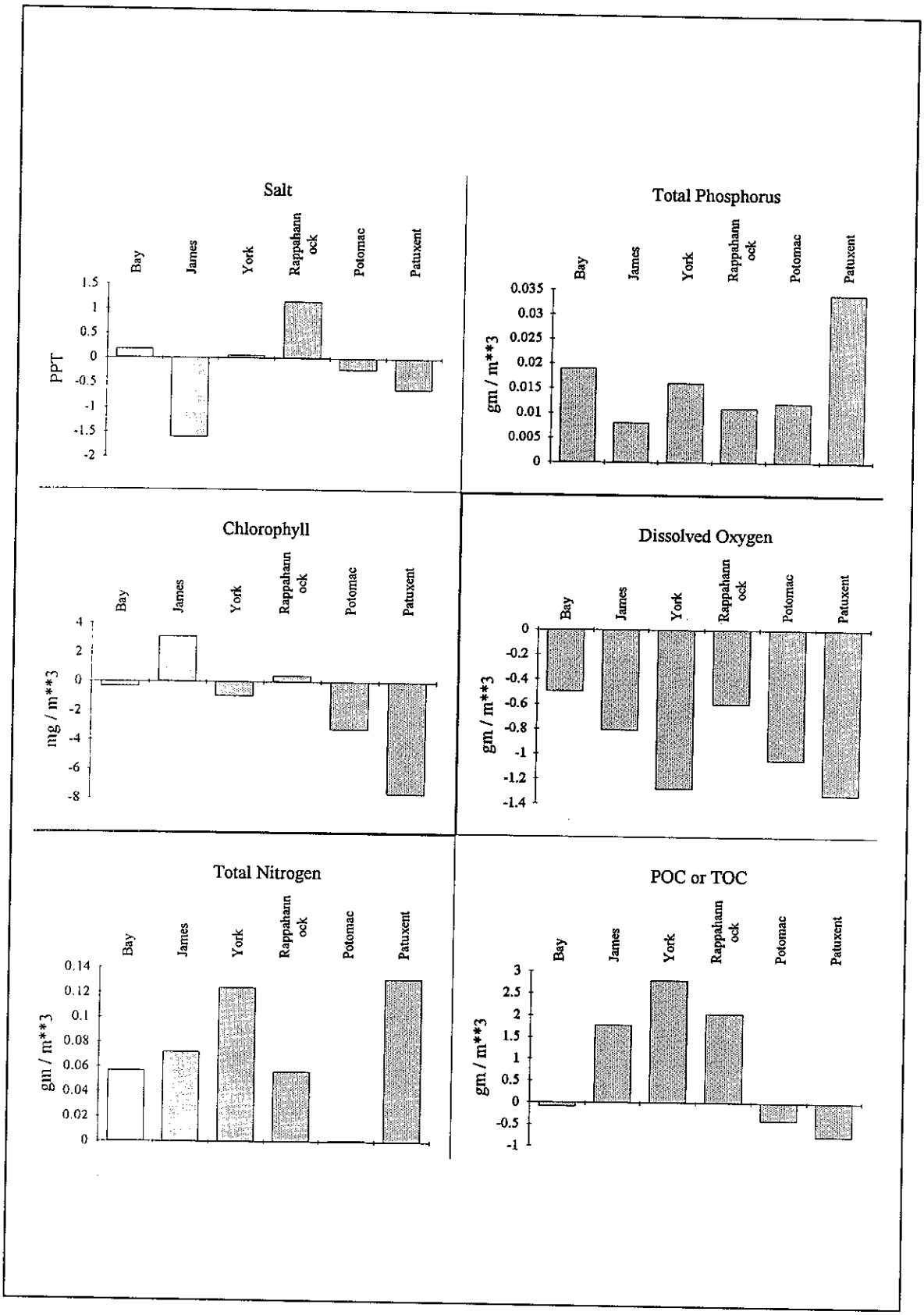

Figure 13-2. Mean Error (Observed - Predicted) in Mainstem Bay and Tributaries

Inland Bays of Delaware, based on measures conducted at Cape Henlopen, is 3.5 gm N m^{-2} yr^{-1} (Cerco et al. 1993). The estimated load to the Inland Bays is more than double the load presently employed in the Chesapeake, 1.5 gm N m^{-2} yr^{-1}. Since atmospheric loads presently comprise 9% of the total nitrogen load, doubling atmospheric loads could easily make up the 5% shortfall in nitrogen.

Mean error summaries indicated observed dissolved oxygen was less than predicted throughout the system. In the mainstem, over-predictions most often occurred in subsurface water characterized by oxygen deficiencies. In the tributaries, over-predictions most often occurred in surface waters nearly saturated with dissolved oxygen.

Absolute Error in Bay and Tributaries

Absolute error in the mainstem was usually less than the tributaries for nutrients, chlorophyll, dissolved oxygen and carbon (Figure 13-3). An exception was absolute salinity error in the mainstem which equalled or exceeded the error in most tributaries. The statistic was surprising since previous analyses indicted salinity predictions in the mainstem were superior. The statistic was apparently an artifact of the lengthy freshwater reaches of the tributaries. In these regions, salinity predictions, essentially zero, were perfect, and biased the absolute error summary for the entire tributary.

Relative Error in Bay and Tributaries

The relative error statistic permitted comparisons between diverse substances and systems (Figure 13-4). Salinity was the substance with least relative error in all bodies. The low error was attributed to the conservative nature of salinity and to the well-known, single source at the ocean. At the other extreme, relative error was greatest for chlorophyll and organic carbon. The high error reflected the non-conservative behavior of algal biomass and organic detritus, the unlimited source of atmospheric carbon, and the approximate nature of mathematical models of biological processes.

Relative error for dissolved oxygen and nutrients was intermediate. Favorable statistics reflected limits on the range of potential values and knowledge of sources and sinks. The atmospheric source of oxygen was unlimited but the range of predicted concentrations was restricted between zero and saturation. The concentrations of total nitrogen and phosphorus were unlimited but dependent on loads which were known to a reasonable extent.

For most substances, relative error was less in the mainstem than in the tributaries. Differences in salinity and dissolved oxygen errors were minor, however. Relative chlorophyll error was clearly much less in the mainstem than in the tributaries. The Potomac and Patuxent stood out as having unusually large chlorophyll errors. In the Potomac, the error reflected the need for

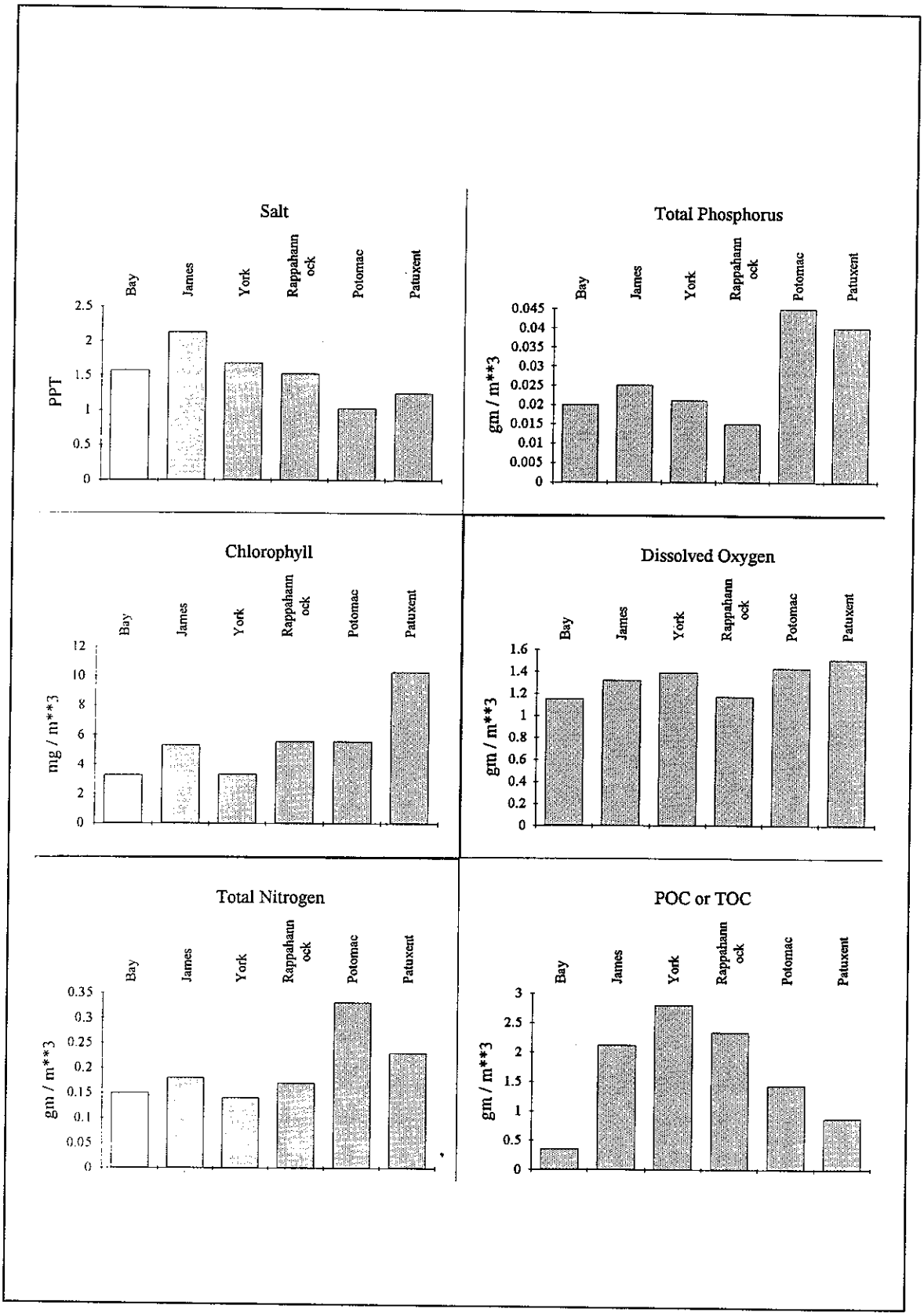

Figure 13-3. Absolute Error in Mainstem Bay and Tributaries

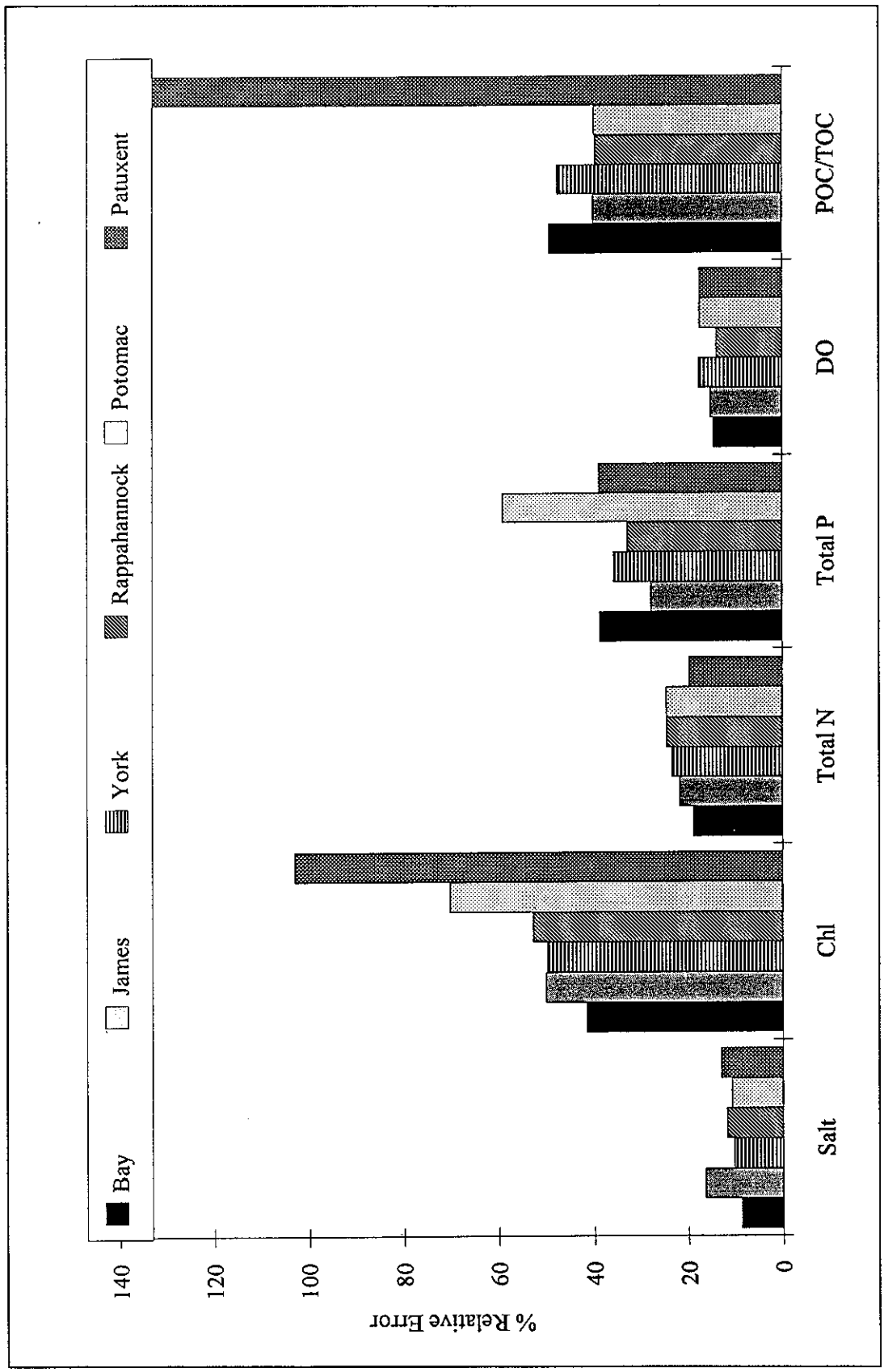

Figure 13-4. Relative Error in Mainstem Bay and Tributaries

improved calibration of cyanobacteria. The origin of the Patuxent error was not apparent.

Total phosphorus provided an exception to the trend of favorable performance in the mainstem relative to the tributaries. The James, York, and Rappahannock Rivers had lower relative error than the mainstem. The apparent superior performance was partially an artifact of the relative error statistic which normalized absolute mean error by mean concentration. In the James and Rappahannock, absolute error exceeded error in the mainstem but mean concentration exceeded the mainstem as well. Consequently, these two tributaries had greater absolute error but less relative error than the mainstem.

Relative Error at Different Stages of Calibration

The model went through four major stages of calibration (Table 13-1). At each stage, modifications were made to the code, loads, or parameter values. Although each change produced qualitative improvements in model-data agreement or in predictive power of the model, statistical behavior of several key constituents was largely unchanged from the initial calibration. Mean errors of total nitrogen, total phosphorus, and dissolved oxygen retained their original biases throughout the calibration period (Figure 13-5). No monotonic decline in magnitude of mean or relative error (Figure 13-6) was apparent for these constituents.

Table 13-1
Major Stages of Calibration

Date	Total Computer Runs	Status
December 1990	100	Initial calibration. Fall–line loads from regression model. Open–mouth boundary conditions based on observations.
April 1991	150	Revised parameter values. Fall–line loads from regression model. Reflected nutrient boundary conditions at open mouth.
December 1991	200	Revised parameter values. Fall–line loads from Phase I EPA Watershed Model. Original boundary condition formulation.
February 1992	220	Revised parameter values. Revisions to sediment model. Fall–line loads from Phase II EPA Watershed Model. Nutrient concentrations at open mouth computed by mass balance.

The persistence of the error statistics and model-data discrepancies indicate important characteristics of the Chesapeake Bay eutrophication model.

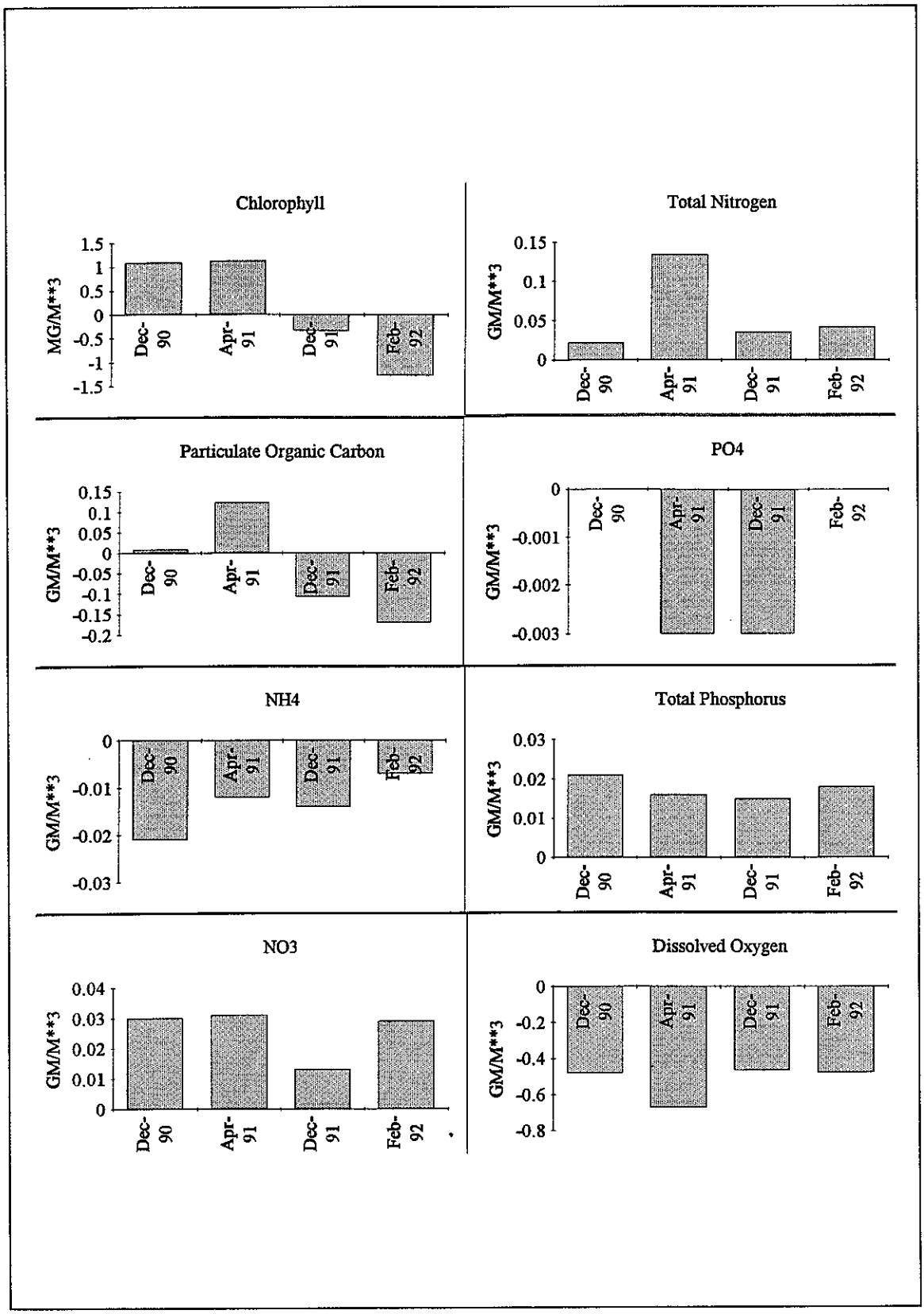

Figure 13-5. Mean Error (Observed - Predicted) in Mainstem Bay at Four Stages of Calibration

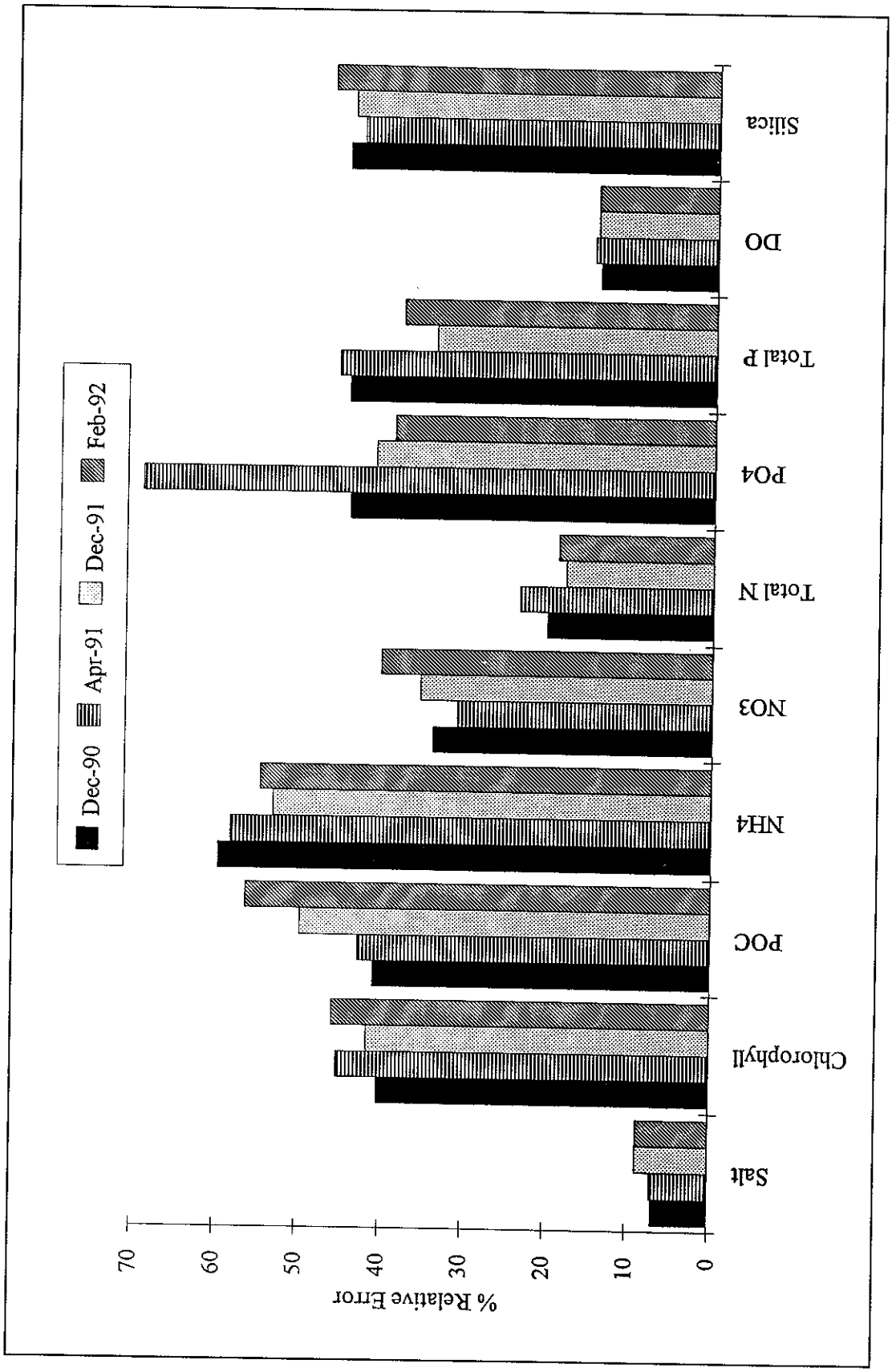

Figure 13-6. Relative Error in Mainstem Bay at Four Stages of Calibration

Predictions are robust and not readily manipulated by the modeler. Deficiencies in loads or formulations are revealed and difficult to counter.

The progress of statistics through 220 model runs indicates that additional calibration of the present model is futile. Improvements in model-data agreement require new estimates of loads to the system or reformulation of model principles.

Sediment Model Performance

The method selected to summarize sediment model performance was determined by the nature of the observations. Due to differences in temporal and spatial scale between the observations and the model, computation of statistics based on direct comparison of model fluxes with corresponding observations was inappropriate. Neither were sufficient observations available for comparisons based on temporal and spatial aggregations. The method selected for evaluation compared the population of observations with the corresponding population of model values.

Populations were compared through cumulative distribution plots (Figure 13-7). These plots indicated, on the vertical axis, the percentage of predictions and observations less than fluxes indicated on the horizontal axis. Ideal correspondence was indicated by lines which overlay directly. Observations were the entire suite of SONE data for 1985 and 1986 in the mainstem and tributaries. Predictions were model results for cells overlying SONE stations for months in which observations were collected.

Correspondence between the distributions of predicted and observed ammonium, nitrate, and phosphate flux was remarkable. Ammonium distributions corresponded through roughly ninety-percent of the populations. Major deviation was limited to the upper ten-percent of the populations in which observed fluxes exceeded the predictions. Nitrate and phosphate exhibited similar behavior. Distributions of predictions and observations corresponded except in the upper extreme. The highest five percent of observed nitrate fluxes exceeded predictions; the highest five percent of predicted phosphate fluxes exceeded observations. For silica, predicted fluxes were less than observed through most of the range. Median predicted flux was 35 mg m^{-2} day^{-1} (16%) less than observed. Predicted sediment oxygen demand was also less than observed. At the median, predictions were 0.2 gm m^{-2} day^{-1} (18%) below observations.

Comparison of predicted and observed sediment oxygen demand was complicated by the dependence of oxygen demand on water-column dissolved oxygen. A more dependable comparison was between predicted and observed carbon diagenesis, the principal component of sediment oxygen demand. Observations of carbon diagenesis were not collected in the SONE program. Estimates of annual-average diagenesis were produced by the standalone

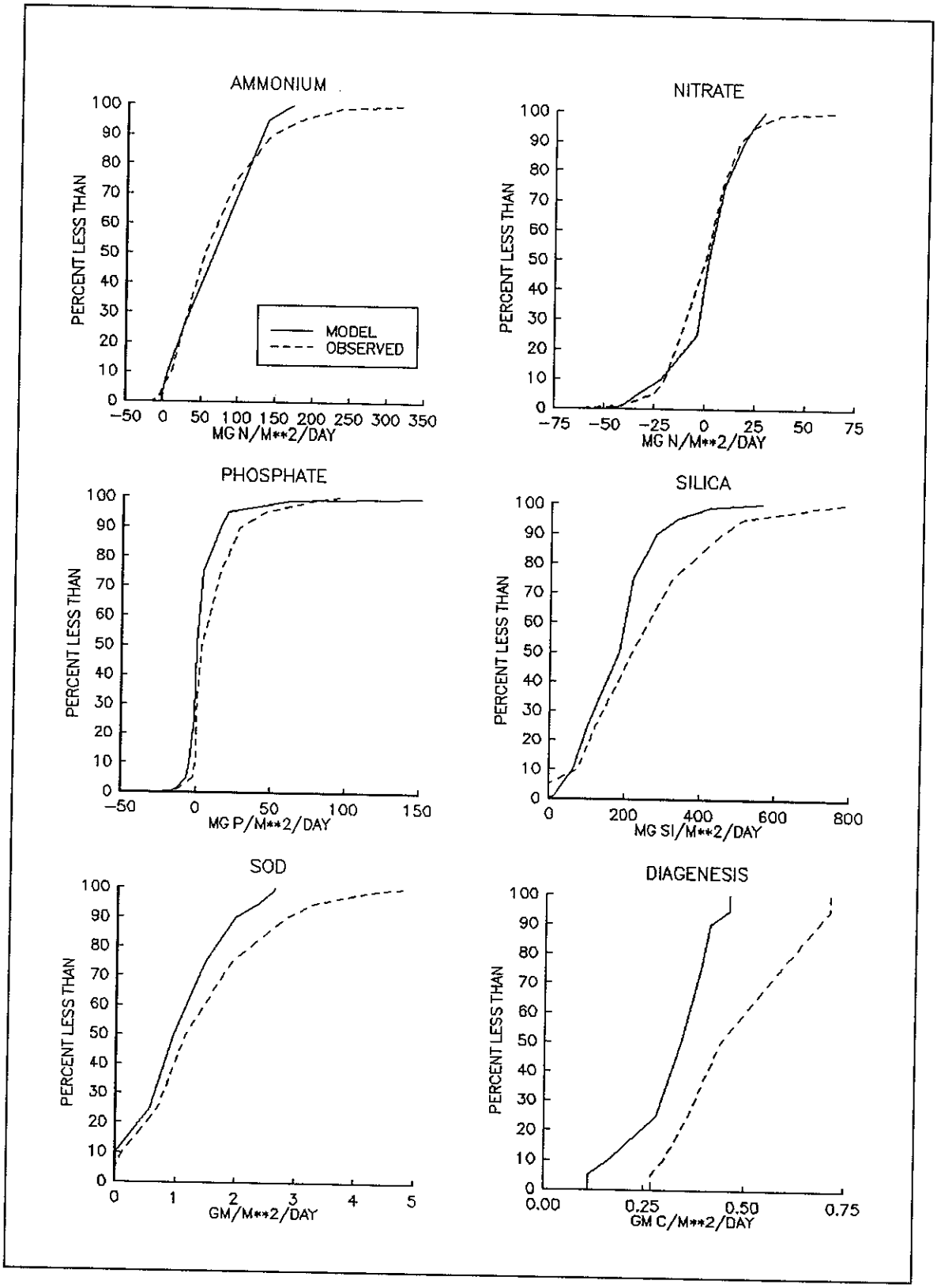

Figure 13-7. Distributions of Observed and Predicted Sediment-Water Fluxes

model, however. These estimates were determined as the diagenesis required for the standalone model to reproduce the observed sediment-water fluxes.

Diagenesis in the standalone and coupled models followed the pattern established in the comparison of observed and predicted sediment oxygen demand. Median diagenesis in the coupled model was 0.1 gm C m^{-2} day^{-1} (23%) less than diagenesis in the standalone model. This comparison confirmed the underestimation of sediment oxygen demand by the model was real rather than an effect of predicted dissolved oxygen on oxygen demand.

The under-prediction of carbon diagenesis in the sediments was consistent with the previously-noted under-prediction of primary production in the water column. Diminished carbon production resulted in less deposition to the sediments. The effect of the under-predicted sediment oxygen demand was partially reflected in the over-prediction of dissolved oxygen in the lower portion of the mainstem water column.

Comparison With Alternate Models

Comparison of statistics between model studies is dangerous. In contrast to classic statistics, no standard definition of model statistics exists. Various treatments of predictions and observations, aggregation for example, affect the magnitude of statistics and complicate comparisons. Since the conflicts and complications cannot be eliminated, review of model application and statistical computation methods is required to fully evaluate comparisons.

Delaware Inland Bays

The Inland Bays model (Cerco et al. 1993) was a two-dimensional application of the hydrodynamic and eutrophication components of the Chesapeake Bay model. The sediment model was not activated. The model was run continuously for three years. Statistics were computed according to the formulae in the present chapter. Reported results were for spatial and temporal aggregations comparable to the present study.

New York Bight

The New York Bight model (Hall and Dortch 1993) was a three-dimensional application of the hydrodynamic and eutrophication components of the Chesapeake Bay model. The sediment model was not activated. The model was run for one summer. Statistics were computed according to the formulae in the present chapter. Reported results were for one-to-one comparisons of predictions and observations.

Steady-State Bay Model

The steady-state model study of Chesapeake Bay (HydroQual 1987) immediately preceded the present study. The model was a three-dimensional eutrophication model applied to summer-average conditions. Statistics were reported individually for three years. Computation of statistics differed from the present chapter. The median absolute error and the median of individual relative errors were selected for comparison with absolute mean error and relative error computed for the present study. The steady-state nature of the model implied temporal aggregation of model and observations.

The Potomac Estuary Model

The Potomac Estuary model (Thomann and Fitzpatrick 1982) included a one-dimensional eutrophication model coupled to a rudimentary sediment model. The median of individual relative errors was reported for six years. Observations collected from June through September in the upper 83 km of the estuary were compared to model results.

Gunston Cove

The Gunston Cove model (Cerco 1985c) was a two-dimensional eutrophication model applied for one summer to an embayment of the tidal Potomac River. For statistical evaluation, observations and model were aggregated spatially but not temporally. The root-mean-square error was used in computation of relative error.

Eau Galle Reservoir

The Eau Galle Reservoir model (Wlosinski and Collins 1985) was a one-dimensional eutrophication model. The model was executed for April through November periods in two years. Relative error was computed:

$$E_{rel} = \frac{|O_{avg} - P_{avg}|}{O_{avg}} \qquad (5)$$

in which:

O_{avg} = mean of observations
P_{avg} = mean of predictions

Lake Ontario

The Lake Ontario model (Thomann et al. 1979) was a two-layer eutrophication model. Median relative error was reported for analysis of ten years of data.

Comparison of Absolute Errors

Absolute salinity error in the present study was clearly less than in alternate models, roughly half the median error in all studies (Figure 13-8). The superior statistic reflected the performance of the CH3D-WES model and the effort expended in linkage of the hydrodynamic and water-quality models.

Absolute dissolved oxygen and chlorophyll errors in the present study were comparable to the median value of all studies. Absolute errors for total nitrogen and total phosphorus exceeded the median value established from all studies.

Comparison of Relative Errors

The sequence of relative errors in the comparisons of all models conformed to the sequence identified for the mainstem and tributaries. Median relative error for dissolved oxygen, 9%, was least of all substances for which comparisons could be made (Figure 13-9). Median relative error for chlorophyll, 30%, exceeded all substances (Figure 13-12). Median relative error for total nitrogen, 12.5% (Figure 13-10), and total phosphorus, 20% (Figure 13-11), were midway between dissolved oxygen and chlorophyll.

Relative error in the mainstem generally exceeded median relative error from all studies. The excess largely reflected the unique nature of the Bay model. The Bay model was run in time-variable, three-dimensional mode, coupled to a predictive sediment model, for three continuous years. None of the alternate models incorporated all features of the Bay model.

Over a decade ago, the median relative error in a summary of dissolved-oxygen models was reported as 10% (Thomann 1982). Despite tremendous improvements in model technology, the standard has not changed. The median derived from models largely completed after 1982 was 9%. The degree of realism has improved tremendously, however. The realism may temporarily diminish statistical performance by removing degrees of freedom the modeler employs to calibrate his model. In the present study, for example, Lagrangian averaging of three-dimensional hydrodynamics eliminated the use of a dispersion parameter to transport mass about the system. The sediment model eliminated tuning of sediment-water material fluxes. Employment of organic carbon as a state variable, instead of BOD, eliminated flexibility in converting short-term to long-term BOD measures and in estimating BOD production by algal life processes.

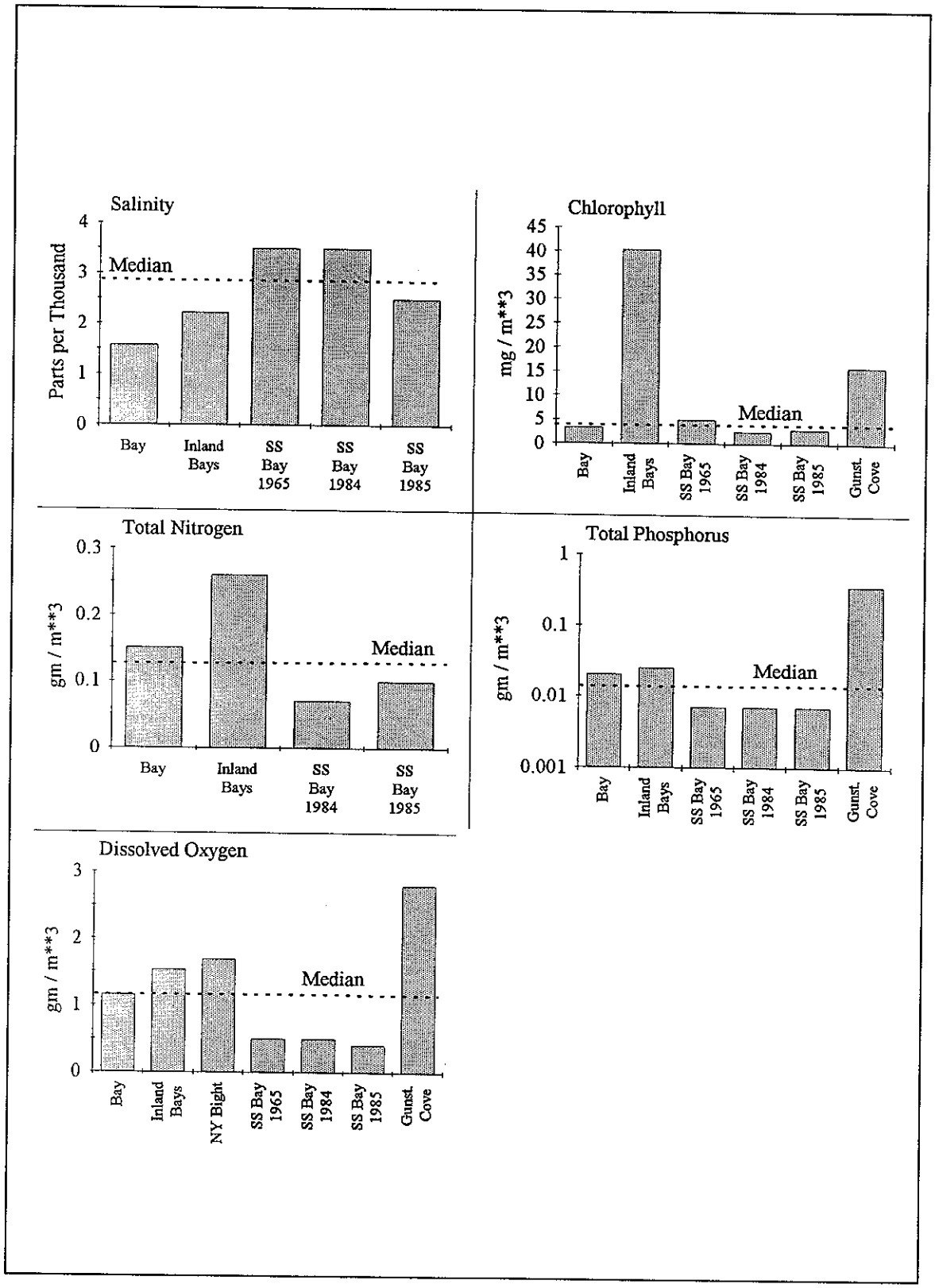

Figure 13-8. Absolute Errors in Several Models

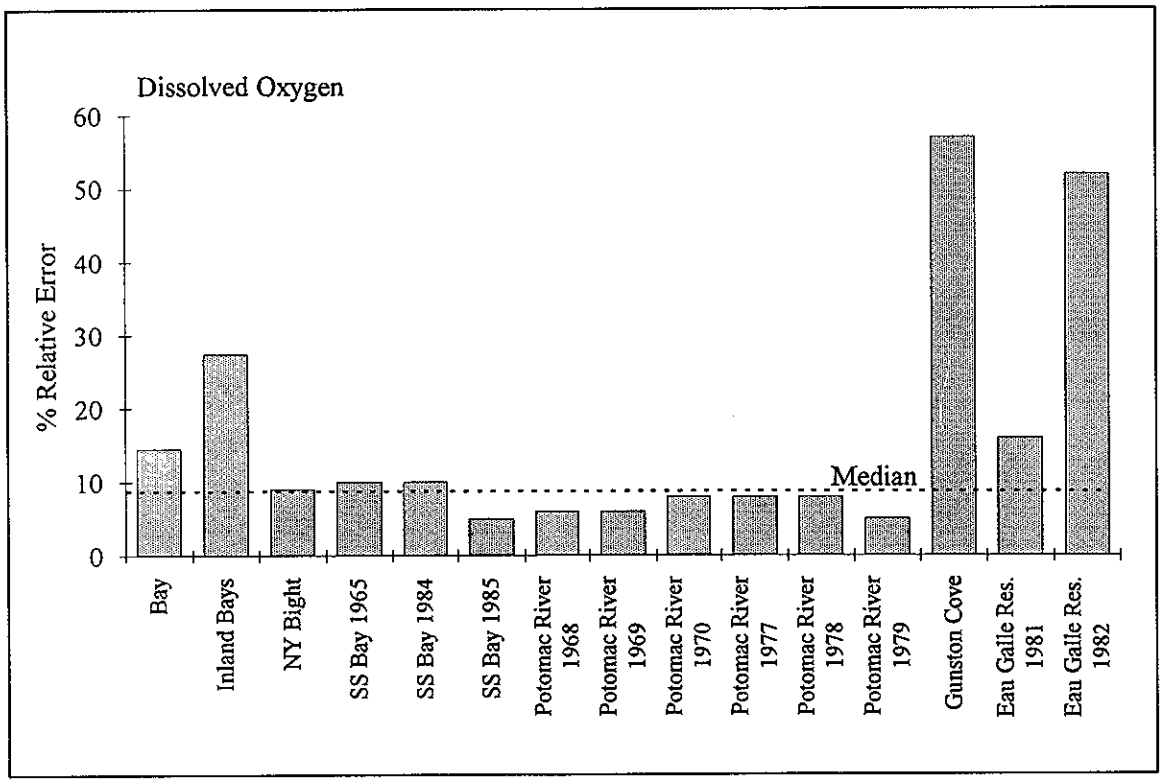

Figure 13-9. Relative Dissolved Oxygen Error in Several Models

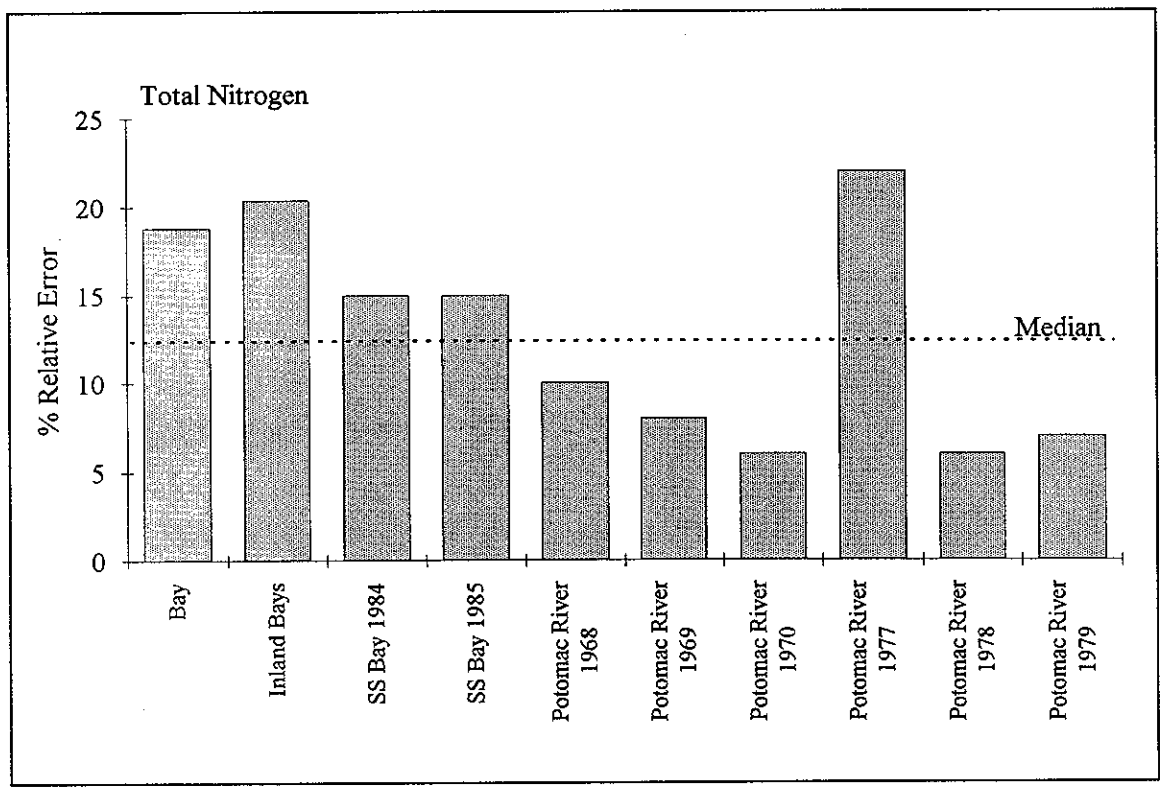

Figure 13-10. Relative Total Nitrogen Error in Several Models

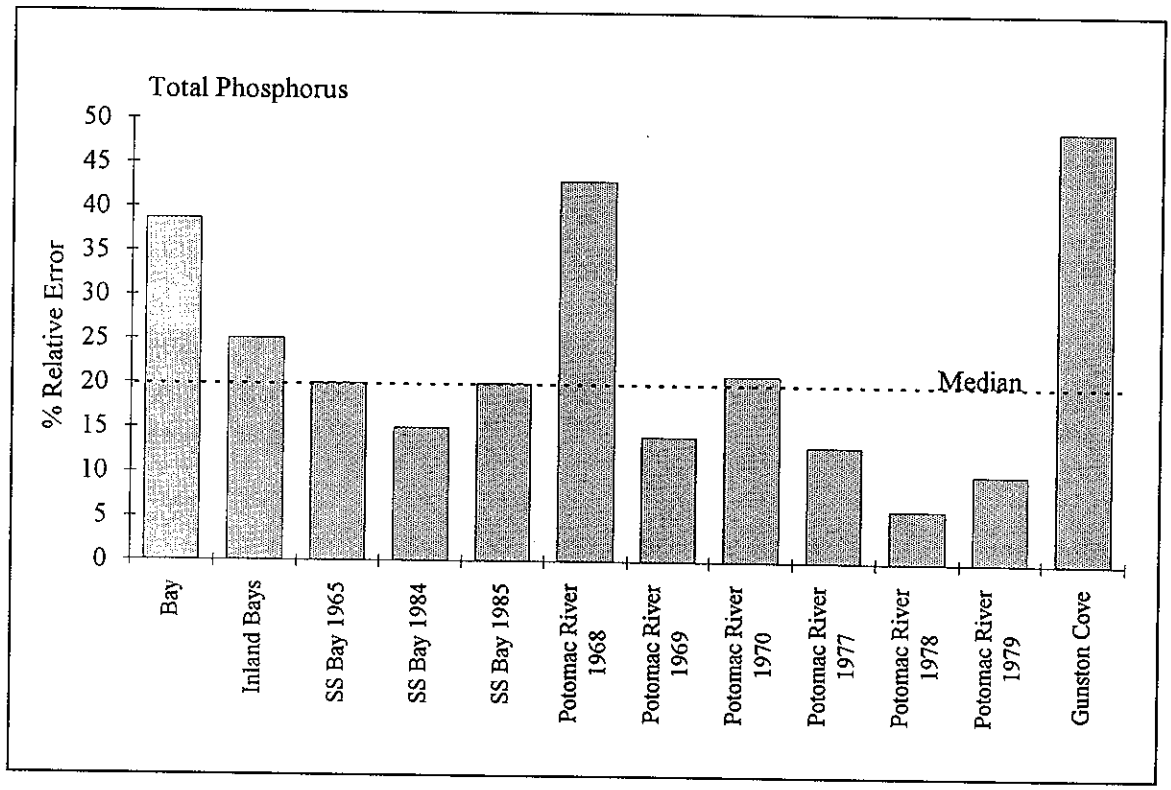

Figure 13-11. Relative Total Phosphorus Error in Several Models

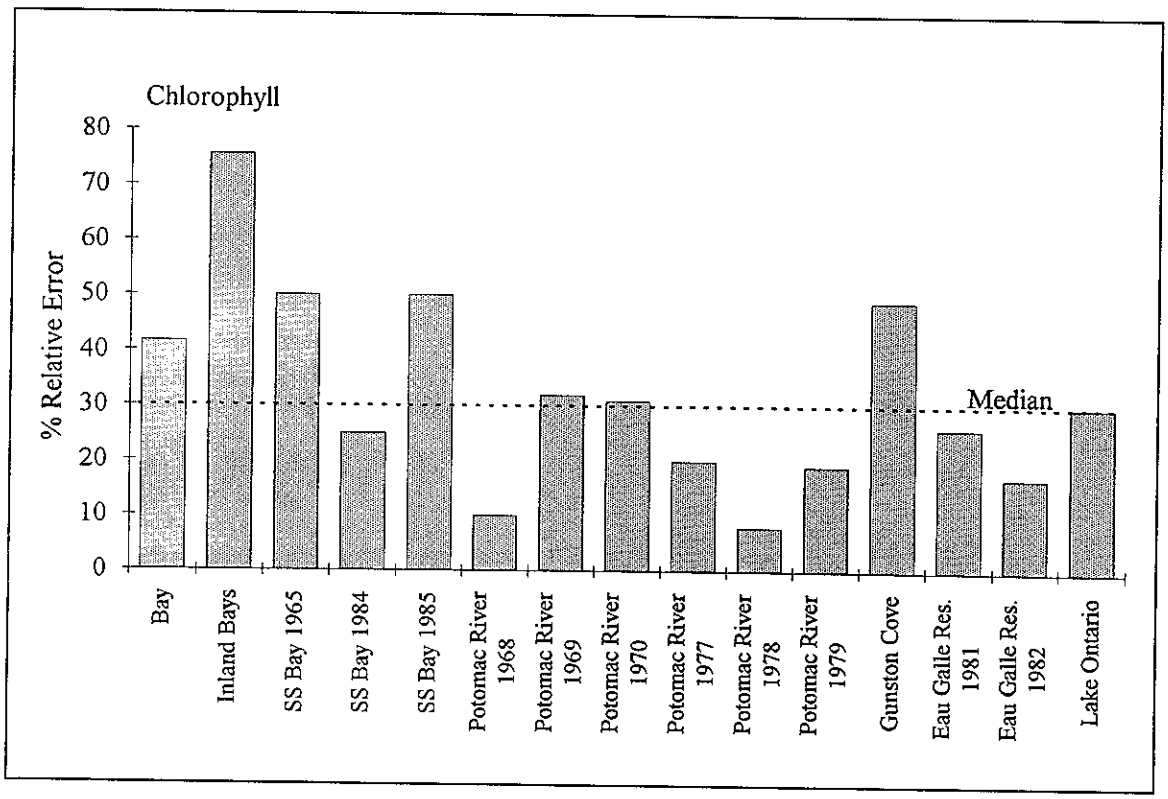

Figure 13-12. Relative Chlorophyll Error in Several Models

Comparison of Mean Dissolved-Oxygen Errors

The majority of models for which data was available over-predicted dissolved oxygen, on average (Figure 13-13). Only one model under-predicted dissolved oxygen. The sample size was small but the data indicated inability to match system minimum dissolved oxygen was a common characteristic of eutrophication models.

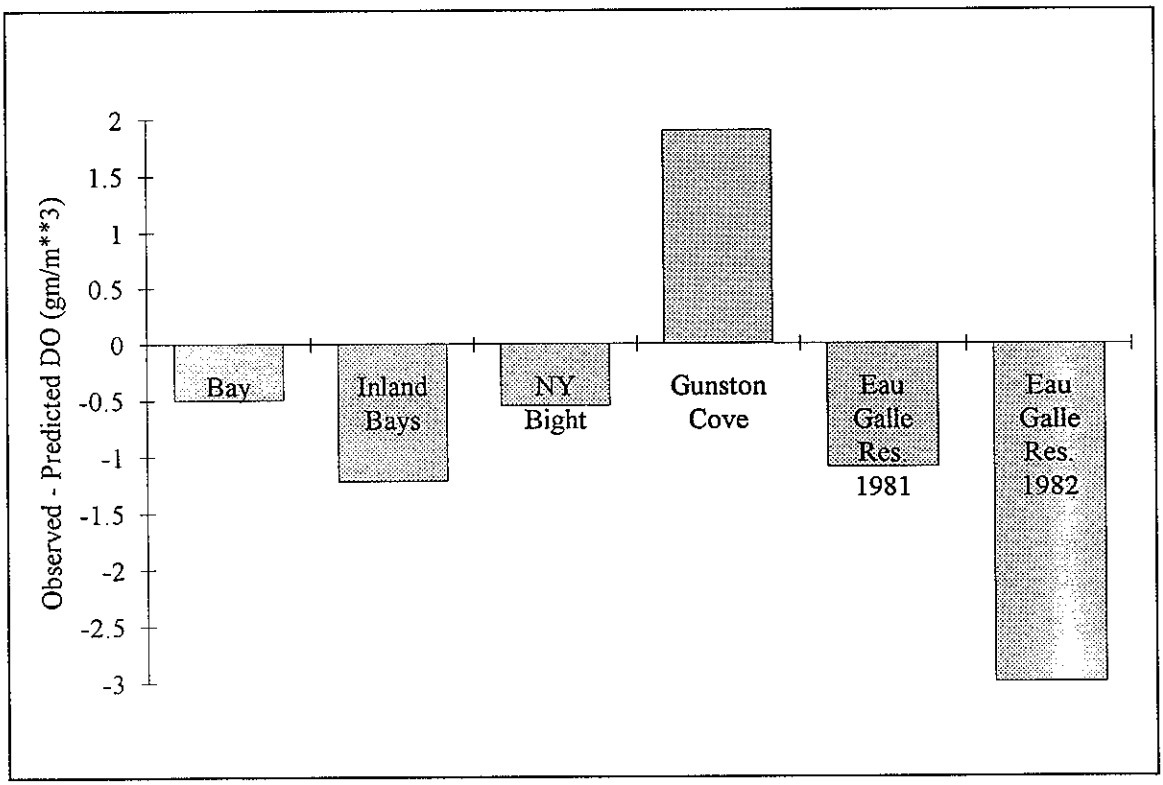

Figure 13-13. Mean Dissolved Oxygen Error in Several Models

Chapter XIV: Thirty-Year Analysis

Introduction

The issue of environmental change, natural and man-induced, is at the forefront of environmental research. Reversal of a perceived decline in Chesapeake Bay water quality, associated with human activity, was a prime motivation of this study. One task specified in the study design was a decades-long simulation of water quality. One purpose of the long-term run was use of the model to explore apparent water quality trends in the Bay. A thirty-year period, 1959-1988, was selected for analysis. At the time the long-term run was initiated, 1988 was the most recent year for which observations were available. The initial year was selected because it was the earliest year for which we could reliably estimate loads to the system.

The Data Base

Dissolved oxygen and chlorophyll data for 1959-1983 were supplied by the EPA Chesapeake Bay Program Office (CBPO). The data set was assembled from observations collected by the Chesapeake Bay Institute, Virginia Institute of Marine Science, EPA Annapolis Field Office, and other agencies. All data in the assembled set were validated by the CBPO, sometimes by reference to original field records. The assembled data set is currently the most complete, accurate source of historic Chesapeake Bay observations. We appended to the data set monitoring data from 1984 to 1987 also supplied by the CBPO. Chlorophyll observations in the historic and monitoring data were inconsistent. Historic observations were total chlorophyll, not corrected for phaeophytin, while monitoring data was phaeophytin corrected. Analysis of the monitoring data indicated phaeophytin averaged 15% of total chlorophyll. We multiplied historic chlorophyll observations by 0.85 to approximate the phaeophytin correction performed on the monitoring data.

Analysis of the data followed the pattern set for analysis of model output and 1984-1986 observations. The mainstem Bay was divided into eight zones along the longitudinal axis (Figure 14-1). A ninth zone encompassed the

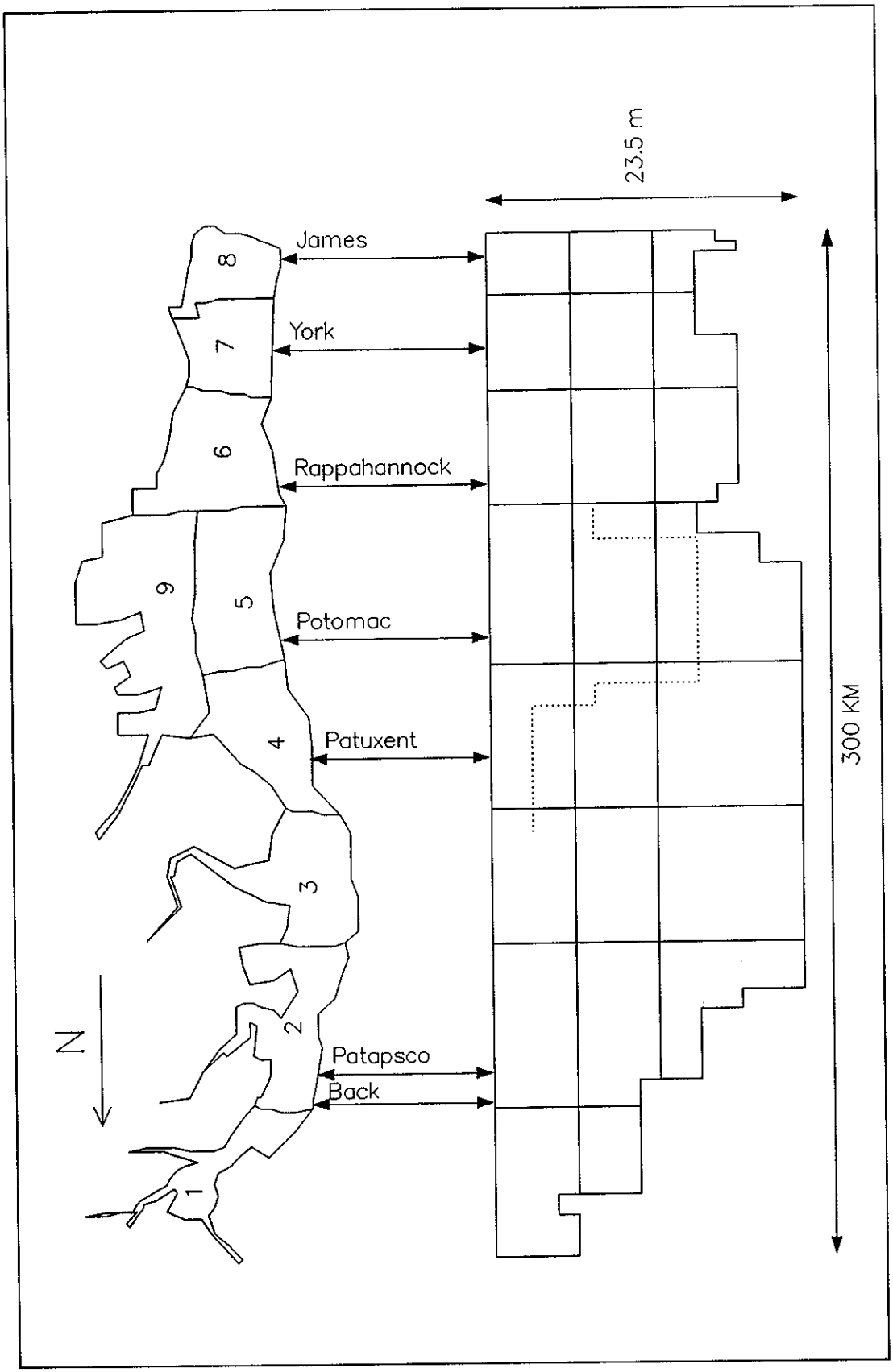

Figure 14-1. Zones for Thirty-Year Analysis

Tangier Sound region in the eastern portion of the Bay. The Bay was also divided into layers that approximated the surface mixed layer (0 to 6.7 m), the pyncnocline region (6.7 to 12.8 m), and a bottom mixed layer (> 12 m). Data analysis was restricted to the period June 1 to September 30 (Season 3) that spans the onset and breakup of anoxia in the Bay. Observations within each zone-level were averaged to produce a mean for the summer of each year.

For initial analysis, the data were further aggregated into decades:

Decade 1	1959-1968
Decade 2	1969-1978
Decade 3	1979-1988

Decade means were the average of individual summer annual means. For some decades in some regions, fewer than ten individual means were available to compute decade means.

The initial analysis indicated summer-average dissolved oxygen less than 3 gm m^{-3} characterized the mainstem between the Back and Rappahannock River entrances at depth greater than 12 m (Figure 14-2). Little variability in this characteristic occurred from decade to decade and no trend was immediately apparent. Elsewhere, summer-average dissolved oxygen generally exceeded 4 gm m^{-3}. More variability was evident than in the region of minimum dissolved oxygen but no pattern was apparent. Least summer-average dissolved oxygen, less than 1 gm m^{-3}, occurred at the bottom of Zone 3. Again, little variability and no trend were apparent.

Ten percent to thirty percent of observations collected in bottom water between the Back and Rappahannock Rivers in recent decades, 1969-1988, exhibited complete anoxia, defined as dissolved oxygen $\leq$ 0.1 gm m^{-3} (Figure 14-3). Complete anoxia was largely restricted to the bottom mixed layer (depth > 12.8m). Observations suggested an increase in the proportion of completely anoxic samples from 1959-1968 to later decades. Judgement should be reserved, however, due to the sporadic nature of early surveys. Twenty-five to seventy-five percent of observations in the same regions and depth interval exhibited dissolved oxygen less than 1 gm m^{-3} (Figure 14-4). Dissolved oxygen less than 1 gm m^{-3} also penetrated into Layer 2 (6.7m < depth < 12.8m) between the Back and Rappahannock Rivers. No temporal trend was apparent in the proportion of observations less than 1 gm m^{-3} dissolved oxygen.

Chlorophyll observations in all decades suggested a spatial trend of higher concentration in the upper Bay and lesser concentration in lower Bay (Figure 14-5). Observations in the first two decades were concentrated in the mainstem above the Rappahannock River entrance. A high degree of variability between decades was apparent in Levels 1 and 2 of the first four zones. Several zone-level combinations indicated that chlorophyll was higher in Decade 1 or Decade 2 than in Decade 3.

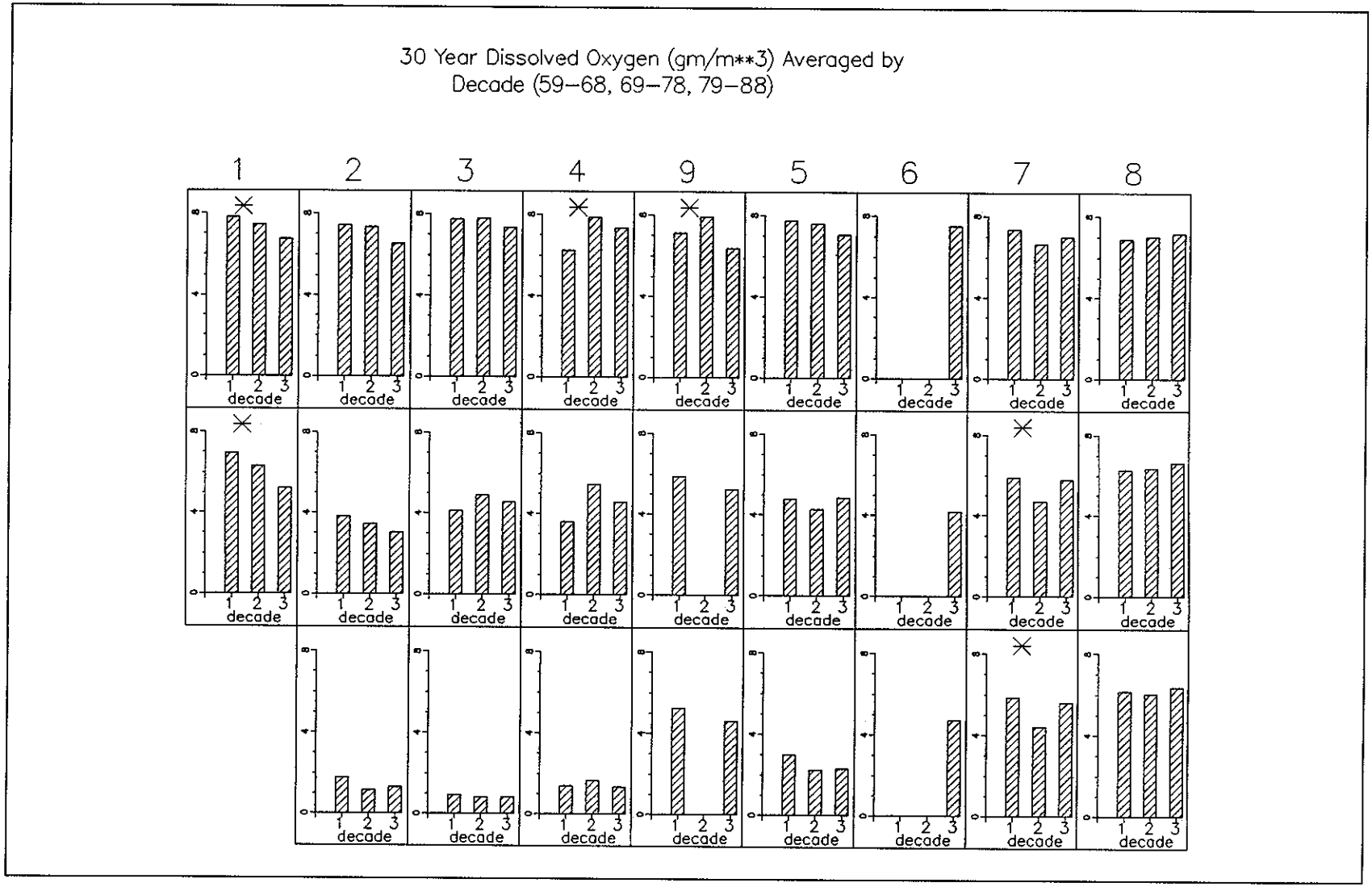

Figure 14-2. Summer-Average Dissolved Oxygen by Zone, Level, Decade (*Indicates Statistically-Significant Difference)

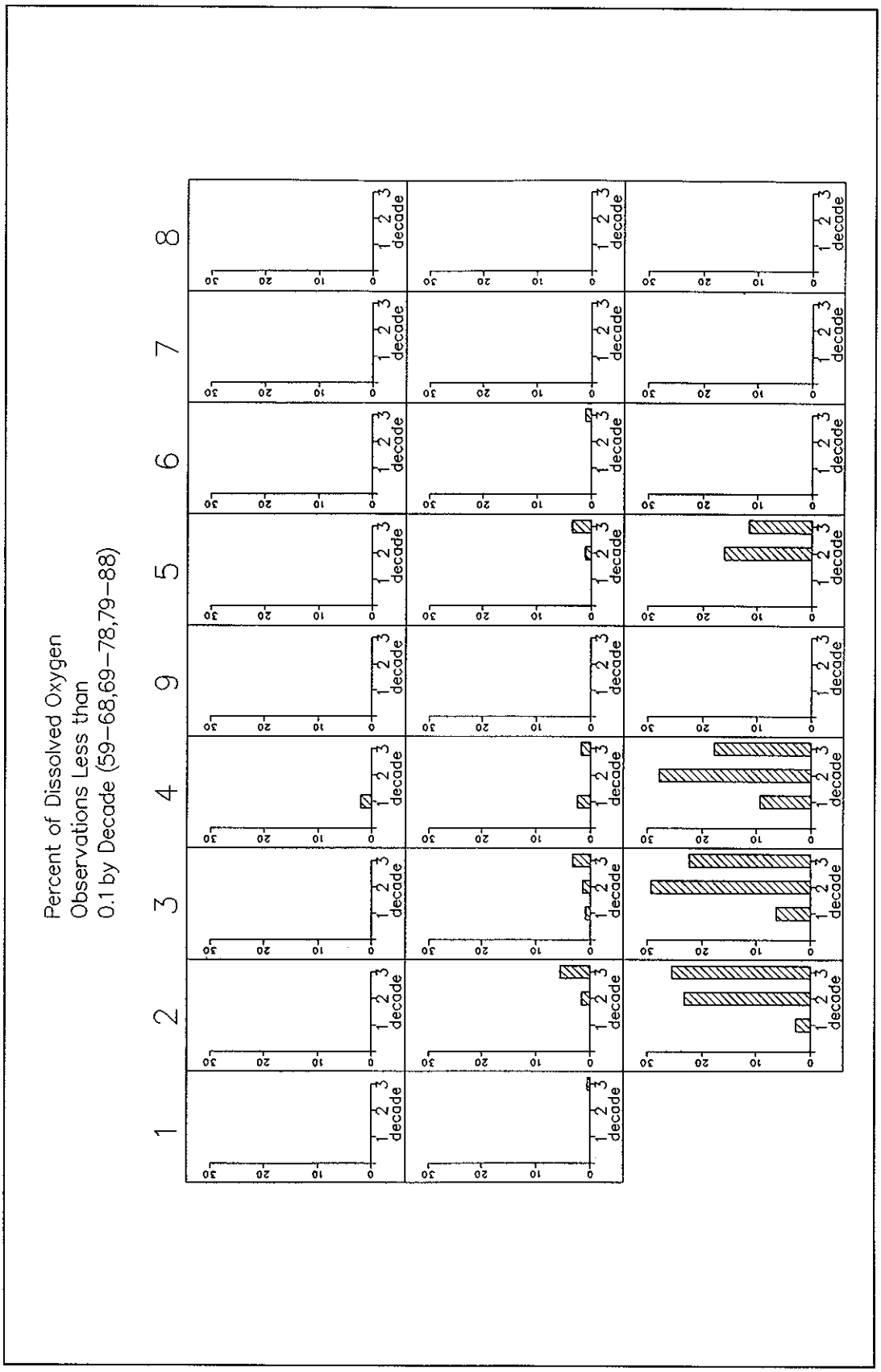

Figure 14-3. Percentage of Dissolved Oxygen Observations Less Than 0.1 gm m^{-3}

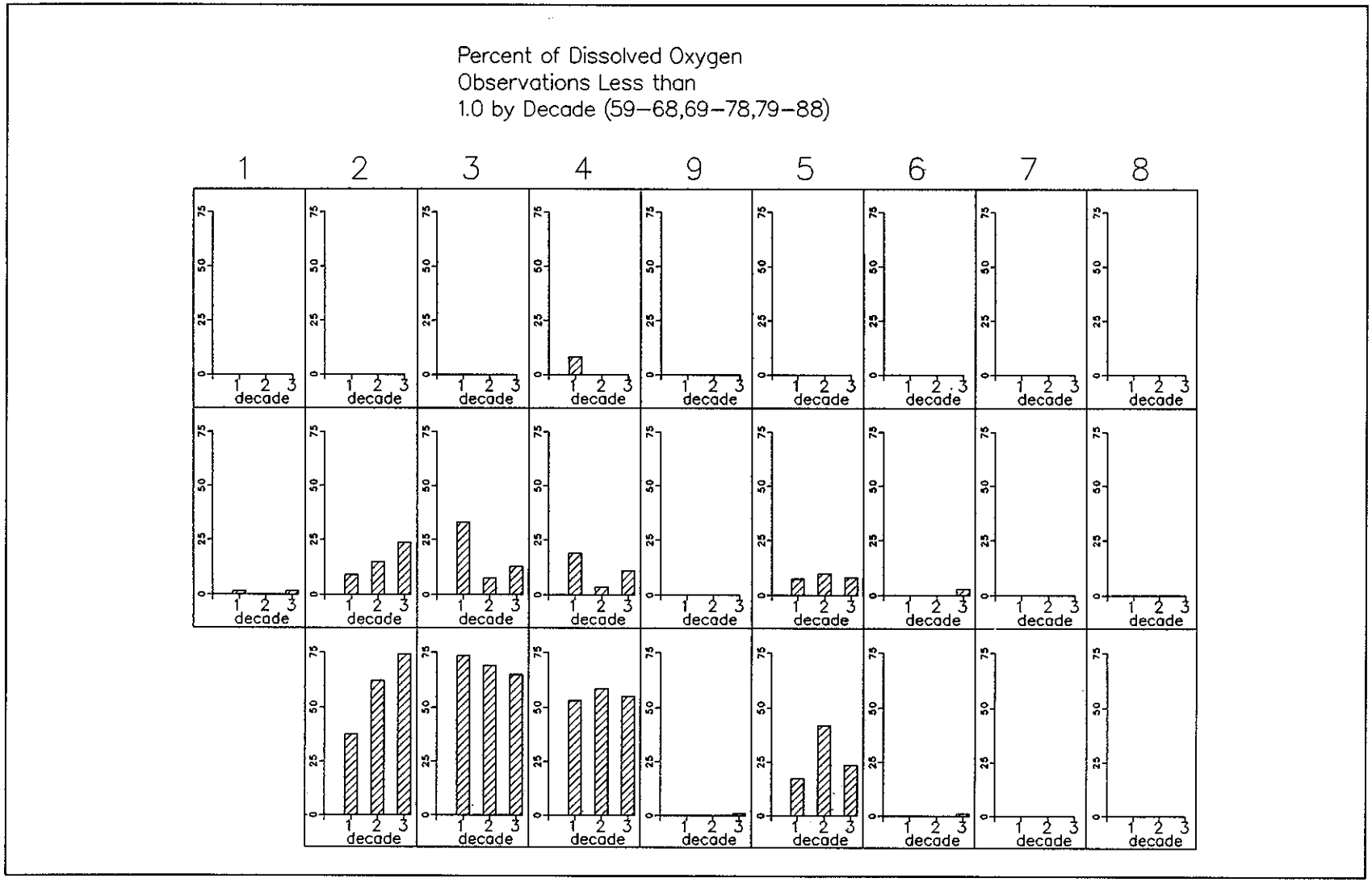

Figure 14-4. Percentage of Dissolved Oxygen Observations Less Than 1.0 gm m^{-3}

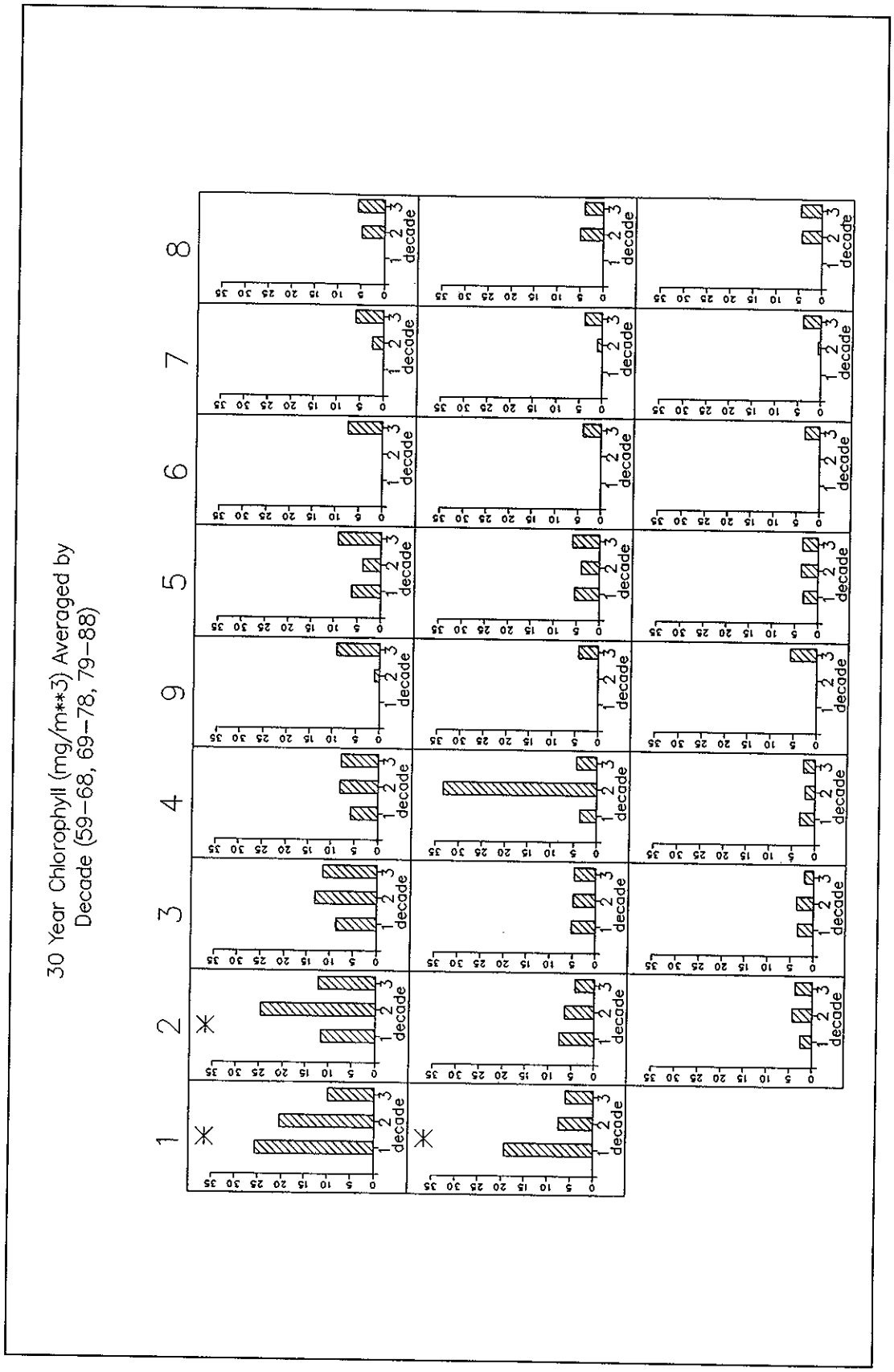

Figure 14-5. Summer-Average Chlorophyll by Zone, Level, and Decade (*Indicates Statistically-Significant Difference)

An analysis of variance (ANOVA) was performed to determine the significance of dissolved oxygen and chlorophyll variations from decade to decade. The ANOVA was performed in each zone-level combination using Decade as the "class" variable (SAS 1988). Each decade contained a maximum of ten observations, each one the annual mean of individual observations within a zone-level. Employment of annual means eliminated the influence on the analysis of varying numbers of surveys in individual years. The Bonferroni t-test ($p < 0.05$) was employed to determine how the decades differed when significant differences were detected.

Two decades were distinguished in the ANOVA. The most recent decade indicated diminished dissolved oxygen, relative to one or both preceding decades, in Zone 1 and in the surface layer of Zone 9. The dissolved oxygen decrease in Zone 1 occurred concurrently with a significant decrease in chlorophyll in Zone 1 and the surface layer of Zone 2. The association of chlorophyll and dissolved oxygen indicates the dissolved oxygen decrease occurred as a result of decreased photosynthetic production.

Decade 2 was distinguished by higher dissolved oxygen, relative to Decades 1 or 3, in surface layers of Zone 4 and 9. The dissolved oxygen behavior in Zone 4 corresponded to trends in average chlorophyll concentration. Most likely, the elevated dissolved oxygen in both Zones 4 and 9 was associated with enhanced algal production during Decade 2. Detection of a significant associated chlorophyll trend was impossible, however, due to the sparse observations in the first two decades. Decade 2 also indicated lower dissolved oxygen, relative to preceding and following decades, in Zone 7 below 6.7 m. Zone 7 also indicated diminished chlorophyll in Decade 2 although, as with Zones 4 and 9, no statistical significance was associated with the apparent chlorophyll trend. The apparent positive correlation between algal production in the euphotic zone and dissolved oxygen in water greater than 12 m deep was unexpected.

The dissolved oxygen differences we detected occurred mostly in water containing 5 gm m^{-3} or more dissolved oxygen. We observed no distinct trend towards unhealthy oxygen levels in any portion of the Bay. Averaged by decade, concentrations in the bottom levels of zones demonstrating minimum dissolved oxygen were unchanged over the three decades.

Approach and Objectives

Numerous investigators have examined essentially the same data base as we and reached disparate conclusions regarding dissolved oxygen trends in the Bay. An alarm was sounded when Flemer et al. (1983) detected an order-of-magnitude increase in the volume of anoxic Bay water from 1950 to 1980. In contrast, Heinle et al. (1980) concluded "Oxygen concentrations in the open Bay have not changed greatly, with the possible exception of extreme conditions, as during periods of extensive ice cover". Seliger and Boggs (1988)

reported a large yearly variance in anoxic volume but no significant increase in anoxia. They determined anoxic volume was highly correlated (r = 0.92) to spring runoff volume in the Susquehanna River. Most recently, Bahner, Reynolds, and Batiuk (1990) detected a small increase (roughly 25%) from 1950 to 1990 in July anoxic volume in the Maryland portion of the Bay. They noted large variance in anoxic volume between years but reported only a weak, qualitative link between anoxic volume and Susquehanna runoff.

The disparate conclusions resulted partially from characteristics inherent in the assembled historic data set. From year to year, sampling location varied as did the number and timing of surveys. The investigators' treatment of the non-synoptic data influenced outcome of the analyses. A review by Boicourt (1992), for example, illustrated how judgement influenced the differing conclusions reached by Flemer et al. versus Seliger and Boggs.

Our approach to the problem of determining trends in the Bay departs from exclusive examination of the data. We will apply the verified three-dimensional eutrophication model to simulate the thirty-year period 1959-1988. Results of the simulation will be examined for trends and other eutrophication characteristics. This approach offers advantages from several standpoints. First, the model represents the thirty-year time period continuously in space and time. No techniques are required to fill in gaps in observations. The model computations are exact. No statistical analyses are necessary to allow for random sampling error. The model is not affected by short-term, local environmental variations that influence the observations and cloud analysis. A significant advantage is that the model provides information for which no long-term observations exist. For example, the time series of total nitrogen and total phosphorus in the Bay can be reconstructed. Finally, the model can be used in a sensitivity mode to examine the factors that influence detected trends.

Hydrology and Hydrodynamics

The Susquehanna River contributes 62% of the gauged freshwater flow to the Chesapeake Bay. Consequently, Susquehanna runoff is a prime determinant of residence time and density stratification in the mainstem. The Susquehanna hydrograph is a good surrogate for a hydrograph of total runoff to the system. Examination of the Susquehanna hydrograph for 1959-1988 (Figure 14-6) indicates flows for 1959-1968 were mostly at or below the mean flow (1957-1989) of 1087 m^3 sec^{-1}. The period 1959-1968 can be characterized as a "dry" decade. Nine out of ten years in the period 1969-1978 were at or above the mean flow. The years 1972 and 1975 were the number one and two highest flows in the period of record (1900-1989). The period 1969-1978 can be characterized as a "wet" decade. Flows in the period 1979-1988 were uniformly distributed above and below average. No distinct characterization is appropriate for this period.

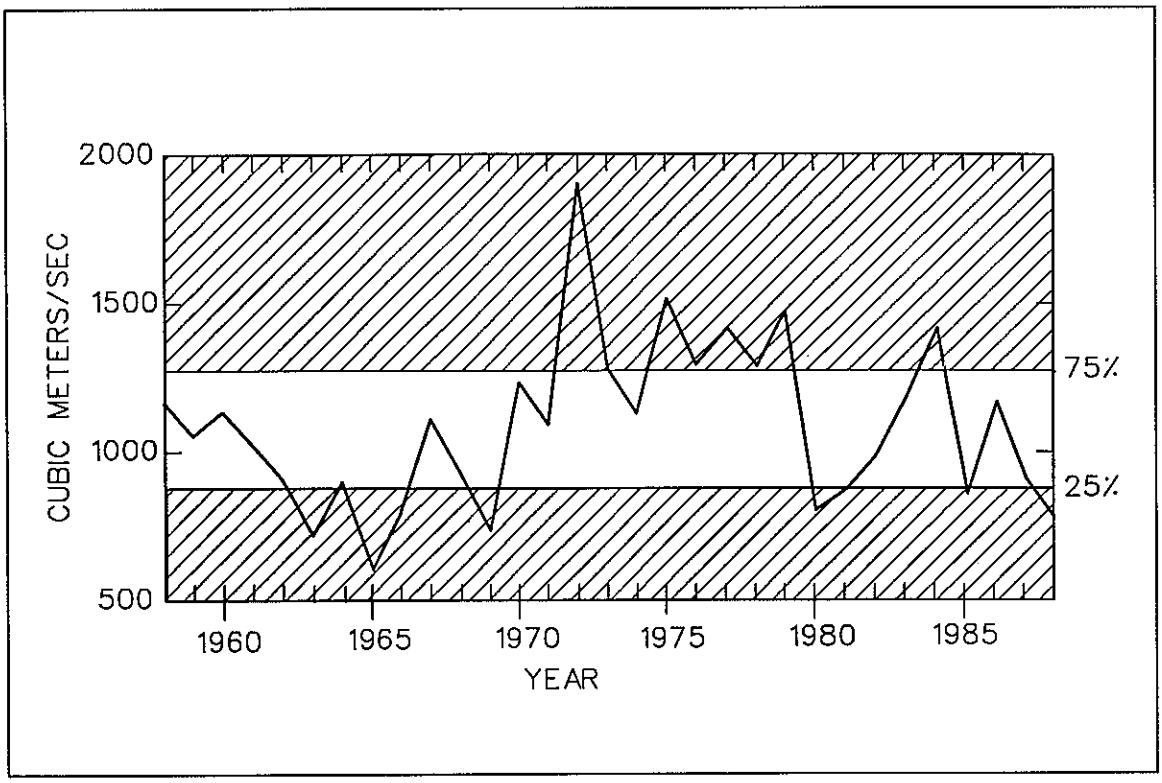

Figure 14-6. Flow at Susquehanna Fall Line, 1958-1988

Hydrodynamics for the thirty-year simulation were obtained by sequencing the annual hydrodynamic series produced for the model calibration. Years in the period 1959-1988 were classified as "wet," "average," or "dry" based on annual flow in the Susquehanna. Wet years were at or above the 75th percentile of annual flows in the period of record (Figure 14-6). Average years were between the 25th and 75th percentile. Dry years had flows below the 25th percentile. Mean flow for 1984, 1410 m^3 sec^{-1}, exceeded flow for 90% of the years on record. Consequently, 1984 hydrodynamics were employed for "wet" years in the thirty-year simulation. Mean flow for 1986, 1168 m^3 sec^{-1}, was at the 60th percentile in the period of record. Hydrodynamics from 1986 were used to represent "average" years in the simulation. Flow in 1985, 863 m^3 sec^{-1} was less than 80% of the years in the period of record. Modified 1985 hydrodynamics were employed for most "dry" years in the simulation. The modification was necessary to remove from the "dry" hydrodynamics the November 1985 storm which flooded the western tributaries and, to a lesser extent, the Susquehanna. A special hydrodynamic model run was completed in which the storm runoff was removed from the fall-line flows specified as boundary conditions. The modified hydrodynamics were employed for all "dry" years in the simulation except 1985. Actual hydrodynamics including the storm were employed for 1985. A listing of classification and hydrodynamics is provided in Table 14-1.

Table 14-1
Inputs to Thirty-Year Run

Year	Hydrology	Hydrodynamics	Fall-Line Loads, Below-Fall-Line Loads	Point-Sources
1959	Average	1986	1959	1965
1960	Average	1986	1960	1965
1961	Average	1986	1961	1965
1962	Average	1986	1962	1965
1963	Dry	1985 (modified)	1963	1965
1964	Average	1986	1964	1965
1965	Dry	1985 (modified)	1965	1965
1966	Dry	1985 (modified)	1966	1965
1967	Average	1986	1967	1965
1968	Average	1986	1968	1965
1969	Dry	1985 (modified)	1969	1970
1970	Average	1986	1970	1970
1971	Average	1986	1971	1970
1972	Wet	1984	1972	1970
1973	Wet	1984	1973	1970
1974	Average	1986	1974	1970
1975	Wet	1984	1975	1970
1976	Wet	1984	1976	1970
1977	Wet	1984	1977	1980
1978	Wet	1984	1978	1980
1979	Wet	1984	1979	1980
1980	Dry	1985 (modified)	1980	1980
1981	Dry	1985 (modified)	1981	1980
1982	Average	1986	1982	1980
1983	Average	1986	1983	1980
1984	Wet	1984	1984	1985
1985	Dry	1985	1985	1985
1986	Average	1986	1986	1985
1987	Average	1986	1987	1985
1988	Dry	1985 (modified)	1988	1985

A key distinction in the three sets of hydrodynamics was in the degree of summer density stratification. During 1984, high freshwater runoff in spring induced relative stratification roughly double the stratification in 1985 or 1986 (Figure 14-7). The "wet" hydrodynamics also qualified as "highly stratified". Despite the distinction as "dry" and "average", little stratification difference existed between 1985 and 1986, however. Both these years were classified as moderately or "normally" stratified.

The hydrodynamic sequencing was appropriate to the simulation objective of trend detection. Since individual hydrodynamics were not employed for each of the thirty years, the simulation was not expected to exactly reproduce water quality within a year. The simulation was expected to reproduce trends, however, and to distinguish the influences of "wet", "average", and "dry" hydrology on eutrophication.

Loads

Point Sources

A listing of point sources and associated loads for the years 1965, 1970, and 1980 was provided by the EPA CBPO. We supplemented this record with 1985 point sources and loads employed in the model calibration. Transition from one set of loads to the next was handled as a step function. Transitions were timed to coincide with a record of treatment upgrades at the Blue Plains treatment facility, Washington, DC. The loads are summarized in Table 14-2. Assignment of loads to individual years is listed in Table 14-1.

Table 14-2
Point-Source Load Summary

Year	Total Nitrogen, kg day^{-1}	Total Phosphorus, kg day^{-1}	Total Organic Carbon, kg day^{-1}
1965	81,068	18,807	155,380
1970	93,984	24,761	159,511
1980	91,249	16,676	98,091
1985	86,313	7,359	15,204

Below-Fall-Line Loads

Relationship of Load to Flow. We noted (Figure 14-8) that below-fall-line loads and flows produced by the Watershed Model often corresponded to the familiar relationship:

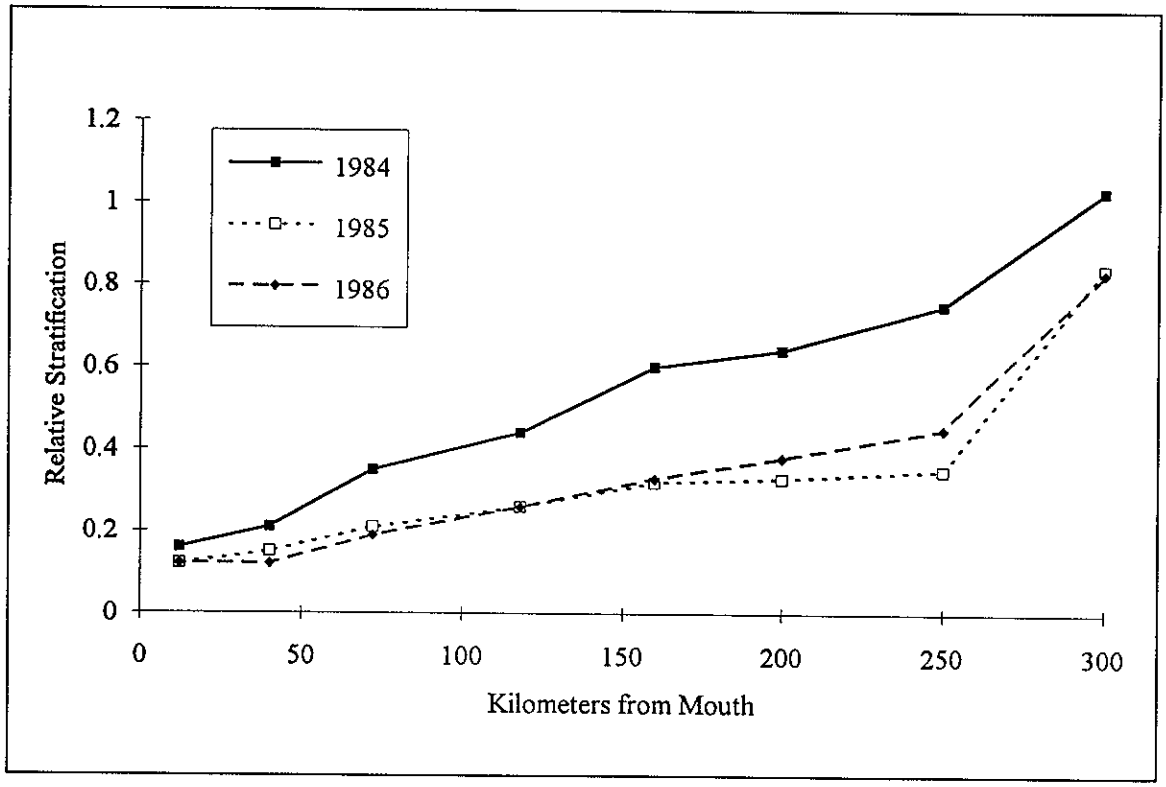

Figure 14-7. Observed Relative Stratification in 1984, 1985, 1986

$$L = a Q^{b} \qquad (1)$$

L = load ($M T^{-1}$)
Q = volumetric flow ($L^3 T^{-1}$)
a, b = constants that relate load to flow

Constants a and b were determined for each below-fall-line watershed using output from the watershed model. Next, the relationship of load to flow was used to derive the thirty-year series of below-fall-line loads.

First, flows and loads were averaged on a seasonal basis into twelve values for the period 1984-1986. Seasons corresponded to the aggregation periods defined for comparison of water quality model predictions and observations (Chapter XI). Equation 1 was transformed:

$$\ln(L) = \ln(a) + b \ln(Q) \qquad (2)$$

Constants a and b were determined by linear regression using seasonal-average flow as the independent variable and seasonal-average load as the dependent variable. The variance of the regression estimates was determined as well.

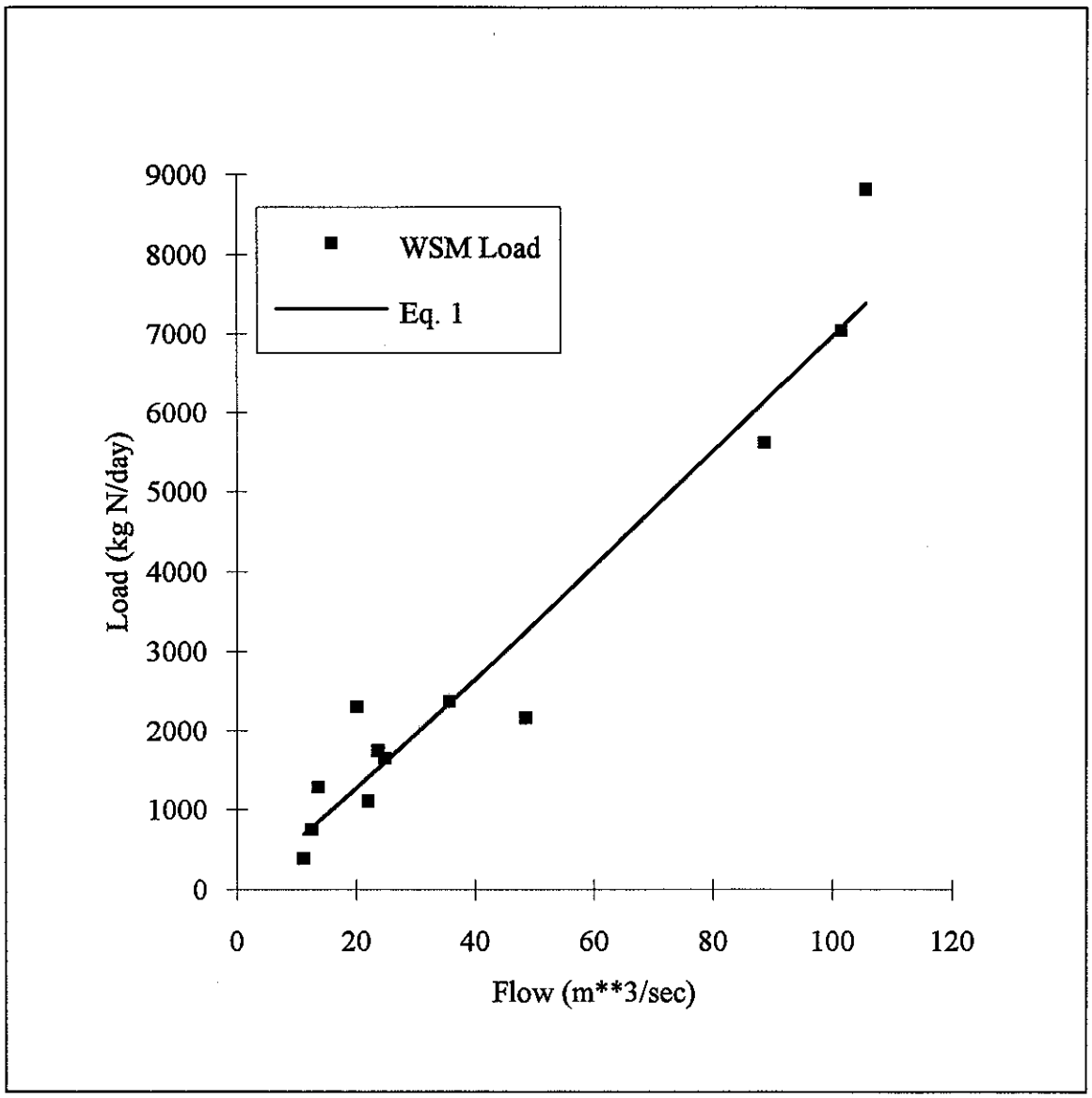

Figure 14-8. Example of Watershed Model Relationship of Load and Flow

$$L = e^{\ln(a) + b\ln(Q) + \frac{s^2}{2}} \qquad (3)$$

Once these parameters were determined, load corresponding to any flow could be computed:

s^2 = variance of regression estimate

Loads for 1984-1986 determined by Equation 3 were checked against loads from the Watershed Model (Figure 14-9). Mean and relative error statistics (Equations 13-1, 13-4) were determined for each watershed. Mean errors for total nitrogen and phosphorus were negligibly small. Relative error for individual seasonal loads was typically 20% for nitrogen and 35% for phosphorus.

Flows. Computation of loads required the thirty-year time series of below-fall-line flows. These were obtained by ratio relationships to stream gauge records. Three stream gauges were identified that characterized flow on the spatial scale defined by Watershed Model below-fall-line watersheds. Gauges on the Pamunkey, Patuxent, and Choptank (Figure 14-10) were selected. According to proximity, below-fall-line watersheds in the Watershed Model were assigned to one of the three gauges. Watershed Model flows for each watershed were averaged seasonally into twelve values for the period 1984-1986. Flows from the stream gauges were also averaged seasonally for the period 1959-1988. Next, flows from the Watershed Model were related to flows at the nearest gauge:

$$Q_i = FR_{ij} G_j \qquad (4)$$

Q_i = flow in below-fall-line watershed i (m^3 sec^{-1})
G_j = flow at stream gauge j (ft^3 sec^{-1})
FR_{ij} = ratio of flow in watershed i to flow at stream gauge j (m^3 ft^{-3})

The flow ratio was evaluated by least-squares relationship of Watershed Model flows, 1984-1986, to gauged flows over the same period. Once the flow ratio was established for each watershed, the thirty-year hydrograph, on a seasonal basis, was constructed by application of Equation 4 to appropriate gauged flows.

Fall-Line Loads

Daily fall-line loads were computed as the product of flow and concentration. Concentrations were estimated by a minimum-variance-unbiased-estimator (MVUE) method (Cohn et al. 1989) using a program supplied by the United States Geological Survey (USGS). The program used least-squares techniques to estimate parameters in an equation that related concentration to flow, season, and time:

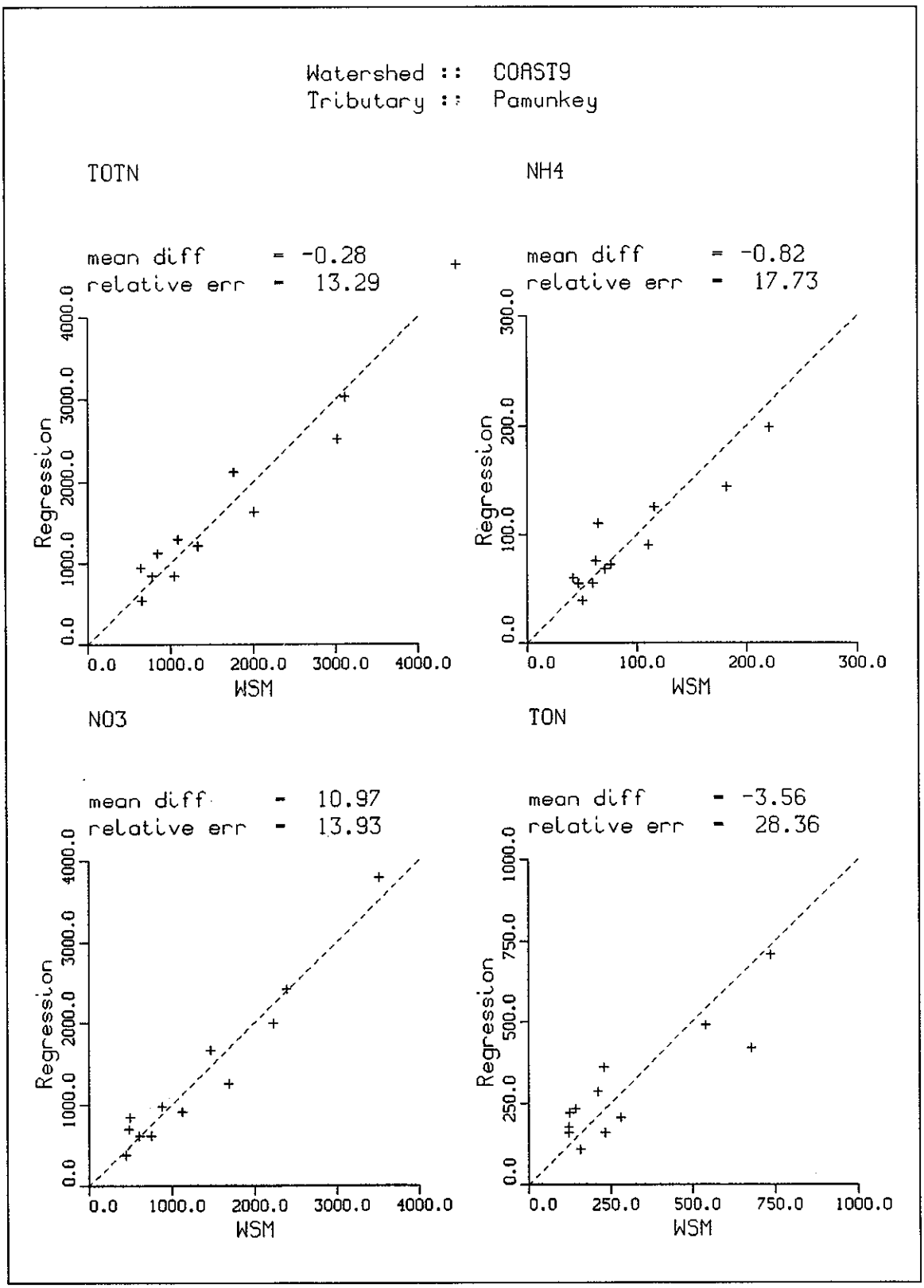

Figure 14-9. Loads in Below-Fall-Line Watershed Coast 9: Watershed Model versus Exponential Regression (Continued)

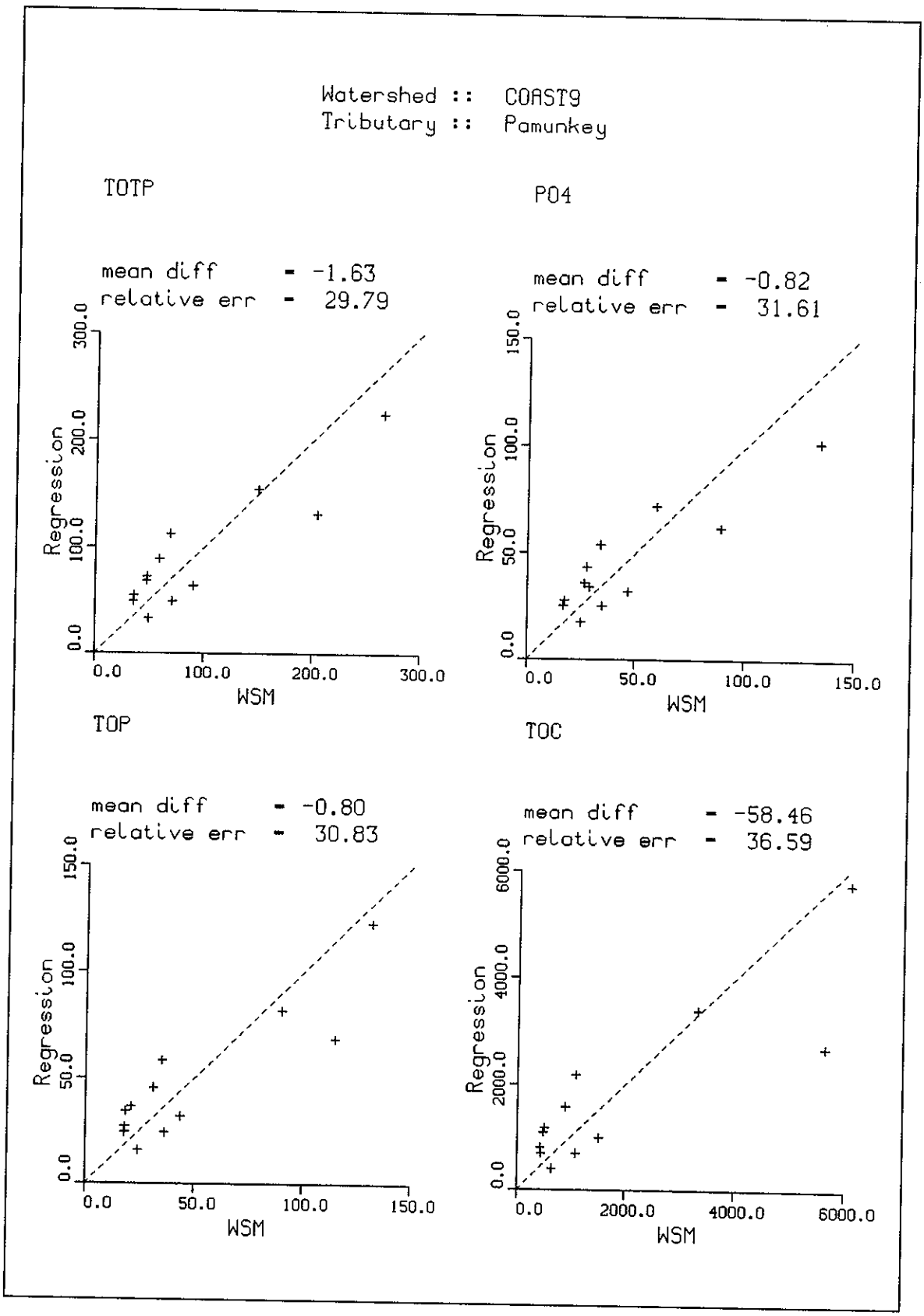

Figure 14-9. (Concluded)

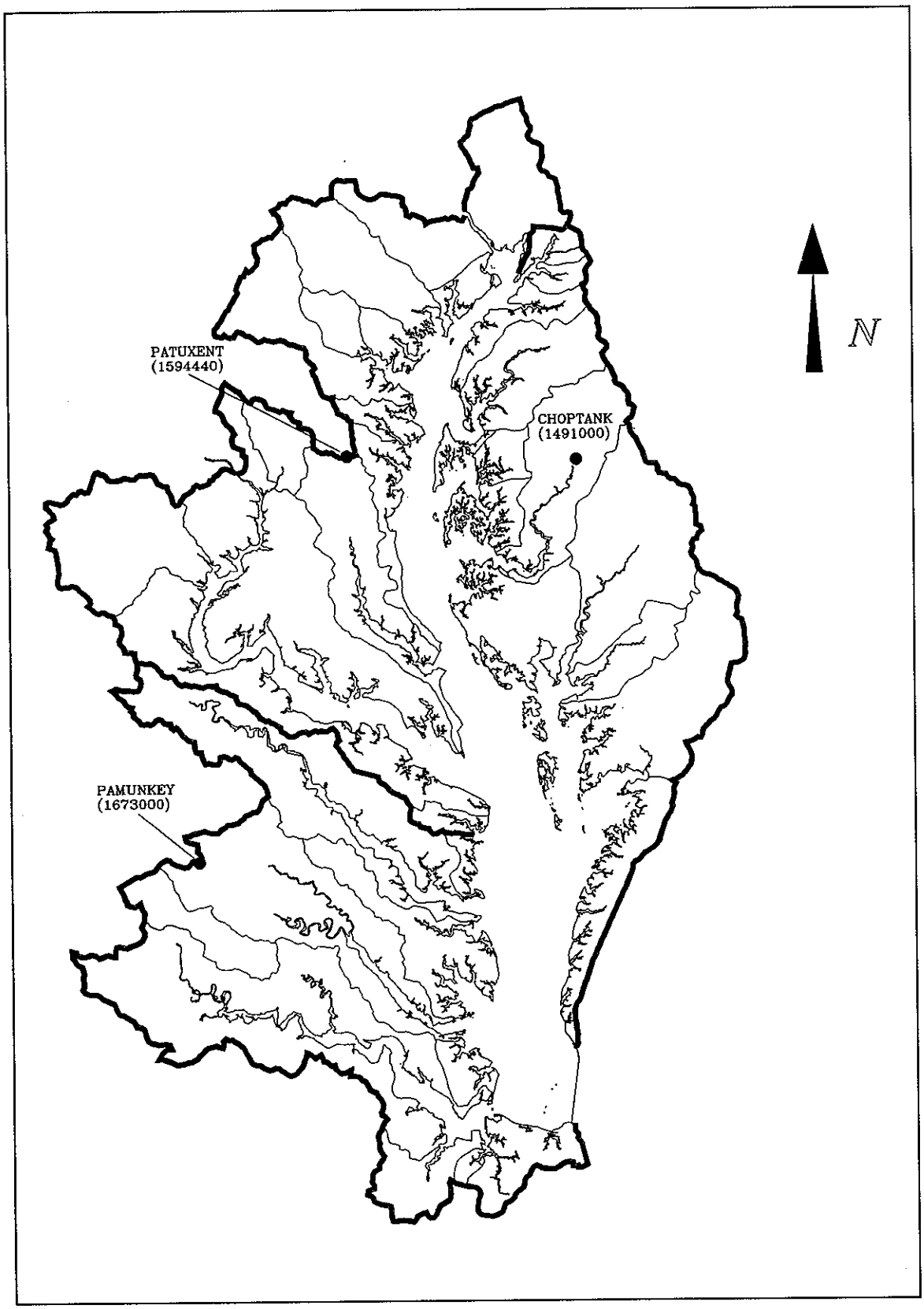

Figure 14-10. Gauges Selected for Analysis of Below-Fall-Line Flows

$$\ln(C) = a_1 + a_2 \ln(Q - Q_c) + a_3 \ln(Q - Q_c)^2 + a_4 (t - t_c) + a_5 (t - t_c)^2 + a_6 \sin(2\pi (t - 1980)) + a_7 \cos(2\pi (t - 1980)) \quad (5)$$

C = concentration
Q = volumetric flow rate
Q_c = an arbitrary flow at the center of the range of flows
t = time in decimal years
t_c = an arbitrary time near the center of the range of times

$a_1, ..., a_7$ = constants that relate concentration to flow, season, and time

Flow and concentration observations for employment in the MVUE estimator were also provided by the USGS. The data set contained observations collected by the USGS and Chesapeake Bay Monitoring Program (CBMP). We supplemented these with EPA data derived from the "TC47 Report" (Guide and Villa 1972). Observational periods of record of fall-line data bases are summarized in Table 14-3.

Table 14-3
Period of Record, Fall-Line Observations

River	TC47	USGS-CBMP
Susquehanna	1969-1970	1978-1988
Patuxent		1978-1988
Potomac	1969-1970	1978-1988
Rappahannock		1980-1989
Mattaponi		1979-1987
Pamunkey		1979-1989
James		1979-1989
Appomattox		1979-1989

The primary indicator of temporal concentration trends was provided by the MVUE program. The program noted the statistical significance of terms in Equation 5. Temporal trends were indicated when the terms containing $(t - t_c)$ and $(t - t_c)^2$ contributed significantly to the least-squares concentration estimate. We also examined trends by testing for differences in the TC47 and USGSCBMP data sets. Residuals were analyzed after flow and seasonal effects were removed from the observations. Following statistical analysis, apparent trends were screened for "reasonableness". Some sparse records

indicated huge trends that were apparently artifacts of the data rather than authentic long-term changes in concentration.

A summary of concentration trends detected at the three major fall-lines is provided in Table 14-4. Concentration differences were determined through evaluation of Equation 5 at the beginning and end of the period of record. Flow and seasonal effects were eliminated by consideration of terms containing a_1, a_4, and a_5 only. Both the Susquehanna and Potomac indicated an increasing trend in nitrogen, primarily in the form of nitrate. Both rivers indicated a decrease in dissolved phosphate although only the Potomac demonstrated a decrease in total phosphorus. Trends in the James were opposite the two larger tributaries. The James demonstrated a decrease in nitrogen and an increase in phosphorus. The James was also the only major tributary to indicate a trend, decreasing, in total organic carbon.

Table 14-4
Concentration Trends at Major Fall Lines

Substance	Susquehanna	Potomac	James
Nitrate	0.33 gm m^{-3} increase from 1969 to 1988	0.26 gm m^{-3} increase from 1969 to 1988	0.074 gm m^{-3} decrease from 1979 to 1988
Total Kjeldahl Nitrogen	0.085 gm m^{-3} increase from 1969 to 1988	No change	No change
Dissolved Phosphate	0.04 gm m^{-3} decrease from 1969 to 1988	0.05 gm m^{-3} decrease from 1969 to 1988	0.064 gm m^{-3} increase from 1979 to 1988
Total Phosphorus	No change	0.07 gm m^{-3} decrease from 1969 to 1988	0.095 gm m^{-3} increase from 1979 to 1988
Total Organic Carbon	No change	No change	2.35 gm m^{-3} decrease from 1979 to 1988

Extrapolation of trends outside the period of record provided dubious results. Trends were allowed only within the period of record. Prior to the earliest fall-line observations, the trend terms in the concentration relationship (Equation 5) were held constant (Figure 14-11). Although the MVUE program included a routine to compute loads, a facility to include trends in only a portion of the record was not available. Consequently, loads were computed by our own program that employed parameter values determined by the MVUE. Comparisons indicated the two programs, supplied with identical parameter values, computed loads that agreed to four significant figures.

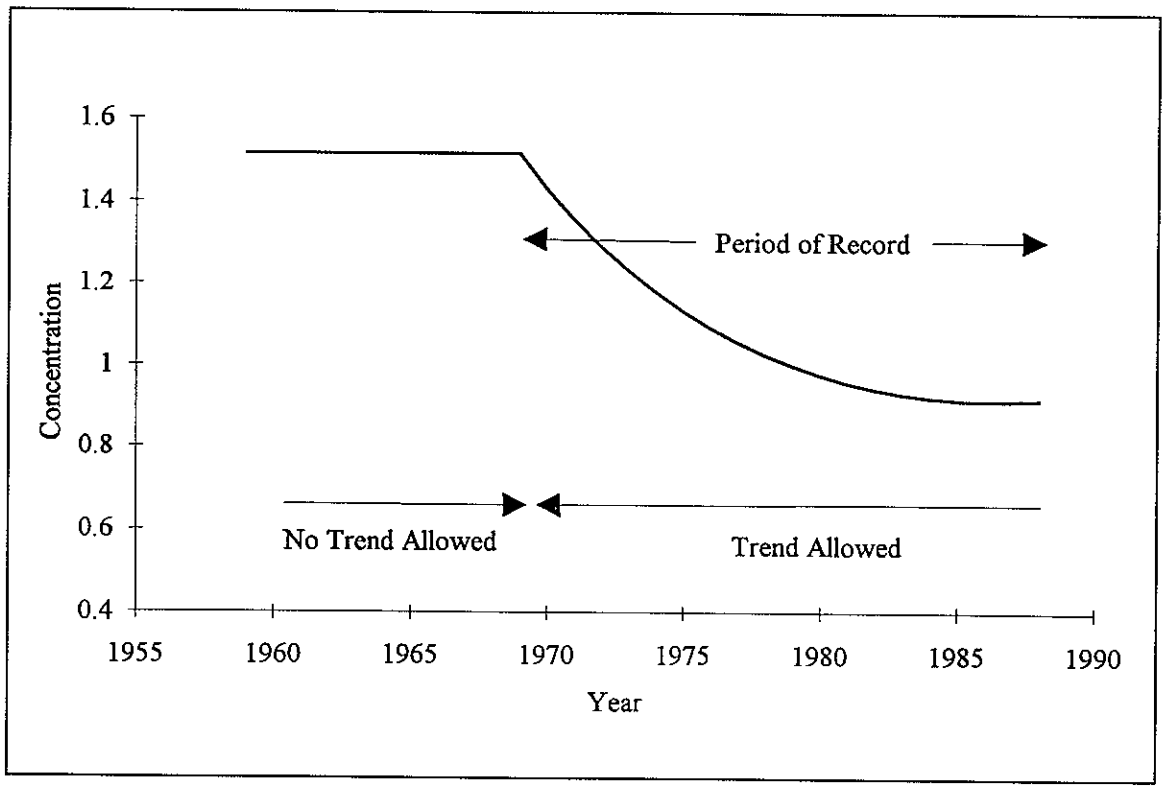

Figure 14-11. Schematic Representation of Concentration Trend at Fall Line

Load Comparison

Annual loads computed at the major fall lines were compared to estimates from other sources (Table 14-5). Alternate estimates of total nitrogen and phosphorus loads were most readily available for the three calibration years 1984-1986. Within this period, our loads were consistent with other estimates (Figures 14-12 to 14-16).

No exact quantification of error in annual load estimates was possible because exact measures of annual loads, against which to compare estimates, were non-existent. Comparison of alternate estimates, however, yielded information that indicated uncertainty in the estimated loads. For each year at each fall line, the coefficient of variation of load was computed:

$$CV = \frac{100\,s}{L_m} \qquad (6)$$

CV = coefficient of variation (%)
s = standard deviation of annual load estimates (kg day^{-1})

Table 14-5
Sources of Fall-Line Load Estimates

Source	Method	Susquehanna	Potomac	James
Maryland Department of the Environment (MDE)	MVUE estimator (Summers 1991)	X	X	
HydroQual Inc. (HDQL)	Regression (HydroQual 1989)		X	
Potomac Estuary Model (PEM)	Unknown (Fitzpatrick 1991)		X	
Metropolitan Washington Council of Governments (COG)	Combined observations and regression (An 1991)		X	
Phase II Watershed Model (WSM)	Predictive model (Donigian et al 1991)	X	X	X
USAE Waterways Experiment Station (WES)	MVUE estimator	X	X	X

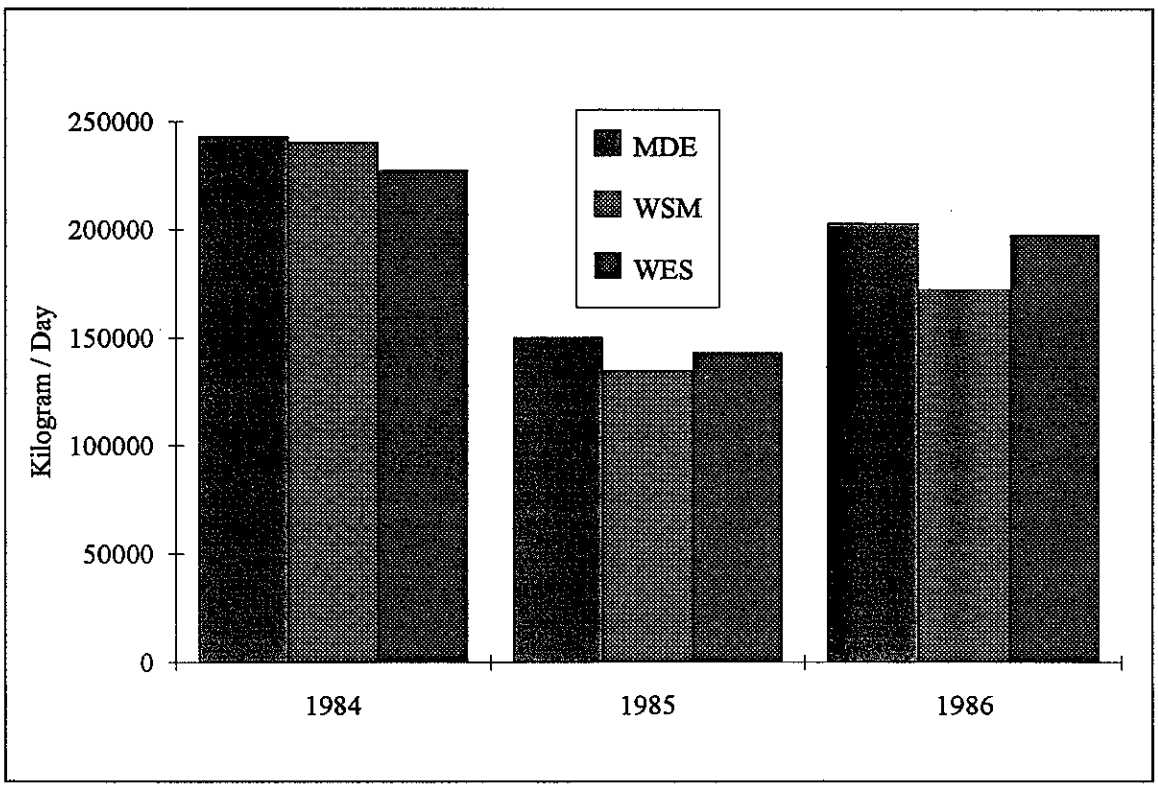

Figure 14-12. Comparison of Nitrogen Load Estimates at Susquehanna Fall Line

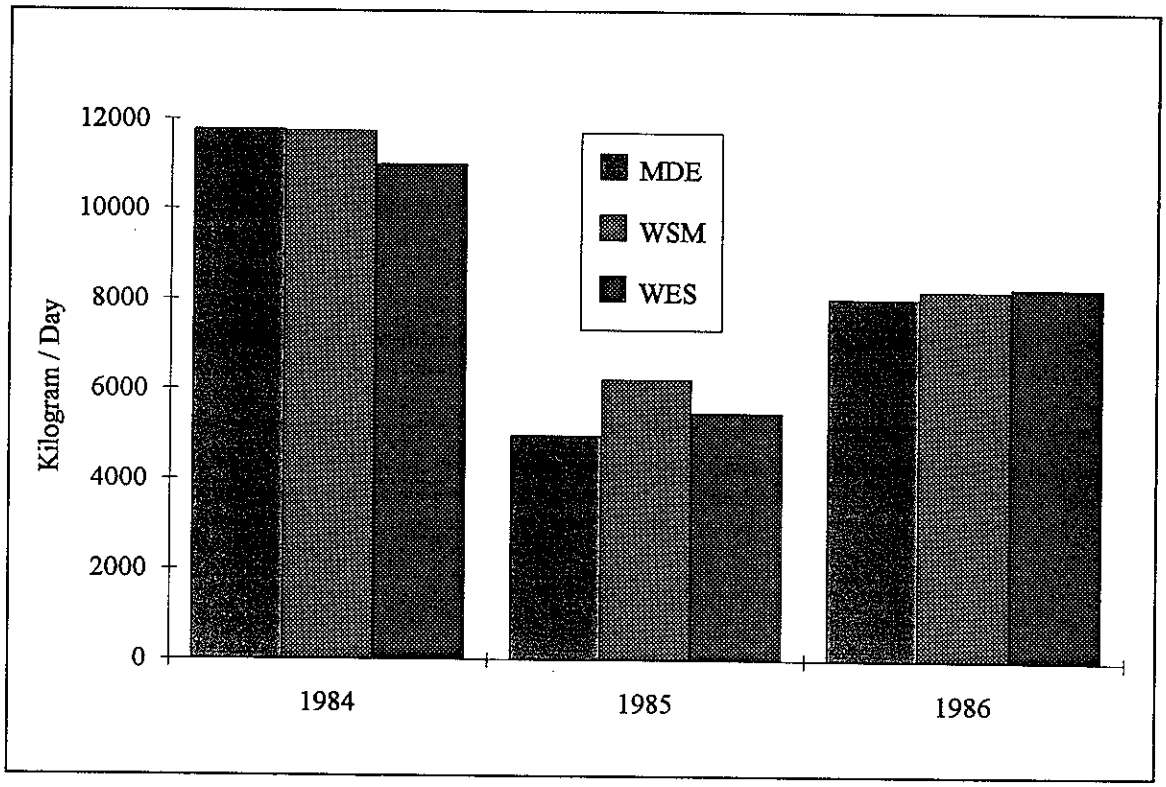

Figure 14-13. Comparison of Phosphorus Load Estimates at Susquehanna Fall Line

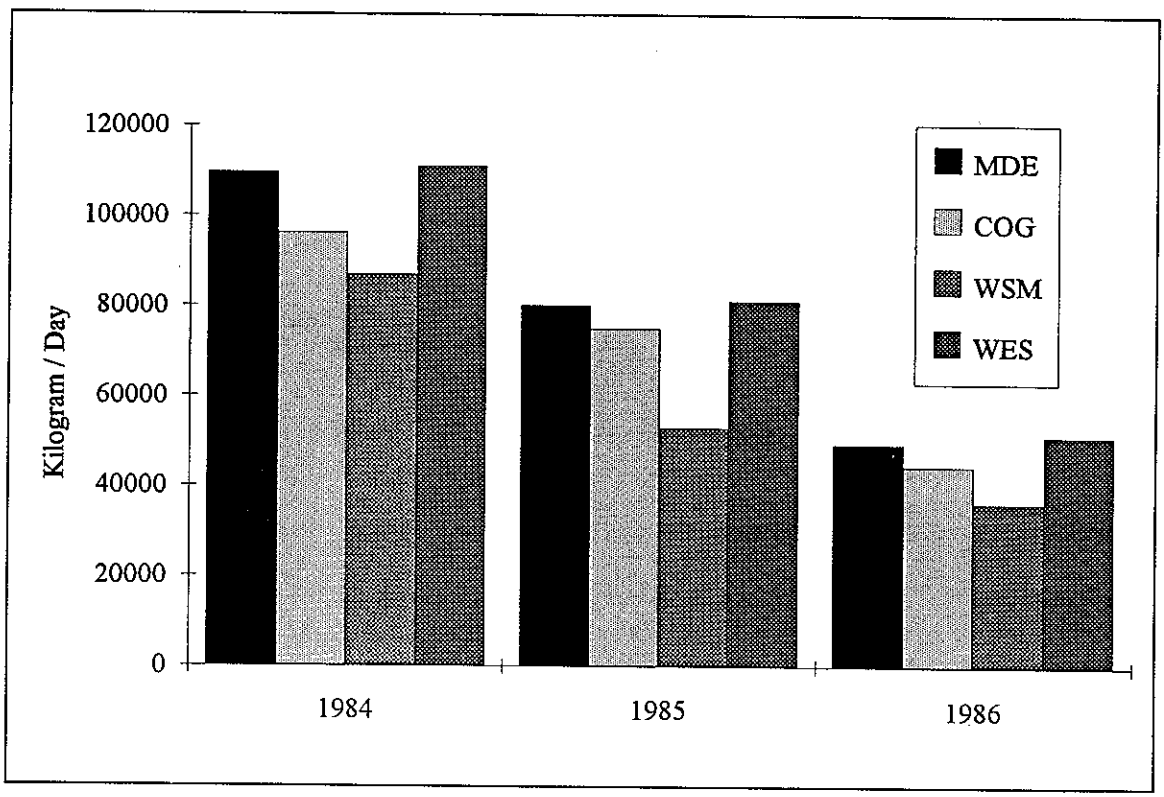

Figure 14-14. Comparison of Nitrogen Load Estimates at Potomac Fall Line

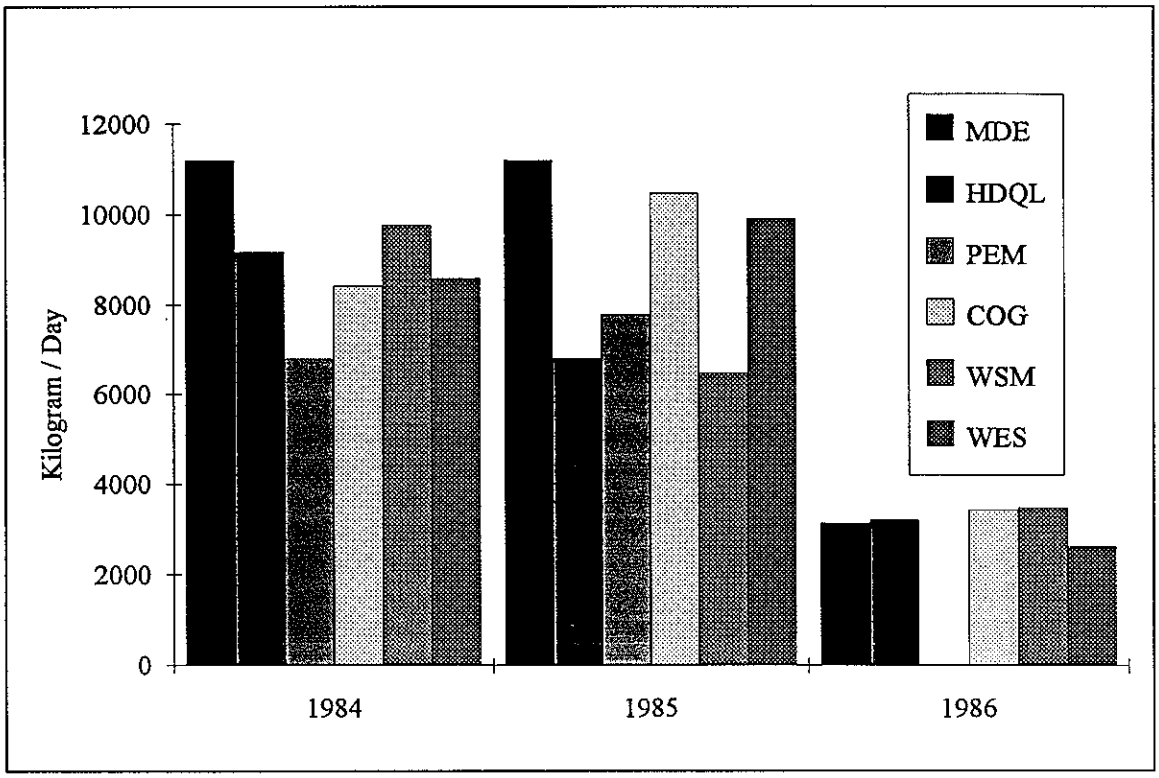

Figure 14-15. Comparison of Phosphorus Load Estimates at Potomac Fall Line

L_m = mean of annual load estimates (kg day^{-1})

The coefficient of variation of nitrogen loads ranged from 3% to 16%. Median value was 7%. The coefficient of variation of phosphorus loads ranged from 1% to 46%. Median value was 15%. The analysis indicated the alternate estimates of nitrogen load agreed well with each other. By implication, nitrogen load estimates were accurate representations of actual loads. Alternate phosphorus load estimates varied more widely than nitrogen. The larger coefficient of variation indicated uncertainty in phosphorus load estimates was double the uncertainty in estimates of nitrogen load.

Atmospheric Loads

No data was available on which to base a thirty-year time series of atmospheric loads to the water surface. Seasonal loads employed in the calibration, 1984-1986, were applied to the thirty years, 1959-1988.

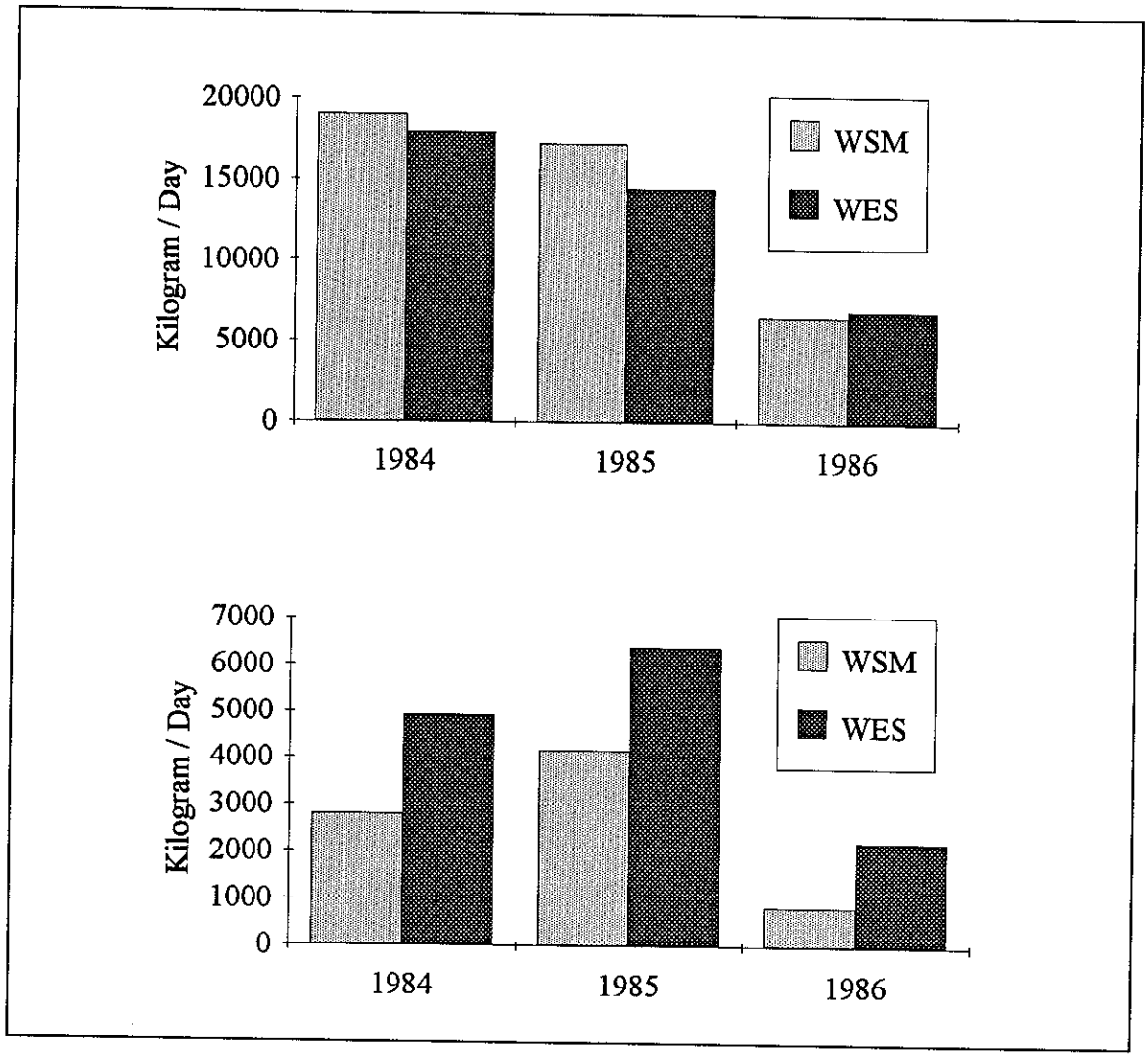

Figure 14-16. Comparison of Nitrogen and Phosphorus Load Estimates at James Fall Line

Load Summary

Total nitrogen loading to the Bay system showed no monotonic trend in the period 1959-1988 (Figure 14-17). Rather, nitrogen loading was strongly correlated to hydrology. Loading was low in the dry years and high in the wet years. Maximum, virtually equal, loads occurred in 1972 and 1979, the years of greatest flow in the Susquehanna River. Minimum load was in 1965, the lowest flow year in the thirty-year series. Virtually all the variation in load was contributed by the fall-line and below-fall-line loads. Variation in point-source loads was comparatively small although the most recent loads, 1984-1988, exceeded the earliest recorded loads. On a decadal basis (Table 14-6), nitrogen loads were least, and below long-term average, in 1959-1968. Loads were greatest, and above average, in 1969-1978. Loads in 1979-1988 were between the extremes.

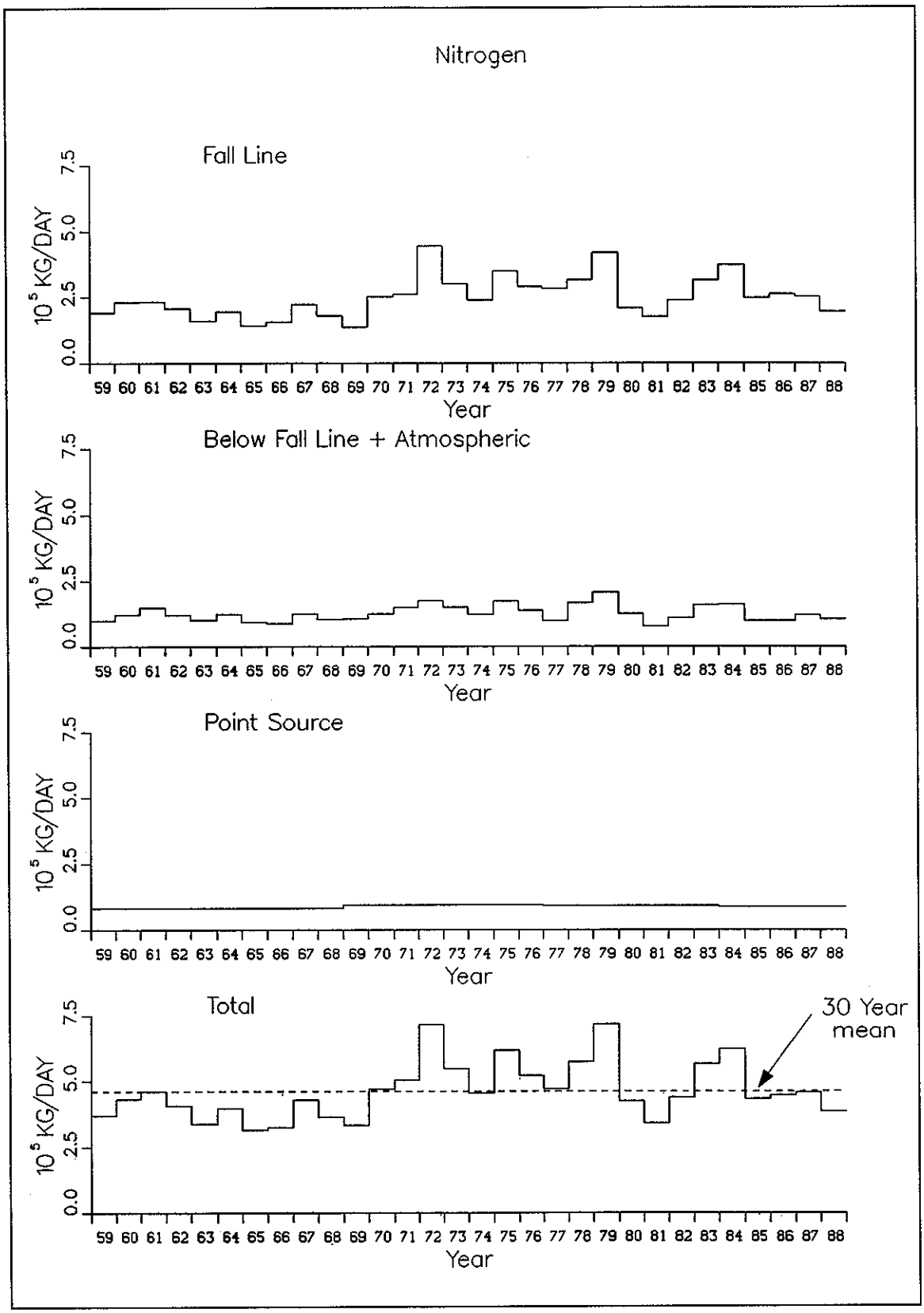

Figure 14-17. Total Nitrogen Loads to Chesapeake Bay System: 1959-1988

Table 14-6
Summary of Loads (kg day^{-1}) by Decade

		Total Organic Carbon	Total Nitrogen	Total Phosphorus
Susquehanna	1959-68	334,720	122,360	6,461
	1969-78	499,398	182,595	9,885
	1979-88	382,374	167,584	7,366
James	1959-68	99,887	11,104	2,243
	1969-78	161,492	15,970	3,643
	1979-88	118,370	13,548	3,888
Potomac	1959-68	119,887	49,115	5,224
	1969-78	186,204	76,108	8,615
	1979-88	172,972	76,343	5,896
Other Fall Line	1959-68	54,126	10,775	1,035
	1969-78	90,663	15,413	1,605
	1979-88	76,299	13,172	1,320
Below-Fall-Line	1959-68	69,319	110,421	6,395
	1969-78	97,259	136,693	7,886
	1979-88	82,999	123,159	7,091
Point-Source	1959-68	155,379	81,070	18,807
	1969-78	147,227	93,438	23,147
	1979-88	113,175	88,802	12,022
Atmosphere	1959-68	0	42,885	1,819
	1969-78	0	42,885	1,819
	1979-88	0	42,885	1,819
Total	1959-68	833,316	427,731	41,985
	1969-78	1,182,243	563,102	56,601
	1979-88	946,188	525,493	39,401

In contrast to nitrogen, total phosphorus loads to the Bay indicated a long-term trend (Figure 14-18). Phosphorus loads peaked in 1972, the year of Tropical Storm Agnes. Loads decreased, with some annual variation, from then to the end of the simulation period. Also in contrast to nitrogen, a large portion of the variation in total phosphorus loads was due to the point-source fraction. Point-source loads from 1984 onward were the least in the thirty years. As a result of average to dry hydrology and point-source control, the lowest loads occurred in the last three years of the thirty-year sequence. On a decadal basis (Table 14-16), phosphorus loads peaked during 1969-1978.

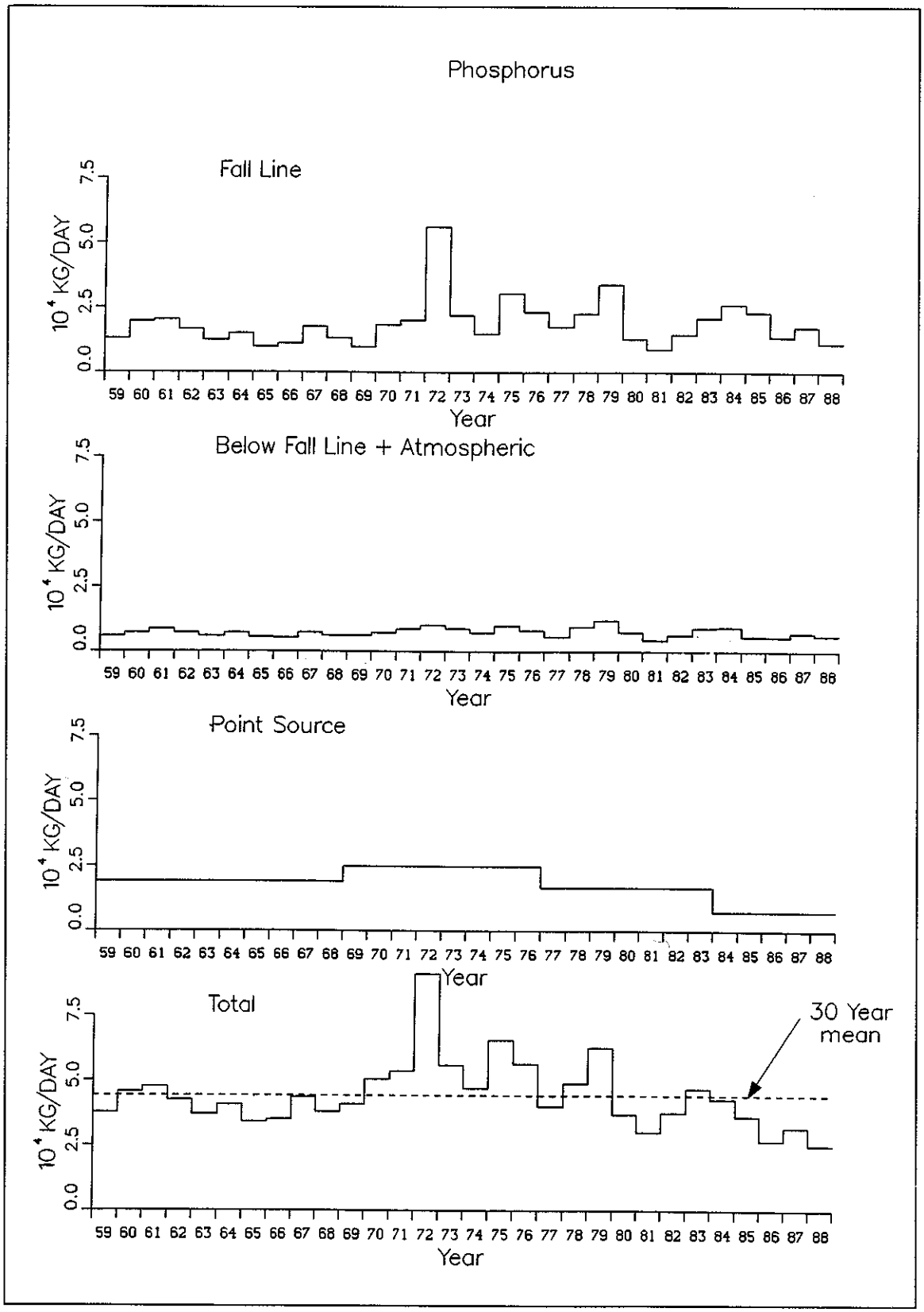

Figure 14-18. Total Phosphorus Loads to Chesapeake Bay System: 1959-1988

Loads were usually below average and showed little variability in 1959-1968. Lowest load by decade occurred in 1979-1988 but the range of loading was wider than in 1959-1968.

Carbon loading behaved much like nitrogen. Loads were strongly correlated with hydrology and showed no distinct long term trend (Figure 14-19). Compared to variability in fall-line loading, point-source variation was negligible. Highest loading occurred in the wettest decade, 1969-1978 (Table 14-16). Lowest load, by decade, occurred in 1959-1968. Loads during 1979-1988 were variable, according to hydrology. Loading during the driest years of the decade, 1981 and 1988, were comparable to loads in 1959-1968.

Thirty-Year Simulation Results

Comparison to Three-Year Simulation

Concentrations predicted for the years 1984-1986 in the thirty-year simulation were compared to observations and to the model calibration results for the same years. The objective was to validate the performance of the model in the long-term simulation. Comparisons were of season-zone-level aggregations used to evaluate the model calibration. Four zones were selected for examination: Zones 2 and 5 in the mainstem Bay (Figure 14-1), Zone 1 in the upper James River (Figure 10-2), and Zone 1 in the upper Potomac River (Figure 10-2).

In the mainstem, output from the two simulations was nearly coincident (Figures 14-20, 14-21) although some differences in phosphorus were evident in Zone 2. Concentration differences were more apparent in the upper Potomac (Figure 14-22). Dissolved inorganic phosphorus in the thirty-year simulation clearly differed from the calibration run and provided superior agreement to the observations. Concentration differences were also evident in the upper James (Figure 14-23) although only for total organic carbon was one prediction, the thirty-year simulation, superior to the other. The differences in the two model runs originated in the fall-line loads. The calibration was driven by Watershed Model loads. The thirty-year simulation was driven by regression-based loads. Origins of the discrepancies were sometimes subtle. In the Potomac, for example, the regressions indicated 17% of total phosphorus was dissolved. The watershed model indicated 38% was dissolved. The discrepancy in dissolved fraction, more than discrepancy in total load, determined the difference in phosphorus predictions in the upper Potomac.

Away from the fall lines, internal processes predominated in determining water column concentrations and fractions. Overall, results of the calibration and thirty-year simulation agreed well, as evidenced by a comparison of relative error statistics for the mainstem (Figure 14-24). The comparison demonstrated that a thirty-year model run can be executed and perform as well as a model run of order-of-magnitude less duration. Results of the thirty-year

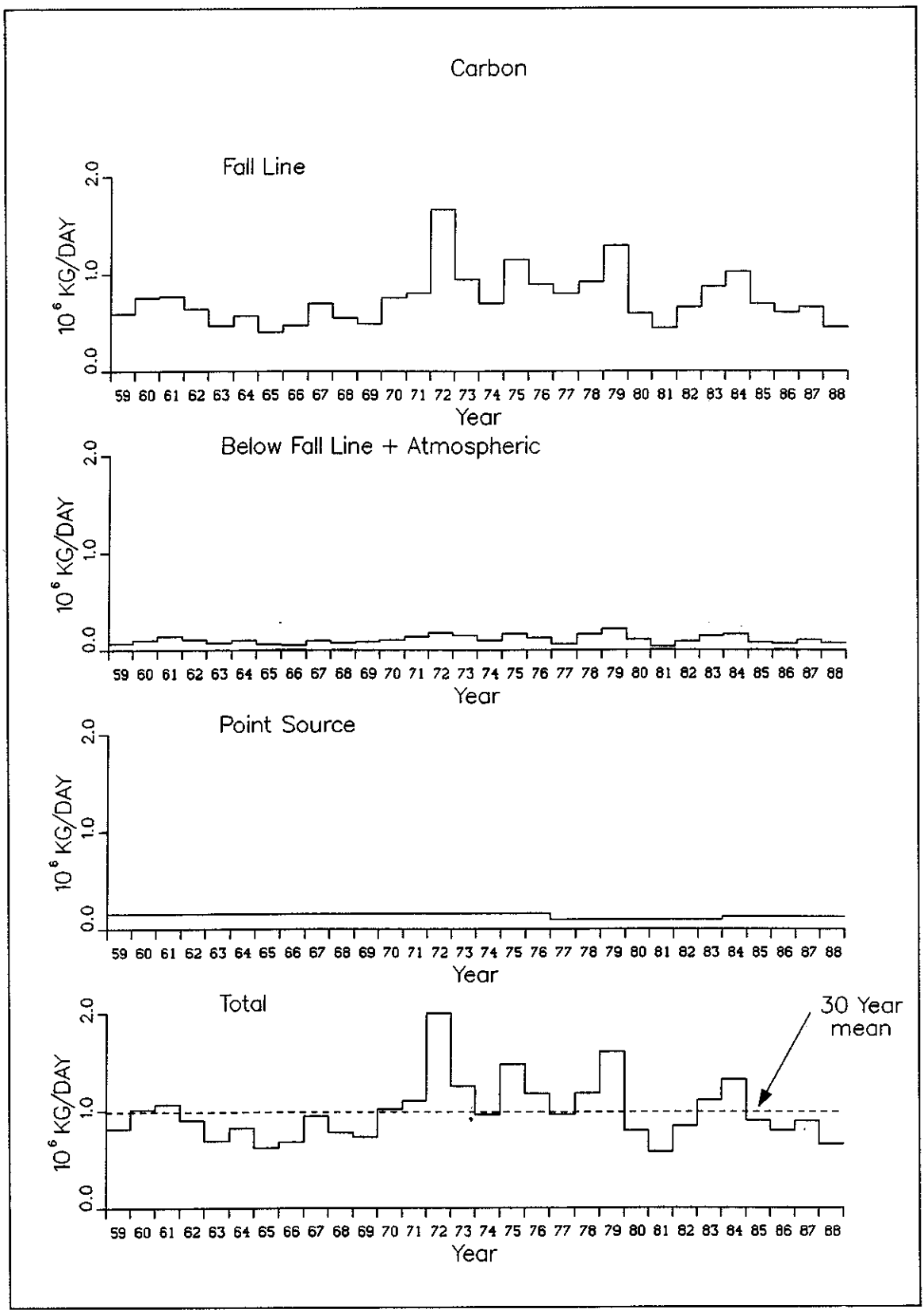

Figure 14-19. Total Organic Carbon Loads to Chesapeake Bay System: 1959-1988

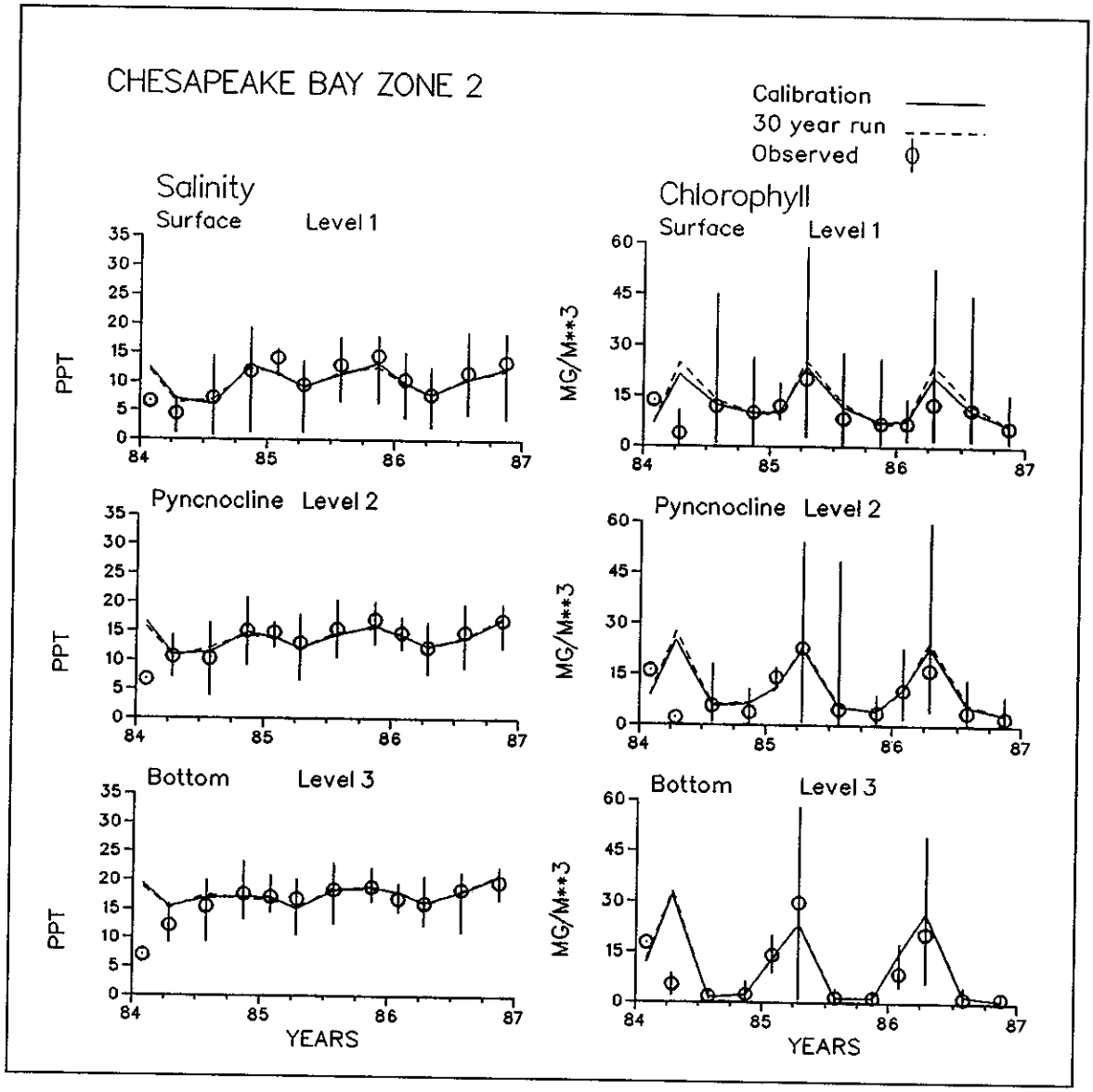

Figure 14-20. Observations in Bay Zone 2, 1984-1986, Compared to Model Calibration and Thirty-Year Simulation (Sheet 1 of 5)

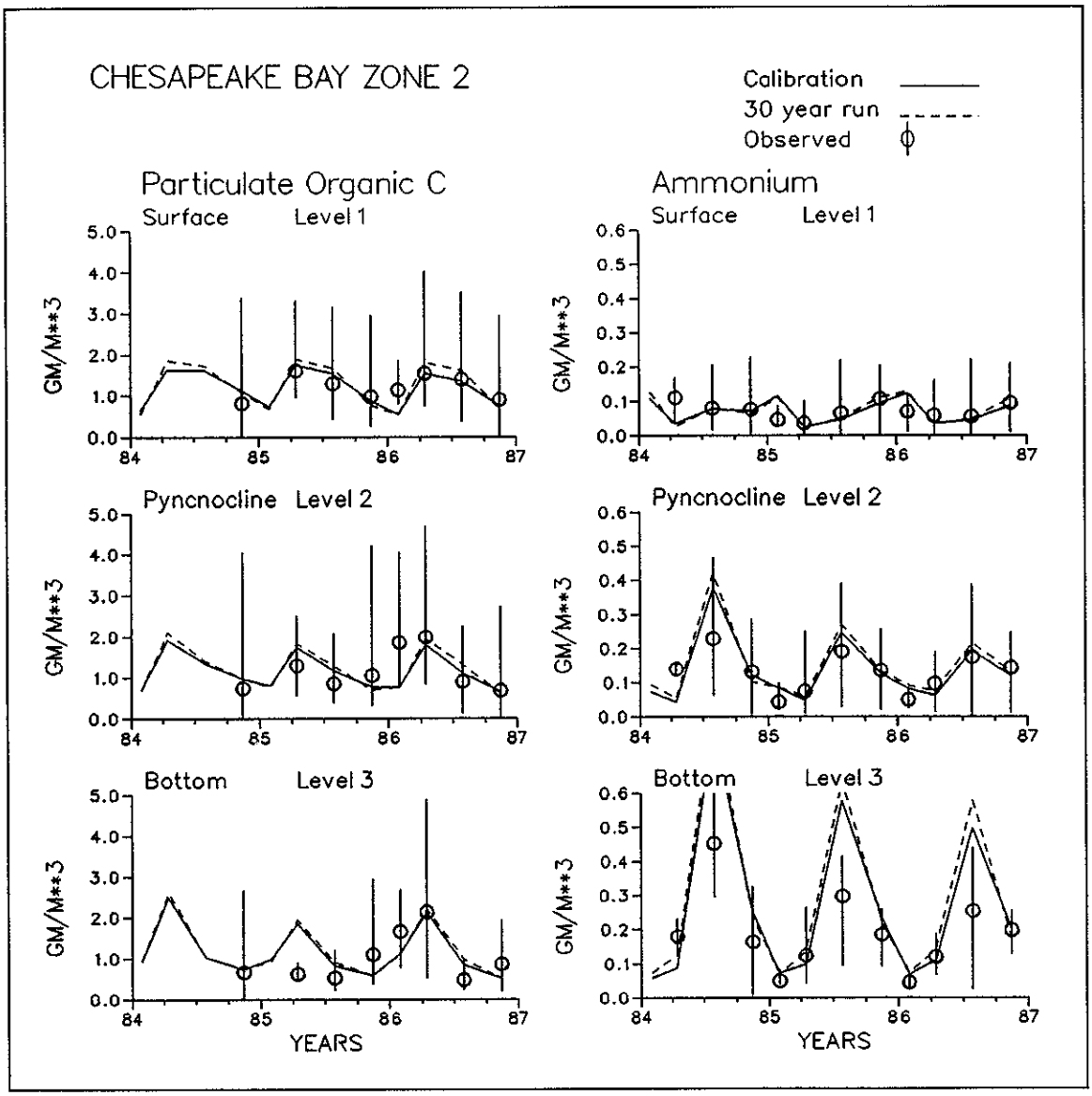

Figure 14-20. (Sheet 2 of 5)

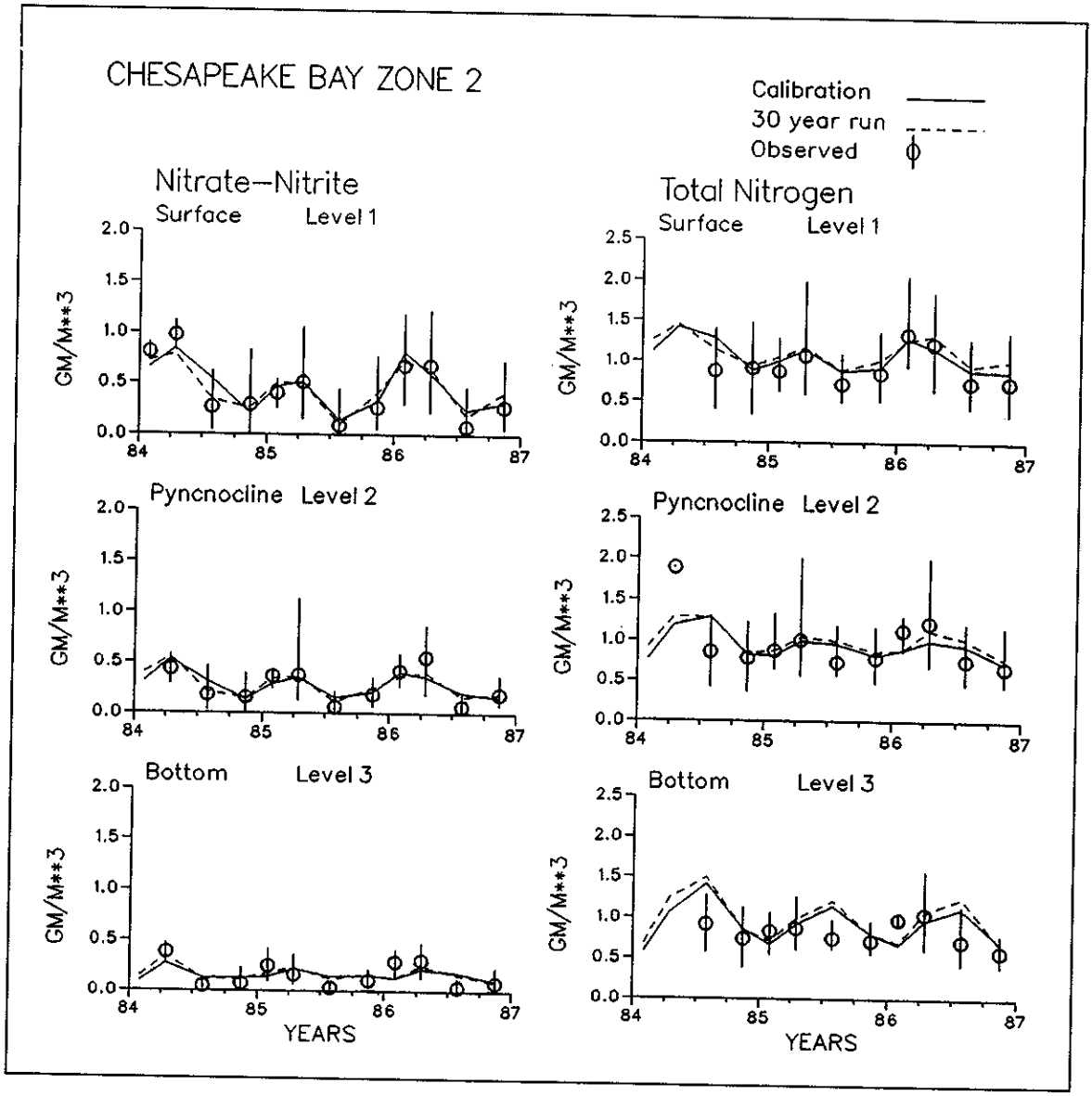

Figure 14-20. (Sheet 3 of 5)

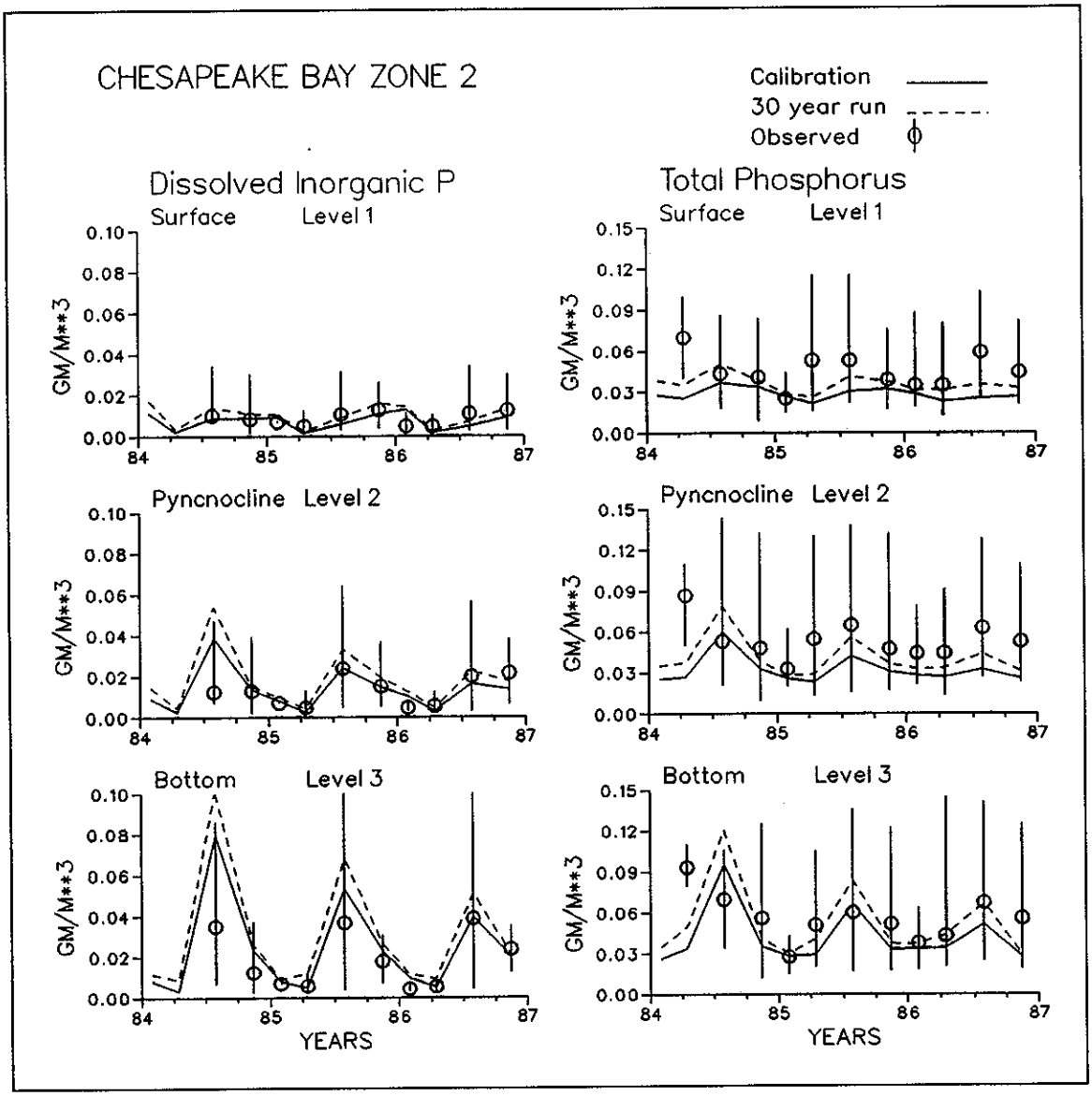

Figure 14-20. (Sheet 4 of 5)

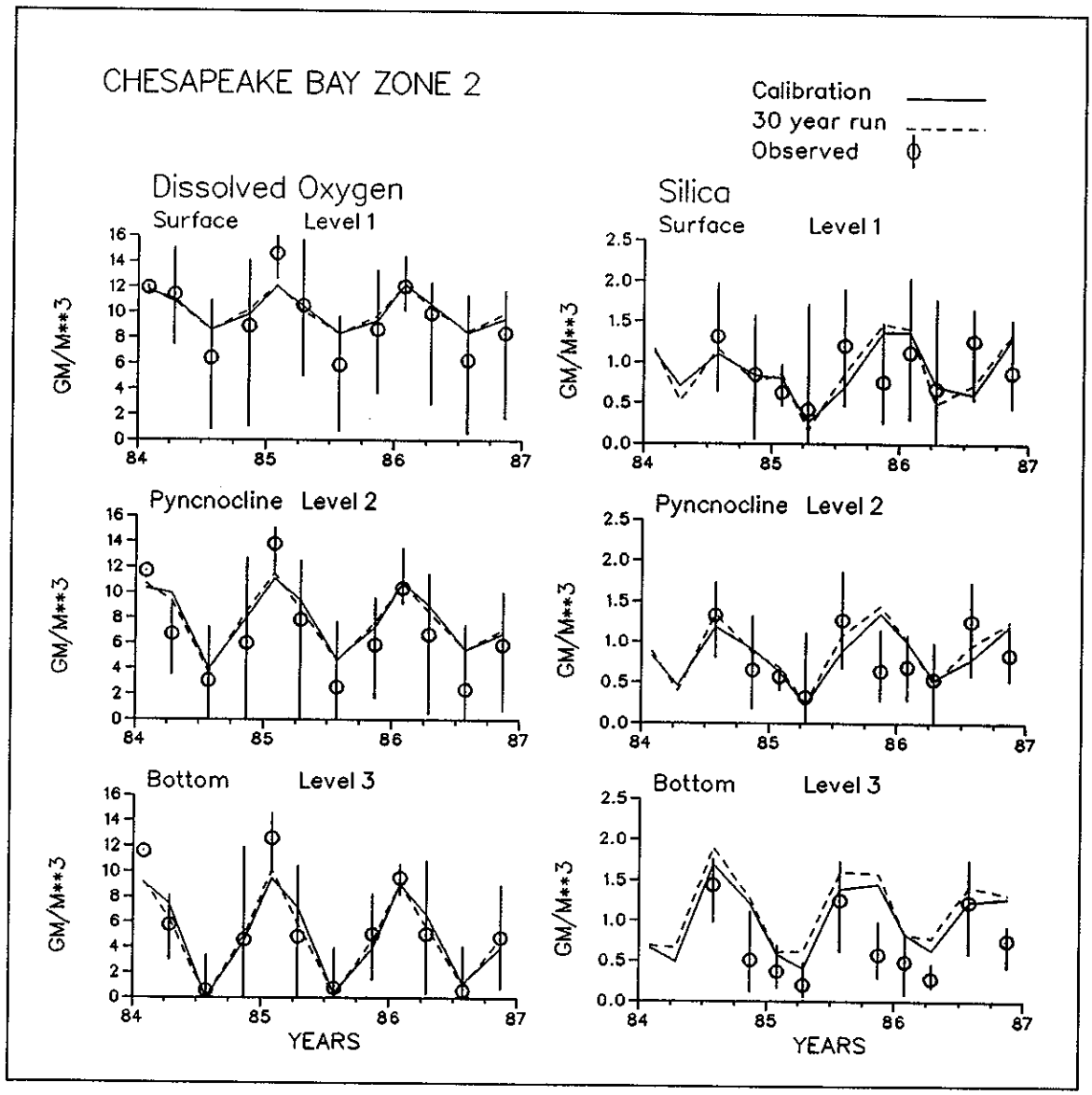

Figure 14-20. (Sheet 5 of 5)

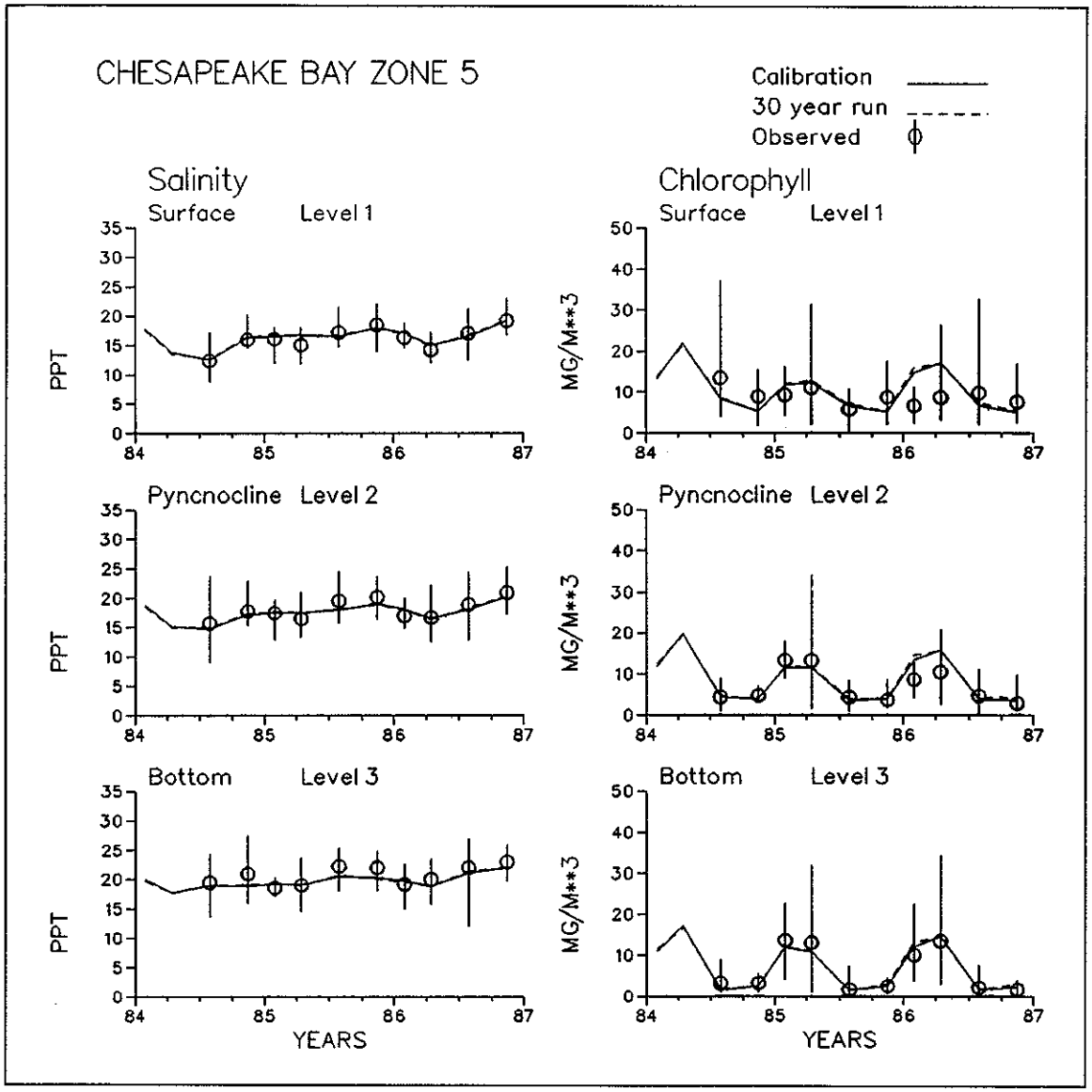

Figure 14-21. Observations in Bay Zone, 1984-1986, Compared to Model Calibration and Thirty-Year Simulation (Sheet 1 of 5)

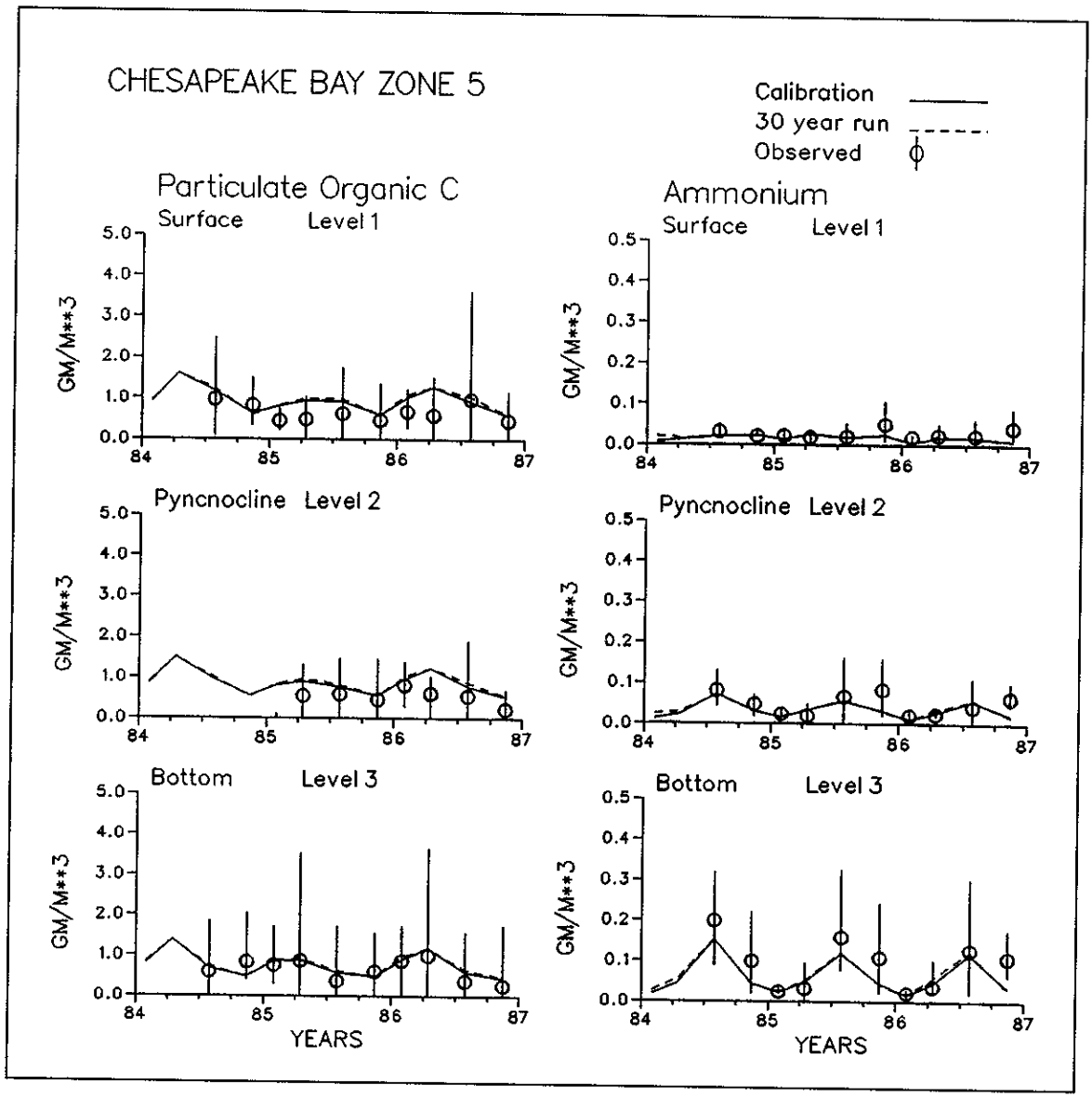

Figure 12-21. (Sheet 2 of 5)

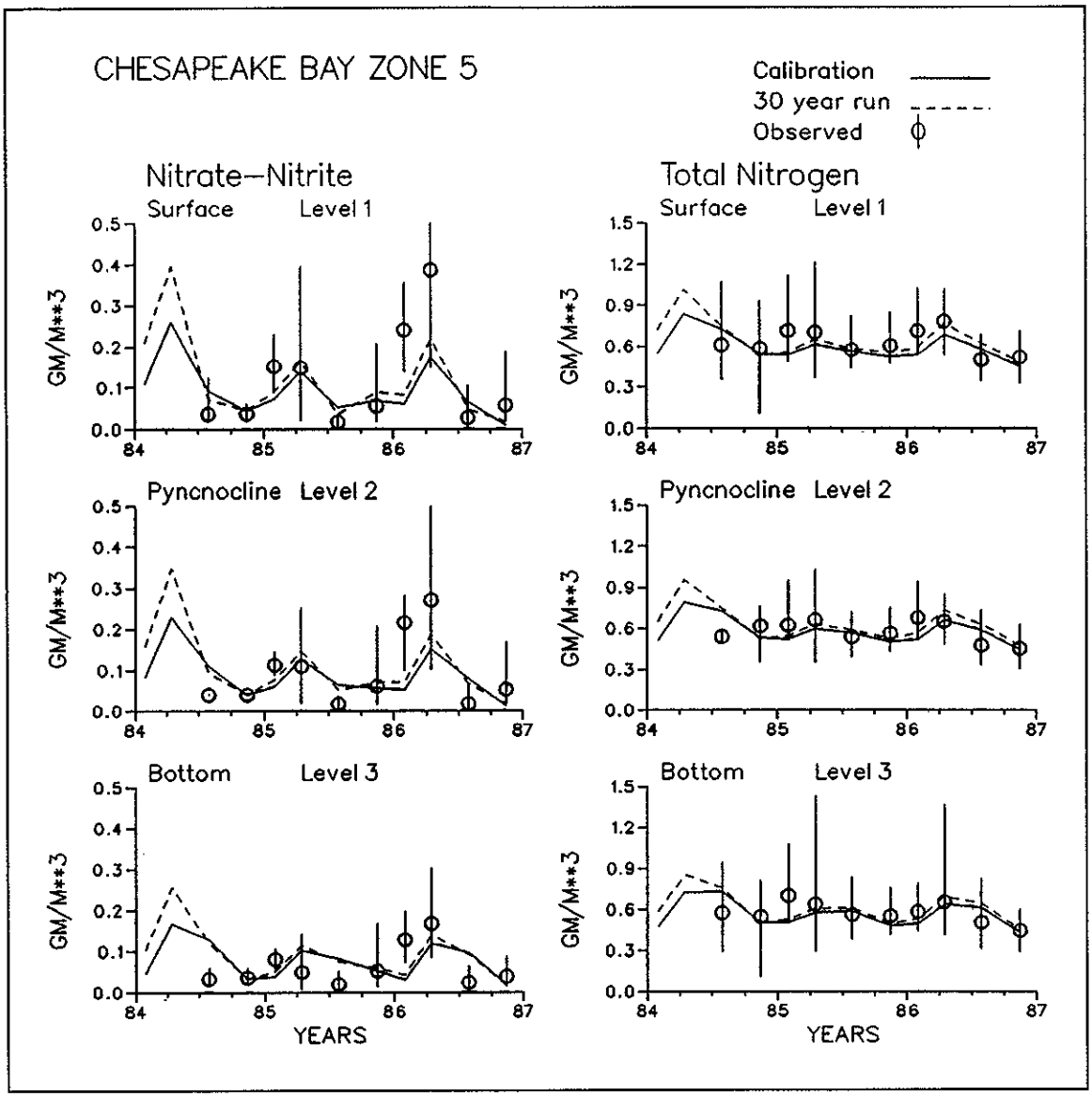

Figure 14-21. (Sheet 3 of 5)

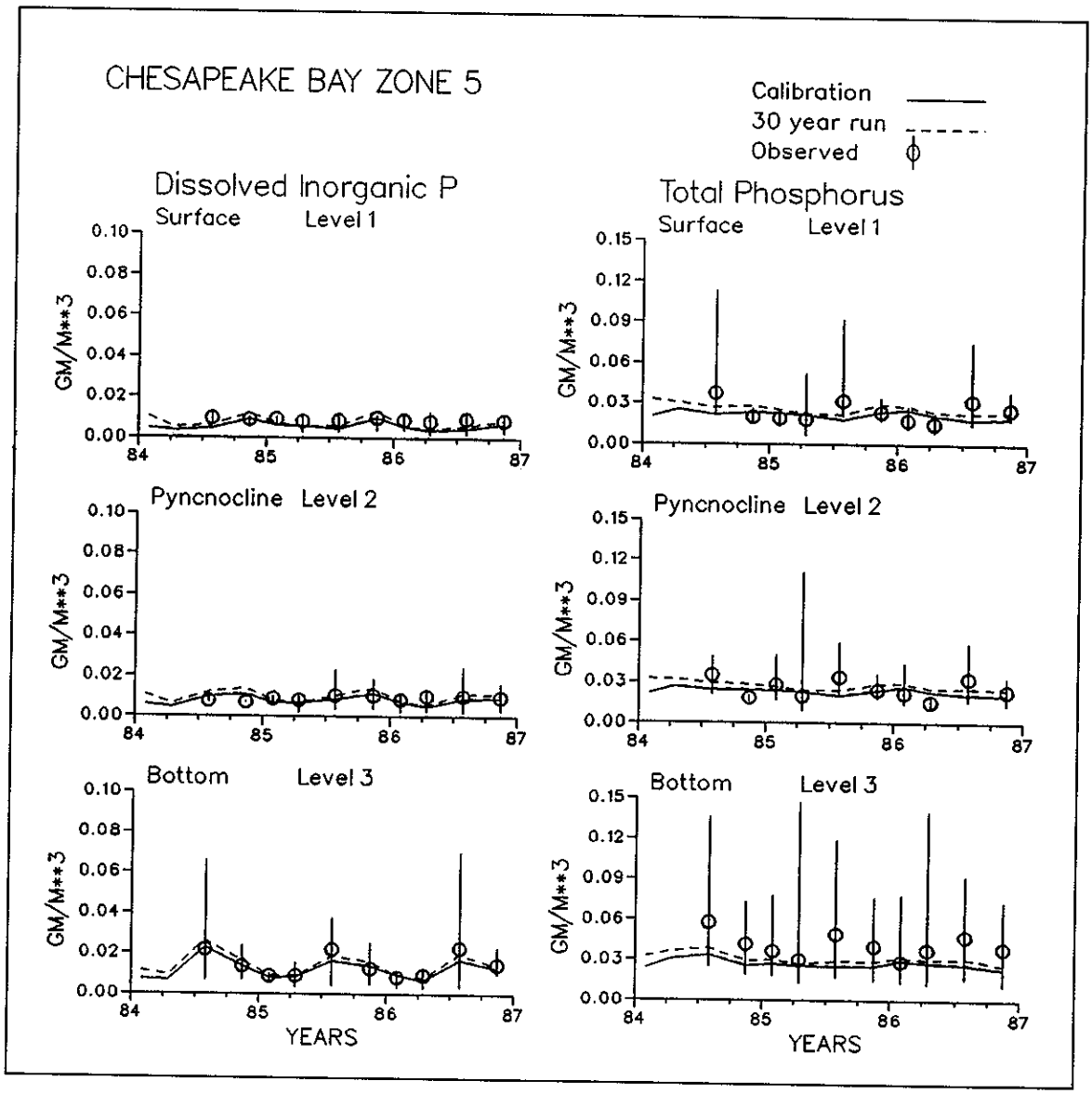

Figure 14-21. (Sheet 4 of 4)

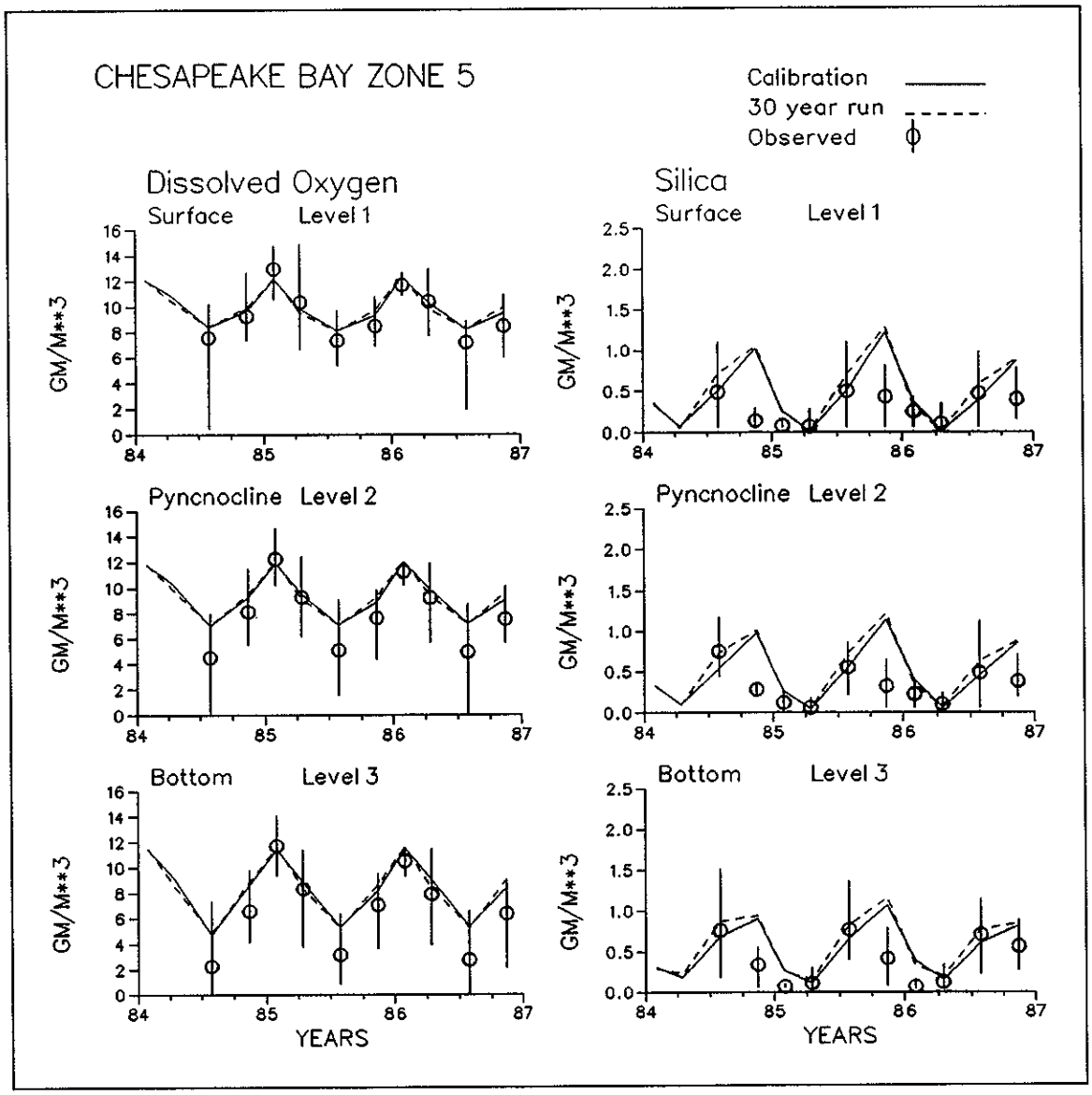

Figure 14-21. (Sheet 5 of 5)

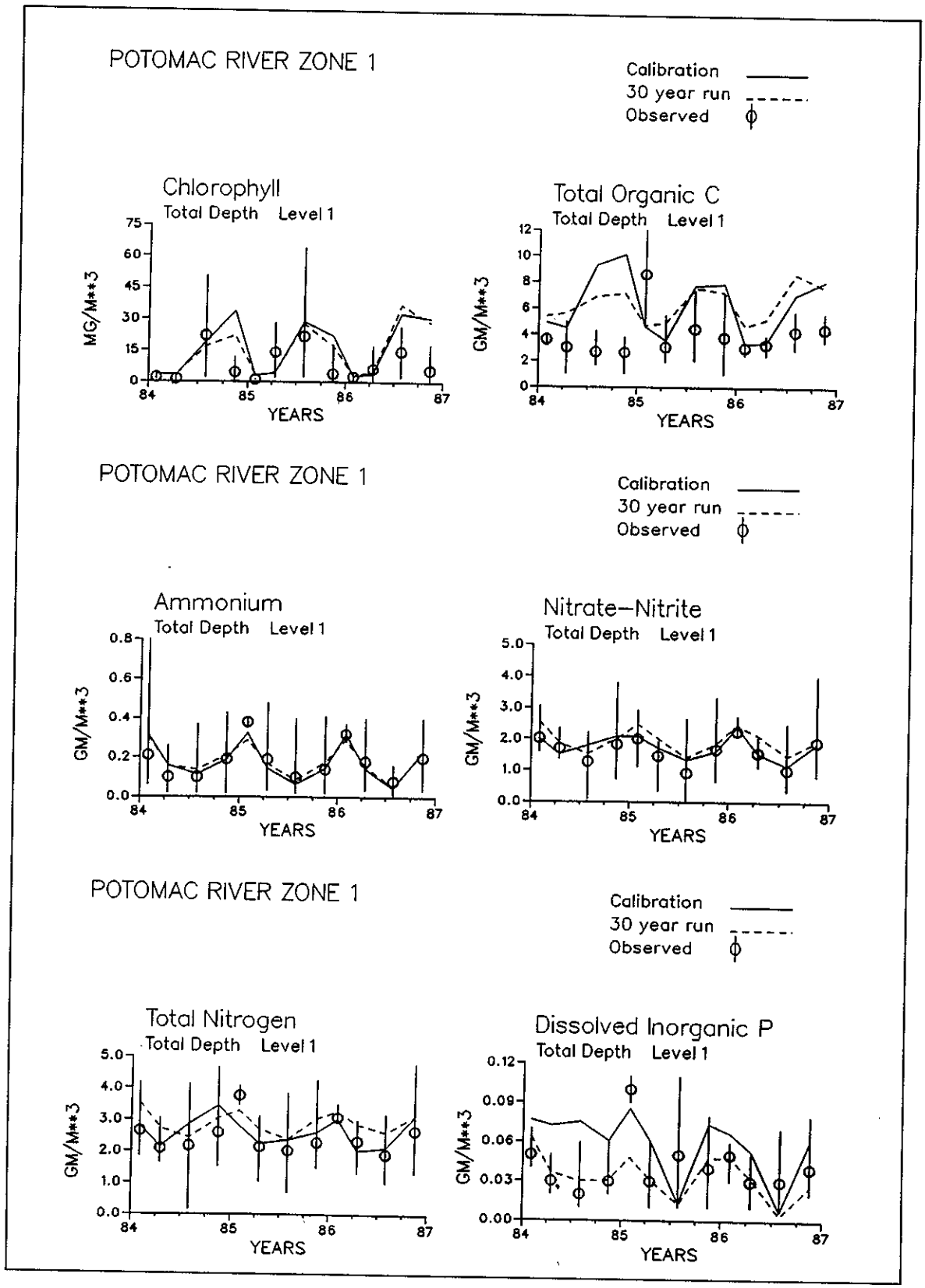

Figure 14-22. Observations in Potomac Zone 1, 1984-1986, Compared to Model Calibration and Thirty-Year Simulation (Continued)

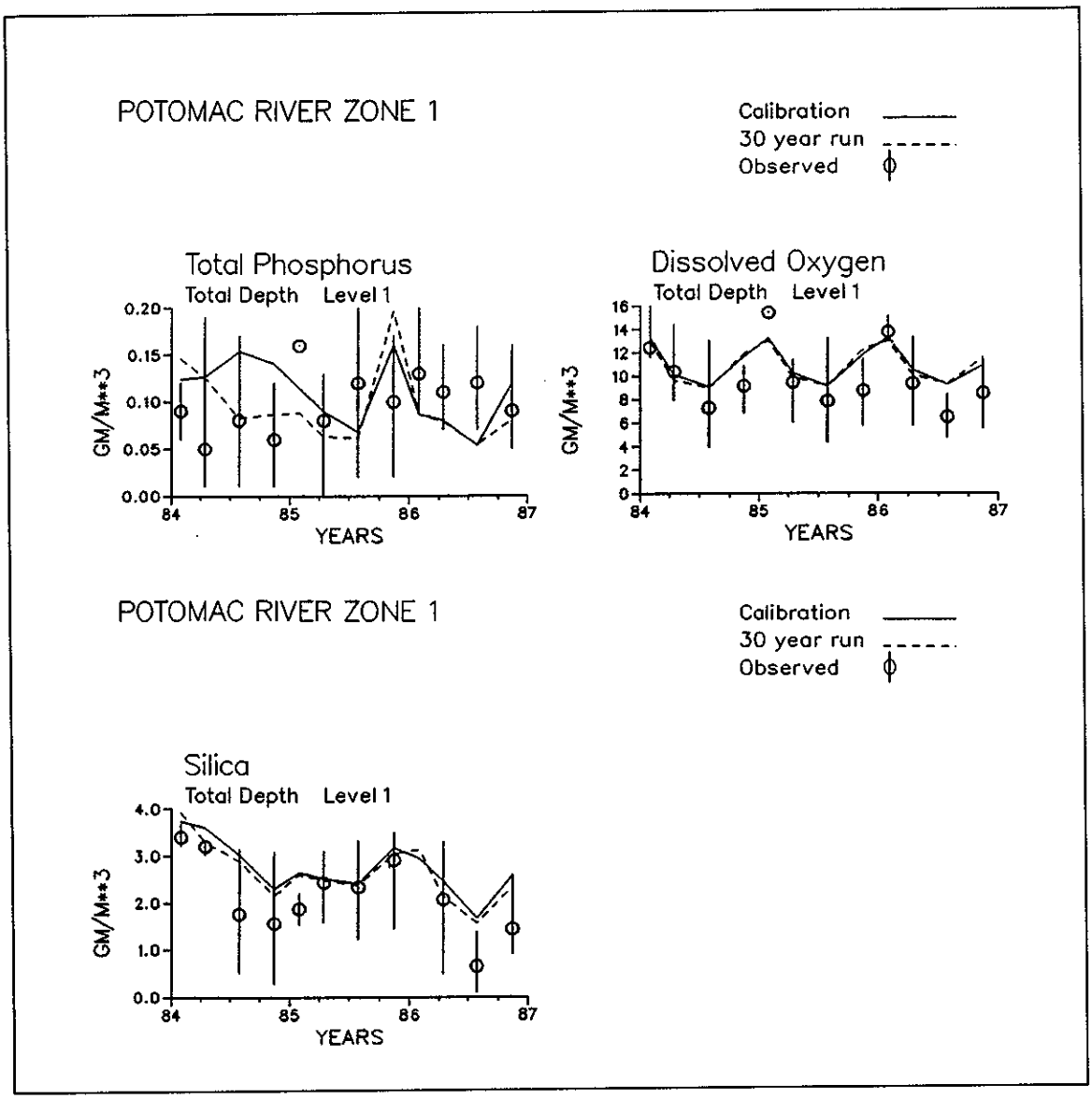

Figure 14-22. (Concluded)

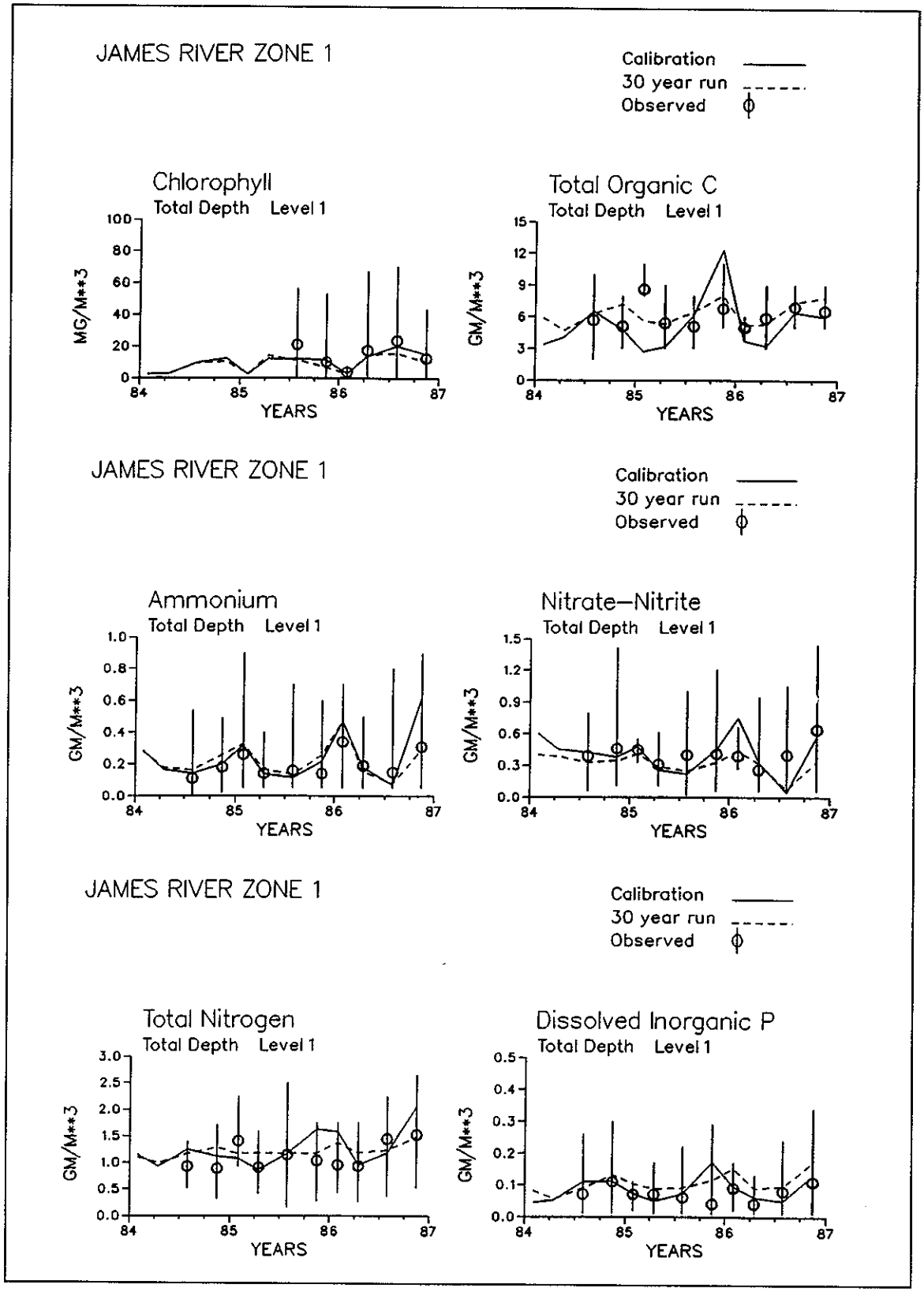

Figure 14-23. Observations in James Zone 1, 1984-1986, Compared to Model Calibration and Thirty-Year Simulation (Continued)

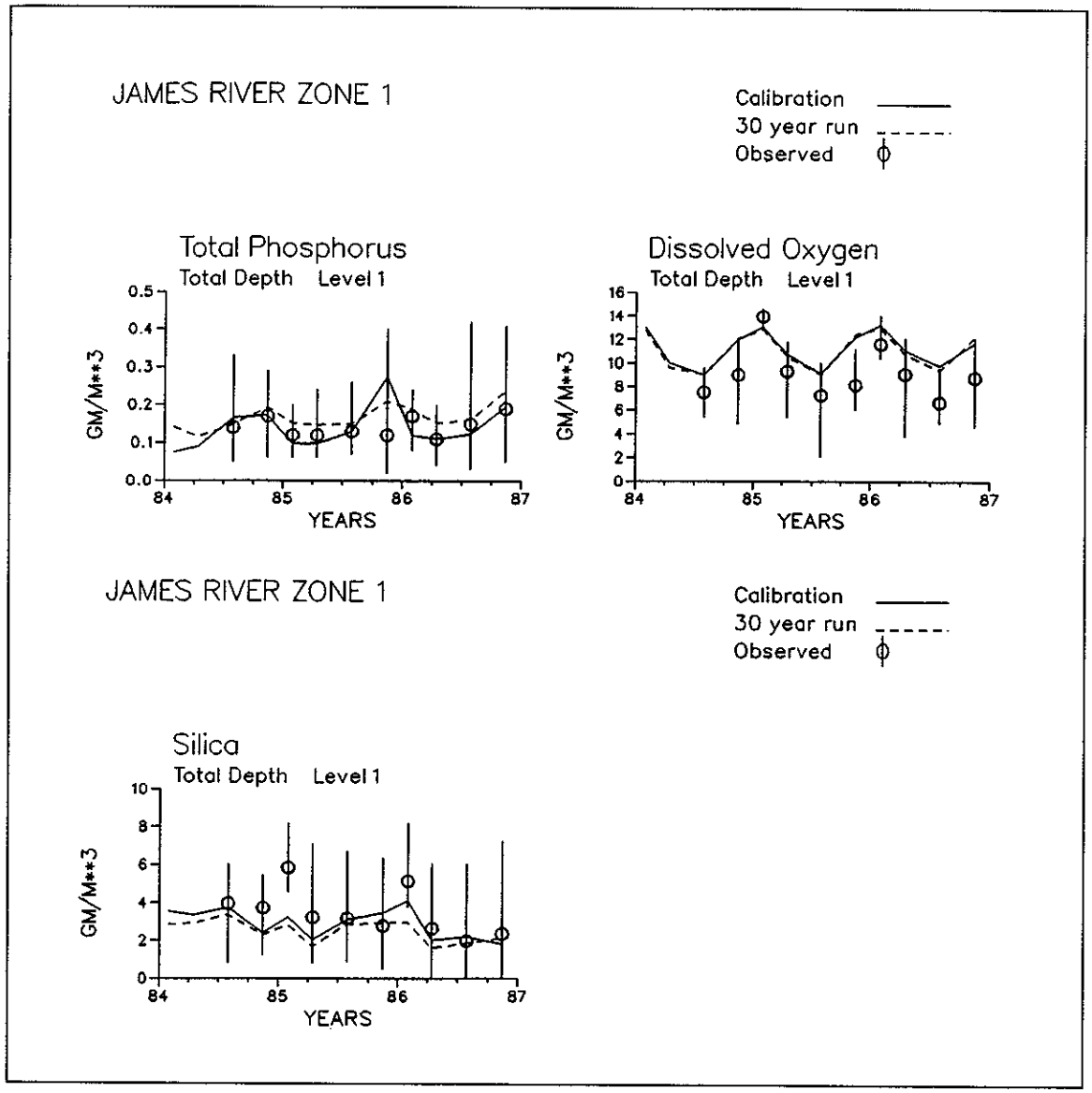

Figure 14-23. (Concluded)

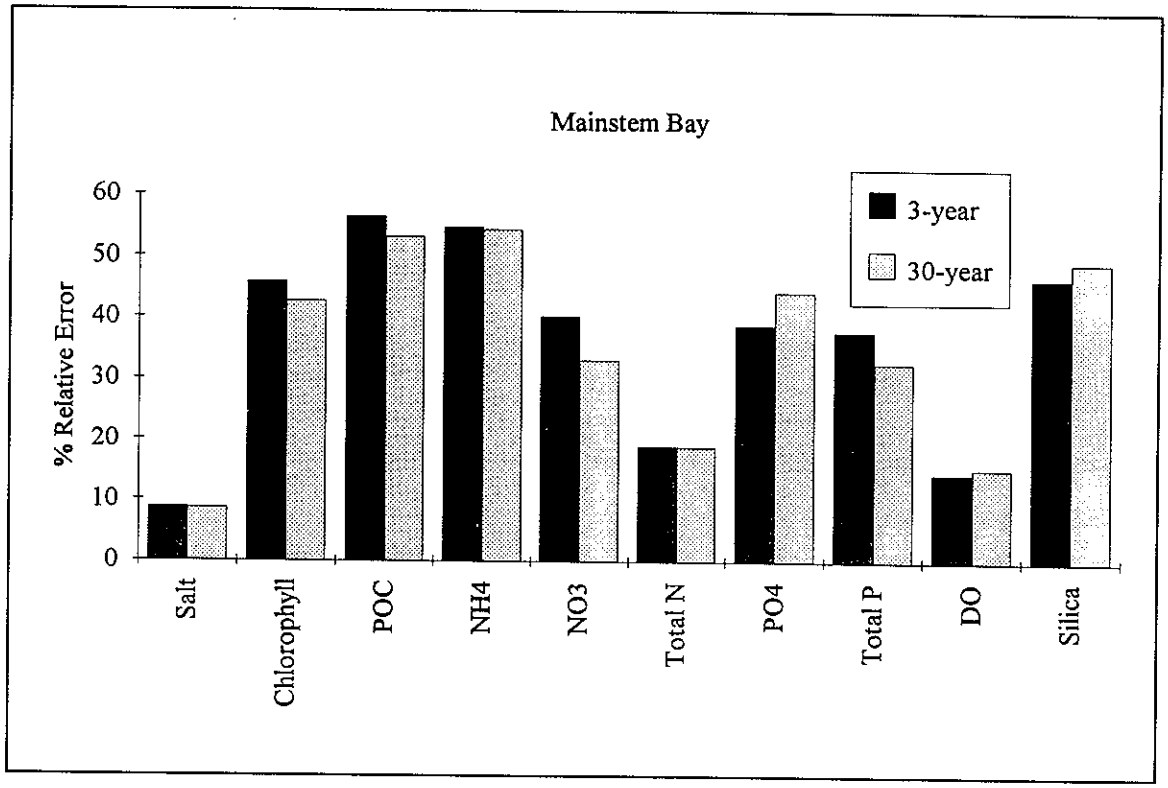

Figure 14-24. Relative Error in Model Calibration and Thirty-Year Simulation

simulation are as reliable as results of the calibration run and can be interpreted with the same degree of confidence.

Thirty-Year Time Series

Output from the thirty-year run was first examined as time series. Two time series were produced for each major water-quality constituent. One time series was an annual average for the mainstem Bay. The second time series was a summer average (June 1 - September 30) only. Concentrations were averaged over the entire volume of the mainstem except for chlorophyll and dissolved oxygen. Since chlorophyll occurs primarily in the photic zone, chlorophyll concentration was averaged in the surface layer (depth < 6.7 m) only. Since dissolved oxygen depletion occurs primarily in bottom waters, dissolved oxygen was averaged in the bottom layer (depth > 12.8 m) only.

None of the time series indicated clear monotonic trends over the thirty-year period although several substances indicated trends of lesser duration. Correlations to hydrology and/or loads were occasionally evident.

Chlorophyll concentrations (Figure 14-25) were minimum in years 7 to 11 (1965-1969) of the simulation, years of average to dry hydrology. Total organic carbon (Figure 14-26), closely tied to algal production, showed the

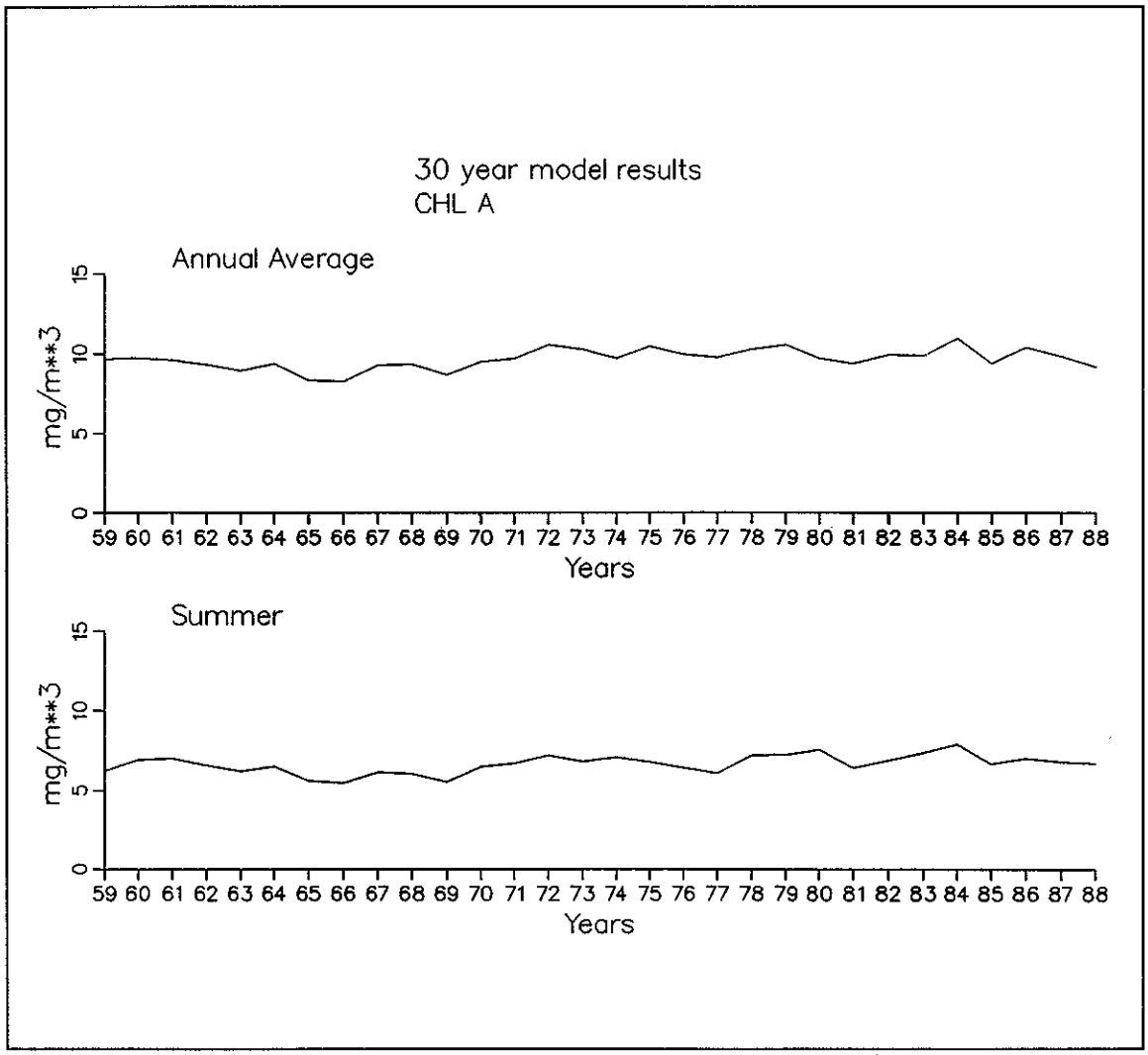

Figure 14-25. Thirty-Year Chlorophyll Concentration in Mainstem Layer 1

same behavior. Neither substance was distinctly higher at the end of the simulation than at the beginning, however.

Ammonium (Figure 14-27) was closely tied to hydrology, especially in the summer months. Ammonium was higher in wet hydrology than in dry to average hydrology. The origin of the ammonium peaks was the larger volume of anoxia that occurred in the wet years. Due to increased anoxia, more ammonium was released from bottom sediments than in less anoxic periods when a larger fraction of sediment ammonium was denitrified to gaseous nitrogen. Ammonium concentration was also clearly higher, $\approx$0.004 gm m^{-3} on an annual basis, at the end of the simulation than at the beginning. The concentration increase correlated with the observed increase in total kjeldahl nitrogen at the Susquehanna fall line (Table 14-4).

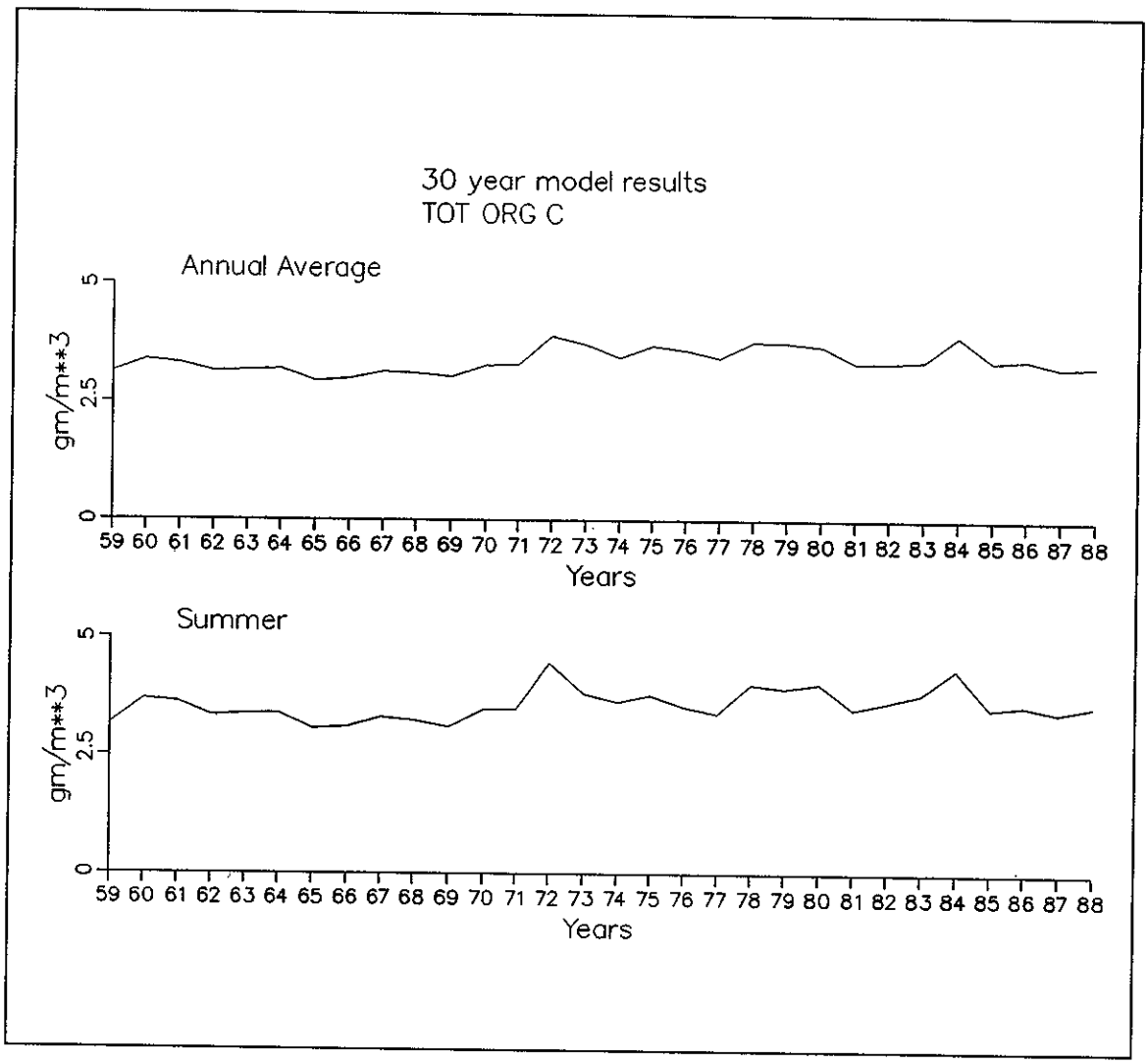

Figure 14-26. Thirty-Year Total Organic Carbon Concentration in Mainstem Bay

Nitrate (Figure 14-28) also demonstrated a correlation with hydrology. As with ammonium, concentration was highest during wet years. The dependence was due to larger loads during wet years rather than a sediment-water interaction, however. Minimum nitrate concentration occurred during the dry years 7 to 11 (1965-1969). On an annual basis, nitrate indicated an increasing trend from 1959 to 1988. Nitrate in the years of average hydrology 1986-1987 was $\approx$0.04 gm m^{-3} higher than in the years of similar hydrology 1959-1960. The nitrate increase correlated with concentration increases detected at the Susquehanna and Potomac fall lines (Table 14-4), the two largest sources of runoff to the Bay.

Total nitrogen concentration and trends (Figure 14-29) mirrored nitrate. Greater concentrations occurred in wet years with high runoff. Minimum total nitrogen was in dry years 7 to 11 (1965-1969). Total nitrogen at the end of

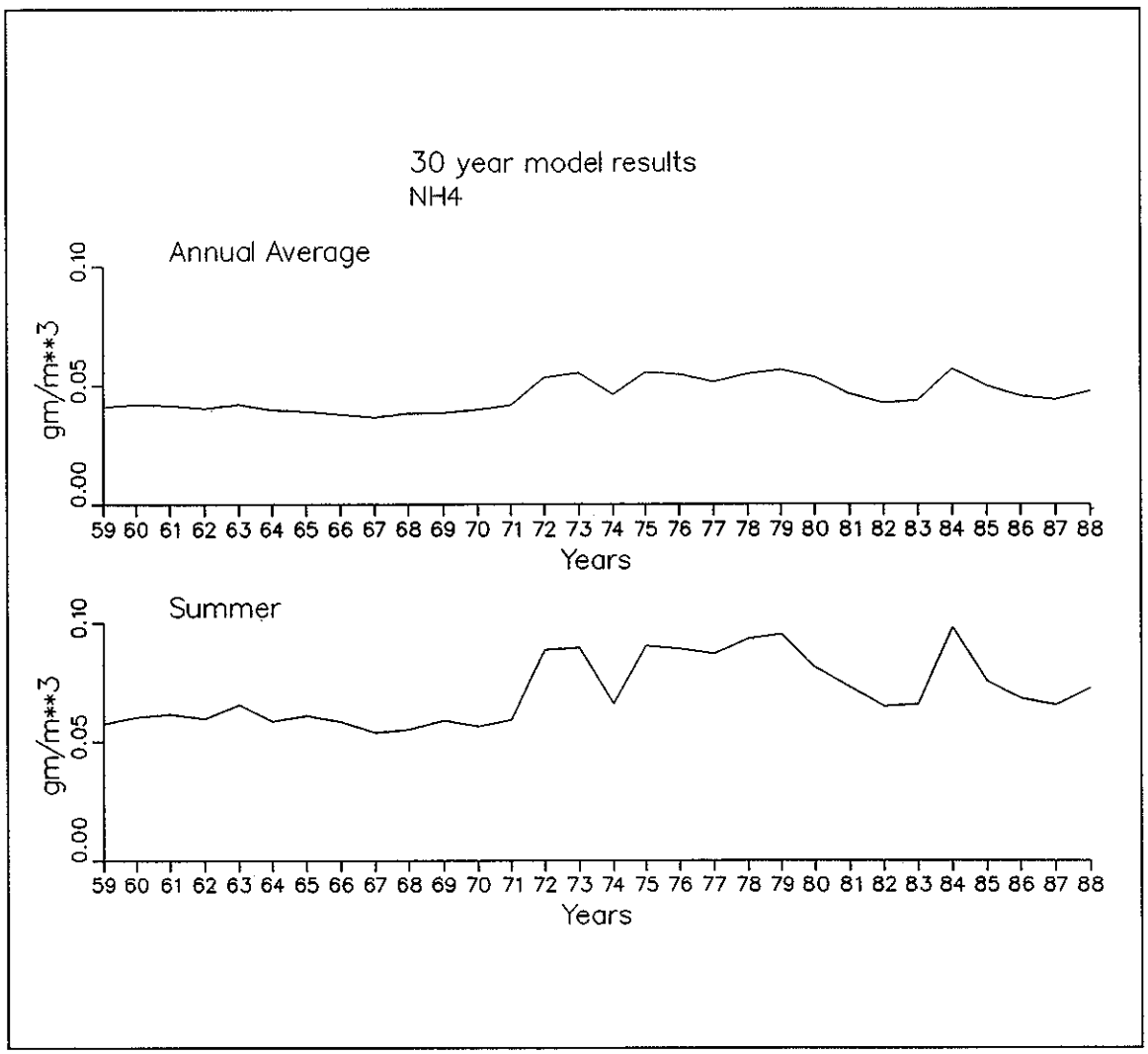

Figure 14-27. Thirty-Year Ammonium Concentration in Mainstem Bay

the simulation was higher, ≈0.06 gm m^{-3} on an annual basis, than at the beginning.

Annual average phosphate (Figure 14-30) and total phosphorus (Figure 14-31) exhibited peak concentrations in years 14 and 15 (1972 and 1973), concurrent with and following the record runoff that occurred in 1972 during Tropical Storm Agnes. Following the storm, phosphate and total phosphorus generally decreased through the end of the simulation. Decreasing concentrations at the Susquehanna and Potomac fall lines (Table 14-4) contributed to the decline as well as hydrologic factors. Phosphorus was correlated with point-source loads as well as hydrology. Point source loads peaked in years 11 to 18 (1969-1976) and were at the thirty-year minimum in years 26 to 30 (1984-1988). As a result of point-source and nonpoint-source controls, on an annual basis, phosphate declined by ≈0.004 gm m^{-3} and total phosphorus declined by ≈0.006 gm m^{-3} from beginning to end of the simulation.

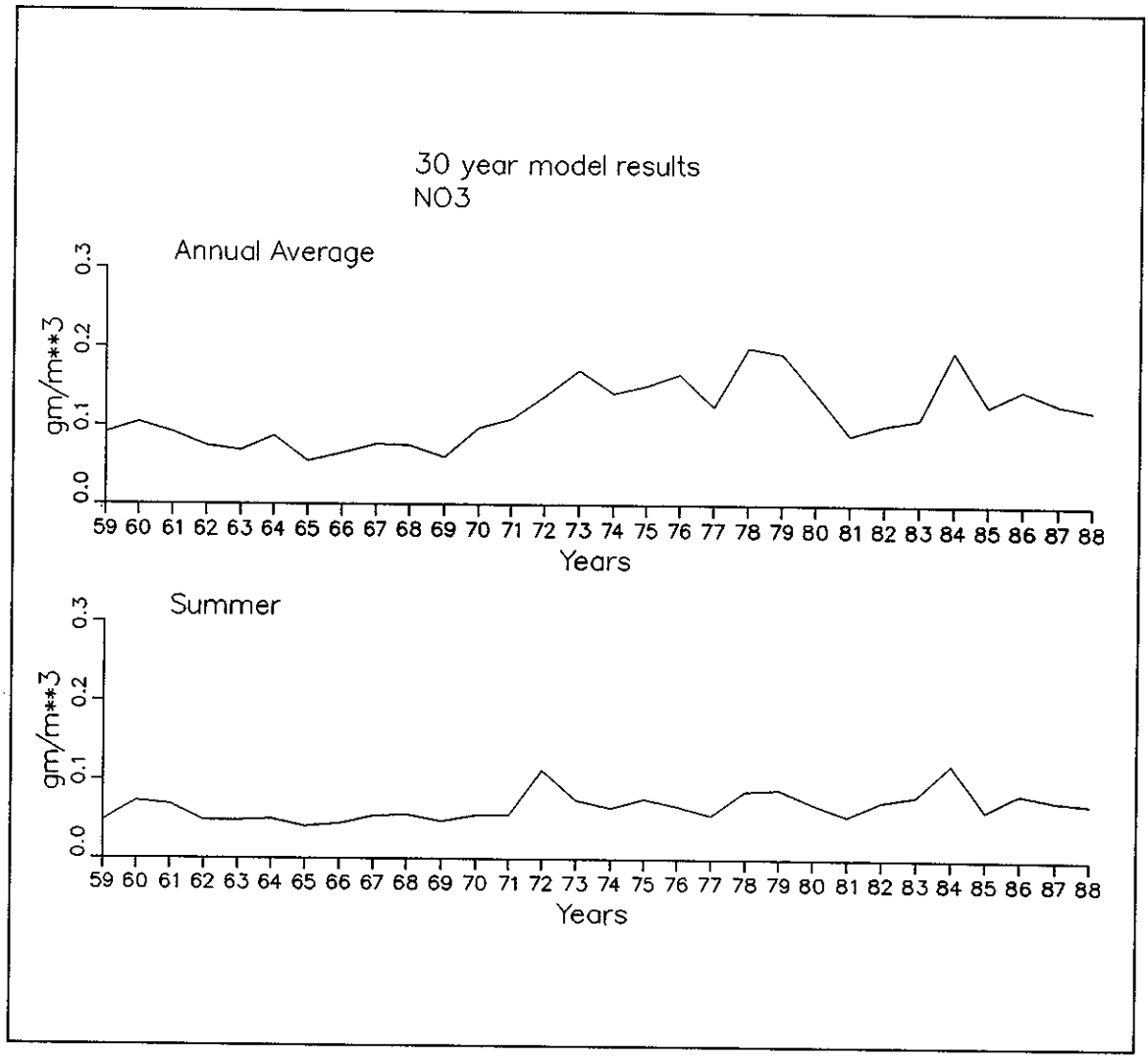

Figure 14-28. Thirty-Year Nitrate Concentration in Mainstem Bay

During summer, bottom dissolved oxygen (Figure 14-32) was closely related to hydrology. Wet years had the least dissolved oxygen as a result of strong stratification and runoff-induced loads. Least summer-average bottom dissolved oxygen in the thirty-year series was in year 21 (1979) a wet year at the end of a wet decade. No clear trend was evident but summer-average bottom dissolved oxygen at the end of the simulation was ≈0.25 gm m^{-3} less than at the beginning of the simulation.

Analysis by Decade

Analysis of simulated time series was subject to some of the same pitfalls as analysis of observed time series. Although observational uncertainty was absent in the simulation, distinction and analysis of trends was still obscured by the deterministic variability that occurred from year to year due to variation

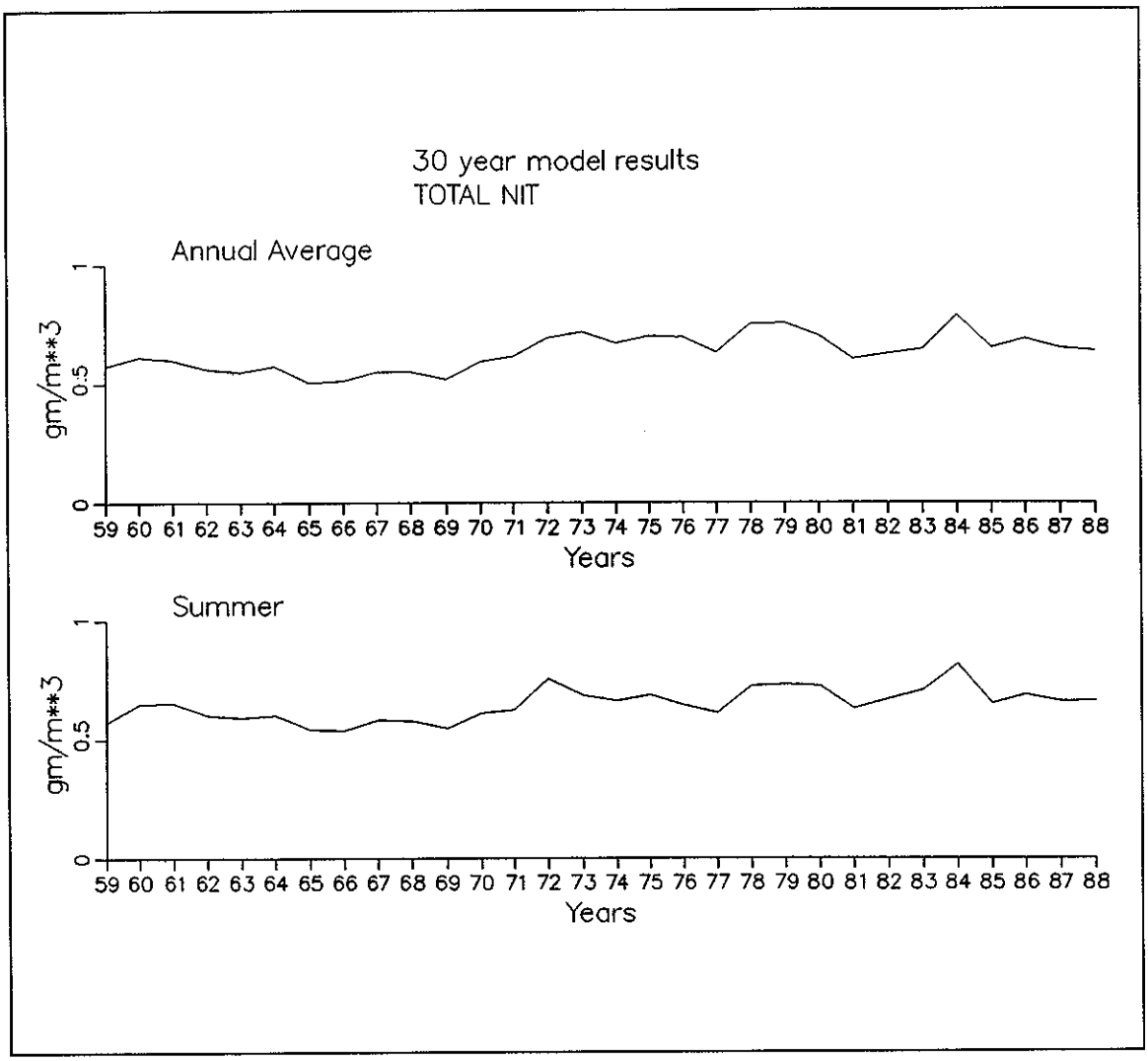

Figure 14-29. Thirty-Year Total Nitrogen Concentration in Mainstem Bay

in loading and hydrology. An improved picture resulted when simulation results were aggregated by decade for summer only. Summer was selected since it is the season critical water quality, as evidenced by bottom-water anoxia. Model results were averaged by zone and level and presented identically to the analysis of the long-term observational record.

In surface waters throughout most of the Bay, summer chlorophyll (Figure 14-33) attained its maximum in the decade 1979-1988. This result is surprising since nitrogen and phosphorus loads were lower in this decade than in the preceding decade. One explanation is that runoff-induced nitrogen and phosphorus loads that dominate the annual total arrive in spring and fall rather than summer. The increasing nitrogen trend at the Susquehanna and Potomac fall lines occurs throughout the year so that the summer loads may be higher in 1979-1988 despite generally lower annual loads than in 1969-1978. Hydrodynamic events appear to predominate in Zone 1, immediately below the

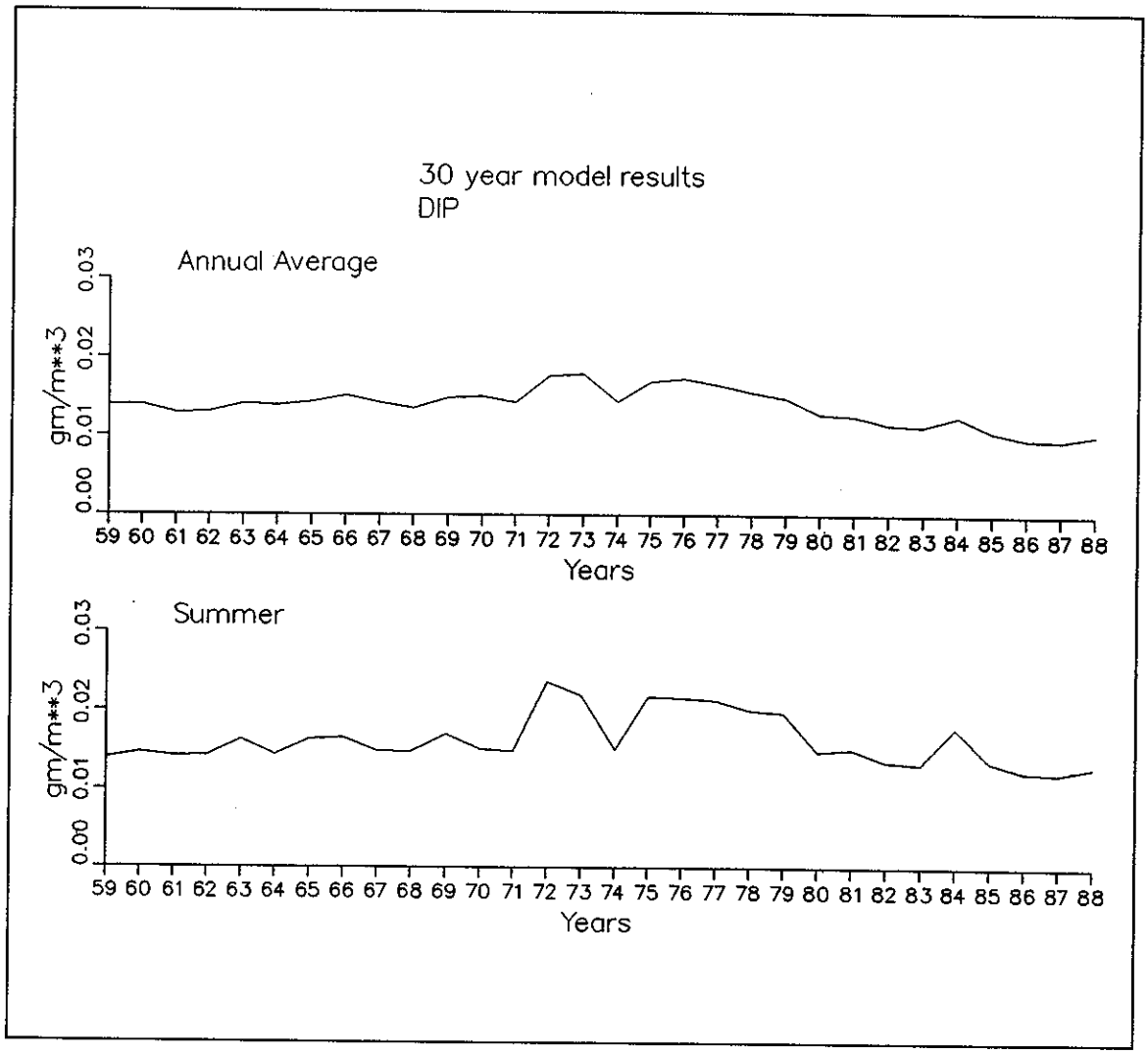

Figure 14-30. Thirty-Year Dissolved Phosphate Concentration in Mainstem Bay

Susquehanna fall line. Algae were highest in the driest decade, 1959-1968, lowest in the wettest decade, 1969-1988, and moderate in the decade of variable flows, 1979-1988.

The model did not show the immense chlorophyll concentrations evident in the data in Zones 1 and 2 during 1959-1978 (Figure 14-5). Our results agreed with a previous model application to the years 1965, 1984, and 1985 (HydroQual 1987). The HydroQual model performed well in 1984 and 1985 but underestimated upper-Bay chlorophyll during 1965. Both models demonstrated one uniform set of algal growth kinetics are not applicable to the upper Bay over three decades. A change in algal species or some other factor affecting algal growth has occurred in the past decade.

On a decadal basis, summer total nitrogen (Figure 14-34) increased monotonically over the three decades. The increase was most noticeable near the

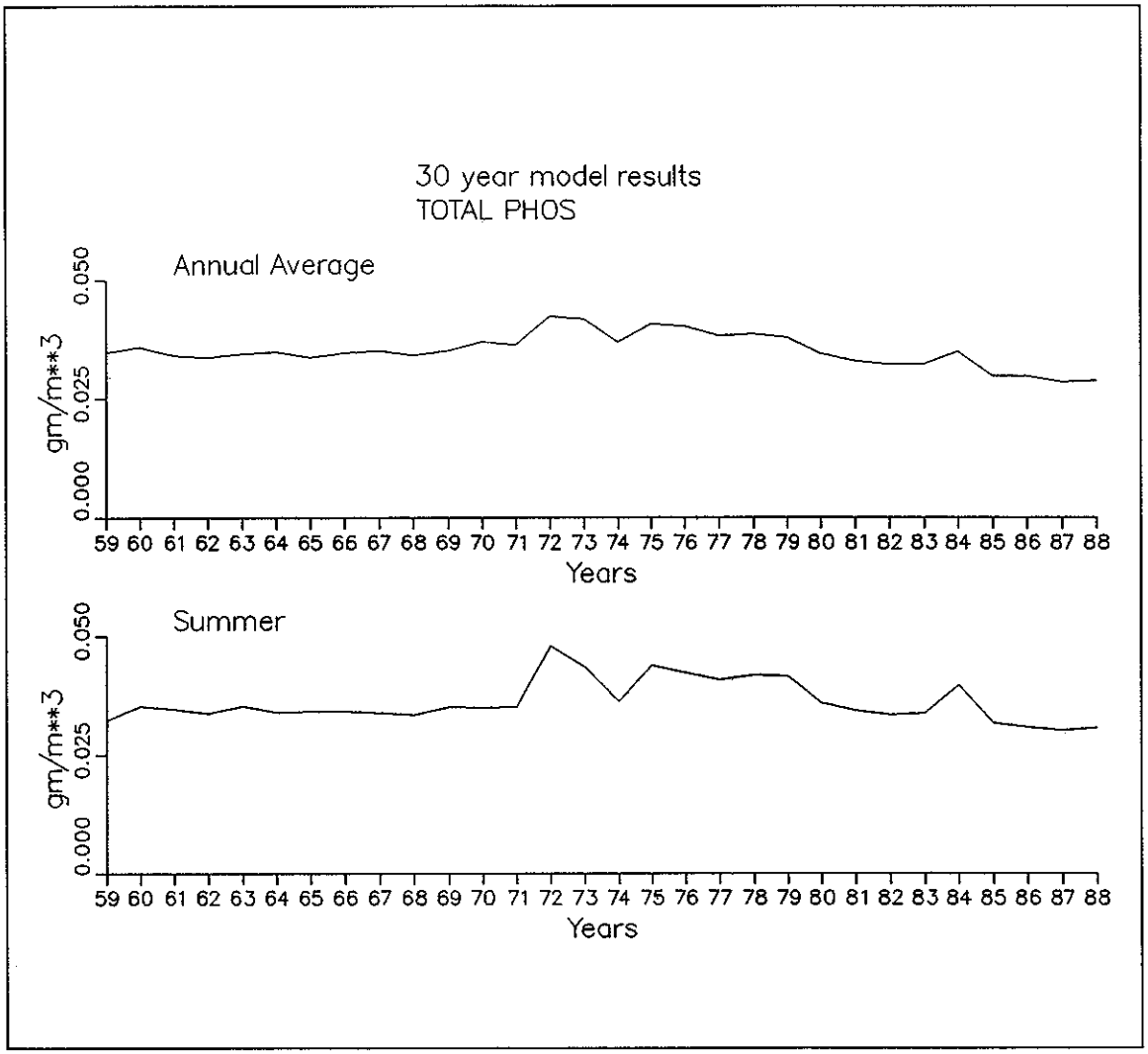

Figure 14-31. Thirty-Year Total Phosphorus Concentration in Mainstem Bay

Susquehanna fall line. As noted previously, the increase correlated with the increasing nitrogen in Susquehanna runoff.

In Zones 1 through 4 and in Zone 9, total phosphorus correlated with decade-averaged loads (Figure 14-35). Phosphorus was highest during 1969-1978 and less in the preceding and subsequent decades. Little or no difference among decades was noted downstream of Zones 4 and 9. An additional influence on total phosphorus, especially evident in bottom waters, was the occurrence of anoxia. Bottom water anoxia was greatest during 1969-1978. The anoxia induced enhanced release of sediment phosphorus that was trapped in surficial sediments during more oxygenated periods.

Dissolved-inorganic-nitrogen (DIN) to dissolved-inorganic-phosphorus (DIP) ratios were analyzed by decade (Figure 14-36). The analysis indicated surface waters in Zones 1 and 2 have been phosphorus limited, relative to

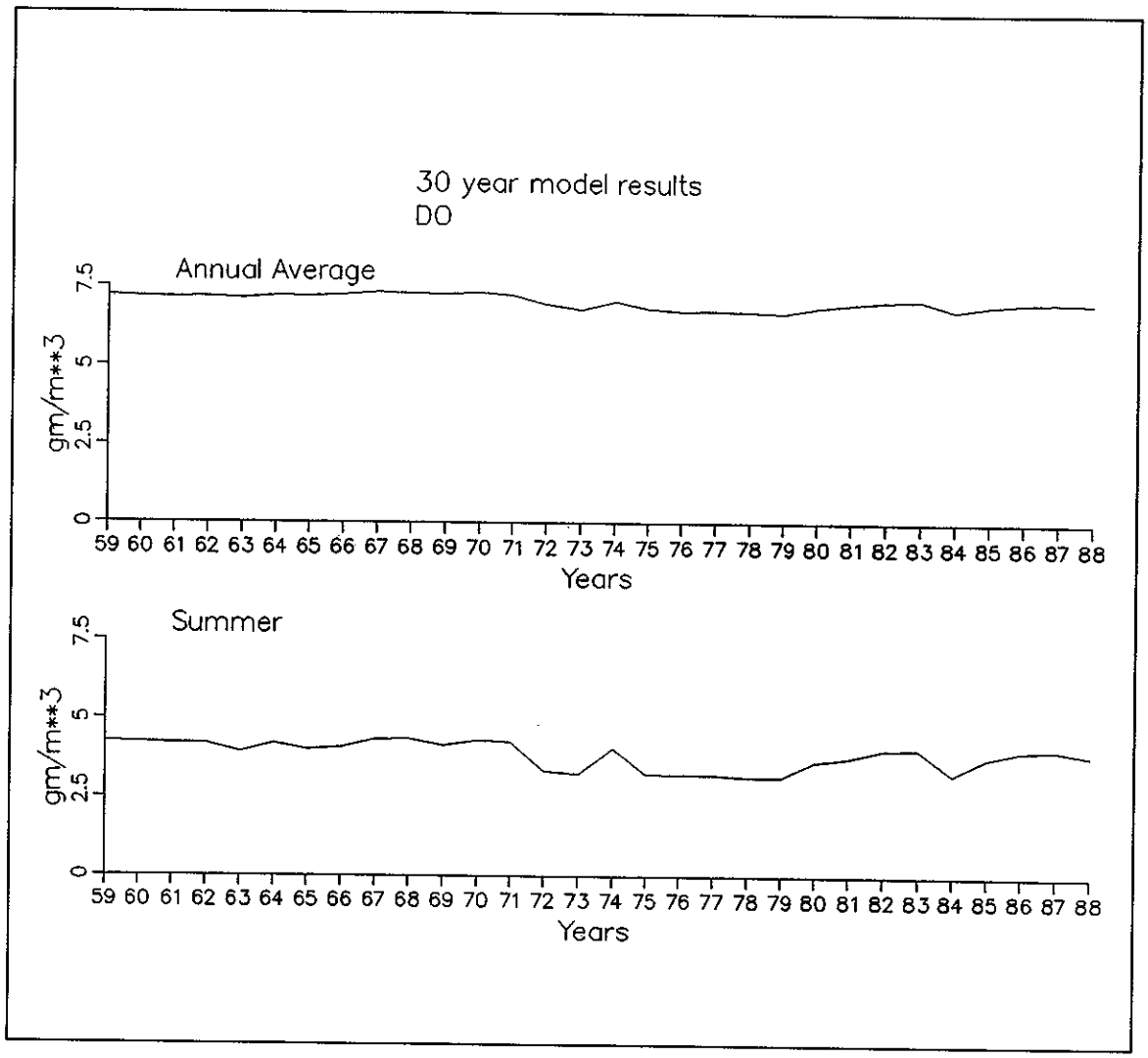

Figure 14-32. Thirty-Year Dissolved Oxygen Concentration in Mainstem Layer 3

Redfield stoichiometry, since the 1959-1968 decade. The limitation leaped during the 1979-1988 decade due to decreased dissolved phosphorus and increased nitrogen in fall-line loads. The effective nitrogen enrichment, reflected in the DIN/DIP ratio, may have induced the apparent algal species change in the upper Bay. This theory is substantiated by observations that diatoms rapidly replaced flagellates when Patuxent River water was nitrogen enriched (Sanders et al. 1987). Zones 3 through 5 and 9 were nitrogen limited during 1959-1978 but approached phosphorus limitation in the last decade due to diminished phosphorus loading. Downstream of Zone 5, the Bay was and remains strongly nitrogen limited.

Dissolved oxygen variation by decade was limited to the second and third layers analyzed (Figure 14-37). Surface dissolved oxygen was saturated and constant throughout the three decades. The most significant variations occurred in the bottom layer of Zones 2 through 4 and Zone 9. These

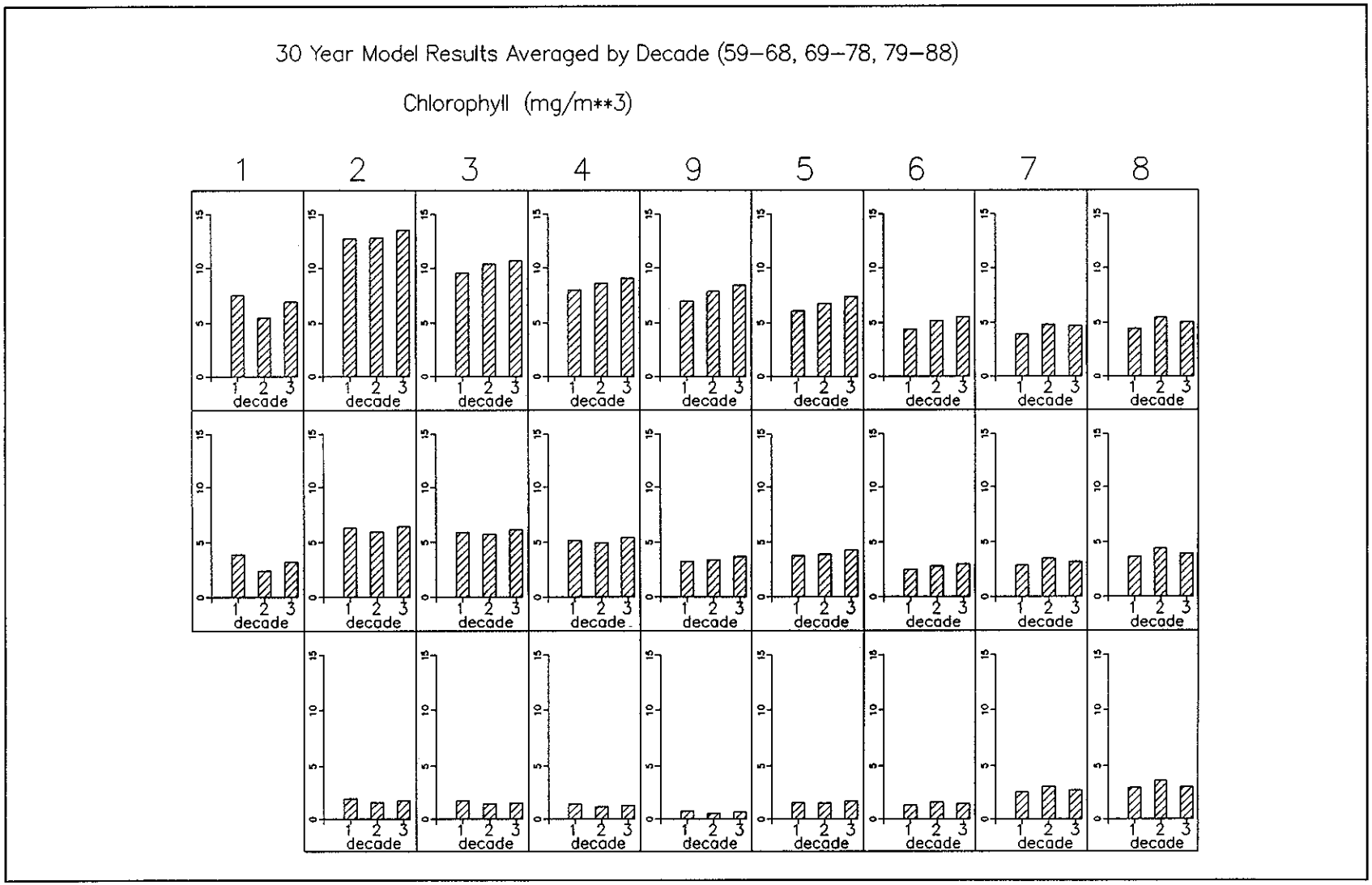

Figure 14-33. Simulated Summer-Average Chlorophyll by Zone, Level, Decade

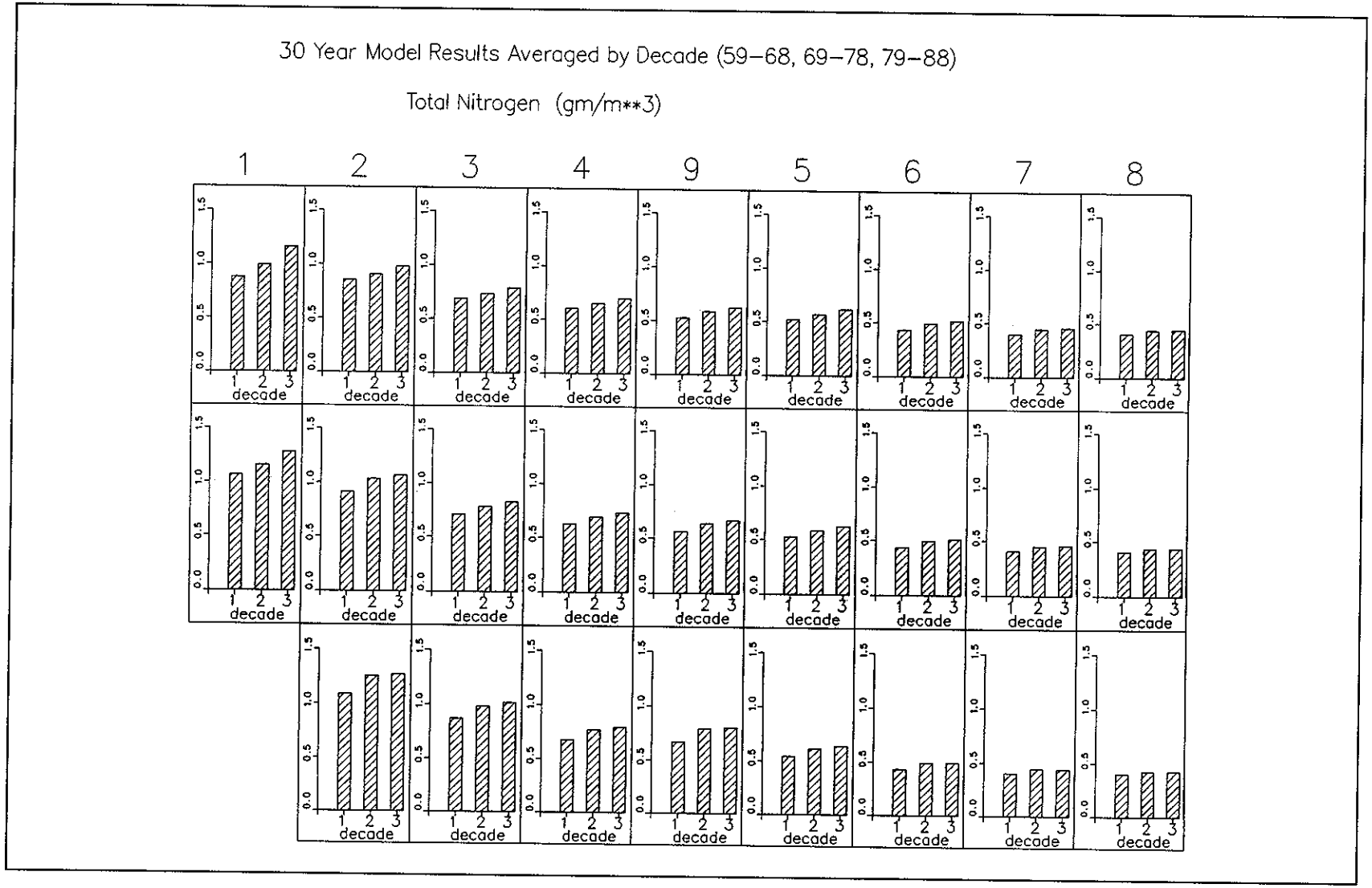

Figure 14-34. Simulated Summer-Average Total Nitrogen by Zone, Level, Decade

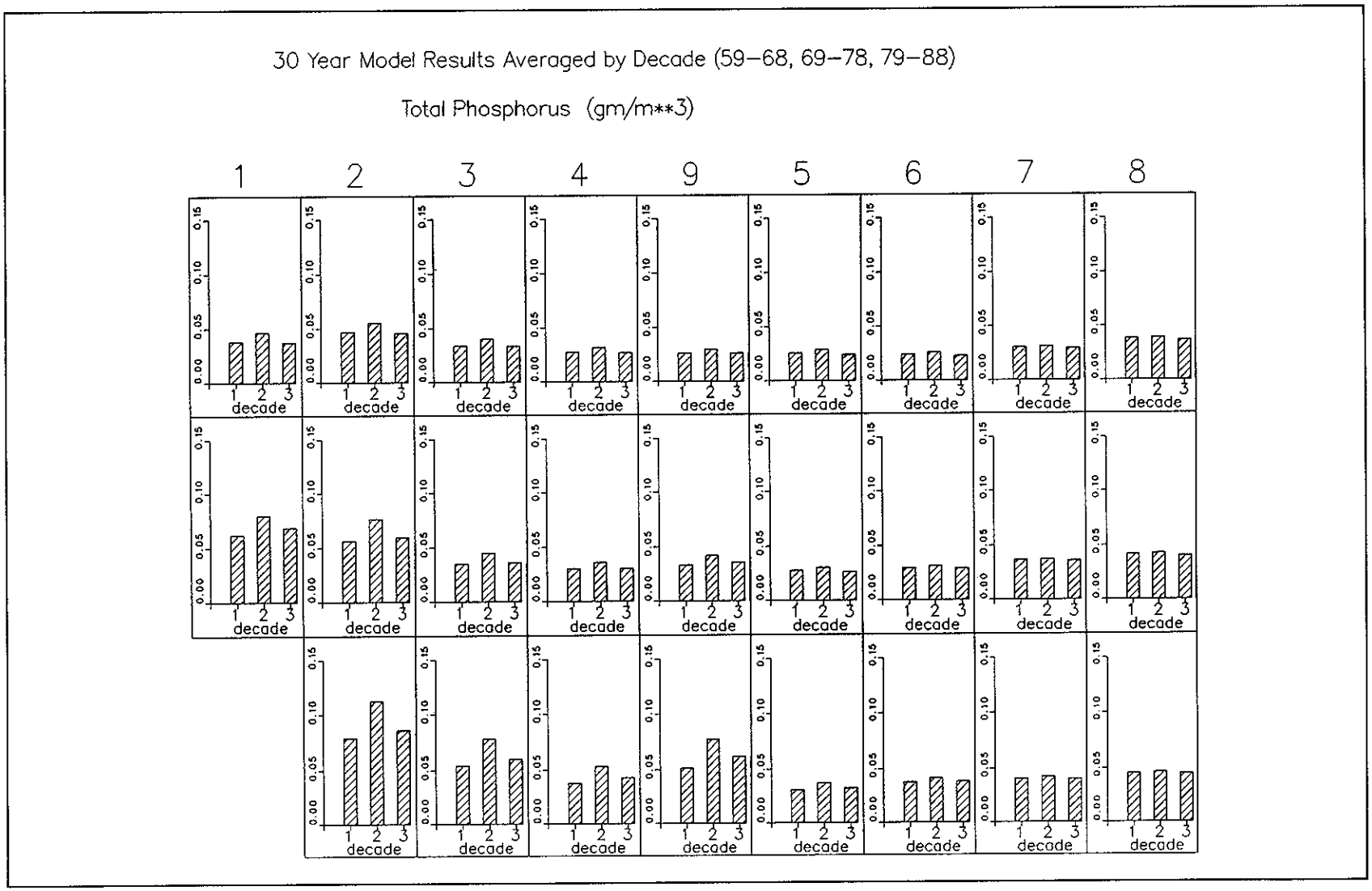

Figure 14-35. Simulated Summer-Average Total Phosphorus by Zone, Level, Decade

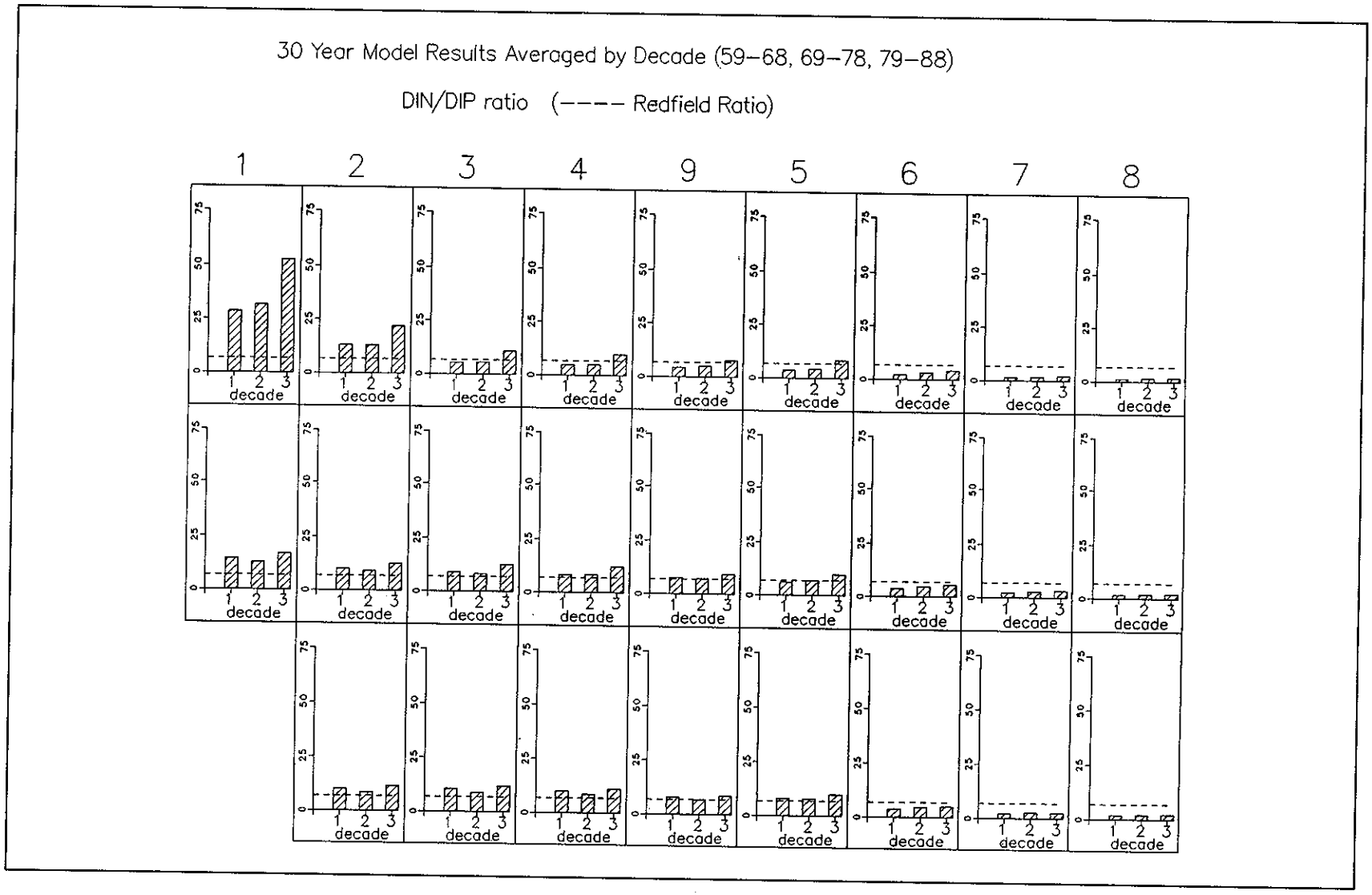

Figure 14-36. Simulated Summer-Average DIN/DIP Ratio by Zone, Level, Decade

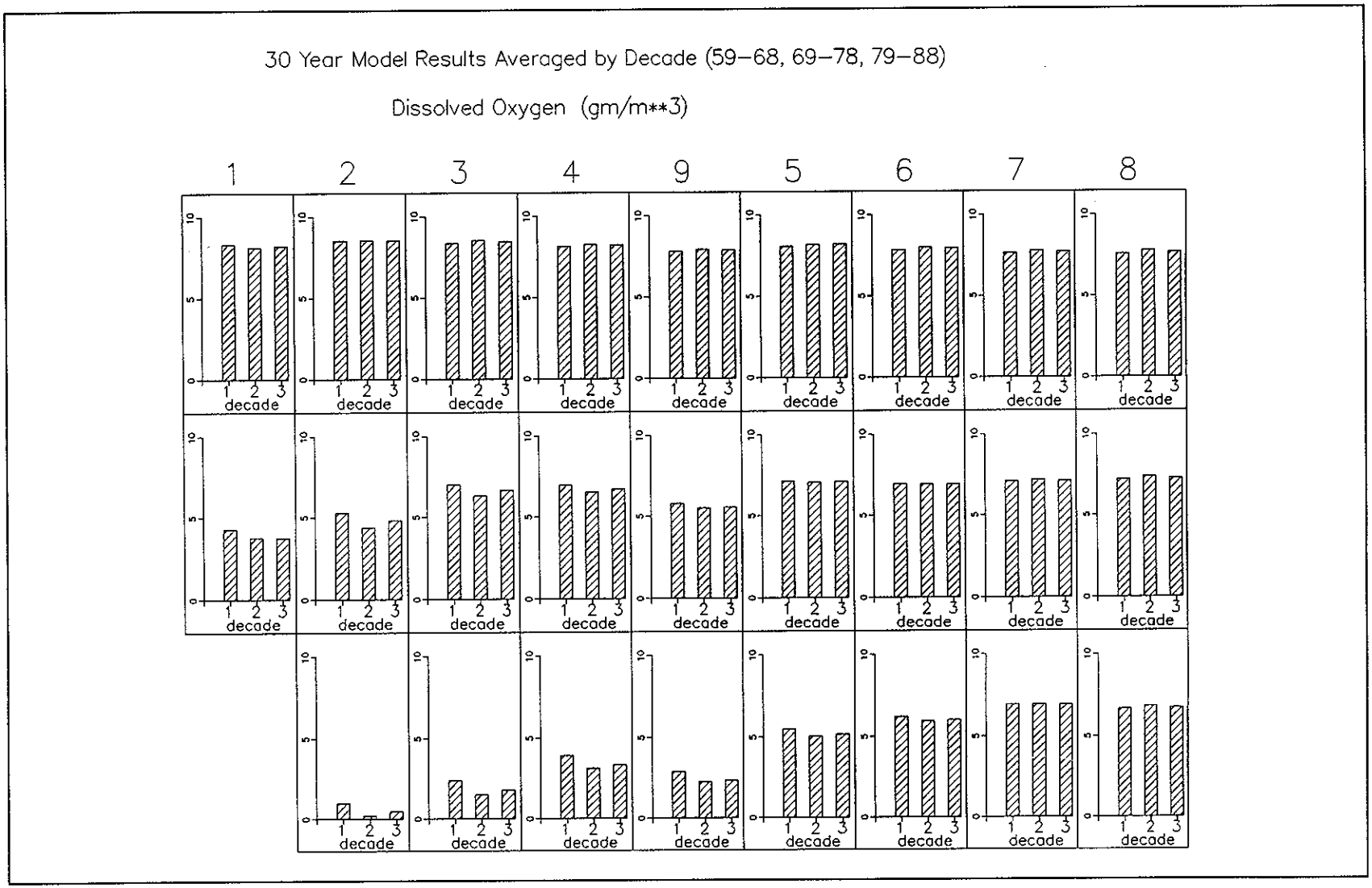

Figure 14-37. Simulated Summer-Average Dissolved Oxygen by Zone, Level, Decade

included the regions that showed the lowest average dissolved oxygen and the highest incidence of anoxia in the historic record. Simulation results indicated 1959-1968 was the decade of highest dissolved oxygen in these regions. The years 1969-1978 were the worst decade. Since then, conditions improved in the decade 1979-1988 but not to levels in the first decade. A tentative conclusion was that bottom water dissolved oxygen improved by a small amount, ≈ 0.5 gm $^{-3}$, in the most recent decade. The initial conclusion did not explain the origin of the improvement, however. Was the improvement due to diminished nutrient loads or changes in predominant hydrodynamics in the decade 1979-1988 relative to 1969-1978? The answer to the question was obtained by comparing only "average" hydrologic years in each decade. Comparison of only average years eliminated effects of stratification from the analysis and mitigated the influence of flow-driven load events. Analysis of average years only indicated a steady, monotonic decline in bottom-water dissolved oxygen (Figure 14-38) from the Back to Rappahannock Rivers and in Tangier Sound. The decadal change was minimal, however: less than 0.3 gm m^{-3} from 1959-1968 to 1979-1988. The analysis indicated that improvement in dissolved oxygen from 1969-1978 to 1979-1988 was primarily due to hydrodynamic effects rather than load effects. When hydrodynamic effects were removed, dissolved oxygen diminished from 1969-1978 to 1979-1988.

Anoxic Volume Days. To compare the occurrence of anoxia among decades, a statistic was created that combined measures of the volume of anoxic water and the duration of the anoxic period. The "anoxic volume days" statistic was defined:

$$AVD = \sum_{i=1,j=1}^{n,m} V_i \Delta t_j \quad \text{if} \quad DO \leq 1 \qquad (7)$$

AVD = anoxic volume-days (m^3 day)
V_i = volume of model cell (m^3)
Δt_j = finite-difference integration time step (day)
DO = dissolved oxygen concentration (gm m^{-3})
n = number of model cells
m = number of time steps in year

Anoxic water was considered to be water with dissolved oxygen concentration less than 1 gm m^{-3}. Anoxic volume days were computed for each zone-level combination and for the entire mainstem Bay.

Examination of anoxic volume (Figure 14-39) mirrored the examination of dissolved oxygen concentration. The decade 1959-1968 had the least anoxic volume; the decade 1979-1988 had the most. Analysis of years of average hydrology only, however, indicated anoxia increased steadily in the Bay throughout the three decades (Figure 14-40). In years of average hydrology, anoxic volume was ≈18% greater in 1979-1988 than in 1959-1968.

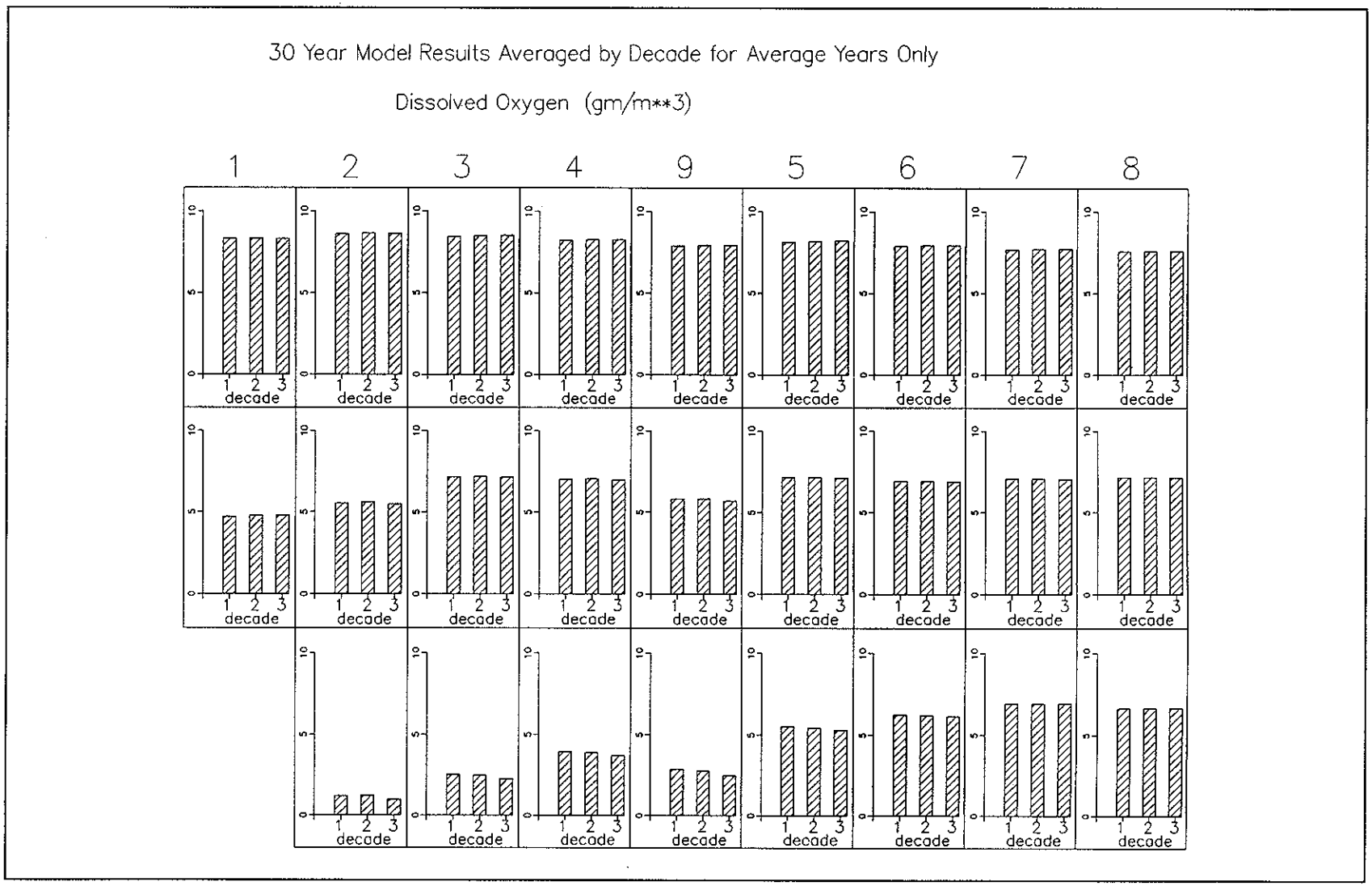

Figure 14-38. Simulated Summer-Average Dissolved Oxygen in "Average" Hydrodynamic Years by Zone, Level, Decade

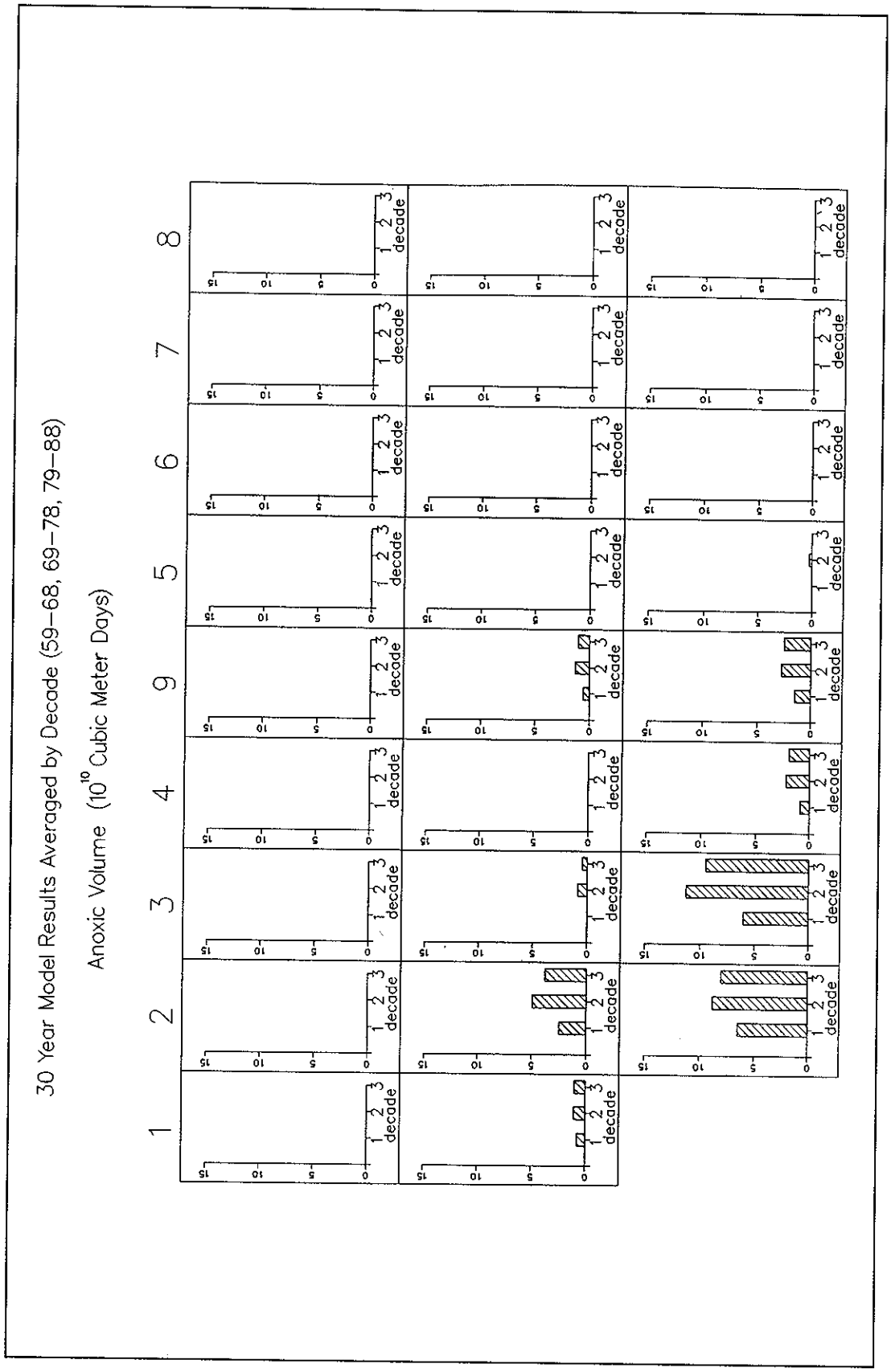

Figure 14-39. Simulated Anoxic Volume Days by Zone, Level, Decade

Examination of Recent Trends

The monitoring program in place since mid-1984 provided a data base with vastly improved capacity for trend detection. The monitoring program conducted regular surveys at consistent locations and analyzed for a wider range of constituents than chlorophyll and dissolved oxygen alone. A portion of the data base has been processed and analyzed for trends (Bahner, Reynolds and Batiuk 1990; Computer Sciences Corporation 1991, Chesapeake Bay Program 1992). Processing consisted of spatial interpolation of the observations and computation of a Bay-wide average concentration representative of each survey. We obtained Bay-wide average total nitrogen and total phosphorus concentrations from the Chesapeake Bay Program Office. In computation of these averages, below-detection-level observations were set at half detection level. We obtained mass estimates of chlorophyll, dissolved inorganic nitrogen, and phosphate and volume estimates of anoxia from Bahner, Reynolds, and Batiuk (1990). Treatment of below-detection-level observations was not detailed in the publication. Mass estimates were converted to concentration using mainstem Bay volume provided in the report. Anoxic volumes were temporally integrated into annual anoxic volume days.

Observations and simulation results from 1984 to 1988 were compared and examined for trends. Trends were determined through application of the model:

$$C = b_1 + b_2 \sin(2\pi(yr - 1984)) + b_3 \cos(2\pi(yr - 1984)) + b_4(yr - 1984) \quad (8)$$

C = observed or simulated Bay-wide average concentration (gm m^{-3})
b_1 = seasonally-independent concentration at beginning of 1984 (gm m^{-3})
b_2, b_3 = constants that determine amplitude of seasonal cycling (gm m^{-3})
b_4 = constant that indicates linear temporal trend (gm m^{-3} yr^{-3})

Constants were evaluated through least-squares linear regression. A trend was detected when the constant b_4 had a statistically significant non-zero value. Observations indicated decreasing trends in three substances: dissolved inorganic nitrogen, phosphate, and total phosphorus (Table 14-7). The simulation confirmed the direction of the observed trends and agreed, within a factor of two, in magnitude. The simulation also indicated decreasing trends in chlorophyll, total nitrogen, and anoxic volume not detected in the observations.

The variance attributed to the chlorophyll slope term in the simulation was negligibly small such that, for practical purposes, neither the observations or the model showed a temporal trend. In the observations, the seemingly random magnitude of the spring bloom precluded trend detection (Figure 14-41). In the simulation, initial inspection indicated a decreasing trend in

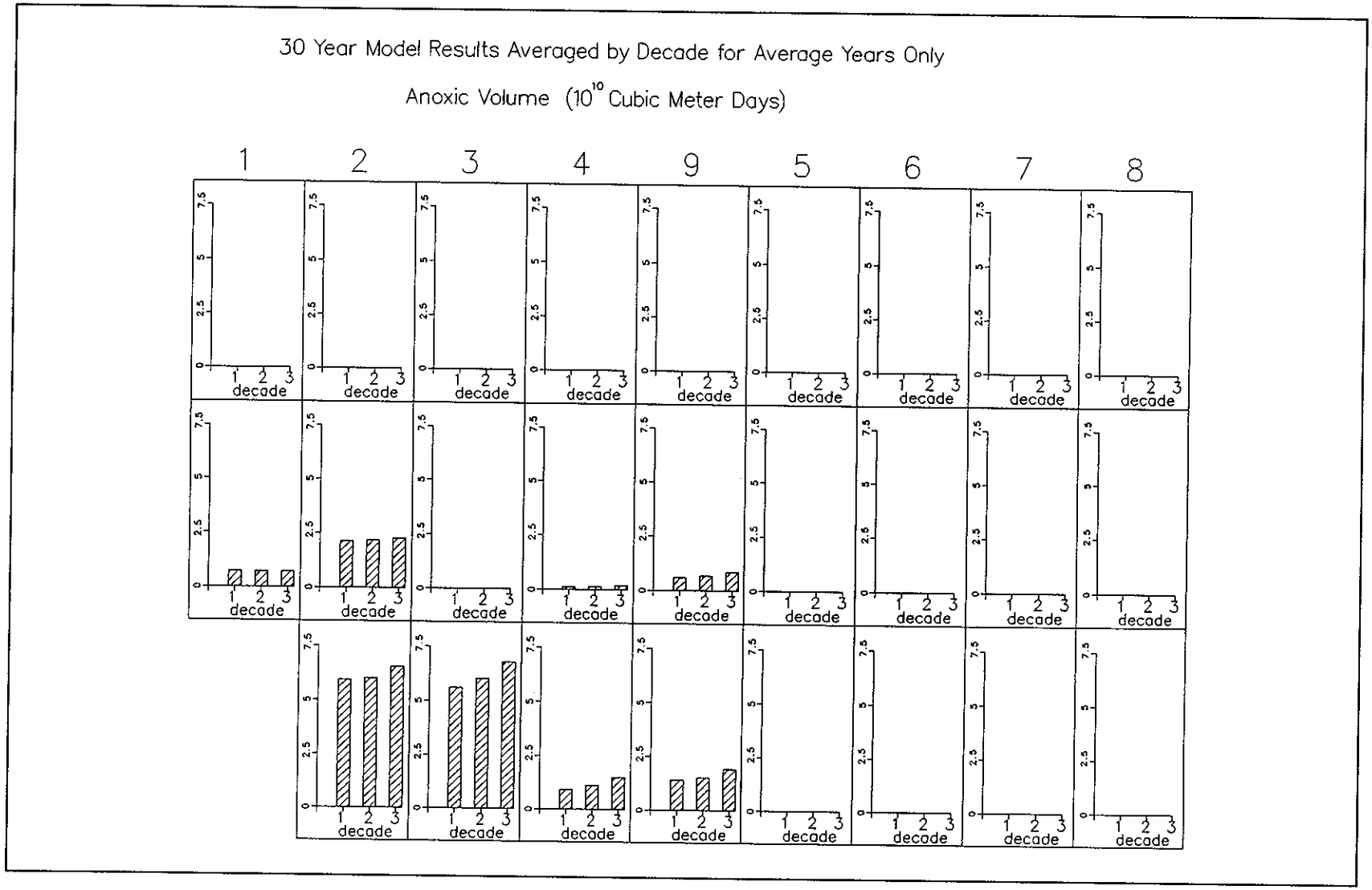

Figure 14-40. Simulated Anoxic Volume Days in "Average" Hydrodynamic Years by Zone, Level, Decade

Table 14-7
Observed and Simulated Trends, 1984-1988

Substance	Observed Trend	Partial R^2, p	Simulated Trend	Partial R^2
Chlorophyll	none		-0.33 mg m^{-3} yr^{-1}	0.01
Dissolved Inorganic Nitrogen	-1.0 x 10^{-2} gm m^{-3} yr^{-1}	0.03, $p < 0.02$	-1.7 x 10^{-2} gm m^{-3} yr^{-1}	0.11
Total Nitrogen	none		-3.0 x 10^{-2} gm m^{-3} yr^{-1}	0.18
Phosphate	-1.3 x 10^{-3} gm m^{-3} yr^{-1}	0.18, $p < 0.0001$	-5.1 x 10^{-4} gm m^{-3} yr^{-1}	0.05
Total Phosphorus	-2.9 x 10^{-3} gm m^{-3} yr^{-1}	0.17 $p < 0.0001$	-1.3 x 10^{-3} gm m^{-3} yr^{-1}	0.34
Anoxic Volume	none		-5.2 x 10^{10} m^3 days yr^{-1}	0.58

magnitude of the spring bloom from 1984 through 1988. The decreasing spring trend was offset by increasing summer concentrations from 1985 through 1988, however. The diminished bloom but enhanced summer chlorophyll fit neatly with the idea that the bloom is phosphorus limited but summer populations are nitrogen limited. Decreased phosphorus loads to the system (Table 14-6) diminished the simulated bloom while nitrogen concentration trends in the Susquehanna and Potomac fall lines (Table 14-4) induced proportional increases in simulated summer chlorophyll. The comparison also continued the theme that chlorophyll in the simulation behaves deterministically while prototype chlorophyll, as evidenced by magnitude of the spring bloom, has a large stochastic component. Unaccountable stochastic behavior was also indicated by the apparent species change in the upper Bay from the mid 1960's to the mid 1980's.

Although the trend term in observed dissolved inorganic nitrogen was highly significant (Table 14-7), the variance attributable to the term was negligibly small. The suggestion that nitrogen decreased from 1984 to 1988 was reinforced by the decreasing trend in simulated dissolved inorganic (Figure 14-42) and total nitrogen (Figure 14-43), however. Detection of the trend illustrated the advantage of the simulation in trend detection over exclusive reliance on observations. The simulated trend detected also illustrated one pitfall of trend examination on short data sets, simulated or otherwise. The simulation indicated decreasing nitrogen from 1984 to 1988 despite an increase in total nitrogen over thirty years (Figures 14-28, 14-29) and increasing concentration at two major fall lines (Table 14-4). The paradox was caused by inclusion of 1984, the wettest year of the decade, in the five-year time series. Total nitrogen did decrease following this abnormal year. If the record considered started earlier or omitted 1984, however, a different trend would have resulted.

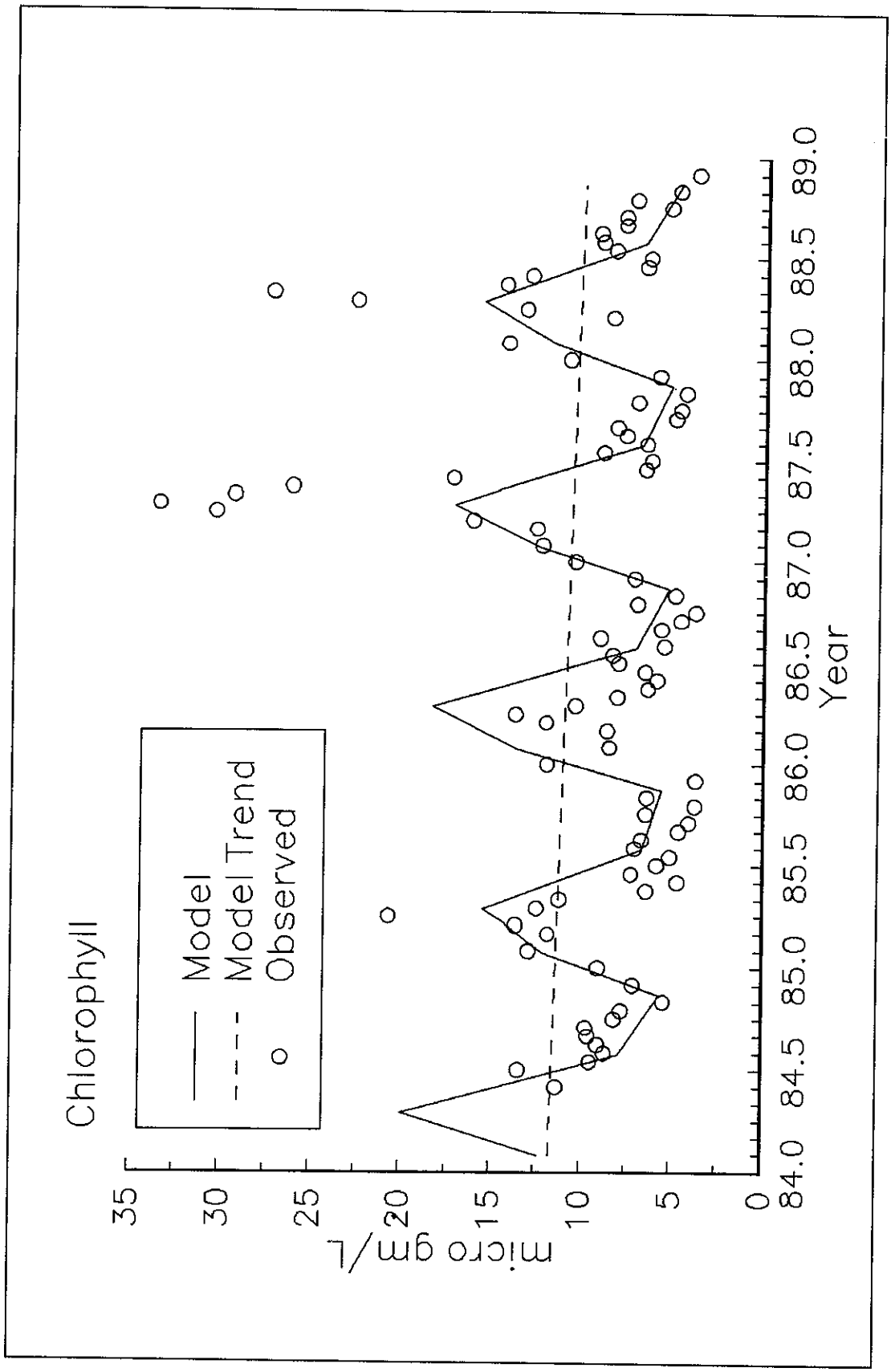

Figure 14-41. Chlorophyll Trends, 1984-1988

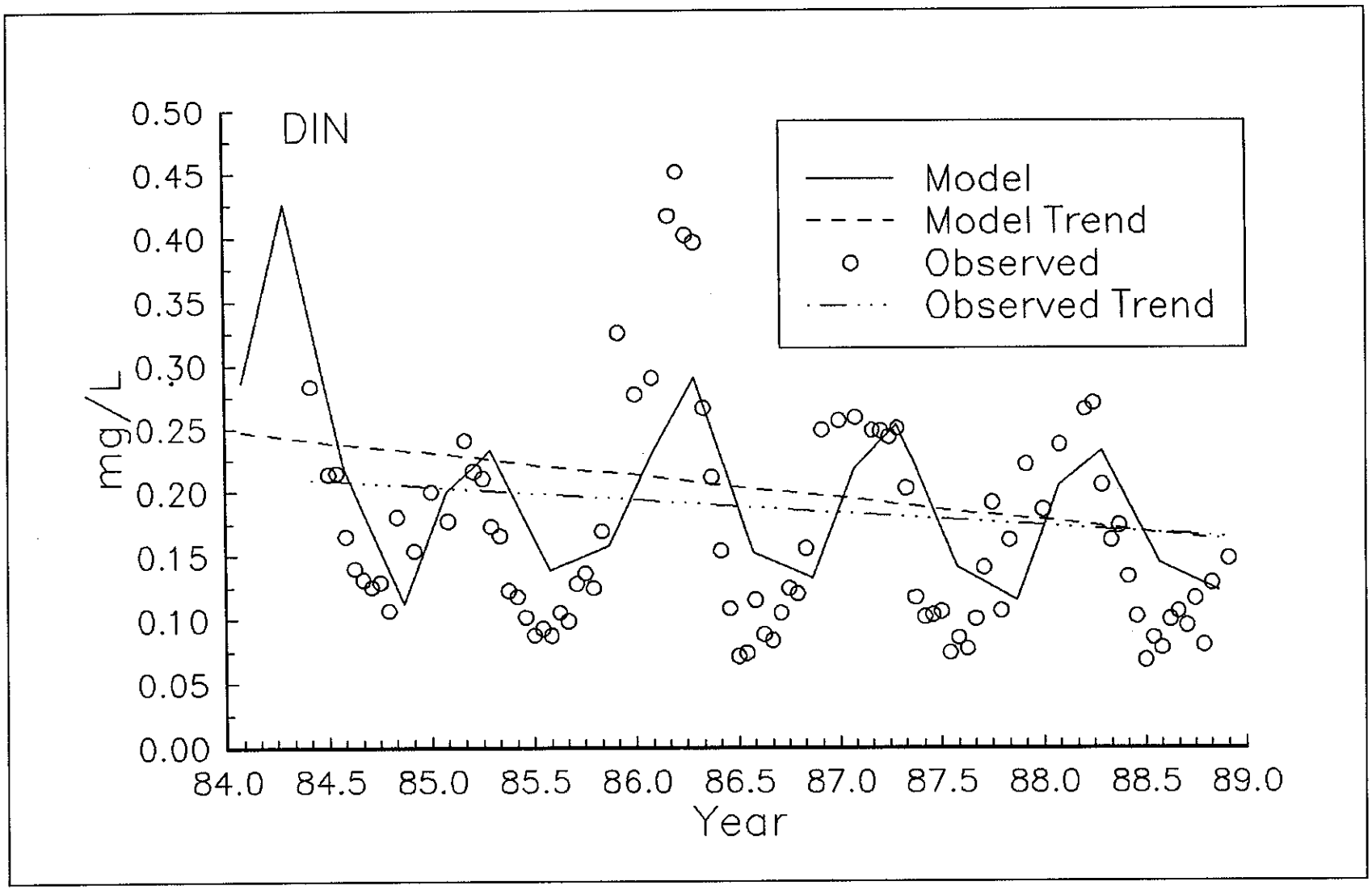

Figure 14-42. Dissolved Inorganic Nitrogen Trends, 1984-1988

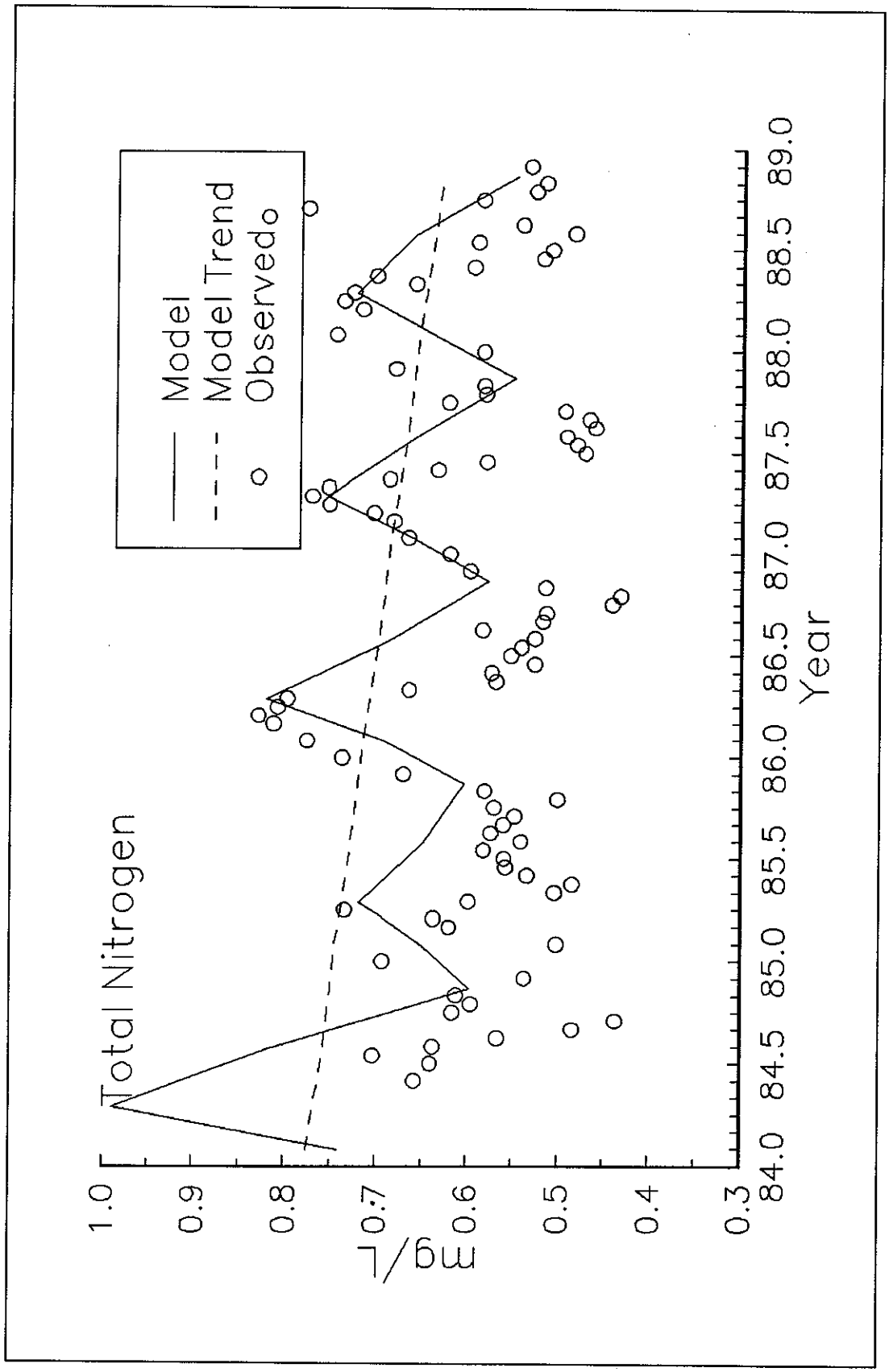

Figure 14-43. Total Nitrogen Trends, 1984-1988

Both the observations and the simulation demonstrated decreasing phosphorus from 1984 through 1988 (Figures 14-44, 14-45). The trends accounted for a reasonable amount of variance (5 to 34%) and were consistent with the decreasing phosphorus loads to the system and the decreasing runoff from 1984 to 1988. One interesting phenomenon in the observations not reflected in the model was the large seasonal variance in total phosphorus (Figure 14-45). The amplitude of the observed seasonal component was roughly four times the amplitude of the simulated component.

Observations showed no five-year trend in anoxic volume (Table 14-7). Detection of a trend was precluded by the small anoxic volume observed in 1985, much less than in preceding or subsequent years (Figure 14-46). By contrast, the simulation indicated decreasing anoxia following the large nutrient loads and high stratification that occurred in 1984. Absent 1984, however, the simulation demonstrated no monotonic trend in anoxic volume.

Trends in the Tributaries

Portions of several tributaries were analyzed by the decade following the pattern set by analysis of the mainstem Bay. Regions were selected because they exhibited water quality problems in the past and/or because they were subject to load-reduction activities. Regions analyzed were the tidal fresh portion of the James River (Zone 1 in Figure 10-2), the tidal fresh portion of the Potomac River (Zone 1 in Figure 10-2) and Baltimore Harbor. Baltimore Harbor was considered to be the Patapsco and Back Rivers (Zone 10 in Figure 9-2).

Of the tributary regions, only Baltimore Harbor had observations included in the historic data set. Observed dissolved oxygen in Baltimore harbor (Figure 14-47) exhibited the same characteristics as Zones 1 and 2 of the mainstem (Figure 14-2). The third decade, 1979-1988, had lower dissolved oxygen in surface and pyncnocline waters (depth < 12.7 m) than either of the preceding decades. No significant change was noted in dissolved oxygen in the bottom layer (depth > 12.7 m) of the harbor. The decrease in dissolved oxygen was associated with an apparent but statistically insignificant decrease in chlorophyll (Figure 14-47). As in the upper mainstem, the decreasing surface dissolved oxygen was most likely due to decreased algal photosynthetic production in the last decade.

The model indicated negligible difference in Baltimore Harbor chlorophyll over the three decades (Figure 14-48). As in the mainstem, the huge concentrations observed during 1969-1978 were not reproduced. The same change in speciation proposed to have taken place in the mainstem apparently affected the Harbor as well.

The simulation indicated hydrologic control of chlorophyll in the upper Potomac (Figure 14-48). Concentrations were roughly equivalent in 1959-1968 and 1979-1988, dry and variable decades. Chlorophyll was least in

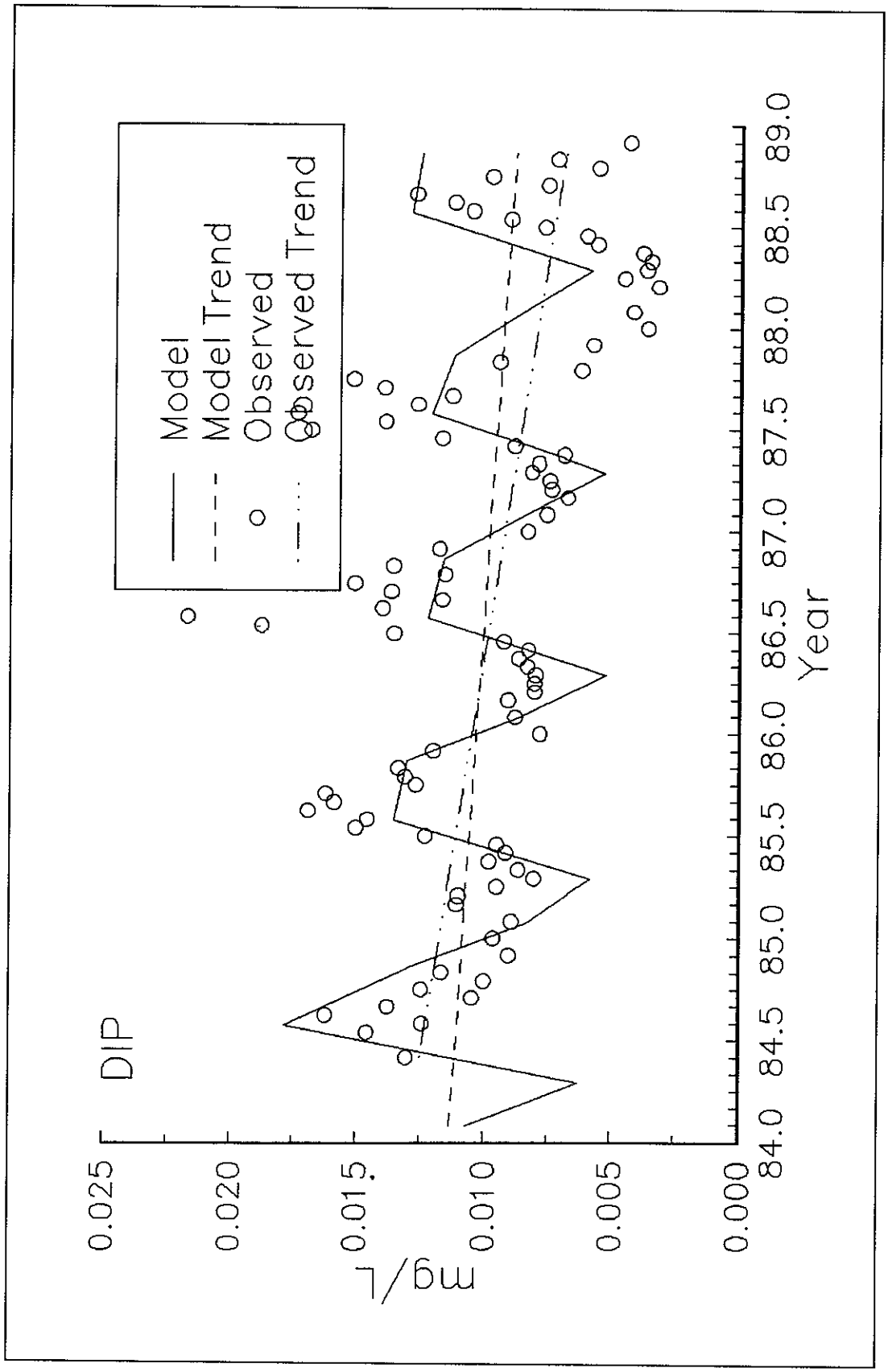

Figure 14-44. Dissolved Phosphate Trends, 1984-1988

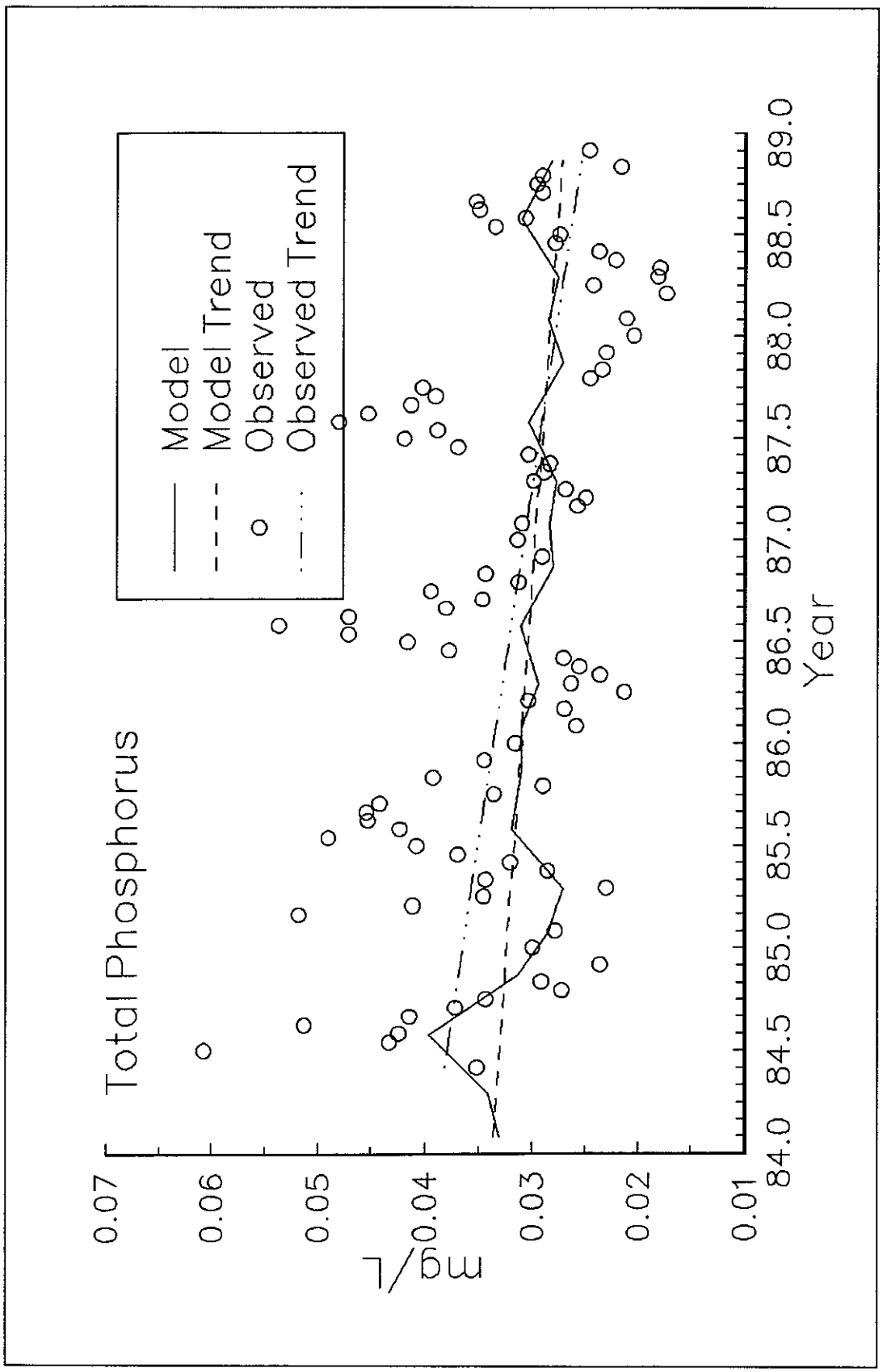

Figure 14-45. Total Phosphorus Trends, 1984-1988

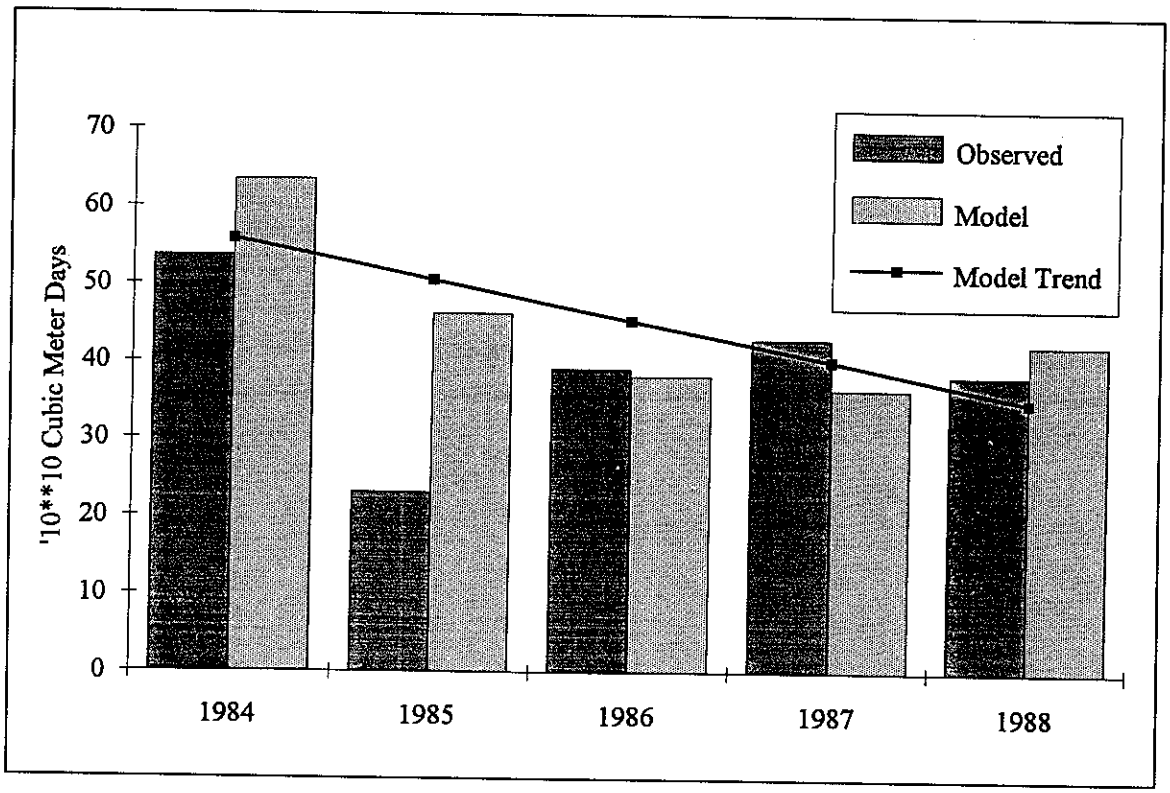

Figure 14-46. Anoxic Volume Trends, 1984-1988

1969-1978, the decade of highest flows. The result was consistent with the concept that high flows and turbulent water are not favorable to the blue-green algae predominant in the upper Potomac (Thomann et al. 1985). The simulation also indicated negligible change in chlorophyll in the upper James (Figure 14-48).

Negligible trend or change in total nitrogen was noted in the upper James or Baltimore Harbor (Figure 14-49). The upper Potomac, however, exhibited a monotonic increase in total nitrogen by decade (Figure 14-49). The increase reflected the increasing trend in nitrate concentration noted at the Potomac fall line (Table 14-4).

Baltimore Harbor exhibited peak total phosphorus in the decade 1969-1988 (Figure 14-50). In surface and mid-depth waters, total phosphorus was roughly equivalent in 1959-1968 and 1979-1988. The trends in Baltimore Harbor coincided with the overall behavior of point-source phosphorus loads. Loading peaked in 1969-1978 and was less prior and after that decade (Table 14-6). The James (Figure 14-50) showed monotonically increasing total phosphorus which corresponded to the fall-line trend (Table 14-4). In the upper Potomac, total phosphorus in 1979-1988 was less than half the two preceding decades (Figure 14-50), as a result of point-source control and declining concentration at the fall line.

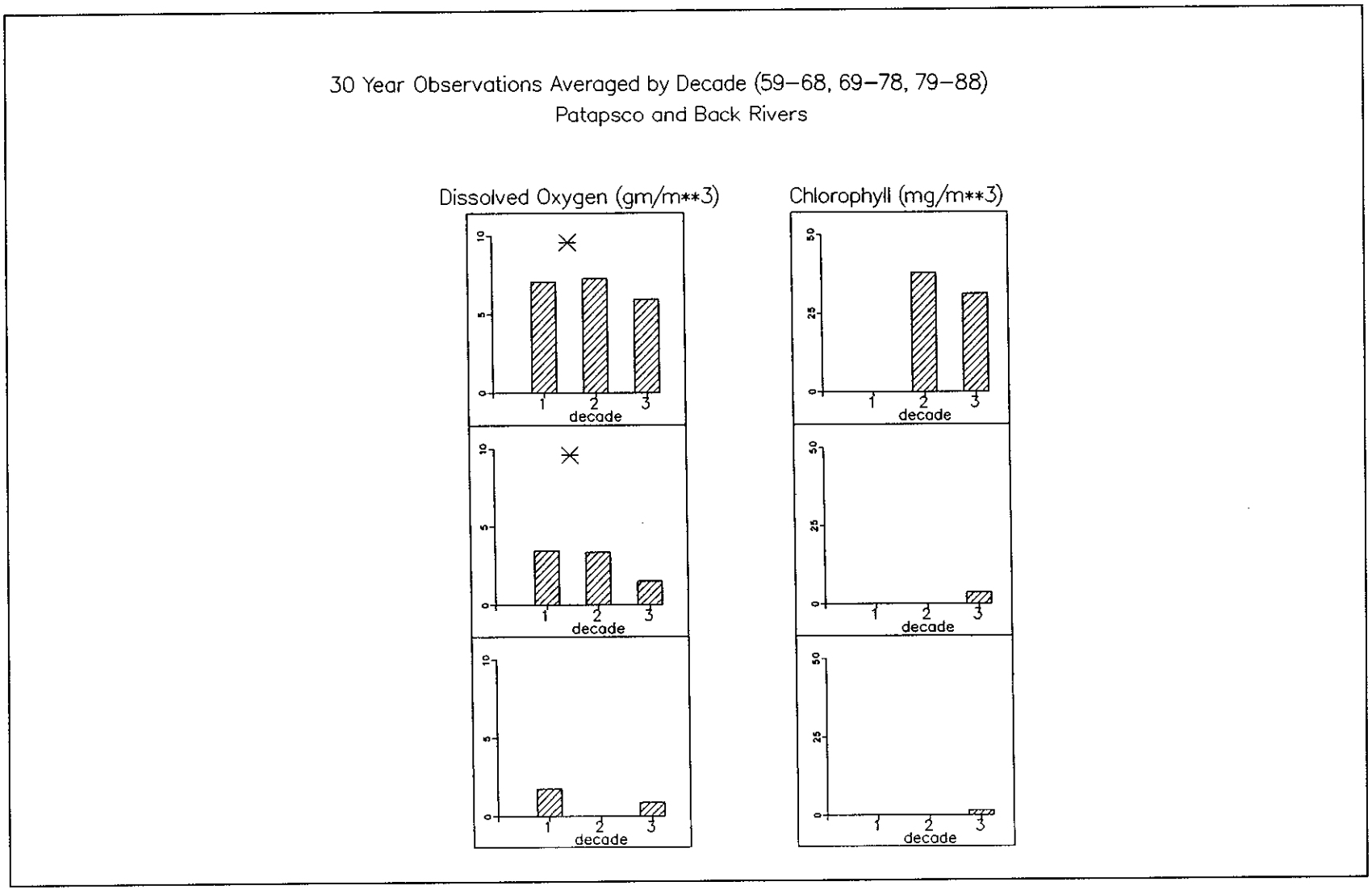

Figure 14-47. Summer-Average Chlorophyll and Dissolved Oxygen in Baltimore Harbor by Level and Decade

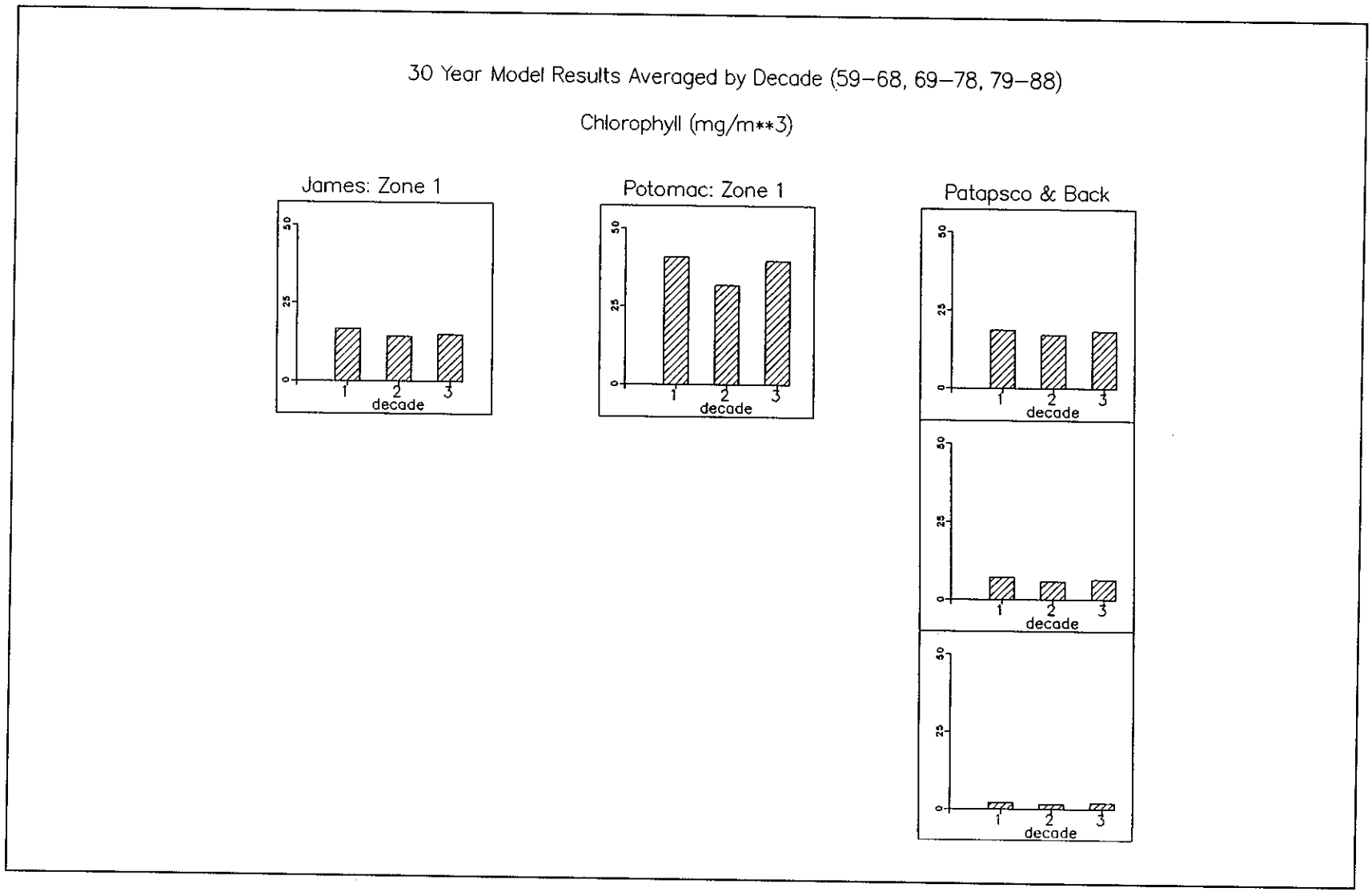

Figure 14-48. Simulated Summer-Average Chlorophyll in Upper James, Upper Potomac, and Baltimore Harbor by Level, Decade

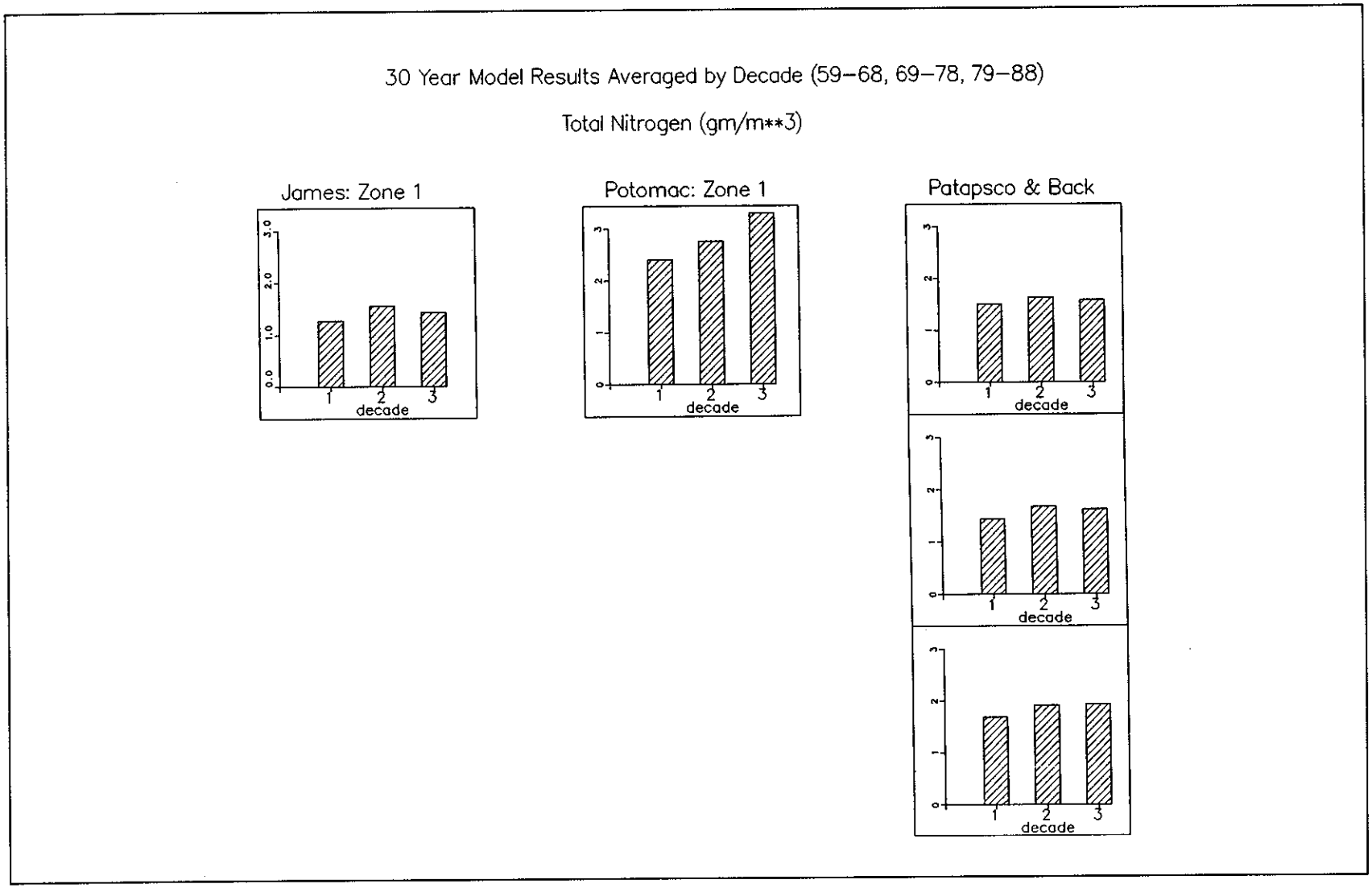

Figure 14-49. Simulated Summer-Average Total Nitrogen in Upper James, Upper Potomac, and Baltimore Harbor by Level, Decade

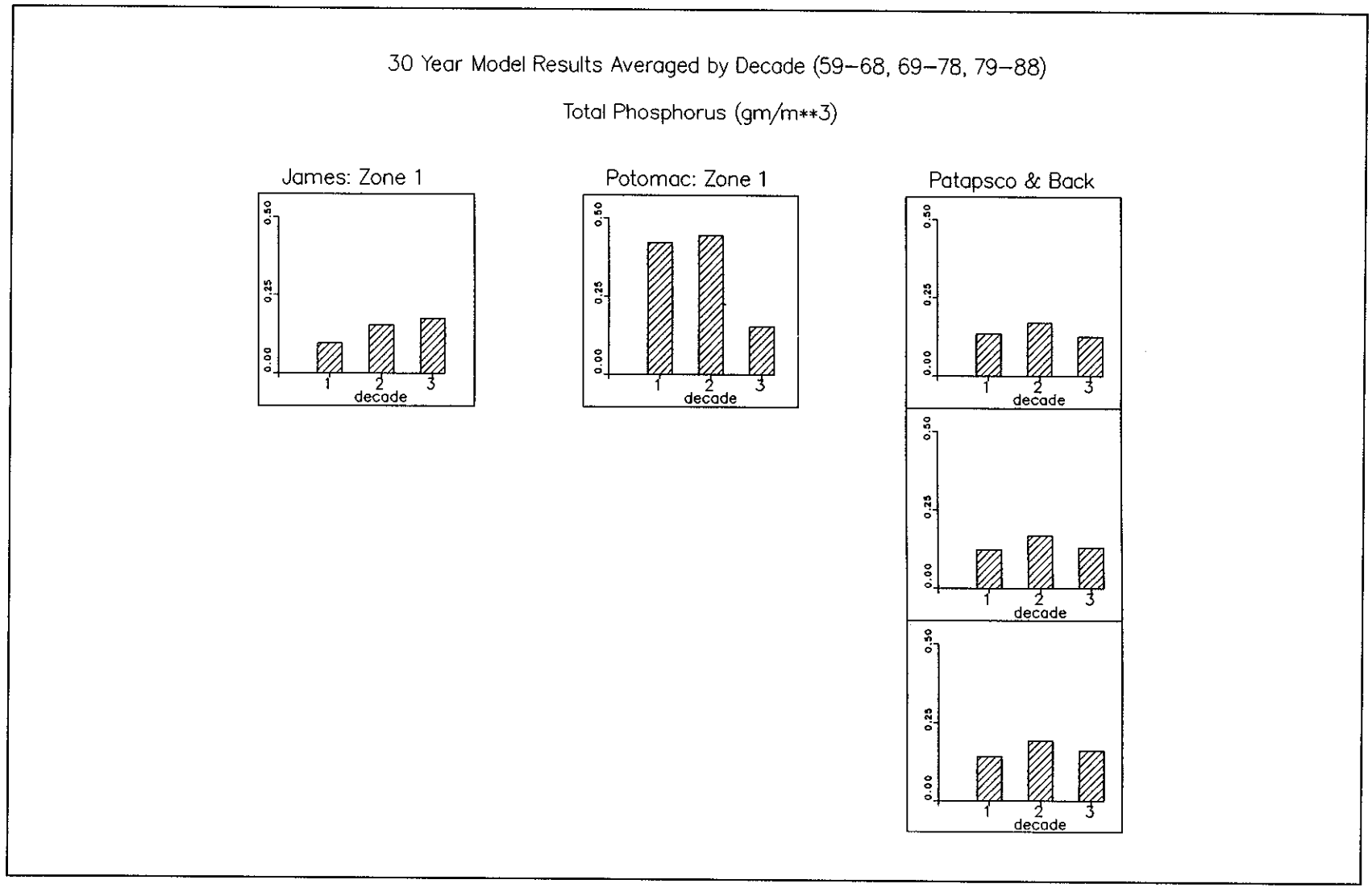

Figure 14-50. Simulated Summer-Average Total Phosphorus in Upper James, Upper Potomac, and Baltimore Harbor by Level, Decade

Phosphorus control coupled with increasing nitrate at the fall line had a major impact on DIN/DIP ratio in the upper Potomac (Figure 14-51). The ratio in the decade 1959-1968 was less than the classic Redfield ratio of 7-to-1. Nitrogen limitation was favored in the earliest decade. In 1969-1978, DIN/DIP was nearly at the Redfield ratio. In 1979-1988, the ratio zoomed to over 50-to-1, strongly favoring phosphorus limitation of algal population. An opposite trend occurred in the upper James (Figure 14-51), largely as a result of concentration trends in the fall line (Table 14-4). In the first two decades, the DIN/DIP ratio favored phosphorus as the limiting nutrient. In the most recent decade, however, nitrogen was more limiting. The DIN/DIP ratio in Baltimore Harbor indicated phosphorus as more limiting from the earliest decade (Figure 14-51). The limitation increased by a small amount in the most recent decade.

Surface waters of all three tributaries indicated little or no dissolved oxygen variation over the three decades (Figure 14-52). Only Baltimore Harbor had sufficient depth for analysis of more than one layer. In the mid-depth, the simulation indicated 1959-1968 was the best decade for dissolved oxygen. The 1979-1988 decade was the worst. The decade 1979-1988 was midway between the two. The bottom layer was anoxic throughout the three decades and showed no change. Dissolved oxygen trends in Baltimore Harbor were consistent with the adjoining mainstem segment and originated in the same phenomenon. High stratification and loads in the wet decade caused lowest dissolved oxygen. Since the bottom of Baltimore Harbor was completely anoxic under even the best conditions, however, the effect of loads and hydrodynamics showed in the middle layer only.

Neither the upper James or Potomac exhibited any anoxia in the three decades (Figure 14-53). In Baltimore Harbor, anoxia occurred in all three layers. Consistent with the dissolved oxygen record, largest anoxic volume was in 1969-1978. Least volume was in 1959-1968. The anoxic volume was influenced by both loading and stratification. When hydrologic effects were removed by considering only average years, the difference between decades was negligibly small. The simulation indicated Baltimore harbor has experienced no fundamental trend in dissolved oxygen over three decades.

Hydrodynamics or Loads?

The correlation between hydrology and anoxia is apparent. The "wet" hydrodynamic years were distinguished by dissolved oxygen minima (Figure 14-32). The wettest decade, 1969-1978, had the largest anoxic volume (Figure 14-39). It's worth noting that the correlation in our simulation between hydrodynamics and anoxic volume, $r = 0.92$, was identical to the correlation reported by Seliger and Boggs (1988) between spring runoff and anoxic volume. Two factors combine to make wet years high in anoxia. First, nutrient loads at and below the fall lines are large (Table 14-6). Large nutrient loads feed algae which settle to the bottom, decay, and consume dissolved

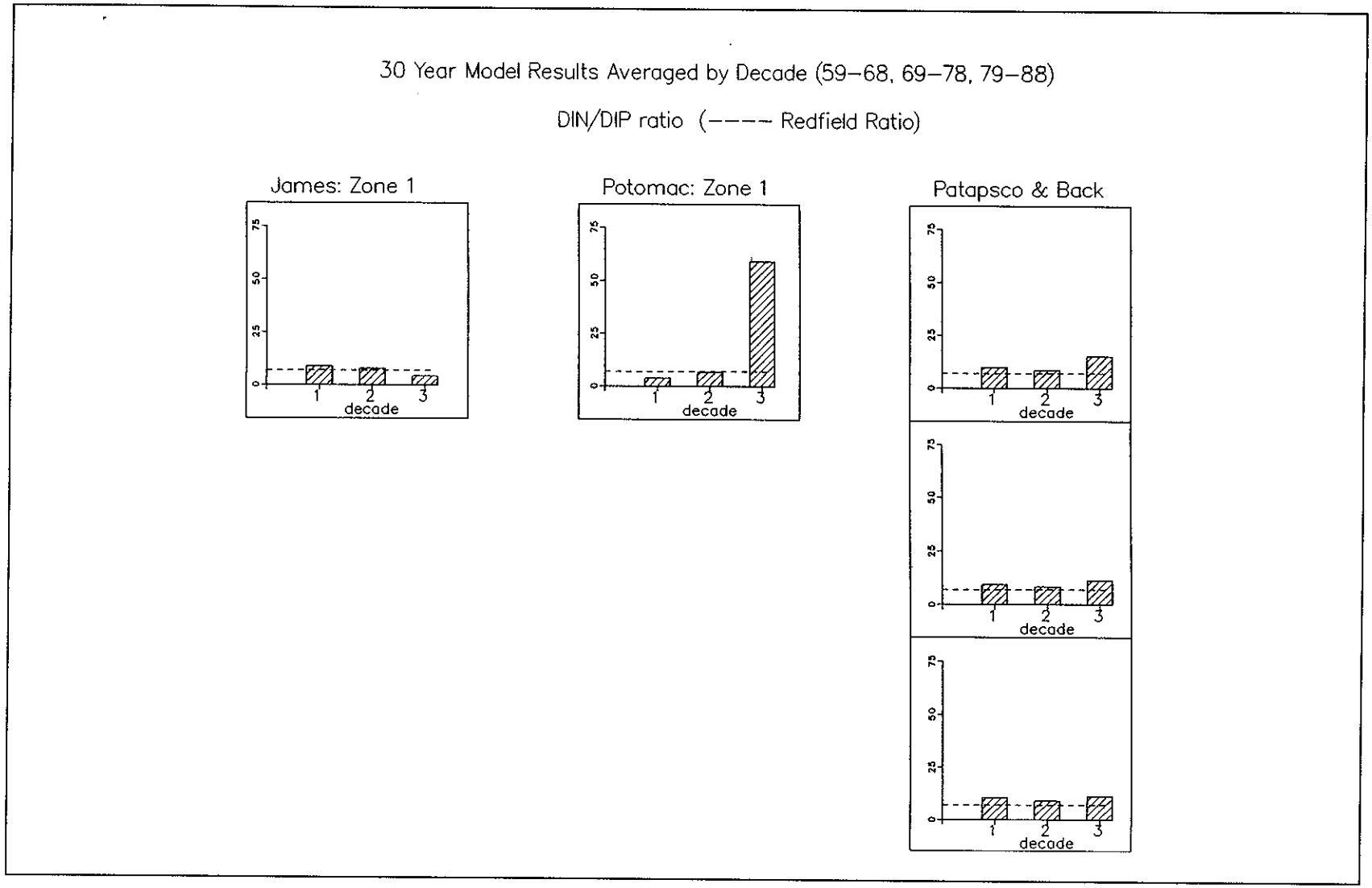

Figure 14-51. Simulated Summer-Average DIN/DIP Ratio in Upper James, Upper Potomac, and Baltimore Harbor by Level, Decade

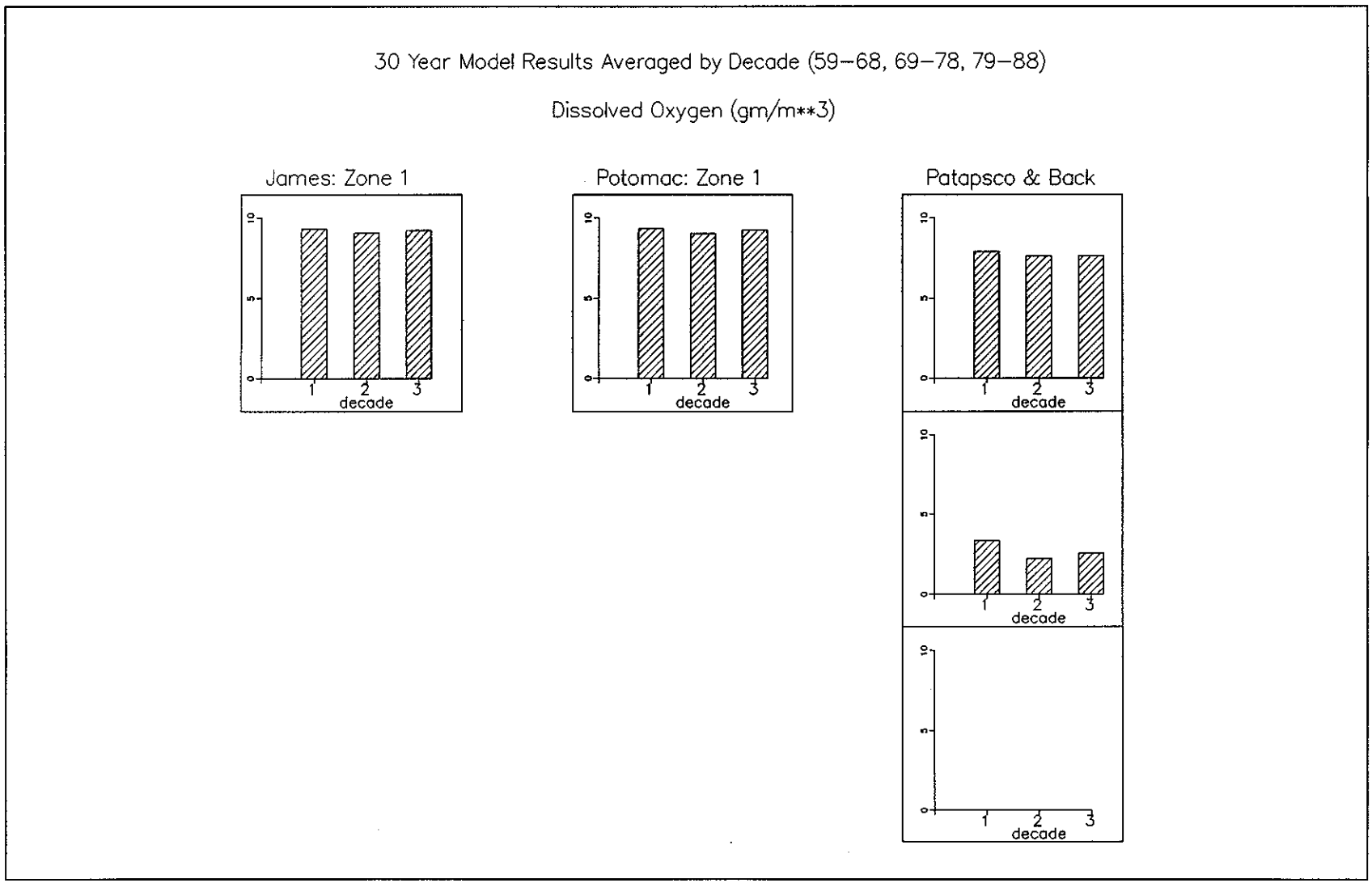

Figure 14-52. Simulated Summer-Average Dissolved Oxygen in Upper James, Upper Potomac, and Baltimore Harbor by Level, Decade

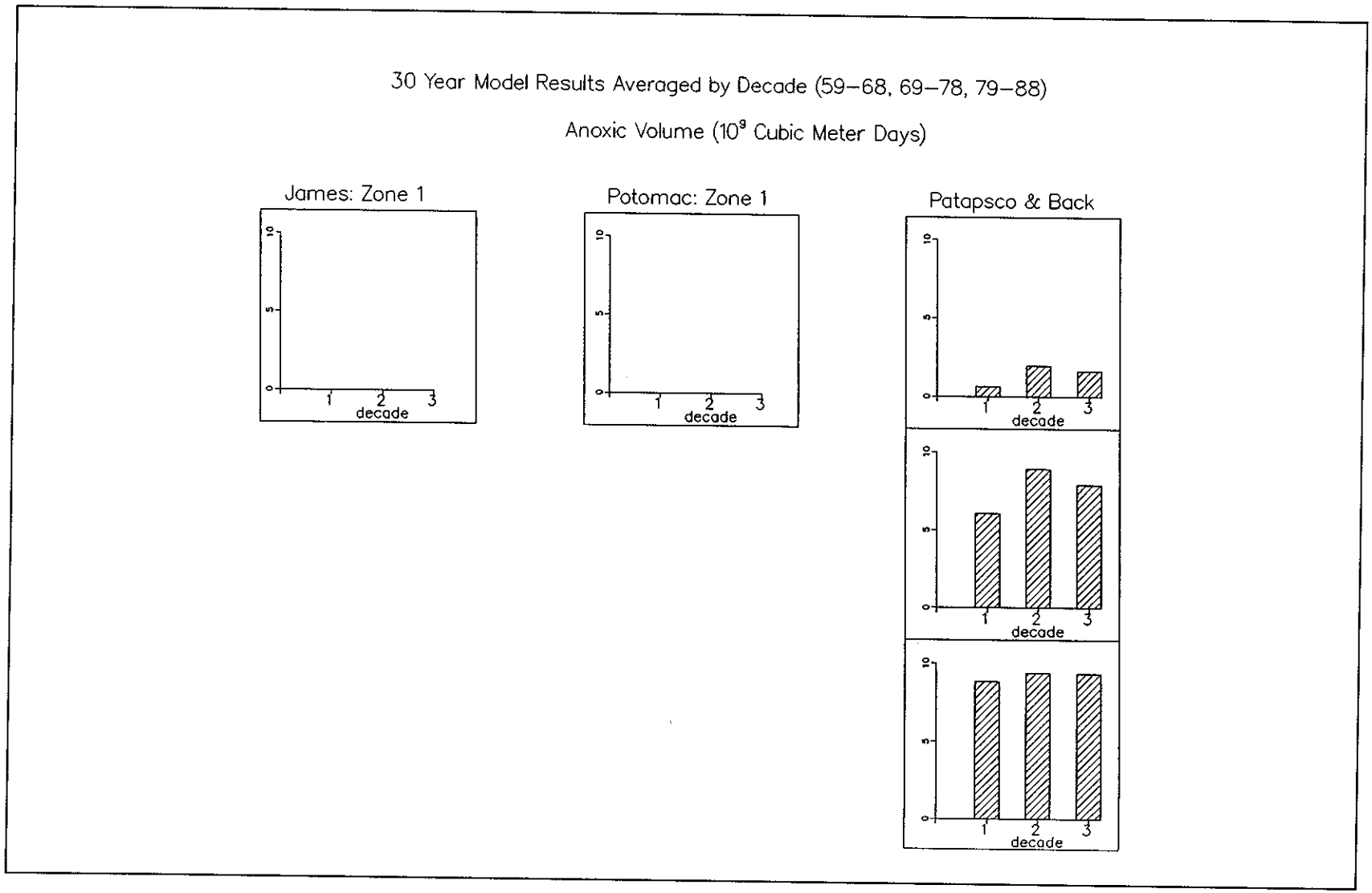

Figure 14-53. Simulated Summer-Average Anoxic Volume Days in Upper James, Upper Potomac, and Baltimore Harbor by Level, Decade

oxygen. Second, the water column is more stratified in wet years (Figure 14-7). Strong stratification isolates the bottom from the surface and prevents oxygen in surface water from diffusing to the bottom. The fundamental question is: "Which of the two processes is most important in creating bottom-water anoxia?" A special model run was made to provide the answer to that question. All loads were left as in the thirty-year simulation but thirty years of average, 1986, hydrodynamics were employed.

Comparison of the "wet-dry-average" simulation with the "average only" simulation indicates stratification is the major determinant of anoxia (Figure 14-54). Wet, 1984, hydrodynamics added 28 x 10^{10} cubic meter days of anoxia to the anoxic volume, 33 x 10^{10} cubic meter days, that occurred when average, 1986, hydrodynamics were employed. The potential variation in anoxia due to loads alone was indicated by the "average only" simulation. The difference between the most and least anoxic years was 18 x 10^{10} cubic meter days. Over thirty years, the maximum variation attributable to loads, 18 x 10^{10} cubic meter days, was only 65% of the anoxia caused by high stratification. The disparate influences of hydrodynamics and loads was even more evident if the typical year-to-year variation in anoxic volume attributable to loads, 4 x 10^{10} cubic meter days, was considered rather than the maximum variation over thirty years.

An unexpected result of the comparison was that dry years (1985 hydrodynamics) exhibited 8 x 10^{10} cubic meter days (≈23%) more anoxia than average years. This result was not explained by stratification since stratification in 1985 and 1986 was roughly equivalent (Figure 14-7). In a study of Virginia tributaries, Kuo and Neilson (1987) linked anoxia to gravitational circulation. The York and Rappahannock Rivers, which had low runoff rates and weak circulation, exhibited more anoxia than the James River, which had highest runoff and strongest circulation. Their analysis indicated the phenomenon was related to residence time. In the presence of weak circulation, water parcels were exposed for a longer period to bottom oxygen demand. An analogous process appears to occur in the Bay. In low flow periods, circulation is weak and anoxia is greater than in periods of higher flow and stronger circulation. In periods of extremely high flow, however, stratification is sufficient to overcome the beneficial effects of strong circulation.

Nitrogen or Phosphorus?

The next important question is: "Which nutrient, nitrogen or phosphorus, most influences the fraction of anoxia which is load induced?" The "average only" simulation, in which hydrodynamic variations were removed, provided some insight. Superimposed time series of anoxic volume and phosphorus loads (Figure 14-55) indicated a decrease in load from 1972 to the end of the simulation. No concurrent decline in anoxic volume was evident, however, indicating the link of anoxia to phosphorus loads was small. The visual

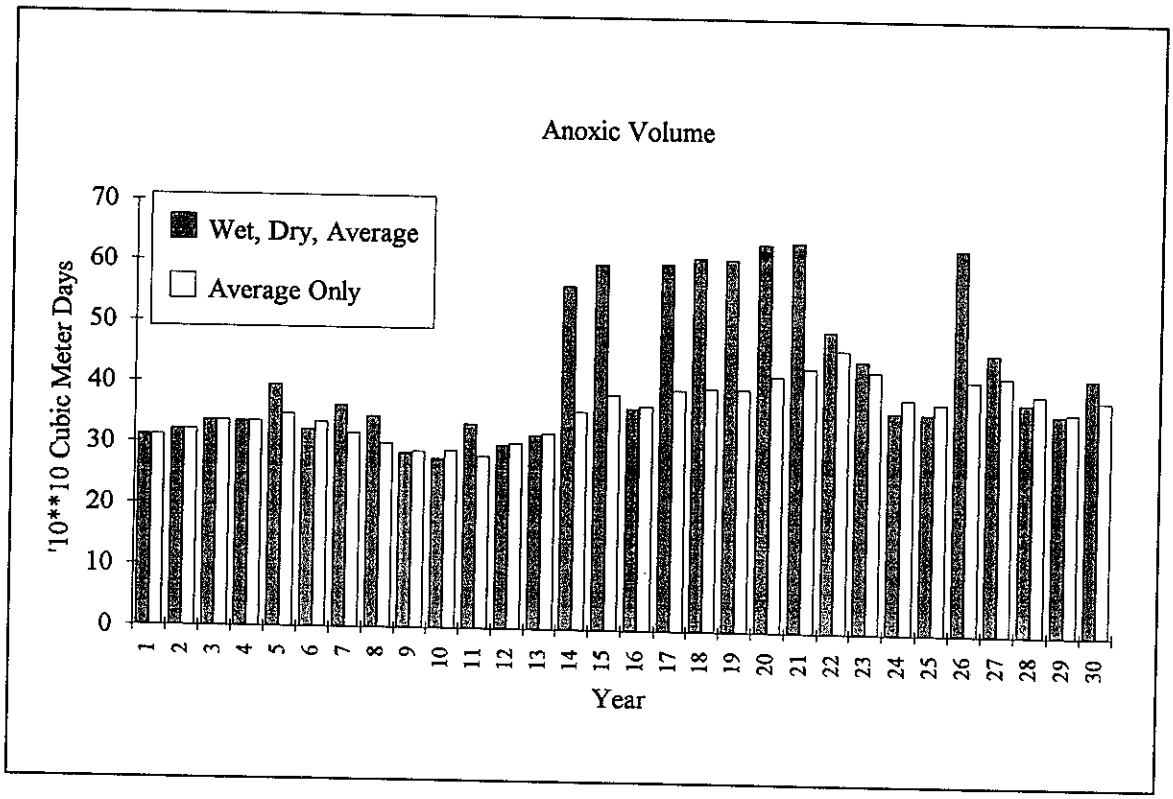

Figure 14-54. Effect of Hydrodynamics on Anoxic Volume Days

correlation of anoxic volume and nitrogen load was much more evident (Figure 14-56). Correlation analysis indicated, in fact, that anoxia was most strongly related to nitrogen load in the preceding year (r = 0.68). A carry-over of the same time scale was revealed by Kemp and Boynton (1992). They noted algal productivity and sediment oxygen demand were closely related to two-year mean river flow but barely to flow in the same year. The one-year time delay is clearly evident in the plot. Load peaks in Years 14, 21, and 26 were followed by anoxic maxima in Years 15, 22, and 27. The build-up or carry-over of nitrogen was also sufficient to cause large anoxic volumes in Years 22-23 and 26-27 despite load reductions in those years.

Summary and Conclusions

The major trend discerned in the analysis of historic dissolved oxygen and chlorophyll observations was a decrease in surface dissolved oxygen in the upper Bay. The decrease was associated with reduced chlorophyll concentration and was most likely due to diminished algal production. The chlorophyll decline was concurrent with decreasing dissolved phosphorus concentration in the Susquehanna River and reduced point-source phosphorus loads. Model simulation indicated a large increase in DIN/DIP ratio occurred in the upper Bay concurrent with the observed decline in chlorophyll. No trend in

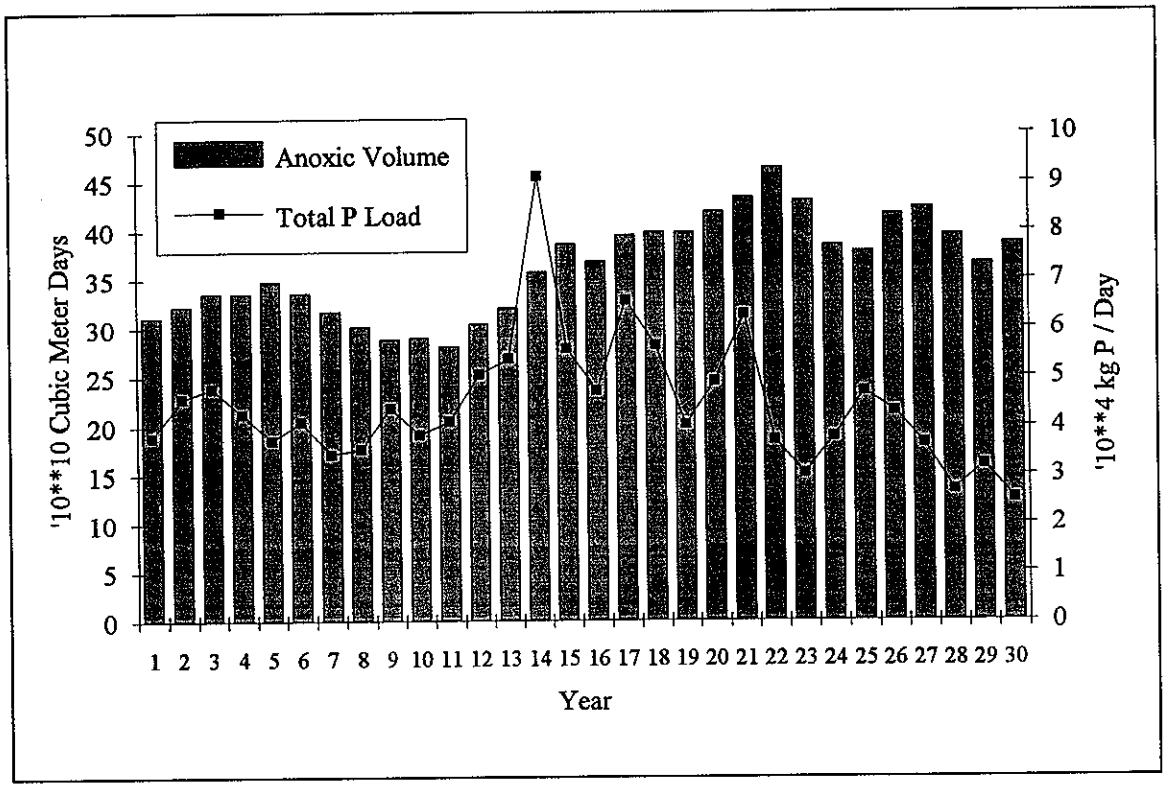

Figure 14-55. Phosphorus Loads and Load-Induced Anoxic Volume Days

bottom-water dissolved oxygen concentration or anoxic volume was evident in the observations.

Nutrient loads to the Bay were maximum in the decade 1969-1978. Nitrogen loads in the decade 1979-1988 were 7% less than in the preceding decade. The reduction was primarily due to hydrologic effects; runoff was less in the most recent decade than in the preceding decade. The underlying trend was for increasing nitrogen concentration at the two major fall lines. Phosphorus loads to the system have decreased steadily since Tropical Storm Agnes in 1972. Phosphorus loads in the decade 1979-1988 were 30% less than in the 1969-1978 decade. The reduction was due to point-source control, declining concentration at the Potomac fall line, and decreased runoff.

The model simulation initiated in 1959 reproduced observations collected in 1984-1986 to the same degree of accuracy as the three-year run calibrated to the 1984-1986 data set. Eutrophication trends observed since regular monitoring started in 1984 were reproduced in the simulation. The model demonstrated long-term stability and accuracy. The simulation provided a useful, valid tool for detection and diagnosis of long-term eutrophication trends in the Bay.

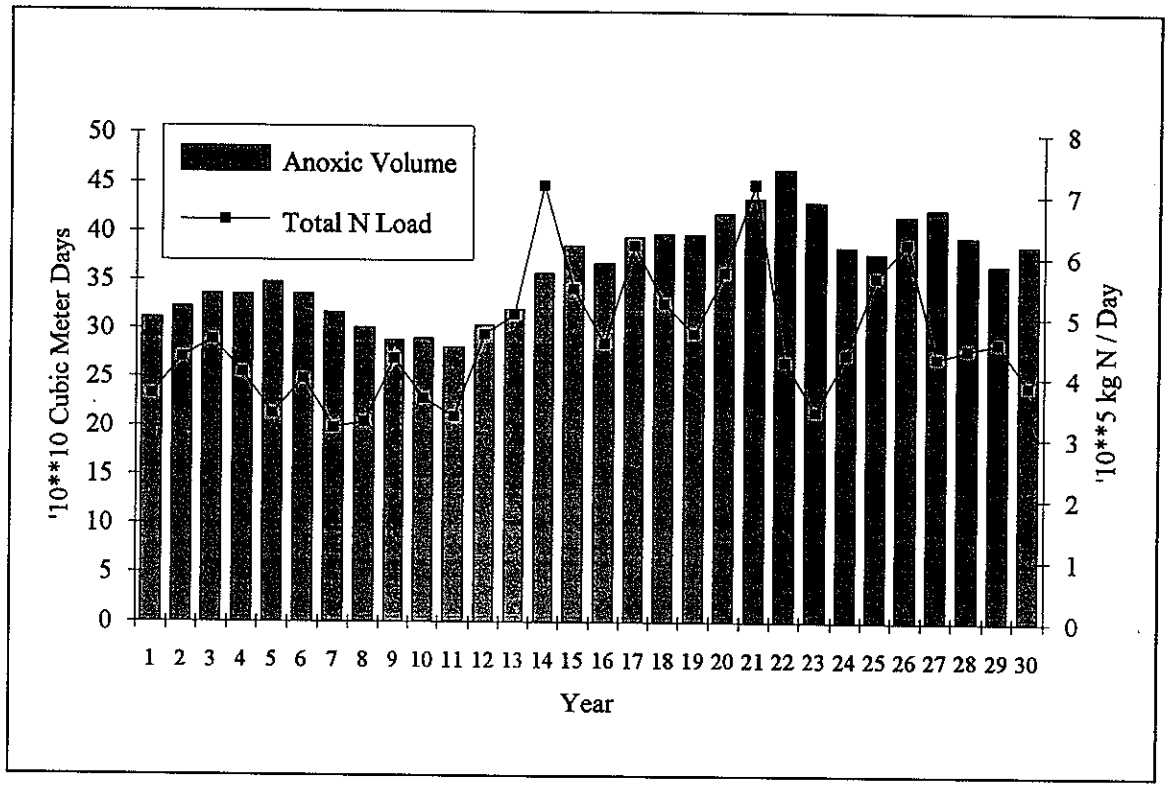

Figure 14-56. Nitrogen Loads and Load-Induced Anoxic Volume Days

Simulated chlorophyll concentrations were closely tied to hydrology. Over most of the Bay, wet years with high nutrient runoff had greatest chlorophyll concentrations. Immediately below the Susquehanna fall line, however, hydrodynamic effects caused chlorophyll to be less in wet years. Summer chlorophyll concentration was greatest in the most recent decade. Increasing summer chlorophyll was linked to an underlying increase in nitrogen concentration in the Susquehanna fall line.

Observations indicated chlorophyll attained maximum concentrations in the upper Bay during the 1969-1978 decade. The maximum concentrations were not reproduced by the model. Apparently, a species change has occurred in the region in the last decade. The species change was most likely induced by an immense increase in DIN/DIP ratio near the Susquehanna fall line.

On an annual basis, total nitrogen concentration in the Bay was closely associated with hydrology. Wet years had higher concentrations than dry years. Total nitrogen in the Bay is increasing due to concentration trends at the two major fall lines. Over thirty years, total nitrogen in the Bay increased by ≈ 0.06 gm m^{-3}.

Total phosphorus concentration in the Bay peaked in 1972 and 1973, following the Tropical Storm Agnes event. Since then, total phosphorus in the Bay has declined steadily. Combined effects of point-source and

nonpoint-source controls have reduced average total phosphorus concentrations by 0.006 gm m^{-3} over thirty years.

Dissolved oxygen trends in the Bay were subtle and unlikely to be detected solely by analysis of observations. On a decadal basis, dissolved oxygen in the Bay was least during 1969-1978. Summer-average bottom dissolved oxygen improved by 0.5 gm m^{-3} in the 1979-1988 decade. The improvement was primarily due hydrodynamic effects, however. Lesser runoff in the most recent decade induced lesser vertical density stratification. When only years of "average" hydrology were compared, bottom dissolved oxygen declined by ≈0.3 gm m^{-3} from 1959-1968 to 1979-1988.

Anoxic volume trends in the Bay mirrored dissolved oxygen trends. The decade 1969-1978 had the largest anoxic volume. Anoxic volume was less in the 1979-1988 decade indicating an improvement in water quality. As with dissolved oxygen however, the improvement was primarily due to hydrodynamic effects. When only years of "average" hydrology were considered, anoxic volume increased by 18% from the 1959-1968 decade to the 1979-1988 decade.

The extreme variation in anoxic volume over thirty years was approximately a factor of two. Highest anoxic volume was in 1979, 64 x 10^{10} cubic meter days. Least anoxic volume was in 1968, 28 x 10^{10} cubic meter days. Order-of-magnitude variations or trends in anoxic volume over the space of two to three decades are highly unlikely.

Analysis indicated hydrodynamics were the predominant influence on anoxic volume. Anoxic volume induced by high stratification, as in 1984, was 50% greater than the range of load-induced anoxia over the thirty-year period.

Trends in anoxia were tied to trends in nitrogen concentration in the two major fall lines. The simulation indicated summer-average nitrogen loads are increasing, thereby supporting increased algal biomass. The algae settle to the bottom, decay, and consume oxygen. A one-year lag occurs so that anoxia is more closely correlated with nitrogen loads in the preceding year than in the current year. Phosphorus load reductions since 1972 had no discernable effect on anoxia although the simulation indicated the magnitude of the spring bloom was diminished. Phosphorus load reductions also were the apparent cause of the observed reduction of summer chlorophyll concentrations near the Susquehanna fall line.

Chapter XV: Scenarios and Load Sensitivity Analyses

Introduction

A primary purpose behind development of the eutrophication model was employment of the model in scenario analysis. The model was intended for use in developing and testing load-management strategies aimed at limiting eutrophication processes in the Bay. Many of the requirements listed prior to model development were specified with scenario analysis in mind. For example, the model capability to simulate the effect of the spring algal bloom on summer anoxia. The sediment model was developed so that the magnitude and time scale of sediment response to management actions could be determined. Loads were linked to the model in a fashion that facilitated examination of temporal and regional load controls.

Before scenarios could be run, however, a scenario methodology had to be developed. The primary issue was duration of the scenarios. Length had to be sufficient for the sediments to respond to management actions. A second issue involved scenario hydrology and hydrodynamics. The scenarios had to account for effects of these dynamic processes on water quality.

Once the strategy was developed, a suite of specific management-strategy scenarios was executed. A second suite of more general load-response scenarios was also executed. The second suite included a scenario which examined the Bay under conditions of an all-forested watershed.

The present chapter describes the analyses and experiments which determined response time of the sediments. Next, the scenario strategy, including hydrology, hydrodynamics, and loads, is described. A description of management and load-response scenarios follows. Load-response and selected management scenarios are described in detail. Finally, Baywide nutrient budgets are developed for three key conditions.

How Long to Steady State?

Analytical Approach

Prior to the development of the eutrophication model, sediment-water interactions were identified as crucial components of the eutrophication process in the Bay (HydroQual 1987). Means were not available, however, to predict the ultimate response of the sediments to management actions or the time for the response to occur. In response to these issues, the decision was made to develop a predictive sediment submodel (DiToro and Fitzpatrick 1993). Following formulation of the sediment model and coupling to the water-quality model, means were available to predict, on an analytical basis, the sediment response time and to test the analysis via execution of the coupled models.

Three time scales affecting the response time of the Bay can be identified. These are the residence time of the water column, the time scale for diagenesis within the sediments, and the time scale for removal of diagenetically-produced material from the sediments.

Residence Time in Water Column

An approximation of residence time of the Bay can be determined by considering the Bay to be a well-mixed system subject to a step-function load change. Concentration in the system is:

$$C = C_o e^{-\frac{Qt}{V}} + C_{in}\left(1 - e^{-\frac{Qt}{V}}\right) \qquad (1)$$

in which:

C = concentration

C_o = initial concentration

C_{in} = inflowing concentration

Q = volumetric flow rate

V = volume

t = time

The simplest case is consideration of an abrupt halt in loading (C_{in} = 0) for which Equation 1 becomes:

$$\frac{C}{C_o} = e^{-\frac{Qt}{V}} \qquad (2)$$

The time to steady state is determined by the term $e^{-Qt/V}$. The volume of the Bay is $\approx 7.9 \times 10^{10}$ m^3. The appropriate flow for this computation is the volumetric flow through the Bay mouth. Lagrangian average flow for the period 1984-1986, as computed by the CH3D hydrodynamic model, is 14400 m^3 sec^{-1}. (The volumetric flow at the mouth is ≈ 7 times the freshwater flow due to density-driven circulation within the Bay.) Employing these parameter values, the time to several benchmarks can be computed (Table 15-1). The conclusion is the time for the Bay water column alone to respond to load changes is less than a year.

Diagenesis Time Scale

The sediment model considers three classes of organic matter:

G1 = labile (decay rate ≈ 0.03 day^{-1})

G2 = refractory (decay rate ≈ 0.002 day^{-1})

G3 = inert (decay rate = 0 day^{-1})

Consider a mass balance within the sediments for the G1 class only:

$$\frac{\delta G1}{\delta t} = \frac{a_1 D}{H} - K_1 G1 - \frac{W}{H} G1 \qquad (3)$$

in which:

G1 = concentration of labile organic matter (M L^{-3})

a_1 = labile fraction of deposited organic matter ($0 \leq a_1 \leq 1$)

D = organic matter loading rate (M L^{-2} T^{-1})

H = thickness of active sediment layer (L)

K_1 = decay rate of G1 organic matter (T^{-1})

W = burial velocity (L T^{-1})

The first term on the right hand side of Equation 3 represents deposition of organic matter from the water column; the second term represents decay; the third term represents burial beyond the active sediment layer.

Table 15-1
Analytical and Empirical Times to Steady-State

Water Column Residence Time (Years)

% Steady State	Analytical	Mainstem Bay	Upper Potomac	
50	0.12	0.35	0.05	
67	0.17	0.5	0.08	
90	0.40	1.16	0.18	
95	0.52	1.5	0.24	
99	0.80	2.3	0.36	

Sediment Diagenesis (Years)

% Steady State	Analytical	Mainstem Bay	Upper Potomac	
50	0.16	2 to 3	< 1	
67	0.29	3 to 4	1.5	
90	2.5	9 to 10	4	
95	3.9	12	6	
99	6.9	17	12.5	

Sediment Phosphate Concentration (Years)

% Steady State	Analytical, Oxic	Analytical, Anoxic	Mainstem Bay (Zone 2)	Upper Potomac
50	9 to 12	1.2	7	12
67	13 to 14	1.6	8.5	15
90	> 20	3.3	20	5
95		4.2	> 20	> 20
99		6.2		

Sediment-Water Phosphate Flux (Years)

% Steady State	Analytical, Oxic	Analytical, Anoxic	Mainstem Bay	Upper Potomac
50	9 to 12	1.2	2 to 16	> 20
67	13 to 14	1.6	4 to > 20	
90	> 20	3.3	7 to > 20	
95		4.2	9 to > 20	
99		6.2	12 to > 20	

Combining terms and simplifying yields:

$$\frac{\delta G1}{\delta t} + \alpha_{11} G1 = \alpha_{21} \qquad (4)$$

in which:

$$\alpha_{11} = K_1 + \frac{W}{H}$$

$$\alpha_{21} = a_1 \frac{D}{H}$$

for which the solution is:

$$G1 = G1_o e^{-\alpha_{11} t} + \frac{\alpha_{21}}{\alpha_{11}} \left(1 - e^{-\alpha_{11} t}\right) \qquad (5)$$

in which:

$G1_o$ = initial concentration of G1 organic matter

$$= \frac{a_1 D}{K_1 H + W}$$

As with residence time, the simplest case is for a cessation of loading ($\alpha_{21} = 0$) in which case:

$$\frac{G1}{G1_o} = e^{-\alpha_{11} t} \qquad (6)$$

By analogy, the G2 concentration is:

$$\frac{G2}{G2_o} = e^{-\alpha_{12} t} \qquad (7)$$

in which:

$$\alpha_{12} = a_2 \frac{D}{H}$$

a_2 = refractory fraction of deposited organic matter

$G2_o$ = initial concentration of G2 organic matter

$$= \frac{a_2 D}{K_2 H + W}$$

Total diagenesis, normalized by initial diagenesis is:

$$\frac{Gt}{Gt_o} = \frac{G1_o e^{-\alpha_{11} t} + G2_o e^{-\alpha_{12} t}}{G1_o + G2_o} \qquad (8)$$

Solution to Equation 8 is based on parameter values characteristic of the sediment model operating in coupled mode with the water quality model (Table 15-2). Some differences exist between parameter values input to the sediment model and parameter values derived from coupled operation. In particular, annual average diagenesis rates are lower than diagenesis rates at 20 C°. Solution (Figure 15-1) indicates a rapid die off, corresponding to depletion of G1 organic matter, followed by a slower depletion of G2 organic matter. Less than four years are required to deplete 95% of the initial organic matter present (Table 15-1).

Table 15-2
Parameters in Analytical Sediment Model

Symbol	Definition	Magnitude
a_1	labile fraction of deposited organic matter	0.45
a_2	refractory fraction of deposited organic mater	0.30
fd_1	dissolved fraction of total substance in upper layer	6.66×10^{-5} (oxic), 0.0196 (anoxic)
fd_2	dissolved fraction of total substance in lower layer	0.0196
fp_1	particulate fraction of total substance in upper layer	$1 - fd_1$
fp_2	particulate fraction of total substance in lower layer	$1 - fd_2$
H	thickness of active sediment layer	10 cm
K_1	decay rate of G1 organic matter	0.025 day^{-1}
K_2	decay rate of G2 organic matter	0.0013 day^{-1}
KL	diffusion velocity for dissolved substances	0.01 m day^{-1}
s	sediment-water mass-transfer coefficient	0.15 m day^{-1}
W	burial velocity	0.25, 0.37, 0.5 cm $year^{-1}$
α	decay rate of combined G1 G2 organic matter	0.0025 day^{-1}
ω	particle mixing velocity	0.0012 m day^{-1}

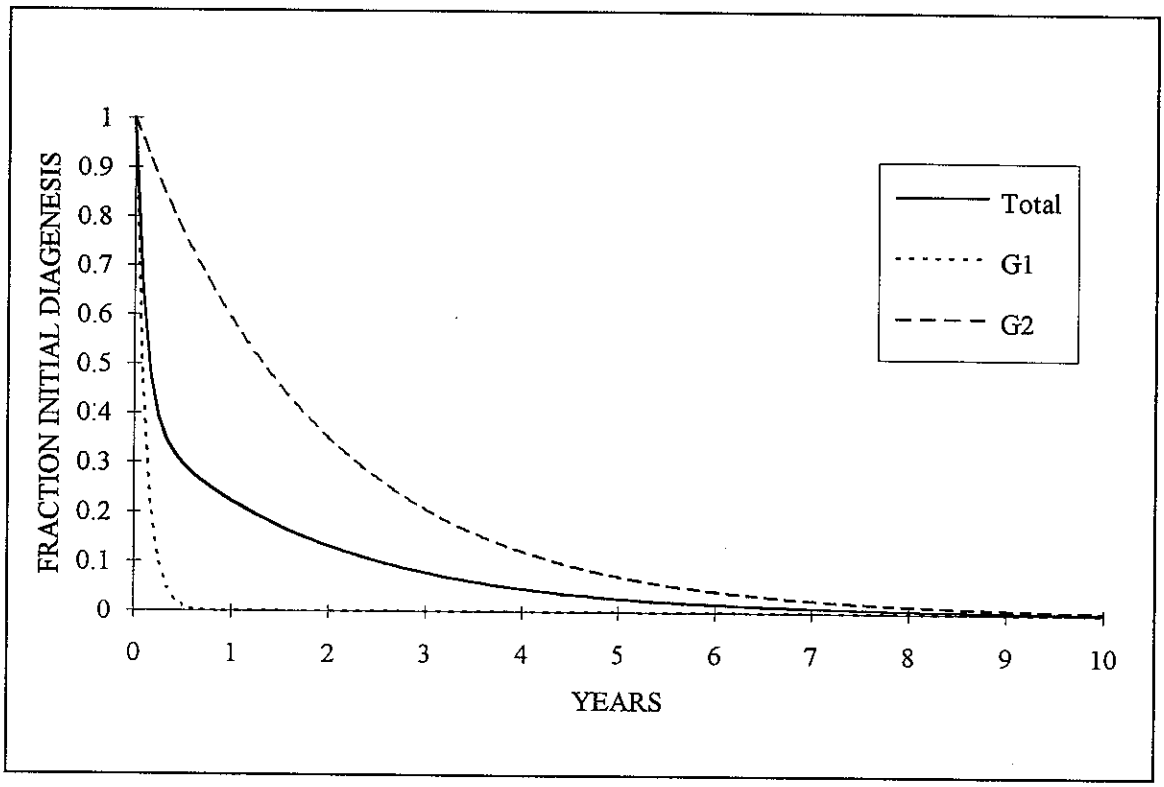

Figure 15-1. Analytical Time to Steady State for G1, G2, and Total Diagenesis

Time Scale for Mass-Transfer and Burial

The diagenesis time scale provides a good approximation of the time scale for sediment-water fluxes of nutrients (e.g. ammonium) that do not undergo significant interchange with inorganic sediment solids. For substances that do undergo interchange (e.g phosphorus), however, residence time in the sediments depends upon sorption characteristics and solids transport within and out of the sediments.

Conceptualization and notation for this analysis are based on documentation of the sediment submodel (DiToro and Fitzpatrick 1993). The sediments are viewed as a two-layer system (Figure 15-2). The upper layer is in contact with the water column and may be oxic or anoxic depending on conditions in the overlying water. The lower layer is permanently anoxic. The upper layer is thin such that concentration within the layer instantly equilibrates with fluxes in and out. Diagenesis within the upper layer is negligible. The thickness of the lower layer approximates the total depth of the active sediments. All diagenesis takes place in the lower layer. The mass-balance equation for the upper layer is:

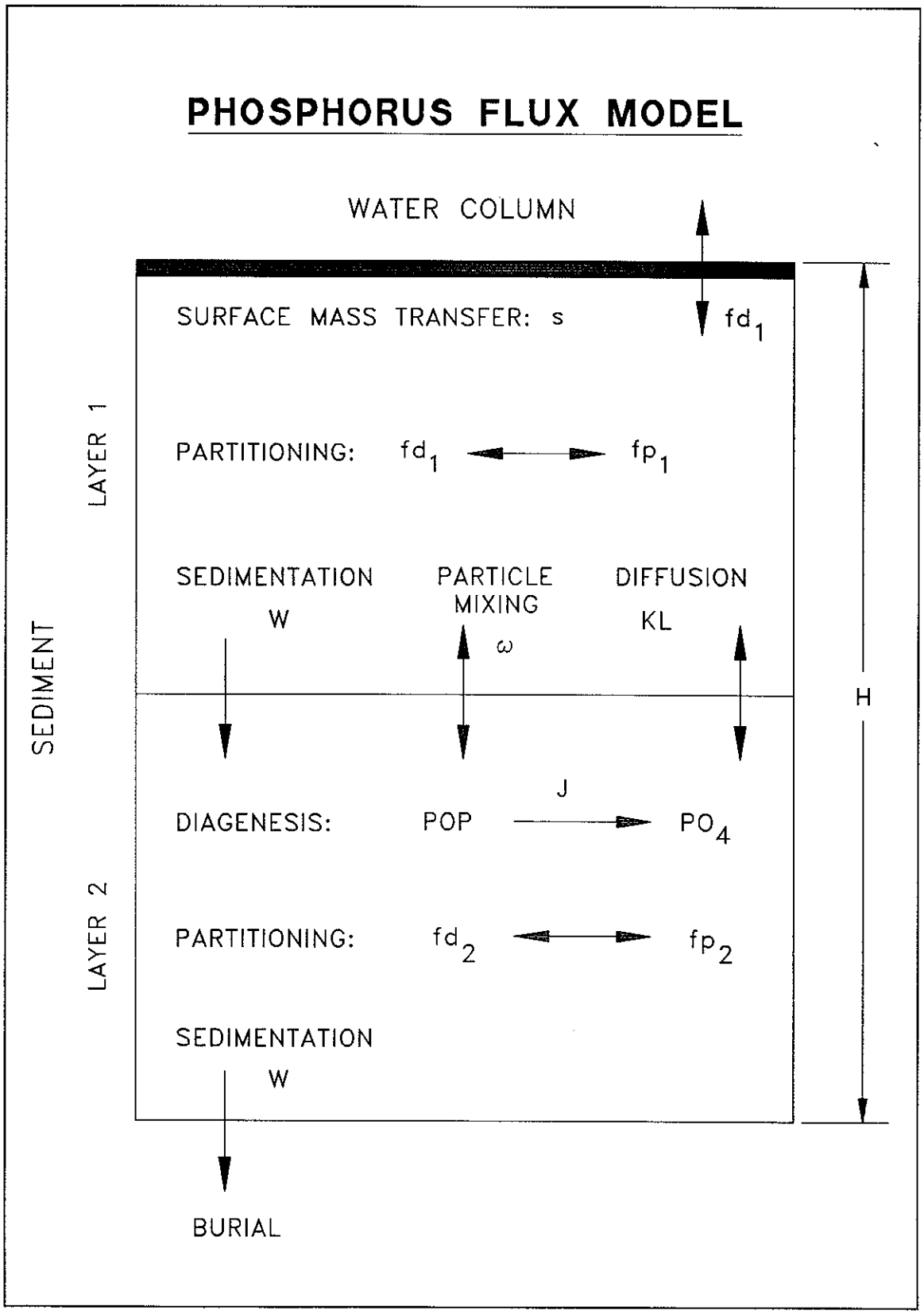

Figure 15-2. Schematic Diagram of Sediment Phosphorus Model

$$s\, fd_1\, Ct_1 = \omega\left(fp_2\, Ct_2 - fp_1\, Ct_1\right) + KL\left(fd_2\, Ct_2 - fd_1\, Ct_1\right) - W\, Ct_1 \quad (9)$$

in which:

Ct_1 = total substance concentration in upper layer ($M\ L^{-3}$)

Ct_2 = total substance concentration in lower layer ($M\ L^{-3}$)

fd_1 = dissolved fraction of total substance in upper layer ($0 \leq fd \leq 1$)

fd_2 = dissolved fraction of total substance in lower layer

fp_1 = particulate fraction on total substance in upper layer

$= 1 - fd_1$

fp_2 = particulate fraction on total substance in lower layer

s = sediment-water mass-transfer coefficient ($L\ T^{-1}$)

ω = particle mixing velocity ($L\ T^{-1}$)

KL = diffusion velocity for dissolved substances ($L\ T^{-1}$)

The left hand side of Equation 9 represents flux to the water column under the assumption that dissolved concentration in the water column is negligibly small compared to the sediments. The terms on the right hand side are mass transport due to particle mixing, diffusion of dissolved substance, and deposition to the lower layer. The equation states that flux to the water column and deposition from surficial sediments are balanced by mixing and diffusion from deeper sediments.

Total concentration in the upper layer can be determined explicitly in terms of concentration in the lower layer:

$$Ct_1 = \frac{\omega\, fp_2 + KL\, fd_2}{s\, fd_2 + \omega\, fp_1 + KL\, fd_1 + W}\, Ct_2 \quad (10)$$

The mass balance equation for the lower layer is:

$$\frac{\delta Ct_2}{\delta t} = \frac{J}{H} - \frac{\omega}{H}\left(fp_2\, Ct_2 - fp_1\, Ct_1\right) - \frac{KL}{H}\left(fd_2\, Ct_2 - fd_1\, Ct_1\right) + \frac{W}{H}\left(Ct_1 - Ct_2\right) \quad (11)$$

in which:

J = diagenetic phosphate production ($M\ L^{-2}\ T^{-1}$)

The first term on the right of Equation 11 represents the diagenetic source of total substance. The second term represents exchange of the particulate fraction with the upper layer. The third term represents exchange of the dissolved fraction with the upper layer. The last term represents deposition of total substance from the upper layer to the lower layer and burial from the lower layer to deep, inactive sediments.

Define two constants:

$$\beta_1 = \omega\ fp_1 + KL\ fd_1$$

$$\beta_2 = \omega\ fp_2 + KL\ fd_2$$

and express Ct_1 in terms of Ct_2. Then:

$$\frac{\delta Ct_2}{\delta t} = \frac{J}{H} - \frac{Ct_2}{H}\left(\beta_2 + W - \frac{\beta_2(\beta_1 + W)}{s\,fd_1 + \beta_1 + W}\right) \qquad (12)$$

The quantity in brackets on the right of Equation 12 represents the net effect of all transport processes on Ct_2. Define this quantity as a new constant γ. Then:

$$\frac{\delta Ct_2}{\delta t} + Ct_2\frac{\gamma}{H} = \frac{J}{H} \qquad (13)$$

Diagenesis within the sediments, J, is a function of time. As before, consider an immediate cessation of organic deposition. For simplicity, consider also that decay of G1 and G2 organic matter can be approximated by a single time constant. The final expression for total substance in the lower layer is:

$$\frac{\delta Ct_2}{\delta t} + Ct_2\frac{\gamma}{H} = \frac{J_o}{H}e^{-\alpha t} \qquad (14)$$

in which:

J_o = initial diagenesis rate ($M\ L^{-2}\ T^{-1}$)

α = decay rate of combined G1+G2 organic matter.

The solution to Equation 14 is:

$$Ct_2 = \frac{J_o}{\gamma - \alpha H}\left(e^{-\alpha t} - e^{-\gamma \frac{t}{H}}\right) + Ct_{2o}\, e^{-\gamma \frac{t}{H}} \qquad (15)$$

in which:

Ct_{2o} = initial concentration in lower layer ($M\ L^{-3}$)

$$= \frac{J_o}{\gamma}$$

Two time scales are present. The first, α, is the scale for diagenesis of organic matter initially existing in the sediment. The second, γ/H, is the time for mass transfer and burial of diagenetically produced material. Quantities associated with the exponentials on the right of Equation 15 represent, respectively, production due to diagenesis, mass transfer and burial of the diagenetically produced material, and mass transfer and burial of initial total substance.

Once total concentration in the lower layer is known, concentration in the upper layer and flux to the water column are computed:

$$Ct_1 = \frac{\beta_2}{s fd_1 + \beta_1 + W} Ct_2 \qquad (16)$$

and

$$F = s fd_1 Ct_1 \qquad (17)$$

in which:

F = transfer from sediment to water column

Owing to the assumption of instantaneous equilibrium in the upper layer, the time constants for upper layer concentration and sediment water flux are the same as the constants for concentration in the lower layer.

Several parameters in Equation 15 are highly dynamic including fd, ω, and KL. For time scale analysis, extreme limits of fd, representing oxic and anoxic water, are coupled with characteristic values of ω and KL (Table 15-2). Solution is examined for the range of W employed in the coupled model (Figure 15-3).

The primary determinant of sediment response is the partitioning of solid and dissolved phases in the surficial sediments. For oxic overlying water in which a large solid-phase fraction exists, the time scale of sediment response is

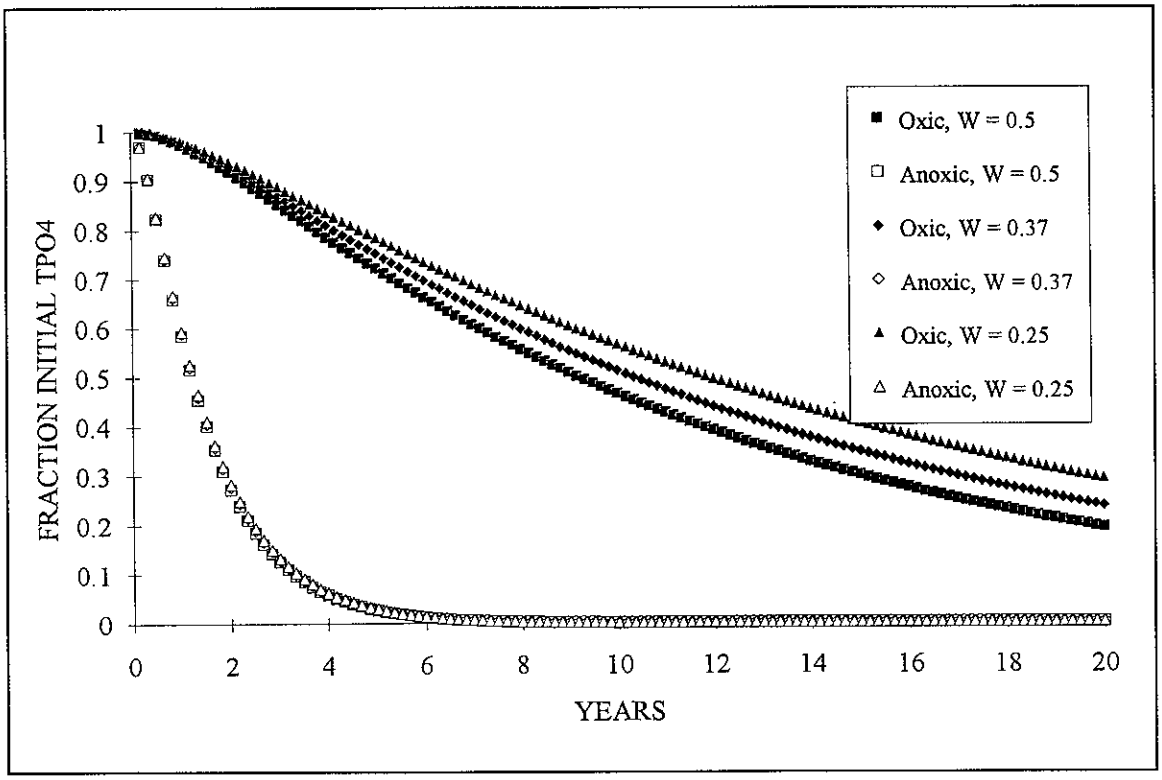

Figure 15-3. Analytical Time to Steady State for Sediment Total Phosphate

lengthy. Decline initially reflects the production of phosphorus due to diagenesis of residual organic material present in the sediments. Following the initial decay period, concentration declines in an exponential fashion. Burial rates have little effect on concentration for the first five years. Beyond that time, concentration is differentiated by the burial rate; the lowest concentration occurs at the highest burial rate. After two decades, twenty to forty percent of the original concentration remains. Time scales for Ct_1 and F are identical to the time scale of Ct_2.

For anoxic overlying water, little effect of residual diagenesis is evident. Neither is the influence of burial rates obvious since most material is released to the water rather than buried. Concentration exhibits an exponential decline which is rapid compared to oxic overlying water. Concentration attains 95% of equilibrium in less than five years (Table 15-1)

Empirical Approach

The Experiment

The analytical approach provided estimates of the time to steady state of Bay waters and sediments. These estimates were tested by performing an experiment with the time-variable, coupled water-sediment model. Loads of nitrogen and phosphorus were halved from existing loads in an average year. Ocean boundary conditions were computed via the mass-balance algorithm described in Chapter 8. The model was run, employing average-year hydrodynamics, for twenty years. Sediment and water-column concentrations and fluxes were output on a seasonal basis and averaged over zones and levels previously defined for model-data comparisons.

Four zones were selected for presentation: Bay Zones 2, 4, and 6, and Potomac Zone 1 (Figure 15-4). The Bay zones were saline and received relatively small direct nutrient loads. Bay Zone 2 was located at the head of the trench that runs up the mainstem and was the site of recurrent bottom-water anoxia. Bay Zone 4 was midway between the fall line and ocean and was subject to intermittent anoxia. Bay Zone 6, in the lower Bay, rarely exhibited anoxia. Potomac Zone 1, adjacent to the fall line, was tidal freshwater and received large nutrient loads from the above fall line and local point sources. This portion of the Potomac exhibited no anoxia. Results are presented for Season 3, Julian days 150 to 270. Season 3 is of most interest since it encompasses the period of bottom-water anoxia. This format also facilitates detection of long-term changes since annual fluctuations are not illustrated.

Water-Column Response

Chlorophyll in the surface waters of the Bay exhibited a smooth, asymptotic decline to steady state (Figure 15-5). Response of chlorophyll to the load reduction was roughly one-to-one; chlorophyll concentration was halved when loads were halved. In the upper Potomac, the response approximated a step function. Virtually all change occurred in one year with little decline thereafter. The Potomac was also distinguished in that the ultimate chlorophyll reduction was proportionately less than the load reduction.

Total nitrogen in Bay and Potomac waters (Figures 15-6, 15-7) mirrored the response of chlorophyll. Total nitrogen declined smoothly in the Bay and in a step function in the Potomac. Both the Bay and tributary exhibited a one-to-one decline of concentration in response to loads, however.

The established pattern of smooth change in the Bay and step-function change in the Potomac was evident for phosphorus (Figures 15-8, 15-9). The Potomac response was clearly two-phased, however. The step function was followed by a drawn-out smooth decline that continued beyond the twenty-year simulation period. Correspondence of load reduction and concentration was evident in the upper Bay and the Potomac. In the rest of the Bay, however,

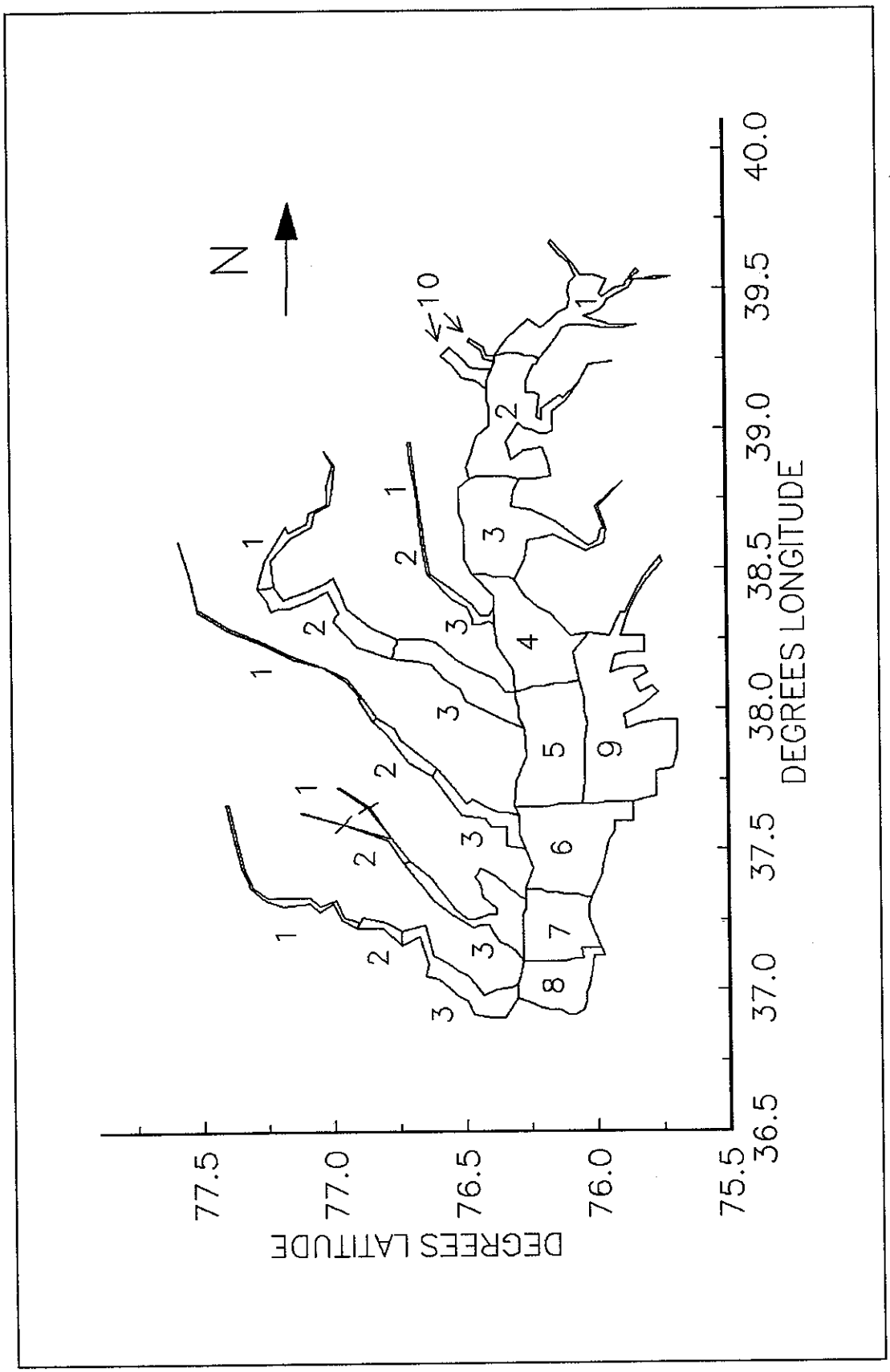

Figure 15-4. Bay and Tributary Zones Selected for Analysis

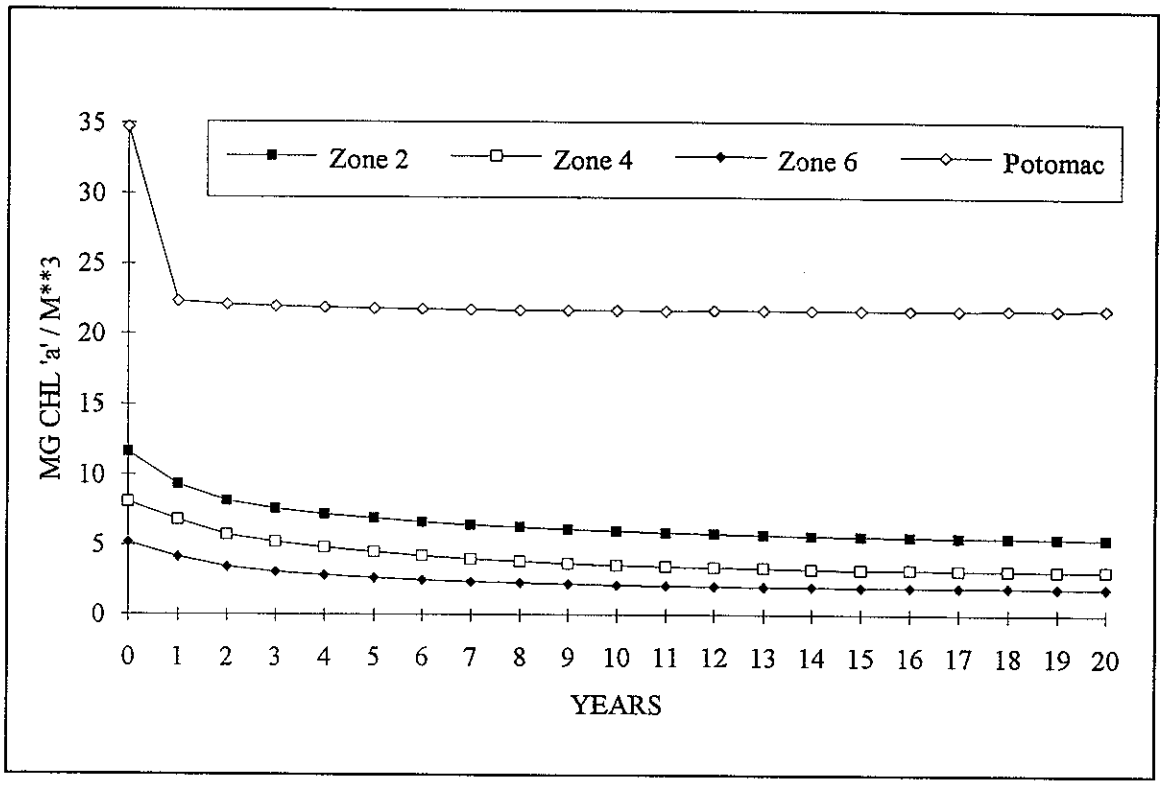

Figure 15-5. Times Series of Surface (Depth ≤ 6.7 m) Chlorophyll in Coupled Model

the reduction in phosphorus concentration was much less than the load reduction.

Dissolved oxygen (Figure 15-10) also conformed to the previously established pattern. In the Bay, dissolved oxygen smoothly increased in response to load reductions. The increase was greatest where the dissolved oxygen deficit was initially most severe. In the Potomac, a minor step-function decrease, most likely due to a decline in algal production, was followed by nearly constant dissolved oxygen concentration.

Sediment Response

The time series of carbon deposition to Bay sediments (Figure 15-11) strongly resembled the time series of chlorophyll in surface waters. A smooth, asymptotic decay occurred and the ultimate reduction in deposition roughly corresponded to the reduction in loads. In the Potomac, initial response of deposition was much more rapid than in the Bay and reflected the step-function change in chlorophyll. As with water-column chlorophyll and phosphorus, the initial decline in deposition was followed by a drawn-out response of small magnitude. The ultimate reduction in deposition was less than the reduction in loads.

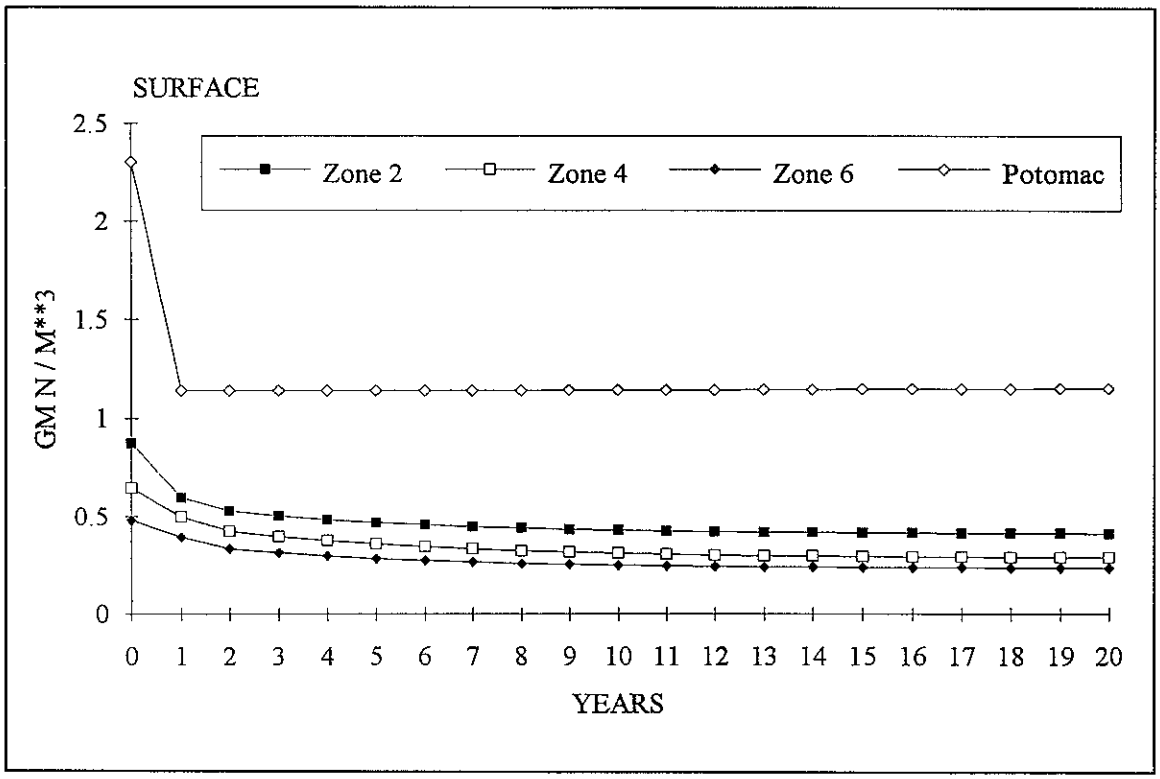

Figure 15-6. Times Series of Surface (Depth ≤ 6.7 m) Total Nitrogen in Coupled Model

Sediment carbon diagenesis responded more slowly than deposition to load reductions (Figure 15-12) since both G1 and G2 carbon forms were deposited. Sediment oxygen demand reductions (Figure 15-13) corresponded in time to diagenesis reductions. Zone 2 SOD stood out in that SOD declined much less, in proportion, than diagenesis. This phenomenon occurred because SOD, under base conditions, was depressed by low dissolved oxygen in the overlying water: a large fraction of sediment diagenesis previously escaped as COD release. Under load reductions, contrary influences affected SOD. SOD was simultaneously diminished by declining diagenesis and enhanced by increased dissolved oxygen in the overlying water. The experiment indicated that diagenesis is preferable to SOD as an indicator of the effects of load reductions.

Time scales for sediment ammonium release (Figure 15-14) also corresponded to diagenesis time scales. In the Bay, the ultimate decline in ammonium release exceeded the decline in diagenesis, however. This phenomenon occurred because larger fractions of ammonium were nitrified-denitrified as the overlying water became more oxygenated.

In the first year after load reductions, total sediment phosphate increased in Zones 2 and 4 of the Bay and in the Potomac (Figure 15-15). The increase was followed by a smooth decline which was not completed within the twenty-year length of the simulation. No increase occurred in Zone 6, however.

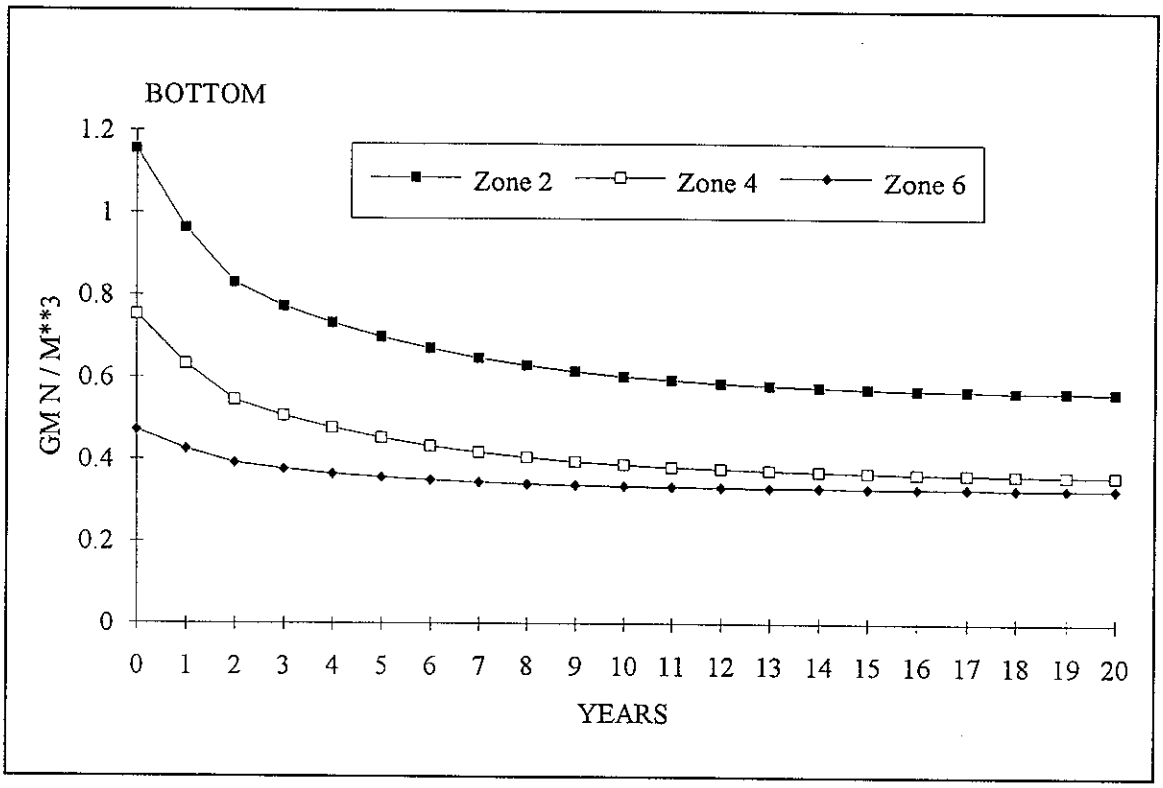

Figure 15-7. Times Series of Bottom (Depth > 12.7 m) Total Nitrogen in Coupled Model

Rather, total phosphate declined in a barely perceptible fashion throughout the simulation.

Sediment-water phosphate flux was characterized by a transient, of one-year duration and varying magnitude, followed by a smooth decline (Figure 15-16). Bay Zone 2 and the Potomac both exhibited an initial increase in flux corresponding to the increase in sediment phosphate. In the Potomac, the increase was sufficient to switch the direction of sediment-water phosphate transfer. In the base case, the sediments imported phosphate; following load reduction, the sediments exported phosphate. Phosphate release never increased in the middle Bay. The transient was clearly evident, however. In the lower Bay, the transient was barely detectible.

The transient originated in several processes. The most evident process was a decrease in sediment-water mass transfer coefficient. The mass-transfer coefficient was defined:

$$s = \frac{SOD}{DO} \qquad (18)$$

in which:

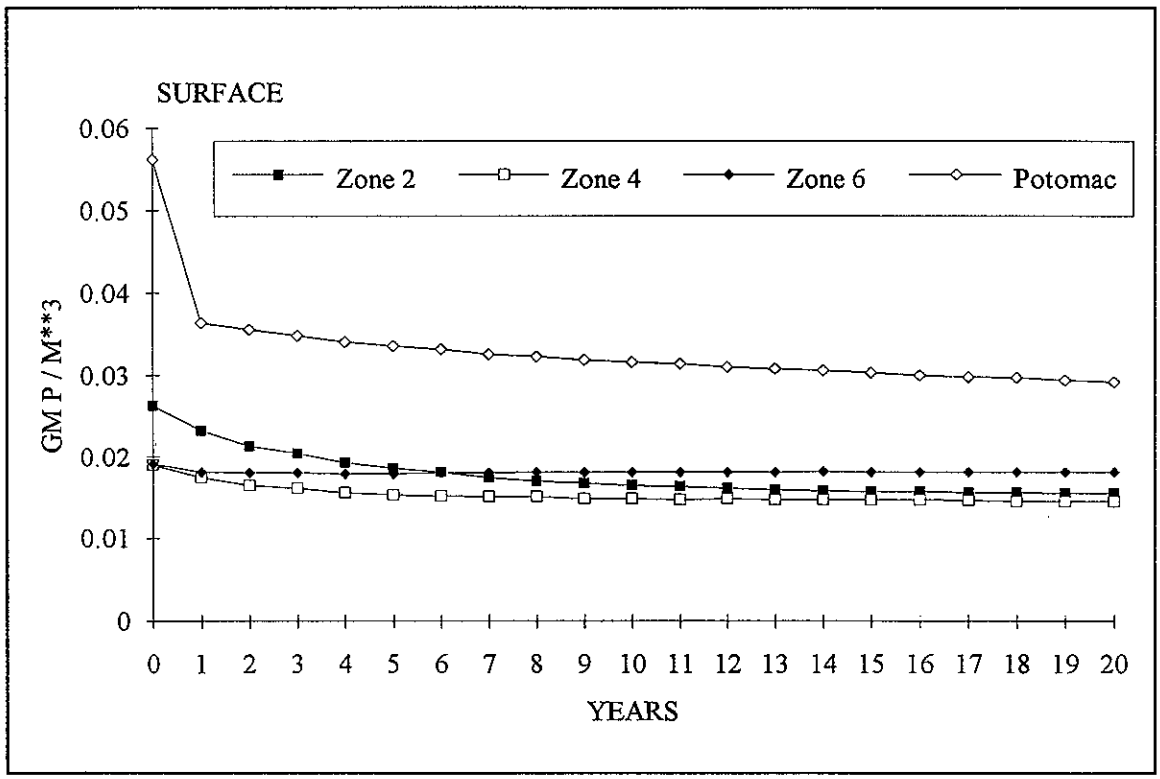

Figure 15-8. Times Series of Surface (Depth ≤ 6.7 m) Total Phosphorus in Coupled Model

s = mass transfer coefficient ($L\ T^{-1}$)

SOD = sediment oxygen demand ($M\ L^{-2}\ T^{-1}$)

DO = dissolved oxygen concentration ($M\ L^{-3}$)

Increases in dissolved oxygen and decreases in SOD concurrent with load reductions reduced the magnitude of the mass-transfer coefficient. Reduced mass transfer induced a build-up of sediment phosphate despite reductions in phosphorus deposition to the sediments. The phosphate concentration in the sediment increased until a new equilibrium was established with the water column. After equilibrium was established, phosphate flux declined in smooth fashion. A second phenomenon that increased flux was reduced particle mixing between the oxic and anoxic sediment layers. Particle mixing moved sorbed phosphate downwards from surficial to deeper sediments. Particle mixing was a function of G1 carbon in the sediment, a surrogate for benthic biomass. Sensitivity runs on an early version of the sediment model indicated reduced carbon deposition in the sediments diminished particle mixing such that phosphate in surficial sediments escaped to the water column rather than being mixed downward. This phenomenon was countered by specification of minimum particle mixing in the current sediment model. The phenomenon may still have acted to a lesser extent, however. Finally, diminished phosphate

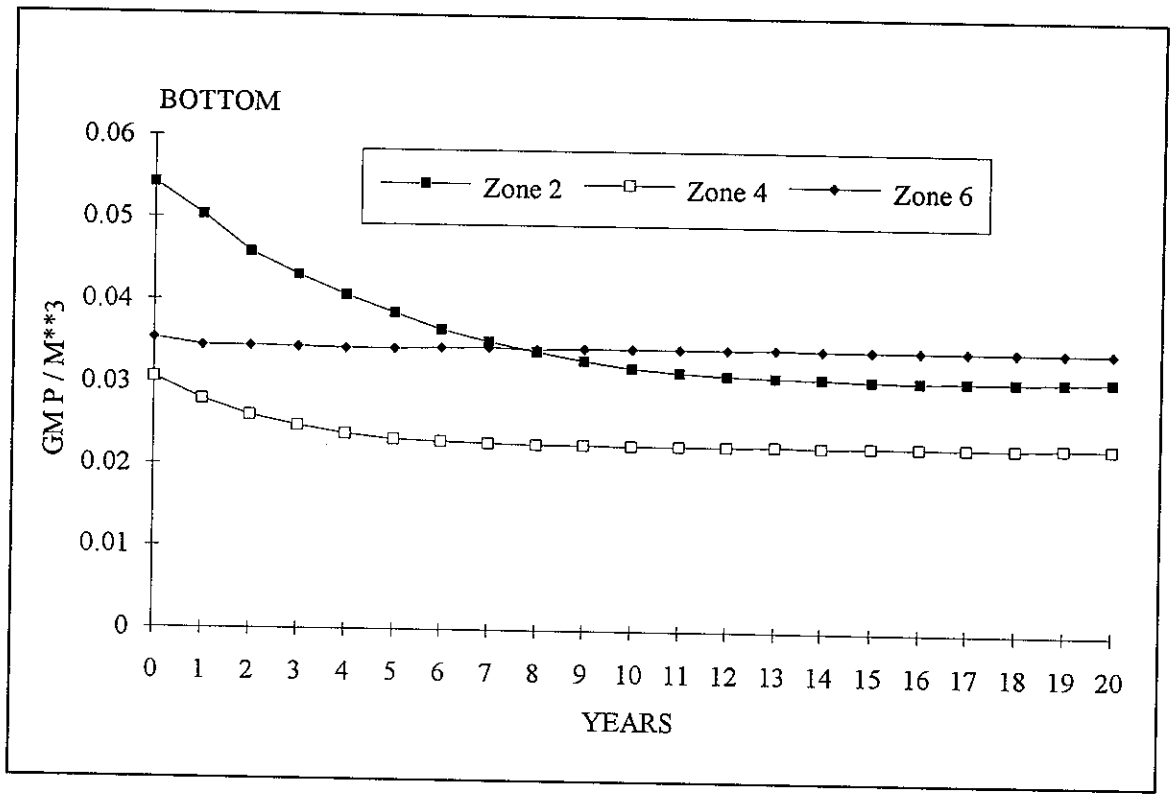

Figure 15-9. Times Series of Bottom (Depth > 12.7 m) Total Phosphorus in Coupled Model

in the water column enhanced gradient-induced transport across the sediment-water interface.

Comparison of Analytical and Empirical Results

The analytical approach examined response to a complete cessation in loading. The experiment examined response to a fractional reduction in loads. Results were compared through normalization of the form:

$$\frac{C - C_\infty}{C_0 - C_\infty} = f(t) \qquad (19)$$

in which:

C = concentration

C_o = initial concentration

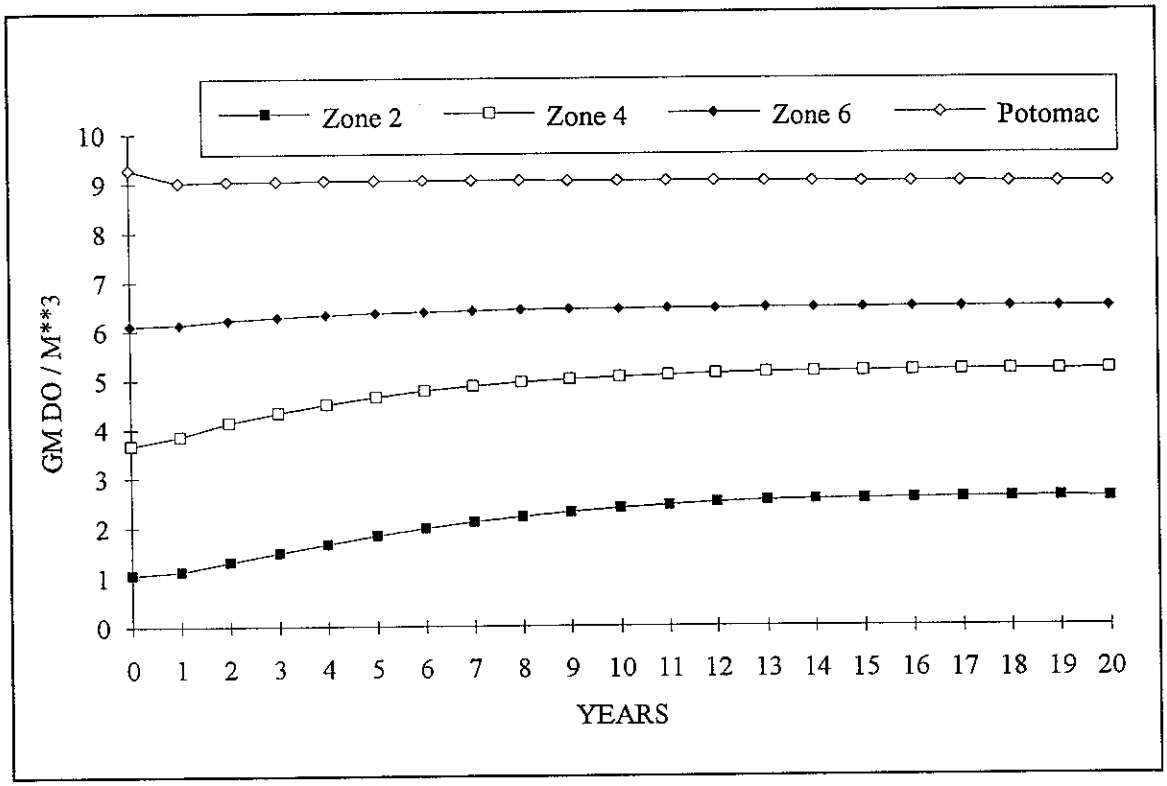

Figure 15-10. Time Series of Dissolved Oxygen in Coupled Model. Depth-Average for Potomac, Depth > 12.7 m for Bay

C_∞ = concentration as time --> ∞

f(t) = analytical or empirical temporal response of C

At time = 0, the normalized function has a value of unity. As time --> ∞, the normalized function --> 0. An identical normalization was defined for sediment-water flux.

Analytical solutions expressed by Equations 2, 8, and 14 are special cases of Equation 19 for which $C_\infty = 0$. For most concentrations and fluxes in the experiment, results after twenty years were at steady state or sufficiently close such that $C(t=20) \approx C_\infty$. For some phosphorus concentrations and fluxes, an alternate approximation was made.

Water-Column Comparisons

Comparison of water-column concentrations in the complete Bay model with a well-mixed ideal were typified by total nitrogen and total phosphorus in surface waters. Viewed once annually over a twenty-year period, the well-mixed model approximated a step function in which initial concentration was

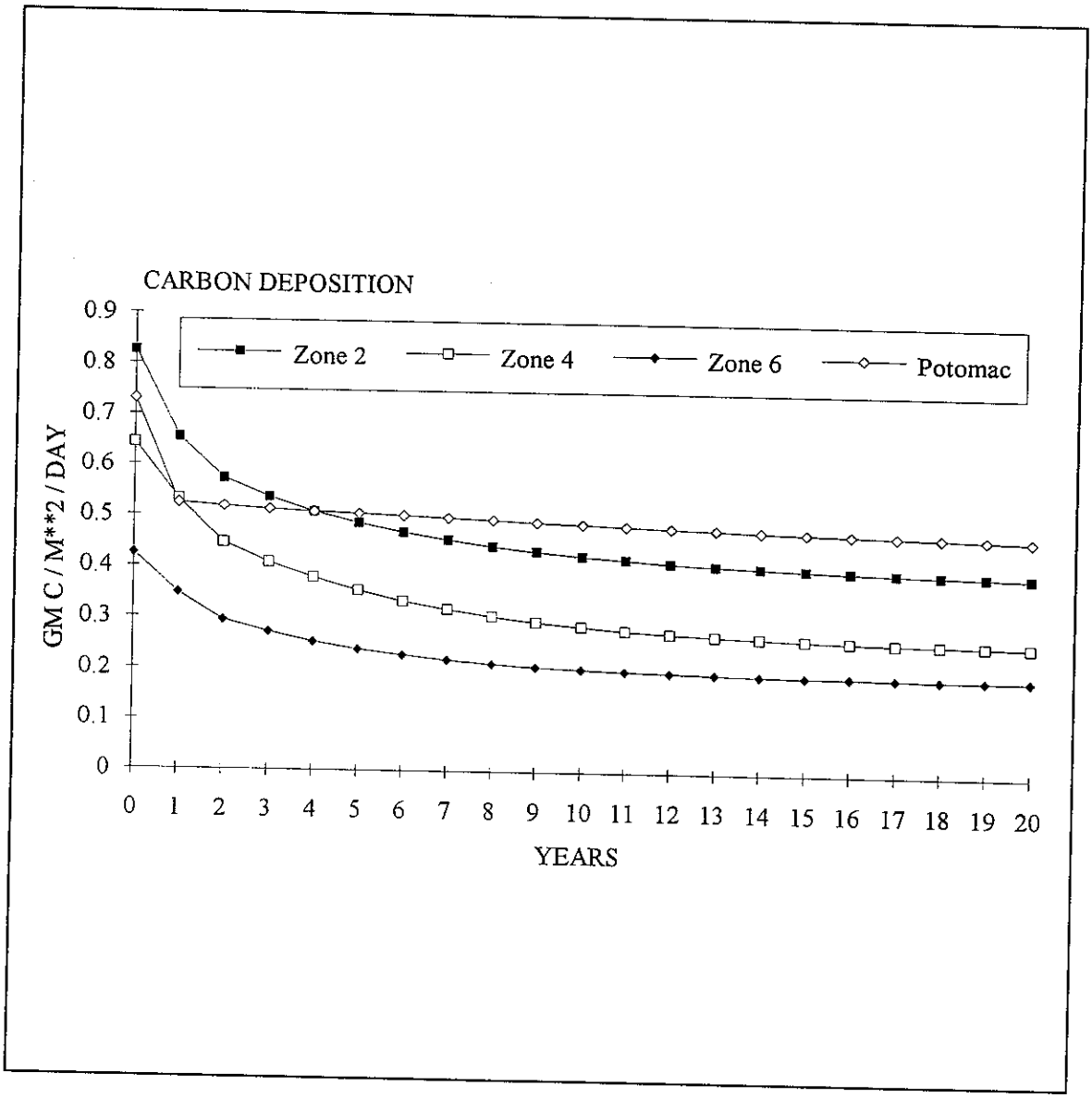

Figure 15-11. Time Series of Particulate Carbon Deposition in Coupled Model

depleted in one year. This ideal was attained in the upper Potomac for total nitrogen; following load reduction, the transition to steady state was complete in one year (Figure 15-17). For the Bay stations, however, the transition was gradual and extended for a period much more lengthy than predicted by residence time.

Zones exhibiting step-function and gradual responses were distributed differently for total phosphorus than total nitrogen. Total phosphorus in the lower Bay declined immediately to its steady-state value, in conformance to the analytical model (Figure 15-18). The Potomac exhibited a large initial decline but the complete response was drawn out as were the gradual responses in the middle and upper Bay.

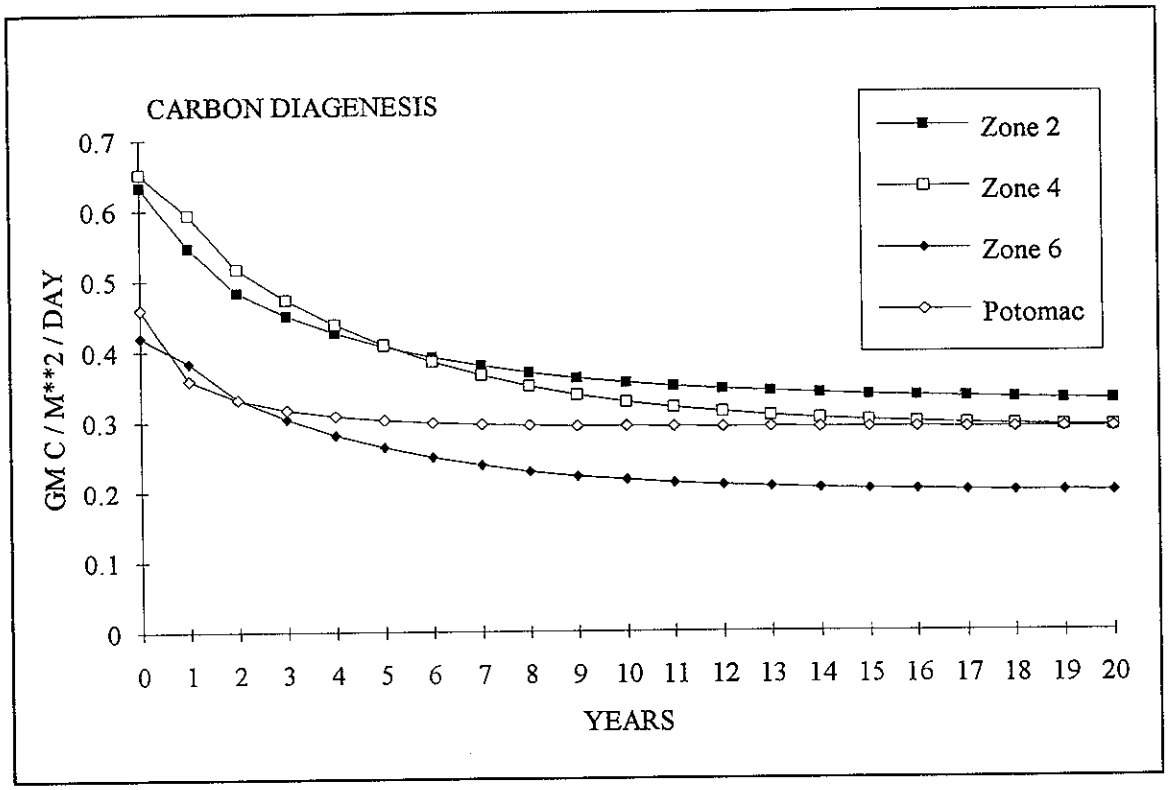

Figure 15-12. Time Series of Sediment Carbon Diagenesis in Coupled Model

Sediment Response

Following load reduction, the analytical model indicated a large, rapid decline in sediment diagenesis as G1 carbon was depleted followed by a more gradual decline until G2 carbon was exhausted (Figure 15-1). The analytical model indicated the transition to steady-state was virtually complete within five years. The Potomac tributary approximated this transition although response was more lengthy (Figure 15-19). The Bay zones behaved not at all according to the analytical model. The initial, precipitate decline was not apparent and the response period was much longer than five years.

The diagenesis time scale exhibited by the model was a good indicator of time scales for SOD and ammonium flux as well but not for phosphate flux (Figure 15-20). The lengthy response times for sediment phosphate and phosphate flux rendered the assumption that $C(t=20) \approx C_\infty$ inappropriate. Steady-state values of sediment phosphate were obtained by fitting the following function to the smooth portion of the sediment phosphate temporal response:

$$\frac{C - C_\infty}{C_0 - C_\infty} = e^{-Kt} \qquad (20)$$

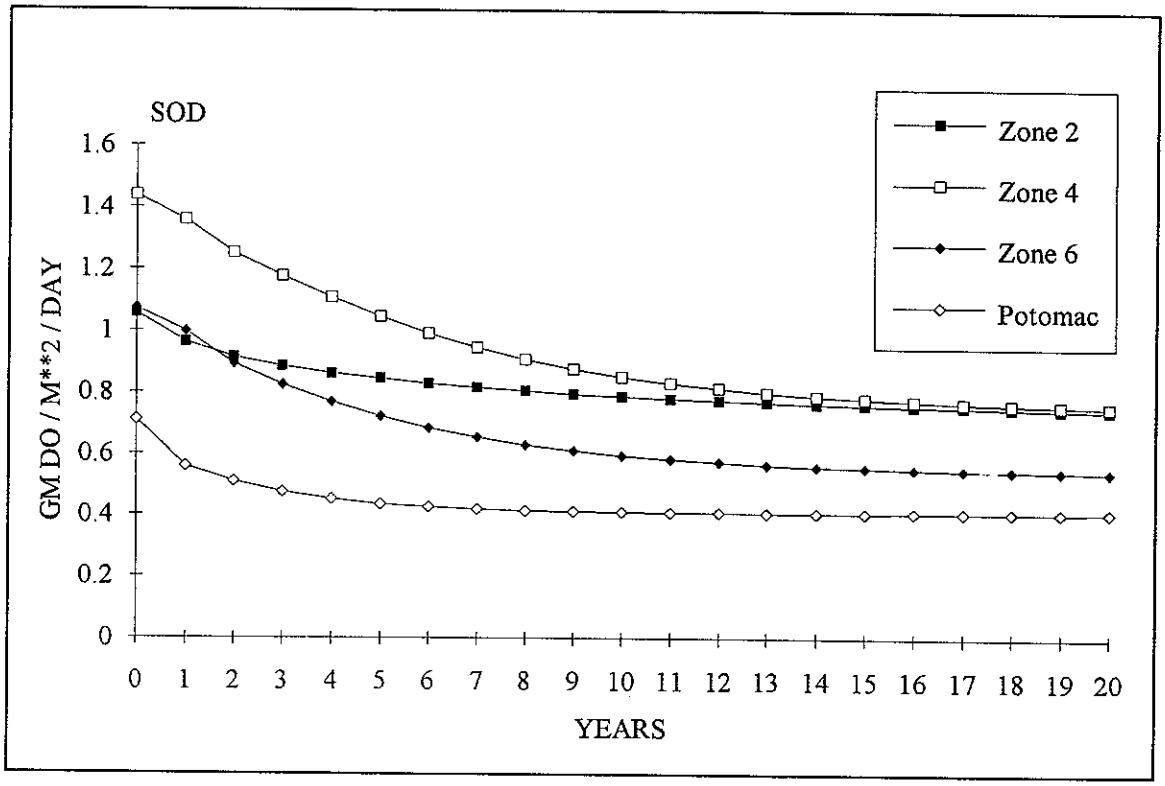

Figure 15-13. Time Series of Sediment Oxygen Demand in Coupled Model

Nonlinear regression was used with t considered the independent variate, C the dependent variate, C_0 as a known parameter and K and C_∞ as unknowns. Fit of the exponential function to the model results in Bay Zone 2 and in the upper Potomac was outstanding (Figure 15-21) with residuals $\leq 0.2\%$. No convergence was obtained for Zones 4 and 6, however, resulting in no estimate of C_∞ for these regions. Worth noting is that parameter K corresponds to γ/H in Equation 15-15. Regression of model results indicated $K \approx 0.05$ year^{-1} compared to $\gamma/H = 0.09$ year^{-1} in the analytical model. Nonlinear regression was also employed to determine steady-state phosphate flux in Bay Zones 2, 4, and in the Potomac. Fit was less ideal than for sediment phosphate but still good (residuals $\leq 10\%$). The decay constant for phosphate flux was larger than for sediment phosphate ($K \approx 0.09$ to 0.37 year^{-1}).

Normalized comparisons between analytical and empirical time to steady state were possible only for Bay Zone 2 and the Potomac. In Bay Zone 2, departure from expected response occurred when sediment phosphate increased the first year following load reduction (Figure 15-22). Following the transient, sediment phosphate declined at a rate such that concentration at the end of the simulation lay between concentrations expected for oxic and anoxic surficial sediments. The change in sign at the beginning of the normalized Potomac response was due to the increase in sediment phosphorus following load reduction. Following the transient, sediment phosphorus in the Potomac declined to roughly the expected fraction of equilibrium after twenty years.

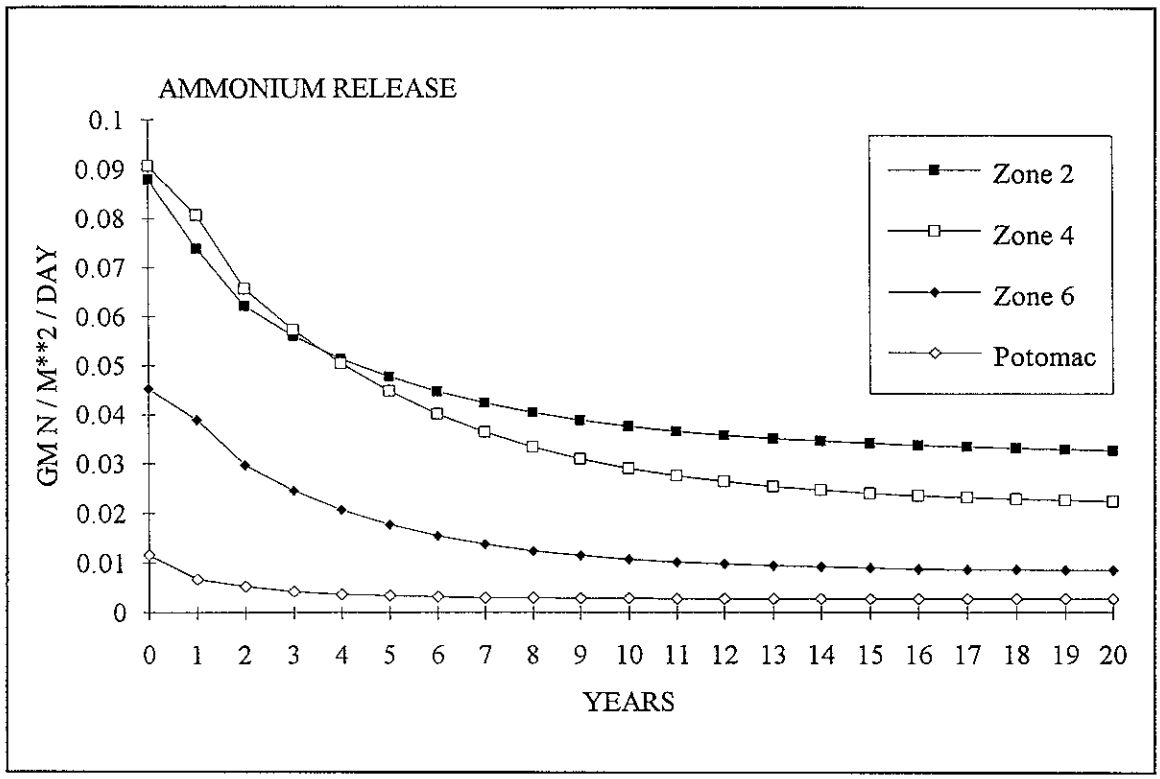

Figure 15-14. Time Series of Sediment Ammonium Release in Coupled Model

Analytical phosphate flux exhibited two characteristic patterns (Figure 15-23). For anoxic surficial sediments, flux rapidly died off in a monotonic pattern. For oxic surficial sediments, flux diminishment was slowed for one to two years while diagenetic production of phosphorus partially countered loss of phosphate from the sediments. Once digenetic production was depleted, flux died off in exponential fashion but at a rate much less than for anoxic sediments. Sediments in the experiment roughly conformed to these two characteristic patterns but the distinction between the two was not based on oxygen. Rather, flux in the middle Bay declined rapidly, although at a rate less than for anoxic sediments, while sediments in the upper Bay and Potomac exhibited a response prolonged beyond the time scale for oxic sediments. Rates of decline in these regions approximated the expected rate for oxic sediments, however. The prolonged response was a displacement due to the initial increase in flux. As a result, the decline to expected values was delayed roughly five years.

Comparison with "Standalone" Sediment Model

Concurrent with this analysis, an independent analysis of time to steady state was conducted employing the sediment model in a "standalone" mode (DiToro and Fitzpatrick 1993). Analytical solutions for diagenesis and

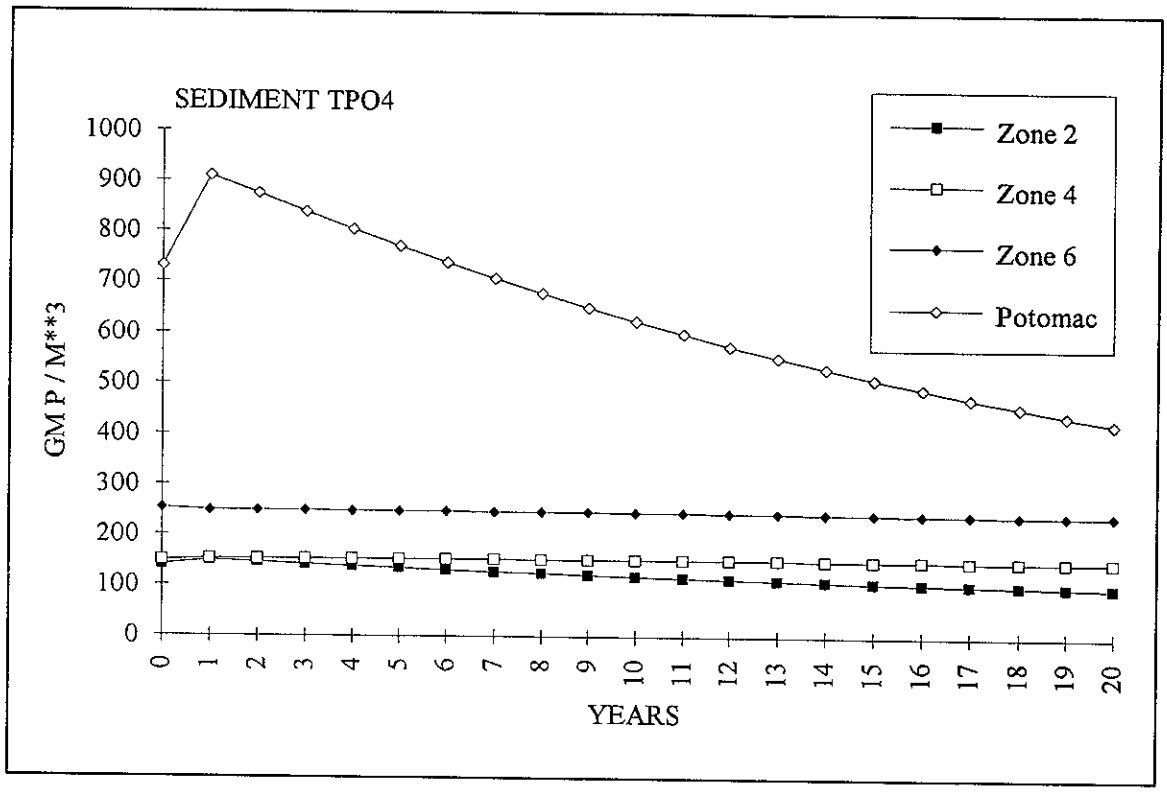

Figure 15-15. Time Series of Sediment Total Phosphate in Coupled Model

phosphorus flux nearly identical to the ones reported here were developed. Conclusions from the analytical solutions were nearly identical as well. The time to 95% equilibrium of diagenesis was reported as 4.5 years. For aerobic sediments, the time to 95% equilibrium of phosphate flux was determined to be 37 years. For anaerobic sediments, the time was 4 to 5 years. Following analytical solution, the analysis paralleled the analysis here; solutions were tested employing the model in a time-variable mode. The sediment model was applied in a standalone mode in which water column conditions were specified as boundaries. The time-variable analysis indicated a time to steady state of ten years for sediment diagenesis, ammonium flux, and SOD. Under aerobic conditions, the time to steady state for phosphate flux extended beyond twenty years. The upper bound for phosphorus time to steady state was expressed in terms of the burial rate. For parameters employed here, the upper bound was 60 to 120 years for 95% equilibrium.

Discussion

The most salient feature of the analysis was the prolonged time scale of diagenesis in the coupled model relative to expectations based on diagenetic decay rates. Analysis indicated diagenesis should attain 95% of equilibrium within four years. In the coupled model, the Bay required 12 years to attain

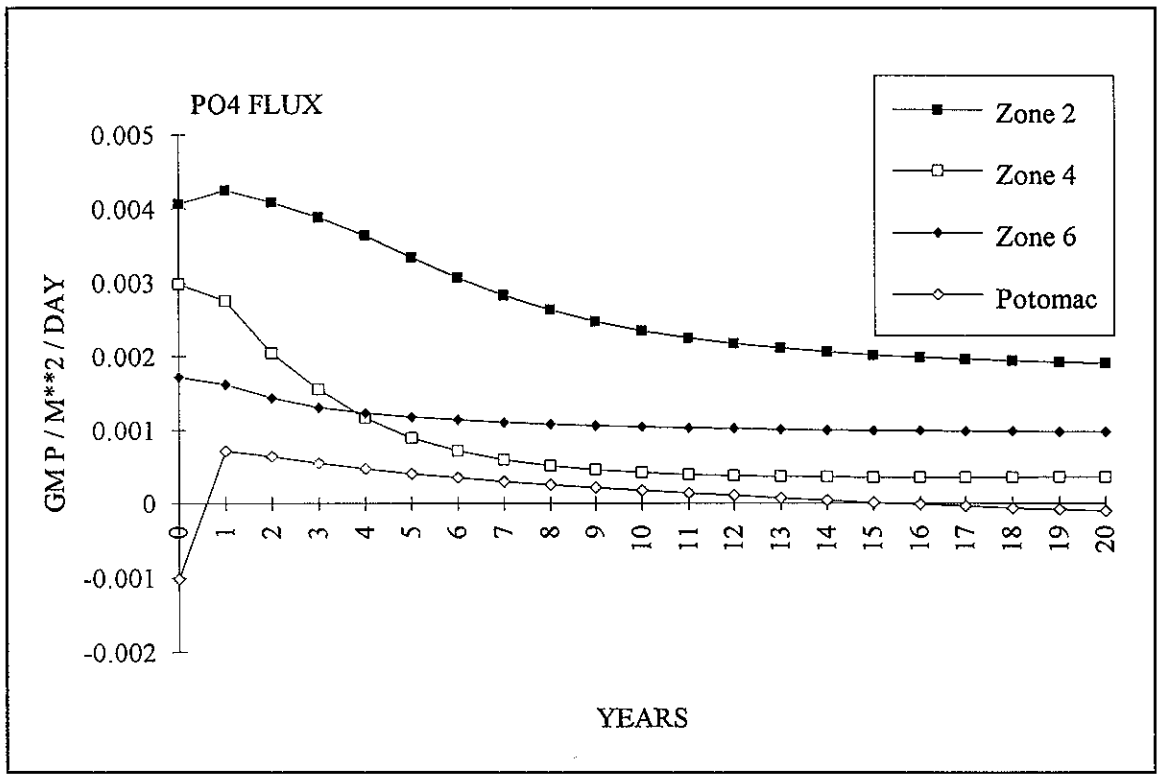

Figure 15-16. Time Series of Sediment-Water Phosphate Flux in Coupled Model

this level (Table 15-1). Although equilibrium was delayed in the upper Potomac, this Zone agreed reasonably with expectations. What was the reason for the delay in the mainstem? The answer lay in the effective residence time of the Bay. Tracer studies conducted with the coupled model indicated the flushing time of the Bay (time to 95% equilibrium) was 1.5 years compared to the well-mixed ideal of 0.5 years (Figure 15-24). As a consequence of the extended residence time, material that left the sediments via diagenesis did not instantly leave the system. Rather, the material was assimilated by algae and recycled back to the sediments, in part as G2 with a multi-year time constant. This effect can be seen in the time series of deposition. Despite the step-function decrease in loading, deposition trailed off for a decade or more before attaining steady state (Figure 15-11). Oceanic flushing of the upper Potomac was negligible but the flushing time was short (0.23 years to 95% equilibrium) and comparable to a well-mixed ideal, due to freshwater throughflow (Figure 15-25). The time series of deposition in the Potomac approximated a step function (Figure 15-11) because nutrients released from the sediments were washed downstream before they were recycled back to the sediments.

Analysis indicated the time scale to equilibrium for phosphate flux was lengthy and for much of the Bay and the Potomac, this proved to be true. Beyond the prediction of lengthy time scales, however, the utility of the analytical approach was limited. Execution of the coupled model was required to

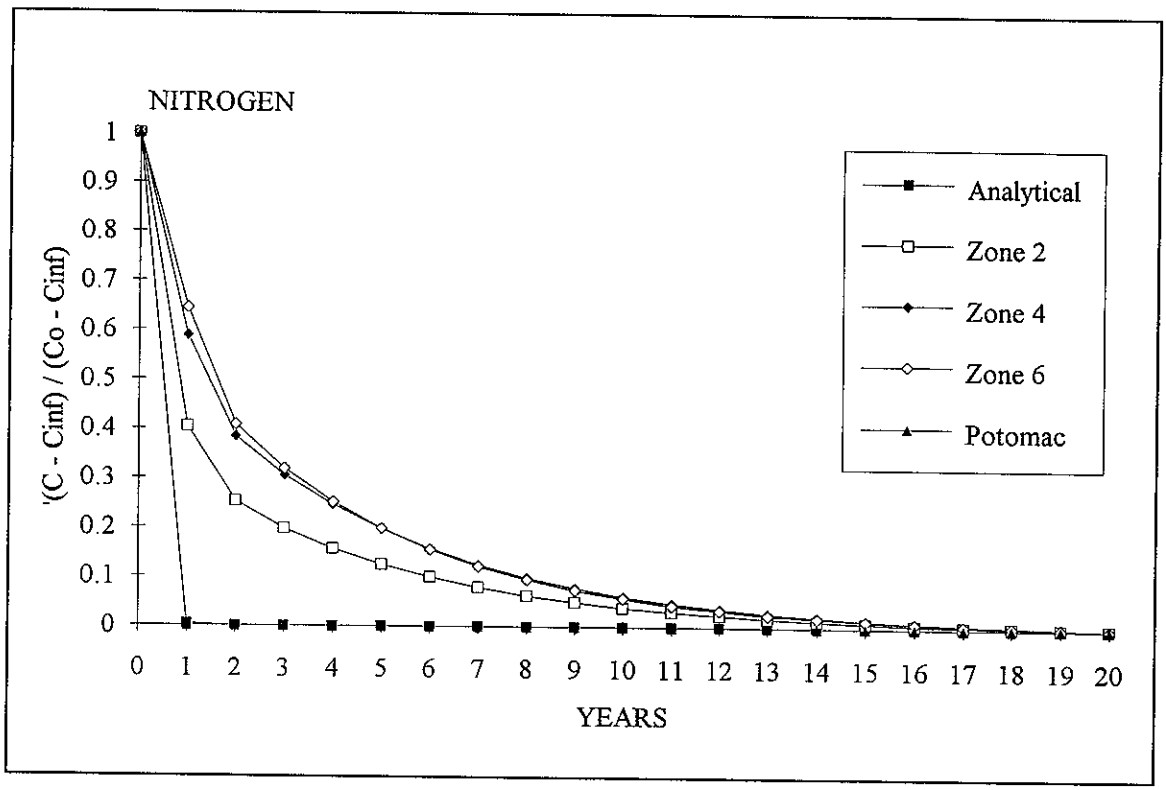

Figure 15-17. Water Column Nitrogen (Depth ≤ 6.7 m) Time to Steady State in Analytical and Coupled Models

examine nature, extent, and time scale of response. In the upper Bay and the Potomac, a transient occurred that temporarily increased sediment phosphate and sediment phosphorus release. In the Potomac, sediments switched from a sink to a source of phosphorus for a period of 16 years (Figure 15-16). Beyond the transient, two time scales appeared in these regions. The first, ≈ 0.05 yr^{-1}, applied to total sediment phosphate, and was equivalent to the burial rate, 0.5 cm yr^{-1}, divided by the thickness of the active sediment layer, 10 cm. The second, ≈ 0.09 yr^{-1}, applied to phosphorus release, and corresponded closely to the decay constant predicted by the analytical model. The analysis did not, however, account for the different time scales of sediment phosphorus concentration and flux. (Perhaps the assumption of instantaneous equilibrium in the surficial sediments was not a good one.) The ultimate effect of the transient was to delay the time to steady state of phosphorus flux beyond the expectation from analysis.

In the middle and lower Bay, negligible change in sediment phosphate occurred (Figure 15-15). These zones demonstrated more noticeable diminishment in phosphorus release (Figure 15-16). A time scale to equilibrium could be identified only for phosphorus release in Zone 4. This time scale was short, however, compared to analysis and to behavior elsewhere in the system (Figure 15-23). Zone 4 achieved complete equilibrium within 15 years. Reasons for the short time scale in the middle Bay were not immediately apparent. The

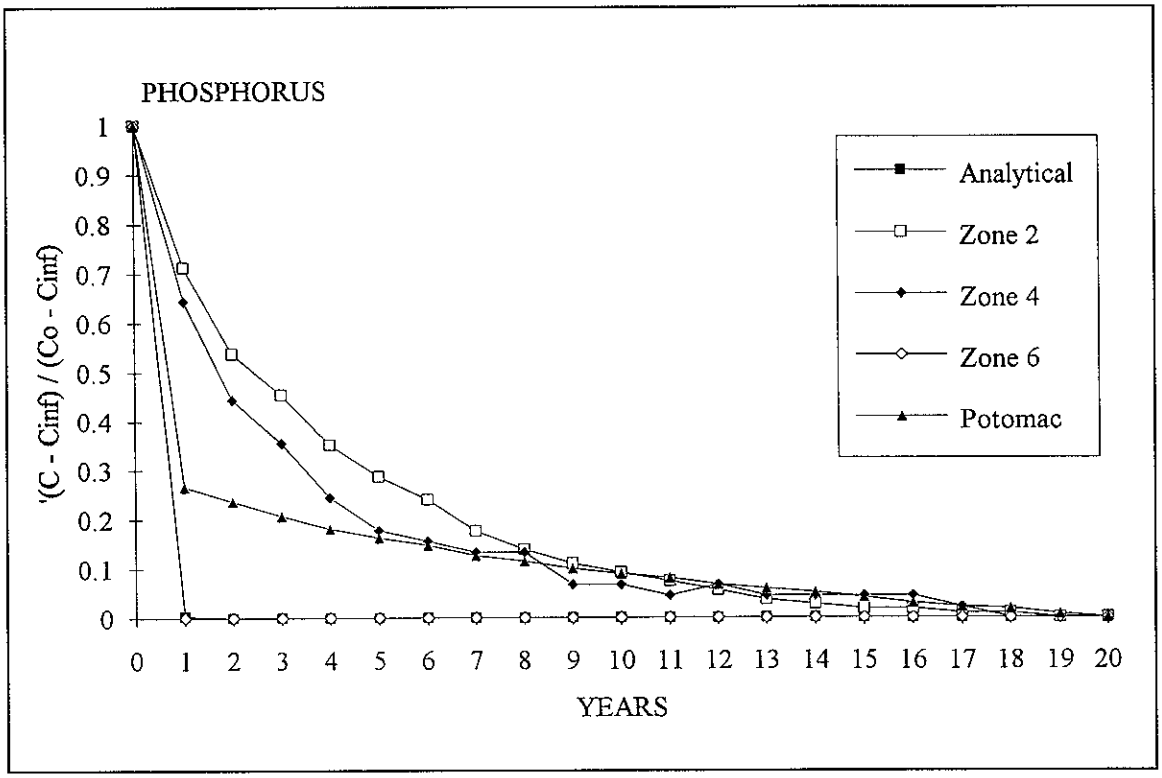

Figure 15-18. Water Column Phosphorus (Depth ≤ 6.7 m) Time to Steady State in Analytical and Coupled Models

region that achieved equilibrium most rapidly was one that was least perturbed, however, suggesting that the time scale for response was associated with the magnitude of the forcing function as well as the properties of the system. Also, the analytical approach ignored phosphorus concentration in the water column which may be significant, relative to the sediments, in the middle and lower Bay.

Scenario Design--Duration, Hydrology, and Hydrodynamics

Design of load-reduction scenarios for the Bay involved numerous considerations. Foremost among these was the duration of the scenarios which was determined by the time for the Bay to respond to load reductions. A second consideration was the dynamic nature of the estuary. Conditions in the estuary respond to a variety of forcing functions which act on time scales of days (e.g. passage of storms) to seasons (e.g. temperature) to years (e.g. hydrology). Information on the range of conditions expected in response to management actions was desirable scenario output.

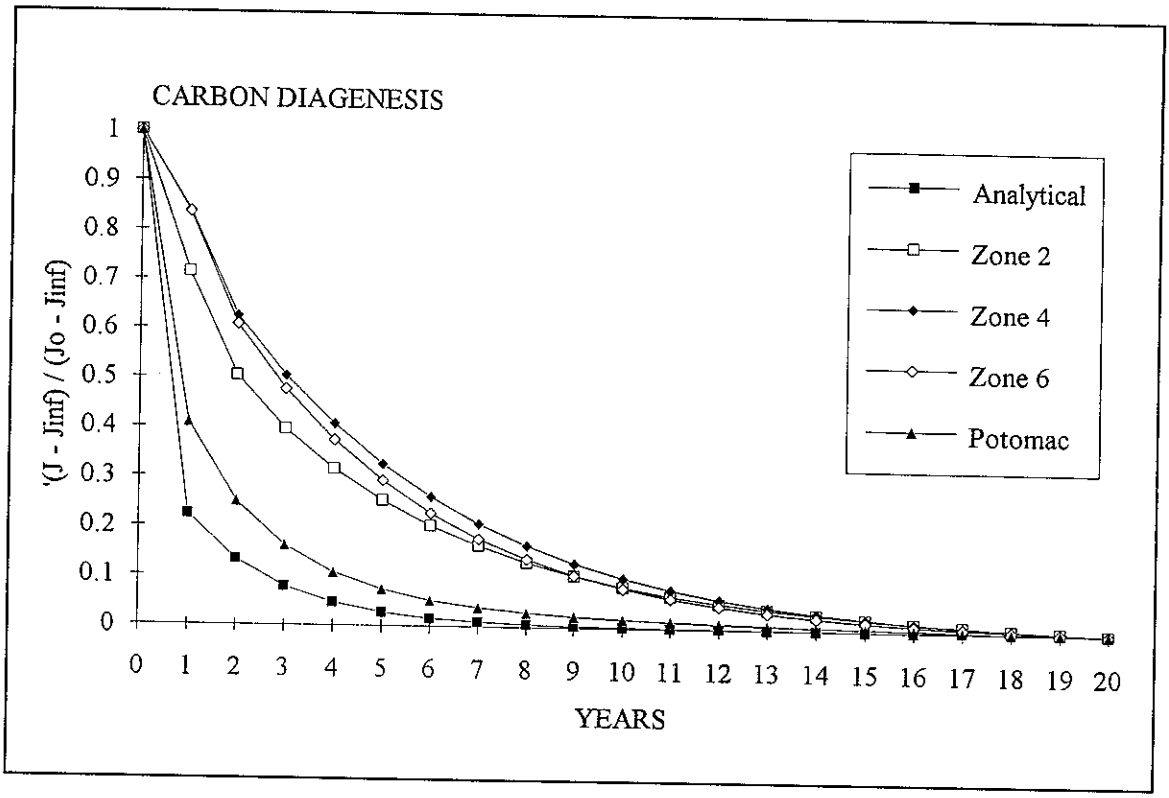

Figure 15-19. Sediment Diagenesis Time to Steady State in Analytical and Coupled Models

Duration of Scenarios

Response of the estuary to load reductions approached completion asymptotically. The rate at which completion was approached depended on the process or substance of interest and on the location within the system. Carbon and nitrogen state variables and processes approached steady state more rapidly than phosphorus. Processes in the upper tributaries approached steady state more rapidly than in the mainstem Bay. The period for a high degree (e.g 99%) of completion of all processes in all locations was multiple decades.

The determination of scenario duration was basically a decision as to when the degree of response to load reductions was sufficiently close to completion. Involved in the decision was a tradeoff between ultimate accuracy of the solution and the number of scenarios to be run within the time available. Running scenarios extensively to a high degree of completion meant that fewer scenarios could be run. The decision also depended on the nature of information desired from the scenario. One goal of the management process was the elimination of anoxia from the Bay. Consequently, the scenarios had to be of sufficient duration to indicate whether this goal was achievable based on the reductions specified in the scenario.

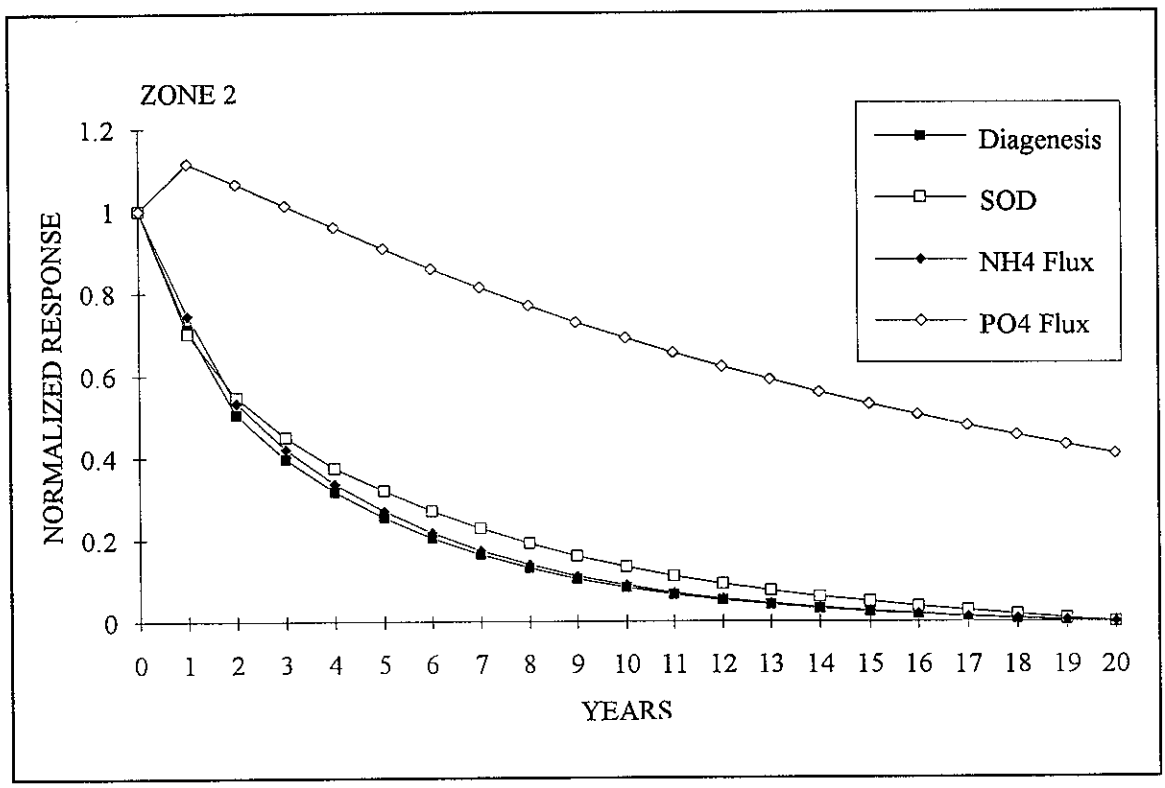

Figure 15-20. Time to Steady State of Sediment Diagenesis, Sediment Oxygen Demand, Sediment Ammonium Release, Sediment-Water Phosphate Flux, Zone 2 Coupled Model

During the model calibration process, empirical investigations of time to steady state and numerous preliminary scenarios were run. Based on these investigations, a ten-year time span was selected for scenario execution. Subsequent, detailed analyses indicated that the ten-year duration allowed water column nitrogen to attain roughly 95% of complete response to load reductions (Figure 15-17). Water column phosphorus attained 90% to 100% of complete response. Degrees of completion of water column chlorophyll (Figure 15-5) and oxygen (Figure 15-10) were in similar ranges. The ten-year duration was employed for all but a few special scenarios for which the highest degree of completion was desired.

Hydrology and Hydrodynamics

Freshwater runoff is a primary determinant of Bay water quality. Runoff at and below the fall lines carries the largest fraction of nutrients introduced to the Bay. Consequently, in wet years, the Bay receives higher nutrient loads than in dry years. Runoff also influences the degree of stratification in the Bay. In wet years, the water column is more highly stratified than in dry years. High stratification diminishes the diffusive supply of atmospheric oxygen to bottom waters and enhances anoxia. Runoff also influences residence

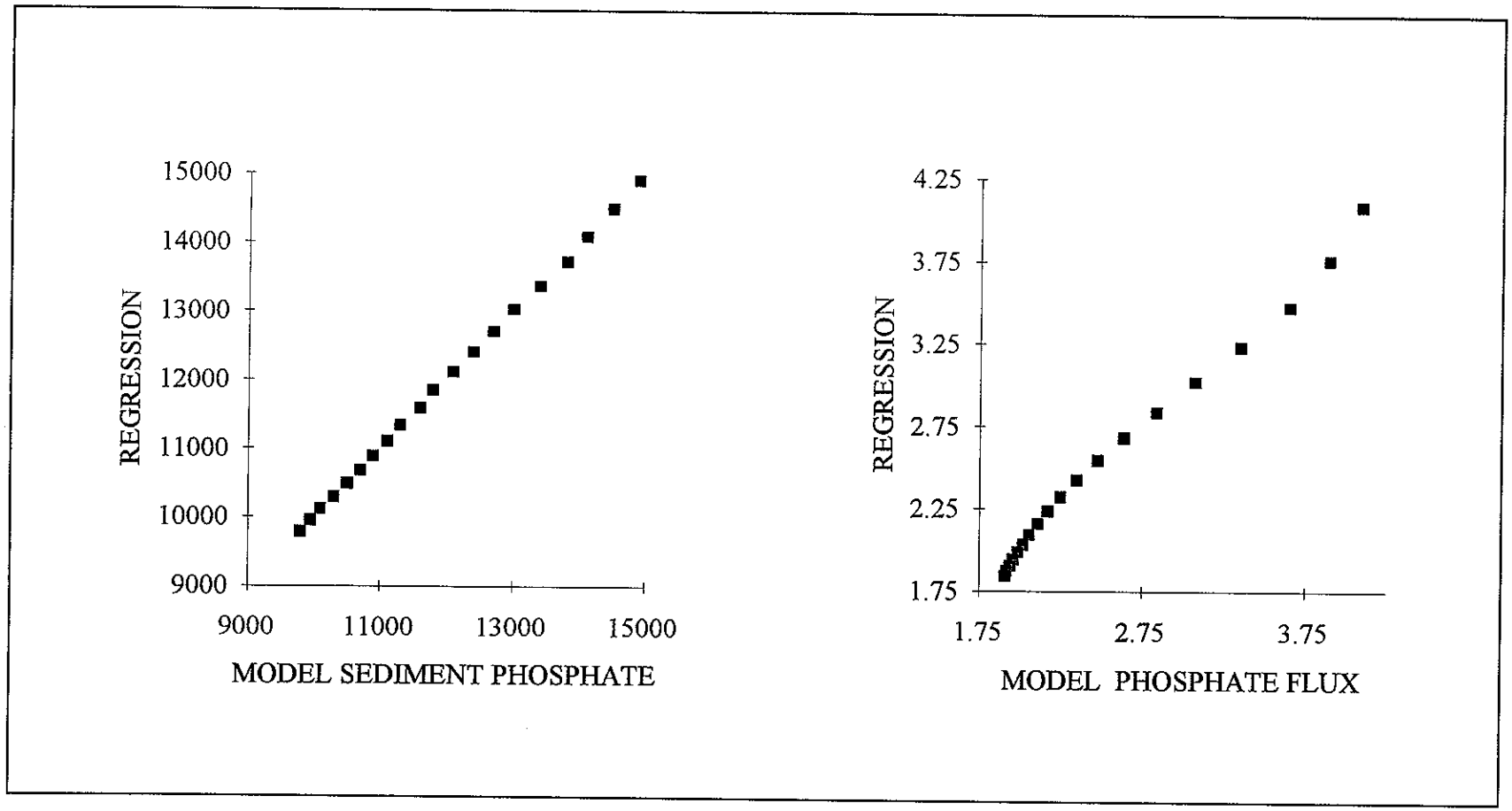

Figure 15-21. Model versus Regression Sediment Phosphate and Sediment Water Phosphate Flux, Zone 2

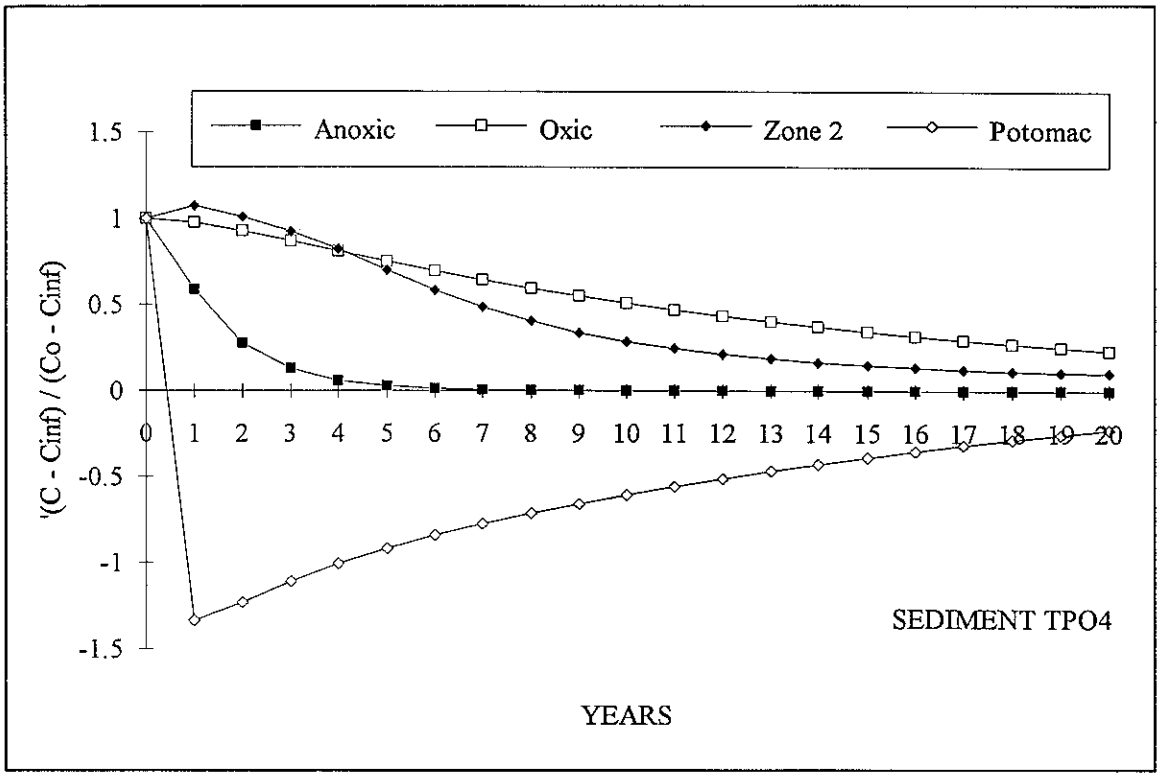

Figure 15-22. Sediment Total Phosphate Time to Steady State in Analytical and Coupled Models

time of the Bay. During wet years, the large volume of runoff moving through the Bay diminishes residence time relative to dry years.

Desire to indicate the direct and indirect influences of hydrology on water quality led to a decision to run the scenarios using variable hydrology. The decade 1979-1988 was selected as providing typical sequence and occurrence of varying annual hydrology. A decade of hydrodynamics was created by sequencing calibration hydrodynamic data sets as in the thirty-year run. Years in the period 1979-1988 were classified as "wet", "average", or "dry" based on annual flow in the Susquehanna. Wet years were at or above the 75th percentile of annual flows in the period of record (Figure 15-26). Average years were between the 25th and 75th percentile. Dry years had flows below the 25th percentile. The 1984 calibration hydrodynamics were employed for "wet" years in the scenarios. Hydrodynamics from 1986 were used to represent "average" years. Modified 1985 hydrodynamics were employed for all "dry" years in the simulation. The modification was necessary to remove from the "dry" hydrodynamics the November 1985 storm which flooded the western tributaries and, to a lesser extent, the Susquehanna. A special hydrodynamic model run was completed in which the storm runoff was removed from the fall-line flows specified as boundary conditions. A listing of hydrologic classification and hydrodynamic data sets employed in scenarios is provided in Table 15-3.

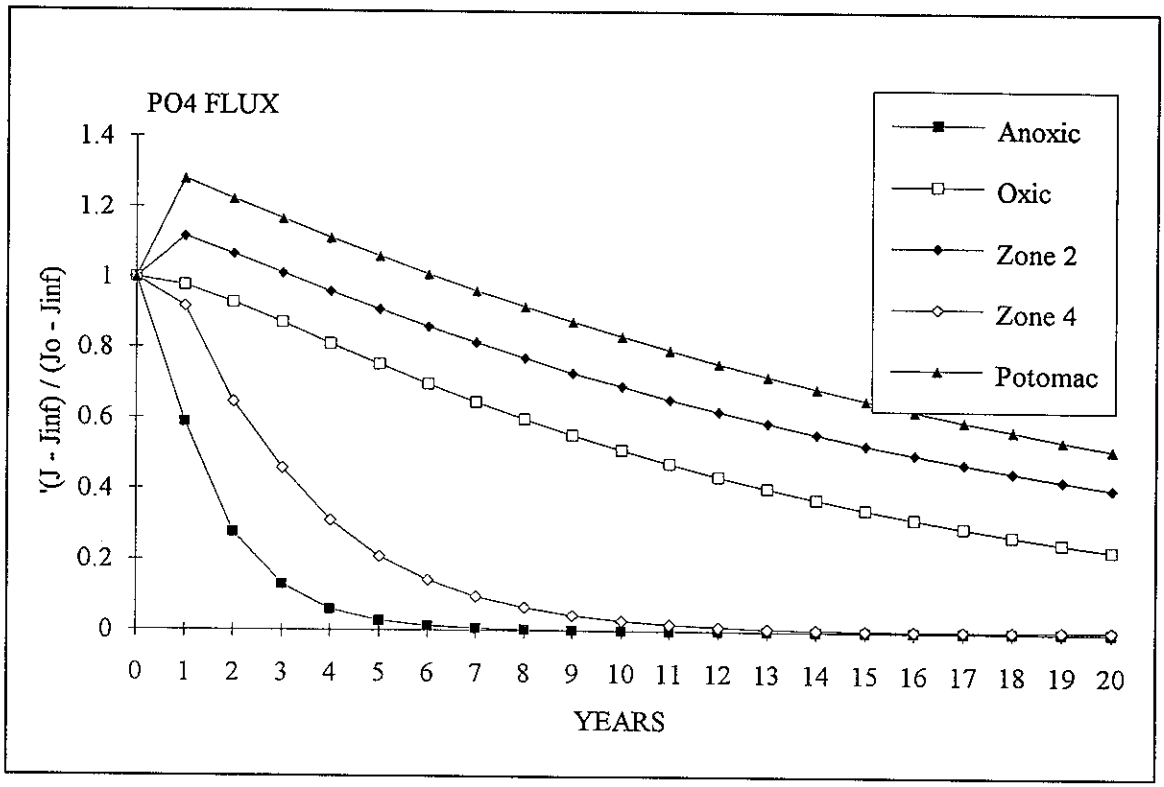

Figure 15-23. Sediment-Water Phosphate Flux Time to Steady State in Analytical and Coupled Models

Scenario Nutrient Loads

Point Sources

Existing

Point-source loads from 1985, identical to the loads used in the model calibration, were employed as existing loads in the scenario process.

Limit-of-Technology

Point-source loads at limit-of-technology (LOT) nutrient removal were supplied by the EPA Chesapeake Bay Program Office. LOT point-source loads were based on the following concentrations:

LOT Point-Source Nutrient Concentrations	
Total Nitrogen	3 gm m^{-3}
Total Phosphorus	0.075 gm m^{-3}

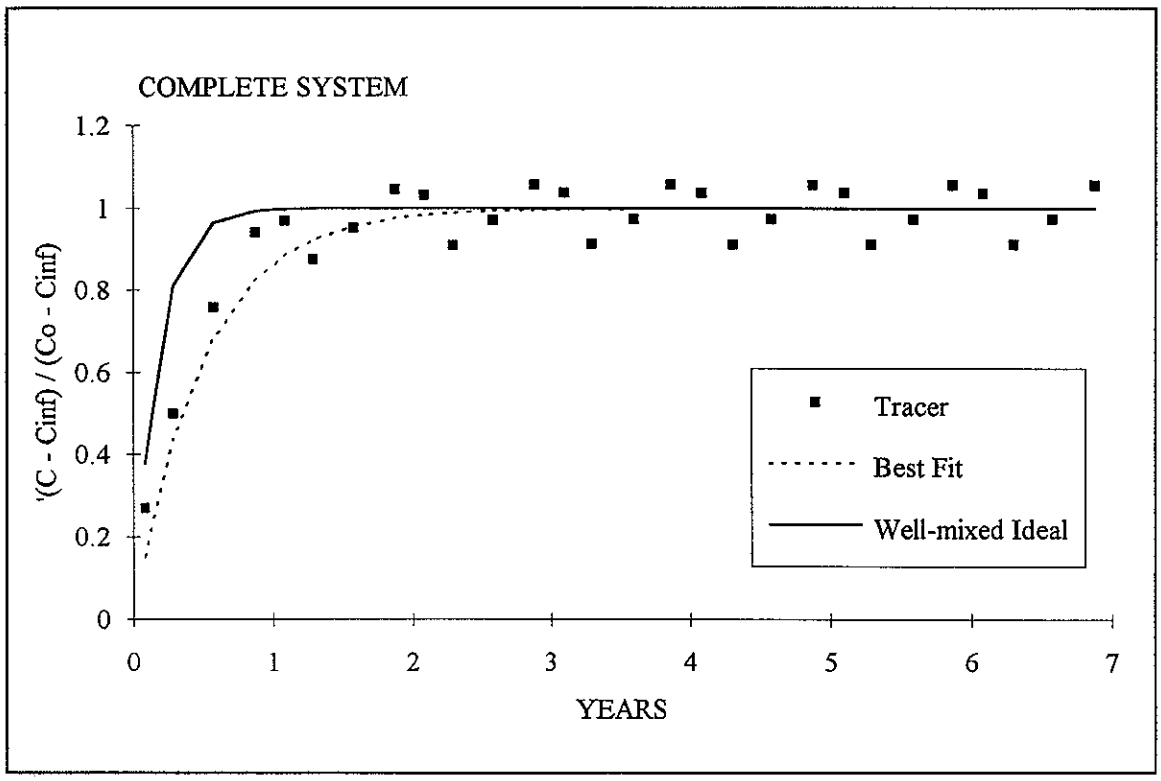

Figure 15-24. Residence Time of Bay in Coupled Model Compared to Analytical Estimate

Total nutrients were split into fractions according to the following protocol:

Nutrient Splits for LOT Point Sources				
Total	**goes to:**	**Fraction**	**Fraction**	**Fraction**
Nitrogen	------>	50% Ammonium	35% Nitrate	15% Organic
Phosphorus	------>	85% Phosphate	15% Organic	

Point-source LOT carbon loads were left at existing levels under the assumption that nutrient removal has no definitive effect on carbon concentration.

The list of point-source dischargers under limit-of-technology conditions differed from the existing list. The LOT list reflected the point sources expected to be on line at the time LOT controls may be implemented. A list of LOT dischargers, loads, and model segments is provided in the Appendix.

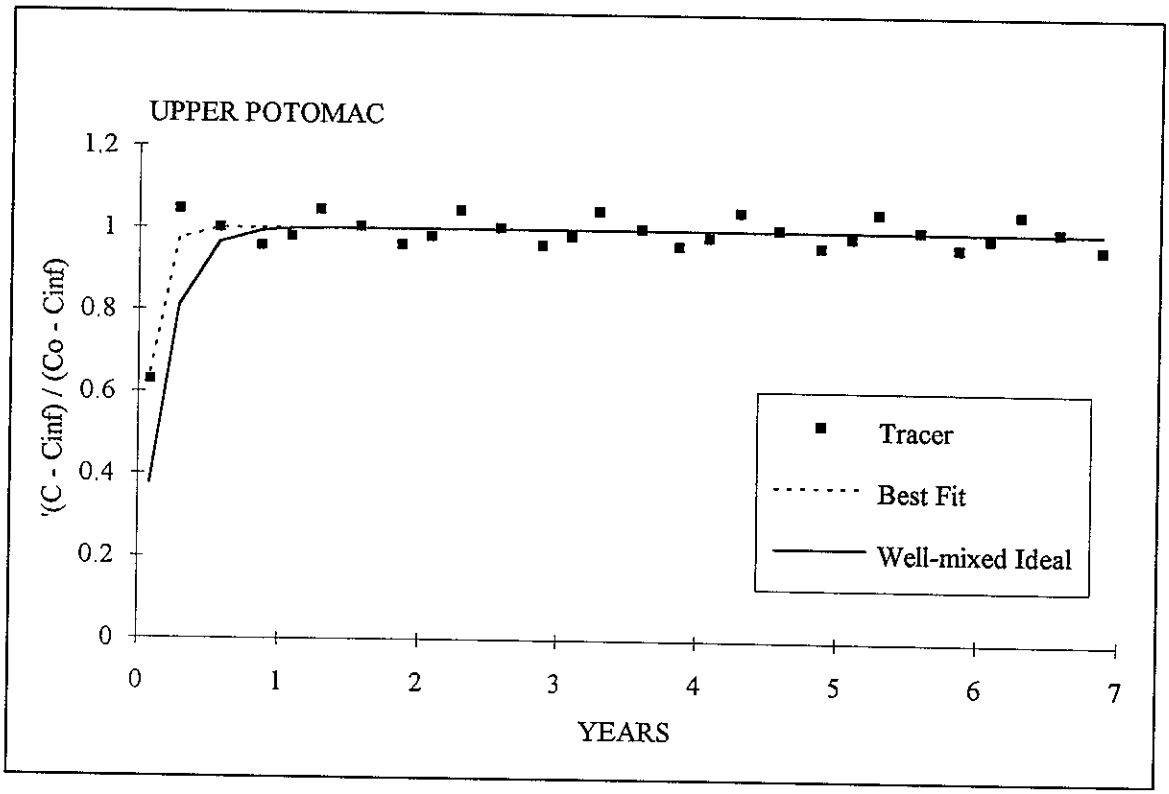

Figure 25. Residence Time of Upper Potomac in Coupled Model Compared to Analytical Estimate

Fall-Line Loads

Existing

Existing fall-line loads for scenarios were obtained from the EPA Phase II Watershed Model (Donigian et al. 1991). Loads for "wet" scenario years were the loads used in model calibration for 1984. Loads for "average" scenario years were the loads used in model calibration for 1986. Loads for "dry" years were largely the loads used in model calibration for 1985. As with hydrodynamics, an adjustment was made to the dry-year loads to remove the autumn 1985 storm. At each fall line, loads from intervals with flows similar to the synthetic dry-year flows were substituted for the storm loads (Table 15-4). Load substitution was also performed on the Appomattox River although the Appomattox is considered a below-fall-line watershed in the coupling of the Water Quality and Watershed Models.

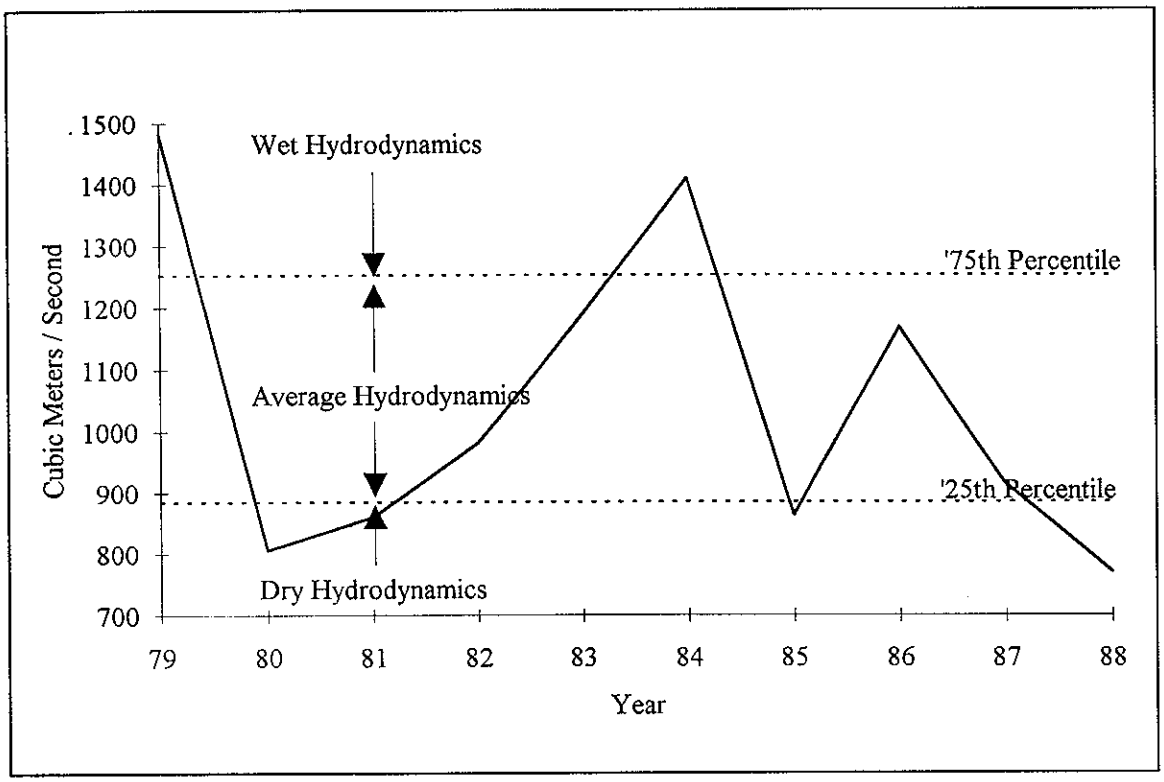

Figure 15-26. Scenario Hydrology and Hydrodynamics

Table 15-3
Scenario Hydrology and Hydrodynamics

Scenario Year	Calendar Year	Hydrology	Hydrodynamics
1	1979	Wet	1984
2	1980	Dry	1985 (modified)
3	1981	Dry	1985 (modified)
4	1982	Average	1986
5	1983	Average	1986
6	1984	Wet	1984
7	1985	Dry	1985 (modified)
8	1986	Average	1986
9	1987	Average	1986
10	1988	Dry	1985 (modified)

Table 15-4
Substitution of Low-Flow Loads for 1985 Storm

River	Loads From	With Flows (m^3 sec^{-1}) in the Range	Were Substituted for Loads From	With Flows (m^3 sec^{-1}) In the Range
James	1984, Julian Days 295-365	96 - 215	1985, Julian Days 295-365	154 - 1360
Mattaponi	1984, Julian Days 295-365	4 - 19	1985, Julian Days 295-365	17 - 100
Pamunkey	1984, Julian Days 295-365	9 - 31	1985, Julian Days 295-365	26 - 163
Rappahannock	1984, Julian Days 295-365	9 - 24	1985, Julian Days 295-365	43 - 312
Potomac	1984, Julian Days 295-365	231 - 613	1985, Julian Days 295-365	80 - 1867
Patuxent	Dry flows were similar to gauged flows. No load substitution was performed.			
Susquehanna	1984, Julian Days 295-336	147 - 508	1985, Julian Days 295-336	337 - 2672
Susquehanna	1984, Julian Days 1-28	488 - 1315	1985, Julian Days 337-365	1099 - 2126
Appomattox	1984, Julian Days 295-365	7 - 17	1985, Julian Days 295-365	32 - 229

Limit-of-Technology

Fall-line loads under LOT conditions were generated by the Watershed Model. The Watershed Model run was based on the application of best management practices to control nonpoint sources of nutrients in the above-fall-line watersheds. These practices included conservation tillage of cropland, removal of highly erodible land from tillage, implementation of structures such as vegetated filter strips, reduction of waste from animal feedlots, and control of urban loads. LOT point-source loads above the fall line were determined as the loads resulting from effluent concentrations of 3 gm m^{-3} total nitrogen, 0.075 gm m^{-3} total phosphorus, and 1 gm m^{-3} BOD.

LOT point-source and nonpoint-source controls were implemented only in jurisdictions covered by the 1987 Chesapeake Bay Agreement (Maryland, Virginia, Pennsylvania, District of Columbia). Loads from portions of the Bay watershed in New York, Delaware, and West Virginia remained at existing levels under LOT controls above the fall line.

The Watershed Model LOT run was based on the same hydrology used to generate the existing 1984-1986 loads. For employment in scenarios, LOT

loads were sequenced according to hydrology and the autumn 1985 storm was removed by substitution of loads from alternate periods.

All-Forested Conditions

A Watershed Model run simulated fall-line loads under all-forested conditions in the Bay watershed. The all-forest run included the entire watershed, not only Bay-agreement jurisdictions. As with existing and LOT fall-line loads, all-forest loads were sequenced according to hydrology and the autumn 1985 storm was removed from the "dry" year loads.

Below-Fall-Line Loads

Existing

Nonpoint-source loads under existing conditions were the 1984-1986 loads provided by the Watershed Model for calibration of the Water Quality Model. Loads for 1984, 1985, and 1986 were assigned to "wet", "dry", and "average" years and sequenced identically to hydrodynamics from those years. Since the autumn 1985 storm passed west of the fall lines of the major tributaries, no correction for the effect of this storm on below-fall-line nonpoint-source loads was necessary except for the Appomattox River.

Limit-of-Technology

Nonpoint-source loads under LOT controls were generated by the same Watershed Model run that generated the fall-line loads. The Watershed Model run was based on the application of best management practices to control nonpoint sources of nutrients in the below-fall-line watersheds. LOT loads for 1984, 1985, and 1986 were assigned to "wet", "dry", and "average" years and sequenced identically to hydrodynamics from those years.

All-Forested Conditions

Nonpoint-source loads under all-forested conditions were generated by the same Watershed Model run that generated the fall-line loads. The Watershed Model run was based on complete coverage by forest of below-fall-line watersheds. All-forest loads for 1984, 1985, and 1986 were assigned to "wet", "dry", and "average" years and sequenced identically to hydrodynamics from those years.

Atmospheric Loads

Atmospheric loads to the water surface under existing and LOT conditions were the 1984-1986 loads employed in calibration of the Water Quality Model. No atmospheric loads to the water surface were considered under all-forested conditions.

Oceanic Nutrient Loads

Although the ocean is not usually considered a load source, the ocean does supply nutrients to the Bay. Nutrient loads to the Bay from the ocean may be considered as gross or net. Gross loads are solely the loads that enter from the ocean. Net loads are loads entering from the ocean less nutrients exported by the Bay to the ocean. Gross loading is always positive into the Bay and is independent of other loads to the system. Net loading may be positive (into the Bay) or negative (out of the Bay) depending on the magnitude of the export relative to the import. Sensitivity studies have shown the export decreases as loads decrease. Consequently, net loading at the mouth is dependent on loading from sources other than the ocean. For scenario analysis, the constant, gross oceanic nutrient load was computed and compared to other nutrient sources. Net loading was reported as a dependent variate: a result of system response to loading and other factors.

The computation of the gross oceanic nutrient load follows from the analysis of Mass-Balance Boundary Conditions (Chapter 8). The quantity of nutrients entering the Bay from the well-mixed volume adjacent to the mouth (Figure 8-3) is:

$$L_t = Q_b C_b \qquad (21)$$

in which:

L_t = total load entering at mouth ($M\ T^{-1}$)

Q_b = volumetric flow from well-mixed volume into Bay ($L^3\ T^{-1}$)

C_b = concentration in well-mixed volume ($M\ L^{-3}$)

Concentration of water entering the Bay is a mixture of concentrations in shelf water and in water leaving the Bay:

$$C_b = \alpha C_u + (1 - \alpha) C_{sh} \qquad (22)$$

in which:

C_u = concentration of water leaving the Bay mouth (M L^{-3})

C_{sh} = concentration of continental shelf water (M L^{-3})

α = proportionality constant

The portion of the entering load that originates on the continental shelf is the product of the flow into the mouth and the fractional concentration attributed to the shelf:

$$L_{sh} = Q_b (1 - \alpha) C_{sh} \quad (23)$$

in which:

L_{sh} = gross load originating on the continental shelf (M T^{-1})

The remainder of the load entering at the mouth, $Q_b \alpha C_u$, is recycled water that has previously left the Bay mouth. This mass is not considered in the gross load.

Variates that make up the computation of gross shelf load are presented in Table 15-5. Loads for wet, dry, and average years are tabulated along with scenario loads.

Table 15-5
Computation of Oceanic Nutrient Loads

Hydrology	Qb (m^3 sec^{-1})	Total Nitrogen (gm m^{-3})	(1 - α)	Load (gm sec^{-1})	Load (kg day^{-1})
Wet	13800	0.37	0.38	1940	168000
Dry	13000	0.37	0.38	1830	158000
Average	13500	0.37	0.38	1900	164000
Hydrology	**Qb (m^3 sec^{-1})**	**Total Phosphorus (gm m^{-3})**	**(1 - α)**	**Load (gm sec^{-1})**	**Load (kg day^{-1})**
Wet	13800	0.053	0.38	278	24000
Dry	13000	0.053	0.38	262	22600
Average	13500	0.053	0.38	272	23500

Load Summary

Existing

Sensitivity analyses showed eutrophication processes were insensitive to variations in external loads of oxygen-demanding material. Carbon formed internally, through primary production, was by far the major source of oxygen demand in the system. Consequently, load summaries focus on nutrients that support primary production.

Existing nutrient loads to the Bay are summarized for "wet", "dry", and "average" years and as a ten-year average (Table 15-6). The ten-year average is for the mix of hydrologies employed in the scenarios (Table 15-3). Under existing conditions, the major nitrogen source to the system is fall-line loading (Figure 15-27). The second largest nitrogen source is gross loading from the ocean. In a dry year, the oceanic source is equivalent to the fall-line load. Averaged over a decade, point sources are the next largest source of nitrogen although below-fall-line nonpoint sources exceed point sources in a wet year. Atmospheric nitrogen sources are the least of the loads.

For phosphorus, the role of the oceanic source is striking (Figure 15-28). Gross loading from the ocean is by far the major phosphorus source in average and dry years and rivals fall-line loads in wet years. Averaged over a

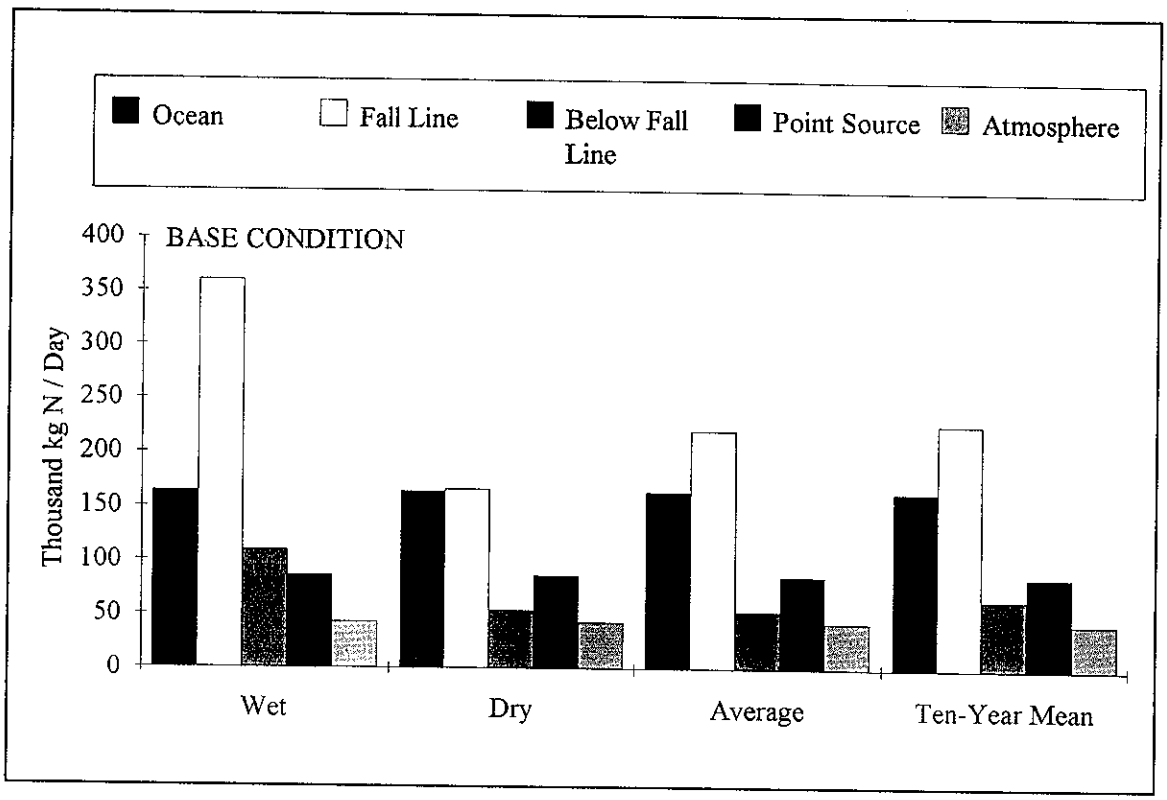

Figure 15-27. Scenario Nitrogen Loads Under Existing Conditions

Table 15-6
Scenario Nutrient Loads (kg day^{-1}) for Existing Conditions

Nitrogen	Wet	Dry	Average	Ten-Year Mean
Fall Line	360,463	166,182	220,823	226,895
Below Fall Line	109,824	53,971	53,208	64,836
Point Source	86,357	86,357	86,357	86,357
Atmosphere	43,025	43,025	43,025	43,025
Total	599,669	349,535	403,413	421,113
Ocean	164,000	164,000	164,000	164,000
Total	763,669	513,535	567,413	585,113
Phosphorus	**Wet**	**Dry**	**Average**	**Ten-Year Mean**
Fall Line	25,792	11,584	13,050	15,012
Below Fall Line	6,386	5,142	3,779	4,846
Point Source	7,359	7,359	7,359	7,359
Atmosphere	1,823	1,823	1,823	1,823
Total	41,360	25,908	26,011	29,040
Ocean	23,500	23,500	23,500	23,500
Total	64,860	49,408	49,511	52,540

decade,fall-line loading is the second largest phosphorus source, followed by point-source loading. Below-fall-line nonpoint sources are less than point sources under all hydrologic conditions and atmospheric loading is least of all.

Limit-of-Technology

Under LOT conditions, the fall line remains the largest nitrogen source to the system (Table 15-7, Figure 15-29) although the ocean is dominant in "dry" hydrology. The major difference between LOT and existing loads is that point sources decline to the least of the load sources. Not surprisingly, the largest load reduction, on absolute (Figure 15-30) and percent bases (Figure 15-31), comes from the point sources. The second largest reduction, in absolute terms, is from fall-line loads. The least absolute load reduction is from below-fall-line nonpoint sources. On a percentage basis, reductions in fall-line and below-fall-line loads are roughly equivalent but much less than point-source reductions.

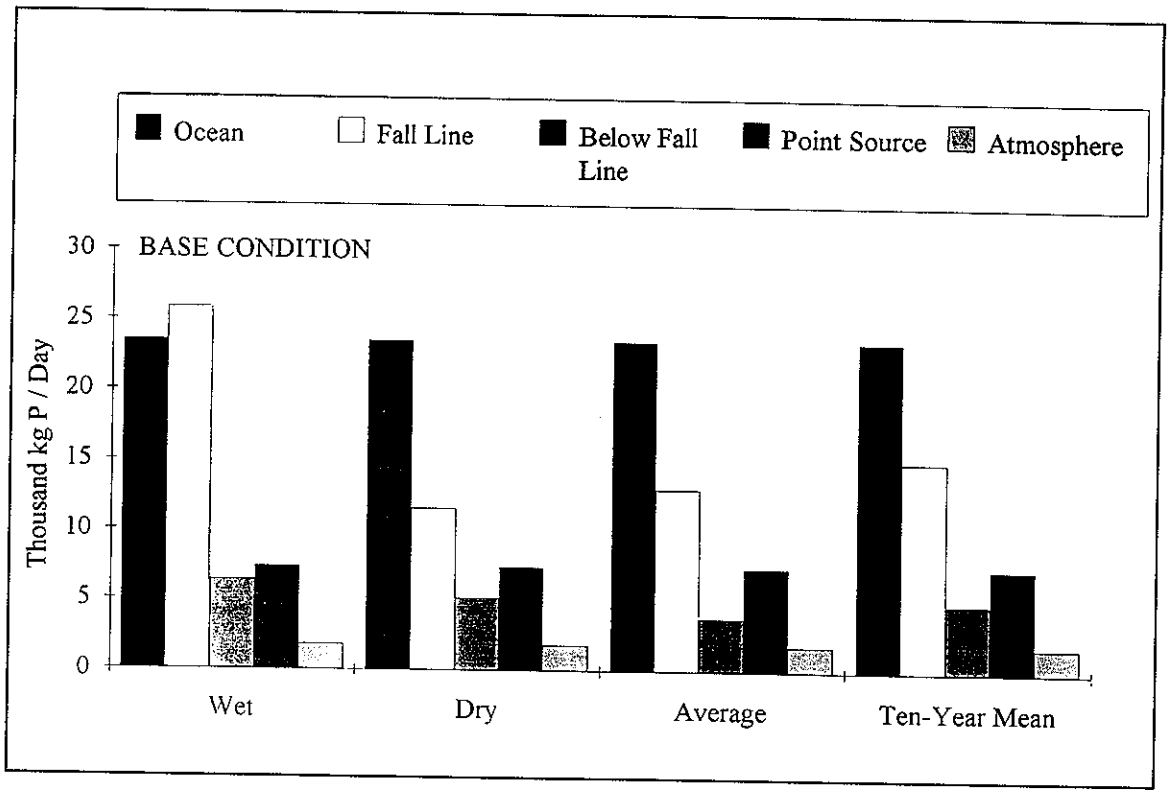

Figure 15-28. Scenario Phosphorus Loads Under Existing Conditions

The dominant role of the ocean in phosphorus loading is magnified in LOT scenarios (Figure 15-32) relative to existing conditions. Fall-line loads remain the second largest phosphorus source. As with nitrogen, point sources are the smallest load fraction under LOT conditions. Absolute load reductions from fall lines and point sources are roughly equivalent (Figure 15-33) although the largest percentage comes from point sources (Figure 15-34). Least load reductions come from below-fall-line nonpoint sources.

All-Forest Conditions

The relative roles of oceanic and fall-line nitrogen loads reverse under all-forest conditions (Table 15-8, Figure 15-35). The ocean is the largest nitrogen source. Below-fall-line nonpoint sources are the least load source. Point sources and atmospheric loads do not exist under all-forest conditions. Examination of the difference between all-forest and existing nitrogen loads indicates the largest excess over all-forest loads occurs in the fall-line category (Figure 15-36). The next largest excess is in point source loads. Excess below-fall-line and atmospheric loads are roughly equivalent. On a percentage basis, all-forest fall-line nitrogen loads are roughly half existing loads (Figure 15-37) while all-forest below-fall-line loads are less than half existing loads.

Table 15-7
Scenario Nutrient Loads (kg day^{-1}) Under Limit-of-Technology Controls

Nitrogen	Wet	Dry	Average	Ten-Year Mean
Fall Line	301,733	140,227	186,722	191,126
Below Fall Line	87,772	43,629	42,371	51,954
Point Source	13,153	13,153	13,153	13,153
Atmosphere	43,025	43,025	43,025	43,025
Total	445,683	240,034	285,271	299,259
Ocean	164,000	164,000	164,000	164,000
Total	609,683	404,034	449,271	463,259
Phosphorus	**Wet**	**Dry**	**Average**	**Ten-Year Mean**
Fall Line	16,165	5,971	6,712	8,306
Below Fall Line	4,359	3,245	2,524	3,179
Point Source	274	274	274	274
Atmosphere	1,823	1,823	1,823	1,823
Total	22,621	11,313	11,333	13,583
Ocean	23,500	23,500	23,500	23,500
Total	46,121	34,813	34,833	37,083

Under all-forest conditions, fall-line and below-fall-line phosphorus loads virtually disappear compared to the oceanic source (Figure 15-38). All-forest

loads in these categories are roughly ten percent of existing loads (Figure 15-40). Point-source and atmospheric loads do not exist. When existing and all-forest loads are compared, existing fall-line loads represent the largest excess over all-forest conditions (Figure 15-39). Existing point-source loads represent the next largest excess.

Scenario Descriptions

Introduction

Two categories of scenarios were performed. "Management Scenarios" were aimed primarily at determining the response of the Bay to feasible ranges of nutrient controls. "Response Scenarios" were aimed at examining the behavior of the Bay under a wide range of nutrient loads, many of which fell outside the range of feasibility. Management scenarios were specified by the

Table 15-8
Scenario Nutrient Loads (kg day^{-1}) Under All-Forest Conditions

Nitrogen	Wet	Dry	Average	Ten-Year Mean
Fall Line	157,406	84,273	116,211	111,675
Below Fall Line	31,661	21,896	20,793	23,408
Point Source	0	0	0	0
Atmosphere	0	0	0	0
Total	189,067	106,169	137,004	135,083
Ocean	164,000	164,000	164,000	164,000
Total	353,067	270,169	301,004	299,083
Phosphorus	**Wet**	**Dry**	**Average**	**Ten-Year Mean**
Fall Line	2,460	787	646	1,065
Below Fall Line	430	381	284	352
Point Source	0	0	0	0
Atmosphere	0	0	0	0
Total	2,890	1,168	930	1,417
Ocean	23,500	23,500	23,500	23,500
Total	26,390	24,668	24,430	24,917

Chesapeake Bay Program Office and its Model and Research Subcommittee. A description of these scenarios is in the present chapter. Analysis of the management scenarios was the subject of a report published by the CBPO (Modeling Subcommittee 1993) and is not repeated here. An exception is presentation of the "Limit-of-Technology Nutrient Control" scenario which is of special interest.

Management Scenarios

Base Scenario. The Base Scenario specified existing conditions in the Bay. It was run with the model exactly as calibrated for 1984-1986 and with loads from that period. The Base Scenario provided the datum against which water quality improvements due to load reductions were determined.

Ninety-Percent Load Reduction. In this scenario existing fall-line, below-fall-line, and point-source loads of nitrogen, phosphorus, and carbon were reduced by ninety percent. Atmospheric nutrient loads were eliminated. The primary purpose of this scenario was to test the response of the model to

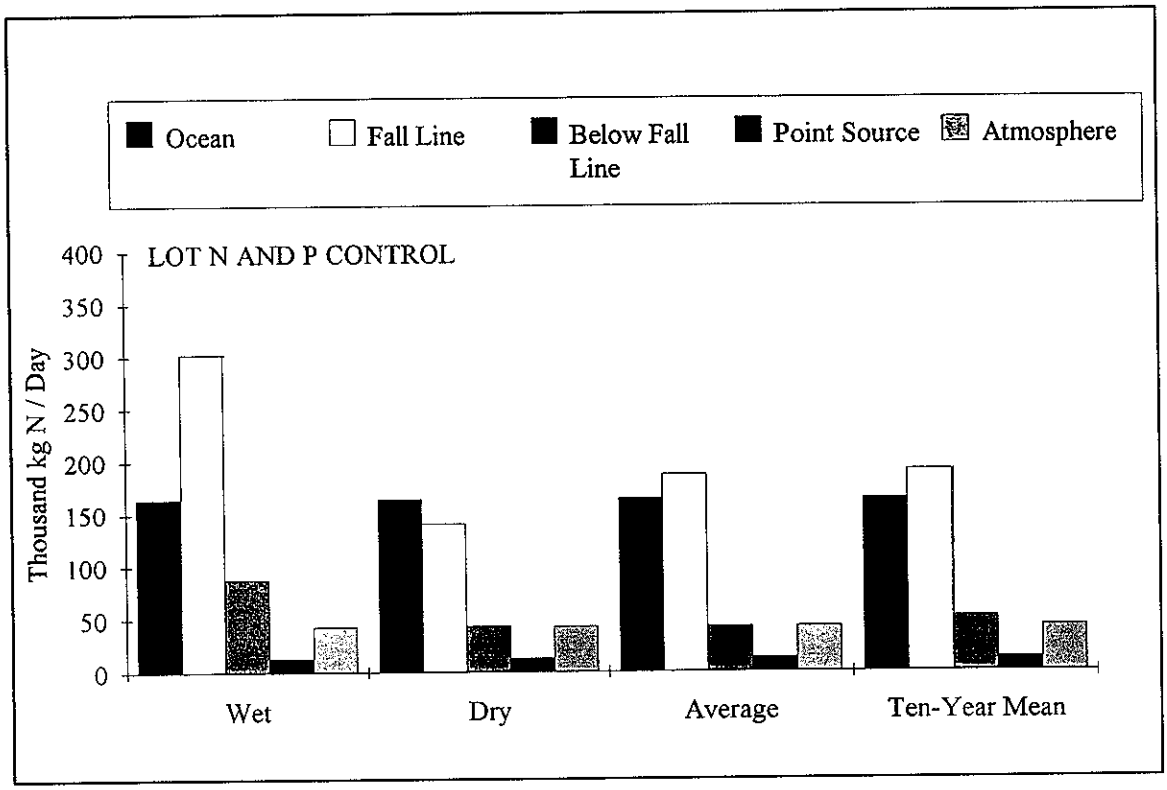

Figure 15-29. Scenario Nitrogen Loads Under Limit-of-Technology Controls

extreme nutrient load reductions. These reductions were well outside the feasible range. The scenario also indicated the maximum improvement that could be expected in Bay water quality and doubled as one of the response scenarios.

Forty-Percent Reduction in Controllable Nitrogen and Phosphorus Loads. This scenario examined the response of the Bay to load reductions specified in the 1987 Chesapeake Bay Agreement completed by the executive officers of the major Bay watershed jurisdictions (Maryland, Virginia, Pennsylvania, District of Columbia). Controllable loads were defined as loads in excess of loads from an all-forested watershed in these jurisdictions . Loads from the portions of the Bay watershed in New York, Delaware, and West Virginia were considered non-controllable and remained at base levels. Reduced loads were determined by the relationship:

$$SL = AF + (1 - FR)(BASE - AF) \quad (24)$$

in which:

SL = scenario load

AF = all-forested load

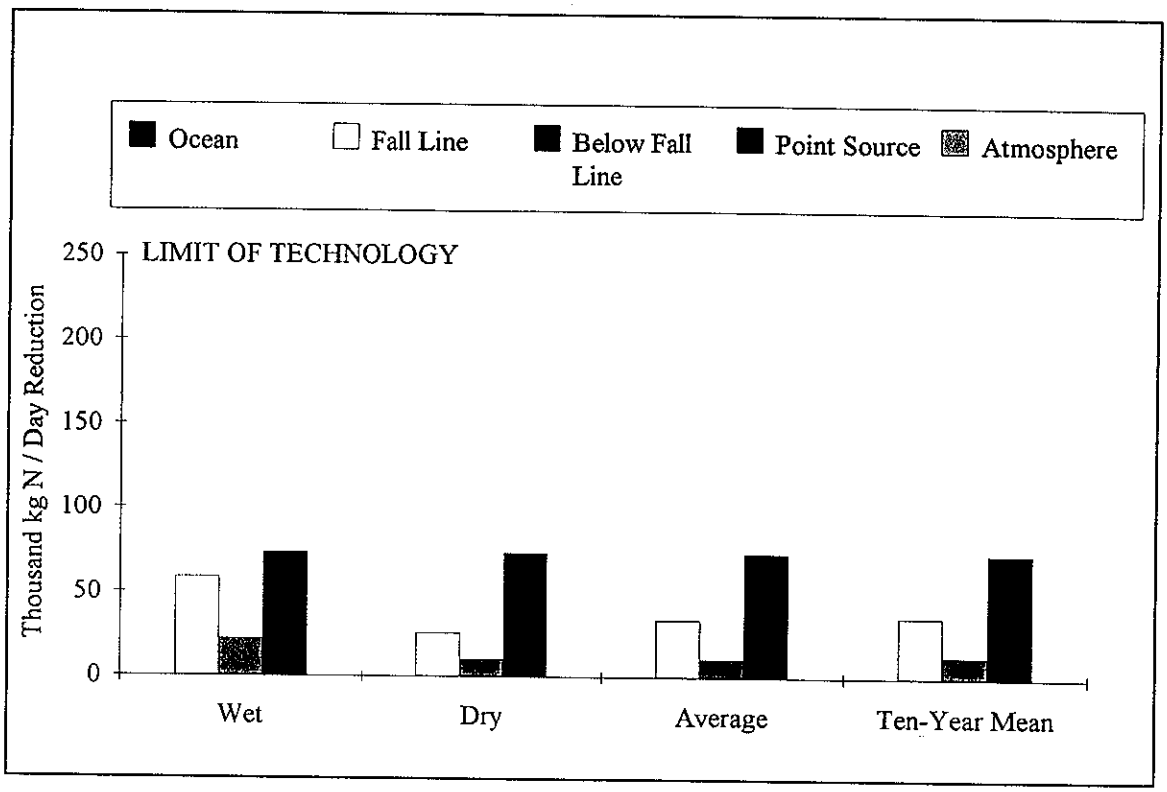

Figure 15-30. Absolute Nitrogen Load Reductions Under Limit-of-Technology Controls

FR = fraction load reduction (= 0.4)

$BASE$ = existing load

The relationship expressed in Equation 24 was applied to all forms of nitrogen, phosphorus, and carbon at each fall line, at each point source, and in each model cell receiving nonpoint-source loading. All-forested (in Bay agreement jurisdictions) fall-line and below-fall-line loads were provided by a run of the EPA's Chesapeake Bay Watershed Model (Donigian et al. 1991). Point-source loads under all-forest conditions were considered zero. Atmospheric nutrient loads remained at existing levels.

Limit-of-Technology Nitrogen and Phosphorus Loads. The Limit-of-Technology scenario was performed using loads described in a previous section of the present chapter. The LOT scenario represents the optimal condition that can be obtained through management controls of point-source and nonpoint-source nutrient loads above and below the Bay fall lines, within Bay-agreement jurisdictions.

Limit-of-Technology Nitrogen Control. For this scenario, LOT nitrogen controls were implemented above the fall line in Bay-agreement jurisdictions and universally below the fall line. Loads provided in the Watershed Model output were routed into Water Quality Model Input decks. Below-fall-line

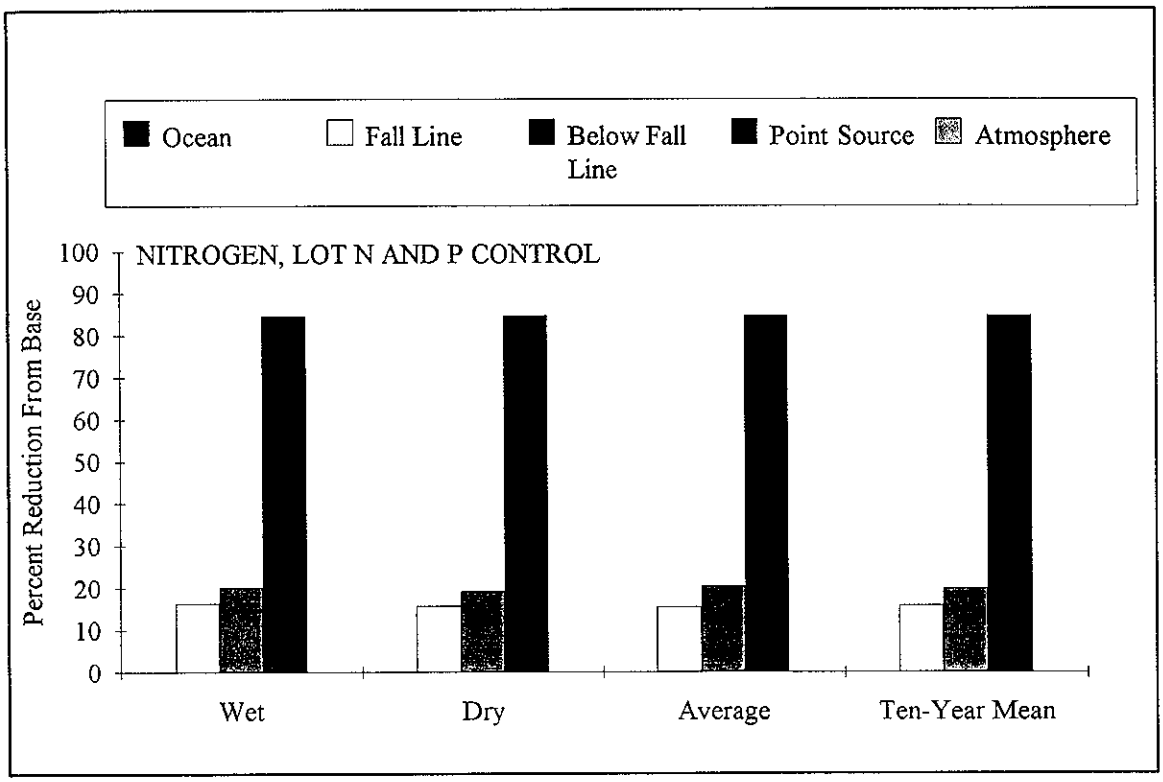

Figure 15-31. Percent Nitrogen Load Reductions Under Limit-of-Technology Controls

point-source nitrogen loads from the LOT Scenario were paired with existing phosphorus loads from the Base Scenario. This scenario included phosphorus load reduction that occurred as a by-product of nonpoint-source nitrogen controls.

Limit-of-Technology Phosphorus Control. For this scenario, LOT phosphorus controls were implemented above the fall line in Bay-agreement jurisdictions and below the fall line. Watershed Model output was routed into Water Quality Model input. Below-fall-line point-source phosphorus loads from the LOT Scenario were paired with existing nitrogen loads from the Base Scenario. Analogous to the LOT nitrogen control scenario, diminished nitrogen loads occurred as a by-product of phosphorus controls.

Regional LOT Nutrient Control: Region I. This was the first of several scenarios that investigated the effect of regional nutrient controls. Three region were defined:

Region I: Conowingo Dam to Above Back River,
Region II: Back River to Above Rappahannock River,
Region III: Rappahannock River to Bay Mouth.

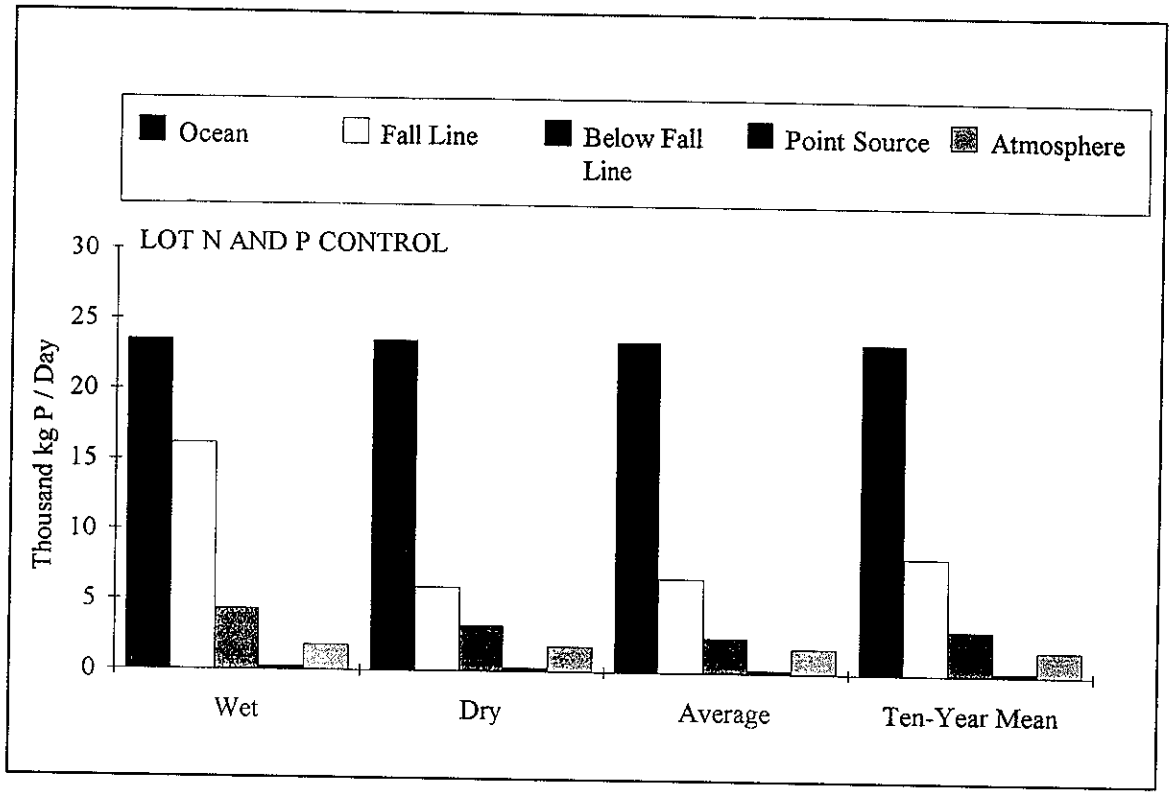

Figure 15-32. Scenario Phosphorus Loads Under Limit-of-Technology Controls

In each regional run, fall-line loads in tributaries to the region, below-fall-line loads within the region and point-source loads within the region were subjected to LOT nutrient controls. Fall-line loads and below-fall-line nonpoint-source loads were computed through implementation of controls in appropriate watersheds of the Watershed Model. For the Region I LOT scenario, controls were implemented in the portion of the Susquehanna watershed represented by Bay-agreement jurisdictions and in one below-fall-line Chesapeake Bay watershed.

Regional LOT Nutrient Control: Region II. For the Region II LOT Scenario, controls were implemented above fall line in the Patuxent and Potomac Rivers and along the Bay and tributary shoreline from above the Back River to below the Potomac River. Point-source load reductions included the Baltimore and Washington metropolitan areas.

Regional LOT Nutrient Control: Region III. For the Region III LOT Scenario, controls were implemented above fall line in the Rappahannock, Mattaponi, Pamunkey, Appomattox, and James Rivers and along the Bay and tributary shoreline from above the Rappahannock entrance to the Bay mouth. Point-source load reductions included the Richmond and Hampton Roads metropolitan areas.

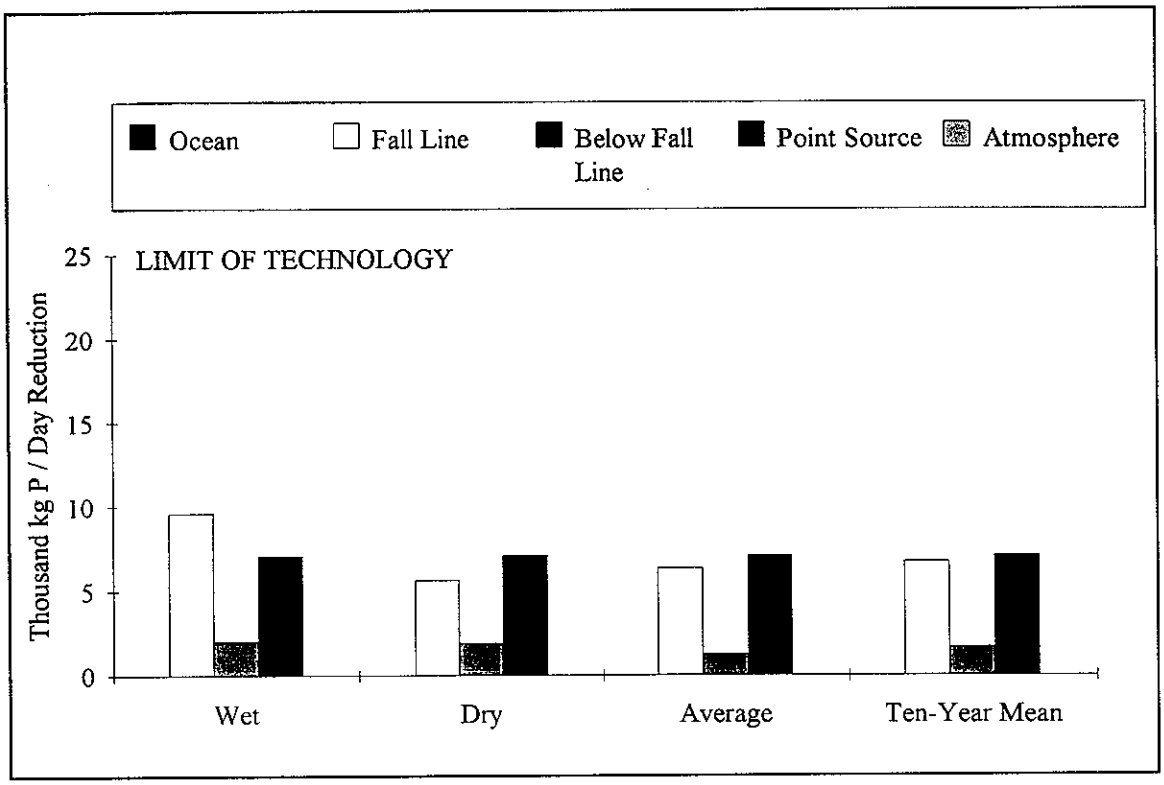

Figure 15-33. Absolute Phosphorus Load Reductions Under Limit-of-Technology Controls

Ninety-Percent Phosphorus Load Reduction. In this scenario, all phosphorus loads to the system, including atmospheric loads, were reduced ninety percent. This run was performed to examine the limit of Bay response to phosphorus load reductions. A ninety-percent phosphorus reduction is beyond the range of feasibility. This run doubled as one of the Response Scenarios.

Forty-Percent Reduction in Controllable Nitrogen and Phosphorus Loads Plus Clean Air Act. In this scenario, a reduction in controllable loads from Bay-agreement jurisdictions was supplemented with a reduction in nitrogen loads estimated by the CBPO to result from implementation of the Clean Air Act. Atmospheric nitrate loads to the water surface were reduced fourteen percent. Nitrate loads at fall lines were reduced two to nine percent. The overall additional reduction in nitrogen loads was roughly three percent.

Forty-Percent Reduction in Controllable Nitrogen and Phosphorus Loads From Entire Watershed Plus Clean Air Act. This scenario was identical to the previous scenario except the forty-percent reduction in controllable nitrogen and phosphorus loads was not limited to Bay-agreement jurisdictions. The reduction was implemented throughout the Bay watershed. As previously, controllable loads were defined as loads in excess of loads from an all-forested watershed.

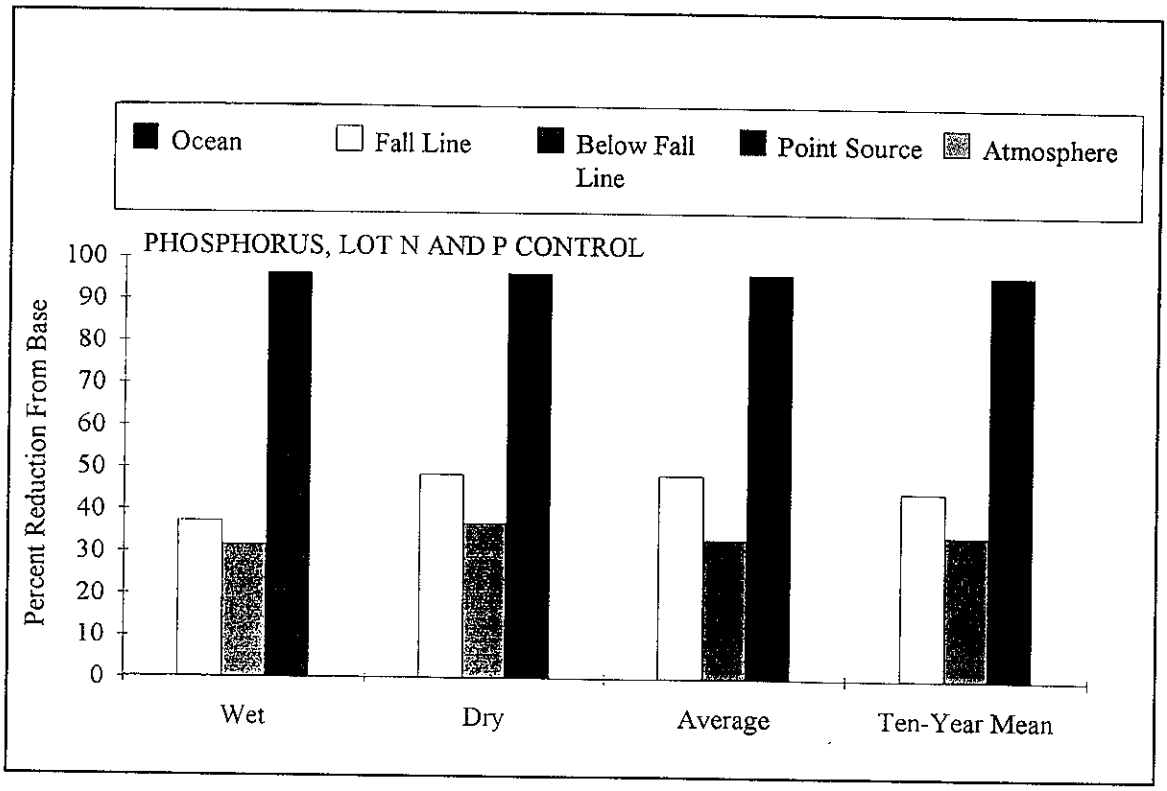

Figure 15-34. Percent Phosphorus Load Reductions Under Limit-of-Technology Controls

Regional LOT Nutrient Control: Region IIa. This scenario was identical to the Region II LOT scenario except the fall-line, below-fall-line, and point-source loads in the Potomac were excluded from controls.

Biological Nutrient Removal at Point Sources, LOT Controls on Nonpoint Sources. In this scenario, biological nutrient removal was simulated at above- and below-fall-line point sources. Due to the nature of the biological nutrient removal process, this scenario amounted to seasonal controls on point source nitrogen discharges. Nitrogen loads were reduced for the months May through November. Year-round point-source phosphorus controls were implemented. Above-and below-fall-line nonpoint sources were subjected to LOT control actions.

Management Scenario II. In this scenario, a variety of management actions were combined according to guidelines developed from previous scenarios. In Region I, loads were first reduced by 73% of the improvement expected from LOT nutrient controls:

$$SL = LOT + (1 - FR)(BASE - LOT) \qquad (25)$$

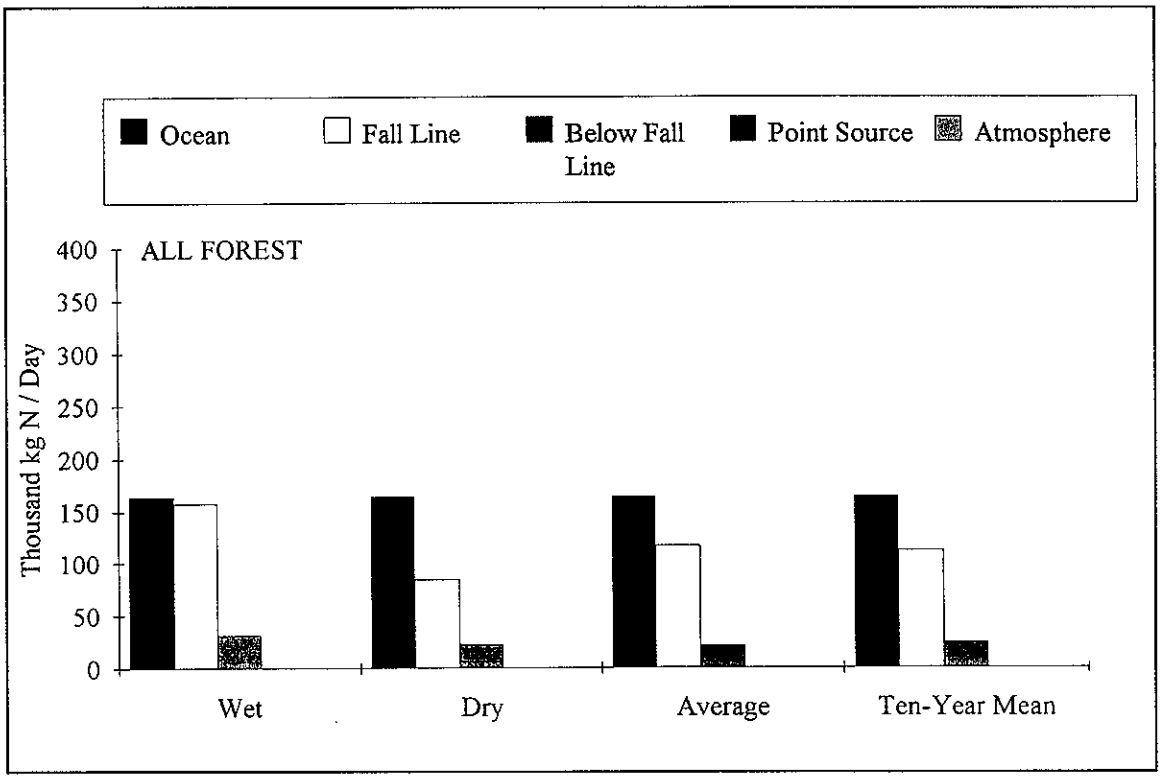

Figure 15-35. Scenario Nitrogen Loads Under All-Forest Conditions

in which:

SL = scenario load

LOT = limit-of-technology load

FR = fraction load reduction (= 0.73)

BASE = existing load

Next, additional quantities of nitrate, specified by the Chesapeake Bay Program Office, were subtracted from the Region I load to account for effects of the Clean Air Act.

In Region II, a process identical to Region I was carried out except the fraction reduction, FR, was 0.72. In Region III, loads from Scenario 12, the Forty-Percent Reduction in Controllable Nitrogen and Phosphorus Loads Plus Clean Air Act Scenario, were implemented. Atmospheric nitrogen loads to the water surface were reduced ten percent.

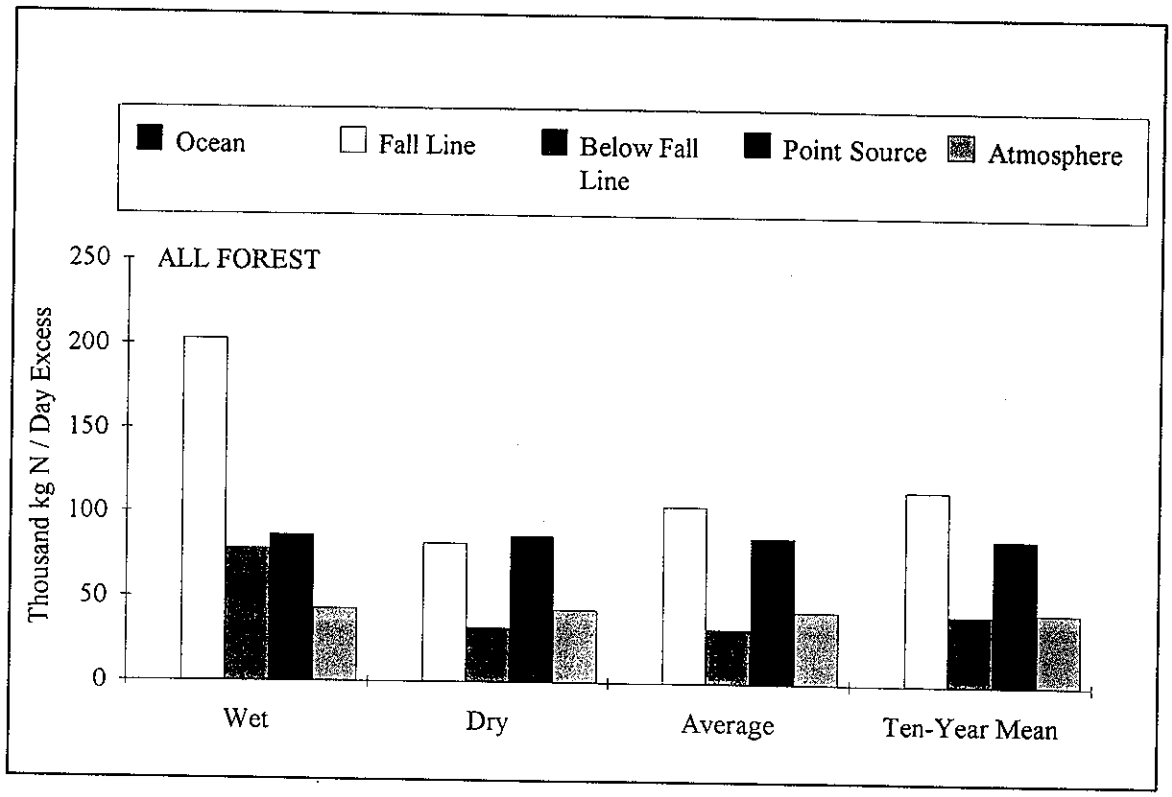

Figure 15-36. Excess of Existing Nitrogen Loads Over All-Forest Conditions

Response Scenarios

Nitrogen Load Reductions. Nitrogen loads to the system were reduced thirty, sixty, and ninety percent in three scenarios. Load reductions were taken uniformly from fall-line loads, below-fall-line loads, point-source loads, and atmospheric loads. For these scenarios, the ocean was not considered a loading source.

Phosphorus Load Reductions. Phosphorus loads to the system were reduced thirty, sixty, and ninety percent in three scenarios. Load reductions were taken uniformly from fall-line loads, below-fall-line loads, point-source loads, and atmospheric loads. For these scenarios, the ocean was not considered a loading source. The ninety-percent phosphorus reduction doubled as one component of the management suite.

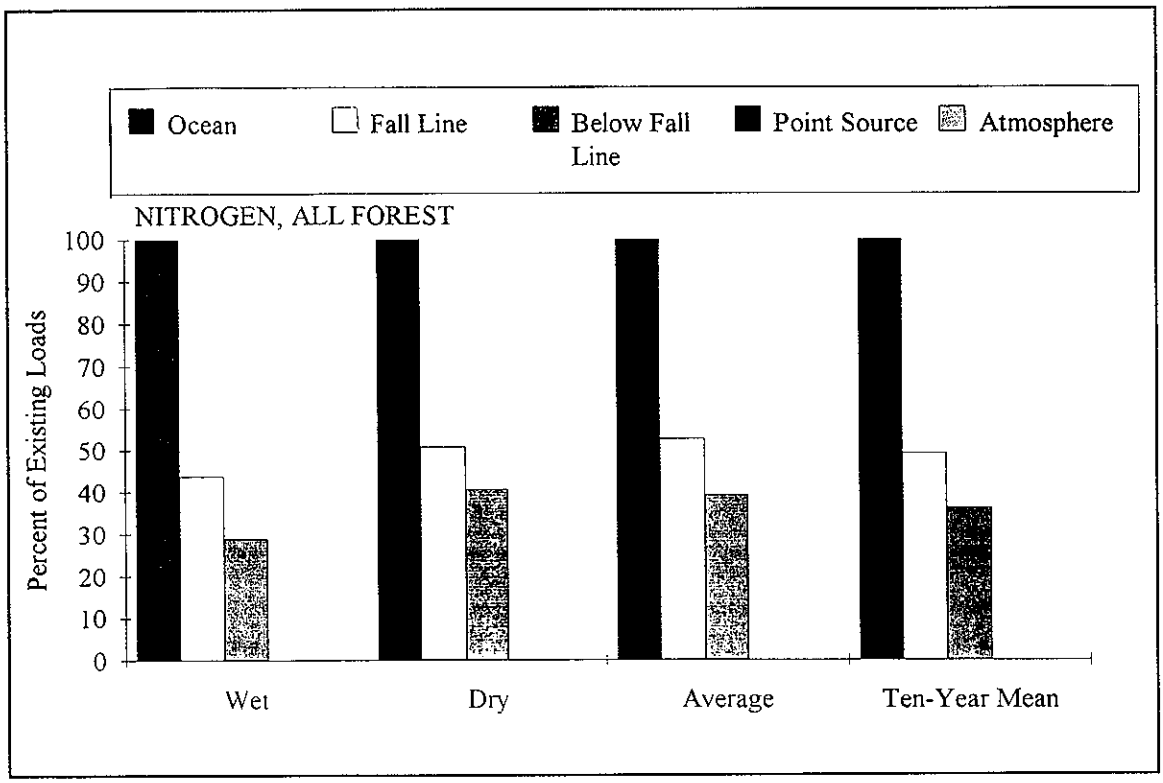

Figure 15-37. All-Forest Nitrogen Loads as Percentage of Existing Loads

All-Forest Scenario. In this scenario, nutrient loads to the Bay were obtained from an all-forest run of the Watershed Model. The all-forest loads were for all regions in the Bay watershed, not only Bay-agreement jurisdictions. Point-source loads were eliminated as were atmospheric nutrient loads to the water surface. In early planning stages of the scenario process, this run was called the "Pristine Run" since it was intended to simulate the Bay under pristine conditions. The "pristine" title was dropped, partly because estimates of pristine loads were not available from the Watershed Model. The all-forest loads from the Watershed Model incorporated existing atmospheric nitrogen loads to the Bay watershed. These loads are thought to be considerably higher than atmospheric loads under pristine conditions. This excess of nitrogen loading to the watershed was countered in the scenario by elimination of atmospheric loads to the water surface. Even under pristine conditions, some loads to the surface exist. Consequently, atmospheric loads to the watershed exceeded pristine loads while atmospheric loads to the water surface were less than pristine loads. This all-forest run comprised the best estimate of Bay water quality under natural conditions.

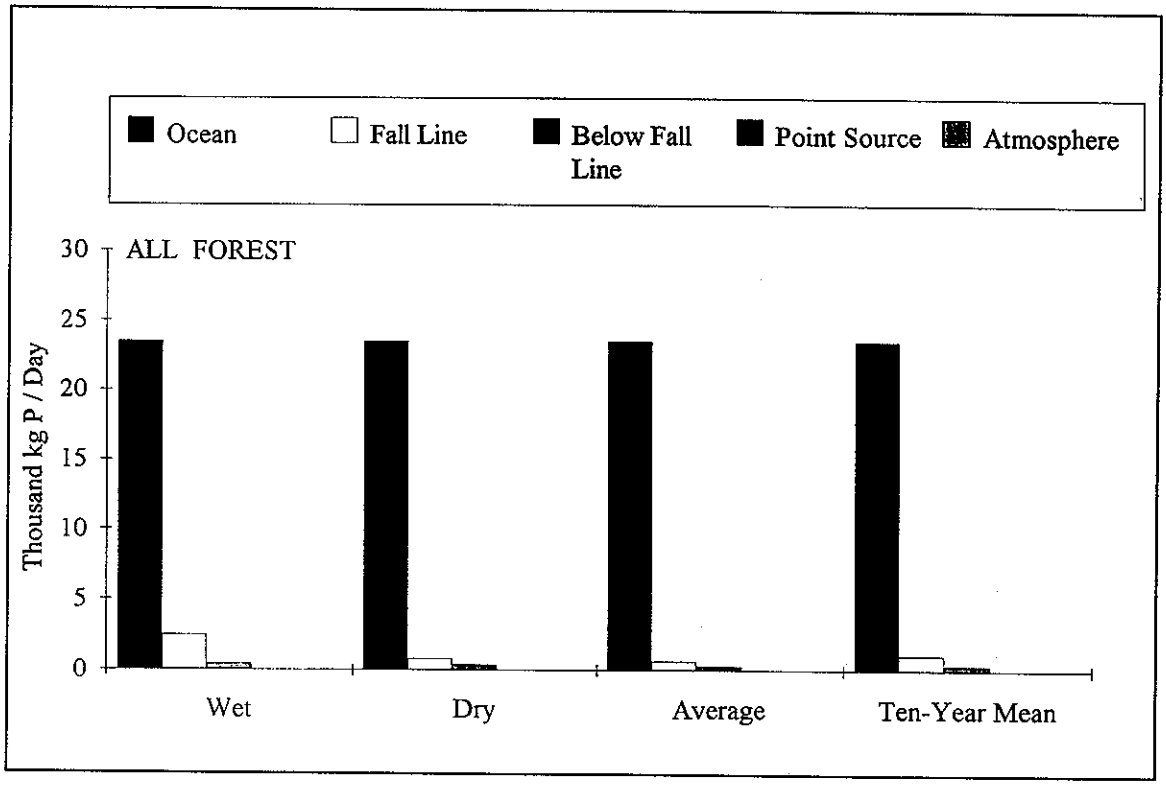

Figure 15-38. Scenario Phosphorus Loads Under All-Forest Conditions

System Response to Nitrogen and Phosphorus Loads

Introduction

Response scenarios were first examined for system-wide effects of nitrogen and phosphorus loads. The load-reduction scenarios, the Limit-of-Technology scenario, and the all-forest scenario were compared.

Presentations are for scenario year 9. Year 9 had average hydrology and achieved 90% or more of steady-state for most processes. Concentrations are presented as volumetric, annual averages including mainstem and tributaries. Sediment fluxes are areal, annual averages including mainstem and tributaries.

Presentation format is primarily as three figures. The upper figure illustrates the effect of nitrogen loads, in kg day^{-1}. The middle figure illustrates the effects of phosphorus loads, in kg day^{-1}. The lower figure illustrates percent change as a function of percent change in nitrogen and phosphorus loads.

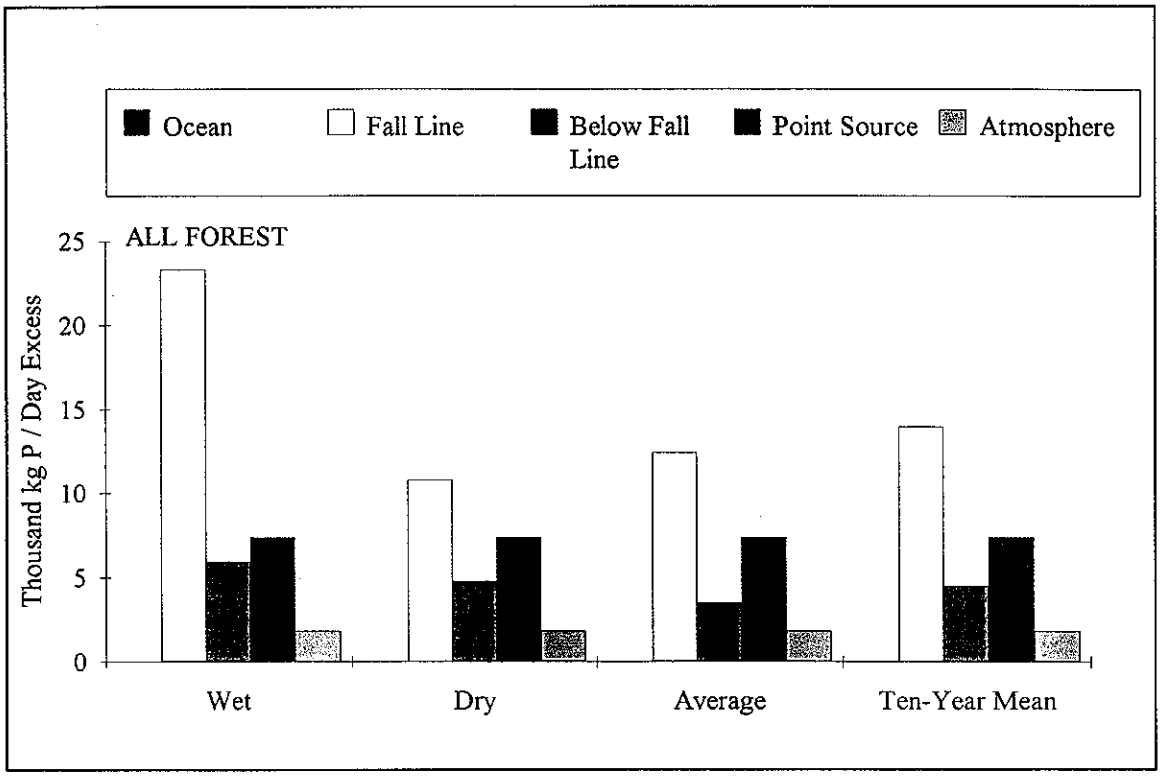

Figure 15-39. Excess of Existing Phosphorus Loads Over All-Forest Conditions

Total Nitrogen Concentration

Total nitrogen concentration was proportional to nitrogen load (Figure 15-41). When load was reduced, concentration declined nearly linearly and roughly in one-to-one proportion to loading. The phosphorus load reductions included in LOT and all-forest scenarios resulted in a small increase in total nitrogen concentration above the level expected based on nitrogen loads alone. The phosphorus reductions diminished algae beyond the control produced by nitrogen alone. As a result of the additional control of algal growth, less nitrogen was removed from the water column, through algal settling, than when phosphorus loads remained at existing levels.

Phosphorus load reductions alone decreased nitrogen concentration by a small amount. The mechanism for the decrease was indirect. Phosphorus load reductions caused a small increase in bottom-water dissolved oxygen. Increased dissolved oxygen caused sediments to retain and denitrify a greater fraction of deposited nitrogen and release a lesser fraction to the water column.

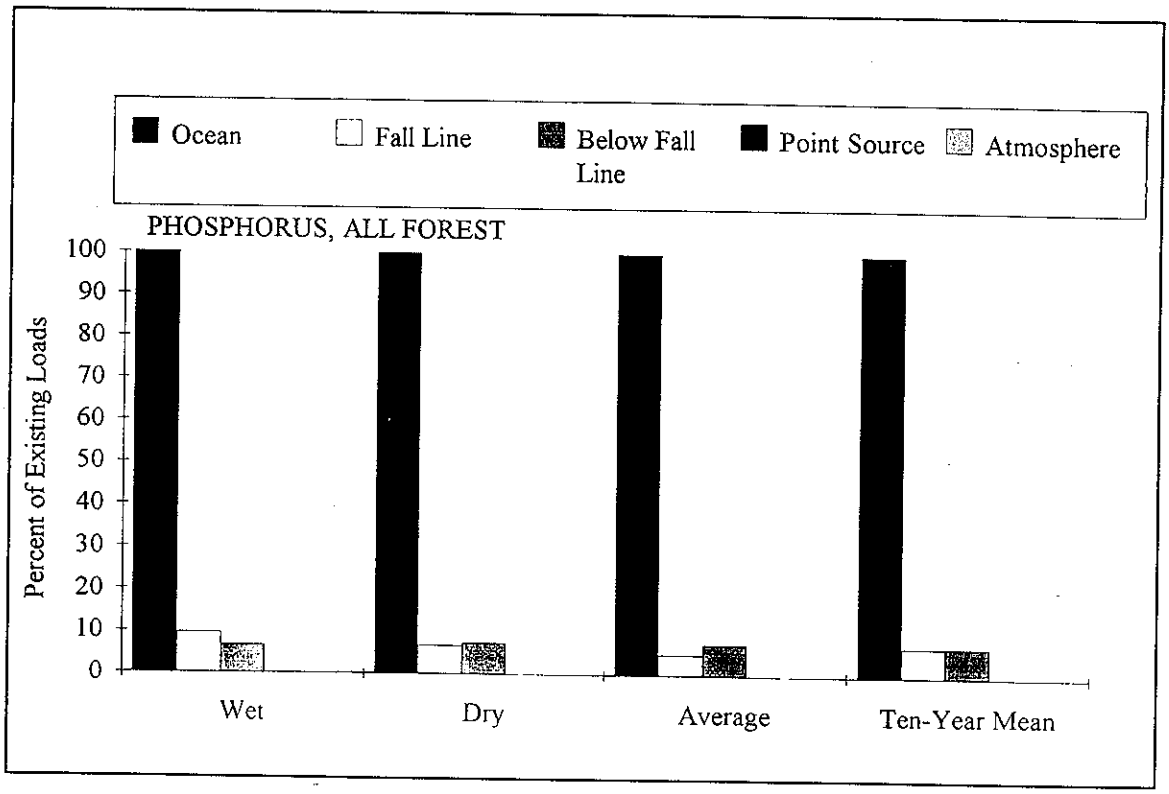

Figure 15-40. All-Forest Phosphorus Loads as Percentage of Existing Loads

Total Phosphorus Concentration

Total phosphorus concentration was linearly proportional to phosphorus loading (Figure 15-42). Total phosphorus under LOT and all-forest conditions corresponded exactly to expectations based on load, despite additional nitrogen reductions under these scenarios. Reduction in phosphorus concentration relative to load was much less than one-to-one due to the large oceanic phosphorus source.

Phosphorus concentration was non-linearly related to nitrogen load. As nitrogen load was reduced, phosphorus concentration increased. The increase became pronounced for load reductions greater than sixty percent. The increase in phosphorus was related to nitrogenous nutrient limitation of algae. As nitrogen load decreased, algal uptake of both nitrogen and phosphorus diminished. Diminished algal uptake caused less transport of phosphorus, via settling of algae and algal detritus, into bottom sediments. The sensitivity to nitrogen load illustrated the role of algae in the transfer of phosphorus out of the water and into bottom sediments.

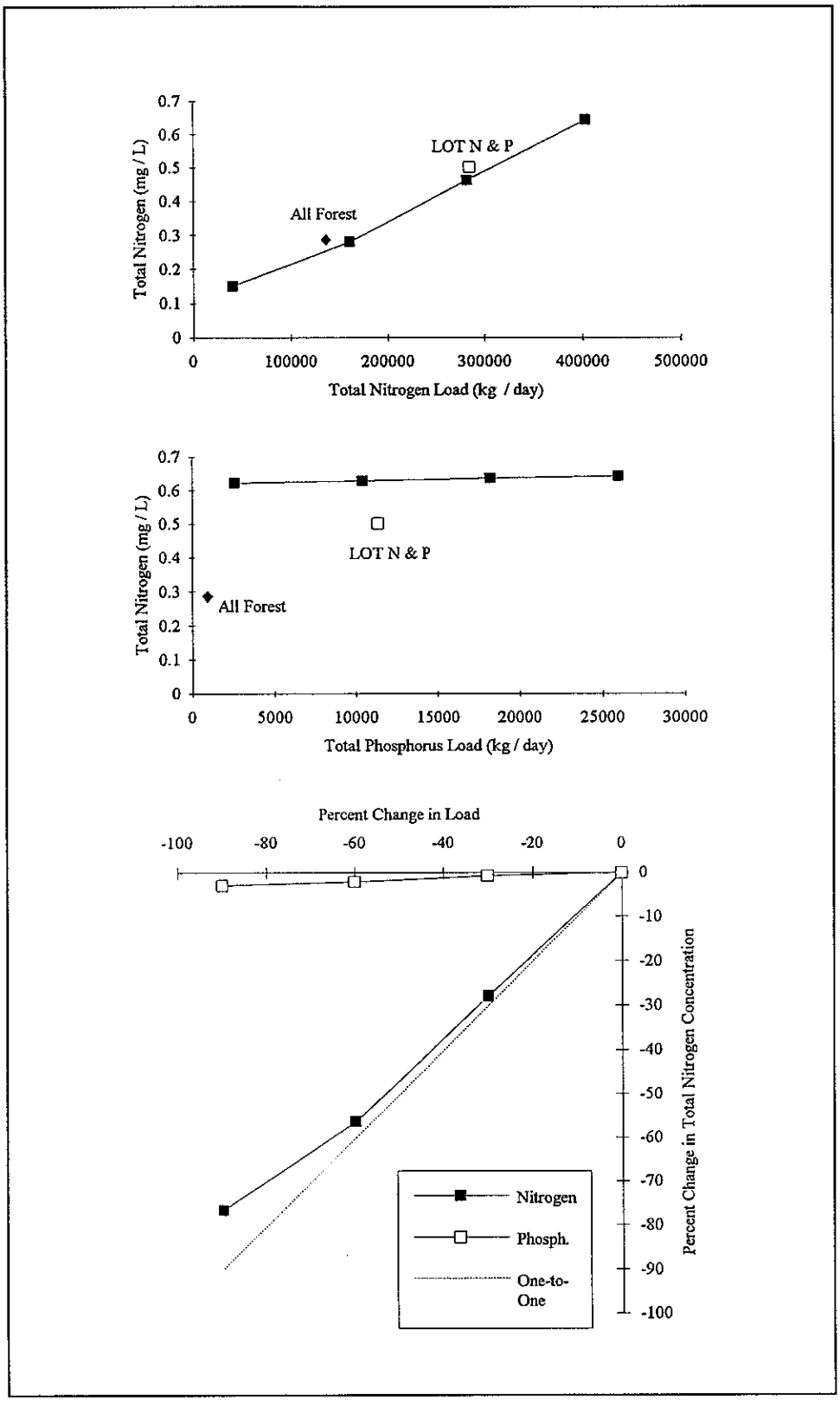

Figure 15-41. Response of System Total Nitrogen Concentration to Nutrient Load Reductions

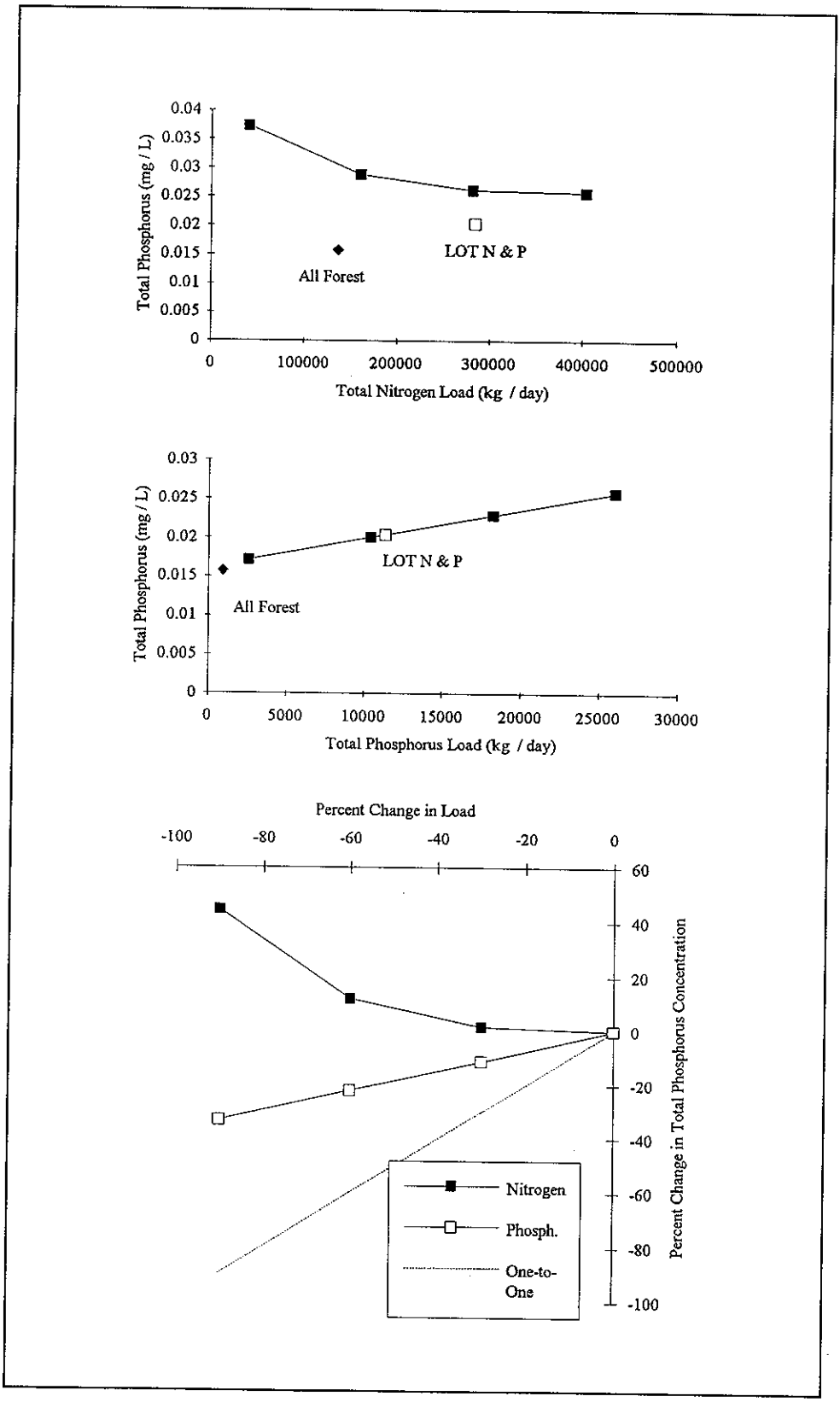

Figure 15-42. Response of System Total Phosphorus Concentration to Nutrient Load Reductions

Dissolved Inorganic Nitrogen

Dissolved inorganic nitrogen concentration was proportional to nitrogen load (Figure 15-43). The relationship to load was non-linear, however. Dissolved inorganic nitrogen was one of the few substances or processes to show a greater than one-to-one response to load reductions. The accelerated response occurred because sediment nitrogen release was diminished by nitrogen load reductions. Nitrogen load reductions caused an increase in bottom-water dissolved oxygen. Increased dissolved oxygen caused sediments to retain and denitrify a greater fraction of deposited nitrogen and release a lesser fraction to the water column.

Phosphorus load reductions caused an increase in dissolved inorganic nitrogen. The increase occurred as algae production became phosphorus limited. The limitation diminished uptake of both nitrogen and phosphorus by algae and resulted in build up on dissolved inorganic nitrogen formerly consumed by algae.

Dissolved Inorganic Phosphorus

Relationship of dissolved inorganic phosphorus to phosphorus loads was nearly linear (Figure 15-44). Reduction of concentration in proportion to loads was much less than one-to-one, however, due to the supply of oceanic phosphorus.

Dissolved inorganic phosphorus increased as nitrogen loads were diminished. The increase was accelerated such that the fractional increase in dissolved inorganic phosphorus was much greater than the fractional decrease in nitrogen load. The increase originated in a phenomenon noted earlier. As one nutrient required by algae became limited, concentration of the other nutrient increased due to diminished algal uptake.

Algal Biomass

Algal biomass, quantified as chlorophyll concentration, was proportional to both nitrogen and phosphorus loads (Figure 15-45). The relationship to nitrogen load was nearly linear and nearly one-to-one. Fractional reductions in nitrogen load resulted in nearly identical fractional reductions in chlorophyll concentration. The relationship to phosphorus loads was less linear and much less than one-to-one. The phosphorus load reductions included in the LOT induced no noticeable decrease in chlorophyll beyond the decrease in nitrogen load reductions alone. The nitrogen reductions in these scenarios diminished chlorophyll beyond the concentration induced by phosphorus reductions alone, however. These results indicated that algae were much more responsive to nitrogen controls than phosphorus controls.

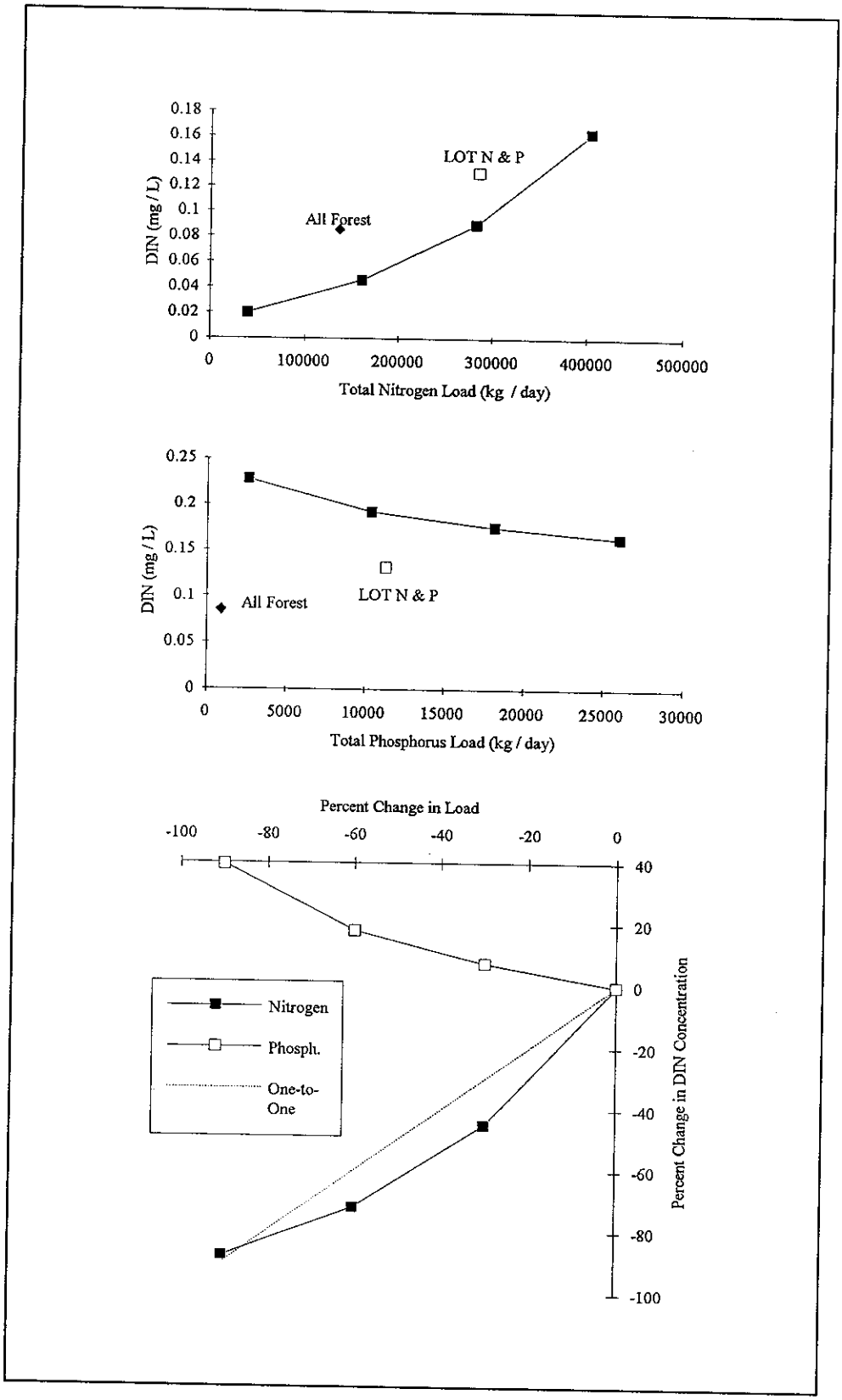

Figure 15-43. Response of System Dissolved Inorganic Nitrogen Concentration to Nutrient Load Reductions

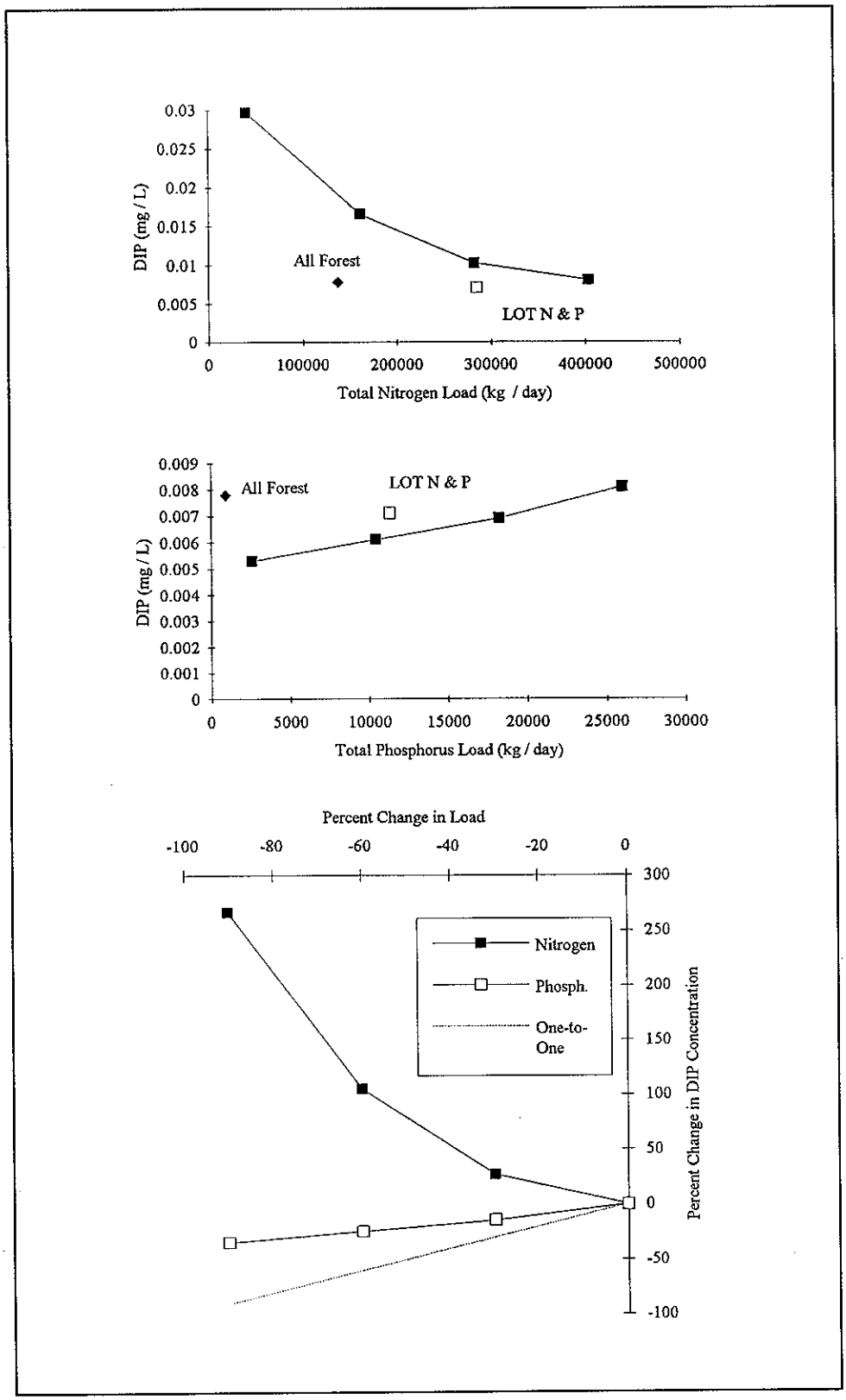

Figure 15-44. Response of System Dissolved Inorganic Phosphorus Concentration to Nutrient Load Reductions

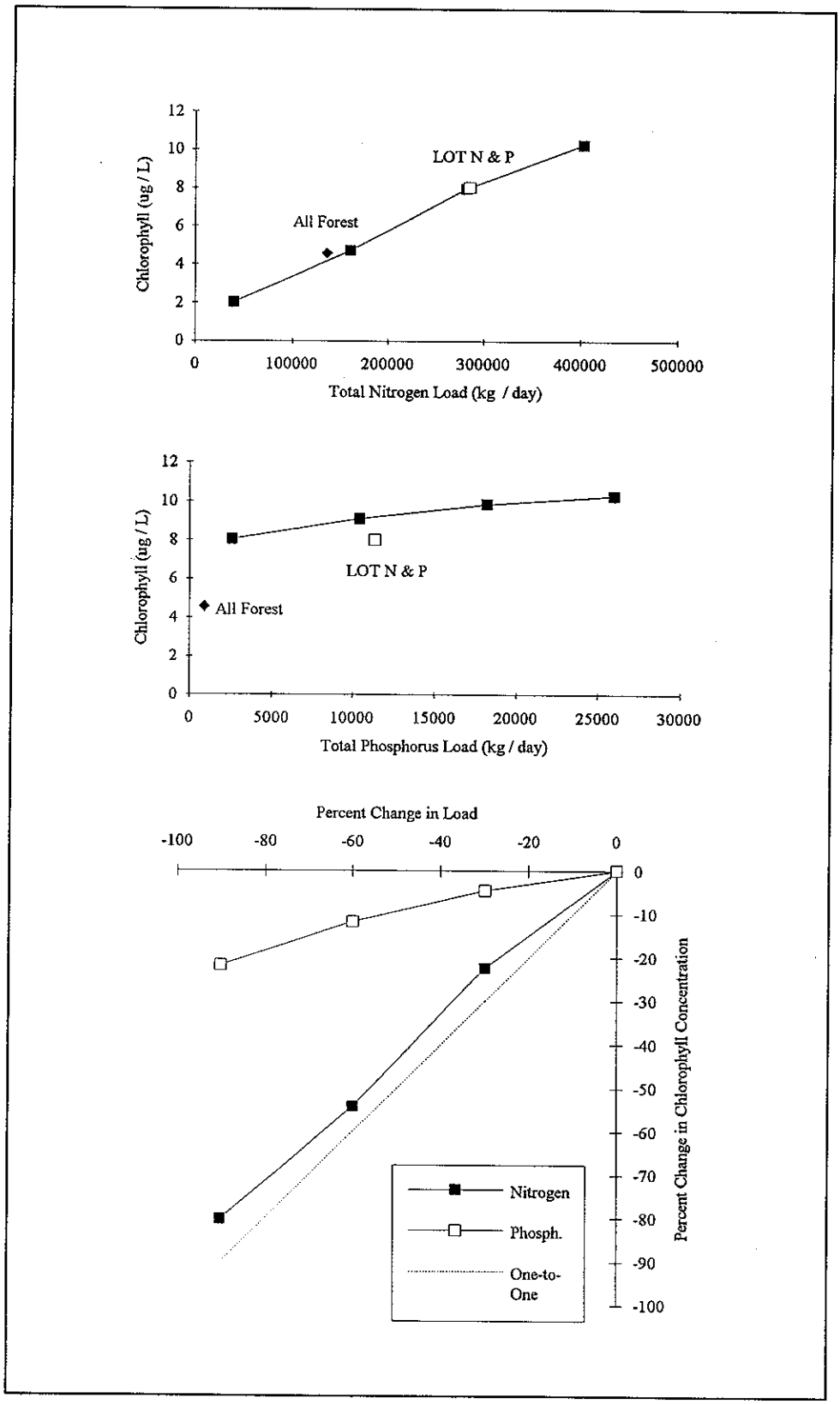

Figure 15-45. Response of System Chlorophyll Concentration to Nutrient Load Reductions

Anoxic Volume Days

The relationship of anoxic volume to nitrogen loads was linear throughout most of the range of loads explored (Figure 15-46). For much of the range of loads, proportional reduction in anoxic volume was greater than the reduction in nitrogen loads. The accelerated response was due to increased sediment denitrification during load reductions. Nitrogen load reductions caused an increase in bottom-water dissolved oxygen. Increased dissolved oxygen caused sediments to retain and denitrify a greater fraction of deposited nitrogen and release a lesser fraction to the water column. The diminished nitrogen release further limited algal production. Less production of algae caused less settling to the bottom and less oxygen consumption upon decay. The scenarios indicated nitrogen reductions exerted two limits on algal production: a direct limit due to load reductions and an indirect limit due to diminished sediment release.

The relationship of anoxic volume to phosphorus loads was nearly linear but proportional reduction in anoxic volume was much less than the fractional reduction in phosphorus loads. The influence of phosphorus load reductions was limited by the supply of oceanic phosphorus. These results indicated that anoxia, as with algae, was much more responsive to nitrogen controls than phosphorus controls.

Sediment Oxygen Demand

The relationship of sediment oxygen demand to nutrient loads (Figure 15-47) was much like the relationship determined for anoxic volume. One difference was that reduction in sediment oxygen demand in response to nitrogen load reductions was less than one-to-one. For anoxic volume, the relationship was greater than one-to-one.

The less than one-to-one correspondence of sediment oxygen demand to load reductions occurs because exertion of sediment oxygen demand depends on dissolved-oxygen concentration. In the absence of oxygen, sediment oxygen demand is zero although release of chemical oxygen demand to the water may be substantial. As dissolved oxygen increases, due to load reductions, sediment oxygen demand may increase, due to oxygen availability, and chemical oxygen demand will decrease. Consequently, the decrease in sediment oxygen demand due to loading is countered, to some extent, by the increase in exertion due to oxygen availability. As a result of two influences acting in different directions, the proportional reduction in SOD is less than the reduction in anoxic volume.

Sediment Ammonium Release

Release of nitrogen from sediments decreased in nearly linear proportion to reduction in nitrogen load (Figure 15-48). Correspondence was greater than

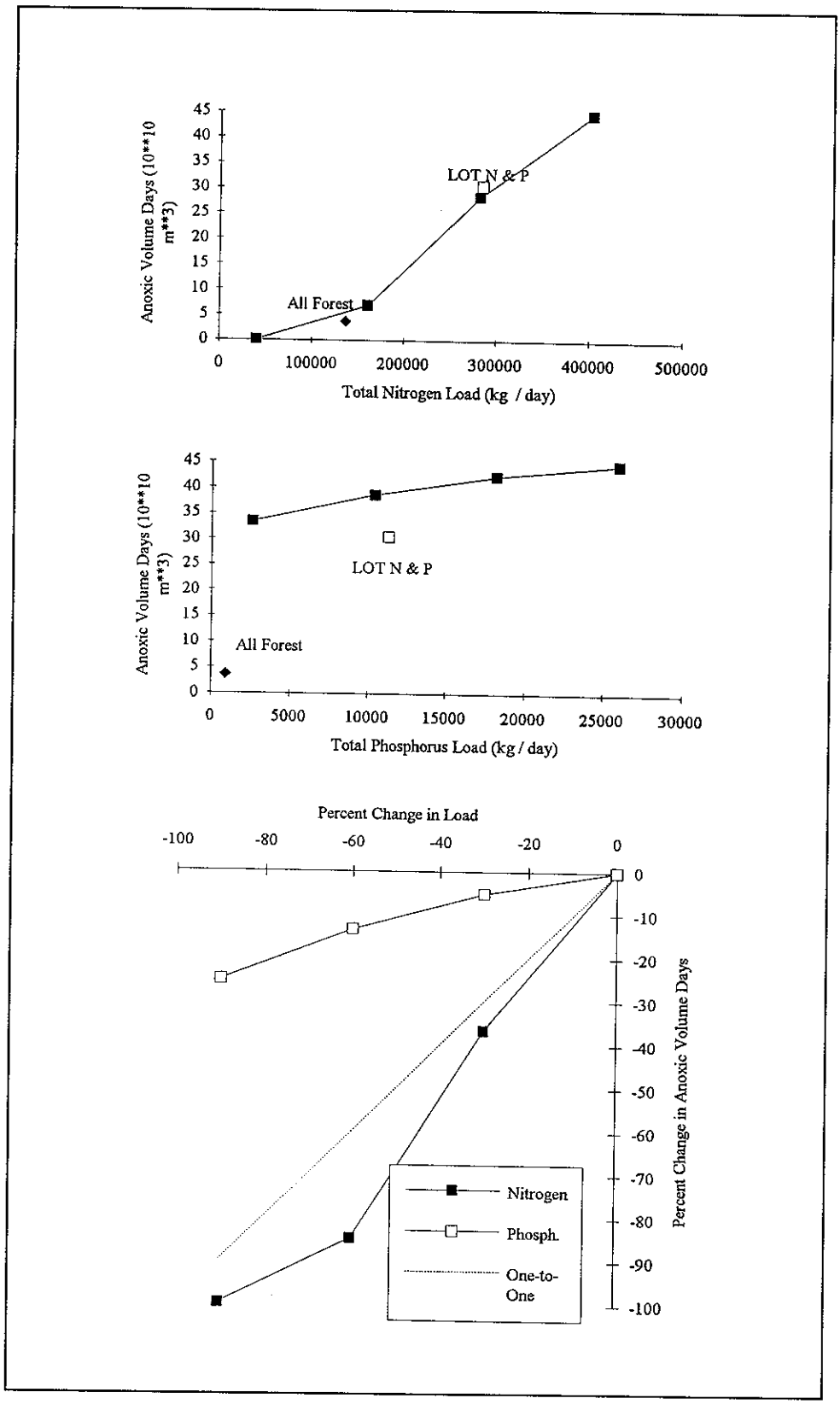

Figure 15-46. Response of System Anoxic Volume Days to Nutrient Load Reductions

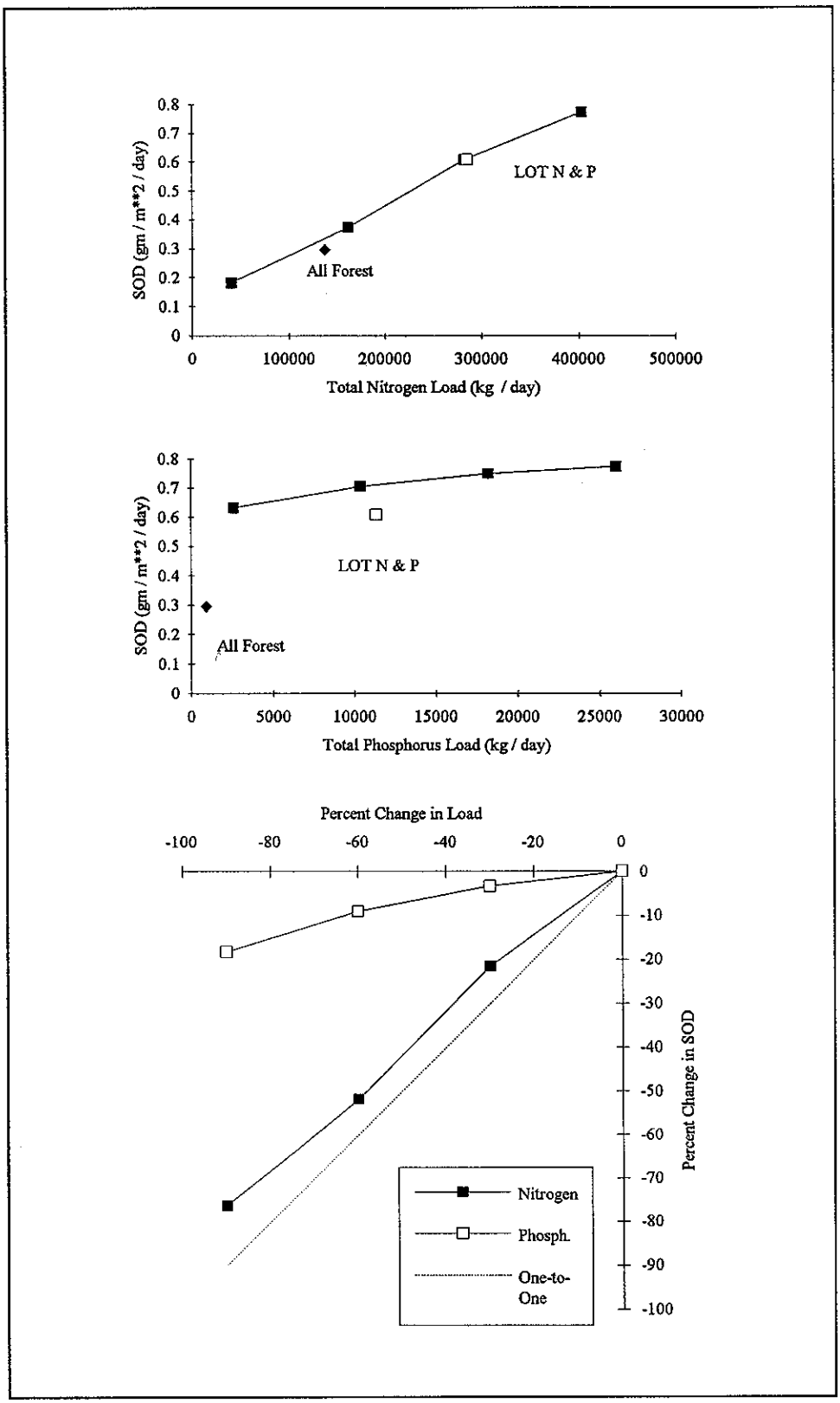

Figure 15-47. Response of System Sediment Oxygen Demand to Nutrient Load Reductions

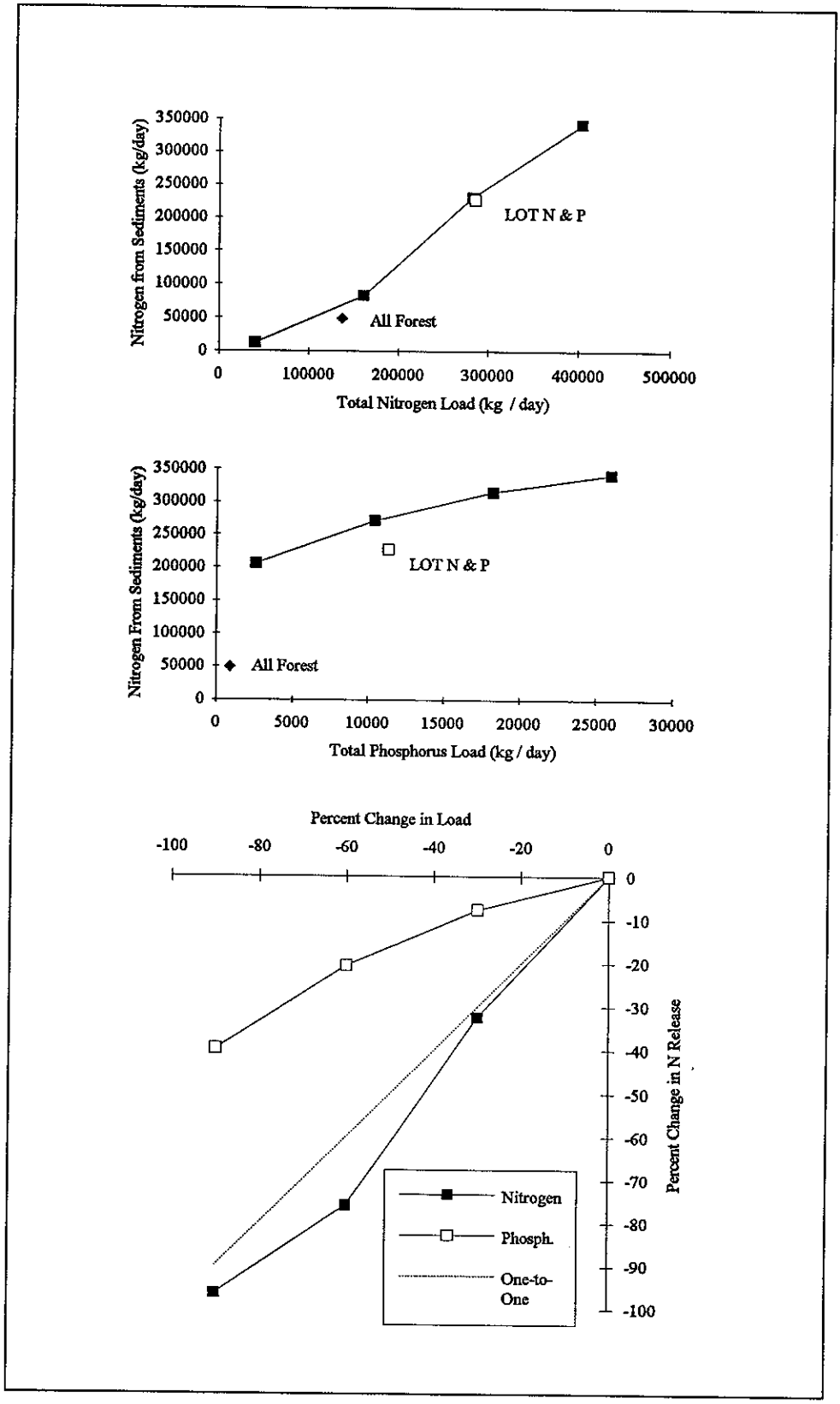

Figure 15-48. Response of System Sediment Ammonium Release to Nutrient Load Reductions

one-to-one, however. The enhanced reduction in nitrogen release was due to denitrification. Reduction in load both decreased deposition to the sediment, as algae and detritus, and increased dissolved oxygen. As oxygen increased, a larger fraction of deposited nitrogen was denitrified. Diminished deposition and increased denitrification caused release to diminish in greater than one-to-one proportion to load reductions.

Sediment nitrogen release also declined in proportion to reduction in phosphorus load. The processes were the same as for nitrogen load reduction: diminished deposition and enhanced denitrification. Nitrogen release declined in much less than one-to-one proportion to phosphorus load, however, indicating that phosphorus was less effective in controlling algal nutrient uptake and in diminishing anoxic volume.

Sediment Phosphorus Release

Reduction in nitrogen loading exerted a strong effect on sediment phosphorus release (Figure 15-49). Release declined in greater than one-to-one proportion to load reductions. Two factors contributed to the influence of nitrogen on phosphorus release. First, nitrogen control limited algal uptake of both nitrogen and phosphorus. Less algal uptake resulted in less deposition to sediments and less diagenetic production of phosphorus. In addition, the sediments retained a greater fraction of deposited phosphorus. The added retention was due to diminishment of anoxia associated with nitrogen reductions. Less anoxic sediment phosphorus release occurred.

Reduction in phosphorus loads had little effect on sediment phosphorus release. In fact, release increased, to a small extent, as load was reduced. The incremental release was primarily a diffusion effect. The transfer of phosphorus from sediments to water was proportional to the concentration difference between sediment interstitial water and the water column. Concentration in interstitial was buffered at a nearly constant level by sorption/desorption on to particles. When concentration in the water was diminished by load reductions, the sediment-water concentration gradient increased and more phosphorus diffused out of the sediments.

The effect can be seen clearly in the plot of phosphorus release versus nitrogen load (Figure 15-49). The thirty-percent load reduction and the LOT control scenario have equivalent nitrogen loads. Phosphorus release is greater under the LOT scenario, however. The reason is that phosphorus controls under LOT load reductions reduce phosphorus concentration beyond the concentration induced by nitrogen load reductions alone (Figure 15-42). The effect of diminished concentration on release can also be seen in a plot of sediment phosphorus release versus water column concentration (Figure 15-50). As concentration declines, due to phosphorus controls, release increases.

The relationships of sediment oxygen demand, ammonium release, and phosphorus release to nitrogen load indicate that reduction of fluxes in

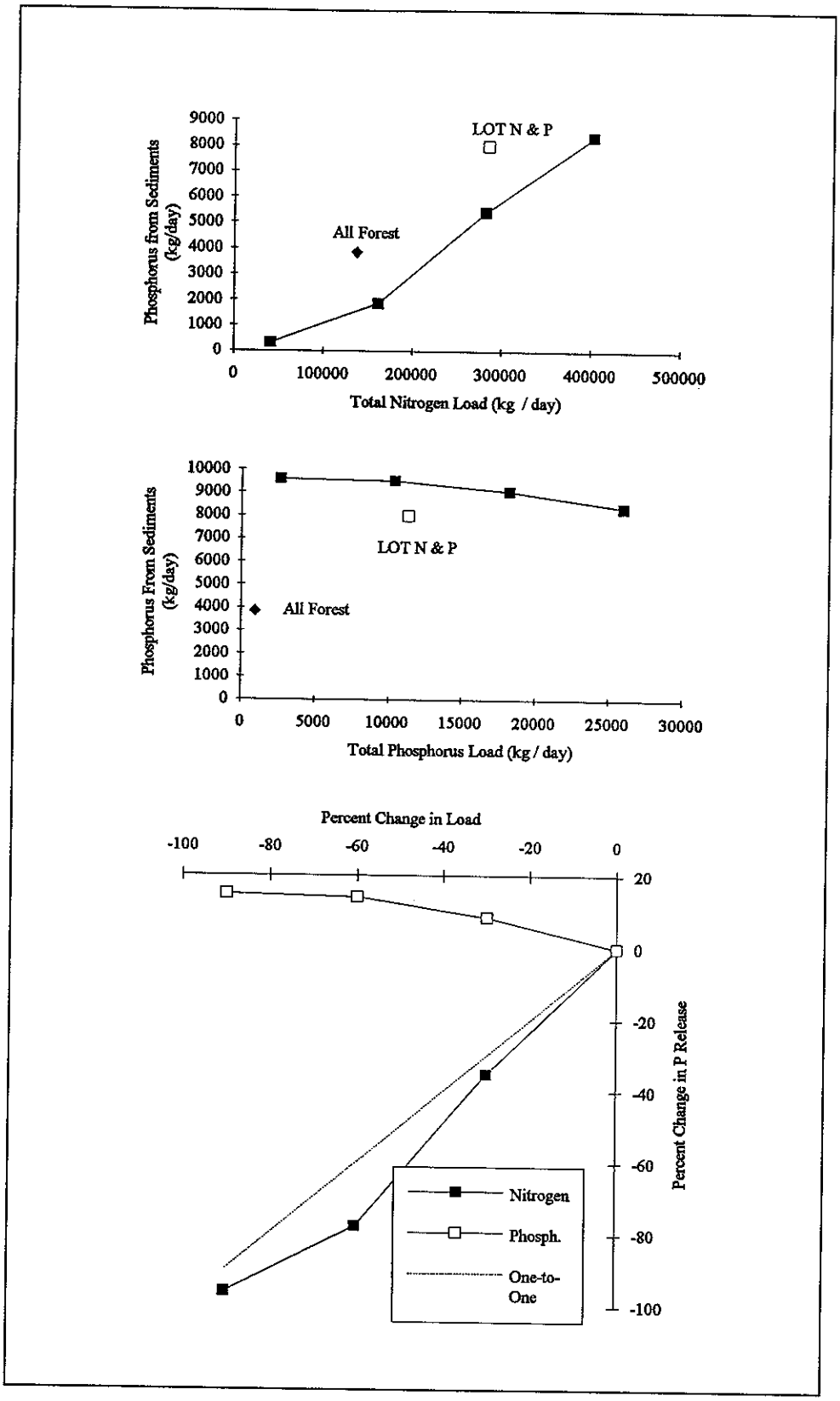

Figure 15-49. Response of System Sediment Phosphorus Release to Nutrient Load Reductions

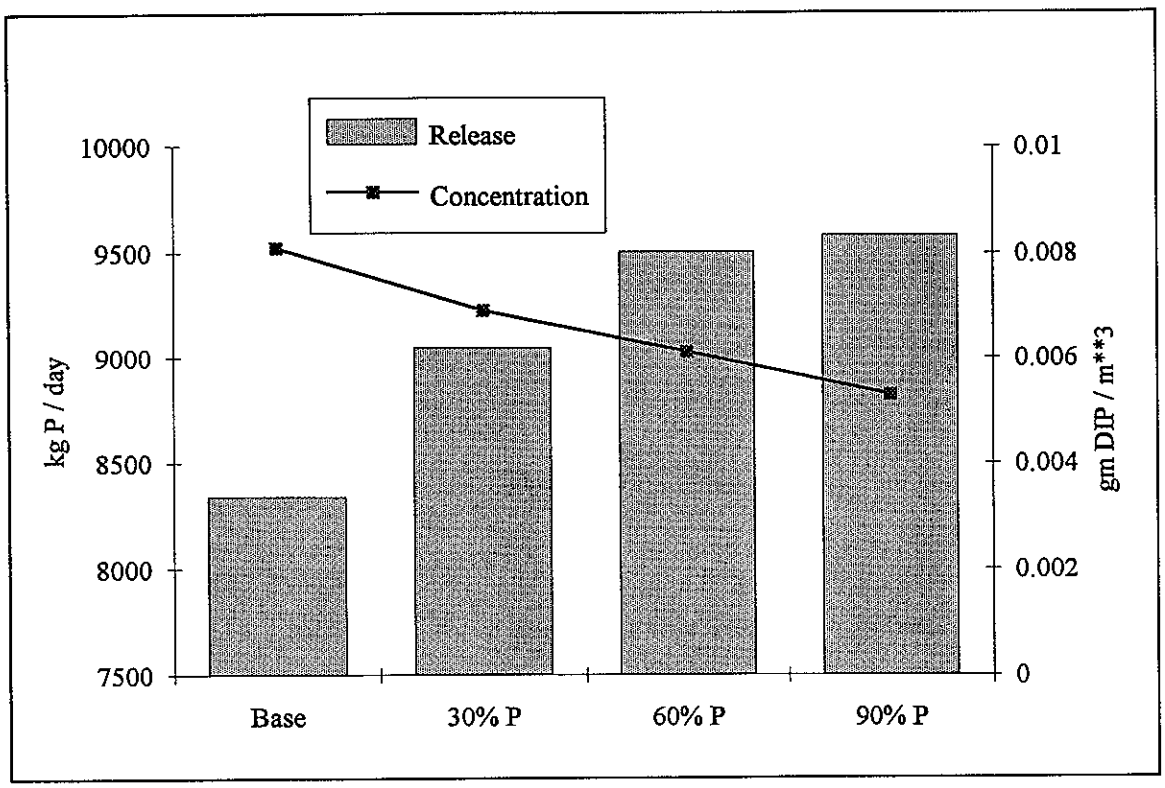

Figure 15-50. System Dissolved Inorganic Phosphorus Concentration and Sediment Phosphorus Release as a Function of Phosphorus Load Reductions

proportion to nitrogen load is a useful first-order approximation for estuarine models lacking a predictive sediment component. The alteration in fluxes in response to reduction of phosphorus loads is less predictable, however. In particular, sediment phosphorus fluxes may not diminish at all in response to load reductions.

Nutrient Inflow Concentrations

A special mass-balance boundary condition was developed to account for the effects of nutrient reductions on concentration of nitrogen and phosphorus flowing into the Bay (Chapter 8). Employment of the algorithm indicated inflowing nitrogen concentration would decline by ten percent in response to a ninety-percent reduction in nitrogen load (Figure 15-51). Inflowing phosphorus concentration would decline by five percent in response to a ninety-percent phosphorus load reduction. The minimum phosphorus inflow concentration was also attained under LOT nitrogen and phosphorus controls. Equivalence in inflow concentration occurred because system total phosphorus concentration was equivalent under 90% phosphorus reduction or LOT nitrogen and phosphorus controls (Figure 15-42).

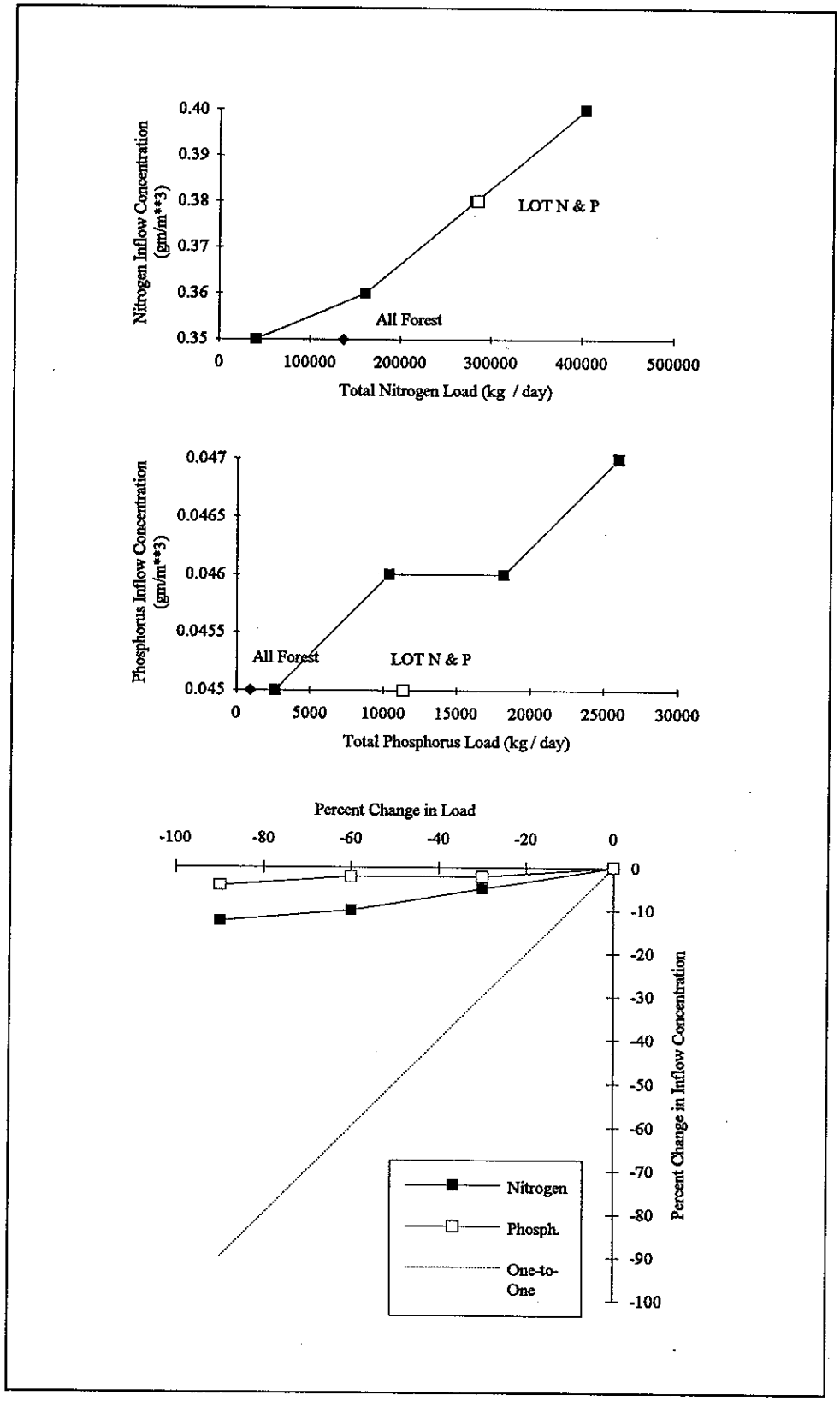

Figure 15-51. Response of Inflow Nutrient Concentrations to Nutrient Load Reductions

Minimal response of inflow concentrations to load reductions indicate the observed diminishment of inflow concentration (Table 8-3) cannot be related to load reductions. For nitrogen, the trend in observations was affected by changes in analytical methodology and is, apparently, an artifact of the changes. The trend in phosphorus was not affected by analytical changes, however. If the phosphorus trend is real, it may reflect large-scale changes in circulation outside the Bay mouth or in concentration of the oceanic reservoir. A sophisticated model of circulation outside the Bay mouth and an extensive data base is required for further resolution of the apparent trend in inflow phosphorus concentration.

Denitrification

A positive feedback loop has been proposed (Harding, Leffler, and Mackieman 1992) in which diminishment in anoxia leads to enhanced nitrification and denitrification in the sediments. The loss of additional nitrogen through denitrification to gaseous form would further improve dissolved oxygen by inducing additional nitrogen limitation on algal carbon production (Figure 2-16). Results from the model indicate the fraction of deposited nitrogen denitrified does increase as a result of load reductions (Figures 15-52, 15-53). Substantial increases in denitrification require load reductions beyond the feasible range, however. Under LOT nutrient controls, the fraction of deposited nitrogen denitrified increases to 37% compared to 30% under base conditions. Under all-forest conditions, however, the fraction increases to 63%.

Mainstem Bay Under LOT and All-Forested Conditions

Introduction

The analyses of system response to nutrient load reductions provided insights into the range of responses and the mechanisms behind them. Spatial and temporal details of responses were not revealed, however. The 30%, 60%, and 90% load reductions had no direct correspondence to past or potential conditions. Two scenarios, the all-forested condition and the limit-of-technology load reduction, did correspond to past and potential future conditions. Spatial and temporal behavior of these scenarios were examined in greater detail than the response scenarios.

In view of the importance of these scenarios, they were run for periods longer than the ten-year duration of the response scenarios. The all-forested condition was run for twenty years. The LOT scenario was run for thirty years. The additional time allowed these scenarios to approach complete response to the altered loads.

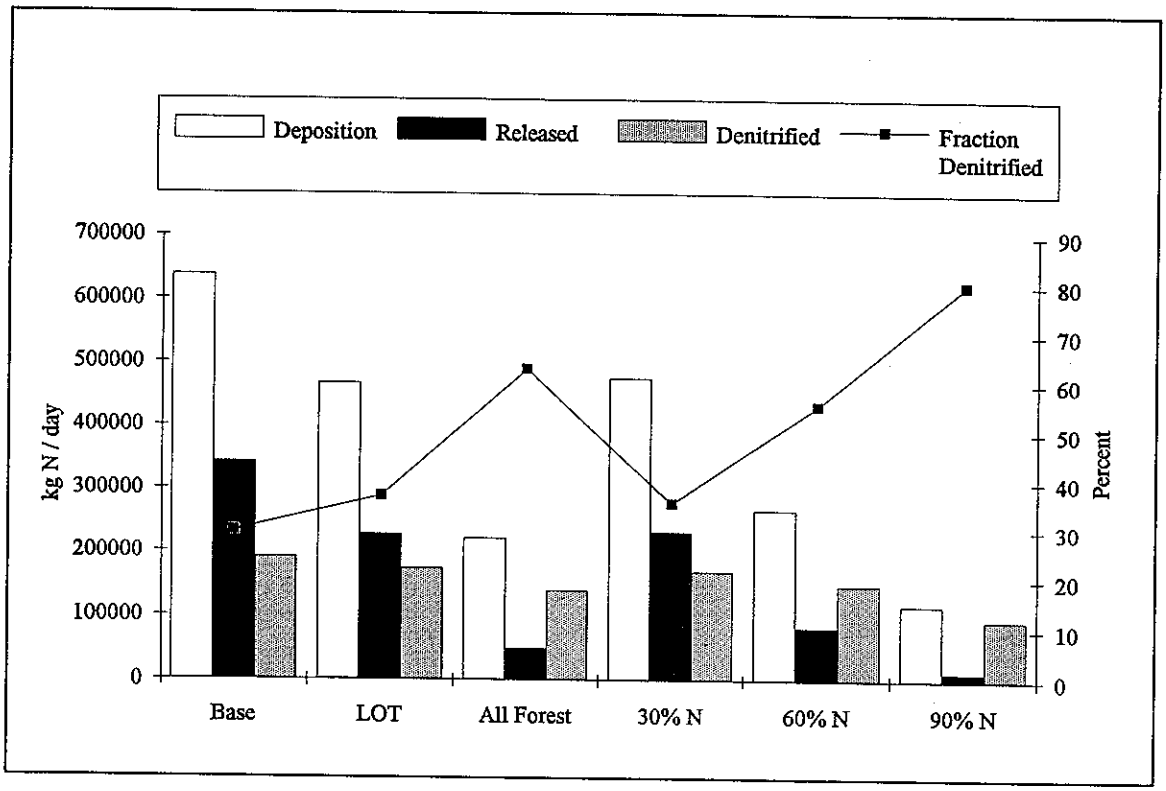

Figure 15-52. Sediment Nitrogen Fluxes as a Function of Nitrogen Load Reductions

Presentations correspond to treatment of calibration results in the mainstem. Concentrations are averaged by season and level and plotted against distance from the mouth of the Bay. Nutrient limitations in the surface layer, primary production, and sediment-water fluxes are also seasonally-averaged. Calibration plots of fluxes and diagnostic information are simplified from the calibration presentation, however, to emphasize differences between existing and scenario conditions. Year 9 in the base scenario is compared to year 19 in the all-forest scenario and year 29 of the LOT scenario. Hydrology in the comparison years is identical and corresponds to the average hydrology of 1986.

The Spring Bloom Period

Concentrations. Algal biomass, as chlorophyll, during the spring bloom in the all-forested condition was roughly half the bloom biomass during the existing condition (Figure 15-54). Chlorophyll under the LOT scenario was midway between the extremes of the existing and all forested conditions. Effects of the LOT reductions were less noticeable in the lower 150 km of the Bay, however.

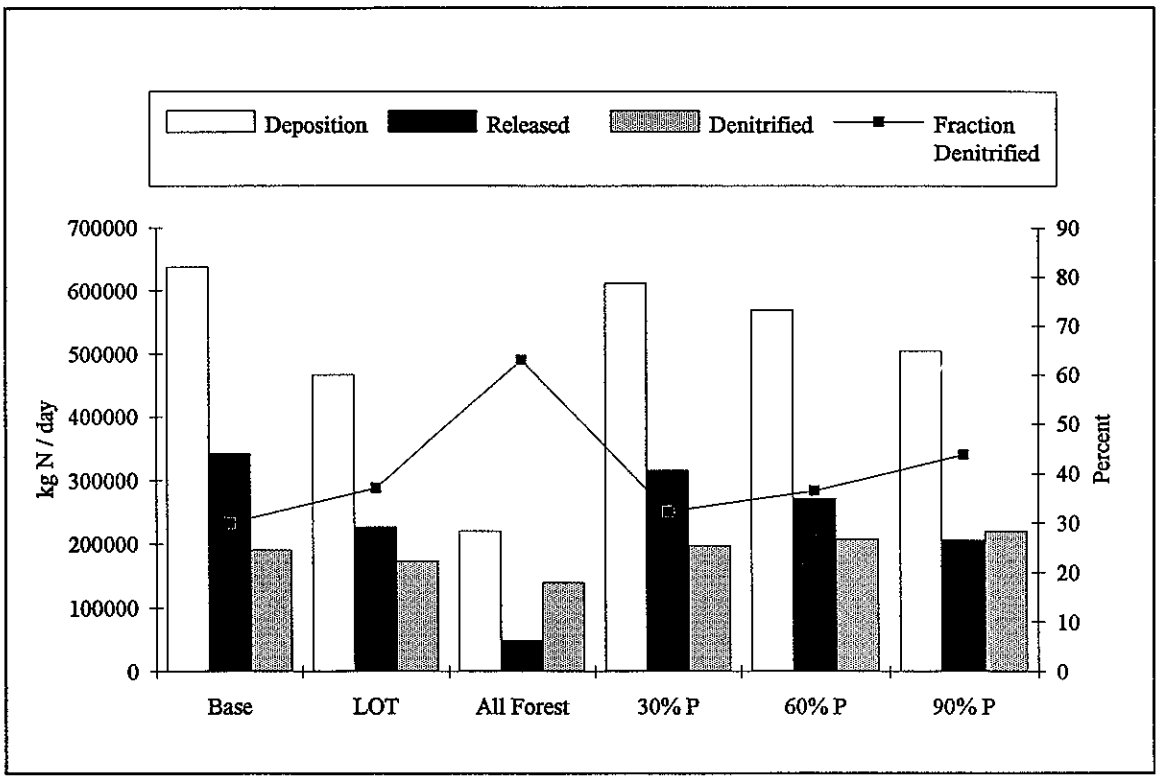

Figure 15-53. Sediment Nitrogen Fluxes as a Function of Phosphorus Load Reductions

Response of particulate organic carbon mirrored chlorophyll. The correspondence occurred because most particulate carbon was algae or algal detritus. Dissolved organic carbon responded much more strongly in the upper Bay than in the lower Bay. The spatial gradient in response was related to specification of boundary conditions at the mouth. Concentration at the mouth was fixed and equal in all scenarios. In the upper Bay, however, concentration could freely respond to variations in algal production. Consequently, diminishment of dissolved carbon was a function of both nutrient loading and distance from the fixed boundary. The scenarios indicated that dissolved organic carbon in the lower Bay depended more on the oceanic reservoir of this substance than on local algal production.

Total nitrogen concentration declined under both LOT and all-forested conditions. Under all-forested conditions, total nitrogen was roughly half the level under existing conditions. Total nitrogen at the open mouth was computed by mass balance but did not vary greatly. Minimal response was reasonable since the concentration weighting function employed in the boundary condition (Table 8-4) attributed more than half the inflow concentration during spring to the ocean reservoir.

Total phosphorus responded strongly to the scenarios. Under existing conditions, concentration was greater near the fall line than at the ocean boundary. Under LOT nutrient reductions, total phosphorus was equivalent at the two

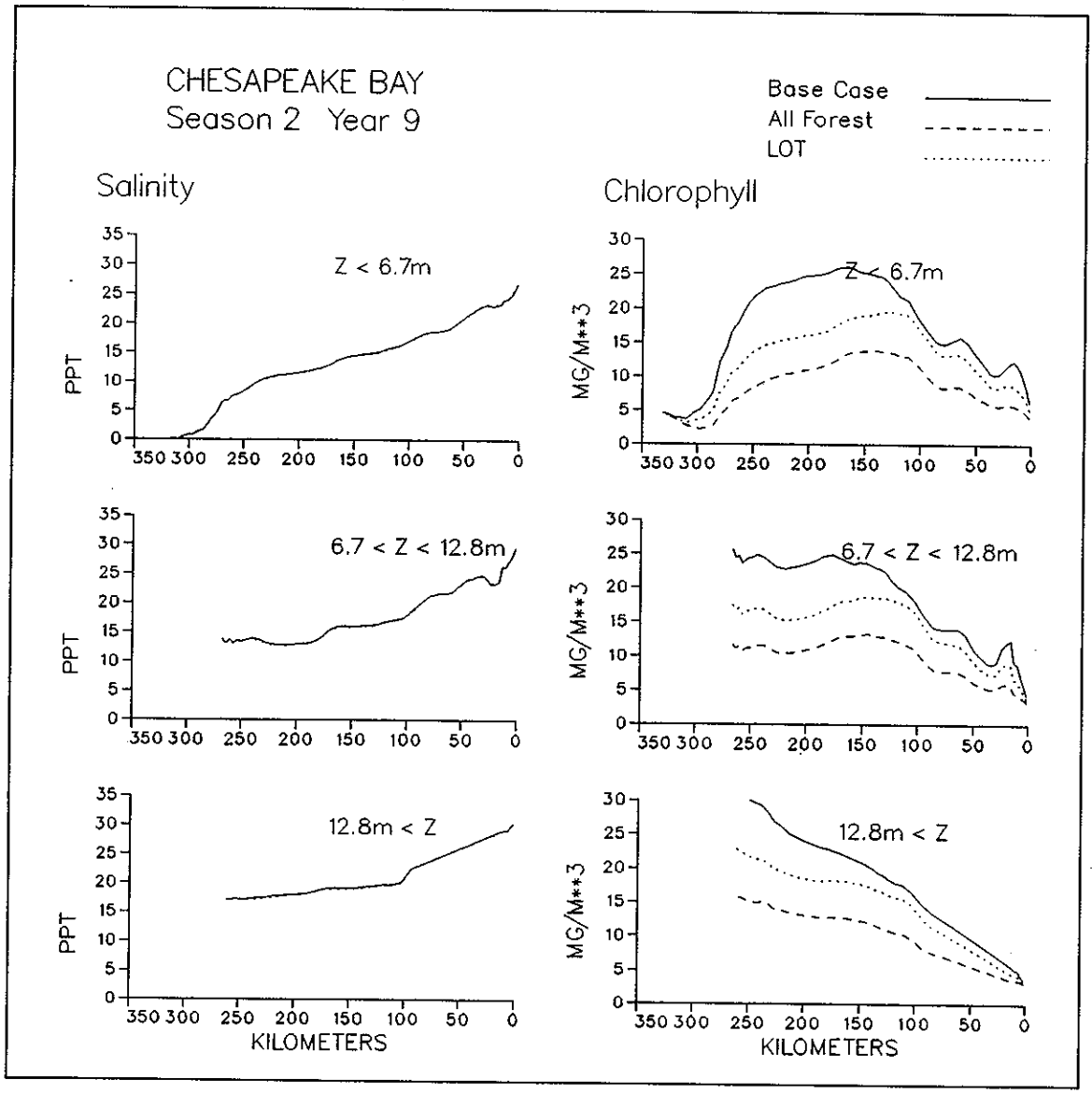

Figure 15-54. Concentrations Along Mainstem Bay Longitudinal Transect for Three Scenarios, Spring Bloom Period (Sheet 1 of 8)

ends of the mainstem. Under all-forest conditions, total phosphorus was nearly absent from the upper Bay. As with nitrogen, total phosphorus was computed by mass balance at the mouth but varied little.

Behavior of nitrogen and phosphorus fractions differed from total concentrations of these substances. Nitrate was unchanged and ammonium little affected by LOT conditions. Decline of nitrate under all-forest conditions was less than total nitrogen. Response of dissolved inorganic nitrogen was affected by the phosphorus limitation in the upper Bay (Figure 15-56). As phosphorus became more limiting, algal nitrogen uptake diminished, partially offsetting the effect of diminished nitrogen loads at the fall line.

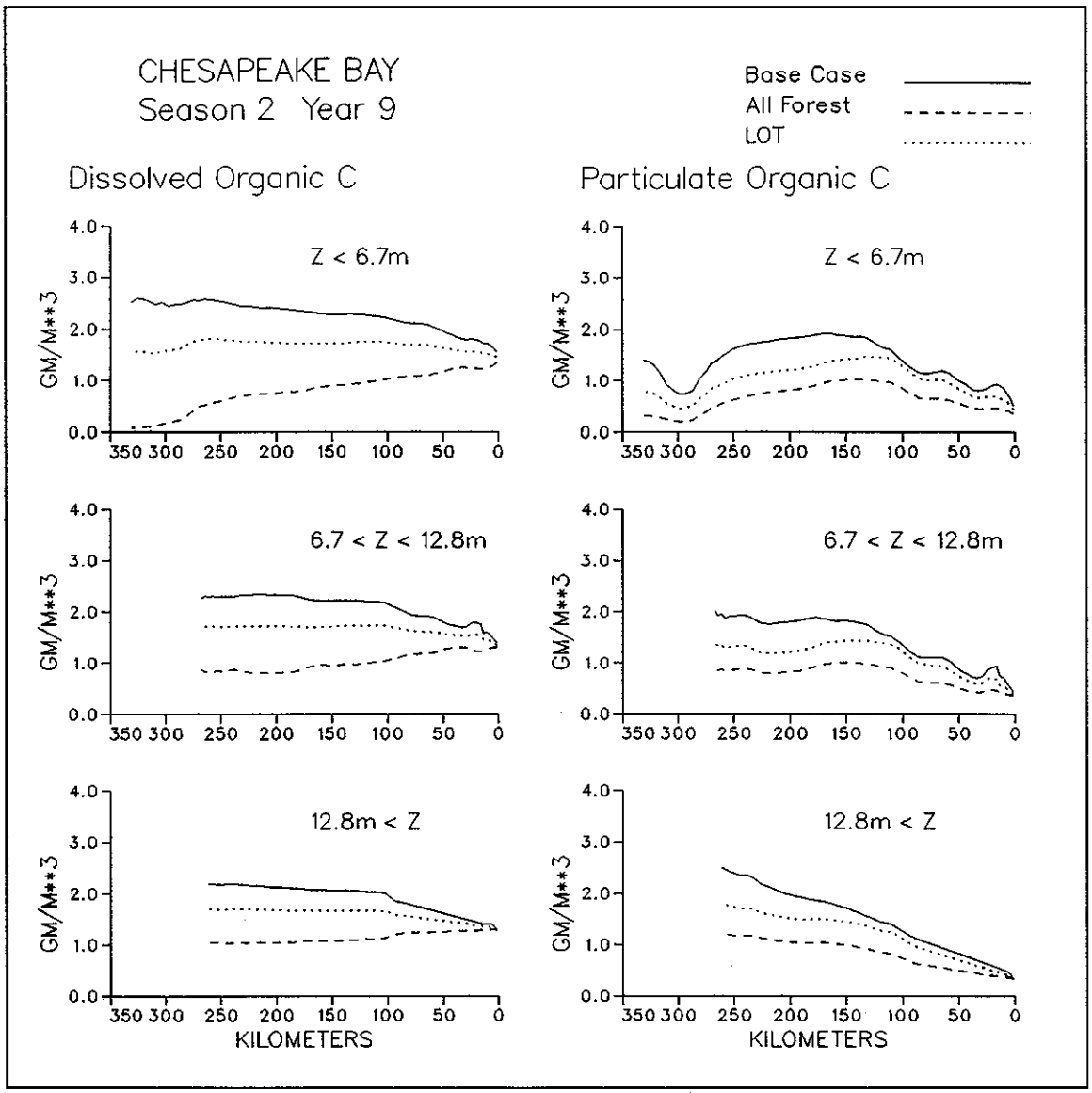

Figure 15-54. (Sheet 2 of 8)

Particulate and dissolved organic nitrogen mirrored the behavior of organic carbon. Particulate organic nitrogen concentration declined in proportion to chlorophyll. Dissolved organic nitrogen concentration was much less in the upper Bay, reflecting diminished algal production, than in the lower Bay, where concentration was maintained by the oceanic reservoir.

Changes in dissolved phosphate were small. In the upper Bay dissolved phosphate was less under all-forest and LOT conditions than under existing conditions. Near the mouth of the bay, dissolved phosphate increased under all-forest conditions. The increase occurred because nitrogen limitation was

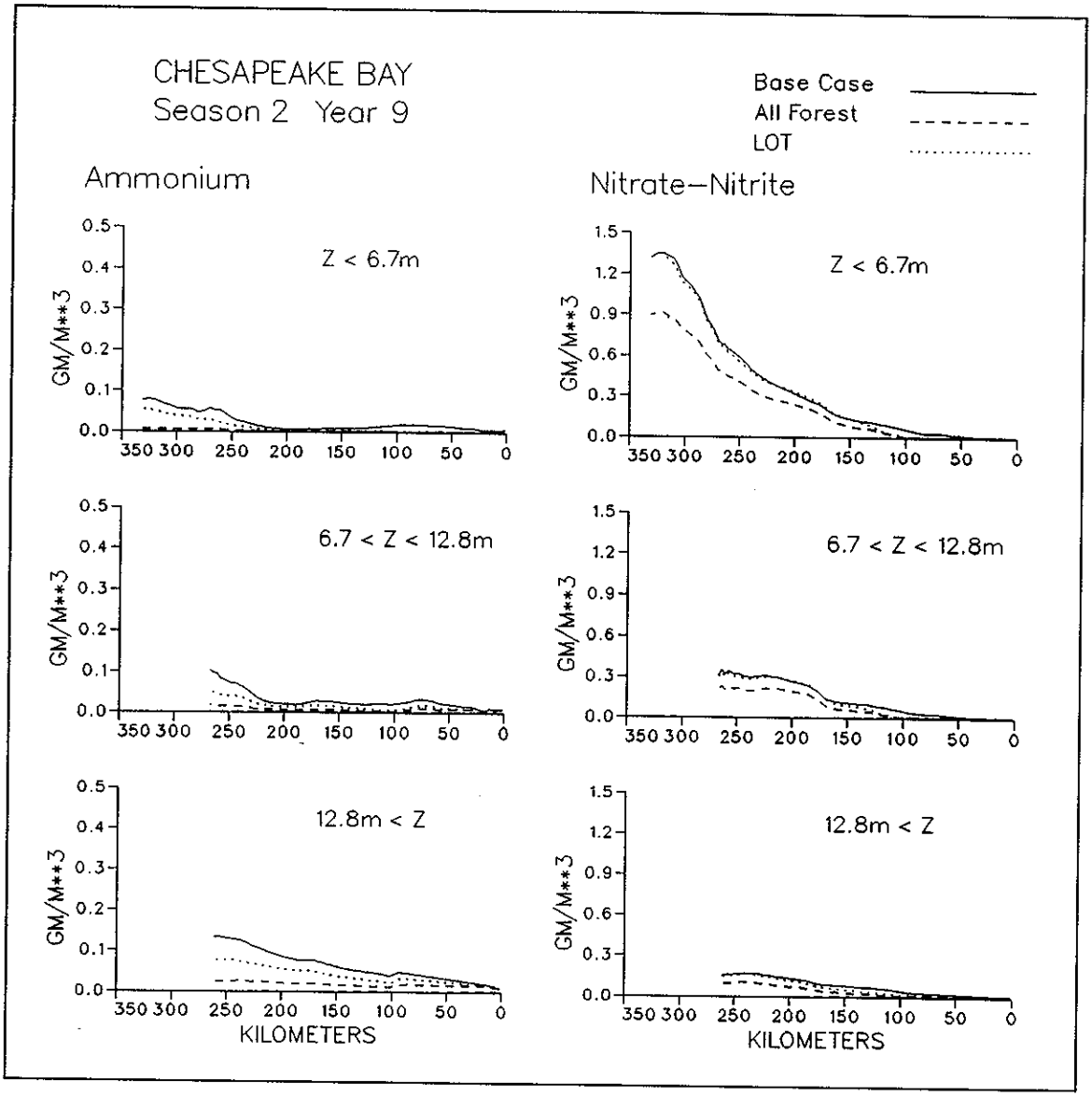

Figure 15-54. (Sheet 3 of 8)

more severe in the lower Bay (Figure 15-56). Nitrogen limitation meant less phosphate was taken up near the mouth and more remained in the water column.

Dissolved organic phosphorus behaved like the equivalent fraction of carbon and nitrogen. Concentration was diminished more in the upper Bay, due to diminished algal production, than in the lower Bay, where concentration was maintained by the oceanic reservoir. Particulate organic phosphorus was not directly related to chlorophyll concentration, however. Concentration declined most near the fall line, reflecting the large particulate component of phosphorus loads.

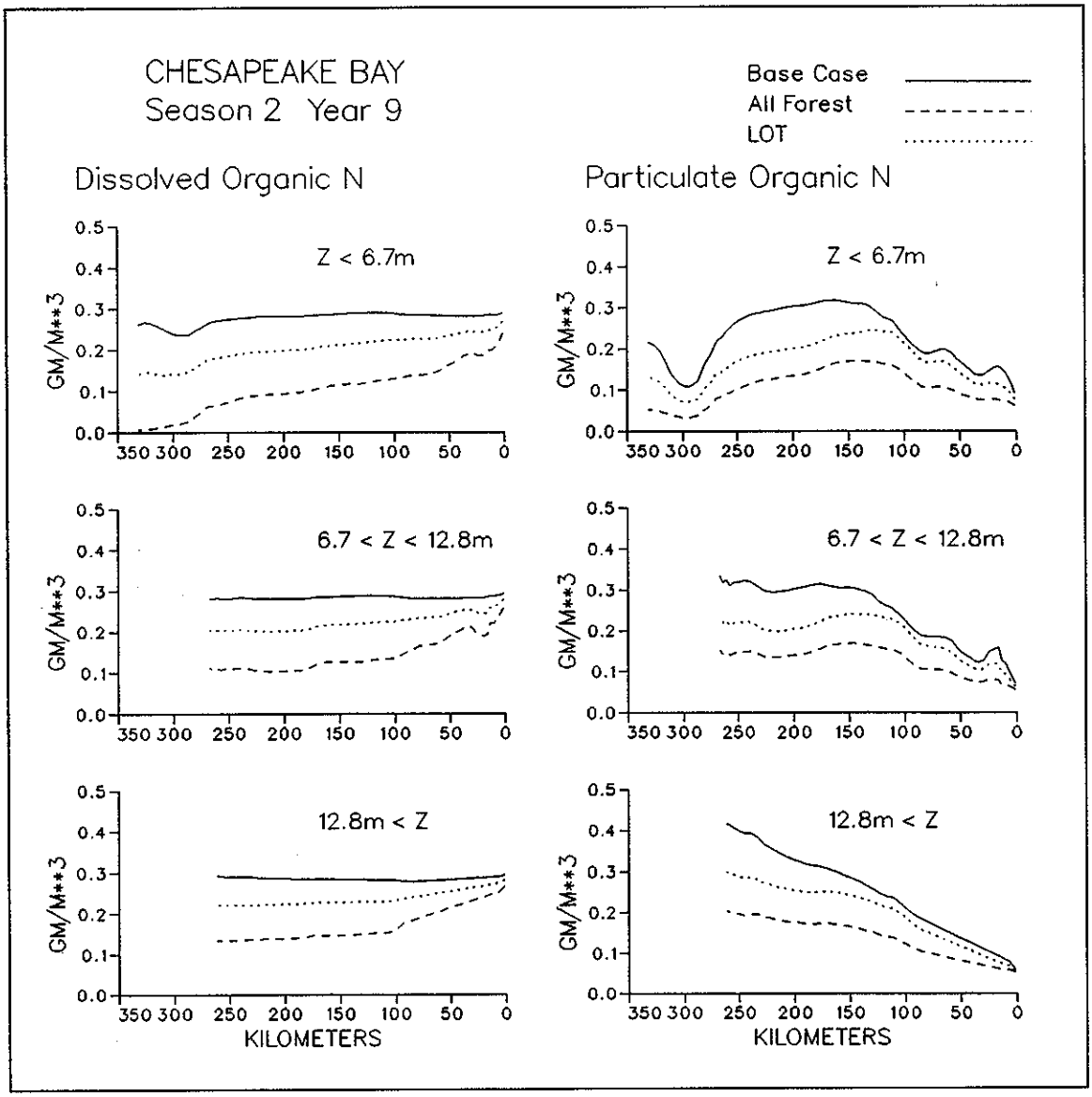

Figure 15-54. (Sheet 4 of 8)

Surface dissolved oxygen was identical under all conditions. Bottom dissolved oxygen improved under LOT and all-forest conditions. For most of spring, however, bottom dissolved oxygen was nearly equal to surface dissolved oxygen. The apparent improvement reflected changes at the onset of the summer anoxic period.

Silica increased under both LOT and all-forest conditions although silica load was unchanged. The increased concentration reflected diminished algal uptake by phosphorus- or nitrogen-limited algae.

Sediment-Water Fluxes. Under existing conditions, deposition to sediments exhibited two peaks (Figure 15-55). Maximum deposition was adjacent to the

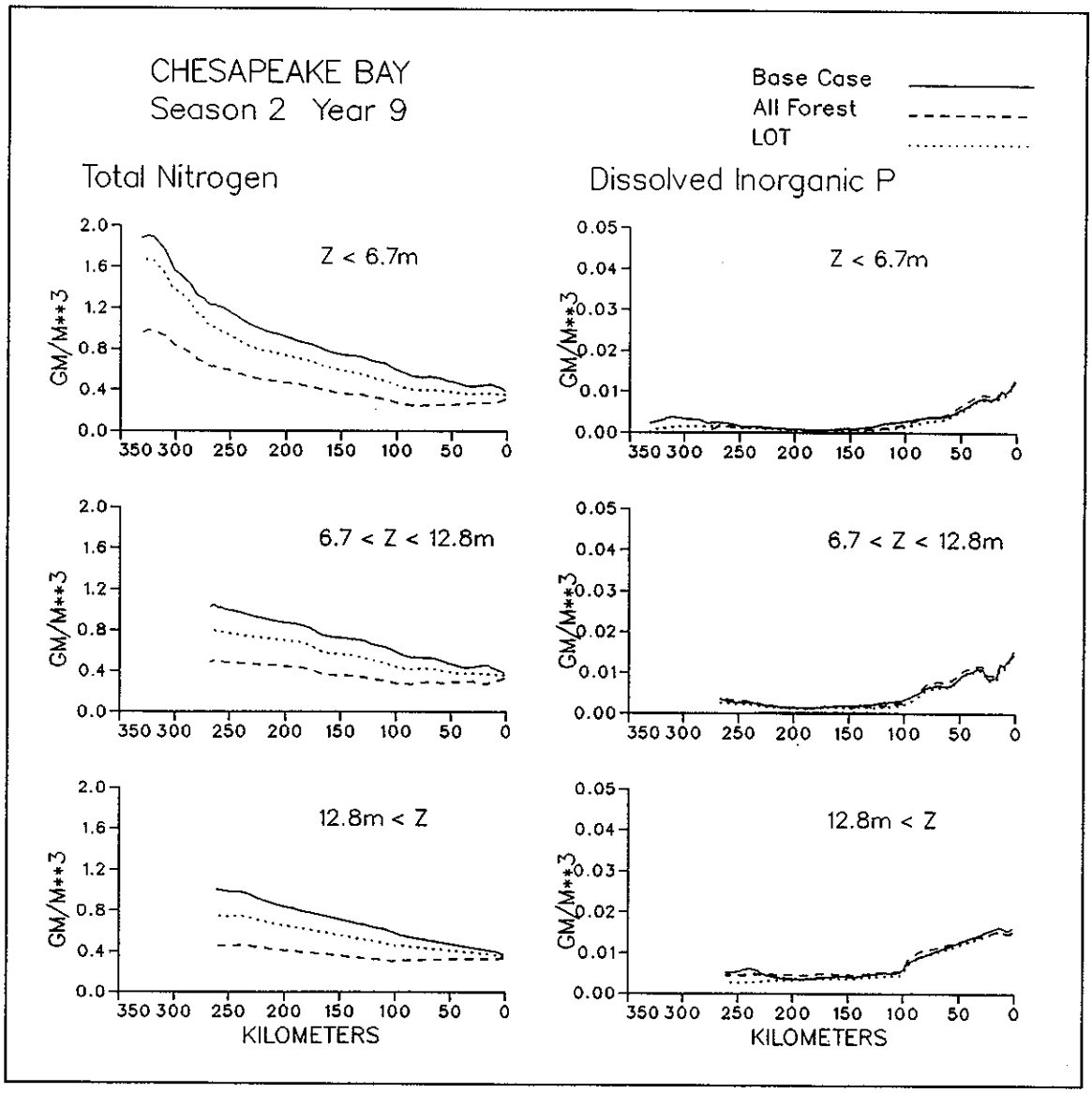

Figure 15-54. (Sheet 5 of 8)

Susquehanna fall line and consisted primarily of river-borne material. The second peak was near km 250, at the head of the deep trench. Material deposited at the head of the trench was a mixture of fall line particles, algal detritus settling from water immediately above, and detritus advected from further downstream. Under LOT conditions, deposition retained the existing spatial distribution but was uniformly less, due to reduction in fall-line loads and algal production. Under all-forest conditions, only a single, diminished peak was evident at the head of the trench. Deposition near the fall line was negligible due to load reductions.

The spatial distribution of sediment oxygen demand differed from deposition. Sediment oxygen demand was minimal adjacent to the fall line despite

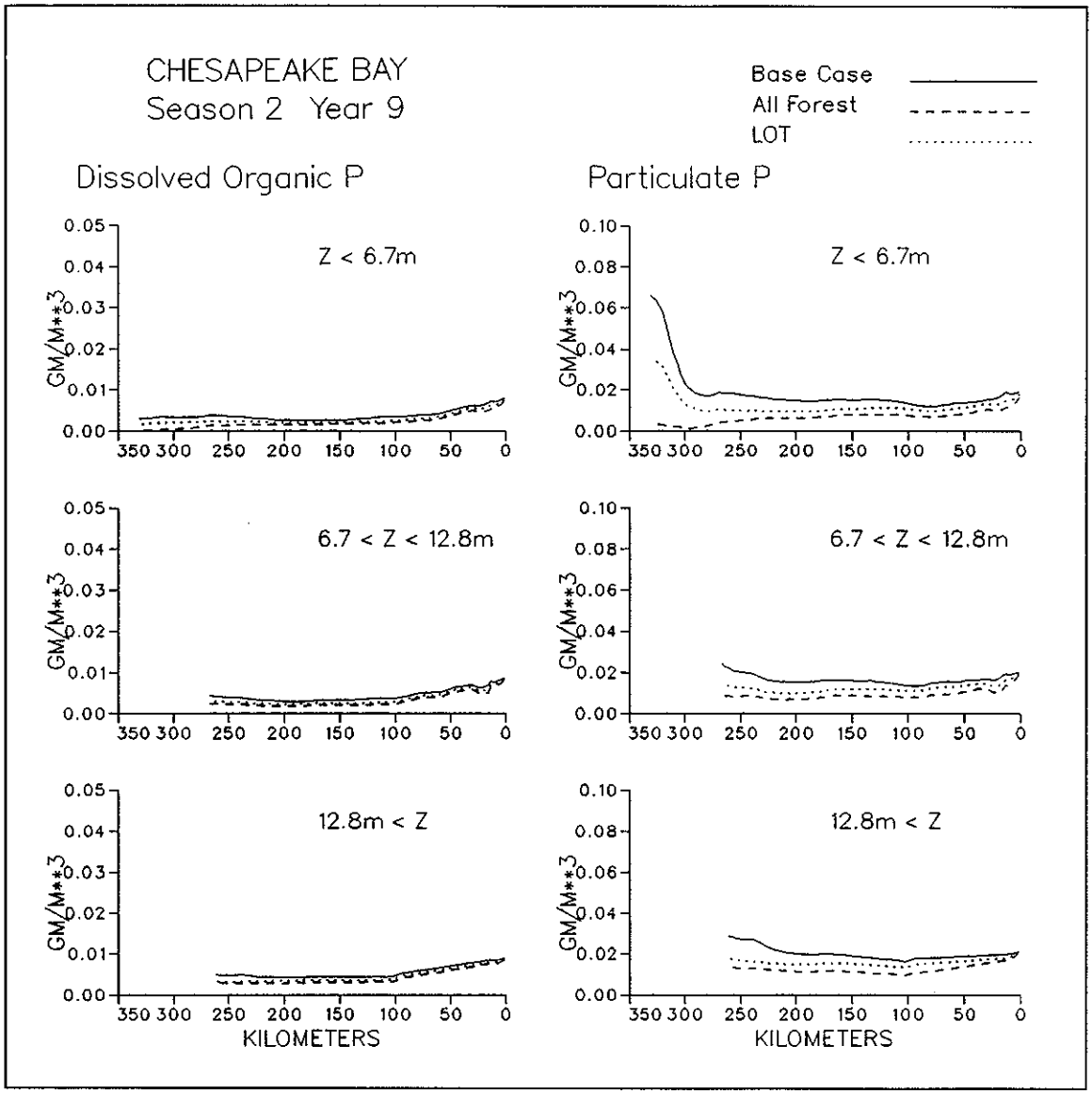

Figure 15-54. (Sheet 6 of 8)

large deposition under existing and LOT conditions. Deposition did not generate sediment oxygen demand because most of the fall-line material was of refractory nature. The refractory portion of fall-line loading also limited, to a lesser extent, sediment oxygen demand at the head of the trench. Maximum sediment oxygen demand occurred around km 200 where deposition was moderate but most material was fresh algal detritus. At all locations, sediment oxygen demand diminished from existing conditions to LOT conditions, to all-forest conditions.

Ammonium release mirrored sediment oxygen demand. Maximum release occurred around km 200, due to deposition of fresh material from the spring

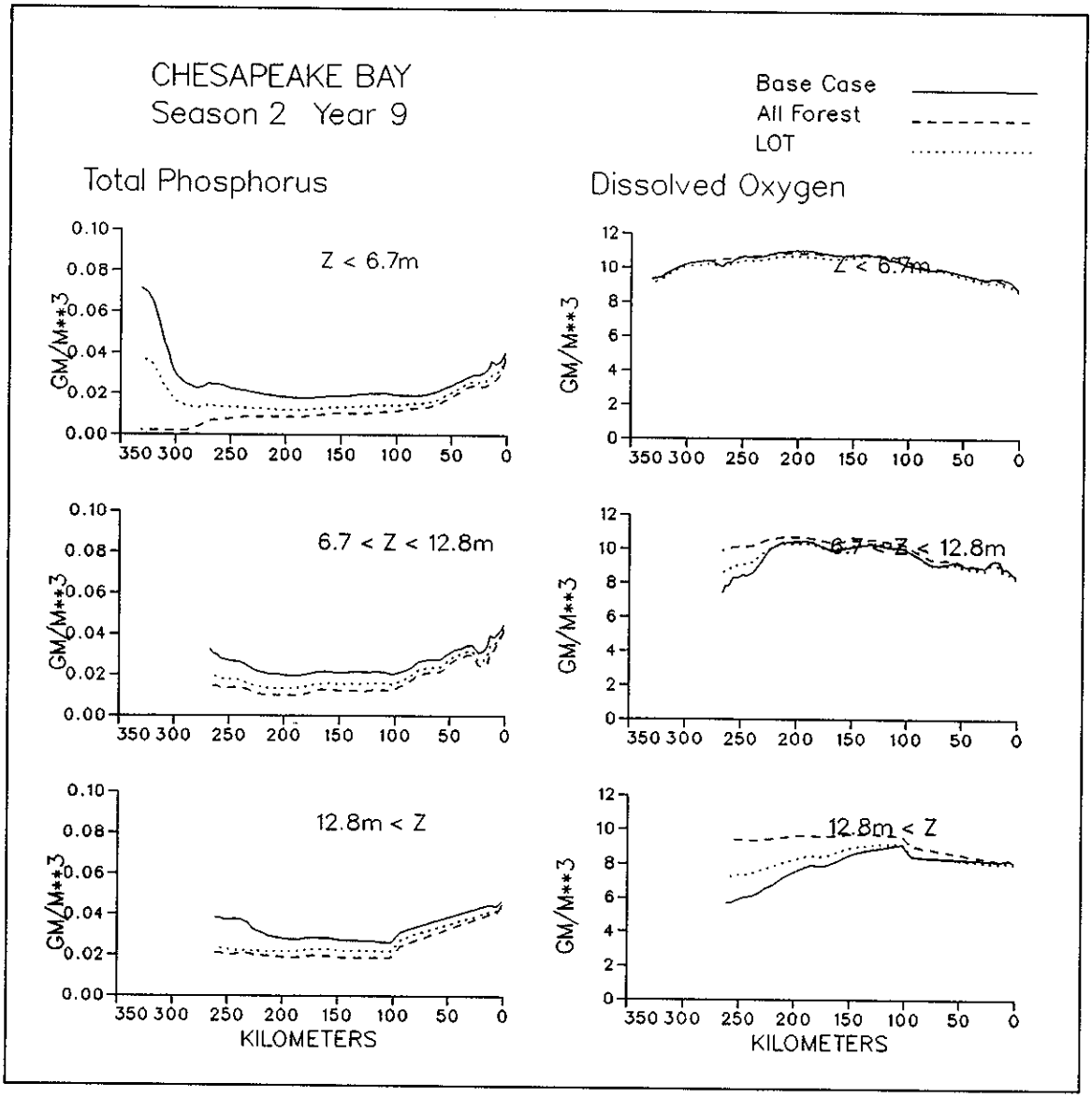

Figure 15-54. (Sheet 7 of 8)

bloom. Release diminished through the sequence from existing to LOT to all-forest conditions.

Sediment-water phosphate flux exhibited a unique pattern in spring. In the central portion of the mainstem, under existing and LOT conditions, dissolved phosphorus diffused from the water column into the sediments. The release, under existing conditions, near km 250 occurred at the onset of anoxic conditions, at the end of the season. Diffusion into sediments indicated a pathway for sediment storage and release of phosphorus in addition to deposition and mineralization of algal detritus. Uptake was negligible under all-forest conditions. The origin of diminished diffusion under all-forest conditions was not clear. Most likely, the sediment-water concentration gradient

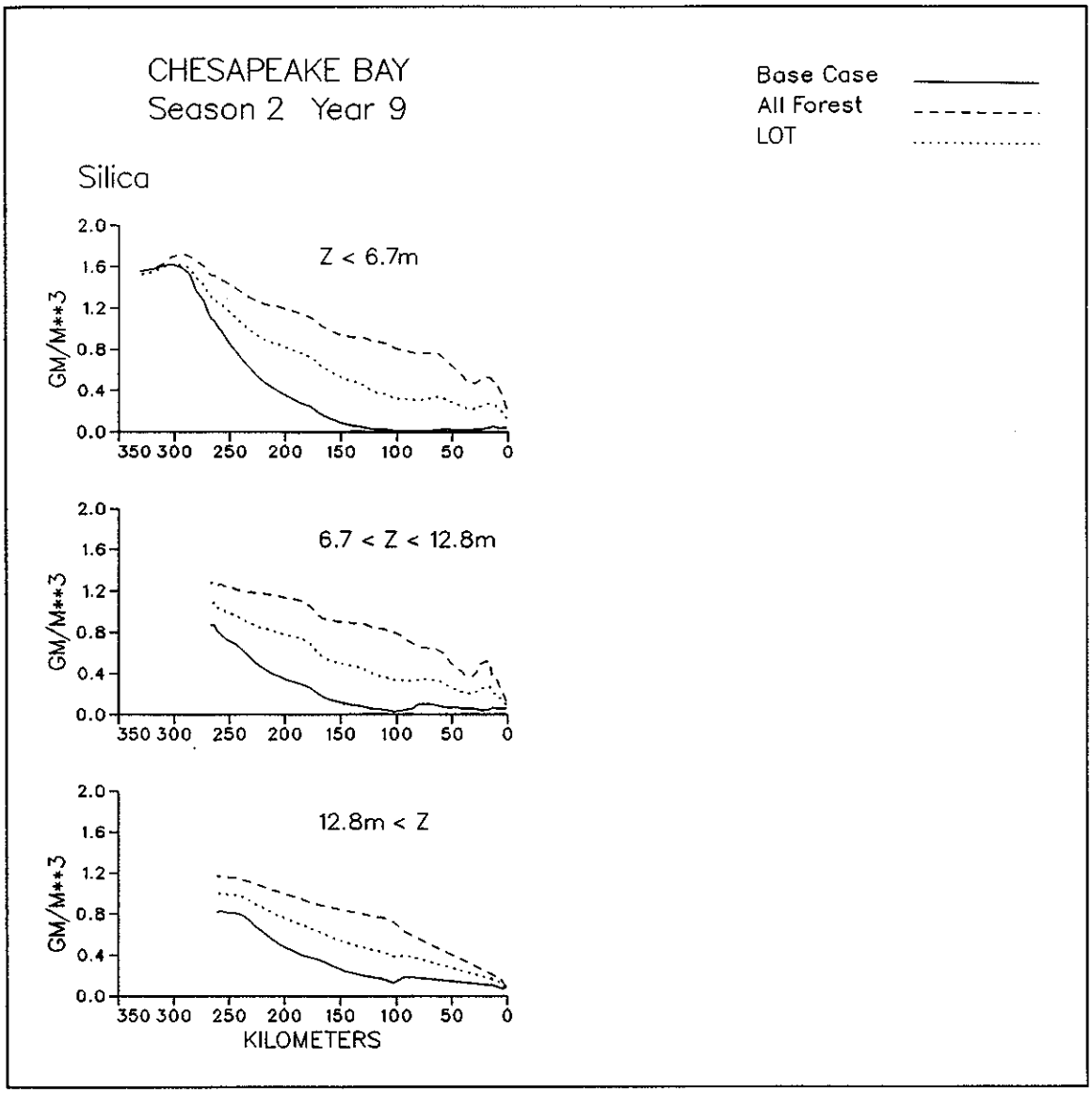

Figure 15-45. (Sheet 8 of 8)

was less although substantial difference in bottom-water phosphate under all-forest conditions, relative to existing conditions, was not evident.

Nutrient Limitations and Primary Production. The LOT and all-forest conditions affected the magnitude, spatial distribution and nature of the limiting nutrient (Figure 15-56). Under base conditions, phosphorus was the limiting nutrient above km 150. Below km 150, silica limitation predominated. Under LOT conditions, the region of phosphorus limitation moved downstream to km 100. Below km 100, limiting nutrient switched to nitrogen. The switch occurred because LOT-induced phosphorus limitation in the upper Bay diminished diatom silica uptake. Less uptake meant more silica travelled downstream towards the mouth. The additional silica in the lower Bay relieved the

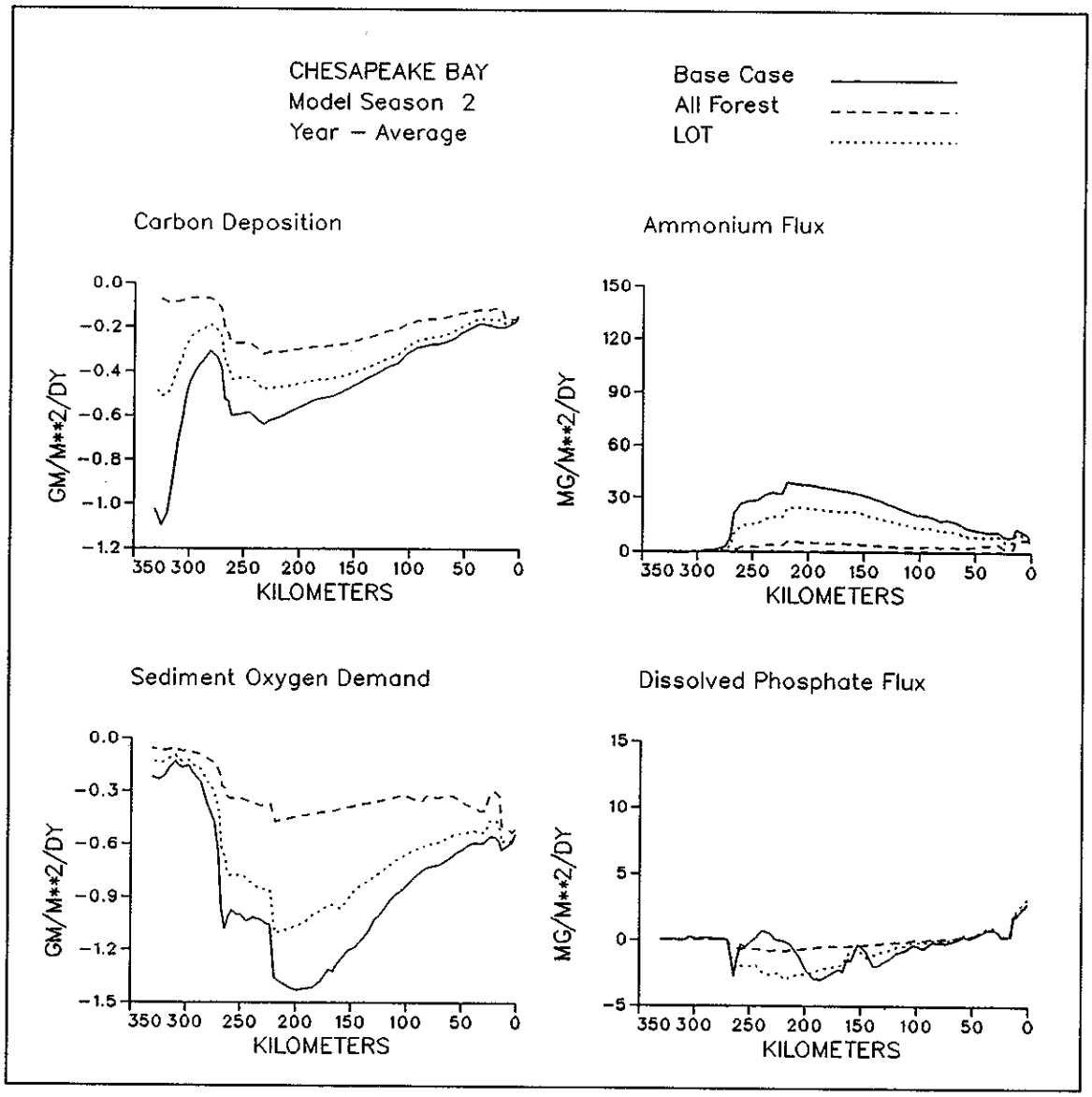

Figure 15-55. Sediment-Water Fluxes Along Mainstem Bay Longitudinal Transect for Three Scenarios, Spring Bloom Period

silica limitation that existed under base conditions. Under all-forest conditions, the spatial extent of phosphorus limitation was unchanged from LOT conditions but the phosphorus limit in the upper Bay became extreme. Adjacent to the fall line, algal production was completely eliminated by phosphorus limitation.

Primary production was diminished more in the upper Bay than the lower Bay under all-forest and LOT conditions. Between km 100 and km 150, a small increase in production occurred under LOT and all-forest conditions. The increase was caused by relaxation of the silica limitation in the lower Bay.

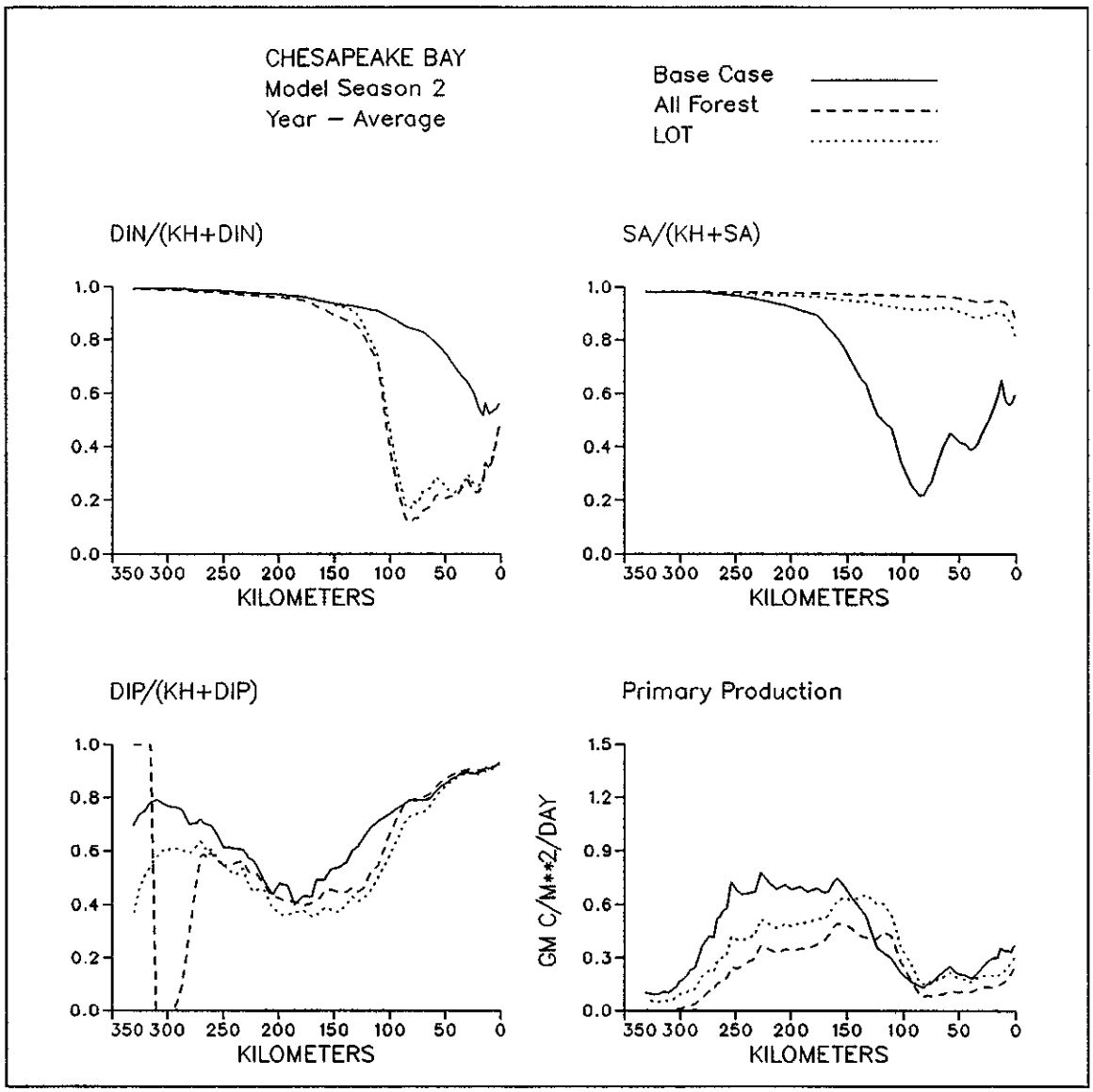

Figure 15-56. Nutrient Limitations and Primary Production Along Mainstem Bay Longitudinal Transect for Three Scenarios, Spring Bloom Period

The Summer Period

Concentrations. Algal biomass, as chlorophyll, diminished under both LOT and all-forest conditions (Figure 15-57). Two factors contributed to the reduction. The first was direct reduction of external nutrient loads. The second was diminished sediment nutrient release. The load reductions resulted in increased bottom dissolved oxygen which, in turn, enhanced sediment retention of nitrogen and phosphorus (Figure 15-58). Enhanced nitrification and denitrification occurred and anoxia-induced phosphorus release was diminished. The

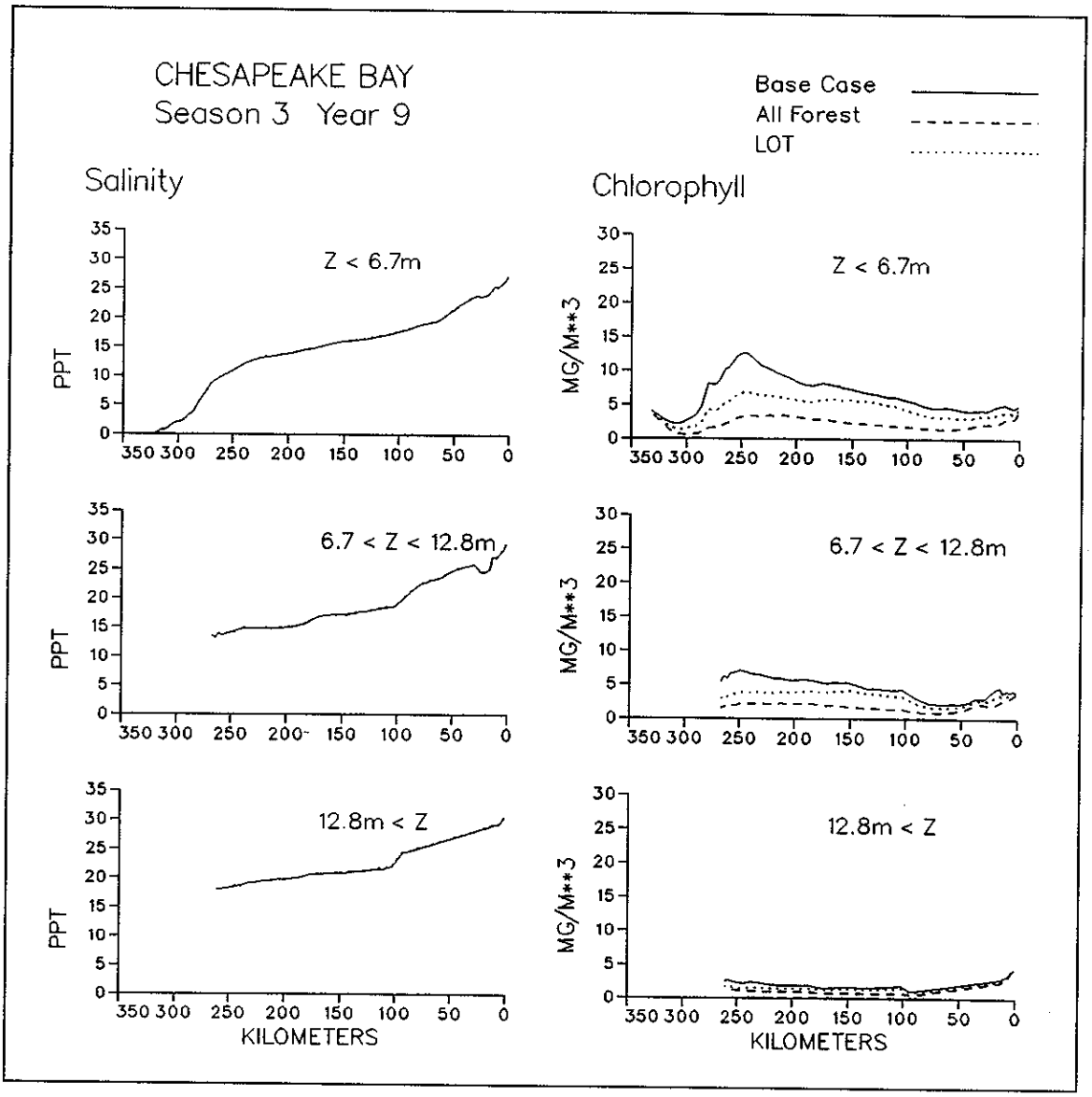

Figure 15-57. Concentrations Along Mainstem Bay Longitudinal Transect for Three Scenarios, Summer Period (Sheet 1 of 8)

reduction of chlorophyll was pronounced near km 150, above the region of greatest sediment release under base conditions.

Behavior of organic carbon was similar to the spring season. Particulate carbon reductions corresponded to algal reductions. Dissolved carbon was diminished greatly in the upper Bay but unaffected at the mouth due to the fixed boundary condition.

Total nitrogen exhibited a unique pattern under all-forest conditions. A longitudinal sag appeared with higher concentrations at the fall line and mouth

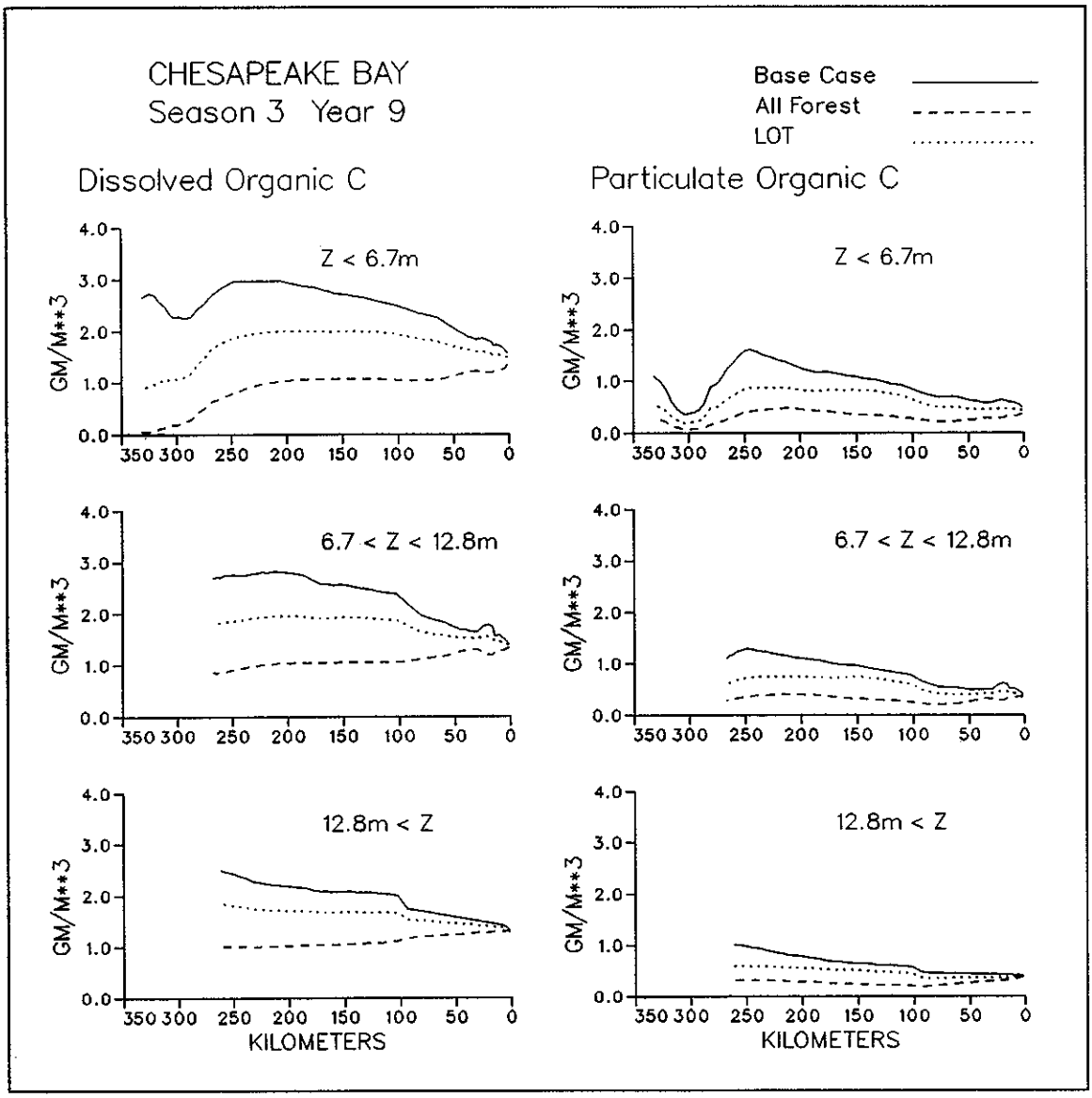

Figure 15-57. (Sheet 2 of 8)

than in the central Bay. The sag implied that the Bay was a net importer of nitrogen during summer under all-forest conditions.

Under existing conditions, total phosphorus concentration was greatest adjacent to the fall line and at the mouth. An internal peak occurred around km 250 due to sediment release (Figure 15-58). Under LOT controls, total phosphorus was greater at the mouth than at the fall line and the internal peak was diminished. Under all-forest conditions, phosphorus virtually disappeared immediately downstream of the fall line and the internal peak was not evident.

Behavior of nutrient fractions did not always correspond to total nutrient concentration. Under LOT controls, nitrate concentration increased above

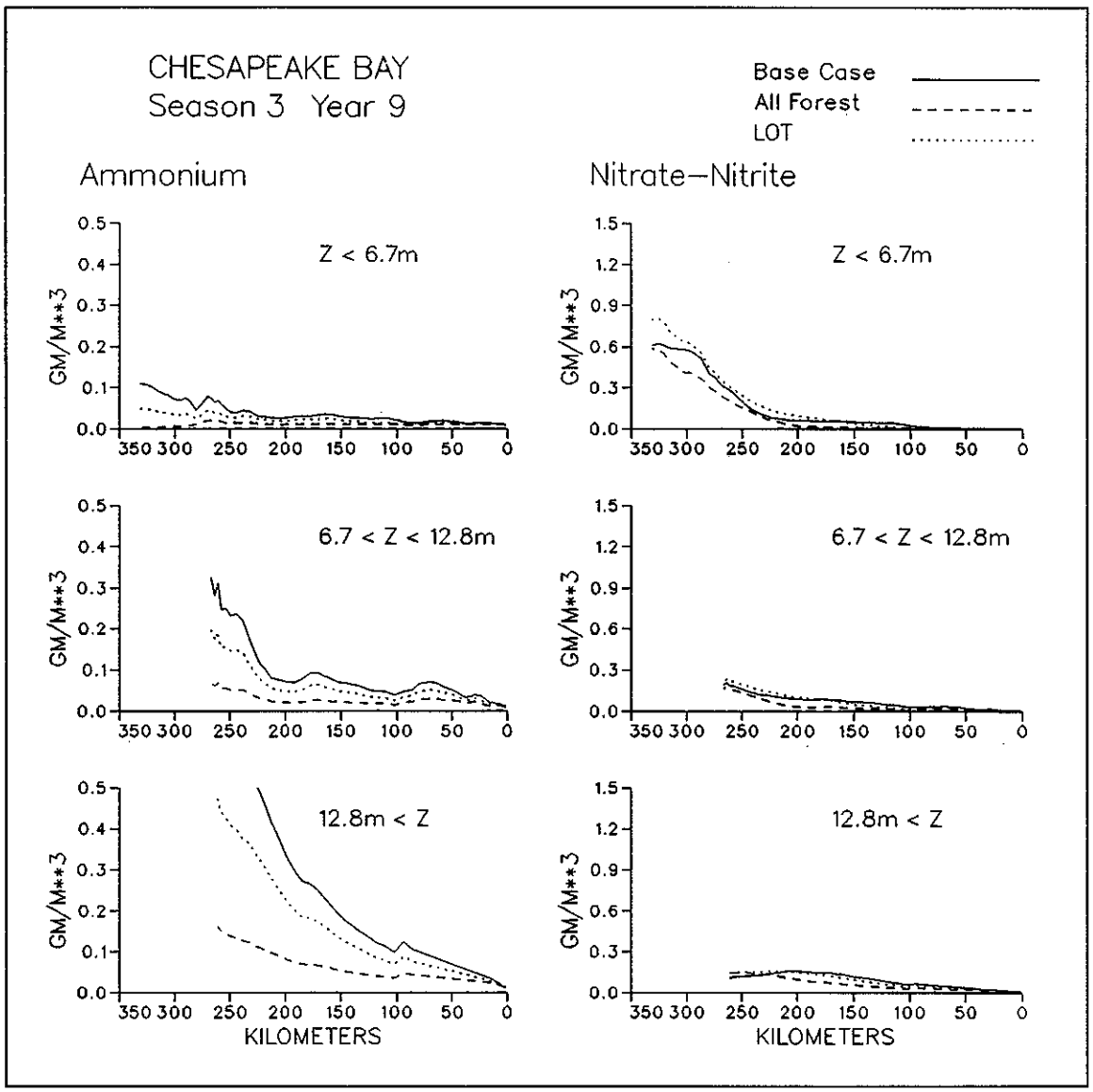

Figure 15-57. (Sheet 3 of 8)

km 150. The increase in nitrate reflected diminished algal uptake due to heightened phosphorus limitation above km 150 (Figure 15-59). Nitrate was less under all-forest conditions, however. Ammonium diminished under both LOT and all-forest conditions. Less ammonium was largely attributable to diminished sediment release.

Organic nitrogen behaved as organic carbon. Particulate nitrogen declined in proportion to algal biomass. Dissolved organic nitrogen declined greatly in the upper Bay and to a lesser extent in the lower Bay. The decline in organic fractions represented, by far, the majority of the total nitrogen decline in surface waters.

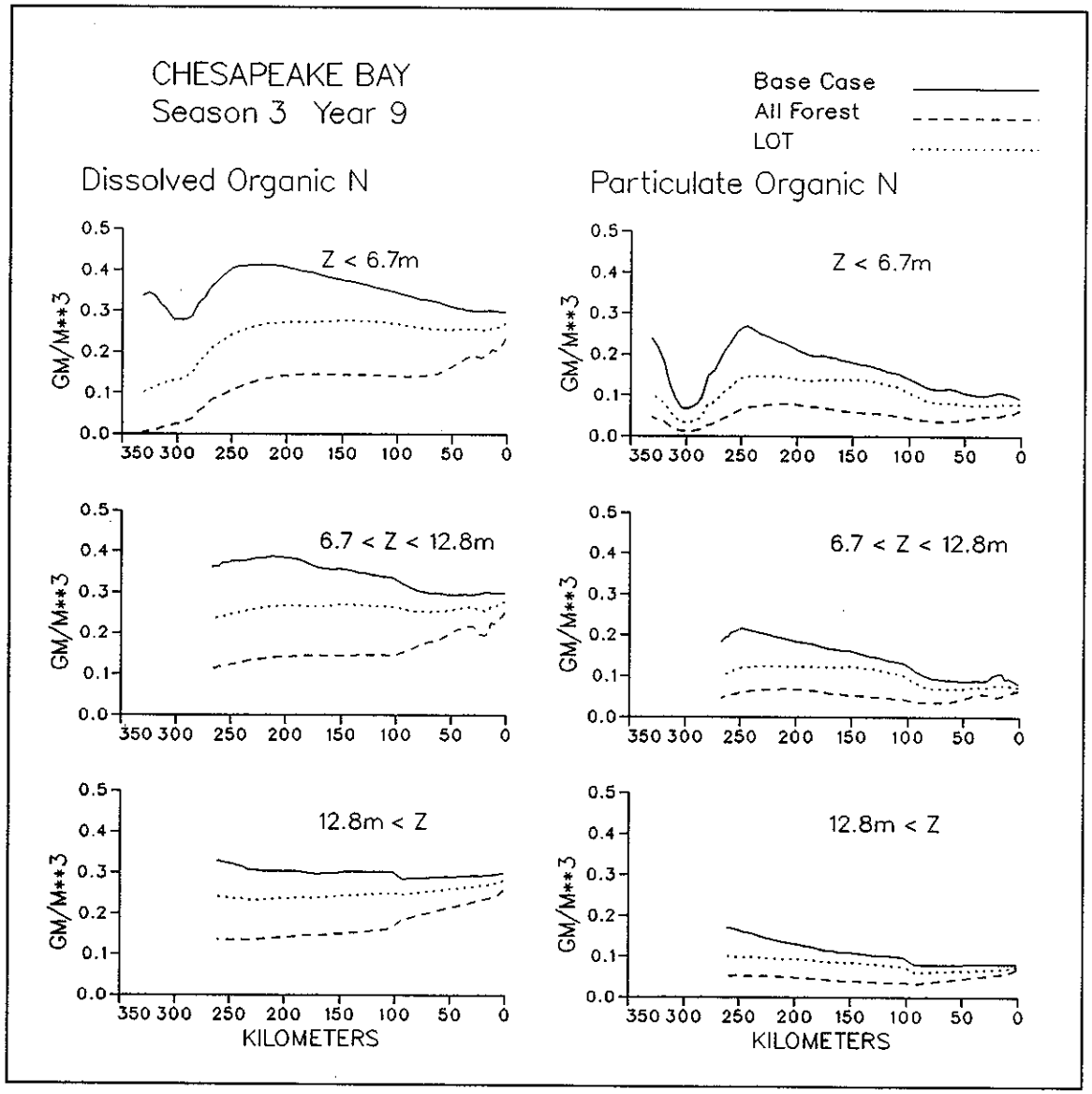

Figure 15-57. (Sheet 4 of 8)

Dissolved phosphate in surface waters was nearly identical under base and LOT conditions. Some decline was noted above km 250. The shape of the response indicated the decrease was from an internal source rather than fall-line loading. Diminished sediment release was most likely responsible although decreased point-source loading from the vicinity of Baltimore may also have been evident. Under all-forest conditions, decline near the fall line continued. The altered shape of the longitudinal distribution indicated the internal source was no longer active. Under all-forest conditions, dissolved phosphorus increased below km 150 due to enhanced nitrogen limitation of algae in the lower Bay.

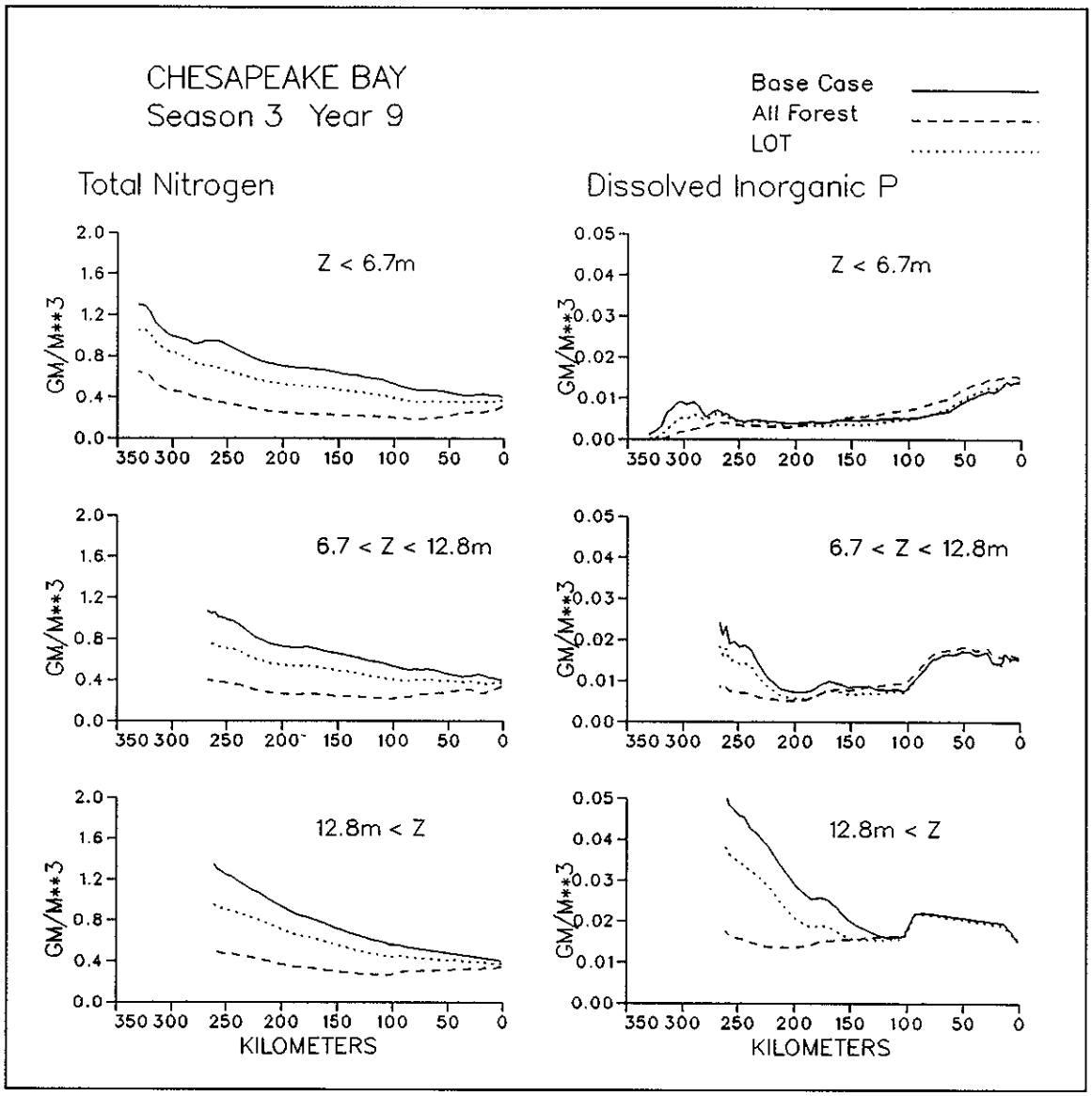

Figure 15-57. (Sheet 5 of 8)

Dissolved organic phosphorus declined in the upper Bay due to diminished algal production. Decline was less near the mouth due to effects of the oceanic source. Most decrease in particulate phosphorus near the fall line was due to diminished loading. A decrease at km 250, due to reduction in algal biomass was also evident.

Under LOT nutrient controls, bottom dissolved oxygen increased by ≈ 0.5 gm m^{-3} throughout much of the mainstem below 12.8 m depth. A substantial volume of water with dissolved oxygen concentration below 1 gm m^{-3} persisted, however (Figure 15-60). System anoxic volume days decreased from 44.6×10^{10} m^3 days under base conditions to 26.7×10^{10} m^3 days under LOT conditions.

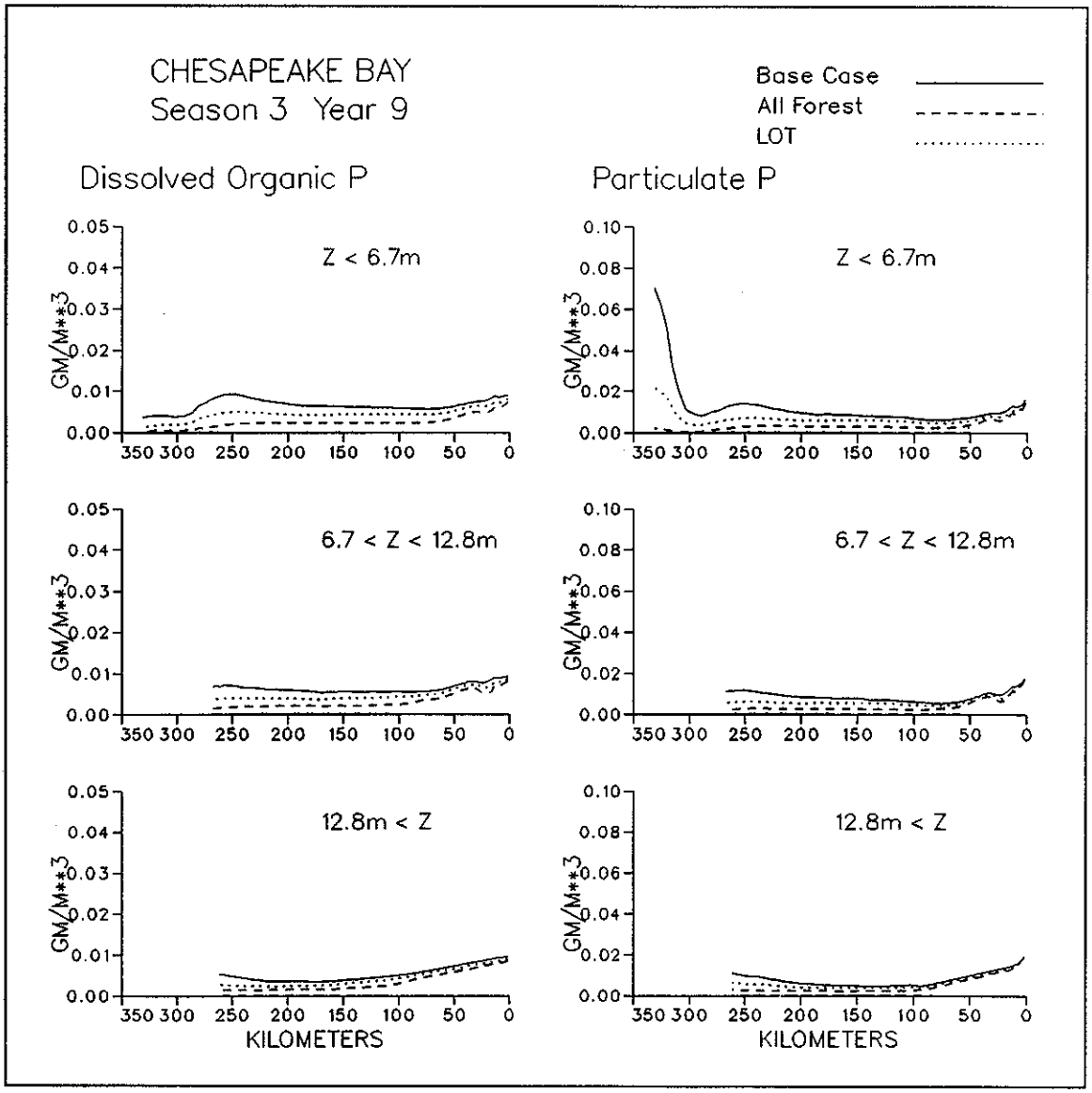

Figure 15-57. (Sheet 6 of 8)

Under all-forest conditions, minimum seasonal-mean dissolved oxygen increased to ≈ 2.7 gm m^{-3}. Dissolved oxygen improved in the pyncnocline as well as near the bottom. Occurrences of dissolved oxygen less than 1 gm m^{-3} were virtually banished under average hydrologic conditions (Figure 15-60). Dissolved oxygen less than 1 gm m^{-3} still occurred under wet hydrology, however. The volume was greatly diminished from 77.1×10^{10} m^3 days under base conditions to 19.4×10^{10} m^3 days under all-forest conditions.

Sediment-Water Fluxes. Deposition during the summer exhibited two peaks, as in spring (Figure 15-58). During summer, however, maximum deposition was at the head of the trench rather than at the fall line. The disparity between deposition in the trench, primarily algal detritus, and deposition near the fall

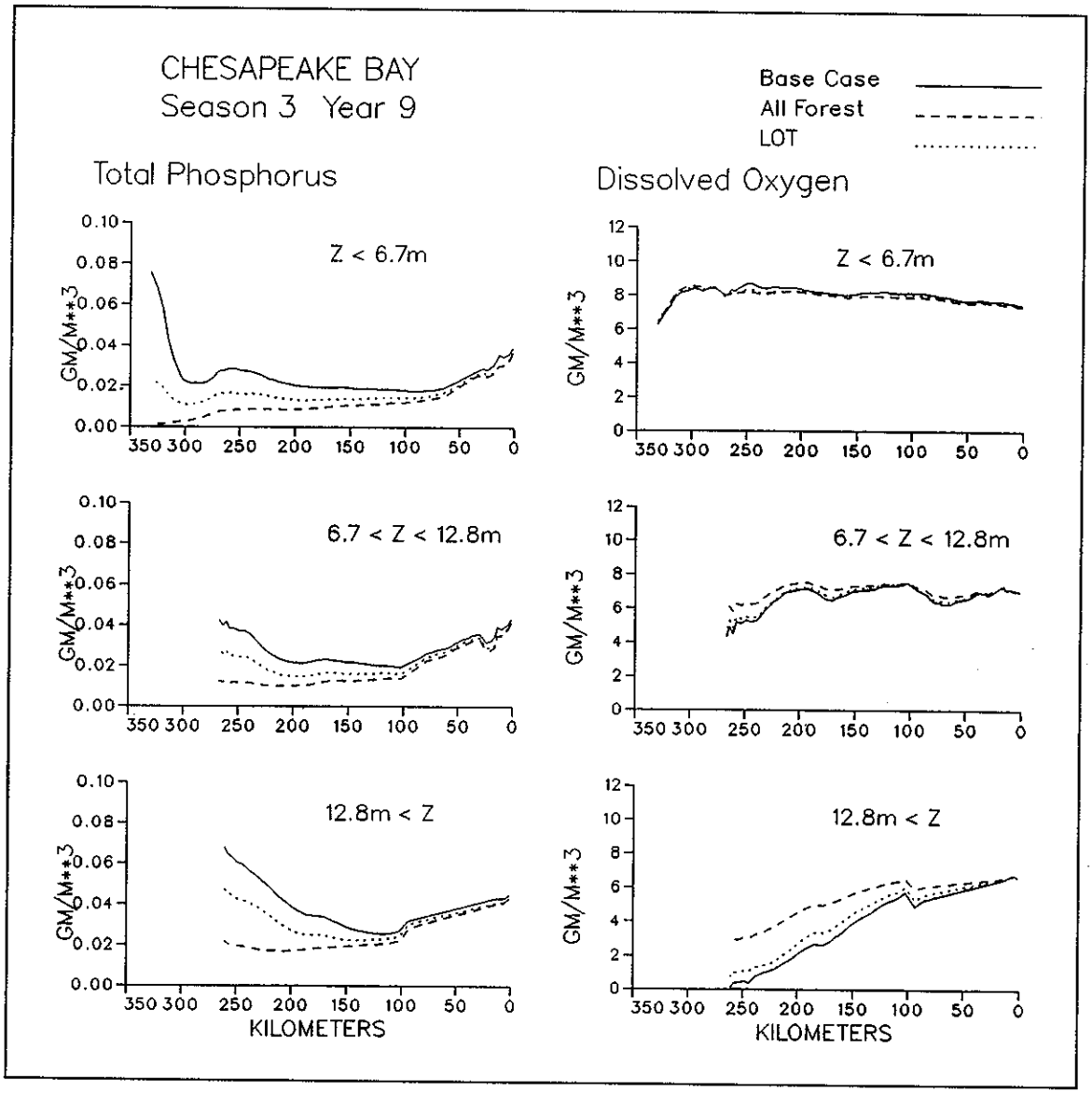

Figure 15-57. (Sheet 7 of 8)

line, primarily river-borne material, was especially evident for the LOT and all-forest scenarios.

Under existing conditions, the spatial distribution of sediment oxygen demand was influenced by dissolved-oxygen concentration in the overlying water. Sediment oxygen demand at the head of the trench, in the region of maximum deposition, was depressed to near zero by absence of oxygen in the water above. Oxygen demand was instead released to the water column in the form of sulfide. Maximum sediment oxygen demand occurred above km 250, upstream of the steep descent into the trench, and around km 100, downstream of the region of recurrent bottom-water anoxia.

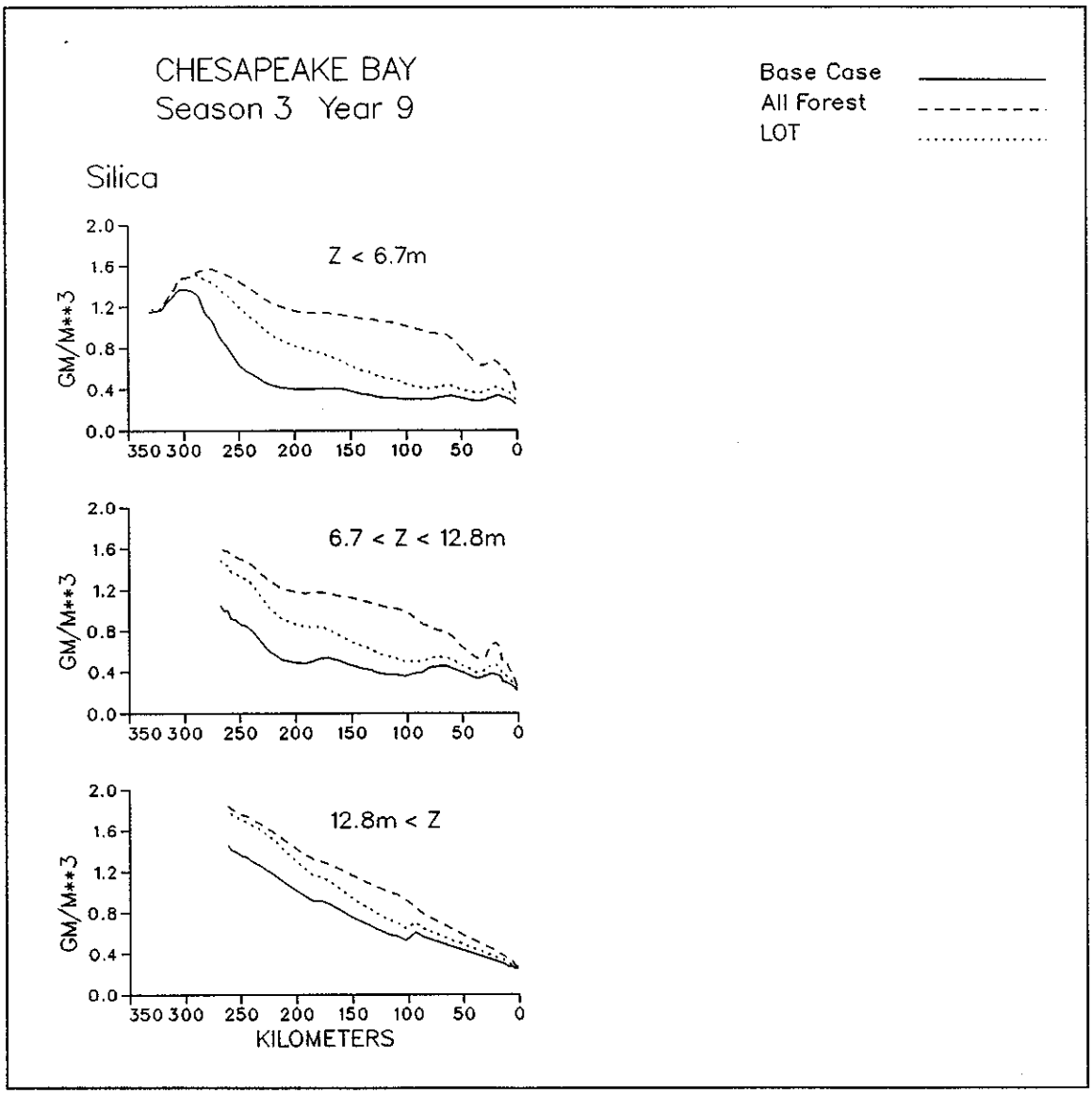

Figure 15-57. (Sheet 8 of 8)

The spatial distribution of sediment oxygen demand under LOT conditions was similar to existing conditions. Demand increased near km 200, however, due to availability of additional oxygen in bottom water. Enhanced oxygen consumption in the sediments meant that less sulfide was released to the water column. Sediment oxygen demand diminished in the lower Bay due to diminished deposition.

Due to absence of oxygen depletion under all-forest conditions, the spatial pattern of sediment oxygen demand conformed largely to the pattern of deposition of labile material. Maximum demand occurred around km 200.

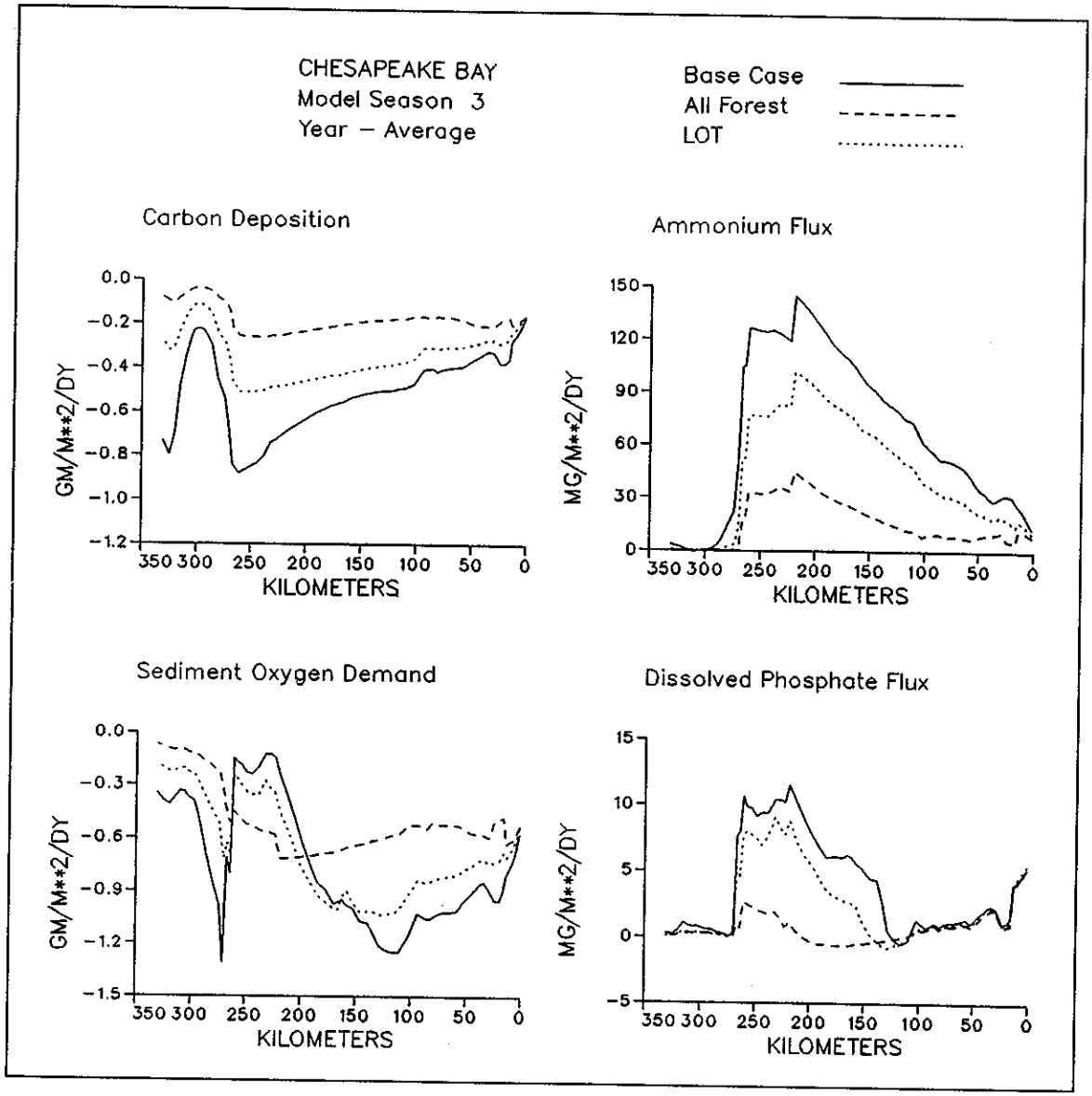

Figure 15-58. Sediment-Water Fluxes Along Mainstem Bay Longitudinal Transect for Three Scenarios, Summer Period

Maximum sediment ammonium release occurred around km 200, slightly downstream of the location of maximum deposition. The offset between maximum deposition and maximum release occurred because deposition at the head of the trench was partially refractory river-borne material. Release responded both to load reductions and increased oxygen in bottom water. As oxygen increased, a larger fraction of sediment nitrogen was denitrified rather than released to the water column.

Under existing and all-forest conditions, maximum sediment phosphorus release occurred between km 200 and 250. Release was influenced by patterns of deposition and by anoxia in the overlying water. Anoxia suppressed

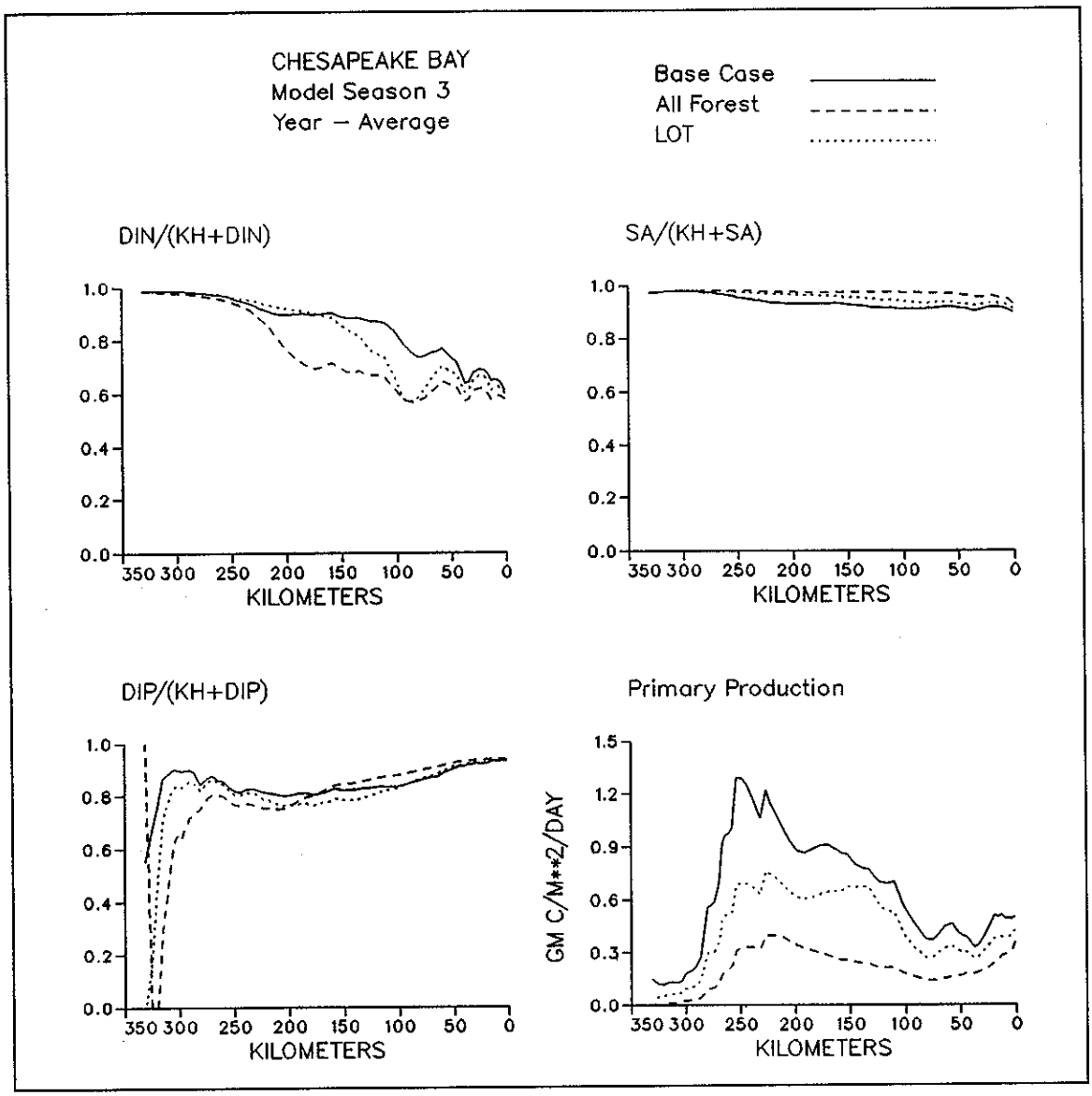

Figure 15-59. Nutrient Limitations and Primary Production Along Mainstem Bay Longitudinal Transect for Three Scenarios, Summer Period

sorption to sediment particles and allowed phosphorus to flow freely from sediments to water. Over the season, however, no more phosphorus could be released than was produced by diagenesis of deposited material.

Under all-forest conditions, maximum phosphorus release was greatly diminished but the location of the maximum was unchanged. Near the fall line and downstream of km 125, sediment phosphorus release was unchanged in any of the scenarios. No change (or release) occurred near the fall line because much material deposited under existing conditions was refractory. Reduction of the load of this material did not alter the amount of phosphorus mineralized in the sediments. In the lower Bay, no change occurred because

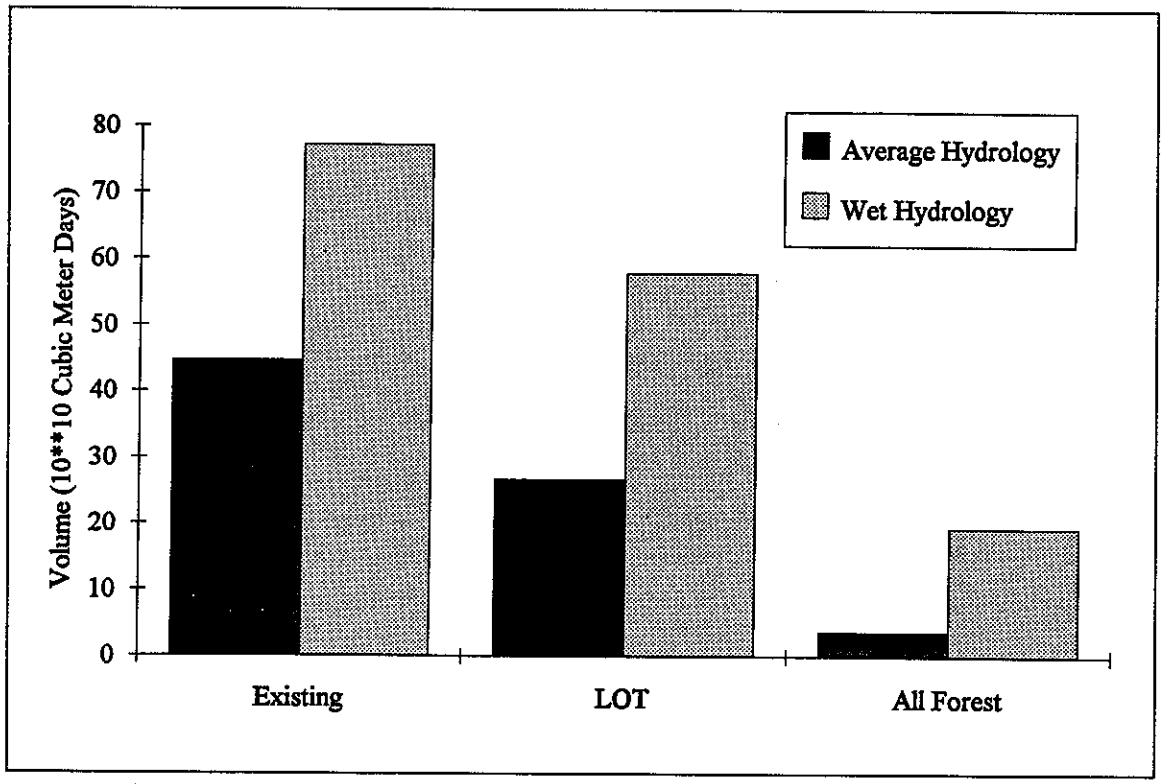

Figure 15-60. Total System Anoxic Volume in Wet and Average Hydrologic Conditions for Three Scenarios

much sediment phosphorus originated in the uncontrolled ocean source and because negligible alteration took place in water-column dissolved oxygen.

Nutrient Limitations and Primary Production. Under base conditions, phosphorus was the limiting nutrient above km 250 and nitrogen was the limiting nutrient below km 100. In the central region, phosphorus, nitrogen, and silica limitations were roughly equivalent. The role of the silica limitation was not significant, however, since diatoms were a small fraction of the total algal biomass.

Under LOT controls, the phosphorus limitation in the upper Bay became more severe and was clearly dominant above km 150. Nitrogen limitation became more severe above km 50. Reductions in primary production occurred primarily above km 150.

Phosphorus limitation in the upper Bay became yet more severe under all-forest conditions. Algal production was absent adjacent to the fall line. The region of nitrogen limitation moved upstream, however, to km 200.

System Annual Nutrient Budgets

System-wide annual nutrient budgets were constructed for the average hydrologic year. Budgets were constructed in two formats. In the first format, mass fluxes were presented. In the second format, fluxes were presented as fractions, normalized by load. Load was considered to be the sum of loads from all fall lines, nonpoint sources, point sources, the atmosphere, and the continental shelf. Recycled Bay water entering the mouth was not considered in the sum.

The nitrogen budget for existing conditions (Figures 15-61, 15-62) provided more detail than the mainstem budget prepared as part of the calibration (Figures 11-41, 11-42). The budget indicated that fall-line loading was the largest nitrogen source to the system. The budget confirmed that the Bay was a net exporter of nitrogen through the mouth. Two-thirds of the nitrogen entering the mouth was recycled nitrogen that originated in the Bay. One-third the nitrogen entering the mouth was from the uncontrollable shelf reservoir. The shelf load exceeded all loads to the system except fall-line loading. Lesser loading sources were point sources, nonpoint sources, and the atmosphere, respectively. The detailed budget revealed that half the atmospheric nitrogen load was returned to the atmosphere as a result of water-column denitrification.

Sediments were the greatest nitrogen sink, exceeding by far the net amounts lost to the ocean and through water-column denitrification. Within the sediments, denitrification exceeded burial and was the single largest pathway for nitrogen removal from the system.

The phosphorus budget for existing conditions (Figures 15-61, 15-62) revealed that new phosphorus from the continental shelf was the largest load to the system, comprising nearly half the total load. Lesser loads came from the fall line, point sources, nonpoint sources, and the atmosphere. The greatest phosphorus sink was through burial. The only secondary sink was loss through the mouth. More than two-thirds of the phosphorus lost through the mouth was recycled and returned to the Bay.

Nitrogen deposition to the sediments exceeded load to the system (Figure 15-62). Excess of deposition over loading indicated nitrogen was rapidly cycled from the sediments to the water column and back to the sediments. On the annual basis, nearly half the deposited nitrogen was returned to the water column.

Phosphorus deposition was also substantial but represented a lesser fraction of total loads than for nitrogen (Figure 15-62). Of more significance, only twenty-percent of the deposited phosphorus was returned to the water. The retention was due to the strong tendency for phosphate to sorb onto sediment particles. By contrast, sorption provided negligible retention of ammonium.

The relative magnitudes of nitrogen sources was the same for LOT as for existing conditions (Figures 15-63, 15-64). The continental shelf represented a

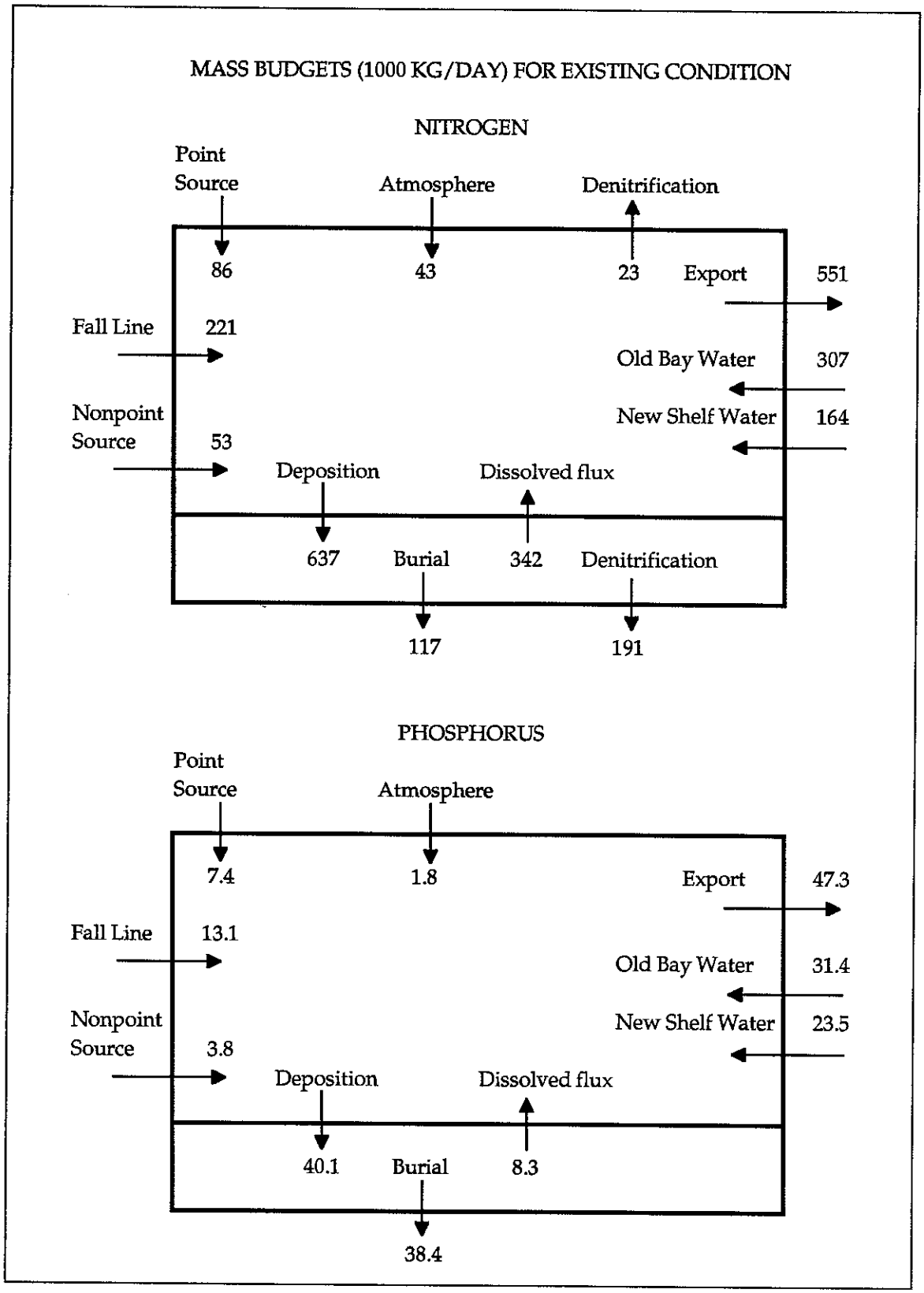

Figure 15-61. Total System Annual Nitrogen and Phosphorus Mass Budgets for Existing Conditions

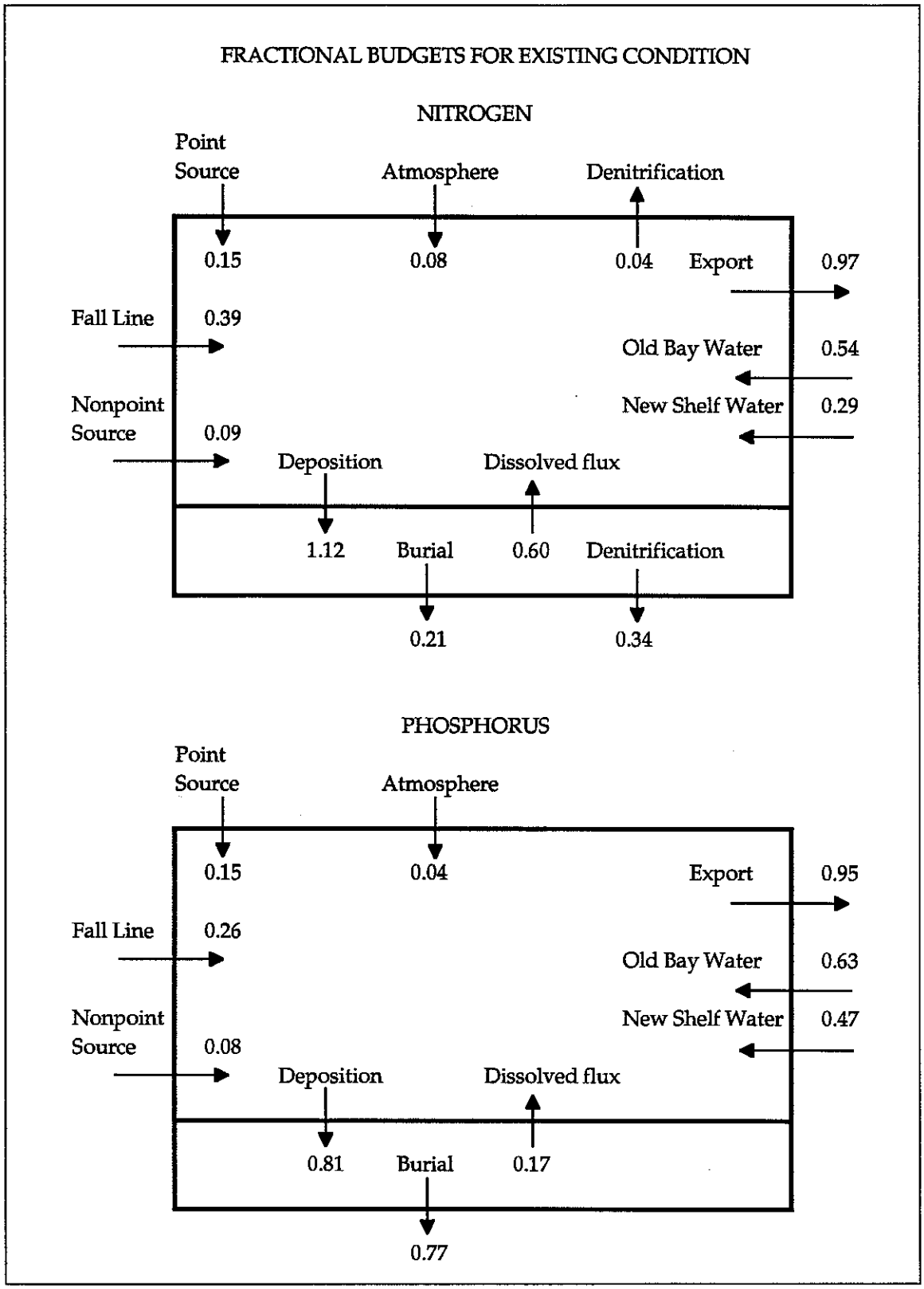

Figure 15-62. Total System Annual Nitrogen and Phosphorus Fractional Budges for Existing Conditions

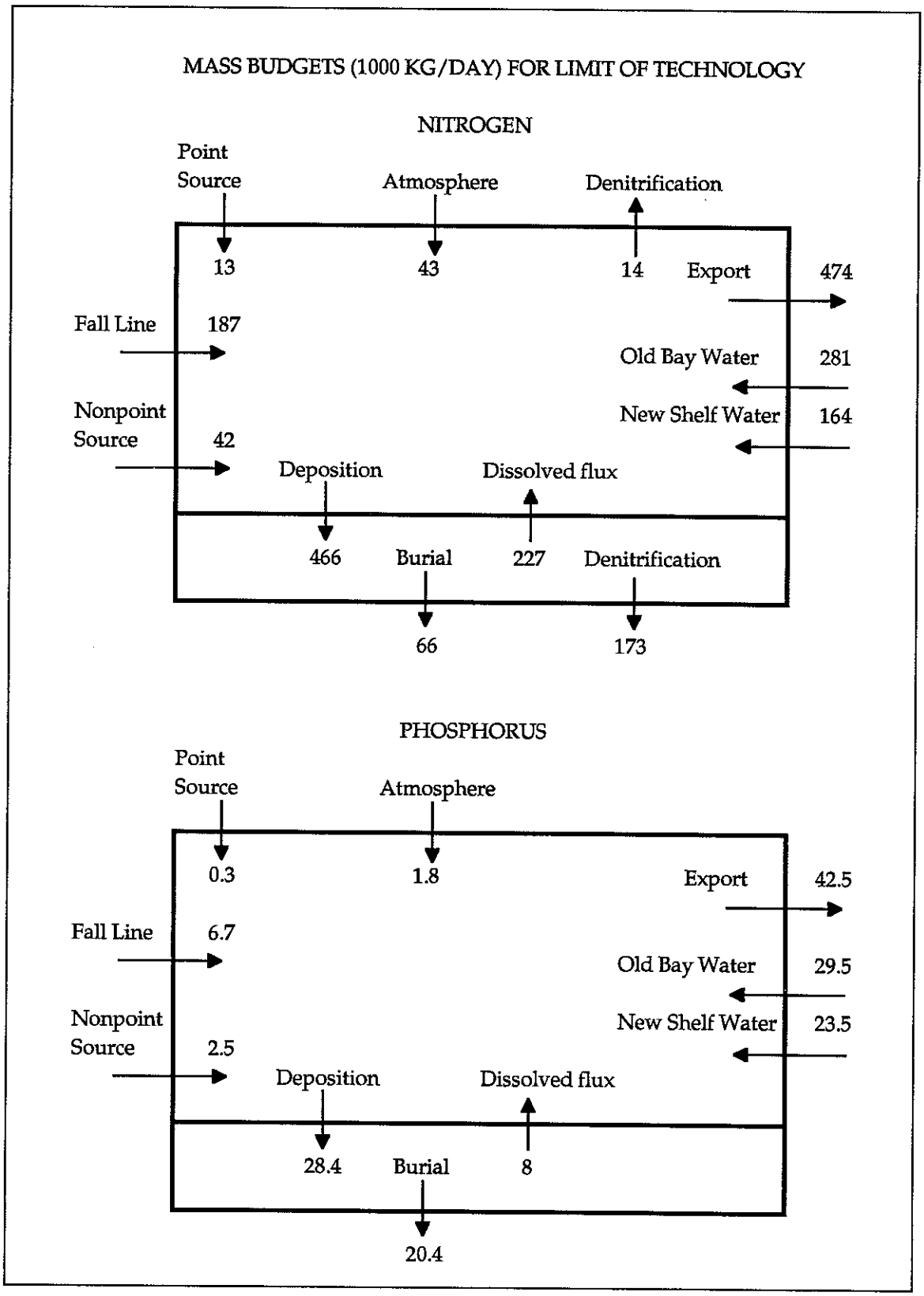

Figure 15-63. Total System Annual Nitrogen and Phosphorus Mass Budgets for LOT Conditions

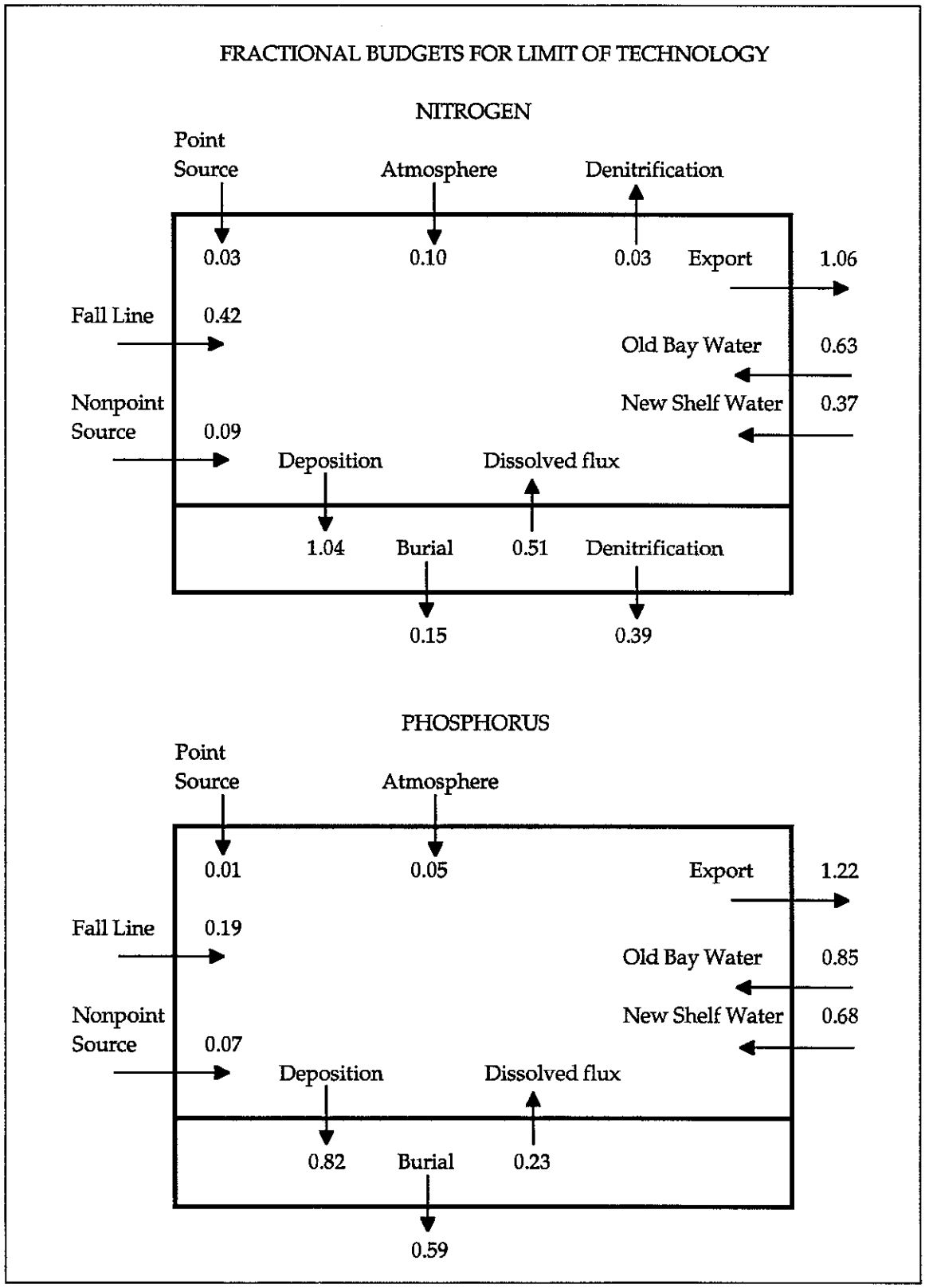

Figure 15-64. Total System Annual Nitrogen and Phosphorus Fractional Budgets for LOT Conditions

larger fraction of the total, however. The Bay remained a net exporter of nitrogen to the shelf. Sediments remained the largest nitrogen sink. The fraction lost to denitrification increased as a result of improved bottom-water dissolved oxygen.

Relative magnitudes of phosphorus loads under LOT were also the same as for existing conditions. Under LOT, however, the continental shelf provided more than two-thirds the total system phosphorus load. Although phosphorus release to the water column declined, the fraction of loading represented by release increased. The increased fraction represented additional diffusion induced by lower phosphate concentration in the water column.

In the sediments, neither the nitrogen or phosphorus budgets were in balance. The imbalance was especially pronounced for phosphorus, for which burial (35,000 kg day^{-1}) exceeded deposition. Burial of nitrogen (105,000 kg day^{-1}) was less than deposition, but still caused a negative balance in the budget. The reported burial fluxes for the LOT and all-forest scenarios were adjusted to balance the sediment budgets.

The time scale for sediment equilibration to LOT loads, in excess of thirty years, raises the question if the sediments are ever in steady state. The time scale indicates phosphorus presently available from Bay sediments reflects loads during the 1970's peak. The lengthy time scale for equilibration also raises questions about the extent to which estimates of burial, which reflect deposition over decades, can be employed in annual nutrient budgets based on loads from a single year.

Relative magnitudes of nitrogen loads under all-forest conditions differed substantially from existing and LOT conditions (Figures 15-65, 15-66). Under all-forest conditions, the continental shelf displaced the fall lines as the primary nitrogen source. The Bay became a net importer of nitrogen from the shelf. Sediments remained the major nitrogen sink. The fraction lost to denitrification, rather than burial, increased, due to the elimination of bottom-water anoxia.

Under all-forest conditions, the continental shelf was virtually the only source of phosphorus to the system. Less phosphorus was deposited and buried than under existing conditions. Deposition was diminished because the strongly nutrient-limited algae took up less phosphate from the water column. As a consequence, half the phosphorus which entered the system was lost out the mouth of the Bay.

Influence of Nitrogen and Phosphorus on Anoxia

Least summer-average dissolved oxygen consistently occurs at the head of the deep trench, around km 250 (Figure 15-57). Water overlying the dissolved-oxygen minimum is clearly phosphorus-limited in spring (Figure 15-56) and tends towards phosphorus limitation in summer (Figure 15-59). During

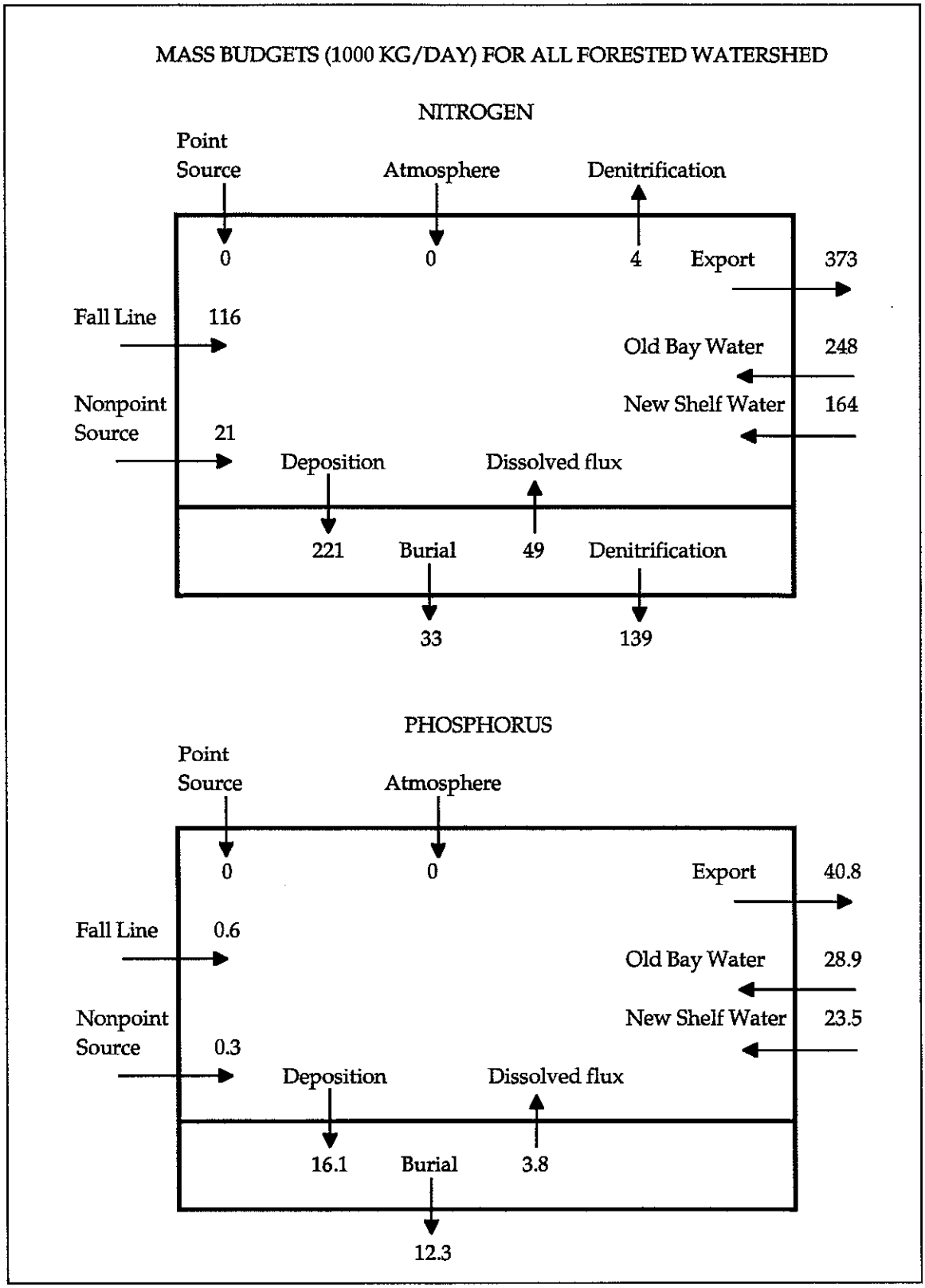

Figure 15-65. Total System Annual Nitrogen and Phosphorus Mass Budgets for All-Forest Conditions

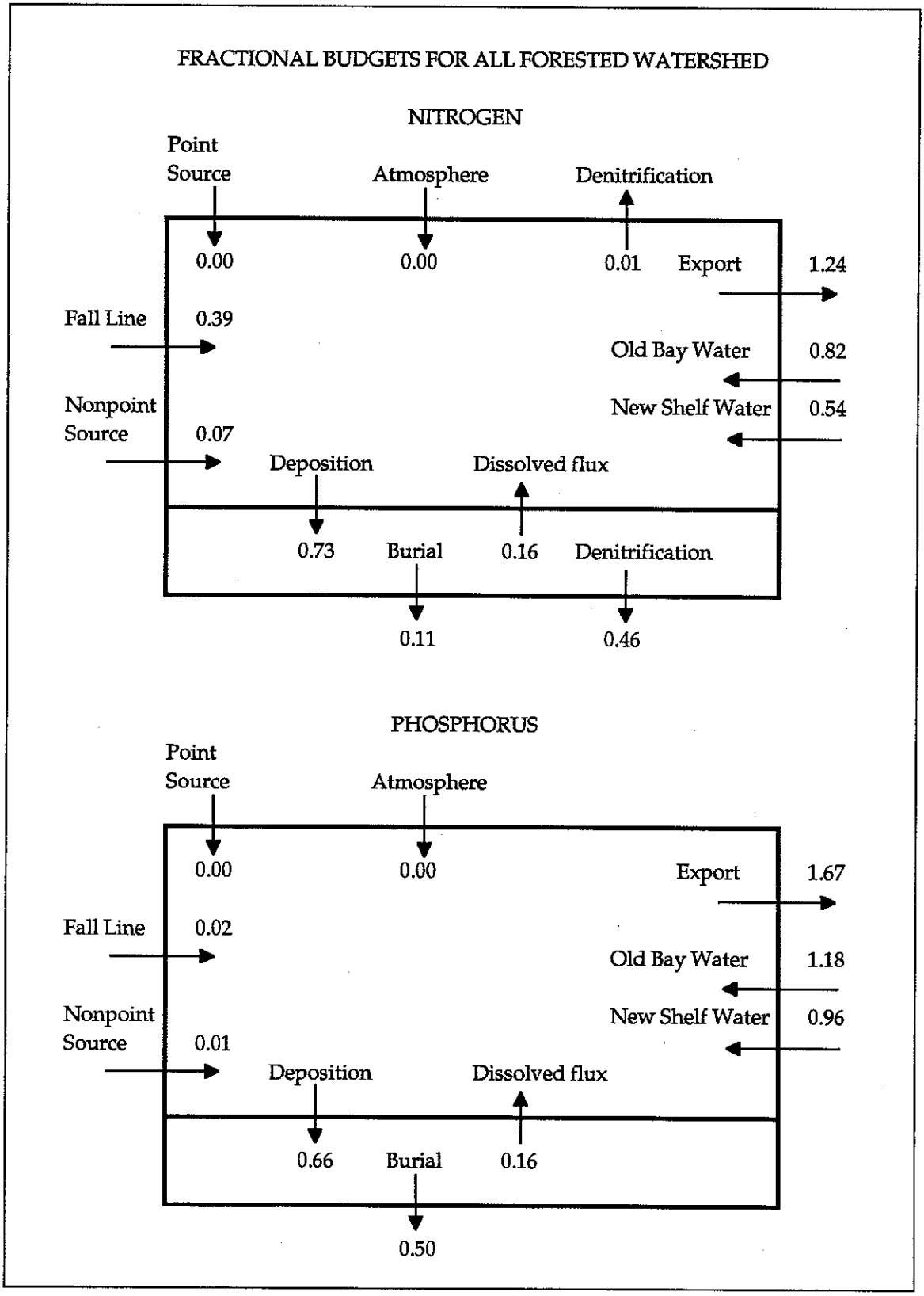

Figure 15-66. Total System Annual Nitrogen and Phosphorus Fractional Budgets for All-Forest Conditions

summer, clearly defined, severe nitrogen limitation occurs only below km 150. Yet the anoxic volume of the system is much more sensitive to reductions in nitrogen load than phosphorus load. Solution to the paradox in which anoxia in phosphorus-limited water responds to nitrogen load reductions was first suggested by the committee examining results of the management scenarios (Thomann et al. 1994). Anoxia at the head of the trench cannot be viewed solely as the result of deposition of oxygen demanding material from waters above. Rather, the deficit at the head of the trench represents the summation of oxygen losses experienced as bottom water travels from the mouth of the Bay upstream. Consequently, minimum dissolved oxygen is determined by oxygen demand from the mouth of the Bay to the head of the trench. And much of the region between the mouth and the head of the trench is influenced by nitrogen limitation rather than phosphorus.

An analytical model for examination of factors influencing estuarine bottom-water anoxia was proposed by Kuo, Park, and Moustafa (1991). The model employed a Lagrangian approach which tracked the dissolved-oxygen deficit of a water parcel moving upstream. As the parcel moved upstream, dissolved oxygen was removed by oxygen demand and supplied by diffusion from surface waters (Figure 15-67). The model was:

$$D(x) = D_o + \int_0^x \left(B(x') - Kz(x') \frac{D(x')}{h(x')} \right) \frac{dx'}{u(x')} \qquad (26)$$

in which:

D = dissolved oxygen deficit (gm m^{-3})

D_o = dissolved oxygen deficit at mouth of estuary (gm m^{-3})

B = oxygen demand in bottom water (gm m^{-3} day^{-1})

Kz = vertical exchange coefficient (m day^{-1})

h = distance between surface and bottom layers (m)

u = Lagrangian velocity (m day^{-1})

x = Eulerian coordinate measured upstream from mouth of estuary (m)

x' = Lagrangian coordinate measured upstream from mouth of estuary (m)

The model expressed the deficit at any location as the initial deficit plus accumulated oxygen losses from benthic processes less diffusion from above. The model indicated that deficit at any location declined as vertical diffusion or upstream velocity increased. Vertical diffusion provided more oxygen from above. Greater velocity decreased the time a water parcel was exposed to

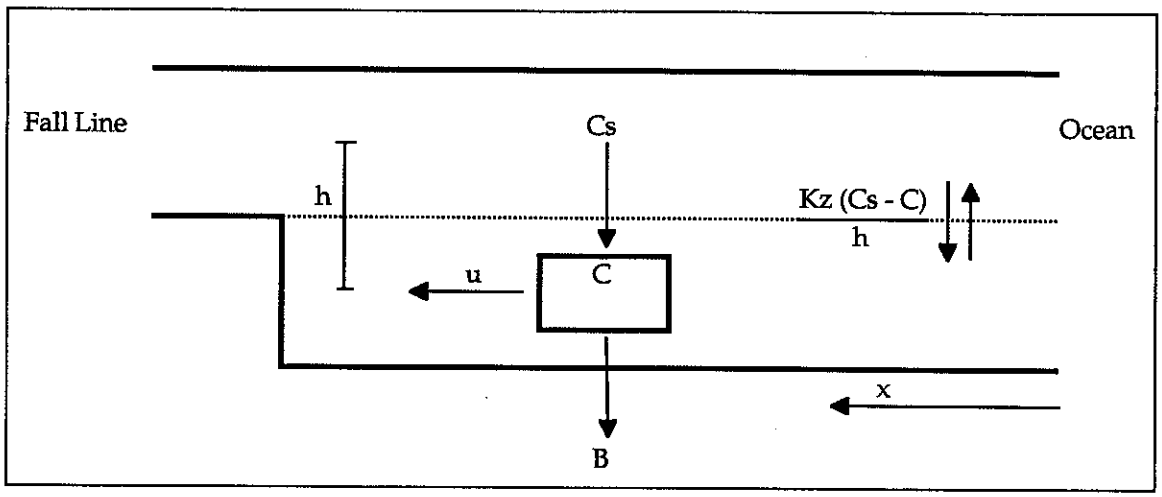

Figure 15-67. Lagrangian Dissolved Oxygen Analysis (C = dissolved oxygen concentration in lower layer; Cs = dissolved oxygen concentration in upper layer; other terms defined in text)

benthic oxygen demand. The model indicated deficit at any location increased in proportion to depth. Greater depth increased the diffusional distance between surface water and bottom water.

To test the hypothesis of the Modeling Subcommittee, the Lagrangian model was expressed in discrete form:

$$D(x) = D_o + \sum \frac{1}{h}\left(B - Kz\frac{D}{h}\right)\frac{\Delta x_i}{u} \qquad (27)$$

in which:

B = oxygen demand from benthic processes (gm m^{-2} day^{-1})

Kz = vertical diffusion (m^2 day^{-1})

Δx_i = length of zone defined along main Bay axis (Figure 15-4)

Other terms are as defined for Equation 26.

Excellent agreement with dissolved oxygen observed between the mouth and the head of the trench (Figure 15-68) was obtained using values presented in Table 15-9.

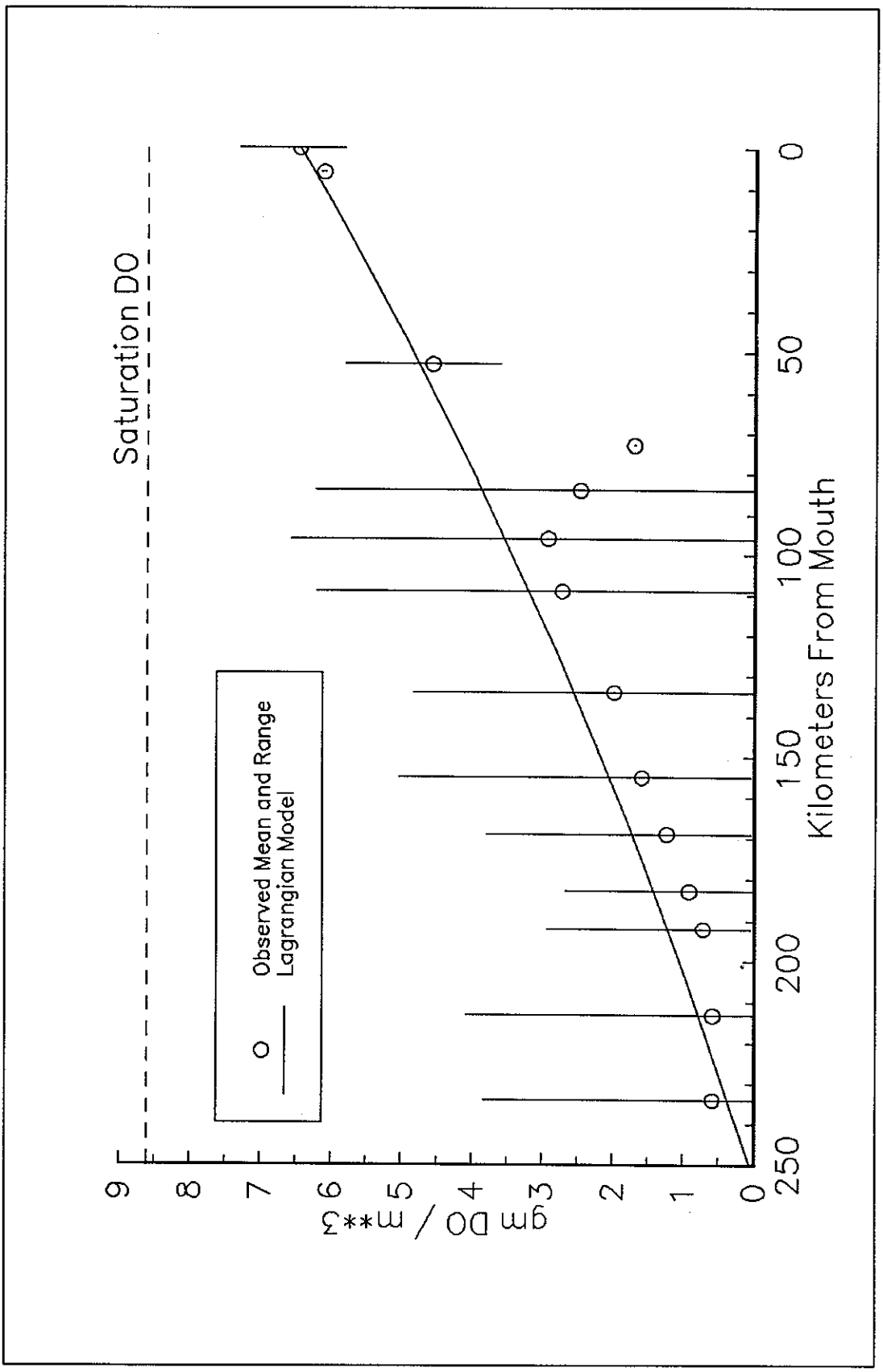

Figure 15-68. Bottom Dissolved Oxygen in Summer With Average Hydrology: Observed (1986) and Predicted by Lagrangian Analysis

Table 15-9
Parameters in Lagrangian Dissolved Oxygen Model

Parameter	Value
D_o	2.2 gm m^{-3}
B	1.5 gm m^{-2} day^{-1}
Kz	0.1 cm^2 day^{-1}
h	9.1 m
u	5 cm day^{-1}

In addition to affirming the validity of the hypothesis, the analysis revealed bottom water at the mouth of the Bay had a dissolved oxygen deficit of 2.2 gm DO m^{-3}. This deficit was imposed by physical and biological processes outside the Bay. At km 150, the upstream limit of severe nitrogen limitation, the accumulated deficit was 6 gm DO m^{-3}. The limited sensitivity of anoxia to phosphorus control was logical when it was revealed that 6 gm DO m^{-3} were lost before water entered the phosphorus-limited portion of the Bay.

Summary

Time to Steady State

The time for the water column and sediments to respond to changes in nutrient loading is influenced by interactions of the water and sediments. Analytical models of water or sediments alone are of limited utility in determining response time of the coupled system. Due to recycling of material between the water column and sediments, response time is usually longer than predicted by basic analytical models.

Concentrations of total nitrogen and total phosphorus in the mainstem attain 90% of their steady-state values in ten years. Diagenesis in the sediments, sediment oxygen demand, and sediment ammonium release also achieve 90% completion in ten years. For much of the Bay, the time for sediment phosphorus release to attain 90% of its steady-state value is much greater than ten years, due to retention of particulate phosphate in the sediments. The time for sediment phosphorus concentration to attain steady-state exceeds thirty years. The limiting process is the rate of burial to deep, isolated sediments. The effect of the slowly diminishing phosphorus release on concentration in the water column is barely observable, however. Consequently, ten years is proposed as the time scale for the Bay to respond to loading changes.

Loads and Budgets

Under existing conditions, fall-line loads are the greatest source of nitrogen to the system. The second largest source is nitrogen introduced from the continental shelf. Despite the large load originating on the shelf, however, the Bay is a net exporter of nitrogen to the shelf. Remaining nitrogen sources, in order of importance are point sources, nonpoint sources, and the atmosphere. The major nitrogen sink is denitrification in the sediments, followed by burial to deep, isolated sediments, net export to the shelf, and denitrification in the water column.

Under existing conditions, the major source of phosphorus to the system is the continental shelf. Due to the shelf source, the Bay is a net importer of phosphorus. Remaining phosphorus sources, in order of importance, are fall-line loads, point sources, nonpoint sources, and the atmosphere. The sole net phosphorus sink is burial to deep, isolated sediments. Phosphorus is lost to the shelf, but more is introduced than is lost.

Under LOT nutrient controls, the fall lines and continental shelf remain the primary nitrogen sources. Nonpoint sources replace point sources as the next largest source. The shelf comprises a larger fraction of the total load than under existing conditions but the Bay persists as a net exporter of nitrogen. Denitrification in sediments continues as the major pathway for loss followed by burial and net export.

The shelf and fall lines are the primary phosphorus sources under LOT nutrient controls. As with nitrogen, point sources of phosphorus fall behind nonpoint sources. The major pathway for phosphorus loss remains burial to deep, isolated sediments.

Under all-forest conditions, the Bay was a net importer of nitrogen. The shelf was the major nitrogen source followed by fall lines and nonpoint sources. Denitrification was the major loss pathway.

Under all-forest conditions, the shelf was the major phosphorus source. All other sources were negligible in comparison. Burial was the major loss pathway for phosphorus introduced from the shelf.

Effects of Nitrogen and Phosphorus on Anoxia

Nitrogen exerts a greater influence than phosphorus on anoxic volume. The reduction of anoxic volume in proportion to reduction in direct (=no shelf) nitrogen loads exceeds one-to-one. By contrast, reduction in anoxic volume in proportion to reduction to direct (=no shelf) phosphorus loads is roughly one-to-four.

Mainstem minimum dissolved oxygen occurs at the head of the deep trench, under surface waters in which algae are phosphorus-limited. Dissolved oxygen deficit at the head of the trench, however, is the sum of losses acquired as bottom water moves upstream from the mouth of the Bay. In summer, nitrogen is the limiting nutrient in much of the lower Bay. Under average hydrologic conditions, bottom water acquires more then 6 gm m^{-3} dissolved oxygen deficit before entering the phosphorus-limited region of the Bay. Consequently, nitrogen controls are of more influence than phosphorus controls on anoxic volume.

Additional Effects of Nitrogen Controls

Nitrogen load can be viewed as a "master variable" which strongly influences concentrations and fluxes throughout the system. System algal biomass is diminished in nearly one-to-one proportion to nitrogen load reductions. Sediment oxygen demand, sediment ammonium release, and sediment phosphorus release also diminish in roughly one-to-one proportion to nitrogen reductions.

Additional Effects of Phosphorus Controls

In the mainstem, the primary effect of phosphorus controls is reduction of algal biomass in the upper half of the Bay. On a system-wide basis, chlorophyll is reduced in roughly one-to-four proportion to reduction in phosphorus loads. The proportional reduction in algal biomass is equivalent to the proportional reduction in anoxic volume.

Nitrogen Versus Phosphorus Control

Although nitrogen control exerts a greater influence than phosphorus control on the entire system, nitrogen control alone is not desirable. Nitrogen control alone increases the system-wide concentrations of total and dissolved inorganic phosphorus. The increase occurs because algal uptake of phosphorus is diminished when production is strongly limited by nitrogen controls. Increased dissolved phosphate is detrimental to living-resource goals established for submerged aquatic vegetation.

Dissolved Oxygen

Under LOT nutrient controls, the volume of anoxic (dissolved oxygen $\leq$ 1 gm m^{-3}) water in an average hydrologic year is reduced by forty percent from existing conditions. Minimum summer-average dissolved oxygen increases from 0.13 gm m^{-3} under existing conditions to 0.75 gm m^{-3} with LOT nutrient controls. Although the concentration increase is small in absolute terms, the increased concentration and diminished anoxia can have a

beneficial effect on benthic organisms adapted to low-oxygen conditions. In the absence of nutrient controls, dissolved oxygen in the Bay will continue to deteriorate due to trends in nitrogen concentration at two major fall lines.

Under all-forest conditions, anoxia was virtually absent from the Bay during average hydrologic conditions. Anoxia was present in unusually wet years accompanied by high stratification. The anoxic volume was only twenty-five percent of the volume under existing conditions with the same hydrology, however.

Chapter XVI: Summary and Conclusions

Background

The present study commenced with a series of technical workshops held in Annapolis and Baltimore, Maryland, in autumn, 1987. The roots of the study extend back to 1983, however. In that year, a technical synthesis (Flemer et al. 1983) reported that the volume of anoxic water in the Bay had increased by an order of magnitude from 1950 to 1980. The conclusion was (and remains) controversial. Other indicators, however, including diminished fisheries harvest and shrinking distribution of submerged aquatic vegetation, supported the judgement that natural resources of the Bay were deteriorating. The potential loss of Bay resources spawned increased activity in Bay monitoring, ecological research, and modeling for management purposes.

One modeling effort (HydroQual 1987) applied three-dimensional hydrodynamic and eutrophication models to data collected in 1965, 1984, and 1985. Summer-average, steady-state conditions were modeled independently in each year. The model provided credible representations of historic and contemporary conditions in the Bay and tributaries. Conclusions of the study emphasized the role of sediment-water interactions in determining water quality.

Despite the success of the modeling effort, limitations were apparent. The chief limitation was absence of a predictive model of sediment-water interactions. A second limitation was the steady-state nature of the analysis. The steady-state model computed no influence of conditions in previous years or seasons on summer-average water quality.

The HydroQual study provided the technical basis for the 1987 Chesapeake Bay Agreement. In the agreement, the chief executives of Pennsylvania, Maryland, Virginia, and the District of Columbia pledged to reduce by forty percent the amounts of nitrogen and phosphorus entering the mainstem of Chesapeake Bay. In view of uncertainties associated with the model study, however, a portion of the Chesapeake Bay Agreement called for a 1991 reevaluation of the forty-percent nutrient reduction goal.

Requirements for Present Study

The EPA Chesapeake Bay Program Office formulated requirements for a model to address remaining technical issues in time for the 1991 reevaluation. Requirements included:

Ability to analyze the current origins and extent of anoxia.

Ability to predict the future of the Bay as a result of management action or inaction.

Ability to reconstruct the processes that have led the Bay to its present condition.

Eight capacities were envisioned in order for a model to meet the requirements. These were:

Simulation of responses of water quality and sediment processes to point and nonpoint-source control actions.

Performance of short-term (annual) and long-term (decades) simulations.

Determination of the effect of spring runoff events on summer anoxia.

Simulation of lateral water quality variations.

Determination of Bay response to area-specific management activities.

Determination of response time of the Bay to management actions.

Evaluation of frequency of critical water-quality events.

Evaluation of historical changes in anoxia.

The Technical Workshops

Negotiations between the EPA Chesapeake Bay Program Office, the U.S. Army Engineer District, Baltimore, and the U.S. Army Engineer Waterways Experiment Station led to selection of the Waterways Experiment Station to conduct the next phase of eutrophication modeling in the Bay. Four workshops were convened to guide formulation of a technical approach for the model study. The workshops were attended by members of government, academia, and industry within and outside the Bay community. Topics addressed in the workshops included water column state variables and aquatic processes,

sediment processes and sediment modeling, hydrodynamic and water-quality model interfacing, and long-term modeling of Chesapeake Bay.

The Chesapeake Bay Model Package

A package of interactive models (Figure 16-1) was assembled to comply with requirements and recommendations for the eutrophication model study. The CH3D-WES hydrodynamic model (Johnson et al. 1991) produced three-dimensional predictions of velocity, diffusion, surface elevation, salinity, and temperature on an intratidal (five-minute) time scale. A processor appended to CH3D-WES filtered intratidal details from hydrodynamic output but maintained intertidal (twelve-hour) transport (Dortch 1990). Intertidal flows, vertical diffusion, and surface elevation were written to disk for subsequent use by the water-quality model, dubbed CE-QUAL-ICM. The water-quality model interacted dynamically with a predictive sediment diagenesis model (DiToro and Fitzpatrick 1993). Fall-line loads and below-fall-line non-point source loads were supplied to the eutrophication model by the EPA's Chesapeake Bay Watershed model (Donigian et al. 1991).

The present report is the primary reference for the formulation of the CEQUAL-ICM water quality model and application to Chesapeake Bay. Development and calibration of the model were conducted through application to the three-year period, 1984-1986. Subsequently, a thirty-year period, 1959-1988, was simulated.

The Study System

Physical Description

The Chesapeake Bay system (Figure 16-2) consists of the mainstem bay, five major western-shore tributaries, and a host of lesser tributaries and embayments. Urban centers along the Bay and tributaries include Norfolk and Richmond Va., Washington, D.C., and Baltimore, Md. The mainstem is roughly 300 km long, 8 to 48 km wide, and 8 m average depth. A deep trench with depths to 50 m runs up the center of the mainstem.

Total drainage area of the Bay is 166,000 km^2. The primary source of freshwater to the system is the Susquehanna River ($\approx$ 64% of total gauged freshwater flow) which empties into the northernmost extent of the Bay. Other major freshwater sources are the Potomac ($\approx$ 19%) and James Rivers ($\approx$ 12%). The remaining western-shore tributaries, the York ($\approx$ 3%), the Rappahannock ($\approx$ 3%), and the Patuxent ($<$ 1%) contribute only small fractions of the total freshwater flow to the Bay.

The mainstem Bay and major tributaries are classic examples of partially-mixed estuaries (Pritchard 1967). When flows in these estuaries are averaged over lengthy time periods, generally more than fifteen days, a net longitudinal

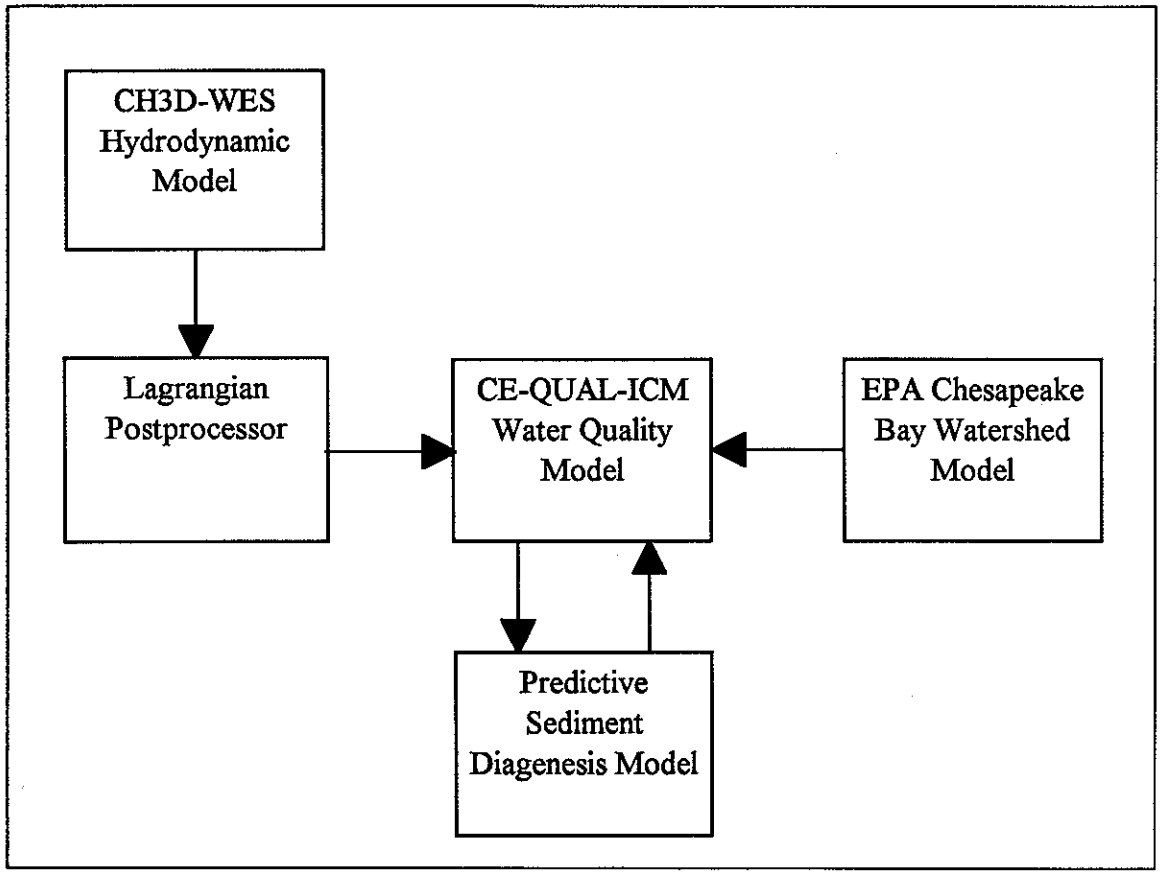

Figure 16-1. The Chesapeake Bay Model Package

circulation is evident. Longitudinal density gradients push bottom water upstream and enhance flow of surface water downstream. The volume of the density-induced flow vastly exceeds the volume of freshwater runoff.

Hydrology

An annual runoff cycle exists in the major bay tributaries. Peak flows typically occur in March or April while minimum flows occur in August and September. Both floods and droughts cause daily and monthly flows to deviate from the long-term pattern. The occurrence of maximum annual flow is particularly susceptible to flood events. As a result of tropical storms, maximum flow may occur in late summer or in autumn rather than in spring.

Mean Susquehanna runoff in 1984 was well above mean flow in the period of record, 1959-1988. In fact, mean flow exceeded 90% of the annual mean flows on record. The year 1984 was a "wet" year. By contrast, flow in 1985 was unusually low. Roughly 80% of the years on record had mean flow which exceeded 1985. The year 1985 was a "dry" year. Mean flow in 1986

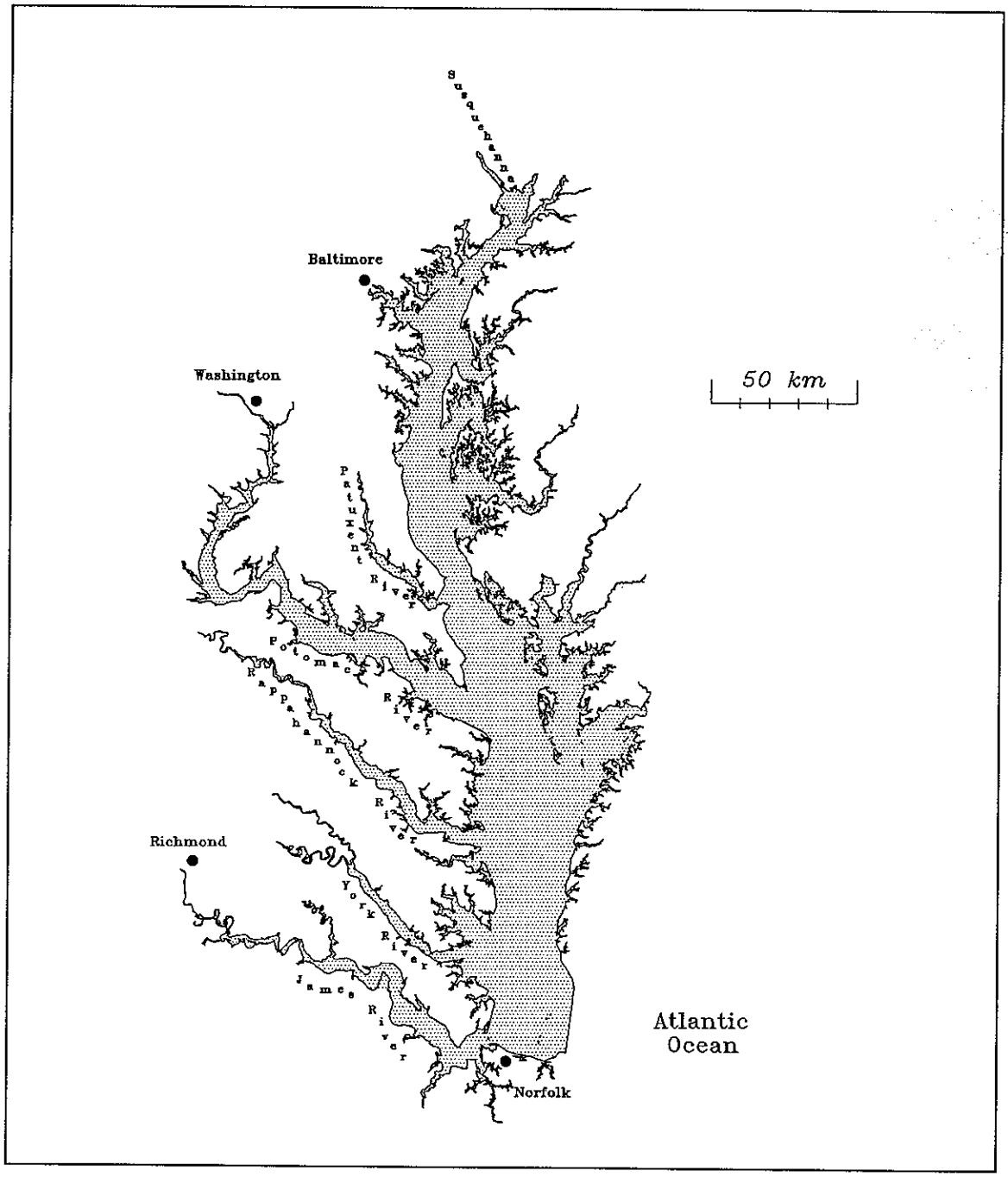

Figure 16-2. The Chesapeake Bay System

was near the mean long-term flow. Susquehanna hydrology in 1986 was "average".

Mean flow in the major tributaries for 1984 was also well above average. The relative order of 1985 and 1986 was reversed from the Susquehanna, however. Highest mean flows were in 1984, moderate flows in 1985, and

lowest flows in 1986. In most tributaries, the defining event of 1985 was an autumn flood in which highest flows in the study period, 1984-1986 occurred.

Eutrophication Processes

Bottom-Water Hypoxia. During the summer months, bottom waters of the mainstem bay are characterized by hypoxic (low dissolved oxygen) or anoxic (no dissolved oxygen) conditions. Longitudinal and lateral extent of hypoxia are determined by the geometry of the trench that runs up the center of the Bay. On occasion, hypoxic water extends from the bottom to within a few meters of the surface but summer-average oxygen concentration within the surface mixed layer is usually 6 gm m^{-3} or greater.

Bottom-water hypoxia occurs at recurrent, predictable time intervals. The onset is in late May when spring warming enhances respiration in benthic sediments. Decay of material deposited in spring and in previous years removes oxygen from bottom water. Density stratification prevents mixing of oxygenated surface water downwards. Low-oxygen conditions continue through the summer, maintained by respiration in bottom water. In mid-September, autumn winds end the hypoxic period by mixing surface water down to the bottom.

Spring Phytoplankton Bloom. A second recurring phenomenon in the Bay is the spring phytoplankton bloom. The bloom usually commences in February, reaches a maximum in April, and ends precipitously in May. The bloom is characterized by high chlorophyll concentrations throughout the water column. At times, a subsurface chlorophyll maximum occurs. Elevated chlorophyll throughout the water column marks the spring bloom as the period of maximum algal biomass.

Strong consensus exists that the occurrence and magnitude of the spring bloom are linked to subsequent bottom-water anoxia. A spring peak in carbon deposition to sediments occurs coincident with the algal bloom (Boynton et al. 1988). The deposition and decay of fresh organic matter contributes to oxygen demand during the onset of the anoxic period. A second link is through a nutrient trapping mechanism (Malone et al. 1988). Nutrients in spring runoff are taken up by algae during the bloom. Predation and algal mortality result in the transfer of nutrients, in particulate organic form, to benthic sediments. In summer, the nutrients are mineralized in the sediments and released to the water column. Nutrients released from the sediments support summer algal production. Carbon produced by algae settles to bottom waters, decays, and consumes oxygen.

Nutrient Limitations. Algae require three major nutrients for growth: carbon, nitrogen, and phosphorus. Diatoms require silica, as well, from which they synthesize their distinctive skeletons. Algal production is diminished or eliminated in the prolonged absence of one or more of the required nutrients. Inorganic carbon is seldom in short supply and is usually not considered in

analyses of nutrient limitations. Silica receives little emphasis in management studies since the supply from natural sources is beyond control and usually abundant. Tremendous emphasis is placed on limitations by nitrogen and phosphorus since the supply of these nutrients can be altered through management of releases.

A "rule of thumb" is that phosphorus is the limiting nutrient in freshwater systems (Hecky and Kilham 1988) while nitrogen is limiting in estuarine (Boynton, Kemp, and Keefe 1982) and marine waters. The principle of phosphorus limitation in freshwater and nitrogen limitation in saltwater presents a reasonable pattern for the Chesapeake Bay system. Phosphorus tends to be limiting in tidal fresh water and near the Susquehanna fall line. In the lower tributaries and in much of the mainstem nitrogen is of more importance as the limiting nutrient.

Seasonality is also apparent in the nutrient limitations. Bioassays (D'Elia, Sanders, and Boynton 1986) and data analyses (Fisher et al. 1992) indicate phosphorus is important as a limiting nutrient in estuarine waters in late winter and spring while nitrogen is more important in summer. The seasonal switch from phosphorus to nitrogen indicates much of the system is phosphorus-limited during the spring bloom and nitrogen-limited during the period of summer maximum productivity. The spring bloom is also a period of potential silica limitation.

Sediment-Water Interactions. Over time scales of years, benthic sediments are sinks of oxygen, nitrogen, phosphorus, and silica removed from the water column. Oxygen is consumed, directly or indirectly, in the oxygenation of organic carbon and in the nitrification of ammonium. Substantial fractions of particulate nitrogen, phosphorus, and silica that settle into surficial sediments are buried to deep sediments from which recycling to the water column is impossible.

Over seasonal time scales, sediments can be significant sources of dissolved nutrients to the overlying water. The role of sediments in the system-wide nutrient budget is especially important in summer when seasonal low flows diminish riverine nutrient input. During summer, warm temperature enhances biological processes in the sediments. Diagenesis (decay) of organic matter produces ammonium, phosphate, and silica that are released to the water column. Sediment ammonium release supplies an estimated 13% to 40% of algal nutrient requirements during August in Chesapeake Bay (Boynton and Kemp 1985). Silica nutrient limitation is not seen in summer because sediment release exceeds fluvial input by a factor of five or more (D'Elia, Nelson, Boynton 1983).

Oxygen consumption in the sediments (or of sulfide released from sediments) is generally about one-third of total oxygen consumption in the system (Kemp et al. 1992). At times, however, sediment processes account for the majority of oxygen consumption. Oxygen consumption due to sediment

processes predominates during the spring peak, and in late summer concurrent with maximum sulfide release.

Nitrogen and Phosphorus Budgets. In the past decade, several annual nutrient budgets for the bay have been performed. All budgets reviewed for the present study agreed that fall-line loads were the major nitrogen source. All budgets indicated that fall-line loading was a significant phosphorus source but not as dominant as for nitrogen. All budgets agreed that the system exports nitrogen to the ocean. Estimates of the fraction exported varied widely however, from a negligible quantity to the majority of the load. Both direction and magnitude of net phosphorus flux at the mouth were controversial. Three budgets examined indicated negligible import, significant export, and significant import. The contradictory results were strongly affected by estimates of burial and the requirement to balance the budget.

Hydrodynamic Model and Computational Grid

Modeling the physics, chemistry, and biology of the Bay required a package of models. Transport processes were modeled by a three-dimensional hydrodynamic model which operated independently of the water quality model. Transport information from the hydrodynamic model was processed and stored on magnetic media for subsequent use by the water quality model.

The Hydrodynamic Model. The CH3D-WES (Computational Hydrodynamics in Three Dimensions - Waterways Experiment Station) hydrodynamic model was a substantially revised version of the CH3D model originally developed by Sheng (1986). Model formulation was based on principles expressed by the equations of motion, conservation of volume, and conservation of mass. Quantities computed by the model included three-dimensional velocities, surface elevation, vertical viscosity and diffusivity, temperature, salinity, and density. Details of the model formulation and application to Chesapeake Bay were presented by Johnson et al. (1991).

Computational Grid. The basic equations of CH3D-WES were solved via the finite-difference method. The finite-difference solution algorithm replaced continuous derivatives in the governing differential equations with ratios of discrete quantities. Solutions to the hydrodynamics were obtained using five-minute intervals for the discrete time steps. The spatial continuum of the Bay was divided into a grid of discrete cells. To achieve close conformance of the grid to Bay geometry, cells were represented in curvilinear rather than rectangular coordinates. Velocities were computed on the boundaries between cells. Temperature, salinity, and density were computed at the center of each cell.

One grid was employed for both the hydrodynamic and water-quality models. The grid contained 729 cells, roughly 5 x 10 km, in the surface plane (Figure 16-3). Number of cells in the vertical ranged from two to fifteen.

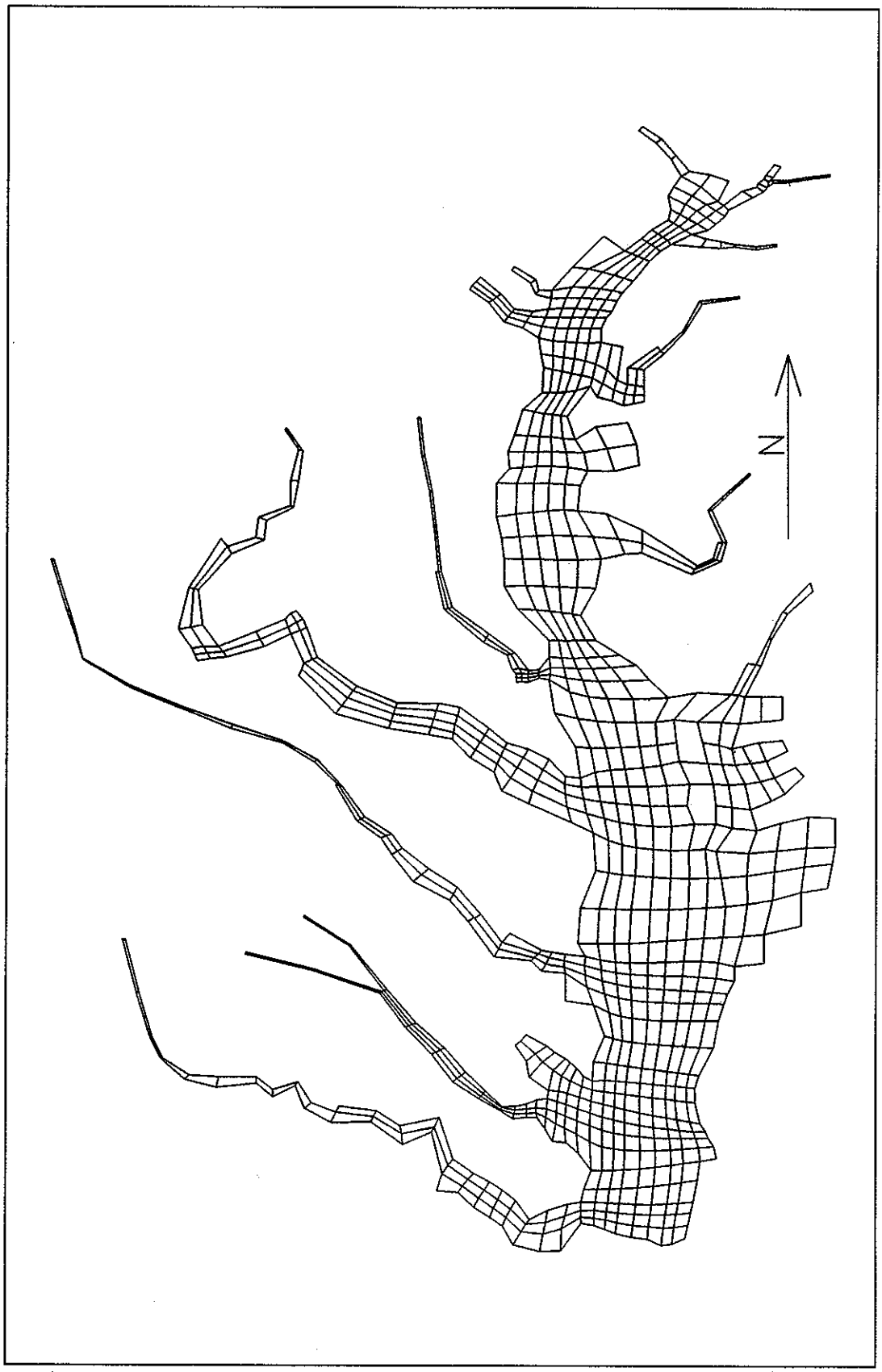

Figure 16-3. Plan View of computational Grid

Surface cells were 2.14 m thick. All other cells were 1.53 m thick. Total number of grid cells was 4029.

Calibration and Verification. The hydrodynamic model was calibrated and verified against a large body of observed tidal elevations, currents, and densities. Particular attention was devoted to replication, in the model, of Bay processes during an April 1983 spring runoff event and an October 1983 wind mixing event. The final check on performance was demonstrated by comparison of modeled and observed salinity over a three-year period 1984-1986. Details of model performance were presented by Johnson et al. (1991).

Linkage to the Water Quality Model. Hydrodynamics for employment in the water quality model were produced for three years, 1984, 1985, 1986. Each year was a single, continuous production run. A processor imbedded in the CH3D-WES code transformed velocities, surface elevations, and vertical diffusivities computed on a five-minute basis into tidal-average values output every 12.4 hours. Lagrangian averaging (Dortch 1990) was performed so that employment of a tidal dispersion coefficient, to compensate for tidal averaging, was not required. Employment of the Lagrangian algorithm reduced the storage requirements for the hydrodynamic output by an order of magnitude.

Volumetric Flows. To aid in interpretation of predictions from the water quality model, various summaries of transport processes were produced. One summary was an examination of volumetric flow between regions of the Bay. Nine regions were defined (Figure 16-4). Eight were along the main axis of the Bay and the ninth comprised the Tangier sound adjacent to the Eastern Shore. Flows were summarized for the summer months, June to September, of 1986. The year 1986 was selected since it was a year of average flow in the Susquehanna River.

At each transect, summaries of upstream, downstream, and net flows were produced. Magnitude of upstream and downstream flows was greatest in the lower Bay and diminished with distance upstream towards the Susquehanna River (Figure 16-5). Lateral volumetric exchanges between the mainstem and Tangier Sound were less than longitudinal flows along the mainstem in mid-Bay.

Net flows (Figure 16-6) were usually an order of magnitude less than upstream and downstream flows. Net flows revealed an interesting phenomenon. Strong net lateral flows occurred from the mainstem into Tangier Sound. Primary downstream transport was through Tangier Sound. A net upstream flow occurred along the mainstem adjacent to the Sound.

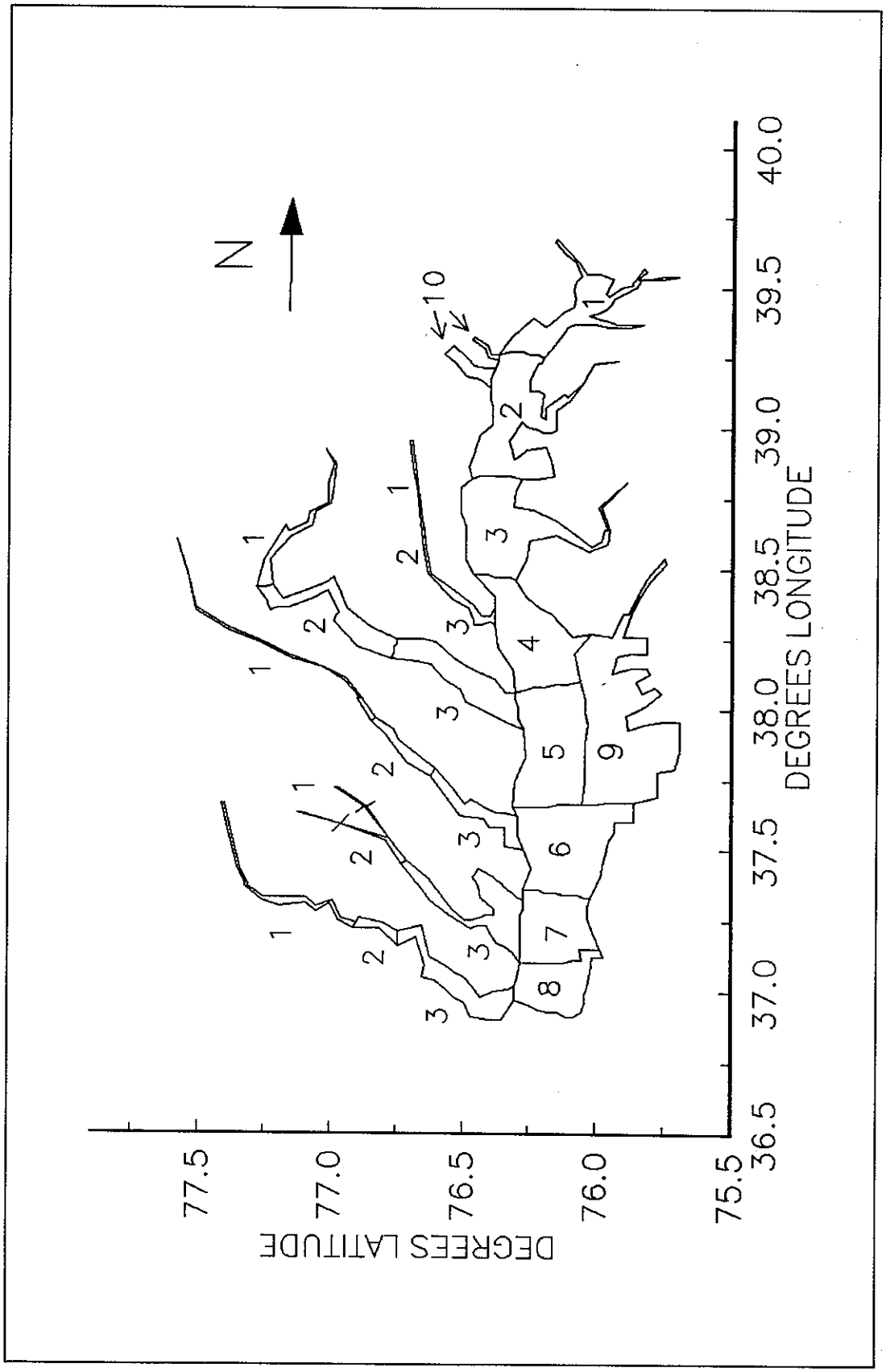

Figure 16-4. Zones for Summaries of Volumetric Flows

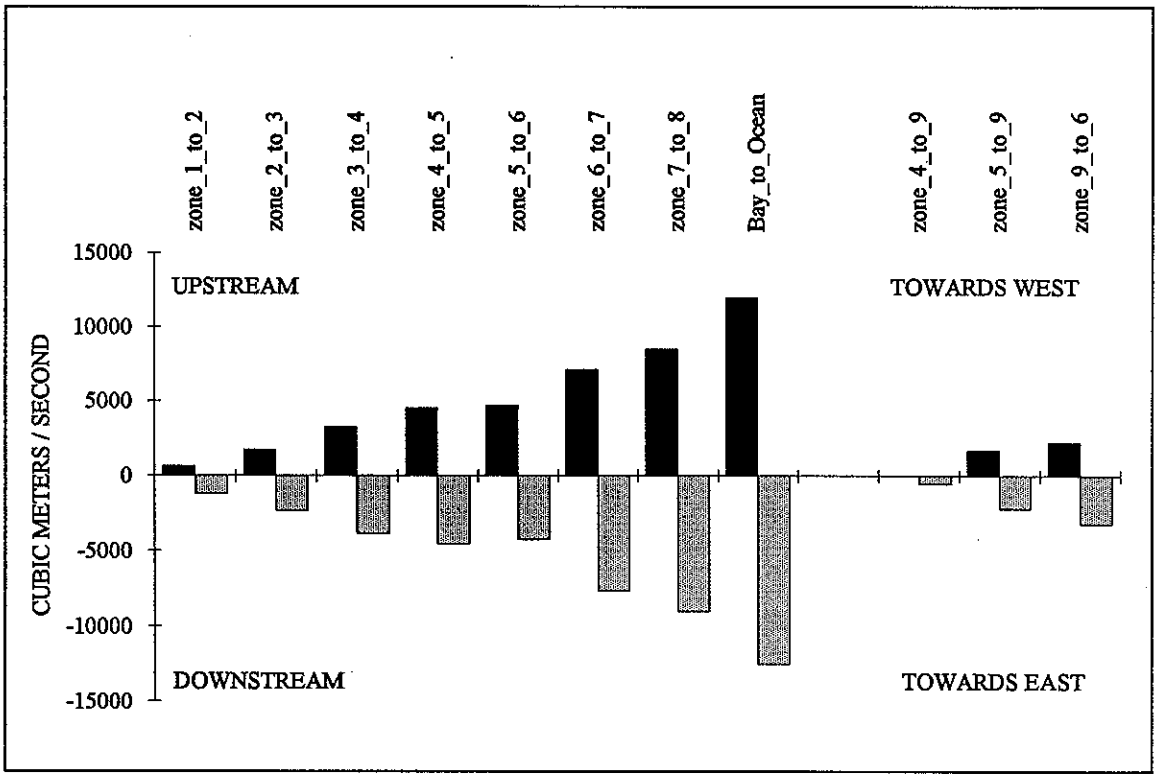

Figure 16-5. Upstream and Downstream Flows at Bay Transects Summer 1986

The Water Quality Model

Conservation Of Mass Equation. The foundation of CE-QUAL-ICM is the solution to the three-dimensional mass-conservation equation for a control volume:

$$\frac{\delta V_i C_i}{\delta t} = \sum_{j=1}^{n} Q_j C_j^* + \sum_{j=1}^{n} A_j D_j \frac{\delta C}{\delta x_j} + \sum S_i \qquad (16\text{-}1)$$

in which:

V_i = volume of ith control volume (m^3)

C_i = concentration in ith control volume (gm m^{-3})

Q_j = volumetric flow across flow face j of ith control volume (m^3 sec^{-1})

C^*_j = concentration in flow across flow face j (gm m^{-3})

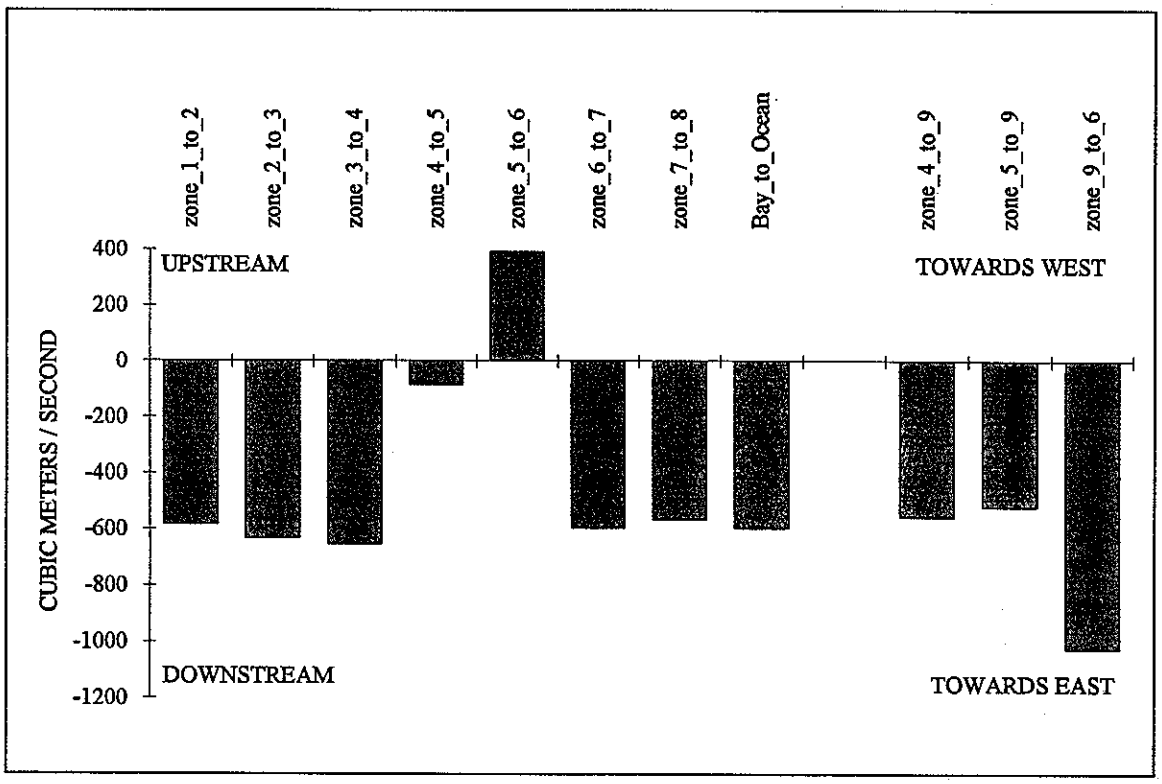

Figure 16-6. Net Flows at Bay Transects, Summer 1986

A_j = area of flow face j (m^2)

D_j = diffusion coefficient at flow face j (m^2 sec^{-1})

n = number of flow faces attached to ith control volume

S_i = external loads and kinetic sources and sinks in ith control volume (gm sec^{-1})

t, x = temporal and spatial coordinates

Control volumes in CE-QUAL-ICM correspond to cells in x-y-z space on the CH3D grid. CE-QUAL-ICM solves the conservation of mass equation in each volume for each model state variable. Solution to the mass-conservation equation is via the finite-difference method using the QUICKEST algorithm (Leonard 1979) in the horizontal directions and a Crank-Nicolson scheme in the vertical direction.

State Variables. A suite of twenty-two state variables was required to model eutrophication processes in the water column (Table 16-1).

Table 16-1
Water Quality Model State Variables

Temperature	Salinity
Total Active Metal	Cyanobacteria
Diatoms	Green Algae
Dissolved Organic Carbon	Labile Particulate Organic Carbon
Refractory Particulate Organic Carbon	Ammonium
Nitrate	Dissolved Organic Nitrogen
Labile Particulate Organic Nitrogen	Refractory Particulate Organic Nitrogen
Total Phosphate	Dissolved Organic Phosphorus
Labile Particulate Organic Phosphorus	Refractory Particulate Organic Phosphorus
Chemical Oxygen Demand	Dissolved Oxygen
Particulate Biogenic Silica	Available Silica

Eutrophication Processes. Kinetic interactions affecting the state variables were described in over 80 partial differential equations that required evaluation of over 140 parameters. The kinetics described carbon, phosphorus, nitrogen and silica cycles and the dissolved oxygen balance.

The model carbon cycle (Figure 16-7) consists of the following elements:

Phytoplankton production
Phytoplankton exudation
Predation on phytoplankton
Dissolution of particulate carbon
Heterotrophic respiration
Denitrification
Settling

Algal production is the primary carbon source although carbon also enters the system through external loading. Predation on algae releases particulate and dissolved organic carbon to the water column. A fraction of the particulate organic carbon undergoes first-order dissolution to dissolved organic carbon. The remainder settles to the sediments. Dissolved organic carbon produced by phytoplankton exudation, by predation, and by dissolution is respired or denitrified at a first-order rate to inorganic carbon. No carbon is recycled from the sediments to the water column although oxygen demand created by carbon diagenesis is included in the model.

The model phosphorus cycle (Figure 16-8) includes the following processes:

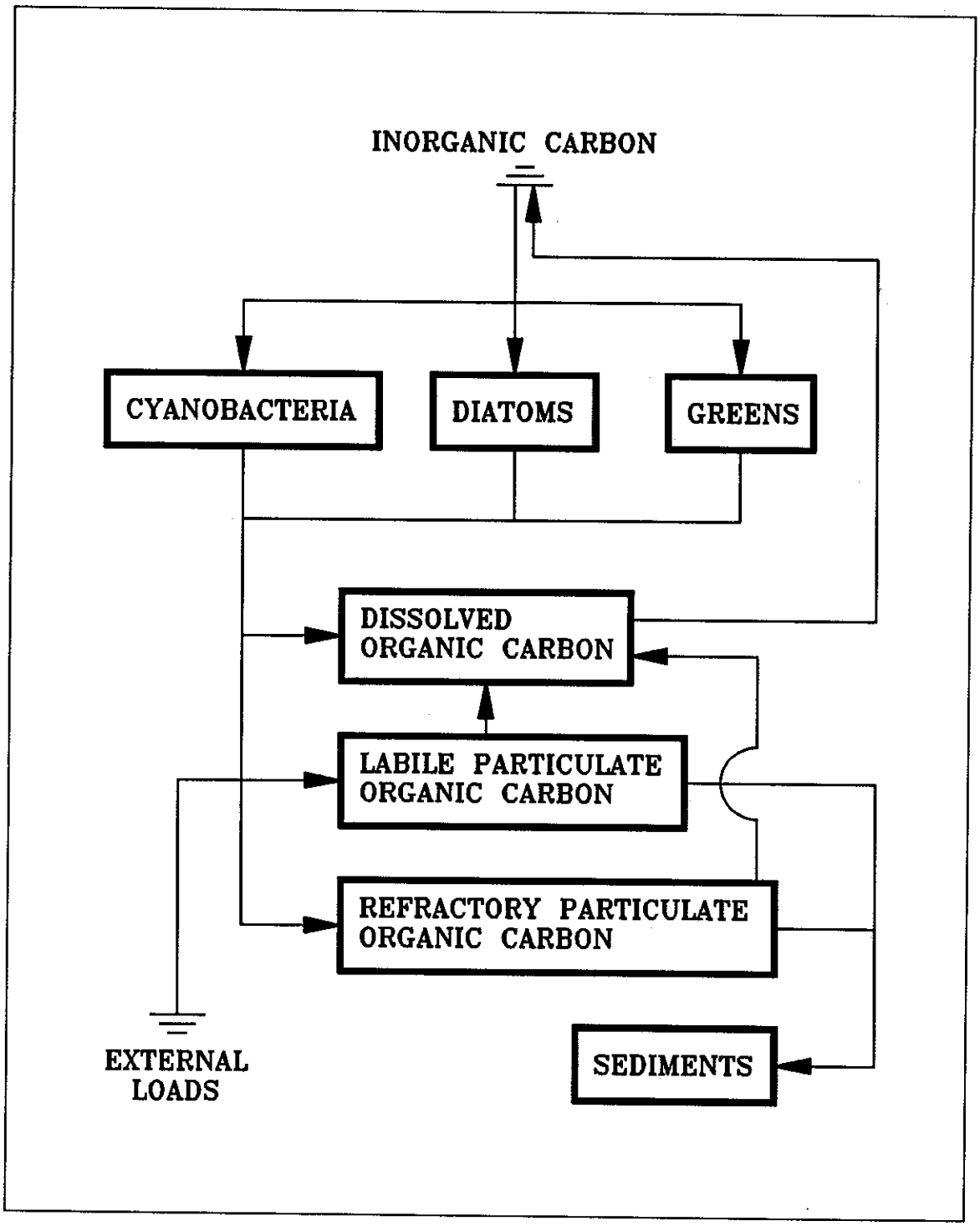

Figure 16-7. The Model Carbon Cycle

Algal production and metabolism
Predation
Hydrolysis of particulate organic phosphorus
Mineralization of dissolved organic phosphorus

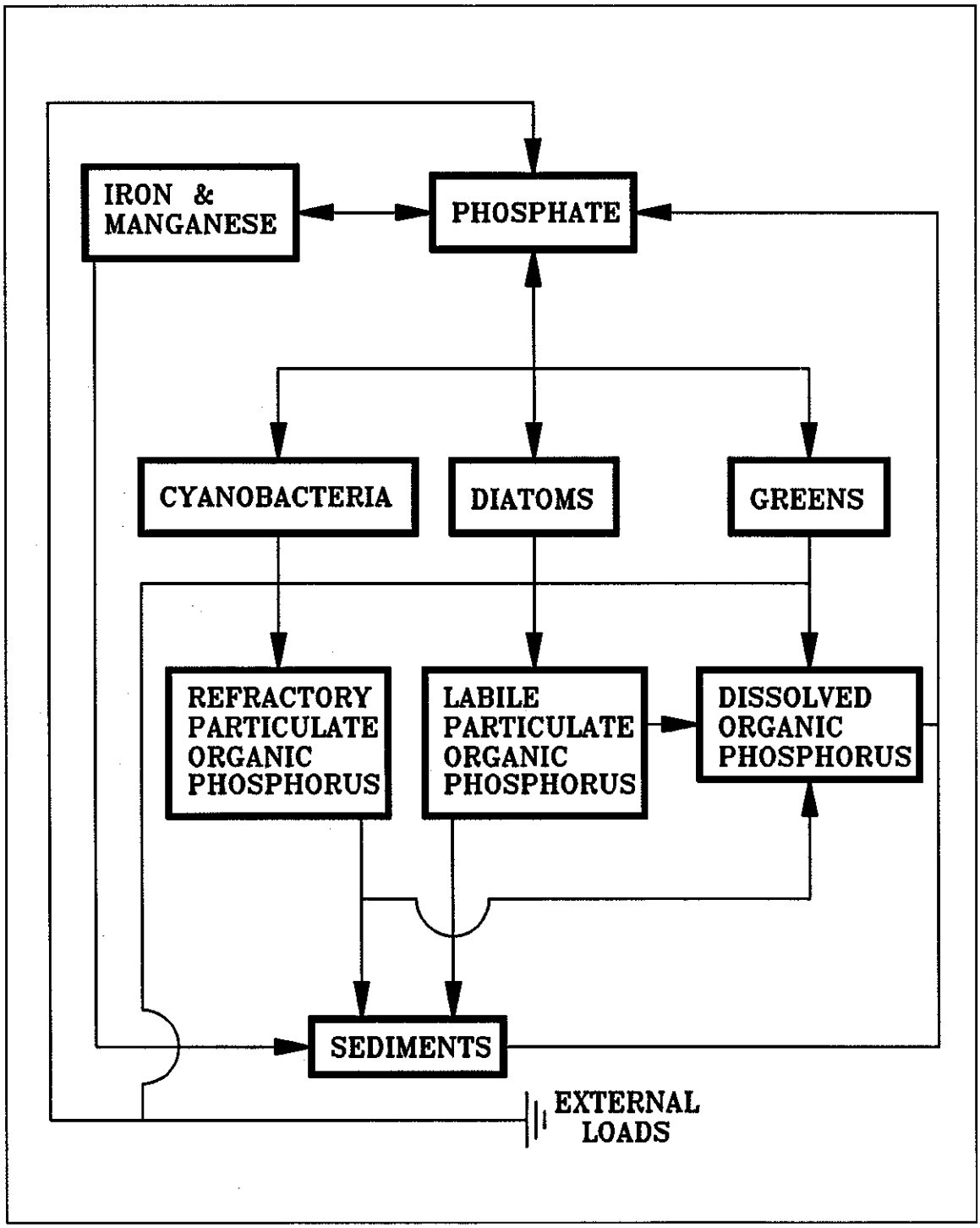

Figure 16-8. The Model Phosphorus Cycle

Settling
Exchange with inorganic solids

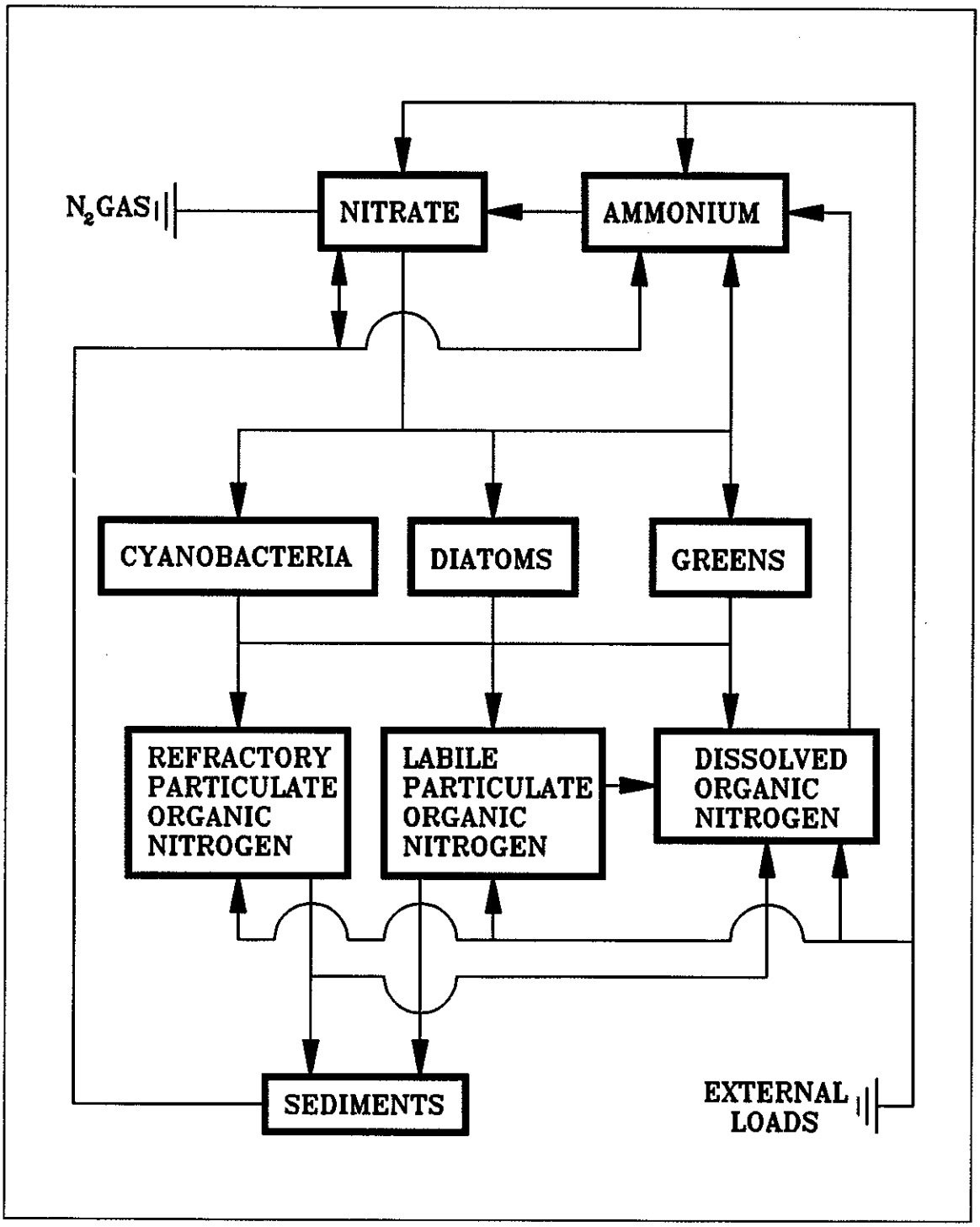

Figure 16-9. The Model Nitrogen Cycle

External loads provide the ultimate source of phosphorus to the system. Dissolved phosphate is incorporated by algae during growth and released as phosphate and organic phosphorus through respiration and predation. A portion of the particulate organic phosphorus hydrolyzes to dissolved organic

phosphorus. The balance settles to the sediments. Dissolved organic phosphorus is mineralized to phosphate. A portion of the phosphate sorbs to inorganic solids and settles to the sediments. Within the sediments, particulate phosphorus is mineralized and recycled to the water column as dissolved phosphate.

The model nitrogen cycle (Figure 16-9) includes the following processes:

Algal production and metabolism
Predation
Hydrolysis of particulate organic nitrogen
Mineralization of dissolved organic nitrogen
Settling
Nitrification
Denitrification

External loads provide the ultimate source of nitrogen to the system. Inorganic nitrogen is incorporated by algae during growth and released as ammonium and organic nitrogen through respiration and predation. A portion of the particulate organic nitrogen hydrolyzes to dissolved organic nitrogen. The balance settles to the sediments. Dissolved organic nitrogen is mineralized to ammonium. In an oxygenated water column, a fraction of the ammonium is subsequently oxidized to nitrate through the nitrification process. In anoxic water, nitrate is lost to nitrogen gas through denitrification. Particulate nitrogen that settles to the sediments is mineralized and recycled to the water column, primarily as ammonium. Nitrate moves in both directions across the sediment-water interface, depending on relative concentrations in the water column and sediment interstices.

The silica cycle (Figure 16-10) is a simple one in which diatoms take up available silica and recycle available and particulate biogenic silica through the actions of metabolism and predation. Particulate silica dissolves in the water column or settles to the bottom. A portion of the settled particulate biogenic dissolves within the sediments and returns to the water column as available silica. Sources and sinks represented are:

Diatom production and metabolism
Predation
Dissolution of particulate to dissolved silica
Settling
Exchange with inorganic solids

Sources and sinks of dissolved oxygen in the water column (Figure 16-11) include:

Algal photosynthesis
Atmospheric reaeration
Algal respiration
Heterotrophic respiration

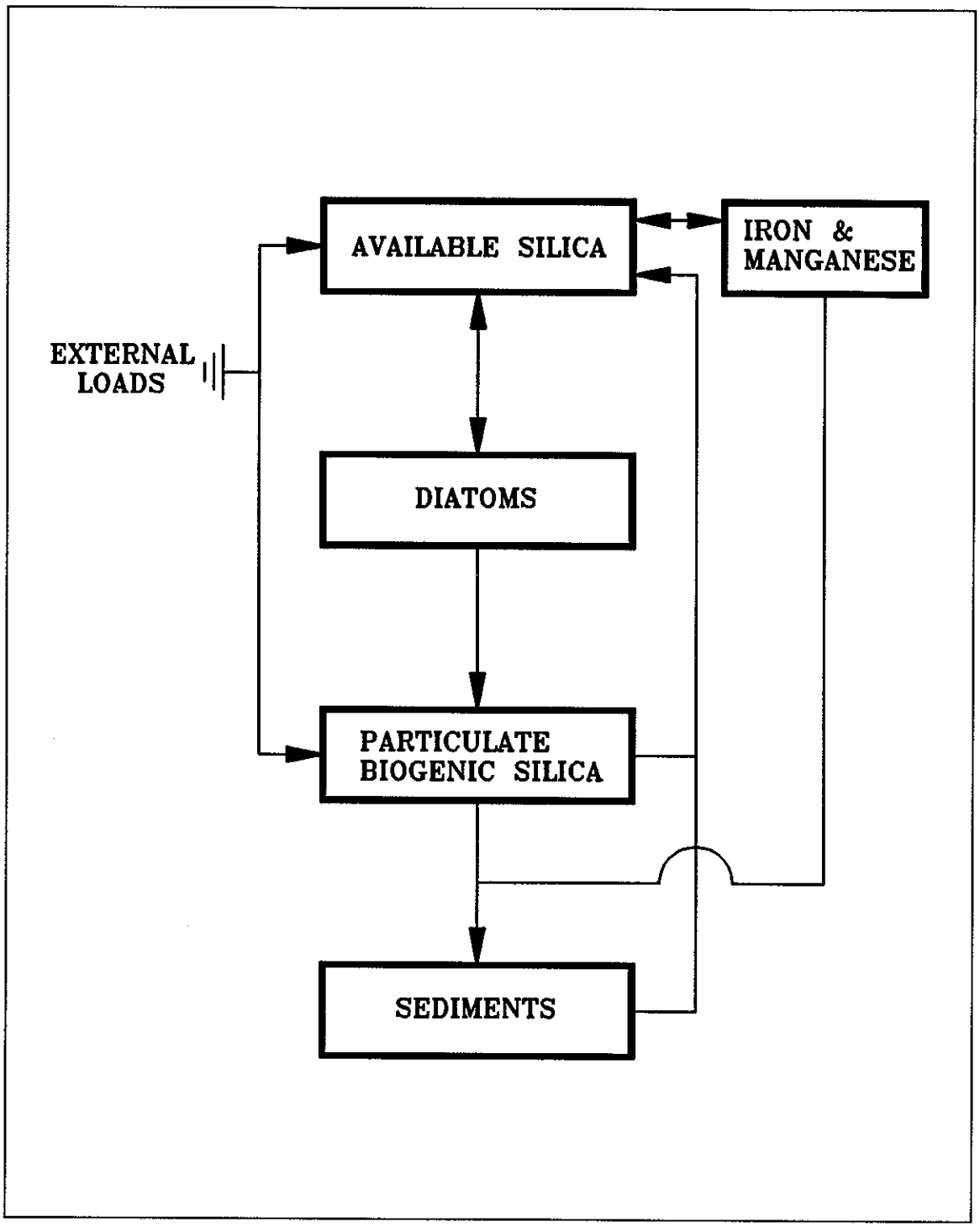

Figure 16-10. The Model Silica Cycle

Nitrification
Chemical oxygen demand

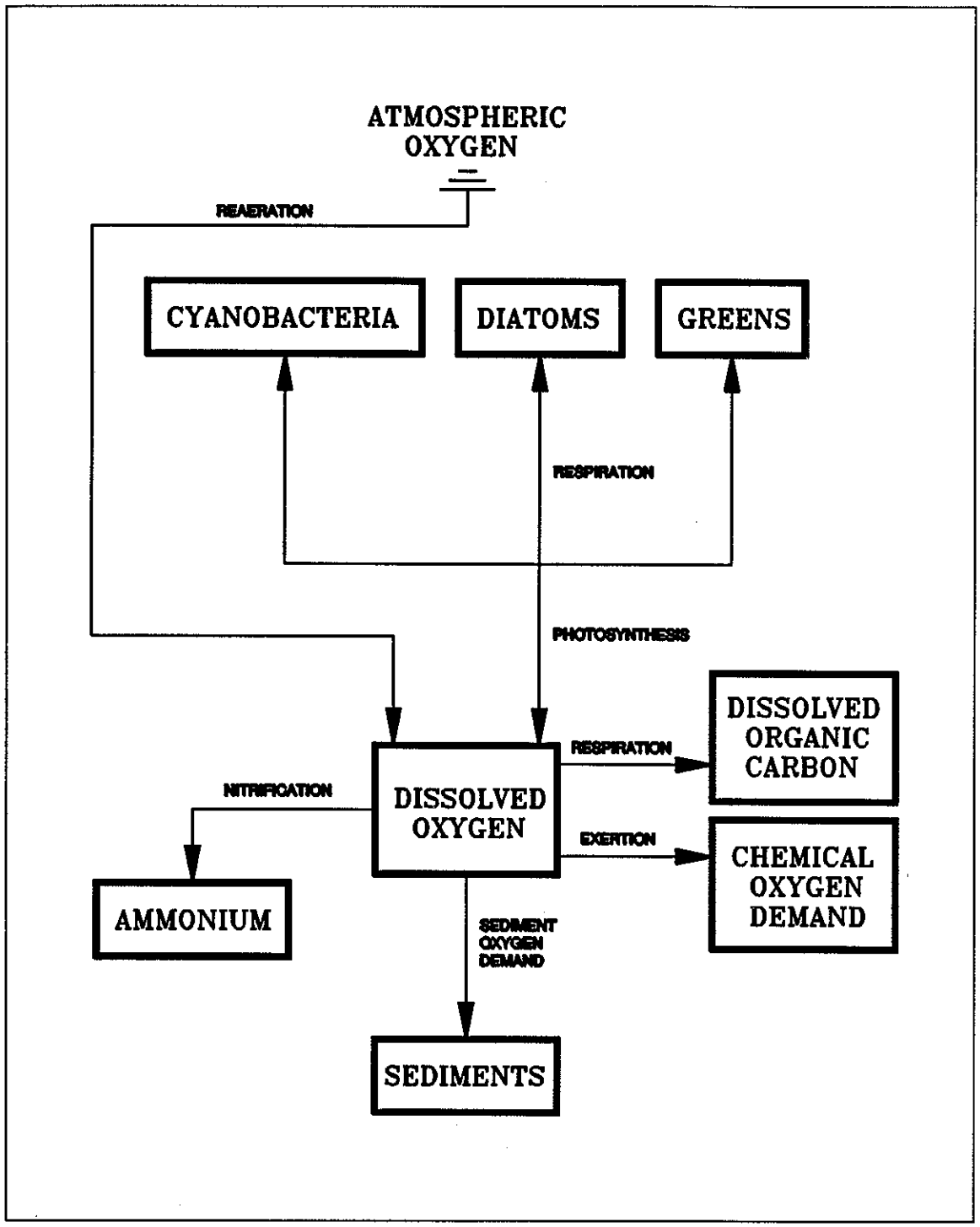

Figure 16-11. Dissolved Oxygen Sources and Sinks

Existing Loads to the System

External loads of nutrients and oxygen demand were divided into four classes. Fall-line loads were carried by freshwater flows that entered the Bay and tidal tributaries at the upper limit of tidal excursion. Location of this limit, the fall line, defined the transition from freeflowing to tidal water bodies. Below-fall-line, nonpoint-source loads were associated with distributed overland flows that entered the Bay and tidal tributaries directly. Point-source loads were discharges from municipal treatment plants, industries, and similar facilities. Atmospheric loads were transfers from the atmosphere to the water surface via rainfall, wind, and other processes.

Fall-Line Loads. Carbon, nitrogen, and phosphorus were the only substances treated as mass loads at the fall lines. Inflows of algae, dissolved oxygen, and silica were treated through specification of concentration boundary conditions. Fall-line loads were generated by the EPA Chesapeake Bay Watershed Model (Donigian et al. 1991). Loads provided by the watershed model resulted from computation of loading, transport, and transformations throughout the Chesapeake Bay watershed above the fall lines. The domain of the watershed model included portions of New York, Pennsylvania, Virginia, West Virginia, District of Columbia, and Delaware.

Below-Fall-Line Nonpoint-Source Loads. Below-fall-line loads of carbon, nitrogen, and phosphorus were also provided by the watershed model. Loads of algae, dissolved oxygen, and other substances were considered negligible. The watershed model generated daily loads for twenty-nine watersheds along the shore of the Bay and tidal tributaries. Loads from each watershed were distributed evenly into adjoining water quality model cells in the surface plane of the grid. Daily loads were averaged into monthly loads prior to input to the water quality model.

Point-Source Loads. Point-source dischargers to the Chesapeake range in size from one of the world's largest, the Blue Plains Treatment Facility, down to trailer parks and highway rest stops. Municipal dischargers in Maryland and the District of Columbia were considered in the model only if daily flow exceeded 0.4 mgd (million gallons per day). Industrial dischargers were considered if BOD load exceeded 100 ppd (pounds per day), if nitrogen load exceeded 40 ppd, or if phosphorus load exceeded 12 ppd. All identifiable point sources in Virginia were considered. In total, nearly 150 point sources were represented in the model. Point-source loads from each facility were computed as the product of flow rate and concentration. Quantification of loads was conducted on a monthly basis.

Atmospheric Loads. Atmospheric loads were divided into two categories. "Wetfall" was the loading associated with dissolved substances in rainfall. Settling of dust particles and similar processes comprised "dryfall".

Annual mean concentrations of ammonium and nitrate in wetfall were obtained from data published by the National Atmospheric Data Program

(NADP 1989). Seasonal wetfall concentrations of organic nitrogen, phosphate, and organic phosphorus were obtained from the Chesapeake Bay Program Technical Synthesis (USEPA 1982). Dryfall nitrogen load was assumed equal to the wetfall nitrate load. Dryfall phosphorus load was assumed to be negligible. Atmospheric loads employed in the water-quality model were identical to loads employed in the watershed model.

Summary by Basin. Direct nutrient loads to the mainstem Bay and major tributary basins were summarized. Total nutrient loads to each basin were largely proportional to drainage area. Largest nitrogen loads were to the mainstem, Potomac, and James (Figure 16-12). These reflected the fall-line loads to each basin although point sources were a significant contributor in the James. Nitrogen loads to Baltimore Harbor were almost entirely from point sources. Nitrogen loads to remaining basins were minor due to small drainage area and few point-source dischargers.

The mainstem also received the largest direct phosphorus load (Figure 16-13) due to runoff from the Susquehanna. Under average hydrologic conditions, total phosphorus load in the James exceeded the Potomac despite the lesser drainage area of the James. The exceedance was due to the large disparity in point-source loading between the two basins. Phosphorus loads to remaining basins were much less than the first three and roughly equivalent.

Summary by Source. The predominant nitrogen load to the system was at the fall lines (Figure 16-14). Fall-line loads were proportional to runoff volume. The year of highest runoff, 1984 had the greatest load. Loads in 1985 and 1986 were equivalent despite the description of 1985 as "dry" year and 1986 as an "average" year. Annual fall-line loads in 1985 were influenced by the autumn storm in the western tributaries. Loads in the Susquehanna, the primary runoff source to the mainstem were less in 1985 than in 1986. In 1985 and 1986, point sources were the second largest nitrogen source although nonpoint sources exceeded point sources in 1984. Atmospheric nitrogen loads were the least of all sources.

Fall-line loading was also the predominant phosphorus source (Figure 16-15). Despite lesser flow in the Susquehanna in 1985 than in 1986, total fall-line loading was greater in 1985. Excess load in 1985 was due to the autumn storm that affected the tributaries. Second largest phosphorus loading was from point sources in all years. Atmospheric phosphorus loads were the least of all sources.

Annual Summary. On an annual basis, total nitrogen loads to the system (Table 16-2) reflected runoff volume in the Susquehanna. Nitrogen loads were largest in 1984, less in 1986 and least in 1985. Total phosphorus loads were also largest in 1984 but the least loads occurred in 1986 rather than 1985. The excess loading in 1985 was due to the loading associated with the major autumn storm in the western tributaries.

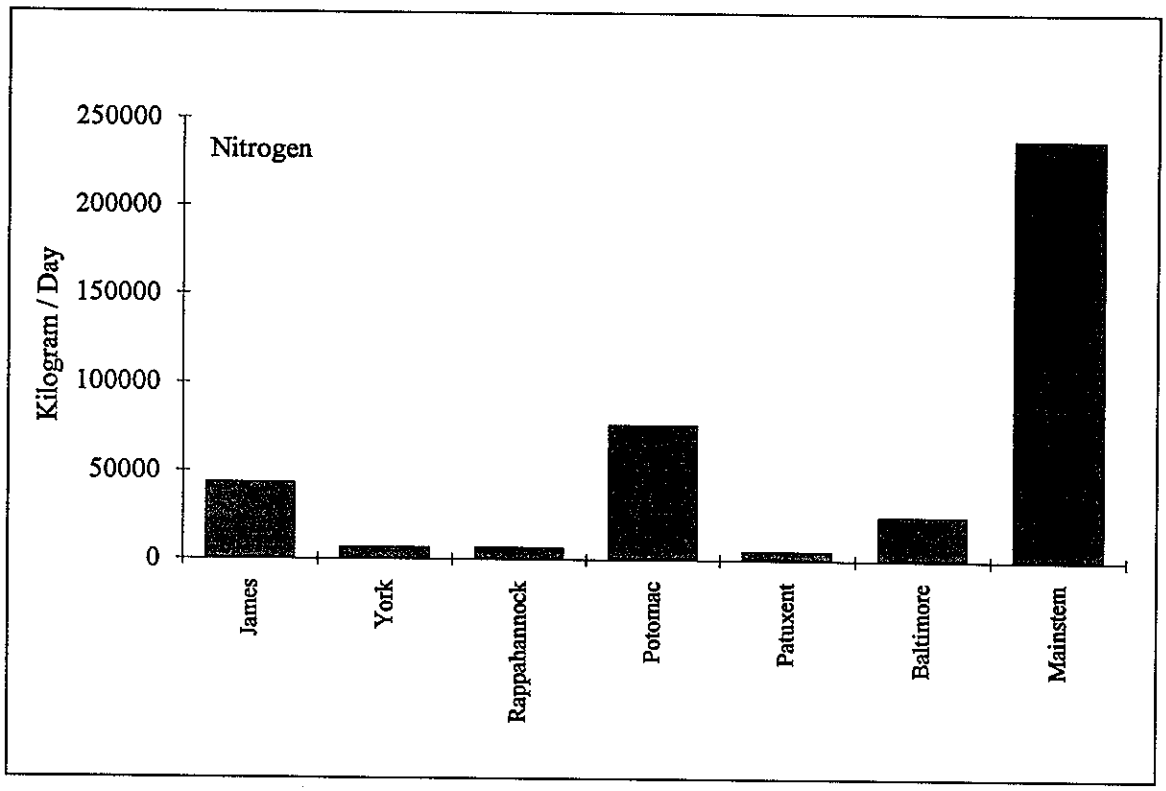

Figure 16-12. Nitrogen Loads by Basin, 1986

Table 16-2
Total Direct Loads to System, 1984-1986

Year	Carbon	Nitrogen	Phosphorus
1984	1,611,667	598,677	41,794
1985	1,004,384	398,317	32,374
1986	725,085	402,886	25,496

The Data Bases

Monitoring Data. The primary source of water-column observations was the monitoring data base maintained by the Chesapeake Bay Program Office. Monitoring data were available from initiation of the program, in June 1984, through the end of 1986. Observations were collected in bay-wide surveys conducted twice monthly in March through October and once monthly in the remaining months. In the Maryland portion of the Bay and in the Virginia portion of the Bay overlying the deep trench, four samples were collected at each station: one meter below the surface, one meter above the bottom, above the pyncnocline, and below the pyncnocline. At the remaining Bay stations and in the tributaries, surface and bottom samples only were collected. Stations sampled and employed in the present study are shown in Figure 16-16.

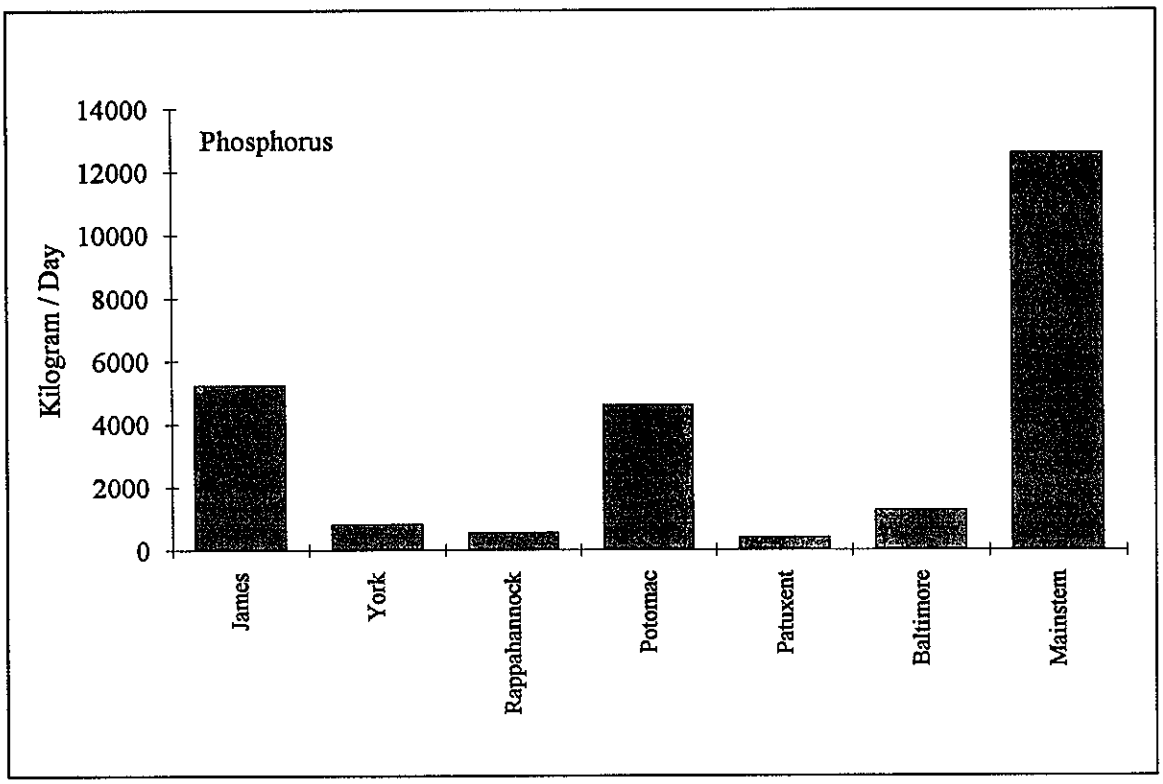

Figure 16-13. Phosphorus Loads by Basin, 1986

Sample analyses differed depending upon sample location and analytical laboratory. Substances directly analyzed (or derived from direct analyses) in the mainstem bay are presented in Table 16-3.

Table 16-3
Sampled or Derived Substances in Chesapeake Bay

Temperature	Salinity
Chlorophyll 'a'	Dissolved Organic Carbon
Particulate Organic Carbon	Ammonium
Nitrate+Nitrite	Dissolved Organic Nitrogen
Particulate Organic Nitrogen	Total Nitrogen
Dissolved Phosphate	Dissolved Organic Phosphorus
Particulate Phosphorus	Total Phosphorus
Dissolved Oxygen	Dissolved Silica
Disk Visibility	

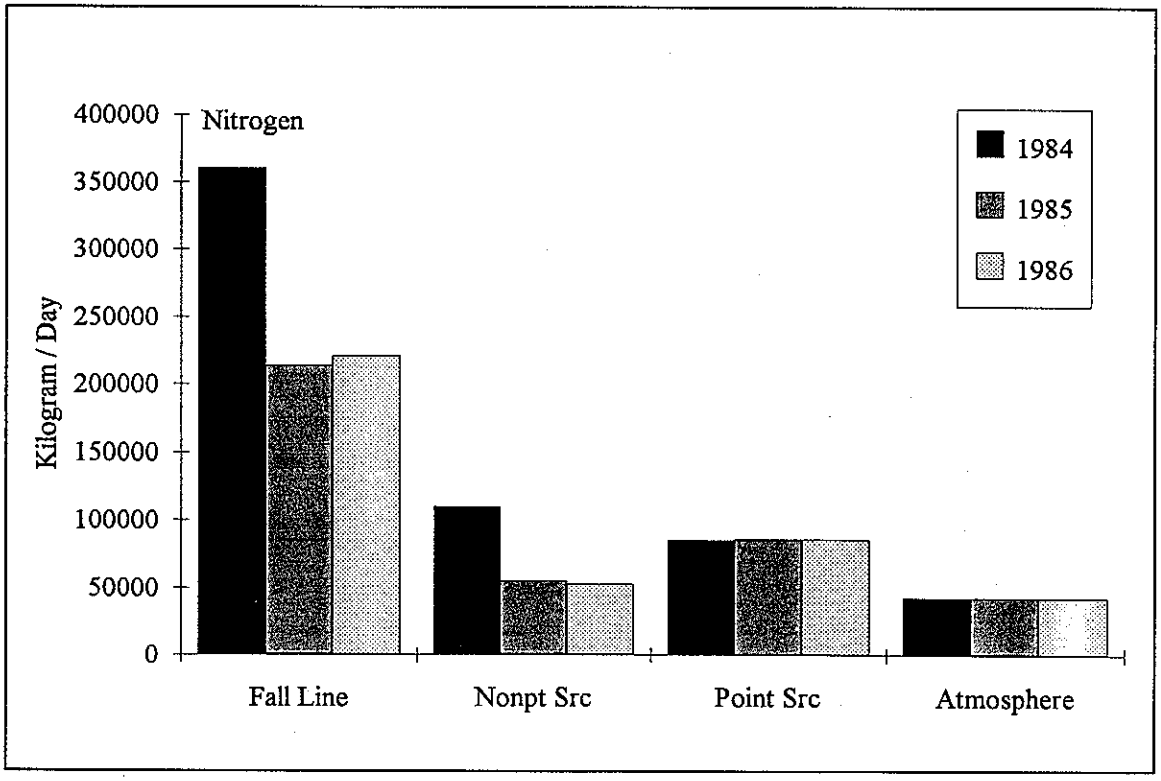

Figure 16-14. Total Nitrogen Loads, 1984-1986

Coupling with the Sediment Model

The need for a predictive benthic sediment model was made apparent by the results of the steady-state model study (HydroQual 1987) which preceded the present effort. The study indicated sediments were the dominant sources of phosphorus and ammonium during the summer period of minimum dissolved oxygen. An increase in sediment oxygen demand and nutrient release was implicated in a perceived decline in dissolved oxygen from 1965 to 1985. For management purposes, a model was required with two fundamental capabilities:

Predict effects of management actions on sediment-water exchange processes, and

Predict time scale for alterations in sediment-water exchange processes.

A sediment model to meet these requirements was created for this study. The model (Figure 16-17) was driven by net settling of organic matter from the water column to the sediments. In the sediments, the model simulated the

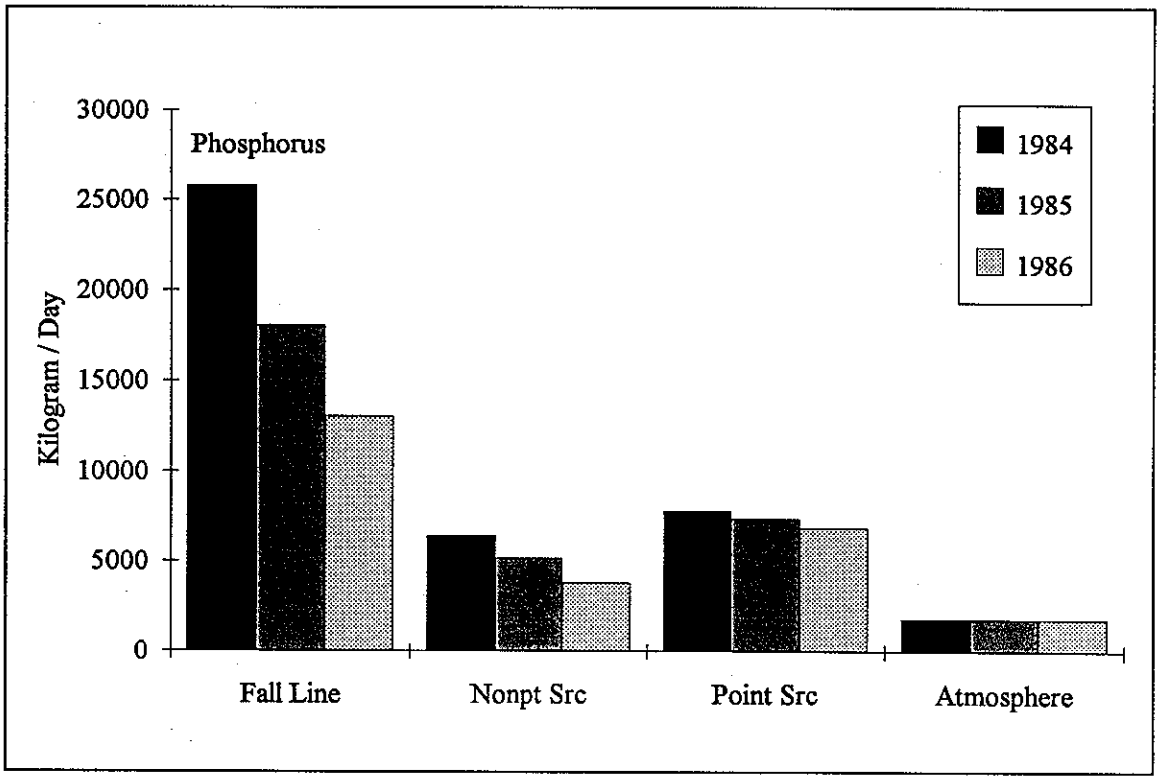

Figure 16-15. Total Phosphorus Loads, 1984-1986

diagenesis (decay) of the organic matter. Diagenesis produced oxygen demand and inorganic nutrients. Oxygen demand, as sulfide (in saltwater) or methane (in freshwater), took three paths out of the sediments: export to the water column as chemical oxygen demand, oxidation at the sediment-water interface as sediment oxygen demand, or burial to deep, inactive sediments. Inorganic nutrients produced by diagenesis took two paths out of the sediments: release to the water column, or burial to deep, inactive sediments. A listing of sediment model state variables and predicted sediment-water fluxes is provided in Table 16-4.

SONE and BEST Programs. Sediment water flux measures employed in model development, calibration, and performance evaluation were obtained from two programs. The SONE (sediment oxygen and nutrient exchange) program (Boynton et al. 1986) provided observations of sediment oxygen demand, and ammonium, nitrate, phosphate, and silica exchange at eight stations in the upper Bay, Patuxent and Potomac Rivers. Observations were collected four times per year during 1985 and 1986. The methodology employed intact sediment cores incubated in triplicate immediately upon collection.

Data collected in the SONE program alone were insufficient to develop and calibrate the sediment model. The more extensive BEST (benthic exchange

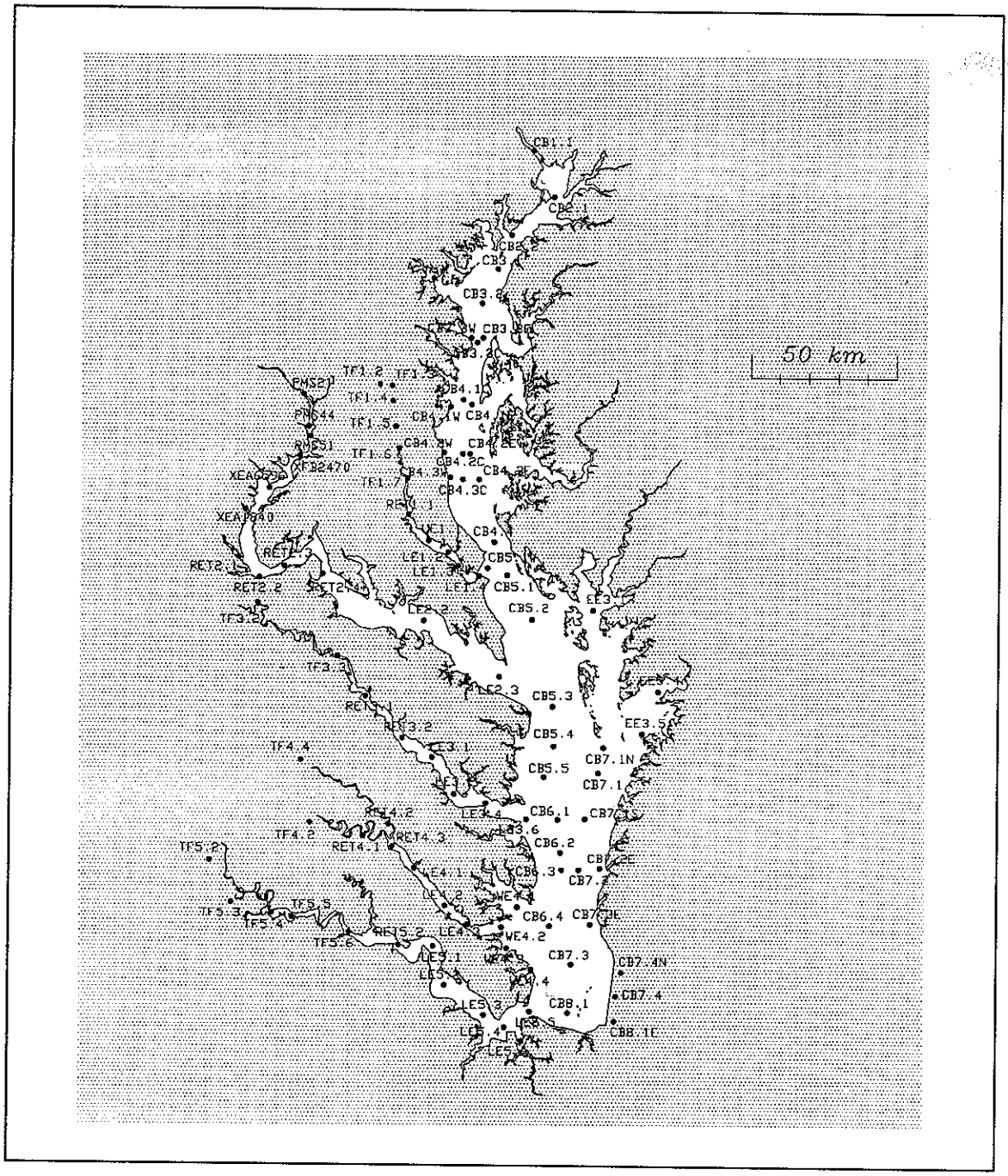

Figure 16-16. Monitoring Program Stations

Table 16-4
Sediment Model State Variables and Fluxes

State Variable	Sediment-Water Flux
Temperature	
Particulate Organic Carbon	Sediment Oxygen Demand
Sulfide/Methane	Release of Chemical Oxygen Demand
Particulate Organic Nitrogen	
Ammonium	Ammonium Flux
Nitrate	Nitrate Flux
Particulate Organic Phosphorus	
Phosphate	Phosphate Flux
Particulate Biogenic Silica	
Available Silica	Silica Flux

and sediment transformations) program (Garber et al. 1988) employed SONE methodology to measure sediment-water exchanges at fourteen stations throughout the mainstem Bay during 1988.

Mainstem Bay Calibration

Summary of Results

Comparison of model predictions with observations indicated the following characteristics:

Comparisons of predicted and observed salinity were excellent (Figure 16-18). Predicted surface salinity conformed to the observed pattern in which salinity is higher on along the eastern shore than along the western shore (Figure 16-19). The comparisons verified that transport in the hydrodynamic model was accurately replicated in the water-quality model.

The recurrence and magnitude of the spring bloom were replicated (Figure 16-18). Annual variability in magnitude and location of peak biomass were difficult to predict, however.

Physical and biological phenomena in the water column and sediments that cause summer bottom-water anoxia were reproduced. The model accurately represented the recurrence of anoxic water at the head of the deep trench (Figure 16-20). Minimum dissolved oxygen concentration was well predicted. Summer-average observations were frequently less than predictions, however.

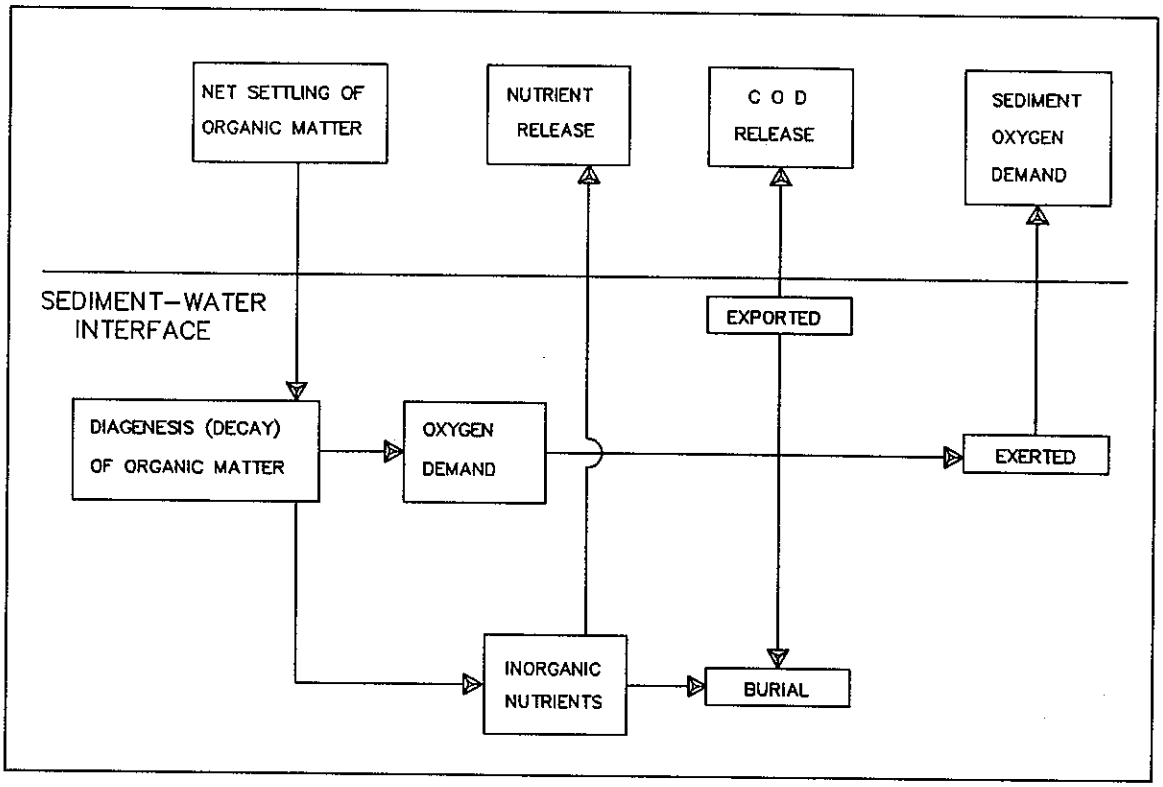

Figure 16-17. Sediment Model Schematic

The interactions between system geometry and hypoxia were well-represented in the model (Figure 16-21). Lowest predicted dissolved oxygen concentrations occurred at the head of the deep trench and penetrated up the channel into Baltimore Harbor. Hypoxia followed the trench down the Bay and penetrated into the connecting channel at the mouth of the Potomac.

Substantial anoxia was also indicated in the secondary channel that runs along the Eastern Shore. Hypoxic water was virtually absent from shoal areas of the mainstem although hypoxia was indicated in shallow portions of some tributaries.

Suggested Improvements

The model provided a realistic representation of eutrophication processes in the mainstem Bay. Spatial and temporal trends and magnitude of the observations were well reproduced. The extensive effort allotted to calibration indicated no improvement in model-data agreement was possible with the present model. Two improvements were suggested to enhance realism and, potentially model accuracy. These were addition of zooplankton and particulate inorganic phosphorus to the model.

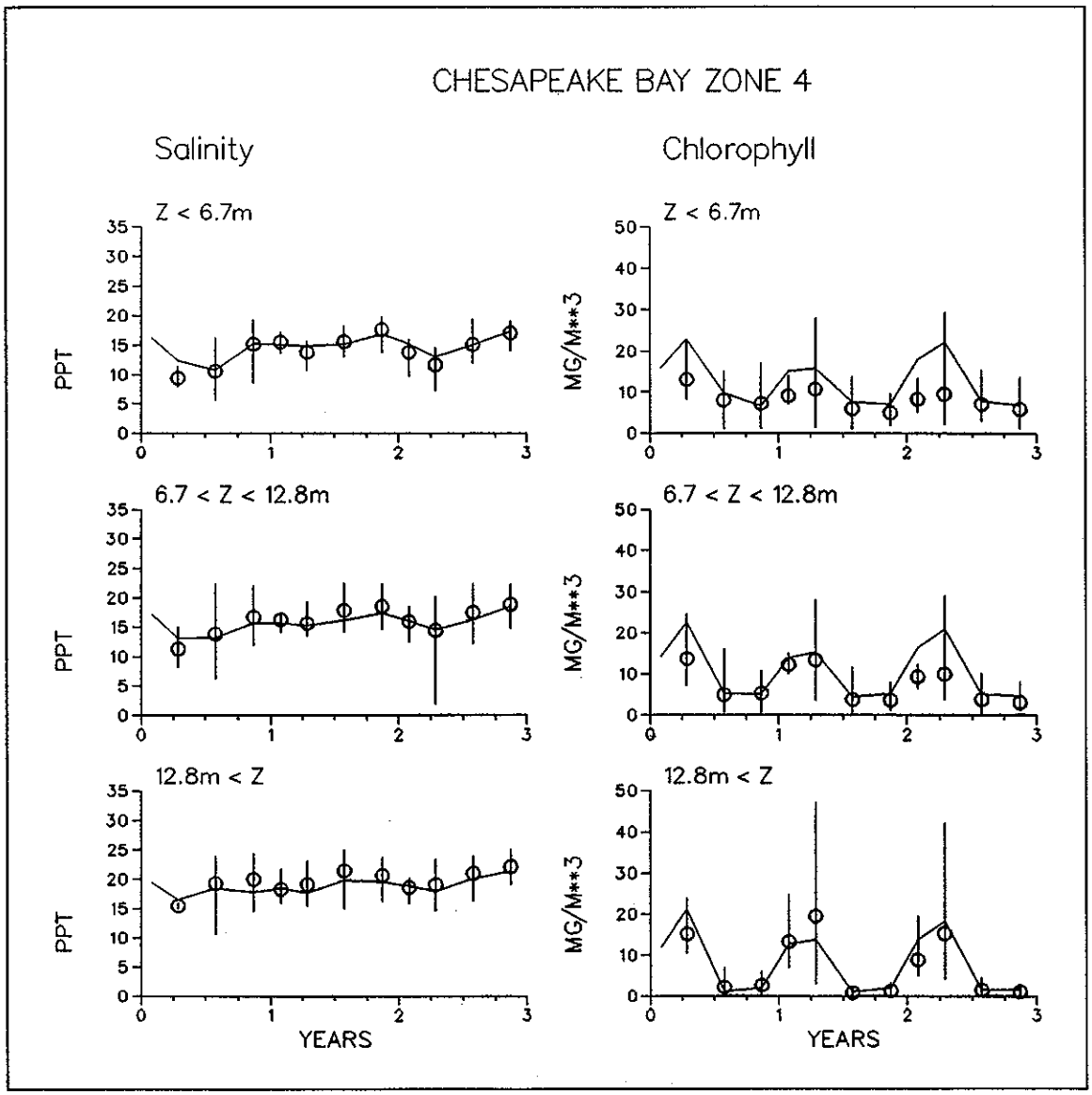

Figure 16-18. Time Series of Predicted and Observed Salinity and Chlorophyll Concentrations in Zone Four

Tributary Calibration

Five major tributaries were sampled and modelled in detail sufficient to warrant individual presentation. These were the James, York, Rappahannock, Potomac, and Patuxent Rivers. Model performance in the two largest tributaries, the James and the Potomac, was largely satisfactory although model-data discrepancies occurred. Correspondence between predictions and observations was less satisfactory in the remaining tributaries. Performance in all tributaries was influenced by the diminished spatial scale relative to the mainstem. The

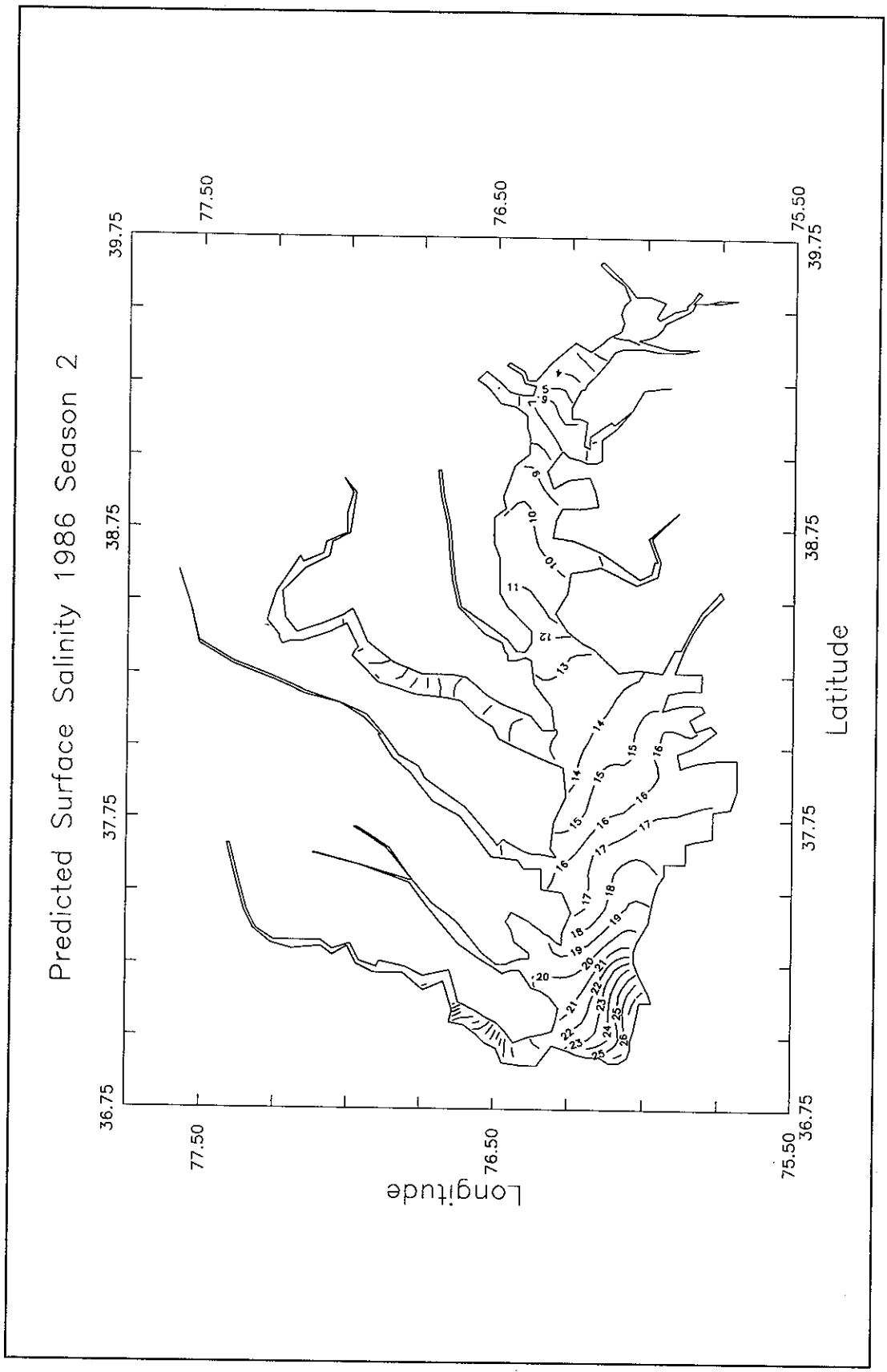

Figure 16-19. Predicted Surface Salinity, Spring 1986

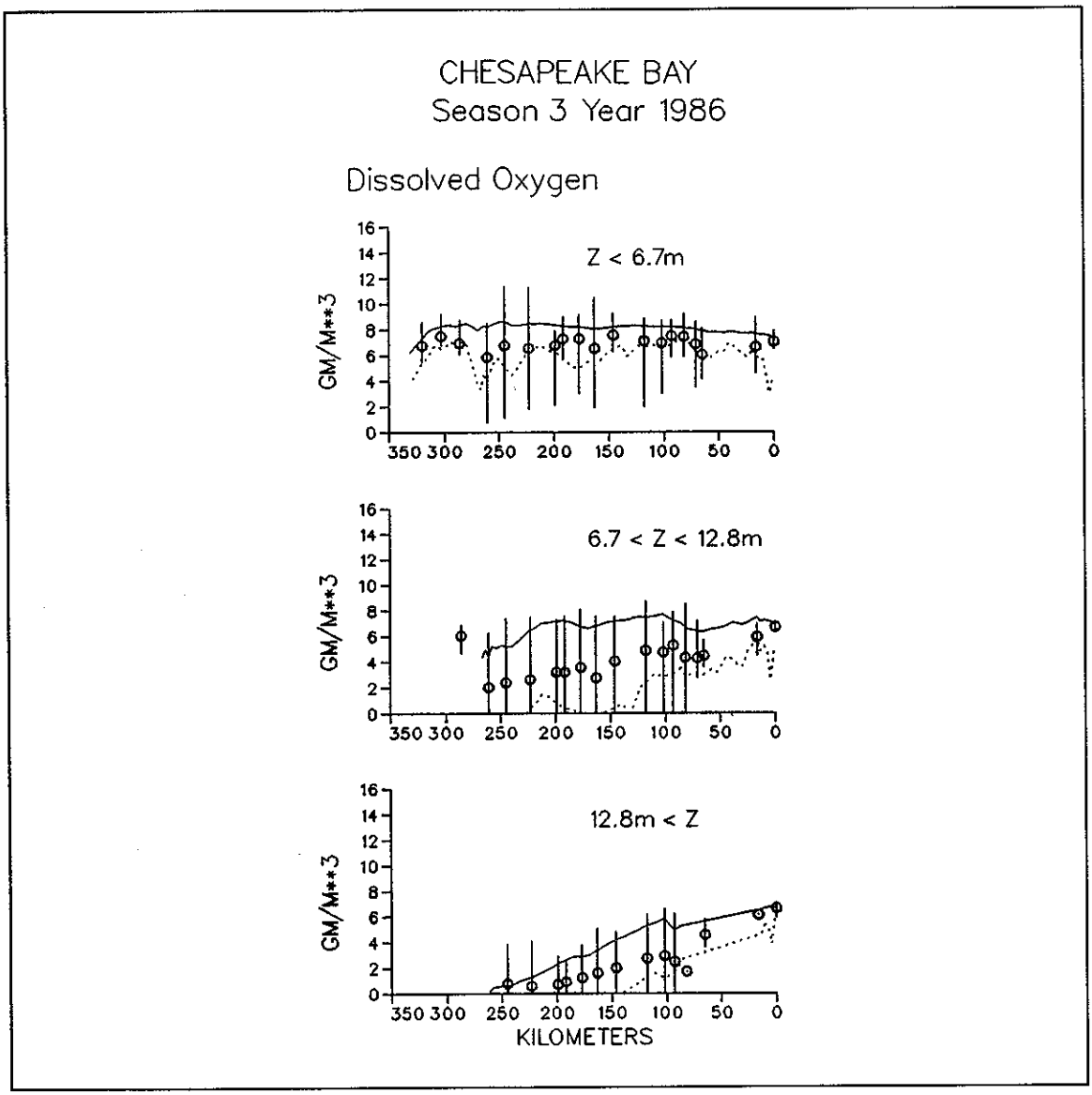

Figure 16-20. Predicted and Observed Dissolved Oxygen Concentration Along Mainstem Bay Transect, Season Three, 1986

diminished scale required finer grid resolution and more detailed specification of loading than were available in the current model framework.

The function of the tributaries as conduits of loads to the mainstem is simulated in the present model. The model may also be used for first-order analysis of tributary response to load reductions. The existing representation is of limited utility, however, for detailed analysis and management of eutrophication processes within the tributaries.

Starting points for improved representation, common to all tributaries, have been identified. These are:

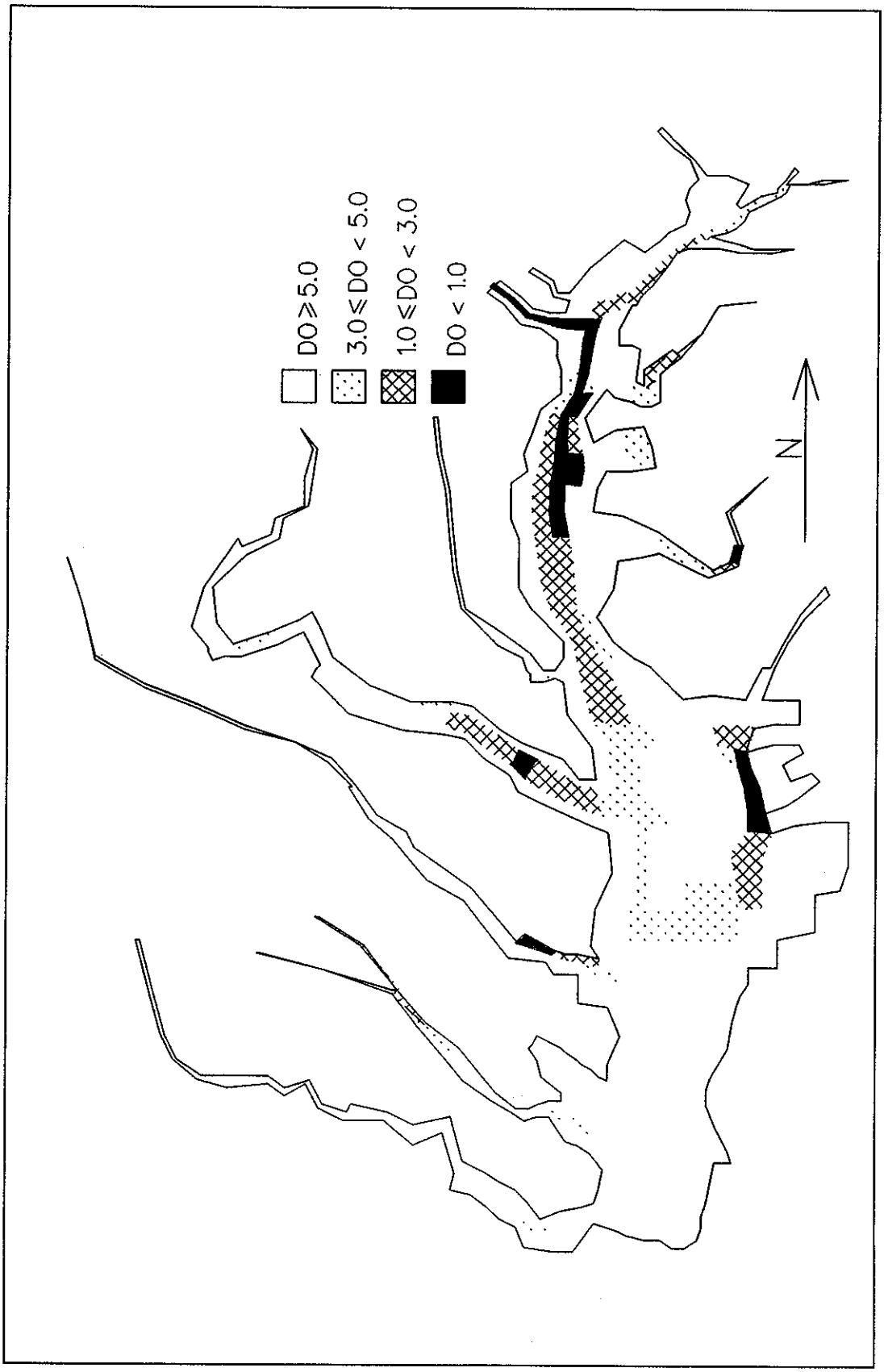

Figure 16-21. Plan View of Predicted Bottom Dissolved Oxygen, Season Three, 1986

1) Magnitude and composition of loads must be quantified with extreme accuracy.

2) Phenomena occurring near the limit of salt intrusion must be represented. These include convergent flows, physical concentration of particulate phosphorus, and the chlorophyll maximum.

3) Longitudinal and lateral resolution of the tributary grids should be improved.

Statistical Summary of Calibration

Graphical and statistical summaries of model performance in the mainstem and individual tributaries were produced.

Mean Error in Bay and Tributaries

The mean error statistic in the mainstem and tributaries identified a shortfall in predicted total phosphorus throughout the system. In the mainstem, the mean error was 38% of the observed mean concentration. The mean error indicated a deficiency in total phosphorus loading. Bank erosion was the likely origin of the missing phosphorus. Estimated erosion loads, 6000 kg day^{-1} (CBPO 1991), were roughly 18% of the loads presently considered in the model.

Mean error summaries indicated observed dissolved oxygen was less than predicted throughout the system. In the mainstem, over-predictions most often occurred in subsurface water characterized by oxygen deficiencies. In the tributaries, over-predictions most often occurred in surface waters nearly saturated with dissolved oxygen.

Relative Error in Bay and Tributaries

Salinity was the substance with least relative error in all bodies (Figure 16-22). The low error was attributed to the conservative nature of salinity and to the well-known, single source at the ocean. At the other extreme, relative error was greatest for chlorophyll and organic carbon. The high error reflected the non-conservative behavior of algal biomass and organic detritus, the unlimited source of atmospheric carbon, and the approximate nature of mathematical models of biological processes.

Relative error for dissolved oxygen and nutrients was intermediate. Favorable statistics reflected limits on the range of potential values and knowledge of sources and sinks. The atmospheric source of oxygen was unlimited but the range of predicted concentrations was restricted between zero and saturation.

The concentrations of total nitrogen and phosphorus were unlimited but dependent on loads which were known to a reasonable extent.

For most substances, relative error was less in the mainstem than in the tributaries. Differences in salinity and dissolved oxygen errors were minor, however. Relative chlorophyll error was clearly much less in the mainstem than in the tributaries. The Potomac and Patuxent stood out as having unusually large chlorophyll errors. In the Potomac, the error reflected the need for improved calibration of cyanobacteria. The origin of the Patuxent error was not apparent.

Relative Error at Different Stages of Calibration

The model went through four major stages of calibration. At each stage, modifications were made to the code, loads, or parameter values. Although each change produced qualitative improvements in model-data agreement or in predictive power of the model, statistical behavior of several key constituents was largely unchanged from the initial calibration. The progress of statistics through 220 model runs indicated that additional calibration of the present model is futile. Improvements in model-data agreement require new estimates of loads to the system, additions to the suite of state variables, or additional grid resolution.

Sediment Model Performance

The method selected to summarize sediment model performance compared the population of observations with the corresponding population of model values. Populations were compared through cumulative distribution plots (Figure 16-23). Ideal correspondence was indicated by lines which overlay directly.

Correspondence between the distributions of predicted and observed ammonium, nitrate, and phosphate flux was remarkable. Ammonium distributions corresponded through roughly ninety-percent of the populations. Nitrate and phosphate exhibited similar behavior. Distributions of predictions and observations corresponded except in the upper extreme. For silica, predicted fluxes were less than observed through most of the range. Median predicted flux was 16% less than observed. Predicted sediment oxygen demand was also less than observed. At the median, predictions were 0.2 gm m^{-2} day^{-1} (18%) below observations.

Comparison With Alternate Models

Median relative error for the mainstem Bay in the present study was in the midrange of reported errors in comparable studies. The statistics did not reflect, however, the unique nature or the high degree of realism in the present

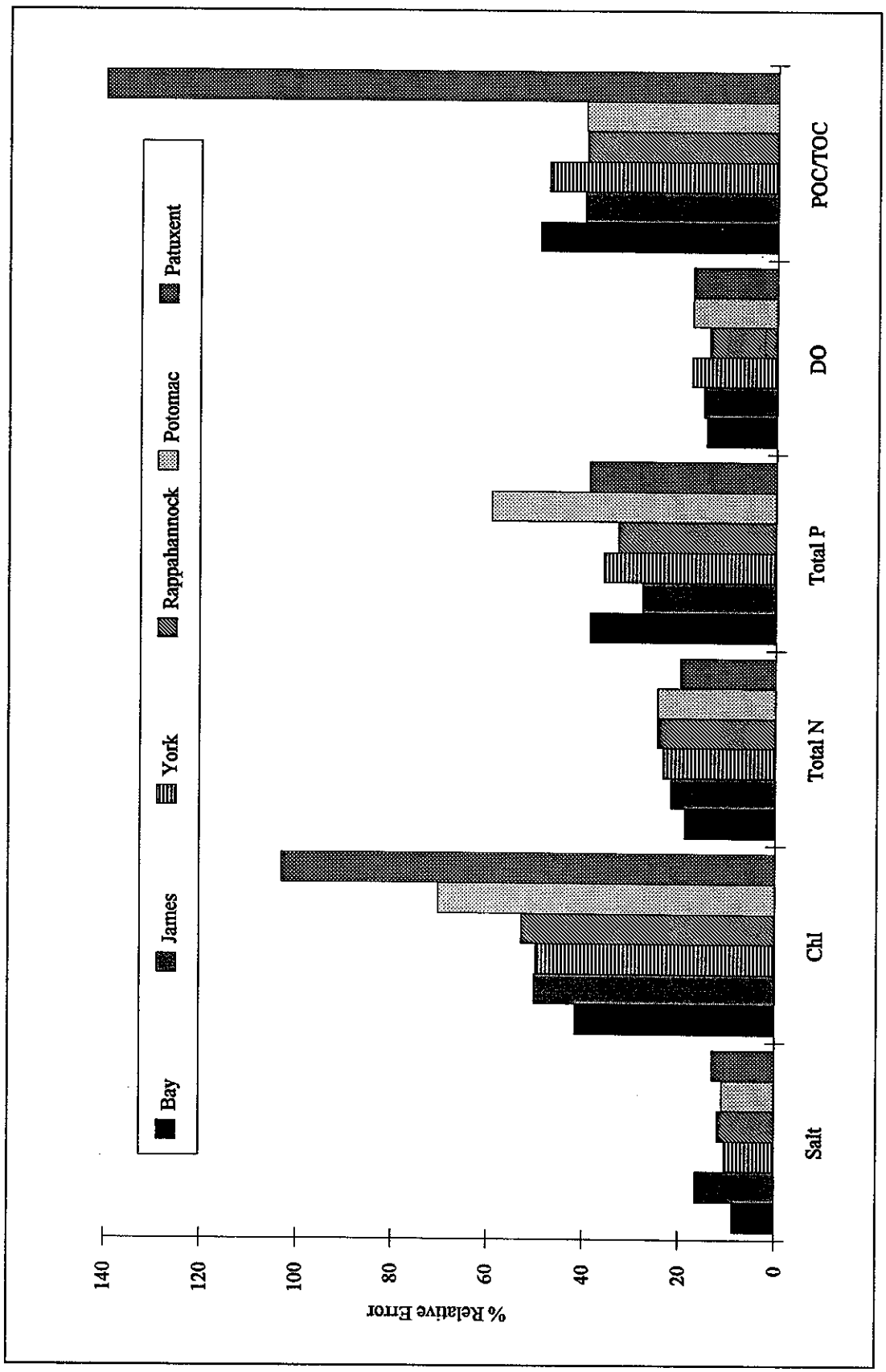

Figure 16-22. Relative Error in Mainstem Bay and Tributaries

study. The realism affected statistical performance by removing degrees of freedom conventionally employed in model calibration. In the present study, for example, Lagrangian averaging of three-dimensional hydrodynamics eliminated the use of a dispersion parameter to transport mass about the system. The sediment model eliminated tuning of sediment-water material fluxes. Employment of organic carbon as a state variable, instead of BOD, eliminated flexibility in converting short-term to long-term BOD measures and in estimating BOD production by algal life processes.

Thirty-Year Analysis

Introduction

The verified three-dimensional eutrophication model was employed in a simulation of the thirty-year period 1959-1988. Results of the simulation were examined for trends and other eutrophication characteristics.

Hydrology and Hydrodynamics

Hydrodynamics for the thirty-year simulation were obtained by sequencing the annual hydrodynamic series produced for the model calibration. Years in the period 1959-1988 were classified as "wet", "average", or "dry" based on annual flow in the Susquehanna. Wet years were at or above the 75th percentile of annual flows in the period of record. Average years were between the 25th and 75th percentile. Dry years had flows below the 25th percentile. Hydrodynamics from 1984 hydrodynamics were employed for "wet" years in the thirty-year simulation. Hydrodynamics from 1986 were used to represent "average" years in the simulation. Modified 1985 hydrodynamics were employed for most "dry" years in the simulation. The modification was necessary to remove from the "dry" hydrodynamics the November 1985 storm which flooded the western tributaries and, to a lesser extent, the Susquehanna.

The hydrodynamic sequencing was appropriate to the simulation objective of trend detection. Since individual hydrodynamics were not employed for each of the thirty years, the simulation was not expected to exactly reproduce water quality within a year. The simulation was expected to reproduce trends, however, and to distinguish the influences of "wet", "average", and "dry" hydrology on eutrophication.

Loads

Point Sources. A listing of point sources and associated loads for the years 1965, 1970, and 1980 was provided by the EPA CBPO. We supplemented

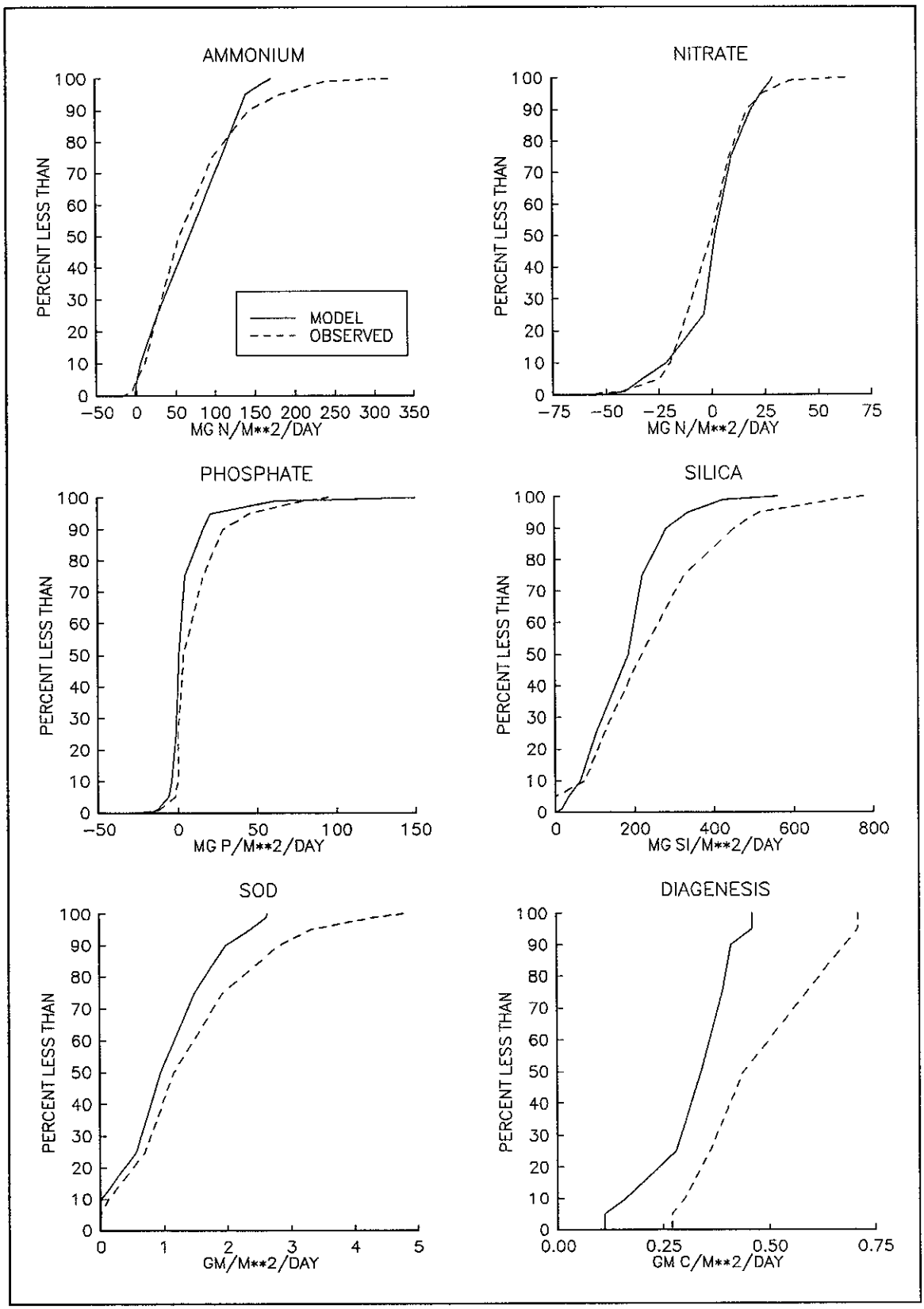

Figure 16-23. Distributions of Observed and Predicted Sediment-Water Fluxes

this record with 1985 point sources and loads employed in the model calibration. Transition from one set of loads to the next was handled as a step function.

Below-Fall-Line Loads. Below-fall-line nonpoint-source loads were derived from loads provided by a predictive watershed model (Donigian et al. 1991). Watershed model loads were available for the years 1984-1986. From these, load-runoff relationships were created for each below-fall-line watershed. Next, a thirty-year record of flow in each watershed was constructed by ratio relationships to long-term gauge records. The flow records were employed in the load-runoff relationships to determine a thirty-year time series of nonpoint-source loads.

Fall-Line Loads. Fall-line loads were computed as the product of flow and concentration. Concentrations were estimated by a minimum-variance-unbiased-estimator (MVUE) method (Cohn et al. 1989) using a program supplied by the United States Geological Survey (USGS). The program used least-squares techniques to estimate parameters in an equation that related concentration to flow, season, and time.

Atmospheric Loads. No data was available on which to base a thirty-year time series of atmospheric loads to the water surface. Contemporary loads employed in calibration of the eutrophication model, 1984-1986, were applied to the thirty years, 1959-1988.

Conclusions

Nutrient loads to the Bay were maximum in the decade 1969-1978 (Figure 16-24). Nitrogen loads in the decade 1979-1988 were 7% less than in the preceding decade. The reduction was primarily due to hydrologic effects; runoff was less in the most recent decade than in the preceding decade. The underlying trend was for increasing nitrogen concentration at the two major fall lines. Phosphorus loads to the system have decreased steadily since Tropical Storm Agnes in 1972. Phosphorus loads in the decade 1979-1988 were 30% less than in the 1969-1978 decade. The reduction was due to point-source control, declining concentration at the Potomac fall line, and decreased runoff.

On an annual basis, total nitrogen concentration in the Bay was closely associated with hydrology. Wet years had higher concentrations than dry years. Total nitrogen in the Bay is increasing due to concentration trends at the two major fall lines. Over thirty years, total nitrogen in the Bay increased by $\approx$0.06 gm m^{-3} (Figure 16-25).

Total phosphorus concentration in the Bay peaked in 1972 and 1973, following the Tropical Storm Agnes event (Figure 16-25). Since then, total phosphorus in the Bay has declined steadily. Combined effects of point-source and

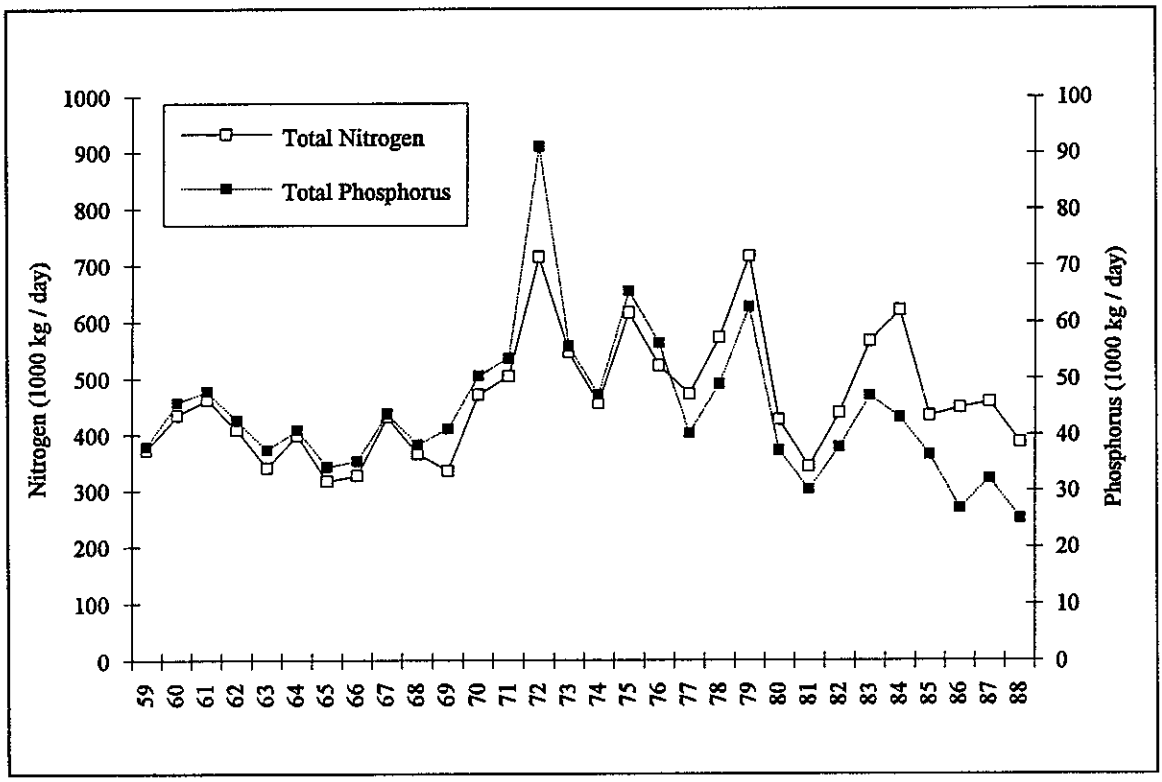

Figure 16-24. Total Nitrogen and Phosphorus Loads to Chesapeake Bay System: 1959-1988

nonpoint-source controls have reduced annual-average total phosphorus concentrations by 0.006 gm m^{-3} over thirty years.

Simulated chlorophyll concentrations were closely tied to hydrology. Over most of the Bay, wet years with high nutrient runoff had greatest chlorophyll concentrations (Figure 16-26). Immediately below the Susquehanna fall line, however, hydrodynamic effects caused chlorophyll to be less in wet years. Summer chlorophyll concentration was greatest in the most recent decade. Increasing summer chlorophyll was linked to an underlying increase in nitrogen concentration at the Susquehanna fall line.

Dissolved oxygen trends in the Bay were subtle and unlikely to be detected solely by analysis of observations (Figure 16-26). On a decadal basis, dissolved oxygen in the Bay was least during 1969-1978. Summer-average bottom dissolved oxygen improved by 0.5 gm m^{-3} in the 1979-1988 decade. The improvement was primarily due hydrodynamic effects, however. When only years of "average" hydrology were compared, bottom dissolved oxygen declined by ≈0.3 gm m^{-3} from 1959-1968 to 1979-1988.

Anoxic volume trends in the Bay mirrored dissolved oxygen trends. The decade 1969-1978 had the largest anoxic volume (Figure 16-27). Anoxic volume was less in the 1979-1988 decade indicating an improvement in water

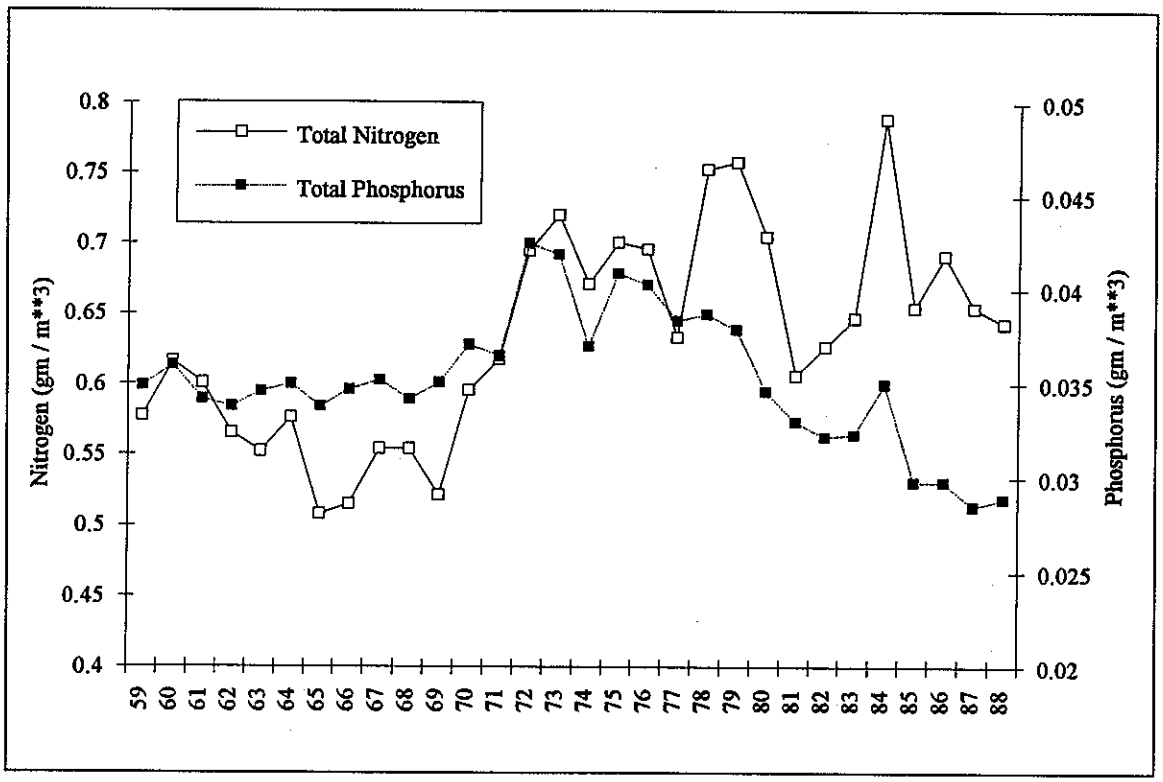

Figure 16-25. Annual-Average Total Nitrogen and Phosphorus Concentration in Mainstem Bay, 1959-1988

quality. As with dissolved oxygen however, the improvement was primarily due to hydrodynamic effects. When only years of "average" hydrology were considered, anoxic volume increased by 18% from the 1959-1968 decade to the 1979-1988 decade.

Trends in anoxia were tied to trends in nitrogen concentration in the two major fall lines. The simulation indicated summer-average nitrogen loads are increasing, thereby supporting increased algal biomass. The algae settle to the bottom, decay, and consume oxygen. Phosphorus load reductions since 1972 had no discernable effect on anoxia although the load reductions apparently caused observed reduction of summer chlorophyll concentrations near the Susquehanna fall line.

Analysis indicated hydrodynamics were the predominant influence on anoxic volume. Anoxic volume induced by high stratification, as in 1984, was 50% greater than the range of load-induced anoxia over the thirty-year period. The extreme variation in anoxic volume over thirty years was approximately a factor of two. Highest anoxic volume was in 1979, 64 x 10^{10} cubic meter days. Least anoxic volume was in 1968, 28 x 10^{10} cubic meter days. Order-of-magnitude variations or trends in anoxic volume over the space of two to three decades are highly unlikely.

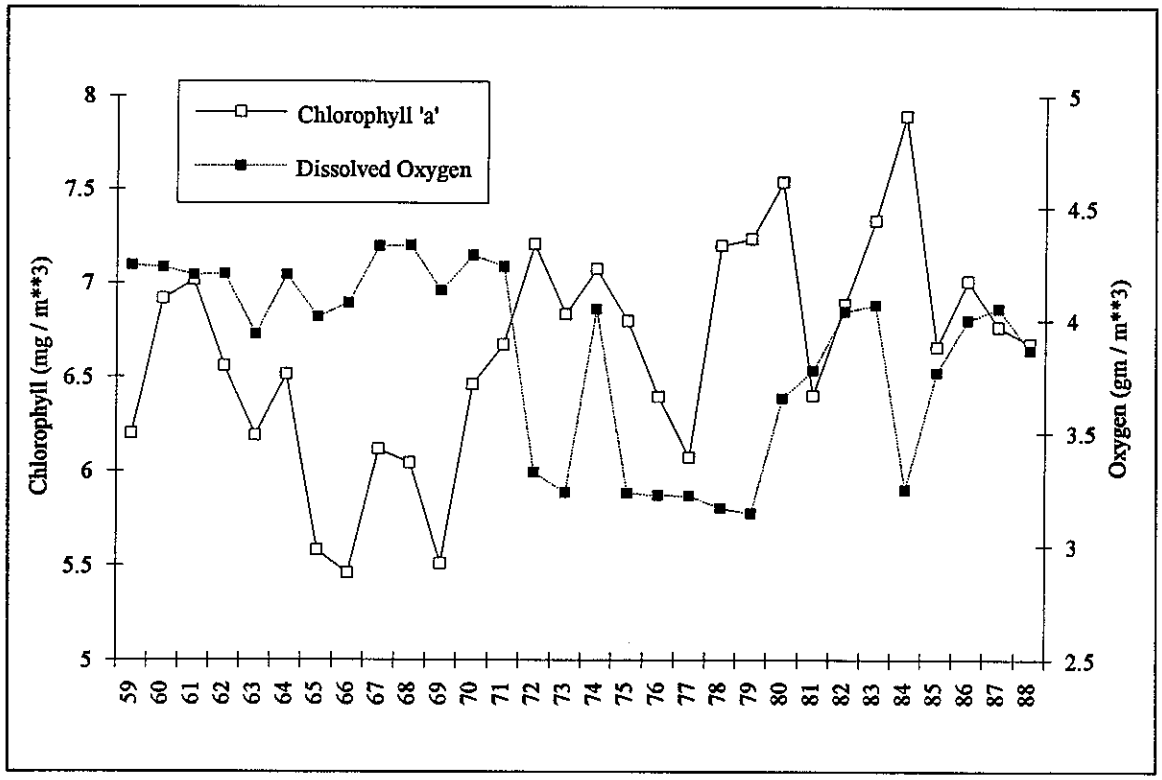

Figure 16-26. Summer-Average Surface Chlorophyll and Bottom Dissolved Oxygen in Mainstem Bay, 1959-1988

Scenarios and Load Sensitivity Analyses

A primary purpose behind development of the eutrophication model was employment of the model in scenario analysis. The model was intended for use in developing and testing load-management strategies aimed at limiting eutrophication processes in the Bay. Before scenarios could be run, however, a scenario methodology had to be developed. The primary issue was duration of the scenarios. Length had to be sufficient for the sediments to respond to management actions. A second issue involved scenario hydrology and hydrodynamics. The scenarios had to account for effects of these dynamic processes on water quality.

Duration, Hydrology, and Hydrodynamics

During the model calibration process, empirical investigations of time to steady state and numerous preliminary scenarios were run. Based on these investigations, a ten-year time span was selected for scenario execution. The ten-year duration was employed for all but a few special scenarios for which the highest degree of completion was desired.

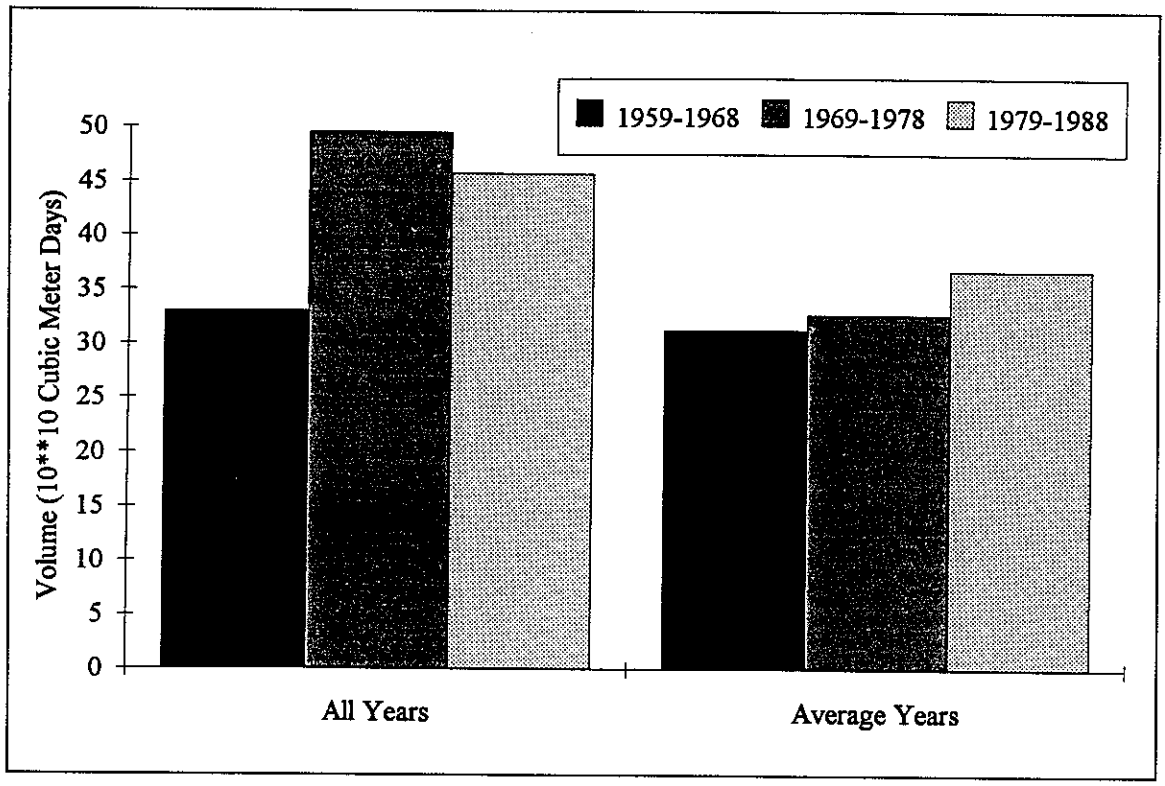

Figure 16-27. Anoxic Volume Days by Decade

Desire to indicate the direct and indirect influences of hydrology on water quality led to a decision to run the scenarios using variable hydrology. The decade 1979-1988 was selected as providing typical sequence and occurrence of varying annual hydrology. A decade of hydrodynamics was created by sequencing calibration hydrodynamic data sets as in the thirty-year run. Years in the period 1979-1988 were classified as "wet", "average", or "dry" based on annual flow in the Susquehanna. The 1984 calibration hydrodynamics were employed for "wet" years in the scenarios. Hydrodynamics from 1986 were used to represent "average" years. Modified 1985 hydrodynamics were employed for all "dry" years in the simulation. The modification was necessary to remove from the "dry" hydrodynamics the November 1985 storm which flooded the western tributaries and, to a lesser extent, the Susquehanna.

Scenario Descriptions

Two categories of scenarios were performed. "Management Scenarios" were aimed primarily at determining the response of the Bay to feasible ranges of nutrient controls. "Response Scenarios" were aimed at examining the behavior of the Bay under a wide range of nutrient loads, many of which fell outside the range of feasibility. Analysis of the management scenarios was the subject of a report published by the CBPO (Modeling Subcommittee 1993) and

is not repeated in the present document. An exception is presentation of the "Limit-of-Technology Nutrient Control" scenario which is of special interest.

Base Scenario. The Base Scenario specified existing conditions in the Bay. It was run with the model exactly as calibrated for 1984-1986 and with loads from that period. The Base Scenario provided the datum against which water quality improvements due to load reductions were determined.

Limit-of-Technology Nitrogen and Phosphorus Loads. The Limit-of-Technology (LOT) scenario represented the optimal condition that can be obtained through management controls of point-source and nonpoint-source nutrient loads above and below the Bay fall lines, within Bay-agreement jurisdictions.

All-Forest Scenario. In this scenario, nutrient loads to the Bay were obtained from an all-forest run of the Watershed Model. The all-forest loads were for all regions in the Bay watershed, not only Bay-agreement jurisdictions. Point-source loads were eliminated as were atmospheric nutrient loads to the water surface. This all-forest run comprised the best estimate of Bay water quality under natural conditions.

Nitrogen and Phosphorus Load Reductions. Nitrogen loads to the system were reduced thirty, sixty, and ninety percent in three scenarios. Phosphorus loads to the system were reduced thirty, sixty, and ninety percent in three additional scenarios. Load reductions were taken uniformly from fall-line loads, below-fall-line loads, point-source loads, and atmospheric loads. For these scenarios, the ocean was not considered a loading source.

Summary of Results

Time to Steady State. Concentrations of total nitrogen and total phosphorus in the mainstem attain ≈90% of their steady-state values in ten years (Figure 16-28). Diagenesis in the sediments, sediment oxygen demand, and sediment ammonium release also achieve ≈90% completion in ten years (Figure 16-29). For much of the Bay, the time for sediment phosphorus release to attain 90% of its steady-state value is much greater than ten years, due to retention of particulate phosphate in the sediments. The time for sediment phosphorus concentration to attain steady-state exceeds thirty years. The limiting process is the rate of burial to deep, isolated sediments. The effect of the slowly diminishing phosphorus release on concentration in the water column is barely observable, however. Consequently, ten years is proposed as the time scale for the Bay to respond to loading changes.

Loads and Budgets. Under existing conditions, fall-line loads are the greatest source of nitrogen to the system. The second largest source is nitrogen introduced from the continental shelf. Despite the large load originating on the shelf, however, the Bay is a net exporter of nitrogen to the shelf. Remaining nitrogen sources, in order of importance are point sources, nonpoint sources,

and the atmosphere. The major nitrogen sink is denitrification in the sediments, followed by burial to deep, isolated sediments, net export to the shelf, and denitrification in the water column.

Under existing conditions, the major source of phosphorus to the system is the continental shelf. Due to the shelf source, the Bay is a net importer of phosphorus. Remaining phosphorus sources, in order of importance, are fall-line loads, point sources, nonpoint sources, and the atmosphere. The sole net phosphorus sink is burial to deep, isolated sediments. Phosphorus is lost to the shelf, but more is introduced than is lost.

Under LOT nutrient controls, the fall lines and continental shelf remain the primary nitrogen sources. Nonpoint sources replace point sources as the next largest source. The shelf comprises a larger fraction of the total load than under existing conditions but the Bay persists as a net exporter of nitrogen. Denitrification in sediments continues as the major pathway for loss followed by burial and net export.

The shelf and fall lines are the primary phosphorus sources under LOT nutrient controls. As with nitrogen, point sources of phosphorus fall behind nonpoint sources. The major pathway for phosphorus loss remains burial to deep, isolated sediments.

Under all-forest conditions, the Bay was a net importer of nitrogen. The shelf was the major nitrogen source followed by fall lines and nonpoint sources. Denitrification was the major loss pathway.

Under all-forest conditions, the shelf was the major phosphorus source. All other sources were negligible in comparison. Burial was the major loss pathway for phosphorus introduced from the shelf.

Effects of Nitrogen and Phosphorus on Anoxia. Nitrogen exerts a greater influence than phosphorus on anoxic volume (Figure 16-30). The reduction of anoxic volume in proportion to reduction in direct (=no shelf) nitrogen loads exceeds one-to-one. By contrast, reduction in anoxic volume in proportion to reduction to direct (=no shelf) phosphorus loads is roughly one-to-four.

Nitrogen Versus Phosphorus Control. Nitrogen load can be viewed as a "master variable" which strongly influences concentrations and fluxes throughout the system. System algal biomass is diminished in nearly one-to-one proportion to nitrogen load reductions. Sediment oxygen demand, sediment ammonium release, and sediment phosphorus release also diminish in roughly one-to-one proportion to nitrogen reductions.

In the mainstem, the primary effect of phosphorus controls is reduction of algal biomass in the upper half of the Bay. On a system-wide basis, chlorophyll is reduced in roughly one-to-four proportion to reduction in phosphorus loads. The proportional reduction in algal biomass is equivalent to the proportional reduction in anoxic volume.

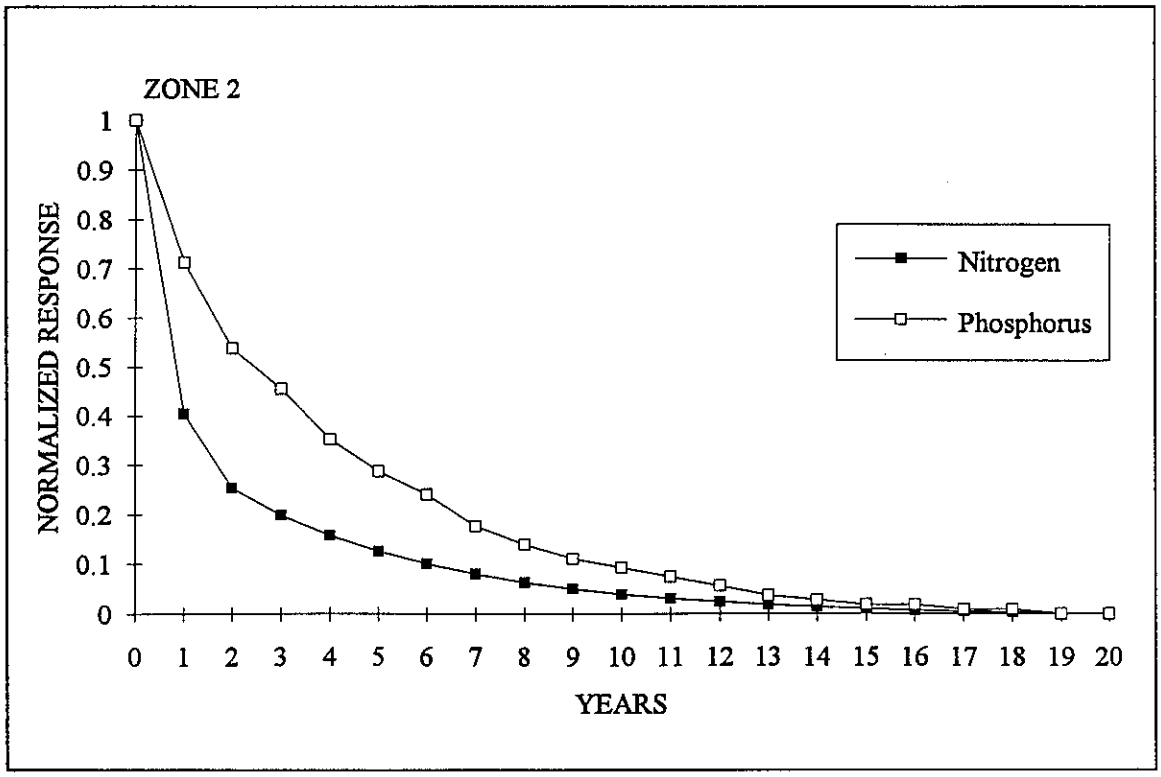

Figure 16-28. Water Column Nitrogen and Phosphorus - Time to Steady State at Head of Deep Trench

Although nitrogen control exerts a greater influence than phosphorus control on the entire system, nitrogen control alone is not desirable. Nitrogen control alone increases the system-wide concentrations of total and dissolved inorganic phosphorus. The increase occurs because algal uptake of phosphorus is diminished when production is strongly limited by nitrogen controls. Increased dissolved phosphate is detrimental to living-resource goals established for submerged aquatic vegetation.

Dissolved Oxygen. Under LOT nutrient controls, the volume of anoxic (dissolved oxygen $\leq$ 1 gm m^{-3}) water in an average hydrologic year is reduced by forty percent from existing conditions. Minimum summer-average dissolved oxygen increases from 0.13 gm m^{-3} under existing conditions to 0.75 gm m^{-3} with LOT nutrient controls (Figure 16-31). In the absence of nutrient controls, dissolved oxygen in the Bay will continue to deteriorate due to trends in nitrogen concentration at two major fall lines.

Under all-forest conditions, anoxia was virtually absent from the Bay during average hydrologic conditions. Anoxia was present in unusually wet years accompanied by high stratification. The anoxic volume was only twenty-five percent of the volume under existing conditions with the same hydrology, however.

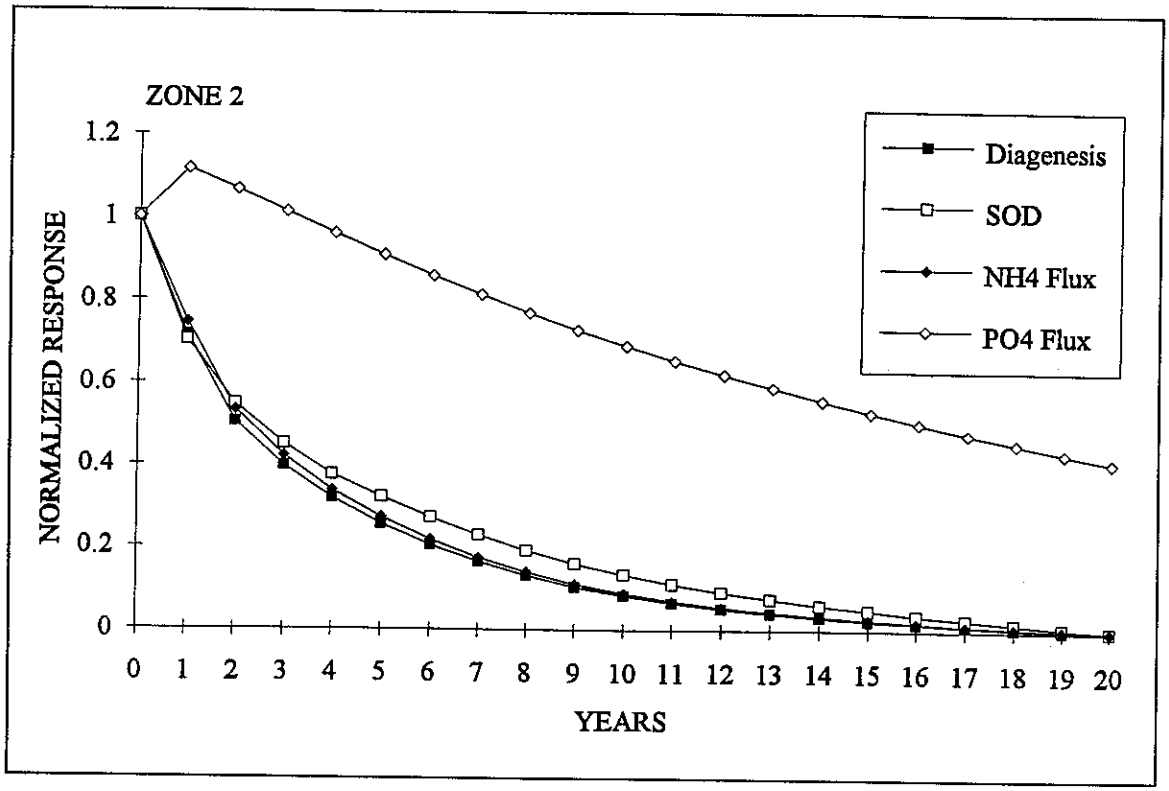

Figure 16-29. Sediment Diagenesis and Fluxes - Time to Steady State at Head of Deep Trench

Comparison With Current Paradigms

In 1992, a workshop convened to examine oxygen dynamics in Chesapeake Bay. The consensus of the workshop was published in summary form (Harding, Leffler, and Mackiernan 1992). A very high degree of correspondence exists between the workshop consensus and the independent conclusions of this report.

The Historic Record. The workshop concluded oxygen depletion has increased since colonial times. The present study indicated minimum summer-average bottom dissolved oxygen, under average hydrology, has declined from 2.7 gm m^{-3} in all-forest conditions to 0.13 gm m^{-3} under existing conditions.

Anoxic Volume. The workshop concluded anoxic volume is determined largely by spring flow in the Susquehanna River and intensity of vertical stratification. The present study indicated a correlation coefficient r = 0.92 between anoxic volume and hydrodynamics. The study also indicated stratification is a more significant determinant of anoxic volume than runoff-borne nutrient loads.

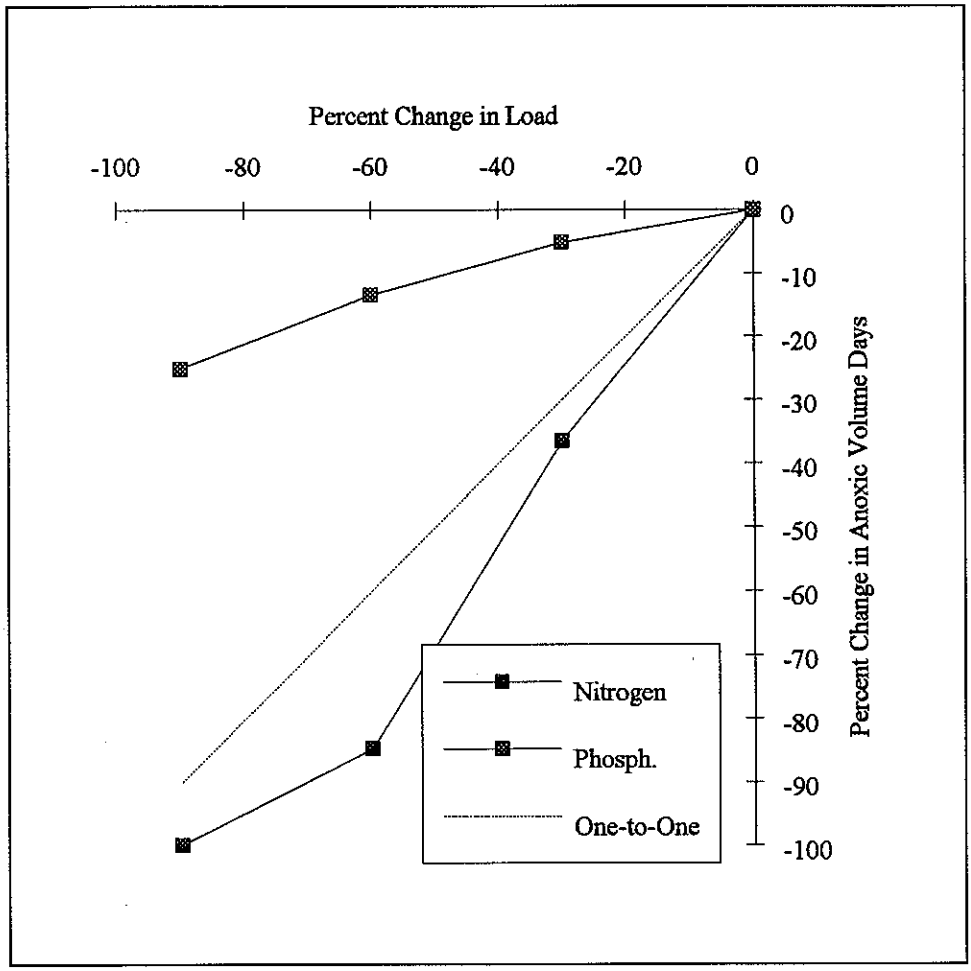

Figure 16-30. Response of Anoxic Volume to Reduction in Nitrogen and Phosphorus Load

Spring Biomass Versus Summer Production. The workshop reported spring is the period of maximum algal biomass but summer is the period of maximum algal production. This characteristic was reproduced by the model.

Nitrification/Denitrification. The workshop reported oxygen depletion in bottom waters inhibits the coupled nitrification-denitrification sequence in sediments. The model indicated the decline of dissolved oxygen from all-forest to existing conditions was accompanied by a decline in denitrification. The fraction of deposited nitrogen denitrified decreased from 63% under all-forest conditions to 30% under existing conditions.

Potential Dissolved Oxygen Improvements. The workshop indicated 40% to 50% load reductions were likely to improve bottom dissolved oxygen by <0.5 to 1-2 gm m^{-3}. The present study indicated the maximum dissolved oxygen improvement from LOT nutrient controls (≈30% nitrogen reduction, ≈50% phosphorus reduction) is 0.62 gm m^{-3}.

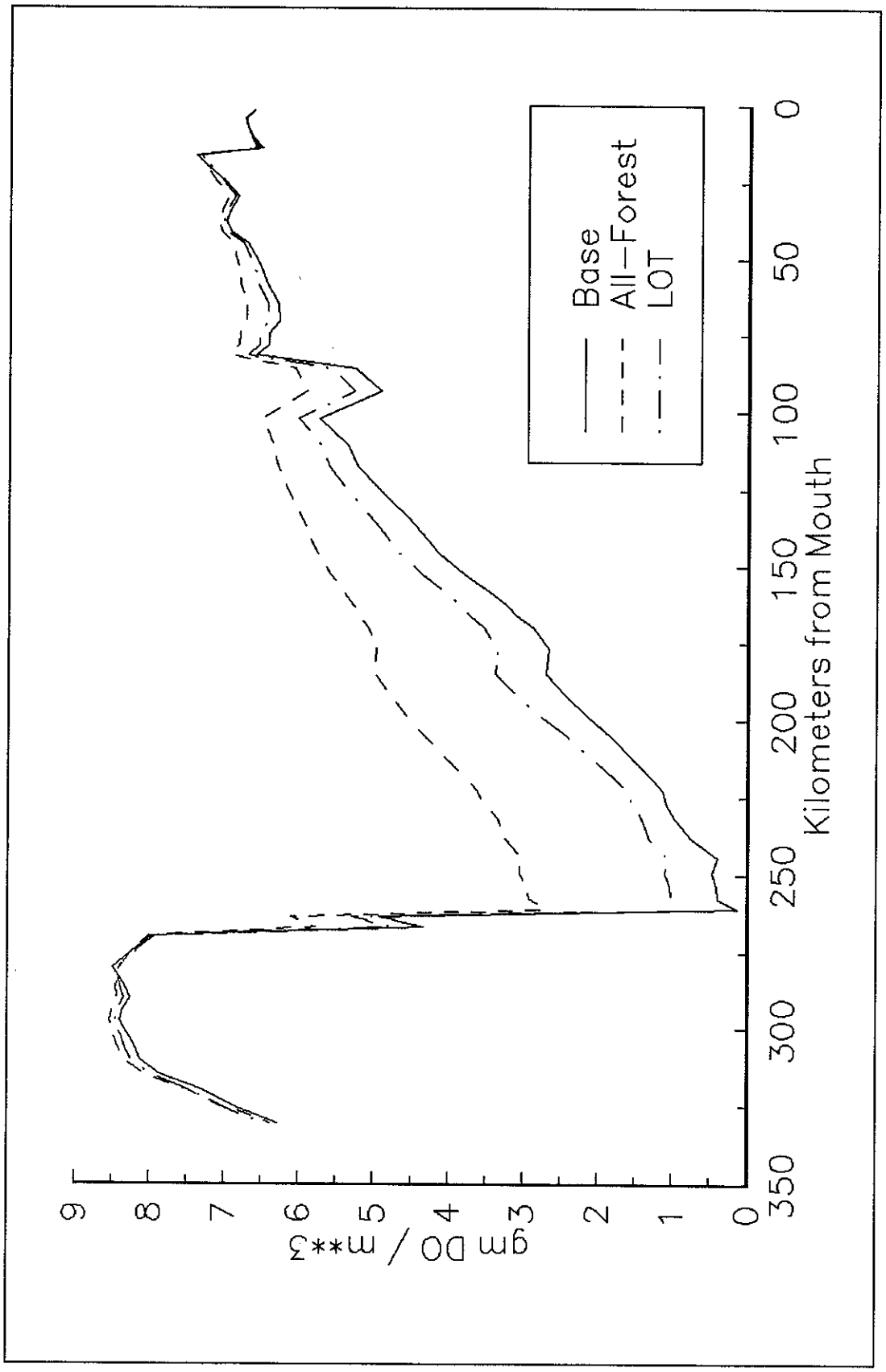

Figure 16-31. Summer-Average Bottom Dissolved Oxygen Under Average Hydrologic Conditions

In Conclusion

The present model represents the state of the art in eutrophication modeling. The model provides three significant advances over the previous state of the art. The first is coupling of the model to a three-dimensional, time-varying hydrodynamic model. The second is coupling to a fully-predictive sediment oxygen demand and nutrient flux model. The third is continuous, multi-year application on an intertidal time scale.

The model meets or exceeds the goals specified at the initiation of the study. The model exhibits a high degree of correspondence to observations of the system and to current consensus regarding eutrophication processes in the Bay. The model is fully acceptable as a tool for management of eutrophication in the mainstem portion of Chesapeake Bay.

References

Almgren, T., and Hagstrom, I. (1974). "The oxidation rate of sulphide in seawater," *Water Research*, 8, 395-400.z

American Society of Civil Engineers. (1961). "Effect of water temperature on stream reaeration," *Journal of the Sanitary Engineering Division*, 87(SA6), 59-71.

Ammerman, J., and Azam, F. (1985). "Bacterial 5'-nucleodase in aquatic ecosystems: A novel mechanism of phosphorus regeneration," *Science*, 227, 1338-1340.

An, T. (1991). Personal communication.

Anderson, G. (1986). "Silica, diatoms and a freshwater productivity maximum in Atlantic coastal plain estuaries, Chesapeake Bay," *Estuarine, Coastal and Shelf Science*, 22, 183-197.

Bahner, L., Reynolds, R., and Batuik, R. (1990). "Volumetric analysis of dissolved oxygen trends in the Chesapeake Bay: Preliminary findings," U.S. Environmental Protection Agency, Chesapeake Bay Program Office, Annapolis, MD.

Baler, W. (1982). "On the distribution of iron and manganese at the sediment/water interface: thermodynamic versus kinetic control," *Geochimica et Cosmochimica Acta*, 46, 1153-1161.

Beers, J. (1986). "Organisms and the food web," *Plankton dynamics of the southern California Bight*, Lecture Notes on Coastal and Estuarine Studies 15, Springer-Verlag, 84-175.

Beers, J., and Brownlee, D. (1988). "Laboratory observations on the reproduction and feeding of a marine pelagic Strombinid Ciliate," submitted to *Marine Microbial Food Webs.*

Bergstrom, P. (1989). Personal communication.

Berounsky, V., and Nixon, S. (1985). "Eutrophication and the rate of net nitrification in a coastal marine ecosystem," *Estuarine, Coastal and Shelf Science*, 20, 773-781.

Bieber, S., and Magnien, R. (1991a). "An assessment of nitrogen concentrations at the mouth of Chesapeake Bay and adjacent coastal waters," Maryland Department of the Environment, Baltimore, MD.

Bieber, S., and Magnien, R. (1991b). "An assessment of phosphorus concentrations at the mouth of Chesapeake Bay and adjacent coastal waters," Maryland Department of the Environment, Baltimore, MD.

Bird, D., and Kalff, J. (1984). "Empirical relationships between bacterial abundance and chlorophyll concentration in fresh and marine waters," *Canadian Journal of Fisheries and Aquatic Science*, 41, 1015-1023.

Boicourt, W., Chao, S., Ducklow, H., Glibert, P., Malone, T., Roman, M., Sanford, L., Fuhrman, J., Garside, C., and Garvine, R. (1987). "Physics and microbial ecology of a buoyant estuarine plume on the continental shelf," *Eos*, 68(31), 666-668.

Boicourt, W. (1992). "Influences of circulation processes on dissolved oxygen in the Chesapeake Bay," *Oxygen dynamics in the Chesapeake Bay*, Smith, Leffler, and Mackiernan eds., Maryland Sea Grant, College Park, MD., 7-60.

Boni, L., Carpene, E., Wynne, D., and Reti, M. (1989). "Alkaline phosphatase activity in *Protogonyaulax tamarensis*," *Journal of plankton research*, 11, 879-885.

Bowie, G., Mills, W., Porcella, D., Campbell, C., Pagenkopf, J., Rupp, G., Johnson, K., Chan, P., Gherini, S., and Chamberlin, C. (1985). "Rates, constants, and kinetics formulations in surface water modeling," 2nd ed., EPA/600/3-85/040, U.S. Environmental Protection Agency, Athens, GA.

Boynton, W., Kemp, W., and Keefe, C. (1982). "A comparative analysis of nutrients and other factors influencing estuarine phytoplankton production," *Estuarine comparisons*, Academic Press, 69-90.

Boynton, W., and Kemp, W. (1985). "Nutrient regeneration and oxygen consumption along an estuarine salinity gradient," *Marine Ecology Progress Series*, 23, 45-55.

Boynton, W., Kemp, M., Garber, J., and Barnes, J. (1986). "Ecosystem processes component (EPC) level I data report no. 3," [UMCEES]CBL Ref. No. 86-56, University of Maryland System Center for Environmental and Estuarine Studies, Solomons, MD.

Boynton, W., Kemp, M., Barnes, J., Matteson, L., Watts, J., Stammerjohn, S., Jasinski, D., and Rohland, F. (1991). "Ecosystem processes component (EPC) level I data report no. 8," [UMCEES]CBL Ref. No. 91-110a, University of Maryland System Center for Environmental and Estuarine Studies, Solomons, MD.

Brush, G. (1984). "Patterns of recent sediment accumulation in Chesapeake Bay (Virginia-Maryland, U.S.A.) tributaries," *Chemical Geology*, 44, 227-242.

Brush, G. (1989). "Rates and patterns of estuarine sediment accumulation," *Limnology and Oceanography,* 34(7), 1235-1246.

Byrne, R., Hobbs, C., and Carron, M. (1983). "Baseline sediment studies to determine distribution, physical properties, sedimentation budgets and rates in the Virginia portion of the Chesapeake Bay," Virginia Institute of Marine Science, Gloucester Point, VA.

Canale, R., and Vogel, A. (1974). "Effects of temperature on phytoplankton growth," *Journal of the Environmental Engineering Division,* 100, 231-241.

Cerco, C. (1985a). "Sediment-water column exchanges of nutrients and oxygen in the tidal James and Appomattox rivers," Virginia Institute of Marine Science, Gloucester Point, VA.

_____. (1985b). "Effect of temperature and dissolved oxygen on sediment-water nutrient flux," Virginia Institute of Marine Science, Gloucester Point, VA.

_____. (1985c). "Water quality in a Virginia Potomac embayment: Gunston Cove," Virginia Institute of Marine Science, Gloucester Point, VA.

_____. (1989). "Estimating estuarine reaeration rates," *Journal of the Environmental Engineering Division,* 115(5), 1066-1070.

Cerco, C., Bunch, B., Cialone, M., and Wang, H. (1993). "Hydrodynamic and eutrophication model study of Indian River-Rehoboth Bay Delaware," U.S. Army Engineer Waterways Experiment Station, Vicksburg, MS.

Charley, R., Hooper, D., and McLee, A. (1980). "Nitrification kinetics in activated sludge at various temperatures and dissolved oxygen concentrations," *Water Research,* 14, 1387-1396.

Chen, H., Hyer, P., and Unkulvasapaul, Y. (1984). "Summary report on calibration of water quality models of the Chesapeake Bay system," Virginia Institute of Marine Science, Gloucester Point, VA.

Chesapeake Bay Program Office. (1991). "1990 progress report for the baywide nutrient reduction strategy," U.S. Environmental Protection Agency, Chesapeake Bay Program Office, Annapolis, MD, pp 42.

_____. (1992). "Trends in nitrogen in the Chesapeake Bay 1984-1990," CBP/TRS 68/92, U.S. Environmental Protection Agency, Chesapeake Bay Program Office, Annapolis, MD.

Chrost, R., and Overbeck, J. (1987). "Kinetics of alkaline phosphatase activity and phosphorus availability for phytoplankton and bacterioplankton in Lake Plubsee (north German eutrophic lake)," *Microbial Ecology,* 13, 229-248.

Cohen, R., Dresler, P., Phillips, E., and Cory, R. (1984). "The effect of the Asiatic clam, *Corbicula Fluminea,* on phytoplankton of the Potomac River, Maryland," *Limnology and Oceanography,* 29, 170-180.

Cohn, T., DeLong, L., Gilroy, E., Hirsch, R., and Wells, D. (1989). "Estimating constituent loads," *Water Resources Research,* 25, 937-942.

Cole, J., Findlay, S., and Pace, M. (1988). "Bacterial production in fresh and saltwater ecosystems: A cross-system overview," *Marine Ecology Progress Series,* 43, 1-10.

Collins, C., and Wlosinski, J. (1983). "Coefficients for use in the U.S. Army Corps of Engineers reservoir model CE-QUAL-R1," Technical Report E-83-5, U.S. Army Engineer Waterways Experiment Station, Vicksburg, MS.

Computer Sciences Corporation. (1991). "Trends in phosphorus in the Chesapeake Bay 1984-1990," CBP/TRS 67/91, Chesapeake Bay Program Office, U.S. Environmental Protection Agency, Annapolis, MD.

_____. (1992). "Investigation of low DO," Unpublished manuscript, Chesapeake Bay Program Office, U.S. Environmental Protection Agency, Annapolis, MD.

Conley, D., and Malone, T. (1992). "Annual cycle of dissolved silicate in Chesapeake Bay: Implications for the production and fate of phytoplankton biomass," *Marine Ecology Progress Series,* 81, 121-128.

Cooper, S., and Brush, G. (1991). "Long-term history of Chesapeake Bay anoxia," *Science,* 254, 992-996.

Davies-Colley, R., and Vant, W. (1988). "Estimation of optical properties of water from Secchi disk depth," *Water Resources Bulletin,* 24, 1329-1335.

Davis, C., Breitner, N., and Harrison, P. (1978). "Continuous culture of marine diatoms under silicon limitation. 3. A model of Si-limited diatom growth," *Limnology and Oceanography,* 23, 41-52.

D'Elia, C., Nelson, D., and Boynton, W. (1983). "Chesapeake Bay nutrient and plankton dynamics: III. The annual cycle of silicon," *Geochimica et Cosmochimica Acta,* 47, 1945-1955.

D'Elia, C., Sanders, J., and Boynton, W. (1986). "Nutrient enrichment studies in a coastal plain estuary: phytoplankton growth in large-scale, continuous cultures," *Canadian Journal of Fisheries and Aquatic Sciences,* 43, 397-406.

DiToro, D., O'Connor, S., and Thomann, R. (1971). "A dynamic model of the phytoplankton population in the Sacramento-San Joaquin Delta," *Non-equilibrium systems in water chemistry,* American Chemical Society, Washington, DC, 131-180.

DiToro, D. (1980). "Applicability of cellular equilibrium and Monod theory to phytoplankton growth kinetics," *Ecological Modelling,* 8, 201-218.

DiToro, D., Paquin, P., Subburamu, K., and Gruber, D. (1990). "Sediment oxygen demand model: methane and ammonia oxidation," *Journal of Environmental Engineering,* 116(5), 945-986.

DiToro, D., and Fitzpatrick, J. (1993). "Chesapeake Bay sediment flux model," Contract Report EL-93-2, U.S. Army Engineer Waterways Experiment Station, Vicksburg, MS.

Donigian, A., Bicknell, B., Patwardhan, A., Linker, L., Alegre, D., Chang, C., and Reynolds, R. (1991). "Watershed model application to calculate bay nutrient loadings," Chesapeake Bay Program Office, U.S. Environmental Protection Agency, Annapolis, MD.

Dortch, M. (1990). "Three-dimensional, Lagrangian residual transport computed from an intratidal hydrodynamic model," Technical Report EL-90-11, U.S. Army Engineer Waterways Experiment Station, Vicksburg, MS.

Droop, M. (1973). "Some thoughts on nutrient limitation in algae," *Journal of Phycology*, 9, 264-272.

Eaton, A. (1979). "The impact of anoxia on Mn fluxes in the Chesapeake Bay," *Geochimica et Cosmochimica Acta*, 43, 429-432.

Edinger, J., Brady, D., and Geyer, J. (1974). "Heat exchange and transport in the environment," Report 14, Department of Geography and Environmental Engineering, Johns Hopkins University, Baltimore, MD.

Effler, S. (1985). "Attenuation versus transparency," *Journal of the Environmental Engineering Division*, 111(4), 448-459.

Fisher, T., Carlson, P., and Barber, R. (1982). "Sediment nutrient regeneration in three North Carolina estuaries," *Estuarine, Coastal and Shelf Science*, 4, 101-116.

Fisher, T., Peele, E., Ammerman, J., and Harding, L. (1992). "Nutrient limitation of phytoplankton in Chesapeake Bay," *Marine Ecology Progress Series*, 82,51-63.

Fitzpatrick, J. (1991). Personal communication.

Flemer, D., Mackiernan, G., Nehlsen, W., and Tippie, V. (1983). "Chesapeake Bay: A profile of environmental change," U.S. Environmental Protection Agency, Region III, Philadelphia, PA.

Flemer, D., Biggs, R., Tippie, V., Nehlsen, W., Mackiernan, G., and Price, K. (1987). "Characterizing the Chesapeake Bay ecosystem and lessons learned," *Estuarine and Coastal Management - Tools of the Trade*, Lynch and McDonald eds., The Coastal Society, Bethesda, MD., 153-177.

Foree, E., and McCarty, P. (1970). "Anaerobic decomposition of algae," *Environmental Science and Technology*, 4, 842-849.

Garber, J. (1984). "Laboratory study of nitrogen and phosphorus remineralization during the decomposition of coastal plankton and seston," *Estuarine, Coastal and Shelf Science*, 18, 685-702.

Garber, J., Boynton, W., Barnes, J., Matteson, L., Robertson, L., Ward, A., Watts, J. (1988). "Ecosystem processes component (EPC) and benthic exchange and sediment transformation (BEST)," [UMCEES]CBL Ref. No. 88-90, University Of Maryland System Center for Environmental and stuarine Studies, Solomons, MD.

Gardner, W., Seitzinger, S., and Malczyk, J. (1991). "The effects of sea salts on the forms of nitrogen released from estuarine and freshwater sediments: does ion pairing affect ammonium flux?," *Estuaries,* 14(2), 157-166.

Gavis, J., and Grant, V. (1986). "Sulfide, iron, manganese, and phosphate in the deep water of the Chesapeake Bay during anoxia," *Estuarine, Coastal and Shelf Science,* 23, 451-463.

Genet, L., Smith, D., and Sonnen, M. (1974). "Computer program documentation for the Dynamic Estuary Model," U.S. Environmental Protection Agency, Systems Development Branch, Washington, DC.

Goodrich, D., van Montfrans, J., and Orth, R. (1989). "Blue crab megalopal influx to Chesapeake Bay: Evidence for a wind-driven mechanism," *Estuarine, Coastal and Shelf Science,* 29, 247-260.

Goodwin, S., Schultz, B., Parkhurst, D., Simon, N., and Callender, E. (1984). "Methods for the collection of geochemical data from the sediments of the tidal Potomac River and estuary and data for 1978-1980," Open-File Report 84-074, U.S. Geological Survey, Reston, VA.

Graham, W., Bender, M., and Klinkhammer, G. (1976). "Manganese in Narragansett Bay," *Limnology and Oceanography,* 21, 665-673.

Grill, E., and Richards, F. (1964). "Nutrient regeneration from phytoplankton decomposing in seawater," *Journal of Marine Research,* 22, 51-69.

Guide, V., and Villa, O. (1972). "Chesapeake Bay nutrient input study," Technical Report 47, Annapolis Field Office, U.S. Environmental Protection Agency, Annapolis, MD.

Hall, R., and Dortch, M. (1993). "New York Bight study report 2 - development and application of a eutrophication/general water quality model," Technical Report EL-93-xx, U.S. Army Engineer Waterways Experiment Station, Vicksburg, MS.

Harding, L., Meeson, B., and Fisher, T. (1986). "Phytoplankton production in two east coast estuaries: Photosynthesis-light functions and patterns of carbon assimilation in Chesapeake and Delaware Bays," *Estuarine, Coastal and Shelf Science,* 23, 773-806.

Harding, L., Leffler, M., and Mackiernan, G. (1992). "Dissolved oxygen in Chesapeake Bay: A scientific consensus," UM-SG-TS-92-03, Maryland Sea Grant, University of Maryland, College Park, MD.

Hecky, R., and Kilham, P. (1988). "Nutrient limitation of phytoplankton in freshwater and marine environments: A review of recent evidence on the effects of enrichment," *Limnology and Oceanography,* 33(4), 796-822.

Heinle, D., D'Elia, C., Taft. J., Wilson, J., Cole-Jones, M., Caplins, A., Cronin, E. (1980). "A historical review of water quality and climatic data from Chesapeake Bay with emphasis on effects of enrichment," CBP-TR-002E, U.S. Environmental Protection Agency, Chesapeake Bay Program, Annapolis, MD.

Helder, W. and DeVries, R. (1983). "Estuarine nitrite maxima and nitrifying bacteria (Ems Dollard Estuary)," *Netherlands Journal of Sea Research,* 17, 1-18.

Holmes, R. (1970). "The Secchi disk in turbid coastal water," *Limnology and Oceanography,* 15, 688-694.

Horrigan, S., Montoya, J., Nevins, J., McCarthy, J., Ducklow, H., Goericke, R., and Malone, T. (1990). "Nitrogenous nutrient transformations in the spring and fall in the Chesapeake Bay," *Estuarine, Coastal and Shelf Science,* 30, 369-391.

HydroQual. (1987). "A steady-state coupled hydrodynamic/water quality model of the eutrophication and anoxia process in Chesapeake Bay," Final report, HydroQual Inc., Mahwah, NJ.

_____. (1989). "Estimation of fall-line water quality concentrations for the Chesapeake Bay basin," U.S.CE0201, HydroQual Inc., Mahwah, NJ.

_____. (1991). "Water quality modeling analysis of hypoxia in Long Island Sound," HydroQual Inc., Mahwah, NJ.

Jenkins, M., and Kemp, W. (1984). "The coupling of nitrification and denitrification in two estuarine sediments," *Limnology and Oceanography,* 29(3), 609-619.

Johnson, B., Kim, K., Heath, R., and Butler, L. (1991). "Development and verification of a three-dimensional numerical hydrodynamic, salinity and temperature model of Chesapeake Bay," Technical Report HL-91-7, U.S. Army Engineer Waterways Experiment Station, Vicksburg, MS.

Kator, H. (1990). Personal communication.

Keefe, C. (1993). "The contribution of inorganic compounds to the particulate carbon, nitrogen, and phosphorus in suspended matter and surface sediments of Chesapeake Bay," *Estuaries,* in press.

Kemp, W., Sampou, P., Garber, J., Tuttle, J., and Boynton, W. (1992). "Seasonal depletion of oxygen from bottom waters of Chesapeake Bay: Roles of benthic and planktonic respiration and physical exchange processes," *Marine Ecology Progress Series,* 85, 137-152.

Kemp, W., and Boynton, W. (1992). "Benthic-pelagic interactions: Nutrient and oxygen dynamics," *Oxygen dynamics in the Chesapeake Bay,* Smith, Leffler, and Mackiernan eds., Maryland Sea Grant, College Park, MD., 149-222.

Kerhin, R., Halka, J., Hennessee, E., Blakeslee, P., Wells, D., Zoltan, N., and Cuthbertson, R. (1983). "Physical characteristics and sediment budget for bottom sediments in the Maryland portion of Chesapeake Bay," Contract No. EPA R805965, Office of Research and Development, U.S. Environmental Protection Agency, Washington, DC.

Kremer, J., and Nixon, S. (1978). *A coasta marine ecosystem simulation and analysis,* Springer Verlag, New York, NY.

Kuo, A., and Neilson, B. (1987). "Hypoxia and salinity in Virginia estuaries," *Estuaries,* 10(4), 277-283.

Kuo, A., Park. K., and Moustafa, Z. (1991). "Spatial and temporal variabilities of hypoxia in the Rappahannock River, Virginia," *Estuaries,* 14(2), 113-121.

Laws, E., and Wong, D. (1978). "Studies of carbon and nitrogen metabolism by three marine phytoplankton species in nitrate-limited continuous culture," *Journal of Phycology,* 14, 406-416.

Laws, E., and Archie, J. (1981). "Appropriate use of regression analysis in marine biology," *Marine Biology,* 65, 13-16.

Leonard, B. (1979). "A stable and accurate convection modelling procedure based on quadratic upstream interpolation," *Computer Methods in Applied mechanics and Engineering,* 19, 59-98.

Lipschultz, F., Wofsy, S., and Fox, L. (1986). "Nitrogen metabolism of the eutrophic Delaware River ecosystem," *Limnology and Oceanography,* 31, 701-716.

Luther, G., Ferdelman, T., and Tsamakis, E. (1988). "Evidence suggesting anaerobic oxidation of the bisulfide ion in Chesapeake Bay," *Estuaries,* 11, 281-285.

Malone, T., Crocker, L., Pike, S., and Wendler, B. (1988). "Influences of river flow on the dynamics of phytoplankton production in a partially stratified estuary," *Marine Ecology Progress Series,* 48, 235-249.

Matavulj, M., and Flint, K. (1987). "A model for acid and alkaline phosphatase activity in a small pond," *Microbial Ecology,* 13, 141-158.

Millero, F. (1991). "The oxidation of H_2S in the Chesapeake Bay," *Estuarine, Coastal and Shelf Science,* 33, 521-527.

Monod, J. (1949). "The growth of bacterial cultures," *Annual Review of Microbiology,* 3, 371-394.

Moon, C., and Dunstan, W. (1990). "Hydrodynamic trapping in the formation of the chlorophyll "a" peak in turbid, very low salinity waters of estuaries," *Journal of Plankton Research,* 12(2), 323-336.

Morel, F. (1983). *Principles of Aquatic Chemistry,* John Wiley and Sons, New York, NY, 150.

National Atmospheric Deposition Program (IR-7)/National Trends Network. (1989). NADP/NTN Coordination Office, Natural Resources Ecology Laboratory, Colorado State University, Fort Collins, CO.

Nixon, S. (1981). "Remineralization and nutrient cycling in coastal marine ecosystems," *Estuaries and Nutrients,* Neilson and Cronin eds., Humana Press, Clifton, NJ., 111-138.

_____. (1987). "Chesapeake ay nutrient budgets - a reassessment," *Biogeochemistry,* 4, 77-90.

O'Connor, D., and Dobbins, W. (1958). "Mechanisms of reaeration in natural streams," *Transactions of the American Society of Civil Engineers,* 123, 641-666.

O'Connor, D. (1983). "Wind effects on gas-liquid transfer coefficients," *Journal of the Environmental Engineering Division,* 190, 731-752.

_____. (1988). "Models of sorptive toxic substances in freshwater systems. I: Basic equations," *Journal of the Environmental Engineering Division,* 114(3), 507-532.

Odum, E. (1971). *Fundamentals of Ecology,* 3rd ed., W. B. Saunders, Philadelphia, PA, pp 106-107.

Office of Environmental Programs. (1987). "Monitoring for management actions - Chesapeake Bay water quality monitoring program - first biennial report," Maryland Department of Health and Mental Hygiene, Baltimore, MD.

Officer, C., Lynch, D., Setlock, G., and Helz, G. (1984). "Recent sedimentation rates in Chesapeake Bay," *The estuary as a filter,* Academic Press, 131-157.

Otsuki, A., and Hanya, T. (1972). "Production of dissolved organic matter from dead green algal cells. I. Aerobic microbial decomposition," *Limnology and Oceanography,* 17, 248-257.

Owens, N. (1986). "Estuarine nitrification: A naturally occurring fluidized bed reaction?," *Estuarine, Coastal and Shelf Science,* 22, 31-44.

Parsons, T., Takahashi, M., and Hargrave, B. (1984). *Biological oceanographic processes,* 3rd ed., Pergamon Press, Oxford.

Pennock, J. (1985). "Chlorophyll distributions in the Delaware Estuary: Regulation by light-limitation," *Estuarine, Coastal and Shelf Science,* 21, 711-725.

Pett, R. (1989). "Kinetics of microbial mineralization of organic carbon from detrital *Skeletonema Costatum* cells," *Marine Ecology Progress Series,* 52, 123-128.

Pritchard, D. (1967). "Observations of circulation in coastal plain estuaries." *Estuaries.* G. Lauff ed., American Association for the Advancement of Science, Washington, 37-44.

Raven, J., and Beardall, J. (1981). "Respiration and photorespiration," *Physiological Bases of Phytoplankton Ecology*, Bulletin 210, Canadian Bulletin of Fisheries and Aquatic Sciences.

Redfield, A., Ketchum, B., and Richards, F. (1966). "The influence of organisms on the composition of sea-water." *The Sea Volume II*. Interscience Publishers, New York, 26-48.

Ricker, W. (1973). "Linear regressions in fishery research," *Journal of the Fisheries Research Board of Canada*, 30, 409-434.

Roman, M., Ducklow, H., Furhrman, J., Garside, C., Gilbert, P., Malone, T., and McManus, G. (1988). "Production, consumption, and nutrient cycling in a laboratory mesocosm," *Marine Ecology Progress Series*, 42, 39-52.

SAS Institute Inc. (1988). *SAS/STAT User's Guide, Release 6.03 Edition*, SAS Institute Inc., Cary, NC.

Sanders, J., Cibik, S., D'Elia, C., and Boynton, W. (1987). "Nutrient enrichment studies in a coastal plain estuary: Changes in phytoplankton species composition," *Canadian Journal of Fisheries and Aquatic Sciences*, 44, 83-90.

Scavia, D. (1980). "An ecological model of Lake Ontario," *Ecological Modeling*, 8, 49-78.

Seitzinger, S., Nixon, S., and Pilson, M. (1984). "Denitrification and nitrous oxide production in a coastal marine ecosystem," *Limnology and Oceanography*, 29(1), 73-83.

Seliger, H., and Boggs, J. (1988). "Long-term pattern of anoxia in the Chesapeake Bay," *Understanding the Estuary: Advances in Chesapeake Bay Research*, Chesapeake Research Consortium, Baltimore, MD., 570- 585.

Sellner, K., Lacoutre, R., and Parrish, C. (1988). "Effects of increasing salinity on a Cyanobacteria bloom in the Potomac River Estuary," *Journal of Plankton Research*, 10, 49-61.

Sellner, K. (1989). Personal communication.

Sharma, B., and Ahlert, R. (1977). "Nitrification and nitrogen removal," *Water Research*, 11, 897-925.

Sheng, Y. (1986). "A three-dimensional mathematical model of coastal, estuarine and lake currents using boundary fitted grid," Report 585, ARAP Group of Titan Systems, Princeton, NJ.

Skrabal, S. (1991). "Clay mineral distributions and source discrimination of upper quaternary sediments, lower Chesapeake Bay, Virginia," *Estuaries*, 14(1), 29-37.

Steele, J. (1962). "Environmental control of photosynthesis in the sea," *Limnology and Oceanography*, 7, 137-150.

Storms, S. (1974). "Selective feeding, ingestion and assimilation rates, and distribution of the Copepod *Acartia* in Chesapeake Bay," Ph.D. dissertation, Johns Hopkins University, Baltimore, MD.

Stratton, F., and McCarty, P. (1967). "Prediction of nitrification effects on the dissolved oxygen balance of streams," *Environmental Science and Technology*, 1, 405-410.

Strickland, J. (1960). "Measuring the production of marine phytoplankton," *Fisheries Research Board of Canada Bulletin*, 122, 172.

Summers, R. (1991). Personal communication.

Taft, J., Taylor, W., and McCarthy, J. (1975). "Uptake and release of phosphorus by phytoplankton in the Chesapeake Bay estuary, U.S.A," Marine Biology, 33, 21-32.

Tchobanoglous, G., and Schroeder, E. (1987). *Water quality*, Addison Wesley, Reading, MA.

Thomann, R., Winfield, R., and Segna, J. (1979). "Verification analysis of Lake Ontario and Rochester Embayment three-dimensional eutrophication models," EPA-600/3-79-094, U.S. Environmental Protection Agency, Duluth, MN.

Thomann, R. (1982). "Verification of water quality models," *Journal of the Environmental Engineering Division*, 108(EE5), 923-940.

Thomann, R., and Fitzpatrick, J. (1982). "Calibration and verification of a mathematical model of the eutrophication of the Potomac Estuary," Hydro-Qual Inc., Mahwah, NJ.

Thomann, R., Jaworski, N., Nixon, S., Paerl, H., and Taft, J. (1985). "The 1983 algal bloom in the Potomac Estuary," Report prepared for the Potomac Strategy State/EPA Management Committee.

Thomann, R., Collier, J., Butt, A., Casman, E., and Linker, L. (1994). "Technical analysis of response of Chesapeake Bay water quality model to loading scenarios," Chesapeake Bay Program Office, U.S. Environmental Protection Agency, Annapolis, MD.

Tuffey, T., Hunter, J., and Matulewich, V. (1974). "Zones of nitrification," *Water Resources Bulletin* 10, 555-564.

Tuttle, J., Malone, T., Jonas, R., Ducklow, H., and Cargo, D. (1986). "Nutrient-dissolved oxygen dynamics in Chesapeake Bay: The roles of phytoplankton and micro-heterotrophs under summer conditions," [UMCEES]CBL 86-125a, University of Maryland Center for Environmental and Estuarine Studies, Solomons, MD.

U.S. Environmental Protection Agency. (1982). "Chesapeake Bay Program technical studies, a synthesis," U.S. Environmental Protection Agency, Washington DC.

Vanderborght, J., Wollast, R., and Billen, G. (1977), "Kinetic models of diagenesis in disturbed sediments, part I, mass transfer properties and silica diagenesis," *Limnology and Oceanography*, 22(5), 787-793.

Walker, T. (1982). "Use of a Secchi disk to measure attenuation of underwater light for photosynthesis," *Journal of Applied Ecology*, 19, 539-544.

Wang, D., and Elliott, A. (1978). "Non-tidal variability in the Chesapeake Bay and Potomac River: Evidence for non-local forcing," *Journal of Physical Oceanography*, 8, 225-232.

Webb, K. (1988). Personal communication.

Wen, C., Kao, J., Wang, L., and Liaw, C. 1984). "Effect of salinity on reaeration coefficient of receiving waters," *Water Science and Technology*, 16, 139-154.

Westrich, J., and Berner, R. (1984). "The role of sedimentary organic matter in bacterial sulfate reduction: The G model tested," *Limnology and Oceanography*, 29, 236-249.

Wezernak, C., and Gannon, J. (1968). "Evaluation of nitrification in streams," *Journal of the Sanitary Engineering Division*, 94(SA5), 883-895.

Wheeler, P., Gilbert, P., and McCarthy, J. (1982). "Ammonium uptake and incorporation by Chesapeake Bay phytoplankton: Short-term uptake kinetics," *Limnology and Oceanography*, 27, 1113-1128.

Wilmot, P., Cadee, K., Katinic, J., and Kavanagh, B. (1988). "Kinetics of sulfide oxidation by dissolved oxygen," *Journal of the Water Pollution Control Federation*, 60, 1264-1270.

Wlosinski, J., and Collins, C. (1985). "Confirmation of the water quality model CE-QUAL-R1 using data from Eau Galle Reservoir, Wisconsin," Technical Report E-85-11, U.S. Army Engineer Waterways Experiment Station, Vicksburg, MS.

Wollast, R. (1974). "The silica problem," *The Sea Vol. 5*, Wiley-Interscience, New York, NY, 359-392.

Yamada, S., and D'Elia, C. (1984). "Silica acid regeneration from estuarine sediment cores," *Marine Ecology Progress Series*, 18, 113-188.

REPORT DOCUMENTATION PAGE

Form Approved
OMB No. 0704-0188

Public reporting burden for this collection of information is estimated to average 1 hour per response, including the time for reviewing instructions, searching existing data sources, gathering and maintaining the data needed, and completing and reviewing the collection of information. Send comments regarding this burden estimate or any other aspect of this collection of information, including suggestions for reducing this burden, to Washington Headquarters Services, Directorate for Information Operations and Reports, 1215 Jefferson Davis Highway, Suite 1204, Arlington, VA 22202-4302, and to the Office of Management and Budget, Paperwork Reduction Project (0704-0188), Washington, DC 20503.

1. AGENCY USE ONLY (Leave blank)	2. REPORT DATE	3. REPORT TYPE AND DATES COVERED
	May 1994	Final report

4. TITLE AND SUBTITLE
Three-Dimensional Eutrophication Model of Chesapeake Bay; Volume I, Main Report

5. FUNDING NUMBERS

6. AUTHOR(S)
Carl F. Cerco, Thomas M. Cole

7. PERFORMING ORGANIZATION NAME(S) AND ADDRESS(ES)
U.S. Army Engineer Waterways Experiment Station
3909 Halls Ferry Road
Vicksburg, MS 39180-6199

8. PERFORMING ORGANIZATION REPORT NUMBER
Technical Report
EL-94-4

9. SPONSORING/MONITORING AGENCY NAME(S) AND ADDRESS(ES)
Chesapeake Bay Program Office, U.S. Environmental Protection Agency, Annapolis, MD 21403; U.S. Army Engineer District, Baltimore, P.O. Box 1715, Baltimore, MD 21203-1715

10. SPONSORING/MONITORING AGENCY REPORT NUMBER

11. SUPPLEMENTARY NOTES
Available from National Technical Information Service, 5285 Port Royal Road, Springfield, VA 22161.

12a. DISTRIBUTION/AVAILABILITY STATEMENT
Approved for public release; distribution is unlimited.

12b. DISTRIBUTION CODE

13. ABSTRACT (Maximum 200 words)

A three-dimensional, time-variable, eutrophication model, CE-QUAL-ICM, was applied to Chesapeake Bay. The model incorporated 22 state variables that included physical properties, multiple forms of algae, carbon, nitrogen, phosphorus, and silica, and dissolved oxygen. The model was part of a larger package that included a three-dimensional hydrodynamic model and a benthic sediment diagenesis model.

The model was initially applied to a 3-year period, 1984-1986. The model successfully simulated water-column and sediment processes that affected water quality. Phenomena simulated include formation of the spring algal bloom subsequent to the annual peak in nutrient runoff, onset and breakup of summer anoxia, and coupling of organic particle deposition with sediment-water nutrient and oxygen fluxes.

The model was next applied in a 30-year simulation of water quality, 1959-1988. The model indicated long-term trends in water quality and affirmed the role of stratification in determining anoxia. Final application of the model was in a series of nutrient load-reduction sensitivity analyses.

The study demonstrated that complex eutrophication problems can be addressed with coupled three-dimensional hydrodynamic and water quality models.

14. SUBJECT TERMS			15. NUMBER OF PAGES
Chesapeake Bay	Eutrophication	Phosphorus	658
Dissolved oxygen	Models	Sediments	16. PRICE CODE
Estuaries	Nitrogen		

17. SECURITY CLASSIFICATION OF REPORT	18. SECURITY CLASSIFICATION OF THIS PAGE	19. SECURITY CLASSIFICATION OF ABSTRACT	20. LIMITATION OF ABSTRACT
UNCLASSIFIED	UNCLASSIFIED		